www.AIVC 2010.org

AIVC International Conference 2010

The 31st AIVC Conference
26-28 October 2010
Seoul, Korea

PROCEEDINGS

Host Organizations

Architectural Institute of Korea(AIK)

Korea Institute of Construction Technology(KICT)

IEA Energy Conservation in Buildings and Community Systems(ECBCS)

Air Infiltration and Ventilation Center(AIVC)

International Network for Information on Ventilation and Energy Performance(INIVE)

05 Program in Detail

Click on the titles to view the papers!

October 26(Tue) 2010

Time	Program		Location	
08:00~18:00	Registration		4F, Hotel Renaissance Seoul	
09:30~09:40	Welcome Speech *(Hway-Suh Kim, Korea)*		4F, UNIVERSAL	
09:40~10:20	Keynote Speech Ⅰ *(Hal Lavin, USA)*			
10:20~10:30	Break		PRE FUNCTION AREA	
	Session 1A Air Distribution Venue Topaz (Renaissance Seoul Hotel 4F) Chairs Yoshino Hiroshi, Geun Young Yun	Session 1B Chemical pollutants & Particles Venue Universal (Renaissance Seoul Hotel 4F) Chairs Carrie Francois Remi, Jaedong Chang		
10:30~10:55	1A-1 Year-round Energy Saving Potential for a Stratum Ventilated Subtropical Office *Zhang Lin (City University of Hong Kong)*	1B-1 Health Hazards in Indoor Air *Max H. SHERMAN (LBNL)*	4F, TOPAZ	4F, UNIVERSAL
10:55~11:20	1A-2 Numerical Prediction of Airflow and Temperature Distribution in Large-Scale Agricultural PVC Greenhouse *Keita Hattori (Kyushu University)*	1B-2 Experimental method for determining removal efficiency of house dust by mechanical ventilation *Kurihara Genta (Tohoku University)*		
11:20~11:45	1A-3 Exposure Risk Assessment by Coupled Analysis of CFD and SIR model in Enclosed Space *Takayuki Fukuoka (Kyushu University)*	1B-3 Distribution of CO in 30 Homes with Unvented Gas Fireplaces *Paul W. FRANCISCO (University of Illinois)*		
11:45~12:10		1B-4 Numerical prediction of particle transport passed through ventilator by CFD with Lagrangian method *Nguyen Lu Phuong (Kyushu University)*		
12:10~13:30	Lunch		3F, DIAMOND	
13:30~14:10	Keynote speech Ⅱ (Masanori Shukuya, Japan)		4F, UNIVERSAL	
14:10~14:20	Break			
	Session 2A Health Indoor Air Quality and Productivity 1 Venue Topaz (Renaissance Seoul Hotel 4F) Chairs Wouter Borsboom, Sumin Kim	Session 2B HVAC System 1 Venue Universal (Renaissance Seoul Hotel 4F) Chairs Pierre Deroubaix, Youngshik Kim		
14:20~14:45	2A-1 A Study on Indoor Environments Made by Thin Line Type Ventilators in Apartment Houses *Keun-Je CHO (Hongik Graduate School)*	2B-1 Rotary heat exchanger model for control and energy calculations *Bjørn R. SØRENSEN (Narvik University College)*	4F, TOPAZ	4F, UNIVERSAL
14:45~15:10	2A-2 A study on eco friendly furniture for mitigation of the indoor air pollution *Hyunsun AN (KICT)*			
15:10~16:10	Coffee break and Poster presentation		PRE FUNCTION AREA	
	Session 3A Health Indoor Air Quality and Productivity 2 Venue TOPAZ (Renaissance Seoul Hotel 4F) Chairs Ohba Masaaki, Janghoo Seo	Session 3B HVAC System 2 Venue Universal (Renaissance Seoul Hotel 4F) Chairs Li Angui, Jinwoo Moon		
16:10~16:35	3A-1 A Study on the field survey of the IAQ in the childcare center *Jung Ha PARK (Chung Ang University)*	3B-1 Measured Duct Leakage and Resulting Envelope Pressure Differences *Paul W. FRANCISCO (University of Illinois)*	4F, TOPAZ	4F, UNIVERSAL
16:35~17:00	3A-2 Case-Control study for the Association Between Indoor Environmental Factors and Children's Health Problems in Japan-Part1 a nationwide questionnaire study among 1664 primary school students *Ando Naoya (Tohoku University)*	3B-2 Calculation of Dehumidification Coeffecients for Numerical Simulation of Desiccant Wheel *Yoshihisa MOMOI (Osaka University)*		
17:00~17:25	3A-3 Case-Control study for the Association Between Indoor Environmental Factors and Children's Health Problems in Japan – Part 2 Results of Measurements during Rainy Season and Winter *Hamada Kensuke (Tohoku University)*	3B-3 Development of a heat pump system with the heat source network model using solar, ground and air heat source *Yujin NAM (The University of Tokyo)*		

05 Program in Detail

Click on the titles to view the papers!

Time	Program		Location	
17:25~17:50	3A-4 A Study on Incomplete Ventilation in High-Rise Residential Building *Jungmin Seo (Sungkyunkwan University)*	3B-4 Energy Saving Potentials of Dedicated Outdoor Air System in High-rise Apartment Buildings *Kim Min-Hwi (Sejong University)*	4F, TOPAZ	4F, UNIVERSAL
18:00~20:00	Welcome Party		3F, DIAMOND	

October 27(Wed) 2010

Time	Program			Location		
08:00~18:00	Registration			4F, Hotel Renaissance Seoul		
09:00~09:40	Keynote speech Ⅲ *(Yingxin Zhu, China)*			4F, TOPAZ		
09:40~09:50	Break					
	Session 4A Natural Ventilation 1 Venue TOPAZ (Renaissance Seoul Hotel 4F) Chairs Sherman Max, Jaehun Jo	Session 4B Computer Simulation 1 Venue Universal (Renaissance Seoul Hotel 4F) Chairs Op t Veld Peter, Jin chul Park	Workshop Workshop on Airtightness Measurement Techniques Venue Lily(Renaissance Seoul Hoteal 23F)			
09:50~10:15	4A-1 Prediction of Heat Emission Effect at Small Single-sided Openings in Apartment Houses *Keigo Nomura (The Univ. of Tokyo)*	4B-1 STUDY ON THE VENTILATION EFFICIENCY IN URBAN STREET CANYONS USING CFD ANALYSIS Influence of the Configuration of Consecutive Street Canyons and Atmospheric Stability *Byoungchull OH(The Univ. of Tokyo)*	6C-1 Recent developments with the revision of ISO 9972 *Hirsohi Yoshino (JAPAN)*	4F, TOPAZ	4F, SAPPHIRE + RUBY	23F, Lily
10:15~10:40	4A-2 Design Method of Vertical Ventilation with Wind Chimney on Roof Driven by Wind and Buoyancy *Toshio Yamanaka (Osaka University)*	4B-2 Energy Demand Prediction Method in the Operating Stage of the Office Building Using Real-Time Data *Young-Hoon Kwak (University of Seoul)*	6C-2 Estimating the uncertainty of an airtightness measurement *Max Sherman (USA)*			
10:40~10:50	Break			PRE FUNCTION AREA		
	Session 5A Natural Ventilation 2 Venue TOPAZ (Renaissance Seoul Hotel 4F) Chairs Charvat Pavel, Han Hwataik	Session 5B Computer Simulation 2 Venue SAPPHIRE+RUBY (Renaissance Seoul Hotel 4F) Chairs Willem de Gids, Gyeong Seok Choi				
10:50~11:15	5A-1 Effect of Intermittent Operation of Ventilation System on Indoor Air Quality in Apartments *Cheol-woong Shin (Hanyang University)*		6C-3 Common problems with building preparation *Stefanie Rolfsmeier (DENMARK)*	4F, TOPAZ	4F, SAPPHIRE + RUBY	23F, Lily
11:15~11:40	5A-2 Development of Zonal Model for Predicting Temperature Distribution inside an Office Room with Hybrid Air-conditioning System *Eunsu LIM (Osaka University)*	5B-2 Modularizing and Validating CFD Parts of Four-way Cassette Type Outlets *Hidekazu Tanaka (University of Tokyo)*	6C-4 Recent experience with tests on large buildings *Colin Genge (CANADA)*			
11:40~12:05	5A-3 Modelling wind driven airflow rate with CFD and verification of approximation formulas based on wind pressure coefficients *S. Leenknegt (K.U.Leuven)*	5B-3 Fungal Growth Prediction on Building Materials by Reaction-Diffusion Model Coupled with Heat and Moisture transfer *Kazuhide Ito (Kyushu University)*	Discussion			
12:05~13:30	Lunch			4F UNIVERSAL		

Click on the titles to view the papers!

Time	Program		Location	
	Session 6A Natural Ventilation 3 Venue TOPAZ (Renaissance Seoul Hotel 4F) Chairs Ito Kazuhide, Jae-Weon Jeong	Session 6B-1 Envelope Air Tightness Case Study Building Venue SAPPHIRE+RUBY (Renaissance Seoul Hotel 4F) Chairs Yun Gyu Lee, Hyuenjoon Moon		
13:30~13:55	6A-1 The influence of stochastic modeling of window actions on simulated summer comfort in office buildings *Wout PARYS (K.U.Leuven)*	6B-1 Ventilation and RH control in museum showcases *Marco PERINO (Politecnico di Torino)*	4F, TOPAZ	4F, SAPPHIRE + RUBY
13:55~14:20	6A-2 Influence of natural ventilation usage on cooling energy consumption and cooling capacity of an air conditioner *Hiromi HABARA(Hiroshima Institute of Technology)*	6B-2 Effective flow area estimation method using a gas *Koji Fujita(Kobe University)*		
14:20~14:45	6A-3 Implementation of measurement and quality frameworks in the french regulation for achieving airtight envelopes *F.R. Carrié (CETE de Lyon)*	6B-3 Development of Infiltration Modeling Parameters for a SIPs Building *Francisco Paul (University of Illinois)*		
14:45~15:10		6B-4 Analysis on CO2 Emissions Reduction Effect of Zero Energy Multi-famiy Housing to cope with UNFCCC *Yoon Yong Sang (KICT)*		
15:10~15:50	Coffee break and Poster display		PRE FUNCTION AREA	
	Session 7A Natural Ventilation 4 Venue TOPAZ (Renaissance Seoul Hotel 4F) Chairs Shen Henggen, Myungsouk Yeo	Session 7B Others Venue SAPPHIRE+RUBY (Renaissance Seoul Hotel 4F) Chairs Sun Sook Kim, Jaedong Chang		
15:50~16:15		7B-1 Robustness and True Performance of Demand Controlled Ventilation in Educational Buildings – Review and Needs for Future Development *Mads Mysen (SINTEF)*	4F, TOPAZ	4F, SAPPHIRE + RUBY
16:15~16:40	7A-2 Velocity Measurement Inside and Outside a Cross-Ventilated Building by Means of PIV *Hisashi KOTANI (Osaka University)*	7B-2 Energy Requirements of a Multi-Sensor Based Demand Control Ventilation System In Residential Buildings *Nam Chul Seong (Kyoungwon University)*		
16:40~17:05	7A-3 Building simulation on utilization of roof window in detached house by using cross-ventilation *Ohba Masaaki (Tokyo Polytechnic University)*	7B-3 Experimental Evaluation of the Moisture Buffering Effect of Hygrothermal Material *Suzuki Hiroaki (Tohoku University)*		
17:05~17:30	7A-4 The climatic potential for a double skin facade integrated with cross ventilation *Won-Jun Choi (University of Seoul)*			
18:00~20:00	Banquet (optional)		3F, DIAMOND	

05 Program in Detail

Click on the titles to view the papers!

October 28(Thu) 2010

Time	Program		Location	
08:00~18:00	Registration		4F, Hotel Renaissance Seoul	
09:00~09:40	Keynote speech Ⅳ *(Peter Wouter, Belgium)*		4F, TOPAZ	
09:40~09:50	Break			
	Session 8A Post Occupancy Evaluation and Surveys in Building Ventilation Venue TOPAZ (Renaissance Seoul Hotel 4F) Chairs Wouter Peter, SeungMin Lee	Session 8B Sustainable Technologies for Building Ventilation Venue SAPPHIRE+RUBY (Renaissance Seoul Hotel 4F) Chairs Schild Peter, Lee Keon Ho		
09:50~10:15	8A-1 Potential of the Solar Thermal Desiccant Cooling in Asia-Pacific Region *N. ENTERIA (SERIS, National University of Singapore)*	8B-1 Natural Ventilation in Thai Hospitals: A Field Study *Vorapat INKAROJRIT (Chulalongkorn University)*	4F, TOPAZ	4F, SAPPHIRE + RUBY
10:15~10:40	8A-2 Dynamic Insulation System applied to Window Frames (Part 1) Evaluation of the thermal insulation efficiency of the proposed window frames *Sihwan Lee (University of Tokyo)*	8B-2 Study on Optimum Air-Conditioning Control System for Energy Conservation Field Assessment of the Thermal Comfort of Occupants in Office *Utsumi Yasuo (Sendai Naitonal College of Technology)*		
10:40~11:05	8A-3 Dynamic Insulation System applied to Window Frames (Part 2) Energy saving effects of the proposed system in residential buildings *Miho Tanaka(The University of Tokyo)*	8B-3 Measurement of temperature distribution and CO2 concentration in a space-heated classroom *Shuzhao Liu (Tohoku University)*		
11:05~11:45	Closing session		4F, TOPAZ	

Click on the titles to view the papers!

Detail Program : Poster Sessions

Poster ID	Topic	Title	Location
A-1	Air Distribution	EXHAUST EFFECTIVENESS BASED ON RESIDUAL LIFETIME OF CONTAMINANT IN A VENTILATED SPACE *Jang Kyungjin, Samgong, Republic of Korea*	PRE FUNCTION AREA
A-2	Air Distribution	Improvement of Temperatures Stratification caused by Air-conditioner by means of Ceiling Fan in Classroom *Wakamatsu Natsuka, Osaka University, JAPAN*	
B-1	Health Indoor Air Quality and Productivity	Experimental Assessment of Humidity Controlling the Performances of Moisture Adsorbing/Desorbing Building Materials *Kim Hea-Jeong, Hanyang University, Republic of Korea*	
B-2	Health Indoor Air Quality and Productivity	Characteristics on indoor air pollutant emission from wood-based flooring by environmental-friendly natural adhesive using CNSL *Lee Jeong-Hun, Soongsil University, Republic of Korea*	
B-3	Health Indoor Air Quality and Productivity	Environment-friendly Hwangtoh composites using water soluble resin for interior materials *Jisoo Jeon, Sumin Kim, Soongsil University, Republic of Korea*	
B-4	Health Indoor Air Quality and Productivity	Adaptation process of human olfactory under continues exposure to odor of ethyl acetate based on subjective estimation of odor intensity *Nagatsugu Hitoshi, Osaka University, JAPAN*	
C-1	Natural Ventilation	Experimental Investigation and Accuracy Study of CFD Analysis for Airflow around Cross-Ventilated Building *Asai Kaori, University of Tokyo, JAPAN*	
C-2	Natural Ventilation	Thermal Environment Generated by Occupant's Opening Control of Window at Naturally Ventilated Building *Kami Kyoko, Osaka University, JAPAN*	
C-5	Natural Ventilation	Study of cross- ventilated indoor air flow characteristics by frequency analysis *Endo Tomoyuki, Kanto Gakuin University, JAPAN*	
C-6	Natural Ventilation	The effect of ventilation rates and window areas on building energy use *Yun Geun Young, Kyung Hee University, Republic of Korea*	
C-7	Natural Ventilation	Performances of new innovative domestic ventilation systems in combination with low temperature floor heating *Op t Veld Peter, Cauberg-Huygen RI bv, NETHERLANDS*	
D-1	Mechanical Ventilation	Prediction of Plume above Residential Cooking Range by means of CFD analysis *Tsumura Yuji, Osaka University, JAPAN*	
D-2	Mechanical Ventilation	Influence of Partition Curtain on Vertical Profile of Temperature and Contaminant Concentration in Sickroom with Displacement Ventilation *Inagaki tatsuya, Osaka University, JAPAN*	
D-3	Mechanical Ventilation	CFD Analysis on Capture Efficiency in Commercial Kitchen using Low Radiative Cooking Equipment with Concentrated Exhaust Chimney *Toyomura Koki, Osaka University, JAPAN*	
E-1	Hybrid Ventilation	A Proposal of Hybrid Ventilation System Using Stack Effect in High-rise Buildings *Yoon Sung Min, Sungkyunkwan Univ., Republic of Korea*	
F-1	HVAC System	Simple error reduction in tracer-gas field-measurements of air handling units *Schild Peter, SINTEF, NORWAY*	
F-2	HVAC System	Investigation of the Usage of Ground Source Heat Pump System on Wall Heating *Yoru Yilmaz, YTU, TURKEY*	
F-3	HVAC System	Thermostat/Hygrometer vs ANN-Based Predictive/Adaptive Environmental Control Strategies *Chang Jae, University of Kansas, UNITED STATES*	
F-4	HVAC System	A Study on the Hybrid Air-conditioning system Coupled with Radiant Floor Cooling and Ventilation System *Park Jae-Hyung, BTU, Republic of Korea*	
F-5	HVAC System	Energy-saving Effect of Thermal Energy Storage Using Introduced Outdoor Air *Asano Yuka, Osaka University, JAPAN*	
F-6	HVAC System	Field Survey on Indoor Thermal Environment in Small to Medium Sized Building with Packaged Air Conditioners *Nakasone Haruka, Osaka University, JAPAN*	
F-7	HVAC System	Evaluation on the Availability of Treated Sewage Water as an Unused Energy Source in a Super High-rise Complex Building *Jae-Han Lim, Ewha Womans University, Republic of Korea*	
G-1	Case Study Building	School Eco-Renovation Method for Improvement of Thermal Environment in Large Workshop of High School without Air-Conditioning System *Yamada Junya, Osaka University, JAPAN*	
G-2	Case Study Building	Indoor Thermal Environment and Vertical Temperature Gradient in Large Workshop of School without air-conditioning *Yasui Saori, Osaka University, JAPAN*	
G-3	Case Study Building	A Study of Design principle and Technology performance applied in Passive House - Focused on cases of the apartment type of Passive Houses in European - *Shin sung-eun, KICT, Republic of Korea*	
H-1	Chemical pollutants & Particles	Prediction of mass transfer rate on the surface of tested building material using CFD analysis *Seo Janghoo, Chosun Univ., Republic of Korea*	
H-2	Chemical pollutants & Particles	Sensitivity Analysis of Parameters affecting Indoor Air Quality related to HCHO and TVOC Reduction *Kim Mi Yeon, Chung Ang University, Republic of Korea*	
I-1	Computer Simulation	Analytical estimation of optimal minimum airflow for air circulation *Park Jin-Hyeon, Yeungnam UNIV., Republic of Korea*	
I-2	Computer Simulation	Evaluation on the Daylighting performance of 'generative facade components' In the digital simulation *Yi Hwang, SAMOO corp., Republic of Korea*	
J-2	Envelope Air Tightness	Effective flow area estimation test using CO2 *Iwamoto Ken, Kobe University, JAPAN*	
J-3	Integration Performance of Building Envelope and Services	PCM cold storage under various ventilation conditions *Charvat Pavel, Brno University of Technology, CZECH REPUBLIC*	
J-4	Sustainable Technologies for Building Ventilation	Study on the Feasibility of Heat Pump Desiccant System Combined with Cogeneration System in Heating and Humidification Mode *Park Beungyong, University of Tokyo, JAPAN*	
J-5	Envleope Air Tightness	Air Leakage Tests for the requirements of the LEED in two high-rise residential buildings *Hyun Kook Shin, Chungbuk National University, Dept. of Architectural Engineering, Cheongju, Korea*	

Year-round Energy Saving Potential for a Stratum Ventilated Subtropical Office

C.K. Lee Zhang Lin K.F. Fong

Building Energy & Environmental Technology Research Unit,

School of Energy and Environment & Division of Building Science and Technology,

City University of Hong Kong, Kowloon, Hong Kong

Abstract

Stratum ventilation has been proposed to cope for elevated indoor temperature recommended by governments in East Asia. TRNSYS is used for computation of the space cooling load and system energy consumption. A typical Hong Kong office is investigated. Compared with mixing ventilation and displacement ventilation, stratum ventilation derives its energy saving potential largely from the following two factors: a reduced ventilation load and increased coefficients of performance (COP) for chillers. The year-round energy saving is found to be substantial at 25% and 44% when compared with displacement ventilation and mixing ventilation respectively.

Keywords: stratum ventilation, displacement ventilation, mixing ventilation, annual, energy saving, TRNSYS simulation

Introduction

Minimizing the energy consumption by air conditioning systems would help to reduce CO_2 emission. Proactive actions in this regard have been taken by several governments in East Asia [1,2,3,4,5]. In order to cope with the recommended elevated room temperatures, stratum ventilation, a new ventilation method, was proposed by Lin et al. [6] with the following characteristics:

1. reversed temperature gradient in the occupied zone;
2. higher air speed at the head-chest level for the same air supply volume;
3. higher supply air temperature; and
4. higher evaporating temperature of the associated chiller, thus higher coefficient of performance (COP) of the chiller.

Tian et al. investigated the diffusion of CO_2 released by the manikin and thermal comfort under stratum ventilation experimentally [7]. The results demonstrated the flow pattern formed by stratum ventilation was able to provide good IAQ in the breathing zone.

System Description

Mixing ventilation (MV), displacement ventilation (DV) and stratum ventilation (SV) may be used to cool a building zone. Figure 1 shows the schematic diagram for the three systems. For MV, air is supplied to the building zone at high velocity at ceiling level which mixes fully with the room air before being extracted from the building zone (usually at ceiling level). The air temperature and pollutant concentration is assumed to be homogeneous within the building zone. For DV, air is supplied at/near the floor level at low velocity which fills the entire floor area and then displaces upward for extraction at ceiling level. The temperature (and usually also the pollutant concentration) increases with the height. For SV, air is supplied at an intermediate level close to the breathing zone/head level which keeps the temperature and pollutant concentration to a low level within the breathing zone. Consequently, a positive temperature and pollutant

concentration gradient is established above the breathing zone while a negative gradient is developed below the breathing zone [8].

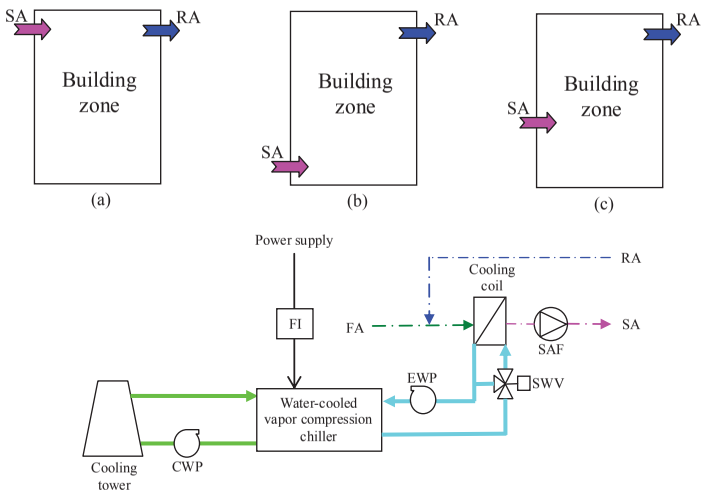


Figure 1 Schematic diagrams of (a) mixing ventilation, (b) displacement ventilation and (c) stratum ventilation systems equipped with an air-handling unit and a variable-speed water-cooled vapor compression chiller

An air-handling unit (AHU), consisting of a cooling coil and a supply air fan (SAF), and a water-cooled vapor compression chiller are used to provide the cooled supply air (SA) to the building zone. The chilled water entering the cooling coil is controlled by a three-way supply chilled water valve (SWV) based on the reference zone air temperature in the cases of DV and SV, or the return air (RA) temperature in the case of MV. The AHU controller generates a linear signal from 0 to 1 corresponding to nil to full flow to the coil when the zone temperature varies between the temperatures within $\pm 1^{o}C$ of the set point. To avoid instability when simulating the cooling coil, the valve will open at least 30% when the output from the AHU controller is greater than zero. The operation of the chiller, the condenser water pump (CWP) and the cooling tower is governed by a return chilled water thermostat with a dead band of $3^{o}C$. The cooling tower is additionally controlled by a return condenser water thermostat triggered between 15 and $20^{o}C$. The fresh air (FA) amount is based on $0.01 m^3/s$ per occupant. The AHU and the chilled water pump (EWP) will always be running within the daily occupancy schedule. A typical Hong Kong office is investigated. The zone loadings are calculated based on the varying ambient conditions and the pre-defined internal heat sources. Hence, the annual performance of the system can be studied.

Model Formulations

Lee presented a model for a variable-speed ground-source heat pump which is also applicable to a variable-speed chiller [9]. A parametric model as used by Jin and Spitler was adopted for the compressor where the various parameter values including the swept volume, volumetric coefficient, polytropic compression coefficient and the mechanical efficiency were determined using a parameter estimation technique based on performance data from the manufacturer (www.emersonclimate.com) [10]. The performance of the condenser and evaporator coils were calculated by dividing each coil into a maximum of three portions corresponding to the different states of the refrigerant in the coils. By employing different temperature effectiveness formulations for the coil portions, the performance of the entire coil was then solved by an iterative method. A thermostatic expansion valve was used which maintained a constant degree of superheat at the compressor suction. The solution for the complete chiller cycle was then

determined based on the energy and refrigerant mass balances for the entire cycle as proposed by Domanski and Didion [11].

For DV, Skistad proposed a rule-of-thumb which stated that the room temperature sufficiently distant from the supply air terminal at 0.1m above the floor is approximately the mean between the supply and return/exhaust air temperatures. Moreover, the room temperature increased linearly from the floor to the ceiling. The reference zone temperature was defined at 1.1m above the floor [12]. Hence,

$$T_{fl} = \frac{T_s + T_e}{2} \quad , \qquad T_r = T_{fl} + T_{grad} \tag{1}$$

where
$$T_{grad} = \frac{T_e - T_{fl}}{H_{room} - 0.1} \tag{2}$$

and
$$Q_{sen} = mc(T_e - T_s) \tag{3}$$

Equations (1) to (3) can be solved if the supply air conditions and the building load are known.

For SV, the correlation of the reference zone temperature to the supply and exhaust air temperatures are represented by a dimensionless temperature defined as

$$\theta_r = \frac{T_r - T_s}{T_e - T_s} \tag{4}$$

based on experimental results [13]. Equation (3) also applies for SV. The same form of mathematical expression was also used to present experimental results both for temperature gradient and for humidity ratio gradient [14]. In estimating the reference zone humidity for both DV and SV, the humidity ratio is deemed to vary in the same fashion as the temperature along the room height.

System Specification

Figure 2 shows the configuration of the typical office used in this study. The office is divided into two zones, namely the individual room and the open concourse with two AHU's used. The west external wall of the individual room zone, with a window area ratio of 0.5, is 8.4 m long. All other partitions are assumed to be thermally symmetrical, meaning that there is no heat transfer across those boundaries.

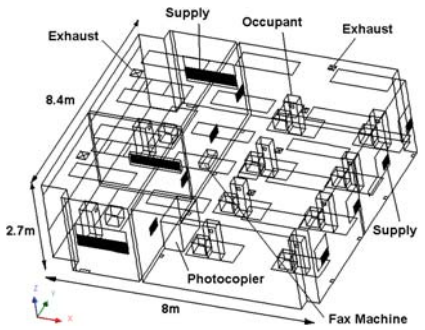


Figure 2 Configuration of typical office

Design loads are summarized in Table 1. The equipment load is assumed to be 30% radiative and 70% convective.

Table 1 Summarized design loads

Type	Room	Concourse
Occupant	2	8
Lighting ($W \cdot m^{-2}$)	19	19
Computer (W per occupant)	150	150
Equipment (W)	0	1850

Figures 3 and 4 show the daily operating schedules. Combined with the design loads stated in Table 1, the peak cooling load can be calculated.

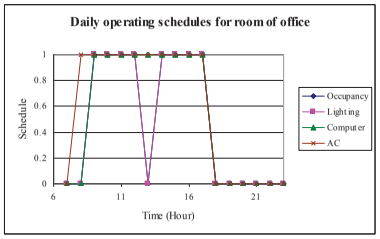


Figure 3 Daily operating schedules for individual office rooms

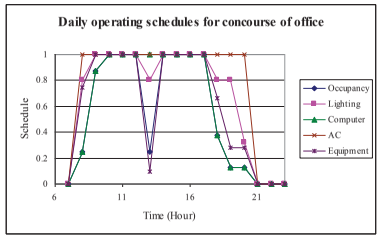


Figure 4 Daily operating schedules for office concourse

The thermal neutral temperatures under the three ventilation methods are different. The design temperatures for rooms ventilated with these methods should therefore not be identical. As a starting point, the design methods of DV and SV consider sensible loads only - no design relative humidity is defined. The corresponding settings are 24°C/54% for MV, 25°C for DV and 26.5°C for SV. The design outdoor condition is 33.5°C/68%. Table 2 summarizes the design cooling loads and required supply air conditions for the various cases. To allow better comparison of energy consumption, the design air flow rate of the MV case is also applied to the DV and SV cases. The system load includes the ventilation load resulting from the fresh air intake. The zone loads of the SV systems are the lowest followed by those of the DV systems, though the differences are less than 4% when compared with those of the MV systems. This is because the higher design indoor temperatures adopted, the less heat transmits through the external wall. The systems loads drop much more than the zone loads with the adoption of DV and SV systems. This is because the exhaust air or RA temperatures are substantially higher for the DV and SV systems which results in a large reduction in the ventilation loads. With a smaller chiller capacity, the corresponding requirements for the water pumps, the cooling tower and the cooling coil can also be reduced which means that both carbon foot print and cost in the construction stage can be lowered. This is also true in the operation stage.

Table 2 Summarized design requirements for the air-conditioning systems

Case	Total zone load (kW)	System load (kW)	Supply airflow rate ($m^3 \cdot s^{-1}$)	Supply air temperature (°C)
Office rooms, MV	3.265	4.167	0.259	13.97
Office rooms, DV	3.201	3.834	0.259	18.17
Office rooms, SV	3.137	3.510	0.259	21.69
Office concourse, MV	4.342	7.943	0.315	13.62
Office concourse, DV	4.324	6.854	0.315	17.81
Office concourse, SV	4.306	5.732	0.315	21.53

With the system requirements fixed, the various parameters for the chiller are to be selected. As the supply air temperatures for the different systems vary significantly, the design chilled water supply temperature should also be different. The higher design supply air temperatures of the DV and SV systems allow higher chilled water temperatures to be adopted. This improves the coefficient of performance (*COP*) of the chiller and offers significant energy saving. To provide the same reasonable difference between the air temperature and chilled water temperature at the cooling coil, the corresponding design chilled water return temperatures are 13°C for MV systems, 18°C for DV systems and 21°C for SV systems. The design condenser water return temperature is 30°C in all cases. To set a comparable baseline in selecting the chiller parameters, *COP* of the chillers are assumed to achieve a rated of 3 when the chilled water return temperature is 13°C in all cases. The design *COP* can then be determined based on the design chilled water return temperature (only applicable for the DV and SV systems). The condenser and chilled water flow rates are selected so that the temperature changes across the chiller are around 5°C. Table 3indicates the various parameter values selected for the air-conditioning systems under different ventilation methods. Only single chiller is used for each case. The supply air fan head is taken as 750 Pa with a fan efficiency of 70% in all cases. The cooling tower fan head is taken as 200 Pa with a fan efficiency of 65%. All water pump efficiencies are assumed to be 60%.

Table 3 Parameter values for the chiller system

	MV	**DV**	**SV**
Chiller			
Condenser water mass flowrate ($kg \cdot s^{-1}$)	0.77	0.68	0.59
Chilled water mass flowrate ($kg \cdot s^{-1}$)	0.58	0.51	0.44
Swept volume of compressor (litre)	0.651	0.576	0.465
Volumetric coefficient of compressor	-0.225	-0.225	-0.239
Compressor polytropic compression coefficient	2.218	1.897	2.131
Electro-mechanical efficiency of compressor (%)	98.41	95.26	93.11
Degree of superheat at compressor suction (°C)	11.1	11.1	11.1
Volume of refrigerant in condenser coil (litre)	3.00	3.00	2.50
Volume of refrigerant in evaporator coil (litre)	3.00	3.00	2.50
Volume of refrigerant in liquid line (litre)	0.20	0.15	0.15
Overall heat transfer value of condenser coil ($kW \cdot K^{-1}$)	1.18	1.00	1.00
Overall heat transfer value of evaporator coil ($kW \cdot K^{-1}$)	0.88	0.75	0.70
Refrigerant charge (kg)	1.38	1.00	1.38
Design *COP*	3.00	3.24	3.42
Auxiliary equipment			
Cooling tower air volume flowrate ($m^3 \cdot s^{-1}$)	0.611	0.556	0.472
Condenser water pump head (kPa)	150	138	130
Chilled water pump head (kPa)	130	125	118

Methodology of Analysis

The TRNSYS simulation software is used for the analysis. New TRNSYS component is developed for the variable-speed chiller. System simulations are made for one year based on the typical weather data of Hong Kong [15] using a simulation time step of 3 minutes. The total primary energy consumption and system performance for the various cases with and without the part-load control are compared. An energy efficiency of 33% is assumed for the electric power plant in relation to the primary energy input.

Results and Discussions

Table 4 summarizes the year-round total energy consumption for the cases investigated. The percentage primary energy saving is at least 25% with the adoption of a DV system and 44% with the use of a SV system when compared with a MV system. A SV system offers at least 21% energy saving when compared with a DV system. The saving is substantial even taking account additional dehumidification of the fresh air might be needed.

Table 4 Year-round total primary consumption

MV (kWh)	35,248
DV (kWh)	26,221
SV (kWh)	19,609
Saving from MV to DV	25.61%
Saving from DV to SV	25.22%
Saving from MV to SV	44.37%

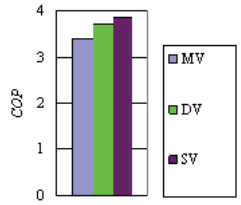


Figure 5 Year round mean COP for the different cases

Figure 5 shows the year-round-averaged *COP* for the different cases investigated. Figures 6 and 7 indicate the variation of the monthly-averaged zone conditions for the different ventilation methods. The temperature change only mildly throughout the year under the temperature control, but the relative humidity varies widely which reaches a maximum in the peak-load season. With the adoption of a DV or SV system, the relative humidity increases significantly due to the higher supply air temperatures used. With cooling-only dehumidification, the higher supply air temperature, the more moisture is introduced into the building zone. A high relative humidity impairs the indoor air quality besides the thermal comfort. On the other hand, the higher the zone temperature, the higher moisture content in the air for a specific relative humidity. This reduces the dehumidification load for SV.

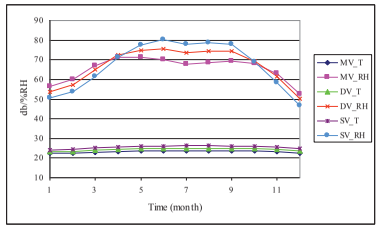


Figure 6 Monthly-averaged zone conditions for office rooms

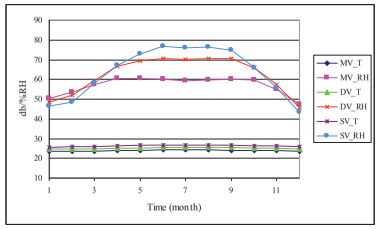


Figure 7 Monthly-averaged zone conditions for office concourse

Conclusion

The energy simulation software TRNSYS is used for computation of the space cooling load and system energy consumption. Year-round energy consumptions of three systems of stratum ventilation, displacement ventilation and mixing ventilation are compared for a typical office configuration in Hong Kong. The energy saving potential of stratum ventilation is derived mainly from two factors: the reduced ventilation load and increased COP of chillers. Because of the higher supply air temperature of stratum ventilation the energy consumed for the treatment of fresh air is much reduced. The increased COP reduces chiller energy in stratum ventilation. Through the year-round energy simulation of the typical office in Hong Kong, stratum ventilation has shown to be able to provide substantial energy saving when compared with conventional ventilation methods. The figure is 25% and 44% when compared with displacement ventilation and mixing ventilation respectively.

Nomenclature

c	Specific heat capacity of air ($kJ \cdot kg^{-1} \cdot K^{-1}$)
COP	Coefficient of performance
H_{room}	Zone height (m)
m	Supply air mass flow rate ($kg \cdot s^{-1}$)
Q_{sen}	Sensible load of building zone (kW)
T	Temperature (^oC)
T_{grad}	Temperature gradient along the zone height ($^oC \cdot m^{-1}$)
θ_r	Dimensionless temperature coefficient as defined in Equation (4).

Subscript

e	Exhaust air
fl	Zone air at 0.1m above floor
r	Reference zone point
s	Supply air

Abbreviation

AHU	Air-handling unit
CWP	Condenser water pump
DV	Displacement ventilation
EWP	Chilled water pump
FA	Fresh air
FI	Frequency inverter
MV	Mixing ventilation
RA	Return air
SA	Supply air
SAF	Supply air fan
SWV	Supply chilled water valve
SV	Stratum ventilation

Acknowledgement

The work described in this paper was fully supported by a Strategic Research Grant of the City University of Hong Kong, Hong Kong Special Administrative Region, China (Project No. 7002481).

References

[1] Electrical and Mechanical Services Department (EMSD), Government of Hong Kong S.A.R., "Energy Conservation Charter 2006- Suitable Room Temperature", http://www.energyland.emsd.gov.hk/blue_sky/eng/index.htm.

[2] National Development and Reform Commission (NDRC), the State Council of China, Citizen's Pact for Deed of Thrift", http://www.ndrc.gov.cn/gzdt/ t20051223_54462.htm.

[3] NOW news, Taiwan, "Campaign in office of president for saving energy and reducing carbon emissions", http://www.nownews.com/2008/05/24/10844 -227 9584.htm.

[4] Ministry of Knowledge and Economy, the Republic of Korea. The standard of energy management, December 29, 2008. http://www.mke.go.kr/info/law/gosiView.jsp? (Item No. 2008-219).

[5] Japanese Ministry of the Environment (MoE), "National Campaign to Fight Global Warming", http://www.env.go.jp/en/press/2005/0428b.html.

[6] Z. Lin, T.T. Chow, C.F. Tsang, K.F. Fang, L.S. Chan, 2009, Stratum ventilation - a potential solution to elevated indoor temperature, Building and Environment, 44(11): 2256-2269.

[7] Tian L, Lin Z, Wang QW J. Comparison of gaseous contaminant diffusion under stratum ventilation and under displacement ventilation, *Building and Environment* 2010**,** in press.

[8] Zhang Lin, Lin Tian, Ting Yao, Qiuwang Wang, TT Chow, Experimental and numerical study of room airflow under stratum ventilation, *Building and Environment* 2010**,** in press.

[9] Lee, C.K. (2010), Dynamic performance of ground-source heat pumps fitted with frequency inverters for part-load control, *Applied Energy,* doi: 10.1016/j.apenergy.2010.04.029.

[10] Jin, H. and J.D. Spitler (2002), A parameter estimation based model of water-to-water heat pumps for use in energy calculation programs, *ASHRAE Transactions,* 108 (1) (2002) 3-17.

[11] Domanski, P. and D. Didion (1984), Mathematical model of an air-to-air heat pump equipped with a capillary tube, *International Journal of Refrigeration,* 7(4), 249-255.

[12] Skistad, H. (1994), *Displacement Ventilation,* Research Studies Press Ltd., Taunton.

[13] Tian, L. (2009), Experimental and numerical study of indoor environment under stratum ventilation, *Doctoral Thesis,* Xi'an Jiaotong University.

[14] Kosonen, R. (2010), Displacement ventilation for room air moisture control in hot and humid climate Air distribution techniques (Air distribution techniques 5), HVAC Handbook - Displacement Ventilation in Hot and Humid Climate.

[15] Chan, A.L.S., T.T. Chow, S.K.F. Fong and J.Z. Lin (2006), Generation of a typical meteorological year for Hong Kong, *Energy Conversion and Management*, 47(1), 87-96.

Numerical Prediction of Airflow and Temperature Distribution in Large-Scale Agricultural PVC Greenhouse

Keita Hattori[1] and Kazuhide Ito[2]

[1] Graduate student, IGSES, Kyushu University, Fukuoka, Japan
[2] IGSES, Kyushu University, Fukuoka, Japan

Abstract

Large-scale greenhouses are usually adopted to control the indoor climate conditions in agriculture. The envelope of agricultural greenhouses generally consists of a PVC (polyvinyl chloride) sheet, which produces a so-called greenhouse effect and protection from harmful insects. In winter, a supplementary heating device in greenhouses is needed because of the lower outdoor temperature and the non-uniform distribution of indoor temperature. Existing research concerning indoor environmental conditions formed in PVC greenhouses is insufficient and precise numerical predictions of airflow and temperature distribution in large-scale vinyl houses are important to develop effective designs from the viewpoint of energy-saving and the development of suitable indoor environments for agricultural products.

To this end, coupled numerical analysis of CFD (computational fluid dynamics) and air-conditioning system was also carried out and the sensor position in the greenhouse and operation of a stirred fan were confirmed to have great impact on energy consumption.

Keywords: PVC greenhouse, CFD, Stirred fan, Flow and temperature distribution

Introduction

Greenhouses are widely used throughout the world owing to the ease of control of indoor environment, low cost, and simple structure. However, during the night-time in winter, supplementary heating equipment, namely, a hot-air furnace system or other air-heating devices, may be necessary to control the cultivation temperature in PVC greenhouses when the outside temperature decreases rapidly. For large-scale PVC greenhouses, thermal stratification from the lower part of the vegetation zone to the upper part near the ceiling is usually formed and a high-temperature and stagnant flow region is observed, especially in the upper part, in greenhouses. The target zone of airflow and temperature control must be the vegetation zone, which is generally the lower part of greenhouses; therefore, the formation of thermal stratification indicates that the heating efficiency of a supplementary heating device is inefficient in winter.

This research focuses on an actual large-scale PVC greenhouse located in Japan, coupled CFD analysis of convection, radiation, and air-conditioning system is carried out in order to estimate the quantitative effects of the use of a stirred fan for air-mixing and an additional PVC screen for partitioning the upper and lower spaces on energy consumption.

Outline of target PVC greenhouse

The target greenhouse is a tunnel-type greenhouse, with two parallel tunnel-type sections, located in Japan. The inner dimensions of one side of the greenhouse are a width of roughly 6.3 m, a length of 86.0 m, and a maximum height of 3.4 m, as shown in Figure 1. There is no

partitioning wall between the two basic greenhouse units and a single non-partitioned space is present. The thickness of the PVC sheet acting as the outer wall is 0.1 mm. A photograph of the exterior, plan, and section are also shown in Figure 1.

In this parallel setting PVC greenhouse, an additional PVC screen can be installed for spatial partitioning of upper and lower zones. Additionally, stirred fans are also present in the upper part of the PVC greenhouse. The airflow rate of each stirred fan is 2,300 m^3/h and a heating source is not built into the fan; that is, it can just be operated to mix air.

A supplementary heating device, a hot-air furnace system, is placed in the greenhouse and temperature-controlled air is supplied through an air duct at six supply openings located at ground level during the night-time in winter. The total airflow rate of the hot-air furnace system is 27,600 m^3/h and the total heat output is 145 kW.

Outline of numerical analyses

The numerical analyses of airflow and temperature distribution in the PVC greenhouse during night-time in winter were carried out by Computational Fluid Dynamics (CFD). Additionally, CFD simulation that incorporated a feedback control routine of supply inlet temperature was carried out.

The flow fields were analyzed using the RNG k-ε model. The second-order upwind scheme was adopted for the convection term, and a SIMPLE algorithm was used for steady-state analyses. The temperature fields were analyzed on the basis of the coupled simulation of CFD, convective, conductive, and radiative heat transfers. Boussinesq approximation was adopted to reproduce the buoyancy effect. The view factors were analyzed by a hemicube method, and an iterative solution of radiosity method was used to analyze mutual radiation. For the PVC wall and the ground, one-dimensional heat-conductive analyses were carried out.

An outline of the analyzed space is given in Figure 1 and an unstructured tetramesh was used for a total of 558,794 meshes for CFD simulation.

CFD simulations in this study were performed with a commercial CFD software package, ANSYS FLUENT 12 (ANSYS, 2009). Table 1 indicates the boundary conditions for numerical analyses.

Feedback control method of supply inlet temperature

In order to estimate the optimal position of temperature sensors, a feedback routine between supply inlet air temperature and sensor temperature was incorporated into the CFD model.

The control method of the supply inlet air temperature is simple proportional control (P-control), as shown in equation 1.

$$T_{in}^{r} = T_{in} - K \times (T_{out} - T_{tar}) \quad (1)$$

Here, T_{tar} indicates target temperature (=15 °C in this analysis), T_{in} is supply inlet air temperature of each duct, T_{out} is the sensor temperature in space, and K denotes a proportional constant (=0.1 in this analysis).

The changes in supply inlet temperature and heat loads of the hot-air furnace in case the sensor position was changed were analyzed. The points of temperature sensors are depicted in Figure 1 (points A-C).

Numerical cases

Cases analyzed are shown in Table 2. The parameters of this analysis are with or without an additional PVC sheet for separating upper and lower parts of the greenhouse, a stirred fan for mixing air and eliminating thermal stratification, and a feedback control system between temperature sensors in the vegetation zone and supply inlet air temperature. A total of 8 analytical cases were arranged. The temperature sensor positions (points A, B, and C, and the average temperature of the vegetation zone) are indicated in Figure 1. The inlet velocity of stirred fans is controlled at 5.5 m/s and turbulent intensity is 5% (recirculating airflow rate of each stirred fan is 2,300 m^3/h).

The temperature-conditioned air is supplied from duct openings, which are located at six points in the PVC greenhouse. The supply airflow rate of each inlet was set to 4,600 m^3/h and the average velocity was set to 5.0 m/s.

Results of numerical analysis

Results of flow and temperature fields

The prediction results of flow fields and temperature distribution for basic cases (Case 1-S – Case 2-S) are shown in Figures 2 and 3. In Case 1 without an additional PVC screen and a stirred fan, a stagnant flow field was formed in the entire space of the greenhouse, except for the vicinity of the supply inlet, and a non-uniform temperature distribution including a local high-temperature region was observed. In Case 2 with six operated stirred fans and an additional PVC screen, flow and temperaure fields were well mixed in the vegetation zone. The upper convection and diffusion of a supply jet from the stirred fan were restricted and the Coanda effect along the surface of the PVC screen was confirmed.

In all cases, the temperature-controlled air was supplied through supply inlets from six locations in the greenhouse; therefore, clear thermal stratification was not observed in the space. Gradual thermal stratification was confirmed in the vicinity of each supply inlet from the hot-air furnace.

Results of coupled analysis for CFD and feedback control of inlet air temperature

Table 3 and Figure 4 show summaries of the numerical results of average temperature and heat load of the hot-air furnace with incorporation of feedback control between supply inlet air temperature and sensor temperature. The flow and temperature distributions hardly changed from those of basic analytical cases (Cases 1-S-2-S).

In Case 1-A and Case 2-A in which the temperature sensor was located at position A as shown in Figure 1, relatively low-temperature air was supplied from the supply inlet (from a hot-air furnace). In Case 1-C and Case 2-C in which the temperature sensor was located at position C as shown in Figure 1, relatively high-temperature air was supplied from the supply inlet as a result of feedback control, regardless of the presence or absence of an additional PVC screen or a stirred fan. The maximum temperature difference of about 9 °C was caused by the difference in sensor positions in the greenhouse.

In Case 2 in which an additional PVC screen and stirred fan were incorporated, the average temperature in the vegetation zone became higher than the average temperature of the whole space. The introduction of an additional PVC screen into the greenhouse was effective for restricting the air-conditioning domain and increasing the heating efficiency.

The estimation results of supply heat load for each case are also shown in Table 3. The supply heat load was calculated by the following two methods: (i) all outdoor air is supplied to a hot-air furnace and there is no air returned to the hot-air furnace from the room, (ii) all returned air is supplied to the hot-air furnace and there is no outdoor air supplied to the hot-air furnace.

If the temperature sensor was set at point A, the supply heat load of the hot-air furnace decreased. In this case, the average temperature in the vegetation zone did not reach the target temperature of 15 °C. In contrast, with sensor point C, the supply heat load of the hot-air furnace increased relative to the previous example. In this case, the average temperature in the vegetation zone exceeded the target temperature by about 2 °C.

Differences of 30% to 40% in supply heat load were confirmed with the change of location of the temperature sensor.

The estimation results of fuel consumption of the hot-air furnace are shown in Table 4. The fuel consumption was estimated by the order of the supply heat load. Type A heavy oil

(Bunker A) was set as the fuel of the hot-air furnace. The ratio to the fuel consumption of a basic case is also shown in Table 4.

In the comparison between Case 1-A and Case 1-C, there was a 35% difference in fuel consumption. Since the averaged temperature in the vegetation zone in Case 1-A was about 3 °C lower than that in Case 1-C, the difference in energy consumption did not automatically indicate an energy-saving performance.

Conclusions

In this study, we reported the result of numerical analysis for flow and temperature distribution in a large-scale PVC greenhouse in winter. The findings obtained in this work can be summarized as follows:

(1) The space of environmental control became reduced in size upon the introduction of an additional PVC screen in the upper part of the vegetation region. The installation of the screen inside the large-scale vinyl house was a simple and energy-effective method of indoor environmental control.

(2) The air-mixing in a vertical direction and also in a horizontal direction in the large-scale PVC greenhouse was stimulated by the introduction of stirred fans in the upper region.

(3) From the viewpoint of heat load of the hot-air furnace system, the energy-saving effects of about 10 – 30% were confirmed upon introduction of a vinyl screen and a stirred fan in a large-scale PVC greenhouse. Because of the non-uniform distribution of temperature in the greenhouse, the position of temperature sensors strongly affected the energy consumption in the case where a feedback control system for the hot-air furnace was introduced.

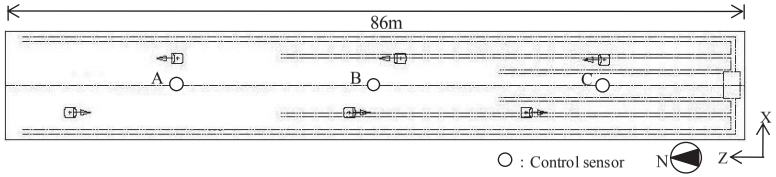
Acknowledgement

This research was partly supported by a Grant-in-Aid for Scientific Research (JSPS KAKENHI for Young Scientists (S), 21676005). The authors would like to express special thanks to the funding source.

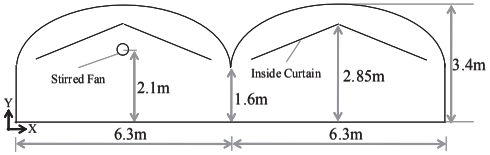
References

ANSYS, 2009. ANSYS FLUENT 12, ANSYS Japan Ltd.

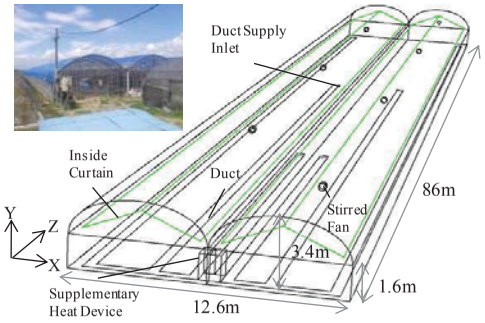
Reichrath, S., Davies, T W., 2002. Using CFD to model the internal climate of greenhouses: past, resent and future, *Agronomie*, 22, pp3–10



(1) Plan



(2) Section



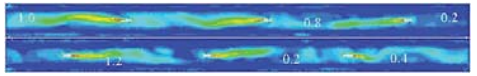
(3) Schematic geometry and photo of exterior

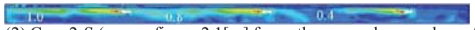
Figure 1 Outline of target greenhouse





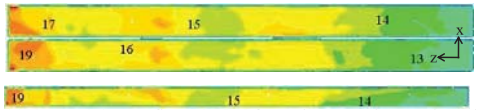
(1) Case 1-S (upper fig. : 2.1[m] from the ground, x-z plane / lower fig. : west center y-z section)



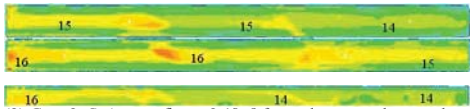


(2) Case 2-S (upper fig. : 2.1[m] from the ground, x-z plane / lower fig. : west center y-z section)

Figure 2 Air flow distribution (Results of CFD analyses)



(1) Case 1-S (upper fig. : 2.1[m] from the ground, x-z plane / lower fig. : west center y-z section)



(2) Case 2 -S (upper fig. : 2.1[m] from the ground, x-z plane / lower fig. : west center y-z section)

Figure 3 Temperature distribution (Results of CFD analyses)

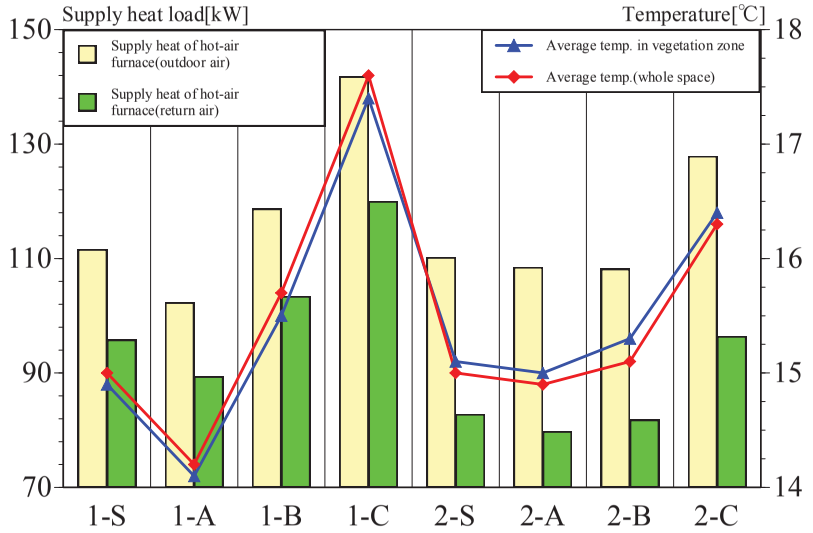


Figure 4 Results of total supply heat from hot-air furnace in case of coupled analysis with feedback simulation

Table 1 Boundary conditions for numerical analyses

Inflow	TI=5[%], L_{turb}=0.1 D_{IE}
Outflow	U_{out}=Free slip, k_{out}=Free slip, ε_{out}=Free slip
Outer Air	Sol-air temperature SAT : 4[°C] Outdoor air temperature : 9[°C] Convective heat transfer rate : 20[W/m^2/K]
Ground	Soil temperature at 1 m below ground : 10[°C], Thermal conductivity of soil : 1.0[W/m/k]
Inside Curtain	Thickness of PVC : 0.1[mm]
Duct	35[°C] constant as surface temperature
Duct Inlet	U_{in}=5.0[m/s], angle 30°
Wall Surface	Velocity : generalized log low Emissivity : 0.9

Table 2 Cases analyzed

Cases	PVC sheet for space partitioning	Stirred fan		Temperature sensor position	Supply air temperature of hot-air furnace
		Installed quantity	U_{inf} [m/s]		
Case 1-S	Not installed	0	-	Space average of vegetation zone	P-type control
Case 1-A				A (see Fig.1(1))	
Case 1-B				B (see Fig.1(1))	
Case 1-C				C (see Fig.1(1))	
Case 2-S	Installed (see fig. 1(3))	6	5.5	Space average of vegetation zone	
Case 2-A				A	
Case 2-B				B	
Case 2-C				C	

Table 3 The results of average air velocities and temperatures for Cases 1-S – 2-C (cases of feedback simulation)

Cases	PVC sheet for space partitioning	Stirred fan		Temp. sensor position	Average temp. in vegetation zone [°C]	Average temp. (whole space) [°C]	Supply inlet temp. from hot-air furnace	Supply heat of hot-air furnace (outdoor air temp. / return air temp.) [kW]	
		Installed quantity	U_{inf} [m/s]						
Case 1-S	Not installed	0	-	Space average of vegetation zone	14.9	15.0	25.7	111.6	95.8
Case 1-A				A (Fig.1(1))	14.1	14.2	23.6	102.3	89.4
Case 1-B				B (Fig.1(1))	15.5	15.7	27.3	118.7	103.4
Case 1-C				C (Fig.1(1))	17.4	17.6	32.5	141.8	120.0
Case 2-S	Installed	6	5.5	Space average of vegetation zone	15.1	15.0	25.7	110.2	82.8
Case 2-A				A	15.0	14.9	25.3	108.5	79.8
Case 2-B				B	15.3	15.1	25.4	108.2	81.8
Case 2-C				C	16.4	16.3	29.8	127.9	96.4

Table 4 The estimation results of fuel consumption of hot-air furnace

Cases	Consumption of heavy oil (type A) (outdoor air temp. / return air temp.) [L/h]		Ratio to Case 1-S (outdoor air temp. / return air temp.)	
Case 1-S	12.5	10.7	1.00	1.00
Case 1-A	11.4	10.0	0.92	0.93
Case 1-B	13.3	11.6	1.06	1.08
Case 1-C	15.8	13.4	1.27	1.25
Case 2-S	12.3	9.3	0.99	0.86
Case 2-A	12.1	8.9	0.97	0.83
Case 2-B	12.1	9.1	0.97	0.85
Case 2-C	14.3	10.8	1.15	1.01

Exposure Risk Assessment by Coupled Analysis of CFD and SIR model in Enclosed Space

Takayuki Fukuoka [1], Kazuhide Ito[2,]

[1] Graduate student, IGSES, Kyushu University, Fukuoka, Japan
[2] IGSES, Kyushu University, Fukuoka, Japan

Abstract

The indoor environment can play a significant role in the transmission and exposure of various contaminants. In some emerging aerial infections, such as influenza virus, tuberculosis virus, and other biological and chemical contaminants, the airborne route of transmission is thought to be important to evaluate exposure health risk. In this paper, first, we present the relationship between the classic SIR model proposed by Kermack & Mckendrick and the Wells-Riley model; then, we introduce the analytical procedure of coupled analysis of computational fluid dynamics (CFD)-based prediction of unsteady contaminant concentration distribution and the basic SIR model to predict exposure risk of residents in an enclosed space.

The classic SIR model consists of three differential equations coupling changes in the population of susceptibles (S), the population of infectors (I), and the population of recovery to an immune state (R). The Wells-Riley model can predict the number of susceptibles (S) as a function of infectious contaminant concentration and exposure time by respiration. Through the analysis of infectious contaminant concentration level in a large enclosure with CFD, prediction of the changes of S, I, and R becomes possible.

The results of sensitivity analysis with changes in ventilation rate and other parameters of infections for targeting a large enclosure with simple geometry showed non-uniform distribution of S, I, and R in enclosed spaces and indicated strong dependence on unsteady and inhomogeneous contaminant distribution.

Keywords: CFD, SIR, Infectious disease, Exposure risk

Introduction

The numbers of tuberculosis carriers and fatalities in Japan over recent years have been extremely high among those of developed countries. Tuberculosis is an airborne infectious bioaerosol and its exposure risk is strongly affected by air flow conditions indoors. In 2009, the epidemic of influenza A (H1N1) became a serious issue and indoor air pollution problems caused by other airborne infectious bacteria, viruses, and pathogens were also recognized as social and public health concerns.

Concerning the exposure route between the generation source of infectious bioaerosols and residents, there are various pathways of transmission: transmission by direct contact, droplet contact, viral droplet nuclei transmission, fecal-oral transmission, oral transmission, and so on. In general, droplet contact and viral droplet nuclei transmission are called airborne route transmissions and the development of a prediction method for these transmission routes indoors is important with regard to the design of healthy indoor environments.

In this paper, first, we present the structure of fundamental epidemiological models, namely, the classic SIR model proposed by Kermack and Mckendrick and the Wells-Riley model; we also introduce the analytical procedure of coupled analysis of computational fluid dynamics (CFD)-based prediction of unsteady contaminant concentration distribution and the classic SIR model to predict exposure risk of residents in enclosed spaces. Generally, airborne infectious pathogens are transported by air movement indoors and coupled analysis of CFD and an epidemiological model is a significant predictive tool of health risk for indoor environmental design.

In this study, we focus on the coupled simulation of unsteady and non-uniform contaminant concentration distribution and infectious risk, which directly indicates the changes of population densities of susceptible, infectious, and recovered subjects in large enclosed spaces.

Outline of Epidemiological Model

The SIR model is a fundamental epidemiological model that represents propagation of transmission and was proposed by Kermack and McKendrick. The classic SIR model consists of three differential equations coupling the changes in the population of susceptibles (S), the population of infectors (I), and the population of recovery to an immune state (R). The basic equations of the SIR model are indicated in Table 1 (Equations (1) – (3)). The original SIR model defined by Kermack and McKendrick consists of only reaction term, and equations (1) – (3) constitute an extended model including the diffusion term. β is the contact rate between susceptibles and infectors [1/person/s], and γ is the recovery rate [1/s]. Basic reproductive ratio R_o is defined from β and γ as shown in equation (4), and has been used widely as a parameter that describes the average number of new cases that an infector produces in a particular population. R_o>1 denotes that the infection rate is larger than the recovery or removal rate, which may lead to an epidemic and the spread of the infection. R_o<1 indicates that the infection rate is smaller than the recovery rate, which may lead to an endemic situation. Here, the equation $S+I+R=N$ ($=S_0$) is used.

On the other hand, a prediction model that quantitatively evaluates airborne infection risk was proposed by Wells in 1955 and modified by Riley et al. This model is known as the Wells-Riley equation as shown in equation (6) and it can predict the number of susceptibles (S) as a function of infectious contaminant concentration and exposure time by respiration. In equation (6), P_I is the probability of infection; C denotes the number of new cases of infectors; Q is the ventilation rate in a room [m^3/s]; q indicates the quanta production rate per infector [quanta/s]; p is the pulmonary ventilation rate of susceptibles [m^3/person/s]; and t is the duration of exposures [s]. Recently, numerical prediction results based on the Wells-Riley model in the case of a SARS outbreak in a hospital were reported by researchers in Hong Kong.

Here, the consistency between the traditional SIR model and the Wells-Riley equation is examined. Under the condition that (I) was much smaller than (S) and assumed to be constant, equation (1) in Table 1 became equation (7). Equation (7) became equation (8) for cases where $S_0=S+I$ and finally equation (9) was derived. Comparing the Wells-Riley equation shown in equation (6) and equation (9) derived from the SIR model, these equations were found to be analogous and equation (10) was introduced. Here, q/Q denotes the unit of concentration and β is a function of the concentration and pulmonary ventilation rate of susceptibles. The numerical prediction of the Wells-Riley model adopting the result of

unsteady and non-uniform concentration distribution estimated by CFD was essentially the same as the numerical prediction of the SIR model coupled with CFD analysis that took the early stage of infection spread into consideration.

Through the analysis of infectious contaminant concentration level and distribution in a large enclosure with CFD, the prediction of the number changes of (S), (I), and (R) becomes possible through the analysis of β.

Coupled Analysis of CFD and SIR Model in this Study

It was possible to predict unsteady and non-uniform concentration distribution by solving the scalar (aerial infectious contaminant) transport equation shown in equation (5) on the basis of flow field analysis by CFD. The time change of contact rate β distributions through unsteady concentration simulation in enclosed spaces and then equations (1)-(3) were solved using this time-dependent β. In the case that the infectors (I) emit infectious contaminant, namely, new contaminant sources, the source term S_ϕ that denotes the formation of scalar (new infectious contaminant) in equation (5) must be considered. In this study, S_ϕ and feedback from SIR analysis to scalar transport equation were disregarded.

The SIR model in Table 1 is an enhancing model that considers diffusion terms in (S), (I), and (R), and the movement of susceptibles or infectious could be reproduced approximately by giving the diffusion coefficient.

In particular, when the grid size of CFD is set to larger than human scale, the numerical results of diffusion and propagation of infectors become reasonable analyses that reproduce an actual phenomenon. In this case, SIR parameters indicate population density, that is, [population/m^2].

In this study, unsteady and non-uniform concentration distribution was analyzed in three dimensions by CFD and governing equations of the SIR model were analyzed in two dimensions at a height of 1.6 m (y) from floor level (breathing zone level) as shown in Figure 1.

Outline of Sensitivity Analysis for Targeting Large Enclosed Spaces

Comparatively large enclosed spaces with a size of 10 m (x)×10 m (z)×3 m (y) and with a supply inlet opening with a size of 0.27 m×0.44 m near the floor and an exhaust outlet opening of the same size near the ceiling were assumed in this sensitivity analysis. The outline of the target enclosed space is shown in Figure 1. The infectious bioaerosols were assumed to be instantaneously generated in the center domain measuring 4 m (x) × 4 m (z) × 3 m (y) in the target enclosed space. The bioaerosols were assumed to be approximately passive contaminants and the unsteady and non-uniform distributions were analyzed during 24 hours with instantaneous generation. Flow fields were analyzed by the RNG k-ε model.

Table 2 denotes the numerical and boundary conditions of this sensitivity analysis. In this

sensitivity analysis, the population of infectors did not recover (γ=0) and they were assumed to die at a constant rate after infection. The γ in equation (9) was replaced with death rate (μ) in this analysis. The initial population of susceptibles S_0 was set at 100 and I_0 was assumed to be 10^{-2}. These values were not intended to reflect a specific or actual phenomenon. Ventilation rate (n) and pulmonary ventilation rate (p) were set to two levels and the contact rate (β) was calculated by pulmonary ventilation rate (p) and prediction results of contaminant concentration in the breathing zone. Death rate (μ) was set to ten times the contact rate (β).

CFD simulation is preferable to understand a non-uniform distribution in a comparatively short time scale. On the other hand, SIR-type epidemiology model is often used for infection transmission prediction for a long time scale, such as weeks or months. In this sensitivity analysis, the condition for highly infectious bioaerosols generated in the target space was assumed, and unsteady analyses were carried out for 24 hours. In accordance with the report by Fine (1993), the orders of basic reproductive ratio (R_o) were summarized as follows: R_o=12-18 for measles, R_o=12-17 for whooping cough (pertussis), R_o=8-10 for varicella, and R_o=6-7 for rubella. In this analysis, basic reproductive ratio (R_o) was set to 10 and other parameters including the contact rate (β) were determined appropriately.

Table 3 shows the cases analyzed. In Case 1 - Case 4, both susceptibles (S) and infectors (I) are assumed to remain stationary and do not move. In Case 5 - Case 8, both susceptibles (S) and infectors (I) are assumed to move at a constant diffusion coefficient. In Case 9 - Case 12, it is assumed that only susceptibles (S) move by diffusion and infectors (I) remain stationary and do not move.

Results of Numerical Analysis

Figure 2 shows the results of flow field at y=1.6 m height for the case of a relatively low ventilation rate (n=0.01 h^{-1}). This x-z plane does not contain supply and exhaust openings. A non-uniform distribution of flow field was confirmed and re-circulating flow was observed in the center of the analytical domain.

Figure 3 indicates the time series of contaminant concentration ϕ in the target space. The value of ϕ denotes the volume-averaged concentration for the whole space. In the case of a low ventilation rate (n=0.01 h^{-1}), the nominal time constant was 100 h and the contaminant concentration ϕ was almost constant through the 24 h of analysis. In the case of a relatively high ventilation rate (n=0.1 h^{-1}), contaminant concentration ϕ decreased exponentially and became 1/10 of the initial concentration level at 24 h from the beginning of the analysis.

Figure 4 shows the contaminant concentration ϕ distribution at 24 hours for two ventilation rates. Non-uniform concentration distributions were formed in the space. In the case of the low ventilation rate (n=0.01 h^{-1}) in particular, the contaminant continuously stayed and accumulated at the center of the space and a high concentration zone was confirmed.

Figure 5 shows (S) and (I) distribution in the x-z plane at y=1.6 m height at 24 hours for three representative cases: Case 3, Case 7, and Case 11. In Case 3 as shown in Figure 5 (1) and (2), the distributions of (S) and (I) were similar, which was because (S) and (I) were assumed to be motionless and converted from (S) to (I) at the same points. (S) and (I) distributions indicated inhomogeneous distribution caused by non-uniform distribution of contaminant. In other words, there were inhomogeneous distributions of infection risk in the room. In Case 7, for which the diffusion of (S) and (I) was adopted, the distributions of (S) and (I) were spread throughout the entire space by movement. In Case 11, for which only the diffusion of (S) was analyzed, the distribution of (S) was almost the same as the result in Case 7. However, concerning (I), the distribution of (I) was similar to the result of Case 3, where the absolute value of (I) became large. This was because (S) moved to a high contaminant concentration region by diffusion and was converted to (I).

Figure 6 shows the time series of average values of (S) and (I) for each case. For Case 1 and Case 5, for which the ventilation rate was set to a relatively high level, namely, n=0.1 h^{-1}, and the pulmonary ventilation rate was set to a low level, namely, p=1.0×10^{-5}, β became almost zero in a short time scale and the time series of (S) and (I) showed constant values (the same as the initial values). In other cases, the time profile of (I) had a local maximum value and then decreased gradually. Considering the diffusion of (S) and (I), the number of (S) was decreased and that of (I) was increased compared with those for Case 1 - Case 4. In the condition of Case 9 - Case 12 in which only (S) moved, time profiles of (S) and (I) were similar to those of Case 5 - Case 8, but the infection risk was estimated to be lower than that of Case 5 – Case 8, for which diffusions of both (S) and (I) were adopted.

Discussion

In this study, numerical analyses of unsteady and non-uniform concentration distribution by three-dimensional CFD and the procedures of coupled simulation between CFD and SIR-type epidemiological models were carried out. On the basis of these proposed procedures, the time dependence and distribution of infectious risk in indoor environments could be predicted quantitatively.

Contaminant concentration in the breathing zone was strongly influenced by the setting of the ventilation rate and therefore contact rate (β) was estimated as unsteady and inhomogeneous; then, space distributions of (S) and (I) were greatly changed in accordance with the boundary condition.

The scale of target spaces in this analysis was limited and grid scale was much smaller than the human scale. Analyses for larger spaces will be necessary in the future.

Furthermore, as shown in equations (1)-(3), constant (linear) and isotropic diffusion coefficients were adopted to reproduce movement of residents. In order to model human movement accurately, it is necessary to adopt a non-isotropic diffusion model and analysis by

cellular automata. This will also be investigated in the future.

Conclusion

In this study, the procedure of coupled analysis of unsteady and non-uniform concentration distribution based on CFD simulation and SIR-type epidemiology model was presented. Furthermore, the results of sensitivity analysis related to the exposure risk assessment of aerial infectious contaminants were shown for large enclosed spaces.

The findings obtained from this study can be summarized as follows:

(1) The Wells-Riley equation, which was used for the oral exposure assessment and is a part of the classic SIR model by Kermack and McKendrick, indicated an initial infectious expansion period. In the assumption of a constant linear rate of pulmonary ventilation rate and contaminant concentration in the breathing zone, contact rate β can be directly estimated. Through the analysis of infectious contaminant concentration level and non-uniform distribution in a large enclosure with CFD, the prediction of the number changes of (S), (I), and (R) becomes possible through the analysis of β.

(2) As a result of sensitivity analysis, the contaminant concentration in the breathing zone was found to be strongly dependent on the ventilation rate and then the distributions of (S) and (I) were greatly changed in accordance with initial and boundary conditions. We believe that the prediction procedures of coupled analysis of CFD and SIR model are effective for infectious risk assessment in indoor environments with sufficient accuracy.

Acknowledgement

This research was partly supported by a Grant-in-Aid for Scientific Research (JSPS KAKENHI for Young Scientists (S), 21676005). The authors would like to express special thanks to the funding source.

References

[1] Kermack, WO. and McKendrick, AG. (1927) A contribution to the mathematical theory of epidemics, *Proceedings of the Royal Society of London Series A*, ***115***, 700-721
[2] Wells, WF., (1955) Airborne contagion and air hygine, Cambridge, MA, Harvard University Press
[3] Riley, EC., Murphy, G. and Riley, RL. (1978) Airborne spread of measles in a suburban elementary school, *American Journal of Epidemiology*, ***107***, 421-432
[4] Li, Y., Huang, X., Yu, I.T.S., Wong, T.W., Qian, H. (2004) Role of air distribution in SARS transmission during the largest nosocomial outbreak in Hong Kong, *Indoor Air*, 15 (2) pp83-95
[5] Hua Qian, et al., (2009) Spatial distribution of infection risk of SARS transmission in a hospital ward, *Building and Environment*, ***44*** (8), 1651-1658
[6] Noakes, C.J., Beggs, C.B., Sleigh, P.A., and Kerr, K.G. (2006) Modeling the transmission of airborne infections in enclosed spaces, *Epidemiol. Infect.*, ***134***, 1082-1091
[7] Fine, P.E.M., (1993) Herd immunity: history, theory, practice, *Epidemiological Review* ***15 (2)***: 265-302

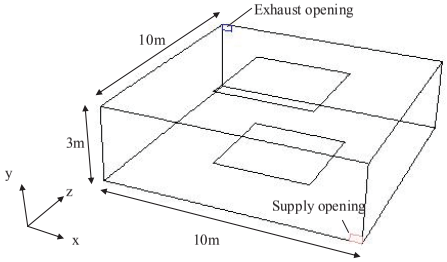


Figure 1 Outline of target spaces

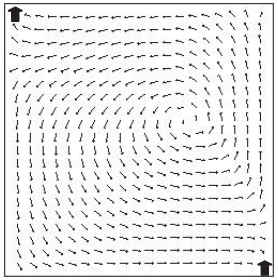


Figure 2 Results of flow field (n=0.01 h^{-1}, y=1.6 m height, x-z plane)

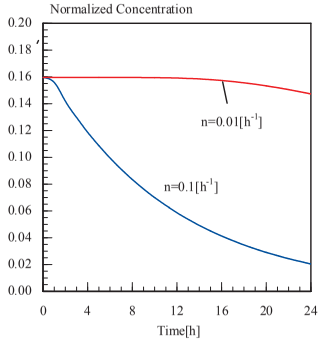
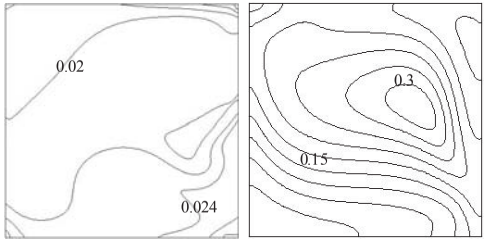
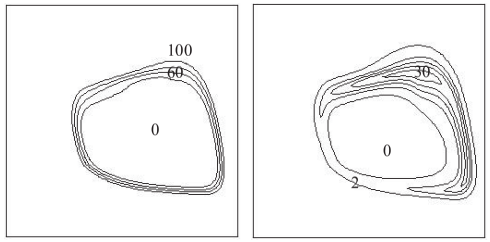


Figure 3 Time series of contaminant concentration ϕ for two ventilation rates (volume-averaged concentration, y=1.6 m, x-z plane)

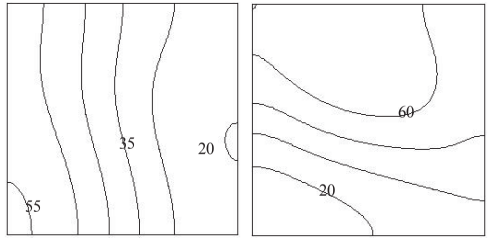


(1) ϕ (n=0.1 h^{-1}) (2) ϕ (n=0.01 h^{-1})

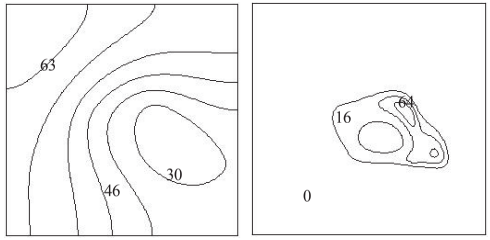
Figure 4 Normalized concentration distribution (t=24 h, y=1.6 m, x-z plane)



(1) S (Case 3) (2) I (Case 3)

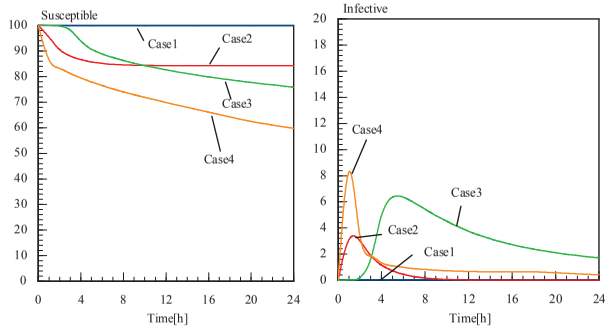


(3) S (Case 7) (4) I (Case 7)



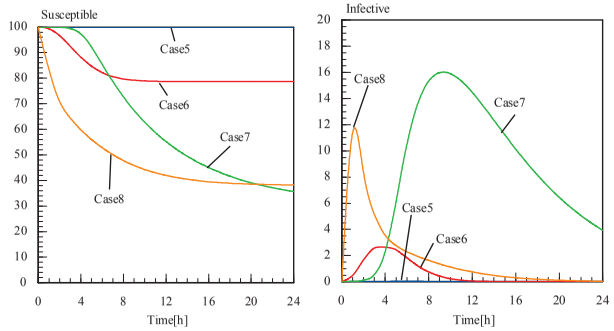
(5) S (Case 11) (6) I (Case 11)

Figure 5 Population density distributions of (S) and (I) (y=1.6 m, t=24 h, x-z plane)



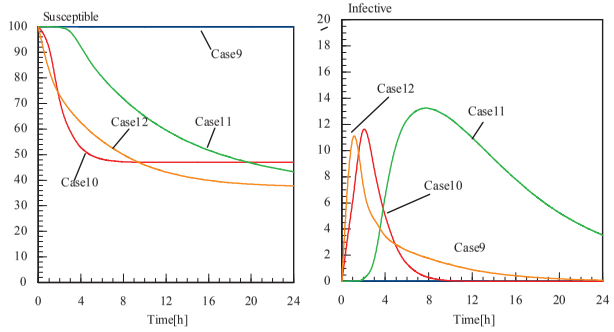
(1) *S* (Cases 1 - 4)

(5) *I* (Cases 1 - 4)



(2) *S* (Cases 5 - 8)

(6) *I* (Cases 5 - 8)



(3) *S* (Cases 9 - 12)

(7) *I* (Cases 9 - 12)

Figure 6 Time series of population density of (*S*) and (*I*) for each case

Table 1 SIR Model and Wells-Riley Model

[1] SIR (Kermack and McKendrick) model

$$\frac{dS}{dt} = -\beta SI + \nabla(D_S \nabla S), \quad \beta = p\phi \tag{1}$$

$$\frac{dI}{dt} = -\gamma I + \beta SI + \nabla(D_I \nabla I) \tag{2}$$

$$\frac{dR}{dt} = \gamma I + \nabla(D_R \nabla R) \tag{3}$$

$$R_o = \frac{\beta}{\gamma} S_0 \tag{4}$$

[2] Scalar transport equation

$$\frac{\partial \phi}{\partial t} + \nabla \phi \mathbf{u} = \nabla(D \nabla \phi) + S_\phi \tag{5}$$

[3] Wells-Riley model

$$P_I = \frac{C}{S} = 1 - \exp(-\frac{Iqpt}{Q}) \tag{6}$$

[4] Relations between each constant of Wells-Riley and SIR

$$S = S_0 \exp(-\beta It) \tag{7}$$

$$I = S_0 - S_0 \exp(-\beta It) \tag{8}$$

$$P_I = \frac{I}{S_0} = 1 - \exp(-\beta It) \tag{9}$$

$$\beta = \frac{qp}{Q} \tag{10}$$

Table 2 Numerical and Boundary Conditions

Turbulence Model	RNG k-ε model (3-dimensional Cal.)
Scheme	Convection Term: QUICK
Inflow Boundary	U_{in}=0.07 [m/s] for n=0.1[h^{-1}], U_{in}=0.007 [m/s] for n=0.01[h^{-1}], k_{in}=3/2× (U_{in}×0.1)^2, ε_{in}=$_\mu^{3/4}$×$k_{in}^{3/2}$/l_{in}, C_μ=0.09, l_{in}=0.044 [m]
Outflow Boundary	U_{out}= free slip, k_{out}= free slip, ε_{out}= free slip
Wall Treatment	Velocity; generalized log low
Contaminant	Passive Contaminant
SIR Model	S_0=100, I_0=10^{-2}, R_o=10

Table 3 Cases analyzed

Case	Ventilation Rate n [h^{-1}]	Pulmonary Ventilation Rate p [m^3/s]	Diffusion Coefficient	
			D_S [m^2/s]	D_I [m^2/s]
Case 1	0.1	1.0×10^{-5}	0	0
Case 2	0.1	5.0×10^{-5}	0	0
Case 3	0.01	1.0×10^{-5}	0	0
Case 4	0.01	5.0×10^{-5}	0	0
Case 5	0.1	1.0×10^{-5}	2.8×10^{-3}	2.8×10^{-3}
Case 6	0.1	5.0×10^{-5}	2.8×10^{-3}	2.8×10^{-3}
Case 7	0.01	1.0×10^{-5}	2.8×10^{-4}	2.8×10^{-4}
Case 8	0.01	5.0×10^{-5}	2.8×10^{-4}	2.8×10^{-4}
Case 9	0.1	1.0×10^{-5}	2.8×10^{-3}	0
Case 10	0.1	5.0×10^{-5}	2.8×10^{-3}	0
Case 11	0.01	1.0×10^{-5}	2.8×10^{-4}	0
Case 12	0.01	5.0×10^{-5}	2.8×10^{-4}	0

Health Hazards in Indoor Air

Jennifer M. LOGUE[1], Max H. SHERMAN[1], Brett C. SINGER[1]

[1] Energy Performance of Buildings Group, Indoor Environment Dept., Environmental Energy Technologies Division, Lawrence Berkeley National Laboratory

Abstract

Indentifying pollutants that pose a potential hazard indoors is an important first step to reducing risks. We reviewed key published studies reporting measurements of chemical pollutants in residences. Summary results were compiled and used to calculate representative mid-range and upper-bound concentrations relevant to chronic exposures for over 300 pollutants and peak concentrations relevant to acute exposures for a few episodic activity-associated pollutants. For the over 100 pollutants with available criterions, the measured concentrations are compared to available chronic and acute health-hazard standards and guidelines. Fifteen pollutants are identified as potential chronic or acute health hazards for many homes. A subset of pollutants are identified as priority chemical pollutants and suggestions are made for effectively reducing indoor concentrations.

Keywords: Indoor air quality; hazard analysis; residential; criteria pollutants; VOCs; air toxics

Introduction

The importance of the residential environment to cumulative air pollutant exposures has been demonstrated in numerous studies [1-2]. As outdoor air pollutant concentrations decrease and residential air exchange rates are lowered with improved air tightness [3], the contribution of indoor pollutant sources to overall exposure is expected to become increasingly more significant. The first step to reducing indoor health risks is to identify the pollutants driving risks indoors and to understand their sources.

Ventilation standards aim to deliver acceptable indoor air quality through whole house and spot ventilation. Some of these hazards can be controlled through dilution ventilation, but for many that may not be an optimal strategy. Since the sources of many of the identified hazards are known, relevant control measures can be considered.

This paper presents the results of a hazard analysis designed to identify chronic and acute chemical contaminants of concern in U.S. residences. We undertook a literature review to identify and compile data on measured pollutant concentrations for volatile organic compounds (VOCs), semi-volatile organic compounds (SVOCs), metals, and criteria pollutants. From these data, we determined broadly representative mid-range and upper-bound concentrations relevant to assessing chronic pollutant exposures. We also compiled data on elevated short-term and peak concentrations resulting from episodic activities. These

concentrations were compared to chronic and acute health guidelines or standards set by various agencies including the U.S. Environmental Protection Agency (USEPA), the World Health Organization (WHO), and the California Environmental Protection Agency (CalEPA). This analysis yielded a list of acute and chronic health hazards, from which priority pollutants were identified. For each priority pollutant, indoor sources are identified and suggestions are made for indoor pollutant mitigation.

Objectives

The objectives of this work were:

1) Determine representative and upper-bound indoor pollutant concentrations

2) Identify pollutants that pose a potential health hazard indoors

3) Ascertain likely sources of indoor pollutants; and

4) Suggest methods for the effective reduction of pollutant concentrations indoors

Approach

Literature Review and Data Compilation

Our literature review identified 86 articles that were relevant to acute and chronic exposure in residences. Our review considered all chemical contaminants measured in residential air regardless of source. The contaminants considered thus include some emitted purely from indoor sources, some that enter predominantly from outdoors, and some having both indoor and outdoor sources.

Seventy-four studies had data relevant to chronic exposures indoors. The studies were of occupied homes and generally designed to avoid extreme emission sources. Sixty-seven studies used sampling durations on the order of one or more days. Eight studies used shorter sample durations but took steps to reduce the impact of any recent pollutant-generating occupant activities. Based on these 75 reports, we compiled a database of summary statistics for chronic-exposure relevant concentrations for SVOCs, VOCs, metals, and criteria pollutants. From this database, we calculated weighted (by sample size) summary statistics for each pollutant.

Eleven studies had data relevant to acute exposures in residences. These studies reported concentrations measured during scripted events or during occupant activities such as cooking or cleaning that happened to occur during sampling. The reported concentrations were either calculated from time-resolved measurement or from short duration integrated samples collected with the express intent of measuring air quality following specific events or activities. These sampling periods tended to be on the order of a few hours, however some studies reported peak concentrations from highly time resolved data.

Hazard Assessment

We conducted the hazard assessment by comparing the compiled summary statistics for representative mid-range and upper-bound chronic-relevant concentrations to available chronic and the activity-associated short-term concentrations to acute health standards. Various governmental organizations publish standards or guidelines that specify either safe or hazardous pollutant concentrations for chronic and acute exposures. Such standards or guidelines are available for diverse sets of chemicals including criteria pollutants, hazardous air pollutants, and toxic air contaminants.

The U.S. Environmental Protection Agency (USEPA) sets National Ambient Air Quality Standards (NAAQS) for six criteria pollutants specified in the 1970 Clean Air Act: carbon monoxide (CO), nitrogen dioxide (NO_2), ozone, particulate matter (PM), lead, and sulfur dioxide. Title III of the 1990 Clean Air Act Amendments established a new regulatory category for chemical air contaminants that are known or suspected to cause serious health effects; 189 chemicals were named to the initial list of hazardous air pollutants (HAPs, also called “air toxics”), of which 187 are still on the list. The USEPA is charged to maintain and update this list, which includes VOCs, SVOCs, metals, and polycyclic organic matter (POM). The CalEPA maintains a separate list of toxic air pollutants referred to as Toxic Air Contaminants (TACs). There is considerable overlap between the CalEPA TAC and the USEPA HAP lists, but there are some key differences. For a subset of these pollutants the USEPA has listed chronic non-cancer reference concentrations (*RfCs*) and cancer unit risk estimates (*UREs*) through its Integrated Risk Information System (IRIS) and Health Effects Assessment Summary Tables (HEAST). Non-cancer *RfCs* report the exposure concentrations that are assumed to represent a safe level in that they are unlikely to cause health effects even for sensitive subgroups of the population. *URE*s estimate the incremental increase in cancer risk that accrues for each 1 g m^{-3} increase in chronic exposure. The California Office of Environmental Health Hazard Assessment (OEHHA) publishes non-cancer Reference Exposure Levels (*REL*s) and its own cancer *URE*s. In addition to the California and USEPA values, the U.S. Occupational Safety and Health Administration (OSHA) sets reference concentrations for workplace exposures, and the Agency for Toxic Substances and Disease Registry (ATSDR) publishes *RfCs* for chronic exposure. Since OSHA regulations are intended to protect generally healthy adult workers, their allowable concentrations tend to be higher than those set for HAPs/TACs by the USEPA and CalEPA.

Whereas exposure concentration limits are specified for acute effects and for chronic non-cancer endpoints, concentration-based standards are not uniformly available for cancer. The European Union and the CalEPA have estimated no-effect concentration levels based on an acceptable level of risk. The USEPA has not defined a generally acceptable cancer risk level

for HAPs. However, a case-specific determination was made in the 1989 Benzene National Emission Standard for Hazardous Air Pollutants (NESHAP). This rule set an upper limit of acceptability of 1 in 10^4 lifetime cancer risk for highly exposed individuals and the goal of reducing lifetime risk to 1 in 10^6 for the general public. In consideration of this range, we used available cancer UREs to calculate acceptable exposure concentration for cancer risk that correspond to a lifetime incremental risk of 1 in 10^5 assuming 70 years of continuous exposure. The resulting cancer-based exposure concentration values are health protective and comparable to but not necessarily equivalent to the *RfC*s.

As a final point, although the our analysis focuses on the method of comparing measured concentrations to health-based standards to establish hazard, we note that there are three indoor air hazards that are already well established—radon, second-hand tobacco smoke, and carbon monoxide (CO).

Potential Health Hazards from Chronic Exposures

In Figure 1 we compare our representative indoor air concentrations to the relevant standards for chronic health hazards. The bars indicate the representative mid-range concentration with a line that extends to the representative upper bound concentration. The graph is arranged, in decreasing order, by the ratio of the mid-range concentration to the lowest available health standard.

The figure identifies 2 criteria pollutants and 20 HAPs/TACs that have mid-range or upper bound concentrations higher than at least one health standard. The majority of the 20 pollutants have indoor concentrations that exceed cancer standards only; only four of the pollutants have indoor concentrations that exceed a non-cancer standard.

Table 1 summarizes the results of the hazards analysis. The table subdivides the chronic hazards into three groups: hazards in most homes, hazards in some homes (on the order of 5-50%) and hazards in very few homes (on the order of a few percent or less) based on what percentage of the available data has concentrations greater than available standards. These groupings are based on our representative mid-range and upper-bound concentrations that generally derive from weighted median and 95th percentile values of reported concentrations in homes. The table also indicates the type of hazard (cancer or non-cancer), the number of available studies, and the level of certainty. The level of certainty reflects whether we believe that the available data is representative of the current state of US homes and was based on the number of available studies, whether reported concentrations were above a standard in U.S. homes or only in homes outside of the U.S, and, in a few cases, information about concentrations outdoors.

Of the 15 compounds identified in most homes, nine were identified as priority chronic hazards in U.S. residences: acetaldehyde, acrolein, benzene, 1,3-butadiene, 1,4-dichlorobenzene, formaldehyde, naphthalene, NO_2, and $PM_{2.5}$. These are nine of the ten pollutants identified as hazards with a high level of certainty in most homes. The tenth pollutant, carbon tetrachloride, was used extensively as a refrigerant in the past, but was banned as part of the Montreal Protocol and has been largely phased out. Due to a long atmospheric lifetime, carbon tetrachloride is still present in the atmosphere at hazardous concentrations.

Several studies have looked at specific events or activities in the home that give rise to high transient pollutant concentrations. The highest concentration for each pollutant was compared to acute standards from WHO, USEPA, and CalEPA. The results are summarized in table 1. The pollutants identified as acute hazards are, for the most part, a subset of the pollutants identified as chronic pollutants. Chloroform was additionally identified as posing a potential acute hazard.

Our results are similar to those identified by the reviews done by Dawson et al.[4], Koistinen et al.[5], and Loh et al.[6] with some distinct differences. Loh et al. [6] identified a similar subset of high priority VOC and SVOC chemical air pollutants using a combination of measurements and modeling. Our review identified a similar set of VOC and SVOC priority pollutants with the addition of acrolein, which was not included in their study. Dawson et al. [4] identified benzene as a having an elevated cancer risks in most homes by comparing concentrations of 10 VOCs to available standards. Koistinen et al. [5] identified 5 priority pollutants in European homes, formaldehyde, CO, NO_2, benzene, and naphthalene. With the exception of CO, these pollutants were identified as priority pollutants in this study as well. The difference appears to be due to higher long term concentrations in European homes.

Identifying Pollutant Sources and Mitigation Strategies

In the residential environment there are 3 main options for reducing indoor concentrations: 1) spot ventilation, 2) removal through whole house ventilation, and 3) reducing or eliminating the use of pollutant containing materials. The most effective method varies from pollutant to pollutant based on the major indoor sources. Table 2 lists the known sources of the nine priority pollutants indoors as well as the strategies that would most effectively reduce indoor pollutants.

The main indoor source of naphthalene, 1,4-dichlorobenzene, benzene, and 1,3-butadiene are specific products. Naphthalene and 1,4-dichlorobenzene are used in mothballs and deodorizers. Solvents, paints, stored fuel and other household products can emit benzene into the indoor environment. Removing these products from the living space would be the most effective method of reduction indoor concentrations.

Cooking and combustion appliances are large contributors to acrolein and NO_2 respectively indoors indicating that spot ventilation is the most effective risk reduction scheme. Outdoor infiltration is a dominate contributor to $PM_{2.5}$ mass indoors although cooking and cleaning are large indoor contributors to the number of particles comprising $PM_{2.5}$ and has been shown to cause short-term concentrations above acute standards. Spot ventilation can effectively reduce the $PM_{2.5}$ risk due to cooking. Reducing outdoor concentration or turning off whole house ventilation during high $PM_{2.5}$ time period will also reduce risks.

The main source of formaldehyde indoors is home furnishings and manufactured wood products, however cooking can also be a source of short term elevated concentrations. Therefore, a combination of spot and whole house ventilation should be used to reduce formaldehyde concentrations in the short term. In the long term, steps should be taken to reduce concentrations in products and materials in homes.

Lastly, acetaldehyde has numerous sources indoors including cooking, indoor combustion, emissions from materials and products. It is unclear which of these pathways is dominant. Whole house ventilation, spot ventilation in kitchens, and reducing the use of products that emit acetaldehyde will all reduce concentrations, but it is unclear which method would be most effective.

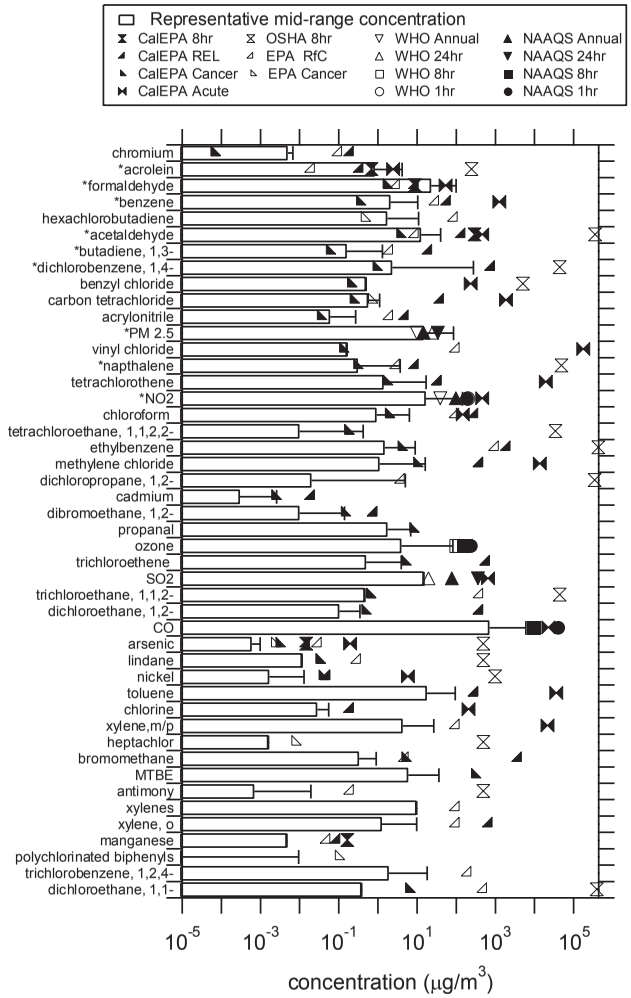


Fig. 1 Representative indoor air concentrations compared to relevant national and international standards. Line extends to the upper bound indoor concentration. Cal AREL is the CalEPA acute reference exposure level (1hr). Cancer, RfC, and REL standards are for chronic long term exposure (70 years). OSHA standards are for workday exposure for a significant portion of a lifetime. (CAL=CalEPA, EPA=USEPA) . (CAL=CalEPA, EPA=USEPA). Priority pollutants are identified with an asterisk.

Table 1 Pollutants that potentially pose an adverse indoor health risks.

Chronic Health Hazard

Hazards in most homes	*# of studies (# of data points, midpoint, upper bound)*	*Hazard**	*Level of certainty*
acetaldehyde**	**12 (1578, 965)**	**C/NC**	**high**
acrolein**	**5 (1241,965)**	**NC**	**high**
benzene**	**21 (6897, 3240)**	**C**	**high**
butadiene, 1,3-**	**8 (328, 7)**	**C**	**high**
dichlorobenzene, 1,4-**	**12 (1691, 1626)**	**C**	**high**
formaldehyde**	**18 (1916, 965)**	**C/NC**	**high**
naphthalene**	**9 (2043, 1544)**	**C/NC**	**high**
NO2**	**19 (7797, 1642)**	**NC**	**high**
PM2.5**	**18 (2822, 1141)**	**NC**	**high**
carbon tetrachloride	5 (861, 554)	C	high
acrylonitrile	1 (75, 75)	C	medium
chromium	4 (284, 334)	C	medium
hexachlorobutadiene	1 (443,400)	C	low
benzyl chloride	1 (39, --)	C	low
vinyl chloride	1 (447, 447)	C	low
Hazards in most homes	*# of studies (# of data points, midpoint, upper bound)*	*Hazard**	*Level of certainty*
chloroform	12 (1217, 1107)	C	high
ETS	not applicable	C/NC	high
ethylbenzene	18 (5689, 2640)	C	high
methylene chloride	8 (1538, 1130)	C	high
radon	not applicable	C	high
tetrachlorothene	13 (3648, 3158)	C	high
cadmium	3 (275, 372)	C	medium
dichloropropane,1,2-	2 (75, 538)	NC	medium
ethanol	2 (444, 227)	C	medium

Table 1(Cont.) Pollutants that potentially pose an adverse indoor health risks.

Acute Health Hazards

Hazards in most homes	*# of studies (# of data points, midpoint, upper bound)*	*Hazard**	*Level of certainty*
acrolein	3	SI	high
formaldehyde	7	SI	high
CO	2	H	high
PM2.5	15	R/H	high
NO2	6	R	high
chloroform	1	RD	low

Table 2 Priority pollutant sources and effective mitigation methods indoors

Priority Pollutants	**Indoor Sources**	**Mitigation Methods PU**	**SV**	**WHV**
acetaldehyde	combustion, products, materials, infiltration	X	X	X
acrolein	combustion, materials		**X**	X
benzene	combustion, infiltration, products	**X**	X	
butadiene, 1,3	products (ETS)	**X**		
dichlorobenzene, 1,4-	products	**X**		
formaldehyde	combustion, materials		**X**	**X**
naphthalene	products	**X**		
NO2	combustions, products		**X**	X
PM2.5	combustion, secondary reactions, infiltration	X	**X**	

PU=reducing product use, SV=spot ventilation, WHV=whole house ventilation

References

1. Edwards, R.D., et al., *VOC concentrations measured in personal samples and residential indoor, outdoor and workplace microenvironments in EXPOLIS-Helsinki Finland.* Atmospheric Environment, 2001. **35**: p. 4531-4543.
2. Weisel, C.P., et al., *Relationships of Indoor, Outdoor, and Personal Air (RIOPA) Part I. Collection Methods.* 2005, Health Effects Institute, Mickely Leland National Urban Air Toxics Research Center and Descriptive Analysis.
3. Sherman, M.H. and N.E. Matson, *Air tightness of new U.S. houses: A preliminary report.* 2002, Lawrence Berkeley National Laboratory, LBNL-48671.: Berkeley, Ca.
4. Dawson, H.E. and T. McAlary, *A compilation of statistics for VOCs from post-1990 indoor air concentration studies in North American residences unaffected by subsurface vapor intrusion.* Ground Water Monitoring & Remediation, 2009. **29**(1): p. 60-69.
5. Koistinen, K., et al., *The INDEX project: executive summary of a European Union project on indoor air pollutants.* Allergy, 2008. **63**(7): p. 810-819.
6. Loh, M.M., et al., *Ranking cancer risks of organic hazardous air pollutants in the United States.* Environmental Health Perspectives, 2007. **115**(8): p. 1160-1168.
7. Logue, J.M., McKone, T.E., Sherman, M.H., and Singer, B.C. *Hazard Assessment of Chemical Air Contaminants Measured in Residences.* Under review by Indoor Air, 2010

Experimental method for determining removal efficiency of house dust by mechanical ventilation

Kurihara Genta, Yoshino Hiroshi, Yonekura Hiroshi, Takaki Rie, and Lu Yang

Tohoku University, Department of Architecture and Building Science, Japan

Abstract

Biological contamination has recently become an important issue in the residential indoor environment. In fact, one of the leading causes of allergic diseases is the presence of mold and mites in house dust that accumulates on the floors, near the breathing zone for infants and toddlers. In this research, experimental studies were carried out in order to examine particle removal efficiency in a room with two ventilation systems: a ceiling exhaust system and a slit exhaust system. The results indicated that there was no clear relationship between removal efficiency and two different outlet locations. It was found that the use of fluorescent particles to simulate house dust was effective for determining the removal efficiency of ventilation systems.

Keywords: particle removal, airborne particles, measuring method, ventilation system

1. Introduction

Today's houses are designed to be well insulated and airtight to reduce energy use and improve thermal comfort. However, this high performance is accompanied by an increase in indoor humidity and condensation due to the lack of ventilation, and is the likely cause of microorganism pollution due to mites and mold. House dust includes mold spores as well as mite excrement and corpses. Existing studies have revealed that indoor air pollution by microorganisms could cause building-related illnesses such as asthma, allergies and atopic dermatitis [1, 2]. The number of patients exhibiting such health problems has been increasing

every year in Japan. Since house dust easily accumulates on the floors, there is a high possibility of allergic reactions in infants and toddlers whose breathing zone is near the floor surface.

Although ventilation is one of the best ways to remove house dust, the required energy consumption must be considered. Therefore, it is important to know what type of ventilation system is most effective for removing house dust.

The objective of this study was to examine how effectively house dust is removed in relation to the location and type of indoor air exhaust system. In this paper, we first describe the experimental measurement method using a box. Then, we present the measurement results for dust removal efficiency using a test house.

2. Experimental measurement method using a box

2.1 Detection equipment

For this study, IMD (instantaneous microbial detection; IMD-A 200-1, BioVigilant Systems) was used to measure the dust particles. IMD is based on optical fluorescence sensor technology and is capable of detecting the size of particles in the environmental air as well as determining whether or not each particle is biological [3]. Particle size can be detected within the range of six stages (0.5–1.0, 1.0–3.0, 3.0–5.0, 5.0–7.0, 7.0–10.0, and 10–15 μm).

2.2 Particles used for measurement

In an existing study [4] on the behavior of mite allergens, JIS-11 test particles were used as simulated particles (Figure 1a). In this case, however, existing particles in the background air might have influenced the measurement results. Therefore, riboflavin (Vitamin B2) was used as harmless biological particles that would not be present in the background air (Figure 1b).

2.3 Measurement of particles in a box

A plastic box measuring 450 mm wide, 350 mm long and 350 mm high was used for examining the measurement method. The box was set in the test house and the cover was put on the box. Then, the air in the box was sucked out and the particles in the air were measured by IMD at measurement intervals of one minute. Figure 2 shows the measurement results of the particles in the air of the box for a 24-h period. Long-term observation of the particle count for 0.5–1.0 μm showed a significant change. For example, the average existing nonbiological particle count in the first half of the measurement period was 802 particles/L for 0.5–1.0 μm and 80 particles/L for 1.0–3.0 μm. In the second half of the measurement period, the count was 1323 particles/L for 0.5–1.0 μm and 68 particles/L for 1.0–3.0 μm. On the other hand, for the biological particles, the total count in all sizes after 12 h was very small. The biological particles were useful for determining the removal efficiency of house dust by the ventilation system.

2.4 Method of supplying particles to the box

The method for supplying particles to the box was examined. A flask containing 1 g of particles at the bottom was set up in the box. As shown in Fig. 3, N_2 gas with a constant flow of 2 L/minute was injected through a tube to the particles at the bottom of the flask.

2.5 Results of measurement

1) JIS-11 test particles

Figure 4 shows the results in the case of using the JIS-11 test particles. The average particle count before supply was 1753 particles/L for 0.5–1.0 μm and 170 particles/L for 1.0–3.0 μm. The particle count for all sizes increased rapidly just after the supply of particles and then decreased to the same level as that before the supply of particles. The decay speed of the particles in the size range 0.5–1.0 μm was slower than that of the other particle sizes. This is because particles smaller than 0.5–1.0 μm were erroneously counted as particles of that size during times of high particle density.

2) Riboflavin particles

Figure 5 shows the results in the case of using the riboflavin particles. The particle count before supply was very low compared with the count for JIS-11 test particles (Figure 4). For particles in the size range 0.5–1.0 μm, the peak count appeared immediately after the supply of particles. As the riboflavin is biological, the existing particle count was very low. The riboflavin can be used to simulate house dust particles for the experiment.

3. Experiment on removal efficiency using a test house

3.1 Outline of test house and ventilation systems

The test room (L×W×H = 5.37×2.74×2.25 m) was located on the second floor of a two-storey experimental house situated at Tohoku University, Japan. Insulation boards were installed on all window surfaces to reduce the effect of cold drafts. The equivalent air leakage measured by the pressurization method was 3.17 cm^2/m^2.

Figure 6 shows the test room. The two mechanical ventilation systems tested in this study are shown in Figure 7. An exhaust is located on the ceiling (ceiling exhaust) in case 1 and slits (5-mm width) are set at the corners between the walls and floor (slit exhaust) in case 2. For both cases, the air inlet is located at the center of the ceiling.

3.2 Pretest for determining the measurement method

(1) Method of supplying the particles

For supplying the riboflavin particles, a flask containing riboflavin (4 g) was set up in the test room as shown in Fig. 6. The indoor air was circulated by two fans, one of which was set in

front of the flask. N_2 gas was injected into the flask for 1 h. The ventilation system was operated after the particles fell freely to the floor due to gravity force. The measurement point was located 1.0 m above the floor between the outlet and the inlet (Figure 6).

(2) Results of the pretest

Figure 8 shows the change in particle count for 90 h after the supply of particles. The particle count increased dramatically just after the supply and reached over 10,000 particles/L for those with diameter of 1.0–3.0 μm. For particles with diameter of 0.5–1.0 μm, the decay of the particle count was not constant for 12 h. It is possible that at times of high particle density some particles were detected as larger particles due to an error in simultaneous counting. Therefore, the volume of riboflavin set in the flask was decreased from 4 g to 1 g.

Also, there was no particle generation from the floor when the ventilation system was operated.

(3) Measurement method

As a result of the pretest, the procedure for measuring removal efficiency was determined as follows:

1) Measurement of particles in the background for at least 12 h before the start of supply.

2) The riboflavin particles (1 g) are supplied to the test room by means of N_2 gas injection into the flask through a tube.

3) The room air is circulated by two fans while particles are supplied for 1 h.

4) After 1 h, the gas injection is stopped and the fans are turned off.

5) Operation of the ventilation system begins when the particle count decreases to 100-1000 particles/L.

3.3 Experimental conditions

Table 1 shows the experimental conditions for four cases. Two kinds of ventilation systems were tested under two different rates of air change per hour (ACH).

3.4 Results of the experiment

(1) Particle count variation in the decay period

Figures 9 and 10 show the measurement results for the slit type and ceiling type of ventilation at 2.5 ACH, respectively. There is not much difference in the decay of particle count between the two ventilation systems. Figure 11 shows the decay count using a log-scale for the y-axis for the two systems. It can be seen that there was no difference between the two systems. The

results at 0.75 ACH show almost the same tendency. There is no difference in the particle removal efficiency between the two ventilation systems from the decay period results.

Also, the measured value was divided by the value at the start of ventilation operation. Figures 12 and 13 show the results for the two ventilation systems in the case of 2.5 and 0.75 ACH, respectively. The decay speed at 2.5 ACH was faster than that at 0.75 ACH.

(2) Particle count variation after the decay

Figures 12 and 13 show the particle count variation after the decay. In the case of the ceiling exhaust, the particle count was higher than that in the case of the slit exhaust.

Figure 14 shows that the particle count variation including the period when a person entered the room for cleaning purposes. In this period, the particle count reached a level of about 40% of the value at the start of particle supply. This clearly indicates that particles were raised from the floor by the walking motion.

4. Conclusions

1. As a result of measurement using a box, the biological riboflavin particles were useful for measuring the particle removal efficiency by ventilation because riboflavin is not present in the background air. The harmless riboflavin can be used to simulate house dust particles for the experiment.

2. Pretest results showed that particles were not generated from the floor when the ventilation system was operated.

3. The experimental results during the decay period indicate that there was no difference in particle removal efficiency between the two ventilation systems.

4. From the results after the decay, the particle count in the case of the ceiling exhaust was higher than that in the case of the slit exhaust.

5. The particle count reached a level of about 40% of the value at the start of supply when a person entered the room for cleaning purposes. It is clear that particles were raised from the floor by the walking motion.

Acknowledgments

This research was supported by the Ministry of Land, Infrastructure, Transport and Tourism as part of the “Program to promote technology related to residential construction” and “Technological development on reducing health problems caused by house dust” and Inter Central corporation consignment research. Sincere appreciation is extended to everyone involved in this research.

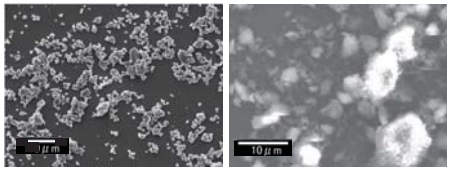
References

1. M. Zureik, et al. “Sensitisation to airborne moulds and severity of asthma: cross sectional study from European Community respiratory health survey”, *BMJ*, 2002, Vol. 325, No. 7361

2. L. Elliott, et al. “Dust weight and asthma prevalence in the national survey of lead and allergens in housing (NSLAH)”, *Environmental Health Perspectives*, 2007, Vol. 115, No. 2, pp. 215-220

3. K.Vishvesh, et al. “Evaluation of an Instantaneous Microbial Detection System in Controlled and Cleanroom Environments”, *BioPharm International*, 2007

4. R. Watanabe, et al. “Effects of Heating Systems on Scattering of Der 1 Based on Experiments and CFD Analysis”, *Architectural Institute of Japan*, 2006, pp. 887-888 (in Japanese)



a: JIS-11 test particles **b:** Riboflavin particles

Figure 1 Scanning electron micrograph of particles

Table 1 Experimental conditions

CASE	Exthust method	Ventilation timing	Particle amount	Flow rate	Date
SE 1	Slit	settling	1.0g	2.5ach*	2009/12/26
CE 1	Ceiling	settling	1.0g	2.5ach	2009/01/08
SE 2	Slit	settling	1.0g	0.75ach**	2009/01/26
CE 2	Ceiling	settling	1.0g	0.75ach	2009/01/15

- Velocity of wind on slit : * 0.12m/s ** 0.42m/s

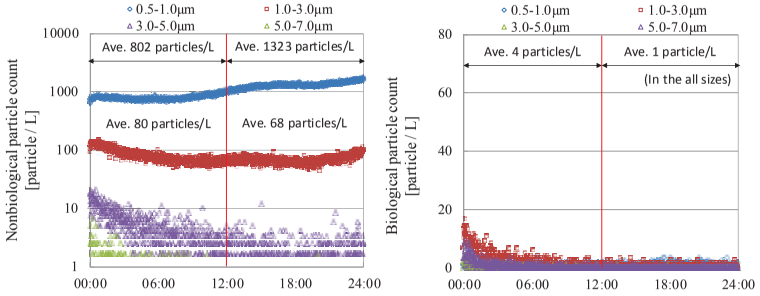


Figure 2 Change in existing particle count

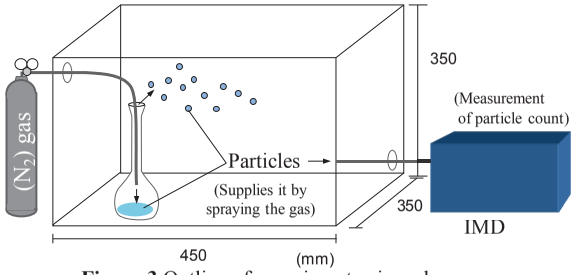


Figure 3 Outline of experiment using a box

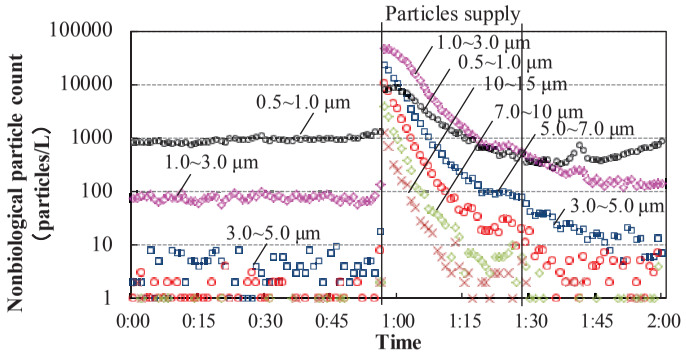


Figure 4 Change in particle count
(JIS11 test particles, September 18)

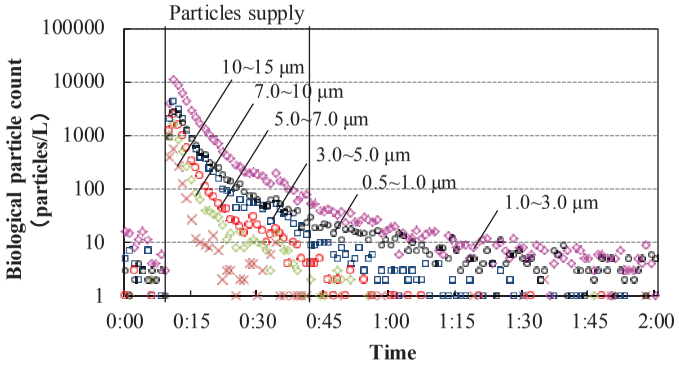


Figure 5 Change in particle count
(Riboflavin particles, October 27)

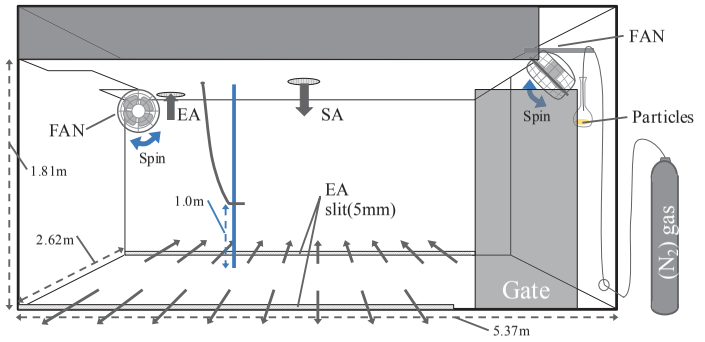


Figure 6 Outline of the test room

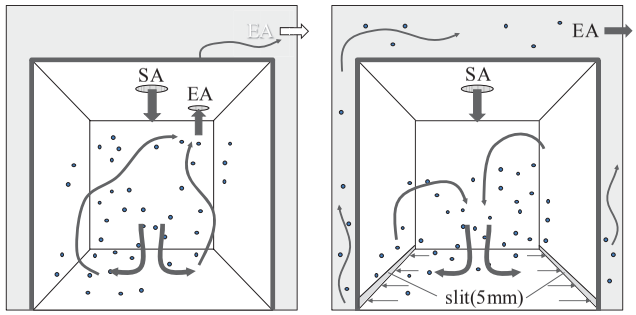


Figure 7 Exhaust methods

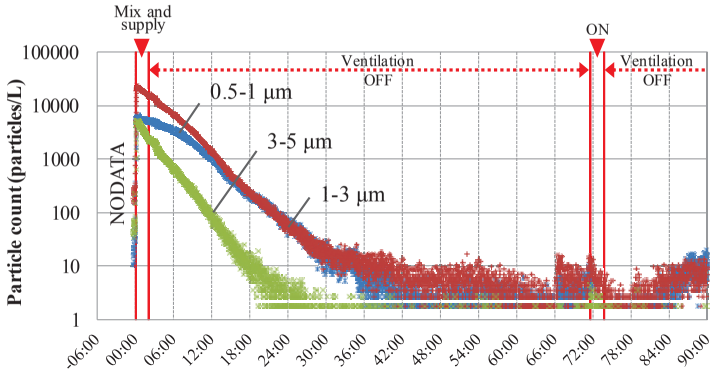


Figure 8 Change in particle count (Ceiling exhaust, 2.5 ACH)

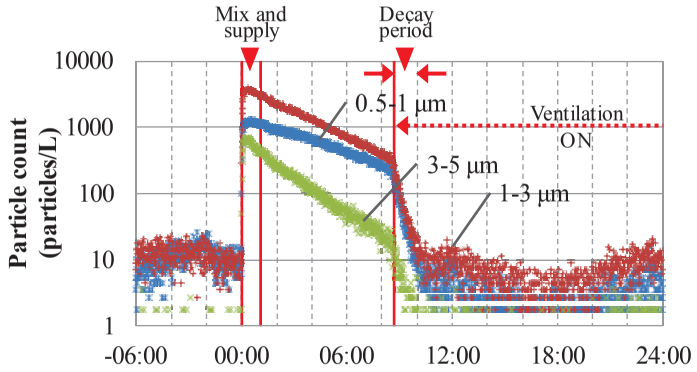


Figure 9 SE1 (Slit exhaust, 2.5 ACH)

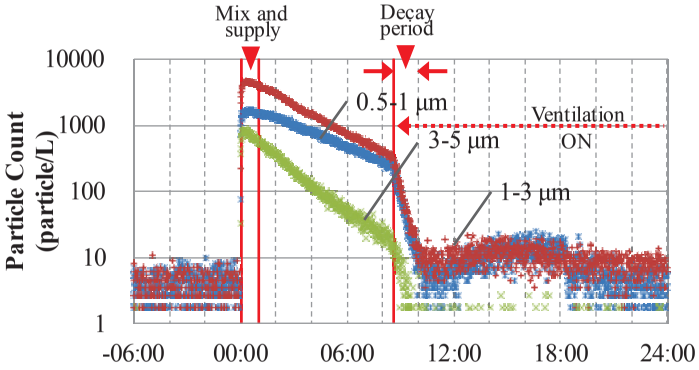


Figure 10 CE1 (Ceiling exhaust, 2.5 ACH)

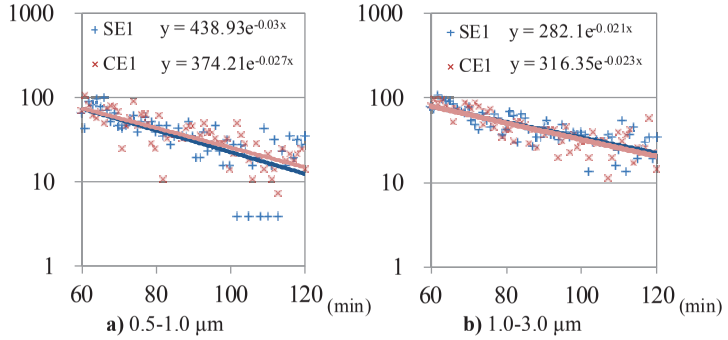


Figure 11 Decay of SE1, CE1 (60–120 min)

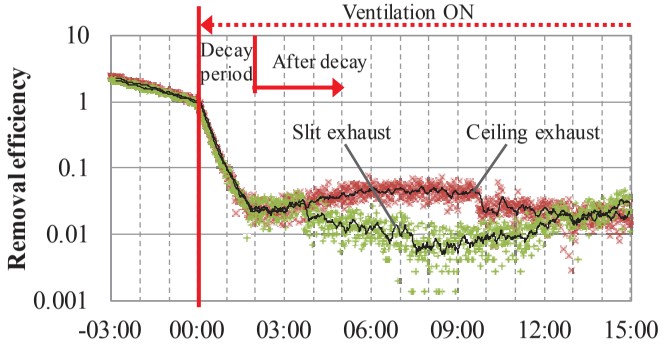


Figure 12 Air change rate 2.5 ACH (SE1, TD2: 0.5–3.0 µm)

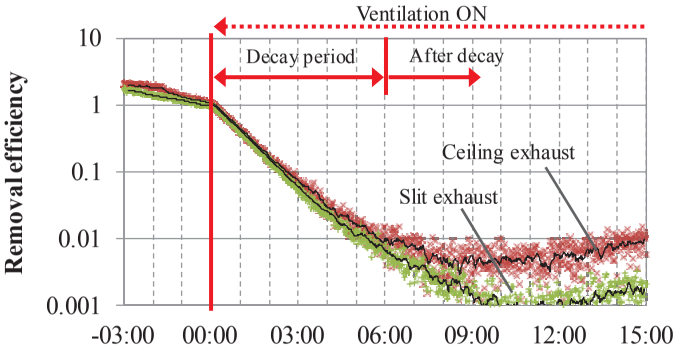


Figure 13 Air change rate 0.75 ACH (SE2, CE2: 0.5–3.0 µm)

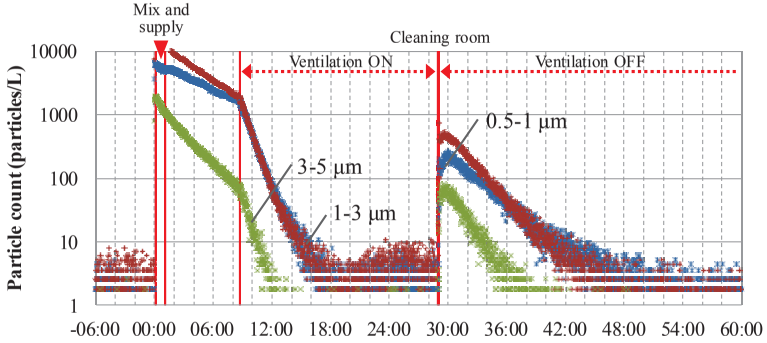


Figure 14 SE2 (Slit exhaust: 0.75 ACH)

Distribution of CO in 30 Homes with Unvented Gas Fireplaces

Paul W. FRANCISCO[1], Jeffrey R. GORDON[1], and William B. ROSE[1]

[1] University of Illinois at Urbana-Champaign, Building Research Council, Champaign, IL

Abstract
As part of a field measurement project of unvented gas fireplaces in 30 homes, portable carbon monoxide sensors were located in several places in each home. This was done to assess the degree to which combustion by-products became distributed throughout the home. The sensors indicated that carbon monoxide levels began rising throughout the home almost immediately, at or near the one-minute sampling interval. The results show that, on average, the reading in the middle of the fireplace room was about 95% of the reading at the mantel. Readings throughout the rest of the home are comparable to each other and are between 75-80% of the reading at the mantel at peak concentrations. These results indicate that carbon monoxide concentrations from unvented fireplace combustion spread rapidly and rather uniformly throughout the house.

Keywords: unvented combustion, residential, field measurement, IAQ

Introduction

Unvented gas heating appliances are similar to other space heating and hearth products, with one exception – they don't have a chimney, flue or vent. For builders and homeowners this is appealing because no hole in the roof or walls is required, allowing for substantial installation savings and preventing potential leaks at the point of venting. Since the installation of unvented gas fireplaces does not require a chimney or any other vents, they can be easily installed almost anywhere. However, since unvented gas fireplaces release combustion products with potentially adverse health effects to the living space, they have remained controversial among the building science community.

From 2005-2007 field testing was performed in 30 homes that utilized these appliances. Testing at each home lasted for 3-4 days, and included measurements of carbon monoxide (CO), carbon dioxide (CO_2), oxides of nitrogen (NO_x) and its components nitric oxide (NO) and nitrogen dioxide (NO_2), oxygen (O_2) depletion, and water vapor (H_2O) in a location approximately 6 feet away from the fireplace. Data were recorded every minute. Summary results from this project can be found in Francisco et al.[1]

In addition to the sampling location near the fireplace, water vapor and CO were also recorded using portable passive sensors in 5 locations throughout the home to assess the distribution of combustion products throughout the home. The results from the water vapor sensors have been published previously[2]. This paper presents the results from the portable CO sensors.

Methodology

At each home sensors were placed on the fireplace mantel, in the middle of the room in which the fireplace was located, on the opposite side of the room in which the fireplace was located, in an adjacent room (often, but not always, a kitchen), and a distant room (often, but not always, a bedroom).

In order to analyze the CO data for distribution throughout the house, the data from the CO sensors at each house were first viewed graphically to determine which fireplace usage cycle produced the largest CO signal. The primary reason why a single cycle was used is that the resolution of the sensors is about 0.5 ppm. Therefore, in order for the comparison between sensors to be as strong as possible the CO levels needed to be as high as possible. Figure 1

shows an example of the data and the selection of a cycle to analyze. This figure, which includes the data from both the mantel and distant sensor locations, shows several important features pertinent to this analysis. First, the distant bedroom sensor consistently indicated a lower CO concentration at that location than at the mantel. Second, the CO levels began to rise and fall at essentially the same time, within the 1-minute sampling interval, thus obviating the need to adjust for any time lag. Third, the rise in the evening of Feb. 4, which shows both a lower concentration than earlier periods and a greater difference between the mantel and the distant bedroom, was actually unrelated to the fireplace but rather was due to cooking in the kitchen.

Once a cycle was selected, the maximum CO concentration for each sensor location was determined. Selecting the maximum has two advantages. First, the sensor resolution is the smallest possible fraction of the signal. Second, it is at these maximum levels at which there is the greatest concern about exposures.

The resulting maximum values for each sensor location was regressed linearly on the mantel sensor values. The coefficient of the regression is an estimate of the percentage of the CO concentration at the mantel that reaches each of the other locations, i.e. for each additional ppm of CO at the mantel the coefficient indicates how much the concentration rises at each location.

In addition to the sample-wide results three homes are discussed individually. These homes each demonstrate interesting characteristics that are not reflected in the overall sample but which are worth discussion.

There were some homes in the sample at which results could not be determined. There were various causes of this, including extremely short cycles, very low concentrations (e.g. under 2 ppm such that the resolution of the sensors was a very large percentage of the signal), and failed sensors such that no data were recorded. The resulting dataset for this analysis comprised 18 homes.

Sample Characteristics

The homes in the study represented a sample of convenience. Homes were solicited via a university newsletter and word of mouth. The average age of the homes was about 35 years old, with a minimum of 3 years and a maximum of about 100 years. The average age of the fireplaces was over 6 years, with a minimum of 4 weeks and a maximum of 15 years. The average floor area of the homes was about 167 m^2, with a minimum of about 111 m^2 and a maximum of about 279 m^2. The average leakage of the homes was about 11.3 air changes at 50 Pa (ACH50) with a minimum of about 5.5 ACH50 and a maximum of about 23.4 ACH50.

Results

Figure 2 shows the maximum concentrations for each sensor location vs. the maximum concentration at the mantel, along with a regression line. These data are for the entire 18 home sample presented in this paper. Figure 2a shows the sensor in the middle of the fireplace room; 2b shows the sensor at the opposite side of the fireplace room; 2c shows the sensor in the adjacent room; and 2d shows the sensor in a distant room.

These regressions show that the CO concentration in the middle of the fireplace room is about 11% higher than the concentration at the mantel, though with a constant of about -2 ppm. The regression shows that the t-statistic on the constant is 2.43, which borders on statistical significance. If the regression was forced through zero then the coefficient would be 0.97. With either analysis, the data indicate that the concentration in the middle of the room with the fireplace is comparable to the concentration at the mantel.

The graphs for the opposite side of the fireplace room, adjacent room, and distant room all show that the concentration at these locations is typically lower than the concentration at the mantel. As the location is further from the mantel the degree of scatter increases, as evidenced by the lower R^2 values.

For the opposite side of the fireplace room and the adjacent room the concentration is about 80% of the value at the mantel. This drops to about 75% at the distant room. These results show that the concentration is typically fairly uniform throughout the house except in the immediate vicinity of the fireplace, at about 75-80% of the level near the fireplace. This is consistent with the results of Ferro et al.[3] who showed that concentrations of point-source contaminants may be only 20-30% lower in other rooms with open doors. High levels of airflow and/or mixing through open doors have also been shown by Miller and Nazaroff[4] and Sherman and Walker[5].

Figure 3 shows the CO data at Sites 26 (Figure 3a) and 31 (Figure 3b), for the mantel, opposite side of the fireplace room, and distant room.

In Site 26 the fireplace was located in the basement. This basement had been tightened but not insulated. The CO sensor in the distant bedroom was upstairs on the first floor.

There are two primary features of the data at this home. First, despite being upstairs, the CO concentration in the bedroom was comparable to the concentration at the opposite side of the fireplace room for most of the test, with the primary exception being the night of Jan. 23 and the morning of Jan. 24. It is likely that the door between the basement and the first floor was closed at this time.

The other feature of this graph is that there are very few times when there is not transient behavior. This makes it reasonable to compare the concentrations in different locations for the entire test period, not just one cycle. Regressions of each sensor on the mantel sensor show that concentration in the middle of the fireplace room was about 94% of the concentration at the mantel, the concentration at the opposite side was about 62% of the concentration at the mantel, and the two sensors upstairs (adjacent and bedroom) were about 54% and 56% that of the mantel, respectively. These percentages are lower than the sample average, but the qualitative result of the sensors beyond the middle of the fireplace room being comparable is consistent with the other homes.

In Site 31 the fireplace was in the living area, and the distant sensor was in the basement. The basement door was typically kept closed.

In this home the concentration at the opposite side of the fireplace room was about 90% that at the mantel, but the concentration in the basement rarely showed substantial evidence of a response to the fireplace operation. These data show the potential impact of closed doors on

the concentration, especially when airflow driving forces (in this case, stack effect) do not promote transport of the CO to the other space (in this case, the basement).

Figure 4 shows the CO concentration and the air temperature at the mantel of Site 29. The temperature indicates when the fireplace was on.

This home was split into two parts, with the lower floor having been turned into an apartment. Both the apartment and the main residence had unvented gas fireplaces. The data indicate that the fireplace in the apartment was turned on for extended periods of time and that stack effect caused the by-products to rise and enter the main residence. This shows not only the potential impact of stack effect to transport CO to higher living areas, but also suggests substantial air leakage between the main residence and the apartment.

Conclusions

The data presented here demonstrate that it is typical for concentrations of combustion by-products from an unvented gas fireplace point source to rise throughout the house with little to no time lag. Concentrations on the opposite side of the fireplace room and throughout the house are typically about 70-80% that of the area in the immediate vicinity of the fireplace.

Individual homes show that door closures can have a substantial impact on the transport of the pollutant, and that transport mechanisms such as stack effect can have a significant impact on the vertical distribution of the pollutant.

References

1. Francisco, P.W., J.R. Gordon, and W.B. Rose. 2010. "Measured Concentrations of Combustion Gases from the Use of Unvented Gas Fireplaces", Indoor Air, in press.

2. Francisco, P. W., J. R. Gordon and W. B. Rose. 2009. "Indoor Moisture in 30 Homes Using Unvented Gas Fireplaces." *ASHRAE Transactions* **115**(1): 914-923.

3. Ferro, A.R.; Klepeis, N.E.; Ott, W.R.; Nazaroff, W.W.; Hildemann, L.M.; Switzer, P. 2009. "Effect of Interior Door Position on Room-to-Room Differences in Residential Pollutant Concentrations After Short-Term Releases", *Atmos. Environ.* **43**: 706-714.

4. Miller, S.L.; Nazaroff, W.W. 2001. "Environmental Tobacco Smoke Particles in Multizone Indoor Environments", *Atmos. Environ.* **35**: 2053-2067.

5. Sherman, M.H.; Walker, I.S. 2009. "Measured Air Distribution Effectiveness for Residential Mechanical Ventilation Systems", *HVAC&R Research J.* **15**: 211-230.

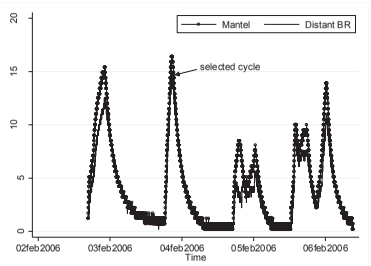


Figure 1. Example of carbon monoxide data and cycle selection for analysis.

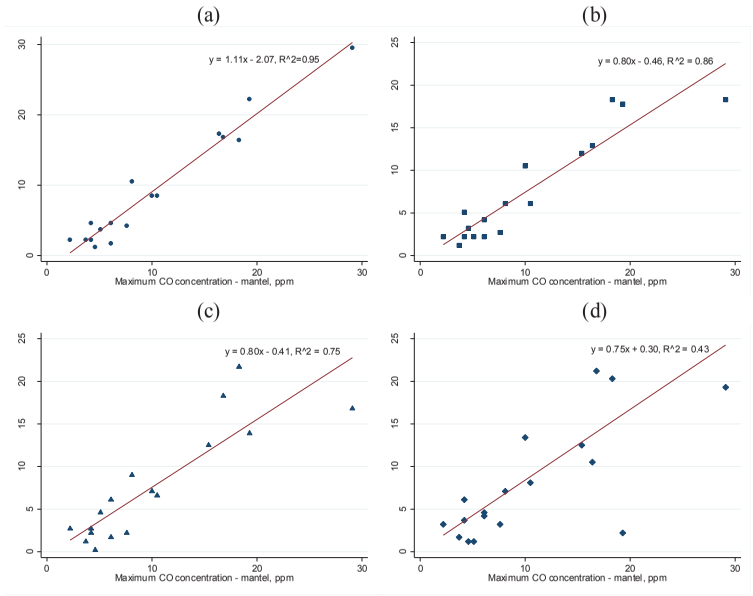


Figure 2. CO concentrations at each sensor location compared to at the mantel.

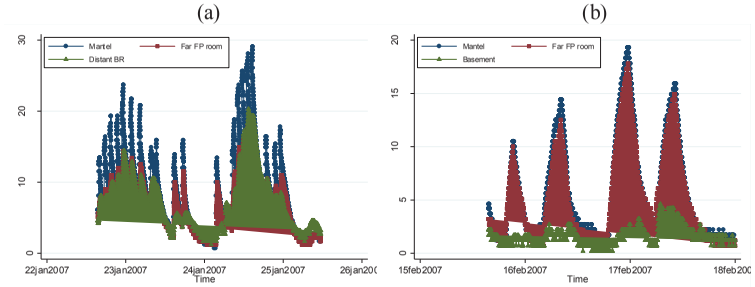


Figure 3. CO concentrations at Site 26 (3a) and 31 (3b).

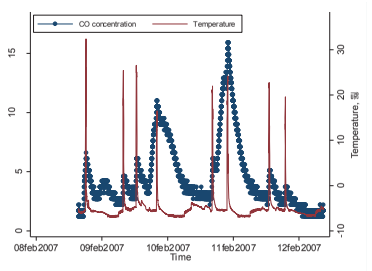


Figure 4. CO concentration and temperature at the mantel at Site 29.

Numerical prediction of particle transport passed through ventilator by CFD with Lagrangian method

Nguyen Lu Phuong[1], Kazuhide Ito[2], Shigeki Onishi[1, 3]

[1]Interdisciplinary Graduate School of Engineering Science, Kyushu University

6-1 Kasuga-koen, Kasuga, Fukuoka, 816-8580 Japan

[2]Associate Professor, Dr.Eng.

Interdisciplinary Graduate School of Engineering Science, Kyushu University

[3]Mitsubishi Electric Corporation

Abstract

The use of CFD technique for predicting the properties of airflow fields and particle movement is effective to carry out parametric study intended for a wide range of particle sizes. In this study, particle dispersions due to turbulent flow and thermophoretic effect were analyzed for a simplified ventilator model. Numerical results that comprise a classification of particle motion, temperature difference and particle diameter were reported. The residence time of particles in the ventilator was confirmed to depend on temperature differences and particle sizes under the condition of constant supply inlet velocity. Large particles (100 μm) were strongly affected by gravitational force and settling to the inlet opening located lower part of the ventilator while smaller particles (10 μm) tended to follow the convective air streamlines. Particle removal by gravitational settling has possibilities by optimizing the flow path and velocity in the ventilator as functions of the target particle size.

Keywords

Computational fluid dynamics, Suspended particle, Lagrangian approach, Ventilation system, Vertical duct, Indoor environment.

Introduction

Indoor air can play a significant role in the transmission of various contaminants and infiltration of a ventilator may be one of the dominant transport routes of contaminants from outdoors to indoors. In particular, adverse health effects of particulate matter, such as aerosolized infectious agents, organic aerosols and yellow sand, are of increasing concern with the increase in allergic diseases.

In order to prevent contamination of particulate matter in indoor environments, the control of the transmission of particles from outdoors to indoors through ventilators is important. Toward this end, the overarching objective of this study is to analyze particle movement in a vertical ventilation duct connected with a ventilator under various boundary conditions.

Particle movements in a ventilation duct are normally affected by flow fields causing pressure differences, thermal conditions between warm and cold zones, gravitational force or by the characteristics of the particles themselves.

In summer, the side of a vertical ventilator that faces the outdoor environment develops a relatively high temperature while the other side of the ventilator facing the indoor environment may be maintained at a relatively low temperature owing to the air-conditioning system. In winter, the outdoor surface of the ventilator becomes relatively cold while the indoor surface of the ventilator is kept warm. These temperature differences between outdoor side and indoor side

of a vertical ventilator or a ventilation duct play an important role in the transportation phenomenon of particles.

Particles with different sizes have different aerodynamic mechanisms, so the behavior of dispersed particles of 10 μm and 100 μm is reported in this paper.

From the viewpoint of effective separation or removal of particles from outdoor air in ventilators and ducts, it is important to analyze the particle transport phenomenon when particles pass through a ventilation duct connected with a ventilator under various flow fields and thermal conditions.

Outline of Target Vertical Ventilation Duct Connected with Ventilator

The outline of the target vertical ventilation duct connected with a ventilator is presented in Figure 1. The target ventilator consists of two parts: a vertical ventilation duct with dimensions L × W × H = 100 × 100 × 2200 mm and a horizontal ventilator with dimensions 700 × 200 × 200 mm. The wall surface of the vertical ventilation duct faces the outdoor environment and the other faces the indoor environment. The horizontal ventilator is set in the ceiling of a residential room.

In this analysis, particles are introduced from an inlet opening of the vertical ventilation duct and transported indoors through the horizontal ventilator.

Research Methodology

Turbulent Model and Numerical Methods

The computational fluid dynamics (CFD) technique was used to predict both air flow and particle behavior. The Navier-Stokes governing equations were discretized by a finite-volume-based commercial CFD code ANSYS/ FLUENT 12. Steady flow fields were analyzed using the low Reynolds number-type k-ε model (Abe Kondo Nagano model). The QUICK scheme was used for the convection term, and a SIMPLE algorithm was used. To analyze the flow field in the boundary layer, the center of the computational cells closest to the wall surface should be at a non-dimensional distance (wall unit) of $y^+<1$, where $y^+ = u^* y_1/\nu$ and y_1 is the distance normal to the wall surface, ν is the kinematic viscosity and $u^* = \sqrt{\tau_w/\rho}$ is the friction velocity. Here, ρ is the air density and τ_w is the wall shear stress.

Flow fields in the ventilator were analyzed by Eulerian approach.

Boundary Conditions

A uniform free stream velocity of 0.3 m/s and *TI*= 5% of air flow were applied for supply inlet boundary conditions. On the solid surfaces no slip boundary condition was applied. For temperature conditions, three types of conditions were set: isothermal, summer and winter conditions. For the wall surface of the outdoor side of the ventilation duct considered here, t_w=40 °C in summer season and t_w=5 °C in winter season, while the indoor wall surface was kept at 25 °C in both seasons. The inlet air temperatures were t_{air} = 30 °C in summer and t_{air} = 0 °C in

winter. The temperature differences between the indoor and outdoor wall were Δt_{summer} = 15 °C and Δt_{winter} = 20 °C. Other wall surfaces of the vertical ventilator were assumed to be adiabatic.

Particle Tracking Method

The Lagrangian method is applied to predict the trajectory of discrete phase particles. The particle transport in fluid flows is treated as a discrete phase made of spherical particles, which are dispersed in the continuous phase. The particle volume loading is usually assumed to be negligible, so that particles have no feedback effect on the carrier gas and particle-particle interactions are also neglected. The Lagrangian approach starts from solving the transient momentum equation for each particle:

$$\frac{d\vec{u}_p}{dt} = \vec{F}_D\left(\vec{u}-\vec{u}_p\right)+\vec{F}_g+F_T \tag{1}$$

The first term on the right-hand side, $\vec{F}_D\left(\vec{u}-\vec{u}_p\right)$, is the drag force per unit particle mass and u is the fluid phase velocity, while u_p indicates particle velocity. F_D is expressed as follows:

$$\vec{F}_D = \frac{18\mu}{\rho_p D_p^2}\cdot\frac{C_D\cdot Re_p}{24} \tag{2}$$

Here, μ is the molecular viscosity of the fluid, ρ is the air density, ρ_p is the density of the particle, and D_p is the particle diameter. Re_p is the Reynolds number defined using fluid viscosity μ as follows:

$$Re_p = \frac{\rho\left|\vec{u}_p-\vec{u}\right|D_p}{\mu} \tag{3}$$

C_D in equation (2) is the drag coefficient, which can be derived from

$$C_D = \frac{24(1-1.6807)Re_p^{0.6529}}{Re_p} - \frac{0.8271\cdot Re}{8.8798+Re_p} \tag{4}$$

$\vec{F}_g$ represents the force of gravity and is presented in equation (5).

$$\vec{F}_g = \frac{\left(\rho_p-\rho\right)}{\rho_p}\vec{g} \tag{5}$$

Particle motions in the flow field with a temperature gradient are affected by an external force proportional to the temperature gradient; this phenomenon is known as thermophoresis, F_T.

$$F_T = -D_{T,p}\frac{1}{m_p T}\frac{\partial T}{\partial x} \tag{6}$$

Here, $D_{T,p}$ denotes the thermophoretic coefficient, which can be defined as follows:

$$D_{T,p} = \frac{6\pi d_p\mu^2 C_s\left(K+C_t K_n\right)}{\rho\left(1+3C_m K_n\right)\left(1+2K+2C_t K_n\right)} \tag{7}$$

where K_n is Knudsen number (= $2\lambda/d_p$), λ is mean free path of the fluid, K indicates the ratio of thermal conductivity of fluid and thermal conductivity of particle, m_p is particle mass, and T is local fluid temperature. C_S, C_t and C_m are model parameters and set as 1.17, 2.18 and 1.14, respectively, in this study.

In order to reproduce the particle turbulent dispersion due to turbulent fluctuations in the flow, discrete random walk (DRW) model is adopted. Turbulent fluctuations in the flow field are represented by defining an instantaneous fluid velocity.

$$\vec{u}_i = \vec{u}_i + u'_i \quad (8)$$

$$u'_i = \sigma\sqrt{2k/3} \quad (9)$$

Here, σ is a normally distributed random number; k is the turbulent kinetic energy. Previous studies have confirmed that the isotropic DRW model is effective and accurate in modeling particle dispersion and distribution in various flows (Lai and Chen, 2007; Zhang and Chen, 2007).

In this analysis, a total 10,000 particles were injected instantaneously (one-shot) at a lower part of the duct (y=100 mm) and assumed to have zero initial velocity. Particle concentrations were assumed to be low enough to ignore particle-particle interactions. Particle tracking was carried out for 30 seconds using pre-analyzed steady flow fields. The wall deposition of particles was not considered. The details of particle parameters are described in Table 1.

Cases Analyzed

Cases analyzed in this study are shown in Table 1. A total of six cases were set using parameters of particle diameter (d_p=100 μm, 10 μm) and temperature condition ($\Delta t_{isothermalr}$ = 0 °C, Δt_{summer} = 15 °C and Δt_{winter} = 20 °C).

Results and Discussion

Flow and Temperature Field

Henceforth, we focus on the results for targeting the vertical ventilation duct due to limitations of space.

Figure 2 denotes the results of velocity distribution at a vertical section of the ventilation duct in three temperature conditions and normalized velocity magnitude of air flow at the central line at y=1600 mm, z=50 mm, is presented in Figure 3. The air flow from supply inlet of the lower part to exhaust outlet of the upper part was formed in the vertical duct for the three cases. For isothermal condition, a flow field similar to a simple channel flow was formed. Concerning the summer and winter cases, upward flow was accelerated by a buoyancy effect in the wall on the high-temperature side and the air stream spread out slightly and followed the wall surface of the duct in an upward direction owing to the Coanda effect. In the region of an L-type bend in the vicinity of the exhaust outlet, separation and re-circulation flow were observed.

The temperature distributions in the ventilator at the central line (y=1600 mm, z=50 mm) are presented in Figure 4. A downward trend of temperature from the hot surface to the cool surface in summer was confirmed. In the case of winter, the supply air temperature was set at 0 °C and then the temperature profile in a crosswise (x) direction became convex downward. Combining

Figures 2, 3 and 4, the impact of temperature gradient against a flow field in the vertical ventilation duct was confirmed.

Path Line of Particle Tracking

Figure 5 illustrates the path line of 30 representative particles of Case 1-1, Case 2-1 and Case 3-1 (cases of D_p= 100 μm). The particle motion at a size of 100 μm was governed by gravitational settling and injected particles were not transported toward the exhaust outlet, which was located in the upper part of the domain. As shown in Figure 5, some of the particles near the left surface dropped down right away after the injection and were directly transported to the supply inlet opening located in the lower part of the ventilation duct. Meanwhile, the rest of them on the right surface were accelerated by inertial force and subsequently fell down to the injection surface by gravitational settling.

Figure 6 shows the spatial distribution of path line of 30 representative particles of Case 1-2, Case 2-2 and Case 3-2 (cases of D_p= 10 μm). While the majority of the particles with D_p= 100 μm were exhausted through the supply inlet opening, the particles with D_p=10 μm tended to follow a streamline of carrier air flow and were transported toward the upper part of the duct. Generally, the small particles (D_p=10 μm) moved in accordance with the convective flow of air, and the effect of the discrete random walk model was relatively prominent compared with thermophoresis for particle motion. The influence of temperature gradient on particle motion was not clear in this analytical condition.

Particle Residence Time in Duct

Residence time of particles inside the vertical ventilation duct is one of the most important parameters of particle motion. This residence time of each particle was counted from injection time (t=0) until leaving the domain or reaching the maximum time step. Figure 7 indicates the residence times of particles in comparison with nominal time constant of gas stream τ_n in six cases. τ_n is defined by the volume of the device [m^3] and the supply air flow rate [m^3/s]. Figure 7 a) denotes the results of small particles (D_p=10 μm) and a large amount of particles stayed in the ventilation duct longer than the nominal time constant (τ_n=7.7 sec). In Cases 1-1, 2-1 and 3-1, the percentages of exhausted particles from the ventilation duct at the point of nominal time constant τ_n were 27.7% in the isothermal case, 29.3% in the summer case and 25.5% in the winter case. Small particles (D_p=10 μm) took longer than τ_n to pass through the vertical duct. At t=30 sec from particle injection, the percentages of exhausted particles from the ventilation duct were 70% for Case 1-2 (isothermal), 73% for Case 2-2 (summer) and 67% for Case 3-2 (winter). At this time point, there remained a number of particles in recirculation or a stagnant region in the duct. Moreover, the number of particles in Case 1-2 (summer) that had left the domain was greater than those of 2-2 and 3-2 at the same residence time. One of the reasons for this difference was that the difference of flow field caused buoyancy and thermophoresis caused a temperature gradient.

Figure 7 b) shows the results of relatively large particles (D_p=100 μm) for staying time in the vertical duct. In this case, the residence times of most particles were shorter than the nominal time constant τ_n because the gravitational force became dominant and acted downward and then particles passed through the supply inlet opening quickly. The percentages of exhausted particles

from the supply inlet opening located in the lower part of the ventilation duct at the point of nominal time constant τ_n were 93.9% for Case 1-1 (isothermal), 94.6% for Case 2-1 (summer) and 92.7% for Case 3-1 (winter).

For a representative inspection plane, 8 plane surfaces (x-z plane) at heights of y=350 mm, y=600 mm, y=850 mm, y=1100 mm, y=1350 mm, y=1600 mm, y=1850 mm, and y=2100 mm were created to compare the particle information like instantaneous velocity, temperature, mass flow, and residence time of particle. Figure 8 a) and 8 b) indicates the distribution of mean velocity components (u of x-direction, v of y-direction) of all of the particles passing each inspection plane during the calculation time (30 sec). The values were normalized by inlet air velocity (U_{in}= 0.3 m/s). Although the difference of u-velocity component of particles in summer and winter conditions is not significant, the discrepancy between the results of the isothermal condition and the other two cases (summer and winter) indicates the effect of temperature differences: buoyancy and thermophoretic force as shown in Figure 8 a). In Figure 8 b), the mean v-velocity component in summer can be seen to increase owing to buoyancy effect from the air flow.

From Figure 8 c), which denotes the average temperature of all of the particles passing each inspection plane during the calculation time (30 sec), the average temperature of particles can be seen to gradually increase along with updraft and the temperature differences between lower plane (y=350 mm) and upper plane (y=2100 mm) were 1.7 °C in summer and 7.7 °C in winter.

Conclusions

CFD modeling of convective air flow and particle motion in a ventilation device heated by a seasonal condition has been presented in this paper. The Lagrangian approach has been used to compute particle trajectories, concentration distributions and residence time of particles in the ventilator. The temperature gradient between hot and cold wall surfaces greatly influenced air flow pattern and temperature distribution, and had a certain impact on particle movement. Small particles (D_p=10 μm) were likely to follow the air flow while large particles (D_p=100 μm) were deposited and exhausted through the supply inlet opening.

Analyses for other particle size, flow and temperature conditions are future research work.

Acknowledgement

This research was partly supported by a Grant-in-Aid for Scientific Research (JSPS KAKENHI for Young Scientists (S), 21676005). The authors would like to express special thanks to the funding source.

References

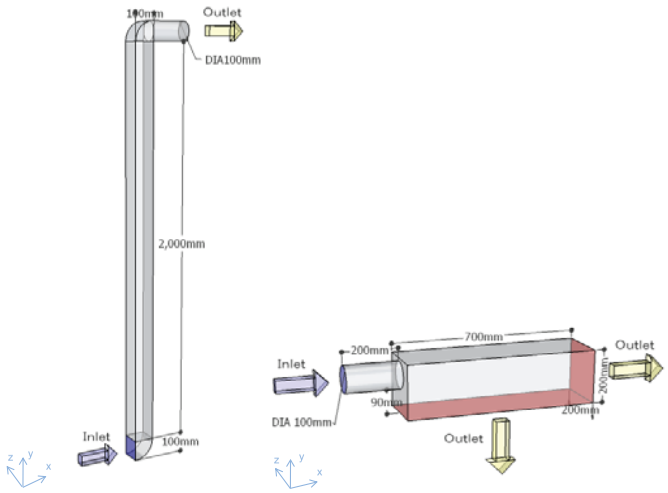
(1) FLUENT, 2006. Fluent 6.3 User's guide. Fluent Inc., Lebanon.

(2) Abe, K., Kondoh, T., Nagano, Y. A new turbulence model for predicting fluid flow and heat transfer in separating and reattaching flows—I. Flow field calculations, Int. J. Heat Mass Transfer 37 (1) (1994) 139–151.

(3) Lai, A.C.K., Chen, F.Z., 2007. Comparison of a new Eulerian model with a modified Lagrangian approach for particle distribution and deposition indoors. Atmospheric Environment 41, 5249–5256.

(4) Zhang, Z., Chen, Q., 2007. Comparison of the Eulerian and Lagrangian methods for predicting particle transport in enclosed spaces. Atmospheric Environment 41 (25), 5236–5248.

(5) Zhang, Z. and Chen, Q. 2009. Prediction of particle deposition onto indoor surfaces by CFD with a modified Lagrangian method, Atmospheric Environment, 43(2), 319-328.



(1) Vertical ventilation duct (2) Horizontal ventilator

Figure 1 Outline of target ventilator

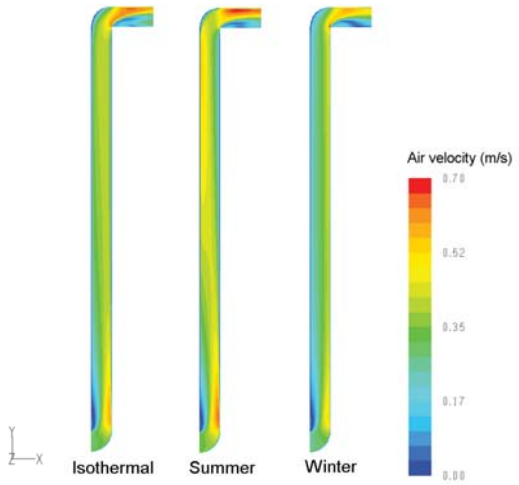


Figure 2 Velocity magnitudes inside the vertical ventilator (m/s) (*x*-*y* plane at the center of spanwise (z=50 mm) direction)

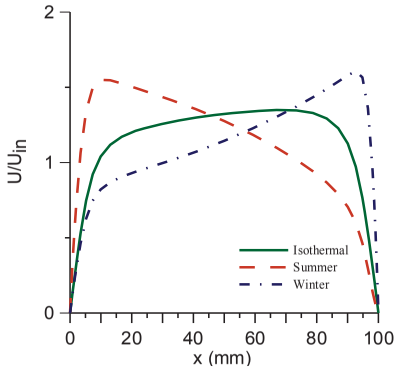


Figure 3 Normalized velocity magnitude of air flow along *x* direction (at y=1600 mm, z=50 mm)

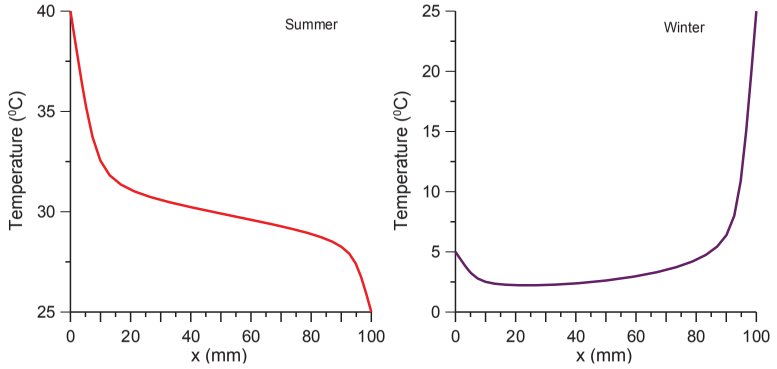
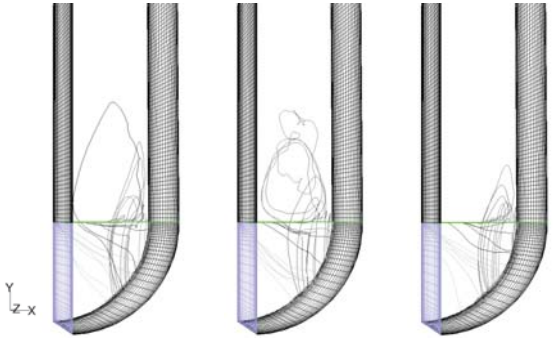
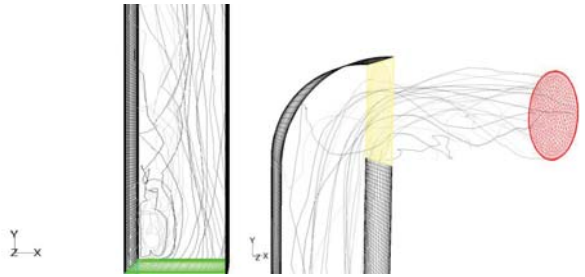


Figure 4 Temperature distribution along *x* direction at y=1600 mm, z=50 mm, in summer (left side fig.) and winter (right side fig.).

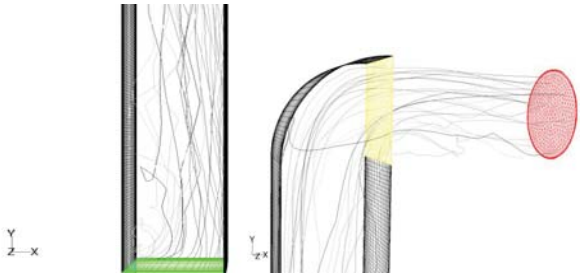


a) Case 1-1 (isothermal) b) Case 2-1 (summer) c) Case 3-1 (winter)

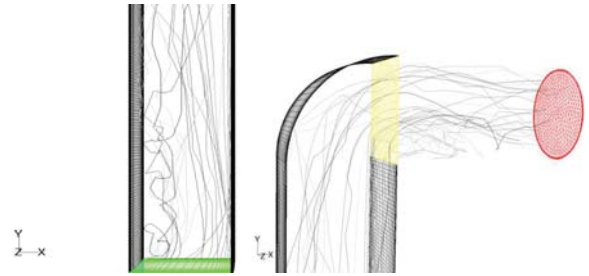
Figure 5 Predicted path line of particles (D_p= 100 μm) in the ventilator



a) Case 1-2 (isothermal)

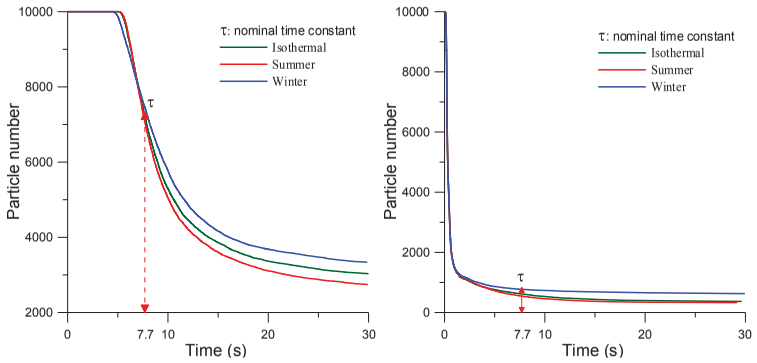


b) Case 2-2 (summer)



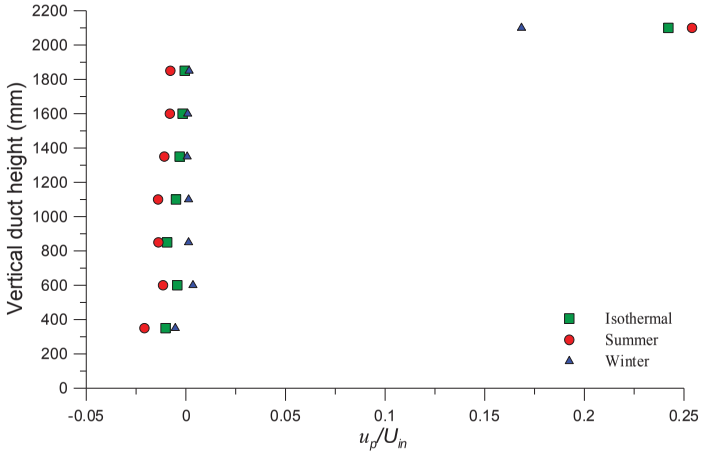
c) Case 3-2 (winter)

Figure 6 Predicted path line of particles (D_p= 10 μm) in the ventilator in the vicinity of inlet (left side fig.) and outlet (right side fig.) of ventilator

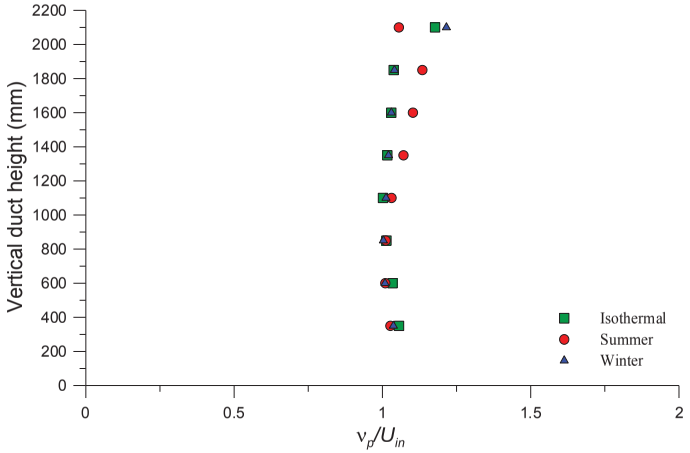


a) Particle size of 10 μm b) Particle size of 100 μm

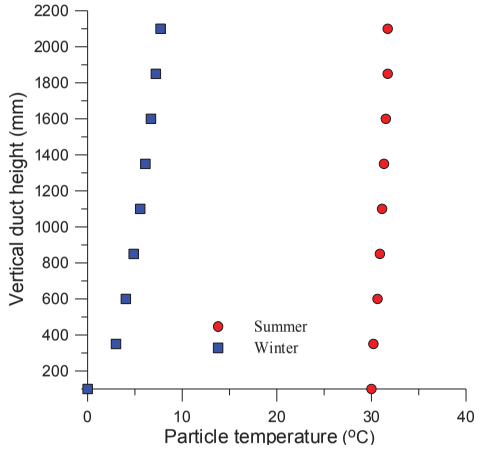
Figure 7 Residence time of particles in the vertical ventilation device



a) Distribution of the mean particle velocity component *u* of *x*-direction at 8 y-planes



b) Distribution of the mean particle velocity component *v* of *y*-direction at 8 y-planes



c) Distribution of the mean particle temperature at 8 y-planes

Figure 8 Distribution of mean velocity component (u, v) and temperature of particles along the vertical ventilator

Table 1 Cases analyzed

Case	Temperature condition	Particle properties
Case 1-1	Isothermal	D_p=100[μm],ρ_p=9.93×10^2[kg/m^3], 520 [ng/particle]
Case 1-2		D_p=10 [μm], ρ_p=9.55×10^2[kg/m^3], 0.5 [ng/particle]
Case 2-1	Summer	D_p=100[μm],ρ_p=9.93×10^2[kg/m^3], 520 [ng/particle]
Case 2-2		D_p=10 [μm], ρ_p=9.55×10^2[kg/m^3], 0.5 [ng/particle]
Case 3-1	Winter	D_p=100[μm],ρ_p=9.93×10^2[kg/m^3], 520 [ng/particle]
Case 3-2		D_p=10 [μm], ρ_p=9.55×10^2[kg/m^3], 0.5 [ng/particle]

A Study on Indoor Environments Made by Thin Line Type Ventilators in Apartment Houses

Hyun-Jae CHANG[1], Keun-Je CHO[2], Tae-Hwoan CHOI[3]

[1] Hongik University, School of Architectural Engineering, Jochiwon, Korea 339-701

[2]Hongik Graduate School, School of Architectural Engineering, Jochiwon, Korea 339-701

[3]LG Hausys, Research and Development. Window Tech Center 150, Songjeong-dong, Hungduk-gu,Cheongju-City, Chungbuk, Korea 261-721,

Abstract

Total heat recovery type ventilators that are connected to each room with ducts are mainly installed in Korea, but they raise concern over duct pollution. In this study, indoor environments made by thin line type ventilators installed in dwelling units of apartment houses are investigated by CFD. Results show the case that thin line type ventilators installed in each room - including kitchens - make the best indoor environment that maintains air velocity at under 0.25m/s, and evenly distributes the age of air in all areas.

Keywords: Ventilator, CFD, Age of air

Introduction

Sick house syndrome (SHS) has been a big social issue in Korea recently, and many people are interested in the indoor air quality (IAQ). Hence, apartment house suppliers were obliged to install ventilators that comply with regulations on architectural equipment standards enacted on February 13, 2006. Under consideration of energy conservation, total heat recovery type ventilators were mainly installed. This type of ventilators is usually connected to each room with a duct. However, ventilators connected with ducts raise concerns over duct pollution and cannot be adjusted to respond to different demands in each room. Thin line type ventilators examined in this paper are installed on window frames in each room and do not need to be connected with ducts (see Fig. 1). The ventilators are composed of total heat exchangers, fans, filters and thin line slots. In this study, air flow fields, temperature fields and the distribution of age of air in a dwelling unit of an apartment house that is equipped with a thin line type ventilator are investigated by computational fluid dynamics (CFD).

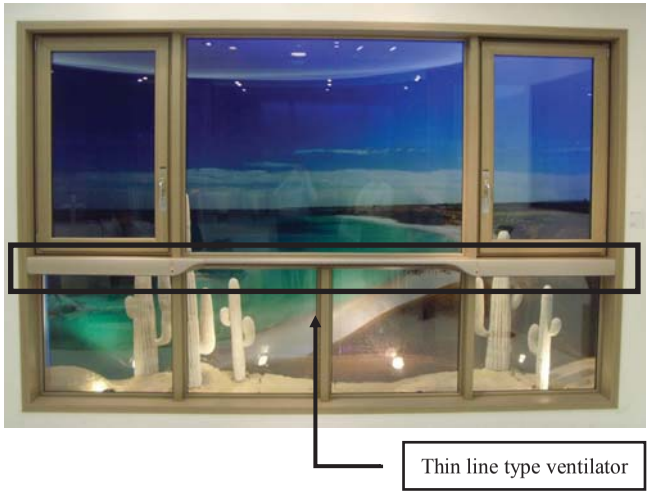


Fig. 1 Thin line type ventilator installed on a window frame

Methods

Air flow characteristics of a thin line type ventilator installed on window frames were investigated by CFD simulation in a dwelling unit of apartment house as shown in Fig. 2. The dwelling unit was composed of one living room, one dining kitchen and three bedrooms. Meshes for CFD simulation were made of hexahedron meshes as shown in Fig. 3 except Case A (see Table 1), in which they were made of tetrahedron meshes; the number amounted to about 600,000 in each. The CFD simulation was conducted using the standard k-ε model as the turbulence model.

Simulation cases and boundary conditions are as shown in Table 1. In case A, a duct type ventilator, which is the general type in Korea is applied. Supply and exhaust air volume in all cases except Case D are adjusted to 150 CMH to satisfy the air change rate of 0.7 h^{-1} which is a legal guideline in Korea. Under this condition, a thin line type ventilator is installed in each room except the living room, where two ventilators are installed. In Case D, a thin line type ventilator is installed on the window frame of the kitchen, whereas in Case B and Case C, there is no ventilator in the kitchen. Supply air temperature was calculated applying 75% of sensible heat recovery efficiency under winter conditions with an outdoor air temperature of 11.3℃. Indoor space is heated by *Ondol* system - a Korean traditional floor heating system. Indoor air temperature and exhaust air temperature are at 20℃.



Fig. 2 Floor plan of apartment house

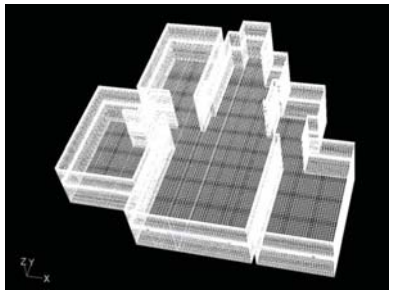


Fig. 3 Meshes for CFD simulation

Table 1 Simulation cases and boundary conditions.

Cases	Features	Supply /exhaust Air volume [CMH]	Air change rate [h^{-1}]	Supply air velocity [m/s]	Return air velocity [m/s]	Supply air temperature [℃]
Case A	Duct type with pan diffuser	150	0.72	1.45	2.36	12.175
Case B	Thin line type, except kitchen, horizontal supply (30CMH ×5 EA)	150	0.72	2.0	1.19	12.175
Case C	Thin line type, except kitchen 30° upward supply, (30CMH × 5EA)	150	0.72	2.0	1.19	12.175
Case D	Thin line type, kitchen included, 30° upward supply, (30CMH × 6EA)	180	0.87	2.0	1.19	12.175

Results and Discussion

Air flow fields, temperature fields and age of air distributions of each case are as shown in Table 2 and Table 3.

1) Duct type ventilator with pan diffuser (Case A)

In this case, pan type supply diffusers are installed on the ceiling near the windows in each bedroom, and two diffusers are installed in the living room. Two return diffusers are installed on the ceiling of the kitchen, near the entrance, whereas there is no return diffuser in the rooms. As shown in Table 2, in all areas except near supply diffusers, air velocity is maintained under 0.25m/s which is the recommended air velocity for preventing draught by ASHRAE. The temperature field at the horizontal section shows about 18℃ in room 1 and room 2, even though the average indoor air temperature is maintained at 20℃. The reason to this may be because the area rate of windows by room in those rooms is relatively large in comparison to the other rooms. The age of air distribution at the horizontal section shows a relatively even distribution. Age of air is under 70 minutes near windows where supply diffusers are installed on the ceiling in the neighborhood; under 80 minutes in the inner space of each room and the living room; and about 100 minutes in the kitchen where only return diffusers are installed.

2) Thin line type ventilator with horizontal supply (Case B)

In this case, thin line type ventilators are installed on window frames of each room except the kitchen. Air is supplied horizontally at 2m/s, a relatively high speed. A spot 1.2m away from the supply slot shows air velocity of about 0.3m/s, and dwellers may be able to feel a draught. The temperature field at the horizontal section shows an area of about 16℃ according to the air flow supply, even though the average indoor air temperature is maintained at 20℃. The age of air distribution at the horizontal section shows relatively even distribution.

3) Thin line type ventilator with 30° upward supply (Case C)

In this case, air is supplied in a 30° upward direction under the same conditions of Case B. Supplied air is pushed up by the air flow induced from the lower part of the indoors (See Table 3). By this way, supplied air flows first to the ceiling, and then to the inner part of indoor space. Air velocity is under 0.25m/s in all indoor space except in front of the supply slot, and the draught is no longer an issue. Temperature field at the horizontal section shows relatively even distribution, and the reason may be because the relatively cold air supplied in an upward direction at about 12℃ is mixed well with indoor air near the ceiling, before it

Table 2 Results of CFD analysis in Case A and Case B

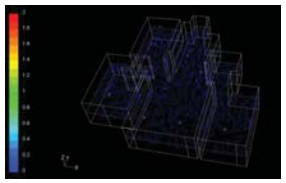
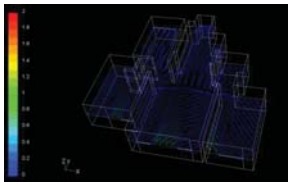
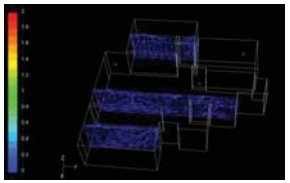
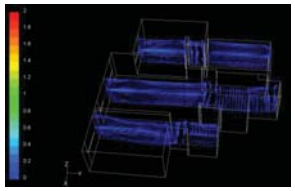
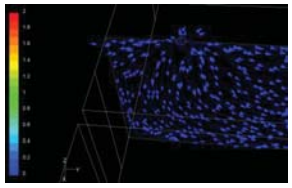
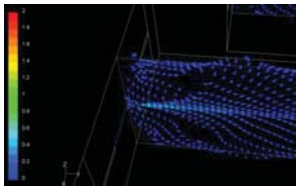
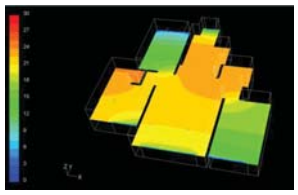
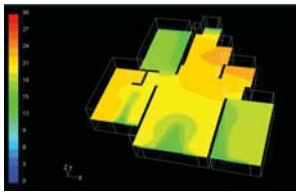
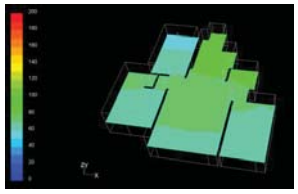
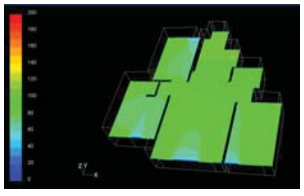
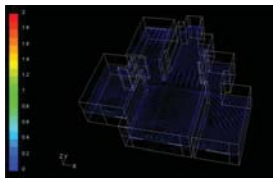
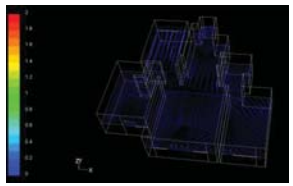
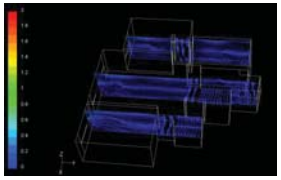
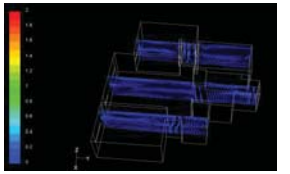
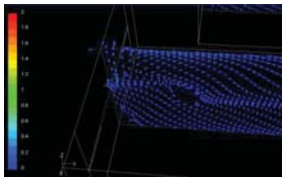
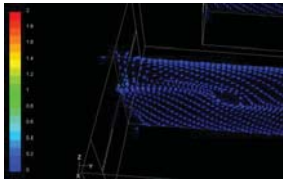
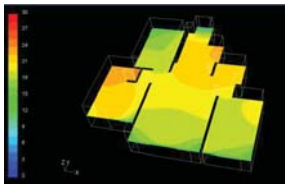
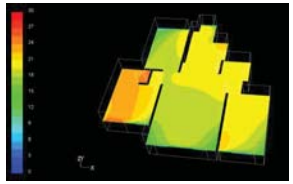
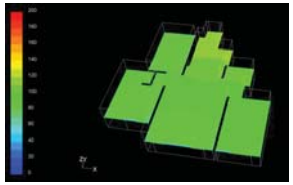
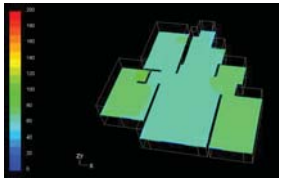
Cases	Case A	Case B
Air velocity field at a horizontal section		
Air velocity field at a vertical section		
Air velocity field magnified at a vertical section		
Temp. field at a horizontal section		
Age of air distribution at a horizontal section		

Table 3 Results of CFD analysis in Case C and Case D

Cases	Case C	Case D
Air velocity field at a horizontal section		
Air velocity field at a vertical section		
Air velocity field magnified at a vertical section		
Temp. field at a horizontal section		
Age of air distribution at a horizontal section		

flows into the inner part of indoor space. This air flow pattern affects the distribution of age of air, and shows a relatively even distribution. However, the age of air reaches about 120 minutes in the kitchen because there is no ventilator.

4) Thin line type ventilator with 30° upward supply, kitchen included (Case D)

In this case, a ventilator is installed in the kitchen under the same condition of Case C. Air at about 12℃ is supplied in a 30° upward direction from the slot of the ventilator installed on the kitchen windows. As seen in Table 3, air flow field and temperature field show almost identical results with Case D. The age of air is improved in all areas including the kitchen at about 70 minutes.

Conclusions

1) In the case of the duct type ventilator, air velocity is maintained under 0.25m/s, and the age of air is under 70 minutes near windows and about 100 minutes in the kitchen where only return diffusers are installed.

2) In the case of the thin line type ventilator with horizontal supply, dwellers may be able to feel a draught.

3) In the case of the thin line type ventilator, in which air is supplied in a 30° upward direction but not installed in the kitchen, air velocity is under 0.25m/s in all the indoor space except in front of the supply slot. However, the age of air shows about 120 minutes in the kitchen which is relatively high.

4) In the case of the thin line type ventilator, in which the kitchen is included, air velocity is under 0.25m/s and the age of air is improved in all areas.

References

1. ASHRAE FUNDAMENTAL HANDBOOK, American Society of Heating, Refrigeration and Air-Conditioning Engineers, Atlanta, GA, 2005.
2. H.B. Awbi, Ventilation of Buildings, E&FN SPON, 1995.
3. Stein, Reynolds, Mechanical and Electrical Equipment for Buildings, John Wiley & Sons, 1992.

A study on eco friendly furniture for mitigation of the indoor air pollution

Hyunsun AN[1], and Yungyu LEE[1]

[1] Korea Institute of Construction Technology, Builiding Planning & Enviroment Research Division, Goyang, Korea 411-712

Abstract

Furniture can raise indoor air contaminants with toxic emissions of VOC and formaldehyde.. While furniture is classified as a subject of safety and has quality labeling, there is a lack of domestic regulations related to contaminant emissions with the exception of sinks. When looking at the analysis on environment-related patients related to the smell or odors from furniture every year, patients suffering from asthma, allergic rhinitis, and atopic dermatitis are on the rise. Likewise, because there was an urgent need to prepare control standards, there was a prior notice of legislation for the introduction of a contaminant emission labeling system from 2010 onwards. This study conducted an analysis on the emission characteristics of VOCs and formaldehyde, an indoor air contaminant emitted from furniture. After an analysis was conducted on contaminant emission characteristics on conventional furniture versus eco-friendly furniture that can reduce harmful elements with closets, which are special-offer products, and office desks which are general market products, improvements were shown which indicate materials were working continuously to reduce indoor air contamination factors. Because of the comparative analysis on characteristics of the furniture of which has eco-friendly engineering against conventional furniture engineering, contaminants had been reduced in furniture using the eco-friendly engineering methods.

Keywords: Furniture, Formaldehyde, VOC, emission, chamber, harmful elements, eco-friendly, indoor air, contaminants

Introduction

According to the materials announced by the Ministry of Environment in February 2008, it appeared that furniture had the possibility of working as an indoor air contamination factor unlike existing construction materials by gradually reducing its formaldehyde emissions, a major indoor air contaminant. However, it is a reality that there is a lack of awareness that furniture is a source of indoor air contamination.[2]

According to the survey conducted by the Korea Consumer Agency, the number of consumer complaints received in relation to smells or odors from furniture for about 4 years from 2002 to 2005, was 264 and is on the rise every year.[2] Furthermore, in the analysis on major environmental disease patients from the National Health Insurance Corporation, environmental diseases such as asthma, allergic rhinitis, and atopic dermatitis are also on the rise every year.[2] Thus, there was an urgent need to prepare related control standards. Therefore, the

extensively in home appliances such as furniture made since 2010 and there was a prior notice of legislation on the introduction of the “Contaminant Emission Labeling System” on various construction materials.[3] The Korea Environment Institute announced that the cause of atopic dermatitis, an environmental disease, exists not only indoors but also outdoors, and contaminated indoor air can be fatal to infants and children under the of age 4.[2] In order to solve the root cause of these problems stemming from contaminants of indoor space, the characteristics of indoor air contaminants like formaldehyde and VOC emissions from furniture must be analyzed, and securing sufficient data about it must be a priority. Likewise, the analyses on the characteristics of contaminant emission on furniture and eco-friendly furniture that can reduce harmful substances desperately require the commercialization of eco-friendly products due to the technological development of materials.

Therefore, this study aimed to analyze the characteristics on eco-friendly furniture that can reduce formaldehyde and VOC emissions.

Methods

A large chamber (24㎥) was used in this study. A test product was purchased personally for the emission test, and the storage period was minimized by receiving earliest possible delivery of products that corresponded with the test schedule. The chamber was washed prior to installing the test product and the background concentration was maintained below standard levels. Measurement of the background concentrations was done by the collection of air inside the chamber using Tenax-TA and a DNPH cartridge after sufficiently ventilating the washed chamber for over 24 hours. The test was conducted after checking if the analyzed background concentration was below the standard levels of TVOC 20㎍/㎥ and HCHO 5㎍/㎥.

It is a general rule to use Tenax-TA and a DNPH cartridge for the collection of VOCs and formaldehyde. The emission test on contaminants emitted from the furniture was first conducted by installing test products that had a verified background concentration on the center of the chamber while all the drawers were opened. The sampling was done after 24 hours, after 72 hours, after 120 hours, and after 168 hours from the point of installing the test product. The test aimed to check the characteristic of contaminant emissions of the product by measuring the emission concentration according to the previously mentioned intervals. The number of times that ventilation was conducted was maintained to 0.5 times/h.

The sampling conditions for VOCs and formaldehyde is shown on Table 1, and the analysis of VOCs after sampling used GC/MS as the conditions for Table 2. In addition, the analysis on formaldehyde used HPLC as conditions shown in Table 3.

Table 1 Sample Collection Conditions

	formaldehyde	TVOC
Absorption Pipe	DNPH-silica cartridge (Ozone scrubber)	Tenax-TA(60/80mesh) 200 ㎎충전(ATD/TCT Tube)
Flow	500 ㎖/min × 30min	100 ㎖/min × 30min
Collected Amount	15ℓ	3ℓ

Table 2 Analysis condition of TD-GC/MS

TD	Turbo matrix 400(Perkinelmer)
Valve temperature	195℃
Desorption temperature	290℃
Desorption time and flow	10min, 30 ㎖/min
Cold trap low temperature	-30℃
Cold trap high temperature	300℃
Transfer line temperature	240℃
Split ratio	10:1
GC/MS	GCMS-QP2010(Shimadzu)
Column	DB-1(0.25 ㎜×1.0 ㎛×60.0m)
Carrier gas	He, 1.0 ㎖/min
Oven temperature	35℃(5min) - 5℃/min - 200℃(17min) - 10℃/min - 250℃(20min)
Electron energy	EI(70eV)
Mass range	m/z 35 - 300

Table 3 Analysis of condition for HPLC

HPLC	Waters 1525 / 717 plus
Column	Ace5 C-18(150 ㎜×4.6 ㎜)
Eluent	Acetonitrile/Water
Flow rate	1.0 ㎖/min
Gradient elution	ACN/Water(40/60→70/30(28min)→40/60(30min))
Injection volume	20 ㎕
Detector	UV@360 ㎚, Waters 2487

Test conditions were in accordance with KS I 2007, and the objective of the test results were ensured by setting the temperature/humidity conditions and ventilation conditions of the general indoor space in a similar fashion.

- Temperature : (25 ± 1) ℃
- Humidity : (50 ± 5) %
- Number of Ventilations : (0.5 ± 0.05) times/h
- Air Velocity : 0.1 ~ 0.3 m/s
- Test Period : 7 days

Results

The test was conducted using a large chamber (24㎥) for the evaluation of furniture material through contaminant emission analysis. It targeted the measurement of contaminants of the emitting component applied with sufficient ventilation within the large chamber. Measurement and analysis was conducted on special products such as closets, which are special-offer products, and office desks, which are general market products.

Table 4 Harmful elements emission of VOCs and Formaldehyde on the closets

mg/(unit . h)

Compound Name	CAS No.	general product	eco-friendly product	functional product	general product	all edge-bonding product
Formaldehyde	50-00-0	5.686	0.278	0.515	0.146	0.080
TVOC	-	2.435	1.419	4.010	18.057	17.813
Chloroform	67-66-3	0.005	0.005	0.005	0.043	0.052
Ethane, 1,1,1-trichloro-	71-55-6	0.002	0.001	0.002	0.015	0.017
Benzene	71-43-2	0.010	0.009	0.006	0.052	0.056
Toluene	108-88-3	**0.509**	**0.080**	**1.542**	**1.531**	**1.002**
Ethylbenzene	100-41-4	0.024	0.005	0.061	0.018	0.038
m,p-Xylene	106-42-3	0.025	0.005	0.100	0.061	0.089
Styrene	100-42-5	0.007	0.003	0.006	N.D	0.004
o-Xylene	95-47-6	N.D	N.D	N.D	0.020	0.025
1,4-cyclohexadiene	**99-85-4**	**N.D**	**N.D**	**N.D**	**8.607**	**5.718**
Benzene, 1,2,4-trimethyl-	95-63-6	0.009	0.002	0.003	N.D	N.D
Benzene, 1,3,5-trimethyl-	108-67-8	0.002	N.D	0.002	N.D	N.D

Benzene, 1,3-dichloro-	541-73-1	0.002	N.D	N.D	N.D	N.D

The TVOC emission of closets appeared in the order of functional products, general products, and eco-friendly products. The amounts of toluene emissions were same as the order of TVOC emissions and the major emission substance was toluene. The formaldehyde emission of closets appeared in the order of general products, functional products, and eco-friendly products. This test was able to confirm that the amount of TVOC and formaldehyde emissions were reduced in the eco-friendly products compared to conventional products. Eco-friendly products are products made with air purification technology, all edge bonding treatment of 4 sides, air circulation engineering, and eco-friendly materials.

Regarding closets, comparative analysis was conducted on conventional products and all edge-bonding products with interval of 1 month. This was to have comparative analysis of all edge-bonding treated and conventional products applied with just one engineering method among three types of engineering methods of eco-friendly products. Even in the engineering method applied with just one method out of three,, it was able to confirm that lower amounts of contaminants were emitted in all edge bonding products than the conventional products. The TVOC emission of a general closet was 18.057mg/unit・h, and the TVOC emission of all edg-bonding treated closets appeared to be 17.813mg/unit・h. It was reasoned that contaminants are emitted from the part where there is no edge-bonding treatment. Furthermore, the emissions of 1,4-cyclohexadiene was detected more. This is thought to have occurred through the finishing materials from the sub materials. However, contaminant emissions of toluene are thought to appear with major emission substances in most furniture products.

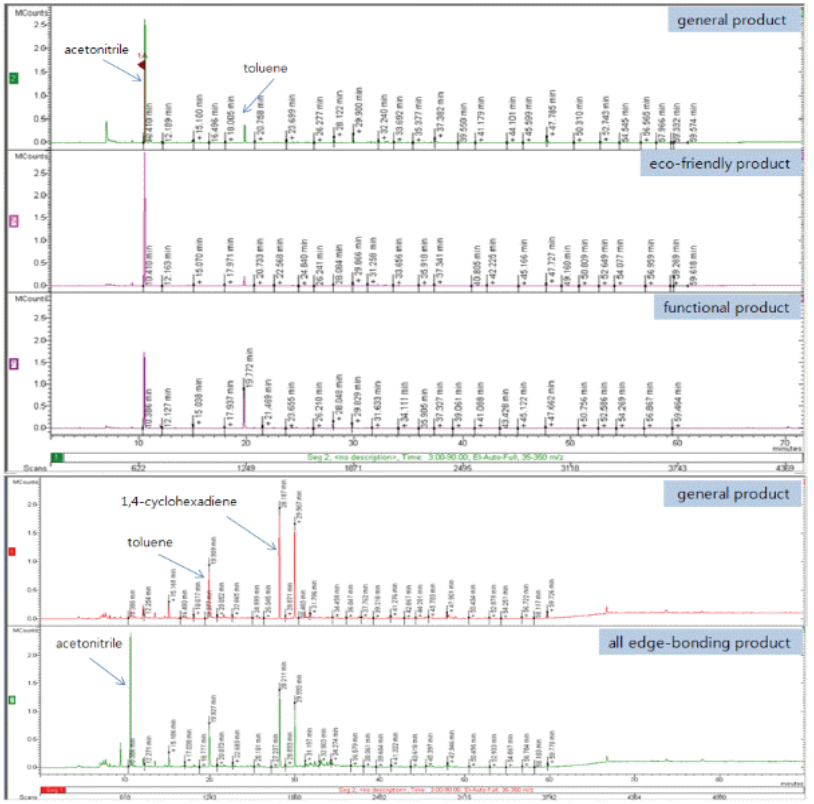


Fig.1 Gas Chromatogram of the closets

For TVOC emissions of office desks, conventional products appeared to be 2 times higher than silver nano sheet products. The toluene emissions was same as the order of TVOC emissions, and cyclohexene and 1-methyl-4-(1-methylidene) which does not come from silver nano sheet products were detected from conventional products. The reason such harmful substances were identified from the general products is because it has been determined that harmful substances are included in the ingredients of bonding agents and finishing

materials which are sub materials.

Table 5 Harmful elements emission of VOCs and Formaldehyde on the office desks

Compound Name	CAS No.	mg/(unit.h) silver nano sheet product	general product
Formaldehyde	50-00-0	0.063	0.071
TVOC	-	0.251	0.506
Chloroform	67-66-3	0.005	0.004
Benzene	**71-43-2**	**0.006**	**0.008**
Toluene	108-88-3	**0.100**	**0.069**
Ethylbenzene	100-41-4	N.D	0.001
m,p-Xylene	106-42-3	N.D	N.D
Styrene	100-42-5	N.D	N.D
Cyclohexene, 1-methyl-4-(1- methylidene)	586-62-9	**N.D**	**0.092**

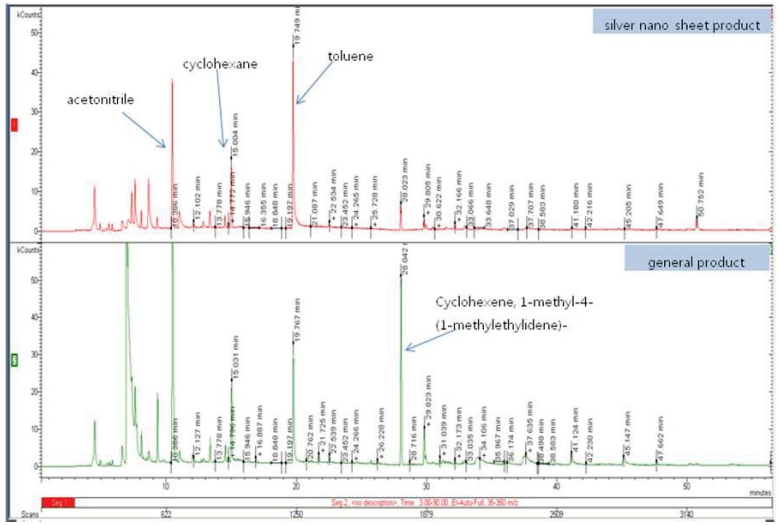


Fig.2 Gas Chromatogram of the office desks

Results and Discussion

This study measured and analyzed closets, which are special-offer products and office desks, which are general market products for the development of eco-friendly furniture in order to reduce indoor harmful substances, and the results are as follows.

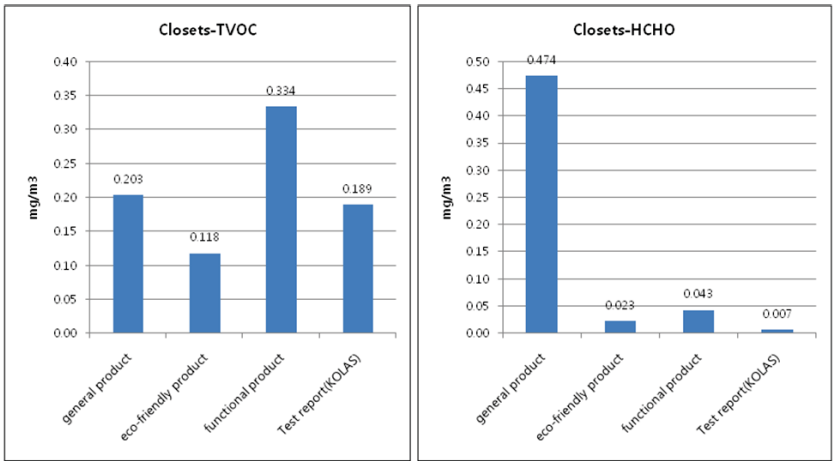


Fig. 3 Harmful elements emission of VOCs and Formaldehyde on the Closets

For closets, a total of 6 specifications were analyzed, and out of those, this is a chart comparing 4 products excluding any overlapping products. The four products include conventional products, eco-friendly product #1, functional products, and eco-friendly product #2. General products use E1 grade wood-based panels, and the finishing materials for the furniture body use PVC-vinyl materials and a one side edge-bonding method is used

for edge bonding as its engineering method. Moreover, there is no many line boring due to the application of fixed shelves, and it is applied to the rear side of the body and an original PVC ventilation grill device. Eco-friendly products use Eo grade wood-based panels, and use a LPM material as the finishing material for the body. For their engineering method, the edge bonding side is bonded with 4 side edges, and the moveable shelf many line boring is done in many line boring. Ventilation holes was fabricated using the mop tray on the bottom of the body, charcoal green deodorant was applied to the side of the body interior and a square PVC ventilation grill was applied to the rear plate. Last of all, functional products are products were covered with yellow earth charcoal during its production process.

While it is deemed that harmful substances, including TVOC, occur during the production process with the use of bonding agents to cover the yellow earth charcoal, it appears that contaminants are not emitted from formaldehyde. It could be determined that less contaminant were emitted in closets with improvements using eco-friendly materials and engineering methods.

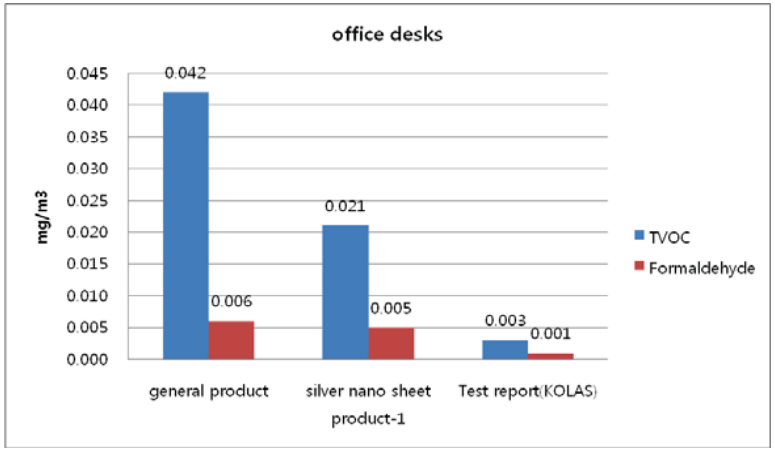


Fig. 4 Harmful elements emission of VOCs and Formaldehyde on the office desks

Measurement and analysis was conducted on the office desk, the market product of Wooami regarding conventional products and functional products. Functional products used the engineering method of a silver nano sheet coating during the production process. As shown in picture 4, it was confirmed that there was less emission of contaminants of VOC and formaldehyde from functional products using the engineering method for coating it with a silver nano sheet. This enabled confirmation that harmful substances were reduced in furniture due to the use of the silver nano sheet engineering method.

Conclusions

As a result of conducting a research on the actual conditions of furniture materials and products sold in Korea, wood based panels are classified into E2, E1, E0, and SE0 grade according to the amount of HCHO emissions,

and its use is identified as maintaining its level at the E1 level. However, in recent times, major developed nations like Japan, the U.S., and Taiwan are strengthening the control of formaldehyde emitted from wood based panel products to the level of SE0, and along with this, they are expanding their control to even major VOCs such as benzene and toluene. Therefore, it is deemed that only when the performance of wood based panel products used as major furniture materials is improved to the E0 or SE0 level, it can then make a contribution to the eco-friendliness of domestic furniture products.

In this study, the amount of contaminant emissions on major home appliances produced and sold in Korea was measured and analyzed using a 24m^3 large chamber.

In order to do this, samples of closets among furniture that can potentially emit indoor air contaminants in excessive amounts were produced using materials of E1 grade and E0 grade respectively, and the level of contaminant emissions were then analyzed. In addition, in order to identify the extent of any performance changes according to differences in production methods, an experiment was conducted on the S Construction specification with eco-friendly engineering methods partially applied and furniture with general specifications equivalent to this. To identify performance for the reduction of harmful substances according to the application of materials related technology such as functional materials, samples using yellow earth charcoal and silver nano sheet was produced, and its performance was then measured.

Through this study, the analysis on the characteristics of contaminant emissions of eco-friendly furniture products ultimately developed was conducted using a 24㎥ large chamber. In order to measure contaminants of indoor furniture products, closets, a special-offer product among furniture products was selected. For the measurement and analysis of TVOC and HCHO, office desks which are general market products were chosen.

The emission of closets with improved manufacturing methods has shown TVOC emissions were 2 times lower than in conventional products, and formaldehyde emissions also appeared to have a significantly lower value. However, closets with yellow earth charcoal emissions appeared to have a somewhat large amount of TVOC emissions. It concludes that harmful chemical substances were emitted from bonding agents used during the process of coating the yellow earth charcoal.

For office desks, which are products on the market, a comparative analysis was carried out on conventional products and silver nano sheet products. From functional products produced by covering silver nano sheets during the production process, TVOC, individual VOCs and formaldehyde (HCHO) appeared to have a low amount of contaminant emissions.

It could be identified that VOCs and formaldehyde emissions emitted from furniture were reduced by applying eco-friendly engineering methods for the reduction of indoor harmful substances. As a result of this study, eco-friendly engineering methods can be utilized in the engineering method for the reduction of contaminant emissions from furniture.

Acknowledgments

This research was supported and invested by a grant business of development for products safety technology from 'Korea Electrical Products Safety Association', funded by 'Ministry of Knowledge Economy' of affiliated Korean government.

References

1. Eun-gyu Lee., "Performance Evaluation of Indoor Air Quality in Apartment Houses due to the Use of Eco-friendly Construction Materials," 2009

2. Korea Institute of Construction Technology, "Development of Evaluation Standards for Contaminants emitted from Home Products(based on electronic appliances) by Large Chamber – Annual Report, Ministry of Environment," Apr. 2009

3. Ministry of Land, Transport and Maritime Affairs, "Construction condition, development, researching of clean-health house for improving Sick house syndrome," Dec. 2009

4. Ministry of Environment, "Study on the Current Status of Contaminants emitted from Home Products and Control Plans," Mar. 2006

5. Ministry of Environment, "Study on Environmental & Economic Benefit Analysis of Eco-friendly Products," 2007

6. Ministry of Environment, "Study on Indoor Air Quality Control Measures," 2004

7. Ministry of Environment, "Basic Plans for Indoor Air Quality Control," 2009

8. National Institute of Environment Research (NIER), "Study on Indoor Survey and Control Plan of Functional Construction Material," 2008

9. Construction Materials Research Group for Environment Assessment, "Survey on Processing of Surface Material of Domestic Furniture Products," 2006

10. Furniture Journal Press Release Material, 2008

11. Korea Air Cleaning Association, "Development of Certification System for Living Products by Large Chamber," 2009. 12

12. Korea Institute of Construction Technology, "Evaluation on Amount of Contaminant Occurrence from Major Construction Materials and Establishment of Basic Data," 2004.

13. Measurement Method of Form Aldehyde and VOC Emission of KS I 2007 (2009) Furniture – Large Chamber Law

14. Ministry of Environment, "Test Method for Indoor Air Quality Process," Jun. 2004.

15. ASTM D 6670-01 (2007) Standard Practice for Full-Scale Chamber Determination of Volatile Organic Emissions from Indoor Materials/ Products

16. JIS A 1903 (2008) Determination of the emission of volatile organic compounds (VOC) for building products - Passive method

17. ISO/DIS 16000-24 (2008) Performance test for evaluating the reduction of volatile organic compounds and carbonyl compounds without formaldehyde concentrations by sorptive building materials

18. WHO, Air Quality Guideline for Europe 2nd Edition 2001

Rotary heat exchanger model for control and energy calculations

Bjørn R. SØRENSEN [1], and Raymond RIISE [1]

[1] Narvik University College, P.O.Box 385, N-8505 Narvik, Norway

Abstract

Rotary heat recovery exchangers are widely used in ventilation systems, and the units are known for their high efficiency and almost maintenance-free operation. Temperature efficiencies above 80% are not uncommon. Performing dynamical analyses of rotary heat exchangers are in many situations advantageous, especially in connection to installation of such equipment in VAV systems. Efficiencies and flows are varying parameters that are crucial for energy calculations, but also for control. The dynamical analysis can effectively be carried out by addressing a dynamical model. This paper presents a simplified model for a rotary heat recovery unit that can be used both in CAV or VAV systems for control and energy analysis. The model is based on a further development of existing models, and is able to account for varying leakage, varying flows and temperatures. The model has been implemented in the Matlab Simulink environment. Simulations show that the results represent real conditions in an adequate way. This has been verified through comparison with measurements.

Keywords: Rotary heat exchanger, modeling, simulation, energy, control.

Introduction

There are many types of heat recovery units (HRU) which are in use in ventilation systems. Examples are rotary heat recovery wheels, plate heat exchangers, water/glycol coil heat exchangers and heat pumps. Rotary heat recovery exchangers are widely used, and the units are known for their high efficiency and almost maintenance-free operation. Temperature efficiencies above 80% are not uncommon. Usually, for balanced systems, this means that the recovered power can be at the same rate. Unfortunately these units are also infamous for transmission of polluted air from exhaust to supply. Due to the rotation of the device, there will always be a possibility of direct connection between exhaust and fresh supply air. Cross-contamination due to rotary heat recovery units comes from two mechanisms; (1) Leakage, (2) Carryover. The former is dependent on the differential static pressure across the wheel, and latter (carryover) occurs as a result of air being entrained within the wheel volume. The degree of carryover air is strongly dependent on whether the unit has a purge section or not. A rotating HRU in a comfort ventilation system is usually built of plane and corrugated aluminum fins mounted in parallel to the rotational axis, forming numerous parallel, axial passages (directional oriented flow). The small diameter of the passages may initiate a transition to laminar flow. Heat is transferred from warm exhaust air to cold supply air by rotating the heated part of the wheel into the cold supply air. Rotary HRUs are continuously regenerative, since heat is carried from one fluid to another by a third medium. The rotor speed is normally relatively low and in a range of 3-15 rpm.

Accurate physical description of transient heat transfer within a rotary HRU is extremely complex. In addition to heat transfer from the surface to the surrounding air, both crosswise

and long side, radial heat conduction within the wheel should be addressed. Important design parameters are:

- Diameter and depth of the wheel, and the size of the duct or AHU.
- Media mass and material properties.
- Surface structure.
- Flow regime and pressure conditions.

In this work, focus has been on establishing a simple model that is sufficiently accurate for control and energy calculations, which can be used integrated in system simulation as well.

Mathematical model

Parts of the modeling approach presented below have been adopted from Børresen et al. [1], and further developed to accommodate varying flow rates.

Model assumptions:

- Balanced ventilation. Exhaust air flow rate is equal to supply air flow rate.
- Non-hygroscopic, regenerative rotor
- The heating media can be separated into two halves, one for exhaust and one for supply. The temperature in each half is uniform.
- The media temperature on the supply side is approximately equal to the supply air temperature.

Model description (also refer to Fig. 1):

Simple heat balance:

$$\frac{d}{dt}\left(\frac{m_R}{2} C_R T_R\right) = Q \cdot \rho_A C_A (1-x)\left(T_O + T_E - T_S - T_D\right) \quad \text{(Eq. 1)}$$

m_R and C_R are the rotor mass and specific heat capacity respectively. Q is the air flow rate, and ρ_A and C_A are the density and specific heat capacity of air. x is assumed to be the share of leakage through the unit ($\geq$0), and a positive value indicates that air is leaking from exhaust to supply. Combining Eq.1 with the temperature efficiency (η_T) for balanced ventilation eliminates the discharge temperature and gives the following expression:

$$\frac{m_R C_R}{2 \cdot Q \cdot \rho_A C_A (1-x)} \frac{dT_S}{dt} = (1-\eta_T) \cdot T_O + \eta_T T_E - T_S \quad \text{(Eq. 2)}$$

Leakage through rotary heat exchangers can in some cases represent significance for the dynamic performance and energy efficiency of the unit. Pressure conditions around the wheel (fan placements) are important, as well as carryover of air within the wheel. Earlier studies have shown that carryover is important especially for VAV systems, where the share of carryover become large at low flow rates [2], [3]. In the model, this has been compensated for simply by introducing a bypass factor. This means that a certain amount of air bypasses the

wheel, and the flow rate through the wheel is reduced accordingly. Hence, after computing supply temperature, it should be corrected for the flow rate bypassing the rotor (leakage), i.e.

$$T_{S,kor} = (1-x)\cdot T_S + x \cdot T_E \qquad \text{(Eq. 3)}$$

Temperature efficiency depends both on rotational speed and flow rate. In general, there are nonlinear relationships between efficiency and speed, and between efficiency and flow rate. At constant rotor speed, efficiencies at low air velocities are higher than efficiencies at high velocities. On the other hand, efficiencies at high rotor speeds are higher than those at low speeds, at constant flow rate. The relationship between efficiency and rotational speed, for a given flow rate, is assumed to be on the form expressed by Eq.4 and Eq.5.

$$\eta_T(n,Q) = \eta_T(n)\cdot\eta_T(Q) = \eta_n \cdot \eta_Q \qquad \text{(Eq. 4)}$$

$$\eta_n = 1 - e^{-C\cdot n} \qquad \eta_Q = A + B\cdot Q \qquad \text{(Eq. 5)}$$

n is the rotational speed of the heat recovery wheel and A, B and C are scaling/calibrating factors which must be determined from known data. Thus some (3) data sets must be available to calibrate the model correctly. Since better efficiencies are obtained for lower flow rates (assuming constant rotor speed), we know that η_Q will descend slightly as Q increases (negative B). To find A and B, we use two sets of data taken from the product catalog of the unit for the same rotor speed; (Q_1, η_1) and (Q_2, η_2), and we assume further that the derivative of η_Q is constant for all rotor speeds. To find C we use yet another set at an arbitrary flow rate (n_3, η_3), so that Eq.4 becomes:

$$\eta_T(n,Q) = \left(\eta_2 - \frac{\eta_2-\eta_1}{Q_2-Q_1}\cdot(Q-Q_1)\right)\cdot\left(1-(1-\eta_3)^{\frac{n}{n_3}}\right) \qquad \text{(Eq. 6)}$$

Together with Eq.2 and 3, Eq.6 represents the governing model for the rotary heat recovery unit. The model can also be used for variable flow rates (VAV systems).

Limiting the rate of heat transfer due to rotation of the wheel:

Consider that the exhaust temperature is altered instantly, for instance as a step. On the supply side of the wheel, the full effect of altered exhaust conditions cannot be seen instantly. That is due to the time it takes to transfer heat from the exhaust side, by the media, to the supply side. The rate at which heat is transferred is restricted by the rotational speed of the wheel. Thus, introducing a signal rate limiter on the exhaust inlet of the model seems appropriate.

Block diagram:

The block diagram of the model is shown in Fig. 2 and includes the efficiency estimation part. First the efficiency is calculated and put through a multiplexer together with other model

input data. The exhaust temperature is fed through a first order filter in order to estimate ramp behavior. Finally the output (supply air temperature) is calculated.

Measurement setup

Data from laboratory measurements have been collected and used to validate the performance of the model. Measurements were performed in a laboratory on an AHU system containing an ABB EC2000 unit with a non-hygroscopic rotary wheel and no purge section. A DAQ-system was used together with Lab-view software to collect the temperature data. Logging was performed for different fan speeds (40%-100%, corresponding to 0.09- 0.25 m^3/s air flow) and rotor speeds (0-12 rpm). The measurement setup was as shown in Fig. 3, but only the measurement points T0, T4, A0 and A4 have been used for comparison to the simulated model output. Flow rates were measured using Brüel & Kjær gas analyzator and multiplexer system. Leakage over the heat recovery unit was calculated from the measured tracer gas concentrations. In this particular setup, fan placements were unfavorable with regards to leakage, causing a relatively large amount of air to flow from the exhaust to the supply side (refer to Fig. 4).

Results and Discussion

As suggested by the comparisons between measurements and simulations shown in Fig. 5 and Fig. 6, the performance of the model is reasonable. Deviations between measurements and simulations are shown in Fig.7. The sample correlation coefficients for both datasets are close to 97%, which again suggests good fit. Dynamically the model performs adequately. From Fig.5 we realize that the step responses follow measurements quite good. For steady state conditions the model shows deviations, especially for the low rotor speeds. This indicates that the efficiency description can be improved. However, more measurement data for different rotary units are required to improve the efficiency model further. Furthermore, assuming a linear relationship for between efficiency and flow rate introduce errors in the performance. A major disturbance in the measurement data is the large amount of re-circulating air (leakage). Modeling leakage using a simplified model may not be properly done, and the comparison indicates that the model performs better when the share of leakage air is small compared to the total flow rate. When the rotor speed is zero, heat will be transported from the exhaust to the supply by conduction through the rotor material. Pure conduction can to some degree be compensated for by introducing a minimum value of the temperature efficiency. This is however not addressed by the model at this stage.

Considering the simplified nature of the model, its performance naturally cannot take into account all possible variations that may occur. Nevertheless, it reflects the major tendencies caused by the most important parameters acting on the system. Thus it will be reasonable to conclude that the model is suitable for simulating different control scenarios, and it may also be used for detecting possible errors and problems. An example of application is tuning the control loops for sequential control of 'cooling coil-rotary heat recovery unit-heating coil', which may represent a challenge in VAV systems. The model can also be used for estimating energy performance.

Conclusions

A dynamical model of a rotary heat exchanger has been developed and accommodated for control and energy simulations. The model can also be used for varying flows (VAV systems). The temperature responses of the model have been compared to measurement data, and performance should be adequate for control and energy simulations. Considering the simplified nature of the model, its performance naturally cannot take into account all possible variations that may occur. Nevertheless, it reflects the major tendencies caused by the most important parameters acting on the system. The model can be used alone or as part of a larger simulation system, as a tool for revealing or preventing possible problems and errors during operation of similar real equipment.

.**References**

1. Børresen, B. A., Thunem A. J., "HVAC control models" Sintef report STF48 F84019, 1984, NTNU, Norway.

2. Sørensen, B. R., "Rotary heat exchangers and VAV systems" Proceedings of Indoor Air 2008, Copenhagen, Denmark.

3. Sørensen, B. R., "Temperature distribution of rotary heat recovery units" Proceedings of the 9th REHVA world congress, Clima 2007, Helsinki, Finland.

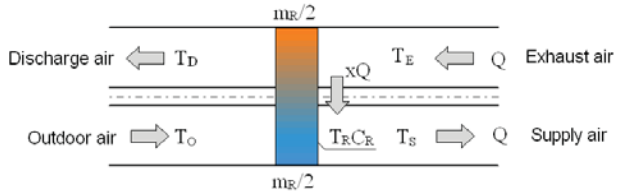


Fig. 1 Model outline

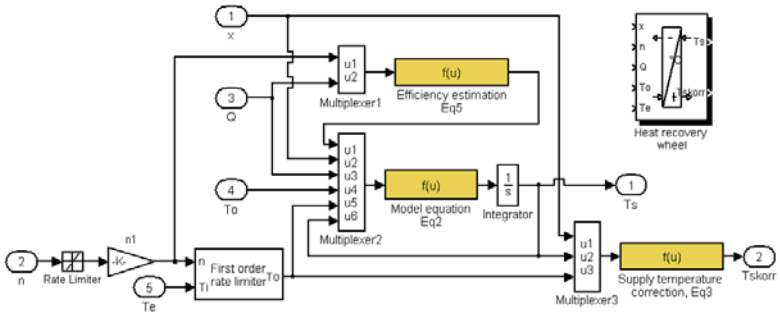


Fig. 2 Model block diagram (Matlab Simulink)

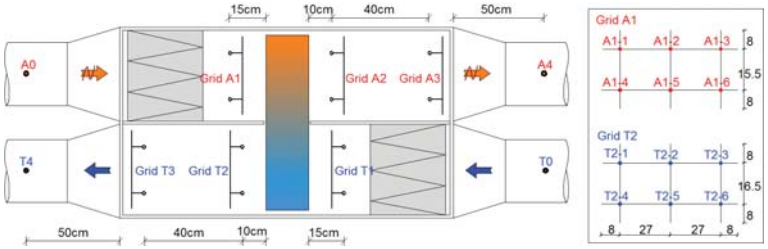


Fig. 3 Measurement setup

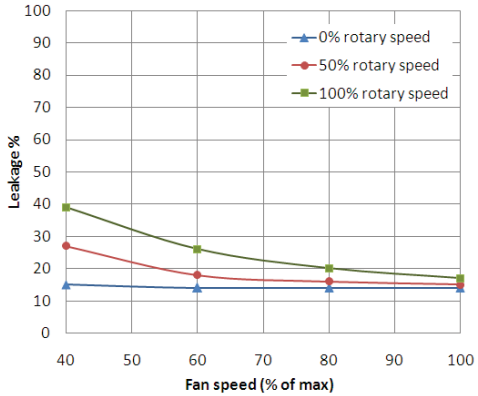


Fig. 4 Leakage [2]

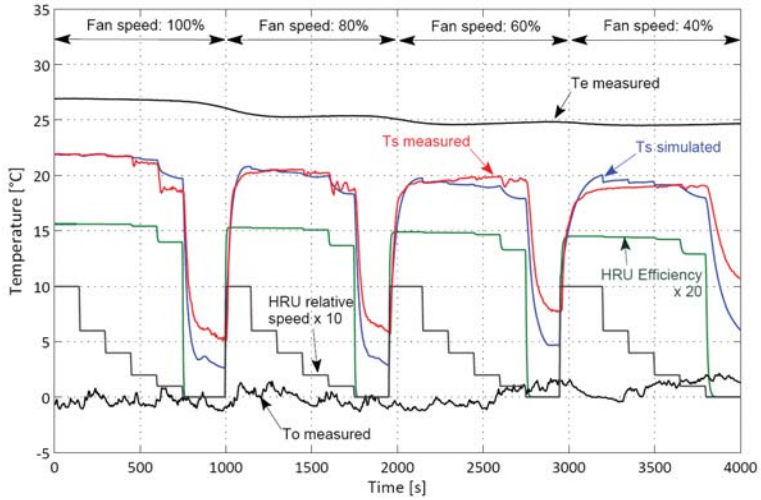


Fig. 5 Measurement and simulation data comparison (dataset 1)

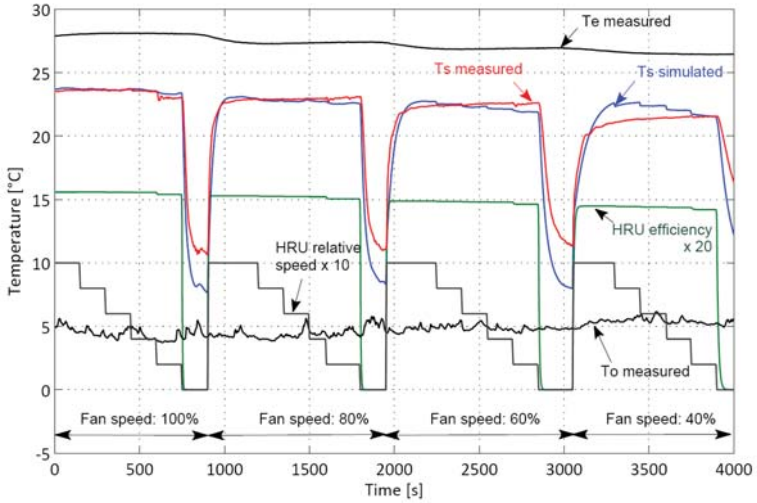


Fig. 6 Measurement and simulation data comparison (dataset 2)

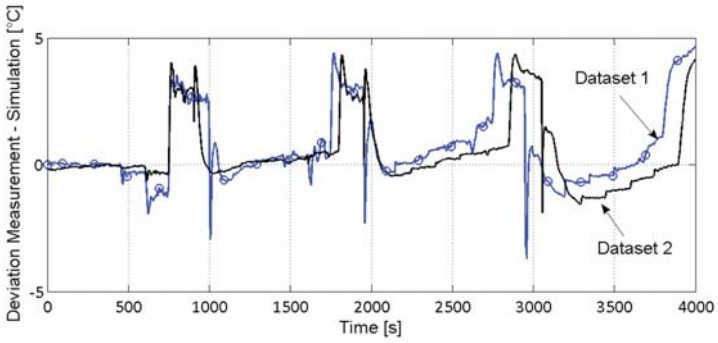


Fig. 7 Deviation between measurement and simulation data

A Study on the field survey of the IAQ in the childcare center

Jung Ha PARK[1], Jin Chul PARK[2] and Eon Ku RHEE[3]

[1] Graduate Program, Dept. of Architecture, Chung Ang University, Korea
[2] Professor, Dept. of Architecture, Chung Ang University, Korea
[3] Professor, Dept. of Architecture, Chung Ang University, Korea

Abstract

Child care center, one of the public facilities, has recently been increased. It is because of the government's childbirth policy. In particular, infants and children who use this place are frequently exposed in danger because of their biological characteristics. They stay in child care center over 7 hours a day in average. Therefore, the importance of the child care center's indoor air has been increased. Thus, survey and investigation of the child care center's indoor air are conducted in this study. Moreover, preliminary data will be suggested for management of the child care center's indoor air quality. The measurement items are PM_{10}, Asbestos, CO, CO_2, NO_2, VOCs, HCHO, Rn and Ozone. And fact finding was conducted in 30 child care centers. Moreover, the survey about the consciousness and administration of satisfaction and interest in indoor air quality targeting 161 teachers who worked in child care centers.

Keywords: Indoor air quality, childcare center, survey

Introduction

1.1 Purpose of Study

Modern men spend 80~90% of their days inside and the matter regarding indoor air pollution is becoming a big social issue due to increment of building airtightness according to energy saving, despite the recent increasing use of construction materials using complex chemicals. The number of patients with environmental disease such as Sick House Syndrome (SHS) has increased from 5.52 million in 2002 up to 7.14 million in 2007. Due to increasing concerns for Well-being, along with the recognition of social issue, the importance of managing building indoor air quality is becoming greater.

Childcare center is a facility expending according to the government's childbirth policy. The importance of indoor air of childcare centers will especially be important, since there is a high possibility for infants at childcare centers to suffer fatal diseases from very little germs, for they are in the stage of full physical growth and their immunity is inferior to that of ordinary grown-ups.

Hence this study carried out research on the actual condition as well as survey centering 5 items of indoor air quality maintenance standard, targeting childcare centers, and attempted to apply such as the foundation for preparing system and policy to protect environment and health of future childcare centers.

1.2 Method and Procedure of Study

The study is to investigate the indoor air condition of childcare centers and suggest basic data for indoor air condition of childcare centers based on such. The following is the summary of the study's procedure.

1) Research on the actual indoor air condition of childcare centers

To investigate the indoor air condition of childcare centers through investigation of actual childcare centers, temperature, humidity and 5 matters of indoor air quality maintenance standard according to the "Law Of Indoor Air Quality Control In Crowd Facilities" were measured on the spot at 30 childcare centers in Dongjak-gu, Seoul.

2) Survey targeting childminders

Targeting 161 childminders of the relevant childcare centers, 26-question survey questioning degree of satisfaction, awareness, detectable symptoms regarding indoor air quality as well as childcare center management and awareness of indoor air quality improvement was carried out.

3) Study on current indoor air condition of childcare centers

Based on the result of survey targeting childminders and indoor air quality measurement of childcare center, characteristics of current indoor air quality condition of the childcare centers were analyzed.

Measurement of air quality of interior facility

2.1 Outline of measurement

The study simultaneously carried out survey and field measurement on indoor air pollutant to inspect the actual condition of indoor air condition of childcare centers. Items to measure for indoor air quality are classified into thermal environmental factor and contaminating factor; temperature, humidity and 5 matters of indoor air quality maintenance standard of crowd facilities were measured. When collecting samples, it measured in nursing rooms where the most facility users are with the same general environmental condition as the relevant in nursing rooms, in daytime. The outline of field measurement of indoor air quality and its measurement items and instruments are shown in Table 1.

Table 1 Outline of intdoor air quality measurement

Classification	Contents
Measurement subject	30 childcare centers in Dongjak-gu (15 Public childcare centers, 15 Private childcare centers)
Measurement period	4. 3. 2009. ~ 6. 5. 2009.
Measurement items	maintenance standard of indoor air quality of crowd facility for 5 contaminants (PM_{10}, CO_2, HCHO, TBC, CO)
Measurement method	Ministry of Environment Notification No. 2004-80 Based on the official test method of indoor air quality

Measurement items	Measurement instrument	Sample collection method and time
Formaldehyde (HCHO)		Flow velocity of 700mL/min, DNPH In DNPH cartridge for 30minutes Collect and analyze with HPLC analysis

Total Bacteria Colony (TBC)		Measure 2 times for 30 minutes with total collection amount of 450L using Air Sampler
Carbon dioxide (CO_2)		Measure for 1 hour using AIRBOXX
Particle Matter (PM_{10})		Microvolt 1100 Low Measure for 8 hours using Flow-Rate Air Sampler with velocity of 3mL/min
Carbon monoxide (CO)		Measure for 1 hour using carbon monoxide measuring instrument
Temperature and Humidity		Measure the average in time zone of 9~11

2.2 Measurement result

The condition of temperature and humidity of each measured childcare center is shown in Table 2. And the result of 5 matters of indoor air quality maintenance standard of crowd facilities is shown in Table 3, Table 4, Table 5, Table 6 and Table 7.

Table 2 Measurement result of temperature and humidity of childcare center (°C,%)

Classification	Heukseok H		Heukseok K		Daebang B	
	Temperature	Humidity	Temperature	Humidity	Temperature	Humidity
Indoor	24.8	32.9	24.6	26.7	22.2	31.1
Outdoor	15.7	38.7	14.8	34.8	20.6	35.4
Classification	Daebang E		Noryangjin N		Sangdo B	
	Temperature	Humidity	Temperature	Humidity	Temperature	Humidity
Indoor	25.1	28.5	25.9	27.4	25.2	61.7
Outdoor	22.9	25.3	28.6	25.3	23.3	60.2
Classification	Sadang Y		Sadang M		Daebang S	
	Temperature	Humidity	Temperature	Humidity	Temperature	Humidity
Indoor	26.5	33.2	20.9	47.2	21.4	49.9
Outdoor	24.9	31.6	15.5	48.5	24.6	46.3
Classification	Dongjak C		Sangdo R		Sangdo G	
	Temperature	Humidity	Temperature	Humidity	Temperature	Humidity
Indoor	24.9	44.7	23.5	53.2	24.8	44.8
Outdoor	27.6	41.5	25.3	43.3	26.8	42.3
Classification	Sadang D		Sadang K		Sadang C	
	Temperature	Humidity	Temperature	Humidity	Temperature	Humidity
Indoor	20.5	45.0	26.8	24.9	24.9	24.9
Outdoor	15.4	50.2	16.8	37.8	17.9	32.5
Classification	Sangdo H		Sadang H		Sangdo J	
	Temperature	Humidity	Temperature	Humidity	Temperature	Humidity
Indoor	24.0	45.3	28.1	28.4	27.7	24.0
Outdoor	25.6	38.5	30.6	23.2	31.2	22.5
Classification	Sindaebang G		Sindaebang B		Sangdo L	
	Temperature	Humidity	Temperature	Humidity	Temperature	Humidity
Indoor	22.3	37.2	27.6	24.3	26.0	51.7
Outdoor	21.7	30.7	23.6	28.5	25.6	52.6
Classification	Sangdo N		Daebang K		Sindaebang L	
	Temperature	Humidity	Temperature	Humidity	Temperature	Humidity
Indoor	27.5	33.4	21.3	42.1	23.2	35.8
Outdoor	28.1	26.4	24.6	38.3	22.9	25.3
Classification	Sadang O		Sindaebang Y		Sangdo S	
	Temperature	Humidity	Temperature	Humidity	Temperature	Humidity
Indoor	29.7	32.5	27.5	32.8	29.4	32.6
Outdoor	31.2	28.6	28.3	28.5	31.3	23.4
Classification	Sadang M2		Noryangjin D		Sangdo N2	
	Temperature	Humidity	Temperature	Humidity	Temperature	Humidity
Indoor	27.4	42.8	26.2	36.3	26.2	49.8
Outdoor	27.8	32.3	30.4	32.0	29.2	26.3
Classification	Temperature		Humidity			
Indoor	25.2		37.5			
Outdoor	24.4		35.0			

Table 3 Measurement result of particle matter of childcare center ($\mu g/m^3$)

Childcare centers	Heukseok H	Heukseok K	Daebang B	Sindaebang G	Sindaebang B	Sadang D	Sadang K	Sadang C
Indoor 1	27.8	25.9	41.7	26.3	44.4	55.6	41.7	40.7
Childcare centers	Daebang E	Noryangjin N	Sangdo B	Sangdo L	Sangdo N	Sangdo S	Sadang M2	Sangdo H
Indoor 1	76.2	67.8	45.5	55.6	38.5	46.3	43.3	41.7
Childcare centers	Sadang Y	Sadang M	Daebang S	Daebang K	Sindaebang L	Sadang H	Sangdo J	Noryangjin D
Indoor 1	18.5	37.8	64.2	80.6	47.2	36.3	112.4	34
Childcare centers	Dongjak C	Sangdo R	Sangdo G	Sadang O	Sindaebang Y	Sangdo N2	Average	
Indoor 1	37.6	46.4	75	52	39.2	41	48.04	

Table 4 Measurement result of carbon dioxide of childcare center (ppm)

Childcare centers	Heukseok H	Heukseok K	Daebang B	Sindaebang G	Sindaebang B	Sadang D	Sadang K	Sadang C
Indoor 1	851	518	568	568	682	780	507	437
Indoor2	985	678	342	560	615	352	440	764
Outdoor	335	336	347	342	336	342	339	352
Childcare centers	Daebang E	Noryangjin N	Sangdo B	Sangdo L	Sangdo N	Sangdo S	Sadang M2	Sangdo H
Indoor 1	1348	611	647	501	623	773	690	690

Indoor2	1498	1548	586	640	704	887	622	890
Outdoor	345	339	346	337	341	329	340	336
Childcare centers	Sadang Y	Sadang M	Daebang S	Daebang K	Sindaebang L	Sadang H	Sangdo J	Noryangjin D
Indoor 1	934	844	786	936	801	870	848	1345
Indoor2	947	424	737	1137	909	862	548	847
Outdoor	346	332	326	332	341	326	335	329
Childcare centers	Dongjak C	Sangdo R	Sangdo G	Sadang O	Sindaebang Y	Sangdo N2	Average	
Indoor 1	535	902	1001	1504	755	1710	818.8	
Indoor2	815	964	1118	972	632	1162	806.2	
Outdoor	323	331	327	345	323	335	336.4	

Table 5 Measurement result of formaldehyde of childcare center (㎍/㎥)

Childcare centers	Heukseok H	Heukseok K	Daebang B	Sindaebang G	Sindaebang B	Sadang D	Sadang K	Sadang C
Indoor 1	35.8	20.55	20.77	26.57	17.65	42.4	22	23.6
Indoor2	37.26	25.19	23.15	21.25	13.53	47.5	27.8	26.2
Childcare centers	8.84	12.25	9.36	15.85	14.5	11.85	11.5	10.8
Childcare centers	Daebang E	Noryangjin N	Sangdo B	Sangdo L	Sangdo N	Sangdo S	Sadang M2	Sangdo H
Indoor 1	26.65	20.48	41.91	23.51	43.19	53.37	36.6	76
Indoor2	25.39	44.98	24.73	19.34	48.78	31.22	42.3	79.51
Childcare centers	8.25	15.3	14.3	12.8	11.5	12.3	8.3	13.9
Childcare centers	Sadang Y	Sadang M	Daebang S	Daebang K	Sindaebang L	Sadang H	Sangdo J	Noryangjin D
Indoor 1	49.15	80.13	20.84	43.25	67.72	69.26	83.5	53.2
Indoor2	53.39	23.68	27.38	70.33	20.93	57.58	60.7	67.5
Childcare centers	13.34	12.26	13.7	11.5	12.62	15.84	16.52	22.48
Childcare centers	Dongjak C	Sangdo R	Sangdo G	Sadang O	Sindaebang Y	Sangdo N2	Average	
Indoor 1	81.42	45.4	25.9	42.3	35.93	61.7	43.0	
Indoor2	78.53	78.18	19.64	56.3	46.58	59.3	41.9	
Childcare centers	15.76	16.72	14.67	12.3	10.9	26.3	13.5	

Table 6 Measurement result of total bacteria colony of childcare center (CFU/㎥)

Childcare centers	Heukseok H	Heukseok K	Daebang B	Sindaebang G	Sindaebang B	Sadang D	Sadang K	Sadang C
Indoor 1	88	29	238	32	28	34	70	289
Indoor2	8	5	230	33	18	19	174	58
Childcare centers	Daebang E	Noryangjin N	Sangdo B	Sangdo L	Sangdo N	Sangdo S	Sadang M2	Sangdo H
Indoor 1	134	119	153	96	78	106	720	215
Indoor2	113	85	85	80	57	64	500	148
Childcare centers	Sadang Y	Sadang M	Daebang S	Daebang K	Sindaebang L	Sadang H	Sangdo J	Noryangjin D
Indoor 1	179	150	210	139	121	100	236	594
Indoor2	97	22	131	129	101	218	379	566
Childcare centers	Dongjak C	Sangdo R	Sangdo G	Sadang O	Sindaebang Y	Sangdo N2	Average	
Indoor 1	260	153	44	290	220	553	189.2	
Indoor2	120	147	54	494	330	347	160.4	

Table 7 Measurement result of carbon monoxide of childcare center (ppm)

Childcare centers	Heukseok H	Heukseok K	Daebang B	Sindaebang G	Sindaebang B	Sadang D	Sadang K	Sadang C
Indoor 1	0.35	0.25	0.62	0.64	0.4	0.72	0.4	0.35
Indoor2	0.33	0.22	0.72	0.46	0.35	0.45	0.25	0.34
Outdoor	0.32	0.21	0.33	0.3	0.38	0.4	0.29	0.31
Childcare centers	Daebang E	Noryangjin N	Sangdo B	Sangdo L	Sangdo N	Sangdo S	Sadang M2	Sangdo H
Indoor 1	0.32	0.4	0.63	0.4	3.04	0.59	0.46	0.19
Indoor2	0.31	0.3	0.56	0.6	1.28	0.64	0.43	0.2
Outdoor	0.28	0.32	0.38	0.41	0.45	0.41	0.37	0.17
Childcare centers	Sadang Y	Sadang M	Daebang S	Daebang K	Sindaebang L	Sadang H	Sangdo J	Noryangjin D
Indoor 1	0.63	0.39	0.34	0.75	0.37	0.22	0.54	0.49
Indoor2	0.54	0.31	0.18	0.44	0.47	0.06	0.47	0.52
Outdoor	0.31	0.28	0.17	0.32	0.28	0.19	0.25	0.34
Childcare centers	Dongjak C	Sangdo R	Sangdo G	Sadang O	Sindaebang Y	Sangdo N2	Average	
Indoor 1	0.13	1.09	0.45	0.35	0.31	0.53	0.55	
Indoor2	0.1	0.75	0.54	0.42	0.28	0.58	0.44	
Outdoor	0.1	0.35	0.37	0.28	0.2	0.4	0.31	

2.3 Discussion

In this chapter, the actual condition of indoor air pollution of childcare centers was to be grasped by analyzing the result of field measurement of 5 pollutants, the indoor air quality maintenance standard of childcare center. The measurement result can be summarized like the following.

1) Among indoor air quality maintenance standard items of childcare center, formaldehyde (HCHO), total bacteria colony (TBC) and carbon monoxide (CO) showed distributions within the limit. Also, as for particle matter (PM_{10}), all facilities, except one with many occupants, were measured to be in less than the limit, showing fair indoor air condition of childcare centers. It is judged to be by the regular cleaning and management of air cleaner use for clean environment maintenance.

2) In case of carbon dioxide (CO_2), the number of relatively many occupants in 6 childcare centers exceeded the limit and it is thought that maintenance of the appropriate number of occupants indoors to be more necessary for childcare center management.

Survey on indoor air quality of childcare facility

3.1 Outline of survey

Unlike other large scale crowd facilities like subway station, hospital and stores, professional indoor air condition management is difficult for childcare center, thus duties of childminders at childcare centers are greater in managing indoor air condition. Hence, survey subjecting 161 childminders of 30 childcare centers in Dongjak-gu was taken place to minutely inspect the actual indoor air condition. Items of the survey were related to general characteristics of childminders and indoor air pollution. The survey subjecting 161 childminders of the relevant childcare centers was carried out along with indoor air pollutant measurement and took the method

of self-responding and withdrawing. The questionnaire was constituted of 26 questions researcher revised and supplemented based on the existing questionnaire regarding indoor air quality and the contents are like the following.

1) General characteristics of childminders such a gender, age, educational background, work experience, physical condition and matter of education: 6 questions
2) Childminders' degree of interest and satisfaction in indoor air quality: 6 questions
3) Physical detectable symptoms of childminders: 3 questions
4) Childminders' awareness of indoor air quality improvement: 3 questions
5) Actual management condition of indoor air quality of childcare facility: 8 questions

3.2 Result of survey

Table 8, Table 9, Table 10, Table 11 and Table 12 show the survey result.

Table 8 General characteristics of childminders

(n=161)

Characteristics		n(%)
Gender	Female	161(100.00)
Age	Under 30	104(64.60)
	30 ~ 39	43(26.70)
	Above 40	14(8.70)
Educational background	High school graduate	12(7.45)
	Junior college graduate	77(47.83)
	College student and graduate	65(40.38)
	Masters course enrollment and higher	7(4.35)
Major at final school	Childcare	34(20.86)
	Early Childhood Education	62(38.04)
	Social Welfare	18(11.04)
	Paedology	26(15.95)
	Home Management	4(2.45)
	Education	3(1.84)
	Other	16(9.82)
Work experience	Less than 4 years	79(49.07)
	4 years or more	82(50.93)
Physical condition	Healthy	115(71.43)
	Worse than average	46(28.57)
Does indoor air quality influence education?	Yes	32(19.88)
	No	129(80.12)

※†: Multiple responses

Table 9 Childminders' degree of interest and satisfaction in indoor air quality

(n=161)

Characteristics		n(%)
Satisfaction in indoor air quality	Very unpleasant	0(0.00)
	Unpleasant	3(1.86)
	Average	53(32.92)
	Pleasant	90(55.90)
	Very pleasant	15(9.32)
Total		161(100.00)
Urge to check the actual condition of air quality of the childcare center	Have	122(75.78)
	Don't have	38(23.60)
	No response	1(0.62)
Total		161(100.00)
Influence air pollution of childcare center has on body	No influence at all	1(0.62)
	Not much influence	18(11.181)
	Average	32(19.88)
	Influence in general	79(49.07)
	Great influence	31(19.25)
Total		161(100.00)
Which is worse: outdoor air pollution or indoor air pollution	Outdoor air pollution	93(57.76)
	Indoor air pollution	68(42.24)
Total		161(100.00)
Indoor air pollutants in knowledge †	Particle matter	149(92.55)
	Ozone	38(23.60)
	Carbon monoxide	55(34.16)
	Carbon dioxide	65(40.37)
	Nitrogen dioxide	22(13.66)
	Formaldehyde	46(28.57)
	Asbestos	85(52.80)
	Radon	12(7.45)
	Volatile Organic Compounds	34(21.12)
	Total Bacteria Colony	41(25.47)
	Other	1(0.62)

※†: Multiple responses

Table 10 Physical detectable symptoms of childminders

(n=161)

Characteristics	n(%)				
General symptoms †					
	Always	Often	Average	Sometimes	None
Inflamed eye	6(3.7)	7(4.3)	20(12.4)	30(18.6)	98(60.9)
Itchiness/ sting in eye	4(2.5)	10(6.2)	18(11.2)	42(26.1)	87(54.0)
Headache	1(0.6)	19(11.8)	20(12.4)	42(26.1)	79(49.1)
Dizziness/ vertigo	1(0.6)	12(7.5)	18(11.2)	28(17.4)	102(63.4)
Respiratory disease	2(1.2)	14(8.7)	19(11.8)	25(15.5)	101(62.7)
Vomiting/ nauseous	0(0.0)	4(2.5)	13(8.1)	14(8.7)	130(80.7)
Cough/ sneeze	5(3.1)	12(7.5)	31(19.3)	64(39.8)	49(30.4)
Skin irritation	1(0.6)	8(5.0)	11(6.8)	22(13.7)	119(73.9)
Chilling effect	3(1.9)	7(4.3)	13(8.1)	17(10.6)	121(75.2)
Insomnia	1(0.6)	3(1.9)	8(5.0)	7(4.3)	142(88.2)
Chemical smell	0(0.0)	1(0.6)	6(3.7)	12(7.5)	142(88.2)
The time zone when symptoms occur (relevant responders)					
Morning	9(6.72)				
Afternoon	125(93.28)				
Total	134(100.00)				
Visited doctor with such symptoms (relevant responders)					
Yes	45(30.41)				
No	103(69.59)				
Total	148(100.00)				

※†: Multiple responses

Table 11 Actual management condition of indoor air quality of childcare center

(n=30)

Characteristics	n(%)
Times of ventilation a day	
1~2 times	1(6.67)
3~4 times	11(36.67)
5~10 times	8(26.67)
More	9(30.00)
Equipment in possession†	
Ventilator	19(63.33)

Air cleaner					24(80.00)
Humidifier					16(53.33)
Air conditioner					30(100.00)
Filter cleaning cycle (relevant facilities)	1 time /week	1time /month	1 time /2~3 months	1 time /season	Do not clean
Air cleaner	12(50.0)	8(33.3)	2(8.3)	1(4.2)	1(4.2)
Air conditioner	10(33.3)	8(26.7)	5(16.7)	7(23.3)	0(0.0)
Cook indoors					
Yes					20(66.7)
No					10(33.3)
Cooking hours (relevant facilities)					
Less than 1hour					1(5.0)
1 hour ~ less than 2 hours					2(10.0)
2 hours ~ less than 4 hours					8(40.0)
4 hours or more					9(45.0)
Ventilation time after cooking (relevant facilities)					
Less than 30 minutes					4(20.0)
30 minutes ~less than 1 hour					1(5.0)
1 hour ~ less than 2 hours					4(20.0)
2 hours or more					11(55.0)

※†: Multiple responses

Table 12 Childminders' awareness of indoor air quality improvement

(n=161)

Characteristics		n(%)
Measures to improve air pollution within childcare centers†	Ventilation installation	76(37.44)
	Cleaning system improvement	48(23.65)
	Prohibition of running indoors	25(12.32)
	Plaything improvement	2(0.99)
	Carpet, curtain improvement	34(16.75)
	Other	18(8.86)
Total		203(100.00)
Fields the government ought to manage most urgently for national health†	Air pollution	74(26.81)
	Water pollution	66(23.91)
	Indoor air pollution	54(19.57)
	Ground pollution	22(7.97)
	Waste (garbage)	59(21.38)
	Other	1(0.36)
Total		276(100.00)
Reason why environmental issues of childcare centers are not improved	Lack of parental interest	1(0.62)
	Lack of director's interest	5(3.11)
	Lack of administrative and financial support	116(72.05)
	Lack of teachers' awareness and attempts to improve	17(10.56)
	Other	22(13.66)
Total		161(100.00)

※†: Multiple responses

3.3 Discussion

For subjective judgment on the actual indoor air condition of childcare, survey subjecting 161 childminders of 30 childcare centers regarding awareness and actual management of indoor air pollution, physical detectable symptoms and such was taken place.

As the survey result, more than 60% of the childminders responded they are satisfied with the indoor environment of the childcare centers and more than 75% responded to be interested in indoor air quality of childcare centers, showing quite a high satisfaction and interest in indoor air quality. Also, it was appeared childcare centers carries on a certain level of management to improve general indoor air quality through a certain level of ventilation, use of air cleaner, cleaning and ventilation after cooking.

Nevertheless, there are only 20% educated about indoor air quality, showing the lack of education regarding indoor air quality, and childminders' awareness of indoor air quality is also caught short. In fact, as the result of research on physical detectable symptoms occurred while working in childcare centers, the usual indoor air pollution in childcare centers seems possible, for more than 90% said to have the symptoms caused by indoor air pollutant in the afternoon as indoor hours accumulates, yet only 30% visited doctors and they seem to not think much of indoor air pollution, for relatively less childminders found indoor air pollution less important then other pollutions to the question regarding awareness of indoor air quality improvement. Hence, it is thought that education on indoor air quality to childminders needs to be increased more.

Conclusions

The study has its purpose on suggesting basic data for improvement and management of indoor air quality of future childcare centers through survey subjecting childcare centers accommodating physically weak children and investigation on the actual indoor air condition. The result of the study can be summarized like the following.

1) As the result of field measurement of pollutants for indoor air maintenance standard of childcare centers, it is thought that they are safe according to the indoor air quality maintenance standard of crowd facility, for items of formaldehyde (HCHO), total bacteria colony (TBC), carbon monoxide (CO) and particle matter (PM_{10}), except for particle matter exceeding the limit, were measured to be in less than the limit, showing indoor air condition of childcare centers is fair by regular cleaning and management of air cleaner use for clean environment maintenance.

2) Among the measured items, carbon dioxide (CO_2) appeared to be exceeding in 6 facilities out of 30 and it is judged that more effort should be made to maintain the appropriate capacity and ventilation in managing indoor air quality in future childcare centers.

3) As the result of survey subjecting 161 childminders of 30 childcare centers, 76% responded to be interested in indoor air quality of childcare centers and 64% responded they are satisfied with the current environment. However, teachers who received education on indoor air condition were only 19.8% and it was grasped only 30% visited doctors due to physical detectable symptoms when exposed in pollution level. This is judged that indoor air quality of childcare centers has potential danger due to insufficient management of childminders and the education on indoor air condition which only 19.8% has completed should be promoted.

References

1. Son, Busun, The actual indoor air quality condition of childcare centers, Air Cleaning Technology, 19(3), 2006
2. Ministry of Gender Equality & Family, Research report on national childcare. education, 2005
3. Korea Institute of Child Care and Education, www.kicce.re.kr
4. Jang, Minseon, Study on the actual indoor air quality condition of childcare centers and improvement, Hanyang University Master's thesis, 2009
5. Jeon, Gwanghee, 'Reason and resolution of low fertility in Korea', 2009
6. Korean Educational Development Institute, 'Education Development', 2002
7. Ministry of Environment, ' Indoor Air Quality Control In Crowd Facilities', 2008
8. Ministry of Environment, 'Manual of indoor air quality design and maintenance management of childcare centers', 2008
9. Ministry of Environment, 'Indoor air quality management policy', 2009
10. Ministry of Environment, 'Indoor air quality official test method', 2004
11. Ministry of Environment, General planning of indoor air quality ventilation (blueprint), 2004
12. Air Quality Guideline for Europe 2nd Edition, WHO, 2001

Case-Control study for the Association Between Indoor Environmental Factors and Children's Health Problems in Japan-Part1 a nationwide questionnaire study among 1664 primary school students.

Ando Naoya[1], Yoshino Hiroshi[1], Hasegawa Kenichi[2], Abe Keiko[3], Ikeda Koichi[4], Kato Noriko[5], Kumagai Kazukiyo[6], Hasegawa Ayumi[7], Mitamura Teruaki[8], Yanagi U[9], Matsuda Asako[2], Takamatsu Mari[2], Hamada Kensuke[1]

1 Tohoku University, Department of Architecture and Building Science, Japan
2 Akita Prefectural University, Dept. of Archi.& Env. Sys. Faculty of Sys. Sci.& Tech., Japan
3 Institute of Environmental Biology, Japan
4 Nihon University, Department of Architecture, College of Science and Technology, Japan
5 Researcher, National Institute of Public Health, Japan
6 California Department of Public Health, Environmental Health Laboratory Branch, USA
7 Sumika Chemical Analysis Service, LTD, Japan
8 Ashikaga Instutute of Technology Department of Architecture, Japan
9 Kogakuin University, Department of Architecture, Japan

Abstract

Recent studies show the number of people affected by biological contaminants have increased every year in Japan. An epidemiological investigation on 4th and 5th grade primary school students was conducted in order to clarify the relationship between indoor environment and children's health problems. A case-control study adopted ATS-DLD-American Thoracic Society-Division of Lung Diseases- questionnaire for evaluation of respiratory symptoms and allergies was conducted for 2574 primary school students (1664 responded) across Japan. The visible presence of mold both living room and children's bedroom excluding window (such as wall, floor or closet) was observed to be significantly associated with bronchial hypersensitivity (OR=3.05 95% Cl: 1.38-6.73). Also, the occurrence of respiratory symptoms and allergic symptoms were significantly associated in homes using humidifier.
These results showed that home environmental factors had serious risk factors for allergic symptoms. In particular, indoor mold and water stain were strongly influence on respiratory symptoms among children in Japan.

Keywords: Allergic diseases, Indoor environmental factors, Case-Control study, Mold or dampness

Introduction

A large number of epidemiological studies reveal that there has been an increase of allergic diseases over the past 40 year worldwide [1]. As for Japan, recent studies show that the number of people affected by biological contaminants has increased every year [2]. The Ministry of Health, Labor and Welfare reported that about 36% of children up to 14 years old had some allergic symptoms [3]. This fact cannot be explained by genetic predisposition, because the time interval was too short to change the genetic factor. Therefore environmental factors including housing characteristics or indoor environmental conditions were considered as risk factors. Since people spend more than 90% of their time in an indoor environment, especially at their own homes [4], the indoor environmental conditions might be a possible risk factor for allergic symptoms.

Nowadays building dampness is one of the indoor environmental problems. Fisk showed that exposure to dampness and mold raises the risk for various respiratory symptoms by 30-50% [5]. A resent report in 2009 by the World Health Organization (WHO) concluded that excess level of dampness problems in indoor environment is a potential health hazard [6]. Also, a large number of epidemiological studies in many countries have revealed an association between home dampness and respiratory symptoms [7] [8] [9]. On the other hand,

epidemiological evidence between indoor environmental factors and children's adverse health is still very low in Japan.

In order to clarify the association between indoor biological contaminant exposure and health problems such as respiratory symptoms and allergic diseases, a nationwide epidemiological investigation has been conducted for 4th and 5th grade primary school children in Japan from 2007 to 2009.The investigation had three phases. This paper reports the outcomes from the case-control study by a questionnaire survey (Phase2). The survey was analyzed to make clear the effect of the dampness and residential factors on children health problems.

Methods

Study Design

This nationwide epidemiological study was divided into three phases (Figure1). The objects of this survey were 4th and 5th grade primary school children in Japan, because children have a higher incidence of allergies due to environmental factors than adults. In Phase 1, a questionnaire survey using postcards was conducted to grasp the prevalence of health problems and its causal factors among 7401 children. Phase 2 was a case-control study through a questionnaire survey to clarify the association between indoor environmental factors and adverse health effects. Phase 3 was a case-control study including house inspections and field measurements.

Number of Respondents and Contents of Questionnaire

The questionnaire survey was carried out from the winter of 2008 to April 2009. Firstly, in Phase 1, school teachers were asked to cooperate for this survey. When school teachers agreed, parents were requested to reply to the questions showed in postcards from August 2007 to January 2009. About 26400 parents were asked to join this survey, and 7401 parents out of them agreed to do it. Out of them, 2625 parents replied to participate in phase 2, and a second questionnaire was distributed to all or them. The completed questionnaires were returned by posted mail within one to three weeks. As shown in Figure 2, this study distributed questionnaires in six areas including 64 cities all over Japan. The total number of respondents was 1,664. The response ratio was 63.2%. The response ratios in the six individual areas were 55.2% (Hokkaido), 63.7% (Tohoku), 63.9% (Tokyo), 68.4% (Tokai), 62.1% (Kansai and Cyugoku) and 43.3% (Kyusyu and Okinawa).

The questionnaire contained 78 questions about building information, installed equipment, lifestyle, building performance, occupant characteristics and health problems. Three questions about dampness indicators regarding to 'condensation', 'visible mold growth' and 'water stains' were asked. Also, the location where the damages occurred (e.g. wall, closet, windowpane or window glass, floor, selling) was asked. Based on this information, a

dampness index was calculated for estimating the association between dampness damage levels and allergic symptoms.

Symptoms of children's adverse health effects were determined by the American Thoracic Society-Division of Lung Diseases (ATS-DLD) questionnaire [10], which considered different allergic symptoms by a combination of positive answers to specific questions. In this paper, three allergic symptoms such as bronchial hypersensitivity, current asthma and allergic rhinitis are analyzed with the influencing factors including age, breastfeeding, parent's smoking habits, pets, cleaning habits, living area and so on. Parents' allergic symptoms were defined as the parent's history of asthma, atopy, allergy, hey fever and hives.

Statistical Analysis Methods

The association between each of the three symptoms (bronchial hypersensitivity, current asthma and allergic rhinitis) and housing characteristics including mold and condensation was analyzed by logistic regression models. The data was initially analyzed by binary logistic regression. After that, adjusted odds ratios (OR) with 95% confidence intervals (95% Cl) were calculated for each of the housing characteristics by using the multivariate logistic regression models, which controlled potentially confounding factors. The analyses were considered to be statistically significant when $p<0.05$. All analyses were conducted with SPSS software for Windows (SPSS, Chicago, IL, USA)

Results

Allergic Symptoms and Gender

Figure 3 presented the allergic symptoms of children and parents. The percentage of boys and girls were almost equal. Almost half of the children have at least one of allergic symptom. The prevalence of bronchial hypersensitivity, current asthma and allergic rhinitis were 12.1%, 5.1% and 58.5%, respectively. Except for current asthma the prevalence of bronchial hypersensitivity and allergic rhinitis among boys was significantly higher than that of girls.

Housing Characteristics and Occupant's Behavior

Housing characteristics and occupant's behaviors were given in Figure 4. Most of the houses in each area were located in residential areas. Detached houses in each area accounted for more than half of the investigated dwellings. The percentage of houses which were over five years old was 82.3% and majority was aged from 10 to 20 years. In Hokkaido and Tohoku areas, double panes were installed in more than half of the houses. In other areas, single panes were more popular. Mechanical ventilation systems were installed in about 40% of the houses. The ratio of houses where the mechanical ventilation was always in operation was less than 40%.

Figure 5 showed the regional differences in condensation, visible mold and visible water stains among the six areas. More than 90% of the families reported at least one dampness problem in either living room or children's bedroom. The occurrence of condensation, visible mold and visible water stains in both rooms was 58.1%, 31.1% and 14.4%, respectively. Such dampness problems were found in the children's bedrooms more frequently than the living rooms. Condensation or mold growth was found most frequently on window panes. Mean values of the dampness index, which integrated occurrence of condensation, visible mold growth and visible water stains for living rooms and children's bedrooms were 1.32 and 1.39, respectively. In Tohoku area, the value was 1.51. Humidifiers were used in 23.1% of the living rooms. In Hokkaido and Tohoku areas, the ratio of houses where the laundry was dried by hanging in the rooms was higher than that of other areas.

Association Between Indoor Environmental Factors and children's Allergic Symptoms

Table 1 shows the multivariate relationship between dampness indicators and children's allergic symptoms. After OR was adjusted for potential confounders, it was found that condensation occurrence on walls, floors, ceilings or closets in both living rooms and children's bedrooms excluding windows was significantly associated with current rhinitis (OR: 2.26 95%Cl: 1.29-3.95). Also, visible presence of mold growth in both living rooms and children's bedrooms excluding windows was strongly associated with current asthma (OR: 3.05 95%Cl 1.38-6.73) and bronchial hypersensitivity (OR: 1.99 95%Cl: 1.10-3.59). Occurrence of water stains was more strongly associated with allergic symptoms than condensation or visible mold. As the values of the dampness index increased (Table2), OR for bronchial hypersensitivity and current asthma increased. Statistically significant OR was found in houses with the occurrence of all three dampness indicators. For bronchial hypersensitivity and current asthma, the OR of children's bedrooms was higher than that of living rooms.

The adjusted OR for occupant's characteristics are shown in Table 3. The use of humidifiers in children's bedrooms was related to bronchial hypersensitivity (OR: 1.76 95%Cl: 1.15-2.70) and current asthma (OR: 2.07 95%Cl: 1.14-3.76). The association between dehumidifiers used in bedrooms and allergic symptoms was found in the crude analysis, but there was no association in the multivariate logistic regression analysis. For allergic rhinitis, these characteristics did not appear.

Discussion

Prevalence of Allergic Symptoms and Dampness Indicators

This survey tried to clarify the association between indoor environments and children's health problems among 4th and 5th grade primary school children in Japan. As a result of statistical analysis, significant relations were found between moisture and mold growth, and allergic

symptoms. For instance, the presence of indoor dampness in children's bedrooms was significantly associated with airway symptoms. More importantly, there was a strong relationship between the high prevalence of respiratory symptoms and the value of the dampness indicator. Also the use of humidifiers in children's bedrooms was an important risk factor for increasing the prevalence of allergic symptoms.

The prevalence of bronchial hypersensitivity, current asthma and allergic rhinitis were 12.1%, 5.1% and 58.5%, respectively. These trends are similar to the findings of a survey in Miyagi and Akita Prefecture in Japan, which are defined for allergic symptoms through ATS-DLD questionnaire [11][12]. Compared to other countries, 12 southern Californian communities in U.S. reported a prevalence of current asthma of 7.3-9.5% [13].

The prevalence of reported condensation, visible mold and visible water stains at any place in both living room and children's bedroom was 58.1%, 31.1% and 14.4%, respectively. Parents reported such contamination occurred often in the children's bedrooms compared to the living rooms. It is estimated that reported prevalence rates of home dampness problems ranged widely (typical range 10-50%).

Similar findings were reported in other Japanese studies, in which condensation on window panes and/or walls occurred in 51.8% of the detached houses and visible mold growth accounted for 39.8% of residences [14]. The reason why the dampness contamination occurred more often in children's bedrooms compared to living rooms was not clear. But one possible reason is that ventilation rates are low in the bedrooms due to small window areas and high moisture environments more easily created in the bedrooms compared to the living rooms.

The Indoor Environmental Factors Influenced to Allergic Symptoms

Self-reported dampness indicators are significantly associated with self-reported respiratory symptoms, with OR ranging from 1.73 to 3.03. The association between 'dampness' and various symptoms was reported by a large number of other studies. In many countries, the number of people susceptible to the effects of dampness and mold in homes has been increasing. In the USA, about 4.6million cases were estimated to be attributable to dampness and mold exposure. The annual economic cost of asthma attributed to those reasons was estimated to be $3.5 billion [15]. Furthermore, exposure to dampness and mold raises the risk of various respiratory symptoms by 30-50% [4]. Actually, the high air humidity may cause microbial growth, which may result in a greater occurrence of spores, allergens, volatile organic compounds [16], and endotoxins [17] in indoor environments. High air humidity has attributed to the increase of house dust mite. The other study showed that moisture-related structural damage combined with polyvinyl chloride materials may lead to chemical emissions and affected the higher prevalence of symptoms among children [18]. Our study

showed that a dose-response relationship between the occurrence of symptoms and the increasing number of dampness indicators was observed in both livings room and bedrooms. A similar trend was identified from the building related symptoms [19]. Our study concluded that reported visible mold or water damage in houses has strong correlation to occurrence of respiratory symptoms.

It was found in this Study that the presence of humidifiers installed in children's bedrooms was associated with both bronchial hypersensitivity and current asthma among children. Another parent-reported study identified that humidifier use increased the risk of wheezing (OR: 1.41 95%Cl 1.11-1.79) [20]. Some microorganisms can grow in air humidifiers, which caused respiratory symptoms [21]. Humidifier usage could especially be related to the increases of fungi concentration [22]. It is also a possibility for the cause of rising concentrations of the dust mite allergen. Therefore if not properly maintained and operated, it could trigger some dampness problems and then effect health.

Several Biases in Statistical Study

This survey has some limitations. First, the influence of selection bias had already been included in Phase 1. In Phase 2, non-responders accounted for more than 30% of dwellings. It was estimated that the real prevalence rate would be lower than the results. The second limitation of this study was dependence on self-reported questionnaires for both health outcomes and independent variables. Thus, it included potential recall bias, which leaded to overestimate or underestimate the environmental exposures among symptomatic subjects. Parents who have experienced asthma or allergic symptoms are likely to report mold or dampness problems more often compared to those without such health problems in family members. Furthermore, parents living in damp buildings concerned about health problems are possibly over-reporting symptoms. However, it was found by other researchers that the tendency to overestimate dampness in houses was independent of whether asthmatic children were present or not [23].

Conclusions

This study documented that mold and water stains in living rooms and children's bedrooms were strongly associated with the risk of rhinitis and airway symptoms in Japan. It was found that dampness and Indoor mold were important risk factors for allergic symptoms among young children. Also, homes installed with humidifiers were harmful for children's health and the evidence of association was found more in children's bedrooms than in living rooms.

The survey provides this information as further measurement for the next step of this study, which reveals the relationship between allergic symptoms and indoor environmental pollutant in detail.

Acknowledgments

The authors would like to thank the occupants who were involved in this study for their helpful cooperation. This project was conducted as one of the activities of the Research Project for Creation of Housing that Promotes Health and Well-being (Chair: Prof. Shuzo Murakami). This study was supported partly by the Housing Research Foundation, TOSTEM Foundation for Construction Materials Industry Promotion and the Kajima Foundation Research Grant.

Reference

1 Holgate ST, The epidemic of allergy and asthma, Nature, 402, B2-4, 1999.

2. Nishima, S, et al, Surveys on the prevalence of pediatric bronchial asthma in Japan: A comparison between the 1982, 1992, and 2002 surveys conducted in the same region using the same methodology, Allergolory international, 58, pp.37-53, 2009.

3. Ministry of Health, Labour and Welfare, Outline of health welfare trend investigation (2003) Allergic symptom, Ministry of Health, Labour and Welfare, 2003.

4. Shiotsu, M, Yoshizawa, S, Ikeda, K, S and Nozaki, A, Survey on Human Activity Patterns According to Time and Place, Part 1 Basic Research on the Exposure Dose to Indoor Air Pollutant, Journal of Architecture, Planning and Environmental Engineering(Transaction of AIJ), No.511, pp.45-52, 1998. (in Japanese)

5. Fisk, W.J, Lei-Gomez, Q and Mendell, M.J. Meta-analyses of the associations of respiratory health effects with dampness and mold in homes, Indoor Air, 17, pp284-296, 2007.

6. World Health Organization (WHO), WHO guidelines for indoor air quality: dampness and mould,WHO, 2009

7. Bornehag, C.G, Sundell, J and Sigsgard, T. Dampness in Buildings and Health: Report from an Ongoing Epidemiological Investigation on the Association Between Indoor Environmental Factors and Health Effects Among Children in Sweden, Indoor Air, 14, pp.59-66, 2004.

8. Haverinen-Shaughnessy, U, Pekkanen, J, Hyvärinen, A, Nevalainen, A, Putus, T, Korppi, M, Moschandreas, D. 2006. Children's Homes-determinants of Moisture Damaged and Asthma in Finnish Residences, Indoor Air, 16, pp.248-255, 2006.

9. K W, Chew, Zuraimi, MS, Tham, FT and Ooi, PL, Association between home dampness and presence of molds with asthma and allergic symptoms among young children in the tropics, Pediatr Allergy Immunol, 18, pp.418- 424, 2007.

10. Japan Public Health Association. Environment Agency consignment business report in 1978, Research on influence on health investigation technique due to air pollution - Research on new method of epidemiological surveillance-, 1979. (in Japanese)

11 Yoshino, H, Hojo, S, Takada, M and Kakuta, K. Relationship between Living Environment and Children Health Problems in Miyagi Prefecture, Journal of Environmental Engineering (Transactions of AIJ), No.558, pp.87-94, 2002 (in Japanese)

12. Hasegawa, K, Matsumoto, S and Genjo, K.. Questionnaire Survey on Relationship between Indoor Environmental Factors and Children Health Problems in Northern Cities of Japan, the proceedings of IAQVEC, II, p.275-281, 2007

13. Peters, JM, Avol, E, et al, A study of twelve southern California communities with differing levels and types of air pollution. 1. prevalence of respiratory morbidity, Am J Respir Crit Care Med, 159, pp.760-767, 1999.

14. Kishi, R, Saijo, Y. and et al. Regional difference in residential environments and the association of dwelling and residential factors with sick house syndrome: a nationwide cross-sectional questionnaire study in Japan, Indoor Air, 19, pp243-254, 2009.

15. Mudarii, D. and Fisk, W.J. Public health and economic impact of dampness and mold, Indoor Air, 17, pp.226-235,2007

16. Schleibinger, H, Laussmann, D, Bornehag, C.G, et al, Microbial volatile organic compounds in the air of moldy and mold-free indoor environments, Indoor Air, 18, pp.113-124, 2008.

17. Andersson, K, et al, Bacteria, molds, and toxins in water-damaged building materials, Appl Environ Microbiol, 63, 387-393.

18. Bornehag, C.G, et al, Phthalates in indoor dust and their association with building characteristics, Environ Health Perspect, 113, pp.1399-1404, 2005.

19. Engvall, K, Norrby, C. and Norback, D. Sick building syndrome in relation to building dampness in multi-family residential buildings in Stockholm, Int Arch Occup Environ Health, 74, pp.270-278, 2001.

20. Gent, J.F, et al, Levels of household mold associated with respiratory symptoms in the first year of life in a cohort at risk for asthma, Environ Health Perspect, 110, pp.A781-A786, 2002.

21. Flannigan, B, and Morey, P, Control of moisture problems affecting biological indoor air quality, ISIAQ guideline, Ottawa, International Society of Indoor Air and Climate, 1996.

22. Ren, P, Jankun, T.M, Belanger, K, et al, The relation between fungal propagules in indoor air and home characteristics, Allergy, 56, pp.419-424, 2001.

23. Williamson, IJ, Martin, CJ, McGill, G, et al, Damp housing and asthma : a case-control study, Thorax, 1997, 52, pp.229-234.

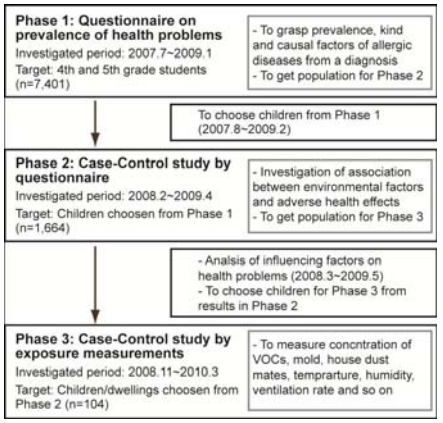


Fig. 1 Design of Epidemiological Survey

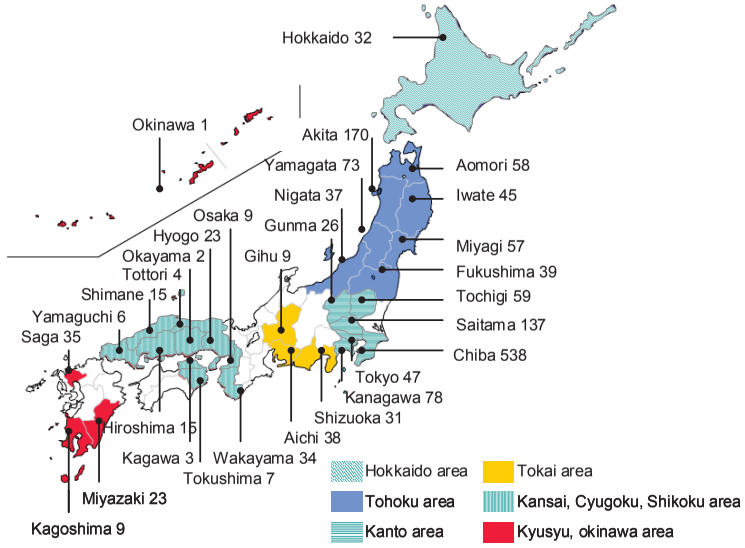
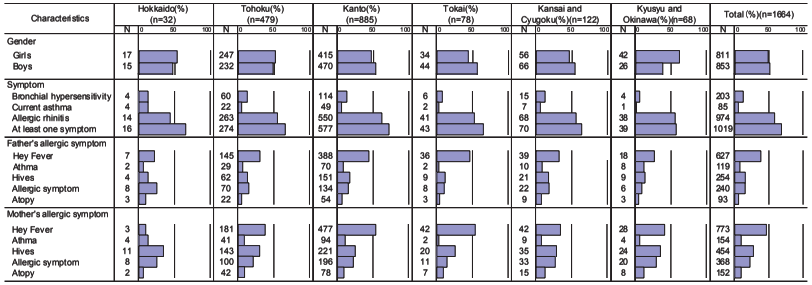
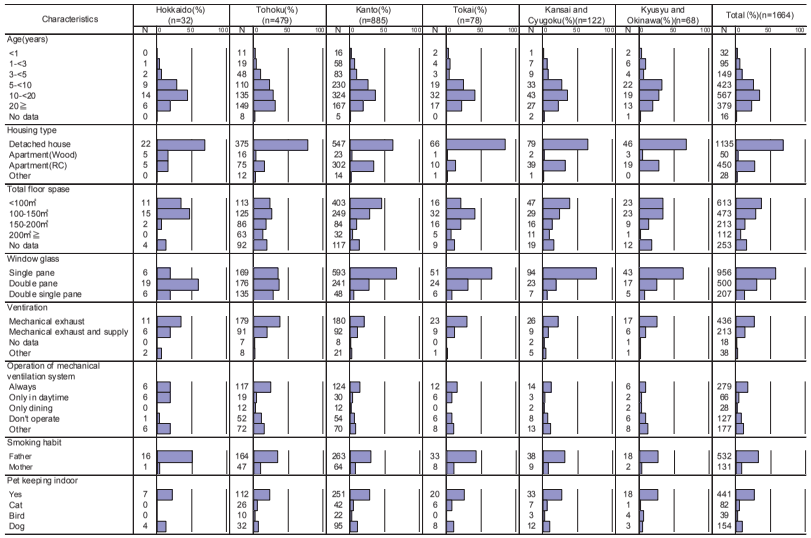


Fig. 2 Investigated locations and number of questionnaires respondents



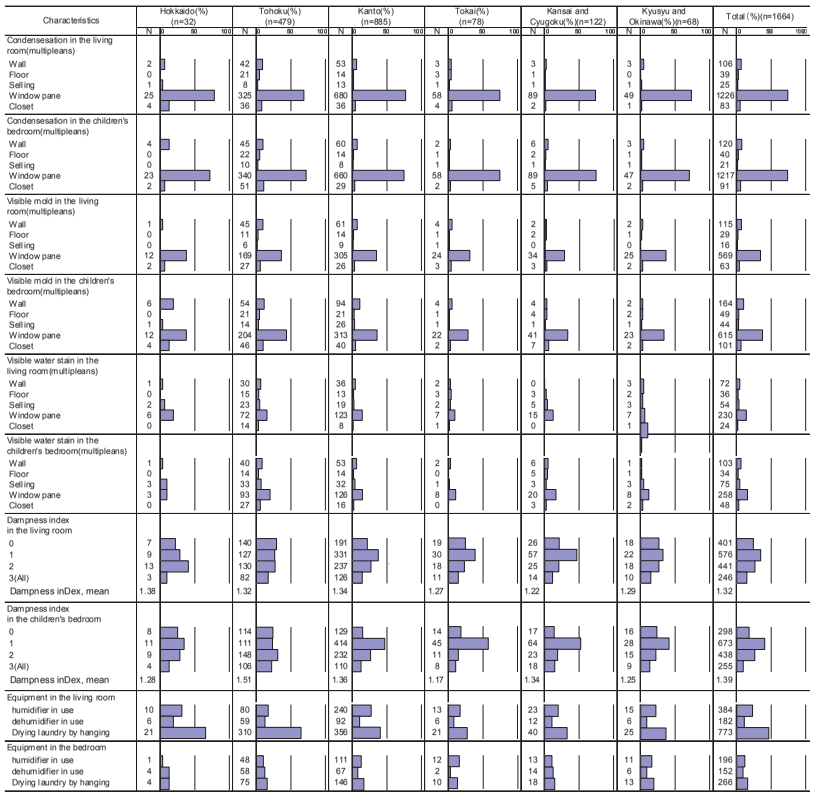
Characteristics	Hokkaido(%) (n=32)		Tohoku(%) (n=479)		Kanto(%) (n=885)		Tokai(%) (n=78)		Kansai and Cyugoku(%)(n=122)		Kyusyu and Okinawa(%)(n=68)		Total (%)(n=1664)	
	N	0 50 100	N	0 50 100	N	0 50 100	N	0 50 100	N	0 50 100	N	0 50 100	N	0 50 100
Gender														
Girls	17		247		415		34		56		42		811	
Boys	15		232		470		44		66		26		853	
Symptom														
Bronchial hypersensitivity	4		60		114		6		15		4		203	
Current asthma	4		22		49		2		7		1		85	
Allergic rhinitis	14		263		550		41		68		38		974	
At least one symptom	16		274		577		43		70		39		1019	
Father's allergic symptom														
Hey Fever	7		145		388		36		39		18		627	
Athma	2		29		70		2		10		8		119	
Hives	4		62		151		9		21		9		254	
Allergic symptom	8		70		134		8		22		6		240	
Atopy	3		22		54		3		9		3		93	
Mother's allergic symptom														
Hey Fever	3		181		477		42		42		28		773	
Athma	4		41		94		2		9		4		154	
Hives	11		143		221		20		35		24		454	
Allergic symptom	8		100		196		11		33		20		368	
Atopy	2		42		78		7		15		8		152	

Fig. 3 Prevalence of children and parents allergic symptoms and gender (n=1664)



Characteristics	Hokkaido(%) (n=32)		Tohoku(%) (n=479)		Kanto(%) (n=885)		Tokai(%) (n=78)		Kansai and Cyugoku(%)(n=122)		Kyusyu and Okinawa(%)(n=68)		Total (%)(n=1664)	
	N	0 50 100	N	0 50 100	N	0 50 100	N	0 50 100	N	0 50 100	N	0 50 100	N	0 50 100
Age(years)														
<1	0		11		16		2		1		2		32	
1-<3	1		19		58		4		7		6		95	
3-<5	2		48		83		3		9		4		149	
5-<10	9		110		230		19		33		22		423	
10-<20	14		135		324		32		43		19		567	
20≧	6		149		167		17		27		13		379	
No data	0		8		5		0		2		1		16	
Housing type														
Detached house	22		375		547		66		79		46		1135	
Apartment(Wood)	5		16		23		1		2		3		50	
Apartment(RC)	5		75		302		10		39		19		450	
Other	0		12		14		1		1		0		28	
Total floor spase														
<100㎡	11		113		403		16		47		23		613	
100-150㎡	15		125		249		32		29		23		473	
150-200㎡	2		86		94		16		16		9		213	
200㎡≧	0		63		32		5		11		1		112	
No data	4		92		117		9		19		12		253	
Window glass														
Single pane	6		169		593		51		94		43		956	
Double pane	19		176		241		24		23		17		500	
Double single pane	6		135		48		6		7		5		207	
Ventiration														
Mechanical exhaust	11		179		180		23		26		17		436	
Mechanical exhaust and supply	6		91		92		9		9		6		213	
No data	0		7		8		0		2		1		18	
Other	2		8		21		1		5		1		38	
Operation of mechanical ventilation system														
Always	6		117		124		12		14		6		279	
Only in daytime	6		19		30		6		3		2		66	
Only dining	0		12		12		0		2		2		28	
Don't operate	1		52		54		6		8		6		127	
Other	6		72		70		8		13		8		177	
Smoking habit														
Father	16		164		263		33		38		18		532	
Mother	1		47		64		8		9		2		131	
Pet keeping indoor														
Yes	7		112		251		20		33		18		441	
Cat	0		26		42		6		7		1		82	
Bird	0		10		22		0		3		4		39	
Dog	4		32		95		8		12		3		154	

Fig. 4 Housing Characteristic and occupant's behavior (n=1664)



Characteristics	Hokkaido(%) (n=32)		Tohoku(%) (n=479)		Kanto(%) (n=885)		Tokai(%) (n=78)		Kansai and Cyugoku(%)(n=122)		Kyusyu and Okinawa(%)(n=68)		Total (%)(n=1664)	
	N	0 50 100	N	0 50 100	N	0 50 100	N	0 50 100	N	0 50 100	N	0 50 100	N	0 50 100
Condensesation in the living room(multipleans)														
Wall	2		42		53		3		3		3		106	
Floor	0		21		14		3		1		0		39	
Selling	1		8		13		1		1		1		25	
Window pane	25		325		680		58		89		49		1226	
Closet	4		36		36		4		2		1		83	
Condensesation in the children's bedroom(multipleans)														
Wall	4		45		60		2		6		3		120	
Floor	0		22		14		1		2		1		40	
Selling	0		10		8		1		1		1		21	
Window pane	23		340		660		58		89		47		1217	
Closet	2		51		29		2		5		2		91	
Visible mold in the living room(multipleans)														
Wall	1		45		61		4		2		2		115	
Floor	0		11		14		1		2		1		29	
Selling	0		6		9		1		0		0		16	
Window pane	12		169		305		24		34		25		569	
Closet	2		27		26		3		3		2		63	
Visible mold in the children's bedroom(multipleans)														
Wall	6		54		94		4		4		2		164	
Floor	0		21		21		1		4		2		49	
Selling	1		14		26		1		1		1		44	
Window pane	12		204		313		22		41		23		615	
Closet	4		46		40		2		7		2		101	
Visible water stain in the living room(multipleans)														
Wall	1		30		36		2		0		3		72	
Floor	0		15		13		3		3		2		36	
Selling	2		23		19		2		5		3		54	
Window pane	6		72		123		7		15		7		230	
Closet	0		14		8		1		0		1		24	
Visible water stain in the children's bedroom(multipleans)														
Wall	1		40		53		2		6		1		103	
Floor	0		14		14		0		5		1		34	
Selling	3		33		32		1		3		3		75	
Window pane	3		93		126		8		20		8		258	
Closet	0		27		16		0		3		2		48	
Dampness index in the living room														
0	7		140		191		19		26		18		401	
1	9		127		331		30		57		22		576	
2	13		130		237		18		25		18		441	
3(All)	3		82		126		11		14		10		246	
Dampness inDex, mean	1.38		1.32		1.34		1.27		1.22		1.29		1.32	
Dampness index in the children's bedroom														
0	8		114		129		14		17		16		298	
1	11		111		414		45		64		28		673	
2	9		148		232		11		23		15		438	
3(All)	4		106		110		8		18		9		255	
Dampness inDex, mean	1.28		1.51		1.36		1.17		1.34		1.25		1.39	
Equipment in the living room														
humidifier in use	10		80		240		13		23		15		384	
dehumidifier in use	6		59		92		6		12		6		182	
Drying laundry by hanging	21		310		356		21		40		25		773	
Equipment in the bedroom														
humidifier in use	1		48		111		12		13		11		196	
dehumidifier in use	4		58		67		2		14		6		152	
Drying laundry by hanging	4		75		146		10		18		13		266	

Fig. 5 Dampness indicator

Table 1 Adjusted odds ratio[a] and 95%CI for the association between dampness indicator and children allergic symptoms.

Characteristics	Adjusted OR(95%CI)[a]		
	Current asthma(N=85)	Bronchial hypersensitivity (N=203)	Current rhinitis(N=974)
Condensation			
No	1.0	1.0	1.0
Only occurance on window pane	0.86(0.42-1.73)	1.01(0.62-1.65)	1.32(0.97-1.80)
Living or bedroom excluding window[b]	1.80(0.73-4.43)	1.64(0.85-3.15)	1.33(0.83-2.13)
Both rooms excluding window[b]	0.90(0.29-2.85)	1.37(0.66-2.86)	**2.26(1.29-3.95)****
Visible mold			
No	1.0	1.0	1.0
Only occurance on window pane	1.21(0.69-2.11)	0.99(0.68-1.45)	1.27(0.98-1.64)
Living or bedroom excluding window[b]	1.26(0.62-2.56)	1.46(0.93-2.28)	1.13(0.81-1.58)
Both rooms excluding window[b]	**3.05(1.38-6.73)****	**1.99(1.10-3.59)***	1.30(0.80-2.11)
Visible water leakage			
No	1.0	1.0	1.0
Only occurance on window pane	1.33(0.65-2.71)	1.33(0.83-2.12)	1.37(0.96-1.95)
Living or bedroom excluding window[b]	**2.35(1.23-4.48)****	**1.73(1.08-2.76)***	1.26(0.88-1.81)
Both rooms excluding window[b]	**2.62(1.11-6.20)***	**2.48(1.36-4.50)****	1.02(0.61-1.71)

a: OR adjusted for gender, age, parental allergic symptoms, surrounding environment,parental smoking, pet, construction age, type of house, ventilation system and distributed area, and each dampness indicator was separately introduced in the model.
b: wall, floor, ceilling or closet
p-value: *** p<0.001, ** p<0.01, * p<0.05

Table 2 Adjusted odds ratio[a] and 95%CI for the association between dampness index[b] and children allergic symptoms.

Characteristics	Adjusted OR(95%CI)[a]		
	Current asthma(N=85)	Bronchial hypersensitivity (N=203)	Current rhinitis(N=974)
Dampness index in the living room			
0	1.0	1.0	1.0
1	0.65(0.32-1.30)	0.96(0.61-1.52)	1.26(0.94-1.68)
2	1.21(0.61-2.41)	1.18(0.73-1.90)	**1.57(1.14-2.16)****
3	1.75(0.83-3.68)	**1.74(1.03-2.92)***	1.44(0.98-2.09)
Dampness index in the children's bedroom			
0	1.0	1.0	1.0
1	0.71(0.35-1.45)	0.89(0.54-1.45)	0.99(0.73-1.34)
2	0.96(0.46-2.02)	1.23(0.74-2.03)	**1.41(1.01-1.97)***
3	**2.12(1.00-4.51)***	**1.99(1.17-3.41)***	1.43(0.97-2.11)

a: OR adjusted for gender, age, parental allergic symptoms, surrounding environment, parental smoking, pet, construction age, type of house, ventilation system and distributed area, and each dampness index was separately introduced in the model.
b:Dampness index was calculated for estimating by summing the presence or absence of three dampness indicators in each room.
p-value: *** p<0.001, ** p<0.01, * p<0.05

Table 3 Adjusted odds ratio[a] and 95%CI for the association between occupant's characteristics and children allergic symptoms.

Characteristics	Adjusted OR(95%CI)[a]		
	Current asthma(N=85)	Bronchial hypersensitivity (N=203)	Current rhinitis(N=974)
Humidifier in the living room			
No	1.0	1.0	1.0
Yes	0.68(0.38-1.23)	0.99(0.69-1.43)	1.01(0.79-1.31)
Humidifier in the children's bedroom			
No	1.0	1.0	1.0
Yes	**2.07(1.14-3.76)***	**1.76(1.15-2.70)***	1.33(0.95-1.86)
dehumidifier in the living room			
No	1.0	1.0	1.0
Yes	0.84(0.40-1.75)	1.16(0.74-1.84)	1.09(0.77-1.53)
dehumidifier in the children's bedroom			
No	1.0	1.0	1.0
Yes	1.69(0.87-3.28)	1.53(0.95-2.45)	0.90(0.62-1.31)
Laundry inside the living room			
No	1.0	1.0	1.0
Yes	1.01(0.62-1.63)	0.94(0.68-1.30)	1.05(0.84-1.31)
Laundry inside the children's bedroom			
No	1.0	1.0	1.0
Yes	1.58(0.91-2.74)	0.95(0.62-1.44)	1.08(0.81-1.45)

a: OR adjusted for gender, age, parental allergic symptoms, surroundings,parental smoking, pet, construction age, type of house, ventilation system, distributed area and visible mold, and each indicator was separately introduced in the model.
b: OR did not calculate
p-value: *** p<0.001, ** p<0.01, * p<0.05

Case-Control study for the Association Between Indoor Environmental Factors and Children's Health Problems in Japan – Part 2 Results of Measurements during Rainy Season and Winter

Hamada Kensuke[1], Yoshino Hiroshi[1], Hasegawa Kenichi[2], Abe Keiko[3], Ikeda Koichi[4], Kato Noriko[5], Kumagai Kazukiyo[6], Hasegawa Ayumi[7], Mitamura Teruaki[8], Yanagi U[9], Matsuda Asako[2], Takamatsu Mari[2], Ando Naoya[1]

1 Tohoku University, Department of Architecture and Building Science, Japan
2 Akita Prefectural University, Dept. of Archi.& Env. Sys. Faculty of Sys. Sci.& Tech., Japan
3 Institute of Environmental Biology, Japan
4 Nihon University, Department of Architecture, College of Science and Technology, Japan
5 Researcher, National Institute of Public Health, Japan
6 California Department of Public Health, Environmental Health Laboratory Branch, USA
7 Sumika Chemical Analysis Service, LTD, Japan
8 Ashikaga Instutute of Technology Department of Architecture, Japan
9 Kogakuin University, Department of Architecture, Japan

Abstract

In order to clarify the association between indoor environmental factors and children's health problems, indoor air quality was investigated during the winter and rainy seasons in Japan. The total of 209 houses was classified into case and control groups whether the child have allergy symptom or not. The number of the houses in case and control groups is 133 and 76, respectively. This survey included measurement of indoor temperature, humidity, the pollution of chemical compound and mite allergen (Der 1). These measurements were conducted in the living room and children's room. It was found that the excess rate of relative humidity 70% in the case group was higher than that of the control group. During rainy season, in most houses (87.5%) Der 1 concentrations exceeded the proposed thresholds of allergic sensitization. The Der 1 concentration of the case group was higher than the control group. It was concluded that the chemical concentration including HCHO was less than the recommended value in many houses. On the other hand, Der 1 exceeded the proposed thresholds of allergic sensitization in the winter and rainy seasons.

Keywords: Children's Health, Allergic Symptoms, Exposure Measurement, Aldehyde, VOC, Mite Allergen

Introduction

Recently, the total number of children affected by allergic diseases has increased in Japan. In order to clarify the relationship between indoor environmental factors and children's allergic diseases, epidemiological surveys for 4th and 5th grade primary school children have been carried out all over Japan since July 2007. In the Phase 2 survey, which surveys the building characteristics, the indoor environment, and factors related to the children's health were investigated using a questionnaire. From houses in the Phase 2 survey, some houses were selected for the houses investigated in the Phase 3 survey, in which the relationship between the indoor environment and children's health was investigated in detail by measuring the indoor environment of houses. This paper reports the results of the Phase 3 survey, which reveals the actual situations of indoor temperature, humidity, the concentration of the chemical compounds including formaldehyde, and the mite allergens. Moreover, the influence of the pollution concentration of these factors on the children's health were examined by the case-control study.

Objectives

(1) Surveyed houses

The measurements were conducted during the winter (November 2008 ~ March 2009) and rainy seasons (July ~ August 2009) in houses where occupants agreed to participate in the Phase 3 survey. These houses were selected from the prior questionnaire survey (Phase 2).

The number of surveyed houses varied depending on the prefecture and measurement items (Table 1). Temperature and humidity were measured in 104 houses during the winter and in 105 houses during the rainy season. Out of them, 68 houses were measured twice in both seasons. Concentrations of the chemical compounds were measured in 95 and 46 houses during the winter and rainy seasons, respectively. All houses measured in the rainy season had already been measured once in the winter. Concentration of the mite allergen was measured in 24 houses in both seasons. Out of them, 17 houses were measured twice in the winter and rainy seasons.

(2) Definitions of case and control groups

The case group includes the children who have the symptom of some allergic diseases evaluated by the ATS-DLD interview sheet (former Environment Agency)[1)] that is used for the preliminary questionnaire survey (Phase2). The control group includes children who have no symptoms at the time of investigation or used to have symptoms in the past. The case group accounted for 70% of the total houses investigated in both seasons.

(3) Measurement items

This survey included the measurements of indoor temperature, humidity, concentration of various chemical compounds in the air and concentration of mite allergens in the house dust. The measurement kits including measuring devices, such as temperature and humidity sensors with recorders (TR 72 U, T&D Corporation), two chemical samplers (VOC-SD and DSD-DNPH, SUPELCO, Inc.) were sent to each house. Residents were requested to set up the equipment in particular places. In some houses, investigators visited the house and collected the house dust from the floor surfaces using a vacuum cleaner. All measurements were conducted in the living room and the children's rooms.

(a) Indoor temperature and humidity

In winter, temperature and humidity were placed near the center (approximately 1.0 m above the floor surface) and northeast corner of both the living room and children's rooms. The total of measurement points per house is four. In rainy seasons, the sensors were placed only near the center of the living rooms and the children's room. The temperature and humidity were monitored for two weeks in the winter and four weeks in the rainy season. The data was recorded every 10 minutes during the measurement period.

(b) Chemical compound concentration

In order to measure the concentration of chemical compound in rooms, two chemical samplers were suspended from the ceiling and indoor air was absorbed passively in a period of 24 hours. These samplers were used for the measurement of volatile organic compound (VOC) and carbonyl compound respectively. After samplers were collected, the chemical concentrations were analyzed using solvent extraction and gas chromatography by the private company.

(c) Concentration of dust mite allergen

The house dust was collected for two minutes using a special vacuum cleaner from 1m^2 floor area. Concentration of Group1 allergens (i.e. Der f 1 and Der p 1) derived from mite excrement particles were analyzed using the ELIZA method by the private company.

(4) Statistical analysis

The factors which influence on allergic symptoms are clarified by the case-control study. Mann-Whitney U test was used for a statistical analysis method. The software SPSS 16.0J for Windows was used to run the analysis.

Results and Discussion

(1) Indoor temperature and humidity

Figures 1(a) and (b) show the statistical values of the temperature and the humidity of the living rooms and the children's rooms for both cases in winter. For the temperature shown in Figure 1(a), the mean value of the control group was higher than that of the case group in the living rooms and the children's rooms in both November and February. However, the average temperature of the case group was higher than the control group in December. Figure 1(b) shows the result of the relative humidity. Relative humidity for both groups in the children's room are higher than the living rooms through in these months. The average relative humidity of the case group exceeds the control group in December. Even though the mean value of relative humidity in the living rooms have similar values between both groups for the months of November and February, the difference between the maximum value and the minimum value was greater in the case group. Such tendency isn't limited to the relative humidity. It is also seen in the result of the temperature in February.

The ratio for the relative humidity exceeded 70%rh for the measurement period is divided into the case group and the control group. It is shown in Figure 2 with the percentile rank. The 70%rh excess rate in each house was calculated because it was reported that the high level of relative humidity that exceeded 70%rh will influence the growth rate of mold [2)]. As a result, relative humidity 70%rh excess rates of the vicinity of the center of the room and the northeast corner in the case group tend to be higher than those in the control group for both living rooms and children's rooms in the winter. Figure 2(a) illustrates the results for the northeast corners of the living room. The difference between the case and the control groups was big. It was confirmed that the relative humidity 70%rh excess rate of the case group is higher than that of the control group in 50% of the houses. This value of case group is statistically (t-test) significantly higher than the control group ($p<0.05$). It was found in Figure 2(b) that the overall values of the case group in the vicinity of the center of the living rooms during rainy seasons tend to be higher ($p<0.2$) than those of the control group..

(2) Chemical compound concentration

Table 2 shows the measurement results of the chemical compound concentrations in 95 houses (190 rooms) during the winter. The TVOC concentration was assumed to be a total value of the chemical compound identified in both the winter and rainy seasons. The

concentration was expressed as 0 μg/m^3 in the case that the measurement value was below the lowest values that were able to be detected. The Ministry of Health, Labour and Welfare in Japan indicated the guideline values of the chemical compounds concentrations shown in Table 2. There were some houses with values of acetaldehyde and p-dichlorobenzene exceeded the guidelines during the winter. The excess rate of acetaldehyde and p-dichlorobenzene was 30.0% and 3.7%, respectively. Other chemicals didn't exceed the guideline. The excess rate of TVOC was 17.4%.

Table 3 shows the measurement results of the chemical compound concentration in 46 houses (92 rooms) during the rainy season. There were few houses where formaldehyde, acetaldehyde and p-dichlorobenzene exceeded the guideline values. However the number of locations where the value exceeded was less than five points for each chemical compound. These excess rates were not high. On the other hand, for p-dichlorobenzene concentration, there was a house where the values were more than 5000μg/m^3. In this house, the high value of p-dichlorobenzene concentration was also measured in the winter. This house used mothballs in the living room and the closet. The child living in this house has atopic dermatitis, and it is possible that the existence of these sources of p-dichlorobenzene affect the symptom. The excess rate of the tentative target value of TVOC was 7.6%, and this value was lower than that of the rainy season.

Figure 3 shows the comparison of the measured concentrations between the case group and the control group during the winter. It was found that the mean TVOC concentration of the case group was higher than that of the control group. However, this result was not significant. For other chemical compounds, a significant difference between the case and the control groups was not also found. It was only seen that the mean formaldehyde concentration of the case group was significantly lower than that of the control group ($p<0.01$). The best explanation was that parents with children affected by allergic diseases likely tried to create better indoor environments for the children in order to reduce the symptoms. However, both values were lower than the guideline value. In the rainy season, there wasn't a significant difference between the case and control groups.

(3) Concentration of mite allergen (Der 1)

1) Winter season

Figure 4 shows the result of measuring the concentration of house dust mite allergen (Der 1) during winter. The WHO standard shows 2μg of the allergic subject Der 1 is a sensitization level. There were 11 houses where this value was exceeded (the excess rate: 45.8%). Among these houses, a high concentration value more than 10μg/g was detected in a house (aki-4) in Akita Prefecture. The child living in this house had serious rhinitis problem. It seems that high concentration value of Der 1 contributes to the symptom severity. In the houses where the standard value had been exceeded, the concentration value in the children's room was higher than that of the living room. The situation of an indoor environment in a bedroom with

a carpet, bedding and closet provide the appropriate environment for growth of the mites.

2) Rainy season

Figure 5 shows the measurment results of the concentration of dust mite allergen (Der 1) during the rainy season. There were 21 houses (87.5%) where the sensitization level was exceeded. It was found that the concentration of mite allergen in the rainy season is higher than that in winter. In many houses where the standard value had been exceeded, high concentration was measured in the children's room as the same as the situation of the winter investigation. A case house (aki-5) located in Akita Prefecture showed the highest concentration of mite allergen. There were carpet, stuffed toys and a garnish of bed used. In this house, the existence of these things was the cause for the growing of mites. These findings corresponded with the fact that the child living in this house also had severe allergy symptoms.

It is reported that the frequency of room cleaning is related to the concentration of mite allergens on the floor[3]. However, there is no relation between the cleaning frequency reported by residents and the concentration of mite allergens in both seasons.

Figure 6 shows the accumulation frequency of the Der1 concentration for the case and the control groups. It was found that the houses with high ranks of Der1 concentrations in both seasons belong to the case group. And measured values in the case group are generally higher than those concentrations of the control group in both seasons. However, a significant difference was not seen for the case group and the control groups in both seasons.

Conclusions

The epidemiological survey conducted to 4th and 5th grade primary school children gave the following findings. (1) The excess rate of the relative humidity (70%) in the case group was higher than that of the control group. (2) The value of the chemical concentrations didn't exceed the guideline values in many houses surveyed. (3)The concentration of the formaldehyde in the case group was significantly lower than that of the control group in the winter. However, both values were low compared with the guideline value. (4)The excess rate of the allergic sensitization threshold of the Der1 concentration was 45.8% and 87.5% in the winter and rainy season, respectively. (5)When comparing the Der1 concentrations, the case group tends to be higher than that of the control group. From these results, it is found that the concentration of the mite allergen often exceeds the standard values in many houses but the situation was not found in case of the chemical compounds. So, it is expected that the high concentration of the exposure the mite allergen was the causes of allergic deceases. From the result that the Der1 concentration of the case group tends to be higher than that of the control group, children's health might be influenced by the exposure to more mite allergens. Moreover, from the results that the excess rate of the relative humidity (70%) in the case group was higher than that of the control group, there is a possibility that a high humidity environment suitable for the growth of mold and mite was developed in the houses of the

children who had an allergic symptom. The indoor environmental factors that relates to such dampness may have influences on the symptom.

Acknowledgments

The authors like to thank the occupants of the investigated dwellings for their helpful cooperation. This project is conducted as a part of Research Project for Creation of Housing that Promotes Health and Well-being (Chair: Prof. Shuzo Murakami, Chief Executive, Building Research Institute). This study was supported partially by Japan Society for the Promotion of Science, Housing Research Foundation, TOSTEM Foundation for Construction Materials Industry Promotion and the Kajima Foundation's Research Grant.

References

1. Japan Public Health Association：Environment Agency consignment business report in 1978, Research on influence on health investigation technique due to air pollution -Research on new method of epidemiological surveillance-, 1979.

2. U Yanagi, Koichi Ikeda: A STUDY ON THE BEHAVIOR AND CONTROL OF MICROBIAL CONTAMINATION IN AN AIR CONDITIONING SYSTEM : Part 1 Growth environment and contamination status of microbes, Architectural Institute of Japan plan system thesis collection, No.593, 49-56, 2005.

3. Seung-Hyun Cho, Tiina Reponen, David I.Bernstein, Rolanda Olds, Linda Levin, Xiaolei Liu, Kimberly Wilson, and Grace LeMasters：The effect of home characteristics on dust antigen concectrations and loads in homes, NIH Public Access, 371(1-3), 31-43, 2006.12

Table 1 Number of surveyed houses in prefectures

Prefectural and city governments	Temperature,humidity		Chemical compound		Dust mite allergen (Der 1)	
	Winter	Rainy season	Winter	Rainy season	Winter	Rainy season
Hokkaido	3	4	3	3		
Aomori		7				2
Iwate	3	4	3	1	3	3
Miyagi	4	7	4	4	3	5
Fukushima		2				
Akita	13	11	13	11	10	7
Yamagata		6				
Tochigi		3				1
Gunma		3				1
Saitama	15	11	15	9	8	5
Chiba	49	29	46	18		
Kanagawa	3	1	2			
Niigata	3	6	3			
Shizuoka	4	1	3			
Wakayama	7	4	3			
Hyogo		6				
total	104	105	95	46	24	24

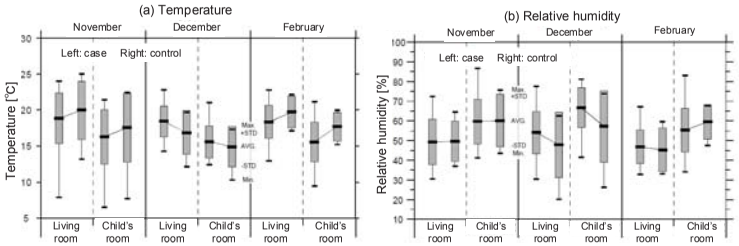


Fig. 1 Statistical values of the temperature and the humidity

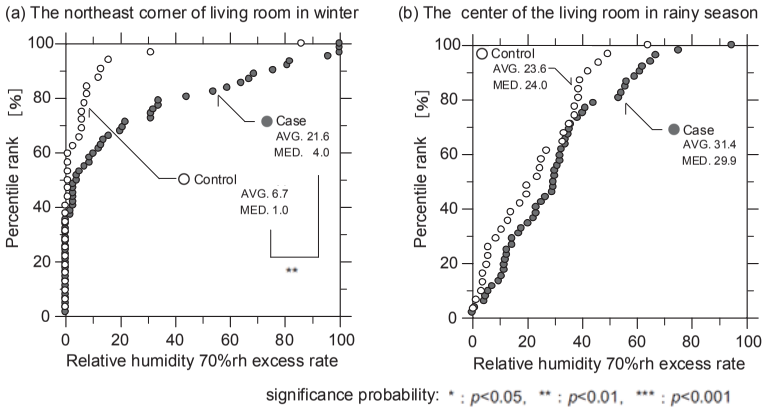


Fig. 2 Percentile rank of relative humidity 70%rh excess rate

Table 2 Measurement results of chemical compound concentration in the winter

	N=190		Indoor concentration (μg/m³)						guideline value in Japan
	Number of detection	Rate of detection	Max	Minimum	Average	Median	Number of excess	Rate of excess	
Formaldehyde	187	98.4%	51.0	0.0	14.4	12.0	0	0.0%	100
Acetaldehyde	190	100.0%	160.0	11.0	44.2	41.0	57	30.0%	48
Toluene	186	97.9%	88.0	0.0	13.1	10.0	0	0.0%	260
Xylene	170	89.5%	171.0	0.0	10.7	5.0	0	0.0%	870
Ethylbenzene	174	91.6%	50.0	0.0	4.0	3.0	0	0.0%	3800
Styrene	28	14.7%	5.0	0.0	0.3	0.0	0	0.0%	220
P-dichlorobenzene	141	74.2%	490.0	0.0	26.1	3.0	7	3.7%	240
TVOC	190	100.0%	1550.0	45.0	291.5	225.0	33	17.4%	400

Table 3 Measurement results of chemical compound concentration in the rainy season

	N=190		Indoor concentration (μg/m³)						guideline value in Japan
	Number of detection	Rate of detection	Max	Minimum	Average	Median	Number of excess	Rate of excess	
Formaldehyde	92	100.0%	146.0	6.1	31.8	25.7	1	1.1%	100
Acetaldehyde	68	73.9%	71.4	0.0	11.5	8.7	2	2.2%	48
Toluene	88	95.7%	125.3	0.0	21.9	17.7	0	0.0%	260
Xylene	17	18.5%	169.3	0.0	8.0	0.0	0	0.0%	870
Ethylbenzene	22	23.9%	42.0	0.0	2.8	0.0	0	0.0%	3800
Styrene	0	0.0%	0.0	0.0	0.0	0.0	0	0.0%	220
P-dichlorobenzene	8	8.7%	5510.0	0.0	84.6	0.0	4	4.3%	240
TVOC	92	100.0%	5757.8	21.1	220.7	90.4	7	7.6%	400

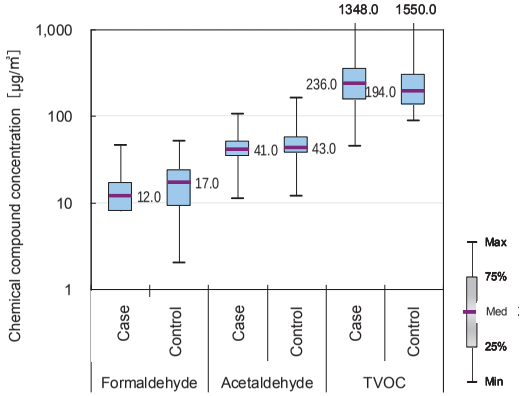


Fig. 3 Statistical value of the chemical compound concentration in winter

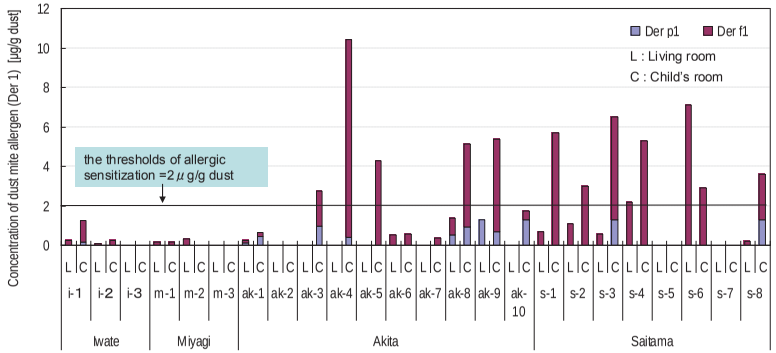


Fig. 4 Concentration of dust mite allergen (Der 1) in the winter

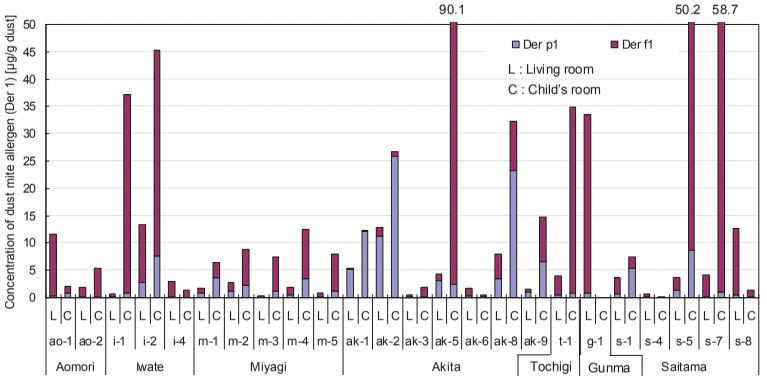


Fig. 5 Concentration of dust mite allergen (Der 1) in the rainy season

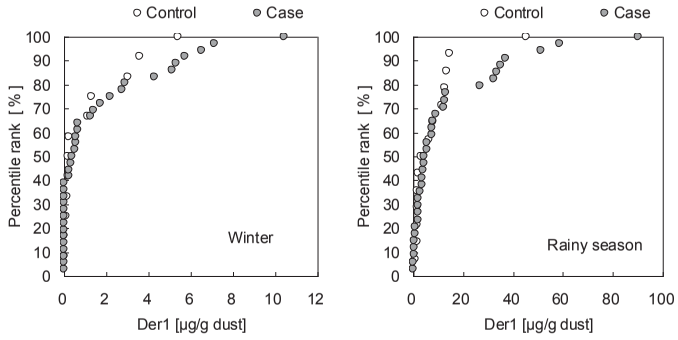


Fig.6 Percentile rank of concentration of dust mite allergen (Der 1)

A Study on Incomplete Ventilation in High-Rise Residential Buildings

Jungmin SEO[1], Sungmin YOON[1], Joonghoon LEE[2] and Doosam SONG[3]

[1]Graduate School, Sungkyunkwan University, Suwon, Korea
[2]Institute of Technology, Samsung C&T Corporation, Seoul, Korea
[3]Dept. of Architectural Eng., Sungkyunkwan University, Suwon, Korea

Abstract

Guideline for ventilation to improve indoor air quality in apartment housings in Korea was recently enacted and natural or mechanical ventilation system has become mandatory. Meanwhile, as the height of residential buildings goes up, the performance of ventilation system is influenced by stack effect especially in winter. This study is to review how stack effect influences ventilation system in high-rise residential buildings through simulations.

Keywords: High-rise Residential Buildings, Stack Effect, Ventilation System

Introduction

As global warming recently drew attention as an international problem, there is a growing interest in reduction of energy consumption and CO2 emission in Korea. In these social trends, there are growing efforts to reduce energy consumption in buildings. Similarly, there have been a lot of efforts to use natural power rather than mechanical power in ventilating buildings. But, as the height of apartment housings goes up, the effect by stack effect on buildings is growing in winter. Stack effect has effect on ventilation systems of high-rise residential buildings as well and there is a difficulty in securing enough performance of ventilation systems. For instance, due to stack effect, there is a difficulty in air supply and exhaust at part of building respectively above and below neutral pressure level.

Therefore, the aim in this study is to verify the influence and characteristics of stack effect on existing ventilation system in high-rise residential buildings and it will be used as reference data for improving the problem.

The research method in this study is to investigate existing ventilation systems used in apartment buildings in Korea and to quantitatively examine the influence of stack effect on the ventilation in high-rise residential buildings using simulation.

Target Building and Ventilation System Overview

1) Target building overview

Figure 1 shows a floor plan of the target building which is typical residential building plan in Korea. The target building of 58m high has 20 stories with 2.9m of floor height. Each floor has two apartments sharing a hall and stairways and elevator are across the hall.

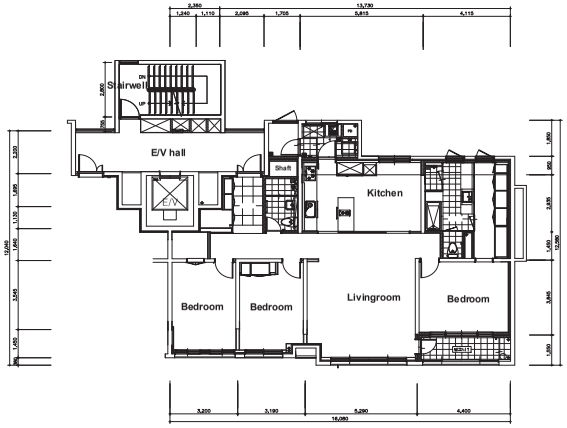


Fig. 1 Floor plan of the target building

2) Ventilation method and ventilation system overview

a) Natural ventilation system

Figure 2 shows a natural ventilation system installed in the balcony window frame. This kind of window is being additionally installed because the laws exclude doors and windows from a natural ventilation system and thus. The natural ventilation system has a natural ventilating opening, which manually or automatically opens, and a filter to remove outdoor dust.

The laws require that a natural ventilation system shall satisfy the ventilation rate of 0.7 times per hour by passing tests such as simulation, mock-up test or real-size test [1]. However, natural ventilation systems have difficulty in stably securing enough ventilation rates due to unstable outdoor wind speed or stack effect.

There are studies being conducted for the guidelines on performance test of natural ventilation systems [5].

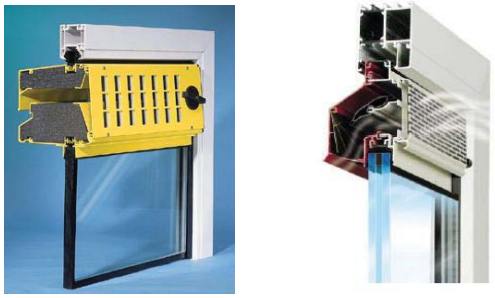


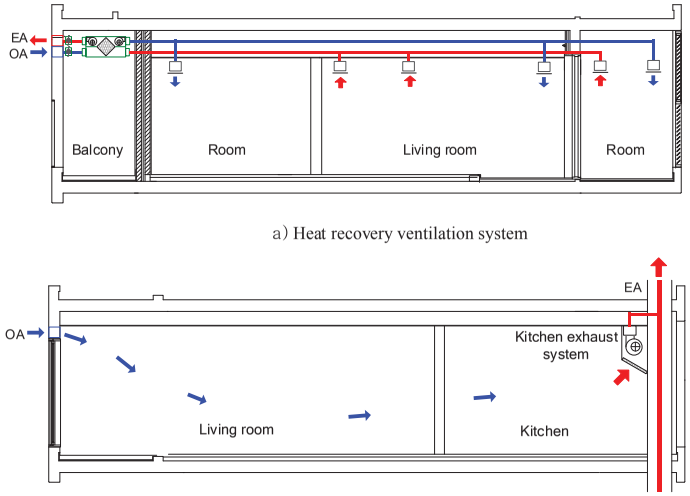
Fig. 2 Natural ventilation system

b) Mechanical ventilation systems

Figure 3-a) shows a heat recovery ventilation system. The heat recovery ventilation system is installed on the wall of balcony and outdoor air supply duct and indoor air exhaust duct are installed there. Air supply and exhaust distribution lines of heat recovery ventilation system are installed inside. The heat recovery ventilation system performs air supply and exhaust at the same time. Jang (2008) [2] measured the performance of heat recovery ventilation system installed in Korea for each brand.

Figure 3-b) shows a kitchen exhaust system. This ventilator emits indoor air exhaust by a kitchen exhaust system apparatus and natural or mechanical ventilator on the wall of balcony

is operated as well. Air exhaust from the kitchen exhaust system goes into a vertical air shaft and gets out of the building through air exhaust duct on the top of the building. However, there are reported problems that food smell from an apartment flowed back into another apartment through a kitchen exhaust system, causing displeasure.



a) Heat recovery ventilation system

b) Kitchen exhaust system

Fig. 3 Concept of mechanical ventilation systems

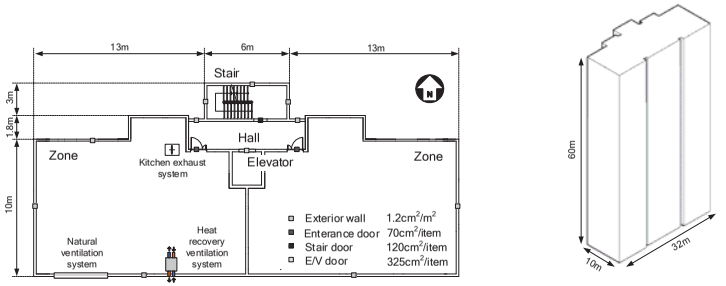
Review of Ventilation Rates and Airflow Characteristics for High-rise Residential Buildings through Network Simulations

This chapter covers airflow network simulations to quantitatively examine the influence of stack effect on the performance of ventilation systems.

1) Simulation overview

a) Simulation model overview

Figure 4 shows a simulation model for high-rise residential buildings. Two apartments, hall, stairways and elevator were modelled for each floor and partitions inside an apartment were ignored. ASHRAE data [4] and measurement data [3] in Korea were referred to for leakage area. Modelling for each ventilation system was conducted for each case.



a) A plane figure b) 3D view

Fig. 4 Simulation model overview

b) Simulation case and input conditions

Table 1 shows a simulation case. Case 1, 2 and 3 are respectively for natural ventilation system, heat recovery ventilation system and kitchen exhaust system. Table 2 shows simulation input conditions. Outdoor temperature condition examined is the temperature of

the coldest day according to weather data. Indoor temperature was assumed at 22℃ due to heating. The temperature of stairways and elevator hall was assumed at 15℃ because they are not air-conditioned. Measurement data [3] and ASHRAE data [4] were referred to for leakage area of exterior walls. Leakage area was inputted as 0m, 1.5m and 3m to consider the variation in infiltration rate according to indoor and outdoor pressure difference for each height on the wall.

Indoor air pollutant is assumed as CO2 generated by residents' breathing and each residence was assumed to have four adult residents. Discharge coefficient of natural ventilation system was assumed at 0.05 m^3/s/Pa to satisfy the ventilation rate of 252 CMH under the pressure difference of 2 Pa based on the research result by Kim (2008) [5]. Kim (2008) [5]'s research shows that even if there were differences among natural ventilation system products, discharge coefficient of natural ventilation system was in the range of 10~25 m^3/h/Pa for the length of 500 mm.

For heat recovery ventilation systems the one showing the best result of fan performance curve as a result of Jang (2008) [2] research was selected. For the kitchen exhaust system, fan performance according to company catalogue was used.

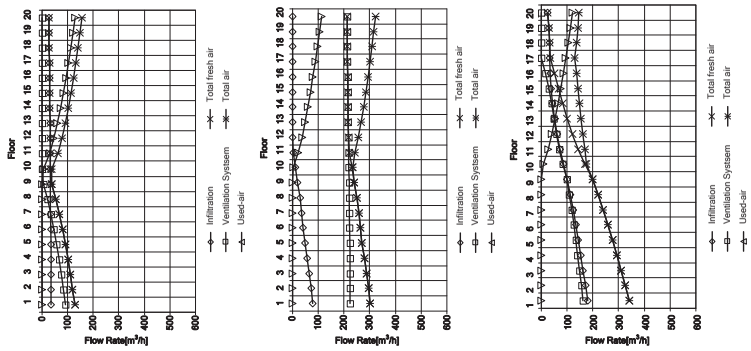
Table 1 Simulation case

	Ventilation system type	Ventilation type
Case1	Natural ventilation system	Natural ventilation
Case2	Heat recovery ventilation system, air supply and exhaust	Mechanical ventilation
Case3	Natural air supply + Kitchen exhaust system	Mechanical ventilation

Table 2 Simulation conditions

Items	Conditions		Remarks
Temperature	Outdoor temperature: -11.3℃ Indoor temperature: 22℃ Non-air conditioned (stairwell, elevator hall): 15℃		Suwon region Weather data
Leakage area	Outer wall(including windows)	1.2 ㎠/㎡	Jo (2007) [3]
	Entrance on the first floor	70 ㎠/item	ASHRAE[4]
	Entrance of each apartment	70 ㎠/item	ASHRAE[4]
	Elevator door	325 ㎠/item	Jo (2007) [3]
	Stairwell door	120 ㎠/item	Jo (2007) [3]
Air pollutant	CO_2 incurring location : all apartments from first floor to twentieth floor Number of residents: assumed as 4 CO_2 emission per person: 0.31[L/min] O_2 consumption per person: 0.373[L/min] Outdoor CO_2 concentration: 0.0005[kg/kg]		ASHRAE Standard 62-1999[6]
Natural ventilation system	$Q=C(\Delta P)^n$, 252 $m^3/h=C(2Pa)^{0.5}$, C= 0.05 m^3/s@1Pa, n=0.5 Front: 0.04 m^3/s@1Pa, Rear 0.01 m^3/s@1Pa, Installed height: 2.3 m		Kim (2008) [5] 13.9~35.78 m^3/h @2Pa, 0.5 m
Mechanical ventilation systems(Fig 3-a))	Heat recovery ventilation system, design capacity 250 m^3/h, pressure loss 150 Pa, Installed height : 2.3 m		Jang (2008) [2]
Mechanical ventilation systems(Fig 3-b))	Natural air supply device: 30 m^3/h@10Pa, 4 item Installed location: 2.3 m kitchen exhaust system catalogue referred to for fan performance data, Installed height: 1.5 m		Performance data provided by a company is referred to

2) Simulation results



a)Case1 b)Case2 c)Case3

Fig. 5 Flow rate for each ventilation method

a) Variation in airflow rate for each ventilation system

Figure 5 shows airflow rate for each apartment. Air supply and exhaust inside an apartment include infiltration through exterior walls, fresh air inflow from ventilation systems and used-air inflow through stairways or elevator halls. Air supply by infiltration and ventilation systems is called fresh air supply and if used-air is also added, it is called total air.

Case1 of natural ventilation system shows that the first and twentieth floors have 128.4 m^3/h and 156.1 m^3/h of total air, respectively, and the eleventh floor has 62.2 m^3/h of it, resulting in mid level having relatively smaller total air than lower or higher level. The first, eleventh and twentieth floors have 128.4 m^3/h, 26.2 m^3/h and 32.5 m^3/h of fresh air, respectively, resulting in relatively insufficient fresh air for mid and higher levels.

Outdoor air supply by natural ventilation systems is greater at lower level, but tends to go down towards higher level.

Case2 of heat recovery ventilation system shows that the first and twentieth floors have 302.6 m^3/h and 323 m^3/h of total air and the eleventh floor has 241.6 m^3/h of it, resulting in lower and higher levels having greater amount of total air than mid level. The first, eleventh and twentieth floors have 302.6 m^3/h, 211.3 m^3/h and 219.8 m^3/h of fresh air, respectively, tending to go down towards higher level. Outdoor air supply by heat recovery ventilation systems a little goes down towards higher level, but it is relatively consistent compared to natural ventilation system.

Case3 of kitchen exhaust system shows that the first, twentieth and eleventh floors have 342 m^3/h, 145.9 m^3/h and 168.3 m^3/h of total air, tending to decrease towards higher level. The first, twentieth and eleventh floors have 342 m^3/h, 24.6 m^3/h and 142.1 m^3/h, showing insufficient fresh air supply at higher level.

Figure 6 shows CO2 concentration variation for each ventilation method. Case1 of natural ventilation system shows the highest CO2 concentration of 3,709ppm at the tenth floor. This is because air supply is insufficient at mid level as shown in Fig. 5-a). Furthermore, due to absolutely insufficient fresh air supply as shown in Fig. 6-a), higher level shows higher CO2 concentration than lower level. However, higher level having lower CO2 concentration than

mid level seems to be because CO2 concentration was diluted by used-air from stairwell or E/V halls.

Case2 of heat recovery ventilation system shows small variation in CO2 concentration. This seems to be because air supply by ventilation systems is consistent and CO2 concentration of used-air went down by indoor air supply and exhaust.

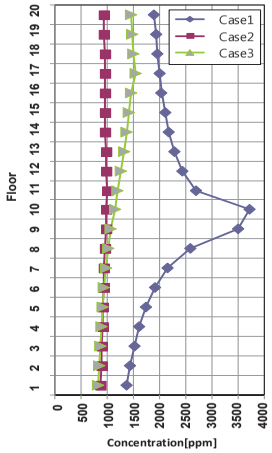


Fig. 6 CO_2 concentrations for each ventilation system

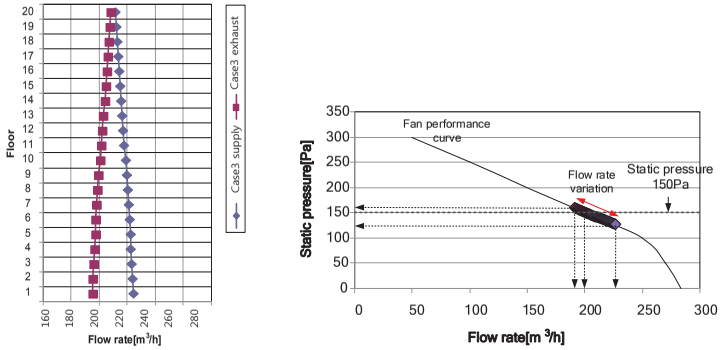
Case3 of kitchen exhaust system shows higher CO2 concentration at higher level than lower level. This is because fresh air supply goes down and used-air goes up towards higher level.

b) Change in fan performance of mechanical ventilation systems

Figure 7-a) shows air supply and exhaust of heat recovery ventilation system for each level.

Case3 shows that air supply goes down and air exhaust goes up towards higher level. This is because due to stack effect, static pressure is applied to indoor from outdoor to help air supply below the neutral pressure level and it is applied to outdoor from indoor above the level to help air exhaust.

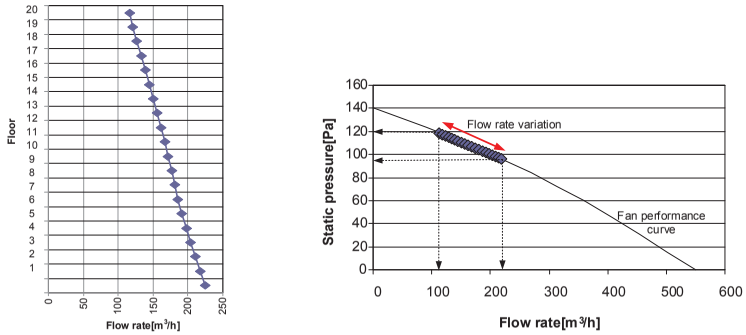
Figure 7-b) shows fan performance curves based on the results of Fig. 7-a). When duct static pressure loss was assumed at 150Pa, air supply should be 200 m^3/h in theory, but it was in the range of 195~224 m^3/h due to stack effect from the simulation result.



a) Supply and exhaust b) Change in fan performance

Fig. 7 Heat recovery ventilation system

Figure 8-a) shows air exhaust of kitchen exhaust system for each level. The first and twentieth floors have 224.1 m^3/h and 116.3 m^3/h of air exhaust, respectively, showing a great difference. Fig. 8-b) shows change in fan performance. Fig. 8-b) shows fan performance decrease towards higher level and it is because of the static pressure increase.



a) Air exhaust b) Change in fan performance

Fig. 8 Kitchen exhaust system

Conclusions

Due to growing concern for energy saving at buildings, there will be growing importance in using natural ventilation. In case of natural ventilation system, ventilation is different for each apartment if it is uniformly applied without considering stack effect.

Mechanical ventilation system showed relatively stable fan performance compared to natural ventilation system, but it is likely to be influenced by stack effect in greater degree as the height of buildings goes up.

Therefore, to secure enough fan performance for high-rise buildings, it is critical to figure out the characteristics of airflow occurring inside the high-rise buildings.

In this study ventilation rates and indoor pollutant concentration distribution were examined for high-rise residential buildings in Korea and then, the problems of existing ventilation systems were reviewed under stack effect in the winter. The results are as follows.

1) Natural ventilation system

Introduction of fresh air in the natural ventilation system is not enough in winter due to stack effect above the neutral pressure level in the building and indoor air pollution or dilution occurs due to used-air introduced into the indoor from the stairwell or E/V shaft as well. Indoor air quality may go poorer due to insufficient ventilation at mid level, and higher level is disadvantageous in securing sufficient fresh air because air supply is not sufficient and used-air constantly flows in through vertical shafts.

2) Mechanical ventilation system

Despite the use of mechanical ventilation systems in winter at high-rise residential buildings, fan performance changes for each level due to stack effect and resulting air pressure. Stack effect goes up towards higher level. Due to stack effect, air exhaust goes down towards higher level in case of kitchen exhaust system. In addition, indoor CO2 concentration increased due to decrease in fresh air supply at higher level.

Acknowledgments

This work was supported by the SRC/ERC program Most(grant R11-2005-056-02004-0) of the Sustainable Building Research Center.

References

1. Lee, Y. G., Kim, S. S., “Trends in the Korean Building Ventilation Market and Drivers for Change,” Air Infiltration and Ventilation Centre, 2008.

2. Jang, H. J., Hong, S. J., “A Study on the Performance of Heat Recovery Ventilation system for Apartment Houses,” Journal of SAREK, Vol.20, No.1, 2008, pp. 26~34.

3. Jo, J. H., et al., “Characteristics of Pressure Distribution and Solution to the Problems Caused by Stack Effect in High-rise Residential Buildings,” Building and Environment, Volume 42, Issue 1, 2007, pp. 263~277.

4. http://www.bfrl.nist.gov/IAQanalysis/CONTAM/libraries.htm.

5. Kim, S. S., Yee, Y. G., “A Study on the Performance Characteristics and Ventilation Performance Evaluation of Natural Ventilators,” Journal of the Architectural Institute of Korea, Vol.24, No.12, 2008, pp. 295~302.

6. American Society of Heating, Refrigerating and Air-Conditioning Engineers, ASHRAE Standard 62.1-1999: Ventilation for Acceptable Indoor Air Quality, 1999.

7. Khoukhi, M., Yoshino, H., Liu, J., “The Effect of the Wind Speed Velocity on the Stack Pressure in Medium-rise Buildings in Cold Region of China,” Building and Environment 42, 2007, pp. 1081~1088.

Measured Duct Leakage and Resulting Envelope Pressure Differences

Paul W. FRANCISCO[1], Scott PIGG[2], Collin OLSON[3], and Bob DAVIS[4]

[1] University of Illinois at Urbana-Champaign, Building Research Council, Champaign, IL
[2] Energy Center of Wisconsin, Madison, WI
[3] The Energy Conservatory, Minneapolis, MN
[4] Ecotope, Inc., Seattle, WA

Abstract

As concern about IAQ has increased, forced-air distribution systems are being viewed as a potentially important factor in preventing the transport of indoor and outdoor pollutants. Duct leakage can be a confounding factor in attempts to use the forced-air system for this purpose. Leakage from outside into the return side of the system brings outdoor air directly into the distribution system through the leak. Supply leakage depressurizes the house which increases infiltration of outdoor air through the envelope. This paper presents results from three projects on field measurements of duct leakage, covering 77 homes in three regions of the U.S.: the Pacific Northwest, Wisconsin, and Central Illinois. These homes range in age from new to over 100 years old. Changes in house pressures due to duct leakage are reported. Duct leakage results are also compared to predicted changes in infiltration based on blower door results and infiltration models.

Introduction

Reduction of air leakage through building envelopes is frequently pursued both as a means of reducing energy use and for preventing contaminants from entering the living space. Typically, this takes the form of air sealing unintentional holes between the living space and outdoors/unconditioned spaces and then providing mechanical ventilation, which allows the air from outdoors to be controlled and, if desired, filtered and/or tempered prior to entering the occupiable space.

As buildings are made tighter, unbalanced airflows have a greater impact on pressure differences between indoors and outdoors as well as between interior zones. Unbalanced flows often take the form of exhaust ventilation or supply ventilation, which are intentional and can be shut off when desired to manage envelope pressures. Unbalanced airflows can also take the form duct leakage in forced-air conditioning systems, which is unintentional. This leakage can either pressurize or depressurize the building relative to outdoors, depending on whether the leakage is greater on the supply or return side. Unbalanced duct leakage can therefore increase the challenge of controlling both pressures and airflows within buildings in order to manage the indoor environment.

This paper presents data that show the influence of duct leakage on building pressures for varying levels of envelope leakage in 77 residential buildings in the United States. While it is generally understood qualitatively that duct leakage can cause pressure changes across the building envelope, and that tighter buildings are more subject to pressure changes from unbalanced flows, these results demonstrate these issues quantitatively. More details of each of these studies can be found in the project final reports[1,2,3].

Methodology

The primary data required for this evaluation are the leakage of the building envelope, the supply and return duct leakages to and from outside, the volume of the house, and the changes in house pressure caused when the air handler for the forced-air system operates. For the evaluation of the impact of duct leakage to inside in homes with basements an assessment of leakage to inside is also required.

A common method of assessing duct leakage to outside is the duct pressurization test, which uses what is essentially a small blower door attached to the duct system with all of the registers or grilles sealed. The test is traditionally performed at a duct pressure of about 25 Pa. When the ducts are pressurized the flow through the fan is an estimate of the leakage at the pressure in the duct system. If a blower door is used to simultaneously pressurize the house to the same pressure as the duct system, then the leakage between the ducts and indoors is eliminated and the remaining measured leakage is to outside only. However, this leakage estimate is unlikely to replicate normal operating conditions and may over- or underestimate the leakage depending on whether the 25 Pa duct pressure is greater or less than the pressure in the ducts at the leaks under normal air handler operation.

As a result, a different method of estimating duct leakage to outside was used for the primary analysis in this paper. This method, called the nulling test, estimates leakage to outside only under normal operating conditions. The basic principle behind the test is to "null" out the pressure change caused by the operation of the air handler fan using a calibrated fan in the building envelope. In principle, a blower door could be used for this fan, but because of the generally very small envelope flows induced by the duct leakage the fan that was used was the same type of fan as is used for the duct pressurization test described above.

The nulling test has two components, one test to get unbalanced duct leakage (i.e. different between supply and return leakage) and one to get estimates of supply and return leakage separately. However, because it is the unbalanced leakage that determines the degree of pressure change due to air handler fan operation only that portion of the test is included in this analysis.

Pressures were measured across the envelope with and without the air handler fan operating. Data collection and fan speed control was automated. The duration of the measurement depended on the amount of wind present during the test. The pressure measurement period was determined largely qualitatively, with the focus being to measure for a long enough period to have the standard error of the envelope pressure measurement be about 0.3 Pa or less. This was generally achievable, but on particularly windy days this was not possible.

Test Sample

The sample presented here includes 50 homes from the Pacific Northwest (PNW, typically within one hour drive of Seattle), 16 from Wisconsin, and 11 from Central Illinois. The PNW and Illinois homes were primarily occupied homes, ranging from recently built to about 100 years old. The Wisconsin homes were all new homes, and most of them were built with the intention of qualifying for energy efficiency credits.

The homes were largely a sample of convenience, with limited physical characteristics required for participation. The PNW and Illinois homes were mostly chosen to have most or all ducts in unconditioned spaces such as vented crawl spaces or attics. The Wisconsin homes were chosen to have at least some ductwork outside of the conditioned space despite the fact that most homes in Wisconsin have all ducts within the conditioned space. Other than these physical characteristics, no effort was made to choose homes with known duct leakage.

Results

Table 1 shows several pertinent characteristics of the test sample, separated by project, including floor area, house leakage, and duct leakage characteristics. The Wisconsin study, being newer homes with most of the ducts located inside the conditioned space, had homes that were larger, tighter, and with less duct leakage to and from outdoors.

Figure 1 shows the change in house pressure caused by unbalanced duct leakage. This figure is broken into four different panels, each representing a different range of building airtightness levels. The upper left panel shows homes that have less than 4 ACH50. The lower right panel shows homes that are greater than 12 ACH50. The remaining two panels show intermediate ranges of airtightness, between 4 and 8 ACH50 for the upper right panel and between 8 and 12 ACH50 for the lower left panel.

These graphs show that the house pressure changes more rapidly with increasing unbalanced duct leakage for the tighter homes and much less rapidly for the leakiest homes. The two intermediate ranges are similar to one another.

The tightest homes were mostly from the Wisconsin study, which also tended to have modest leakage to outside because most of the ducts were in the basement. This limits the unbalanced duct leakage range for this portion of the data. However, there is still a definite trend of a substantially steeper relationship, and a regression of house pressure change on unbalanced duct leakage showed the steeper change to be statistically significant.

Regressions were done on all four of the subsets of data. All four regressions had constants that were not statistically significant, but the regression coefficients were all significant at the 95% confidence level. For the tightest homes, the regression coefficient was -0.020, meaning that the house pressure changed by 0.020 Pa for each cubic foot per minute of unbalanced duct leakage. For the two intermediate levels of house envelope leakage, the results were similar, with the 4 ACH50 to 8 ACH50 homes having a regression coefficient of -0.0077 and the 8 ACH50 to 12 ACH50 homes having a regression coefficient of -0.0081. The leakiest homes had a regression coefficient of -0.0042. These results suggest that the tighter homes have about 5 times the envelope pressure change as the leakiest homes for equivalent unbalanced duct leakage.

Table 2 shows estimates of outdoor air brought in to the home due to duct leakage. These estimates are based on a model developed by Palmiter and Bond[4] which has the feature of considering both the change in airflow through the building envelope and the additional air that comes in directly via the duct work. The portion of the model that accounts for the air that comes in directly through the ductwork uses the return leakage flow rate and then reduces that leakage rate by the fraction of the air handler flow that leaks to outside via leakage in the supply ducts. The estimated natural infiltration was estimated using the leakage from the blower door test and the procedures in ASHRAE Standards 119[5] and 136[6] to account for building height and local weather.

This table shows the expected trend of increasing natural infiltration with leakier building envelopes. It also shows that, on average, the tightest homes also had the lowest unbalanced duct leakage and the homes between 8 and 12 ACH50 had the highest unbalanced duct leakage. As stated previously, the tightest homes were usually the new homes in the Wisconsin study which had most of the ducts inside the conditioned space, so the result that the unbalanced duct leakage to and from outside is the smallest for this group is no surprise.

The trend in the additional outdoor air caused by duct leakage is comparable to the trend seen for the unbalanced duct leakage itself, with the low-unbalanced leakage duct systems of the tightest houses inducing little air and the high-unbalanced leakage duct systems of the 8-12 ACH50 homes having the most induced outdoor air.

The trend is very different with regard to average change in envelope pressure corresponding to these results, however. The leakiest houses, which averaged about six times the unbalanced duct leakage as the tightest houses, averaged a somewhat smaller house pressure change due to the duct leakage. The implication is that, had the tight homes had more ducts in unconditioned spaces and had those ducts been of comparable leakiness to the systems in the leakiest houses, the house pressure changes would have been much greater and had a much greater impact on attempts to manage house pressures.

Conclusions

This paper shows unbalanced duct leakage can cause substantial unintended changes in house pressure. Though the tightest homes in the study had the lowest average unbalanced duct leakage because most of the ductwork in these homes was within the conditioned space of the homes, the pressure changes resulting from unbalanced duct leakage were substantially higher in these homes for comparable levels of unbalanced duct leakage. This could have implications for airflow control using barometric dampers and drafting of atmospherically-drafted combustion appliances. Therefore, it is of great importance to ensure that duct systems in tight houses are also made to have low leakage.

References

1. Francisco, P.W., L. Palmiter, E. Kruse, and B. Davis. 2003. *Field Evaluation of Improved Methods for Measuring the Air Leakage of Duct Systems Under Normal Operating Conditions in 51 Homes*. Final report for the National Energy Technology Laboratory under contract DE-FC26-01NT41257.

2. Pigg, S. and P.W. Francisco. 2008. *A Field Study of Exterior Leakage in New Wisconsin Homes*. Energy Center of Wisconsin, Madison, WI.

3. Francisco, P.W. 2009. *Understanding and Reducing Uncertainties in the Delta-Q Test during Field Testing*. Building Research Council, Champaign, IL.

4. Palmiter, L. and T. Bond. 1992. "Impact of Mechanical Systems on Ventilation and Infiltration in Homes". Proceedings of the 1992 Summer Study Conference of the

American Council for an Energy-Efficient Economy, Pacific Grove, CA, vol. 2, pp. 205-216.

5. ASHRAE. 1994. *ASHRAE Standard 119 – Air Leakage Performance for Detached Single-Family Residential Buildings*. American Society of Heating, Refrigerating and Air-Conditioning Engineers, Atlanta, GA.

6. ASHRAE. 2001. *ASHRAE Standard 136 – A Method of Determining Air Change Rates in Detached Dwellings*. American Society of Heating, Refrigerating and Air-Conditioning Engineers, Atlanta, GA.

Table 1. Test home characteristics.

	Mean	Minimum	Median	Maximum
Floor Area, m^2 (ft^2)				
PNW	153 (1646)	65.7 (707)	151 (1626)	249 (2683)
Wisconsin	353 (3795)	127 (1372)	354 (3810)	586 (6306)
Illinois	157 (1687)	106 (1144)	167 (1800)	204 (2200)
House Leakage, m^3/s @ 50 Pa (CFM50)				
PNW	1.09 (2309)	0.36 (766)	1.00 (2109)	2.32 (4921)
Wisconsin	0.66 (1406)	0.17 (370)	0.65 (1374)	1.44 (3044)
Illinois	1.07 (2277)	0.56 (1181)	1.05 (2223)	1.51 (3193)
House Leakage (ACH50)				
PNW	11.0	3.8	9.3	29.0
Wisconsin	3.3	0.8	2.4	13.2
Illinois	10.3	6.7	11.1	14.7
Supply Leakage, m^3/s (CFM)				
PNW	0.049 (103)	-0.001 (-2)	0.041 (86)	0.168 (356)
Wisconsin	-0.006 (-12)	-0.088 (-186)	0.000 (1)	0.021 (45)
Illinois	0.080 (168)	-0.003 (-7)	0.064 (136)	0.181 (384)
Return Leakage, m^3/s (CFM)				
PNW	0.044 (92)	-0.019 (-40)	0.031 (66)	0.197 (417)
Wisconsin	0.006 (12)	-0.083 (-176)	0.003 (6)	0.086 (182)
Illinois	0.050 (106)	-0.006 (-13)	0.037 (79)	0.173 (367)
Unbalanced Leakage, m^3/s (CFM)				
PNW	0.005 (11)	-0.151 (-320)	0.010 (21)	0.140 (296)
Wisconsin	-0.011 (-24)	-0.080 (-169)	-0.005 (-10)	0.006 (12)
Illinois	0.030 (63)	-0.033 (-69)	0.016 (34)	0.119 (253)

Table 2. Estimated introduced outdoor air based on seasonal average weather, means per tightness group.

	Natural Infiltration, m^3/s (CFM)	Unbalanced Duct Leakage, m^3/s (CFM)	Added outdoor air due to duct leakage, m^3/s (CFM)	Average change in house pressure, Pa
ACH50 < 4	0.032 (69)	0.006 (13)	0.004 (9)	0.39
4 < ACH50 < 8	0.039 (82)	0.032 (67)	0.021 (44)	0.66
8 < ACH50 < 12	0.054 (113)	0.049 (104)	0.035 (75)	0.86
ACH50 >12	0.073 (154)	0.037 (79)	0.023 (48)	0.34

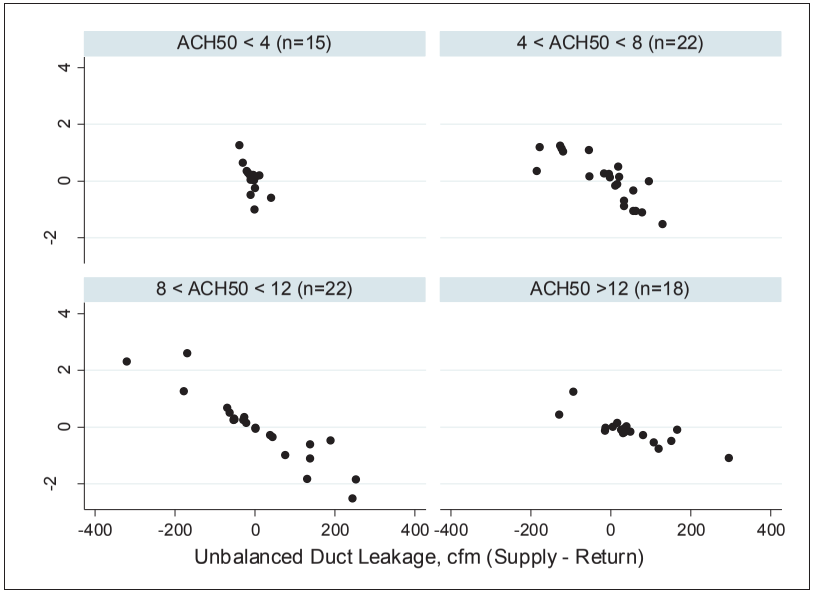


Figure 1. Change in house pressure vs. unbalanced duct leakage for 4 groupings of ACH50. Divide by 2119 to convert from cfm to m^3/s.

Calculation of Dehumidification Coefficients for Numerical Simulation of Desiccant Wheel

Yoshihisa MOMOI[1], Ryuichiro YOSHIE[2], Akira SATAKE[3], and Hiroshi YOSHINO[4]

[1] Division of Global Architecture, Graduate School of Engineering, Osaka University, Japan

[2] Department of Architecture, Graduate School of Engineering, Tokyo Polytechnic University, Japan

[3] Maeda Corporation, Tokyo, Japan

[4] Department of Architecture and Building Science, Graduate School of Engineering, Tohoku University, Japan

Abstract

In the previous study, a numerical method which simulates combined heat and moisture transfer process in solid desiccant materials was investigated. The calculation results successfully reproduced the cyclic process of the moisture adsorption and desorption. The validity of the numerical simulation method for the desiccant wheel was examined by the comparison between the experiment and the numerical simulation of the desiccant dehumidifier.

In this paper, it reports that the dehumidification performance of the desiccant wheel could be expressed as two dehumidification coefficients (effectivenesses of the dehumidifier) in the psychrometric chart, from the result of the air temperature and humidity before and behind the desiccant wheel. One is effectiveness for relative humidity, another one is effectiveness for enthalpy.

It was shown that the average temperature and humidity of the wheel outlet air were predictable without depending on the regeneration air temperature by using the effectivenesses of the dehumidifier.

Keywords: *Desiccant, Dehumidification, Numerical Simulation, Adsorption, Desorption*

Introduction

Desiccant dehumidifiers can remove moisture from air by using desiccant materials (absorbents such as silica gel), without cooling the air below its dew point. As the desiccant material absorbs moisture, it becomes saturated with water. Therefore, the desiccant material must be regenerated periodically. The regeneration air is heated to lower its relative humidity and dries the desiccant materials. In the case of a rotary wheel desiccant dehumidifier, a portion is being regenerated while the remainder is absorbing water for operating adsorption and regeneration at the same time. The wheel rotates between the adsorption part and the regeneration part.

In the previous reports [1, 2], the authors developed a numerical model of a desiccant wheel, derived the heat and moisture transport equations for the inside of the desiccant element. In addition, the authors measured equilibrium moisture content and moisture transfer coefficient, which are important parameters that determine the dehumidification performance. Moreover, numerical analysis inputting these measured values was conducted, and the validity of the numerical analysis was discussed, by comparing the calculation results with the experimental results of a desiccant system. This paper expresses the dehumidification performance of a desiccant wheel with two dehumidification coefficients (effectivenesses of the dehumidifier), by finding out the moisture absorption and desorption phenomena in the desiccant wheel. A

simplified numerical method for predicting the temperature and humidity of the air at the outlet of a desiccant wheel is discussed.

1. Heat and moisture transport equations in the desiccant wheel

As shown in Fig. 1, a desiccant wheel is cylindrical, and its cross-section has a corrugated honeycomb structure. Cutting out an infinitesimal volume from the wheel, a numerical model was produced with reference to the theory of the simultaneous transfer of heat and moisture proposed by Matsumoto [3] and Hokoi et al.

(1) Moisture balance equation for the air of the flow passage in the infinitesimal volume

$$\beta\rho_a \frac{\partial X_a}{\partial t} = -\beta u \rho_a \frac{\partial X_a}{\partial x} + \beta \frac{\partial}{\partial x}\left(\lambda_a' \frac{\partial X_a}{\partial x}\right) - \gamma \frac{\partial w}{\partial t} \quad \text{(Eq. 1)}$$

(2) Heat balance equation for the air of the flow passage in the infinitesimal volume

$$\beta C_a \rho_a \frac{\partial \theta_a}{\partial t} = -\beta u \rho_a C_a \frac{\partial \theta_a}{\partial x} + \beta \frac{\partial}{\partial x}\left(\lambda_a \frac{\partial \theta_a}{\partial x}\right) - \alpha S\left(\theta_a - \theta_d\right) \quad \text{(Eq. 2)}$$

(3) Heat balance equation for the desiccant material in the infinitesimal volume

$$\left(1-\beta\right) C_d \rho_d \frac{\partial \theta_d}{\partial t} = \left(1-\beta\right) \frac{\partial}{\partial x}\left(\lambda_d \frac{\partial \theta_d}{\partial x}\right) + L\alpha' S\left(X_a - X_b\right) + \alpha S\left(\theta_a - \theta_d\right) \quad \text{(Eq. 3)}$$

The moisture content of the desiccant material varies according to the moisture transfer, which is induced by the difference in absolute humidity between the desiccant material surface and the air of the flow passage. Accordingly, it can be expressed by Eq. 4.

$$\gamma \frac{\partial w}{\partial t} = \alpha' S\left(X_a - X_b\right) \quad \text{(Eq. 4)}$$

The above equation system has four equations and five variables X_a, X_b, θ_a, θ_d, and w, and so the equation system is not closed. Then, the system is closed by assuming the local equilibrium in which the absolute humidity and moisture content of the desiccant material surface immediately follow the equilibrium moisture content curve as expressed by Eq. 5.

$$w = f\left(X_a, \theta_a\right) = f\left(X_b, \theta_d\right) \quad \text{(Eq. 5)}$$

where it is assumed that there is no heat loss, air flow is laminar, pressure and flow rate are constant, and temperature and moisture content are homogeneous in the thickness direction of the desiccant material.

2. State variation of the desiccant material during the absorption and desorption processes

Based on the calculation results with the above mentioned numerical calculation model for a desiccant wheel, phenomena that occur in the desiccant wheel during the absorption and

desorption processes is discussed. As shown in Fig. 2, the desiccant wheel was divided into 20 parts in the flow direction for calculation. Calculation was conducted for the adsorption and desorption processes. In the adsorption process, the air with a temperature of 30 degrees Celsius and a relative humidity of 90 % flows from the left side. These values were given as boundary conditions in the left ends of the computational domain. In the desorption process, the air with a temperature of 70 degrees Celsius and a relative humidity of 6.4 % flows from the right side. It was assumed that wheel thickness was 100 mm, moisture transfer coefficient α'S was 3.5, rotational speed was 30 rpm, and air velocity u was 1.16 m/s (which corresponds to the air velocity when 100 m^3/h of air passes through a wheel with a diameter of 300 mm).

The moisture content of the desiccant element changes along the curve of the equilibrium moisture content expressed by Eq. 5, according to the relative humidity at the element surface. Fig. 3 shows the change in moisture content with time at the divided elements x = 1, 10, 20 during the absorption process. Fig. 4 shows the change in the moisture content distribution with time in the thickness direction of the wheel. When the rotational speed of the wheel is 30 rpm, the variation in the moisture content in each element is not so large. Accordingly, it can be concluded that in order to improve the absorption performance, it is important to use a material whose equilibrium moisture content curve has a large gradient and a material whose dehumidification speed is high, that is, moisture transfer coefficient α'S is large.

3. State variation of the air passing through the desiccant wheel during the absorption and desorption processes

This section is focused on the state variation of the air that is dehumidified and humidified by the desiccant wheel. The air passing through the wheel follows the psychrometric chart. When OA passes through the desiccant wheel in the adsorption process, the latent heat of the water vapor adsorbed by the desiccant material emerges as sensible heat. That means the heat of adsorption is generated with the phase change, as shown in Fig. 5. Accordingly, temperature and humidity vary along the isenthalpic line in theory. However, the desiccant wheel is actually exposed to the high-temperature RA until just before the dehumidification process, and so the heat transfer from the regeneration side to the adsorption side occurs. Therefore, the average temperature and humidity of SA at the outlet of the adsorption side become higher than those of the ideal isenthalpic process. In theory, the relative humidity of the dehumidified air SA is equal to that of RA, but in reality, the relative humidity of SA changes with time. It is because the amount of water vapor that can be absorbed by the desiccant material is finite, and the desiccant material becomes saturated with water. Accordingly, actual SA undergoes a different state variation from an ideal process. The state variation of the air in the desorption side is also different from the ideal process. This was also demonstrated by the results of the experiment carried out at Tohoku University.

4. Definition of dehumidification effectiveness

The ideal process for adsorption is shown on the psychrometric coordinates in Figs. 6 and 7. Process air enters the dehumidifier at a state designated by OA, is ideally warmed and dehumidified along the isenthalpic line, exiting the humidifier at the air state labeled SA(ideal). However, as mentioned above, the adsorption and desorption processes are not isenthalpic in reality because the process air and the desiccant material can't be completely dried in a rotary system. Thus, the dehumidification effectivenesses ε_{F1} and ε_{F2} can be expressed as deviation from the ideal process by the following equations [4].

$$\varepsilon_{F1} = \frac{F1_{SA} - F1_{OA}}{F1_{RA} - F1_{OA}} \quad \text{(Eq. 6)}$$

$$\varepsilon_{F2} = \frac{F2_{SA} - F2_{OA}}{F2_{RA} - F2_{OA}} \quad \text{(Eq. 7)}$$

where enthalpy and relative humidity are expressed with the coordinate variables $F1$ and $F2$ in the psychrometric chart. The dehumidification effectiveness for enthalpy ε_{F1} is defined as proportion of the difference between the enthalpy coordinate of SA ($F1_{SA}$) and OA ($F1_{OA}$) to the difference between that of RA ($F1_{RA}$) and OA ($F1_{OA}$). The dehumidification effectiveness for relative humidity ε_{F2} is defined as proportion of the difference between the relative humidity coordinate of SA ($F2_{SA}$) and OA ($F2_{OA}$) to the difference between that of RA ($F2_{RA}$) and OA ($F2_{OA}$). The dehumidification performance increases as ε_{F1} becomes smaller and ε_{F2} becomes larger.

Coordinate transformation is expressed by the following equations, as derived by Jurinak [5] for silica gel desiccant:

$$F1 = -\frac{2865}{T^{1.490}} + 4.344X^{0.8624} \quad \text{(Eq. 8)}$$

$$F2 = \frac{T^{1.490}}{6360} - 1.127X^{0.07969} \quad \text{(Eq. 9)}$$

where T is absolute temperature [K], and X is absolute humidity [kg-H_2O/kg-Dry air].

5. Calculation of dehumidification effectiveness

5.1 Dehumidification effectiveness calculated from the experiment results

Fig. 8 shows the measured variations in temperature and relative humidity at the outlet. When rotational speed is low (at 5 rph), heat transfer from the desorption side to the adsorption side is little and the air undergoes the isenthalpic change as a whole, and so ε_{F1} becomes small. However, the relative humidity of SA is as high as about 26%, and ε_{F2} becomes about 0.6, although ideal ε_{F2} is 1.0. On the other hands, when rotational speed is high (at 60 rph), the

relative humidity of SA decreases to 7.5 %, and so ε_{F2} becomes as high as about 0.9. However, the behavior of air deviates from the isenthalpic line, and ε_{F1} becomes large.

Figs. 9 and 10 show ε_{F1} and ε_{F2} calculated from the experiment results of Tohoku University, respectively. As regeneration temperature increases, ε_{F1} and ε_{F2} decrease slightly. As air flow rate increases from 100 m^3/h to 200 m^3/h, ε_{F1} decreases by about 0.1. This is considered because the heat transferred from the desorption side to the adsorption side is purged immediately when the air flow rate is large. In addition, as air flow rate increases, the relative humidity of SA becomes higher, and so ε_{F2} decreases.

5.2 Dehumidification effectiveness calculated with the numerical calculation model

By conducting the calculation with the numerical calculation model for a desiccant wheel, it is possible to calculate dehumidification effectivenesses under a broad range of conditions. Figs. 11 and 12 show the calculation results of the dehumidification effectivenesses under the assumption that wheel thickness is 100 mm, the temperature and relative humidity of OA are 30 degrees Celsius and 16.0 g-H_2O/kg-Dry air, and the temperature and relative humidity of RA are 60, 70, or 80 degrees Celsius and 16.0 g-H_2O/kg-Dry air. The dehumidification effectivenesses calculated from the numerical simulation don't vary significantly according to regeneration temperature as well as the experiment. As air flow rate increases, both of ε_{F1} and ε_{F2} decrease.

6. Conclusions

Based on the results of the calculation with the numerical calculation model for a desiccant wheel, the spatial distribution and time variation of the moisture content for the desiccant material and the variations in air temperature and relative humidity at the outlet of the desiccant wheel are clarified. And then it is indicated that by analyzing the variations in air temperature and relative humidity before and behind the desiccant wheel with dehumidification effectivenesses, it is possible to easily estimate the air temperature and relative humidity at the outlet of the desiccant wheel. For the future, dehumidification effectivenesses will be further generalized for air flow rate and rotational speed.

Acknowledgments

The authors gratefully acknowledge the New Energy and Industrial Technology Development Organization (NEDO) of Japan through the Project of Solar Energy and New System Technology Resources and Development for funding this research with contract number

05002503-0. Research members include Prof. Mochida, Dr. Takaki, Dr. Lun, Dr. Yonekura, Mr. Enteria (Tohoku University), Mr. Kawahara, Mr. Kubo (Maeda Corporation), Dr. Mitamura (Ashikaga Institute of Technology) and Mr. Baba (Earth Clean Tohoku).

References

1. Yoshie, R., Momoi, Y., Satake, A., Yoshino, H. and Mitamura, T., Numerical Analysis of Heat and Moisture Transfer in Desiccant Wheel for Dehumidification, Proceedings of Clima 2007 WellBeing Indoors Abstract Book, p.531, 2007.

2. Momoi, Y., Yoshie, R., Satake, A., Yoshino, H. and Mitamura, T., Performance Prediction of Rotary Desiccant Wheel, Proceedings of the 29th AIVC Conference, Volume3, pp.297-302, 2008.

3. Matsumoto, M., Simultaneous Heat and Moisture Transfer in Porous Wall and Analysis of Internal Condensation, Energy Conservation in Heating, Cooling, and Ventilating Buildings, Proceedings of 1977 International Seminar of Heat and Mass Transfer, Dubrounik, Vol.1, pp.45-58, 1978.

4. TRNSYS 16.1 User's Manual, 2006.

5. Jurinak, J.J., Open Cycle Desiccant Cooling – Component Models and System Simulations, PhD Thesis, University of Wisconsin, Madison, 1982.

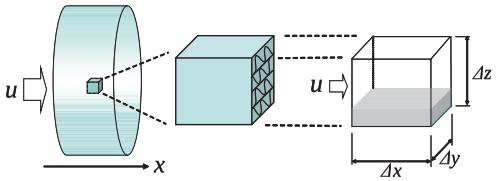


Fig. 1 Modeling of rotary wheel desiccant dehumidifier

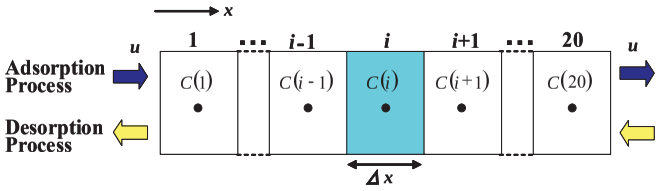


Fig. 2 Divided cells and boundary conditions

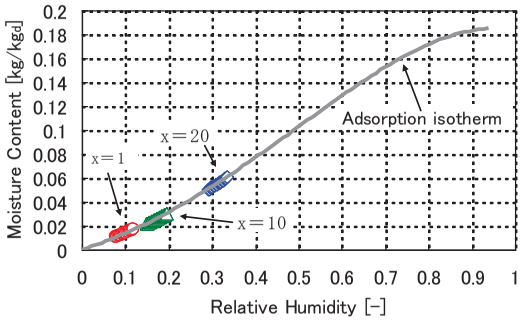


Fig. 3 State variation of the desiccant material on the absorption isotherm

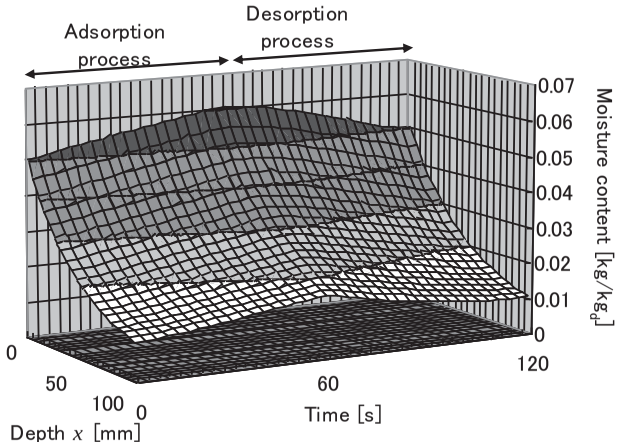


Fig. 4 Time variation of moisture content distribution

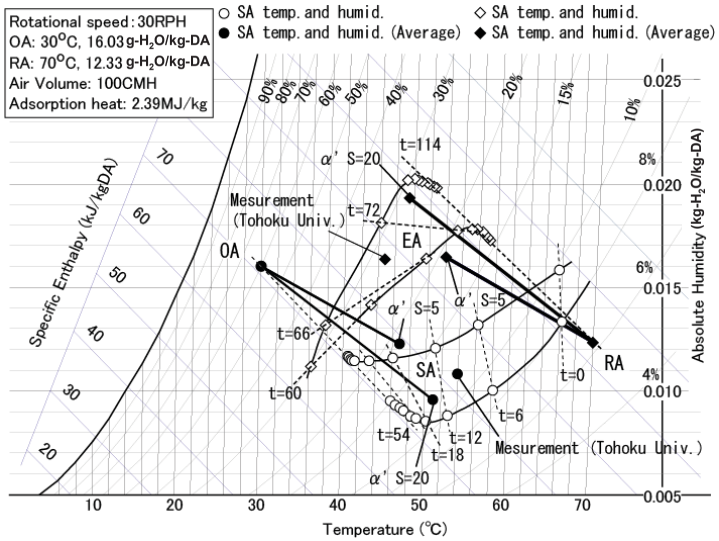


Fig. 5 Air temperature and humidity through the desiccant wheel

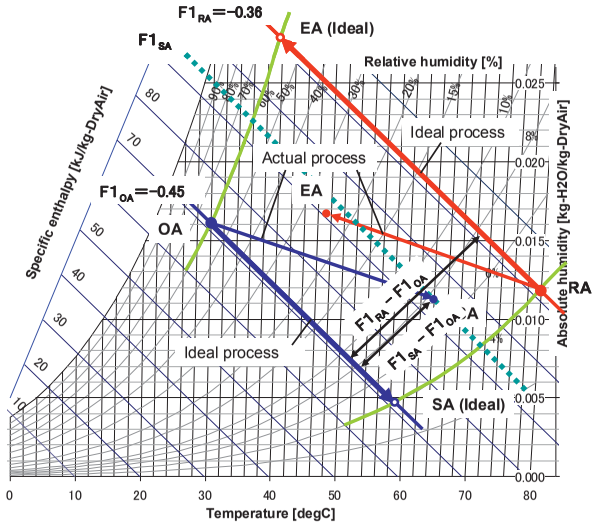


Fig. 6 Dehumidification effectiveness for enthalpy

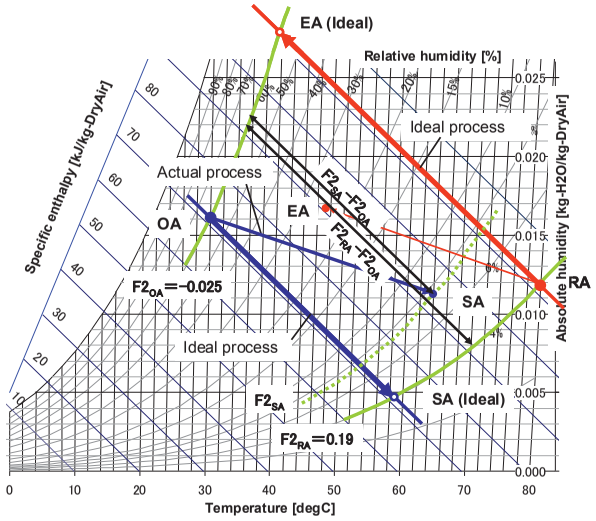


Fig. 7 Dehumidification effectiveness for RH

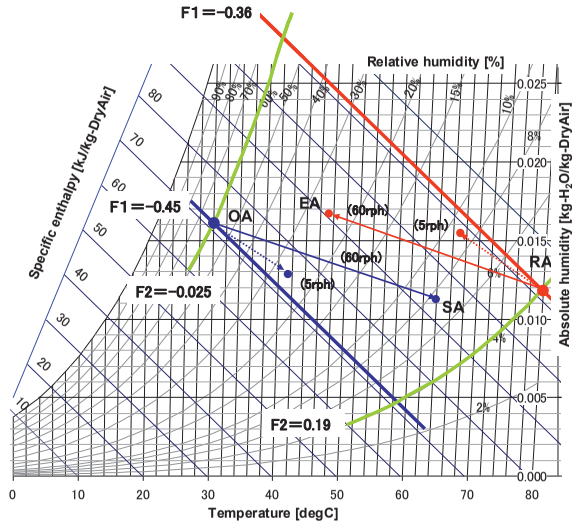


Fig. 8 Effect of rotational speed on humidification effectiveness

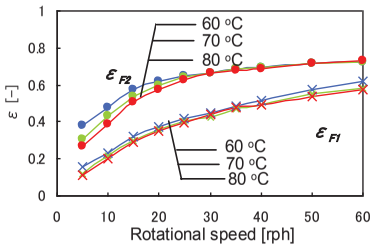


Fig. 9 Relation of rotational speed and dehumidification effectiveness (100 m^3/h)

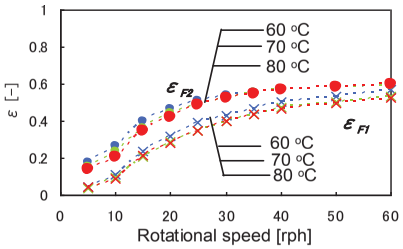


Fig. 10 Relation of rotational speed and dehumidification effectiveness (200 m^3/h)

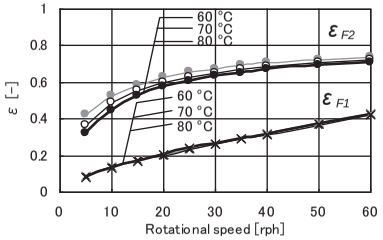


Fig. 11 Dehumidification effectiveness (1.0 m/s)

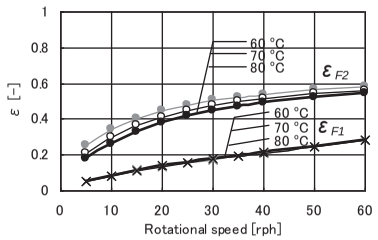


Fig. 12 Dehumidification effectiveness (2.0 m/s)

Nomenclature

ε: porosity (ratio of the air passage area to the cross-sectional area of a wheel) [-]
ρ_a: air density [kg/m^3] ρ_d: desiccant material density [kg_d/m^3] u: air velocity [m/s]
X_a: absolute humidity of flow passage air [kg-H_2O/kg-DA]
X_b: absolute humidity of desiccant material surface [kg-H_2O/kg-DA]
t: time [s] x: coordinate in the direction of the air passage axis [m]
λ_a': moisture conductivity of air [kg/{sm(kg-H_2O/kg-DA)}]
λ_d': moisture conductivity of desiccant material [kg/{sm(kg-H_2O/kg-DA)}]
γ: filling density of desiccant material (the mass of desiccant material per unit volume including the air passage) [kg_d/m^3]
w: moisture content (water vapor adsorption amount per unit mass of desiccant material) [kg-H_2O/kg_d]
α': moisture transfer coefficient on desiccant material surface [kg/{sm^2 (kg-H_2O/kg-DA)}]
α: heat transfer coefficient on desiccant material surface [J/(sm^2K)]
S: desiccant material surface area per unit volume including the air passage [m^2/m^3]
C_a: specific heat of air [J/(kgK)] C_d: specific heat of desiccant material [J/(kgK)]
θ_a: temperature of passage air [°C] θ_d: temperature of desiccant material [°C]
λ_a: thermal conductivity of air [J/(smK)]
λ_d: thermal conductivity of desiccant material [J/(smK)]
L: adsorption/desorption heat [J/kg]

Development of a heat pump system with the heat source network model using solar, ground and air heat source

Yujin NAM[1], Shinsuke KATO[2], and Ryozo OOKA[2]

[1] Research Fellow, Institute of Industrial Science, The University of Tokyo, Tokyo, Japan 153-8505
[2] Professor, Institute of Industrial Science, The University of Tokyo, Tokyo, Japan 153-8505

Abstract

In this research, a heat pump system with a heat source network is suggested which utilizes outdoor air heat, solar heat and ground heat as heat source for cooling, heating, hot water and refrigerating. This paper describes the summary of the suggested system and the results of the annual energy simulation. The heating and cooling loads, the electric consumption and the COP were calculated by TRNSYS 16 and evaluated in the cases of different local conditions and different system compositions. In the results, the superiority of the suggested system has been quantitatively evaluated comparing with the conventional heat pump system using one heat source. Furthermore, it was more significant in cold climate, in which the heating COP was 64% up compared the air source heat pump system, than it in subtropical climate, 46% up.

Keywords: heat pump system, heat source, network model, solar heat, ground heat source

Introduction

Recently, heat pump systems using solar heat or ground heat as a heat source have got a lot of attention for the use of renewable energy. These kinds of systems can achieve more energy-saving than conventional air source heat pump systems by utilizing more efficient heat source.

However, the performance of each system has the limitation of efficiency due to its dependence on the condition of local climate, geology, system composition, etc. In order to achieve more efficient performance, it is necessary to develop a heat pump system which adopts various heat sources and optimizes them. O.Ozgener and A.Hepbasli[1] have conducted performance analysis of heat pump system using solar and ground heat source for heating, and suggested that the combined operation can be more efficient in Mediterranean and Aegean regions of Turkey through the experimental study [2]. Furthermore, superiority of the solar-assisted ground source heat pump system has been confirmed by a parameter study with exergetic modeling [3]. W.B.Yang et al.[4] also calculated the performance of a solar-ground source heat pump system on the condition of various design and operation by numerical simulation. K.Miyauchi et al. [5, 6] developed multi-source and multi-use heat pump (MMHP) system, which utilize air, ground and solar heat sources in heating, cooling and hot water, and estimated the system performance by experimental analysis. However, there are few researches which quantitatively estimate superiority by local characteristic and design tool considering life cycle cost of the system. In order to design and operate such multi-source heat pump systems efficiently, it is necessary to develop the optimal design tool which can be applied to various conditions. In this research, a heat pump system with the heat source network using solar, ground and air heat sources has been developed in order to achieve greater energy-saving and utilize various heat sources optimally in a building. This paper describes about the developed network model and parameter analysis with a heat source network model.

System Summary

Fig. 1 shows a conceptual diagram of the heat pump system with the heat source network model using solar, ground and air heat sources. The system has solar heat collector, air heat exchanger and ground heat exchanger as the equipment of heat source, which are linked by water-loop piping. More effective heat source is selected by a control valve considering with temperature of heat sources and the circulation water of the selected heat source is supplied to the heat pump. Moreover, a thermal storage tank can be additionally used depending on the conditions such as the operation schedule, heat exchange rate, temperature level, etc. In order to keep the annual balance of heat use, the system introduces the multiple uses including heating, cooling, refrigerating and hot water.

Simulation Model

In order to develop a heat source network model and conduct the parameter analysis through the application to the various conditions, a simulation model use TRNSYS 16 (Transient

Systems Simulation Program) with heating and cooling calculation of multi-zone in this research. The water-to-water heat pump model (Type504) is combined with solar collector module (Type73) and ground heat exchanger module (Type557), and meet heating and cooling loads of a building. Fig.2 shows the performance curve of the heat pump. More effective heat source, which is a heat source of lower temperature in cooling and that of higher in heating, is selected by control valve. Fig.3 indicates the control system of heat source. In this paper, air-source heat pump system is not connected to the heat source network model yet, but the performance of only air heat source is calculated in same condition by another model with air-source heat pump system model (Type665).

Calculation Summary

Fig.4 shows a building model (floor plan and elevation partly in section of base floor), the object of space heating and cooling, which is assumed to 8 story office building (total floor space 6,600m^2). External walls consist of wall board (0.012m), polystyrene (0.025m), common concrete (0.35m), cement mortar (0.02m) and tile (0.008m). Internal walls consist of cement mortar (0.02m), common concrete (0.15m) and cement mortar (0.02m). Furthermore, ceilings consist stone (0.012m), wall board (0.009m), common concrete (0.15m) and floor (0.003m). Table 1 presents the condition of building load in this calculation. Indoor heat gain from occupants sets to sensitive heat of 75W and latent heat of 75W (ISO7730). Table 2 shows the calculation conditions in all cases. In this calculation, it is assumed that the heat pump system with solar heat collector and ground heat exchanger supply heating and cooling to two office area of base floor. The assumed locations are Sapporo (annual average temperature 9.1^{o}C) and Kagoshima (annual average temperature 18.9^{o}C) in Japan. Case studies are conducted to find out the system performance in each case and to confirm the superiority of the system using the heat source network. The solar heat collector (SHC) has 0.7 of the efficiency factor of collector fin, 0.28 [W/m^{2}K] of the heat loss factor and 0.8 of the absorptance of absorber plate. Furthermore, the ground heat exchanger (GHX) is the bore-hole type (concrete grouting) with single U-tube (inner diameter 27mm, depth 100m, thermal conductivity 0.41 [W/mK]). The effective thermal conductivity of soil sets to 1.30W/mK.

Calculation Results

Fig.5 and Fig.6 show the calculation results of heating (13th Jan.) in Case1 and Case 7 which include the temperature of ground and solar heat source, the electric consumption (E.C.) of heat pump and COP (coefficient of performance) of heat pump. They are the results of each 20 minutes, and the results of the other time are interpolated. In Sapporo, as shown in Fig. 5, around noon when solar radiation is high, the system uses solar heat source but, ground heat

source in most period. Consequently, the temperature of heat source and the COP of heat pump decreased in the end of operation, but the temperature of GHX became recovered after the operation stops. In the calculation of this period, average COP of heat pump with solar and ground heat source was 5.34, higher than that with only air heat source (2.17) and that with only ground heat source on same condition (4.58). However, in Kagoshima (Fig.6), even though the area of SHC sets to a half of Case 1, the higher temperature of heat source can be acquired due to higher solar radiation at Kagoshima (daily solar radiation 8.55[MJ/m^2]). Finally, the daily average COP with solar and ground heat source is 6.09, higher than that with only air heat source (2.78) and that with only ground heat source on same condition (5.61). Table 3 presents the results of parameter study. The average heating and cooling COP in all cases were calculated in respectively one month, heating from 5th Jan. and cooling from 4th Jul. In the results, the heating COP depends on both the area of SHC and the length of GHX, but the cooling COP depends on only the length of GHX due to lower temperature of ground heat source in summer. The COP of heating and cooling in Case 1, which has the largest SHC and the longest GHX, was higher than it in the other cases of Sapporo. Furthermore, the result of Cases 1 to 3 in which the length of GHX was changed, indicates that it affects on the cooling COP more significantly than the heating COP. Additionally, the difference of heating COP between Cases 3 and 5 (6.3%) was higher than that between Cases 1 and 4 (3.5%), because the length of GHX in Cases 3 and 5 was shorter than that in Cases 1 and 4, that means more dependent on the solar heat source. On the other hands, the COP of heating and cooling in Case 6 was higher than that in the other cases of Kagoshima. The COP of Kagoshima is higher in heating but lower in cooling than it of Sapporo because of higher solar radiation and annual temperature (ground temperature) in Kagoshima. Although Case 9 has a tenth area of SHC in Case 1, the heating COP of Case 9 is higher than it of Case 1. This indicates that it might be more efficient to install small SHC and balanced GHX in the location where solar radiation and annual temperature are high.

Conclusion

In this research, numerical simulation with a heat source network model has been conducted in order to estimate the superiority of the system using solar and ground heat source and develop the optimal design tool. In the results, the performance of the system has been calculated in various conditions, and it founds that the heating COP depends on both the area of SHC and the length of GHX, but the cooling COP depends on only the length of GHX. Furthermore, in the location where solar radiation and annual temperature are relatively high, it might be more efficient to install small SHC and balanced GHX. In the future, more detailed heat pump model which is suitable to the temperature level of solar and ground heat source will be developed by the specific of refrigerant and each device such as an evaporator,

a compressor, condenser, etc. Moreover, this research will consider various operation methods such as the ground thermal storage, the use of storage tank and the application for hot water and refrigerating.

References

1. Ozgener, O. and Hepbasli, A., "A review on the energy and exergy analysis of solar assisted heat pump systems, " Vol. 11, *Renewable and Sustainable Energy Reviwes*, 2007, pp.482~496.

2. Ozgener, O. and Hepbasli, A., "Performance analysis of solar-assisted ground-source heat pump system for greenhouse heating: an experimental study," *Building and Environment*, Vol.40, 2005, pp.1040~1050.

3. Ozgener, O., Hepbasli, A., and Ozgener, L., "A parametric study on the exergoeconomic assessment of a vertical ground-coupled (geothermal) heat pump system," *Building and Environment*, Vol.42, 2007, pp.1503~1509.

4. Yang, W. B., Shi, M. H., and Dong, H., "Numerical simulation of the performance of a solar-earth source heat pump system," *Applied Thermal Engineering*, Vol.26, 2006, pp. 2367~2376.

5. Miyauchi, K. Ooka, R., Nam, Y. J., Hino, T., and Harada, Y., "Feasibility Study and Development of Multi-Source and Multi-Use Heat Pump System," *10th REHVA WORLD CONGRESS, Clima 2010* (CD-Rom), Antalya, Turkey, 2010.

6. Harada, Y., Ooka, R., Sato, H., Nam, Y. J., Hino, T., and Miyauchi, K., "Real-scale Experiment of Multi-Source and Multi-Use Heat Pump System," *10th REHVA WORLD CONGRESS, Clima 2010* (CD-Rom), Antalya, Turkey, 2010.

7. Kjellsson, E., Hellström, G., and Perers, B., "Optimization of systems with the combination of ground-source heat pump and solar collectors in dwellings," *Energy*, Vol.35, 2010, pp.2667~2673.

8. Nam, Y.J., Kato, S., Ooka, R., and Lee, S.H., "Study on a heat pump system using heat source network model with solar and ground source; Development of simulation model," *Annual Conference of Architectural Institute of Japan* (CD-Rom), Toyama, Japan, 2010.

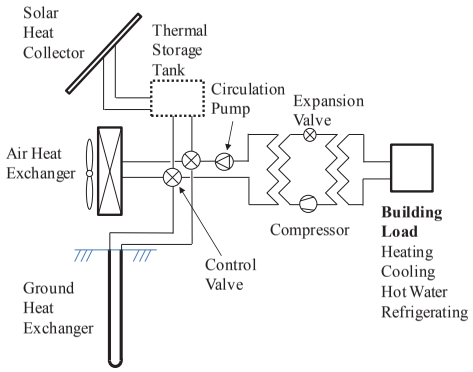


Fig. 1 Conceptual diagram of the heat pump system with heat source network model

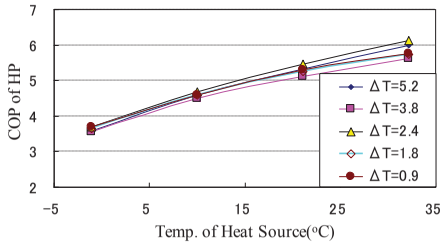


Fig. 2 The performance curve of a Heat pump

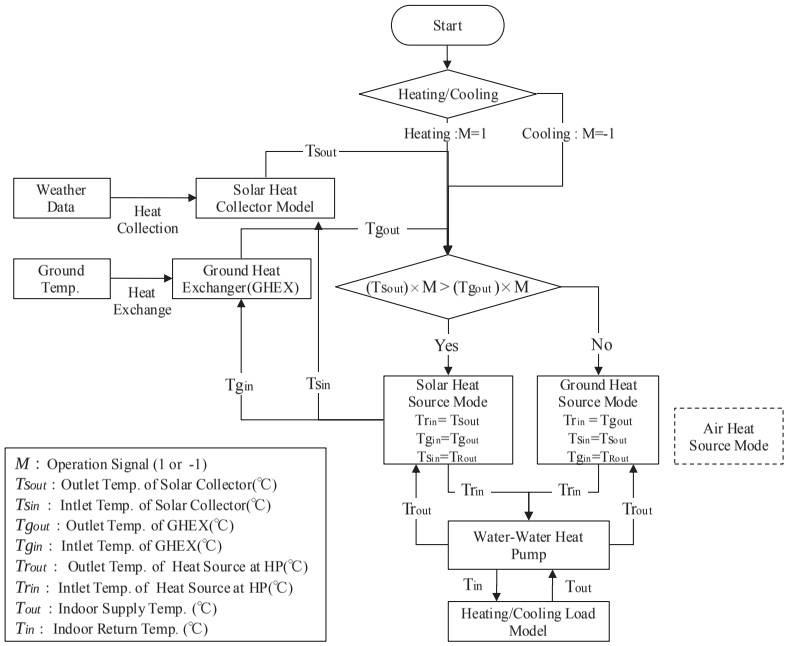


Fig. 3 The control system of heat source

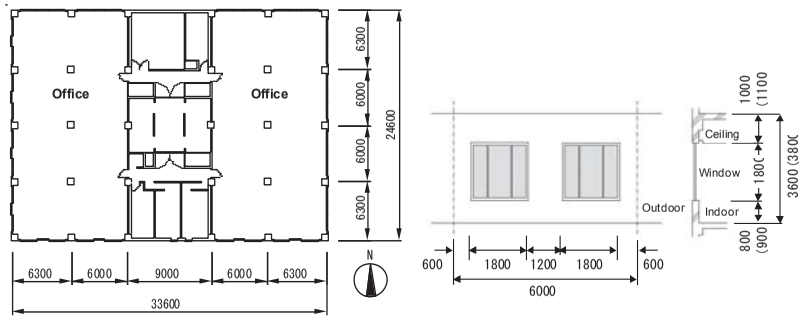


Fig. 4 Building model (floor plan and elevation partly in section of base floor)

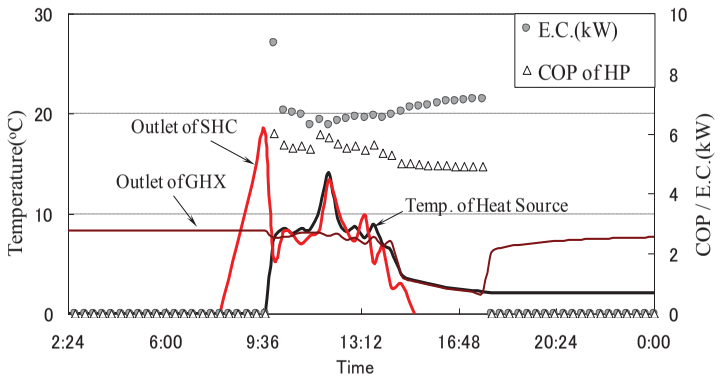


Fig. 5 Calculation result of heating (Sapporo, 13th Jan.)

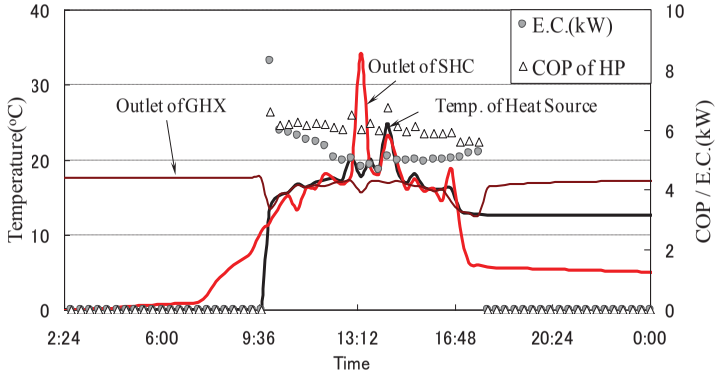


Fig. 6 Calculation result of heating (Kagoshima, 13th Jan.)

Table 1 Calculation Conditions

Location	Sapporo, Kagoshima (Meteonorm Data)
Design Temp. & Hum.	Summer 26°C, 50%, Winter 22°C, 50%
U-Value [W/m²°C]	External Wall 0.71 Glass 5.72 Internal Wall 3.70 Ceiling/Floor 3.08
Operation Time	9 A.M.~6 P.M.
Artificial Lighting Equipment Density of Persons	20 W/m² 10 W/m² 0.20 person/m²
Air Exchange Rate	1.2 Times/h

Table 2 Calculation Cases

Case	Location	Total Area of SHC [m²]	Total Length of GHE [m]
Case1	Sapporo	100	500
Case2	Sapporo	100	300
Case3	Sapporo	100	100
Case4	Sapporo	50	500
Case5	Sapporo	50	100
Case6	Kagoshima	100	500
Case7	Kagoshima	50	500
Case8	Kagoshima	20	500
Case9	Kagoshima	10	500
Case10	Kagoshima	10	100

Table 3 Calculation Results

Case	Location	Heating COP	Cooling COP
Case1	Sapporo	5.45	4.17
Case2	Sapporo	5.32	3.33
Case3	Sapporo	5.12	2.93
Case4	Sapporo	5.26	4.17
Case5	Sapporo	4.80	2.92
Case6	Kagoshima	5.93	3.73
Case7	Kagoshima	5.82	3.73
Case8	Kagoshima	5.73	3.73
Case9	Kagoshima	5.72	3.73
Case10	Kagoshima	5.32	3.08

Energy Saving Potentials of Dedicated Outdoor Air System in High-rise Apartment Buildings

Kim Min-Hwi[1], Kim Jin-Hyo[1], Kwon Oh-Hyun[1], Seok Yoon-Jin[1], Jin Jeong-Tak[1], and Jeong Jae-Weon[1]

[1] Sejong University, Dept. of Architectural Engineering, Seoul, Korea 143-747

Abstract

The main thrust of this paper is to investigate the optimized supply air condition and energy saving potentials of a dedicated outdoor air system (DOAS) applied to a high-rise apartment building. For a typical 132-m^2 apartment unit, it was assumed that two different systems, namely, a centralized DOAS integrated with ceiling radiant cooling panel (CRCP) and a decentralized energy recovery ventilator (ERV) operated with packaged air conditioner, were installed. The transient behavior and control characteristics of each system were modeled numerically using a commercial equation solver program and annual cooling coil load and heating load reduction potential of the two systems were compared. It was found in this research that a DOAS-CRCP system can reduce the cooling coil load by over 21% annually compared to the current energy recovery ventilator-packaged air conditioner pair. In addition, the use of DOAS can reduce the annual ventilation heating load by over 40% when the enthalpy wheel and the sensible wheel of the DOAS unit operate simultaneously. It was also found that the optimized dew point temperature of the DOAS supply air that accommodates the latent load of a space is 11~12°C.

Keywords: DOAS, high-rise apartment building, decentralized ventilation, centralized ventilation

Introduction

Over the last decade, the Korean market has witnessed the rapid planning and construction of high-rise apartment buildings as an alternative to reorganizing and expanding the urban residential environment. As a result of this trend, high-rise apartment building and a multipurpose building has become representative of Korean residential buildings and has become tighter and better insulated. With this development, the energy consumption owing to ventilation can become much greater than that caused by the heat transfer through the building shell. This increases the contradiction between improving the indoor air quality and reducing the energy used for ventilation. On the other hand, decentralized energy recovery ventilator and air-conditioning systems are increasingly being used in high-rise apartment buildings in Korea.

However, the operation of a typical decentralized air-conditioning system is not well understood. This is not because such systems are operated based on subjective decisions, but because building occupants are unknowingly worried about increasing their electric consumption charges and do not understand how to optimally operate a decentralized air-conditioning system to maintain a healthy indoor air environment [1, 2]. In addition, the maintenance of a decentralized air-conditioning system installed in a housing unit includes changing filters and washing a part of the energy recovery ventilator; this maintenance task is costly and time consuming. Therefore, to optimally control and maintain ventilation and air-conditioning system, there has recently been a gradual increase in interest to develop a ventilation system that can be controlled from a central station or a central plant. Compared with existing ventilation systems, a central ventilation system offers many advantages, as it

supplies a sufficient rate of ventilation and can be systematically and economically maintained. In addition, if a central cooling system is used with a central ventilation system, we won't need any additional air-conditioning plant room in each household and we will able to use more additional area in residential building.

The use of a dedicated outdoor air system (DOAS) [3], which has aroused increasing interest in the EU and North America as a high efficiency central ventilation system, is one of the ideal solutions to this issue. With the aim to solve the problems posed by such a system, this research determines the optimized supply air conditions and estimates annual cooling and heating energy consumption when DOAS is applied to a high-rise apartment building. In addition, the resulting energy savings, as compared with the operation of existing air-conditioning systems, are analyzed quantitatively.

Overview of dedicated outdoor air system (DOAS)

When many researchers finally realized that systems were largely based up on the sensible heat transfer function of air in an air-handling system, they began to propose a "decoupled system"; that is, one that decouples the ventilation and the air-conditioning function, or decouples the sensible and latent load functions. After the 1990s, this new concept of a decoupled system prompted much research in North America and the EU. The latent cooling load is always handled by a DOAS. When the sensible cooling load exceeds the maximum capacity of the DOAS, the radiant panels are activated in order to handle the remaining space sensible cooling load. When the total space cooling load exceeds the DOAS cooling capacity, the radiant panel system accommodates the remaining cooling load (Figure 1).

(1) Components of DOAS

In a DOAS/radiant panel cooling system, the entire latent load, a portion of the sensible load, and the OA ventilation cooling load are handled by a combination of the enthalpy wheel and the DOAS cooling coil, which working in series. The radiant panel system accommodates the remaining sensible load. A properly designed DOAS with a parallel sensible system can save considerable energy compared to a conventional system while always supplying the correct amount of ventilation air, as required by the ventilation rate standards, to each space. The components of a DOAS include an enthalpy wheel, a cooling coil, a sensible wheel, and a supply/return fan.

Energy savings for the conditioning of fresh air can be achieved by the application of a DOAS, in which the sensible and latent heat recovered from the exhausted air is transferred to the supply air. At present, two kinds of approaches are available for heat recovery ventilators: sensible heat exchangers, and an enthalpy wheel and sensible wheel. An enthalpy

wheel, which can save latent energy, is problematic due to its rotating moving parts. The OA enthalpy is reduced by the enthalpy wheel during the summer. An enthalpy wheel transfers the excess moisture and sensible heat contained in the OA stream to the relatively dry and cool exhaust airstream, reducing the energy consumed for heating and humidification. Silica gel and molecular sieves are the desiccants that are currently employed for enthalpy wheels. Enthalpy wheels with the familiar honeycomb matrix were made of aluminum, which has high heat transfer characteristics. In heat transfer, the excess moisture and sensible heat contained in the OA stream is transferred to the relatively dry and cool exhaust airstream, through the use of an aluminum wheel treated with a coating such as silica gel or molecular sieves (Figure 3).

A sensible wheel is simple and reliable, but it cannot recover latent energy and is not treated with a coating for the recovery of latent energy. Direct expansion coils or cold water coils are commonly used in cooling coils.

(2) Parallel system

A DOAS treats and supplies to the room only the required ventilation air at a constant volume. When a DOAS cannot handle the entire sensible load, an additional system is needed to handle the remaining cooling or heating load, to be operated along with a DOAS. In the case of Korea, existing residential buildings can use Ondol, which is used in current apartments as a parallel heating system in winter. There are also various parallel cooling systems that can be used in the summer: packaged air-conditioners, fan-coil units, etc. In this paper, it is assumed that ceiling radiant cooling panels are used, as their use with DOAS has received serious attention in investigations that focus on the improvement of their thermal and economic advantages [6, 7].

Estimation of supply air setpoint

The advantage of a DOAS when it is installed in a high-rise apartment building is that it maintains the indoor air quality (IAQ) and thermal comfort requirements by constantly providing the current required standard of ventilation air and removing the latent loads from the outside air (OA) intake and generating it in spaces using a 100% OA ventilation system. To remove the latent loads from the outdoor air intake, the dew point temperature (DPT) that is supplied to each household must be controlled. Consequently, this section addresses the selection of an appropriate DPT in the application of a central ventilation system to a high-rise apartment building.

(1) Determination of DOAS supply air rates

According to the standards of current Korean criteria for ventilation rates, a rate of 0.7 ACH is recommended for new or remodeled buildings that have more than 100 housing units. Therefore, ventilation rates are estimated using the current ventilation standard (Table 1). While the required ventilation for each space is estimated using the minimum ventilation rates recommended by ASHRAE Standard 62.1-2007, additional ventilation rate standards have recently been mandated for housing units that are higher than the 3rd floor. According to Standard 62.1, an apartment building requires 9 CMH of OA per person and 1.1 CMH of OA per unit floor area [4]. Figure 4 shows that the estimated design ventilation rates required for each space increase as the scale of an apartment grows larger; in addition, the difference between the required ventilation rates estimated by Korean standards and the ASHRAE standards increase.

(2) Determination of proper DPT of DOAS supply air during summer

During the cooling period, supply air must be removed from the latent load by the DOAS to supply the minimum required ventilation rates in each conditioned space, and the DPT of the supply air must be controlled in order to remove the latent load. Above all, the required supply air humidity ratio for each housing unit is calculated using Equation 1. This design is determined based on the indoor space latent load (Q_L), the required ventilation rates (V), and the indoor humidity ratio (W). The appropriate DPT can be obtained using a psychrometric chart to determine the humidity ratio of the supply air.

$$Q_L = 3.0 \times \dot{V} \times (W_r - W_\alpha) \quad \text{(Eq. 1)}$$

Where, Q_L = Indoor latent load (W)

$\dot{V}$ = Supply ventilation rates (l/s)

W_r = Indoor humidity ratio (g/kg)

W_α = Supply humidity ratio (g/kg)

Generally, the latent load in an indoor housing unit is produced by the residents, infiltration, and use of the kitchen and bathroom. Among these factors, the latent load from the residents and infiltration is easily estimated using the existing method of load calculation, but the latent load produced by a variety of lifestyles is not as easy to estimate as the patterned lifestyle that is assumed in the existing method. In addition, some of the humidity that is present indoors is absorbed by the furniture, the building interior, and a number of possible unexpected factors.

Therefore, the dryness of the supply air required for each space must respond to different latent loads, which in turn calls for a different quantity of supply air.

On the other hand, a review of the available literature shows various case studies that attempt to predict the latent load in terms of moisture generation per hour or per day for each space, as determined through testing and experimentation. However, most of these studies involve experiments of short duration and a limited experimental area. Above all, the most important problem faced in the use of these data is the lack of consistency in among the previous literatures test results.

In this research, the latent load for each apartment space is estimated using Equation 2 for the maximum predicted latent load equation released by ASHRAE Fundamentals [5]. The proper DPT for a DOAS system is also calculated based on this result.

24°C DBT, 50% RH was selected as the target space condition for setting the supply air DPT. This corresponds to 9.275 g/kg HR. Then, based on the above findings that predicted the maximum latent load using Equation 2 and estimated the supply air HR and DPT using Equation 1, the proper DPT of supply ventilation air for various apartment floor areas can be selected, as listed in Table 2.

$$Q_L = 20 + 0.22 \cdot A_f + 12 \cdot N_{oc} \quad \text{(Eq. 2)}$$

Where, A_f =Indoor floor area (m^2)

N_{oc} =Number of occupants

As listed in Table 2, the proper DPT range of DOAS SA is 11.6−12.2°C, with the application of a domestic ventilation standard and ASHRAE Standard 62.1 in various apartment floor areas during the summer. This means that if a DOAS system can provide a temperature of 11.6−12.2°C to each space, most of the latent load is removed and is controlled only through the provision of the required quantity of ventilation air in a 24-h period.

During the dry season, such as winter or an intermediate season, indoor air conditioning can be controlled without the need for any additional control by using DOAS or by additional humidification if necessary [8]. Therefore, in this research, SA DPT is only estimated during the summer.

(3) Determination of proper supply air temperature of DOAS

In a DOAS system, the supply air DBT is determined in order to reduce the sensible cooling load from the quantity of ventilation rates. In the summer, when the ventilation DBT that is supplied to each room is lower than that of the room condition, it not only increases the indoor comfort level, but also increases the effectiveness of the sensible cooling load (Eq. 3).

$$Q_{S,vent} = 1.23 \times \dot{V} \times (T_r - T_\alpha) \quad \text{(Eq. 3)}$$

Where, $Q_{S,vent}$ =Sensible cooling capacity of ventilation (W)

$\dot{V}$ =Ventilation rates (L/s)

T_r =Indoor DBT (°C)

T_α =DBT of ventilation air (°C)

In cool seasons, however, a DOAS can generally handle only a part of the space sensible load. If the space sensible load exceeds the DOAS sensible cooling capacity, this excess sensible load is handled by a parallel cooling system. The larger the sensible cooling capacity of a DOAS, the smaller the cooling capacity of a parallel system needs to be (Eq. 4).

$$Q_{S,parallel} = Q_s - Q_{S,vent} \quad \text{(Eq. 4)}$$

Where, $Q_{S,parallel}$=Required sensible cooling capacity of parallel cooling system (W)

Q_s =Indoor sensible load (W)

The supply air that a DOAS supplies to each space can be controlled by the temperature of the air leaving the cooling coil (11−12°C) to become a neutral temperature that can better suit residents' comfort level (18−20°C), depending on their needs and preferences. When the supply air which passed through the enthalpy wheel to remove the humidity after that leaved the cooling coil is supplied to each space without any reheating and is cooled to a proper temperature of 11−12°C DPT, it can receive the maximum effect of the sensible cooling and the size of the parallel cooling system can be minimized. In this research, therefore, we selected a proper supply air temperature of 11−22°C, which provided a maximum sensible cooling effect.

On the other hand, when the space cooling load is low in an intermediate season and the space heating load is occurred, a supply air temperature of 18−20°C is selected, which does not affect the comfort level. In this case, the heat needed for supply air reheating is collected from the enthalpy wheel and sensible wheel of the DOAS and no additional energy

consumption is required. However, an additional reheating system is needed, when the OA temperature is too low to provide the proper supply air condition from the sensible wheel and enthalpy wheel by the DOAS.

Energy performance of DOAS-parallel system

In order to further study the energy performance of the cooling coil load required in summer and to increase the quantity of the heating load obtained from ventilation, a typical floor (132 m^2) was modeled with a DOAS-parallel system in order to compare its energy performance with that of an existing decentralized air-conditioning system that is commonly used in high-rise apartment buildings.

(1) Summary of models

A virtual 132-m^2 (9 × 14.7 × 2.4 m) apartment building was selected as a test building for a comparison of a central DOAS cooling system with an existing decentralized air-conditioning system that is commonly used in high-rise apartment buildings (Fig 5). The configuration of each apartment unit that is occupied by 4 residents includes three bedrooms, a living room, a kitchen, and a bathroom. It has a 0.5 $W/m^2 \cdot h \cdot K$ curtain wall, which is commonly applied in apartment building exterior exposure, and 3.0 $W/m^2 \cdot h \cdot K$ double windows [11, 12]. The load calculations for two cases were performed based upon the assumption of the following conditions for the setting. The windows are located in the north and the east in each space, and the test building does not experience infiltration through the window frames or air gaps. The lighting load density is 20 W/m^2, and miscellaneous equipment generates sensible heat of 10 W/m^2. It was also assumed that the latent load in Equation 2 has always been the case in this residential building, as various lifestyles can create unpredictable latent loads.

(2) Summary of ventilation system

- *DOAS-parallel system*

In the central DOAS system, regardless of where the conditioned outdoor air is delivered, the dedicated outdoor air unit should be maintained at the proper DPT (12°C) to supply the appropriate amount of outdoor air required to achieve standard ventilation rates, so that the indoor latent load is eliminated. Among several candidates for a parallel sensible cooling system, a packaged air-conditioning system, which is usually used in high-rise apartment buildings, was selected for this research. A ceiling radiant cooling panel may be the best choice for the DOAS in terms of energy savings, thermal comfort, and indoor air quality.

- *Decentralized air-conditioning system*

It is assumed that a small decentralized air-conditioning system of the kind that is commonly used in high-rise apartment buildings is selected. In order for the indoor and outdoor air to meet the required ventilation rates, the sensible cooling load has to be handled by a packaged air-conditioning system, because a decentralized air-conditioning system does not have components to actively control the DPT and SA temperature as does a DOAS. Therefore, an additional component is essential to provide sufficient cooling and dehumidifying capacity. The target supply air temperature leaving a packaged air-conditioning system selects 16°C commonly used, and DPT for dehumidification is selected as 12°C, the same as that for DOAS.

Thermal performance of DOAS

(1) Comparison of cooling performance

In this study, HAP 4.20a was chosen for the estimation of the model building energy performance, with monthly and hourly peak load and cooling and latent load. The existing energy simulation program, however, cannot be modeled for DOAS. Therefore, a simulation model of DOAS and a decentralized air-conditioning system is presented based on the EES equation solver and the monthly and hourly cooling coil load is estimated using the energy performance of the model building. For the sake of simplicity, the following analysis assumes a 24-h-a-day ventilation mode. The ceiling radiant panel and packaged air conditioner were automatically controlled by meeting the target space conditions (i.e., DBT 24°C and a relative humidity of 50%).

- Cooling Coil Load: DOAS-parallel ceiling radiant panel

The sensible cooling load of the cooling coil is the sum of the DOAS-cooling coil load and the sensible cooling load of the ceiling radiant panel. On the other hand, the latent load of the cooling coil is the outdoor air latent load that is reduced in the cooling coil in order to meet the target DPT (12°C) (Eq. 6). The summation of these coil loads is the total cooling coil load for the DOAS-radiant cooling panel (Eq. 7).

$$Q_{s,cc} = Q_{s,DOAS,cc} - Q_{s,panel} \quad \text{(Eq. 5)}$$

$$Q_{l,cc} = Q_{l,DOAS,cc} \quad \text{(Eq. 6)}$$

$$Q_{t,cc} = Q_{s,cc} - Q_{l,cc} \quad \text{(Eq. 7)}$$

- Cooling Coil Load: decentralized air-conditioning system

In a decentralized air-conditioning system, the sensible cooling coil load is handled by the cooling coil in the air-conditioner units (Eq. 8). The OA latent load and the indoor latent load are handled by the decentralized air-conditioning system. The summation these coil loads is the total cooling coil load for a decentralized air-conditioning system (Eq. 7).

$$Q_{s,cc} = Q_{s,\,packaged,cc} \quad \text{(Eq. 8)}$$

$$Q_{l,cc} = Q_{l,\,packaged,cc} \quad \text{(Eq. 9)}$$

On the other hand, in a packaged air conditioner, when the indoor air is circulated by the cooling coil of the air conditioner, reheating of the load takes place by a process of cooling at the set point temperature and reheating before a supply is provided. Generally, the reheating of the supply air is handled by an electronic resistance heater installed in the packaged air conditioner.

(2) Determination of monthly cooling coil load

Figures 6 and 7 indicate that the thermal loads for these two cases were estimated based on alteration of the hourly cooling coil load for a July and August design day for the test building. There was no difference in the latent load of the coil load in each system. The sensible load of the cooling coil in a decentralized air-conditioning system, however, is higher than that of a DOAS-radiant cooling panel.

This signifies that the airflow rates of a packaged air conditioner are controlled by the sensible cooling load, but the large amount of airflow rates are always supplied by the packaged air-conditioner more than by DOAS-radiant cooling panel, which supplies the minimum required ventilation rates. In addition, reheating the load takes place by a process of cooling at the set point temperature and reheating before providing supply; the reheating energy is consumed by this process. The results for thermal performance are estimated as being the same as in July and August during the summer.

Figure 8 shows the monthly total cooling coil loads estimated for each system. One can see that in each month, the cooling coil load for the decentralized air-conditioning system is 19–24% higher than that for the DOAS-radiant cooling panel.

(3) Annual total cooling coil load

On the other hand, Figure 9 shows that the annual total cooling coil load for a decentralized air-conditioning system is 21% higher than that of a DOAS-radiant cooling panel, and additional reheating energy is needed for the decentralized air-conditioning system.

(4) Comparison of heating loads

When the indoor thermal condition is handled for a target temperature (e.g., 21°C) during the winter, using an enthalpy wheel system as in a decentralized air-conditioning system or DOAS-radiant cooling panel, cold OA for ventilation is preheated by the heat recovery process, and the increasing heating load and cold draft is mitigated for the directly supplied cold ventilation air. In addition, when dry air is used as the ventilation air supplied to a space during the winter, the space can become dry; however, the energy of the exhaust air is recovered by the DOAS or energy recovery ventilator, and a humidification effect can be expected from this process [10].

(5) Temperature change during winter

Figures 10 and 11 show and compare the hourly change in supplied air temperature for ventilation supplied by a decentralized air-conditioning system and a DOAS-radiant cooling panel during December and January design days. The results indicate that the supply air temperature of DOAS is always higher than that of a decentralized air-conditioning system. The source of this difference may be that decentralized air-conditioning systems have only one heat recovery component, while a DOAS-radiant cooling panel has an enthalpy wheel and a sensible wheel, which make a significant difference in the amount of heat recovery energy. Although they are not provided in this paper, data for the other months in the heating season showed a similar result for the supply air temperature. However, it is assumed that setting the target space condition at 21°C and with a 0.7 enthalpy and sensible wheel effectiveness, leaving the decentralized air-conditioning system air at 15.2−20.5°C during entire heating period, but leaving the DOAS-radiant cooling panel air at 17.1−20.7°C. Relatively high SA temperature make affect of heating load reduction owing to required ventilation rates in winter.

(6) Comparison of heating loads for ventilation

It is essential that the heating load be increased for OA ventilation during the winter. Although OA ventilation air is preheated by energy recovery, it is always lower than the

indoor air temperature. However, Figure 12 and Figure 13 show that the amount of increase in the heating load of the relatively high supply air temperature of DOAS is lower than that of a decentralized air-conditioning system.

On the contrary, in a comparison of the monthly increase in heating load shown in Figure 14, it can be seen that a DOAS may experience a 40% lower heating load than a decentralized air-conditioning system in every month. Consequently, this has a significant impact on the annual heating load; the additional annual heating loads for OA ventilation of a decentralized air-conditioning system and a DOAS are 923 kWh and 523 kWh, respectively. The additional load for a decentralized air-conditioning system is thus 59% higher than that of a DOAS-radiant cooling panel.

Conclusion

The aim of this research was to determine the proper supply air condition of a central ventilation system and to compare the energy simulation results of a DOAS radiant panel cooling system with a decentralized air-conditioning system. The main conclusions are as follows:

(1) The proper supply air DPT of a DOAS should be 11−20°C during a cooling period in order to handle the latent load. It is effective for reducing the energy consumption of a parallel cooling system that maintaining lowly the supply air temperature from leaving the cooling coil to neutral temperature.

(2) The annual cooling coil load of a DOAS radiant panel cooling system is 21% less than that of a decentralized air-conditioning system.

(3) Finally, a DOAS radiant panel cooling system can save 40% of the increased heating load compared with a decentralized air-conditioning system, and it can achieve a high supply air temperature because of the double heat recovery produced by the enthalpy wheel and sensible wheel during the winter.

Acknowledgement

This work has been supported by National Research Foundation under contract NRF-2008-331-D00657 with funding from the Korea Ministry of Education, Science and Technology.

References

1. Kim, H. J., Kim, J. H., and Park, J. S., “Effects of Ventilation System on Energy Consumption in Apartments ,” No. 3, *Journal of Korea Institute of Ecological Architecture and Environment*, 2009, pp.170~173.

2. Kim, J. H., et al., “A study on Current Problems of Heat Recovery Ventilator Operated by Occupants in High-rise Apartment Houses,” *Journal of Korean Institute of Architecture*, Vol.25, No.2, 2009, pp.249~256.

3. Emmerich, S. J., and McDowell, T., “Initial Evaluation of Displacement Ventilation and Dedicated Outdoor Air Systems for U.S. Commercial Buildings,” *NISTIR 7244*, 2005.

4. American Society of Heating, Refrigerating, and Air-Conditioning Engineers, *Standard 62.1-2007: Ventilation for Acceptable Indoor Air Quality*, ASHRAE, 2007.

5. American Society of Heating, Refrigerating, and Air-Conditioning Engineers, *ASHARE Handbook Fundamentals*, ASHRAE, 2005.

6. Roth, K. W., et al. “Energy Consumption Characteristics of Commercial Building HVAC Systems, Volume III: Energy Savings Potential,” *Final Report by TIAX LLC to U.S. Department of Energy, Office of Building Technology, State and Community Programs*, 2002.

7. Jeong, J. W., Mumma, S. A., and Bahnfleth, W. P., “Energy Conservation Benefits of a Dedicated Outdoor Air System with Parallel Sensible Cooling by Ceiling Radiant Panels,” *ASHRAE Transactions*, Vol.109, No.2, 2003, pp.627~636.

8. Jeong, J. W., and Mumma, S. A., “Binary Enthalpy Wheel Humidification Control in Dedicated Outdoor Air Systems,” *ASHRAE Transactions*, Vol.113, No.2, 2007, pp.220~226.

9. Lim, J. H., et al., “Prediction Analysis of Condensation on the Interior Curtain-wall Surface of a High-rise Apartment Unit,” *Journal of Korean Institute of Architecture*,Vol.23, No.3, 2007, pp.205~215.

10. Eagon Window & door, http://www.eagon.com/indtroduce/WND_010_070 (May. 3, 2009).

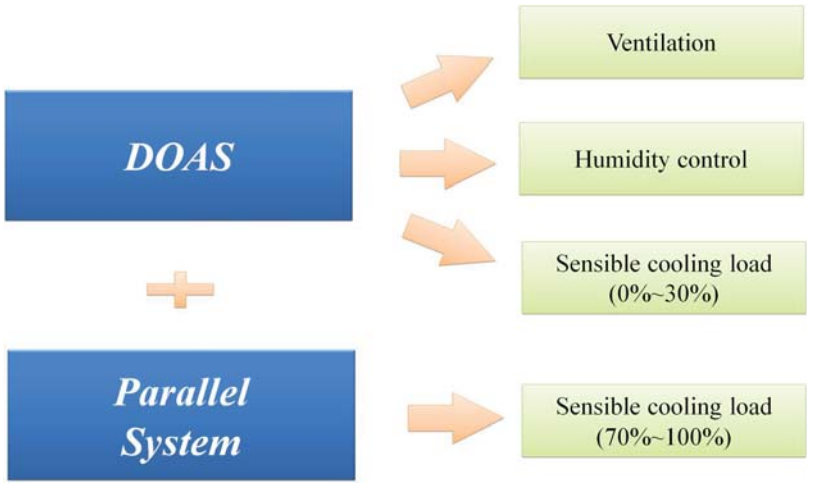


Fig. 1 Concept of DOAS-parallel system

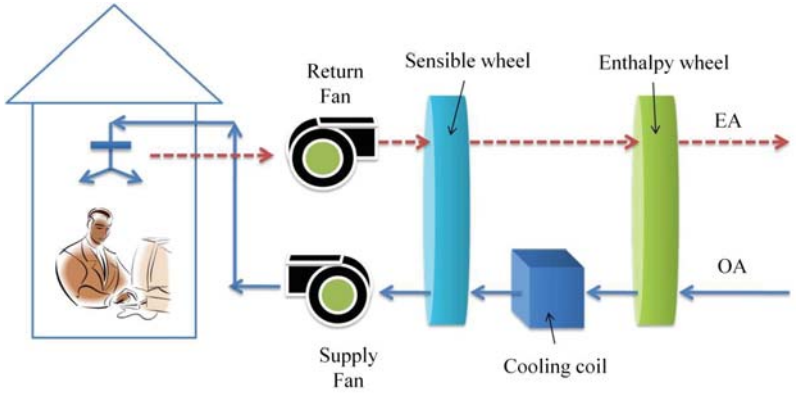


Fig. 2 Components of DOAS

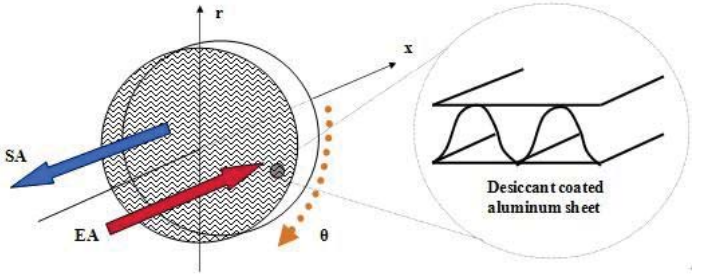


Fig. 3 Rotary-type enthalpy wheel

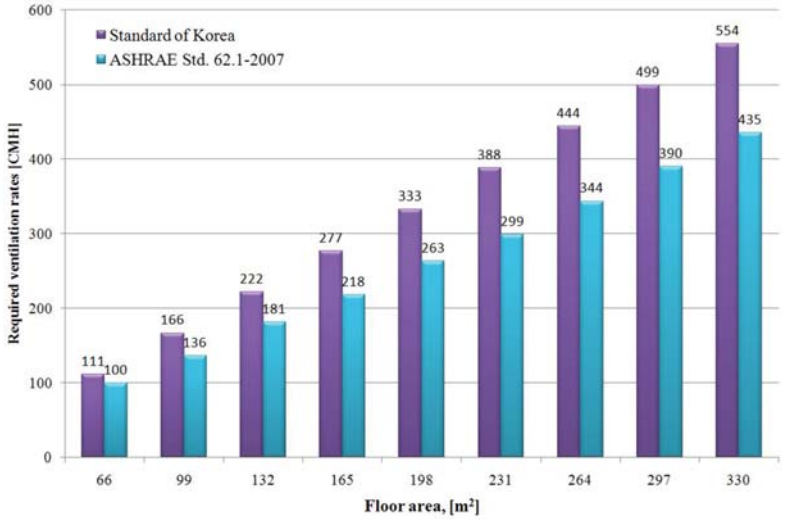


Fig. 4 Comparison of required ventilation rates

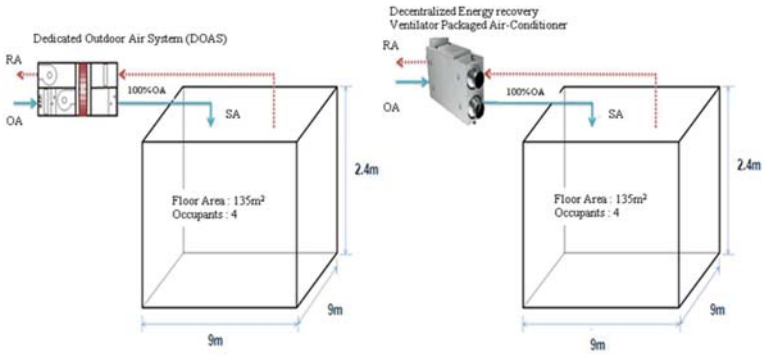


Fig. 5 Simulation model

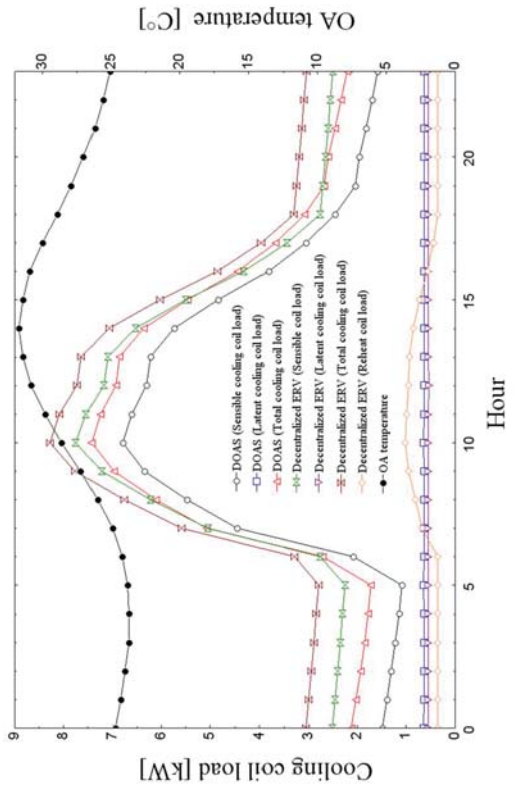


Fig. 7 Hourly design of daytime cooling coil for August

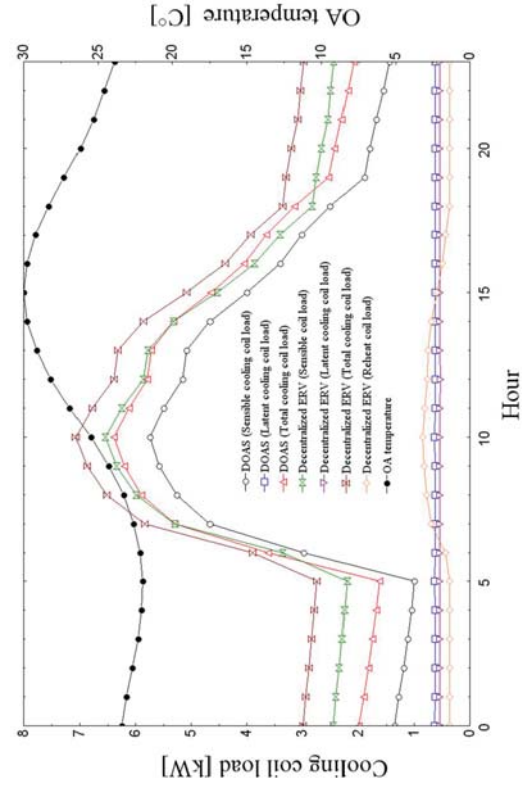


Fig. 6 Hourly design of daytime cooling coil for July



Fig. 9 Annual total cooling coil load

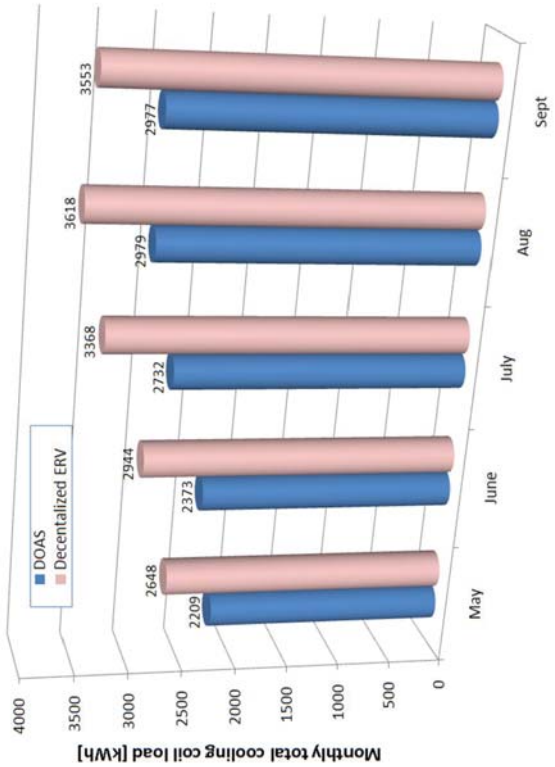


Fig. 8 Monthly total cooling coil load

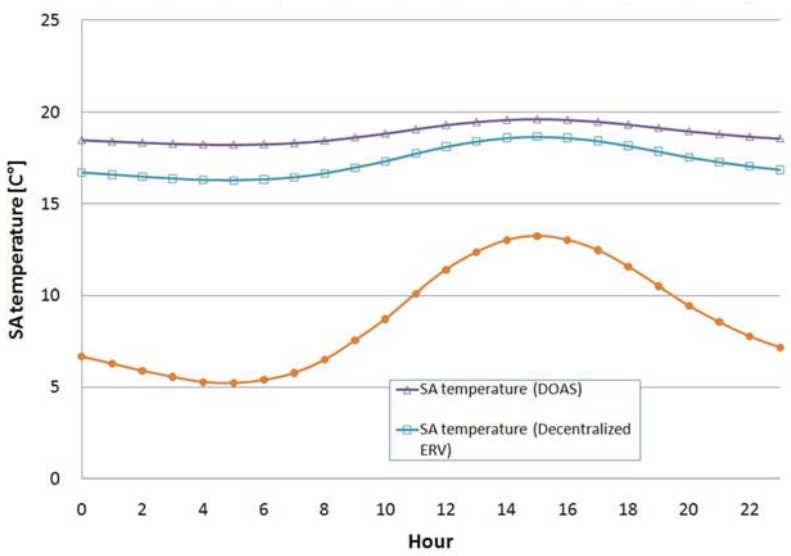


Fig. 10 Design of daytime change in supply air for December

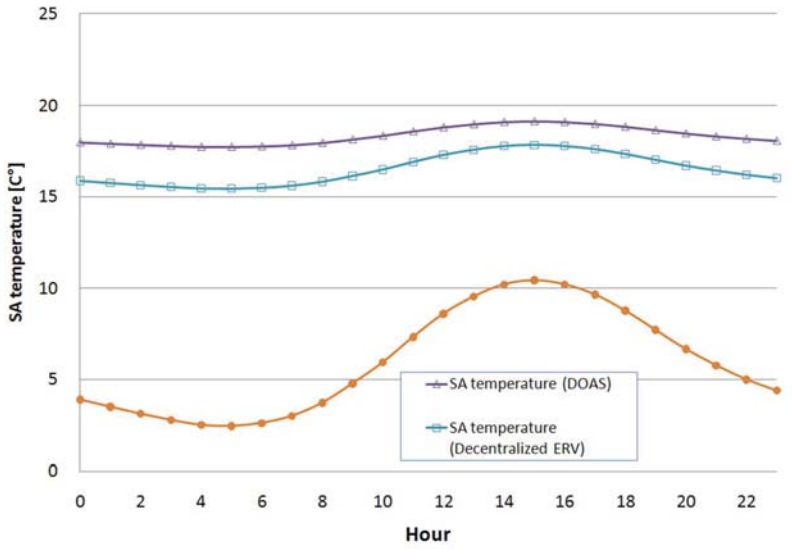


Fig. 11 Design of daytime change in supply air for January

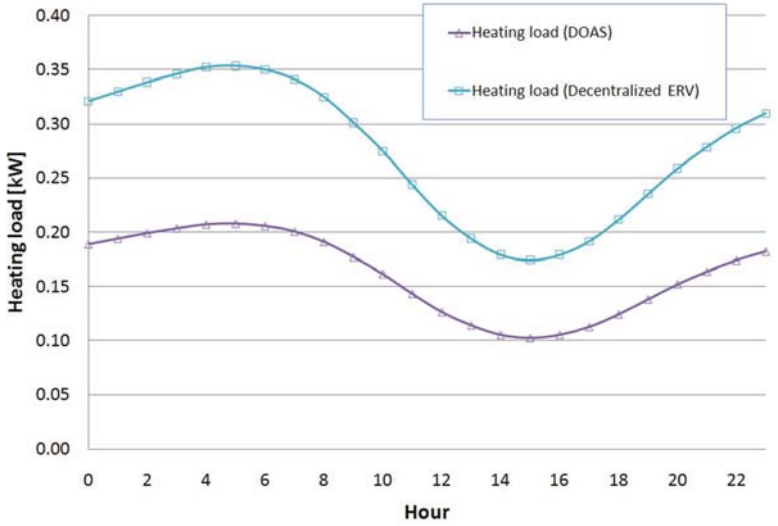


Fig. 12 Design of daytime heating load for December

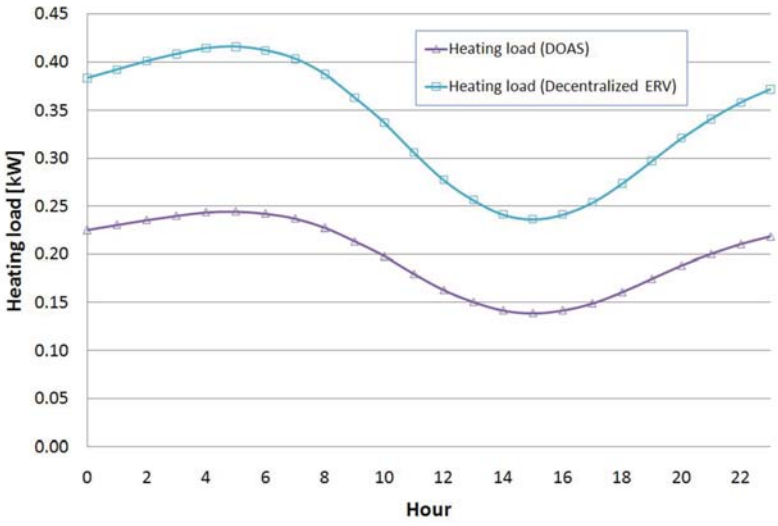


Fig. 13 Design of daytime heating load for January

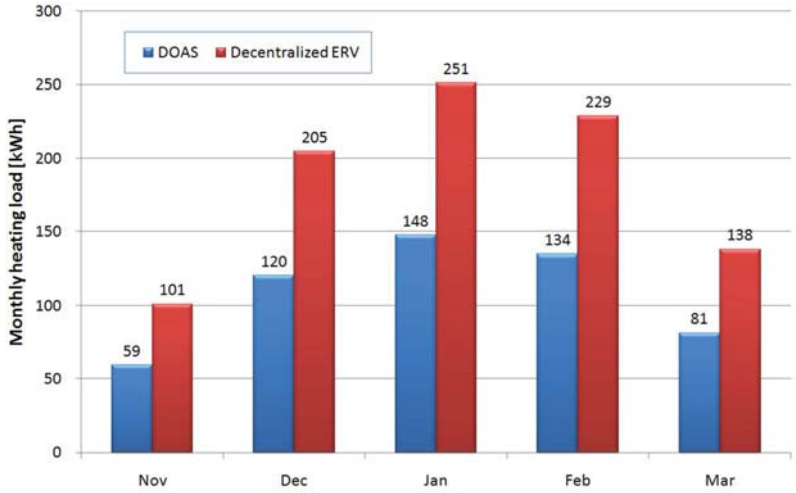


Fig. 14 Increasing rates of monthly heating load

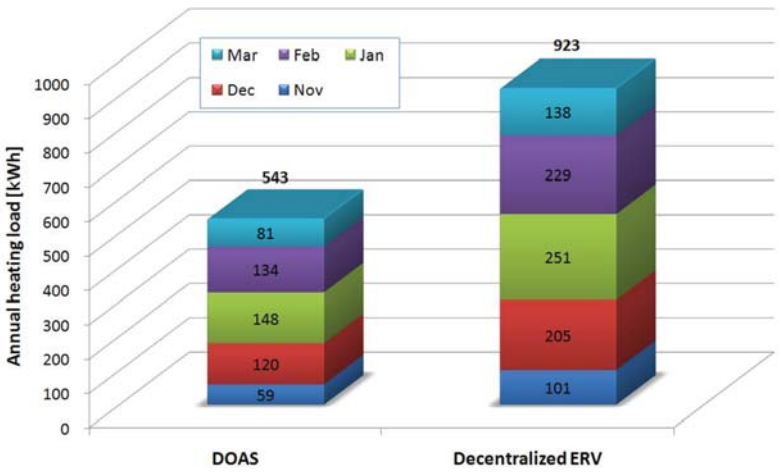


Fig. 15 Increasing rates of annual heating load

Table 1 Required ventilation rates per floor area

Floor area, [m^2]	Volume, [m^3]	Occupants	Required Ventilation rates, CMH	
			Standard of Korea	ASHRAE Std. 62.1-2007
66	158	3	111	100
99	238	3	166	136
132	317	4	222	181
165	396	4	277	218
198	475	5	333	263
231	554	5	388	299
264	634	6	444	344
297	713	7	499	390
330	792	8	554	435

Table 2 Proper DPT of DOAS supply air in a cooling period

Floor area, [m^2]	Latent load, [W]	Required ventilation rates, [l/s]		Supply air humidity ratio, [g/kg]		Proper DPT of supply air, [°C]	
		Standard of Korea	Standard of ASHRAE	Standard of Korea	Standard of ASHRAE	Standard of Korea	Standard of ASHRAE
66	71	31	28	8.50	8.42	**11.6**	**11.4**
99	78	46	38	8.71	8.58	**11.9**	**11.7**
132	97	62	50	8.74	8.62	**11.9**	**11.7**
165	104	77	61	8.82	8.69	**12.1**	**11.8**
198	124	92	73	8.82	8.70	**12.1**	**11.9**
231	131	108	83	8.86	8.74	**12.2**	**11.9**
264	150	123	96	8.86	8.74	**12.2**	**11.9**
297	169	139	108	8.86	8.75	**12.2**	**11.9**
330	189	154	121	8.86	8.75	**12.2**	**11.9**

Prediction of Heat Emission Effect at Small Single-sided Openings in Apartment Houses

Ayako Nishimura[1], Masashi Imano[2], Kei Ogino[3],
Keigo Nomura[3], Yuzo Sakamoto[4]

[1] The Tokyo Electric Power Company, M. Eng.
[2] Assist. Prof., Grad. School of Eng., The Univ. of Tokyo, Dr. Eng.
[3] Graduate Student, Grad. School of Eng., The Univ. of Tokyo.
[4] Prof., Grad. School of Eng., The Univ. of Tokyo, Dr. Eng.

Abstract

In this study, we propose a method for forecasting heat emission effect in a small single-sided slit opening. In order to make a heat flux forecasting model, we carried out field measurement, wind tunnel experiment, and CFD analysis. In the field measurement, we measured heat flux and grasped the relationship of heat flux of the opening and airflow around the building surface. In the wind tunnel experiment, we measured airflow around the opening and grasped turbulence characteristics. In the CFD analysis, we used RANS model of high Reynolds numbers type and considered optimum turbulence model by comparing with the results of wind tunnel experiment. Finally, we used standard k-ε model under non-isothermal conditions and calculated the coefficients of the heat flux forecasting model from the relationship of heat emission quantity at the opening and airflow around the building surface by CFD analysis.

Keywords: apartment houses, single-sided openings, natural ventilation, heat emission, heat flux, field measurement, wind tunnel experiment, CFD, RANS model

1. Introduction

Recently, an expectation of heat emission effect by natural ventilation has risen in terms of energy conservation and comfortableness. However, openings in apartment houses can be installed only on one side wall, and ventilation system using the back and forth differential pressure cannot often be used. Nevertheless, the quantitative findings to estimate the effect under adverse circumstances are few. Warren et al insisted that the ventilation in the room with a single-sided opening mainly resulted in turbulent mixing layer between the indoor stationary air and the wind flowing parallel to the wall, and the ventilation quantity was proportional to the wind velocity around the building's surface. In addition, Kono et al proposed the method to estimate ventilation flow from wind velocity parallel to the wall. It is assumed that turbulent heat flux much contributes to heat transport of a single-sided opening. Therefore, it is necessary to grasp heat emission quantity including turbulent heat flux and solve the heat emission mechanism in order to estimate heat emission effect in the room with a single-sided opening. The purpose of this study is to grasp heat emission quantity of a small single-sided opening especially a slit opening (about 20 cm width) considering crime prevention, and to construct a method for forecasting heat emission effect.

2. Forecasting process of heat emission effect in a single-sided opening

We propose a forecasting process shown in Figure 1 by applying ventilation quantity forecasting method of Kono et al. To practice this method, we examined two matters; the arrangement of CFD analysis condition and making heat flux forecasting model.

The former have been already reported. We report the result of examination about heat flux forecasting model and trial calculation of heat emission effect forecasting process in this report.

3. Measurement of heat flux by field measurement

3.1 Definition of heat flux

Heat flux divided by the heat capacity of air is defined as follows.

Effective heat flux $\overline{u\,\theta}$ (Equation 1): heat transportation moving from inside to outside through an opening It is equal to heat loss per unit area from an opening.

Non-turbulent heat flux $U\Theta$ (Equation 2): heat transportation by mean flow, which is separated into inflow and outflow.

Turbulent heat flux $\overline{u'\,\theta'}$ (Equation 3): It is calculated by subtracting non-turbulent heat flux from effective heat flux. It is heat transportation by turbulent correlation of wind and temperature.

$$\overline{u\theta} = \sum (u_t \cdot \theta_t) \cdot \Delta t / t \qquad \text{(Eq. 1)}$$

$$U\Theta = U_{in}\Theta_{in} + U_{out}\Theta_{out} \qquad \text{(Eq. 2)}$$

$$\overline{u'\theta'} = \overline{u\theta} - U\Theta \qquad \text{(Eq. 3)}$$

3.2 Outline of field measurement

We measured in a room of the third floor of a four-story RC manufacturing apartment houses in Shinjuku, Tokyo after sunset on 6 December 2009. Beforehand, we heated and stirred the air in the room with a heater so that inside temperature is about 1.5 degree higher than outside, for we assumed late summer. We started to measure an hour after stopping the heater. The opening is a slit opening considering crime prevention. It slides outside lengthwise and works as a wind catcher as well. We placed three-dimensional sonic anemometers 50 cm apart from the wall to measure wind velocity around the opening (Figure 4). We measured temperature and wind velocity at opening at the same time by the anemometer and thermocouples in order to gain heat flux. We placed the anemometers to six points, and thermocouples to 5 cm inside and outside from center point of measurement of anemometers. When the air flowed in, we

used the temperature of outside thermocouples. When the air flew out, we used the temperature of inside thermocouples (Figure 5, 6). Measurement interval of wind velocity was 0.1 seconds, and that of temperature was 2 seconds. We analyzed wind velocity and temperature using linear interpolation per 0.1 seconds.

3.3 Results of field measurement and heat flux model

While measuring, 60 percent of the rooftop wind flowed from N, 40 percent flowed from NNW. Average wind speed was 1.7 m/s. The wind of the surface blew down at 45° along the wall from N. The wind velocity was 0.6 to 1.4 m/s. Figure 7 shows mean airflow quantity that flowed in and out, and wind velocity around the building surface of 10 minutes interval. Ventilation quantity was calculated by the product of each wind velocity at 6 points and window area which was equally divided into 6 parts. Although this study assumes wind-driven heat transfer, buoyancy ventilation also occurs in real experiment. So, we need to confirm the order of buoyancy ventilation. The ratio (C_b) of buoyancy ventilation quantity (Q_b) to total ventilation quantity (Q_t) was 20 to 35 percent. Buoyancy ventilation quantity was calculated as follows.

$$Q_b = \frac{1}{3} A C_d \sqrt{\frac{9.8 \Delta\theta h}{\theta}} \qquad C_b = Q_b / Q_t$$

We calculated heat flux by Equation (1)-(3). For these, we divided heat flux by indoor and outdoor temperature difference ($\Delta\ \theta$) (Equation (4), (5)). Then, we multiplied (1-Cb) In order to eliminate the influence of buoyancy, (1-C_b) was multiplied. Equation (4) is the standard heat flux.

$$K_{mean} = (1 - C_b) \cdot U\Theta / \Delta\theta \qquad \text{(Eq. 4)}$$

$$K_{turb} = \overline{u'\theta'} / \Delta\theta \qquad \text{(Eq. 5)}$$

Figure 8 shows the mean standard heat flux of 10 minutes interval gained by field measurement. The turbulent heat flux is 20 to 80 percent of the non-turbulent hear flux. However, the data with weak wind velocity of building surface and unstable wind direction were removed.

Figure 9 shows the relationship between the standardized non-turbulent heat flux (K_{mean}) and scalar wind velocity of building surface (U_R). Figure 10 shows the relationship between the ratio of turbulent heat flux to non-turbulent heat flux (K_{turb} / K_{mean}) and the turbulence intensity at the building surface (I_R). They are roughly proportional.

Thus, we gained equations of forecasting model (Equation (6), (7)) from the slope of straight line in Figure 9-10. From these equations, we led Equation (8) which shows the standardized effective heat flux by U_R and I_R. We measured 50 cm apart from the wall. In order to convert

to the condition of 1m apart from the wall, we multiplied wind velocity by conversion factor 1.07 which was led by Kono et al.

4. Wind tunnel experiment

4.1 Outline of wind tunnel experiment

The experiment was done in the wind environment simulator laboratory, Faculty of Engineering The University of Tokyo. The model was in 1/4 scale. We set up the opening on the wind tunnel floor, and the chamber below (Figure 11). The size of opening was 50×330, and 45 mm thick. The size of the chamber was 700×600×700 mm (the room of 4 and a half mat was assumed). Figure 12 shows two types of openings, a simple opening and a lengthwise sliding opening which was the reproduction of the shape of sash. We disturbed the airflow in the wind tunnel by using turbulent lattice. Figure 13 shows the profile of wind velocity and turbulence intensity. In case of the lengthwise sliding opening, we changed inflow wind direction to the opening by 0°, 45°, 90°. We measured 3 direction wind velocity elements with a split film (low-pass frequency was 1Hz).

4.2 Results of wind tunnel experiment

Comparison in different shape of opening

Figure 14 shows wind velocity vector at the center section of simple opening and the lengthwise sliding opening in the wind direction 0°. In case of simple opening, a whirlpool occurred in the opening. We observed that the wind was drawn and flew into the chamber at the edge of leeward. The standard airflow quantity at the opening was 0.0076. It is about 1/3 of the result of experiment of Kono et al, 0.024. Standard airflow quantity can be calculated by dividing ventilation quantity by area of opening and inflow wind velocity. Ventilation quantity is the total sum of product of wind velocity toward normal direction and the area at each measure point.

We think this is because thicker thickness of opening is; lesser the turbulent mixture layer grows. In case of lengthwise sliding opening, windward airflow that collided with sliding plate was led to inside. However, most of inflow air cut corners because drawn airflow by leeward circulating airflow was strong. The standard airflow quantity at the inside of the opening was 0.032. It was approximately 1/7 of that at the outside of the opening. The standard airflow quantity of lengthwise sliding opening was approximately 4.2 times of that of simple opening.

Comparison in different inflow wind direction

We measured the wind velocity in the plane of outside with lengthwise sliding opening, changing inflow wind direction at 0°, 45°, 90°. Figure 15 shows the anemometry point of

wind velocity, wind velocity of normal direction, and the turbulence energy. In case of 0°, we measured only the upper half, since it's symmetrical. In case of 0° and 45°, the wind flowed in from the windward opening, and flowed out from the leeward opening remarkably. The wind velocity was large, 1 to 1.5 m/s. On the other hand, in case of 90°, the wind flowed in from most of the area of the opening. The wind velocity was small, 0.3 m/s at its most. The turbulent mixture layer grew as the wind went to leeward. In case of 45°, it is assumed that shortcut of the wind will decrease, and substantial ventilation quantity will increase, for flow field isn't symmetrical, different from the case of 0°. Calculation of substantial ventilation quantity by CFD is reported in the next report.

5. CFD analysis

5.1 Outline of CFD analysis

We will calculate the heat flux of opening by CFD analysis in future. Therefore, we inspected the accuracy of calculation of airflow around the opening and compared turbulent models by CFD analysis under non-isothermal condition. Table 2 shows the outline of analysis. We reproduced an area which is centered at the center of the opening of wind tunnel experiment. Its sides of horizontal plane were 1.2m each. We interpolated measurements in wind tunnel experiment and used them as vertical profile of inflow wind. We inspected about three kinds of turbulent models, standard k-ε, RNG k-ε, and Realizable k-ε.

5.2 Results of CFD analysis

Figure 16 shows correlations of results of CFD analysis and wind tunnel experiment of wind velocity toward normal direction in the outside of the opening at each wind direction. Measuring points were shown in Figure 15. The smallest RMSE was at the standard k-ε model. Standard k-ε model accurately reproduced the airflow which collided with sliding plate vertically as in the case of 0°. However, it didn't accurately reproduce the airflow which collided with sliding plate slantingly as in the case of 45°, or in the turbulent mixture layer as the case of 90°. Figure 17 shows correlations of turbulent energy. It shows similar tendency.

6. Heat flux model by CFD analysis

6.1 Outline of CFD analysis

Table 3 shows conditions of temperature field. We assumed uniform heat generation of 20 W/m3 in the chamber. The wall of chamber was assumed to be complete insulation. The inflow wind direction was 0°, 22.5°, 45°, 67.5°, 90° (Figure 18). We reproduced external part (no openings) of the object building and surrounding buildings, and calculated airflow around the building to 16 directions by CFD. Then we gained the wind velocity profile around the building surface. Figure 19 shows this. This profile was weighted by occurrence rate and average was taken.

6.2 Results of CFD analysis

Figure 20 shows airflow quantity that passed through the opening and effective ventilation quantity that was calculated from temperature difference between inside and outside. The airflow quantity that passed through the opening was the largest at 0°, and decreases according to cosine curve. This is assumed that it depends on the vertical projection area of vane. However, the effective ventilation quantity was the largest at 67.5°. This is assumed that the air didn't take a shortcut easily, so flowed inside, and the room was ventilated effectively.

6.3 Calculation of coefficients of heat flux forecasting model

Figure 21 shows the method of calculating coefficients of heat flux forecasting model. Total heat emission quantity is equal to total heat generation in the chamber. Thus, we divided the heat emission quantity by the area of the opening, and calculated effective heat flux. We multiplied mean airflow velocity and mean temperature, and calculated non-turbulent heat flux. We subtracted non-isothermal heat flux from effective heat flux, and gained turbulent heat flux. We calculated coefficients of heat flux forecasting model from the relationship of effective heat flux and U_R, I_R (the height was 25 cm, actual scale was 1 m) (Table 4). These coefficients are used according to wind direction of vertical plane.

7. Conclusions

We proposed the forecasting process of heat emission effect and finally calculated the heat flux forecasting model. We found that standard k- model was the most accurate. In the future, we need to simulate with more accurate model such as LES model, or inspect with more turbulent inflow wind. We also need to examine hereafter the cause that the effective ventilation quantity is the largest at 67.5°

Nomenclature

u	instantaneous wind velocity [m/s]
U	mean wind velocity [m/s]
θ	instantaneous temperature [℃]
Θ	mean temperature [℃]
Q	airflow quantity [m^3/s]
C_b	buoyancy ventilation quantity / all airflow quantity [-]
$\Delta\theta$	indoor and outdoor temperature difference [℃]

I turbulence intensity [m^2/s^2]

A area of the opening [m^2]

k turbulence energy [m^2/s^2]

t time [s]

F heat flux [W/m^2]

K standardized heat flux [m/s]

α , β coefficient of the model [-]

Subscript

t instantaneous value per measuring interval (0.1 seconds)

in inflow

out outflow

b by buoyancy

t total

mean non-turbulence component

turb turbbulence component

eff effective component

R around the building surface

Acknowledgement

The Tokyo Electric Power Company R&D Center and Hidekazu Tanaka, a postgraduate of Sakamoto laboratory of the University of Tokyo supported the field measurement.

References

1. P.R.Warren, “Ventilation through Openings on One Wall Only, Energy Conservation in Heating, Cooling, and Ventilating Buildings,” Vol.1, 1978, pp.189~206.

2. KONO Ryohei, et al, “Prediction of Airflow Rate of Single-sided Room in Cross Wind: The study on characteristics of ventilation with single-sided opening Part 3,” Journal of Environmental Engineering (Transactions of AIJ), 2008.

3. IMANO Masashi, “Development of a CFD Software for Predicting Cross Ventilation Flow in a House Using Adaptive Mesh Refinement and Super-Parallel Calculation,” Transactions of the Society of Heating, Air-conditioning and Sanitary Engineers of Japan, 2005, pp.1097~1100.

①【Calculation of airflow around the building surface by CFD analysis】

We reproduce surroundings and externals part of the object building, and calculate airflow around the building surface

Examination 1: Arrangement of CFD analysis condition in order to get appropriate solutions

②【calculation of standard heat emission quantity】

We substitute U_{CFD} and k_{CFD} that was calculated in 16 wind directions for the heat flux forecasting model that is described later, and calculate standard heat emission quantity per standard wind velocity and temperature difference between inside and outside of the room.

Examination 2: Make of heat flux forecasting model

Fig. 1 Forecasting process of heat emission effect

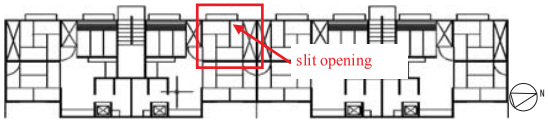


Fig. 2 Object unit (third floor)



Fig. 3 Object building





Fig. 4 Anemometer at the the building surface

Fig. 5 Anemometer and thermocouples at the opening



Fig. 6 Slit opening

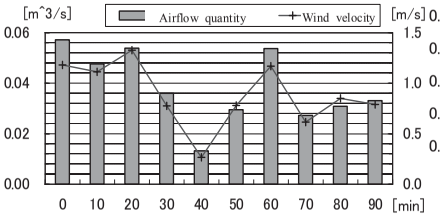


Fig. 7 Wind velocity around the building surface

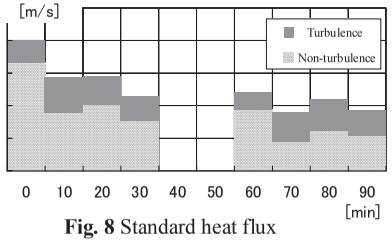


Fig. 8 Standard heat flux

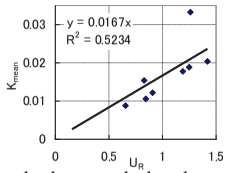


Fig. 9 Standard non-turbulent heat flux and scholar wind velocity around the building surface

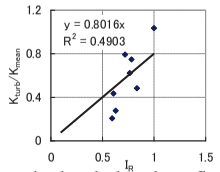


Fig. 10 Standard turbulent heat flux and turbulent energy around the building surface

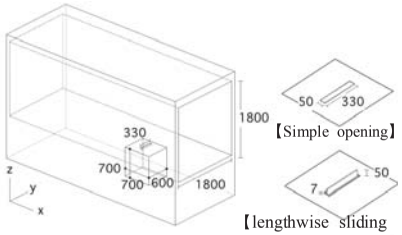


Fig. 11 Wind tunnel model (Unit of length : mm)

Fig. 12 Opening model (Unit of length : mm)

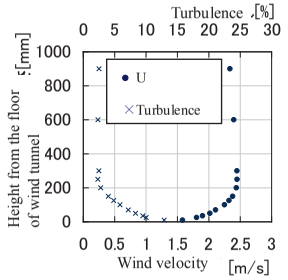


Fig. 13 Wind velocity profile

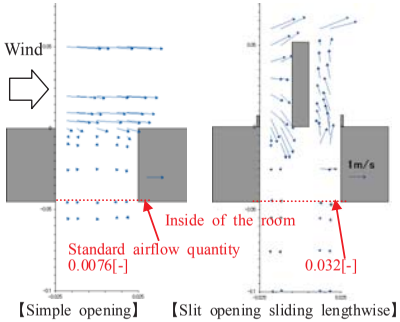


Fig. 14 Wind velocity vector of main wind direction (Inflow was positive at wind velocity.)

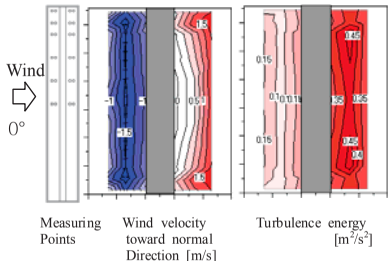


Fig. 15 Plane distribution in the outside of the opening (Inflow was positive at wind velocity.)

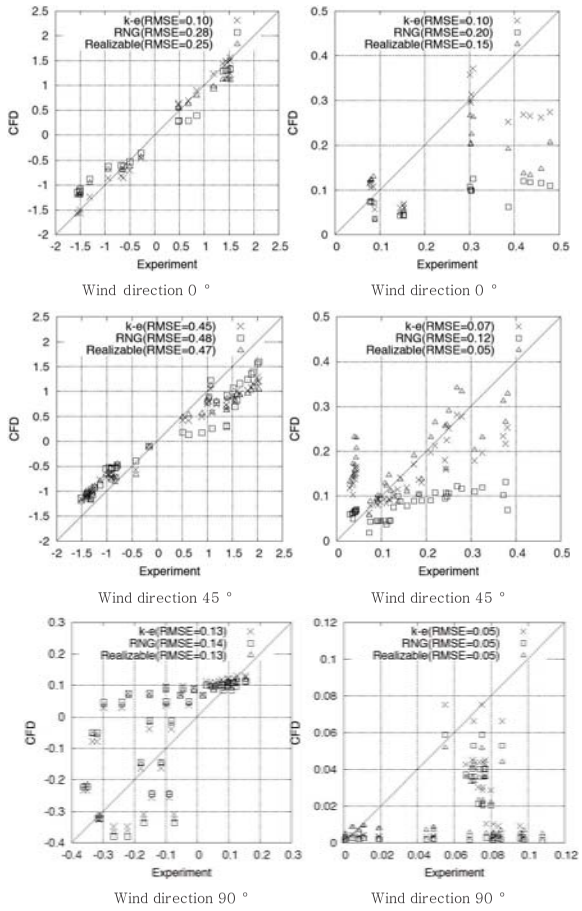
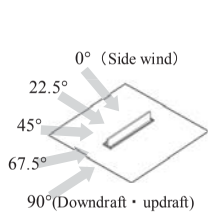
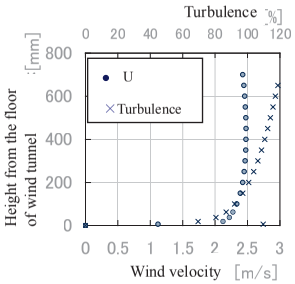


Fig. 16 Correlations of results of CFD analysis and wind tunnel experiment of wind velocity in the outside of the opening

Fig. 17 Correlations of results of CFD analysis and wind tunnel experiment of turbulent energy in the outside of the opening





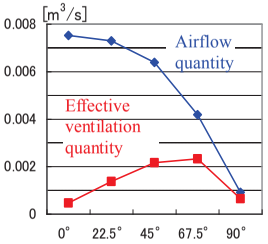


Fig. 18 Inflow wind direction **Fig. 19** Wind velocity profile **Fig. 20** Airflow quantity that passed through the opening and effective ventilation quantity

①【Separation of non-turbulent heat flux and turbulent heat flux】

All heat generation quantity = All heat emission quantity (steady) = Effective heat flux

Average wind velocity of the opening × Average temperature = Non-turbulent heat flux

Effective heat flux – Non-turbulent heat flux = Turbulent heat flux

⇩

②【Calculation of the coefficients of heat flux forecasting model for each direction】

Heat flux forecasting model : $K_{eff} = \alpha(1+\beta I_R) \cdot U_R$

→We divide heat flux by the area of the opening, temperature difference, and scholar wind velocity, and calculate α. $\alpha = F_{mean}/A/\Delta\theta/U_R$

→We divide the ratio of non-turbulent heat flux to turbulent heat flux by turbulent intensity, and calculate turbulence correcting coefficient β. $\beta = F_{turb}/F_{mean}/I_R$

Fig. 21 Method of calculating coefficient of heat flux forecasting model

Table 1 Outline of field measurement

Date of measurement	2009/12/6 19:12～20:52	The late summer was assumed. The room was heated before measurement. (Outside temperature standed at about 11℃.)	
Item of measurement	Measuring instrument	Interval	Remarks
Wind velocity on the roof	Three-dimensional sonic anemometers	0.1 seconds	on the staircase in the south (height 16.24m)
Wind velocity around the building surface	Three-dimensional sonic anemometers	2 seconds	50 cm apart from the wall
Wind velocity, Temperature at the opening	Three-dimensional sonic anemometers, thermocouples	0.1 seconds	Temperature : measured at 2 points for each side of the room, linear interpolation per 2 seconds
Room temperature, Outside temperature	Thermocouples	2 seconds	Room temperature : weighted average of 5 points volume Outside temperatue : the same measuring position as wind velocity around the building surface

Table 2 Outline of CFD analysis

Analysis code	Open source CFD tool : OpenFOAM
Area of calculation	1.2m(x)×1.2m(y)×1.36m(z)
Grid of calculation	Number of grid : 2.5 million, width of grid : 2.5mm～4cm
Solution of calculation	Steady solution, SIMPLE
Turbulence model	Standard k-ε, RNG k-ε
Advection term scheme	TVD (van Leer limiter)
Influx boundary	Profile by wind tunnel experiment
Wall boundary condition	Generarized logarithm rules for slickenside
Sky boundary	Slip boundary condition

Table 3 Outline of CFD analysis

Turbulence model	Standard k-ε model
Condition of non-isothermal flow field	
Buoyancy term	Disregard of influence(=0)
Uniform heat genaration in the room	20W/m^3
Boundary condition	Outside wall of chamber : 0 inclination (insulation)
Constant	Prandtl number=0.7
	Turbulence Prandtl number=0.9

Table 4 Coefficient of model

	α	β
0°	0.014	0.042
22.5°	0.039	0.080
45°	0.061	0.095
67.5°	0.068	0.051
90°	0.014	0.426

Design Method of Vertical Ventilation with Wind Chimney on Roof Driven by Wind and Buoyancy

Toshio Yamanaka[1], Hisashi Kotani[1], Yoshihisa Momoi[1], Kazunobu Sagara[1],

Tomohiro Kobayashi[2] and Yuka Komatsu[3]

[1] Dept. of Architectural Engineering, Osaka University, Suita, 565-0871, Japan

[2] Ritsumeikan University, Dept. of Architecture and Urban Design, Kusatsu, 525-8577, Japan

[3] Panasonic Electric Works Co., Ltd., Tokyo, 105-8301, Japan

Abstract

The calculation system for vertical ventilation with wind chimney on the roof driven by wind and buoyancy is presented and the necessary data is measured. The calculation system is based on the "pressure – airflow rate relationship (Pressure -Volume curve: P-V curve)" and the local velocity and static pressure at the point of chimney top. The P-V curves were measured by wind tunnel test for some typical shapes of wind chimney top. It is turned out that the effect of upper wind velocity can be eliminated by normalization of the pressure at chimney neck and airflow rate through the chimney. The number of tested models are six : simple outlet, two types of wind-break plates, two types of horizontal duct, rainproof type.

Keywords: Wind chimney, Vertical ventilation, Wind tunnel test, Pressure - Volume curve

1. Introduction

In urban area, the cross ventilation through windows is not necessarily possible. In such cases,

vertical ventilation using devices such as chimney is effective. In this paper, the chimney ventilated by wind force is named “wind chimney” as a device for natural ventilation in building superior to simple side windows. In most cases, wind chimney will be assisted by buoyancy caused by the heat emission inside the room.

Nevertheless, there is no established calculation system that enables us to design the wind chimney. In general, wind pressure coefficient is used for the calculation of ventilation rate through windows of a building, but it is not appropriate to apply wind pressure coefficient to the chimneys exposed to natural wind. It is because the mutual action between natural wind and shape of chimney top is quite complicated, and for example the suction effect on the pressure loss through the overall chimney can change depending on wind direction and airflow rate of chimney. The design method of wind chimney, therefore, is quite necessary.

So, the objectives of this study are to present the equations to predict the airflow rate of vertical chimney based on “Pressure – airflow rate relationship” (Pressure -Volume curve: *P-V* curve) and to measure Pressure -Volume curve representative of the ventilation characteristics of each wind chimney with different top-shape by wind tunnel test.

2. Methods

2.1 Equations for calculation of airflow rate of wind chimney

In this section, basic equations to calculate the airflow rate of chimney will be introduced. Based on the equations previously presented by Ishihara[1)], the static pressure at the chimney neck (base of the chimney, see **Fig.1**) p_c [Pa] can be defined as the function of airflow rate of chimney Q [m^3/s], local wind velocity around chimney top V_L [m/s], wind direction angle to the chimney θ [degree]. So the following equation can be written.

$$p_c = f(Q, V_L, \theta) \quad \text{(Eq. 1)}$$

This function f in **Eq.1** is representative of the characteristics of each chimney, which depends on the shape of chimney top. It is essential to determine this function from the experiment in wind tunnel or CFD analysis and so on.

Using this equation and Bernoulli's principle, the following equation can be derived,

$$p_c = f(Q, V_L, \theta) - (\rho_o - \rho_i) g h_c + C_L \frac{\rho_o}{2} V \quad \text{(Eq. 2)}$$

where ρ_o and ρ_i is the density of outdoor air and air inside chimney [kg/m^3], g is gravitational acceleration [m/s^2] (=9.8), h_c is chimney height above chimney neck [m], C_L is local pressure coefficient in the air at chimney top position, V is upper wind velocity independent of air stream around building. (see **Fig.1**) Here, it should be noted that C_L is not the wind pressure on the wall of chimney or building, but the static pressure in the air at the position of chimney top normalized by the dynamic pressure of natural wind at the height of chimney top.

2.2 Measurement of pressure-volume curve using wind tunnel test

In order to measure the *P-V* curve of different chimney types, wind tunnel test was conducted. Scaled model of various chimneys were made, and they were installed on the floor of wind tunnel. **Fig.2** shows the cross-section of test models of chimney, and **Fig.3** shows the appearance of each model. Model A is a simple chimney type, and Model B & C is the simple chimney with wind barrier in front of openings in vertical walls at chimney top. Model C has base plate at the bottom of wind barrier of Model A. Model D allows wind enter the horizontal duct placed on the top of Model A. Model E is the improved type of Model D whose horizontal duct has a constricted section area at the chimney top to introduce Venturi effect. Model F is the designed type for a real building of a college in Japan. This model has an inside opening with a shutter at the bottom of chimney, which can be controlled automatically to prevent rain infiltration.

After the chimney model was set on the floor of wind tunnel, then the air is supplied though flexible duct by fan installed outside the wind tunnel (see **Fig. 4**). The airflow rate was measured by orifice flow meter, and the static pressure at each chimney neck was measured by micro differential pressure gauge. In Fig.5, the details of the neck of chimney model are shown. Velocity of approaching wind is 5 m/s, and the velocity distribution is uniform. Turbulent intensity of approaching wind is less than 0.5%. The reference static pressure and reference dynamic pressure are measured by pitot tube at the center of tunnel section. The height of pitot tube is 0.9m above the floor. Base duct with the length of 20cm was attached to each chimney to place the chimney top at higher position (see **Fig.3**). Sampling frequency is 100Hz, and the pressure and velocity data for 30 seconds were analyzed to obtain mean values. Table 1 shows the experimental conditions, that is, tested wind direction angle defined in Fig.2 for each chimney model.

3. Results

3.1 Effect of upper wind velocity on Pressure-Volume curve (*P-V* curve)

Only in the case of Model A and wind direction angle 0 degree, three wind velocities were tested. The relationship between airflow rate and static pressure at chimney neck is presented in Fig.6(1). On the other hand, in Fig.6(2), airflow rate was normalized by the product of section area of chimney neck and upper wind velocity, and static pressure was normalized by dynamic pressure of upper wind. From these two graphs, *P-V* curves of different wind velocity can be presented by representative one curve independent of velocity effect for each chimney type and wind direction angle. This curve will be called normalized P-V curve of a chimney.

3.2 Comparison of flow characteristics of different chimney top

Fig.7 shows normalized *P-V* curves of the tested chimneys. These curves were derived from the test data in the case that the upper wind velocity is 5 m/s. Some curves for different wind direction angles are drawn in each graph. It is important the static pressure of chimney neck at zero velocity of chimney neck means wind pressure coefficient of the chimney top. If this value of a chimney has large negative value, such chimney is able to induce strong suction effect utilizing dynamic pressure of natural wind. The *P-V* curves of Model A for three wind directions shows relatively low neck pressure at any normalized velocity at chimney neck, and the wind angle of 45 degrees shows lowest neck pressure. The lower the pressure at chimney neck is, the smaller the pressure loss through the chimney becomes.

At Model B, the type with wind barrier, the neck pressure change hardly and quite stable against neck velocity. This tendency is supposed to be brought by the airflow between the chimney top and wind barrier surrounding the chimney openings. At Model B, the wind angle of 45 degree also shows the lowest neck pressure, but the difference due to wind angle seems smaller than that of Model A.

At Model C, the inclination of *P-V* curve is rather larger than that of Model B, but the neck pressure shows the lowest value in these three models, Model A, B &C. It can be said that the largest top area causes blocking effect in the natural wind and makes the largest negative pressure at chimney top.

In the case of Model D, the pressure loss depends on the wind direction angle. From the graph, at v/V >0.3, the order of pressure loss is 0º or 22.5º, 45º, 67.5º, 90º. The wind direction of 90º can produce the lowest pressure due to strong side suction made by large section area of the chimney top. In the case that the approach wind can enter the chimney top without obstacles at wind direction angle of 0º, blocking effect of the airflow in the confined rectangular vent can produce larger pressure loss than the other wind angle.

These tendencies are also true of Model E, and the difference of wind angle is larger than that of Model E. This is, of course, affected by Venturi effect due to the constricted section area of rectangular vent.

Model F is an example of real chimney installed on the roof of school building in Kobe, Japan (see **Fig.8**). These chimneys are connected to the large lecture halls on the 3rd floor of 6-story building. Each lecture hall have two chimneys and 300 students in the class, and the hall will be ventilated by both wind-force and buoyancy. As is seen in Fig.2, Model F has a small opening inside to protect the vertical duct from heavy rain. This opening will produce large pressure loss in P-V curve of **Fig.7**, which seems like a quadratic function. This means total pressure loss coefficient of chimney is almost constant, because of the small opening inside the chimney. The difference by wind direction angle is relatively small. Although Model F was designed with the priority of aesthetic point of view, it is made clear from **Fig.7**

that this model is not superior to other chimney models from the viewpoint of ventilation capacity.

From **Fig.7**, it is concluded that Model C is the best in respect of ventilation capacity utilizing wind force, because this chimney has the lowest neck pressure in wide range of neck velocity. In this paper, only 6 models were examined, but there might be some better shapes of chimney top. It is desired that many useful data of P-V curves of wind chimney will be obtained by further study.

4. Conclusions

The concluding remarks made clear in this paper are as follows:

1) The calculation of airflow rate of wind chimney is enabled by identifying the relationship between airflow rate of chimney and the pressure at the neck of chimney. This relationship is called Pressure-Volume curve (*P-V* curve).
2) The modified Bernoulli's equation was introduced to calculate the airflow rate of chimney, taking account of local pressure coefficient C_L in the air at chimney top position.
3) Six models of chimney with different shapes were tested by supplying air through the chimneys in a wind tunnel with approach wind of 5 m/s to measure the *P-V* curves. This experiment was turned out to be useful to know the ventilation characteristics of wind chimney.
4) By normalizing *P-V* curves, different *P-V* curves can be presented by representative one curve independent of velocity effect for each chimney type and wind direction angle. This is the relationship between the velocity at the chimney neck divided by approach wind velocity and the static pressure at the chimney neck divided by dynamic pressure of approach wind.
5) Among six chimney models, two models with large wind barriers have excellent capacity in comparison with the other models. Especially Model C with wind barriers whose bottom is covered with plates.

Acknowledgments

The authors would like to appreciate the cooperation of Takenaka Research & Development Institute.

References

1. Ishihara M., “Ventilation characteristics of the monitor roof, Transactions of architecture and building science”, AIJ (Architectural Institute of Japan), 1969, Vol.65, pp.66-72 (In Japanese)

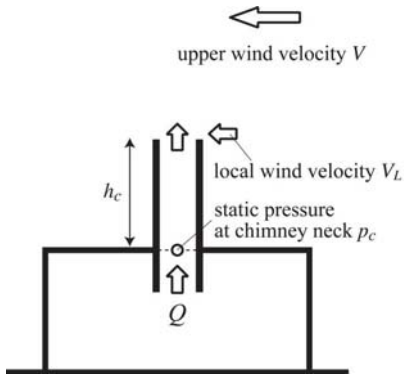


Fig. 1 Explanation of variables

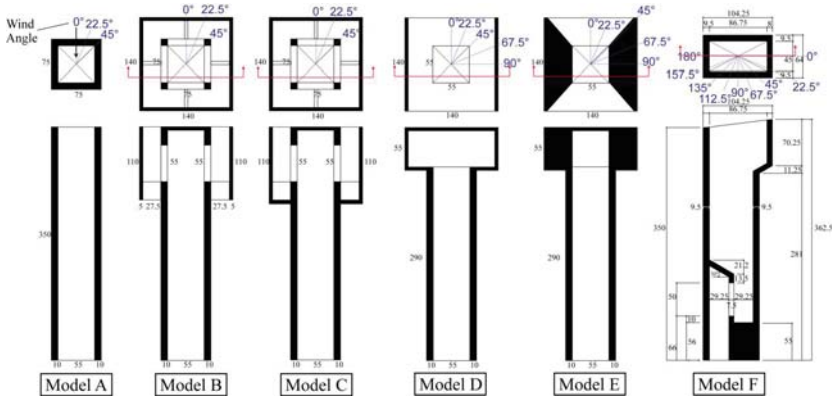


Fig. 2 Cross-section of test models of wind chimney

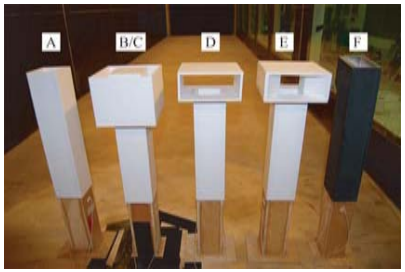


Fig. 3 Tested chimney models with different tops

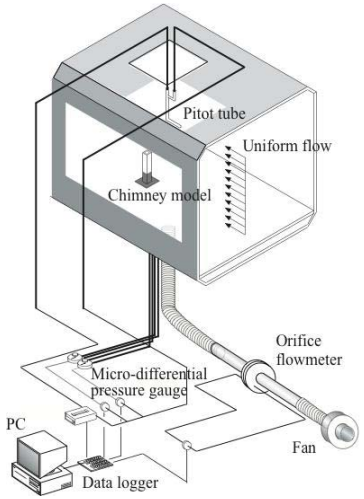


Fig.4 Experimental setup

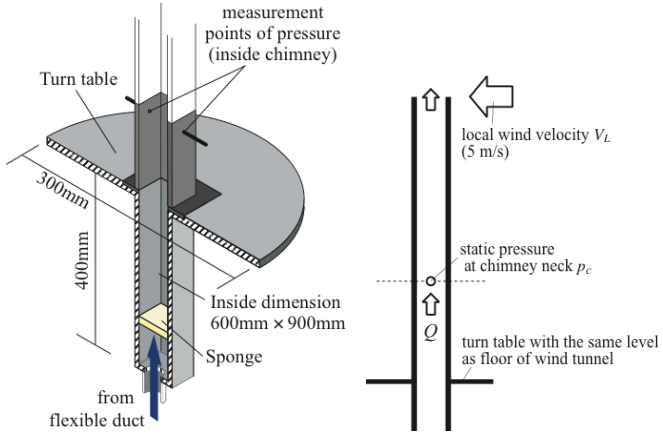
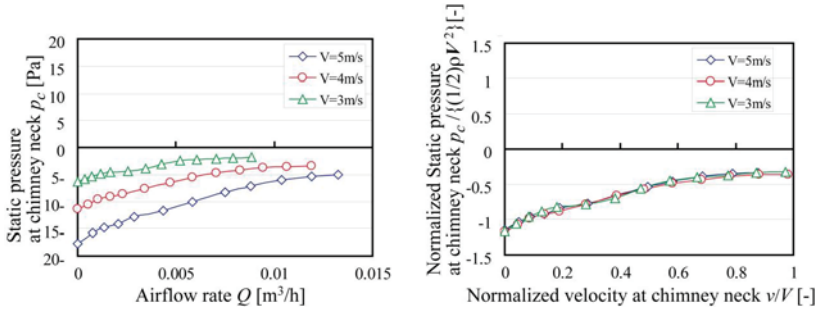


Fig.5 Measurement point of pressure at the neck of chimney



a) Pressure-volume curves b) Normalized pressure-volume curves

Fig.6 Relation between Airflow rate and static pressure at the neck of chimney
(Chimney : Model A, wind direction : 0 degree)

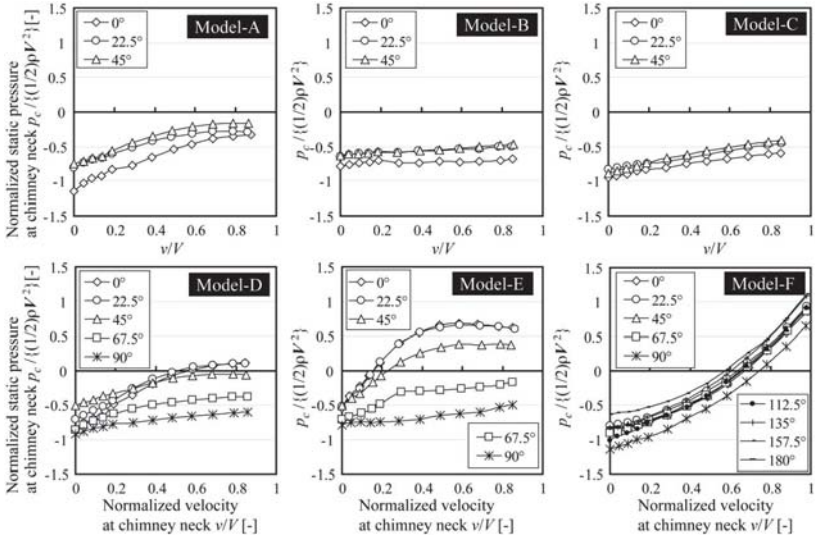


Fig. 7 Comparison of flow characteristics of each chimney



Fig.8 Appearance of chimney (Model F) in real building

Table 1 Experimental conditions

Shape of chimney top	Wind direction angle [degree]
A (simple outlet)	0, 22.5, 45
B (wind-break plate)	0, 22.5, 45
C (wind-break plate with bottom plate)	0, 22.5, 45
D (horizontal duct)	0, 22.5, 45, 67.5, 90
E (horizontal duct introducing contraction flow)	0, 22.5, 45, 67.5, 90
F (rainproof : example applied to a real building)	0, 22.5, 45, 67.5, 90, 112.5, 135, 157.5, 180

Influence of the Configuration of Consecutive Street Canyons and Atmospheric Stability

Byoungchull OH[1], Ryozo OOKA[2], Takeaki KATSUKI[3] and Hideki KIKUMOTO[1]

[1] Graduate Student, The University of Tokyo, Japan

[2] Professor, The University of Tokyo, Institute of Industrial Science, Japan

[3] Project Researcher, The University of Tokyo, Institute of Industrial Science, Japan

Abstract

This research, based on Computational Fluid Dynamics (CFD) analysis, focuses on the wind characteristics and the ventilation performance in the consecutive street canyons produced by various building complex configurations. In this research, the buildings in the street canyon space were distributed in either staggered or normal arrangements and, in consideration of the varying distribution and height of different buildings, high-rise buildings, middle-rise buildings and low-rise buildings were all included. The air flow field and concentration distribution change were compared at various degrees of atmospheric stability. In order to examine the ventilation efficiency and purging flow rate (PFR), 3 different atmospheric conditions were analyzed - a stable case, a weak-unstable case and an unstable case. Based on the analysis results, it was found that in isothermal cases the best pedestrian effect and ventilation efficiency were achieved when buildings with different heights were laid out in a normal arrangement. In non-isothermal cases, the highest ventilation efficiency was found in unstable conditions.

Keywords: CFD, Ventilation performance, Staggered arrangement, Normal arrangement, Atmospheric stability, Ventilation efficiency, PFR, Pedestrian effect

Introduction

Recently, the urban outdoor environment is worsening for air pollution by virtualization and urban congestion. For the purpose of improvement of air quality of urban area, it is necessary to enhance urban ventilation through and ventilation efficiency. In previous research, Yoshie et al. [1] carried out wind tunnel experiment under the conditions of variations of height of building and of gross building coverage ratio and gross floor-area ratio. Moreover, the effect of building height on the wind velocity and temperature at the pedestrian level was examined. The concept of ventilation in the vertical direction is introduced. Uehara et al. [2, 3] examined the flow field and the diffusion field under various the atmospheric stabilities in urban street canyon by wind tunnel experiments. Kim et al. [4] analyzed the influence of aspect ratio of the canyon space and surface temperature on airflow pattern and pollutant dispersion by CFD simulation. Furthermore, Hong et al. [5] examined the urban ventilation efficiency around an elevated highway by use of Visitation Frequency (VF) [6] and Purging Flow Rate (here after PFR) [7, 8] . However, the floor area ratio and the building coverage ratio are limited by legislations on an urban planning and a construction plans in the real urban. In these circumstances, it is difficult to obtain the general result of the ventilation efficiency.

In this study, it was assumed that several similar buildings were arranged in the mainstream direction and that a boundary layer was fully developed over the arrangement of street canyons. Four specific cases, each with a different type of building arrangement and height, were then compared at the same floor area ratio and building coverage-ratio in the same urban street canyon space. The pedestrian effect was evaluated in terms of the absolute wind velocity at pedestrian level, and ventilation was evaluated across a plane area at a standard height of 0.5H (7.5 [m]). CFD results were used to examine the pedestrian effect and ventilation efficiency in each case. Three additional cases, with different degrees of atmospheric stability, were also examined to investigate the influence of atmospheric stability on the flow pattern and the ventilation efficiency.

Description of CFD analysis

1. Analysis Cases

Fig.1 shows the analysis cases used in terms of their target area and Table 1 shows the floor area ratio, building coverage ratio and building size for each case. In Case 4, the building coverage ratio was a little smaller than the other cases. The [maximum] height of all cases was about 6.67H (100 [m]) in terms of computational area. The isothermal cases were Case 1 to Case 4 and the non-isothermal cases were Case 5 to Case 7. The geometric parameters of the non-isothermal cases were the same as those used for Case 1.

2. Numerical conditions

Table 2 shows the governing equations used for CFD simulation. In this study, the standard k-ε model [9] was used as the turbulence model. Table 3 shows the analysis conditions and the boundary conditions. The first-order upwind scheme was used for the differential scheme of the convection term. A second-order central difference scheme was used for the other spatial finite differences. The generation condition of the pollutant was specified as 1 [μg m^{-3} s^{-1}] in the space from ground level up to a height of 0.5H. The transport of pollutant was assumed to be passive scalar. The temperature conditions are shown in Table 3. Table 4 shows the bulk Richardson number and temperature conditions of the non-isothermal cases.

Calculation of ventilation rate and PFR

In this study, ventilation efficiency was estimated from the interface-based ventilation rate and PFR of the target area of the canyon space, from ground level up to a height of 0.5H

(averaging the upper surface of the target area). Equation (1) and equation (2) show the interface-based ventilation rate and PFR.

$$Q[m^3 s^{-1}] = \int_V q dv / \frac{1}{S} \int_S C ds = q_p / Cs \quad (1)$$

$$PFR[m^3 s^{-1}] = \int_v q dv / \frac{1}{V} \int_v C dv = q_p / Cp \quad (2)$$

Here, q is the velocity of the pollutant generation rate per unit volume [μg $m^{-3}s^{-1}$], C is the pollutant concentration [μg m^{-3}], q_p is the velocity of the pollutant generation rate per unit time in the target area [μg s^{-1}], Cs is the horizontally averaged value of the concentration at the upper-interface of the target area [μg m^{-3}], and C_P is the spatially averaged value of the concentration in target area p [μg m^{-3}].

CFD results and discussion

In all the isothermal and non-isothermal cases, the absolute wind velocity, turbulent energy (k), temperature and the concentration of contaminant were examined in the vertical profile throughout the horizontal plane averaged across the target area.

1. Results for absolute wind velocity and turbulence energy, k

The profile of horizontally averaged absolute wind velocity

Fig. 2 and Fig. 3 show the profile of the horizontally averaged absolute wind velocity ($|\mathbf{U}| = \sqrt{U_1^2 + U_2^2 + U_3^2}$) in the isothermal cases and the non-isothermal cases, respectively. The absolute wind velocity in Case 1 was generally larger than the other cases, except near ground level in the canyon space. The absolute wind velocity of Case 2 was the smallest within the canyon space. In the upper region above the canyon, the absolute wind velocity in Case 1 was the largest, while the absolute wind velocity in Case 3 and Case 4 decreased because of the resistance of the high-rise buildings. From the viewpoint of the pedestrian effect, Case 3, which was composed of non-uniform building blocks, proved to be the most efficient. These results are very similar to those of Hagishima et al. [10]. By comparison, in the non-isothermal calculations, there was little difference between Cases 1, 5, 6, and 7 within the canyon space, from ground level up to a height of 1.0H (Fig. 3). In the upper region above the canyon, the absolute wind velocity in Case 1 (neutral) and Case 5 (stable) increased more than Case 6 (weak-unstable) and Case 7 (unstable). This was due to the turbulent kinetic energy and turbulent coefficient of viscosity in Case 6 and Case 7, increased by the buoyancy effect (as explained later). It was concluded that atmospheric stability does not have a great influence on the pedestrian effect.

The profile of horizontally averaged turbulent kinetic energy

The vertical profiles of horizontally averaged turbulent kinetic energy, k, in the isothermal and non-isothermal calculations are shown in Fig. 4 and Fig. 5. The turbulent kinetic energy in Case 3 was the largest and Case 4 was the smallest within the canyon space. Case 3 showed the largest value above a height of 1.0H and Case 4 showed the smallest. In the non-isothermal calculations, Case 7 (unstable) generally showed the largest value and Case 5 (stable) showed the smallest (see Fig. 5). This was due to atmospheric instability causing buoyancy production and increasing turbulent kinetic energy. The atmospheric instability increased the production term of turbulent energy by means of this buoyancy effect.

2. Results for temperature and concentration

The profile of horizontally averaged temperature

Fig. 6 shows the vertical profile of horizontally averaged temperature results for non-isothermal calculations. There was a very large vertical temperature difference within the canyon space in the unstable cases, while the vertical temperature gradients above the canyon were comparatively small.

The profile of horizontally averaged concentration

Fig. 7 shows the vertical profile of horizontally averaged concentration results for the isothermal calculations. Below a height of 1.0H, the concentration in Case 3 was the lowest while the concentration in Case 4 was the highest. This is because the turbulent kinetic energy in Case 4 was small, and the turbulent mixing effect was not active. On the other hand, as the turbulent kinetic energy in Case 3 was large, the concentration decreased. Fig. 8 shows the results of the non-isothermal calculations. The concentration in Case 5 was larger than Case 1, whereas the concentration in Case 6 and Case 7 was smaller than Case 1. There was a clear relationship between atmospheric stability and concentration. This was due to the relationship between atmospheric stability and turbulent energy, i.e., the turbulence mixing effect illustrated in Fig. 5.

The interface-based ventilation rate and PFR per unit ground surface area

In order to analyze ventilation efficiency in the target area, the interface-based ventilation rate and PFR per unit ground surface area of the target area were compared. Here, the interface-based ventilation rate refers to the air exchange rate through the interface, as explained above. The height of the interface was set at 0.5H. Fig.9 shows the results of isothermal and non-isothermal calculations for the interface-based ventilation rate and PFR per unit ground surface area of the target area. These two indices showed the same overall trends, but the interface-based ventilation rate was a little larger than the PFR. This is because the averaged concentration of the interface

area was much lower than the averaged concentration of the canyon space. Based on the isothermal calculations, Case 3 showed the largest ventilation rate and Case 4 showed the smallest. In terms of the PFR, the results for Case 3 were also larger than Case 4.It can, therefore, be concluded that Case 3 produced the most efficient ventilation effect and Case 4 the worst. In terms of the interface-based ventilation rate, the results for Case 5 were smaller than Case 1, and the results for Case 7 were the largest, overall. Likewise, in terms of PFR per unit ground surface area, the results for Case 5 were also smaller than Case 1 and the results for Case 7 were the largest. In conclusion, it can be seen that atmospheric conditions had a significant effect on t he ventilation rate. Therefore, in this study, neutral atmospheric conditions (as shown by Case 1) produced a more efficient ventilation rate than stable conditions (Case 5) while unstable atmospheric conditions produced the most efficient ventilation rate of all. This is because the buoyancy effect, based on atmospheric stability, affects diffusion properties due to the turbulence mixing effect. The relationship between the bulk Richardson number (Rb) in the canyon space and the interface-based ventilation rate per unit ground surface area is shown in Fig. 10. As can be seen, atmospheric instability increased ventilation efficiency and atmospheric stability decreased ventilatin efficiency.

Conclusions

In this study, the ventilation efficiency within street canyons and the effects of wind on pedestrians were evaluated using CFD to compare various building configurations and arrangements. The following conclusions were obtained:

1. In the isothermal calculations, the horizontally averaged velocity in Case 1 (middle-rise buildings in a normal arrangement) was generally quite large within the street canyon. However, near the surface of the ground the velocity in Case 3 (high-rise and low-rise buildings in a normal arrangement) was the largest of all. Above the street canyon level, the horizontally averaged velocity in Case 3 and Case 4 (high-rise buildings in a normal arrangement) was quite small compared with the other cases tested.

2. In the non-isothermal calculations, there was very little difference between Case 1 (neutral), Case 5 (stable), Case 6 (weak-unstable), and Case 7 (unstable). Therefore, it was concluded that atmospheric stability has relatively little effect on wind at the pedestrian level.

3. In the isothermal calculations, the concentration in Case 2 (middle-rise buildings in a staggered arrangement) and Case 4 (high-rise buildings in a normal arrangement) was larger than that of Case 3 (non-uniform building height in a normal arrangement). This is because the non-uniformity of buildings caused a turbulence mixing effect. Therefore, the interface-based ventilation rate and PFR in Case 3 were relatively large.

4. In the non-isothermal calculations, the concentration in Case 5 (stable) was larger than Case 7 (unstable). This was a result of the unstable conditions generating turbulence due to the buoyancy effect and causing turbulent mixing. Therefore, the interface-based ventilation rate and PFR increased in proportion to the intensity of atmospheric instability.

References

1. Yoshie RYUICHIRO, Tanaka HIDEYUKI, Shirasawa TAICHI, Kobayashi TSUYOSHI : Experimental study on air ventilation in a built-up area with closely-packed high-rise buildings, *Journal of Environmental Engineering (Transaction of AIJ).* Vol. 73, No. 627, pp. 661-667. May 2008

2. Kiyoshi UEHARA, Shuzo MURAKAMI, Susumu OIKAI, Shinji WAKAMATSU : Wind tunnel experiments on how thermal stratification affects flows in and above urban street canyons, *Atmospheric Environment 34*, 1553-1562, 2000

3. Kiyoshi UEHARA, Shuzo MURAKAMI, Susumu OIKAI, Shinji WAKAMATSU : Wind tunnel test of concentration fields around street canyons within the stratified urban canyon layer, *J. Archit. Plann. Environ. Eng., AIJ*, No. 499, 9-16, Sep., 1997

4. Jae-Jin KIM, Jong-Jin KIM : A numerical study of thermal effects on flow and pollutant dispersion in urban street canyons, *Journal of Applied Meteorology*, 1999, Vol. 38 pp. 1249-1261

5. Hong HUANG, Shinsuke KATO, Ryozo OOKA, Taifeng JIANG : CFD Analysis of Ventilation Efficiency around an Elevated Highway using Visitation Frequency and Purging Flow Rate, *The Sixth Asia-Pacific Conference on Wind Engineering (APCWE-VI)*, pp.10, 2005.09

6. Csanady G. T. : Dispersal by randomly varying currents, *J. Fluid Mech.* Vol. 132, pp. 375-394, 1983

7. Sandberg, M. : The use of moments for ventilation assessing air quality in ventilated room, *Building Environ., 18*, 1983

8. Sandberg, M. : Ventilation effectiveness and purging flow rate - A review, ISRACVE ASHRAE, pp-17, 1992 *International Symposium on Room Air Convection and Ventilation Effectiveness*, *University of Tokyo*, pp. 1- 21, 1992

9. B. E. Launder, D. B Spalding : The Numerical computation of Turbulent Flows, *Computer Methods in Applied Mechanics and Engineering 3*, pp. 269 – 289, 1974

10. Aya HAGISHIMA, Jun TANIMOTO, Koji NAGAYAMA, Masahiro KOGA : Wind tunnel experiment on drag force coefficient of regular arrangement rectangular blocks with different heights, *Journal of Environmental Engineering (Transaction of AIJ)* , no. 619, pp. 39-46. Sept. 2007

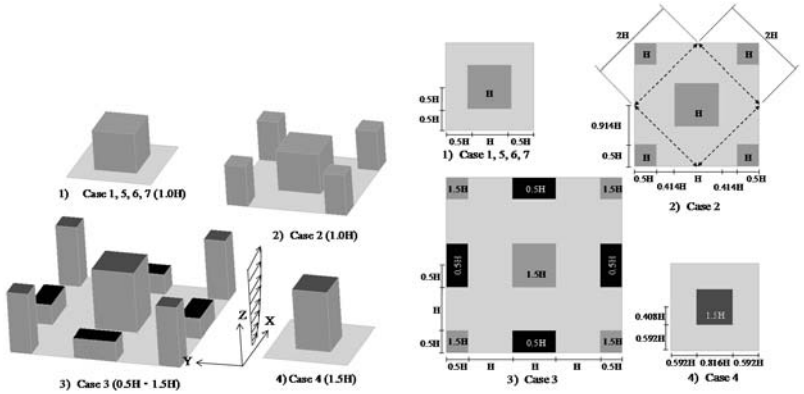


Fig. 1 Details of analysis cases showing target area (1.0H = 15 [m])

Table 1 Details of floor-area ratio, building coverage ratio, and building size

Case	Building size (X × Y × Z)	Building disposition	Floor-area ratio	Building coverage ratio
Case 1, 5, 6, 7	1.0H × 1.0H × 1.0H : Middle-rise	Normal arrangement	125%	25%
Case 2	1.0H × 1.0H × 1.0H : Middle-rise	Staggered arrangement	125%	25%
Case 3	1.0H × 1.0H × 1.5H : High-rise (Ⅰ)	Normal arrangement	125%	25%
	1.0H × 1.0H × 0.5H : Low-rise			
Case 4	0.816H × 0.816H × 1.5H : High-rise (Ⅱ)	Normal arrangement	125%	16.64%

1.0H = 15 [m]

Table 2 Governing equations for the k-ε two-equation turbulence model

$\frac{\partial U_i}{\partial X_i} = 0$	Continuity equation
$\frac{\partial U_i}{\partial t} + \frac{\partial U_i U_j}{\partial X_j} = -\frac{\partial}{\partial X_i}\left(\frac{P}{\rho} + \frac{2}{3}k\right) + \frac{\partial}{\partial X_j}\left\{\nu_t\left(\frac{\partial U_i}{\partial X_j} + \frac{\partial U_j}{\partial X_i}\right)\right\} - g\beta\Delta T\delta_{i3}$	Momentum equation
$\frac{\partial k}{\partial t} + \frac{\partial k U_j}{\partial X_j} = \frac{\partial}{\partial X_j}\left(\frac{\nu_t}{\sigma_1}\cdot\frac{\partial k}{\partial X_j}\right) + (P_k + G_k) - \varepsilon$	Turbulent energy transport equation
$\frac{\partial \varepsilon}{\partial t} + \frac{\partial \varepsilon U_j}{\partial X_j} = \frac{\partial}{\partial X_j}\left(\frac{\nu_t}{\sigma_2}\cdot\frac{\partial \varepsilon}{\partial X_j}\right) + \frac{\varepsilon}{k}(C_1 P_k + C_3 G_k) - C_2\frac{\varepsilon^2}{k}$	Turbulent dissipation rate equation
$\nu_t = C_\mu \frac{k^2}{\varepsilon}$	Equation for deciding ν_t
$P_k = \nu_t\left(\frac{\partial U_i}{\partial X_j} + \frac{\partial U_j}{\partial X_i}\right)\cdot\frac{\partial U_i}{\partial X_j}$	Production term for k
$G_k = -g\beta\frac{\nu_t}{\sigma_3}\cdot\frac{\partial T}{\partial X_i}\delta_{i3}$	Buoyant production term
$\frac{\partial \Phi}{\partial t} + \frac{\partial \Phi U_j}{\partial X_j} = \frac{\partial}{\partial X_j}\left(\frac{\nu_t}{\sigma_3}\cdot\frac{\partial \Phi}{\partial X_j}\right)$	Scalar transport equation

Here $\sigma_1 = 1.0$, $\sigma_2 = 1.3$, $\sigma_3 = 1.0$,
$C_\mu = 0.09$, $C_1 = 1.44$, $C_2 = 1.92$, $C_3 = C_1 (G_K > 0)$ or $C_3 = 0 (G_K \leqq 0)$

Where U_i is the mean of the velocity components in the x (i = 1), y (i = 2), and z (i = 3) directions, respectively. P is the mean static pressure, ρ is the air density, ν_t is the turbulent eddy viscosity, k is the turbulent kinetic energy, ε is the turbulent kinetic energy dissipation rate, g is the gravitational acceleration, β is the thermal expansion coefficient of air, δ_{ij} is the Krönecker delta, and Φ is the scalar such as temperature and concentration.

Table 3 CFD analysis conditions and boundary conditions

	Wind velocity	k	ε	Concentration	Temperature
Sky	$\frac{\partial U_1}{\partial X_3} = 0$, $\frac{\partial U_2}{\partial X_3} = 0$, $U_3 = 0$	$\frac{\partial k}{\partial X_3} = 0$	$\frac{\partial \varepsilon}{\partial X_3} = 0$	C = 0	T = 30 [℃]
Side	$\frac{\partial U_1}{\partial X_2} = 0$, $U_2 = 0$, $\frac{\partial U_3}{\partial X_2} = 0$	$\frac{\partial k}{\partial X_2} = 0$	$\frac{\partial \varepsilon}{\partial X_2} = 0$	$\frac{\partial C}{\partial X_2} = 0$	$\frac{\partial T}{\partial X_2} = 0$
Inlet	Cyclic ($\Delta p/\Delta x$) = 0.008/30 [Pa m^{-1}]	Cyclic			
Outlet					
Ground surface	Z_0 log low (Z_0 = 0.01 [m])	$\frac{\partial k}{\partial X_3} = 0$	$\frac{\partial \varepsilon}{\partial X_3} = 0$	$\frac{\partial C}{\partial X_3} = 0$	T = 29 [℃] (stable) T = 35 [℃] (weak-unstable) T = 40 [℃] (unstable)
Surface		$\frac{\partial k}{\partial Xn} = 0$	$\frac{\partial \varepsilon}{\partial Xn} = 0$	$\frac{\partial C}{\partial X_3} = 0$	

Xn: Vertical direction on wall surface

Table 4. Atmospheric stability and bulk Richardson number for different cases

Case	Atmospheric stability	Atmospheric Temperature [℃] : T	Surface Temperature [℃] : Ts	*Rb*
Case 1	Neutral	30		0
Case 5	Stable	30	29	0.0444
Case 6	Weak- unstable	30	35	-0.3171
Case 7	Unstable	30	40	-0.6511

bulk Richardson number $Rb = gH(T_H - T_S) / \{T + 273\} (U_H)^2\}$

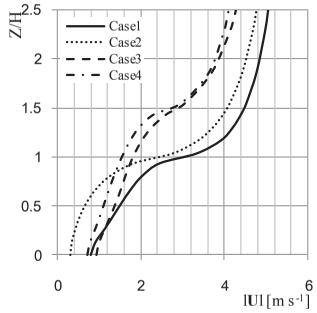


Fig. 2 Vertical profile of horizontally averaged absolute wind velocity (|U|) for isothermal cases

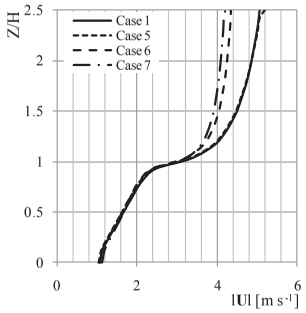


Fig. 3 Vertical profile of horizontally averaged absolute wind velocity (|U|) for non-isothermal cases

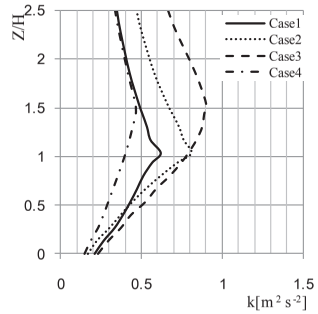


Fig. 4 Vertical profile of horizontally averaged turbulent kinetic energy

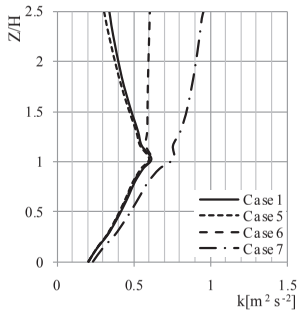


Fig. 5 Vertical profile of horizontally averaged turbulent kinetic energy

for isothermal cases

for non-isothermal cases

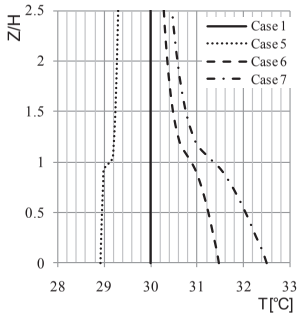


Fig. 6 Vertical profile of horizontally averaged temperature for non-isothermal cases the horizontal plane mean

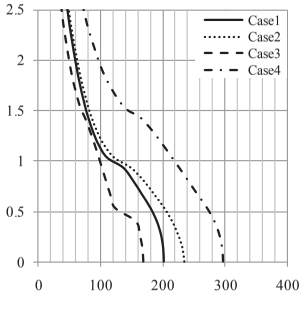


Fig. 7 Vertical profile of horizontally averaged concentration for isothermal cases

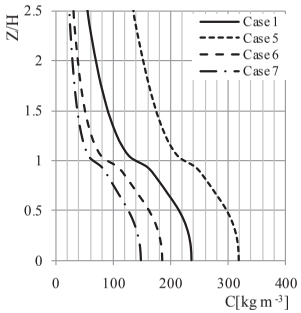


Fig. 8 Vertical profile of horizontally averaged concentration for non-isothermal cases

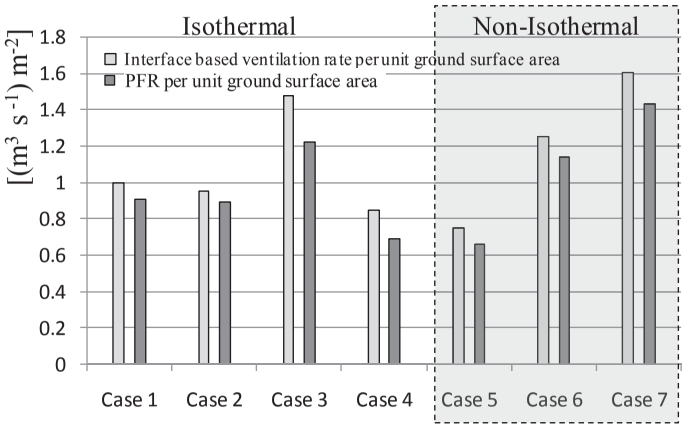


Fig. 9 Interface-based ventilation rate and PFR per unit ground surface area

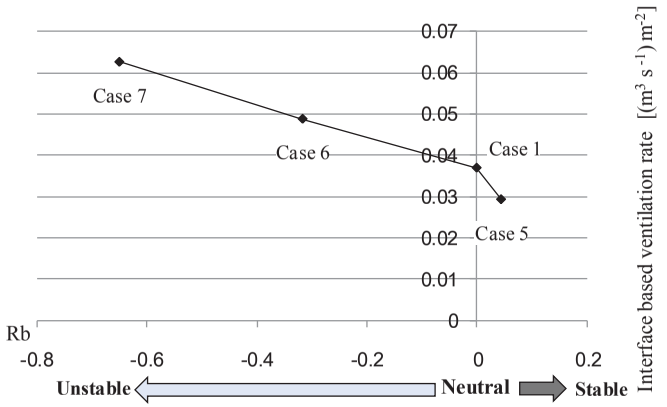


Fig. 10 Rb and interface-based ventilation rate per unit ground surface area

Effect of Intermittent Operation of Ventilation System on Indoor Air Quality in Apartments

Cheol-woong Shin[1], Hyung-Jun Kim[2], Jun-seok Park[3]

[1] Graduate School of Dept. of Sustainable Architectural Engineering, Hanyang University, Seoul, Korea

Master course degree, of Sustainable Architectural Engineering, Hanyang University, Seoul, Korea

3 Dept. Of Architectural Engineering, Hanyang University, Seoul, Korea

Abstract

This study analyzed the effect of intermittent operation of ventilation system on changes of indoor air pollutants' levels through field measurements. The changes of indoor air pollutants' levels, such as, CO2, PM10, TVOCs, and HCHO were monitored during 24 hours at each ventilation condition. One group was the operation time: 2 hours, 8hours, and 24 hours. The other group was the changes of start time of ventilation, before noon, after noon, and night, while the ventilation was operated only two hours. From these results, it was found that the operation time of ventilation significantly affects the levels of pollutants. However, the start time of ventilation did not showed the significant differences between conditions, because of time variations of sources of pollutants. From these results, it is suggested that rational strategy for operation of ventilation system will be developed for indoor air quality and energy savings in the apartments.

Keywords: Apartment, Ventilation system, Intermittent Operation, Indoor Air Quality, improvement.

Introduction

Increasing of mechanical operating of newer apartment has contributed to increasing ventilation energy consumption since the 2006 building standard law on ventilation in Korea.

Many studies had been done on the effect of ventilation system in apartments on indoor air quality and decreasing energy consumption by mock-up tests and computer simulations. As a result in Choi study[2] is to find optimum ventilation time in a newly-built apartment house at which the ventilator installed. It is found that the HCHO and toluene concentrations are remarkably decreased with the elapse of ventilation time and the concentration reduction rate is increased with increment of air change rate after one hour after operating the ventilator. And also, in Hwang study[3], three types of mechanical ventilation system of apartment house including HRV were simulated by multi-zone modeling. Simulation results suggest an appropriate and economical renovation method of apartment house ventilation system for reducing indoor air contamination. Lee study[4] was to evaluate the possible control modes of hybrid ventilation system in applying to general apartments by using TRNSYS simulation program. But there are not many studies on a real-time measurement of ventilation and indoor air quality. In this study, ventilation equipment was installed and actual residents was living in apartment, changes in operating hours and operating times due to changes in indoor air was measured changes in environmental factors and propose an efficient ventilation operation.

Method

Table 1 shows outline of the apartment. It was attempted to select the apartment that was built after the law about the installation of the ventilation system in apartments had legislated. Therefore the apartment that was built before 2007 and has ventilation system was selected. The occupants have moved into the apartment in October 2007 and about 1007 households have lived. These area of residence consisted of from 70 ㎡ to 146 ㎡. The apartment is heated by district heating system.

Table 1 Description of the apartment 1

Item	Contents
Location	GyeongGi-do
Completion	October. 2007
Filed test period	21 Apr 2009 ~ 1 may 2009
Area and Number of occupants	106m^2 / 4 people
Ventilation system	Mechanical supply air / Natural exhaust

Table 2 Ventilation operating condition and IAQ measurement

Condition	Case	Test Period	Ventilation operating condition	Measurement factor	Measurement equipment
Changes of operation time	Case A Case B	5day	① Non-operating ② 2hour operating (18:00 ~ 20:00) ③ 8 hour operating (15:00 ~ 23:00) ④ 24 hour operating (00:00 ~ 24:00)	Temperature [℃] Humidity [%] CO_2 [ppm] PM10 [mg/m^3] TVOCs [μg/m^3] HCHO [μg/m^3]	espec R-11 Q-track Dust track Mini pump (GC/MS)
Changes of start time of ventilation	Case C Case D	4day	① Non-operating ② Before noon (10:00 ~ 12:00) ③ After noon (18:00 ~ 20:00) ④ Night (20:00 ~ 22:00)	Temperature [℃] Humidity [%] CO_2 [ppm] PM10 [mg/m^3]	

The apartment ventilated by mechanical supply fan and there is no exhaust fan. The ventilation rate was over 0.7 ACH. Result of airtightness measurement in 4 households is similar that airtightness and air change rate 4 households are similar to that result of measurement airtightness and air change rate. IAQ measuring point decided in the middle living room to minimize the supply air effect by using simulation. Table 2 shows ventilation operating conditions and IAQ measurement. It was maintain a constant occupant's presence in test households while during IAQ measurement period. Ventilation minimum operation set 2hour with the result that CFD simulation and mass valance

Results

Results of Indoor pollutant concentration of change by ventilation non-operating

Fig 1 shows change of CO2 concentration and temperature during the one day while ventilation not driving. CO2 average concentration of A and B households exceed the CO2 criterion but C and D households to maintain the CO2 criterion concentration. PM10 measurement in 4 Households maintains that to below PM10 criterion concentration 0.15μ

g/m^3. In all household CO2 and PM10 concentration shows that at morning(07:00 ~ 09:00) and evening(18:00 ~ 22:00) has the high concentration patterns. The average temperature of all households was measured from 23.6℃to 24.8℃ and the average humidity was measured from 45% to 61%.

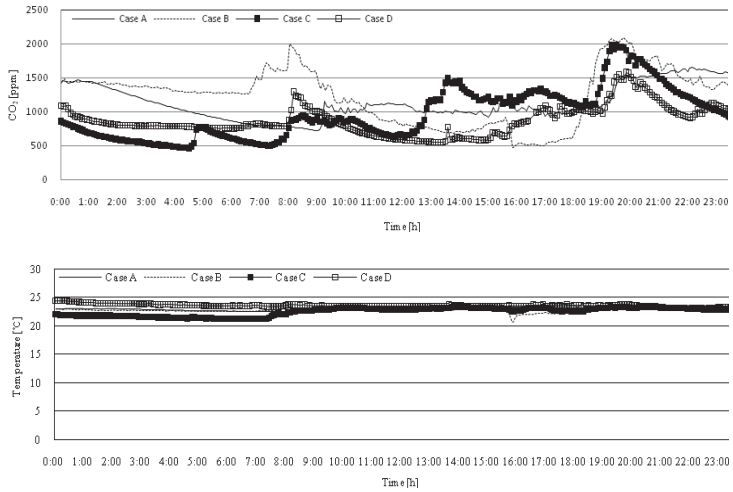


Fig. 1 CO_2 concentration and temperature changes when Ventilation was non-operating

Results of TVOCs and HCHO measurement In A and B household maintain to below TVOCs and HCHO criterion concentration when ventilation not are driving.

Results of IAQ measurement according to increasing ventilation operation time

Fig 2 show change of CO2, PM10 concentration and ventilation operating schedule in A, B households while it is according to increasing ventilation operation time. Avera ge daily CO2 concentration was exceed the criterion concentration by only non-operati ng and 2hour operating of ventilation. Average daily concentration of PM10 maintains below the criterion concentration 0.15μg/m^3 by all ventilation conditions.

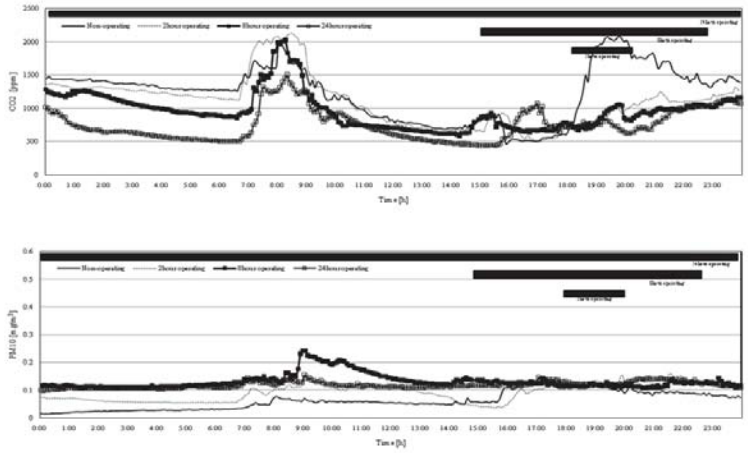


Fig. 2 CO2 and PM10 concentration change by ventilation increasing operation time

According to increasing ventilation operation time in Fig 3 as below, shows overtime of daily by CO2 and PM10 criteria concentration. Criteria pollutant concentration set a CO2 concentration 1000ppm and PM10 0.05mg/m3 for judge the concentration chan ge of pollutant.

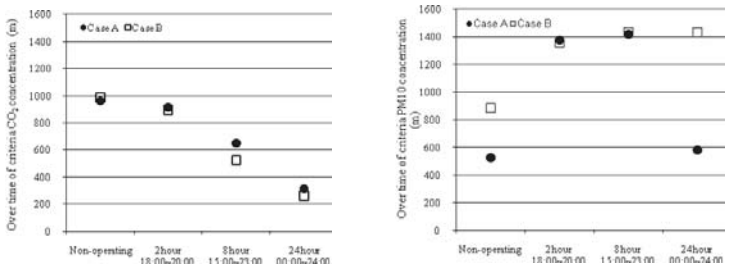


Fig. 3 Overtime of criteria concentration by change of ventilation increasing time

Overtime of daily by CO2 and PM10 criteria concentration analysis shows the CO2 c oncentration shows decreasing trend but PM10 concentration not shows decreasing tren d in A, B households while according to increasing ventilation operation time. The re duction effect of co2 concentration is judged to be effective while according to increa sing ventilation operation time. Fig 4, 5 shows change of VOCs and HCHO concentr ation when before and after operate ventilation. As a result of VOCs and HCHO con centration reduction effect analysis were less effective while ventilation operation time was increasing

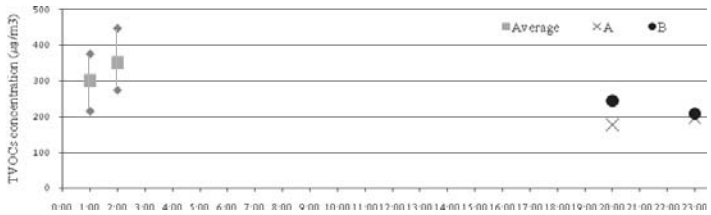


Fig. 4 TVOCs concentration of according to increasing ventilation operation time

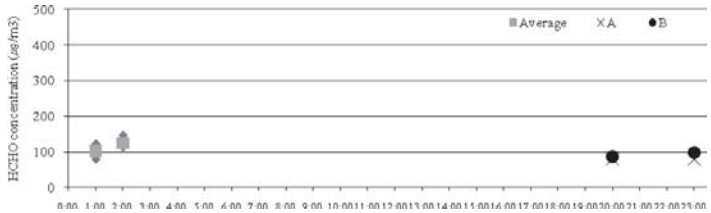


Fig. 5 HCHO concentration of according to increasing ventilation operation time

IAQ measurement according to variation ventilation operation time period

Fig 6 shows change of CO2, PM10 concentration and ventilation operating schedule i n C, D households while according to change of start time of ventilation. CO2 and P M10 concentration is higher at before noon, after noon and daily concentration of PM 10 shows below criterion concentration. CO2 and PM10 concentration was decreases when after ventilation operating at before noon, after noon. According to change of st art time of ventilation in Fig 7 as below, shows overtime of dai l y b y C O 2 a n d P M 1 0 criteria concentration. Over the measure period, difference of overtime on CO2 conc

entration has produced similar results while according to change of start time of venti lation. As a result of PM10 concentration is higher when ventilation operation at after noon. According to change of start time of ventilation shows less effective the effect of PM10 concentration decreasing.

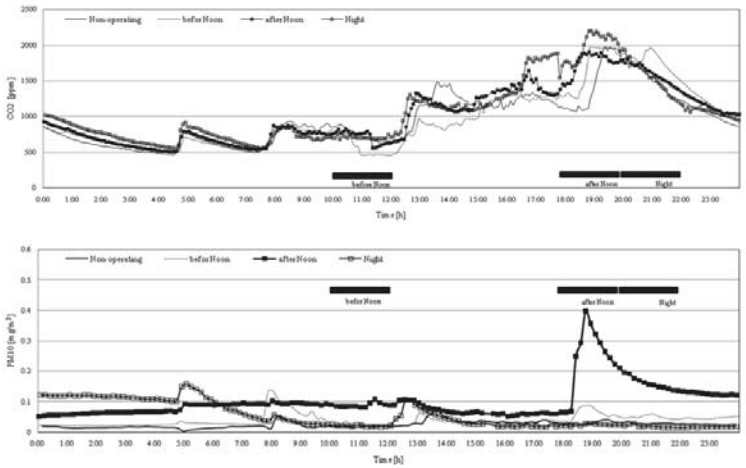


Fig. 6 CO2 and PM10 concentration change by change of start time of ventilation

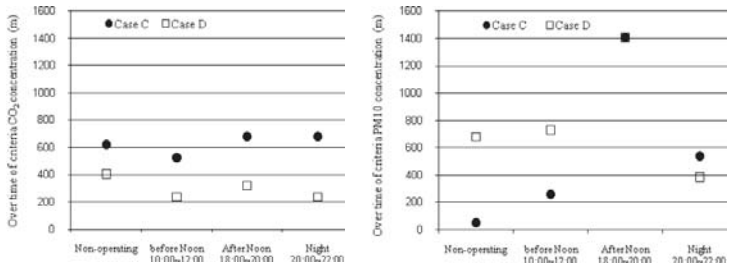


Fig. 7 Over time of criteria concentration by change of ventilation start time

Discussion

Indoor CO2 concentration is higher standard concentration when ventilation operating. For the reason, set 2 hour of ventilation operation time not make a bird of enough ventilation for removal of indoor pollutants. Change of ventilation condition was less effect PM10 concentration change during experimental time. It was not found that effect of occupants activity pattern was lager effect than change of ventilation condition when experimental period. Indoor TVOCs and HCHO concentration change was maintain steady state because apartment had been built 2 years later. It was found that change of ventilation condition had not influence pollutant concentration change.

Conclusions

In this study, the effect of intermittent operation of ventilation system on changes of indoor air pollutants' levels through field measurements was analyzed. And the results of this study are summarized as follows. According to the operation increasing time of ventilation significantly affects the decreasing of CO2 average concentration. Change of ventilation condition less affects the indoor PM10 concentration change. TVOCs and HCHO concentration could maintain regardless of ventilation conditions just by over 2 hour ventilation operating. IAQ

Acknowledgments

This work was supported by Sustainable Building Research Center of Hanyang University

which was supported the SRC/ERC program of MEST (R11-2005-056-02002).

References

1. Hyung-Jun Kim., Jun-Seok Park., "Effects of Ventilation System Operation on Annual Energy Consumption in Apartments," Proceedings of the AIK, Vol. 29, No. 1, 2009, pp.757~760.

2. Seok-Yong Choi., Sang-Hee Kim., Jung-Jae Yee., "The Effect on Indoor Air Quality Improvement by Ventilation Rate in Newly Built Apartment," Korean journal of the SAREK, Vol.18, No.8, 2006, pp.613~687.

3. Tae Chul Hwang., Hyun Woo Lee., Sang Gon Choi., Jin Kwan Hong., "The Study on the Renovation Method of Apartment House Ventilation System for Reducing Indoor Air Contamination," Korean journal of the SAREK, Vol.20, No.6, 2008, pp.409~415.

4. Yong-Jun Lee., Jong-Seo Won., Seung-Bok Leigh., Kyung-Hoi Lee., "An Evaluation of Performance of Hybrid Ventilation System in Apartment focused on Indoor Air Quality," Korean journal of the AIK, Vol.21, No.9, 2005, pp.205~212.

Development of Zonal Model for Predicting Temperature Distribution inside an Office Room with Hybrid Air-conditioning System

Eunsu LIM[1], Toshio YAMANAKA[1]

1 Osaka University, Dept. of Architectural Engineering, Suita, Japan

Abstract

Recently, the hybrid air-conditioning system that used natural ventilation together with a mechanical air-conditioning was proposed. Hybrid air conditioning system is expected to be saving energy and maintain keep indoor thermal environment comfort.

The purpose of this study is to develop a simplified numerical model that predicts distribution of indoor air temperature when the office room is air-conditioned by hybrid air-conditioning. An office room with hybrid air-conditioning system with wind-driven ventilation as natural ventilation was used by object of this study. The temperature distribution can be calculated by solving the equations of air balance and heat balance in each zone. The results of CFD analysis are assumed to be a correct answer in this paper. The air temperature prediction of zonal model was compared with the results of CFD analysis to optimum solution.

Keywords: Hybrid Air-conditioning System, Wind-driven Ventilation, CFD, Zonal Model, Temperature Distribution

Introduction

The natural ventilation is of considerable concern as energy saving method in office room building. Natural ventilation can provide the fresh outdoor air for occupants and maintains

acceptable indoor air quality. However, it is difficult to keep indoor thermal environment comfort only by the natural ventilation. Recently, the hybrid air-conditioning system that used natural ventilation together with a mechanical air-conditioning was proposed. In fact, the number of building with hybrid air-conditioning system is increasing. There have been various investigations of hybrid ventilation and hybrid air-conditioning [1].

The hybrid air-conditioning system is expected as air-conditioning system that can save energy and maintain keep indoor thermal environment comfort. Temperature and airflow distributions inside a room with hybrid air-conditioning system are more complex than those distributions inside a room with only mechanical air-conditioning. It is useful for the design of hybrid air-conditioning system to investigate the indoor airflow characteristics. We have been clarifying the indoor airflow characteristic of the office room with hybrid air-conditioning system [2], [3].

Recently, computational fluid dynamics (CFD) is used extensively in the analysis of airflow, temperature and contaminant distributions. The CFD analysis is able to simulate the detailed prediction of airflow and temperature. However, it takes a lot of time complexities and economical costs to analyze with CFD method. CFD cannot be used at basic design step. It is necessary that temperature and airflow distributions inside room with hybrid air- conditioning are predicted by simple methods.

Objectives

The purpose of this study is to develop a simplified numerical model that can predict distribution of air temperature inside an office room with a hybrid air-conditioning system with wind-driven ventilation as natural ventilation. It is necessary to clarify the indoor air characteristics. CFD analysis was conducted to clarify the air temperature and airflow distribution inside an office room. The results of CFD analysis are used to be correct values in this paper.

The air temperature prediction of zonal model was compared with the results of CFD analysis to optimum solution.

Outline of CFD

Figure 1 shows the area of CFD analysis. The size of office room is 10.8m x 28.8m in plan and ceiling height is 2.6m. The hybrid air-conditioning system of the office room consists of wind-driven ventilation and mechanical air-conditioning system. The wind-driven ventilation opening is settled at near the ceiling. The win-driven opening was called NVO in this paper. The each NVO has the size of 3.6 (W) x 0.1 (H) m and continues. The mechanical

air-conditioned air is supplied to the office room through under floor air distribution (UFAD) and flowed out from the room through return slits. The each UFAD has the size of 0.2 (W) x 0.2 (H) m.

Table 1 shows the setting of CFD analysis. Standard k-ε Model was used as the turbulence model. SIMPLEC was used as pressure-velocity coupling algorithm for the calculation with quick as discretization scheme of advection term. The size of meshes is 0.1 (X) × 0.1 (Y) × 0.1 (Z) m in the office room and the total meshes are 808,704. The boundary conditions of velocity are based on results of the calculated ventilation rate for each opening by network model using measured wind pressure coefficient by means of the wind tunnel test. The air change rate by the natural ventilation was set at 5 ACH. Table 2 shows the boundary conditions. 5 ACH was assumed as a round number from the measurement values in the hybrid ventilated building that the authors measured [4]. The outdoor air was supplied horizontally from NVO and air-conditioned air was supplied vertically from UFAD. Boundary conditions of internal heat loads were shown in Table 3. The office room has occupants, notebook PC, OA loads except notebook PC, and lighting equipment on ceiling as internal heat loads. Total of internal heat loads is 14,668W.

Results of CFD

Distribution of indoor air temperature

Figure 2 shows the CFD analyzed results of the distribution of the temperature at A-A' section (Figure 1). The dark color of figure means a high temperature and the light color of figure means a low temperature. The air temperature changes approximately 22~25 [deg. C] at most areas except the vicinity of the supply openings of air-conditioning and natural ventilation. The temperature rises while going to the leeward side. The temperature difference between the area near the supply natural ventilation openings and the exhaust natural ventilated openings is large and that is about 3~4 [deg. C]. It can be said that the difference of the thermal environment is large by the position of occupant. For provide to occupants the acceptable thermal environment, it is necessary that temperature distribution is predicted by the simplified method when designing a hybrid air-conditioning system.

Distribution of velocity

Figure 3 shows the CFD analyzed results of the distributions of velocity. The speed is equal to or less than 0.2m/s in most areas except the vicinity of the supply openings of air-conditioning and natural ventilation. The velocity of the fresh outdoor airflow reduces after flowing into the room, and the velocity is about 0.5m/s when it drops into the low level of the room from the ceiling.

Figure 4 shows the CFD analyzed results of the vertical distribution of velocity vector and temperature together. At the low level of the room, the outdoor air divided into two directions, flows in the leeward side of natural ventilation and the opposite direction of that. The high temperature of indoor air near the ceiling causes the outdoor airflow along the ceiling to drop in the lower level of the room. The direction of high temperature of indoor air is opposite direction of inflow outdoor air. Because the updraft at about 7m position away from the wall of the leeward side flows until vicinity that the inflow outdoor air is felled from ceiling.

Outline of Zonal model

The office room in the zonal model was assumed to be the area of two dimensions. Figure 5 shows the zone division of the calculated area. The office room was divided horizontally every 3.6m. In addition, the office room was divided vertically into the occupied zone and the non-occupied zone. The occupied zone is area from floor to the height of 1.8m. The office room is consists of 16 zones.

We assumed 4 airflow elements in the office room referring to the results of CFD. The 4 airflow elements in the office room is following as; (1) the airflow of natural ventilation, (2) the supplied airflow from UFAD, (3) the circulating flow caused by convection for wide area of office room, (4) the airflow mixed between occupied zone and non-occupied zone in the each zone. Figure 6 shows the outline of the zonal model.

Several assumptions were made in the zonal model. (1) The outdoor airflow from natural ventilation flow into the office room along the ceiling. The outdoor airflow flowed into the office room along the ceiling. The outdoor airflow entrained the ambient air falls down from the ceiling at X_{max} . The outdoor airflow drops in the occupied zone of the same zone and the close zone. The position of X_{max} is determined by the following equation [5]:

$$X_{max} = \left(0.925 Ar^{-\frac{2}{3}} \right) \cdot H_0 \cdot K \quad (1)$$

where:

H_0 = the height of supply natural ventilation opening

K = centerline velocity constant [6]

The amount of the outdoor air at the X [m] far from natural ventilation supply opening Q_x is described by the equation [7]:

$$Q_x = 0.248 \sqrt{\frac{X}{H_0}} \cdot Q_o \quad (2)$$

where:

Q_0= flow rate of inflow outdoor air

The same flow rate as outdoor airflow rate flows in leeward side at zones except zones near supply and exhaust natural ventilation openings, the flow rate flows out through exhaust natural openings. At zones near supply and exhaust natural ventilation openings, the followings were assumed.

At zones near supply natural ventilation openings, Q_x is called as $Q_{jet(noi)}$ when *X* belongs to zone *NOi*. The amount of jet flow at zone *NOi* $Q_{jet(noi)}$ dropped in occupied zone from non-occupied zone *NOi*, the outdoor airflow $Q_{jet(noi)}$ is flowed in the occupied zone *Oi* of the same zone and the close zone. In this paper, $Q_{jet(noi-1)}$ is flowed in the zone *Oi-1* and *Oi*, and $Q_{jet(noi-1)}$ is described by the following equation:

$$Q_{jet(noi-1)} = Q_{jet(noi-1,oi-1)} + Q_{jet(noi-1,noi)} \quad (3)$$

$$Q_{jet(noi-1,oi-1)} = A \cdot Q_{jet(noi-1)} \quad (4)$$

$$Q_{jet(noi-1,noi)} = (1-A) \cdot Q_{jet(noi-1)} \quad (5)$$

where:

$Q_{jet(i,j)}$ = jet airflow rate that flowed in zone *j* from zone *i*

A = ratio of $Q_{(noi-1,oi-1)}$ to $Q_{jet(noi-1)}$

At zone *O7* near exhaust natural ventilation openings, the same flow rate $Q_{(o6,o7)}$ as outdoor airflow rate is divided airflow rate $Q_{(o7,no7)}$ and $Q_{(o7,o8)}$. The relation is described by the following equation:

$$Q_{(o6,o7)} = Q_{(o7,no7)} + Q_{(o7,o8)} \quad (6)$$

$$Q_{(o7,no7)} = B \cdot Q_{(o6,o7)} \quad (7)$$

$$Q_{(o7,o8)} = (1-B) \cdot Q_{(o6,o7)} \quad (8)$$

where:

$Q_{(o7,no7)}$ = airflow rate that flowed in non-occupied zone *NO7* from occupied zone *O7*

$Q_{(o7,o8)}$ = airflow rate that flowed in occupied zone *O8* from zone *O7*

B = ratio of $Q_{(o7,no7)}$ to $Q_{(o6,o7)}$

(2) The supplied airflow from UFAD does not flow to the near occupied zone, and flow only to non-occupied zone in the same zone. The same amount of supplied air from UFAD in zone *Oi* flows to zone *NOi*, and flowed out the office room through return air opening. This relationship is described as following equation:

$$Q_{SA(oi)} = Q_{RA(noi)} \quad (9)$$

where :

$Q_{SA(oi)}$: flow rate of supply air of air-conditioning in zone Oi

$Q_{RA(noi)}$: flow rate of return air in zone NOi

(3) There is the airflow of the circulating flow on the wide area. This circulating airflow by convection exists in the zone except the close zone of supply opening and exhaust opening of natural ventilation. This circulating airflow rate Q_α is assumed to be in zone 2 ~ zone6 referring to the results of CFD.

(4) There is the mixed airflow rate between occupied zone and non- occupied zone. This airflow is in the whole zone except the close zone of the supply opening and exhaust opening of natural ventilation. The airflow rate that flowed in occupied zone *NOi* from occupied zone *Oi* is designated as Q_{ui}. The airflow rate that flowed in occupied zone *Oi* from occupied zone *NOi* is designated as Q_{di}. This relationship is described as following equation:

$$Q_{di} = Q_{ui} \tag{10}$$

The temperatures for all zones are calculated by solving air balance equation and heat balance equation for each zone. Table 4 shows the parameters that were used to calculate the optimum solution. At first, the temperature differences for all zones between CFD results and zonal model results are calculated by means of the each parameter's combination. The mean absolute value of temperature difference between CFD results and zonal model results ΔT defined by following equation:

$$\Delta T = \frac{\left|T_{CFD(i)} - T_{ZONE(i)}\right|}{N} \tag{11}$$

Where:

$T_{CFD(i)}$: average temperature of zone i calculated by CFD analysis

$T_{ZONE(i)}$: average temperature of zone i calculated by zonal model

N : number of zone

The optimum solutions of Q_α and Q_d were founded as the minimum value of the calculated ΔT on each case. The constant A and B were calculated in the same method. The values were calculated in order of constant A, B.

Results and Discussion

Figure 7 shows the mean absolute value of temperature differences $\Delta T_{(\alpha, d, 0, 0)}$ between CFD results and zonal model results for all zones by combining Q_α and Q_d. Here, constant A and B were 0. $\Delta T_{(\alpha, d, A, B)}$ means that the temperature difference was calculated by using α, d, A and B as Q_α, Q_d, A and B.

The value of ΔT changes 0.7 ~ 1. 2 [deg. C]. The smallest value of $\Delta T_{(\alpha, d, 0, 0)}$ is 0.7 [deg. C] when Q_d is 300 [m^3/h] and Q_α is 1700 [m^3/h]. The values of constant A and B were calculated by these values.

Figure 8 shows the mean absolute value of temperature differences $\Delta T_{(1700, 300, A, 0)}$ between CFD results and zonal model results for all zones when constant A is changed from 0 to 1 at 0.1 intervals. The value of constant B was 0. The smallest value of $\Delta T_{(1700, 300, A, 0)}$ calculated for all zones is 0.47 [deg. C] when A is 0.8. Figure 9 shows the calculated $\Delta T_{(1700, 300, 0.8, B)}$ when constant B is changed from 0 to 1 at 0.1 intervals. The smallest value of $\Delta T_{(1700, 300, 0.8, 0)}$ calculated for all zones is 0.37 [deg. C] when B is 0.3.

Figure 10 shows the temperatures of CFD results and zonal model results when using the calculated values. 1700 [m^3/h], 300 [m^3/h], 0.8 and 0.3 were used by the values of Q_α, Q_d, constant A and constant B. The temperature of the office room has the distribution of 20~26 [deg. C]. The temperature results of zonal model in each zone are similar with CFD results at the most zones. However, in zone 1 of the windward and zone 7, 8 of the leeward side, the temperature difference between zonal model results and CFD results is large. It is necessary to clarify a current of air characteristic around the natural ventilation openings.

Temperature of return air, removed heat load rate by air-conditioning

Figure 11 shows the return air temperatures. The calculated return air temperature by zonal model is lower than that by CFD. Figure 12 shows the comparison of the removal rate of heat load by air-conditioning and natural ventilation. These values were calculated by using air temperature of inflow and outflow side opening of natural ventilation and air-conditioning. The removal rate of the heat load by air-conditioning in CFD results is about 8.5% larger than that by zonal model. Because the temperature of each zone was calculated by assuming complete mixture and it was not able to calculate temperature distribution of the vicinity of ceiling.

Conclusions

We tried to develop the simplified prediction model that can predict temperature distribution inside the office room with hybrid air-conditioning system. CFD analysis was conducted to clarify the air temperature and airflow distribution inside an office room. The results of CFD analysis are used as correct values in this paper.

The temperature distribution predicted from zone model agreed approximately with CFD results at the most occupied zones except the windward and leeward window side. However,

the differences of the return air temperature near the ceiling between CFD results and zone model results are not small. It can be said that the zone model is effective to predict the temperatures of occupied zones. However, the zone model is not effective to predict the removal rate of heat loads by the air-conditioning and the natural ventilation. For applying the zone model to various conditions, more investigations will be needed. Especially, it is necessary to organize data concerning the airflow rates in each zone, constant A, and B.

References

1. Heiselberg, P. (ed.), "T Principles of Hybrid Ventilation," *International Energy Agency Annex 35,* Denmark , *2002*

2. Lim, E., et al., "Airflow Characteristics in Room with Hybrid Air-conditioning System of Task Air Supply and Natural Ventilation," *Proceedings of ROOMVENT*, 2007, B02n, 1267

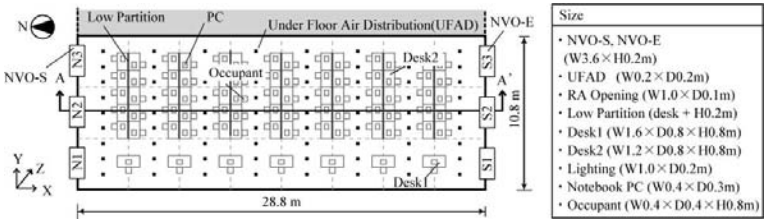
3. Lim, E., et al., "Influence of Supply and Natural Ventilation Openings on Airflow Characteristics in Office Room with Hybrid Air-conditioning System," *Proceedings of ROOMVENT, 2009*, pp. 1783-1790

4. Ushio, T., et al., "Thermal Environment in Office Room Served by Task/ Ambient Air-conditioning System with Natural Ventilation," *Proceedings of Indoor Air Quality, Ventilation & Energy Conservation in Buildings (IAQVEC)*, 2008, pp. 492-499

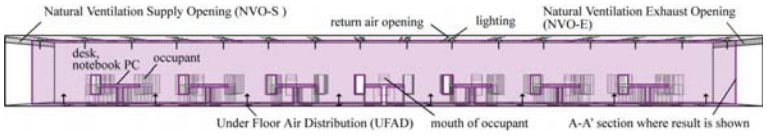
5. Kubota, H., "A BASIC STUDY ON THE ROOM AIR DISTRIBUTION (I) : Separation of the Cool Air from the Ceiling," *Transaction of Architectural Institute of Japan*, 236, 1975, pp. 35-40 [in Japanese]

6. ASHRAE Handbook—Fundamentals 2005, chapter 33, p3

7. Rajaratnam, N., Translated by Y. Nomura, "Turbulent Jet," *Morikita. Pub.*, Tokyo, 1981, P 217 [in Japanese].



(a) Layout of office room



(b) Section where result is shown

Figure 1 Area of CFD analysis

Table 1 Setting of CFD analysis

Turbulence model	Standard k-ε
Algorithm	Steady state (SIMPLEC)
Analysed area	28.8m(X) x 10.8m(Z) x 2.6m(Y)
Meshes	108(X) x 208(Z) x 26(Y)
Discretization scheme for advection term	QUICK
Wall boundary condition	Standard log-low, Adiabatic

Table 2 Boundary conditions

Velocity [m/s]	Air-conditoning (flow rate : 3,261 m^3/h)		UFAD	0.31
			Exhaust Opening	-0.944
	Natural Ventilation (flow rate : 4,032 m^3/h)	NVO-S	N1	0.50
			N2	0.52
			N3	0.54
		NVO-E	S1	-0.51
			S2	-0.52
			S3	-0.53
Temperature [deg.C]	Air-conditoning			20 deg.C
	Natural Ventilation			18 deg.C

Table 3 Internal heat loads

Heat load		Number
Person	60 W	77
Notebook PC	30 W	77
Lighting on ceiling	32W (60% on setting position, 40% on floor and desks)	96
OA loads except PC	30 W/m^2	

Table 4 Parameters that were used to calculate the optimum solution

Q_{α}[m^3/h]	0,500, from 1000 to 3000 at 100 intervals, 3500, 4000
Q_d [m^3/h]	from 0 to 2000 at 100 intervals
A [-]	from 0 to 1 at 0.1 intervals
B [-]	from 0 to 1 at 0.1 intervals

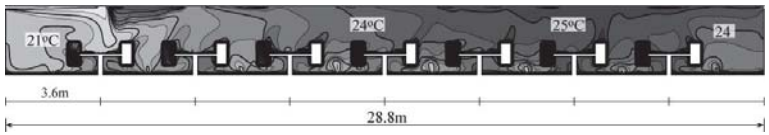


Figure 2 Distribution of Temperature at A-A' Section [deg. C]

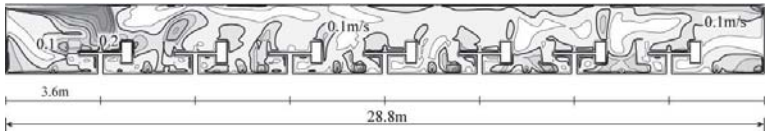


Figure 3 Distributions of velocity at A-A' Section [m/s]

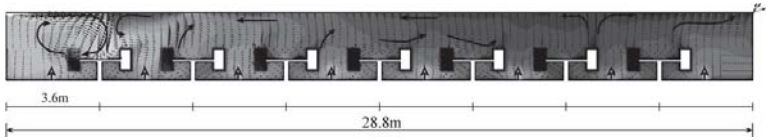


Figure 4 Distributions of velocity vector and temperature at A-A' Section

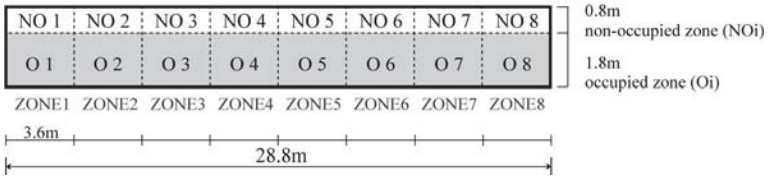


Figure 5 Zone division of the calculated area

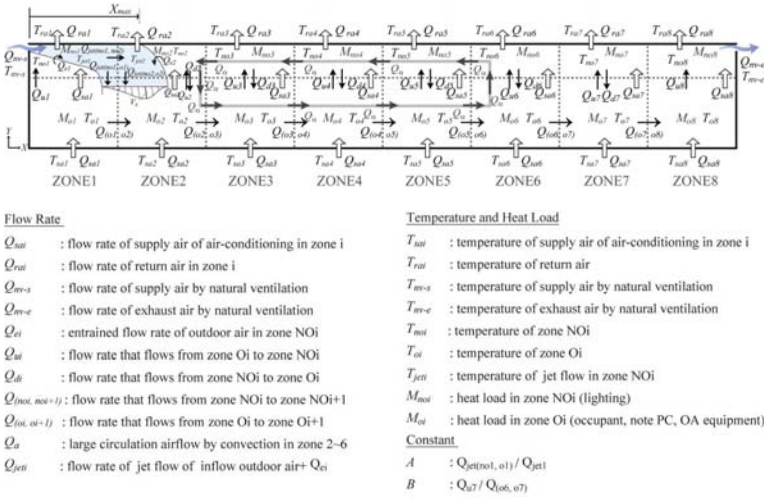


Figure 6 Outline of the zonal model

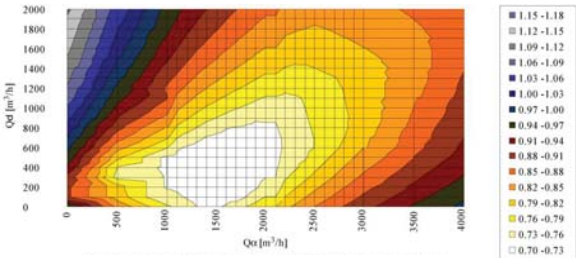


Figure 7 Mean absolute value of temperature differences $\Delta T\,(Q_{\alpha}, Q_{d}, A, B)$ between CFD results and zonal model results for all zones by combining Q_{α} and Q_{d} (constant A=0, B=0)

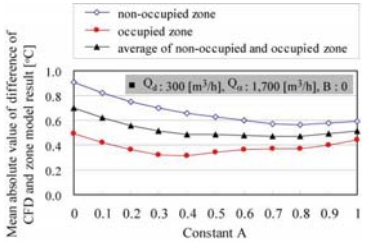


Figure 8 Mean absolute value of temperature differences $\Delta T_{(1700,\ 300,\ A,\ 0)}$ between CFD results and zonal model results for all zones when constant A is changed from 0 to 1 at 0.1 intervals (B=0)

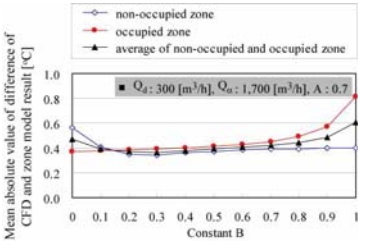


Figure 9 Mean absolute value of temperature differences $\Delta T_{(1700,\ 300,\ 0.8,\ B)}$ between CFD results and zonal model results for all zones when constant B is changed from 0 to 1 at 0.1 intervals

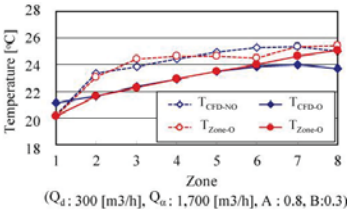


Figure 10 Comparison between temperature of zonal model results and that of CFD results on each zone (Q_{α}=1700, Q_{d}=300, A=0.8, B=0.3)

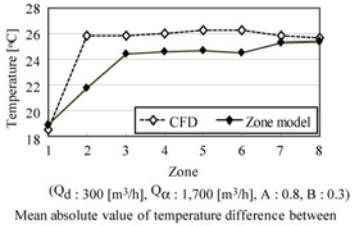


Figure 11 Comparison between return air temperature of zonal model results and that of CFD results

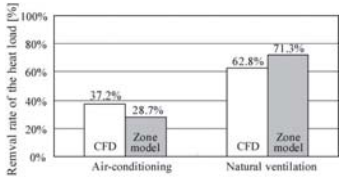


Figure 12 Comparison between removal rate of heat load by air-conditioning and that by natural ventilation

Modelling wind driven airflow rate with CFD and verification of approximation formulas based on wind pressure coefficients

S. Leenknegt[1]*, B. Piret[1], A. Tablada de la Torre[1], D. Saelens[1]

(1) Division of Building Physics, Department of Civil Engineering, K.U.Leuven, Leuven, Belgium

* contact information: sarah.leenknegt@bwk.kuleuven.be

ABSTRACT

An isothermal CFD study was made of a building perpendicular to the wind direction. The building was modelled with a closed façade, and consecutively with one and multiple openings. The sensitivity was investigated for different turbulence models, meshes and near wall treatments, both in 2D and 3D. A large sensitivity was found to the modelling options with regard to the predicted wind pressure coefficients (C_p) distribution, but less with regard to the predicted flow rate through the openings. The distribution of C_p was compared to literature and the influence of the openings on the wind pressure coefficients is investigated. Openings have a large influence on local C_p on the windward side, but only limited on the leeward side. The simulated airflow rates were recalculated using theoretical approximation formulas. The calculated values showed better agreement to the CFD-simulations when the C_p in front of the openings were used, compared the C_p taken at a closed wall.

KEYWORDS

Wind-driven ventilation, CFD, internal airflow, night ventilation

1 Introduction

Night ventilation is a method to cool a building by using the thermal inertia of walls and floors to buffer the heat during day. Wind, thermal buoyancy or fans can be used to achieve the necessary high air change rates during night time to cool down the exposed surfaces [1]. In order to minimize the energy use, ideally, this process is driven by natural driving forces. However, a large uncertainty in the realizable cooling potential is in the prediction of natural ventilation flows [2], [3]. The focus of this paper is on the prediction of wind-driven airflow rates with Computational Fluid Dynamics (CFD) versus approximation formulas from literature. Commonly, a network model is assumed, where the flow rate is predicted based on wind pressure coefficients, combined with a discharge coefficient for the opening to take into account friction losses. In this paper, it is investigated how these wind pressures vary at the location of the openings, and how this influences the predicted flow rate. A rectangular opening is used, with wind direction perpendicular to the opening.

2 Methodology

The object of the study is a building of 25 m high, 20 m wide and 30 m long, which is modelled with CFD (Fluent 6.3 and Fluent 12 (ANSYS)). In a first step, a validation is made for a scaled model of the building (1/200), using wind tunnel measurements from the CEDVAL[1] database provided by the Meteorological Institute of the Technical University in Hamburg [4]. Secondly, the scaled model is rescaled to full scale to determine the wind pressure on the façades. Consequently, one, and later multiple, openings are incorporated in the building, resulting in a modified distribution of the wind pressure coefficient on the façade and air flowing through the opening(s). An illustration is given in Fig. 1.

[1] CEDVAL = Compilation of experimental data for validation of micro-scale dispersion models

First an investigation is made of the sensitivity with regard to the following modelling options. Turbulence modelling is investigated through the following RANS models: realizable k-ε and SST k-ω. Near wall modelling is investigated through standard wall functions, non equilibrium wall functions and enhanced wall treatment. Finally, mesh independency is investigated.

Secondly, a discussion is made on the distribution of the wind pressure coefficients on the facade and the profile at the openings. Also, a discussion is made of the airflow rate, predicted by the simulations and calculated with approximation formulas.

3 Modelling

There are a number of specific challenges to the modelling of wind flow around buildings with CFD [5],[6]. This will not be discussed in detail here; rather the choices made for this research will be recounted. The simulation is isothermal: buoyancy is not taken into account.

3.1 Boundary conditions

The wind velocity at the inlet of the flow domain will vary with the height, as it is located in the lower part of the atmospheric boundary layer (ABL). To use the data from CEDVAL [4] for validation, the velocity profile at the inlet must correspond to the inlet at the wind tunnel, which was achieved with a power law given in equation (1) (scaled model), where $U(y)$ is the profile of the x-velocity over the height (m/s), U_{ref} is the reference x-velocity at reference height h_{ref} (m) and α describes the type of environment upstream from the inlet. The turbulent kinetic energy k and the turbulent dissipation rate ε at the inlet are given by equations (2) and (4).

Vertical x-velocity profile $$U(y) = U_{ref}\left(\frac{y}{h_{ref}}\right)^{\alpha} = 6 \cdot \left(\frac{y}{0.5}\right)^{0.22} \quad (1)$$

Turbulent kinetic energy $$k(y) = 1.5 \cdot I(y)^2 \cdot U(y)^2 \quad (2)$$ [7]

Turbulence intensity $$I(y) = 0.05 + 0.18 \cdot \exp(-0.08u) \quad (3)$$

Turbulent dissipation rate $$\varepsilon(y) = \frac{(u^*)^3}{\kappa(y + y_0)} = \frac{0.377^3}{0.42(y + 7 \cdot 10^{-4})} \quad (4)$$

Friction velocity $$u^*_{ABL} = \frac{U(y_{ref})\kappa}{ln\left(\frac{y_{ref} + y_0}{y_0}\right)} \quad (5)$$

3.2 Roughness

A common problem in CFD wind studies is to simulate a correct progression of the velocity profile over the upstream part of the domain, that is from the inlet towards the area of interest. In reality, this is determined by the roughness of the terrain y_0, while the software package Fluent uses an equivalent sand-grain roughness K_s in the wall functions for the near wall modelling.

For this research, the recommendations from [5] and [8] were followed for the value of K_s. The boundary conditions used in the simulation of the model are summarized in Table 1.

3.3 Mesh and turbulence model

This CFD-study concern two types of flow: free flow around an obstacle and wall bounded flow. For flow in an enclosed environment, [9] gives following conclusions with regard to the most common RANS models. Both standard and RNG k-ε models provide reasonable results, if no special situations occur (e.g. strong buoyancy). The SST k-ω model gives even better results, but still requires further validation.

For wind studies, commonly applied RANS models are the standard k-ε model for its good stability, with as alternatives the realizable or RNG k-ε [8]. As there are no fixed guidelines to the selection of a turbulence model, [8] recommends to perform a sensitivity study and to compare the results to measurement data, relevant to the specific case.

A sensitivity study is made with regard to turbulence models, near-wall treatment and mesh size.

- For the validation study with the scaled building model, five meshes were investigated, as well as four combinations of turbulence model and near-wall modelling; see also respectively Table 2 and Table 3.
- For the 2D full scale study (closed and open), the realizable k-ε (non-equilibrium and standard wall functions) and SST k-ω model were applied, together with the base mesh from the validation (me3) and an extra mesh (mehi) with refinement on all edges by approximately a factor 2.
- Finally, for the 3D study of the open building (one and multiple openings) the realizable k-ε model with standard wall functions was investigated with a base mesh (me3) and a refined mesh (mehi). The SST k-ω was tested only with the base mesh (me3) and one opening. It was also investigated if the calculation domain could be halved by introducing a symmetry plane. As all boundary conditions are symmetric, this is a justified simplification.

In the following paragraph, an overview is given of the validation of the scaled closed building model. The validation is done by comparing x-velocities of the flow throughout the flow domain. The experimental data from CEDVAL only contain velocity profiles, therefore the resulting wind pressure coefficients are verified by using the TNO C_p-Generator [10], which is a database of C_p-coefficients based on systematic wind tunnel experiments and various studies with several validations [11],[12].

3.4 Scaled closed building: validation of velocity profiles

The validation study on the scaled building block is described in detail in [13], and was made using the recommendations of [8]. Generally, the difference between the experimental and simulation data is larger than the difference within the simulation results. The main difference between measurement and simulation is situated at the leeward vortex (behind the building) and the roof, where Fluent predicts leeward vortices that are both too high and longer than in the wind tunnel. Furthermore, there is only limited difference between the different wall treatments of the realizable k-ε model. The k-ε model also performs slightly better than the k-ω model in the prediction of the velocity throughout the flow domain and is more stable.

Finally, also a mesh dependency study was performed with 5 meshes (see Table 2). As the results were relatively independent of the mesh, the resolution of the base mesh (me3) is sufficient to predict to velocities around the closed building.

4 Discussion of results

4.1 Full scale closed building

After the validation of the scaled model, all the dimensions of the small scale building are multiplied by a factor 200 (25/20/30 m). The velocity profile from equation (1) is rescaled by increasing the reference height h_{ref} from 0.5 to 100 m, while α and U_{ref} are unchanged. Consequently, also the k - and ε - profile is resized. There is good correspondence between the velocity profiles for the scaled and full-scale building. However, there are significant differences between the C_p-values, both between scaled and full scale model as between 2D and 3D simulation, which is illustrated in Fig. 2. The values plotted here are taken from the vertical centre line just next to the wall surface, starting at the ground on the windward side, continuing over the windward side, the roof and the leeward side. The TNO C_p-Generator gives higher negative values on the roof and on the leeward side as well as a much higher peak at the windward side of the roof. The full scale model agrees better with the results from the TNO C_p-Generator on the windward side and the roof, but shows still lower values on the leeward side. This indicates that a full scale study is indeed necessary in order to make conclusions.

4.2 Full scale open building: global C_p profile over facade

Fig. 3 shows the C_p-values in the case of one opening, with a comparison of the realizable k-ε model with standard wall functions (ke-stw) and the SST k-ω model (kw). The results from 2D and 3D are compared as well. For reference, the values from the TNO C_p-Generator for a closed building are included. A decrease in the local pressure coefficients is visible at the opening on the windward side. At the leeward side, a shift is visible as well, though less pronounced. A comparison of the base mesh (me3) and the refined mesh (mehi) showed that the base mesh is sufficient.

With regard to the modelling sensitivity, following remarks are made for the case with one opening (Fig. 3):

- **2D versus 3D**: the 2D simulations overestimate the leeward pressure coefficients, as was already mentioned before but is visualised here. Also at the windward side, the correspondence of the 3D-results to the TNO C_p-Generator is better (zone close to roof). This shows that a 3D simulation is required.
- **Turbulence model**: The SST k-ω model gives an unrealistic profile of the under pressure at the roof. Also at windward facade, the values are significantly lower, but at leeward facade, there is a large similarity with the realizable k-ε model.

Fig. 4 shows a similar comparison for the case with multiple (mult) openings. Remarkable is the large influence of the openings on the windward side and the very limited influence on the leeward side. For this case, a comparison was also made between a flow domain with and without symmetry plane, showing that this does not alter the results for this wind direction.

Fig. 5 gives a compilation of the previous three figures. The overall wind pressure coefficient between the openings on the windward side is slightly higher for the case with multiple openings compared to the case with one opening. For all openings, the local pressure drop at the windward side is in the same order of magnitude, for the central opening for example from 0.6 to 0.4.

4.3 Full scale open building: local C_p and velocities at the openings

Fig. 6 and Fig. 7 show respectively the C_p- and x-velocity-profile over the opening: (a) shows the opening at the windward side while (b) shows the opening at the leeward side. Results are given for the internal zone (middle of the building) for the case with one and multiple (mult) openings. Following comparisons are shown in these figures:

- 2D versus 3D
- one versus multiple openings
- the realizable k-ε model with either standard wall functions (ke-stw) or non-equilibrium wall functions (ke-ne) and the SST k-ω model (kw)
- the base mesh (me3), the refined mesh (mehi) and the mesh with symmetry plane (h-)

The C_p-values at the windward side, shown in Fig. 6-a, show good agreement between 2D and 3D. At the leeward side however in Fig. 6-b, the C_p have very large differences between 2D and 3D which is consistent with the previous results.

For the velocities at the windward side (Fig. 7-a) a clear difference is seen between 2D and 3D simulations, but the different turbulence models perform similar (compare 3D_one_ke-stw and 3D_one_kw). For the velocities at the leeward side (Fig. 7-b), there is a large spread over all the displayed results. We see here that there is a large sensitivity to the different turbulence models (compare 3D_one_ke-stw and 3D_one_kw).

The influence of one compared to multiple openings is limited (Fig. 7-b: compare 3D_one_ke-stw and 3D_mult_ke-stw). This indicates that the wind-driven flow through one opening will

have a limited influence from the presence of other openings, and may be investigated individually. This must be verified with further simulations and different opening locations, but could simplify the geometric model significantly.

5 Prediction of airflow rate

5.1 Results from the CFD-study

The airflow rates as predicted by the CFD-simulations are compared in Table 4. The flow rates in the 2D simulation represent an overestimation, as they assume an infinite opening length and ignore the additional friction losses at the vertical opening boundaries. An imbalance between incoming and outgoing flow was observed, which is most likely due to an insufficiently fine mesh at the openings. It is clear that even in the CFD-study, there is uncertainty on the predicted mass flows, but the differences between the 3D-results are limited to maximum +/- 5%.

5.2 Theoretical calculation of airflow rate

Wind-driven flow rates can be estimated with approximation formulas (resistance model), which use the wind pressure in combination with the opening characteristics. Therefore, the discharge coefficient C_d, which is an empirical correction factor to indicate the "flow efficiency" of an opening, is determined for this specific case. Typically, a value of 0.6-0.65 is assumed for rectangular openings, though it is shown that C_d is not a constant [14],[15]. C_d is defined by the so-called orifice equation, given by equation (6).

$$C_d = \frac{G_a}{A \cdot \sqrt{\frac{2\Delta P}{\rho_0}}} \qquad (6)$$

and here:

$\Delta P_{in} = |P_{front} - P_{int}|$
$\Delta P_{out} = |P_{back} - P_{int}|$
G_a [m³/s]

Special care should be taken in the determination of the pressure difference ΔP over the opening. ΔP is well defined in pipe flows, but not straightforward for flow through wall openings [16]. For this comparison, it is particularly important that the same pressure differences are later also applied in the approximation formulas. Here, the pressure difference was taken between the area weighted average static pressure at 20 cm outside the inlet/outlet opening and an internal static pressure P_{int}, which is defined here as the area weighted average of the static pressure in a vertical cross section through the middle of the internal zone.

Table 5 gives an overview of area weighted average values for both 2D and 3D simulations of following parameters: P_{int}, P_1, P_2, ΔP, C_p and the resulting C_d for each opening. Notice that the C_p have a v_{ref} of 6 m/s and were also taken at 20 cm distance from façade and opening.

In a second step, the airflow can be recalculated theoretically for each simulation, using the C_p-values from Table 5. As the simulations are isothermal, pressure differences due to thermal stack are neglected. Two methods are used. The first one is the method of Aynsley [16], which is a simplified empirical method, giving the flow for cross ventilation by equation (7). A second method gives an iterative approach, described by Liddament (2009) [17], where the pressure outside both openings is determined by equation (8). Next, the conservation of mass in equation (9) is iterated for the j *(= 2)* openings, until p_{int} is determined. Both methods use the same basic equations, and should therefore give the same results.

$$Q = \rho \cdot v_{ref} \cdot \sqrt{\frac{C_{p,front} - C_{p,back}}{\frac{1}{A_{front}^2 C_{d,front}^2} + \frac{1}{A_{back}^2 C_{d,back}^2}}} \qquad [kg/s] \quad (7)$$

$$p_{w,front/back} = 0.5 \cdot C_{p,front/back} \cdot \rho \cdot v_{ref}^2 \qquad [Pa] \quad (8)$$

$$\sum_{i=1}^{j} \rho_i \cdot C_{d,i} \cdot A_i \cdot \sqrt{\frac{2}{\rho_i}} \cdot |p_{w,i} - p_{int}|^{n_i} \left[\frac{p_{w,i} - p_{int}}{|p_{w,i} - p_{int}|}\right] = 0 \qquad (9)$$

The results are given in Fig. 8: in (a) default values are assumed for C_d (0.65 for a rectangular opening) and n_i (0.5 for turbulent flow), while (b) shows the results when C_d from the simulations were used. The vertical axis indicates which simulation was used as a reference. The 2D-results are omitted in (b), as C_d can only be determined from a 3D simulation. The results of Aynsley and Liddament are indeed identical.

On Fig. 8-a, there is 9 to 18% difference between the calculated and the simulated flow rate over all the 3D simulations. When the calculated C_d-values are applied in Fig. 8-b, the calculated mass flow rates are nearly identical (difference between 2 to 5%) to the simulations. Notice that for these simplified formulas, the C_p values just in front of the openings were used, though they are usually applied with C_p-values on the closed facade. When comparing to the results with the C_p-values from the closed case (3D_cl_ke-ne_me3), there is a difference of 9 to 11% compared to the 3D CFD-results.

6 Conclusions

Wind-driven ventilation rates are predicted using wind pressure coefficients and the characteristics of the opening. In this paper, a CFD-wind study was made of a building with closed facade, and one and later multiple openings. The sensitivity study showed that the wind pressure must be simulated in a full scale 3D model and that there were large differences between the realizable k-ε and SST k-ω model with regard to the C_p on the windward side and roof. The first model showed better agreement with values from literature. The predicted flow rates were less sensitive to the turbulence model.

The openings in the building cause a local reduction of the C_p in the order of 0.2 on the windward side. In case of multiple openings, the influence on C_p-profile on the leeward side was limited. The local velocity and C_p profile at the openings showed only small influence from the presence of adjacent openings.

The airflow rate through the opening was recalculated with approximation formulas by Aynsley and Liddament. Only 2 to 5% difference was seen between simulated and calculated flow rates when the applied C_p*'s* were taken next to the opening and the applied C_d was deduced from the simulation results.

ACKNOWLEDGEMENTS

This research was funded by the Research Foundation Flanders (FWO Vlaanderen). Their financial contribution is greatly appreciated.

REFERENCES

[1] Artmann, N. (2009), PhD-thesis, *Cooling of the building structure by night-time ventilation*, Aalborg University, Denmark.

[2] Breesch, H. (2006), PhD-thesis, *Night ventilation: uncertainty and sensitivity analysis*, UGent, Belgium.

[3] Artmann et al. (2008), *Parameter study on performance of building cooling by night-time ventilation*, Renewable Energy 33 (12), p. 2589-2598.

[4] University of Hamburg, Meteorological Institute, Compilation of experimental data for validation of microscale dispersion models (CEDVAL).

[5] Blocken et al. (2007), *CFD simulation of the atmospheric boundary layer: wall function problems*, Atmospheric Environment 41, p. 238-252.

[6] Saathoff et al. (1995), *Effects of model scale in estimating pollutant dispersion near buildings*, Journal of Wind Engineering and Industrial Aerodynamics, Vol. 54-55, p 549-559.

[7] Blocken, B., Persoon, J. (2009), *Pedestrian wind comfort around a large football stadium in an urban environment: CFD simulation, validation and application of the new Dutch wind nuisance standard*, Journal of Wind Engineering and Industrial Aerodynamics, Vol. 97, nr. 5-6, p. 255-270.

[8] Franke et al. (2007), *Best practice guideline for the CFD simulation of flows in urban environment*, COST Action 732 – Quality assurance and improvements of microscale meteorological models, 2007.

[9] Zhai et al. (2007), *Evaluation of various turbulence models in predicting airflow and turbulence in enclosed environments by CFD: Part 1: Summary of prevalent turbulence models*, HVAC&R Research 13(6).

[10] TNO Building and Construction Research, TNO Web Application C_p-Generator.

[11] IEA – ECBCS, Annex 35: HybVent (2003).

[12] de Wit, M.S. (1999), *Uncertainty in wind pressure coefficients for low-rise buildings*, Delft University of Technology.

[13] Piret, B. (2009), *CFD-simulation of wind-driven night ventilation in office buildings*, Master Thesis, K.U.Leuven, Leuven, Belgium.

[14] Heiselberg et al. (2001), *Characteristics of airflow from open windows*, Building and Environment, Vol. 36, nr. 7, p. 859-869.

[15] Chu et al. (2009), *Turbulence effects on the discharge coefficient and mean flow rate of wind-driven cross-ventilation*, Building and Environment, nr. 44, p. 2064-2072.

[16] Aynsley, R.M. (1997), *A resistance approach to analysis of natural ventilation airflow networks*, Journal of Wind Engineering and Industrial Aerodynamics, nr. 67-68, p. 711-719.

[17] Liddament, M. (2009), VEETECH Ltd. - Online Tutorials.

Tables

Table 1: Boundary conditions for CFD-simulation of the model (y_0 in the wind tunnel is 0.7 mm, for the full scale building y_0 is 0.14 m)

Faces	**Boundary**	**Parameters**		
Ground	WALL	$K_{s,scaled}$ = 0.0086 m	$K_{s,full}$ = 1.74 m	C_s = 0.8
Building	WALL	$K_{s,scaled}$ = 0 m	$K_{s,full}$ = 0 m	C_s = 0.5
Left side	SYMMETRY	$K_{s,scaled}$ = 0 m	$K_{s,full}$ = 0 m	C_s = 0.5
Right side	SYMMETRY	$K_{s,scaled}$ = 0 m	$K_{s,full}$ = 0 m	C_s = 0.5
Sky	SYMMETRY	$K_{s,scaled}$ = 0 m	$K_{s,full}$ = 0 m	C_s = 0.5
Inlet	VELOCITY INLET	U(y)	equation (1)	input profile
		k(y)	equation (2)	input profile
		ε(y)	equation (4)	input profile
Outlet	PRESSURE OUTLET	p_{gauge} = 0 Pa		
		k(y)	equation (2)	input profile
		ε(y)	equation (4)	input profile

Table 2: Mesh sensitivity analysis, applied to CFD-model of scaled wind tunnel building block

mesh 3	base mesh (me3)	20 $.10^4$ cells
mesh 1	2x more cells/edge	160.10^4 cells
mesh 2	√2x more cells/edge	51 $.10^4$ cells
mesh 4	√2x less cells/edge	14 $.10^4$ cells
mesh 5	2x less cells/edge	2 $.10^4$ cells

Table 3: Model sensitivity

Model	Turbulence model	Near wall modelling
1	Realizable k-ε	enhanced wall functions with pressure gradient
2		non-equilibrium wall functions
3		standard wall functions
4	Standard k-ω	shear flow corrections (SST)

Table 4: Comparison of wind-driven ventilation according to CFD-results: velocity and mass flow

	2D						**3D**				
# OP.	**ONE**			**MULT.**			**ONE**		**MULT.**		
	ke-ne	**ke-stw**	**kw**	**ke-ne**	**ke-stw**	**kw**	**ke-stw_h**	**kw_h**	**ke-stw_h**	**ke-stw**	
$v_{x,in}$	2.98	2.96	2.84	2.92	2.90	3.11	2.27	2.25	2.27	2.22	**m/s**
$v_{x,out}$	2.75	2.77	2.69	2.72	2.70	2.84	2.18	2.20	2.18	2.22	**m/s**
m_{in}	9.117	9.070	8.693	8.946	8.874	9.522	6.941	6.89	6.937	6.811	**kg/s**
m_{out}	8.432	8.480	8.240	8.329	8.255	8.713	6.687	6.74	6.690	6.812	**kg/s**

Table 5: Comparison of wind-driven ventilation according to 3D CFD-results: boundary conditions at the opening

# openings	ONE		MULT.		
case	ke-stw_h-mehi	kw_h-me3	ke-stw_h-mehi	ke-stw_mehi	units
P_{int}	1.35	2.81	0.98	1.93	Pa
P_{front}	8.07	7.56	9.13	7.95	Pa
P_{back}	-3.76	-2.61	-3.33	-4.26	Pa
ΔP_{in}	6.72	4.75	8.15	6.02	Pa
ΔP_{out}	5.11	5.42	4.32	6.19	Pa
$C_{p,f}$	0.37	0.34	0.36	0.41	-
$C_{p,b}$	-0.17	-0.12	-0.19	-0.15	-
$C_{d,in}$	0.68	0.81	0.62	0.71	-
$C_{d,out}$	0.76	0.74	0.82	0.70	-

Figures

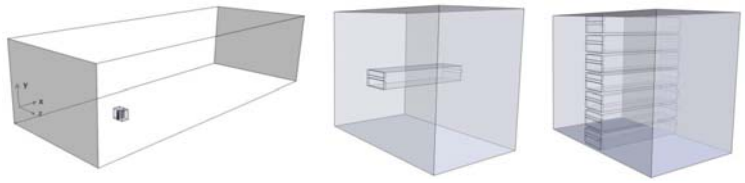


Fig. 1. Overview of (a) building in flow domain and 3D model of the building with (b) one and (c) multiple openings

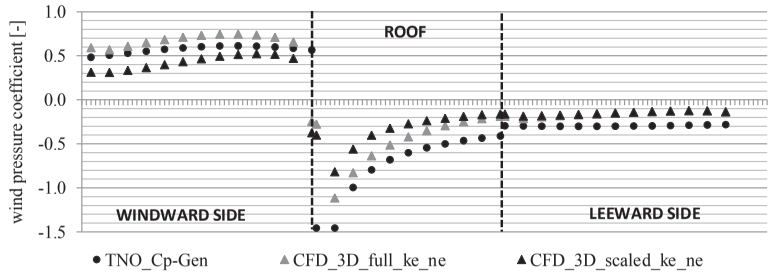


Fig. 2. Comparison of C_p-values between full scale and scaled model of closed building: verification with TNO C_p-Generator

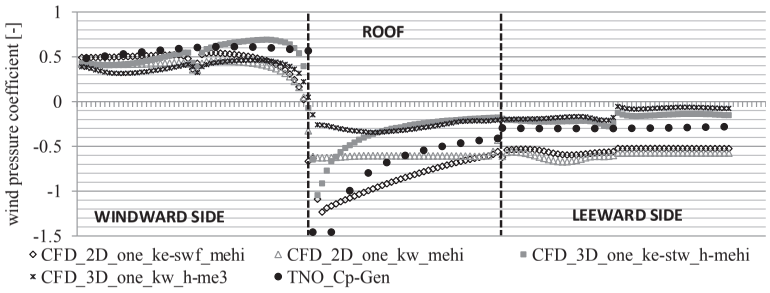


Fig. 3. Comparison of C_p-values: one opening (CFD), closed building (TNO)

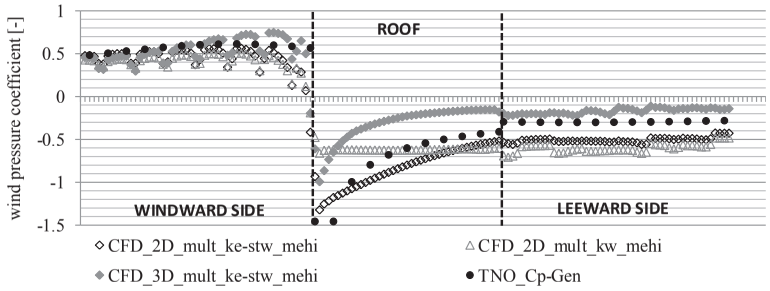


Fig. 4. Comparison of C_p-values: multiple openings (CFD), closed building (TNO)

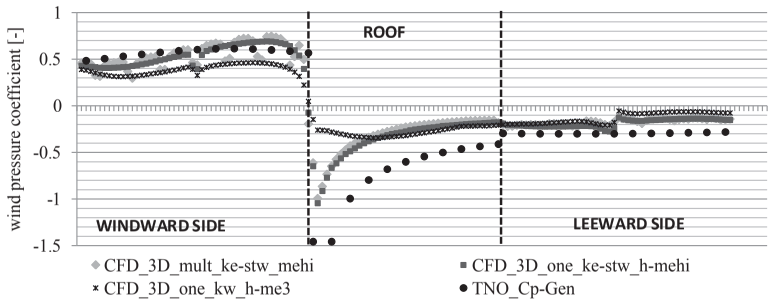
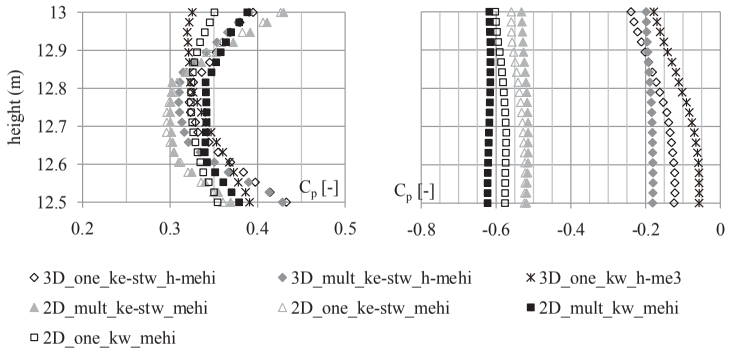
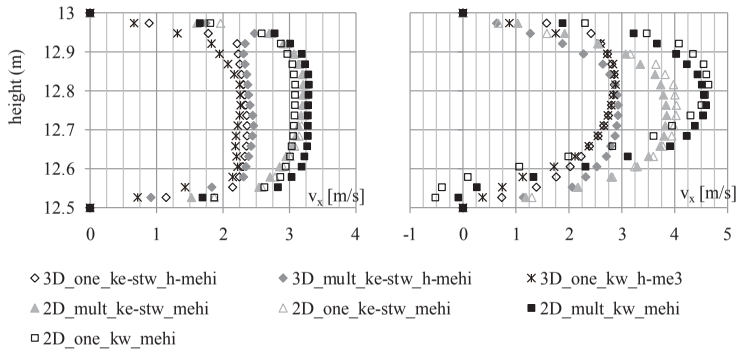


Fig. 5. Comparison of C_p-values: closed versus one or multiple openings (CFD_3D) and closed building (TNO)



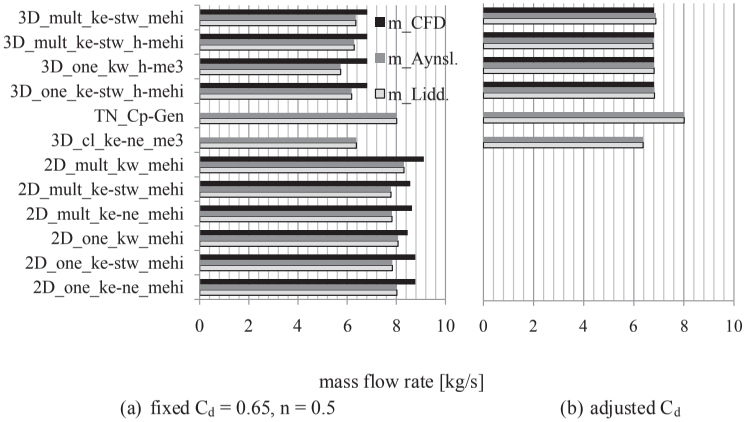
(a) FRONT – 20 cm from opening (b) BACK – 20 cm from opening

Fig. 6: Comparison of C_p-profile at opening



(a) FRONT – at opening (b) BACK – at opening

Fig. 7: Comparison of velocity profile at opening



(a) fixed $C_d = 0.65$, $n = 0.5$ (b) adjusted C_d

Fig. 8: Comparison of resulting mass flow rates – according to CFD or to approximation formulas

Solar Greenhouse and natural ventilation

Elena BIGELLI[1], Luca GUARDIGLI[2], Debora VENTURI[3]

[1]University of Bologna, Dept. of Architecture and Planning, Bologna, 40122, Italy

[2]University of Bologna, Dept. of Architecture and Planning, Bologna, 40122, Italy

[3]University of Bologna, Dept. of Architecture and Planning, Bologna, 40122, Italy

Abstract

The paper presents a study on the thermal behavior of a solar greenhouse set against one apartment of a residential eco-sustainable building in a temperate climate. Particular attention was given to the analysis of the contribution of solar radiation in winter heating in relation to natural ventilation. This study makes use of a transient energy simulation system named ESP-r (Environmentals System Performance - research).

The results so far have revealed that the preferred orientation of the greenhouse to maximize the solar collection in January and February (South) can cause overheating in March, as the temperature inside the room exceeds 25°C (limit of the comfort zone) for 5% of the hours, and in April when the discomfort is for 60% of the time. The final step of the study focuses on the dimensioning of the openings for the reduction of the above mentioned percentage through natural ventilation, identifying a design methodology that integrates low-energy concepts in the design process.

Keywords: Solar greenhouse, thermal comfort, natural ventilation, solar radiation.

Introduction

Representing buffer zones between inside and outside, greenhouses are helpful design solutions for the reduction of energy consumption in low-energy buildings,. Unfortunately, in temperate climates like the Mediterranean greenhouses tend to be useless in most of the months – especially in the central hours of the day – due to their overheating. This the reason why in the past climate sensitive buildings haven't widely exploited such kind of solutions. In this paper we try to analyze the role of natural ventilation in reducing the extra-heat in some of these critical periods of the year for the above mentioned areas.

Of course, a greenhouse should be considered, according to our hypothesis, non only as a heating space and/or a thermal accumulator, but also a living place of a green building where thermal comfort should be achieved. In this perspective, natural ventilation should be able to balance the rise in temperature in some critical months like March, April, September and November (mean seasons). In hot seasons from the beginning of May to the end of September, for the considered climate in the northern emisphere, the greenhouse should be continuously ventilated and protected with solar screens.

1. Design criteria for a solar greenhouse based on its thermal behavior

As a reference, we took the design of an apartment building near Rimini, in the Northern Adriatic coast of Italy. Into the ESP-r software we built a simplified model of the apartment, consisting of two heating zones: a living room of 20 m^2 and the greenhouse of 14 m^2 set against it (fig. 1). In the living space the presence of doors or windows was not considered. In such a way the results would not be influenced by the particularities of size, facing and orientation of these elements.

We connected the two zones and we established the boundary conditions of each surface: the vertical surfaces of the greenhouse are in contact with the external environment, except the wall and the transparent door between the two rooms. For all the other surfaces adjacent to spaces at the same temperature the heat transmission was set to zero. Then, we derived the thermophysical properties of the materials and the composition of the vertical section of the walls from the normally used building technology in the area (fig.2).

The available climate information for the site of Rimini is relative to the year 2005 and contains data recorded on a significant number of years, regarding air temperature [°C], direct and diffuse solar radiation [W/m^2], wind speed [m/s], wind direction and relative humidity [%]. The climatic data refer to the Italian Climatic data collection "Gianni De Giorgio" (IGDG), developed for use in simulating renewable energy technologies, and based on a 1951-1970 period of record (Mazzarella, Politecnico di Milano).

The preliminary study started with the simulation of winter climatic conditions, especially the two coldest months of January and February. In the living room we assumed a constant temperature of 20 [°C] from an operating heating system, and the absence of internal free heat inputs; in this step the contribution of natural ventilation was not considered.

First, we evaluated the behavior in terms of energy balance and temperature variations in January and February with the glass screen facing south, the best orientation for the greenhouse. As shown in the graph, representing

the coldest days of January, the temperature difference between the external environment and the greenhouse varies from 7 [°C] to 18 [°C] (fig.3), creating an almost comfortable zone: the living-room temperature (blue line) exceeds 20 [°C] in the central hours of the day, and the heating demand is significantly reduced.

In a second step, in order to define more clearly some design criteria, we tested different configurations of the envelope and the orientation, varying single parameters from time to time. We identified five types of configuration (A, B, C, D, E), and for each of them four different cases (A1, A2, A3, A4, etc.), varying the position and the size of the glass surfaces and the width of the greenhouse.

As indicative of the greenhouse's thermal efficiency we considered the heating plant consumption [kWh], based on some simplifying assumption made at the beginning of the simulation. The results were collected in a table (fig. 4): every type of greenhouse has one case (the 3rd column: A3, B3, C3,..) that reveals the best performance. In this configuration, where the sides facing east and west are opaque, the energy losses, which outweigh solar gains, are limited by the thermal inertia of the walls, and the reduced glass surface of 14 m^2 is still capable of a reasonable solar captation.

Once identified types A and D as the most suitable for their energy performance, we studied their behavior in the south-east and south-west orientations (± 30° from the south); the results are shown in figure 5. In both types, south and south-west orientations have better performances, compared with south-east. These simulations are relative to January and February, when required tasks of the greenhouse are maximizing solar captation and reducing energy consumption .

In conclusion, south and south-west orientations with opaque sides meet the best performance. However, the south-east orientation should be preferable, because it creates less overheating problems over the whole year.

2. Contribution of natural ventilation

In this step, the evaluations on the behavior of the greenhouse were extended to March and April, introducing the required contribution of natural ventilation in relation to the risk of overheating. This contribution was considered in two different ways: the first considers constant-air-volume changes (ACH) according to the minimum average value of 0,3 [vol/h] set by the national legislation ; the second consists on defining an air flow network through the openings and boundary conditions..

For this simulation we chose the A3 model in the south orientation and an average minimum value of 0,3 [vol/h] for the ventilation in the living-room and in the greenhouse. The graphic of figure 6 shows that in the living-room the temperatures of January and February are contained into comfort limits (from 18 [°C] to 25 [°C]), with a maximum temperature of 23 [°C]. Keeping the same conditions for March, the living-room reaches unacceptable temperatures, going beyond the comfort zone for 7% of total hours (fig. 7). Therefore, we increased the ventilation in the greenhouse up to 0,6 vol/h, obtaining the percentage of 5%, considered more acceptable for comfort. We followed a similar process for April, obtaining an overheating of the living-room for 73% of the hours (fig. 8); increasing the ventilation in the greenhouse up to 0,9 [vol/h], we obtained the relative graphic of temperature where this percentage is reduced down to 60% (fig. 9, 10). This level should be considered unacceptable, and some corrective measurements should be adopted, like a further increase of ventilation or a complete opening of the greenhouse during the day.

The construction of an air flow network comprises 3 elements:

- Nodes: these are placed in each zone to be included in the network as well as external to the building.
- Components: these are the ventilation openings through which air flows (windows, doors, voids and cracks).
- Connections: these determine which nodes are connected by which components.

In our case, the simple air flow network model consists on 3 nodes (1 internal and 2 external to the greenhouse), 2 components (2 window openings) and 2 connections, as seen in figure 11.

The control of the flow components is needed to tell when the windows are open and when they are closed; in our case we decided to open the windows from 9.00 a.m. to 6.00 p.m. through an on/off mechanism when the greenhouse's temperature is above the temperature setpoint of 25 [°C].

In this configuration, we studied a single side ventilation through overlapped openings at an average distance of 2 [m], to maximize the pressure difference of air inlet and outlet (stack effect). As the amount of air moving vertically depends on the size of the ventilation openings, we assumed three different areas: 0,1 [m^2], 1 [m^2], and 5 [m^2] .

The results for the first type of openings are as follows: when windows are open, in the greenhouse there is a difference temperature that goes from 5 to 10 [°C], while the average temperature is about 26 [°C] (fig. 12). In the second case, where openings are of 1 [m^2], the temperature difference varies from 8 to 13 [°C], and the greenhouse's temperature stays around 23[°C] (fig. 13).

In the third case, with the maximum area of openings (5 [m^2]), the temperature difference varies from 10 to 15 [°C] and the average temperature is about 23[°C] (fig. 14).

We can notice that openings of 0,1 [m^2] offer a less effective ventilation and do not contribute significantly to the greenhouse's temperature. The last two cases present very similar effects. This means that for a good ventilation a total opening area of 2 [m^2] is enough. The sharp temperature changes with the on-off

configuration are due to the fact that in March temperature outside is still quite low, especially in some days (red line in figures 12, 13, 14), causing a rapid lowering of the greenhouse's temperature; openings are regulated by an on/off system that is always technically difficult to manage automatically. However, natural ventilation based on this air flow network has clearly helped in lowering the living-room's temperature, which does not exceed 22,4 [° C] during March and 23,4 [° C] during April.

In conclusion, the results on the effectiveness of natural ventilation through an air flow network are more significant than those obtained by ACH system. According to the simulation the automatically controlled single side ventilation gives an important contribution in March and April, reducing the overheating of the living-room and bringing the temperature within the comfort zone. The simulation also showed that for the ventilation of a south oriented greenhouse with a volume of approximately 40 [m^3], and a glazed area of approximately 15 [m^2], two horizontal openings with a total area of 2 [m^2] are enough.

References

1. Buffington D. E ., R. A., Bucklin R. W. Henley and D. B. McConnell, *Greenhouse ventilation*, AE-10, Agricultural and Biological Engineering Department, University of Florida, IFAS Extension, 2010.
2. Givoni B., *Characteristics, design implications, and applicability of passive solar heating systems for buildings Solar Energy*, Volume 47, Issue 6, 1991, Pages 425-435.
3. Mazria Edward, *The Passive Solar Energy Book*, Rodale Press, 1979.
4. Zappone Claudio, *La serra solare*, Sistemi Editoriali, Milano, 2009.

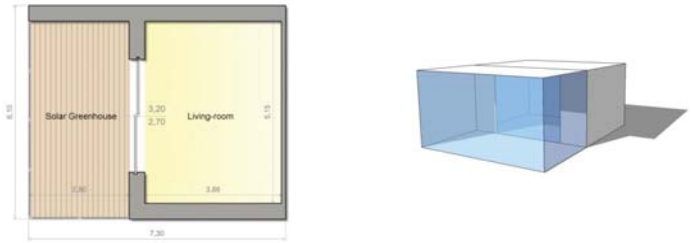
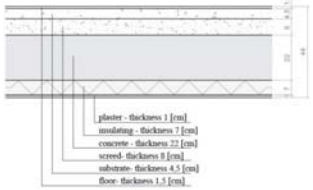
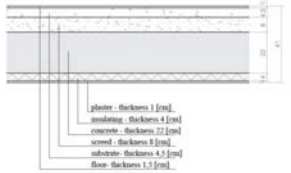


Figure 1 Plan and three-dimensional pattern of the ESP-r model

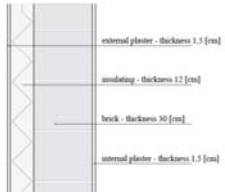
EXTERNAL FLOOR – GREENHOUSE
Transmittance K = 0,42 [W/m^2°C]



INTERNAL FLOOR – LIVING ROOM
Transmittance K= 0,63[W/m^2°C]



EXTERNAL WALL
Transmittance K= 0,18 [W/m^2°C]



INTERNAL WALL
Transmittance K= 0,8 [W/m^2°C]

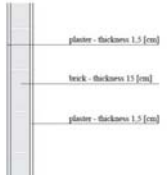


Figure 2 Composition of constructions used in the model

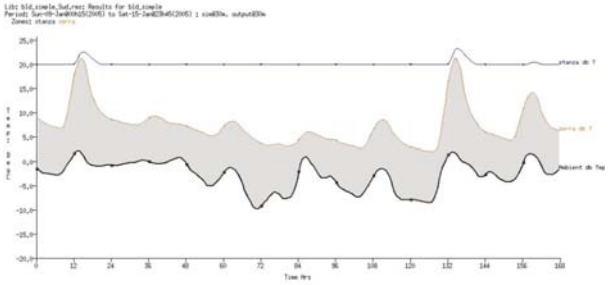


Figure 3 Graph of temperature of the coldest week of January

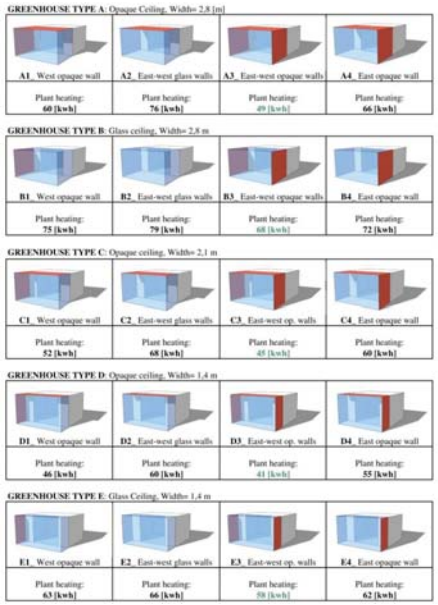
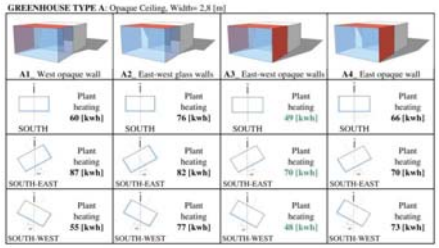


Figure 4 Study on the greenhouse's envelope: results of simulations (Orientation: South, Period: January and February)



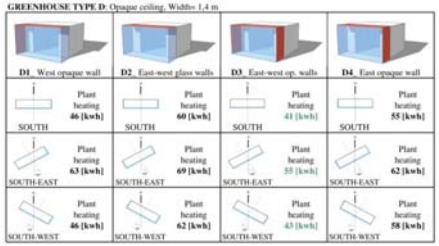


Figure 5 Study on the greenhouse's orientation: results of simulations

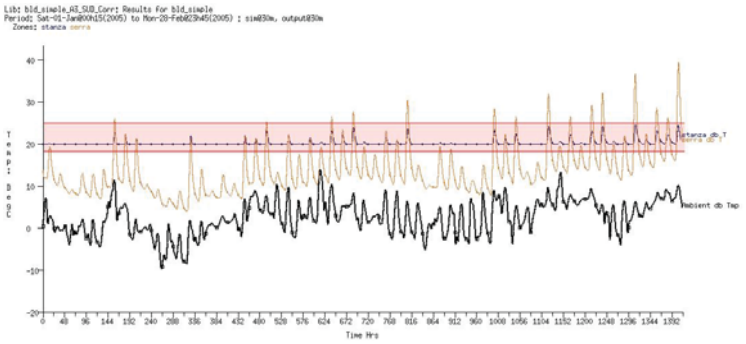


Figure 6 Graphic of January and February temperatures

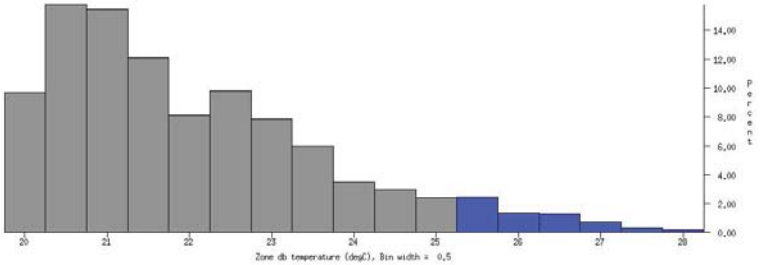


Figure 7 March's temperature distribution in the living-room

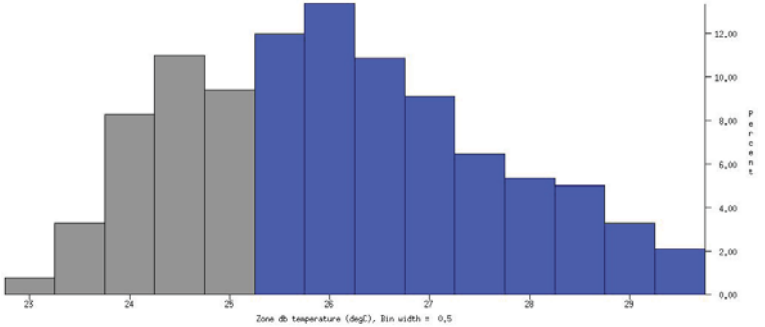


Figure 8 April's temperature distribution in the living-room

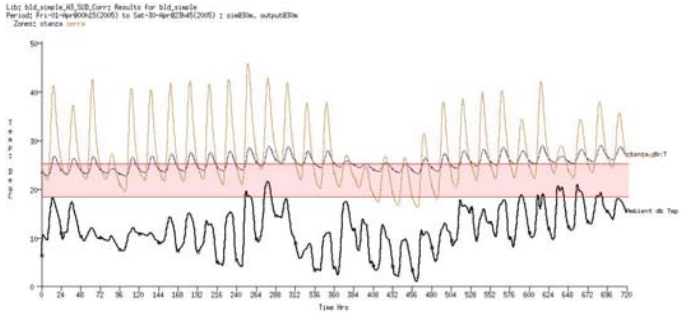


Figure 9 Graphic of April's temperatures

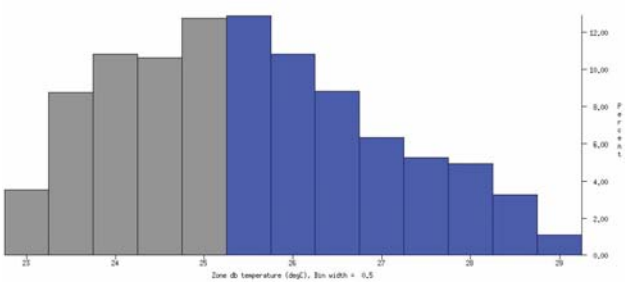


Figure 10. April's temperature distribution in the living-room with a ventilation of 0,9 [vol/h] in the greenhouse.

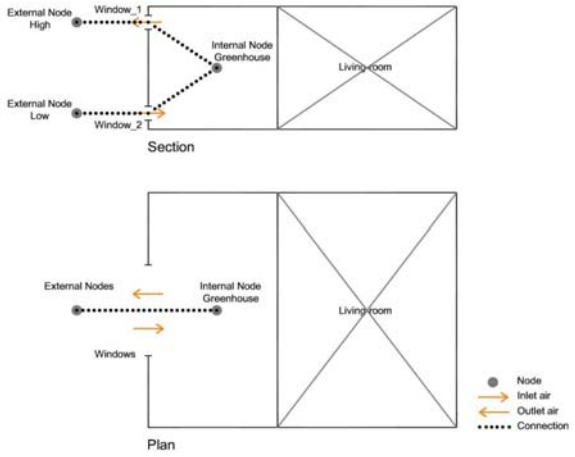


Figure 11. Air flow network scheme.

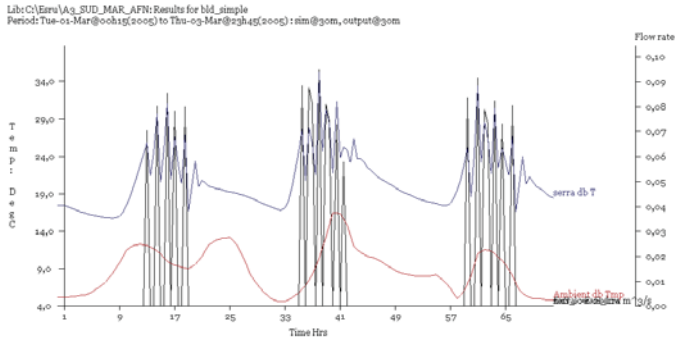


Figure 12. Greenhouse's temperature (blue line), outside ambient temperature (red line) and air flow rate of greenhouse (black lines) during 1, 2, 3 March. Opening area is of 0,1 [m^2].

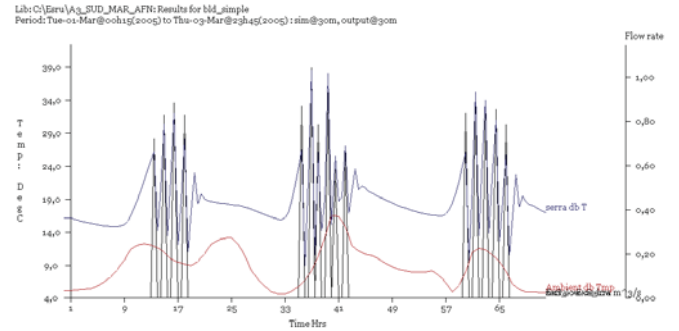


Figure 13. Greenhouse's temperature (blue line), outside ambient temperature (red line) and air flow rate of greenhouse (black lines) during 1, 2, 3 March. Opening area is of 1 [m^2].

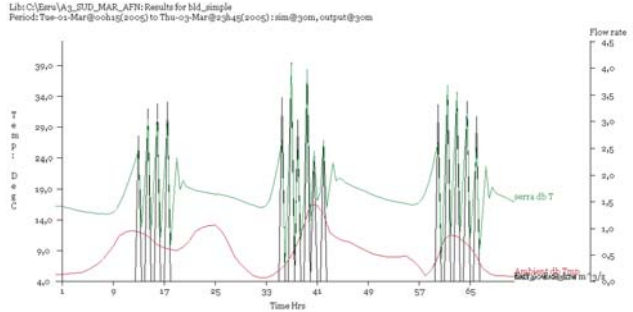


Figure 14. Greenhouse's temperature (green line), outside ambient temperature (red line) and air flow.

Modularizing and Validating CFD Parts of Four-way Cassette Type Outlets

Hidekazu Tanaka[1], Masashi Imano[1], Yuzo Sakamoto[1]

[1] Affiliation, the University of Tokyo, Dept. of Architecture, Tokyo, Japan 113-8656

Abstract:

In this paper, we created the CFD parts of four-way cassette type outlets for predicting easily the thermal environment of an office with packaged unit air-conditioning systems. At first we measured detail distributions of wind velocity around the cassette type outlets in two cases of angles of flap in an experiment room with particle image velocimetry (PIV).

Secondly we created the CFD parts of this type of outlets and performed CFD analysis. As a result of examining the correlation with measured velocity distribution around the outlets, we have confirmed the validity of these CFD parts.

Keywords: CFD, AC unit, PIV

1. Introduction

We created the CFD parts of a four-way cassette type outlet which is the most popular air

conditioning as the internal terminal. The supply-air is one of the important factors of constructing the thermal environment therefore the simulating model which can reproduce the airflow such as the distance of reaching and the way of diffusing is needed. In order to create such a model, we need the minute visualization and measurement of the supply-air. We used the PIV for measuring the minute distribution of average velocity of the airflow. In addition, we checked the characteristics of the turbulence and two-dimensional nature of the wind velocity by using supersonic wind velocimeter. Based on these data, we created the CFD parts of the outlet and analyzed the PIV measuring room with these parts.

2. Measurement of the Supply-Air

2.1. Measurement by PIV

2.1.1. Device and Criteria

The measurement was performed in the two cases of the angle of flaps of a four-way cassette type outlet, ‘Horizontal’ and ‘Vertical’. Then the velocity of wind was 22.0 m/s, and considering the symmetry of the shape, only one side of the outlet was measured (the measurement area is shown in Fig. 1). Pictures of five sections were taken every 50mm intervals, defining the central section as Section 1. The measuring devices were arranged like Fig. 2. The outlet was put upside down and a board simulating a ceiling was put for the convenience of measurement. The source of light was the 120mJ Double Pulse YAG Laser (produced by DANTEC co., Microwave) and exposed as the sheet light 1mm thick. The pictures of the measuring area were taken vertically by a CCD camera (produced by DANTEC co., FlowSenseM2). The vectorial velocity was calculated by Direct Mutual Correlative Method, and defined the check area as 32 times 32 pixels. 100 pictures were taken every section and were averaged in order to capture the steady property of airflow.

2.1.2. Result of Measurement

The result of this measurement is shown in Fig. 3 and 4. The angle of the supply-air is about 30 degrees at ‘Horizontal’ and about 80 degrees at ’Vertical’. From the center to the

edge in these cases, the angle of supply-air changes vertically. The width of airflow is almost the same in these cases, and the dependence on the flaps is considered to be small.

2.2. Measurement by Supersonic Wind Velocimeter

2.2.1. Device and Criteria

Since a PIV is two-dimensional, the factor of velocity vertical to the laser sheet can't be obtained. It seems that the characteristic of supply-air is quite two-dimensional. In order to check it, a measurement by three-dimensional supersonic wind velocimeter is performed (produced by KAIJO, Type WA-590). The velocity is measured at the point shown on Fig.5 in the PIV measuring section 1 to 4. The measuring frequency was 200Hz and the number of measurement on each point was 8008.

2.2.2. Result of Measurement

The results of calculating average wind velocity, turbulence energy, angle from the vertical plane, turbulence intensity and the scale of the length of a vortex (refer to Eq.1, 2 and 3) from the measurement are shown in Table 7 and 8 (refer to the Fig. 6 for the direction of the factor of velocity).

$$I=(2/3K)^{0.5}/U\times 100 \qquad \text{(Eq.1)}$$

$$L_i=U\cdot\sum_j<u_i(t-j\Delta\tau)\cdot u_i(t)>/<u_i(t)^2> \qquad \text{(Eq.2)}$$

$$L=(L_1+L_2+L_3)/3 \text{ when } \Delta\tau(i=1,2,3)_{1)} \qquad \text{(Eq.3)}$$

u,v,w : three-dimensional factor of wind velocity (see Fig.6)

U : scaler wind velocity[m/s] k : turbulence energy[m^2/s^2] I : turbulence intensity[%]

θ : angle from the vertical plane[deg] L : scale of the length of a vortex[mm]

$\Delta\tau$: interval of measurement[s]

The factor of velocity u, vertical to the laser sheet, is at most 0.5m/s and the declination is less than 5 to 10 degrees. It is considered that this factor is so small that there is no problem

by ignoring it in crating a model for simulation.

3. Creating CFD Parts

3.1 Creating the Parts of Measurement Data

The parts of measurement data were created in case of average wind velocity, turbulence intensity and the scale of the length of a vortex from the measurement near the four-way cassette type outlet, measured in 2.1. The parts consist of external files of STL format which describe the body of the outlet in XML format, and external files of VTK format which describe the data of a field of measured average wind velocity, turbulence intensity and the scale of the length of a vortex. Since we assumed the symmetry of plane and rotation in PIV measurement and measured in half of one outlet, we extracted the data according to the symmetry and created the data of a field corresponding to the four outlets. We show the data of the shape and distribution of velocity is shown in Fig. 9, visualized by ParaView, an open-source tool for visualization.

3.2. Creating CFD Parts

The CFD parts were created, which inherit the measurement parts based on the external files of the shape and the external file of the data of a field included in the measurement parts created in 3.1. Then the serial numbers of the measurement parts were put as the reference serial number of the CFD parts in order to show the inheritance of the measurement data. The turbulence energy and the rate of dissipating of the turbulence energy were included in addition to average wind velocity, turbulence intensity and the scale of the length of a vortex, which are normally necessary for analyzing by CFD in a RANS turbulence model. The rate of dissipating of the turbulence energy was calculated from the turbulence energy and the scale of the length of a vortex by assuming the local balance of the energy.

4. Analyzing and Validating with CFD Parts

4.1. Criteria for Analyzing by CFD

The case of PIV measurement experiment on 2.1 by CFD was analyzed with the parts created on 3.2 (the criteria are shown in Table 10). The analyzing area is shown in Fig. 11, but considering the symmetry of the field of flow, only the 1/4 symmetric area shown in the figure is analyzed. When practical analysis of the anemostat type outlets and cassette type outlets by CFD is done, the boundary and criteria of bounds of the AC unit, outlets and inlets are often modeled. The AC unit as rectangular by BOX Method, a kind of modeling, was modeled and analyzed[1].

The Table 12 is the cases of calculation for validating the parts, and we validated it by changing the height of the modeling boundary of this AC unit (the width is fixed) and the interval of the grids. These parts have three-dimensional distribution of velocity, but the BOX Method needs the two-dimensional distribution of velocity at the outlets of modeled boundary. So we interpolated the wind velocity at the outlets of modeled boundary of each case from three-dimensional distribution of field velocity. Since the volume of wind changes when interpolating the wind velocity, we scaled the wind velocity at the boundary in order to adjust the volume of wind to what is described in the parts. We are due to have the interpolation of the data of the field to the modeled boundary and the process for saving the plane integration (wind volume for velocity) implemented by CFD vendors as the function of the parts.

4.2. Validation of the CFD Parts

The correlation (the velocity v and w) between the measured value and the result of CFD analysis of case 1 with RNG K-Epsilon model is shown in the Fig. 13. The square value of R of the measured value and the result of CFD analysis in each wind direction and each case is shown in the Table 14 and 15. The correlation above and on the v side of the PIV measurement area was checked. The correlation of Standard K-Epsilon model was about 0.027(U), 0.021(w) and 0.037(u) worse than that of RNG K-Epsilon model in average. The correlation becomes poor (especially in the case of 'Vertical') in case 2 which has 2.5mm

lower boundary than case 1. In case 3 in which the interval of grids is 5mm, the correlation is quite poor. The case 1, which has a high modeling boundary and fine interval of grids of 2.5mm, shows a good correlation and we find that we should set the height of modeling boundary and interval of grids to such a level in order to analyze by CFD minutely. The interval of grids could be rough in the area far from the outlet, and further validation in the case of measurement in distant points is needed about the interval of grids and correlation of wind velocity in distant points.

5. Conclusion

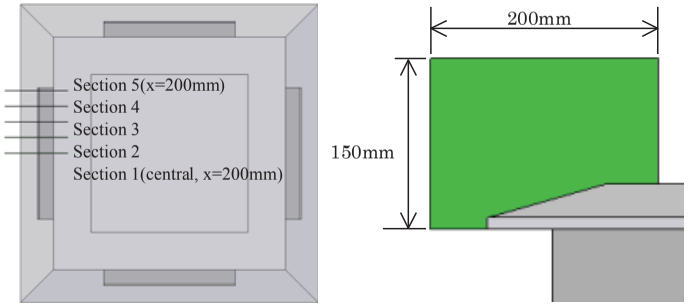
The airflow of a four-way cassette type outlet was measured and the steady characteristic was revealed by PIV. The two-dimensional characteristic was checked and the turbulence factor by a supersonic wind velocimeter was measured. The results of the measurement were converted into CFD parts, the measurement room was analyzed by CFD and the parts were validated. We found out that by moderately taking the height of the modeling boundary and the interval of grids, we can accurately reproduce the distribution of the wind velocity near the outlet.

[acknowledgement]

This paper was written with the help of the members of CFD parts WG in SHASE(the Society of Heating, Air-Conditioning and Sanitary Engineering of Japan). We appreciate the cooperation to the persons concerned.

[references]

MOMOI Yoshihisa, YAMANAKA Toshio, KOTANI Hisashi et al. “**CFD of Airflows in Rooms with Anemostat Type Air Diffuser : Part 5. CFD Simulation Using Measured Values of Velocity and Turbulence Parameters in Large Space as Boundary Conditions**” pp775～776 : 2001



a) Location of Measuring Section b) Size of Measurement Area

Fig.1 Measurement Area

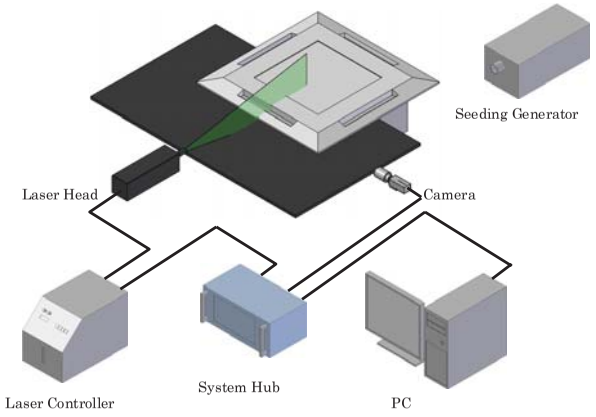
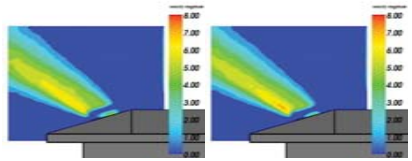
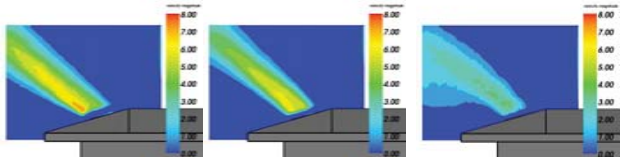


Fig.2 Measuring Devices

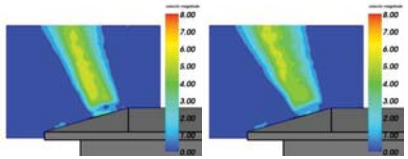


a) Section 1(central, x=0mm) b) Section 2(x=50mm)

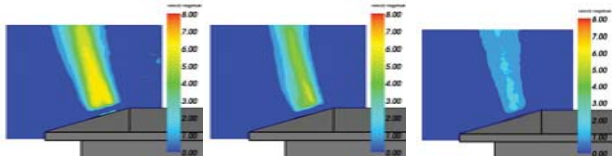


c) Section 3(x=100mm) d) Section 4(x=150mm) e) Section 5(x=200mm)

Fig.3 Distribution of Velocity (Horizontal)



a) Section 1(central, x=0mm) b) Section 2(x=50mm)



c) Section 3(x=100mm) d) Section 4(x=150mm) e) Section 5(x=200mm)

Fig.4 Distribution of Velocity (Vertical)

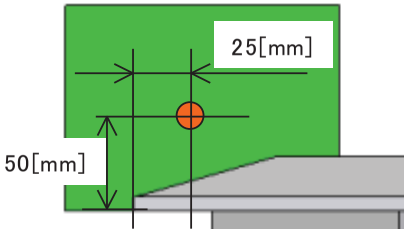


Fig.5 Measuring Point

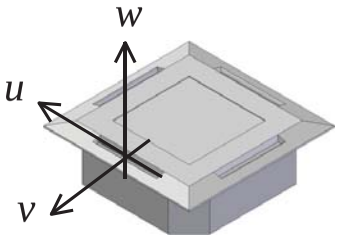


Fig.6 Direction of Factors of Velocity

Table 7 Average Wind Velocity, Factor of Turbulence and Angle from Vertical Section

(Horizontal)

	u [m/s]	v [m/s]	w [m/s]	U [m/s]	k [m^2/s^2]	I [%]	θ [deg]	L [mm]
Section1	0.24	3.21	2.26	3.94	0.11	6.8	3.5	3.6
Section2	0.14	2.44	1.72	2.99	0.12	9.4	2.7	3.1
Section3	0.25	2.55	1.79	3.12	0.13	9.6	4.6	4.1
Section4	0.50	2.36	1.85	3.04	0.18	11.3	5.0	6.0

Table 8 Average Wind Velocity, Factor of Turbulence and Angle from Vertical Section

(Vertical)

	u [m/s]	v [m/s]	w [m/s]	U [m/s]	k [m^2/s^2]	I [%]	θ [deg]	L [mm]
Section1	0.28	1.23	4.58	4.75	0.08	4.9	3.3	3.6
Section2	0.27	1.46	5.41	5.61	0.06	3.6	2.8	3.1
Section3	0.26	0.82	3.73	3.83	0.20	9.5	3.9	4.1
Section4	0.16	0.22	1.25	1.27	0.16	25.7	7.0	6.0

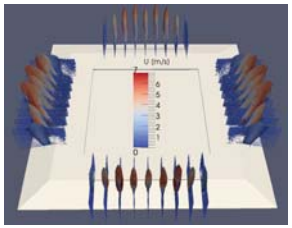


Fig.9 Data of Actual Shape of the Part and Data of Velocity Field

Table 10 Criteria for CFD Analysis

CFD Software	Open Source CFD Tool OpenFOAM
Analyzing Area	1.5m(x)×1.5m(y)×1.5m(z)
Width of Grids	2.5cm or 5cm
Sollution	SIMPLE(Static Solution)
Turbulence Model	RNG $k-\varepsilon$
Advective Term Scheme	TVD Scheme (limited Upwind)
Boundary Wall	Generalled PowerLaw for Smooth Wall
Criteria for Inlet	Pressure Fixed

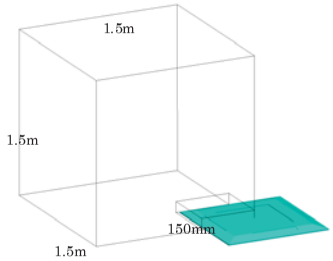
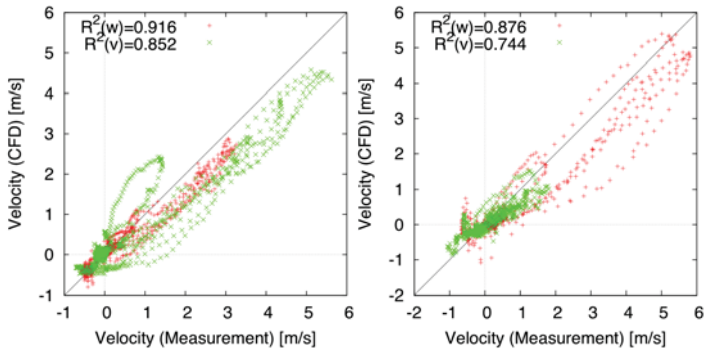


Fig.11 Area of CFD Analysis

Table 12 Cases of CFD Analysis

Case	Height of Model Boundary[cm]	Interval of Grids[cm]
1	10	2.5
2	7.5	"
3	10	5



a) Horizontal b) Vertical

Fig.13 Correlation of Wind Velocity between Measurement and CFD (Case 1, RNG)

Table 14 Square Value of R of Measurement and CFD (Horizontal, RNG)

Case	w(z velocity)	v(y velocity)	U(scaler)
1	0.916	0.852	0.808
2	0.880	0.807	0.747
3	0.702	0.547	0.128

Table 15 Square Value of R of Measurement and CFD (Vertical, RNG)

Case	w(z velocity)	v(y velocity)	U(scaler)
1	0.876	0.744	0.806
2	0.801	0.626	0.714
3	0.648	0.615	0.422

Fungal Growth Prediction on Building Materials by Reaction-Diffusion Model Coupled with Heat and Moisture transfer

Kazuhide Ito[1]

[1] IGSES, Kyushu University, Fukuoka, Japan

Abstract

A mathematical model that reproduces fungal proliferation and morphological colony formation was developed on the basis of a reaction diffusion modeling approach. In this modeling, fungus was separated into two states, active and inactive, and it was assumed that active fungus moves by diffusion and reaction while generating and producing inactive fungus. The effects of temperature and humidity on fungal growth were explicitly incorporated in the reaction term of nutrient consumption/generation of active fungus in this governing equation. The damping function, which reproduces the effects of temperature and humidity on fungal growth, was developed and explicitly based on the fungal index proposed by Abe. In order to estimate the sensitivity of the proposed numerical fungal growth model, fungal growth on the surface of building materials was analyzed for four types of building materials, and the prediction results were compared with the results of WUFI-Bio.

Keywords: Fungi, Reaction diffusion model, Heat and moisture transfer, Indoor environment

Introduction

Fungal growth in indoor environments is strongly related to the indoor physical and chemical conditions, such as atmospheric temperature, relative humidity and nutrients; therefore, a comprehensive prediction method must be developed to estimate the health risk of fungal contamination for exposed individuals. Large numbers of studies have also shown an association between the health risk of fungal contamination and residence in homes with signs of 'dampness'. Wickman et al. reported associations between damp houses and the presence of dust-bound micro-fungi in the homes of healthy children but not in the homes of atopic children (Wickman et al., 1992), and adverse effects on health due to micro-fungi exposure have become a serious problem.

The pollution problems caused by fungi in indoor environments are usually recognized at a stage where colony formation has progressed to a level enabling visual identification In other words, the prediction and control of the adverse effects of fungi on health at an early stage of fungal growth are usually difficult because of the lack of both prediction methods and detailed information regarding the effects of various indoor physical, chemical and biological parameters on the germination of spores and subsequent hyphal growth and colony formation.

In the field of mould/fungi growth prediction by computational simulation, WUFI-Bio is widely used to estimate spore germination and subsequent mould growth on building materials. WUFI is hygro-thermal calculation software developed at the *Fraunhofer Institut für Bauphysik*, Germany, and WUFI-Bio is an additional function of WUFI (add-on software) that was developed to estimate the probability of growth of some species on building surfaces.

This research focuses on the development of a simplified prediction model for two dimensional fungal growth in indoor environments, which incorporates heat and moisture transfer analysis in building materials.

Theory

Reaction diffusion model of fungal growth

In the present study, a mathematical model that reproduces fungal proliferation and morphological colony formation was developed on the basis of a reaction diffusion modeling approach. In this model, the fungus was hypothetically separated into two states, active and inactive. In this modeling, it was assumed that active fungus moves by diffusion and reaction while generating and producing inactive fungus at a constant rate. In terms of the morphology of colony formation, colonies might form a ring shape like a doughnut with the perimeter containing active fungus and the center containing inactive fungus. Concerning the inactive fungus, which is produced by the dynamism of the active fungus, neither extinction nor movement is considered and it is simply modeled as accumulating at the place it was generated.

Using these assumptions, a non-linear reaction diffusion model, which is coupled with temperature and humidity transfer in building materials, was adopted and is expressed by the following partial differential equations.

[1] The transport equation of active fungi, *u*

$$\frac{\partial u}{\partial t} = \nabla \cdot \left(D_c \nabla u\right) + \theta f\left(u,n\right) - a\left(u,n\right)u - \gamma u \tag{1}$$

$$D_c = \sigma_1^{'} \cdot u \cdot n\,, \quad \sigma_1^{'} = \sigma_1\left(1+\delta\right), \quad -0.5 < \delta < 0.5 \tag{2}$$

$$f\left(u,n\right) = \sigma_2\left(\frac{f_1 n}{1+f_2 n}\right) \cdot u \cdot \zeta\left(T,\varphi\right) \tag{3}$$

$$\zeta\left(T,\varphi\right) = a_1 \exp\left(a_2\varphi^2 + a_3 T^2 + a_4\varphi * T + a_5\varphi + a_6 T + a_7\right) \tag{4}$$

$$a\left(u,n\right) = \sigma_3 \cdot \frac{1}{\left(1+\frac{u}{a_1}\right)\cdot\left(1+\frac{n}{a_2}\right)} \tag{5}$$

[2] The transport equation of inactive fungi, *v*

$$\frac{\partial v}{\partial t} = a\left(u,n\right)u \tag{6}$$

[3] The transport equation of nutrients

$$\frac{\partial n}{\partial t} = D_n \nabla^2 n - f\left(u,n\right) \tag{7}$$

[4] The hygro-thermal transport equations

$$\frac{dH}{dT}\cdot\frac{\partial T}{\partial t}=\nabla\cdot\left(\lambda\nabla T\right)+h_v\nabla\cdot\left(\delta_p\nabla\left(\varphi p_{sat}\right)\right) \quad (8)$$

$$\frac{dw}{d\varphi}\cdot\frac{\partial \varphi}{\partial t}=\nabla\cdot\left(D_\varphi\nabla\varphi+\delta_p\nabla\left(\varphi p_{sat}\right)\right) \quad (9)$$

Here, u and v are the hypothetical densities of active and inactive fungi, respectively. The total density of fungus is given by (u+v). n is the concentration of nutrients. The first term on the right side of equation (1) expresses the non-linear diffusion term that indicates the random movement of fungus. The second term is the reaction and generation term, which depends on the density of active fungus, nutrient concentration and other environmental factors. The third term refers to the conversion from active to inactive fungus and the fourth term expresses the rate of death of active fungus. The term on the right side of equation (6) expresses the generation of inactive fungus transformed from active fungus (same as the third term in equation (1)).

Equation (4) shows the damping function of fungal growth as a function of temperature T and relative humidity φ. In this study, the damping function $\zeta(T, \varphi)$ is expressed according to the fungal index proposed by Abe (Abe, 1993). This damping function is incorporated into the reaction and the term relating to the generation of active fungi, and the effect indirectly influences fungal diffusion.

Equation (7) shows the transport equation of nutrients and the first term on the right side of the equation indicates the diffusion of nutrients on the two-dimensional surface, and D_n is the diffusion coefficient of nutrients. The second term denotes the nutrient consumption by active fungus. Although it is thought that various types of nutrients influence fungal growth, nourishment of fungi was assumed in this study.

Equations (8) and (9) show the simultaneous heat and moisture transport and, here, dH/dT denotes the heat storage capacity of the moist building material, $dw/d\varphi$ denotes the moisture storage capacity of the building material, T is temperature and φ is relative humidity.

In the present study, for purposes of simplification, only nutrient concentration, temperature and relative humidity were focused on and these parameters non-homogeneously distributed on the surface of building materials were assumed to be the dominant environmental parameters in fungal growth.

Prediction of spore germination and mould growth by WUFI-Bio

WUFI-Bio was developed at the *Fraunhofer Institut für Bauphysik*, Germany, in order to describe non-steady fungal growth on the surface of building materials. The characteristic WUFI-Bio model is used to determine the moisture content within spores in order to predict bio-hygrothermal phenomena of spore germination and subsequent growth of hypha. The fungal growth rate in the WUFI-Bio model is calculated using isopleth diagrams, which were

determined under constant temperature and humidity conditions. WUFI-Bio is a simulation model coupled with unsteady hygrothermal analysis of building materials and used worldwide.

In this study, the prediction results of WUFI-Bio were used to estimate the sensitivity of the reaction diffusion model.

Prediction of hypha growth by fungal index

Fungal index was proposed as a parameter to characterize the indoor environmental capacity for fungal growth and is widely used in Japan. This fungal index is based on the growth response of a xerophilic fungus *Eurotium herbariorum* as a function of ambient temperature and relative humidity. Fungal index is also based on isopleth diagrams under steady-state environmental conditions. The prediction results of fungal index were also used to evaluate the sensitivity of the reaction diffusion model.

Furthermore, in this research, fungal index was used as the damping function $\zeta(T, \varphi)$, which is expressed by equation (4) for the reaction diffusion model. In the condition that fungal index (mycelium length) is assumed to be a dependent variable and temperature and relative humidity are assumed as independent variables, the approximate expression $\zeta(T, \varphi)$ based on isopleth diagrams of fungal index was assumed using the non-linear and minimum-square approximation method. The parameters in equation (4) were a_1=1.089, a_2=-170.195, a_3=-0.012, a_4=-1.241, a_5=347.922, a_6=1.784 and a_7=-182.404 (R^2=0.929). In this approximation, $\zeta(T, \varphi)$ has the unit of mm/week.

Numerical Analysis

In this analysis, heat and moisture transfer and fungal growth on an indoor wall surface were analyzed for four building materials: (i) concrete single wall, (ii) gypsum plaster single wall, (iii) insulation board and (iv) composite wall consisting of (i), (ii), (iii) and an air layer, under summer climate conditions in Fukuoka, Japan. The building material of case (iv) is shown in Figure 1. Numerical analyses of heat and moisture transfer in building materials were carried out in one-dimension. Numerical predictions of fungal growth of (1) WUFI-Bio model, (2) fungal index proposed by Abe and (3) the reaction diffusion model proposed in this paper were conducted following temperature and relative humidity analyses on the surface of building materials.

Table 1 shows the cases analyzed and Table 2 shows the physical properties of the target building materials, which were obtained from the IBP database.

Concerning the case of the reaction diffusion model, its model parameters were identified using fundamental experimental data of colony formation and set by consideration of the results of previously conducted sensitivity analysis (see Ito and Mizuno, 2008). A two-dimensional plane of 200 mm (y) × 200 mm (z) on a wall surface (indoor side) was targeted as the object surface in this analysis. An equally spaced mesh with 1 mm intervals was adopted for the y and z directions for analysis of the reaction diffusion model. A uniform distribution of nutrient concentration was assumed as the initial condition. As the initial condition of active fungus, u = 1.0 was set at the center of the analytical plane (point x=100 mm and y=100 mm). The initial concentration of inactive fungus was assumed to be zero (v= 0.0). A free slip condition (zero gradient) was assumed as the boundary condition at the edge of the analytical plane. Each transport equation (eqs. (1), (6) and (7)) was discretized by the finite volume method, and unsteady analyses were carried out using the explicit method for solving time-variable partial differential equations. Calculations totaling 168 hours were conducted in real time. Table 3 shows a list of model parameters and other boundary conditions used for the numerical analysis. Stochastic fluctuation as shown in equation (2) was coupled in this analysis.

Results

Time course of temperature/relative humidity on the inner surface of building materials

Figure 2 depicts the time courses of temperature and relative humidity on the surface of target building materials (indoor side) and the outdoor climate conditions in summer. The calculation period covered was the first week of July in Fukuoka, Japan. The initial conditions of room air temperature and relative humidity were set at 25 ºC and 85% RH, respectively, and the room air temperature and relative humidity were fixed at constant values. The heat and moisture transfer analyses were carried out at one hour intervals using WUFI software.

The outside temperature changed within the range of 19 ºC - 32 ºC on the basis of the AMeDAS data of a standard year. Wall surface temperature (indoor side) became constant at about 25 ºC in cases (iii) insulation board and (iv) composite wall. In cases (i) concrete single wall and (ii) gypsum plaster single wall, although the wall surface temperature (indoor side) fluctuated, the temperature changes were smaller than the outdoor temperature fluctuation.

The outside relative humidity in this climate condition changed within the range of 50% RH – 100% RH on the basis of the AMeDAS data. Relative humidity on the wall surface (indoor side) became constant at about 85% RH in cases (iii) insulation board and (iv) composite wall. In the case of (ii) gypsum plaster single wall, relative humidity on the wall surface became relatively high.

Time course of hypha growth by numerical prediction

Figure 3 depicts the time course of fungal growth on each wall surface (indoor side). The prediction results of (1) the WUFI-Bio model overestimated the fungal growth response compared with the results of (2) fungal index. In the cases of (i) concrete wall and (ii) gypsum plaster board in particular, large differences were observed in the fungal growth response after 24 h from the start of analysis, although a difference in hyphal growth could not be confirmed at an earlier stage of analysis in (2) fungal index. For (2) fungal index, a high dependency of fungal growth on the target building materials was confirmed. In other words, the results of (2) fungal index had high sensitivity for the temperature and relative humidity compared with those of (1) the WUFI-Bio model.

The results of (3) the reaction diffusion model proposed in this study showed a similar pattern to the results of (1) the WUFI-Bio model.

Figure 4 shows the time course of colony formation predicted by the reaction diffusion model in Case3(II)g_S and Case3(IV)m_S. The morphological characteristics of the fungal colony were schematically predicted in modeling active and inactive fungi separately. In the early stage of calculation (less than 24 h), fungal colonies grew rapidly and seven days after the test started, the result of numerical analysis showed a tendency to increase constantly, but the amount of active fungus (u) did not appear to change markedly especially in Case3(IV)m_S. In this numerical analysis, the fluctuation of diffusion coefficient, which is expressed by Eq. (2), was coupled and then the phenomena of asymmetry and non-uniform diffusion were reproduced comparatively.

Discussion

There was a substantial difference between the prediction results of the WUFI-Bio model and the fungal index. This was caused by differences of the isopleth diagrams of growth response as a function of temperature and relative humidity. The WUFI-Bio model adopted more than 10 types of fungal growth response data. In comparison, fungal index was based on three types of fungi: *Eurotium herbariorum*, *Altermaria alternate* and *Aspergillus penicillioides*.

The prediction results of the reaction diffusion model were strongly dependent on the values of model parameters (σ_1, σ_2, f_1, f_2, θ, σ_3, a_1, a_2,) and nutrient condition (n_0, D_n). These model parameters were estimated heuristically to correspond to the results of the WUFI-Bio model in this analysis. The theoretical determination of these model parameters is a goal of future research.

Conclusions

The findings obtained in this work can be summarized as follows:

(1) Fungal index had a high sensitivity to temperature and relative humidity on the surface of building materials compared with the results of WUFI-Bio and the reaction diffusion model proposed in this study. From the viewpoint of predicted hypha length, the result of the WUFI-Bio model was the longest and the result of the reaction and diffusion model was similar to that of the WUFI-Bio model.

(2) The morphological characteristics of fungal colony formation could be reproduced on the basis of reaction diffusion expression in modeling active and inactive fungi separately.

(3) As the next step of this research, model parameters must be identified on the basis of detailed experimental data, and it is also necessary to couple numerical analysis with other parameters, for example characteristics of building materials and pH, in the proposed mathematical model.

Acknowledgments

This research was partly supported by a Grant-in-Aid for Scientific Research (JSPS KAKENHI for Young Scientists (S), 21676005). The authors would like to express special thanks to the funding source.

References

Sedlbauer, K. (2001) Prediction of mould fungus formation on the surface of and inside building components, Dissertation University Stuttgart 2001.

Abe, K. (1993) Method for Numerical Characterization of Indoor Climates by a Biosensor using a Xerophilic Fungus, *Indoor Air 3*, 344-348

Ito, K and Mizuno, Y (2009) Numerical Morphological Analysis of Fungal Growth based on a Reaction - Diffusion Model : *Biocontrol Science*, Vol.14, No.1, pp 21-30

Ito, K. (2009) Micro/ Macro Scale Experiments of Fungal Growth for determining Parameters of Mathematical Growth Models, *ROOMVENT 2009,* pp400-407

Mimura, M., Sakaguchi, H., and Matsushita, M. (2000) Reaction-diffusion modeling of bacterial colony pattern. *Physica A, 282*, 283-303

Kawasaki, K., Mochizuki, A., Matsushita, M., Umeda, T., and Shigesada, N. (1997) Modeling spatio-temporal patterns generated by *Bacillus subtilis*. *J. Theor. Biol,. 188*, 177-185

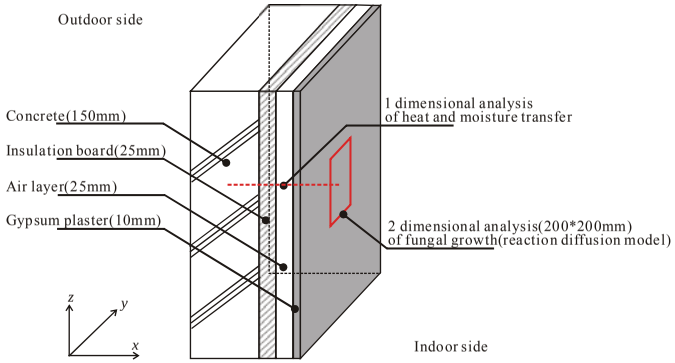


Figure 1 Target building materials (case (iv) composite wall)

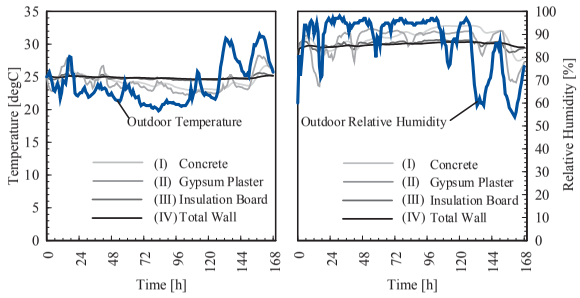
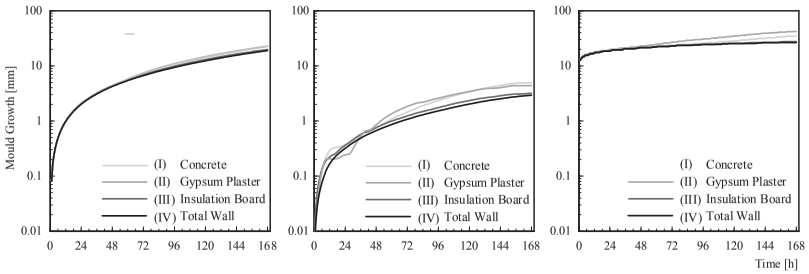
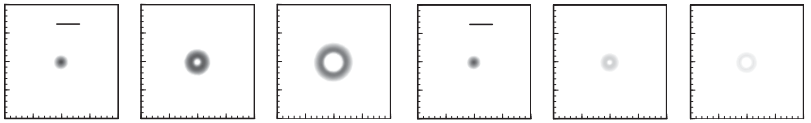


Figure 2 Results of time courses of temperature (left side) / relative humidity (right side fig.)



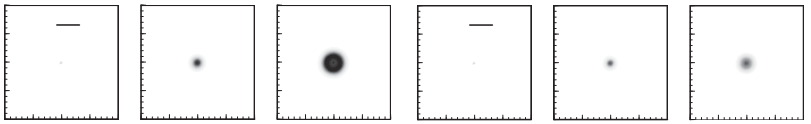
(1) Case 1 (WUFI-Bio) (2) Case 2 (Fungal index) (3) Case 3 (React. diff.)

Figure 3 Results of hypha length prediction [mm]



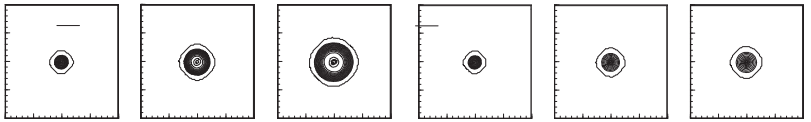
24h 96h 168h 24h 96h 168h

(1) Case3(II)g_S, Active fungi (*u*) (4) Case3(IV)m_S, Active fungi (*u*)



24h 96h 168h 24h 96h 168h

(2) Case3(II)g_S, Inactive fungi (*v*) (5) Case3(IV)m_S, Inactive (*v*)



24h 96h 168h 24h 96h 168h

(3) Case3(II)g_S, Active +Inactive (*u*+*v*) (6) Case3(IV)m_S, Active +Inactive (*u*+*v*)

Figure 4 Results of morphological characteristics of fungal colony formation

Table 1 Cases analyzed

	(I) Concrete (150^{mm})	(II) Gypsum plaster (10^{mm})	(III) Insulation board (25^{mm})	(IV) Composite wall ((i)+(ii)+(iii)+air layer) (210^{mm})
(1) WUFI-Bio	Case 1(I)c_S	Case 1(II)g_S	Case 1(III)a_S	Case 1(IV)m_S
(2) Fungal index	Case 2(I)c_S	Case 2(II)g_S	Case 2(III)a_S	Case 2(IV)m_S
(3) React. diff. model	Case 3(I)c_S	Case 3(II)g_S	Case 3(III)a_S	Case 3(IV)m_S

Table 2 Physical properties of target building materials

Material	Thickness [mm]	Bulk density [kg/m^3]	Porosity [m^3/m^3]	Specific Heat Capacity (dry) [J/kgK]	Thermal Conductivity (dry) [W/mK]	Water Vapor Diffusion Resistance Factor [-]
(I) Concrete	150	2200	0.18	850	1.6	92
(II) Gypsum Plaster	10	1721	0.305	850	0.2	13
(III)Insulation Board	25	28.6	0.99	1470	0.025	170.56

Table 3 Numerical and boundary conditions

Calculation period	Total 168h, Time Steps:1[h], Start:07/01, End:07/09
Initial Condition (wall inside)	Initial Temperature[℃] : 25 ºC, Initial Relative Humidity[-] : 0.6 Initial Water Content[kg/m^3] of Concrete: 41.3, Insulation Board : 0.16, Gypsum Plaster : 1.13
Indoor Climate	Temperature[℃] : 25ºC constant, Relative Humidity[-] : 0.85 constant
Outdoor Climate	Fukuoka; AMeDAS standard year (07/01 to 07/09)
Model parameters of Reaction diffusion model	σ_1=5.0×10^{-5}, σ_2=3.0, f_1=1.0, f_2=1.0,θ=5.0×10^2, σ_3=5.0, a_1=1/2400, a_2=1/120, n_0=1.0 for PDA, D_n=1.0×10^{-9}, u_0 (center)=1.0, v_0=0.0

The influence of stochastic modeling of window actions on simulated summer comfort in office buildings

Wout PARYS[1], Dirk SAELENS[1], Hugo HENS[1]

[1] Division of Building Physics, K.U.Leuven, Kasteelpark Arenberg 40-2447, 3001 Heverlee, Belgium

Abstract

In this study, an attempt is made to define building design variables for a medium-sized office building with individual office cells in order to provide sufficient summer comfort without active cooling in a moderate climate.

Firstly, an approach to take realistic window-opening behavior into account is proposed based on observational data in literature. A stochastic model is defined for an active and a passive user, representing the variability between individuals.

The uncertainty in summer comfort due to the building use and occupant behavior is then assessed. The sensitivity of the simulated summer comfort proves to be substantial. A criterion for robustness of the building design for behavioral aspects is deduced from this analysis.

Finally, it is shown using the proposed criterion that for office cells with external shading where window-opening is allowed, satisfying summer comfort can be guaranteed independent of the building use if the glazing-to-wall-ratio does not exceed 60%.

Keywords: Window-opening, behavioral model, summer comfort, office building, adaptive theory

Introduction

In Belgium, which has a moderate climate, many existing small or middle-sized office buildings are not equipped with active cooling systems, but rely on window-opening for summer comfort [1]. In addition, there is a trend towards constructing low energy and even so-called passive office buildings. In these designs, it is attempted to combine minimized heating demands with passive cooling techniques ([2], [3]). Furthermore, it is now known that occupant satisfaction is higher in office buildings where the user can exercise some control over the environment than in fully air-conditioned offices ([4], [2]). Off course, this cannot be applied in every situation: window-opening or applying external shading is not always possible and manual control in landscape offices is often infeasible due to social interaction.

Meanwhile, the adaptive comfort theory has found its way to the building standards. The European standard EN15251, which provides boundary conditions for the design and the assessment of energy performance of buildings, allows for higher temperatures as a function of running mean outdoor temperature in buildings where the opening of windows is the primary means of regulating the thermal conditions in summer. This is a strong incentive for building designers to develop passive cooling concepts. However, when assessing the expected summer comfort at the design stage through building simulation, the manual control of windows is generally simplified to deterministic thresholds at which windows are assumed to be open ([5], [6]). The influence of the occupant can however be substantial [3].

During the past decades, several researchers have introduced behavioral window-opening models based on observational data for individual or 2-person offices ([7], [8], [9], [10], [11], [12]). Most of these models are Markov chains, with probabilities of transition depending on the physical conditions. There is disagreement between the authors on the selection of driving variables for actions on windows, though the recent publications seem to agree upon the inclusion of the indoor temperature, to explicitly implement the adaptive principle ([11], [12]). Additionally, these recent models include the occupancy state as a driving variable, because it was noticed that most of the actions occurred when the user was arriving at or leaving his office. Quasi all of the data were collected in office buildings without ventilation system, but the indoor air quality is not included as a driving variable in any study. Furthermore, no information on window opening angles was gathered. There is a clear lack of intercomparison and validation of all introduced models, preventing them to safely expand their applicability beyond the observed office building. Some of the models have already been coupled to building simulation software ([3], [10]).

In this study, the summer comfort of a middle-sized office building with varying building parameters will be calculated, taking into account a realistic pattern of window-opening based on the model of [12]. The requirements for the building design to provide sufficient comfort without active cooling for the Belgian climate can thus be identified. In addition, the uncertainty on this result due to occupant behavior will be assessed.

Building Model

The simulations are performed for the climate of Uccle, Belgium. The geometry of the office space is given in Fig. 1. The internal walls are assumed to be adiabatic, so heat losses or gains occur through the external façade only (though heat can be stored in the internal constructions). This façade faces south, representing the worst case scenario. The external wall is a masonry cavity wall; the floor is a heavyweight, concrete construction and the internal walls are lightweight, gypsum board walls. A basic hygienic ventilation rate of 1.2 ACH is supplied at outdoor temperature during office hours. Two levels of internal heat gains from appliances are considered: 5.4 W/m^2 and 16.1 W/m^2, respectively identified as low and moderate/high in [13].

The considered building variables and their ranges are the following:

- U-value of the opaque part of the external façade. This ranges from 0.6 W/m^2K (the legal maximum for new constructions in Flanders) to 0.15 Wm^2K (the Passive House Standard).
- Glazing-to-wall-ratio. This ranges from 21% to 71%.
- Glazing type. 6 glazing types were selected from manufacturer's data (see Table 1). Glazing with U-value higher than 1.1 W/m^2K is rarely placed in Belgian offices nowadays, so this is not considered. Types 1 to 5 represent the whole commercially

available spectrum of visual transmittance (in discrete steps) and associated g-value for double low-e glazing with a gas-filled cavity. Type 6 is a triple glazing.

- Shading device. The considered types are: (a) no shading device, (b) external fixed horizontal louvers. The latter is selected as a shading device, because it is assumed to have a minor influence on the air flows, as opposed to for example screens.

The combination of these variables results in 180 different building designs.

Behavioral Model

The model of [12] is selected for this research, because it is based on the largest dataset and the broadest measuring campaign. It is a Markov chain with probabilities of transition as a function of several physical variables and of the occupancy state.

In reality, there's an important variability in user behavior that should be included in the uncertainty analysis. This is accomplished in this study by defining representative active and passive users [14]. As is stated in [15], the characteristic physical variable A_{50}, for which the probability of action is equal to 0.5, is a fair indicator to compare the individuals. Thus, it is proposed here to define *active* behavior as the 25th percentile and *passive* behavior as the 75th percentile of the set of individual A_{50}-values, where A is the most influential driving variable of the respective probability function. The functions resulting from this methodology are shown in Fig. 2. Since night ventilation is not considered in this study, it is assumed that the windows are closed at the last departure of the day.

From bivariate plots in [15] it can be deduced that people show consistent behavior at different occupancy states, e.g. users that show *active* opening behavior at arrival will also show this *active* behavior at intermediate times. However, people with *active* opening behavior will not necessarily show *active* closing behavior and vice versa. Therefore, two representative user patterns are defined, one with *active* opening and *passive* closing and one with *passive* opening and *active* closing. These two types will yield respectively the largest and the smallest net window opening times in building simulation.

As the behavioral model of window-opening depends on the occupancy state, it is necessary to implement a detailed stochastic occupancy model. Several models are available, but require mostly building specific inputs that cannot be supplied for this generic office building ([16], [17]). A simplified version of the model of [17], called the *Lightswitch* model, was already introduced in [18]. The probabilities of transition for 5 minute time steps are estimated from empirical data (Fig. 3).

To introduce some variability in the occupancy profiles, a parameter is introduced, accounting for the differences amongst office buildings. The probability of temporary absence is multiplied by a *parameter of mobility* M. This is the most important parameter,

because it determines the number of vacant-to-occupied events per day, which influences the window-opening behavior. Based on findings in [17], [16] and [19], a spectrum for the parameter of mobility of 0.1 to 0.7, resulting in an average of 3 to 9 vacant-to-occupied events per day, is established.

Because the behavioral model is stochastic, it will generate different results every time it is run. However, in this research, only one run of the model for every building variant is done in order to limit the calculation time. For one building variant, the behavioral model was run 100 times, to see how large the deviations are. In terms of weighted exceeding hours (see further), the standard deviation due to the stochastic character of the behavioral model was limited to about 15% (Fig. 4).

Thermal and Lighting Model

The summer comfort calculations are performed with TRNSYS version 16 [20], a software package for dynamic building simulation, with a 1 hour time step. The installed lighting power is 11 W/m^2. The lighting is assumed to be switched on at full power at first arrival and switched off on last departure of the occupant. Additionally, an automated daylight dimming control is simulated, which results in lower heat gains. The light simulations are performed with the Daysim software [21]. Finally, the behavioral model is implemented in Matlab and is coupled in real-time to TRNSYS to be able to take possible window-opening as an adaptive action into account.

Air Flow Model

Only single-sided ventilation is considered. This is the most conservative option, resulting in the lowest air flows ([2]) and is therefore appropriate when assessing comfort. Because of this option, it is sufficient to model only one office cell. The air flows when the window is opened are estimated using EN15242:

$$q_{v,win} = 3.6 \cdot 500 A'_{ow} \sqrt{C_t + C_w V_{met}^2 + C_{st} H_{win} |\theta_i - \theta_e|} \qquad \text{(Eq. 1)}$$

Where the coefficients C_t (=0.01), C_w (=0.001) and C_{st} (=0.035) account for respectively the influence of wind turbulence, wind speed and stack effect. V_{met} is the meteorological wind speed at 10m height and H_{win} is the height of the window. A'_{ow} (m^2) is the equivalent open area of the window, depending on the opening angle α and the area of the window A_{ow}:

$$A'_{ow} = \left(2.6 \cdot 10^{-7} \alpha^3 - 1.19 \cdot 10^{-4} \alpha^2 + 1.86 \cdot 10^{-2} \alpha\right) A_{ow} \qquad \text{(Eq. 2)}$$

Two opening angles are considered, 10° and 90°.

This calculation method is simplified, but as was shown in [22], the resulting air flows comply well with air flows calculated with a more sophisticated nodal network. It is therefore

decided to use this simplified equation in the building simulations, since this effects in much smaller computational times.

Summer comfort criteria

The summer comfort of the different building designs is assessed according to the degree hours criteria of the European standard EN15251. In this method, the comfort is considered insufficient if the weighted sum of hours at which the indoor temperature exceeds the limit value is more than 5% of the occupied time, i.e. about 100 hours on a yearly basis. The weighing factor is the difference between the occurring temperature and the limit value. The latter depends on the running mean outdoor temperature (Fig. 5).

Thus, in contrast to [3], the interest of this analysis does not lie in detailed temperature profiles, but rather in aggregated seasonal performance.

Results and Discussion

Different behavioral patterns are simulated for every building design. The level of internal heat gains from appliances, lighting control, occupant mobility, window-opening user type and opening angles are considered here as behavioral variables. For each variable, two more extreme values were chosen, resulting in 32 patterns.

In Fig. 6, the results are shown for a sample of the building designs, ordered according to the mean of the weighted exceeding hours for the 32 patterns. The graph shows the mean value, 25^{th} and 75^{th} percentile in the boxes, while the whiskers show the 10^{th} and 90^{th} percentile.

It is clear that on the one hand, for about half of the designs the simulated summer comfort is independent of the behavioral patterns, either because there are no problems or because there are certain problems to provide satisfying comfort. However, for another part of the building designs, the summer comfort is not guaranteed and is dependent on the occupant behavior. In Fig. 7, this is shown in detail. This raises the question about the necessary robustness of designs for user behavior. Should the building suffice even in the worst case scenario? When considering the rather conservative upper value of the internal heat gains and the fact that a possible correlation between 'activity' of window-opening and individual sensitivity for high temperatures is neglected, this might be too strict. It is therefore proposed for this research that a building satisfies if the 75th percentile of the results for simulations with different behavioral patterns is lower than 100 weighted exceeding hours.

In Fig. 8, the 75^{th} percentile of the weighted exceeding hours is compared for different window-opening patterns for a selection of buildings. This graph indicates that applying a deterministic threshold temperature at which the windows are opened underestimates the potential summer discomfort. Using a deterministic threshold in building simulation appears

to be comparable to assuming an *active* window-opening behavior, which is a too optimistic boundary condition for comfort calculations, as this is only representative for minor part of the building occupants.

In this last paragraph the building designs that can provide satisfying summer comfort without active cooling are identified. The higher established criterion for robustness for building use and occupant behavior is applied, i.e. only buildings where 75% of the behavioral profiles result in less than 100 weighted exceeding hours annually are retained.

Some conclusions can be drawn from Fig. 9. Firstly, respective comparison between the graphs for U-value of the opaque façade of 0.6 W/m^{2}K and 0.15 W/m^{2}K, and the graphs for glazing 5 and 6 -with comparable g-values but different U-values, see Table 1- learns that thermal insulation of the envelope has a negligible influence on the performance of the building in summer conditions.

Secondly, it is possible to achieve good summer comfort without active cooling in a building without solar shading, but only for small glazing-to-wall-ratios (lower than 40%) and glazing with low g-values (lower than 0.40).

Finally, unless for very large glazing-to-wall-ratios (higher than 60%), it is possible to design the individual office cells of an office building in a moderate climate without active cooling, if external solar shading is applied and window-opening by the occupant as an adaptive measure is allowed.

Conclusions

In this study, an attempt has been made to define building design variables for a medium-sized office building with individual office cells in order to provide sufficient summer comfort without active cooling in a moderate climate.

Firstly, an approach to take realistic window-opening behavior into account was proposed based on observational data in literature. A stochastic model, which explicitly includes the adaptive principle, has been defined for an active and a passive user, representing the variability between individuals.

The uncertainty in summer comfort due to the building use and occupant behavior was then assessed, by applying different levels of internal gains, occupancy variability, varying lighting control, *active* and *passive* window users and different window opening angles. The sensitivity of the simulated summer comfort proved to be substantial. A criterion for robustness of the building design for behavioral aspects was deduced from this analysis. The uncertainty on the induced air flow through window-opening was not taken into account.

Finally, it was shown using the proposed criterion that for office cells with external shading where window-opening is allowed, satisfying summer comfort can be guaranteed independent of the building use if the glazing-to-wall-ratio does not exceed 60%. It is also possible without external shading device, but only for small glazing-to-wall-ratios and low g-value glazing.

Acknowledgments

This research was funded by the Institute for Promotion of Innovation trough Science and Technology in Flanders (IWT-Vlaanderen). This support is gratefully acknowledged.

References

1. Belgian Building Research Institute, *Kantoor2000: Study of Energy Use and Indoor Climate in Office Buildings (In Dutch)*, BBRI, 2001.

2. Gratia, E., Bruyere, I., & De Herde, A., "How to use natural ventilation to cool narrow office buildings," Vol. 39, No. 10, *Building and Environment*, 2004, pp. 1157~1170.

3. Yun, G., Tuohy, P., & Steemers, K., "Thermal performance of a naturally ventilated building using a combined algorithm of probabilistic occupant behaviour and deterministic heat and mass balance models," Vol. 41, No. 5, *Energy and Buildings*, 2009, pp. 489~499.

4. Voss, K., Herkel, S., Pfafferott, J., Lohnert, G., & Wagner, A., "Energy efficient office buildings with passive cooling – Results and experiences from a research and demonstration programme," Vol. 81, No. 3, *Solar Energy*, 2007, pp. 424~434.

5. Emmerich, S., & Crum, J., *Simulated performance of natural and hybrid ventilation systems in an office building*, Gaithersburg: Building and Fire Research Laboratory, 2005.

6. Holmes, M., & Hacker, J., "Climate change, thermal comfort and energy: Meeting the design challenges of the 21st century," Vol. 39, No. 7, *Energy and Buildings*, 2007, pp. 802~814.

7. Warren, P., & Parkins, L., "Window-opening behavior in office buildings," Vol. 5, No. 3, *Building Services Engineering Research and Technology*, 1984, pp. 89~101.

8. Fritsch, R., Kohler, A., Nygard-Ferguson, M., & Scartezzini, J., "A stochastic model of user behaviour regarding ventilation," Vol. 25, No. 2, *Building and Environment*, 1990, pp. 173~181.

9. Herkel, S., Knapp, U., & Pfafferott, J., "Towards a model of user behaviour regarding the manual control of windows in office buildings," Vol. 43, No. 4, *Building and Environment*, 2008, pp. 588~600.

10. Rijal, H., Tuohy, P., Humphreys, M., Nicol, J., Samuel, A., & Clarke, J., "Using results from field surveys to predict the effect of open windows on thermal comfort and energy use in buildings," Vol. 39, No. 7, *Energy and Buildings*, 2007, pp. 823~836.

11. Yun, G., & Steemers, K., "Time-dependent occupant behaviour models of window control in summer," Vol. 43, No. 9, *Building and Environment*, 2008, pp. 1471~1482.

12. Haldi, F., & Robinson, D., "Interactions with window openings by office occupants," Vol. 44, No. 12, *Building and Environment*, 2009, pp. 2378~2395.

13. American Society of Heating, Refrigerating and Air-Conditioning Engineers, *ASHRAE Fundamentals*, ASHRAE, 2009.

14. Reinhart, C., "Lightswitch-2002: a model for manual and automated control of electric lighting and blinds," Vol. 77, No. 1, *Solar Energy*, 2004, pp. 121~126.

15. Haldi, F., *Towards a unified model of occupant's behaviour and comfort for building energy simulation*, Ph.D. thesis, Lausanne, 2010.

16. Wang, D., Federspiel, C., & Rubinstein, F., "Modeling occupancy in single person offices," Vol. 37, No. 2, *Energy and Buildings*, 2005, pp. 121~126.

17. Page, J., Robinson, D., Morel, N., & Scartezzini, J., "A generalized stochastic model for the simulation of occupant presence," Vol. 40, No. 2, *Energy and Buildings*, 2008, pp. 83~98.

18. Newsham, G., Mahdavi, A., & Beausoleil-Morrison, I., “Lightswitch: a stochastic model for predicting office lighting energy consumption,” 3th European Conference on Energy Efficient Lighting, Newcastle-upon-Thyne, UK, 1995, pp. 59~66.

19. Rubinstein, F., Colak, N., Jennings, J., & Niels, D., “Analyzing occupancy profiles from a lighting controls field study,” CIE Conference, San Diego, US, 2003.

20. Klein, S., Duffie, J., Mitchell, J., Kummer, J., Thornton, J., Bradley, D., et al., *Trnsys manual, a transient simulation program*, Madison: Solar Engineering Laboratory, University of Wisconsin-Madison, 1996.

21. Reinhart, C., *Tutorial on the use of Daysim simulations for sustainable design*, 2006.

22. KUL-BWF, UG-VAS, KUL-TME, KUL-ELECTA, *IWT GBOU EL2EP - Residential buildings: a methodology for the overall optimization of residential buildings with a very low energy consumption and environmental pollution (in Dutch)*, 2006.

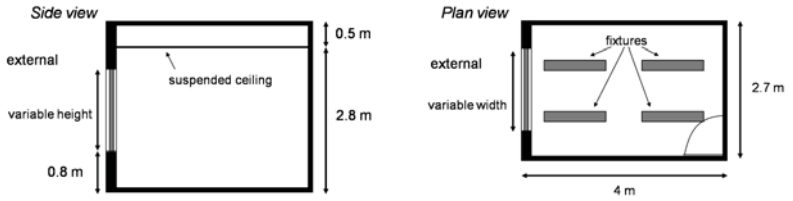


Fig. 1 Office geometry

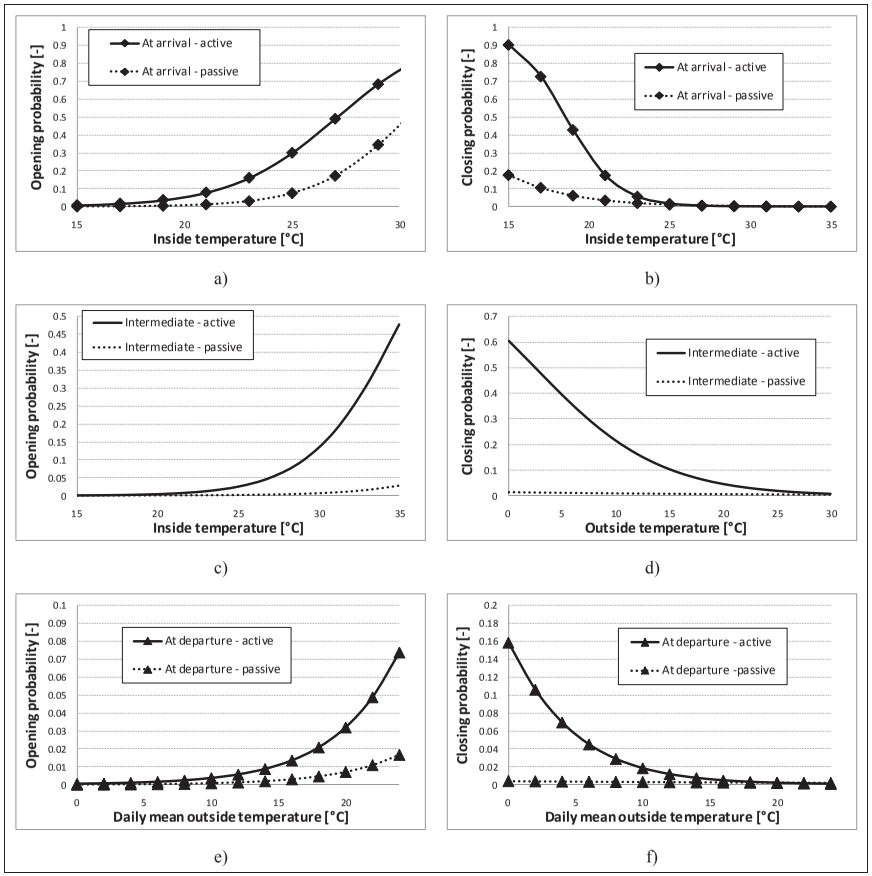


Fig. 2 Probabilities of transition as a function of the main physical stimulus for different occupancy states for active and passive users. a) no rain, previous absence over 8h and

outdoor temperature 15°C b) outdoor temperature 20°C c) no rain, ongoing presence of 2h and outdoor temperature 15°C d) indoor temperature 20°C e) following absence over 8h f) following absence under 8h and indoor temperature 20°C

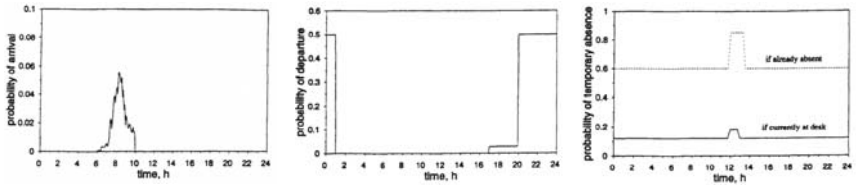


Fig. 3 Probabilities of transition, from [18]

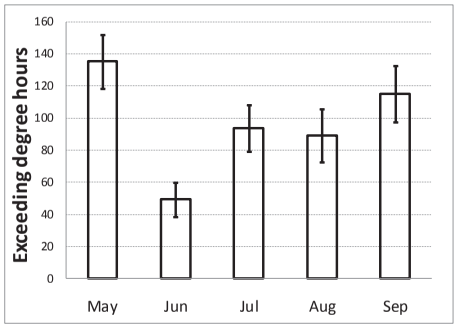


Fig. 4 Average and standard deviations of monthly weighted exceeding hours for 100 runs of the same building with the stochastic behavioral model

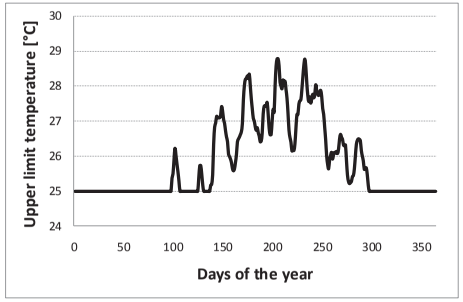


Fig. 5 Upper limit temperature for the climate of Uccle, for class II according to EN15251

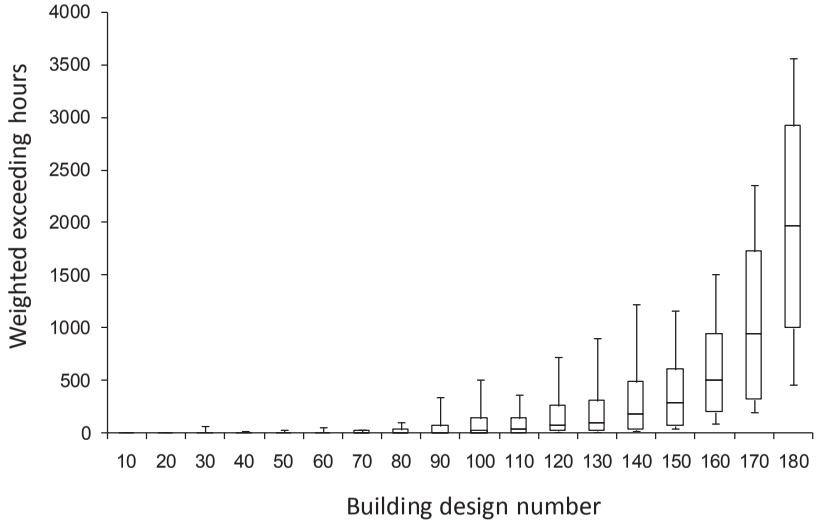


Fig. 6 Uncertainty on simulated summer comfort due to behavioral patterns for a selection of 18 over the whole range of designs

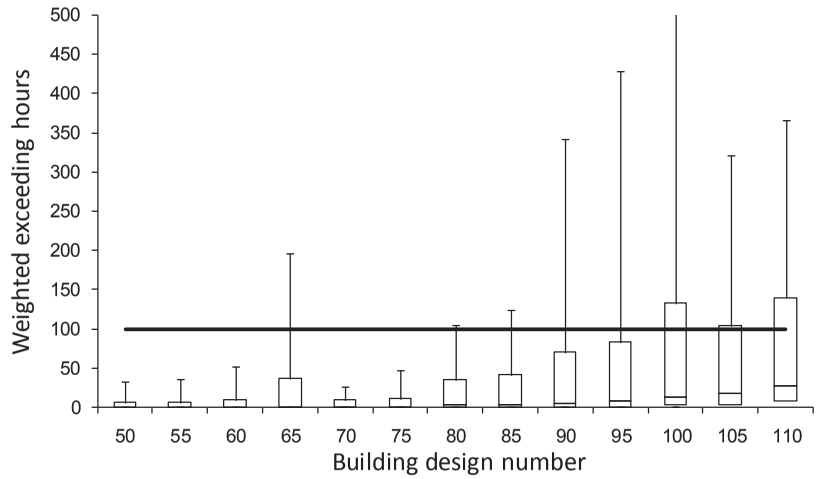


Fig. 7 Uncertainty on simulated summer comfort due to behavioral patterns for a selection of 13 building designs

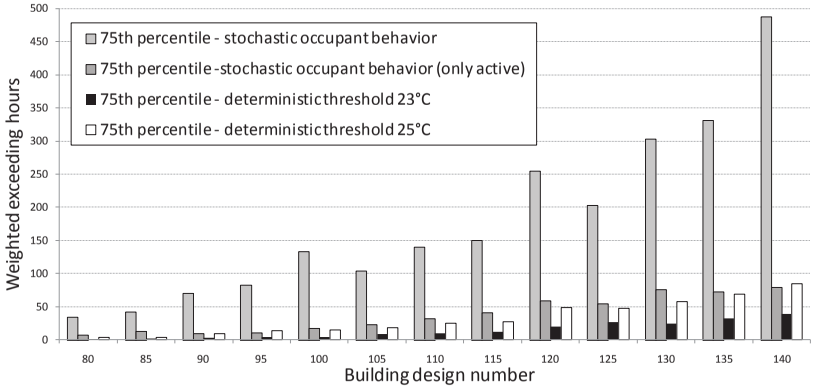


Fig. 8 Sensitivity of the simulated summer comfort to applied window-opening pattern

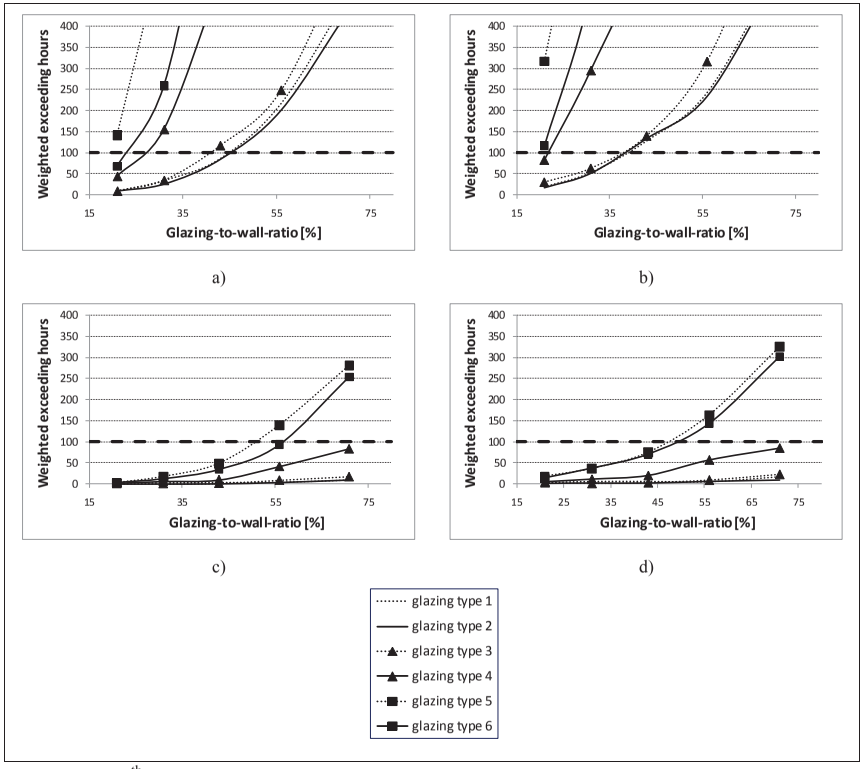


Fig. 9 75th percentile of simulated summer comfort for varying glazing-to-wall-ratio and glazing type. a) No shading device, U_{opaque} = 0.6 W/m^{2}K b) No shading device, U_{opaque} = 0.2 W/m^{2}K c) External horizontal slats, U_{opaque} = 0.6 W/m^{2}K d) External horizontal slats, U_{opaque} = 0.2 W/m^{2}K

Table 1 Various glazing types

Nr.	Visual Transmittance [-]	g-value [-]	U-value [W/m^{2}K]
1	0.36	0.26	1.1
2	0.48	0.29	1.1
3	0.61	0.35	1.1
4	0.59	0.44	1.1
5	0.77	0.59	1.1
6	0.72	0.48	0.8

Influence of natural ventilation usage on cooling energy consumption and cooling capacity of an air conditioner

Hiromi HABARA[1], Shigeki NISHIZAWA[2], Hisashi MIURA[2],
Akinori HOSOI[3], and Takao SAWACHI[4]

[1] Hiroshima Institute of Technology, Hiroshima, Japan
[2] National Inst. of Land and Infrastructure Management, MLIT, Ibaraki, Japan
[3] University of Kumamoto Prefecture, Kumamoto, Japan
[4] Building Research Institute, Ibaraki, Japan

Abstract

In Japan, natural ventilation through large openings has been used for cooling in summer and medium season. However, air conditioner has become popular recently, because it is hot and humid in summer in most parts of Japan. It causes cooling energy consumption to rise continuously. Nowadays, as global warming has become a serious problem, natural ventilation has been considered as a key method for cooling energy conservation. However, there is insufficient knowledge of natural ventilation effectiveness on cooling energy conservation quantitatively. Therefore, in order to verify the effectiveness of natural ventilation through large openings, we have been conducting experiments by automatically simulating various occupants' behaviors, namely cooking, lighting, usage of electric appliances and domestic hot water, operation of air conditioners, windows and curtain opening/closing. In this paper, we have performed experiments with additional several patterns, which have different thermal conditions for on operation of air conditioners, to our previous paper. And based on the experimental results, we analyzed the heat discharge by natural ventilation and the cooling capacity of air conditioner. The result suggests that though natural ventilation sometimes brings the gain of sensible and latent heat, it is not so much as to increase the daily cooling capacity of air conditioner.

Keywords: Natural ventilation, Air conditioner, Residential house

Introduction

In Japan, natural ventilation through large openings has been used for cooling in summer and medium season. However, air conditioner has become popular recently, because it is hot and humid in summer in most parts of Japan. It causes cooling energy consumption to rise continuously. Nowadays, as global warming has become a serious problem, natural ventilation has been considered as a key method for cooling energy conservation. However, there is insufficient knowledge of natural ventilation effectiveness on cooling energy conservation quantitatively.

Therefore, in order to verify the effectiveness of natural ventilation through large openings, we have been conducting experiments by automatically simulating various occupants' behaviors, namely cooking, lighting, usage of electric appliances and domestic hot water, operation of air conditioners, windows and curtain opening/closing. In this paper, we have performed experiments with additional several patterns, which have different thermal conditions for on operation of air conditioners, to our previous paper (H. Habara, 2009). And based on the experimental results, we analyzed the heat discharge by natural ventilation and the cooling capacity of air conditioner.

Experimental Dowelling

The experimental dwelling is a west unit on the third floor of RC construction multi-family house building (T. Sawachi, 2007). Fig. 1 shows the external view of the house building and the internal view of living room. The house building has been built on an open site, and the surroundings have little influence to obstruct the outside wind. The dwelling has 4 occupied rooms (e.g. Living room, Japanese-style room, Child room 1 and Child room 2). Each occupied room has one air conditioner, one inner opening and one window. Table 1 shows the volume of room and the size of opening. These air conditioners and openings except the inner opening of child room 2 are operated automatically by the devises shown in Fig. 2 and Fig. 3. Air conditioners are operated by the infrared signal from the IR adapter which is put on the receiver directly. On the other hand, windows are operated by taking out or up wire with motor on the topside of them. Inner openings are operated by applying the device on the market.

On the assumption that the family is consisted of a couple and their 2 children, we set the 3 patterns of occupants' life-style; for weekday, for holiday that the family stays home and for holiday that the family stays out (T. Sawachi, 2007). In this paper, we analyzed data which was measured in the experiments which were performed with schedule for weekday.

Experimental Condition

Experiments have been conducted with three patterns of thermal control shown in Table 2 during July – October in 2007-2009. The name of pattern is formed from thermal control pattern (CV, AC), Ta and Tb. CV is the pattern that occupants control their thermal environment with cross ventilation between living room and child room 1 in the day time and between Japanese-style room and child room 1 in the night time. On the other hand, AC is the pattern that occupants control their thermal environment with only air conditioner. Ta is the upper limit of room temperature without using air conditioner, and Tb is the preset temperature of air conditioner.

Occupants' thermal control in each room is judged from occupation and room temperature at 900 mm height above the floor every one hour while sleeping and every five minutes while awaking. Table 3 shows the outline of occupants' behavior and decision of operation. First, occupants' thermal control behavior is decided with Table 4. And then, according to the behavior, openings and air conditioners are operated by Table 5. Fig. 4 shows the occupation of each room which is scheduled at 5 minute intervals.

In CV pattern, thermal control behavior is decided by Table 4-(a). According to thermal control behavior decided by Table 4-(a), openings and air conditioners are operated by Table 5-(a), Table 5-(b), Table 5-(c) and Table 5-(d).

In AC pattern, thermal control behavior was decided by Table 4-(b). According to thermal control behavior decided by Table 5-(b), openings and air conditioners are operated by Table 5-(d)

Measurement Method

The measurement items relate with outdoor environment, indoor environment, neighborhood environment, air conditioner and air flow rate. Table 5 shows the summary of measurement items. Fig. 5 shows the measurement points of indoor environment. The items on outdoor environment are temperature, relative humidity, solar radiation, wind velocity, wind direction and rain fall. The items on indoor environment are air temperature, relative humidity, glove temperature, wall surface temperature and wind velocity.

The cooling capacity is measured with temperature and humidity of discharge and intake airflow and rotation frequency of fun. The discharge airflow is estimated on the relationships between rotation frequency of fun and discharge airflow which is obtained in the pre-experiment. And then, the cooling capacity is calculated by multiplying the discharge airflow by the enthalpy difference between discharge and intake air.

The airflow rate is calculated by the product of average air flow velocity though window and area of window.

Results and Discussion

Fig. 6 and Fig. 7 describe the daily variation of heat capacity of air conditioner and heat discharge by natural ventilation with average data in 5 minutes, which was measured in CV 26_26 pattern. During daytime, when cross ventilation was used, the airflow rate was 6 – 15 ACH (300 – 800 m^3/h) and the sensible heat discharge by cross ventilation was 200 – 400 W. This is enough to discharge almost inner heat generation. On the other hand, though the latent heat was gained by around 200 W at the beginning of cross ventilation, it was almost always discharged. During evening and night time, when air conditioner was used, the sensible heat capacity of air conditioner was 400 – 1200 W and the latent heat capacity of air conditioner was 200 – 400 W, which exceeded the inner heat and moisture generation.

Fig. 8, Fig. 9 and Fig. 10 show the relationship of daily average temperature and daily heat capacity / discharge. Fig. 11 shows the relationship of daily average temperature and daily cooling hour. Fig. 12 shows the relationship of daily average temperature and daily electric power consumption. In CV 28_26 pattern, both sensible and latent heat discharge by natural ventilation increased as outside temperature got lower. When outside temperature was below 24 ^oC, total heat discharge was around 10 – 20 MJ, which was as much as the heat capacity of air conditioner. As the sum of heat discharge by natural ventilation and heat capacity of air conditioner in CV 26_26 pattern is almost equal to heat capacity of air conditioner in AC

28_26 pattern, natural ventilation took charge of heat and moisture removal in CV 28_26 pattern. Meanwhile, when outside temperature was above 24 ^{o}C, though natural ventilation didn't contribute to removal of heat and moisture generation, the heat capacity of air conditioner in CV 28_26 pattern was higher than that in CA 26_26 pattern. It is because the daily total cooling hour was reduced, as the upper limit of room temperature without using air conditioner (Ta) in CV 28_26 pattern is 2 degree lower than that in AC 26_26 pattern. According to the decrease of cooling hour, the daily total electric power consumption declined in CV 28_26 pattern.

Through the experiment period, natural ventilation sometimes brought the gain of sensible and latent heat. It was at most 5 MJ, which didn't increase the cooling heat capacity of air conditioner.

Conclusions

In this paper, we discussed the influence of natural ventilation on cooling energy consumption and cooling capacity of air conditioner, based on the experimental result which was performed with three pattern of thermal control behavior. The results suggest that though natural ventilation sometimes brings the gain of sensible and latent heat, it is not so much as to increase the daily total cooling capacity of air conditioner. The heat discharge by natural ventilation can be effective on cooling energy conservation in hot and humid areas. In the future study, in order to apply the technique of cooling energy conservation with heat discharge by natural ventilation, we will research the effects of natural ventilation on cooling capacity of air conditioner in hot and humid condition.

References

1. H. Habara, et al., "Verification of the Effect of Cross Ventilation on Energy Conservation by Simulating Occupant Behavior," Vol. 8, No. 3, *The International Journal of Ventilation*, 2009, pp.201~206.
2. T. Sawachi, et al., "Proposal of the Experimental Method with Lifestyle Simulating Method Aimed at Validating Energy Performance of Promising Measures: Study on the Experimental Validation of Energy Conservation Measures for Residential Buildings Part 1," Journal of environmental engineering, *AIJ*, 621, 2007, pp.69~76.



Fig. 1 External view of the house building and internal view of the living room

Table 1 Volume of rooms and size of opening

	Volume of room [m^3]	Window size [m^2]	Inner opening size [m^2]
Living room	54.0	1.1	1.7
Japanease-style room	22.3	1.1	2.4
Child room 1	23.2	0.5	1.6
Child room 2	18.0	0.4	1.6



Fig. 2 Devise for operation of air conditioner



Fig. 3 Devise for operation of opening

Table 2 Experimental pattern

Thermal control pattern	Upper limit of room temperature without air conditioner (Ta)	Preset temperature of air conditioner (Tb)
CV28_26	28 °C	26 °C
AC26_26	26 °C	26 °C
AC28_26	28 °C	26 °C

Fig.3 Outline of operation logic

Thermal control pattern	Thermal control behavior	Operatin of air conditioner, window and indoor opening			
	Each room	Living room	Japanese-style room	Child room 1	Child room 2
CV	Table 4-(a)	Table 5-(a)	Table 5-(b)	Table 5-(C)	Table 5-(d)
AC	Table 4-(b)	Table 5-(d)			

Table 4 Decision of thermal control behavior

(a) CV

Requirement				Now thremal control behavior	Notes
Now schedule of occupation	Previous thermal control behavior	Now environment		Each room	
		Outside velocity	Room temperature		
Awake or Sleep	N	10m/s ≤	Tb ≤	A	Decide the behavior at the beginning of occupation
			< Tb	C	
		< 10m/s	-	V	
	V	10m/s ≤	Tb ≤	A	Decide the behavior except first 5 minites after the beginning of occupation
			< Tb	C	
		< 10m/s	Ta °C ≤	A	
			20 °C ≤ and < Ta	V	
			< 20 °C	C	
	C	-	Tb ≤	A	
			< Tb	C	
	A	-	-	A	
On occupancy	-	-	-	N	

A: Air conditioner, C: Close window without air conditioner, V: Cross ventilation or single-sided ventilation, N: No occupan

(b) AC

Requirement			Now thremal control behaviour
Now schedule of occupation	Precious thermal control behaviour	Now environment	Each room
		Room temperature	
Awake or Sleep	C or N	Ta °C ≤	A
		< Ta °C	C
	A	-	A
Nn occupancy	-	-	N

Table 5 Decision of operation for openings and air conditioners

(a) Living room in CV

Now thremal control behavior		Operation		
Living room	Japanese-style room	Living room		
		Air conditioner	Window	Inner opening
A	-	on	close	close
V	-	off	open	open
C or N	C	off	close	open
C or N	Except V	off	close	close

(b) Japanese-style room in CV

Now thremal control behavior		Operation		
Japanese-style room	Living room	Japanese-style room		
		Air conditioner	Window	Inner opening
A	-	on	close	close
V	Except A	off	open	open
V	A	off	open	close
C or N	-	off	close	close

(c) Child room 1 in CV

Now thremal control behavior			Operation		
Child room 1	Living room	Japanese-style room	Child room 1		
			Air conditioner	Window	Inner opening
A	-	-	on	close	close
V	-	-	off	open	open
C	-	-	off	close	close
N	A	-	off	close	close
N	V	-	off	open	open
N	C or N	V	off	open	open
N	C or N	Except V	off	close	close

(d) Child room 2 in CV and each room in AC

Now thremal control behavior	Operation		
Each room	Each room		
	Air conditioner	Window	Inner opening
A	on	close	close
V	off	open	close
C or N	off	close	close

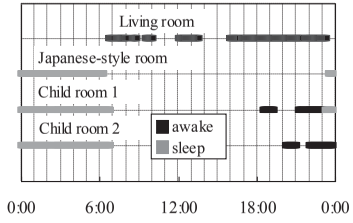


Fig.4 Schedule of occupation in each room

Table 5 Measurement items

Item		Instrument	Number of point	Interval
Indoor environment	Air temperature	Thermal couple	5 per room	5 min
	Relative humidity	Electric hygrometer	1 per room	5 min
	Glove temperature	Thermal couple	1 per room	5 min
	Wall surface temperature	Thermal couple	6 per room	5 min
	Wind velocity	Hot wire anemometer	1 per room	5 min
Outdoor environment	Temperature	Thermister	1 per room	5 min
	Relative humidity	Resistance hygrometer	1 per room	5 min
	Solar radiation	Pyranometer	1 per room	5 sec
	Wind direction	Ultrasonic anemometer	1 per room	5 sec
	Wind velocity	Ultrasonic anemometer	1 per room	5 sec
	Rain fall	Pluviometer	1 per room	5 min
Coolin capacity of air conditioner	Electric power consumption	Clump sensor	1 per appliance	1 min
	Discharge air temperature	Thermal couple	1 per appliance	5 sec
	Discharge air humidity	Electric hygrometer	1 per appliance	5 sec
	Intake air temperature	Thermal couple	1 per appliance	5 sec
	Intake air humidity	Electric hygrometer	1 per appliance	5 sec
	Rotation frequency of fan	Rotation frequency meter	1 per appliance	5 sec
Air flow rate	Air flow velocity	Ultrasonic anemometer	5 per room	0.1 sec

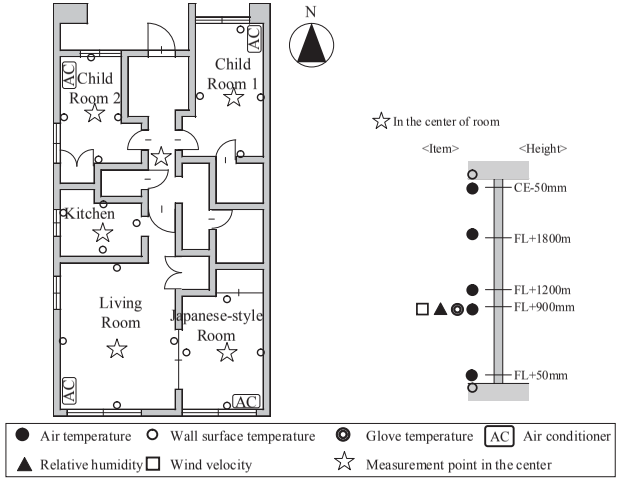


Fig. 5 Measurement points of indoor environment

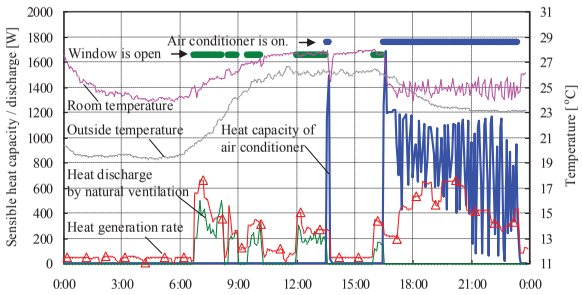


Fig. 6 Daily variation of sensible heat capacity / discharge (19 Sep. 2007)

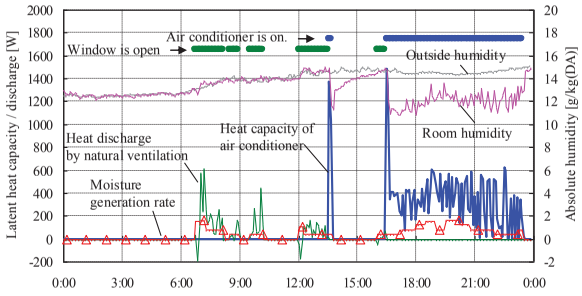


Fig. 7 Daily variation of latent heat capacity / discharge (19 Sep. 2007)

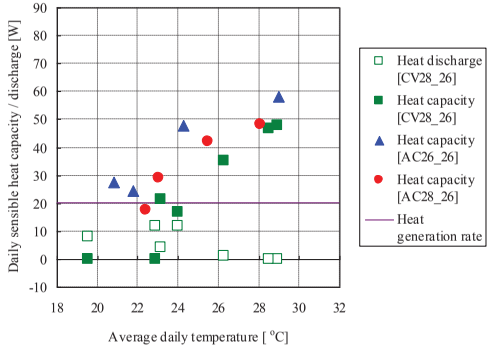


Fig. 8 Daily sensible heat capacity / discharge

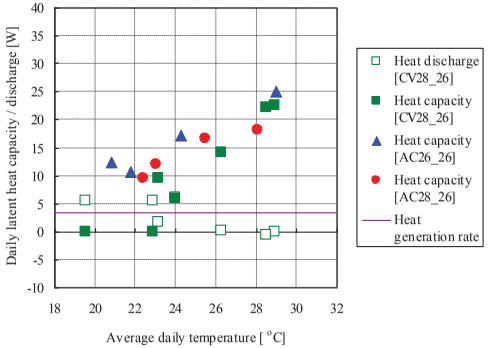


Fig. 9 Daily latent heat capacity / discharge

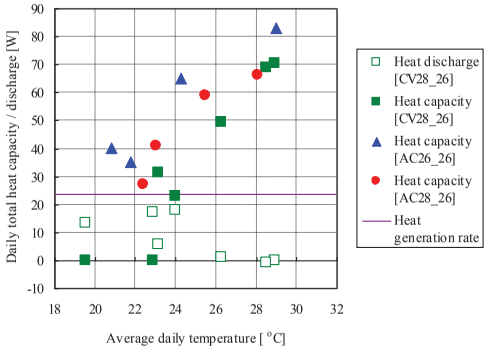


Fig. 10 Daily total heat capacity / discharge

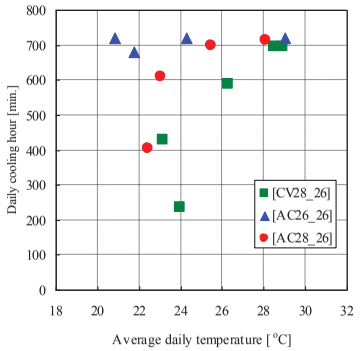


Fig. 11 Daily cooling hour

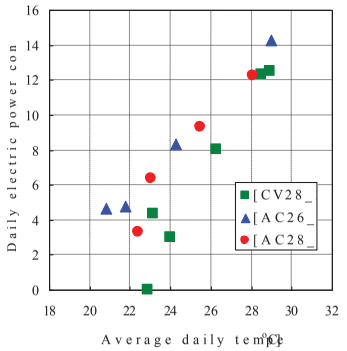


Fig. 12 Daily electric power consumption

IMPLEMENTATION OF MEASUREMENT AND QUALITY FRAMEWORKS IN THE FRENCH REGULATION FOR ACHIEVING AIRTIGHT ENVELOPES

F.R. Carrié, S. Charrier, V. Leprince

Centre d'Etudes Techniques de l'Equipement de Lyon
46 rue Saint Théobald
F – 38081 L'Isle d'Abeau Cedex, France

ABSTRACT

It is foreseen that the 2012 version of the French regulation will include a minimum requirement for the envelope airtightness of residential buildings, with two options to justify its treatment: a) measurement at commissioning or b) adoption of an approved quality management approach. This paper describes the qualification process for authorizing technicians to conduct airtightness measurement when the result is to be used in the EP-calculation method. It also discusses the requirements set for approved quality management approaches. These processes have started in 2008 which allows us to analyze the impacts of the measures taken on the supporting staff and on the market. Our analyses underline the importance of the qualification process to ensure homogenous measurement practice between technicians. They also show the limits of the controls that can be implemented if the process is not appropriately sized to absorb a large number of applications. Regarding the approved quality management approaches, their impact is increasing rapidly with builders engaged in that process who produce hundreds to several thousands of homes a year. Other market players also explore this option, namely industries and contractors.

KEYWORDS

air infiltration, envelope, ductwork, leakage, energy use, low-energy buildings

INTRODUCTION

The objective of the revision of the French energy performance regulation is to generalize low-energy buildings. The threshold is set to 50 kWh of primary energy per m^2 per year for residences, with some modulation depending on climate zone and altitude; this number includes the primary energy use for heating, cooling, domestic hot water, auxiliary equipment, and lighting. Given the severe impact of envelope leakage in such low energy buildings, a minimum requirement will very likely be set for the envelope airtightness of residential buildings in the 2012 energy performance regulation. Two options are foreseen to comply with this minimum requirement : a) measurement at commissioning or b) adoption of an approved quality management approach. The first option raises the question of the quality of the measurements to ensure homogenous measurement practice between technicians, and thereby avoid perverse effects that could put discredit to the whole framework and distort competition. The second implies the definition of a legal framework that describes the requirements for approved quality management approaches. This paper discusses successively the approach envisaged to answer those two problems based on the lessons learnt from experience with the previous framework.

QUALITY FRAMEWORK FOR MEASURERS

Although there exists a European and an International Standard (EN 13829 and ISO 9972) on the measurement of envelope airtightness, there remains unanswered questions when the result is to be used as an input in an energy performance calculation method. One key problem lies in the building preparation, i.e., the openings that have to be sealed or closed during the measurement. One example often cited is the case of a biomass boiler with a combustion air intake in the living space, for which it could be interpreted that method A requires that the intake remains in its normal condition of use, although it may make sense to seal it if the calculation method appropriately takes into account the energy impact of the additional air drawn into the house.

This is the reason why the BBC-Effinergie label defines in more detail the openings that can and cannot be sealed or closed during the test (Table 1). The basic rule is that the building envelope must represent its condition during the season in which the heating or cooling systems are used; however, openings whose contributions are taken into account in the energy calculation method are sealed. This rule is now integrated in an application guide for EN 13829 which has been released in February 2010 (GA P 50-784).

Another major issue lies in the competence of the measurer. Evidence shows that there can be serious misinterpretations of the measurement protocol and analysis that can of course be intentional but that can also be done in good faith, simply because of a lack of basic knowledge on the energy performance regulation, HVAC systems, or airflow and pressure measurement techniques. This can lead to serious errors in the estimations of the derived quantities that are used in the calculation method. For this, the ministry has decided to require that the measurers be authorized to perform such measurement. The authorization is delivered according to a 3-step approach :

The candidate must attend a training which is approved by the ministry based on a referential. Three trainings bodies are now offering these kinds of trainings.
The candidate must succeed to a theoretical and a practical examination. The theoretical examination is based on a multiple-choice questionnaire. The practical part consists in the examination of a test report by the training body. The training body is given a grid to help this evaluation process.
The candidate must submit 5 reports to a commission in charge of advising the ministry to deliver authorizations. The commission is made of about 20 anonymous experts in the field who evaluate the reports. The experts can ask for complements if the mistakes are not fundamental or if clarification is needed. In this case, the authorization is discussed at the following meeting based on the new materials provided by the candidate. An application cannot be evaluated more than 3 times; over 3 trials, the candidate must submit a new application.

As of April 2010, 153 persons have applied for an authorization; 53 have been authorized. Applicants usually have to go through 2 meetings of the commission to obtain their authorization. The mean elapsed time between the application and the authorization is about 5.5 months.

Because of the large number of applications received in the past months (over 60 between January and June 2010), and because the foreseen large number of applications as the 2012 regulation will require this authorization for all measurements if it is used as proof of compliance to the EP-regulation, we are working on a new organisation to be able to deal with over 1000 applications a year. The basic idea is to delegate the process to a private body who will organize the examination of the reports by pool of experts approved by the ministry.

We have also defined a framework to monitor the activity of the authorized measurers. For this, the measurers must file a database for each measurement they perform. This record is a simple table in a spreadsheet, with pre-defined fields. Each measurer must send this record along with his first application; he must also send it every

year to have his authorization prolonged. An interesting project called Web@set is underway to explore the possibility to build a national database with information provided on-line by the measurers as they prepare their reports and who would have access through to other services through the Website, e.g., statistical analyses.

This overall framework is still under construction, but our feeling is that it has greatly helped the measurers' community keep a positive image. The potential discredit that could fall on a new job and a subject which remains controversial among building professionals has been avoided so far.

	Energy Performance Method (French regulation)	**Method A**	**Method B**
Windows, doors, trapdoors	Close	Close	Close
Closets and toilets doors	Close (others doors are left opened)	Close (others doors are left opened)	Close (others doors are left opened)
Mechanical ventilation or air conditioning installations	Seal	Seal	Seal
Openings of natural ventilation without closing device	Seal	Open (1)	Seal
Openings of natural ventilation with closing device	Not allowed by hygienic regulation	Close	Seal
Combustion appliances without closing device	Open or Seal (2)	Open	Seal
Combustion appliances with closing device	Close or Seal (2)	Close	Seal
Water traps	Fill or Seal	Fill or Seal	Fill or Seal
Other voluntary openings without closing device	Open	Open	Seal
Other voluntary openings with closing device	Close	Close	Close

Table 1 : Building preparation. State of openings depending on the purpose of the measurement : method A, method B, or method for the French energy performance calculation. Table inspired from GA P 50-784. (1) If automatically-regulating openings are present, it is likely that the regression will not be satisfactory. (2) Seal if airflow rate impact is taken into account in the energy calculation method.

APPROVED QUALITY MANAGEMENT APPROACHES

The 2005 version of the regulation has introduced the possibility to claim for a better value than the default airtightness value in the EP-calculation, without performing a test, provided that an approved quality management approach be applied.

The basic requirements for the quality management approach to be approved are :
- to identify "who-does-what" and when;
- to trace each step of the approach;
- to prove that the approach is effective based on measurements on a sample;
- to propose a scheme to ensure that the approach will remain effective with time, based on measurements on a sample.

We were originally sceptical about the viability of this option. However, our confidence is growing although this framework needs a careful independent evaluation. This is due to the convincing results obtained by several bodies, especially builders of single-family houses advised by a few consultant firms well-experienced with quality management approaches. Their results consistently show values well-below the relevant limits, although such levels are usually attained in 20 to 30% of houses (Figure 1). These results are based on measurements usually performed by "authorized measurers" in ISO 9001 bodies. Note however that the measurers are not necessarily independent of the contractor.

As of June 2010, 20 quality management approaches have been submitted for approval to the ministry, 11 have been approved, 5 have been approved pending checks (Table 2). Figure 2 shows one overall scheme inspired from an approved approach by a manufacturer of autoclave aerated concrete (AAC, Xella Thermopierre). In sum, this synthesis shows the wide scope of potential applicants for such approach, with a production ranging from about 50 dwellings a year to over 5000 between the applicants, and its compatibility with the status of builder or industry.

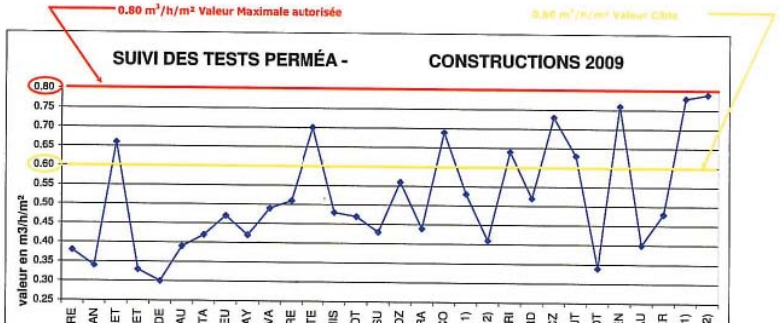


Figure 1 : Excerpt from a monitoring report of a single-family house builder showing air tightness values consistently below the limit of 0.8 $m^3/h/m^2$ (red line). This builder aims to attain 0.6 $m^3/h/m^2$ on a regular basis (yellow line).

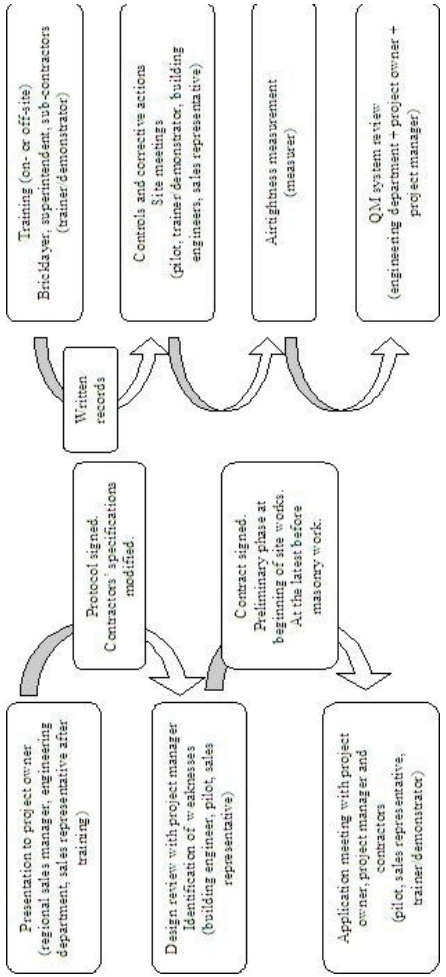


Figure 2 : Overall scheme for approved quality management approach by a manufacturer of AAC. Pilot is site coordinator of QM approach. Translated with permission from Xella Thermopierre.

Application date	Type of applicant	Type of buildings	Production (per year)	Status	Approval date
18/06/06	Federation of manufacturers	Single-family		Rejected	
19/10/07	Builder	Single-family	100	Approved	20/10/08
06/11/07	Builder	Single-family	200	Approved	25/11/08
06/11/07	Builder	Single-family	200	Approved	25/11/08
01/11/08	Manufacturer of AAC	Single-family Multi-family	40 projects (2010) representing 800 dwellings	Approved	26/10/09
24/11/08	Builder	Single-family		Approved	24/04/09
24/02/09	Builder	Single-family	250	Approved pending checks	
20/05/09	Builder	Single-family		Approved	05/08/09
25/05/09	Builder	Single-family	300	Approved	05/08/09
25/05/09	Builder	Single-family		Approved	05/08/09
29/06/09	Builder	Single-family		Approved pending checks	
09/09/09	Builder	Single-family		Approved	19/04/10
09/09/09	Builder	Single-family	50	Approved pending checks	
09/09/09	Builder	Single-family	200	Approved	19/04/10
05/11/09	Builder	Single-family	5000	Approved	19/04/10
09/11/09	Builder	Single-family		In process	
08/03/10	Builder	Single-family	250	Rejected	
08/03/10	Builder	Single-family	900	Approved pending checks	
08/03/10	Builder	Single-family		Rejected	
08/03/10	Builder	Single-family	1500	Approved pending checks	

Table 2 : Overview of quality management approach applications as of June 2010.

CONCLUSION AND PERSPECTIVES

Generalizing airtight constructions is challenging, however, it is absolutely necessary to address this issue given the objective to generalize near-zero energy buildings in 2020. The problem has been tackled in France through several channels, among which the definition of quality frameworks for the measurement and achievement of airtight envelopes. The lessons learnt from these frameworks, operational since the beginning of 2008, are quite interesting. First, the examination of the measurers' reports within the authorization process as well as the feed-back from training shows that there remains an important need for training to ensure homogeneous practice. Insufficient training for measurers could severely distort competition. Second, major market players pay a great deal of attention to quality management approaches. The wide scope of applicants, from small builders to big ones or manufacturers, is quite encouraging, so are the results presented in the yearly reports.

Based on this positive experience, and because the treatment of envelope airtightness will be mandatory in 2012 revision of the energy performance regulation, the ministry has decided to enforce these frameworks within this revision. Therefore, measurements will have to be performed by authorized technicians to be valid to check

compliance with the minimum requirement or with the value used in the energy performance calculation. The use of approved quality management approaches will remain a possible option to prove compliance with the airtightness minimum requirement without a systematic test. With minor changes, the frameworks described in this paper will be re-conducted.

ACKNOWLEDGEMENTS

The contribution of CETE de Lyon to the implementation of these quality frameworks is funded by the ministry for ecology, energy, sustainable development, and sea (MEEDDM).
The sole responsibility for the content of this publication lies with the authors. It does not necessarily reflect the opinion of the Ministry.

REFERENCES

EN 13829 (2000). Thermal performance of buildings - Determination of air permeability of buildings - Fan pressurization method (ISO 9972:1996, modified).
ISO 9972 (2006). Thermal performance of buildings - Determination of air permeability of buildings - Fan pressurization method. Second edition 2006-05-01.
AFNOR. GA P 50-784 (2010). Performance thermique des bâtiments. Guide d'application de la norme NF EN 13829 : 2001. Février 2010.

Ventilation and RH control in museum showcases

Marco PERINO[1] and Chiara BONVICINI[2]

[1] DENER, Politecnico di Torino - Italy
[2] ONLECO S.r.l - Italy

Abstract

Museum showcases represent a peculiar confined space were ventilation and indoor climate conditions play an important role. Conservation of the works of arts, in fact, requires a control of the environmental parameters, with a tolerance usually far tighter than that required for assuring the comfort of people.

A number of laboratory measurements have been performed on small experimental showcases to analyze the influence of air tightness and gas permeability on the passive control of the RH inside the container (pressurization tests, tracer gas measurements and temperature/relative humidity response tests have been performed). Furthermore, real showcases, operating under actual museum conditions, have been studied by monitoring, for medium long time, indoor/outdoor environmental parameters.

In the paper the set-up of the laboratory experimental procedure and the measurement results are presented and critically analyzed. These laboratory experiences are then compared against field measurement results.

Keywords: museum showcases, artworks preservation, air tightness, gas permeability, laboratory measurements, thermo-hygrometric control, environmental conditions monitoring, buffer materials, passive RH control.

Introduction

The conservation of works of art is largely influenced by the conditions of the indoor environment where the objects are exhibited or preserved. In fact, the conservation conditions of materials (both in general and, in particular, for hygroscopic substances, such as paper, wood and canvass) depends strongly on the level of the air temperature and relative humidity of the surrounding environment. Therefore, the environmental control assumes a remarkable role in the preventive conservation. The environmental parameters, such as relative humidity, temperature, but also light and dust, if not properly controlled, can cause or accelerate the deterioration of works of art.

In recent times, in Europe and Italy, the emanation of standards and guide-lines [1, 2, 3] has contributed to rise the attention of museum staff to the microclimatic control. Optimal values of the ambient parameters, that can be used as a reference by curators in absence of other specific indications, have been assessed for different categories of materials.

The actual achievement of these optimal values, however, can be very difficult due to the specific features of museum buildings and their installations. In such conditions, and/or when mixed collections are displayed in the same room, the adoption of suitable museum showcases can be a valid alternative to allow a suitable control of thermo-hygrometric parameters.

In order to perform as expected, museum showcases must, nevertheless, meet several requirements. Among the other it is possible to mention:

- security, that is protection against acts of vandalism and robbery,
- safety, that is protection against various risk (fire, earthquake, …),
- optimal fruition of the displayed collection,
- proper conservation of artworks, that is control of relative humidity, IAQ and temperature.

In relation to the last requirement, it is of paramount importance to design a museum showcase capable of reducing and delaying the time variation of the indoor environmental parameters caused by the external conditions (i.e. the ones in the room). A good showcase envelop, with high thermal insulation and low air (gases and water vapor) permeability, can provide a first, significant measure to make, on the short and medium time,

the internal conditions (micro-environment) the least influenced by the external conditions (macro-environment). Construction materials and techniques play a primary role as far as the envelope performances are concerned [4] and, hence, largely affect the number of air exchanges between showcases and museum indoor environment.

Through the use of a suitably optimized showcase envelopes it is possible to exert a first, effective, control of the environmental conditions for preservation. However, it has to be underlined that, on the long period of time, the values of micro- and macro-environment parameters will tend to be the same (i.e. they will swing around the same average value). In order to further improve the control of the internal temperature and relative humidity the adoption of supplementary measures is therefore required.

To keep inside the showcase an average value of the thermo-hygrometric parameters constantly different from that in the room, two different strategies can be used:

- *passive control* (nowadays this approach is only limited to the relative humidity control),
- *active control* (both relative humidity and temperature are accurately controlled via a mechanical HVAC system).

Passive control is carried out by introducing in the showcase some buffer or hygroscopic materials (typically silica-gel salts) that, pre-conditioned at the desired RH level, adsorb and release water vapour and help in stabilising the relative humidity. This type of devices offers several benefits compared to active control; in particular it requires low operating and maintenance cost and its action is intrinsically safe (a fault in an active control system, in fact, can determine rapid and large variations of temperature and relative humidity inside the showcase, the worst scenario as far as the conservation of works of art is concerned).

However, buffer materials have a limited life span and periodically, the “exhausted” material has to be changed and re-conditioned.

It is well known that the “air change rate” plays a fundamental role in determining the performance of a showcase and the life span of buffer materials [5]. Less obvious is the fact that the usually adopted “air change rate” parameter actually includes, not only the effect of ventilation, but also the diffusive phenomena, i.e. the gas exchange between the indoor/outdoor of the showcase due to the gas permeability of materials.

It has to be noted that the situation is analogous to the building sector, but in this last case the influence of ventilation phenomena is of orders of magnitude larger than diffusion, being the air tightness of rooms far worse than that of showcases. Furthermore, the surface-to-volume ratio increases by decreasing the size of the system and hence, the surface related phenomena (like gas diffusion) will play a major role in case of small enclosures.

Aims of this work were:

- to analyze the influence of air tightness and gas permeability on the passive control of the relative humidity inside museum showcases,
- to set-up, verify and propose test procedures for assessing the showcase performance,
- to deepen the knowledge of buffer material behavior.

For this sake, some experimental showcases, made of different materials and with various construction techniques, have been tested in laboratory. Moreover, investigation were also performed in the field by analyzing the behavior of real museum showcases and by testing different strategies for improving their performance.

Pollutants mass balance and influence of ventilation/diffusion on showcase indoor environment

As it has been discussed in the previous section, the common belief among museum curators is that air tightness of showcases is, practically, the only relevant features as far as the envelope performance are concerned. Consequently great care is paid by manufacturers in building well "sealed" containers. Gasket and adhesive are adopted to seal as best as possible all the air leakage paths. This is certainly an agreeable approach, being the ventilation one of the major factor influencing the mass exchange[1] between the indoor and outdoor environment. However, it has been demonstrated that the most influencing phenomenon in case of museum showcases is , frequently, represented by gas diffusion.

The adoption of the "*air change rate*" word and concept, n [1/h], as a performance parameter, does not certainly help in clarifying the real physical mechanism that takes place and can lead to misunderstandings among the persons involved in the museum works. The reason of this lays in the typical assumptions that are done solving the generic mass balance equation of a pollutant (or water vapor or tracer gas) for a building (sector from which these concepts have been derived). In the built environment, in fact, the contribution of diffusive phenomena to the mass exchange rate is negligible compared to the effect of ventilation (convective transport). The continuity equation of a generic pollutant or gas (assuming constant and uniform density over the volume and no endogenous pollutants production) for a typical room can be written as [6, 7]:

$$\sum_{in} Q_{in} \cdot C_b - \sum_{out} Q_{out} \cdot C_{out} = \frac{\partial \left(V \cdot \langle C \rangle \right)}{\partial \tau} \qquad (1)$$

[1] In case of RH control, the mass balance of water vapor is of interest.

Introducing the ventilation efficiency, $\varepsilon_v = \frac{C_{out} - C_b}{\langle C \rangle - C_b}$, assuming steady-state air flow rate (so that $\sum_{in} Q_{in} = \sum_{out} Q_{out}$) and perfect mixing (ε_v=1), the solution of equation (1) can be written as:

$$\langle C(\tau) \rangle - C_b = \left(\langle C_0 \rangle - C_b \right) \cdot e^{-n \cdot \tau} \qquad (2)$$

Being $n = \frac{Q}{V}$ the air change rate. Therefore, in case of a typical building and/or analogous enclosed spaces, the concentration time history of a generic pollutant can be satisfactorily described through the air change rate concept, as underlined by equation (2).

However, if part of the container envelope (walls and/or floor, roof) is permeable to gaseous pollutants, as it usually happens in case of museum showcases (figure 1), the continuity equation for pollutant (the endogenous source term is again assumed equal to zero) becomes:

$$\sum_{in} Q_{in} \cdot C_b - \sum_{out} Q_{out} \cdot C_{out} + q_d = V \cdot \frac{\partial \langle C \rangle}{\partial \tau} \qquad (3)$$

Neglecting the edge effects and the buffering (unsteady sorption/desorption) of the gas within the permeable material, hypothesizing a diffusion according to the Fick's first law, the q_d term may be modelled as:

$$q_d = \frac{\dot{m}_d}{\rho_{gas}} = - A \cdot D_{gas} \frac{\Delta C}{s} \qquad (4)$$

Combining equation (3) and (4), under the simplifying hypotheses discussed in [8], it is possible to write:

$$- \left(\langle C \rangle - C_b \right) \cdot n - \frac{A \cdot D_{gas} \cdot \left(\langle C \rangle - C_b \right)}{V \cdot s} = \frac{d \left(\langle C \rangle - C_b \right)}{d\tau} \qquad (5)$$

Integrating equation (5) under the same assumptions adopted for equation (1), one obtains:

$$\left(\langle C_{gas}(\tau) \rangle - C_b \right) = \left(\langle C_{gas,0} \rangle - C_b \right) \cdot e^{-\left(n + \frac{A \cdot D_{gas}}{V \cdot s} \right) \cdot \tau} = \left(\langle C_{gas,0} \rangle - C_b \right) \cdot e^{-\alpha \cdot \tau} \qquad (6)$$

By comparing equation (2) and (6) it is possible to see that the effect of the diffusive transport of the pollutant determines an increment to the value of the air change rate, n.

In these conditions the exponent of the concentration decay curve (equations 6 and 7) cannot be called the "air change rate", being:

$$\alpha = n + \left(\frac{A \cdot D_{tracer}}{V \cdot s} \right) = \frac{Q}{V} + \left(\frac{\delta_{tracer} \cdot A \cdot p_{atm}}{V \cdot s \cdot \rho_{tracer}} \right) \quad (7)$$

The concentration time history of pollutants becomes a function of α and not only of the air change rate, $n = \frac{Q}{V}$.

The difference between these two quantities increases when:

- the gas diffusion coefficient D_{gas} increases, or, better, when decreases the gas diffusion resistance of the envelope (defined as $\frac{s}{D_{gas}}$);
- increases the area of the gas permeable surface, A;
- the ratio A/V is high (this condition is likely to happen in case of small containers);
- the ventilation air flow rate is low (in this case the magnitude of n will be comparable or smaller than the term $\frac{A}{V} \cdot \left(\frac{s}{D_{tracer}} \right)^{-1}$, a situation typical in museum showcases).

To avoid a possible misunderstanding in the following sections the quantity α will be addressed as the "equivalent air change rate".

Performance assessment of the museum showcases

Two features need to be addressed in order to fully characterize the ability of the showcase envelope in keeping the indoor environment controlled: one is the air tightness, which exerts its influence on the ventilation[2], the other is the gas permeability, which drives the diffusion.

[2] For a given showcase, the air flow rate due to ventilation depends on the air velocity near the envelope, originated by air movements on the outside facing surface of the container, and on the temperature difference between the indoor/outdoor of the showcase.

An experimental test based on pressurization techniques can be adopted to assess the air tightness [6]. Instead, for quantifying the simultaneous effect of ventilation and gas diffusion, that is, the overall phenomenon describing the pollutant exchange between the micro and macro environment, a tracer decay technique demonstrated to be a suitable approach (see e.g. [8] for a theoretical background).

In order to verify the proposed testing procedures, and to analyze the relative influence of ventilation and diffusion on the RH control in museum showcases, an experimental campaign has been developed in the laboratory.

Three different types of box shaped experimental museum containers (internal size: 0.58 x 0.19 x 0.38 m and volume: 0.042 m^3), with different air tightness and gas permeability values, have been built and analyzed. Measurements were performed both with and without buffer materials (ArtSorb®) inside the showcases.

In particular, the features of the three studied showcases were:

- *SI showcase (air and gas tight)*: completely made of Plexiglas, virtually perfect air and gas tightness;
- *VI showcase (gas tight)*: completely made of Plexiglas, with calibrated airy holes (diameter 5 mm). The holes (maximum 10 in total) can be opened or closed on demand. In the experiments here described 2+2 holes were opened (2 openings on the lower part of a vertical wall, 2 holes on the upper part of the same wall) (symbol: *VI2*);
- *SP showcase (air tight)*: five walls are made of Plexiglas, one wall made of MDF (Medium Density Fiber Board – MDF has a quite high air tightness and gas permeability, [8]).

For each container a preliminary characterization of the envelope has been done by performing both pressurization tests (with positive and negative pressure differences) and tracer decay experiments (figure 2 shows a scheme of the laboratory apparatuses). These campaign allowed to classify the showcases performance and to verify the capability, drawbacks and advantages of the proposed measurements techniques.

The pressurization tests provided the values of C, air permeability of the showcase (the flow exponent was always assumed equal to 0.67 for the assessment of C) and the tracer gas measurements provided the equivalent air change rate, α. Results are resumed in table 1. Examples of pressurization test and tracer decay measurement results are also shown in figures 3 and 4, for an actual museum showcase (test were performed in the field).

On a subsequent phase of the research, the influence of the showcase envelope features on the RH control was analyzed. To this aim, a series of relative humidity response tests have been performed inside a climatic room (climatic room size: 5.05 m × 2.90 m × 2.65 m).

In particular, each container has been subject to a sinusoidal variation of RH (with different periods - 24, 48 or 72 hours - and same amplitude - RH fluctuations between 40 and 70%) at a constant air temperature (T ≈ 25°C). Temperature and relative humidity inside and outside the showcases were continuously monitored by means of a Delta-T Devices DL3000 datalogger (sampling rate: 5 min). Tests were repeated with and without buffer materials inside the showcases.

Figure 5 shows, as an example, the relative humidity versus time for the showcases without buffer materials (period of the sinusoidal variation of RH: 24 hours). Time profiles of RH inside the various showcases with 400 g of buffer materials are shown in figures 6 and 7, for a period of 24 and 72 hours respectively.

Finally, studies on real showcases equipped with buffer materials and operating under actual museum conditions were carried out by monitoring for medium/long time the indoor/outdoor environmental parameters (T and RH. Measurements were performed using Smartreader SR002 and/or Testo 175-H2 microdataloggers).

Results and Discussion

As expected, the performance of the showcase envelope exerts a large influence on the control of the internal relative humidity. A good, air and gas tight, container (like *VI*) allows to decouple the indoor environment from the fluctuations of the outdoor parameters (fig. 5). The influence of the air tightness and of the gas permeability of wall materials on the RH stabilization revealed to be of the same order of magnitude. In terms of amplitude of RH variations, an almost perfectly airtight, but poorly gas tight system (e.g. container *SP*) behave like an air leaky box (e.g. container *VI2*). However, as shown in figure 5, thank to the relatively larger buffer effect of the gas permeable material, the oscillations of RH for the *VP* box are delayed compared to the outdoor variations (i.e. in the climatic room); for the air leaky systems (*VI2*) the two curves are, instead, almost in phase.

As far as the tests with the showcases equipped with buffer materials (ArtSorb ® casset with 400g of beads, pre-conditioned at an RH of 55%) are concerned, figure 6 and 7 shows, as an example, the results of two tests.

For the high performance showcase (*VI*) the buffer materials does not add any detectable benefit, being the envelope alone already able to keep the relative humidity inside the box stable and non influenced by the outdoor variations. Nevertheless, the presence of the Artsor® preconditioned at 55 % allows to modify, in an almost permanent way, the internal value of RH (keeping it at a different value compared to the outdoors. See e.g. fig. 5 and 6 & 7). As far as the *SP* and *VI2* showcases are concerned, instead, the introduction of the buffer

material, as expected, produces an improvement in terms of fluctuations smoothening. It has, however, to be observed that the same mass of buffer materials resulted in a different effect if applied to the *VI2* box and the *VP* box. In the first case the smoothening is larger and it seems to be only marginally influenced by the period (24 or 72 hours) of the outdoor fluctuation of the RH (see fig. 6 and 7). In the latter case, the buffer material can still dampen the amplitude of the outdoor fluctuations (even if less effectively), but the performance is largely influenced by the period of the outdoor fluctuations. Longer periods determine a smaller ability of the Artsorb® in keeping controlled the indoor RH (daily gradient of RH: about 5%).

Finally, in figure 8 the time profiles of the air temperature inside the climatic room and the three experimental showcases are plotted. The variations of temperature are very small (due to the tolerance of the control system of the climatic room. The tests were, in fact, done at a nominally constant temperature), but the thermal inertia of the container introduces some delays between the outdoors and the indoors[3]. These small temperature differences (less than 0.5 °C) are the major responsible of the natural ventilation of the showcases (test were done in practically still air).

Finally, in order to verify the findings of the laboratory measurement campaign, an investigation on a series of actual museum showcases (at the "Museo Nazionale del Cinema" di Torino – Italy) was performed. In particular, the effectiveness of the passive control of RH by means of buffer materials was investigated by comparing the performance of "old" and "new", retrofitted, showcases (whose features are summarized in Table 2). The retrofit always consisted in interventions aimed at improving, to a lesser or larger extent, the overall tightness of the container. Figures from 9 to 14 resume the results of these activity and stress, once again, the conclusions drawn from the laboratory studies.

Conclusions

For a reliable and effective control of the relative humidity inside museum showcases the container envelope has to provide satisfactory performance in terms of tightness. This tightness, as highlighted, must refer to both air tightness and gas tightness. In fact, it has been demonstrated that for typical museum showcases, ventilation and diffusion play an equivalent role in determining the water vapour exchange between the indoors and outdoors of the enclosure.

To assess the overall performance of the container, a tracer decay procedure has revealed to be the most suitable test. Pressurization techniques can only address the quality of the showcases in terms of air tightness (that is, to certify the care with which joints and connections are made), but does not supply any comprehensive information about the ability of the container in preventing unwanted variations of the internal relative humidity due to the variations in the outdoor environment.

A series of measurements performed in the field, on real museum showcases, has confirmed the findings achieved in the laboratory.

Symbols

A = panel area [m^2]

[3] SI and VI2 boxes, all made in Plexiglas, showed a comparable trend. The larger thermal inertia of the MDF board (VP) allowed a larger delay of the temperature profile (fig. 8).

α = equivalent air change rate (exponent of the tracer gas decay curve) [1/s] or [1/h] or [1/day]

C_{out} = volume concentration at the outlets [ppm]

C_b = background concentration [ppm]

<C> = room mean concentration [ppm]

C = concentration [ppm]

C = air permeability [l/(h·Pa$^{0.67}$)]

$$C = \frac{Q}{\Delta p^{0.67}}$$

D_{gas} = gas diffusion coefficient [m^2/s]

δ_{gas} = gas permeability coefficient [kg/(smPa)]

ε_v = ventilation efficiency [-]

Subscripts

atm = atmospheric

in = inlet

$\dot{m}_d$ = mass flow rate [kg/s]

n = air changes [1/s] or [1/h] or [1/day]

n = flow exponent of the curve

$$Q = C \cdot \Delta p^n$$

p = pressure [Pa]

Q = ventilation air flow rate [m^3/s]

q_d = gas volume flow rate[m^3/s]

ρ = density [kg/m^3]

s = wall thickness [m]

τ = time [s]

V = volume of the confined space [m^3]

out = outlet

gas = pollutant, water vapour or tracer gas

References

[1] Atto di indirizzo sui criteri tecnico-scientifici e sugli standard di funzionamento e sviluppo dei musei (D. Lgs. n.112/98 art. 150 comma 6)

[2] UNI 10829:1999 Beni di interesse storico e artistico - Condizioni ambientali di conservazione - Misurazione ed analisi

[3] UNI 10969:2002 Beni culturali - Principi generali per la scelta e il controllo del microclima per la conservazione

[4] 4. Perino, M., Filippi, M., AICAAR Le prestazioni delle vetrine museali ai fini del controllo del microclima – il controllo di frontiera.

[5] Thomson, G., "Stabilisation of RH in exhibition cases: hygrometric half time", Studies in Conservation 11, 1977, pp. 8-30.

[6] Sherman M.H., "Tracer-gas techniques for measuring ventilation in a single zone", Building and Environment, Vol. 25, n. 4, pg. 365-374, 1990.

[7] Charlesworth P.S., "Air Exchange Rate and Airtightness Measurement Techniques – An Application Guide", AIVC Doc. AIC-AG-2-88, August 1988.

[8] Filippi M., Perino M.," Experimental evaluation of gas permeability in common materials and influence of diffusion phenomena on tracer gas techniques", RoomVent 2007 Conference, CD – sect. C06 – "Measurement methods and case studies" , 13-15 June 2007, Helsinki, Finland.

Acknowledgments

Part of this work has been done in the frame of a Research Contract between "Museo Nazionale del Cinema di Torino" and Dipartimento di Energetica del Politecnico di Torino.

Authors are grateful to dr. Donata Pesenti for her contribution and skilful cooperation.

Table 1 - Pressurization tests and tracer gas measurements results (these values are an average of different repeated tests).

Showcase	Pressurization tests		Tracer gas measurements
	ΔP +	ΔP -	
	C [l/(h · $Pa^{0.67}$)]		n [1/day]
SI	Virtually ∞	Virtually ∞	0,008
VI2	219,4	228,2	1,86
SP	1,7	1,7	18,16

Table 2 "Museo Nazionale del Cinema – Torino", tested showcases' features.

Showcase	Dimension	Construction materials	Buffer materials
Old showcase (no longer in use)	0.56m× 0.56m× 0.51m Volume: 0.16 m^3	Plexiglas, MDF, poor airtight joints.	1 box of 400 g of Art Sorb. Pre-conditioned at 55%
New showcase	0.7m× 0.56m× 0.56m Volume: 0.22 m^3	Plexiglas, steel, aluminium alloy, airtight joints.	1 box of 400 g of Art Sorb. Pre-conditioned at 45%
Poster Frame	0.8m× 1.2m× 0.07m Volume: 0.07 m^3	Plexiglas, MDF	1 sheet of 160 g of Art Sorb. Pre-conditioned at 50%
Poster Frame Optimized	0.8m× 1.2m× 0.07m Volume: 0.07 m^3	Plexiglas, MDF, back side with a water vapour barrier (PE sheet)	1 sheet of 160 g of Art Sorb. Pre-conditioned at 50%

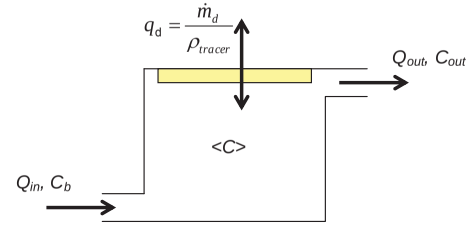


Fig. 1 - Envelope not perfectly tight to the pollutants. Fluid dynamic scheme.

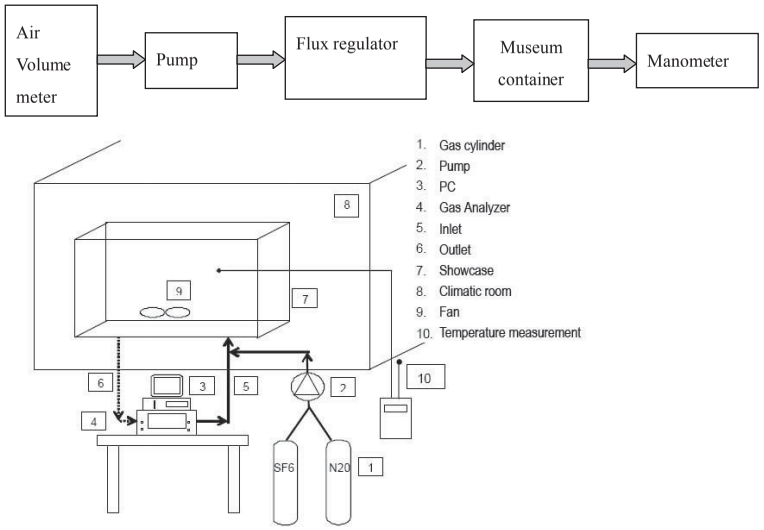


Fig. 2 - Scheme of the laboratory apparatuses used for the showcase characterization (pressurization tests and tracer decay measurements).

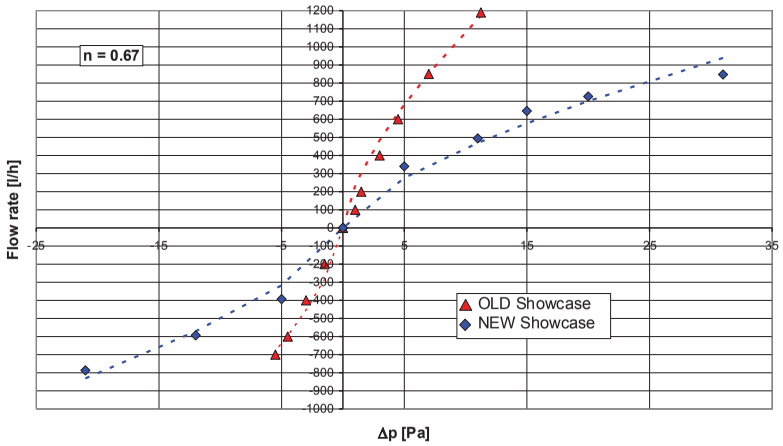


Fig. 3 - Pressurization tests – Actual showcase. Comparison between OLD and NEW Showcases (Δp^{+}: C_{old} = 231 l/(hPa$^{0.67}$); C_{new} = 94 l/(hPa$^{0.67}$) - Δp^{+}: C_{old} = 216 l/(hPa$^{0.67}$); C_{new} = 109 l/(hPa$^{0.67}$)) .

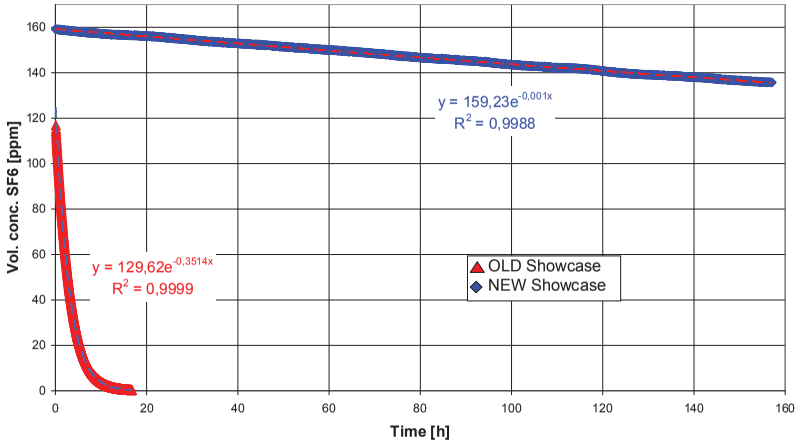


Fig. 4 Gas trace measurements – Actual showcase. Comparison between OLD (α: 8,24 1/day) and NEW (α: 0,02 1/day) showcases results.

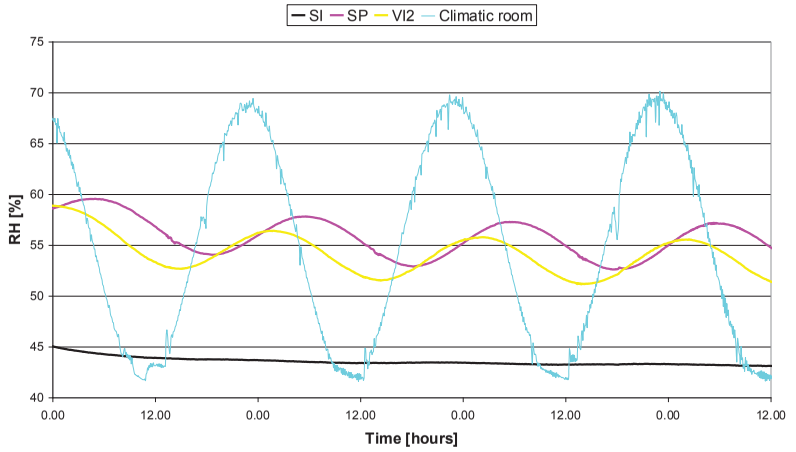


Fig. 5 - Relative humidity vs. time inside climatic room and inside the three tested showcases without buffer materials. RH fluctuations between 40 and 70% - 24 hours period.

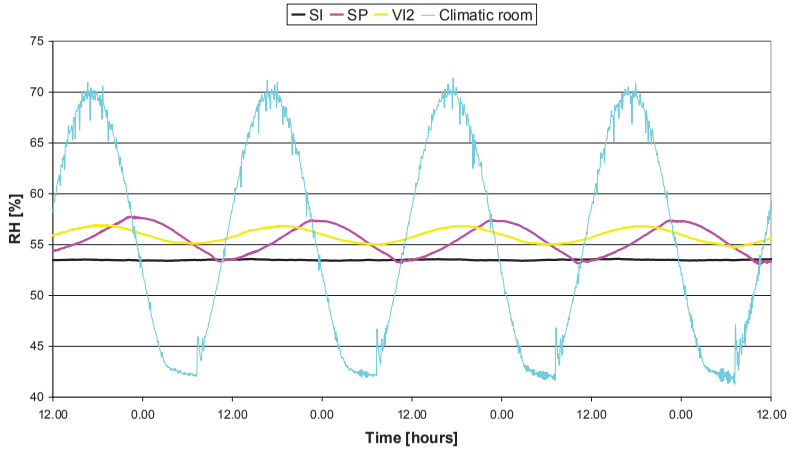


Fig. 6 - Relative humidity vs. time inside climatic room and inside the three tested showcases equipped with 400 g of ArtSorb®. RH fluctuations between 40 and 70% - 24 hours period.

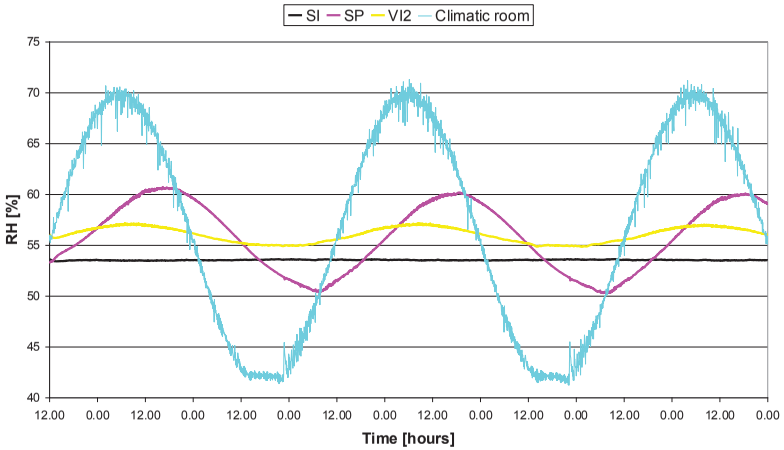


Fig. 7 - Relative humidity vs. time inside climatic room and inside the three tested showcases equipped with 400 g of ArtSorb®. RH fluctuations between 40 and 70% - 72 hours period.

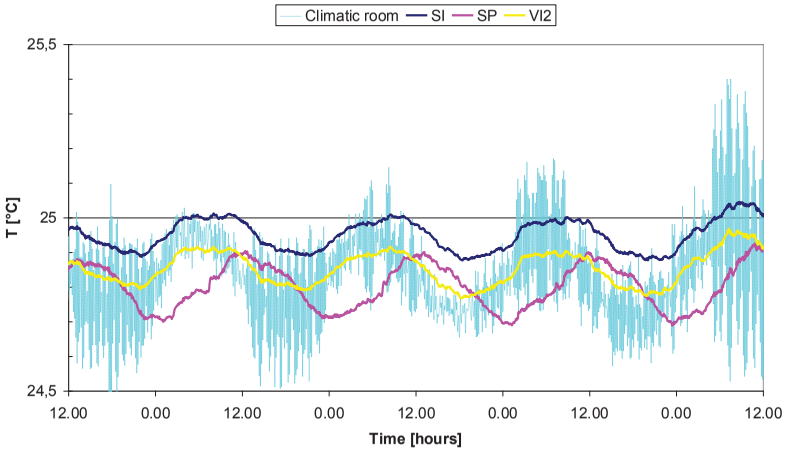


Fig. 8 - Temperature values inside climatic room and inside the three tested showcases.

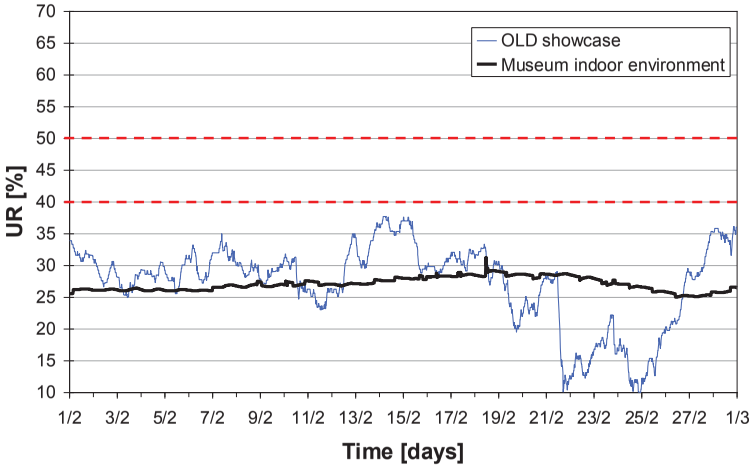


Fig. 9 - OLD Showcase; RH time profile in winter season (February). In red the acceptability interval for conservation.

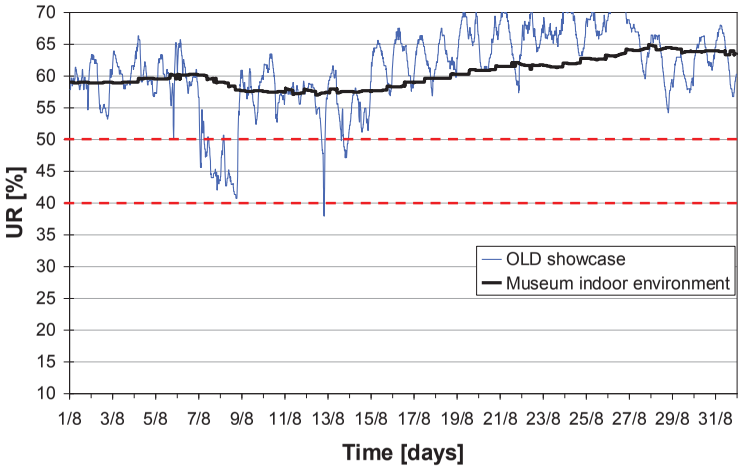


Fig. 10 - OLD Showcase; RH time profile in summer season (August). In red the acceptability interval for conservation.

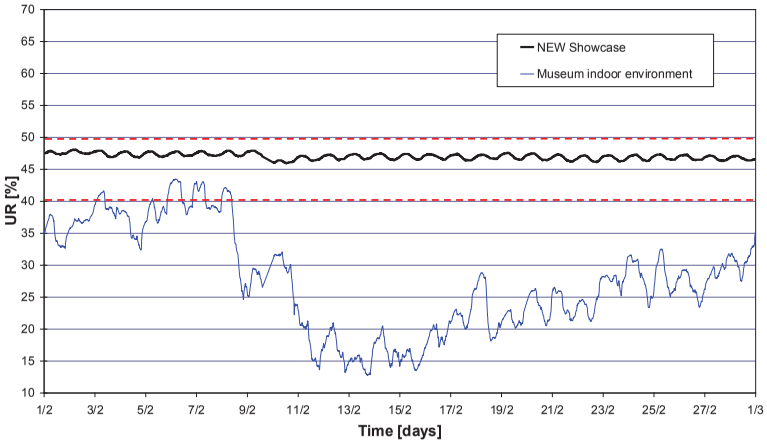


Fig. 11 - NEW Showcase; RH time profile in winter season (February). Acceptability interval for conservation.

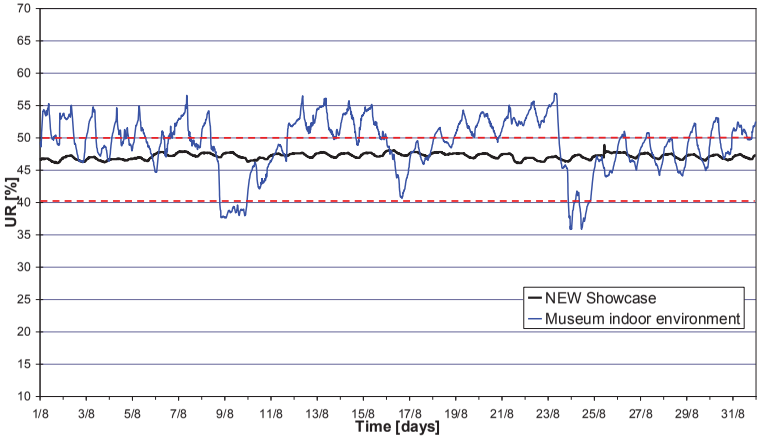


Fig. 12 - NEW Showcase; RH time profile in summer season (August). In red the acceptability interval for conservation.

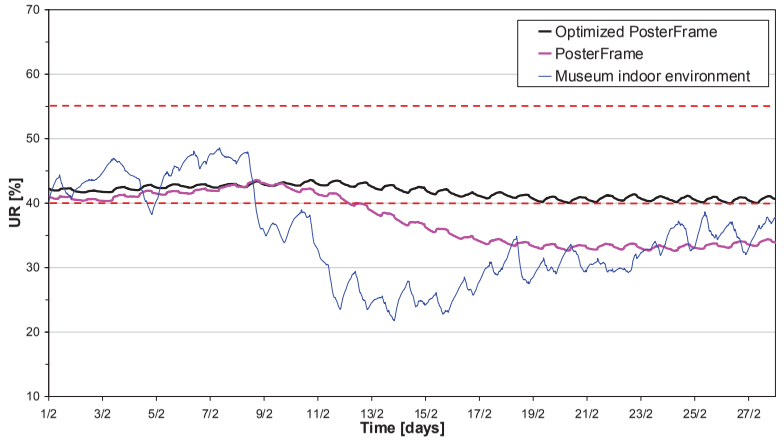


Fig. 13 - Poster Frame; RH time profile in winter season (February). In red the acceptability interval for conservation.

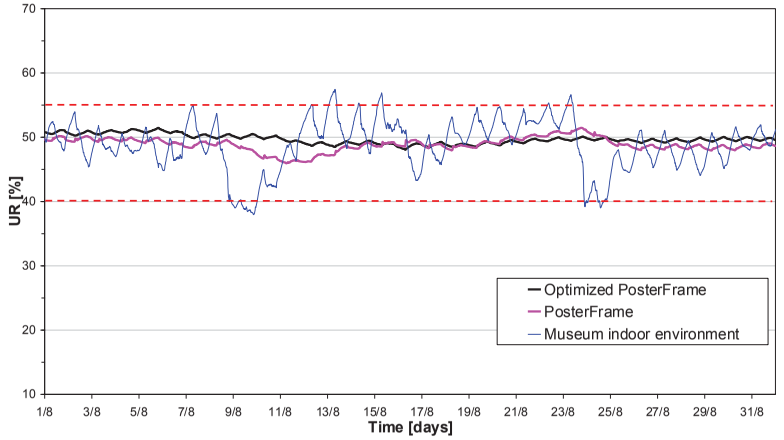


Fig. 14 - Poster Frame; RH time profile in summer season (August). In red the acceptability interval for conservation.

Effective flow area estimation method using a gas

Koji Fujita, Ken Iwamoto, and Takayuki Matsushita

Dept. of Architecture, Graduate School of Eng., Kobe Univ., Kobe, Japan 657-8501

Abstract

The objective of this paper is to present a new method for estimating effective flow areas not only in the external wall of a house but also in the internal walls between rooms using only one type of tracer gas. The discharge coefficient of each wall and the pressure in each room—which are unknown variables—are determined using nonlinear simultaneous equations, which consist of balance equations for the air mass and tracer-gas concentration in the rooms. To verify the validity of this method, we performed a numerical experiment. We defined the values of the discharge coefficient of each wall, and then simulated changes in the temperature and tracer-gas concentration. We then estimated the discharge coefficient of each wall from the simulated temperature and concentration values using the method. Because it was confirmed that the estimated values were equivalent to the defined values, the validity of this method was verified.

Keywords: Effective flow area, Air leakage area, Discharge coefficient, Estimation, Newton's method, numerical experiment.

Introduction

In houses that exhibit a high level of airtightness, it is necessary to provide appropriate ventilation in order to ensure high indoor air quality. Methods to observe the flow of air through rooms using tracer gas have previously been reported [1][2]; however, in these methods, the measured air flow is valid only if the external wind velocity and temperature are the same at the time of measurement, with the same volume of air being supplied or discharged by a machine. If the air velocity, temperature, and supply/discharge volume differ, the air flow will be different too.

To quantify air flow rates under any conditions, it is necessary to determine the effective flow areas (air leakage areas) of the walls that have air leakage areas around doors or in walls. Practical method exists for estimating effective flow area on the basis of the relation between pressure difference and air flow volume [3]. However, this method has mostly been used to estimate effective flow areas in the external walls of a house and not those in the internal walls between rooms. The objective of this paper is to present a method that can estimate effective flow areas not only in the external walls of the house but also in the internal walls between rooms using only one type of tracer gas. In this paper, we present the theoretical

basis of the estimation method and the results of a numerical experiment performed to validate the method.

Balance equations for air mass and tracer-gas concentration

In this paper, we present a method to estimate the effective flow areas of walls whose position, width, and height are known. For example, it is known that air leakage areas exist above and underneath a closed door, in addition to the left and right sides of the door. In order to obtain the effective flow areas of the doorway, we consider the doorway as a "wall" and calculate the effective flow area with respect to its total area.

In houses having multiple rooms, if heat generation and the supply of tracer gas are carried out in an arbitrary room, the balance equations for the air mass and tracer-gas concentration can be expressed as in Equations 1 and 2 below, respectively.

$$\left\{V_n \frac{d\rho_n}{dt}\right\} = -[I]\{w_m\} \quad \text{(Eq. 1)}$$

$$\left\{V_n \frac{d(\rho C)_n}{dt}\right\} = -[I]\{x_m\} + \{S_n\} \quad \text{(Eq. 2)}$$

Here, {} denotes a vector; [], a matrix; the subscript n, the number of the room; and m, the number of the wall.

V : volume of room (m^3),

ρ : air density (kg/m^3),

C : tracer-gas concentration ($kg_{(gas)}/kg_{(air)}$),

w : net mass flow rate of air through a wall that has air leakage areas ($kg_{(air)}/s$),

x : net mass flow rate of tracer gas through a wall that has air leakage areas ($kg_{(gas)}/s$),

S : supply rate of tracer gas ($kg_{(gas)}/s$),

$[I]$: incidence matrix that represents the connections between rooms [4].

The net mass flow rates of the air and tracer gas through a wall that has air leakage areas can be expressed as Equations 3 and 4 below, respectively. We assume that the air flow rate is proportional to the square root of pressure difference across an opening as long as there is no vertical distribution of pressure difference.

$$\{w_m\} = \{f_w(\alpha_m, b_m, h_m, \rho, p_m)\} \quad \text{(Eq. 3)}$$

$$\{x_m\} = \{f_x(\alpha_m, b_m, h_m, \rho, C, p_m)\} \quad \text{(Eq. 4)}$$

where:

α : discharge coefficient of wall that has air leakage areas (-), $\left(= \frac{Q_0}{bh}\left(\frac{\rho}{2}\right)^{0.5}(p_r)^{a-0.5}\right)$ [3],

Q_0 : air leakage coefficient ($m^3/(s\ Pa^a)$) [3],

a : air flow exponent (-) [3],

p_r : reference pressure difference (Pa) [3], (in Japan, 9.8 Pa),

b : width of wall (m),

h : height of wall (m),

p : pressure difference across wall (Pa).

The pressure difference across the wall, as shown in the equation below, is expressed in terms of the pressure in each room and the incidence matrix.

$$\{p_m\} = [I]^T \{P_n\} \qquad \text{(Eq. 5)}$$

where:

P : pressure in room (Pa).

We consider that the air density and tracer-gas concentration in each room are obtained through measurement. Therefore, in the Equations 1 and 2 with the Equations 3, 4 and 5, the discharge coefficient $\{\alpha_m\}$ of each wall and the pressure $\{P_n\}$ in each room are the unknown variables. The effective flow area of each wall is expressed as $\{\alpha_m b_m h_m\}$, and the width and height of the wall are considered as known. Therefore, if $\{\alpha_m\}$ of each wall is known, we can obtain the effective flow area of each wall.

Estimation method using Newton's method

Since the discharge coefficient of the wall and the room pressure have a nonlinear relationship, as apparent in Equations 1 and 2 with the Equations 3, 4 and 5, we use Newton's numerical method to solve the system of nonlinear equations. A flow chart of the method used to estimate the discharge coefficients is shown in Figure 1.

To solve the simultaneous equations, it is necessary for the number of equations to be equal to the number of unknown variables.

For a certain concentration and temperature state, it is possible to derive as many balance equations for the air mass and tracer-gas concentration as the number of rooms. The number of equations that can be derived is given by the following formula:

[number of temperature and tracer-gas concentration states (K) × number of rooms (N) × 2].

The pressure in each room is different for different temperature and tracer-gas concentration states, but the discharge coefficient of each wall does not change with the temperature and concentration state. Therefore, the number of unknown variables is represented by the following formula:

[number of temperature and tracer-gas concentration states (K) × number of rooms (N) + number of walls that have air leakage areas (M)].

In order to make the number of equations equal to the number of unknown variables, we choose KN + M equations out of 2KN balance equations for the air mass and tracer-gas concentration and set up ${}_{2KN}C_{KN+M}$ systems of nonlinear equations (step I). We assign a number to each system of nonlinear equations from y = 1 to ${}_{2KN}C_{KN+M}$ and start solving from y = 1.

Hypothetical values are assumed for the discharge coefficients $\{\hat{\alpha}_m\}$ of each wall (m: 1 through M) and the pressure $\{\hat{P}_n\}_k$ in each room (n: 1 through N) for each temperature and concentration state (k: 1 through K), which are the unknown variables (step II).

The adjustment of the discharge coefficient of each wall and the pressure in each room is repeated according to the method described below until the errors $\{\Delta W_n\}$ (Equation 6) and $\{\Delta X_n\}$ (Equation 7) in mass balance and tracer-gas concentration, respectively, were below the allowable limits (step III through VII).

$$\{\Delta W_n\}_k = -[I]\{w_m + \Delta w_m\}_k - \left\{V_n \frac{d\rho_n}{dt}\right\}_k \quad \text{(Eq. 6)}$$

$$\{\Delta X_n\}_k = -[I]\{x_m + \Delta x_m\}_k + \{S_n\}_k - \left\{V_n \frac{d(\rho C)_n}{dt}\right\}_k \quad \text{(Eq. 7)}$$

where:

$$\{w_m + \Delta w_m\}_k = \{f_w(\hat{\alpha}_m, p_m + \Delta p_m)\}_k, \quad \text{(Eq. 8)}$$

$$\{x_m + \Delta x_m\}_k = \{f_x(\hat{\alpha}_m, p_m + \Delta p_m)\}_k, \quad \text{(Eq. 9)}$$

$$\{p_m + \Delta p_m\}_k = [I]^T \{\hat{P}_n\}_k . \quad \text{(Eq. 10)}$$

By considering that $\{\hat{\alpha}_m\}$ and $\{\hat{P}_n\}_k$ differ from the true values $\{\alpha_m\}$ and $\{P_m\}_k$ by $\{\Delta\alpha_m\}$ and $\{\Delta P_m\}_k$, respectively, we can write the following expressions.

$$\{\hat{\alpha}_m\} = \{\alpha_m + \Delta\alpha_m\} \quad \text{(Eq. 11)}$$

$$\{\hat{P}_n\}_k = \{P_n + \Delta P_n\}_k \quad \text{(Eq. 12)}$$

From Equations 5, 10 and 12, the relation between the error in the room pressure and that in the pressure difference across each wall can be expressed as

$$\{\Delta p_m\}_k = [I]^T \{\Delta P_n\}_k . \quad \text{(Eq. 13)}$$

After substituting Equation 11 into Equations 8 and 9 and performing the first-order Taylor expansion around α_m and p_m, Equations 6 and 7 can be expressed as the following equations using the relation expressed as Equation 13.

$$\{\Delta W_n\}_k = -[I]\{f_{w,k}(\alpha_m, p_m)\} - [I]\left[\frac{\partial f_{w,k}}{\partial \alpha_m}\right]\{\Delta\alpha_m\} - [I]\left[\frac{\partial f_{w,k}}{\partial p_{m,k}}\right][I]^T\{\Delta P_n\}_k - \left\{V_n \frac{d\rho_n}{dt}\right\}_k \quad \text{(Eq. 14)}$$

$$\{\Delta X_n\}_k = -[I]\{f_{x,k}(\alpha_m, p_m)\} - [I]\left[\frac{\partial f_{x,k}}{\partial \alpha_m}\right]\{\Delta\alpha_m\}_k - [I]\left[\frac{\partial f_{x,k}}{\partial p_{m,k}}\right][I]^T\{\Delta P_n\}_k + \{S_n\}_k - \left\{V_n \frac{d(\rho C)}{dt}\right\}_k \quad \text{(Eq. 15)}$$

Here, $\left[\frac{\partial f_{w,k}}{\partial \alpha_m}\right]$, $\left[\frac{\partial f_{w,k}}{\partial p_{m,k}}\right]$, $\left[\frac{\partial f_{x,k}}{\partial \alpha_m}\right]$ and $\left[\frac{\partial f_{x,k}}{\partial p_{m,k}}\right]$ are diagonal matrices of size N.

Using the relations expressed as Equation 1 through 4, Equations 14 and 15 can be expressed as following equations.

$$\{\Delta W_n\}_k = -[I]\left[\frac{\partial f_{w,k}}{\partial \alpha_m}\right]\{\Delta\alpha_m\} - [I]\left[\frac{\partial f_{w,k}}{\partial p_{m,k}}\right][I]^T\{\Delta P_n\}_k \quad \text{(Eq. 16)}$$

$$\{\Delta X_n\}_k = -[I]\left[\frac{\partial f_{x,k}}{\partial \alpha_m}\right]\{\Delta\alpha_m\}_k - [I]\left[\frac{\partial f_{x,k}}{\partial p_{m,k}}\right][I]^T\{\Delta P_n\}_k \quad \text{(Eq. 17)}$$

By setting up Equations 16 and 17 for K temperature and concentration states and N rooms and by rearranging the terms, we can obtain the following equation.

$$\begin{Bmatrix} \{\Delta W_n\}_{k=1} \\ \vdots \\ \{\Delta W_n\}_{k=K} \\ \{\Delta X_n\}_{k=1} \\ \vdots \\ \{\Delta X_n\}_{k-K} \end{Bmatrix} = \begin{bmatrix} [A_{w,k=1}] & [B_{w,k=1}] & [0] & [0] & \cdots & [0] \\ [A_{w,k=2}] & [0] & [B_{w,k=2}] & [0] & \cdots & [0] \\ \vdots & \vdots & \vdots & \ddots & \cdots & \vdots \\ [A_{w,k=K}] & [0] & [0] & [0] & \cdots & [B_{w,k=K}] \\ [A_{x,k=1}] & [B_{x,k=1}] & [0] & [0] & \cdots & [0] \\ [A_{x,k=2}] & [0] & [B_{x,k=2}] & [0] & \cdots & [0] \\ \vdots & \vdots & \vdots & \ddots & \cdots & \vdots \\ [A_{x,k=K}] & [0] & [0] & [0] & \cdots & [B_{x,k=K}] \end{bmatrix} \begin{Bmatrix} \{\Delta\alpha_m\} \\ \{\Delta P_n\}_{k=1} \\ \vdots \\ \{\Delta P_n\}_{k=K} \end{Bmatrix} \quad \text{(Eq. 18)}$$

where:

$$[A_{w,k}] = -[I]\left[\frac{\partial f_{w,k}}{\partial \alpha_m}\right], \quad [B_{w,k}] = -[I]\left[\frac{\partial f_{w,k}}{\partial p_{m,k}}\right][I]^T,$$

$$[A_{x,k}] = -[I]\left[\frac{\partial f_{x,k}}{\partial \alpha_m}\right], \quad [B_{x,k}] = -[I]\left[\frac{\partial f_{x,k}}{\partial p_{m,k}}\right][I]^T.$$

The vector on the left side of Equation 18 represents the errors in the mass balance and tracer-gas concentration balance for N rooms at K different temperature and concentration states. The size of the vector is 2KN. The size of the matrix on the right side is 2KN × (KN + M). In Equation 18, if we eliminate all elements except those related to the KN + M balance equations for the air mass and tracer-gas concentration (selected in step I), the size of the vector on the left size becomes KN + M, while that on the right side becomes (KN + M) × (KN + M). This can be expressed as follows.

$$\{V_{\Delta W,\Delta X}\} = [D]\{V_{\Delta\alpha,\Delta P}\} \quad \text{(Eq. 19)}$$

$\{V_{\Delta\alpha,\Delta P}\}$ can be obtained by multiplying both sides of Equation 19 by the inverse of matrix $[D]$.

$$\{V_{\Delta\alpha,\Delta P}\} = [D]^{-1}\{V_{\Delta W,\Delta X}\} \quad \text{(Eq. 20)}$$

Using $\{\Delta\alpha_m\}$ and $\{\Delta P_n\}_k$ obtained using Equation 20, $\{\hat{\alpha}_m\}$ and $\{\hat{P}_n\}_k$ can be adjusted using Equation 21 and 22.

$$\{\hat{\alpha}_{m,new}\} = \{\hat{\alpha}_m\} - r_\alpha\{\Delta\alpha_m\} \quad \text{(Eq. 21)}$$

$$\{\hat{P}_{n,new}\}_k = \{\hat{P}_n\}_k - r_P\{\Delta P_n\}_k \quad \text{(Eq. 22)}$$

Here, r_α and r_p are constants used to adjust the discharge coefficient and pressure (set to 0.6 in the present research).

Steps II through VIII are repeated until the completion of calculations for all systems of nonlinear equations chosen in step I. The calculated discharge coefficient of each wall may vary with the specific system of nonlinear equations considered. For each wall, the discharge coefficient is estimated as the average of the obtained values.

Examining the validity of the estimation method through a numerical experiment

The validity of the proposed method for estimating effective flow areas is verified by means of a numerical experiment. Figure 2 shows an outline of the numerical experiment. The shape and discharge coefficients of each wall of the building model used in the experiment, the volume of the tracer gas supplied, and the generated heat are provided as inputs to an air flow network calculating program [4] in order to simulate the temperature and tracer-gas concentration in each room. The temperature and tracer-gas concentration values obtained in the simulation are input into a program that uses the effective flow area estimating method and determines the discharge coefficient of each wall. The discharge coefficient values provided as input to the air flow network calculating program and those estimated using the present estimation method are compared for each wall.

Figure 3 shows a building model considered in a numerical experiment. The building contains four rooms, and eight walls that have air leakage areas. The discharge coefficients of the walls provided as inputs to the air flow network calculating program [4] are shown in parenthesis of Figure 3. Table 1 shows the three conditions considered for heat generation and the supply of tracer gas.

Figures 4 and 5 show changes in the temperature and tracer-gas concentration for the three conditions. The flat parts of the curves shown in the Figures are considered to represent steady states and the values are listed in Table 2.

The values of the steady-state temperature and tracer-gas concentration corresponding to the three conditions are input into the program that uses the effective flow area estimation method proposed here, and the discharge coefficient of each wall is obtained. Figure 6 shows the estimated discharge coefficient of each wall. The estimated value is obtained as the average of the discharge coefficients of the wall, which depend on the specific system of nonlinear equations considered. The same figure shows the minimum and maximum values of the discharge coefficient calculated by considering different systems of nonlinear equations. The average, minimum, and maximum values of each wall almost coincide with the true value that is shown in parenthesis of Figure 3 (the value provided as input to the air flow network calculating program). The maximum difference between the maximum or

minimum value and the true value is 7.2%, and the maximum difference between the average and true value is 2.9%.

The total number of combinations of the system of nonlinear equations was 10,626. Out of these systems, 6,653 systems yielded solutions. Of the remaining, 49 were linearly dependent, while 3,924 did not converge and did not yield solutions. If a method can be found to select systems of nonlinear equations that yield solutions, there will be no need to solve all systems. Future studies should focus on the development of such a method.

Summary and conclusions

We present a method for estimating effective flow areas not only in the external wall of a house but also in the internal walls between rooms using only one type of tracer gas. The discharge coefficient of each wall that has air leakage areas and the pressure in each room—which are the unknown variables—are determined using nonlinear simultaneous equations, which consist of balance equations for the air mass and tracer-gas concentration in the rooms. The nonlinear simultaneous equations are solved using Newton's method.

To verify the validity of this method, we performed a numerical experiment. We defined the values of the discharge coefficient of each wall, and then simulated changes in the temperature and tracer-gas concentration. We then estimated the discharge coefficient of each wall from the simulated temperature and concentration values using the method. It was confirmed that the estimated discharge coefficient of each wall was equivalent to the defined value. Thus, the validity of this method was verified.

Acknowledgments

This work was supported by MEXT KAKENHI (No. 21760450).

References

1. F. W. Sinden, "Multi-chamber Theory of Air Infiltration," Building Environment, Vol.13, 1978, pp.21-28.

2. C. F. A. Afonso, E. A. B. Maldonado and E. Skaret, "A Single Tracer-gas Method to Characterize Multi-room Air Exchanges," Energy and Buildings, Vol.9, 1986, pp.273-280.

3. ISO 9972, Thermal performance of buildings - Determination of building air permeability of buildings - Fan pressurization method, 2006.5.

4. J. Rao and F. Haghighat, "A Procedure for Sensitivity Analysis of Airflow in Multi-zone Buildings," Building and Environment, Vol.28, No.1, 1993, pp.53-62.

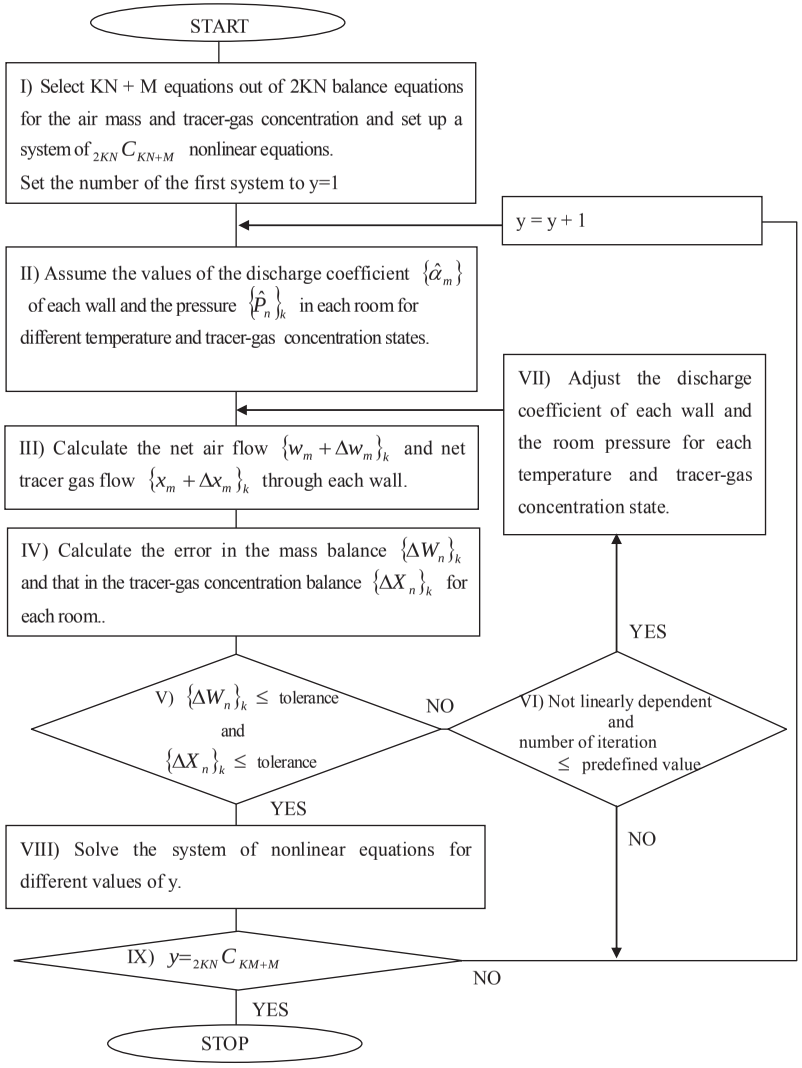


Fig. 1 Flow chart of the method used to estimate discharge coefficients

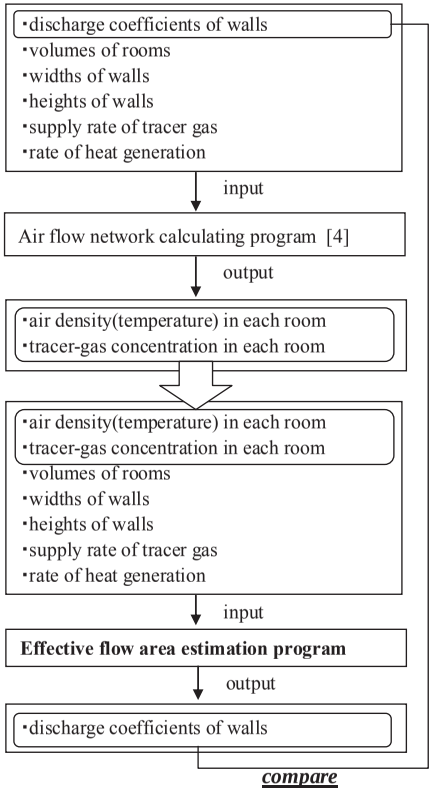


Fig. 2 Outline of numerical experiment

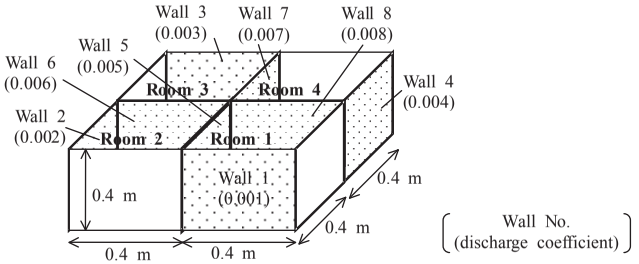


Fig. 3 Building model considered in numerical experiment

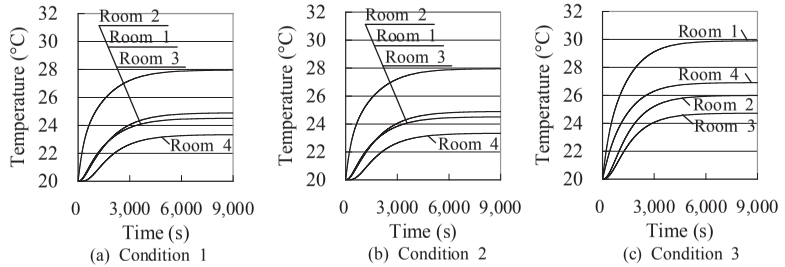


Fig. 4 Temperature

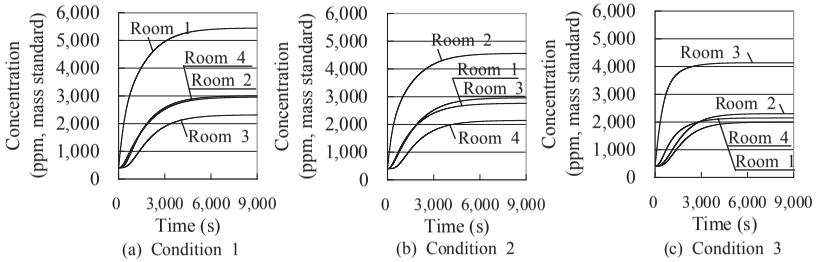


Fig. 5 Tracer-gas concentration

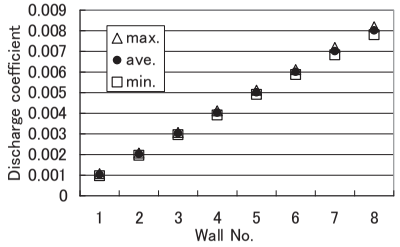


Fig. 6 Estimated discharge coefficients

Table 1 Conditions for heat generation and supply of tracer gas

	Rate of heat generation (W)				Supply rate of tracer gas (g/h)			
	Room 1	Room 2	Room 3	Room 4	Room 1	Room 2	Room 3	Room 4
Condition 1	-	0.8	-	-	1.5	-	-	-
Condition 2	-	0.8	-	-	-	1.5	-	-
Condition 3	0.8	-	-	0.4	-	-	1.5	-

Table 2 Values of the steady-state temperature and tracer-gas concentration

	Temperature (°C)				Tracer-gas concentration (ppm) (mass standard)			
	Room 1	Room 2	Room 3	Room 4	Room 1	Room 2	Room 3	Room 4
Condition 1	24.88	27.95	24.50	23.32	5,443	2,951	2,310	2,999
Condition 2	24.88	27.95	24.50	23.32	2,956	4,558	2,757	2,140
Condition 3	29.89	25.98	24.71	26.90	1,992	2,298	4,134	2,142

Development of Infiltration Modeling Parameters for a SIPs Building

Ty NEWELL[1], and Paul W. FRANCISCO[2]

[1] Newell Instruments, Inc., Urbana, IL
[2] University of Illinois at Urbana-Champaign, Building Research Council, Champaign, IL

Abstract
Reduction of infiltration in the Equinox House, a residence under construction in Urbana Illinois, has been characterized through a series of blower tests as different joints and seams in the building were sealed. Equinox House is constructed with 30 cm thick SIPs (Structural Insulation Panels) wall and roof panels consisting of a Styrofoam core and oriented strand board sheathing on interior and exterior surfaces. Blower door tests were performed as each type of seam in the house was sealed. Wall to foundation connections, wall to roof connections, panel to panel connections, and miscellaneous gaps were examined. The effect of adding wall surfaces (drywall) to the building are also presented. The results show strong correlations between level of infiltration and the amount of labor and the amount of sealant used to lower the infiltration. The house infiltration was reduced to 0.37 ACH at 50 Pa. The correlation parameters, while specific to this type of construction, demonstrate how costs related to infiltration reduction can be formulated and utilized for optimal building design analyses.

Keywords superinsulated, supersealed, infiltration, ventilation, ach

Introduction

Uncontrolled infiltration is undesirable for many reasons. In almost any climate requiring air conditioning and/or space heating, uncontrolled infiltration impacts energy requirements. In the US, where typical residential construction methods result in significant uncontrolled infiltration, the "fresh" air entering the house does so through cracks such as sill plates, window jambs, door frames, flue vents and utility penetrations which are often regions containing dirt, moisture, mold, mildew, and vermin. Additionally, relying on uncontrolled infiltration for fresh air leads to stagnated regions within the residence where air is not purged, creating local regions of poor air quality.

Equinox House is a super-insulated, super-sealed residence recently constructed in Urbana, Illinois. Urbana Illinois is a region with hot, humid summers and cold winters. Figure 1 is a recent picture of Equinox House undergoing placement of exterior siding. After all wall and roof panels were installed, a series of blower door infiltration tests were conducted as silicone caulk was applied to all wall and roof panel seams. The effect of the sealing process and the cost related to the sealant and labor are presented in this paper. The goal was to reach an ACH (air change per hour) less than 0.6 in accordance with Passive House design standards before adding drywall to the interior of the house. The house construction process, sealing and infiltration measurement results, and the cost impact of the sealing effort are described.

Equinox Construction Methods

Equinox is a single story "ranch" type residence with 195 m^2 of indoor floor area and 54 m^2 of attached car garage. Due to the high ceilings, the interior, conditioned volume of the house is 790 m^3. The floor is concrete "slab-on-grade" construction with no insulation placed beneath. In Illinois, an uninsulated floor is generally more economical for maintaining comfort than an insulated slab floor.

The foundation wall surrounding the house was constructed with ICF (Insulated Concrete Form) block which has 7cm of expanded Styrofoam on the exterior and interior sides of the ICF.

Figure 2 is a photo of the ICF being placed around the building perimeter. Reinforced concrete, 15.2 cm thick, is poured between the Styrofoam sides of the ICF block, as shown in Figure 3.

Two layers of treated lumber 31 cm wide by 1.9 cm thick was bolted to the top of the concrete foundation wall, forming the base for the wall panels. Untreated lumber 29.2 cm wide and 3.8 cm thick was screwed and nailed onto the sillplate lumber. SIPs (Structural Insulated Panels) were placed on top of the sillplate lumber. A channel milled into the bottom edge of the SIPs wall panels fit over the 29.2 cm by 3.8 cm lumber, allowing nails to attach the wall panel to the sill. Figure 4 shows the installation of the first SIPs wall panel on the sill.

Figure 5 shows continued placement of SIPs wall panels and Figure 6 shows the last roof SIPs panel being placed on the house. The SIPs can be up to 2.4 meters wide by 7.3 m long with a thickness of 31.4 cm including the two layers of OSB (1.11 cm per OSB layer) and 29.2 cm of Styrofoam. Between each wall panel and each roof panel is a Styrofoam spline with an OSB layer glued on its outside layer. The spline is 7.6 cm thick and plugs into the 3.8 cm deep channels milled into the edge of each SIPs panel. Ringshanked nails are driven on each side of the panel seams into the spline to fix the walls and roof together. The walls and roof of the house required 5 days with approximately 6 to 7 laborers to erect. This consisted of two days to erect the house walls, one day to construct internal structural framing for the roof, and two days to install the roof panels.

During erection of the wall and roof panels, a line of urethane foam sealant was placed between each panel seam, and the splines were coated with a bead of panel adhesive. Generally, these steps should provide a high level of sealing for the house shell, however the construction of Equinox occurred in December, 2009 during wet, freezing weather, causing difficulties in applying the foam and panel adhesive. Therefore, one might find that the level of performance improvement due to additional panel sealing activities discussed in this paper may not yield the same level of performance improvement in SIPs homes installed under better construction conditions.

Infiltration Tests

Six series of infiltration tests were conducted with a Minneapolis Blower Door operated at 50 Pa. The tests were conducted over from March 2010 to June 2010. The first five test series consisted of several tests in which the amount of caulk, the time required to apply the amount of caulk to panel seams of a measured length, and the change of air changes at 50 Pa (ACH50) were measured. The sixth blower door test was conducted after drywall was applied to all interior wall and ceiling surfaces.

Figure 8 shows the change of ACH50 as a function of panel seam length. On average, leakage dropped 0.0067 ACH50 per meter of panel seam length. Some panel seams did show variations in the amount of leakiness. For example, the first 60 meters of seam sealing was the sillplate seam around the perimeter of the house. The sillplate seam shows 0.01 ACH50 reduction per meter of seam length, which is due to some waviness between the layers of wood in the sill plate and the connection to the bottom of the SIPs wall panels. The vertical seams between wall panels with the spline connections have a change of 0.0046 ACH50 per meter length, and are the

data series from 60 meters to 200 meters in Figure 8. The additional seams consist of the wall to roof panel seams, and the roof to roof panel seams. The relatively "flat" regions of the Figure 8 plot at 150 meters, 250 meters, and 350 meters are locations represented by a region of roof panel seams, window perimeter seams, and door perimeter seams that did not display significant leakiness. The roof panel seams were between three panels that apparently had less leakiness than other panel seams. Possibly, the weather was somewhat better than the other construction periods and the foam sealant did a better job during that time. The windows and doors were foam sealed when installed, and these seals were relatively good. The last data point shown in Figure 8 represents the last blower door test performed after drywall was added. The drywall did reduce the infiltration, and most likely the effect of cladding the interior with drywall would have been more significant if the extensive panel seam sealing had not been performed. While this may have saved some cost, the danger of not sealing the panel seams is that moisture can move into various isolated regions of the panel seams and create rot at some time in the future.

Figure 9 shows the amount of silicone caulk applied to the panels seams, expressed in terms of tubes of caulk. A tube of caulk contains 0.283 kg of silicone caulk. The sillplate seam required 0.5 tubes of caulk per meter of seam, which as discussed previously consisted of multiple seams due to the multiple layers of wood that the wall panels are mounted on. The rest of the seams required approximately 0.18 tubes of caulk per meter of panel seam. Figure 10 shows the labor hours as a function of panel seam length. The sillplate seam required 0.1 hours of labor per meter of seam length while the other seams required approximately 0.04 hours of labor per meter of seam.

Impact of Panel Sealing Effort

The cost related to the sealing effort can be quantified in order to determine the payback of the sealing effort. For central Illinois, the cooling and heating seasons consist of 3900 C-day. On a simple basis, assuming that the infiltration under normal conditions can be estimated as ACH50 divided by 20, the uncontrolled house infiltration has been reduced from 120 m^3 per hour to 15 m^3 per hour. This represents a reduction of 3300 kW-hr of sensible thermal energy conditioning, which with a heat pump having a coefficient of performance of 3 represents a reduction of 1100 kW-hr of electric energy. With a value of $0.12 US per kW-hr, the savings is $130 per year.

The silicone caulk costs $4 US per tube for a total of $300 US for 75 tubes of caulk. Construction labor for caulking is valued at $20 US per hour, with a total cost of $340 for 17 hours of labor. The total sealing cost of $640 for caulk and labor therefore results in a simple payback of 5 years.

Summary

This study provides quantitative data related to the effort and cost of super sealing a residence in the US. Although the data are for one house of one particular design, the results show that the effort expended on sealing a house prior to installing the interior finishes can be quantified and that the payback for sealing the house are favorable. Several questions remain to be answered. Several houses of any type of construction should be evaluated for a better statistical measure of sealing effort and costs. Improved construction practices may help reduce the cost associated

with sealing effort and cost. Finally, the durability of a sealing method needs to be examined in order to know whether the effort has a lasting effect or is only effective for a period of time less than the lifetime of the home.



Figure 1 Photo of the Equinox House in Urbana Illinois in May 2010.



Figure 2 ICF (Insulated Concrete Form) foundation wall used for Equinox perimeter.



Figure 3 Concrete poured in ICF foundation wall.



Figure 4 Placement of the first SIPs wall panel on the foundation wall sill plate.



Figure 5 Continued placement of SIPs wall panels around the house perimeter.



Figure 6 Installation of SIPs roof panels on Equinox.



Figure 7 Completed SIPs panel installation with house wrap and windows installed.

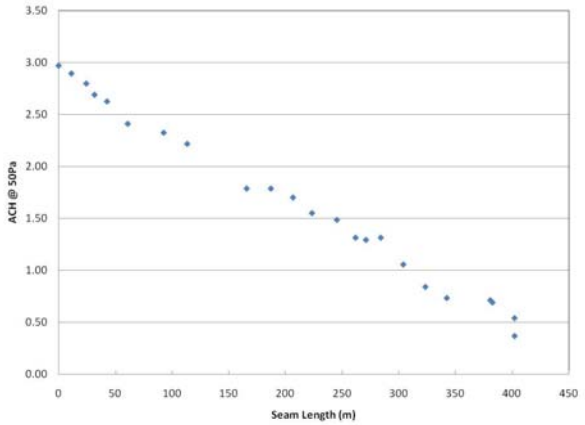


Figure 8 Reduction in infiltration (air changes per hour) as a function of panel seam length.

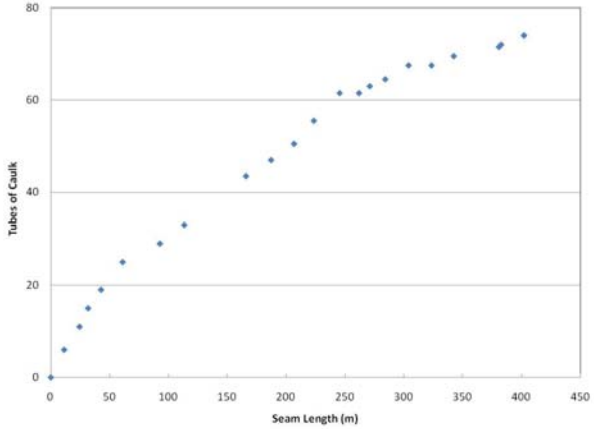


Figure 9 Tubes of silicone caulk (x grams per tube) as a function of panel seam length.

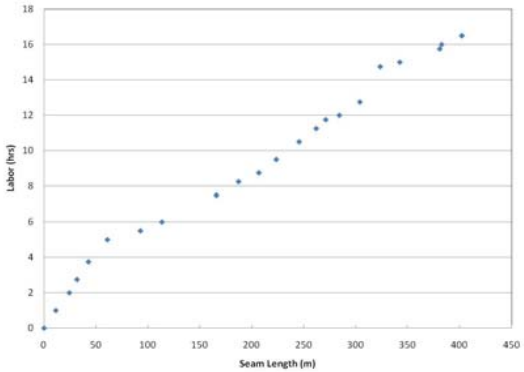


Figure 10 Hours of labor required for sealing panel seams as a function of seam length.

Analysis on CO_2 Emissions Reduction Effect of Zero Energy Multi-famiy Housing to cope with UNFCCC

Yong-Sang Yoon[1], Sun-Hye Mun[2]

[1] Dept.Building&Urban Research. Korea Institute of Construction Technology, Geyeonggi-Do, Republic of Korea, 411-712

[2] Dept.Building&Urban Research. Korea Institute of Construction Technology, Geyeonggi-Do, Republic of Korea, 411-712

Abstract

Korean government established a target to reduce greenhouse gas ("GHG") emissions to 30% by 2020 to cope with the United Nations Framework Convention on Climate Change (UNFCCC) and secure its national competitiveness, and prepared a roadmap to develop this project. Especially, the government set up the objective of Zero Energy Consumption for the newly constructed multi-family housings by 2025 to reduce CO_2 in the building sector.

This Study is aimed at the analysis of CO_2 emissions reduction effect when introducing the component technology for implementing zero-energy multi-family housing building by reflecting this trend at home and abroad. In order to do this, CE3 - Building Energy Performance Evaluation Program was adopted.

Keywords: Green Home, Empirically Demonstrated House, Passive, Renewable energy

Introduction

Global warming threatens survival of human being throughout the world in a variety of results such as drought, typhoon, flood, etc. Ironically, the acts of human being conducted for their survivals like industrial activities threaten survival of human being by emitting CO_2 that is a root cause of expediting global warming. In addition, a nation's CO_2 emissions represent the indicator to measure economy of the nation.

In the case of Korea, temperature has increased by approx. 1.7℃ for the past 96 years (1912~2008), which resulted in the loss of national land in part owing to the rise of sea level along with destruction of ecosystem. Furthermore, some advanced countries intend to use the control of GHG as a trade barrier in such a manner of banning imports from the country having high GHG emissions in the process of production.

Under the international circumstance like this, the issue of global warming became the task to be solved with top priority that cannot be delayed any longer, and Korea, therefore, prepared the plan for GHG reduction centered on Kyoto Protocol as shown in the Graph below.

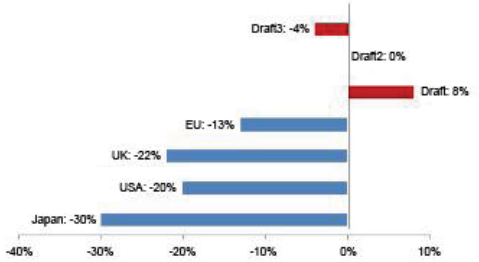


Fig. 1 Comparison of Korea's reduction target against those of the advanced countries

Korea selected the means of reduction by stages as shown in the Table 00 in order to accomplish the largest level of reduction for a developing country like 30% (4% from 2004) against BAU(Business As Usual) by 2020. Such amount of reduction is equivalent to such level of GHG being emitted from 2000cc Sonata for 49,300,000 persons (populations projected in 2020) to travel Seoul through Busan (round trip) for 24.7 times.

Table 1 Means of reducing CO_2 emissions

	Major means of reduction (Each includes policy means of the former scenario)
Draft 1	− Greening of Building/House − Reinforcing demand management such as high-efficiency facility, etc. − Changing into low carbon traffic system − Expanding the portion for new/renewable energy and nuclear sectors new & renewable − Promoting Smart Grid
Draft 2	− Removing fluoride gas that has high global warming potentials − Expanding the distribution of bio fuel − Introducing CCS in part
Draft 3	− Distributing next-generation green car (Electric vehicle, fuel cell electric car, etc.) − Expanding the distribution of high-efficiency product, electric appliances − Promoting strong demand-side management policy

Among the major means of reduction in Draft 1, the field that may most reduce GHG is the building sector. The ratio of residence to the building sector in Korea is 54% showing the highest of all, of which, the multi-family housing house occupies 53%.

That is, in order to accomplish the objective of reducing GHG emissions by 30% from BAU, it is inevitable to reduce CO_2 emissions from multi-family housing building sector. Therefore, Korean government established energy level of newly built multi-family housing houses to zero level by 2025.

This study is intended to analyze the possible reduction of CO_2 emissions from multi-family housing house using CE3 as the first step for quantifying CO_2 emissions and discuss on the method of utilizing the result of study in future.

2. Overview of Energy Performance Evaluation in Multi-family Housing

2.1 Energy Performance Evaluation Tool: CE3

In order to reduce CO_2 emissions, it is essential to forecast energy consumptions of the subject buildings. For this, this study adopted CE3 that is a tool for assessing the energy performance.

CE3 is the Web-based program aimed to assess building energy performance developed specially for domestic circumstance in consideration of EPBD (Energy Performance of Building Directives), International Standard ISO 13790, Germany's DIN V18599.

CE3 is the solution that enables to strategically analyze energy in comprehensive view of interaction of energy flow in accordance with physical or mechanical characteristic of the building on the whole, through which it is possible to suggest optimal direction by grasping the problem in energy performance sector at design stage and forecast the energy cost required for a year or CO_2 emissions.[1]

2.2 Building Energy Performance Level

In this study, energy consumption and CO_2 emissions of the building by stages from the Energy Reduction Design Standard (existing standard) to zero energy house were analyzed.

The subject fields of analysis are the buildings in general that are domestically built subject to 'Building Energy Saving Design Standard'. This standard suggests the obligation and recommendations by fields by categorizing the buildings in a certain scale into building sector, mechanical equipment sector, electrical sector, and new & renewable energy facility sector in order to improve energy efficiency and facilitate the reduction of GHG. The design standard in building sector suggests the standards of layout, plane, and lighting and ventilation plan of the building and recommends the users to observe the insulation performance of window and exterior wall. New & renewable energy facility sector was recently added since the importance of GHG reduction has emerged.

The next subject field of comparison is the case of minimizing energy consumption of the building by introducing passive component technology such as air tightness, high insulation, etc. In order to accomplish the objective established by the government by 2025, that is, Zero

[1] CE3 website: www.kihoo.co.kr

Energy Consumption of the Building, it is necessary to minimize building's energy demand through passive design, and then produce energy by introducing new & renewable energy facility. Currently, passive design standard requires the installation of Heat Recovery Ventilator with the performances of 15kWh/㎡·a for heating energy demand, 120kWh/㎡·a for primary energy demand, 0.6 times (@50Pa) for ventilation & recovery, and at least 85% for ventilation efficiency. In this study, the result of minimizing energy consumption was extracted following gradual introduction of a variety of passive component technology.

2.3 CE3 Input Data

The subject building of analysis was assumed to have dwelling exclusive area in 85m2/household comprising total 14 households for the application of multi-family housing, where two households per floor reside in 7 story building. In addition, the location of the subject building was assumed not to be influenced by the shade of the surrounding buildings when energy is produced by new & renewable energy facility.

The standard meteorological data that is one of the input values and standard operation profile in the analysis of building energy performance is the factor that may greatly influences on the result. In this study, the data of Korea Meteorological Administration clarified through TMY2 technique was adopted as standard meteorological data, while the value used when estimating energy efficiency grade of domestic building was selected for standard operation profile. When the standard meteorological data is applied, space zoning was conducted broadly into air-conditioning space (living room, room, kitchen), non-air conditioning space stair case, and elevator shaft.

Table 2 CE3 Input value by zones

Input value		Air conditioning space	Non air conditioning space
Preset temperature	Heating	20℃	-
	Cooling	26℃	-
Energy demand for hot water supply		129.84Wh/㎡	-
Lighting	Required illuminance	300lx	100lx
	Power consumption	8W/㎡ (LED Lighting)	10W/㎡

Next, the insulation performance by building zones according to the subject building of analysis was as shown in the Table 3. The values applied for performance analysis was set at the level which is being developed in Korea. Phase 1 is the case of enhancing energy performance of the window by introducing vacuum glass, Phase 2 is the case of improving the insulation performance of the wall by applying new insulating material and External Insulation Finishing System, and lastly the phase 3 is the case of installing Heat Recovery Ventilator with the heat recovery efficiency in 85% and electrically driven exterior awning system outside the window.

The value calculated through these input value is the energy demand of the subject building, and as the next stage, the scale of new & renewable energy facility being introduced to fulfill this energy demand. For the new & renewable energy source to be used, photovoltaic and solar heat were taken into account, which are the largest sources distributed in Korea. The scale of introduced system was estimated using the statistic data[2] on the productions of Korea's new & renewable energy sources.

Table 3 Energy Performance Level by Building Elements

		Exterior Wall	Roof	Window	
				K(W/m²K)	SHGC
General Building[3]		0.36	0.24	3.0	0.6
Low Energy House	Phase 1	0.36	0.24	0.88	0.6
	Phase 2	0.1	0.08	0.88	0.6

[2] Korea Energy Management Corporation, 2009
- solar heat: 0.064toe/㎡·yr (745kWh/㎡·yr)
- photovoltaic: 0.292toe/kW (1,358kWh/kW·yr)

[3] The energy conservation design standards. [Annex 4] heat transfer coefficients for building elements, Chungbu area

	Phase 3	0.1	0.08	0.6	0.15~0.75

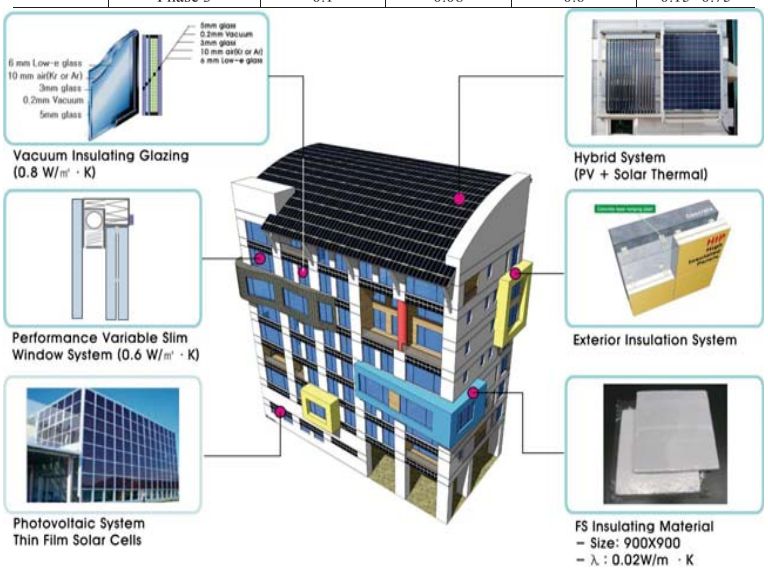


Fig. 2 Empirical Study on Application of Component Technology for the Subject Buildings

3. Results and Discussion

3.1 Energy Performance following Introduction of Component Technology

Results of energy performance evaluation by introducing building component technology by stages through CE3 were clarified as shown in the Table 4 and Figures 3 and 4 illustrate them in graph. As shown in the result, assuming that cooling/heating energy demand of multi-family housing is 100% (166.2kWh/㎡·yr) under the energy saving design standard, if passive component technology is introduced, it becomes 13.6% (22.6kWh/㎡·yr) which means cooling/heating energy demand is reduced by 86.4%. That is, with exterior insulation method and high-performance window applied, it is possible to reduce energy demand of the building by at least 80%. Especially in case of heating energy demand, it was analyzed that it reduces the demand by 90%.

According to the monthly energy demand shown in additional linear graph, in the case of the subject building of comparison, the change in the value of energy demand depending on the season is very low. This represents that the building becomes more independent from outdoor air condition as the energy performance of the building becomes higher.

Table 4 Energy Use of Subject Buildings by Stages

Unit: kWh/㎡·yr

	Standard	Subject Buildings of Comparison		
		Phase 1	Phase 2	Phase 3
Heating	126.1	90.1	18.7	12.5
Cooling	37.8	42.2	20.7	10.1
Total	163.9	132.3	39.4	22.6

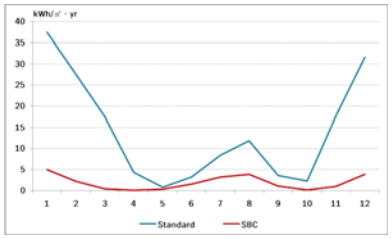


Fig.3 Yearly Cooling/Heating Energy Demand per Unit Area

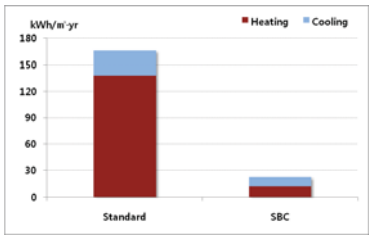


Fig.4 Yearly Cooling/Heating Energy Demand per Unit Area

Next, new & renewable energy facility introduction scale was calculated for the purpose of energy zero at the subject building of comparison. Heating can be covered by the production of hot water supply through solar heat, while cooling was assumed to utilize the power produced by photovoltaic facility. As result of calculating the scale being introduced based on the yearly energy productions by new & renewable energy sources, photovoltaic system in 9 ㎡ is required to meet cooling energy demand in 10.1kWh/m^{2}yr, while solar heat system

capable of 20 m^2 is required to cover heating energy demand in 12.5kWh/m^2yr in order to fulfill energy zero of the building.

3.2 Analysis of CO_2 Emissions Reduction Effect

CO_2 emissions were forecast based on energy demand by the stages of introducing component technology that was already analyzed. CO_2 emissions were calculated through the application of CO_2 conversion coefficient by energy sources. In the case of thermal energy according to domestic statistic data, the consumption of 1toe results in the emission of CO_2 3.178 tons, and 0.4448 ton per MWh for electrical energy. As result of reflecting this in energy demand, if all the component technologies are introduced, CO_2 emissions is found to reach 33% of energy saving design standard. Finally energy demand becomes zero through the introduction of new & renewable energy, and therefore CO_2 emissions from the subject building reaches zero too.

Table 5 Energy Use Reduction Effect by Stages

		Standard	Subject Building of Comparison		
			Phase 1	Phase 2	Phase 3
Energy Demand	Heat (toe)	12.89	9.21	1.91	1.28
	Elec. (MWh)	44.98	50.22	24.63	12.02
CO_2 emission (tCO2)	Heat	40.97	29.27	6.08	4.06
	Elec.	20.01	22.34	10.96	5.35
	total	60.98	51.61	17.03	9.41

4. Conclusions

Energy demand of the building was analyzed to be reduced by 86.4% through the introduction of passive component technology (high level of insulation, high-performance window, etc.) of the building. In addition, the additional introduction of new & renewable energy facility enables to accomplish zero energy demand from the subject building.

CO_2 emissions of the subject building of analysis can be reduced by 85% when passive component technology is introduced, and the energy demand reaches zero when new & renewable energy facility is applied.

In the following studies, the implementation of zero energy in the multi-family housing house including the feasibility analysis of component technology and the area of new & renewable energy facility to be secured for installation, etc. should be considered.

Acknowledgments

This work was supported by the Korea Research Council for Industrial Science and Technology funded by the Korea government (Ministry of Knowledge Economy) (B551179-09-04-00)

References

1. Liping Wang, Julie Gwilliam, Phil Jones, 2009, Case study of zero energy house design in UK, Energy and Buildings 41, pp.1215-1222

2. L. Zhu, R. Hurt, D. Correa, R. Boehm, 2009, Comprehensive energy and economic analyses on a zero energy house versus a conventional house, Energy 34, pp.1043-1053

3. M. Sun-hye, Y. Yong-sang, 2009, A Study on Zero Energy in Multi-House by Applying Renewable Energy Facility, SAREK

4. Promotion of European Passive House (PEP), Passive House Solution, 2006

Velocity Measurement Inside and Outside a Cross-Ventilated Building by Means of PIV

Hisashi KOTANI [1], Tomohiro KOBAYASHI [2], Kaori ASAI [3], Yasue TANAKA [4], and Yasuhiro SHIOZAKI [4]

[1] Department of Architectural Engineering, Osaka University, Suita 565-0871 Osaka, Japan
[2] Dept. of Architecture and Urban Design, Ritsumeikan University, Kusatsu 525-8577 Shiga, Japan
[3] Department of Architecture, The University of Tokyo, 153-8505 Tokyo, Japan
[4] Kanomax Japan, Suita 565-0805 Osaka, Japan

Abstract

Cross-ventilation is regarded to be beneficial control method to obtain thermal comfort in a hot summer without using mechanical devices. Since it is complicated flow phenomenon, details of flow characteristics have not been sufficiently known. The final goal of this work is to establish a new prediction method of flow rate based on energy balance within the stream tube passing through or around the building. To validate numerical results obtained by CFD, they need to be compared with experimental results. This paper presents wind tunnel measurement of flow characteristics inside and outside a cross-ventilated model. Velocity and pressure were measured along the central line of the stream tube for internal flow, and velocity distribution of the external flow was measured by Particle Image Velocimetry (PIV).

Keywords: Cross-Ventilation, Wind Tunnel Test, Particle Image Velocimetry (PIV)

Introduction

The use of renewable energy sources to control internal environment has been attracting practical and academic attentions. Wind-induced cross-ventilation has been beneficial method to moderate hot and humid environment in summer time. To design a building where cross-ventilation functions well, flow characteristics such as flow rate, flow pattern and flow movement must be considered in advance. As Ishihara [1] pointed out, the conventional prediction method of the flow rate based on the orifice equation cannot work for the large opening. This is due to that, for cross-ventilation phenomena, the resistance coefficient of an opening cannot be precisely estimated by the chamber method and the driving pressure cannot be altered by wind pressure coefficient either (see Kobayashi et al. [2]). Ishihara [1] explained this problem as *Interference* of openings and tried to evaluate the overall resistance by introducing *Interference coefficient*. Sandberg [3] introduced geometrical parameter named Catchment area, which can also be regarded as dimensionless flow rate, and showed the relationship with porosity defined as opening area divided by wall area. Kotani and Yamanaka [4] followed Ishihara′s interference coefficient and also proposed a prediction method where vectors normal to the opening and parallel to the wall are added to obtain overall resistance coefficient. Murakami et al. [5], Kato [6] showed the concept of an alternative prediction method based on energy balance inside the selected stream tube passing through/around the building (i.e. power balance model). Axley et al. [7] also showed almost the same principle and formulated the multi-zone flow network model. These prediction concepts seem to be rational because of considering actual phenomenon. However, details of the flow characteristics in the stream tube have not sufficiently been clarified. The final goal of this work is to establish a new prediction method based on energy balance inside the stream tube. To analyze stream tube Computational Fluid Dynamic (CFD) seems to be useful.

The authors have studied power transportation within stream tube for a single room model (see Kobayashi et al. [8]). In this paper, a building model supposed to be composed of nine single-room residences is analyzed. Given the validation of the numerical results that will be obtained by CFD, the flow quantities must be known in advance by means of wind tunnel experiment as the correct value of the calculation. Nishimoto et al. [9] investigated the flow characteristics of a single cross-ventilated room model by means of Particle Image Velocimetry (PIV) system and CFD. This paper pays attention to the airflow around a cross-ventilated building, which includes the complicated flow field as separation and relatively large wake region. It focuses on both internal and external flows of the building model. As for the former, velocity and static pressure are measured along the central line and turbulent kinetic energy is also estimated by anemometer and pressure tube, and the latter, 2-D velocity distribution are obtained using PIV system. In addition to providing qualitative information of the cross-ventilation flow field, these results are to be compared with CFD results that have been obtained in the following work presented by Asai et al. [10].

Method

A closed-circuit wind tunnel in Osaka University whose length, depth, height of the working section was 9.5m, 1.8m, 1.8m respectively was used for the measurement. Fig.1 shows the studied building model which is supposed to be composed of nine one-room residences where central one is provided with two openings on opposite sides. Here, shaded area indicates the attachable orifice plates provided with an opening of which resistance coefficient based on the chamber method is already known (see Kotani and Yamanaka [4]). As studied cases, the side length of the openings (L) was changed as 15, 30, 45, 60, and 90 mm. To analyze fundamental cross-ventilation flow and to see its variation corresponding to the opening size, the test model was located at the center of the wind tunnel with the wind direction perpendicular to the opening. The test model was exposed to a free flow of 10 m/s to keep Reynolds number sufficiently high, where turbulent intensity was approximately 1.0 %. As the reference static pressure in the wind tunnel, that of a Pitot tube installed at the location of 300 mm away from the wall of the wind tunnel was adopted.

As an analysis of the stream tube passing through the room, velocity and static pressure were measured along the central line of the openings. The velocity measurement was conducted by using I-type hot wire anemometer with its sampling frequency and sampling time 1,000 kHz and 30 seconds respectively considering estimation of the turbulent statistics. As for the static pressure measurement, a handmade static pressure tube was used with its sampling frequency 100 Hz for 30 seconds. Both probes are depicted in Fig.2. The probe was attached to an arm provided with a support pole fixed to a 1-D traverser. Velocity and static pressure were

measured between the points of X=-150 and X=1100 mm basically at every 10 mm. In the vicinity of two openings, however, this interval was changed to be 5.0 mm assuming the abrupt variation in pressure and velocity. Fig.3 shows the experimental set-up of the measurement.

Analysis of the external stream tube passing around the building was done using PIV system. PIV is a measurement technique obtaining an instantaneous velocity by detecting the length of spatial shift of seeding particles between two photographs taken within a known time interval. Fig.4 illustrates the experimental set-up. A smoke generator was used and the seeding particles were injected into the wind tunnel through the nozzle. A double-pulse Nd : YAG laser was located outside of the wind tunnel and a laser sheet was radiated to the central section of the model horizontally. A CCD camera was installed above the model. Time interval of two pulses were set at 200 μs with a frequency of 4.0 Hz for 25 seconds. Thus, 100 pairs of photographs were taken to obtain time-average velocity by exactly synchronizing with laser pulses under the control of PIV program operated by PC. Since the wake region was supposed to be large due to the relatively large façade area, both model vicinity and the wake regions were analyzed separately by taking photograph for each region as shown in Fig.5. In estimating velocity, FFT cross-correlation method (Willert [11]) was applied. In addition, to improve the statistical reliability and spatial resolution, the recursive correlation method (Hart [12]) was also adopted. Table 1 summarizes the setting of PIV measurement.

Results and Discussions

Flow quantities along central line

Fig.6 shows the static pressure, X-component of the velocity, and turbulent kinetic energy along the central line of the openings. Shaded area indicates the model and X-axis is the distance from inlet opening divided by the model length. Static pressure was expressed as dimensionless pressure by divided by the total pressure far upstream of the model. The velocity is also dimensionless value where reference velocity is obtained by Pitot tube assumed to be the same as approaching flow. To estimate turbulent kinetic energy, each component of fluctuating velocity was assumed to be the same as;

$$k = \frac{1}{2}(\overline{u'^2} + \overline{v'^2} + \overline{w'^2}) = \frac{3}{2}\overline{u'^2}$$

Assuming that I-type hot wire was measuring two components of velocity, turbulent kinetic energy was estimated based on instantaneous velocity reading ($v'_{hotwire}$) as;

$$k = \frac{3}{2}(\frac{1}{2}\overline{v'^2_{hotwire}}) = \frac{3}{4}\overline{v'^2_{hotwire}}$$

In general, the static pressure increases in front of the model according to the Bernoulli's principle, where velocity becomes small due to the impingement on the windward wall. In the

case of smallest opening, dimensionless static pressure becomes almost 1.0, which means a large part of dynamic pressure of the approaching flow is converted into static pressure without any energy loss. In the case of L=90 mm, meantime, dimensionless static pressure is approximately 0.8, which indicates that the dynamic pressure remains to some extent at the inlet opening. Correspondingly, the lowest velocity value obtained by hotwire differs according to the opening size. After flowing into the room, lower static pressure can be seen inside the room, and large opening case tends to show lower pressure. Considering this pressure drop is regarded as energy loss and conversion into the dynamic pressure, large openings exhibiting large pressure drop generates larger velocity because energy loss seems to become small. Measured dimensionless velocity also exceeds 1.0 except the case of L=15 mm. The case of L=90 mm shows pressure recovery inside the room. Whereas small openings generate a "jet" flow type, this tendency indicates that the dominant stream tube is formed and its cross-sectional area gradually varies. Moving to the leeward side of the model, any significant difference cannot be seen in static pressure among all cases. On the other hand, importantly, velocity extremely differs. The authors have shown that the negative static pressure could become small on the leeward side when the openings are large, where the wake was blown away and no backflow exists on the leeward (see Kobayashi et al. [2][13]). Here, it must be noted that I-type hotwire anemometer cannot measure negative velocity but absolute value. As referred to hereinafter in discussing PIV results, a backflow in the wake can be seen in all the cases studied here. From these results, it can be said that the static pressure on the leeward depends only upon whether or not the wake is blown away.

To analyze turbulent statistics is also important for understanding phenomenon and for studying accuracy of CFD analyses simulating these experiments. Almost no turbulent kinetic energy is produced on the windward side and no significant difference is seen inside the model either. However, there exists notable difference on the leeward side. Although all results show the sharp peak relatively close to the model after discharged from opening, the location is shifted in leeward direction as openings become large. As is seen in velocity vector plots obtained from PIV, the discharged flow collides to the backflow in the wake here, and consequently turbulent kinetic energy is produced. This peak is followed by a moderate increase, and in all cases, the second peak is seen downstream where X-axis is approximately 5.0. A conceivable phenomenon that caused this correspondence of location is confluence of the external flow passing around the test model. From these outcomes, it is believed that the second peak indicates an end of the leeward wake whose size is determined mostly by façade area regardless of the strength of the discharged flow as far as backflow exists on the leeward side. In such a flow field, static pressure on the leeward side is independent of opening size.

External flow field obtained from PIV measurement

Fig.7 shows the velocity vector plots obtained from PIV measurement, where vector plots are omitted to show only one eighth of them are shown. Although obtained velocity inside a room is not reliable due to the light reflection and transmission, this measurement was conducted to analyze external flow; mainly separation and the wake that could have complicated flow characteristics. The angle of separation around the windward corner of the model seems to be almost the same among all cases, and consequently flow pattern in the external flow becomes almost the same. This is due to that the façade area is sufficiently large if compared with opening area. Therefore, the location of the confluence point which seems to exist further downstream is believed to be almost the same.

As for the discharged flow, the collision to the backflow is clearly seen in the wake, as is not confirmed by hotwire measurement. It can also be confirmed that the X-axis of this collision points corresponds to that of the sharp peak in turbulent kinetic energy. Throughout these wind tunnel tests, the qualitative flow characteristics have clarified except static pressure distribution around the model which is also important for power transportation inside the stream tube. This must also be measured by another method. In order to analyze the stream tube passing through/around the building numerical study seems to be essential because it can determine streamlines and provide spatial distribution of velocity and pressure. The wind tunnel experiments introduced in this paper are also simulated by CFD analysis and those results are compared with experimental results presented in this paper to validate CFD in analyzing the stream tube in future work (see Asai et al. [10]).

Conclusions

The authors aim to establish an improved prediction method of the flow rate in cross-ventilation based on energy balance inside the stream tube passing through/around the building based on CFD analyses. This paper presented the wind tunnel experiments analyzing internal and external flow; i.e. measurement of flow quantities along the central line and PIV measurement around the building model, of which purpose is to obtain correct results to be compared with CFD and to understand fundamental flow characteristics in cross-ventilation. From the viewpoint of latter purpose, the following conclusions have been acquired.

1. The size of the wake generated on the leeward side including backflow is determined mostly by building shape (e.g. aspect ratio of length based on façade area to building depth) and independent of opening size.
2. When there exists the wake including backflow, static pressure on the leeward side becomes almost the same when opening size is different despite that the velocity retained by discharged flow can extremely differs; i.e. it is whether or not the wake exists that determines leeward static pressure.

3. The peaks of turbulent kinetic energy can be good indicators of the collision point of discharged flow and backflow, and confluence point of external flow passing around the building.

4. In the case of large openings, quite large static pressure drop occurs in flowing into a room and the velocity becomes large inside. For such internal flow, dominative stream tube is formed and the conventional prediction of flow rate seems not to work appropriately.

This paper presented fundamental flow characteristics in cross-ventilation phenomenon by means of wind tunnel test. Given the analysis of the power transportation inside the stream tube for a new prediction method, CFD analyses of these experiments were also conducted. As a future prospect of this work, after studying the accuracy of the calculation (Asai et al. [10]), the stream tube is to be determined, and the transported power on the sections of stream tube and energy loss inside the control volume are to be analyzed based on CFD.

Acknowledgment

This work was partly supported by Grant-in-Aid for JSPS Fellows (representative T. Kobayashi (20-912)), Japan Society for the Promotion of Science, 2009.

References

1. Ishihara M., "Building Ventilation Design", Asakura shoten, 1969. (In Japanese)

2. Kobayashi T., Sagara K., Yamanaka T., Kotani H., Takeda S., and Sandberg M., "Stream Tube based Analysis of Problems in Prediction of Cross-Ventilation Rate", *The International Journal of Ventilation*, Vol.7, No.4, pp.321~334, 2009.

3. Sandberg M., "Airflow through large openings – A catchment problem?" *Proceedings of ROOMVENT 2002*, pp.541~544, Copenhagen, Denmark, 2002.

4. Kotani H. and Yamanaka T., "Interference coefficient for discharge coefficient in prediction of wind-driven cross ventilation rate through large openings", *Proceedings of the 29th AIVC Conference*, Vol.3, pp.27-32, Kyoto, Japan, 2008.

5. Murakami S., Kato S., Akabayashi S., Mizutani K., Kim Y. D., " Wind Tunnel Test on Velocity Pressure Field of Cross-Ventilation with Open Windows", *ASHRAE Transactions*, Vol.97, Part 1, pp.525-538, 1991.

6. Kato S., "Flow Network Model based on Power Balance as Applied to Cross-Ventilation", *The International Journal of Ventilation*, Vol.2, No.4, pp.395-408, 2004.

7. Axley J.W., and Chung D. H., "POWBAM0 Mechanical Power Balances for Multi-zone Building Airflow Analysis", *The International Journal of Ventilation,* Vol.4, No.3, pp. 95-112. 2005

8. Kobayashi T., Sagara K., Yamanaka T., Kotani H., Takeda S., and Nishimoto N., "Power Transportation Analysis inside Stream Tube of Cross-Ventilated Building", *Proceedings of the 29th AIVC Conference*, Vol.1, pp.249-254, Kyoto, Japan, 2008.

9. Nishimoto N., Sagara K., Yamanaka T., Kotani H., Kobayashi T., and Takeda S., "Measurement of total pressure, static pressure and wind velocity around cross-ventilated building", *Proceedings of the 29th AIVC Conference*, Vol.1, pp.237-242, Kyoto, Japan, 2008.

10. Asai K., Kotani H., Kobayashi T., Yamanaka T., and Momoi Y., "Experimental Investigation and Accuracy Study of CFD Analysis for Airflow around Cross-Ventilated Building", *Submitted to the 31st AIVC Conference*, Seoul, Korea, 2010.

11. Willert C. E. and Adrain R. J., "Digital Particle Image Velocimetry", *Experiments in Fluids*, Vol.10, No.4, pp.191-215, 1991.

12. Hart D. P. “Super-Resolution PIV by Recursive Local-Correlation”, *Journal of Visualization*, Vol.3, No.2, pp.187-194, 2000.

13. Kobayashi T., Sagara K., Yamanaka T., Kotani H., and Sandberg M., “Wind Driven Flow through Openings – Analysis of the Stream Tube”, *The International Journal of Ventilation*, Vol.4, No.4, pp.323-336, 2006.

Table 1 Setting of PIV

Camera Frame Size	625 mm × 471 mm 1,376 pixel × 1,040 pixel
Program	Davis 7.2
Algorithm	FFT Cross-Correlation Method (Recursive Correlation Method)
Interrogation Window Size	Pass 1 : 64 pixel × 64 pixel Pass 2 : 32 pixel × 32 pixel Pass 3 : 32 pixel × 32 pixel
Overlap	50 %
Total Numver of Vectors	5,590 (86×65)
Time Interval of Pulse	200 μs
Sampling Frequency	4.0 Hz
Sampling Time	25 seconds
Laser Output	50 mJ / Pulse
Seeding Size	0.3 - 1.0 μm

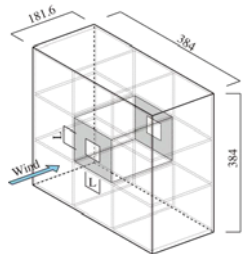


Fig.1 Model configuration

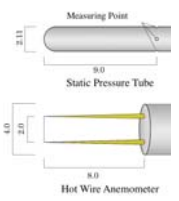


Fig.2 Probe head

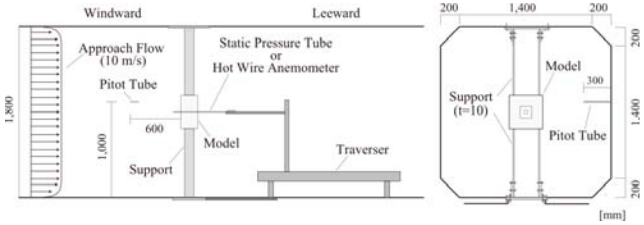


Fig.3 Experimental set-up of the measurement along the central line

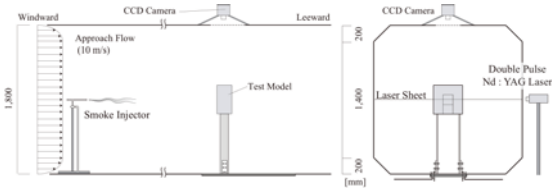


Fig.4 Experimental set-up for PIV measurement

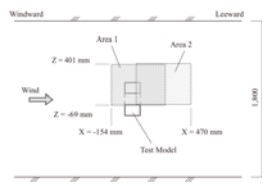


Fig.5 Measured regions in PIV

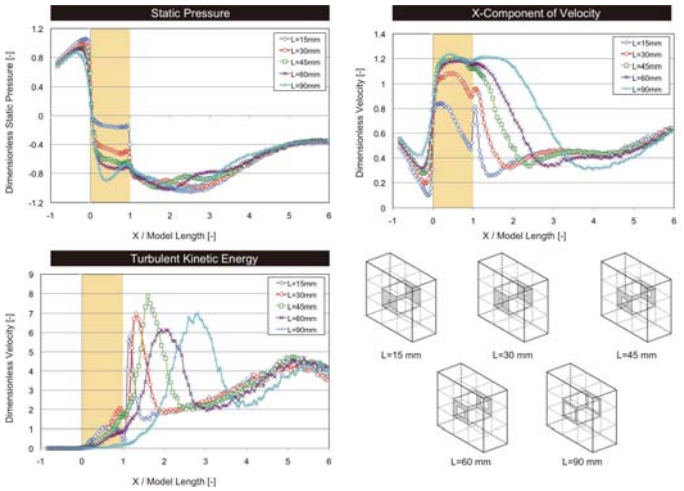


Fig.6 Flow quantities along the central line of the openings

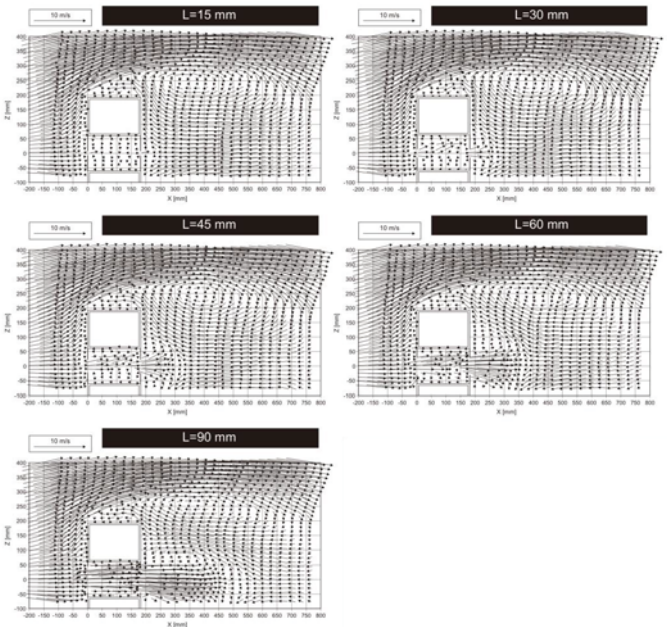


Fig.7. Velocity Vector Plots obtained from PIV

Building simulation on utilization of roof window in detached house by using cross-ventilation

Masaaki OHBA[1], Kenji TSUKAMOTO, Takashi KURABUCHI[2] and Toshihiro NONAKA[3]

[1] Tokyo Polytechnic University, Department of Architecture, 1583, Atsugi-city, Kanagawa, Japan 243-0297
[2] Tokyo University of Science, Tokyo, Japan
[3] Tostem Corporation, Tokyo, Japan

Abstract

The effects of roof window on ventilation flow rates and reduction of cooling loads in densely populated areas were investigated by using building simulations. In May of the intermediate season, when utilizing roof window, the cumulative number of air exchanges increased by 9 % to 12 % compared to that when the windows at side walls remained open only during the daytime. When the building coverage ratio increased from 0 % to 20 %, the cumulative number of air exchanges decreased and the cumulative cooling loads increased. However, when the building coverage ratio increased from 20 % to 40 %, the cumulative number of air exchanges and cooling loads remained almost the same.

Keywords: roof window, cross-ventilation, building simulation, ventilation flow rate, cooling load, local dynamic similarity model(LDSM), COMIS, TRNSYS

Introduction

Cross ventilation is accepted as one of the effective energy conservation techniques. However, in densely built-up residential area such as Tokyo, it is not clear whether this approach can

fully account for the beneficial effects with windows set on wall. It is believed that the influence of building coverage ratio on cross-ventilation could be improved by using roof void opening. Thus, there is a possibility that roof window plays an effective role for cross-ventilation in the area of high building coverage ratio. The objective of this study is to evaluate the advantage of roof window for cross-ventilation in the area of high building coverage ratio.

Simulation Outline

Simulation codes

The calculations of ventilation flow rate and cooling load for a detached house were performed by using a COMIS-LDSM model with a combination of TRNSYS thermal multizone building model. The Local Dynamic Similarity Model (LDSM) gives valuable information on inflow/outflow angles at openings[1]. The ventilation flow rates were calculated by the fundamental formulas (1) to (3) of the LDSM in Table 1. Fig.1 outlines the COMIS-LDSM model and the TRNSYS model[2, 3, 4]. The COMIS code was revised on the basis of LDSM model to calculate the discharge coefficients and airflow rates at inflow/outflow openings. Wind pressure (P_w), tangential dynamic pressure (P_t) and ventilation performances of inflow/outflow openings were provided as input data. Arbitrary room pressure (P_R) was given as an initial condition, and a discharge coefficient corresponding to P_R* was selected from the ventilation performance curve. The calculation was repeatedly conducted with different room pressures until ventilation flow rates of outflow and inflow in each room were balanced.

Residential house model

A typical residential house model[5] defined by the Architectural Institute of Japan was used as an object model. The residential house, cf. Fig.2 and Fig.5, has five rooms; a Living/Dining Room, a Kitchen and 3 bedrooms with a total floor area of 120 m^2, and it is assumed for a family comprising a couple with two children. It was also assumed that the building was insulated according to the next-generation energy saving standards. The residential house model was selected due to the results obtained from a survey by Nakamura et al. in 2000 for the special 23 wards of Tokyo[6]. The survey indicated that there were many two-story buildings which accounted for about 70 % of all buildings, and buildings of 100 m^2 or less for about 80 % of all buildings. The size of roof window is assumed 600mm×600mm. The ventilated space of the entire house is 229 m^3.

Meteorological conditions

The characteristics of meteorological factors in Tokyo were analyzed by using the extended AMeDAS weather data of the standard year. The analysis period was commenced in May including the intermediate season. The hourly mean temperature was recorded between 16.4 °C and 22.3 °C. The relative humidity was 51 % to 73 %. When the wind speed was adjusted to that at the eaves height (5.9 m) of the detached house, the measured mean wind speed was between 1.3 m/s and 2.4 m/s. Southwest winds accounted for 20 % of the period when occupants were asleep, and south to southwest winds accounted for 50 % of the period when occupants were awake.

Building coverage ratios

In the survey done by Nakamura et al. in 2000, the gross building coverage ratio was found from 10 % to 50 % in the central part of Tokyo, and 90 % of that ranged from 15 % to 40 %. The building coverage ratios in this study were therefore set to 0 %, 20 % and 40 %. The wind pressure on an opening (P_w) and the tangential dynamic pressure (P_t) were obtained beforehand from a 1/100 scale model used in a wind tunnel experiment. Dummy models with identical configuration around the object model were arranged. The reference height was set at the eaves height of 5.9 m. The wind profile had a power index of 0.25 as shown in Fig.3. It was assumed that the ventilation performance of rectangular openings was in accordance with the results of Ohba et al. (2008), and the discharge coefficients of room doors were set to 0.63. The effects of adjacent building shadows that may reduce solar radiation loads in the house were, however not taken into account.

Outline of the simulation logic of window and air-conditioning operation

The decision tree of operation of cooling and windows is shown in Fig.4. Fig.5 shows the operation of opening and closing openings in the house[8]. The logic of opening/closing windows was applied to the windows and doors in the habitable rooms and the hall. Four cases were simulated as shown in Table 2. For Case 1, we only used the logic of turning on/off air-conditioners with all windows closed. For Case 2 and Case 3, the basic logic of opening/closing windows was used. Windows were opened in occupied rooms when the temperature exceeded 24 °C and closed when the temperature dropped below 23 °C. Windows were closed when all family members either asleep or when the rooms were not occupied. For Case 4, the active logic of opening/closing windows was used. Even when residents were asleep, we opened the windows 20 % when the room temperature exceeded 24 °C and closed them when the temperature dropped below 23 °C. Doors in habitable rooms

were opened when the windows were opened and the doors were closed when the air-conditioners were turned on and/or the windows were closed.

The schedule of persons at home is shown in Table 3, proposed by AIJ. The same pattern was used during weekdays and weekends. It was assumed that the house was not occupied from 14:00-16:00 and the family was asleep from 23:00-6:00. It was also assumed that the Japanese room and the spare room were unoccupied all the time. According to the logics, the windows were opened and closed, and the air-conditioners were turned on and off at a 15-minute interval according to the temperature of each room.

Simulation results

Cumulative number of air exchanges in entire residential house

Fig.6 shows the cumulative number of air exchanges, which is defined as the number of time that the entire air volume in house changes with outside air. When the building coverage ratio was 0%, i.e. utilizing roof window in Case 3, the cumulative number of air exchanges increased by 9% compared to that of Case 2 when the windows remained open only during the daytime. If the windows remained 20% open and the duration of opening was kept longer, even during the time while occupants were asleep in Case 4, the cumulative number of air exchanges increased by 24 % compared to that of Case 2.

When the roof window was opened (Case 3) with a building coverage ratio of 20%, the cumulative number of air exchanges increased by 12% compared to that of Case 2. When the windows remained 20% open (Case 4), the cumulative number of air exchanges increased by 27 % compared to that of Case 2.

For the case with building coverage ratio of 40%, the cumulative number of air exchanges decreased compared with that when the building coverage ratio was 20%. When roof window was opened (Case 3), the cumulative number of air exchanges increased by 8% compared to that of Case 2. When the windows remained 20% open (Case 4), the cumulative number of air exchanges increased by 21 % compared to that of Case 2.

Cumulative hours of air-conditioner operation time in entire residential house

Fig.7 gives the cumulative air-conditioner operation time of the entire house. For the case of 0% building coverage ratio, it required 360 hours when the windows were closed (Case 1). The cumulative air-conditioner operation time reduced by 43% when the windows were kept

open (Case 2). However, the effect of roof window in Case 3 was very small. When the windows remained 20% open (Case 4), it was reduced by 46%.

For the case of 20% building coverage ratio with the side windows remained open, the cumulative air-conditioner operation time was reduced by 42%. However, the effect of roof window (Case 3) was the same as that with a building coverage ratio of 0%. When the windows remained open 20% (Case 4), the cumulative air-conditioner operation time was reduced by 46%. However, when the building coverage ratio increased from 20 % to 40 %, the cumulative air-conditioner operation time remained almost the same as that with a building coverage ratio of 20%.

Cumulative cooling load in the entire residential house

As shown in Fig.8 and Table 4, with a building coverage ratio of 0%, the cumulative cooling load required 163 kWh when the windows remained closed (Case 1). When the side windows remained open (Case 2), the cumulative cooling load was reduced by 37 % compared to that of Case 1. The effect of roof window (Case 3) was not much significant, cf. Fig.7 and Fig.8. When the windows remained 20 % open (Case 4), the cumulative cooling load was reduced by 42 %.

For the case of 20% building coverage ratio with the side windows remained open, the cumulative cooling load was reduced by 28% compared to that of Case 1. When the windows remained 20 % open (Case 4), the cumulative cooling load was reduced by 38%. However, it remained almost the same even when the building coverage ratio increased from 20 % to 40 %.

Conclusions

We evaluated the effects of roof window on ventilation flow rates and reduction of cooling loads, according to different building coverage ratios by using the COMIS-LDSM model and the TRNSYS model.

- In May of the intermediate season, when utilizing roof window, the cumulative number of air exchanges increased by 9 % to 12 % compared to that when the side windows remained open only during the daytime.
- When the windows remained 20% open at night, the cumulative number of air exchanges increased by 21 % to 27 % compared to that when the windows remained open only during the daytime.
- The cumulative number of air exchanges decreased when the building coverage ratio increased from 0 % to 20 %. However, it remained almost the same even when the

building coverage ratio increased from 20 % to 40 %.

- The cumulative cooling load in the entire house, when the windows remained open in occupied rooms, was reduced by 28 % to 31 % compared to that when the windows remained closed completely. When the side and roof windows remained 20 % open at night, the cumulative cooling load was reduced by 36% to 40 % compared to that in Case 1.
- With a building coverage ratio of 20%, the reduction of cumulative cooling loads by roof window increased by 4% compared to that of the side windows.

Acknowledgments

This study was partially supported by the Korea-Japan Basic Scientific Cooperation program of JSPS ("Optimization Study on the Evaluation and Development of the Ventilation Design Criteria for Constructing the Future Zero-Energy Town," headed by Professor Masaaki Ohba, Tokyo Polytechnic University from 2008 to 2012)

Nomenclature

A	opening area
C_d	discharge coefficient
C_{dS}	basic discharge coefficient
Q	ventilation flow rate
P_R	room pressure
P_R*	dimensionless room pressure
P_{RS}*	dimensionless room pressure in case of $C_d = C_{dS}$
P_t	dynamic pressure tangential to opening
P_W	wind pressure
U_0	reference wind velocity at eave (=7m/s)
λ	building coverage ratio
n	power exponent
ρ	air density
Z_m	height of model
Z_p	height of proto type

References

1. Kurabuchi T, Ohba M, Endo T, Akamine Y and Nakayama F., Local dynamic similarity of cross-ventilation, Part 1 Theoretical framework, *International Journal of Ventilation*, Vol.2, No 4, 2004, pp.371-382.

2. Ohba M., Tsukamoto T., Kurabuchi T., Goto T., Nonaka T. and Endo T., Study on energy conservation effects of wind-induced ventilation in detached house using coupled simulation of semi-empirical ventilation model and network models, *Proceedings of 29th AIVC Conference*, Vol.3, 2008, pp.21-26.

3. Ohba M., Kurabuchi T., Tsukamoto K., Nonaka T. and Goto T., A simulation study on the reduction of cooling loads in a detached house by cross-ventilation using the local dynamic similarity model, *The International Journal of Ventilation*, Vol.8, No 3, 2009, pp.251-264.

4. Tsukamoto K., Ohba M., Kurabuchi T., Nonaka T. and Goto T., Study on reduction of cooling loads in detached house by cross-ventilation using coupled simulation of semi-empirical ventilation model and network models, Proceeding of the 11th International Conference on Air Distribution in Rooms, Korea, 2009, pp.1541-1548

5. Udagawa H., Typical problems for house, 15th Heat Symposium, AIJ, 1985, pp.49-56 (in Japanese).

6. Nakamura O., Miyashita K., Uematsu Y. and Yamada M., Actual conditions of terrain roughness evaluated from numerical data of structural dimensions in Tokyo, Journal of Wind Engineering, No 84, 2000, pp.59-69 (in Japanese).

7. Architectural Institute of Japan, Expanded AMeDAS weather data, Tokyo, Maruzen, 2003.

8. Nagai T., Windows and HVAC operation to reduce cooling requirement by means of cross-ventilation, International Journal of Ventilation, Vol.5, No 1, 2006, pp.151-162.

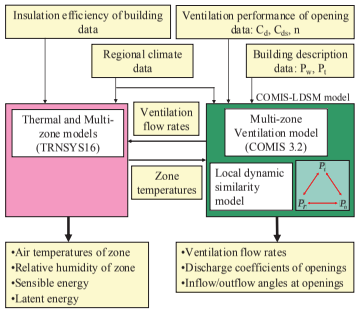


Fig. 1 Block diagram of COMIS-LDSM & TRNSYS model



Fig. 2 AIJ residential house model

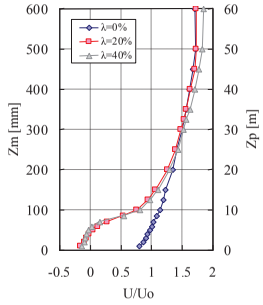
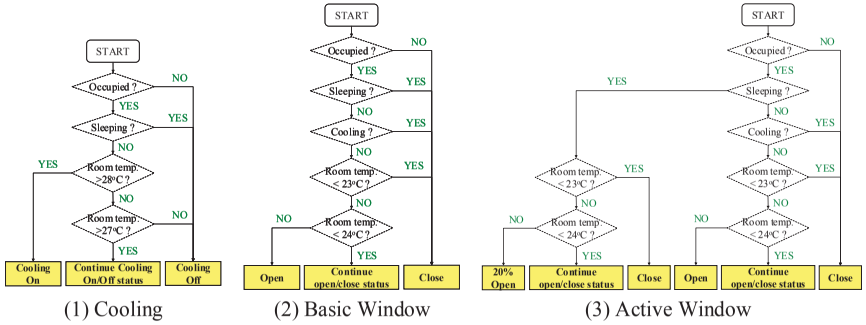


Fig. 3 Wind profile in wind tunnel experiments



(1) Cooling (2) Basic Window (3) Active Window

Fig. 4 Operation of cooling and window

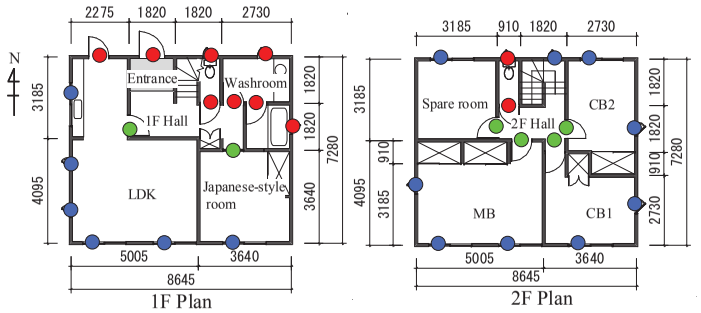


Fig. 5 Location of opening/closing windows

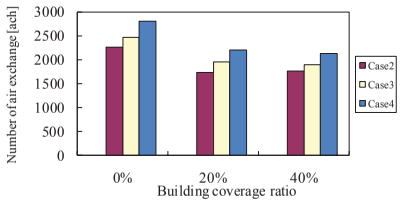


Fig. 6 Cumulative number of air exchanges

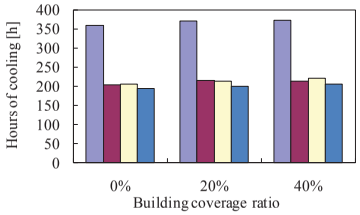


Fig. 7 Cumulative operating hours of air-conditioners

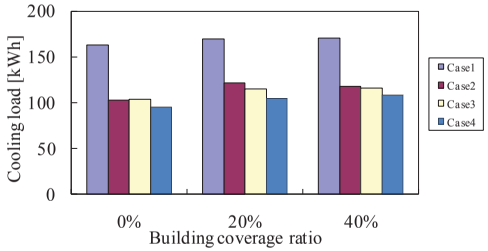


Fig. 8 Cumulative cooling loads

Table 1 Fundamental formulas of local dynamic similarity model

$$P_R^* = \frac{P_R - P_W}{P_t} \quad (1) \qquad Q = C_d A \sqrt{\frac{2}{\rho}|P_R - P_W|} \quad (2) \qquad C_d = C_{dS}\left(\frac{P_R *}{P_{RS} *}\right)^n \quad (3)$$

Table 2 Simulation cases on reduction of cooling loads by cross-ventilation

Case	Air-conditioner operation	Window operation	Window type
1	On/Off	All windows closed	Side windows
2	On/Off	Basic logic of windows Opened/Closed	Side windows
3	On/Off	Basic logic of windows Opened/Closed	Side & roof windows
4	On/Off	Active logic of windows Opened/Closed	Side & roof windows

Table 3 Schedule of occupied time zone

	1	2	3	4	5	6	7	8	9	10	11	12	13	14	15	16	17	18	19	20	21	22	23	24
LDK	0	0	0	0	0	0	1	4	1	1	1	1	1	1	0	0	3	3	3	3	2	2	1	0
MB	2	2	2	2	2	2	1	0	0	0	0	0	0	0	0	0	0	0	0	0	0	0	1	2
CB1	1	1	1	1	1	1	1	0	0	0	0	0	0	0	0	0	0	0	0	0	1	1	1	1
CB2	1	1	1	1	1	1	1	0	0	0	0	0	0	0	0	0	0	0	0	0	1	1	1	1

Table 4 Cooling load reduction ratios of the entire house with each building coverage ratio

Case	λ=0% [kWh]	λ=20% [kWh]	λ=40% [kWh]
Case1	63 (-)	170 (-)	170 (-)
Case2	102 (37.3%)	122 (28.1%)	118 (30.7%)
Case3	103 (36.8%)	115 (32.4%)	116 (32.1%)
Case4	96 (41.5%)	104 (38.4%)	108 (36.3%)

The climatic potential for a double skin facade integrated with cross ventilation

Won-Jun Choi[1], Jae-Wan Joe[1] and Jung-Ho Huh[2]

[1] Graduate Student, Department of Architectural Engineering, University of Seoul, Seoul, 130-743, Korea
[2] Professor, Department of Architectural Engineering, University of Seoul, Seoul, 130-743, Korea

Abstract

When it comes to natural ventilation performance for large space cooling during summer time or intermediate seasons, double skin facade(DSF) integrated with cross ventilation(CV) exhibits more energy efficiency than single-side ventilated DSF. In this case, ventilation performance is remarkably affected by climatic conditions. Therefore, it is important to analyze micro climatic conditions before applying this passive technique.

To date, many studies have been done regarding DSF, however, there are very few studies pertaining to feasibility have existed in Korea. In this paper, a case study of four models with weather data of Seoul was conducted based on the following criteria: existence of DSF, opening/closing modes of the DSF openings, and ventilation types. The results showed that the annual cooling load of the cross-ventilated DSF was less than that of the single-side ventilated DSF by 7.9%, and the ACH of the cross-ventilated DSF was 1.2~6.2 times more than that of the single-side ventilated DSF.

Keywords: Cross-ventilation, Double skin facade, Stack effect, Natural ventilation, Airflow network

1. Introduction

1.1. Background and Purpose

Many architects and clients prefer to implement highly glazed facades for aesthetic reasons or to showcase the transparent image of enterprises(Oesterle et al., 2001). Buildings designed with glass facades exhibit less thermal resistance performance than those with insulated walls and introduce more solar radiation. Considering that office buildings have more occupants and equipments than other buildings, such design characteristics cause higher energy consumption for maintaining an indoor thermal comfort. The double skin facade (DSF) system, which was introduced as an alternative solution to these issues, has become rapidly popular in Europe because not only does it uphold the green image of buildings, it also allows natural ventilation in buildings and performs the role of a thermal buffer space in winter.

Compared to mechanical ventilation, natural ventilation is much harder to control. Therefore, an integrated analysis of the building plan and climatic condition is essential not only to increase energy efficiency but also to create a comfortable indoor environment. The most frequently implemented natural ventilation method used in the DSF system is single-sided ventilation, in which ventilation occurs between the cavity of the DSF and the adjacent indoor space. Single-side ventilated DSF affects only part of the rooms adjacent to the cavity, and yields minimal effect on buildings with deep plan buildings (Straube and Straaten, 2001). Also, the effective depth of external air in single-sided ventilation is limited to 8 m from the opening, at an air velocity of 1 m/s (Gan, 2000). As a result, the effect of natural ventilation in DSF implemented large buildings can be maximized by combining cross-ventilation(CV).

The airflow behavior of single side ventilated DSF is governed mainly by the stack effect caused by the temperature difference. However, the airflow behavior of cross ventilated DSF coupledly depends on stack effect due to solar radiation, wind direction and speed, and operational mode of the upper and lower openings. It has been generally accepted that the ventilation performance is affected largely by the climatic characteristics. Therefore, good DSF design and its performance can be expected only after a thorough analysis of the climatic characteristics of the surroundings.

There have been many DSF studies mainly focusing on the thermal and airflow behavior based on the opening and shading operation modes and the possibility of a load reduction. Most of the studies are on single-sided ventilation and associated with European weather conditions ignoring the humidity effect. However, the humidity must be considered particularly in hot and humid climates such as the summer time in Korea, ventilation performance completely changes from what was considered in previous studies. There have been few studies on the possibility of DSF integrated with CV.

Therefore, this study aims to examine the ventilation performance of DSF combined with CV and its applicability by conducting ventilation performance and building load analysis using a dynamic building energy simulation tool.

1.2. Methodology and procedure

This research was conducted using the following procedure:

(1) Analysis of the factors in the performance of natural ventilation using hourly weather data of Seoul;

(2) Establishment of four models based on the existence of DSF, the opening operational modes in DSF, and the ventilation types;

(3) Simulation of each model based on the weather data analyzed in (1); and

(4) Comparative analysis of the cooling load, ventilation performance, and direction of the airflow for each model.

2. Simulation Tool and Calculation Method

2.1. Airflow network method

Airflow network method evaluates the airflow in a building by assuming airflow as a network of nodes and simplifying the linkage to which airflow passes from one to another node. In the calculation process, the law of conservation of mass is applied to the airflow caused by the pressure difference. While this method can only give quantitative information of airflow and can not offer detailed information of internal air circulation or temperature distribution like CFD, it offers fast evaluation speed.

This study used Airflow Network of EnergyPlus 4.0 for evaluating ventilation performance and applicability of a target model.

2.2. Calculation method

In the airflow network model, each path consists of two nodes, each of which has an inlet and an outlet. Each path is linked by components (i.e., the opening and HVAC system, etc.) that correspond to the airflow and the pressure. If n and m are two continuous nodes, and assuming that the pressure difference between components is governed by Bernoulli's equation, pressure difference can be expressed as below:

$$P = \left(P_n + \frac{\rho v_n^2}{2}\right) - \left(P_m + \frac{\rho v_m^2}{2}\right) + \rho g(z_n - z_m) \quad \text{(Eq.1)}$$

where,

P: The pressure difference between nodes n and m [Pa]

$P_{n,\ m}$: The pressure at nodes n and m [Pa]

ρ: The air density [kg/m^3]

$v_{n,\ m}$: The air velocity at nodes n and m [m/s]

g: The gravity acceleration [Pa]

$z_{n,\ m}$: The height at nodes n and m [m]

If each term is rearranged and the effect of the wind pressure is added, Eq. 1 can be expressed as in the following airflow network model:

$$P = P_n - P_m + P_s + P_w \quad \text{(Eq.2)}$$

where,

P_s: The pressure difference due to the difference of density and height [Pa]

P_w: The pressure difference due to the wind [Pa]

Fig. 1 shows the flowchart of factors that influence airflow distribution in buildings. More detailed calculation algorithm of many components can be found in the COMIS Fundamental Manual (1990) which was the basis of the airflow network implemented in EnergyPlus.

3. Weather Data Analysis

Wind speed and wind direction are important environmental factors in implementing DSF combined with CV. These variables directly affect the wind pressure coefficient of the external surface of a building and must be analyzed before implementing this type of natural ventilation.

The hourly weather data of Seoul used in this study is generated by using the ISO Test Reference Year (TRY) method. This data is based on 20 years data (1985-2005) from the Korea Meteorological Administration (KMA).

Figs. 2 shows the relative frequency of the wind speed and Fig. 3 shows the monthly average wind speed from April to October, when natural ventilation is used. The wind speed of 1-3 m/s occurs most frequently, and the total average wind speed in this period is 2.18 m/s. It is generally believed that wind direction in Korea is northwester in winter due to the Siberian air mass, and the oceanic southeaster in summer. Analysis of the

climatic data used in this study, however, and Yoon's study (2003) on the climatic data collected by the KMA for the 30 years, showed a different result. Fig. 4 shows the relative frequency of each wind direction. The figure shows that the northward wind distribution is relatively more frequent than southward. In natural ventilation that combines DSF and cross-ventilation, most of the DSF is fixed southward to address the stack effect. Therefore, cross-ventilation that introduces outdoor air from the north and exhausts indoor heat to the southward DSF is an effective energy conservation strategy.

4. Simulation

4.1. Simulation model

As shown in Fig. 5, two simulation models were made depending on the existence of DSF. The DSF model in Fig. 5 (a) is again divided into three cases based on the operation mode of the DSF's lower openings and the types of ventilation, as shown in Fig. 6. Table 1 shows the summary of the four cases. Case 1~3 correspond to the model in Fig. 5 (a), and Case 4, to the model in Fig. 5 (b).

The basic information on the target models is in Table 2. Except for the existence of the DSF space, all the models have identical conditions. All the detailed size and structure of model (a) is in Fig. 7. Case 4, in which no DSF was implemented, used ventilation through all the windows, except for the southward curtain-wall facade. The blinds were installed 0.5 m apart from the outer layer of the DSF in Case 1~3, and inside the southward façade in Case 4. The blinds were set to operate under the intensity of solar-radiation over 200 W/m2. It is assumed that the existence of the blinds did not affect airflow in the building.

The thermal characteristics of building envelope, internal heat gain, and HVAC operational conditions are shown in Tables 3, 4, and 5, respectively.

4.2. Control scheme of the opening

Humidity is relatively low in spring and fall in Korea, and does not significantly affect the indoor thermal comfort. However, this can be an important factor in summer. Thus, it is appropriate to apply the enthalpy control scheme, rather than temperature control, to the opening and closing of windows for natural ventilation.

In this study, windows were set to be open, as shown in Fig. 8, when the indoor enthalpy (H_{in}) is higher than the outdoor enthalpy (H_{out}). The windows are fully open at the point of the enthalpy difference between outdoor and indoor (ΔH) is the smallest, and the opening rate decreases proportionally until the ΔH reaches the maximum of 42,000 J/Kg. Regardless of this control scheme, however, the openings of the upper and lower DSF were set to be always open at its maximum from April to October. All the openings are closed during the rest of time period.

5. Results

5.1. Load analysis

Fig. 9 shows the annual cooling loads of the four cases by floor. In all the cases, the profile of the cooling load tends to increase as the floor gets higher. The annual cooling load increased from Case 1 through Case 4 in order.

While the annual total cooling load in Case 1 showed a better result than Case 2, such result is not always the case, as shown in the monthly cooling load in Fig. 10. The cooling load of Case 1 in April and May is less than Case 2, but from June to October, Case 2 exhibits less than Case 1. Case 2, with both the upper and lower openings open, has more airflow rate of cavity zone, and the resulting decrease in the surface temperature in the inner layer of the DSF is believed to have led to the decrease in the cooling load.

The annual cooling loads in Case 1 and 2, in which cross-ventilation was implemented, were less by 7.9% and 5.5%, respectively, than that in Case 3, in which single-sided ventilation was implemented. Cases 1 to 3, in which DSF was applied, showed a decrease in their annual cooling load of as little as 29.4% (Case 3) and as much as 34.9% (Case 1) compared to Case 4, in which the facade was a curtain-wall.

5.2. Analysis of the air change rate (ACH)

Figs. 11 and 12 show the monthly average ACH of the conditioned zone of Cases 1 to 4 between April and October, and the monthly average ACH in the DSF zone in Cases 1 to 3, respectively.

Cases 1, 2, and 4, in which cross-ventilation was implemented, showed a ACH in the conditioned zone that was 1.2 (Case 2 in April) to 6.2 (Case 1 in June) times higher than that in Case 3, in which single-sided ventilation was used. The total average ACH from April to October, when natural ventilation can be used, was highest in Case 1, followed by Cases 2 and 4, each of which showed an average ACH 4.7, 4.2, and 3.7 times higher than that in Case 3, respectively. The ventilation performance was highest in June, and relatively smaller in April and October than in the other months due to the huge difference between the indoor and outdoor enthalpies. The outcome will differ if the ventilation is made without implementing the opening control strategy.

The ACH of the DSF zone was reversed to the amount of ventilation in the conditioned zone. Case 1, with the lower opening closed, showed a lower result than Cases 2 and 3, with both the upper and lower openings open. Such result was also shown in the profile. While the ACH in Case 1 was identical to the profile in Fig. 11, which is the monthly ACH of the conditioned zone. However, the ACH in Cases 2 and 3 were affected by the external wind speed and direction, as analyzed in Figs. 3 and 4, regardless of the ACH profile of the conditioned zone. In other words, the ACH in Case 1 was affected by the opening control strategy based on the temperature and humidity, whereas that in Cases 2 and 3 was affected by the wind speed and direction.

Fig. 13 shows the average ACH in June by floor. The ACH in Cases 1, 2, and 4, with cross-ventilation, exhibited superior ventilation performance compared to that in Case 3, with single-sided ventilation.

The comparison of Cases 1 and 2 showed that the amount of ventilation in Case 1, with the lower DSF opening closed, was larger than that in Case 2. This was due to the air inside the DSF staying longer in Case 1 than in Case 2, thus causing more stack effect. In Cases 1, 2, and 4 with DSF, the stack effect decreased as with the higher stories, and therefore, the amount of ventilation also decreased. In Case 4 without DSF, however, the

amount of ventilation increased as with the higher stories, and this is congruent with the wind speed profile of external boundary.

5.3. Airflow analysis

Fig. 14 shows the airflow between the DSF cavity and the indoor (airflow across the openings of inner layer of DSF), and between the indoor and the outdoor (summation of airflow across the openings of the eastward, westward and northward directions.) A sunny day of June 2nd was selected for this graph.

In the lower floors, the airflow from outdoor to indoor to the cavity is predominant. This is the positive airflow, taking indoor heat into the cavity zone and discharge into the upper opening of DSF. Through this process, the building's cooling load can be reduced. However, as the floor gets higher, the air of DSF cavity flows back to the indoor space (Cavity->Indoor->Outdoor) because of the weakened stack effect. Especially on the fifth and sixth floors, the flow from the cavity to the indoor overwhelms the flow from indoor to cavity. This means the high-temperature air in the DSF cavity reflux to the conditioned zone. This phenomenon is affected not only by height but also by the difference between indoor and outdoor temperature. The air that flows back not only raises the indoor cooling load but also degrades the indoor thermal comfort.

Fig. 15 shows the relative cooling load increase rate of each floor compare to second floor from April to October. In Case 4 without DSF, the cooling load increase rate profile is not as steep as the other cases, whereas the cooling load increase rate in Cases 1 to 3 with DSF increased by a large margin especially fifth and sixth floors. The airflow in the cavity which flows back to indoor is the main reason for the increase of cooling load and this can be a critical factor in the thermal comfort and indoor load. Therefore, it is necessary to conduct research on an appropriate opening control strategy or DSF cavity zoning.

6. Conclusion

This case study of four models with weather data of Seoul was performed based on DSF existence, operational mode of DSF's upper and lower openings, and ventilation types. The conclusions were made as the following.

(1) In large office buildings with DSF, it is more beneficial to implement cross-ventilation than single-sided ventilation for reducing the cooling load.

(2) In natural ventilation combining DSF and cross-ventilation, only the DSF's upper opening exhibited better results than both the DSF's upper and lower openings in terms of the annual cooling load and ACH of the conditioned zone. It is more beneficial, however, to open both the upper and lower openings for the cooling load during summer when there is strong solar radiation.

(3) In multi-story DSFs, the decrease in stack effect on a higher floor not only reduces the amount of ventilation but also increases the cooling load. To prevent this phenomenon, appropriate cavity zoning or a control strategy that reflects the changing environment condition is needed.

Acknowledgments

This work was partially supported by grant no. 07 Urban Renaissance B04 from the Ministry of Land, Transport and Maritime Affairs.

References

1. Oesterle, E. et al., Double-skin facades, New York: Prestel, 2001

2. Straube, J. F., and Straaten, R. V., Technical Merit of Double Facades for Office Buildings in Cool Humid Climates, Building Engineering Group, University of Waterloo, Canada, 2001.

3. Gan, G., Effective depth of fresh air distribution in rooms with single-sided natural ventilation, Energy and Buildings, 31, pp. 65-73, 2000

4. Sinclair, R. et al., Ventilating Façades, ASHRAE Journal, April, 2009

5. Yoon, J. O., The Characteristics of Wind in the 29 cities of Korea, Architectural Institute of Korea, Vol. 19, No. 11, pp. 229-236, 2003

6. Feustel, H.E. and Raynor-Hooson A., COMIS Fundamentals, Air Infiltration and Ventilation Centre, Technical Note 29, Lawrence Berkeley Laboratory Report, LBL-28560, 1990

7. Lixing Gu, Airflow network modeling in EnergyPlus, Proc. Building Simulation, 2007, pp. 964-971, 2007

8. ASHRAE, ASHRAE Handbook Fundamentals. Atlanta: American Society of Heating, Refrigerating and Air-Conditioning Engineers, Inc. 2009

9. DOE, EnergyPlus 4.0 Documentation, US Department of Energy, 2009

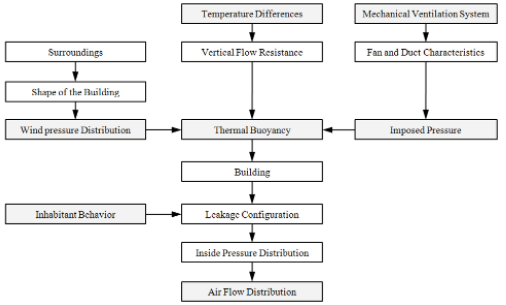


Fig. 1 Influences on the Air-Flow Distribution in Buildings (Feustel 1990)

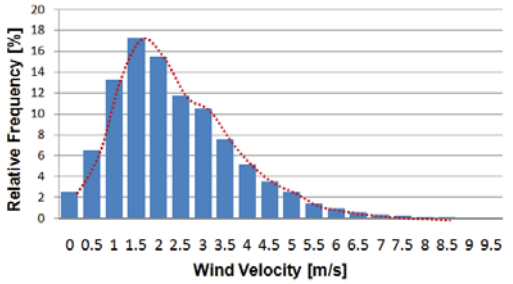


Fig. 2 Relative frequency of wind speed

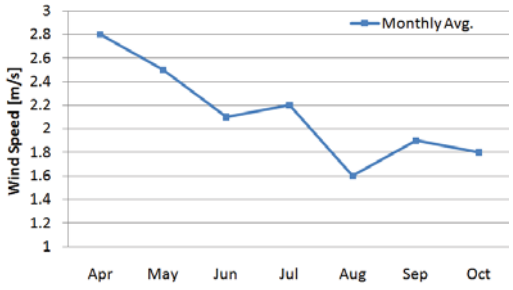


Fig. 3 Monthly average wind speed

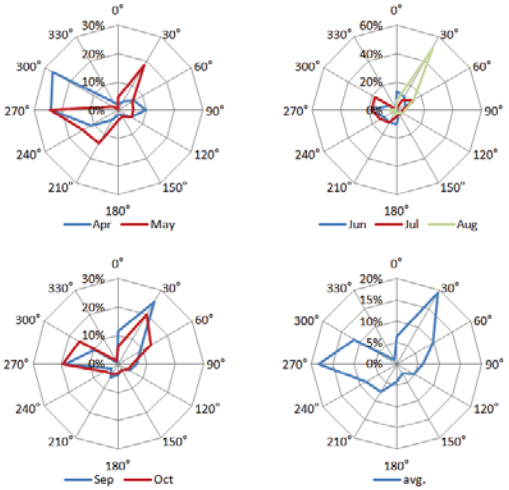
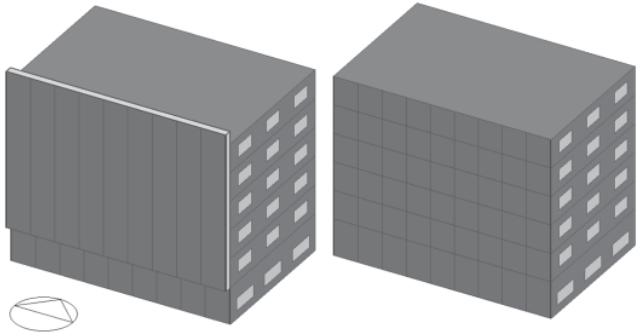
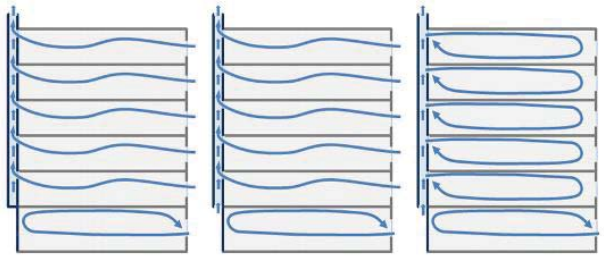


Fig. 4 Relative frequency of wind direction



(a) DSF model (b) Curtain-wall model

Fig. 5 Simulation model



(a) Case 1 (b) Case 2 (c) Case 3

Fig. 6 Conceptual charts of the ventilation types by case

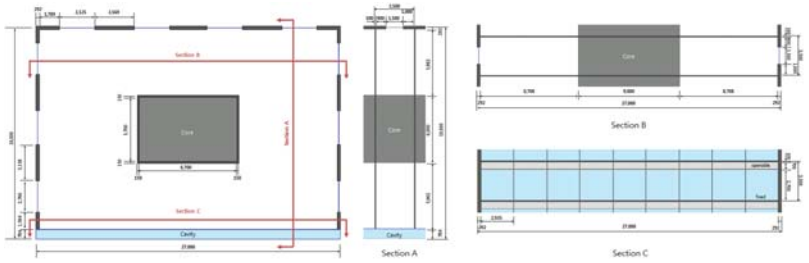


Fig. 7 Floor plan and cross sections

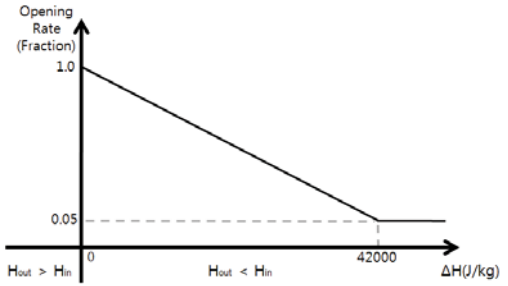


Fig. 8 Opening control strategy

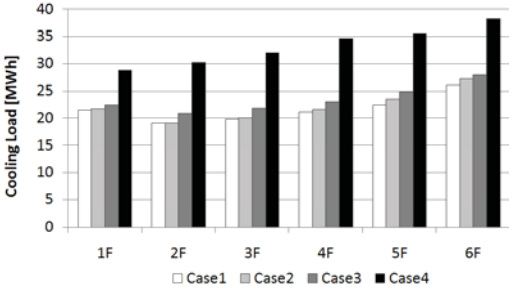


Fig. 9 Annual cooling load by floor

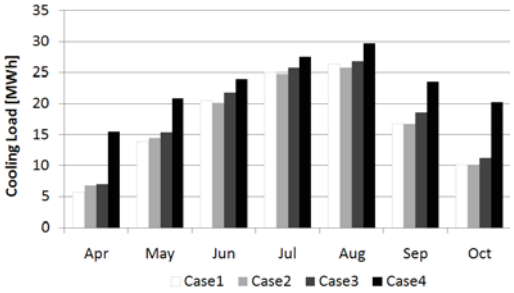


Fig. 10 Monthly cooling load

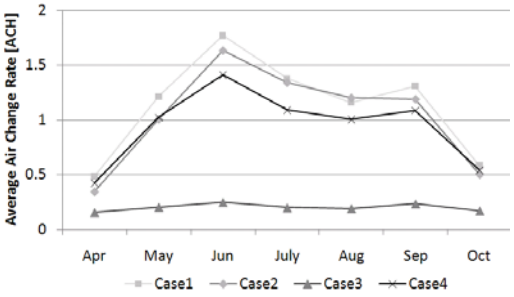


Fig. 11 Monthly average ACH in the conditioned zone

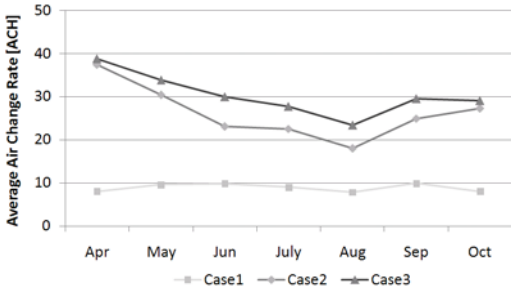


Fig. 12 Monthly average ACH in the DSF zone

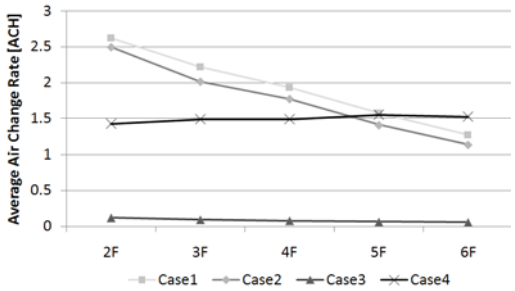


Fig. 13 Average ACH in June by floor

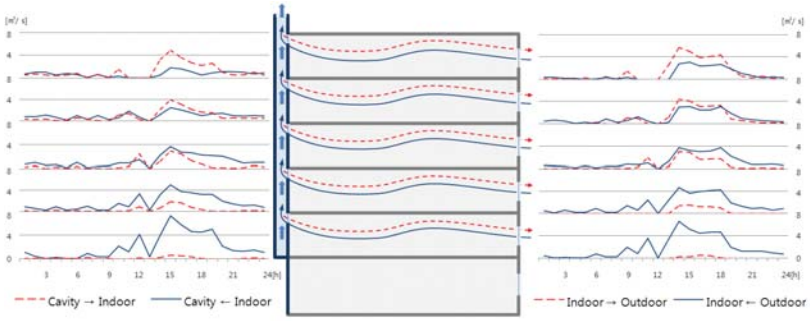


Fig. 14 Airflow between the cavity and the indoor(Left), the indoor and the outdoor(Right)

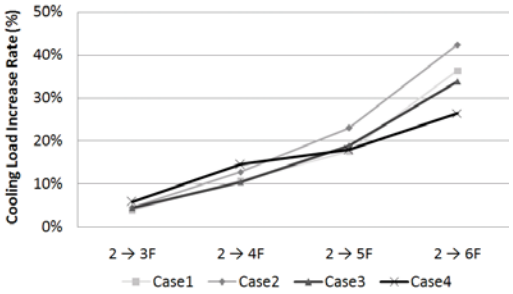


Fig. 15 Cooling load increase rate compare to second floor

Table 1 Simulation cases

Case	DSF	DSF Opening Status	Venting Type
Case1	○	Upper Only	Cross
Case2	○	Upper and Lower Opened	Cross
Case3	○	Upper and Lower Opened	Single
Case4	×	-	Cross

Table 2 Basic information on the model

Stories	6F
Height	22 m+1.5 m(DSF)
Total Building Area	2898.93 ㎡
Net Conditioned Area	2548.78 ㎡
Width of the Air Cavity	784 mm

Table 3 Thermal properties of the simulation model

Component		Thickness (mm)	SHGC	U-Value (W/㎡·k)	Solar Transmittance	Solar Reflectance
Roof Ground Floor		350	-	0.25	-	-
Exterior Wall		292	-	0.35	-	-
DSF	Outer	6-(Clear)	0.810	6.121	0.775	0.071
	Inner	6-(Low-e) 13-(Air) 6-(Clear)	0.563	1.772	0.474	0.17 - 0.071
Outer window		6-(Low-e) 13-(Argon) 6-(Clear)	0.564	1.499	0.474	0.17 - 0.071
Blind		1	0.9*		0.3	0.3

*Thermal Conductivity (W/m·k)

Table 4 Indoor heat gain

People	10W/㎡	Based on ASHRAE Fundamentals (2009)
Equipment	10.76W/㎡	
Lighting	11W/㎡	

Table 5 HVAC operation

	Summer	Winter
Set Point Temperature	26℃	21℃
Period	Apr～Oct	Nov～Mar
Operation Time	08:00～18:00	

Robustness and True Performance of Demand Controlled Ventilation in Educational Buildings – Review and Needs for Future Development

[1,2] Mads Mysen, [2] Peter Schild, [1] Finn Drangsholt

[1] *Oslo University College, Pilestredet 35, NO-0166 Oslo, NORWAY*

[2] *SINTEF Forskningsveien 3b, NO-0314 Oslo, NORWAY*

Abstract

Although theoretical studies show that energy use for ventilation purposes can be reduced by more than 50% with DCV compared to CAV, evaluation of real energy use demonstrates that this potential is seldom met. DCV-based ventilation systems must become more reliable to close the gap between theoretical and real energy-performance. This unfortunate experience with DCV seems to have many causes, including: unclear placement of system responsibility, inadequate specifications and hand-over documentation, balancing report not suitable for DCV, communication errors and lack of knowledge about DCV-systems among decision makers, designers and operators etc. Identified key factors for improvement so far are adequate specifications, hand-over documentation and balancing report for DCV and a clearly defined and placed responsibility for the overall functionality. This paper presents a recently started project that will last until 2013 and aims to develop and disseminate knowledge on systems with improved robustness.

Keywords: Demand controlled ventilation, Energy efficient, Educational buildings, Robustness, Target values, Occupancy, Control systems, Sensors, Communication systems

Introduction

There are many possibilities for the application of DCV and new knowledge about the importance of outdoor air supply, because of awareness of its positive effect on sick leave and productivity [1, 2] should lead to a wish to increase the outdoor air supply in comfort ventilation applications. This will further increase the demand for and profitability of, DCV-systems.

Demand controlled ventilation (DCV) can considerably reduce the ventilation airflow rate and energy use compared to constant air volume (CAV) ventilation [3]. This conclusion is supported by an inspection of 157 classrooms in primary schools in Norway [4]. On average, 74% of the design capacity is utilized when the classroom is in use, in terms of number of occupants. The classrooms are typically used for 4 hours on days with normal school activity. Theoretically, CO_2-sensor based DCV should reduce the ventilation air volume in the average classroom to about 43% of the corresponding air volume for a CAV-system operating with full airflow from 7 AM to 5 PM. The energy use for ventilation purposes is reduced to about 38% of the corresponding energy use for a CAV-system. Ventilation energy consists of fan energy and necessary ventilation heat after heat recovery. Comparison of perceived indoor climate in schools with CAV-systems and DCV-systems does not indicate that well designed CAV-systems add extra quality to the indoor climate [5]. Studies by Wachenfelt [6] support this conclusion. The purpose of extra ventilation with CAV-systems is therefore questionable as it basically leads to additional energy use when rooms are unoccupied.

CO_2-monitoring sensors have been commonly used for controlling the ventilation rate. Several field studies indicate that many CO_2-based demand controlled ventilations system do not meet design goals of saving energy because of poor sensor accuracy, [7]. More accurate sensors together with air flow rate measuring at room level, could even make it possible to "see" important demands such as: "how many occupants are in the room, and are the number increasing or decreasing", information important to optimize indoor environment. New CO_2-sensors with HoloChip have recently been introduced to the market. They are announced to have increased accuracy and long-term stability. Sensor performance and improved sensor requirements will be evaluated in this project.

Infrared occupancy sensors are a cheap alternative to CO_2-monitoring for controlling the ventilation rate. The control strategy is normally bimodal: The ventilation rate is reduced to a minimum when the room is unoccupied, and is increased to the design ventilation rate whenever the room is occupied. The occupancy sensor can also control artificial lighting and solar shading. IR-sensor based demand-controlled ventilation reduces the energy use for ventilation purposes in the average classroom to about 51% of the corresponding air volume for a CAV system operating with full airflow from 7 AM to 5 PM [4]. There are also IR sensors with a stepless output signal that is proportional to the activity level in the sensor's field of view, which is an approximate measure of the number of people in the room.

Case studies in Swedish schools have shown that IR-sensor based DCV can reduce the ventilation energy requirements by approximately 50% [8]. Persily [9] has found that DCV-CO_2 can reduce the energy use for ventilation purposes from about 50 to 75% in a lecture hall. Both of these results are in good agreement with the results of Mysen [4].

Sørensen [10] has estimated the energy savings to be between 30 and 55% with DCV relative to a comparable CAV-system without being specific about the type of building. Drangsholt [11] found that the average occupant load in a university auditorium during the working period was about 36% of maximum allowed occupancy load.

Mysen's results [4] are from schools with a traditional classroom-based education principle. Since the input data for the study of Mysen were collected, newer Norwegian schools are built with more open-plan indoor solutions with individual and group based education. The decision as to which of bimodal IR-sensor based DCV, or CO_2-sensor based DCV, is the most profitable depends on absenteeism and utilization of class capacity together with the

operation time. Information about use is therefore crucial for optimal design of DCV-systems. [10, 12]. We need knowledge about the use of modern indoor school areas to decide important parameters including density (people/m^2), time of use, operation time of air-handling-units, ventilation system and energy saving potential, optimal sensor choice and ventilation system design. This will be evaluated in this project.

Mysen [13] evaluated a simplified ventilation system with direct air supply through the façade in a school in a cold climate. The school had problems with draughtiness and too low temperatures that hopefully can be mitigated with better tuning of the control system. Use of a combined CO_2- and temperature target seems more appropriate for such ventilation concepts. This is supported by the fact that perceived air quality (PAQ) in the school is better in January than June, which we can assume is mainly caused by a lower indoor air temperature in the breathing zone. Figure 1 shows examples of different control strategies. The figure illustrates our suggested improved control strategy with temperature compensation of the CO_2 set-point. The control can be either linear or stepwise. Both are illustrated.

Implementing such a control strategy could improve thermal comfort and reduce energy use for heating without compromising PAQ during cold weather. In addition it could improve indoor air quality (IAQ) during warm weather with only a slight increase in energy use.

The studies of Fang et al. [14] support this assumption. They studied PAQ, SBS-symptoms and performance of office work at three levels of air temperature and humidity and two levels of ventilation rate (20°C/50% RH, 23°C/50% RH, 26°C/60% RH at 10 ℓ/s per person outside air, and 20°C/40% RH at 3.5 ℓ/s per person outside air). This study shows that the impact of PAQ of decreasing the ventilation rate from 10 to 3.5 ℓ/s per person could be counteracted by a decrement of temperature and humidity from 23°C/50% RH to 20°C/40% RH. Several SBS symptoms were alleviated at low levels of temperature and humidity despite a coincident reduction of ventilation rates. This is consistent with several other studies starting with Wyon [15] demonstrating that warm humid air is perceived as less fresh and less acceptable, and that SBS symptoms such as fatigue and headache may be caused by exposure to air at slightly raised temperature and humidity.

Such a strategy might lead to negative consequences for IAQ related symptoms if the pollution load is considerably influenced by factors such as cleaning standard, emissions

from building materials and pollution caused by moisture problems. DCV with CO_2- or temperature-compensated CO_2 control, presuppose that the total pollution load is always dominated by pollution from the occupants, or that the indoor environment is controlled by multisensors. Nano- and microtechnology and industrial production methods have made it possible to produce cheap and robust mulitisensors [16]. The use of temperature-compensated CO_2 control and other intelligent parameter combinations will be investigated further in this project.

Another interesting reflection is that the minimum ventilation rates prescribed in existing ventilation standards do not include the influence of air temperature [17]. These standards can be a barrier to a possibly more optimal ventilation control with temperature-compensated CO_2-set point and the rational basis for this seems dubious. This will be investigated further in this project because it might lead to an unnecessary use of energy during cold weather.

This project focuses on educational buildings, but the results will be applicable for other type of buildings designed for high occupant density.

Methods

The following methods are used:

Literature reviews and focus groups

Critical review will be conducted in the initial stage of the project together with interviews of focus groups will be carried out.

Field studies

Gain relevant knowledge about the use of modern school as basis for evaluate the potential of energy use reduction with DCV.

The results of the field study will be analyzed with statistical tools leading to relevant input data for calculation of energy saving potential controlled for not relevant parameters. The need for sensibility analyses will be continuously considered and, if necessary performed.

The energy saving potential will be analyzed base on the field study results. The variation of the energy potential including relevant uncertainty will be analyzed with statistical tools.

Compose tools

Establish a validated Excel® based tool for simulation of the true reduction in flow rate and fan power in schools, based on the methods described of Mysen (Mysen et al. 2003, Mysen et al 2005) that will serve as appropriate documentation according to the Norwegian building code. The tool should give necessary input data for design, management and maintenance of the DCV system.

Establish guidelines and an Excel based cost-benefit tool for decision makers applicable in the early stage of a project.

Establish system specifications, hand-over documents and balancing report suitable for DCV.

Validation in field and laboratory

Validate the calculation tools through pilot studies and field and laboratory measurements.

Observations and Discussion

There are several factors influencing robustness and energy use related to DCV. The most important factors are:

- Target values (e.g. fresh air flow rates)
- Occupancy and activity
- Design (duct layout, VAV/CAV mixing, ventilation principle)
- Control systems (actuators, sensor location, algorithms and control strategy)
- Sensors (reliability and accuracy, location)
- Communication systems (protocols, transfer rate)

All these factors and their interactions are affected by a rapid development based on knowledge and available technology. There are several different system solutions based on

pressure control, flow control, damper position control with and without optimizer and self regulating DCV diffusers.

In addition, you might have value-added functionality if the sensors control other energy related technology such as artificial lighting, solar shading, heating-/cooling systems and log data about actual use of the rooms/areas.

Although theoretical studies show that energy use for ventilation purposes can be reduced by more than 50% with DCV compared with CAV. Evaluation of real energy use demonstrates that this potential is seldom met. DCV-based ventilation systems must become more reliable to close the gap between theoretical and real energy-performance.

This unfortunate experience with DCV seems to have many causes like:

- unclear placement of responsibility for the overall system functionality
- inadequate specifications and hand-over documentation
- balancing report not suitable for DCV
- components and room-level control that work autonomously but do not communicate properly with BEMS
- lack of knowledge about DCV-systems and components throughout the whole chain from decision makers to operating personnel
- wiring mistakes
- programming errors
- defect sensors or unfortunate placement of them.

This implies that future systems should have some kind of inherent functionality to detect, diagnose and repair faults before it leads to adverse health and energy consequences.

The following success criteria's for well functioning and economical beneficial DCV have been identified through introductory interviews:

- Responsibility for the overall system functionality is clearly defined and placed

- Knowledge about DCV among decision makers, designers, contractors and operating personnel. It's especially crucial that it is designed by an HVAC-consultant with up-to-date expertise within DCV
- Interactive systems communicate smoothly
- Adequate specifications, hand-over documentation and balancing report for DCV have been used
- Components, such as sensors, that have proper functionality and quality throughout their predicted lift expectancy
- Possibility to control the function of crucial components such as fan energy use, VAV-damper positions, air flows at room level etc.
- Maximum diversity factors use for dimensioning and assumed average use for energy calculations, together with specified running conditions during control procedure.
- Prospective economical penalty is agreed upon before performance test during final control procedure

Summary and conclusions

This paper presents initial and coming studies of a recently started project that aims to develop and disseminate knowledge on systems with improved robustness.

Evaluation of real energy use of DCV-systems demonstrates that theoretical potential for energy reduction is seldom met. DCV-based ventilation systems must become more reliable to close the gap between theoretical and real energy-performance.

This unfortunate experience with DCV seems to have many causes. Optimal indoor environment with a minimum use of resources (eq. energy) requires well-functioning DCV. Some success criteria for well functioning and economical beneficial DCV are identified and described above. The following topics will be investigated further:

- *Actual use of modern indoor school areas related to density (people/m^2), time of use, operation time of air-handling-unit*
- *Evaluation of different DCV solutions regarding robustness, energy use and reliable ventilation rates*.
- *Optimal ventilation system design and sensor choice*
- *Use of temperature-compensated CO_2 control and other parameter combinations*

Acknowledgments

The project is funded by contributions from the industry partners **VKE** www.vke.no, **Skanska** www.skanska.no, **Undervisningbygg Oslo KF** www.undervisningsbygg.oslo.kommune.no and **Optosense** www.optosense.com and public funding from the Norwegian Research Council.

References

1. Eriksson, M., "Trends in the Norwegian building ventilation market and drivers for change", AIVC Paper no 01 March 2008.

2. Wargocki, P., Wyon, D.P., Sundell, J., Clausen, G., Fanger, P.O., "The effects of outdoor air supply rate in an office on perceived air quality, sick building syndrome, symptoms and productivity", Indoor Air 10, 2000, pp. 222~236.

3. Fisk, W.J., De Almeida, A.T., "Sensor-based demand-controlled ventilation: A review", Energy and Buildings 29, 1998, pp.35~45.

4. Mysen, M., Berntsen, S., Nafstad, P., Schild, P.G., "Occupancy density and benefits of demand-controlled ventilation in Norwegian primary schools", Energy and Buildings 37, 2005, pp.1234~1240.

5. Mysen, M., "Ventilation Systems and their Impact on Indoor Climate and Energy Use in Schools", Norwegian University of Science and Technology, Doctoral Theses, 2005:111.

6. Wachenfeldt, B.J., Mysen, M., Schild, P.G.. "Air flow rates and energy saving potential in schools with demand-controlled displacement ventilation", Energy and Buildings 39, 2007, pp. 1073~1079.

7. Fisk, W.J., Sullivan, D.P., Faulkner, D., Eliseeva, E., "CO_2 monitoring for demand controlled ventilation in commercial buildings", Environmental Energy Technologies Division, Indoor Environment Department, Lawrence Berkeley National Laboratory, Berkley, CA 94720, March 2010.

8. International Energy Agency, in: Mansson, L.-G. (Ed.), "Demand-controlled ventilating systems: case studies", Swedish Council for Building Research, Stockholm, 1993.

9. Persily, A., Musse, A., Emmerich, S., Taylor, M., "Simulations of indoor air quality and ventilations impacts of demand controlled ventilation in commercial and institutional buildings", National Institute of Standards and Technology, Gaithersburg, USA 2003.

10. Sørensen, B., "Applications and Energy Consumption of Demand Controlled Ventilation Systems. Modelling, Simulations and Implementation of Modular Built Dynamical VAV Systems and Control Strategies", Narvik Institute of Technology. Norwegian University of Science and Technology, Trondheim, Doktor ingeniøravhandling 2002:34.

11. Drangsholt, F., "The applicability of demand controlled ventilating systems for assembly halls", Norwegian University of Science and Technology, Dr. ingeniøravhandling 1992:37.

12. Mysen, M., Rydock, J.P., Tjelflaat, P.O., "Demand controlled ventilation for office cubicles – can it be profitable?", Energy and Buildings 35, 2003, pp. 657~662.

13. Mysen, M., Schild, P.G., Hellstrand, V., Thunshelle, K. (2005), "Evaluation of simplified ventilation system with direct air supply through the facade in a school in a cold climate", Energy and Buildings 35, 2004, pp. 657~662.

14. Fang, L., Wyon, D.P., Clausen, G., Fanger, P.O., "Impact of indoor air temperature and humidity in an office on perceived air quality, SBS symptoms and performance", Indoor Air 14, 2004, (s7), pp. 74~81.

15. Wyon, D.P., Fanger, P.O., Olesen, B.W., "The mental performance of subjects clothed for comfort at two different air temperatures", Ergonomics, Vol. 18, 1975, pp. 359~374.

16. Drysdale, A., Olesen, B., Toftum ,J., Hök, B., Gløersen, P.G., Østbø, N.P., Jensen, G.U., Jensen, J.M., Friis, M.S., "Multi-Sensors for Indoor Environment Control – A feasibility study carried out for the Nordic Innovation Center - Final report", Danish Technological Institute, March 2004.

17. NS-EN 15251:2007, "Indoor environmental input parameters for design and assessment of energy performance of buildings addressing indoor air quality, thermal environment, lighting and acoustics", 2007.

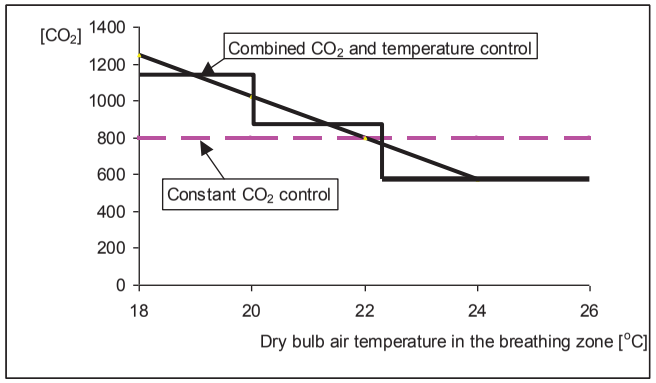


Fig. 1 Three different control strategies for DCV. The conventional constant CO_2 control and the suggested improved control strategy with linear or stepwise temperature compensated CO_2 set-point.

Energy Requirements of a Multi-Sensor Based Demand Control Ventilation System In Residential Buildings

Nam Chul Seong[1], Sung Min Hong[1], Dong Won Yoon[1]

[1] 1Kyoungwon University, Seoul, Korea

Abstract

In Korea, in 2006, the building regulation was revised to apply 0.7 ACH (Air Change Rate) ventilation systems to improve indoor air quality in residential apartment housing. The purpose of this study is to evaluate energy requirement and indoor contaminant level characteristics for residential building applying with sensor-based DCV (Demand Control Ventilation) system. It has been simulated both in a setting of the constant volume of 0.7 ACH intakes as recommended by the Korean Indoor Air Act and in a sensor-based DCV system controlled with CO2 and chemical material such as TVOC (Total Volatile Organic Compound).

Our study demonstrates that the DCV system is energy efficient and maintains better indoor air quality because the indoor contamination level is reduced by controlling the outdoor air intakes. DCV system consists of a hardware module of sensor units and a control algorithm that implements several integrated ventilation strategies to meet the ventilation requirements.

In this study, the energy requirements have been evaluated with two ventilation control strategies; one for the conventional ventilation type and the other for a sensor-based DCV system. DCV is a real time, occupancy and contamination level based ventilation approach that can lead to significant energy saving over the traditional fixed OA (Outdoor Air) intake ventilation system. Our approach enables the incorporated system to maintain proper IAQ (Indoor Air Quality) at all times in a space where adequately ventilated to reduce the indoor pollutant level and thus improves the air quality in an indoor environment.

Keywords: Indoor Air Quality, DCV (Demand Control Ventilation), Sensor-Based Control, Residential Ventilation System, Energy Simulation.

Introduction

Recently, people spend 90% of their time indoors with the majority their life (Klepeis et al, 2001). The apartment house is a domestic residential trend in Korea from industrialization and rapid urbanization.

According to government (Ministry of Land, Transport and Maritime Affairs, MOLTMA) figures, in 2008 the percentage of apartment houses was increasing steadily, and reached 43.89% and that of new construction supply 85.8% during the last five years. For this reason of changing trend in residential buildings, highly air-tight envelopes and lack of operable windows make it difficult to meet the ventilation needs without using mechanical ventilation systems.

Due to the trend, in 2006, Building regulation has been revised to make it mandatory to keep ventilation rate at 0.7 ACH or above air changes during 24 hours to improve Indoor Air Quality in resident buildings. Thus, they have to install a mechanical or natural ventilation system. However, a survey in other research reveals that many mechanical ventilation systems are not often operated by residents because of following. First, it is found that occupants tend to avoid powering their ventilation system in order to save utility cost. Relying on occupants' decision in tuning on or off of their ventilation system may be a bigger problem in the effectiveness of operating current mechanical ventilation systems.

Actually, there has been a variety of research to identify emission characteristic and reduce emission rate of chemical source from building material and product. However, research on energy consumption is still under way to identify their impact. Also, it is insufficient to evaluate and validate the performance of ventilation systems against government regulations.

Purpose

With maintaining comfortable and healthy indoor environment, minimizing the energy consumption of ventilation systems is required. When the mechanical ventilation systems installed in residential buildings, the followings are suggested in this study to improve mechanical ventilation performance concerned energy efficiency and indoor air quality. The purpose of this study is to control appropriate ventilation and maintenance of indoor contaminant levels for reduction of energy consumption in residential building while improvement indoor air quality.

Methods

- Multi-Simulation using Coupled Tools

It has been simulated both of constant volume of 0.7 ACH intakes as guidelines on the Korean indoor air Act and sensor-based DCV system controlled with both of CO_2 and chemical sensor for operating mechanical ventilation system.

CO_2 and chemical contamination level simulation has been performed using CONTAM 2.4 and energy simulation has been performed using Energy Plus Ver. 3.1 with TMY2 (Typical Meteorological Year) format of weather data for Seoul, Korea. Fig 1 is shown the simulation processing in this study. Subject household is selected an apartment house of Korean standard model that has an area of 84 ㎡ and floor plan is as follow Fig 2.

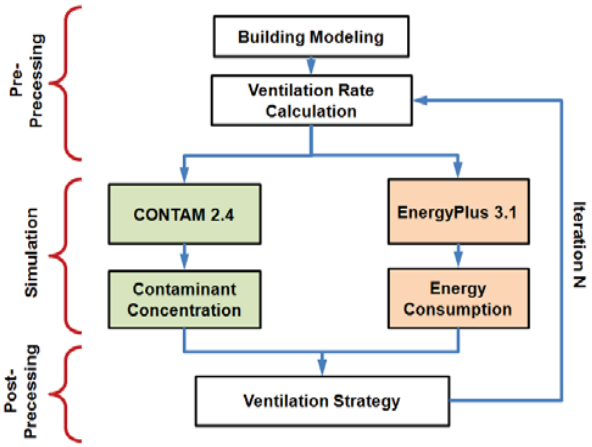


Fig. 1 Simulation Processing

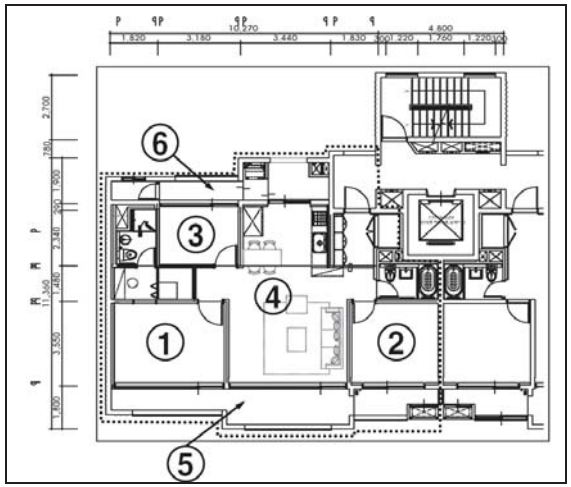


Fig. 2 Floor plan of Subject household (84 ㎡)

Simulation

1) Performance assessment for indoor contaminants control

The modeling to calculate contamination of each zone is as Fig3. for simulation using CONTAM 2.4. Exhaust air is balanced with the supply air. Multi-Zone has an air flow network through the open fraction and infiltration condition is 0.15 air change per hour each Zones. Infiltration condition of unconditioned Zone like balcony is 2.0 airchange per hour because considering to be adjacent outside air.

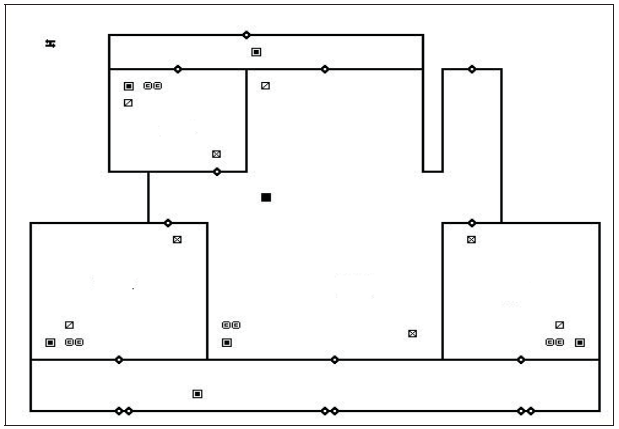


Fig. 3 Multi-zone modeling for subject household using CONTAM 2.4

The initial CO_2 concentration is set to 400ppm. The CO_2 generation rate per person is set to 17liter per hour(ℓ/h) for adult with common indoor activity (ASHRAE Handbook Fundamentals, 2005).

TVOC generation rate is calculated based on data had been already measured in the government case studies.(Study of emitting pollutants from appliance and furniture, Ministry of Environment,2006) It is assumed that TVOC emission rate from finishing material is based on certificated first class material in Korea. The initial

TVOC concentration is set to 1000[㎍/㎥]. Calculation basis of VOCs Emission rate are described in Table 1 and Table 2

Table 1 Calculation basis of VOCs Emission Rate

	Area of wall, ceiling [㎡]	Area of floor [㎡]	First Class Emission rate per hour [mg/㎡·h]	Finishing material [mg/h]	Product [mg/h]	Total Calculated Emission rate per hour [mg/h]
Bedroom	54.94	18.95	0.1	7.389	2.42	9.809
Room 1	44.89	13.97	0.1	5.886	3.57	9.456
Room 2	32.12	9.024	0.1	4.1144	2.87	6.9844
Living Room	86.24	37.29	0.1	12.353	10.625	22.978

Table 2 Calculation basis of VOCs Emission Rate from Product and Appliance

Bedroom [mg/unit·h]	**Furniture**	**Bed mattress**	**Chest of drawers**		
	1.77	0.65	1.77		
Room 1 [mg/unit·h]	**Bed mattress**	**Desk**	**Personal Computer**	**Chest of drawers**	**Chair**
	0.65	1.1	0.58	1.77	0.12
Room 2 [mg/unit·h]	**Bed mattress**	**Desk**	**Chest of drawers**		
	0.65	1.1	1.77		
Living Room [mg/unit·h]	**Kitchen unit**	**Shoe rack**	**TV**		
	7.16	2.875	7.75		

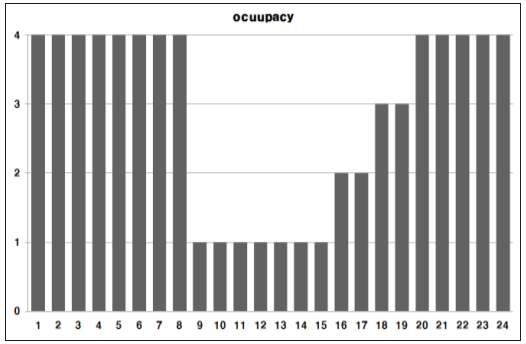


Fig. 4 Occupancy Schedule

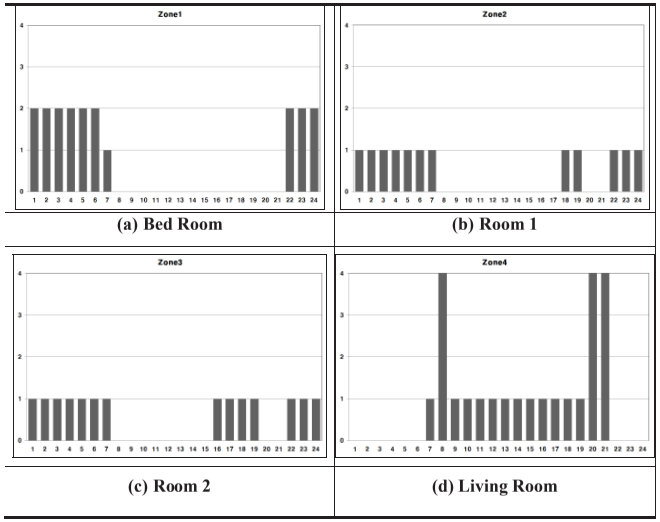


Fig. 5 Occupancy Schedule of each Zone

Occupants in the house are assumed a family of four and occupancy schedule is shown in Fig4 and Fig5.

2) Analysis of Energy Consumption

A thermal dynamic energy simulation has been performed using Energy Plus Ver. 3.1 with TMY2 format of weather data for Seoul, Korea. Energy requirements have been evaluated with both of ventilation control strategies for conventional type and sensor based DCV system. Outputs of energy consumption for heating in winter have been compared with ventilation requirements and also the fractions of energy consumptions on the two different control strategies. Table 3 shows basic conditions for simulation in Energy Plus.

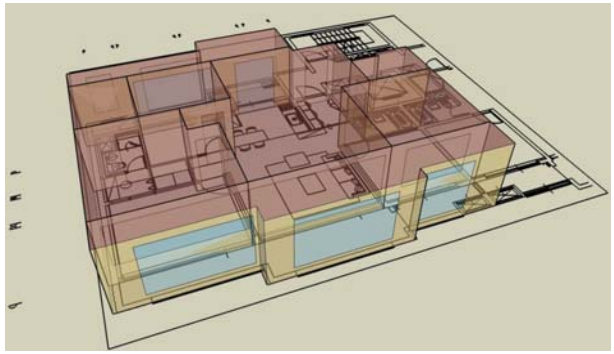


Fig. 6 Modeling and Rendering for subject household using Openstudio

Table 3 Basic Conditions of Simulation in Energy Plus

	Version Identifier	**3.1**
Site	North Axis	0
	Terrain	City
	Heat Balance Algorithm	Conduction Transfer Function
Time Step	Number of Time steps	1 Hour
Site Location	Name	Seoul Design_Conditions
Run Period	Begin Month	11
	Begin Day of Month	1
	End Month	3
	End Day of Month	31

Fig7 shows an overview of the heating modeling schematics. Heating-coil is modeled with coil length per flow, hot water circulation pump flow and head referred to measurement case studies in order to calculate the exact energy consumption. Supply hot water temperature of floor heating system is set to 60 Celsius degree. Also, Fig8 shows an overview of the mechanical ventilation system including heat recovery modeling schematics. Specifications of ventilation system (fan efficiency, pressure-rise) is referred to commercialized products.

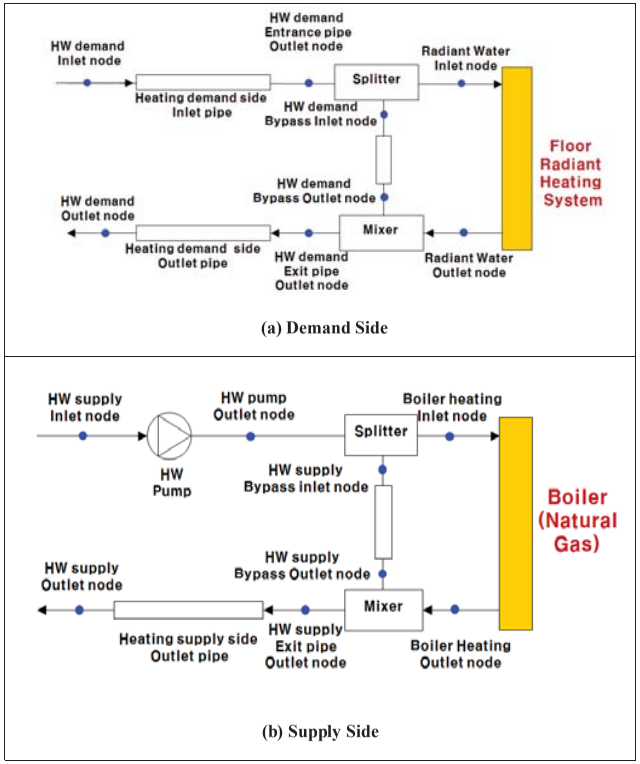


Fig. 7 Schematic of Hot Water Plant (Boiler) and Radiant Floor Heating System

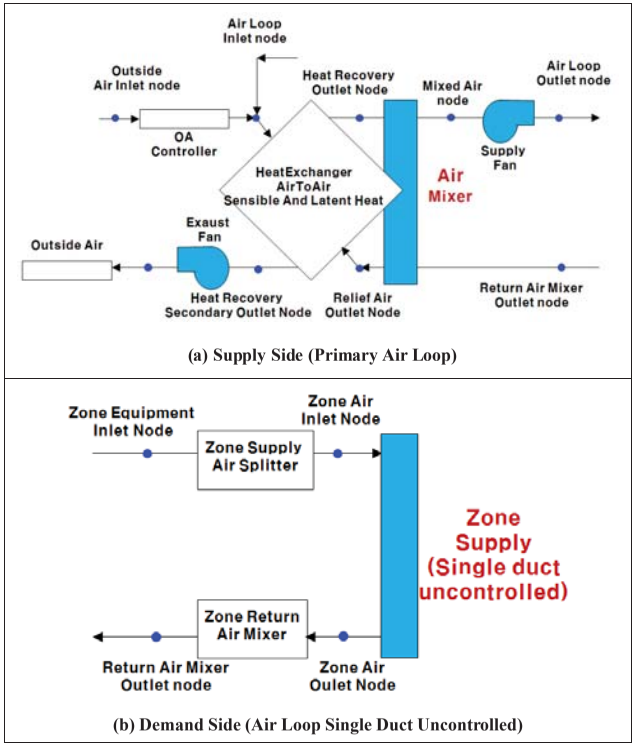


Fig. 8 Schematic of the Air Loop for ventilation included the heat recovery

Table 4 Ventilation Rate of Korean standard for simulation

Zone Name	Volume [㎥]	Ventilation Rate [㎥/h]
		Korea Standard (0.7ACH)
Bedroom	45.48	31.836
Room1	33.52	23.464
Room2	21.66	15.162
Living Room	89.50	62.650

Results

1) Ventilation Rate with Korean standard (0.7ACH)

Fig 9 shows the result of simulation for the current Korean ventilation standard and change of CO_2 concentration. When the ventilation system is not operating concentration of CO_2 is reached about 5000[ppm] in the each room during sleeping time of occupancies but ventilation rate is 0.7[ACH] concentration of CO_2 is maintained below 1600[ppm].

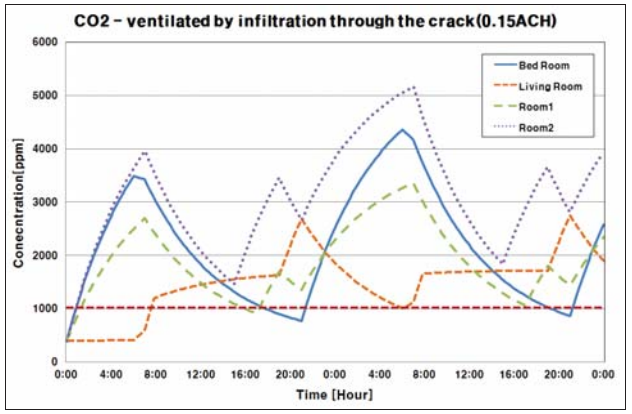


Fig. 9 Change of CO_2 concentration (Non-ventilation)

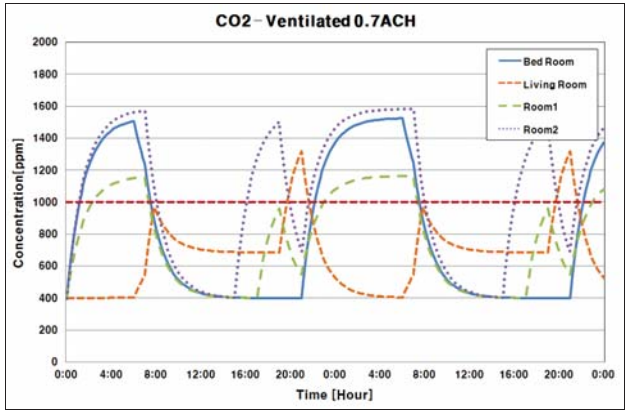


Fig. 10 Change of CO_2 concentration (0.7ACH)

Fig 11 and Fig 12 are results of simulation by comtam2.4 program. It is assumed that infiltration air volume is 0.15[ACH] and the initial concentration of TVOC is 1000[㎍/㎥]. Without ventilation, TVOC concentration level is risen to about 4000[㎍/㎥], and when ventilated by Korean standard, is maintained 600[㎍/㎥]. Table5 is the result of gas consumption simulated using Energyplus each case in winter of Korea.

Table 5 Comparison Boiler gas consumption with each case applied Korean ventilation standard

Boiler Gas Consumption [MJ]		
Month	**No vent-0.15[ACH])**	**(Vent 0.7ACH)**
NOV	676.29	1236.30
DEC	1362.11	2624.25
JAN	1590.46	3209.31
FEB	1354.20	2552.46
MAR	757.36	1584.424
TOT	5740.32	11206.77

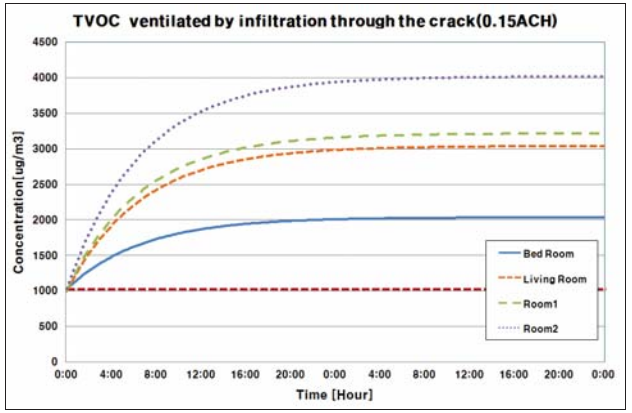


Fig. 11 Change of TVOC concentration (Non-ventilation)

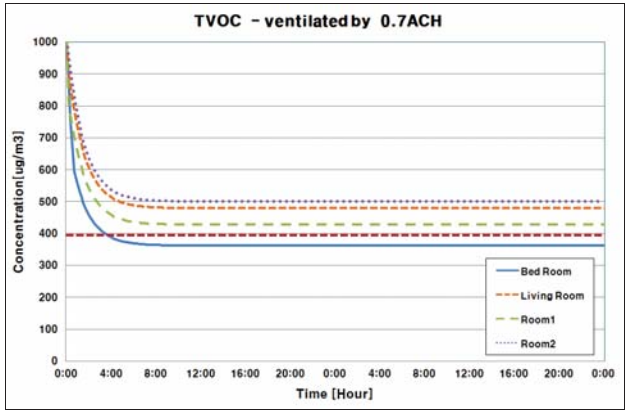


Fig. 12 Change of TVOC concentration (0.7ACH)

2) Ventilation with CO_2 sensor-DCV Type

Fig13 and Fig14 shows CO_2 and TVOC level which are the results of CO_2-DCV to maintain below Korean standard (1000[ppm]) in the commercial building. The air volume is 1.5[ACH] calculated mass balancing equation. When the vent turn off, TVOC concentration rise rapidly.

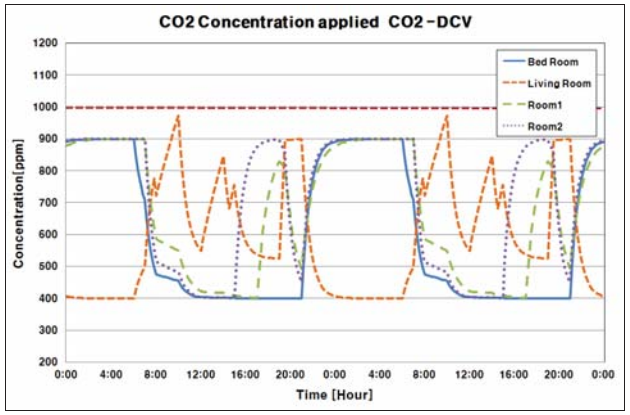


Fig. 13 CO_2 concentration with CO_2-DCV

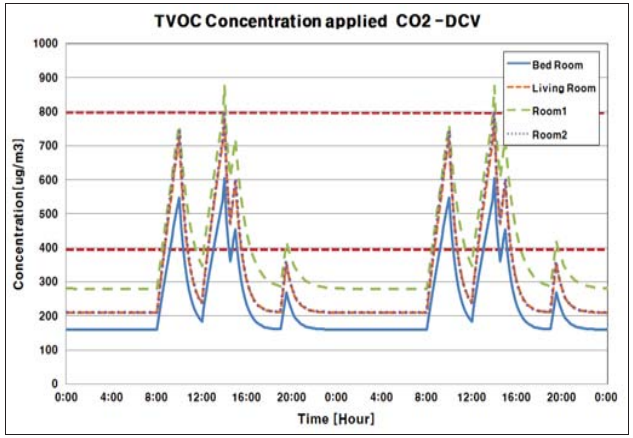


Fig. 14 TVOC concentration with CO_2-DCV

3) Ventilation with TVOC sensor-DCV Type

Fig15 and Fig16 shows the result of TVOC-DCV to maintain TVOC-800[㎍/㎥] each room, the ventilation is operating with regular interval of 0.7[ACH]. CO_2 is maintained irregularly below 2000[ppm] according to the occupant's schedule.

Table 6 is shown energy consumption with the simulation results. When the ventilation is controlled by TVOC-DCV (0.7ACH, On/Off control), the energy consumption has reduced at 26% compared with 24 hour continuous ventilation. In the CO_2-DCV for maintaining 1000ppm as standard concentration, the energy consumption is increased at 17% compared with those of 0.7[ACH], because of increasing of ventilation air volume.

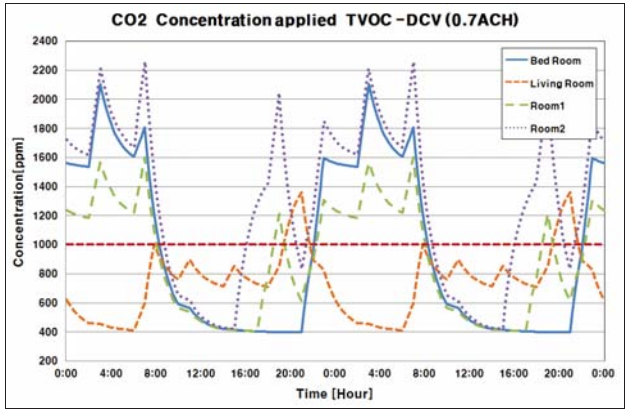


Fig. 15 CO_2 concentration with TVOC-DCV

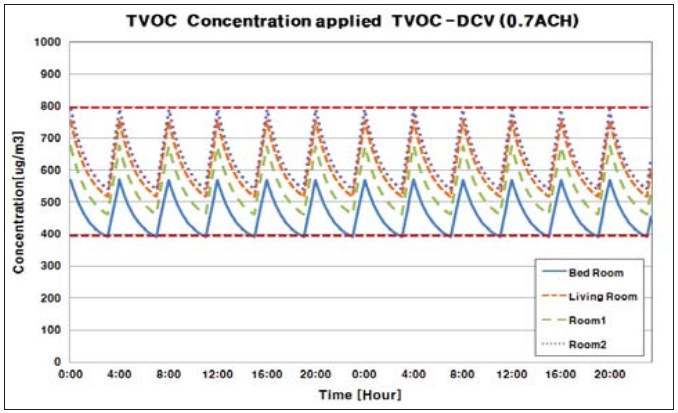


Fig. 16 TVOC concentration with TVOC-DCV

Table 6 Comparison with Energy Consumptions

Boiler Gas Consumption [MJ]			
Month	**0.7ACH**	**TVOC DCV (0.7 ACH)**	**CO_2 DCV (1.5 ACH)**
NOV	1236.31	718.43	1482.65
DEC	2624.26	1949.60	3109.84
JAN	3209.32	2499.72	3695.23
FEB	2552.47	1947.43	2925.38
MAR	1584.42	1220.55	1977.74
TOT	11206.78	8335.72	13190.84

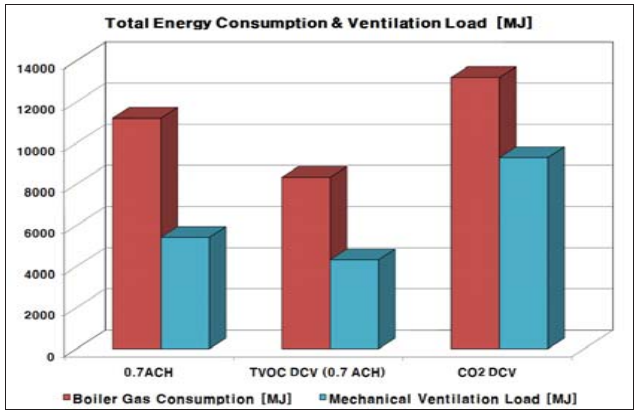


Fig. 17 Comparison with Energy Consumptions and OA Loads

Conclusions

As a Korean Ventilation Regulation, it is an essential to install the mechanical ventilation system or natural ventilation devices with 0.7 ACH rate in every residential apartment house. But there are lack of explanation how to operating ventilation system as confirm the perceived IAQ. Without any sufficient ventilation control strategies, it is difficult to improve IAQ by an occupant ON-OFF control.

If the ventilation unit is operating for 24 hour, the energy consumption would be dramatically increased. Therefore, the sensor based DCV control is very efficient control strategies in the residential building for comfort and energy saving.

From the result of simulations, the Korean Ventilation Regulation in the residential building is dissatisfied to keep the CO_2 levels properly at 1000 [ppm]. In the individual room with door closed, the CO_2 concentration is

rapidly increased during sleeping period as over range of 1000 ppm. Additional air volume is necessary to reduce the CO_2 concentration.

When the TVOC is maintained from 600[㎍/㎥] to 400[㎍/㎥] in the room, it is enough to reduce the chemicals with ventilation rate of 0.7[ACH]. As a result of analysis, CO_2 is not sufficient to use as a surrogate factor in the residential building. The CO_2 concentration is varied with schedule of occupancy in individual room. TVOC concentration is emitted steadily from the finishing materials, CO_2-DCV type can't control the chemical concentration efficiently than TVOC-DCV type.

The current Korean Ventilation Regulation with 0.7[ACH] of ventilation rate is not sufficient to control the CO_2 concentration, but it is enough to reduce TVOC concentration properly. For energy conservation of ventilation system, the sensor-based DCV is very efficient in the residential building, and TVOC is the proper target than CO_2 concentration to control the perceived IAQ for occupant's healthy and comfortable environment.

Acknowledgments

Acknowledgements can be published at the end of the text before references.

References

1. DOE, Energy Plus Input Output Reference. ver 3.1, 2009.
2. NIST, George N. Walton W. Stuart Dols, CONTAM 2.4 User Guide and Program Documentation. , 2008
3. ASHRAE Standard 62.1-2007 Ventilation for Acceptable Indoor Air Quality

Experimental Evaluation of the Moisture Buffering Effect of Hygrothermal Material

Hiroaki SUZUKI[1], Hiroshi YOSHINO[1],
Kenichi HASEGAWA[2], Huibo ZHANG[1] and Ayaka IWATA[2]

[1] Tohoku University, Department of Architecture and Building Science, Graduate School of Engineering, Sendai, Japan
[2] Akita Prefectural University, Department of Architecture and Environment Systems, Yurihonjo, Japan

Abstract

Residential buildings newly constructed in Japan are well insulated and airtight for energy conservation. However, the indoor environment of these houses can suffer from high humidity in the summer and low humidity in the winter. In order to mitigate this problem, hygrothermal materials are installed in some Japanese houses. The test method for small samples of hygrothermal material is prescribed in the Japanese Industrial Standards (JIS). However, the moisture buffering effect of the hygrothermal materials adopted in actual houses is unclear. The purpose of this study was to clarify the effect of hygrothermal material on indoor moisture control. A series of experiments was carried out in two identical rooms. In the room installed with hygrothermal material, variations in relative humidity were controlled and compared with the room without hygrothermal material. This material demonstrated good performance for moisture buffering effect in an actual-scale room.

Keywords: Hygrothermal Materials, Moisture Buffering Effect, Moisture Variation, Moisture Distribution, Experimental House, Loading Ratio

Introduction

Residential buildings newly constructed in Japan are well insulated and airtight for energy conservation. However, the relative humidity (RH) of the indoor environment can be too high in the summer and too low in the winter. Indoor humidity is an important factor for air quality

and occupant health. For this reason, it is necessary to ensure the long life of houses and healthy life of occupants by keeping the indoor humidity within an appropriate range. To control variations in indoor RH, hygrothermal materials with moisture adsorption/desorption properties are installed as finishing materials in some Japanese houses.

The test method for small samples of hygrothermal material is prescribed in the JIS [1, 2]. However, little research has been done on the moisture buffering effect of hygrothermal materials adopted in actual houses. In addition, the indoor humidity environment depends on the combination of many factors, such as moisture sources (occupants, moisture-emitting equipment, plants), ventilation and air infiltration, moisture adsorption and desorption from surrounding surfaces (interior walls, floors, etc.), air flow and temperature distribution, as well as the humidity ratio of the outdoor air. Previous studies have evaluated the moisture buffering effect in a climate chamber [3, 4], but this is different from the actual outdoor climate.

The aim of this study was to clarify the moisture buffering effect and moisture distribution in the full-scale rooms of a test house.

Outline of Experiment

Experimental House

A series of experiments was carried out in an experimental house located on the campus of Akita Prefectural University, Japan, from October to November 2009. **Figure 1** shows a schematic view and the location of measurement points in the house. The experimental house is composed of two wooden stories. The test rooms are situated on both sides of the entrance hall. This experiment was performed in the test rooms on the second floor. Northern rooms were not used. The western room is named “Room A”, and the eastern room is “Room B”. Each room is 4.2 m in width, 4.6 m in depth and 2.9 m in height and the floor area is 19.2 m^2. The internal volume is 55.6 m^3. Each room was equipped with ten sensors (THT-B121, Shinyei Technology Co., Ltd.) for measuring the temperature and RH at 1-min intervals. The outdoor temperature and humidity were measured by psychrometers. At the center of the rooms, temperature and RH sensors were set at 0.05 and 1.5 m high from the floor and at 0.05 m below the ceiling in order to measure the vertical temperature and RH distribution. At the surface of the walls, sensors were set at 1.5 m high from the floor. Each sensor is covered by a cylinder 8 mm in diameter. Therefore, the measured point is 4 mm away from the surface. At the corner between walls a sensor was set at 0.05 m high from the floor level. The other sensors were set at 1.5 m high from the floor level.

Experimental Cases

The interior surfaces of Room A were covered with polyethylene sheets in all experimental cases in order to prevent moisture adsorption and desorption with the building envelope. In Room B, interior surface walls were installed with hygrothermal materials of 12-mm-thick vermiculite board made from unfired vermiculite, calcium hydroxide, silica and pulp by autoclaving at 180°C [5]. The ceiling and floor were covered with polyethylene sheets. As shown in **Table 1**, experiments were carried out for four cases, each with a different loading ratio of hygrothermal materials. The loading ratio means the ratio of the material surface area to the experimental room volume. The surfaces of Room A were covered with polyethylene sheets in all experimental cases. The polyethylene sheets were used to change the area of hygrothermal materials according to the different cases. The loading ratio was different between experiments for Room B.

Moisture was provided by evaporation from a tray (size: 265W×170D×225H mm) with water, which was electrically heated. An electric balance was used for measuring the quantity of humidification. A mechanical fan was installed in the air inlet formed temporarily in the wall between the experimental room and the adjustment northern room. The air change rate was measured by an air volume flow meter (SwemaFlow 65, Kona Sapporo Co., Ltd.). The target air change rate is 0.5 1/h and the target humidification rate is 150 g/h. **Figure 2** shows the schedule for each experimental case. Each experiment consisted of a preconditioning period for 24 h and a constant humidification period of 12 h followed by no humidification for 24 h or more.

Results and Discussion

Quantity of Humidification and Air Change Rate

The measured values for water temperature, moisture production rate and total moisture production are shown in **Table 2**. In order to prevent surface condensation, the water temperature was controlled to below 65°C. There was a slight difference in water temperature, moisture production rate and total moisture production between experimental cases. The water temperature changed in the range of 64.1 to 66.3°C. The moisture production rate changed in the range of 142.2 to 164.4 g/h. The total moisture production changed in the range of 1725 to 1968 g. The values for the air change rate measured by three methods are shown in **Table 3**. The three methods were measurement using an air volume flow meter, calculation by the constant concentration method using water vapor emission rate and calculation by the decay method using absolute humidity (AH) change. The value for the air change rate measured by the air volume flow meter was close to the target value of 0.5 1/h, but the values obtained using the constant concentration method and decay method were slightly different from the target value. The reason is that the ventilation rate was influenced by high-velocity outdoor wind during the experiment.

Humidity Variations and Distribution

(1) Results for Cases 1 and 4

The change in temperature, AH and RH for Case 1 and Case 4 is shown in **Fig. 3** to **Fig. 8**. In the case with hygrothermal materials installed on the four side walls (Case 1), during the preconditioning period in Room A, the RH changed by about 10% due to the influence of the outdoor air RH change over the course of 6 h. The RH in Room B was very stable compared with Room A. During the humidification period in Room A, the RH increased by about 20% over the course of 12 h. In Room B, the RH increased by about 15%. During the following period in Room A, the RH rapidly decreased by 30% after the 12 h. In Room B, the RH gradually decreased by 15%. The same tendency was found for the change in AH.

In the case of hygrothermal materials installed on one side of the walls (Case 4), the moisture buffering effect in Room B was small. It was found that humidity variation was suppressed by the use of hygrothermal materials.

The AH at the center point was higher than that at other points. However, the temperature at the center point was higher than that at other points in the test room. The RH at the center point was lower than that at other points in the test room. The AH of the surface of walls installed with hygrothermal materials in Room B was lower than that at the center point. When hygrothermal materials were installed on the interior surface of the walls, the moisture distribution of AH at the surface of the wall became lower than that at other measured points during the humidification period. However, the moisture distribution of absolute humidity at the corner point was lowest in the experimental room in almost all cases.

(2) Comparison of humidity change between Room A and Room B

A comparison of the average humidity change between Room A and Room B in each case is shown in **Figs. 9** to **12**. These figures show the average of the 10 measurement points for the humidity change, which is shown by the difference from the values at the beginning or the end of humidification. In all cases, AH and RH in Room A were higher than that in Room B during the humidification period and were lower than in Room B during the following period. This means that Room B installed with hygrothermal materials adsorbed and desorbed moisture during the humidification period and during the following period, respectively.

The humidity controlling effect depends on the loading ratio of hygrothermal materials. However, the effect was not directly proportional to the loading ratio.

Evaluation of Moisture Buffering Effect

In order to evaluate the moisture buffering effect, the following index is used.

Index of moisture adsorption effect: $$K_1 = 1 - \frac{S_1'}{S_1}$$ (Eq. 1)

Index of moisture desorption effect: $$K_2 = 1 - \frac{S_2'}{S_2}$$ (Eq. 2)

S_1 is the accumulated area of increased humidity ratio in the experiments in Room A for 12 h after humidification started and S_1' is the same area of increased humidity ratio in the experiments in Room B (**Fig. 13**). S_2 is the accumulated area of decreased humidity ratio in the experiments in Room A for 12 h after humidification ended and S_2' is the same area of decreased humidity ratio in the experiments in Room B (**Fig. 13**). Therefore, K_1 and K_2 mean the ratio of the amount of humidity variation in the case with hygrothermal materials to the case without moisture absorption and desorption.

Relationship between Moisture Buffering Effect and Loading Ratio

The relationship between the moisture buffering effect determined in the previous section and the loading ratio is shown in **Fig. 14**. Except for Case 2, the K_1 and K_2 values increase as the loading ratio increases. These results are reasonable. The values of K_1 are higher than K_2 because the speed of adsorption is higher than that of desorption. However, the result for Case 2 is far from this tendency. One reason is the effect of strong outdoor wind, resulting in a high ventilation rate. The measured results for the ventilation rate shown in Table 3 indicate that the value in Case 2 was higher than that in the other cases. With the high ventilation rate, the decreasing and increasing rate of AH becomes smaller.

Conclusions

Experiments were conducted to investigate the moisture buffering effect and moisture distribution in relation to the use of hygrothermal materials. The results were as follows. Changes in humidity during the humidification period and following period in Room A were suppressed by 9%, and 7%, respectively, compared with Room B without hygrothermal materials. The humidity gradient existed between the central point and the surface of the walls, with hygrothermal materials. As the loading ratio increased, the moisture buffering effect increased. However, the moisture buffering effect in Case 2 was lower than the value expected, due to an increase in the air change rate.

Acknowledgments

The research work described in this paper was supported by Osaka Gas Co., Ltd., and a Grant-in-Aid for Scientific Research (A) (20246092) from the Japan Society for the Promotion of Science.

References

1. Japanese Industrial Association. JIS A 1470 – 1 Determination of water vapor adsorption/desorption properties for building materials – Part 1: Response to humidity variation. 2008.

2. Japanese Industrial Association. JIS A 1470 – 2 Determination of water vapor adsorption/desorption properties for building materials – Part 2: Response to temperature variation. 2008.

3. Yoshino, H., Mitamura, T., and Hasegawa, H., "Moisture buffering and effect of ventilation rate and volume rate of hygrothermal materials in a single room under steady state exterior conditions," Building and Environment 44, 2009, pp. 1418–1425.

4. Zhang, H., Yoshino, H., Hasegawa, H., and Ito, K., "An Experimental Study of Moisture Buffering Effect and Moisture Distribution in a Hygrothermal Materials Furnished Test Chamber," Proceedings of Healthy Buildings 2009, paper 606, 13-17 September 2009, Syracuse, NY USA.

5. Fukuda, Y., Akao, M., and Yamazaki, A., "Next Generation Building Material MOISS," Journal of the Clay Science Society of Japan, Vol. 44, No. 3, 2005, pp. 118–123.

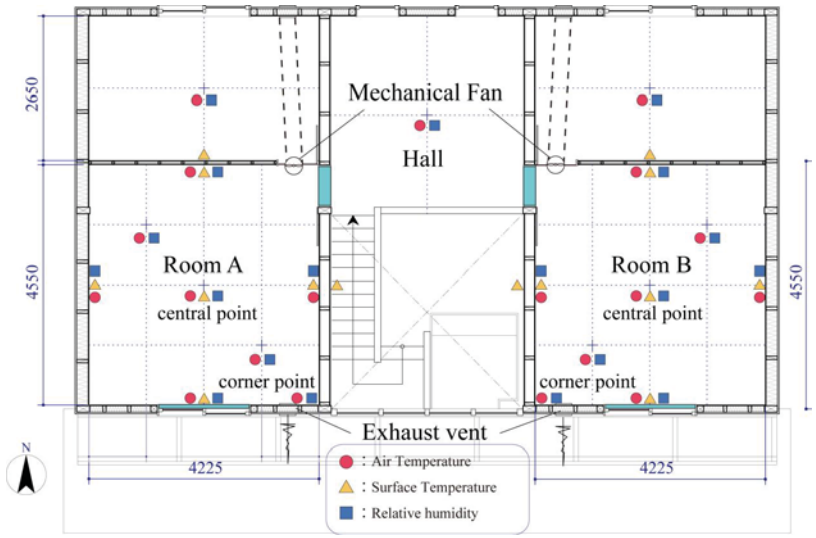


Fig. 1 Schematic view and location of measurement points in the experimental house

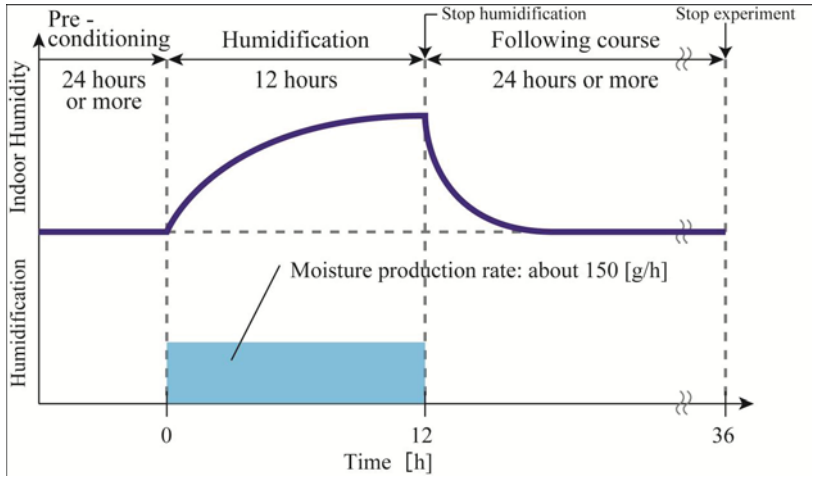


Fig. 2 Schedule for each experimental case

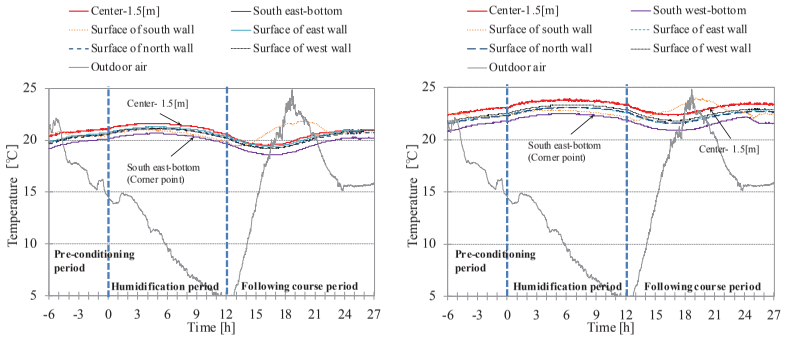


Fig. 3 Temperature variations in Case 1

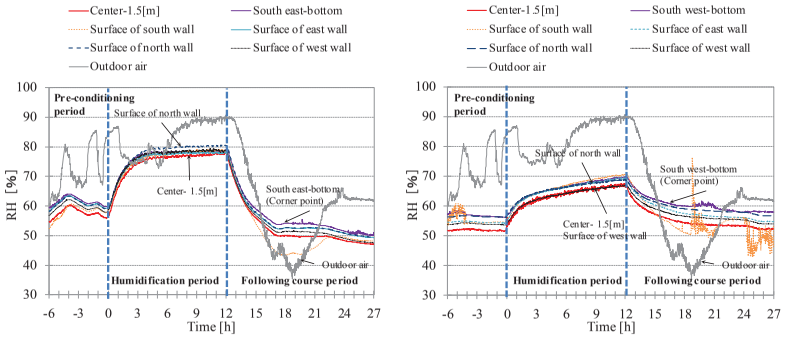


Fig. 4 RH variations in Case 1

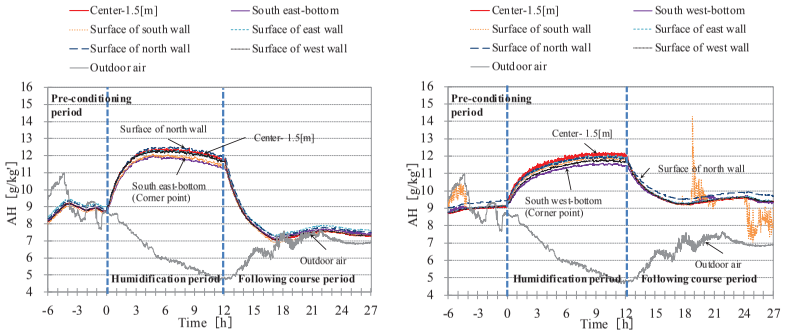


Fig. 5 AH variations in Case 1

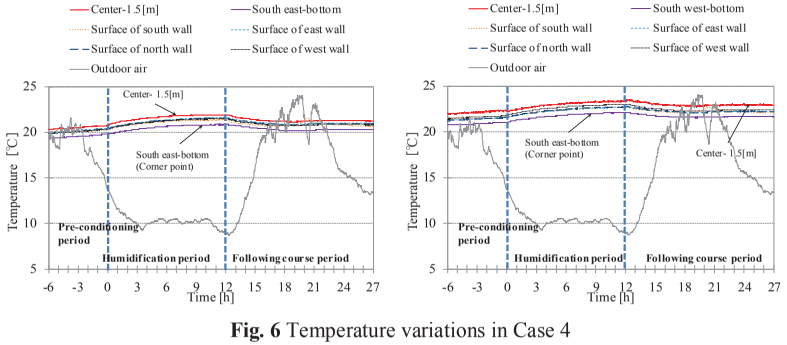


Fig. 6 Temperature variations in Case 4

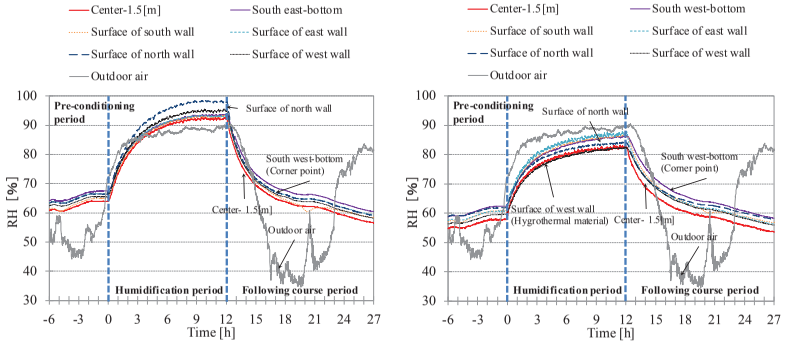


Fig. 7 RH variations in Case 4

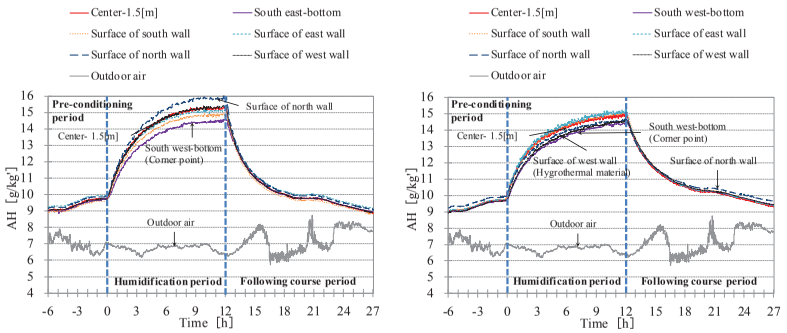


Fig. 8 AH variations in Case 4

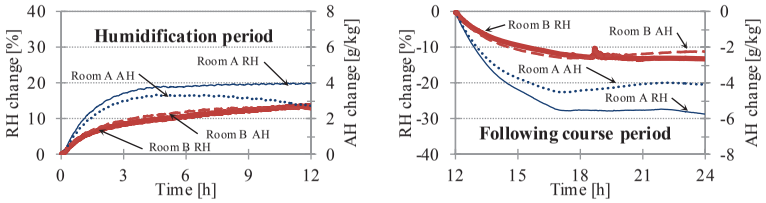


Fig. 9 Comparison of average humidity changes in Case 1

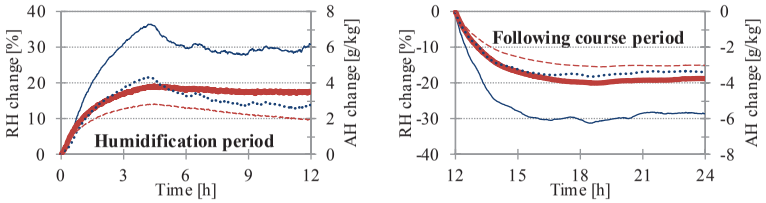


Fig. 10 Comparison of average humidity changes in Case 2

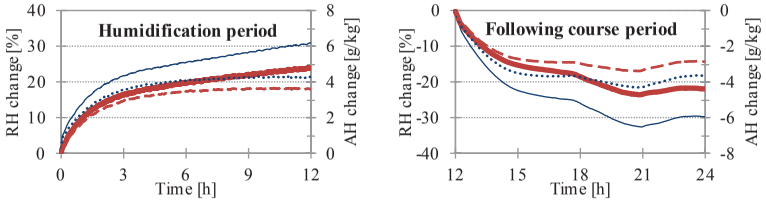


Fig. 11 Comparison of average humidity changes in Case 3

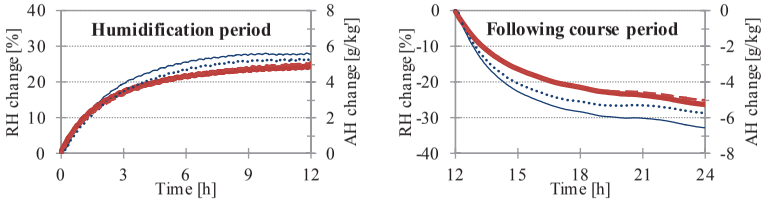


Fig. 12 Comparison of average humidity changes in Case 4

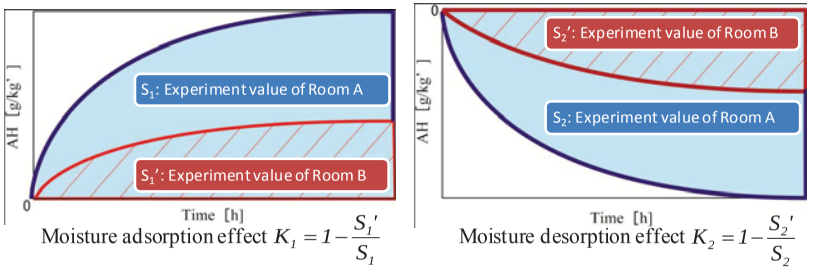


Fig. 13 Schematic of moisture adsorption effect and desorption effect

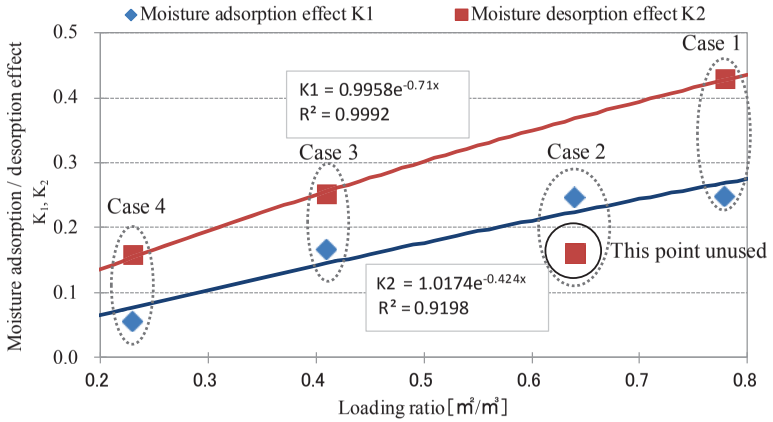


Fig. 14 Relationship between moisture buffering effect and loading ratio

Table 1 Experiments on hygrothermal material location and loading ratio

Experimental cases (Dane day)		Hygrothermal materials	Loading ratio [m³/m³]	Target of ventilation rate [1/h]
Case1 (Oct 30th - Nov 1st)	Room C	none	0	0.5
	Room D	4 sides of walls	0.78	
Case2 (Nov 2nd - 4th)	Room C	none	0	
	Room D	3 sides of walls	0.64	
Case3 (Nov 5th - 8th)	Room C	none	0	
	Room D	2 sides of walls	0.41	
Case4 (Nov 9th - 11th)	Room C	none	0	
	Room D	1 side of walls	0.23	

Table 2 Measured values for water temperature, moisture production rate and total moisture production

Experimental cases		Water temperature [℃]	Moisture production rate [g/h]	Quantities of total moisture production [g]
Case1	Room C	64.2	142.2	1732
	Room D	65.5	150.1	1839
Case2	Room C	64.1	154.6	1833
	Room D	66.3	164.4	1968
Case3	Room C	64.4	143.8	1725
	Room D	66.1	154.6	1855
Case4	Room C	64.1	153.8	1846
	Room D	66.2	158.1	1898

Table 3 Values for air change rate

Experimental cases		Air volume flow mater [1/h]	Constant Consentration Method [1/h]	Concentration Dencay Method [1/h]	Outside wind speed [m/s] (Humidificatio period)	Outside wind speed [m/s] (After the stop of humidification)
Case1	Room C	0.48	0.38	0.38	0.5	1
	Room D	0.49	0.44	(0.22)		
Case2	Room C	0.48	0.59	0.66	2.2	2.7
	Room D	0.49	0.51	(0.31)		
Case3	Room C	0.48	0.37	0.48	0.3	0.7
	Room D	0.49	0.43	(0.35)		
Case4	Room C	0.48	0.28	0.27	0.2	1
	Room D	0.49	0.32	(0.20)		

( ) was installed with hygrothermal materials, therefore, it is only reference value.

Potential of the Solar Thermal Desiccant Cooling in Asia-Pacific Region

N. ENTERIA[1,2], K. MIZUTANI[2], H. YOSHINO[3], R. YOSHIE[2], and A. MOCHIDA[3]

[1]Solar Energy Research Institute of Singapore, National University of Singapore, Singapore, 609924
[2]Environment Group, Wind Engineering Research Center, Tokyo Polytechnic University, Atsugi, 243-0297 Japan
[3]Laboratory for Building Environmental Engineering, Tohoku University, Sendai, 980-8579 Japan

Abstract

The solar thermal desiccant cooling system was numerically investigated for application in the Asia-Pacific Region (East Asia and South East Asia). The system was modeled in transient system simulation (TRNSYS) program and applied in a hypothetical office building. The typical meteorological year (TMY) was used as the basis for the climatic conditions. The system was applied in the region's sixteen major cities covering the temperate, sub-temperate/sub-tropical and tropical climates. The results showed the required flat plate collector area was bigger in the tropical climate compared to temperate climate. The needed air flow rate was higher in tropical climate compared to temperate climate. However, in general, it was shown the potential and applicability of the solar thermal desiccant cooling system in the Asia- Pacific Region.

Keywords: Solar energy; Desiccant system; Dehumidification; Cooling; Simulation; Asia

AIVC 2010 Conference [Korea]

Nomenclatures

C_p	specific heat ($kJ \cdot kg^{-1} \cdot K^{-1}$)
DCOP	desiccant coefficient of performance
E	electric energy (kJ)
h	moist air enthalpy ($kJ \cdot kg^{-1}$)
h_{Evap}	latent heat of evaporation ($kJ \cdot kg^{-1}$)
m	mass flow ($kg \cdot s^{-1}$)
OPEC	off-peak electric energy consumption
Q	heat energy (kJ)
OA	outdoor air
RA	return air, room air
SA	supply air
SCOP	system coefficient of performance
SF	solar fraction
SHR	sensible heat ratio
t	time (s)
T	temperature (^oC)
X	absolute humidity ($Kg_{H2O} \cdot Kg_{Air}^{-1}$)

Subscript

AHC	air heating coil
Aux	heater (daytime)

CL	cooling load
Col	collector
Hea	heater (nighttime)
I	inlet
O	outlet
OA	outdoor air
RA	return air
SA	supply air
Sen	sensible energy
Ther	thermal energy
Tot	total energy
W	water
X	absolute humidity

Introduction

Buildings consume large amount of conventional energy resources [1]. Large amount of building energy consumption is to support indoor thermal comfort conditions. In Europe, 10% of total energy consumption is for the provision of indoor thermal comfort [2]. In Middle East, 70% of the building energy consumption is for the maintenance of indoor thermal environment [3]. In Japan, 3% of total building energy consumption is for indoor cooling [4]. However, during summertime, large percentage of building energy consumption is for air dehumidification and cooling. In South East Asia, it is expected that buildings consume large percentage of electric

AIVC 2010 Conference [Korea]

energy to support comfortable indoor environment due to the climatic conditions (hot and humid for whole year).

There were several studies conducted on the reduction of building cooling energy consumption through the utilization of alternative energy sources, equipment, devices and methods [5,6]. Solar energy is available anywhere at different solar intensities. In most cases, the amount of cooling requirement is in phase with the amount of solar radiation [7]. Nighttime and off-peak electric energy is readily available for utilization [8]. Utilization and application of off-peak electric energy for peak demand have an impact on peak load demand reduction [9].

Thermally driven cooling technologies are potentials both for utilizing the free solar energy and the cheaper off-peak electric energy. Several studies were conducted with regard to the applicability of thermally driven cooling technologies [10]. Desiccant cooling system is a potential for application utilizing available thermal energy resources [11]. Enteria et al., (2009) [12] shows the potential of utilizing nighttime electric energy and daytime solar energy for the operation of the desiccant cooling technology.

There were several researches conducted on the potential of the solar desiccant cooling technologies with and without back-up thermal energy sources [13,14]. System potential in different climatic conditions as in the case of Europe was conducted by Mavroudaki et al., 2002 [15]. For Australian climates, White et al., 2009 [14] conducted numerical investigation comparing the Southern and Northern Australian climates. Fong et al. [16] investigated the applicability of the system in sub-tropical Hong Kong. Kodama et al., 2000 [17] made

investigation for the application in damp climatic conditions. However, no investigation was conducted for application in the greater Asia-Pacific Region which is very hot and humid (East Asia during summer time and South East Asia for whole year).

The East Asian areas have temperate and sub-temperate climates while the South East Asian areas have tropical climate. Since the Asia-Pacific Region is very high in humidity and temperature compared to other regions of the world, day-long air cooling and dehumidification is needed. Katejanekarn et al. 2009 [18] showed that ordinary evaporative cooling alone was not enough to maintain the indoor thermal comfortable condition due to higher air wet bulb temperature. This paper presents the investigation of the solar desiccant cooling system potential in the Asia-Pacific Region (East Asia and South East Asia). This was done through numerical investigation in the transient system simulation (TRNSYS) program using the typical meteorological year (TMY) as the input weather conditions. The system was investigated during the hottest and humid week of the year.

Solar-desiccant cooling system

System description

The solar thermal desiccant cooling system presented in Fig. 1 consists of the solar thermal subsystem and the desiccant cooling subsystem. The solar thermal subsystem composes of the flat plate collector, nighttime electric heater and thermal storage tank. The desiccant cooling subsystem composes of desiccant wheel, cross-flow heat exchangers, evaporative coolers and daytime auxiliary heater (in this case an electric heater). The system (Fig. 1) is an updated design presented by Enteria et al., 2009 [19]. In the original design, no daytime auxiliary heater was

presented. In addition, one evaporative cooler was used in previous design. To make the system practical for application and at the same time enhance the cooling performance, daytime auxiliary heater and one evaporative cooler were added. The solar thermal subsystem and the desiccant cooling subsystem were connected through the air-heating coil.

System operation

The original design of the solar desiccant cooling system was validated by series of numerical and experimental runs [20,21]. The optimum design and operational conditions of the original system was used as the basis for the updated solar desiccant cooling system design presented here. The system operated during nighttime (off-peak) to store thermal energy from nighttime electric heater. The stored nighttime thermal energy was used to support the early operation of the desiccant cooling system. The desiccant cooling subsystem started to operate at 8AM which solar radiation was still not available [12]. As the solar energy increases with advancing daytime, the flat plate collector started to operate to support the operation of the desiccant cooling subsystem. However, in the case of cloudy sky, the daytime auxiliary heater was used to augment the thermal energy requirement. The daytime auxiliary heater used in the study was an electric heater; however, it can be substituted with gas heater and other waste-heat sources. The desiccant cooling subsystem operated until 6PM in the afternoon.

System and building model

Solar desiccant cooling system model

The model of the solar desiccant cooling system was done in TRNSYS [22]. The model considered the heat losses in the water piping [23]. Piping heat losses were considered based on our experimental evaluation [24]. Several solar thermal and desiccant cooling system modeling did not considered these losses.

Building model

The hypothetical building was designed to serve as the thermal load of the solar thermal desiccant cooling system. The building physical description and dimension was the same to Mavroudaki et al., (2002) [15]. However, the building structural components and thermal properties were different.

The building was rectangular in shape with all four walls as external. The building was cool and ventilated using the solar thermal desiccant cooling system from 8AM to 6PM during weekdays. The building had five office workers doing seated, light work such as typing. Each worker had sensible gain of 75W and latent gain of 75W. The worker had each computer with thermal gain of 230W. The office lighting had thermal gain of 17W/m^2. The building had an air infiltration of 0.5 ACH (air change per hour). All the thermal gains from computers, lighting and occupants started from 8AM to 6PM. The hypothetical building with solar thermal desiccant cooling system was applied in sixteen different cities in the Asia-Pacific region (See Table 1 for locations).

Performance indices

Solar thermal subsystem performance

The contribution of the solar energy in the thermal energy requirement of the system operation was expressed as the solar fraction (SF)

$$SF = \frac{Q_{Col}}{Q_{Col} + Q_{Hea} + Q_{Aux}} \quad (1)$$

Where,

$$Q_{Col} = \int_{Start}^{End} \left[m_{Col} C_{P(W)} \left(T_{Col,O} - T_{Col,I} \right) \right] dt \quad (2)$$

$$Q_{Hea} = \int_{Start}^{End} \left[m_{Hea} C_{P(W)} \left(T_{Hea,O} - T_{Hea,I} \right) \right] dt \quad (3)$$

$$Q_{Aux} = \int_{Start}^{End} \left[m_{RA} \left(h_{RA(2)} - h_{RA(1)} \right) \right] dt \quad (4)$$

Desiccant cooling subsystem performance

The ratio of air sensible energy load, latent energy load and total energy load reduced by the desiccant cooling subsystem was expressed as the sensible heat ratio (SHR)

$$SHR = \frac{Q_{Sen}}{Q_{Tot}} \quad (5)$$

Where,

$$Q_{Sen} = \int_{Start}^{End} \left[m_{SA} C_{P(A)} \left(T_{OA} - T_{SA} \right) \right] dt \quad (6)$$

$$Q_{Lat} = \int_{Start}^{End} \left[m_{SA} h_{Evap} \left(X_{OA} - X_{SA} \right) \right] dt \quad (7)$$

$$Q_{Tot} = Q_{Sen} + Q_{Lat} = \int_{Start}^{End} \left[m_{SA} \left(h_{OA} - h_{SA} \right) \right] dt \quad (8)$$

The desiccant cooling subsystem performance in reducing air temperature and humidity content based on thermal energy requirement was expressed as the desiccant coefficient of performance (DCOP)

$$DCOP = \frac{Q_{CL}}{Q_{Ther}} \quad (9)$$

Where,

$$Q_{CL} = \int_{Start}^{End} [m_{SA}(h_{OA} - h_{SA})]dt \quad (10)$$

$$Q_{Ther} = \int_{Start}^{End} [m_{RA}(h_{RA(1)} - h_{HA})]dt + \int_{Start}^{End} [m_{RA}(h_{RA(2)} - h_{RA(1)})]dt \quad (11)$$

System performance

The amount of electric energy consumption by the system operation was expressed as the ratio of off-peak electric energy consumption to total electric energy consumption called off-peak electric energy consumption (OPEC)

$$OPEC = E_{Nighttime} / (E_{Nighttime} + E_{Daytime}) \quad (12)$$

Where,

$$E_{Nighttime} = \int_{Start}^{End} (E_{Hea})dt + \int_{Start}^{End} (E_{Hea,Pump})dt \quad (13)$$

$$E_{Daytime} = \int_{Start}^{End} (E_{Aux})dt + \int_{Start}^{End} (E_{AHC,Pump})dt + \int_{Start}^{End} (E_{Col,Pump})dt + \int_{Start}^{End} (E_{Fans})dt \quad (14)$$

The performance of the system was based on the reduction of the air temperature and humidity content to the system total electric energy consumption expressed as system coefficient of performance (SCOP)

$$SCOP = Q_{CL} / (E_{Daytime} + E_{Nighttime}) \quad (15)$$

Simulation and Evaluation

System Specification

For different climatic conditions, the system had different specifications to maintain the indoor thermal comfort conditions (See Table 2). In this table, it was shown that in Tokyo, Japan, the required flat plate collector area was $8m^2$. The volumetric air flow rate was $330m^3/h$ for outdoor air with $165m^3/h$ supply air.

In the case of other locations and conditions, Table 2 shows the different sizes of the solar thermal system flat plate collector requirements and air flow rates to support room cooling, dehumidification and ventilation. This system size supported the required comfortable condition of the room presented. As shown in the table, northern part of the Asia-Pacific Region (East Asia and upper part of South East Asia) needed $8m^2$ of the flat plate collector except for Korea. In the lower portion of the South East Asia, the required flat plate collector was $12m^2$ except for Timor.

The required air flow rates for the East Asia was 330m^3/h compared to the middle of the East Asia and South East Asia which had 200m^3/h air flow rate. The southern part of the South East Asia required 330m^3/h air flow rate to support the required indoor environmental comfort.

The smaller requirement of flat plate collector area in the East Asia even at higher volumetric air flow rate is due to the lower outdoor air absolute humidity content compared to the South East Asia. Thus, the required thermal energy for dehumidification is lower compared to the South East Asia. In South East Asia, it needs large area of solar collector to support the dehumidification of high volumetric flow rate of air since the absolute humidity content is higher compared to East Asia.

In the case of the lower East Asia and upper South East Asia, smaller size of flat plate collector is needed with lower air flow rate due to the high collection of solar energy compared to north East Asia and not as high absolute humidity content compared to lower South East Asia. Thus, different sizes of the flat plate collectors are needed for different air flow rates to support the needed indoor environmental conditions.

Building Performance

In the case of Jakarta and Port Moresby, the desiccant cooling had an air flow rate of 330m^3/h compared to 200m^3/h in Dili with 12 m^2 flat plate collector (See Table 2). This was due to the higher dehumidification requirement (higher outdoor air absolute humidity content). The average air temperatures (outdoor air, supply air and room air) were presented in Fig. 2.

AIVC 2010 Conference [Korea]

As presented, the outdoor air temperature was higher in the location of Vientiane and Yagon (35^{o}C and above). The outdoor air temperature was decreasing from north to south of the two cities. The supply air temperature was between 17^{o}C and 24^{o}C. With this condition, the room temperature was maintained within 22^{o}C and 25^{o}C with system specifications presented in Table 5. In the case of air absolute humidity contents (outdoor air, supply air and room air), Fig. 3 showed the results.

As presented in the figure, the region outdoor air average absolute humidity was within 15g/kg and 21g/kg. This makes the region one of the most humid climates. The supply air absolute humidity content was maintained within 3g/kg and 7g/kg. With these conditions, the room absolute humidity was maintained within 8g/kg and 11g/kg. This makes the building indoor environment thermally comfortable.

The air equivalent relative humidity (outdoor air, supply air and room air) was presented in Fig. 4. It shows the region average humidity between 45% and 74%.

System Performance

The performance of the solar desiccant cooling system is presented in Fig. 5. It shows the sensible heat ratio (SHR), off-peak electric energy consumption (OPEC) and solar fraction (SF). The solar desiccant cooling system shows reduction of a large amount of air latent energy content. Based on the sensible heat ratio, it was within 20% to 30%. It means almost three-fourth of the air thermal load controlled by the solar desiccant cooling system was an air latent energy (moisture).

The operation of the nighttime electric heater made possible the early day operation of the solar desiccant cooling system. As shown in Fig. 5, the off-peak electric energy consumption reached more than 55% of the entire energy consumed in the operation of the solar desiccant cooling system (For cities of Yagon, Manila and Dili). These cities had high solar radiation with outdoor air temperature and humidity. Seoul has lower OPEC value due to lower solar radiation during the operation and it means daytime electric heater operates to compensate the system thermal requirement.

The evaluation of the thermal energy requirement was based on the solar energy contribution – solar fraction. It showed the high solar fraction was possible in the southern region (South East Asia) which reached 90% compared to the East Asia (less than 80%).

The system thermodynamic performances were presented in Fig. 6 – desiccant coefficient of performance (DCOP) and the system coefficient of performance (SCOP). The desiccant cooling subsystem performance – the desiccant coefficient of performance (DCOP) showed it had value of between 1 and 0.5 (Fig. 6). It means it needed greater amount of thermal energy to produce cooling load. However, as shown in Fig. 5, the solar energy contributed sizable amount of thermal energy requirement of the system. This is due to the contribution of solar fraction (between 70% and 90%).

As presented in the results, the system coefficient of performance was high in the South East Asia compared to the East Asia. The SCOP reached above 3 in Brunei. As shown in Fig. 3,

AIVC 2010 Conference [Korea]

Brunei has highest outdoor air absolute humidity content. The solar fraction in Brunei reached 90% (See Fig. 5). The solar thermal desiccant cooling system has low SCOP in Seoul (SCOP <1.5) due to low available solar radiation. This resulted to high consumption of thermal energy from electric heater (daytime).

Conclusions

The paper showed the potential and applicability of the solar thermal desiccant cooling system in the hot and humid Asia-Pacific Region (East Asia and South East Asia). The studies focused on the application of the developed solar thermal desiccant cooling system based on the numerical investigation in transient system simulation (TRNSYS) program.

The results showed the needed area of the flat plate collector varied depending on locations with available solar radiation, required air flow rates, and dehumidification rates. In addition, the needed air flow rate to maintain the indoor thermal comfort depends on the available solar radiation, outdoor air temperature, and humidity content.

In general, the presented solar thermal desiccant cooling system maintained the required indoor thermal comfortable conditions in the Asia-Pacific Region (East Asia and South East Asia) with specifications dependent to the region's different climatic conditions.

References

1. IEA, "Key World Energy Statistics," *International Energy Agency*, Paris, France, 2008.

2. Kolokotroni, M., Aronis, A., "Cooling-Energy Reduction in Air-Conditioning Offices by Using Night Ventilation," Vol. 63, *Applied Energy*, 1999, 241~253.

3. El-Desssouky, H., Ettouney, H., Al-Zeefari, A., "Performance Analysis of Two-Stage Evaporative Coolers," Vol. 10, *Chemical Engineering Journal*, 2004, 255~266.

4. Murakami, S., Levine, M.D., Yoshino, H., Inoue, T., Ikaga, T., Shimoda, Y., Miura, S., Sera, T., Nishio, M., Sakamoto, Y., Fujisaki, W., "Overview of Energy Consumption and GHG Mitigation Technologies in the Building Sector of Japan," Vol. 2, *Energy Efficiency*, 2009, 179~194.

5. Afonso, C.F.A., "Recent Advances in Building Air Conditioning Systems," Vol. 26, *Applied Thermal Engineering*, 2006, 1961~1971.

6. Kim, D.S., Infante Ferreira, C.A., "Solar Refrigeration Option – A State-of-the-Art Review," Vol. 31, *International Journal of Refrigeration*, 2008, 3~15.

7. Tabor, H., "Use of Solar Energy for Cooling Purposes," Vol. 13, *Solar Energy*, 1962, 395 ~399.

8. Balghouthi, M., Chahbani, M.H., Guizani, A., "Solar Powered Air Conditioning as a Solution to Reduce Environmental Pollution in Tunisia," Vol. 185, *Desalination*, 2005, 105~110.

9. Parker, G.J., "Off-Peak Energy Storage for Domestic Applications in Christchurch, New Zealand," Vol. 44, *Applied Energy*, 1993, 259~281.

10. Wang, R.Z., Oliveira, R.G., "Adsorption Refrigeration – An Efficient Way to Make Good Use of Waste Heat and Solar Energy," Vol. 32, *Progress in Energy and Combustion Science*, 2006, 424~458.

AIVC 2010 Conference [Korea]

11. Jurinak, J.J., Mitchell, J.W., Beckman, W.A., "Open-Cycle Desiccant Air Conditioning as an Alternative to Vapor Compression Cooling in Residential Applications," Vol. 106, *Journal of Solar Energy Engineering,* 1984, 252~260.

12. Enteria, N., Yoshino, H., Mochida, A., Takaki, R., Satake, A., Yoshie, R., Mitamura, T., Baba, S., "Construction and Initial Operation of the Combined Solar Thermal and Electric Desiccant Cooling System," Vol. 83, *Solar Energy*, 2009, 1300~1311.

13. Casas, W., Schmitz, G., "Experiences with a Gas Driven, Desiccant Assisted Air Conditioning System with Geothermal Energy for an Office Building," Vol. 37, *Energy and Buildings*, 2005, 493~501.

14. White, S.D., Kohlenbach, P., Bongs, C., "Indoor Temperature Variations Resulting from Solar Desiccant Cooling in a Building Without Thermal Backup," Vol. 32, *International Journal of Refrigeration*, 2009, 695~704.

15. Mavroudaki, P., Beggs, B.B., Sleigh, P.A., Halliday, S.P., "The Potential for Solar Powered Single-Stage Desiccant Cooling in Southern Europe," Vol. 22, *Applied Thermal Engineering*, 2002, 1129~1140.

16. Fong, K.F., Chow, T.T., Lin, Z., Chan, L.S., "Simulation-Optimization of Solar-Assisted Desiccant Cooling System for Subtropical Hong Kong," *Applied Thermal Engineering*, In Press.

17. Kodama, Andou, K., Ohkura, M., Goto, M. Hirose, T., "Process Configurations and Their Performance Estimations of an Adsorptive Desiccant Cooling Cycle for Use in a Damp Climate," Vol. 36, *Journal of Chemical Engineering in Japan*, 203, 819~826.

18. Katejanekarn, T., Chirarattanaon, S., Kumar, S., "An Experimental Study of a Solar-Regenerated Liquid Desiccant Ventilation Pre-Conditioning System," Vol. 83, *Solar Energy*, 2009, 920~933.

19. Enteria, N., Yoshino, H., Satake, A., Mochida, A., Takaki, R., Yoshie, R., Baba, S., "Development and Construction of the Novel Solar Thermal Desiccant Cooling System Incorporating Hot Water Production," Vol. 87, *Applied Energy*, 2010, 478~486.

20. Enteria, N., Yoshino, H., Satake, A., Mochida, A., Yoshie, R., Mizutani, K., "Numerical Evaluation and Optimization of the Combined Solar Thermal and Electric Desiccant Cooling System," In Proc: *ASME International Mechanical Engineering Congress and Exposition*, 2009.

21. Enteria, N., "Development and Evaluation of the Combined Solar Thermal and Electric Desiccant Cooling System," *Ph.D. Thesis, Tohoku University*, Japan, 2009.

22. TRNSYS 16, Solar Energy Laboratory, University of Wisconsin-Madison, USA.

23. Buckles, W.E., Klein, S.A., "Analysis of Solar Domestic Hot Water Heaters," Vol. 25, *Solar Energy*, 1980, 417~424.

24. Enteria, N., Yoshino, H., Mochida, A., Takaki, R., Yonekura, H., Yoshie, R., Mitamura, T., Baba, S., "Initial Operation and Performance Evaluation of the Developed Solar Thermal and Electric Desiccant Cooling System," *Experimental Heat Transfer*, In Press.

AIVC 2010 Conference [Korea]

Figures:

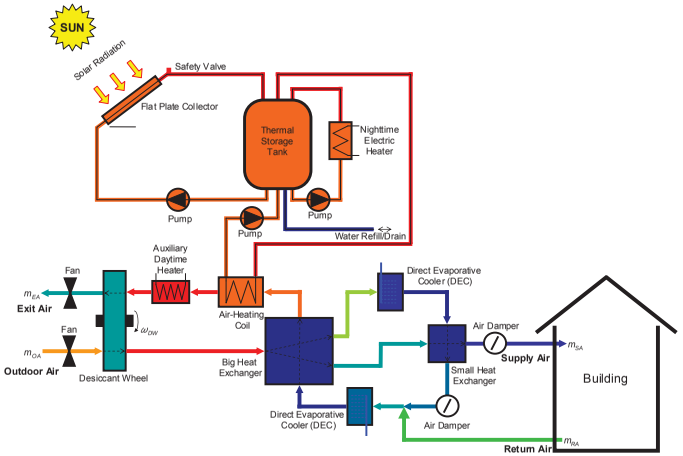


Figure 1 Solar thermal desiccant cooling system used in the study.

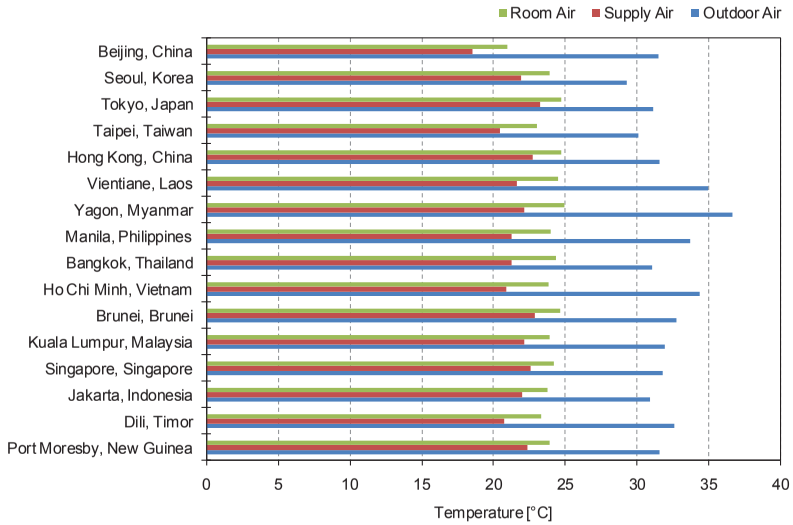


Figure 2 Air temperatures at different locations and weather conditions in the Asia-Pacific Region (East Asia and South East Asia).

AIVC 2010 Conference [Korea]

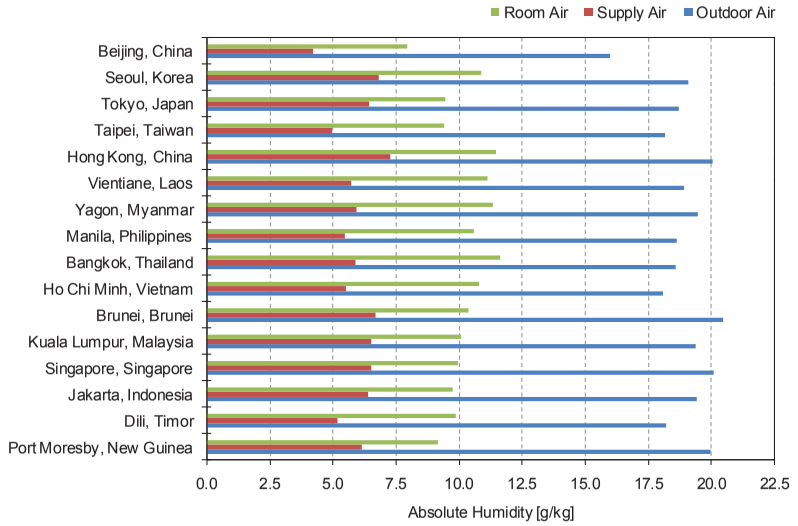


Figure 3 Air absolute humidity at different locations and weather conditions in the Asia Pacific Region (East Asia and South East Asia).

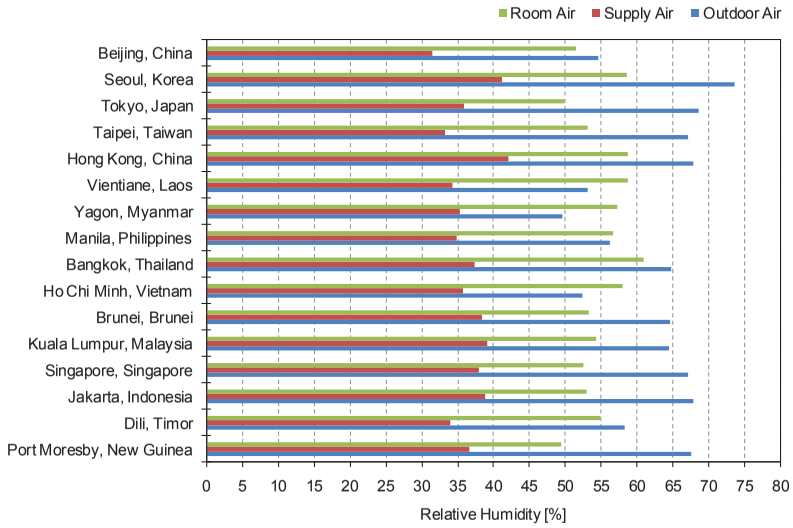


Figure 4 Air relative humidity at different locations and weather conditions in the Asia-Pacific Region (East Asia and South East Asia).

AIVC 2010 Conference [Korea]

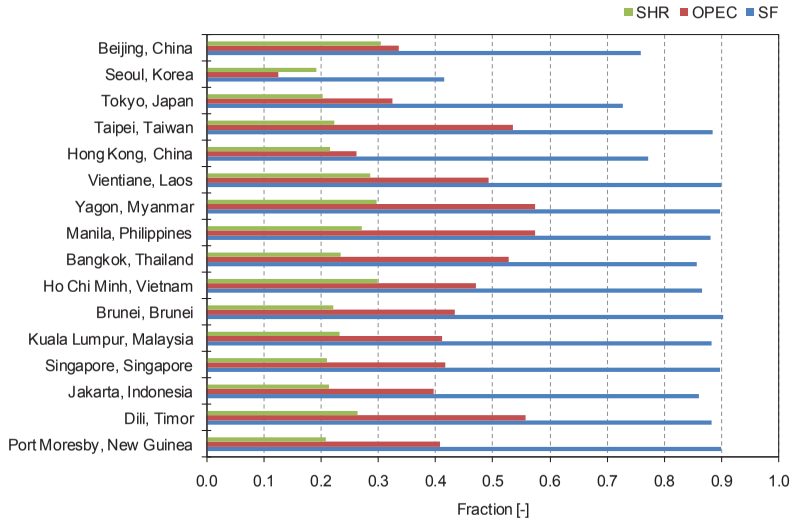


Figure 5 System sensible heat ratio, off-peak electric energy consumption and solar fraction at different locations and weather conditions in the Asia-Pacific Region (East Asia and South East Asia).

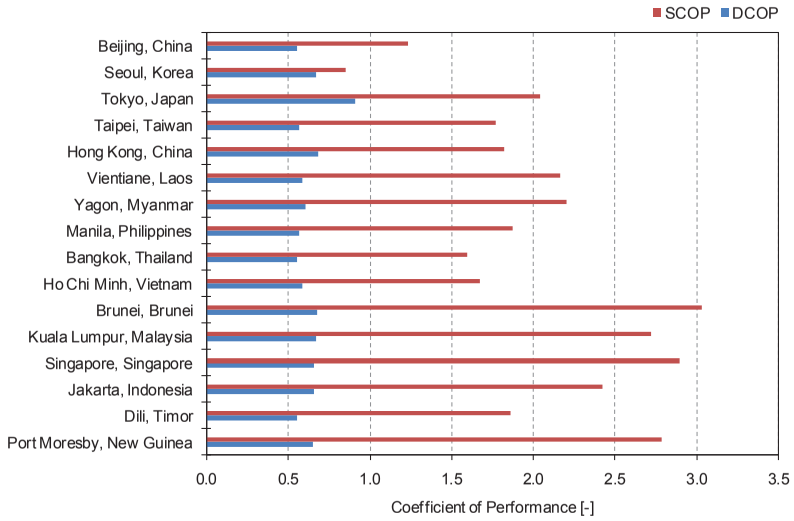


Figure 6 System coefficient of performance at different locations and weather conditions in the Asia-Pacific Region (East Asia and South East Asia).

AIVC 2010 Conference [Korea]

Table 1 Asia-Pacific Region (East Asia and South East Asia) major countries and cities

Country	City	Latitude	Longitude
China	Beijing	39° 54′ 50″ N	116° 23′ 30″ E
Korea	Seoul	37° 34′ 8″ N	126° 58′ 36″ E
Japan	Tokyo	35° 42′ 2″ N	139° 42′ 54″ E
Taiwan/China	Taipei	25° 2′ 0″ N	121° 38′ 0″ E
China (SAR)	Hong Kong	22° 15′ 0″ N	114° 10′ 0″ E
Laos	Vientiane	17° 58′ 0″ N	102° 36′ 0″ E
Myanmar	Yagon	16° 48′ 0″ N	96° 9′ 0″ E
Philippines	Manila	14° 35′ 0″ N	120° 58′ 0″ E
Thailand	Bangkok	13° 45′ 8″ N	100° 29′ 38″ E
Vietnam	Ho Chi Minh	10° 46′ 10″ N	106° 40′ 55″ E
Brunei	Bandar Seri Begawan	4° 53′ 25″ N	114° 56′ 32″ E
Malaysia	Kuala Lumpur	3° 8′ 0″ N	101° 42′ 0″ E
Singapore	Singapore	1° 17′ 0″ N	103° 50′ 0″ E
Indonesia	Jakarta	6° 12′ 0″ S	106° 48′ 0″ E
East Timor	Dili	8° 34′ 0″ S	125° 34′ 0″ E
Papua New Guinea	Port Moresby	9° 25′ 0″ S	147° 17′ 0″ E

Table 2 Specification of the solar thermal desiccant cooling system at different locations and weather conditions

	Flate Plate Collector		Air Flow Rate	
	Inclination [°]*	Area [m²]	Outdoor Air [m³/h]	Supply Air [m³/h]
Beijing, China	39	8	330	165
Seoul, Korea	37	10	330	165
Tokyo, Japan	35	8	330	165
Taipei, Taiwan	25	8	200	100
Hong Kong, China	22	8	330	165
Vientiane, Laos	17	8	200	100
Yagon, Myanmar	16	8	200	100
Manila, Philippines	14	8	200	100
Bangkok, Thailand	13	8	200	100
Ho Chi Minh, Vietnam	10	8	200	100
Brunei, Brunei	4	12	330	165
Kuala Lumpur, Malaysia	3	12	330	165
Singapore, Singapore	1	12	330	165
Jakarta, Indonesia	6	12	330	165
Dili, Timor	8	8	200	100
Port Moresby, New Guinea	9	12	330	165

**Facing Equator*

Dynamic Insulation System applied to Window Frames (Part 1)

Evaluation of the thermal insulation efficiency of the proposed window frames

Sihwan Lee[1], Miho Tanaka[1] and Shinsuke Kato[2]

[1] Graduate Student, The University of Tokyo, Dept. of Architecture, Tokyo, Japan 153-8505
[2] Professor, The University of Tokyo, Institute of Industrial Science, Tokyo, Japan 153-8505

Abstract

In order to insulate buildings more efficiently, many insulation methods have been proposed and successfully applied to the building envelope, including areas such as walls and windows. However, it is also important to insulate window frames efficiently because they usually contribute the greatest heat loss. The authors propose a new dynamic insulation system for window frames, with an active ventilation function and a heat pump for heat recovery. This system is composed of three parts: window frames that use a porous material for dynamic insulation, a mechanical ventilation system, and a heat-recovery heat pump system. This paper describes a computational simulation study of the technical feasibility and the thermal insulation efficiency of the porous material in the proposed system. First, a window frame was designed containing a porous material such as a packed bed of particles (i.e. glass wool, mineral wool, aluminum particles, etc.). Then, to verify its thermal insulation efficiency, the temperature contribution of the window frame was evaluated using computer fluid dynamics with different coupled conditions, such as the indoor/outdoor pressure difference. In addition, to verify the effect of moisture condensation, the relative humidity in the porous material was calculated based on conditions such as the outdoor air temperature, humidity ratio, indoor/outdoor pressure difference, and porosity of the insulation material. The calculated results show the thermal load was inversely proportional to the indoor/outdoor pressure difference. Moisture condensation in the insulation material depends on the outdoor temperature, humidity ratio, and porosity.

Keywords: Dynamic insulation, Thermal insulation efficiency, Computational fluid dynamics

Introduction

In recent years the world has been facing an escalating energy crisis, and reducing energy consumption is a serious concern [1], [2]. This being so, many different energy saving possibilities must be investigated, especially the use and loss of energy in buildings. Most heat loss in buildings occurs by heat conduction through the building envelope, including walls, windows, and window frames. However, heat loss also occurs by infiltration through cracks. Existing residential buildings often have very poor thermal performance, with a high U-value (more correctly called the overall heat transfer coefficient) and numerous cracks, resulting in high energy use for heating, cooling and ventilation. Therefore, buildings built recently are more airtight and use a great deal of insulation to minimize the loss of energy through the building envelope. However, a sole focus on air-tightness and insulation to reduce energy consumption in buildings will make it difficult to maintain indoor air quality (IAQ). Sick building syndrome (SBS) and building-related health concerns have become a driving force for improving IAQ via various technical and policy approaches [3]. One technical solution involves dynamic insulation that blocks heat transport by making the incoming airflow pass through a porous material. Because dynamic insulation reduces heat loss and also helps maintain indoor air quality, several different dynamic insulation systems have been proposed and successfully applied to the building envelope, including walls and windows [4], [5]. Furthermore, the Building Standard Law of Japan has been in force since July 1st, 2003, requiring a minimum indoor ventilation rate of 0.5 replacements per hour for the entire 24 hours. Many studies have shown that it is possible to use dynamic insulation efficiently in residential buildings.

Objectives

In this paper, we propose a new insulation system to insulate window frames efficiently in existing residential buildings, because they usually exhibit the greatest heat loss. The aim of this paper is to evaluate the thermal insulation efficiency of the insulation material in the proposed insulation system in order to confirm its feasibility. Moreover, we evaluate whether it produces excessive moisture condensation, depending on the outdoor temperature, the indoor/outdoor pressure difference, or the porosity of insulation material.

Methods

1. The new system proposed to increase thermal insulation and air-tightness

Figure 1 shows the concept of the new system proposed to increase thermal insulation and air-tightness of window frames in residential buildings. This system is composed of three

parts, including dynamic insulation incorporated in the window frames, a mechanical ventilation system, and a heat-recovery heat pump system.

1.1. Dynamic insulation incorporated in the window frames

In this paper, in order to apply dynamic insulation to window frames, porous insulation material such as a packed bed of particulate material (i.e. glass wool, mineral wool, aluminium particles, etc.) is installed around the window so that fresh air, water vapour and heat can pass through. Figure 2 shows the principle of dynamic insulation. Dynamic insulation refers to the use of porous insulation material through which ventilation air can enter a building, thereby reducing the conductive heat loss through the material to a very low level. Assuming uniform air flow, heat transfer in the dynamic insulation can be described using a 1-D steady-state model, as given by Equation 1 [6].

$$k\frac{d^2T(x)}{dx^2}-u\rho_aC_P\frac{dT(x)}{dx}=0 \qquad \text{(Eq. 1)}$$

where k [W/m·K] is the thermal conductivity of the insulation material, T [K] is the temperature, ρ_a [kg/m^3] and C_P [J/kg·K] are the density and the heat capacity of air, and u [m/s] is the air velocity.

Assuming a constant temperature boundary condition for the indoor and outdoor environments, the following dynamic U-value can be derived to represent the overall heat loss, as given by Equation 2. The dynamic U-value, U_{dyn} is the U-value of the wall modified by the air velocity across it and the insulation thickness.

$$U_{dyn}=\frac{u\rho_aC_p}{e^{\frac{u\rho_aC_pL}{k}}-1} \qquad \text{(Eq. 2)}$$

where L [m] is the insulation thickness. It is clear that the dynamic U-value is a function of the air velocity, or, more exactly, the *Pe* number, as given by Equation 3. This is defined to be the ratio of the rate of advection of a physical quantity by flow to the rate of diffusion of the same quantity driven by an appropriate gradient.

$$Pe=\frac{u\rho_aC_pL}{k} \qquad \text{(Eq. 3)}$$

1.2. Mechanical ventilation system

A mechanical ventilation system is used to maintain an adequate supply of fresh air and to maintain the thermal insulation efficiency of the dynamic insulation. This means that indoor air leaves the room through the ventilation system, while fresh air enters the room through the porous material in the window frames.

1.3. Heat-recovery heat pump system

The heat pump system recovers exhaust heat, enabling the creation of a zero-energy house. However, the heat recovery function of the heat pump system is used only in winter, because

a positive pressure condition must be maintained indoors to prevent moisture condensation in summer.

2. Numerical evaluation of thermal insulation efficiency

Computer fluid dynamics (CFD) was used to model fluid, heat flow, and condensation in the insulation material of the proposed system. CFD has been widely used to simulate air movement, heat transfer, mass transfer, and the interaction between indoor and outdoor environments.

2.1. Calculation model

To determine the thermal insulation efficiency of the proposed system, the temperature contributions of the window frames were calculated using computer fluid dynamics under different coupled conditions, i.e. the indoor/outdoor pressure difference. The calculation model was applied to simulate the insulation material, as shown in Fig. 3(a). The model included an indoor zone, an outdoor zone, a window, and a window frame. Details of the window frame (1.10 m × 1.04 m × 1.04 m) used to for calculation are shown in Fig 3(b). The insulation material applied to the window frame acts as an air supply opening, allowing fresh air into the room. In this study, the effects of the heat pump system and the window are not considered, in order to keep the model simple.

2.2. Flow model and boundary conditions

A high-Reynolds number k-epsilon turbulence model was used for computing the turbulent viscosity and diffusivity. For modeling of fluid, heat flow, and condensation, the boundary conditions required for the simulation were those associated with heat transfer through air and insulation material, and properties such as porosity and diameter. The boundary conditions and material properties for the simulation are summarized in Tables 1, 2, and 3.

2.2.1. Flow model for the porous media

The steady state flow model for simulation of the porous media is represented by a mass conservation equation as follows.

$$\frac{\partial(\rho U_i)}{\partial x_i} = 0 \qquad \text{(Eq. 4)}$$

where U_i is the mean superficial air velocity in the x_i direction. The superficial air velocity (velocity based on volumetric flow rate) is related to the physical velocity V_i (true velocity through pores of the medium for instance) by the porosity, $U_i = \varepsilon V_i$.

The permeability and inertial resistance factor of the porous media were derived from the Ergun equation, as given by Equation [7]. The Ergun equation is applied here for the pressure drop, *dp*, over the length, *dL*, determined by the diameter of the porous material, assuming that the U-value is 0 W/m^2 when the pressure difference is 10 Pa.

$$\frac{dp}{dL} = \frac{150\mu(1-\varepsilon)^2}{\varepsilon^3 \phi_C{}^2 D_P^2} U + \frac{1.75\rho(1-\varepsilon)}{\varepsilon^3 \phi_C D_P} U^2 \quad \text{(Eq. 5)}$$

where φ_C [-] is the shape factor, U [m/s] is the superficial velocity through the medium, ρ [kg/m^3] is the fluid density, D_P [m] is the diameter of the porous material, μ [kg/m·s] is the molecular viscosity, and ε [-] is the porosity or void fraction of the porous medium.

2.2.2. Air density

The density ρ of a mixture of dry air molecules and water vapour molecules can be expressed by Equation 6. To determine the density of the air, it is necessary to know the actual air pressure, the water vapour pressure, and the air temperature.

$$\rho = \frac{P_{dry}}{R_{dry} \times T} + \frac{P_{vapor}}{R_{vapor} \times T} \quad \text{(Eq. 6)}$$

where P_{dry} [Pa] is the pressure of dry air in pascals, P_{vapour} [Pa] is the pressure of water vapour in pascals, R_{dry} [287.05 J/kg·K] is the gas constant for dry air, and R_{vapour} [461.49 J/kg·K] is the gas constant for water vapour.

2.2.3. Thermal conductivity

The effective thermal conductivity of the porous material, k_{eff}, can be expressed as the volume average of the fluid conductivity and the solid conductivity, as shown in Equation 7.

Figure 5 shows the applied thermal conductivity in porous media in terms of porosity.

$$k_{eff} = \varepsilon \times k_{fluid} + (1-\varepsilon) \times k_{solid} \quad \text{(Eq. 7)}$$

where k_{solid} [W/m·K] is the solid medium thermal conductivity, and k_{fluid} [W/m·K] is the fluid phase thermal conductivity.

2.2.4. Mass diffusivity

The diffusion of moisture through building materials is a natural phenomenon, and it has significant effects on the comfort of the indoor environment. The effective diffusion coefficient in porous media, D_e, describes diffusion through the pore space of porous media, as shown in Equation 8 [8]. Figure 6 shows the applied effective diffusion coefficient in porous media in terms of porosity.

$$D_e = \frac{D\varepsilon_t \delta}{\tau} \quad \text{(Eq. 8)}$$

where D [m^2/s] is the diffusion coefficient of the gas or liquid filling the pores, ε_t [-] is the porosity available for transport, δ [-] is constrictivity, and τ [-] is tortuosity. In this study, we calculate the diffusion coefficient D using the following formula [9], [10].

$$D = 2.31 \times 10^{-5} \left(\frac{T}{273.16} \right)^{1.81} \left(\frac{P_a}{P_a + P_v} \right) \quad \text{(Eq. 9)}$$

where P_a [Pa] is the air pressure, in this case the atmospheric pressure, and P_v [Pa] is the vapour pressure.

2.3. Simulated cases

Figure 4 shows the calculated cases for the CFD simulation. These cases were based on the indoor/outdoor pressure difference, the outdoor temperature and the porosity of the insulation material in summer and winter. Table 2 shows the calculated cases in summer operating mode and Table 3 shows the calculated cases in winter operating mode.

Results and Discussion

1. Effect of indoor/outdoor pressure difference

Figures 7(a) and 10(a) show the calculated result of the temperature distribution across the insulation material versus the indoor/outdoor pressure difference in summer and winter. In winter, the air temperature rises slowly as the outdoor air passes through the insulation materials, and it is cooled slowly in summer. The heat loss/gain in the room was reduced with increases in the indoor/outdoor pressure difference, depending upon the estimated pressure drop across the porous material, as shown figure 13(a). However, it is necessary to calculate suitable ventilation rates because it is possible to increase ventilation loads by increasing the indoor/outdoor pressure difference. Therefore, this is the best way to use the heat pump system to recover heat from the exhaust air to realize zero-energy residential buildings.

Figures 7(b), 7(c), 10(b), and 10(c) show the calculated relative humidity and absolute humidity distribution versus the indoor/outdoor pressure difference in summer and winter. The results show that no moisture condensation occurred in any calculated case. Condensation did not occur in summer because no vapour barrier was used in the insulation material. It did not occur in winter either, because lower humidity of the outdoor air entered the indoor environment directly.

2. Effect of outdoor temperature

Figures 8(a) and 11(a) show the temperature distribution across the insulation material versus the outdoor temperature at an indoor/outdoor pressure difference of 10 Pa. The heat loss/gain in the room was smaller with a smaller indoor/outdoor temperature difference, as shown figure 13(b). Furthermore, the variation of the indoor wall surface temperature increased with a decrease in the indoor/outdoor temperature difference at a fixed pressure difference.

Figure 8(b), 8(c), 11(b), 11(c) show the calculated results for the relative humidity and absolute humidity distribution versus the outdoor temperature, showing that no moisture condensation occurred in the porous material in any calculated cases.

3. Effect of porosity

Figures 9 and 12 show the calculated heat loss/gain versus the porosity of insulation material. The heat loss/gain is approximately 0 W/m^2 with a porosity of greater than 50% when the indoor/outdoor pressure difference is 10 Pa, as shown in Figure 13(c). Therefore, we know that thermal insulation efficiency increases with increasing porosity of the insulation material.

Conclusions

This paper proposed a new system of dynamic insulation for window frames to reduce energy consumption, and conducted a feasibility study on its effectiveness using CFD simulation. In this paper, we found that the thermal insulation efficiency of the proposed system increased with increasing indoor/outdoor pressure difference, with decreasing indoor/outdoor temperature difference, and with increasing porosity of the insulation material. A summary of the general findings of this study is as follows.

1. The heat loss/gain in the room was reduced with increasing indoor/outdoor pressure difference, depending upon the estimated pressure drop across the porous material. Furthermore, it was also reduced with decreasing indoor/outdoor temperature difference.

2. According to the calculations on porosity, the heat loss/gain is approximately 0 W/m^2 for porosities greater than 50% when the indoor/outdoor pressure difference is 10 Pa.

3. No moisture condensation occurred in the porous material in any calculated case in summer and winter.

4. The properties of other porous materials should be measured and a new material developed with improved characteristics. Moreover, thermal comfort should be calculated for a realizable room model by examining the effects of any cold drafts and the energy-saving effects of the heat pumps included in the proposed system, and this will be evaluated in future investigations.

Acknowledgments

This study was made possible by the financial support received from the Ministry of the Environment, Japan. Moreover, we would like to thank the staff at Sankyo Tateyama Aluminium Inc., J Architecture System Inc., and Tsuchiya Hometopia Inc. for their generous cooperation.

References

1. IPCC Fourth Assessment Report (AR4), "Climate Change 2007: Synthesis Report", November, 2008, (http://www.ipcc.ch/publications_and_data/publications_ipcc_fourth_assessment_report_synthesis_report.htm).

2. Materials of the International Energy Agency (IEA), "Energy Policies of IEA Countries – Japan 2008 Review", June, 2008, (http://www.oecd.org/LongAbstract/0,3425,en_33873108_33873539_40804559_1_1_1_1,00.html).

3. Spengler J., Samet J., McCarthy J., Indoor Air Quality Handbook, Vol. 1.1–1.1 9, McGraw-Hill Professional Publishing, USA, 2001, pp. 22.1–22.11.

4. A. Dimoudi et al. "Experimental work on a linked, dynamic and ventilated, wall component," Energy and Buildings 36, 2004, pp. 443-453.

5. Arvid Dalehaug et al. "Dynamic Insulation in a wall," Report Collection of Architectural Institute of Japan, No. 66, 1993.

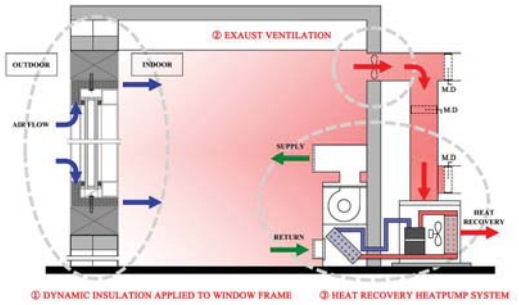
6. Annex 44 A3, "Dynamic Insulation Systems," Annex 44 State-of-the-Art Working Report Part A3, (www.civil.aau.dk/Annex44).

7. Sabri Ergun, "Fluid Flow Through Packed Columns," Vol. 48, No. 2, Chemical Engineering Progress, 1952, pp.89~94.

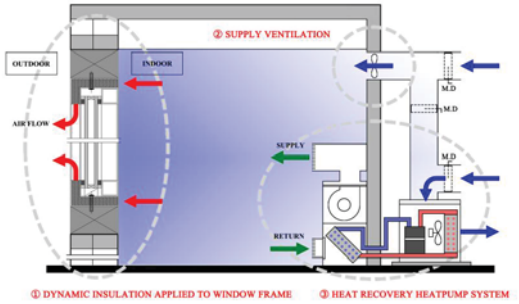
8. P. Grathwohl, "Diffusion in natural porous media: Contaminant transport, sorption / desorption and dissolution kinetics," Kluwer Academic Publishers, 1998.

9. Boynton, W.P., Brattain, W.H., 1929. Interdiffusion of gases and vapors. International Critical Tables 5.

10. Schirmer, R., "The diffusion coefficient water vapour-air mixtures and the rate of evaporation," VDI Beihaft Verfahrestechnik 6, 1938.

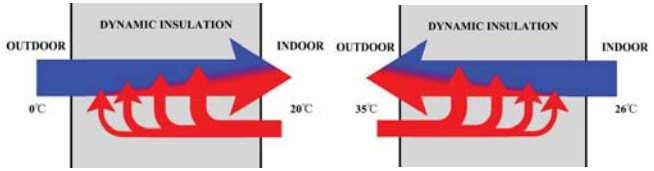


(a) Winter mode [negative indoor pressure]



(b) Summer mode [positive indoor pressure]

Fig. 1 Mechanisms of the proposed system



(a) Winter mode [negative indoor pressure] (b) Summer mode [positive indoor pressure]

Fig. 2 Principle of dynamic insulation

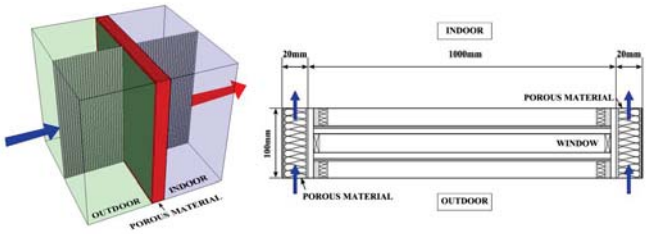
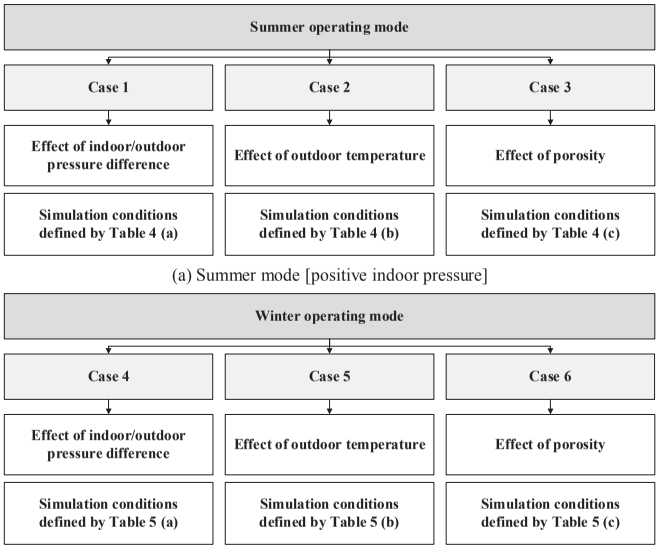


Fig. 3 Calculation model



(a) Summer mode [positive indoor pressure]

(b) Winter mode [positive indoor pressure]

Fig. 4 Simulated Cases

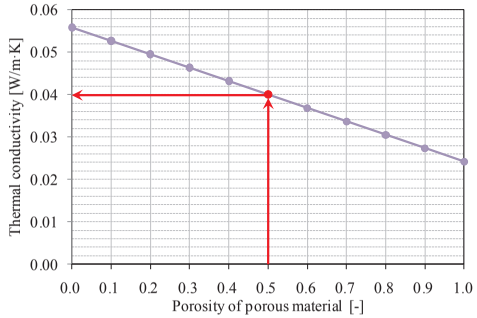
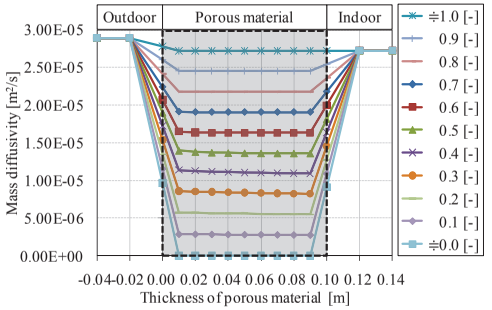
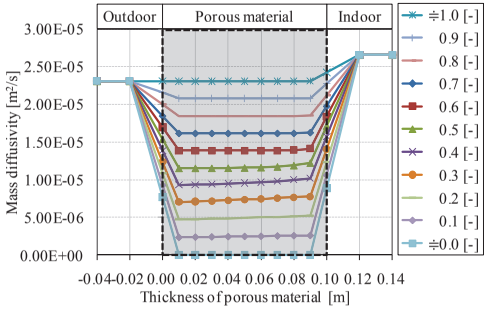


Fig. 5 Thermal conductivity of porous media versus porosity [W/m·K]

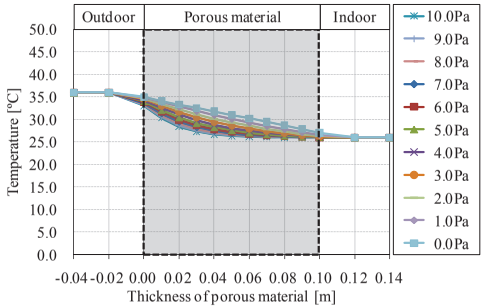


(a) Summer mode

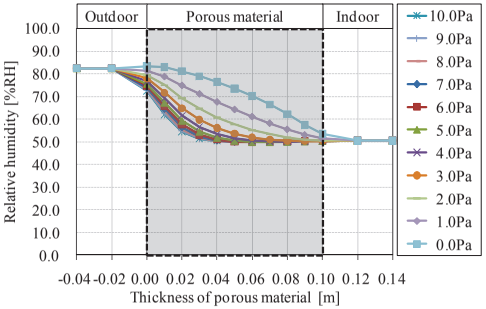


(b) Winter mode

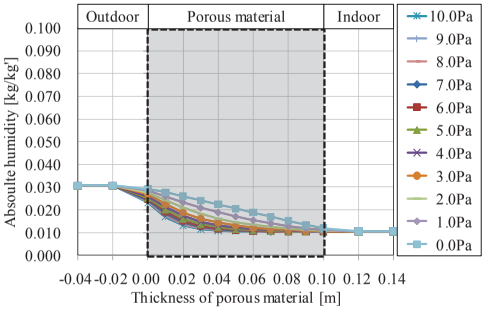
Fig. 6 Mass diffusivity versus porosity [m^2/s]



(a) Temperature distribution

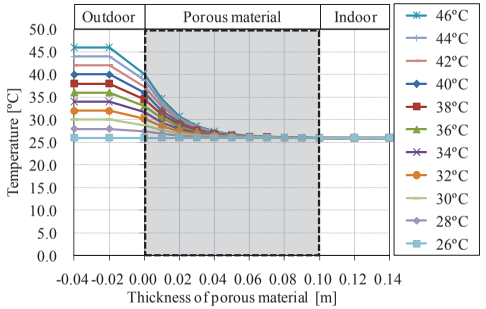


(b) Relative humidity distribution

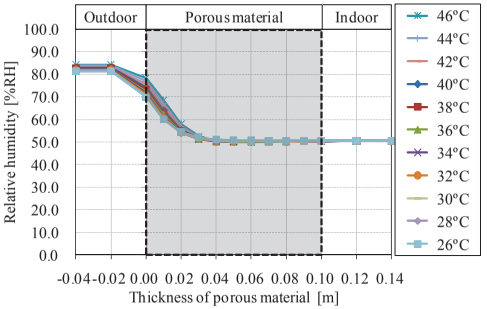


(c) Absolute humidity distribution

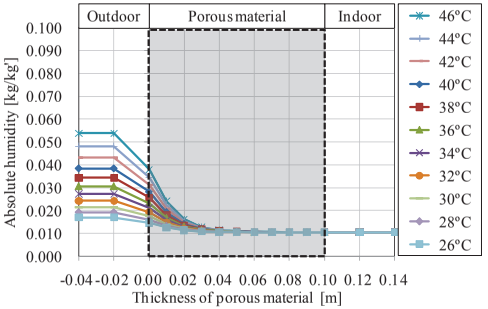
Fig. 7 Simulation results for Case 1



(a) Temperature distribution

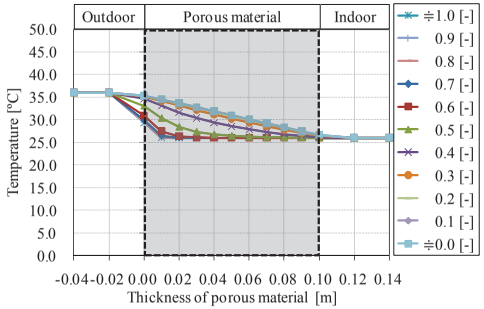


(b) Relative humidity distribution

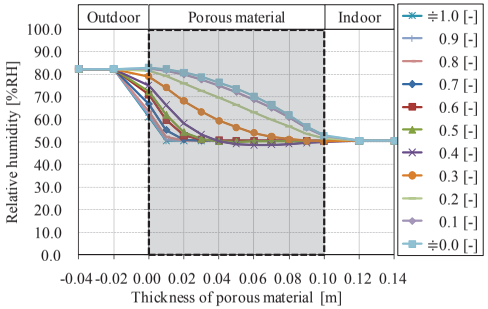


(c) Absolute humidity distribution

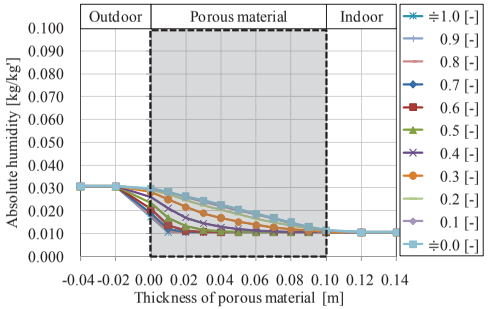
Fig. 8 Simulation results for Case 2



(a) Temperature distribution

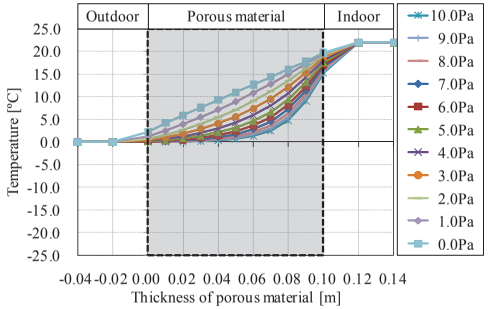


(b) Relative humidity distribution

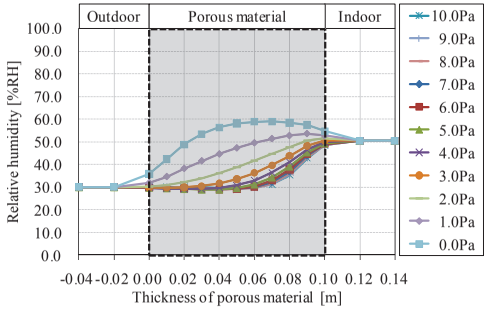


(c) Absolute humidity distribution

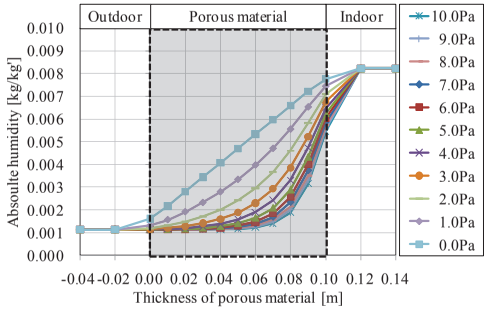
Fig. 9 Simulation results for Case 3



(a) Temperature distribution

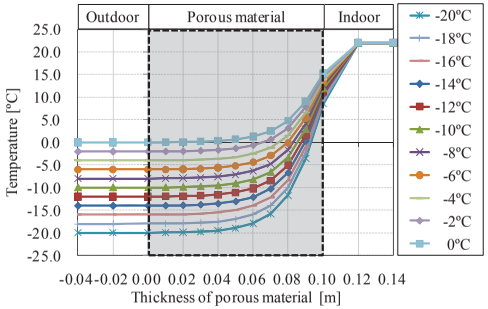


(b) Relative humidity distribution

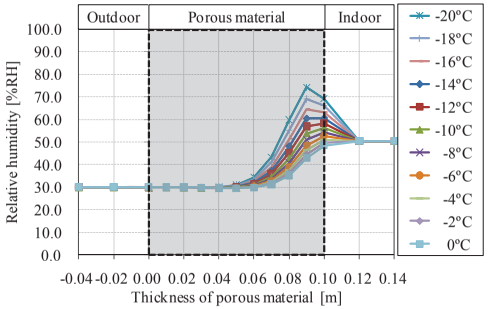


(c) Absolute humidity distribution

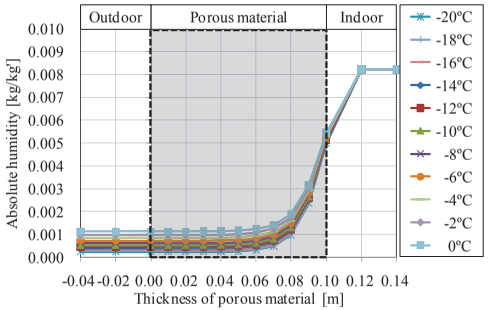
Fig. 10 Simulation results for Case 4



(a) Temperature distribution

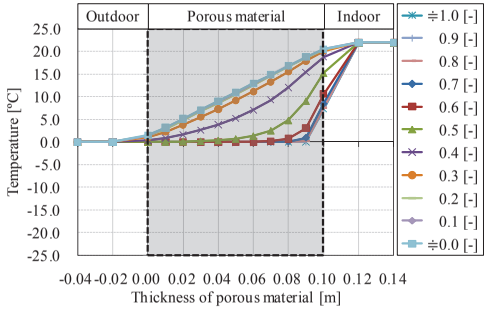


(b) Relative humidity distribution

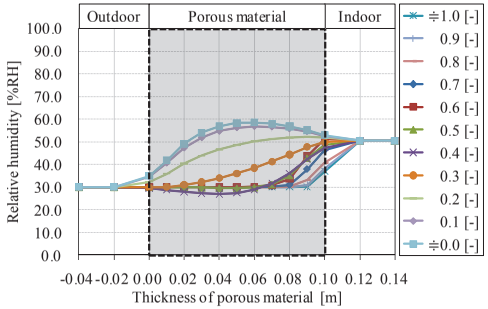


(c) Absolute humidity distribution

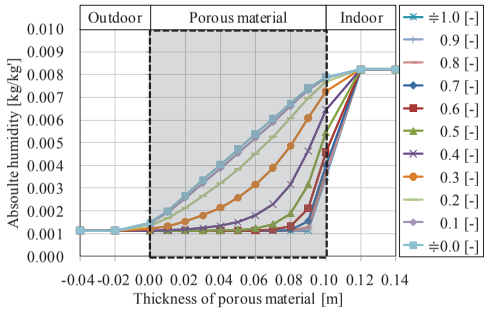
Fig. 11 Simulation results for Case 5



(a) Temperature distribution

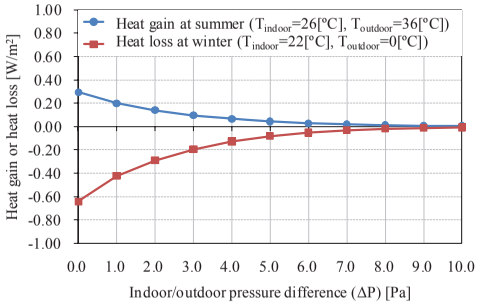


(b) Relative humidity distribution

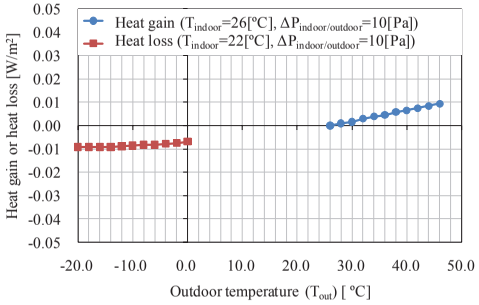


(c) Absolute humidity distribution

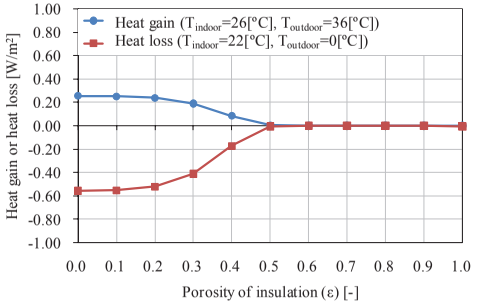
Fig. 12 Simulation results for Case 6



(a) Heat loss versus the indoor/outdoor pressure difference



(b) Heat loss versus the outdoor temperature



(c) Heat loss by the porosity

Fig. 13 Heat loss through the insulation material

Table 1 Boundary conditions

Items	Boundary conditions
Calculation domain	1.10 m(x) × 1.04 m(y) × 1.04 m(z)
Mesh	550,000 nodes with structured mesh
Turbulence model	High-Reynolds number k-epsilon turbulence model
Inlet boundary	0.0816 m^2, 0.002 m/s
Window	1.00 m(y) × 1.00 m(z), Adiabatic
Wall boundary	Defined in the calculated cases

Table 2 Material properties

Items	Air	Water vapour	Insulation material
Specific heat (C_P)	1006.43 [J/kg·K]	2014 [J/kg·K]	2100 [J/kg·K]
Thermal conductivity (λ)	0.0242 [W/m·K]	0.0261 [W/m·K]	0.0558 [W/m·K]
Viscosity (μ)	1.79×10^{-5} [kg/m·s]	1.34×10^{-5} [kg/m·s]	-
Molecular weight (M)	28.97 [kg/kgmol]	18.02 [kg/kgmol]	-

Table 3 Porous media properties

Items	Porous media
Viscous resistance ($1/m^2$)	Defined by Eq. 5
Inertial resistance (1/m)	Defined by Eq. 5
Fluid density (ρ)	Defined by Eq. 6
Thermal conductivity (λ)	Defined by Eq. 7
Porosity (ε)	0.5 [-] (Cases 1, 2, 4, 5) 0.0, 0.1, 0.2, 0.3, 0.4, 0.5, 0.6, 0.7, 0.8, 0.9, 1 [-] (Cases 3, 6)
Diameter (D_p)	0.0003278 [m]
Shape factor (φ_C)	1 [-]
Mass diffusivity (D_e)	Defined by Eq. 8

Table 4 Calculated cases in summer operating mode

(a) Calculated case using the indoor/outdoor pressure difference (Case 1)

Case 1		Summer operating mode
Indoor	Temperature	26 [°C]
	Relative humidity	50 [%RH]
Outdoor	Temperature	36 [°C]
	Relative humidity	80 [%RH]
Indoor/outdoor pressure difference		0, -1, -2, -3, -4, -5, -6, -7, -8, -9, -10 [Pa]
Porosity of insulation material		0.5 [-]

(b) Calculated case using the outdoor temperature (Case 2)

Case 2		Summer operating mode
Indoor	Temperature	26 [°C]
	Relative humidity	50 [%RH]
Outdoor	Temperature	26, 28, 32, 34, 36, 38, 40, 42, 44, 46 [°C]
	Relative humidity	80 [%RH]
Indoor/outdoor pressure difference		-10 [Pa]
Porosity of insulation material		0.5 [-]

(c) Calculated case using the porosity (Case 3)

Case 3		Summer operating mode
Indoor	Temperature	26 [°C]
	Relative humidity	50 [%RH]
Outdoor	Temperature	36 [°C]
	Relative humidity	80 [%RH]
Indoor/outdoor pressure difference		-10 [Pa]
Porosity of insulation material		0.0, 0.1, 0.2, 0.3, 0.4, 0.5, 0.6, 0.7, 0.8, 0.9, 1.0 [-]

Table 5 Calculated cases in winter operating mode

(a) Calculated case using the indoor/outdoor pressure difference (Case 4)

Case 4		Winter operating mode
Indoor	Temperature	22 [°C]
	Relative humidity	50 [%RH]
Outdoor	Temperature	0 [°C]
	Relative humidity	30 [%RH]
Indoor/outdoor pressure difference		0, -1, -2, -3, -4, -5, -6, -7, -8, -9, -10 [Pa]
Porosity of insulation material		0.5 [-]

(b) Calculated case using the outdoor temperature (Case 5)

Case 5		Winter operating mode
Indoor	Temperature	22 [°C]
	Relative humidity	50 [%RH]
Outdoor	Temperature	-20, -18, -16, -14, -12, -10, -8, -6, -4, -2, 0 [°C]
	Relative humidity	30 [%RH]
Indoor/outdoor pressure difference		-10 [Pa]
Porosity of insulation material		0.5 [-]

(c) Calculated case using the porosity (Case 6)

Case 6		Winter operating mode
Indoor	Temperature	22 [°C]
	Relative humidity	50 [%RH]
Outdoor	Temperature	0 [°C]
	Relative humidity	30 [%RH]
Indoor/outdoor pressure difference		-10 [Pa]
Porosity of insulation material		0.0, 0.1, 0.2, 0.3, 0.4, 0.5, 0.6, 0.7, 0.8, 0.9, 1.0 [-]

Dynamic Insulation System applied to Window Frames (Part 2)

Energy saving effects of the proposed system in residential buildings

Miho Tanaka[1], Sihwan Lee[1] and Shinsuke Kato[2]

[1] Graduate Student, The University of Tokyo, Dept. of Architecture, Tokyo, Japan 153-8505
[2] Professor, The University of Tokyo, Institute of Industrial Science, Tokyo, Japan 153-8505

Abstract

This paper describes the energy-saving effects of the proposed system with an active ventilation function and a heat pump for heat recovery. First, the temperature of the air supplied through the porous material versus the outdoor temperature was calculated using computational fluid dynamics to set the boundary conditions for the energy simulation. Then, the cooling/heating loads of a typical residential building in Japan were calculated and comparisons were made with and without the proposed system installed. In addition, in order to evaluate the energy-saving rate under different climatic conditions, the annual air-conditioning loads in several areas (Tokyo and Sapporo in Japan, and Seoul in the northwest of South Korea) were calculated. As expected, dynamic insulation applied to window frames was effective from the point of view of its insulation efficiency. The calculated results indicate that residential buildings making use of the proposed system could achieve energy savings of 14~34%. Especially it is more effective when the outdoor temperature is low in winter. In summer, the energy saving potential depends on the performance of an installed heat pump. A comparison of different climatic conditions showed that the energy-saving rate was especially high in areas with a large annual temperature difference between the indoor and outdoor environment.

Keywords: Dynamic insulation, Thermal insulation efficiency, Energy simulation, Ventilation system

Introduction

How best to reduce home energy consumption in Japan is a serious concern. Although the basic approach to reducing home energy consumption is to insulate and to seal up residences, adequate ventilation must be provided in order to maintain indoor air quality. Therefore, various architectural technologies have been designed to achieve this result. Dynamic insulation blocks heat transport by making the airflow coming into the house pass through a porous material. Because dynamic insulation reduces heat loss and also helps maintain the indoor air quality, many different systems for dynamic insulation have been proposed and successfully applied to the building envelope, including walls and windows [1], [2], [3]. However, it is especially important to insulate the window frame efficiently because it usually contributes the greatest heat loss.

Objectives

In a previous paper, a new dynamic insulation system was proposed and a CFD simulation showed that application of dynamic insulation to window frames was effective in terms of its insulation efficiency [4]. In this paper, using the results of the CFD simulation, the air-conditioning load was calculated by means of a coupled simulation of TRNSYS V16 [5],

with and without the system installed, to show how effectively the system could reduce energy consumption.

Methods

The heating/cooling loads of a typical residential building in Japan were calculated for four cases in terms of the heat pump system, heat recovery ventilator, and dynamic insulation applied to window frames.

1. Building models

Figure 1 shows the plan of the building model used for the calculation, which is proposed as a standard residence in Japan by the Institute for Building Environment and Energy Conservation (IBEC) [6]. The model differs a little according to the climate area: one is for a warmer area (building model type A), and another is for a colder area (building model type B). In this paper, model type A is used for calculations for Tokyo, and model type B is used for calculations for both Sapporo and Seoul.

2. Calculated cases

Table 1 shows the details of all cases. In all cases, the air change rate is 0.5 times per hour. In Case 1, the heat pump system, ventilation system with heat-recovery ventilator, and dynamic insulation are not installed. In Case 2, the model has only a heat recovery ventilator with 70% efficiency as a ventilation system. In Case 3, only a heat pump system is installed. In Case 4, dynamic insulation is applied to window frames with an exhaust heat pump system.

In this paper, for simplicity the cooling/heating loads of only the living room were calculated, using a transient system simulation program with a modular structure, TRNSYS. The calculated results show the differences between the four cases. In addition, in order to evaluate the energy-saving rate under different climatic conditions, the annual air-conditioning loads were calculated. Figure 3 shows a flowchart of all calculated cases.

3. Boundary conditions

Table 2 shows the boundary conditions of the building envelope. The U-value meets the standards established by IBEC [6]. Table 3 shows the boundary conditions of the windows. Dynamic insulation was applied only to the window frames in the living room. The frames contain porous materials. The ventilation air flow rates and the air temperature coming into the living room through the porous material were calculated by CFD simulation in a previous paper, with boundary conditions shown in Table 4 [4]. The porosity of the porous material is 0.5 [-] and the frame area is 15% of the window area. The pressure difference is assumed to

be 10 Pa in this paper, although various cases with different given conditions were calculated in the CFD simulation. This value was selected because heat loss through the porous material surrounding windows is almost 0 W/m^2 when the pressure difference is 10 Pa, as determined by the CFD simulation [4].

The air temperature coming into the living room through the porous material is calculated as follows. First, the relationship of the temperature difference between indoor/outdoor and indoor surface/outdoor is calculated from the results of the CFD simulation [4]. Figure 2 shows the temperature contribution, and leads to Equation 1 as a linear approximation:

$$T_{di} = 0.655 \times [T_{indoor} - T_{outdoor}] + 0.653 + T_{outdoor} \quad \text{(Eq. 1)}$$

where $T_{outdoor}$ [K] is ambient air temperature, T_{indoor} [K] is the indoor air temperature in the living room, and T_{di} [K] is the indoor surface temperature of the porous material.

4. Weather data

Data from AMeDAS (Automated Meteorological Data Acquisition System, developed by the Japan Meteorological Agency) in Tokyo (E139º 45' N35º 41'), Sapporo (E141º 21' N43º 04'), and data from Meteonorm (produced by METEOTEST) in Seoul (E126º 92' N37º 53'), including solar insolation, temperature, wind velocity and wind direction, were used as input data in order to calculate heating/cooling loads.

5. Family structure/schedule

We assumed that the family unit consisted of a father (male, age 46), a mother (female, age 44) and two children (female, age 16; male, age 14). Table 5 (a) shows the family schedule. Tables 5 (b) and (c) show the air-conditioning and lighting/equipment schedules, respectively.

Results and Discussion

1. Annual air-conditioning loads

Figure 4 shows the annual air-conditioning load of a typical residential building in three different areas, based on energy simulations using weather data for Tokyo, Sapporo and Seoul, and comparing the cases. This shows that the dynamic insulation system proposed in a previous paper [4] is more effective for energy saving in the cold climate areas, Sapporo and Seoul. The ratio of the annual air-conditioning loads of Cases 2, 3 and 4 to that of Case 1 is shown in Table 6. In Sapporo, the annual air-conditioning load of Case 4 is decreased 34% relative to Case 1. Under warm climate conditions, in Tokyo, the annual air-conditioning load in Case 3 is less than in Case 4.

2. Heating/cooling loads

Figure 5 shows the different heating/cooling loads of the cases. The heating loads calculated in the three areas decrease in order of increasing case number. The cooling loads of Case 2 are the largest of the three areas.

3. Air-conditioning loads versus heat conduction

Figure 6 shows the air-conditioning load due to heat conduction in the three different areas. In all areas, the conduction load for heating in Case 4 is much less than that of the other cases. The dynamic insulation system proposed is so effective in Case 4 that it contributes very significant heating energy savings. However, conduction loads for cooling in Case 2 are much less than in the other cases, for two reasons. First, in winter solar radiation makes the room warm and heated outdoor air is also supplied by the heat-recovery ventilator. Second, with the cooling mode in summer, the air supplied from the heat-recovery ventilator is warmer than the room temperature when the outdoor temperature is lower than that indoors. These situations make the cooling loads of Case 2 greater than those in Case 1. In all areas, the cooling load due to heat conduction in Case 3 is less than that in Case 4. This means that the dynamic insulation system applied to the window frames in Case 4 insulates the room well, which keeps the indoor temperature warm.

4. Air-conditioning loads versus ventilation

Figure 7 shows the ventilation loads in the three different areas. Ventilation loads of Case 2 are less than those of the other cases in all areas. In Case 3, the indoor/outdoor temperature difference is larger than in Case 1 because the heat pump system makes the living room warm in winter and cool in summer for all 24 hours, which saves air-conditioning load. Compared to Case 3, the heating load versus ventilation in Case 4 is lower because the dynamic insulation system supplies heated outdoor air to the building.

Conclusions

This paper evaluates the energy-saving efficiency of a new dynamic insulation system by examining outdoor conditions and combined systems. A summary of the general findings of this study is as follows.

1. This dynamic insulation system, proposed in a previous paper [4], saves energy in cold climate areas. In Sapporo, residential buildings using the proposed system could achieve energy savings of 34%.

2. With this dynamic insulation system, the cooling load does not decrease as much as the heating load. Residential buildings with the proposed system in a hot and humid climate will be evaluated in future investigations.

3. In this paper, a dynamic insulation system is applied only to the window frames, which reduces the heating/cooling load. This airflow window system and a wall with dynamic insulation will be proposed and evaluated in future investigations.

Acknowledgments

This study was made possible by the financial support received from the Ministry of the Environment, Japan. Moreover, we would like to thank the staff at Sankyo Tateyama Aluminium Inc., J Architecture System Inc., and Tsuchiya Hometopia Inc. for their generous cooperation.

References

1. A. Dimoudi et al. “Experimental work on a linked, dynamic and ventilated, wall component,” Energy and Buildings 36, 2004, pp. 443-453.

2. Arvid Dalehaug et al. “Dynamic Insulation in a wall,” Report Collection of Architectural Institute of Japan, No. 66, 1993.

3. Mohammed Salah-Eldin Imbabi. “Modular breathing panels for energy efficient, healthy building construction,” Renewable Energy 31, pp.729-738, 2006.

4. Sihwan Lee, Miho Tanaka, and Shinsuke Kato, “Dynamic Insulation System applied to Window Frames (Part1),” AIVC2010.

5. http://sel.me.wisc.edu/trnsys/

6. Client’s Criterion for Housing Project, “Heating and cooling load calculation, ”, Institute for Building Environment and Energy Conservation , Chapter. 3, pp. 35-64, 2009.

7. http://en.wikipedia.org/wiki/Tatami/

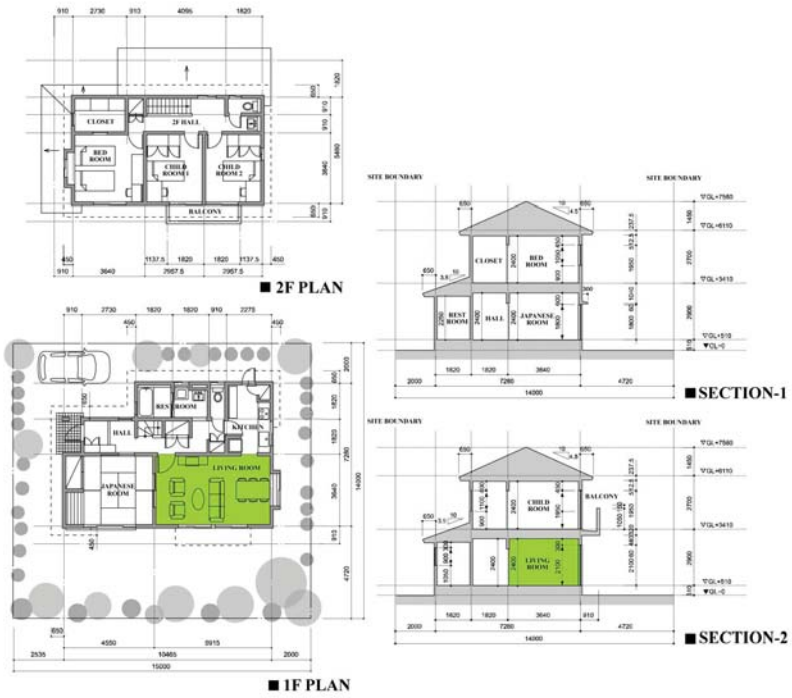


Fig. 1 Calculation model (model type A in warmer area in Japan by IBEC [6])

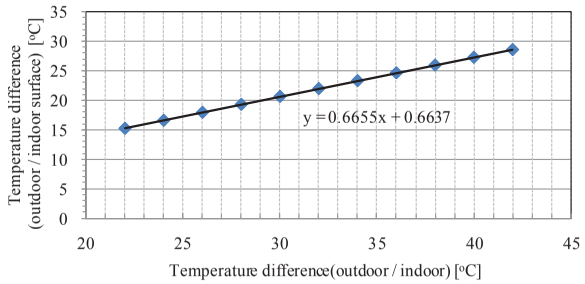


Fig. 2 Calculated supply air temperature through insulation by temperature difference

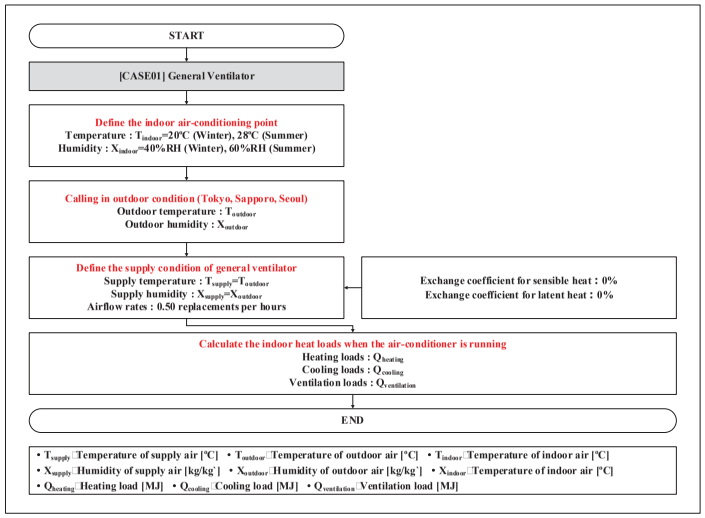


Fig. 3 (a) Flowchart of calculation (Case 1)

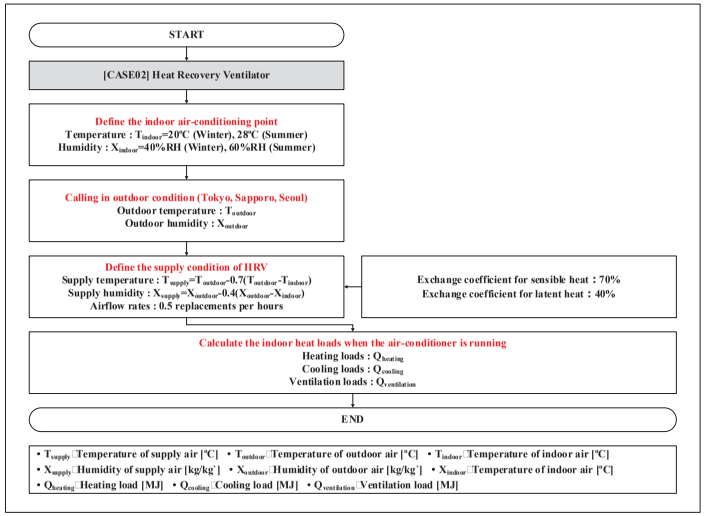


Fig. 3 (b) Flowchart of calculation (Case 2)

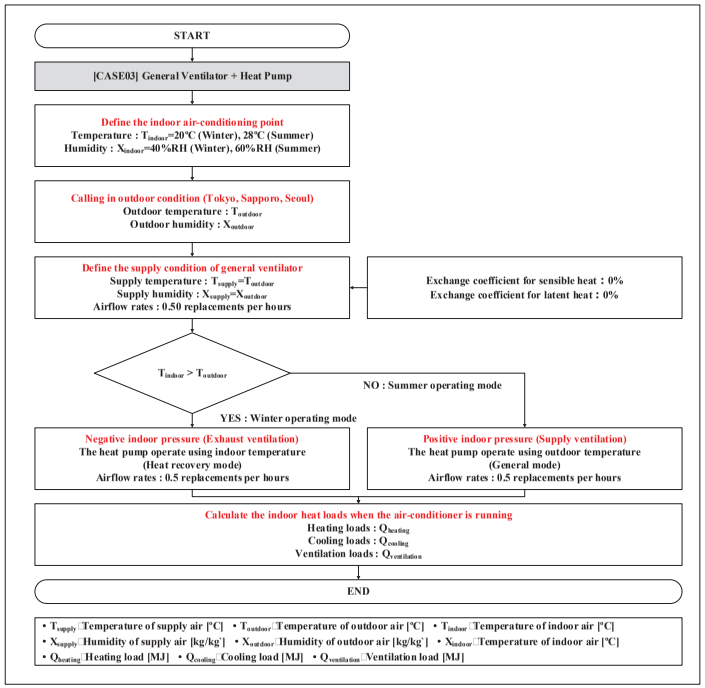


Fig. 3 (c) Flowchart of calculation (Case 3)

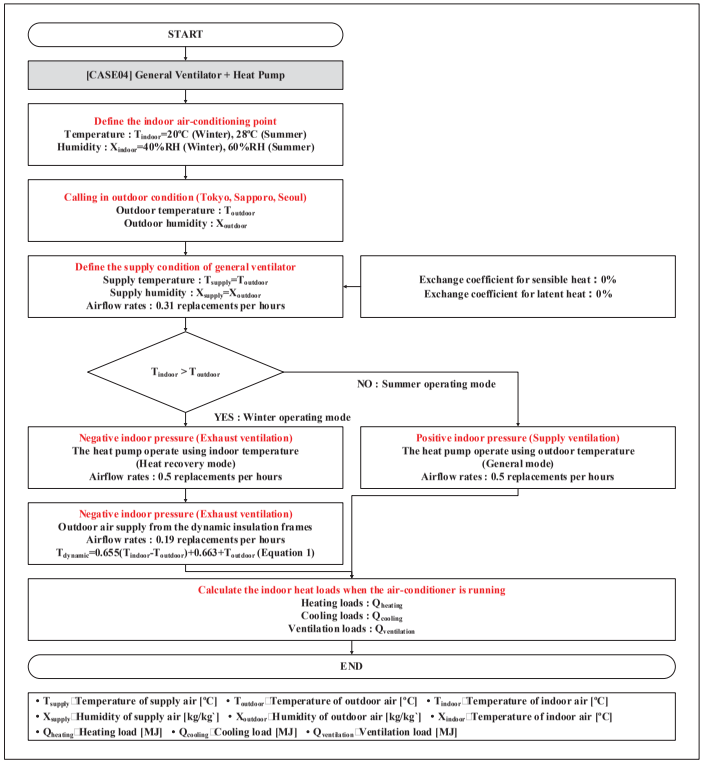


Fig. 3 (d) Flowchart of calculation (Case 4)

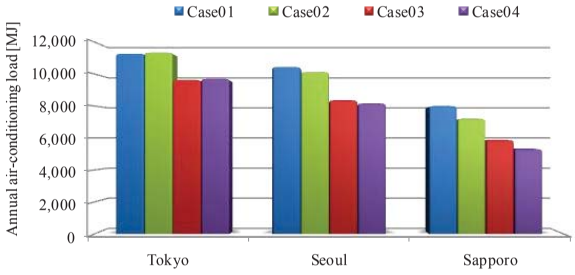
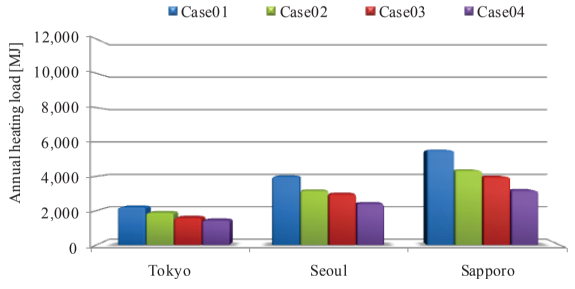
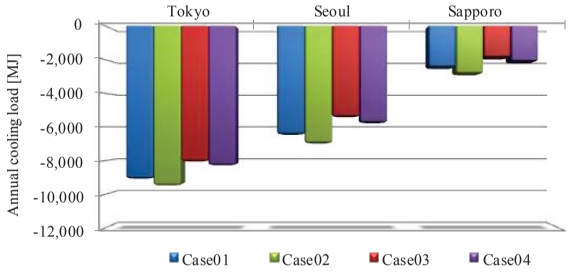


Fig. 4 Annual air-conditioning loads of each case

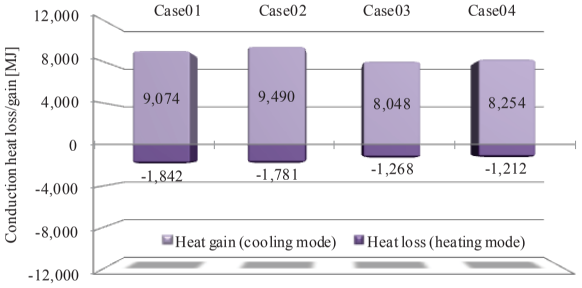


(a) Annual heating load

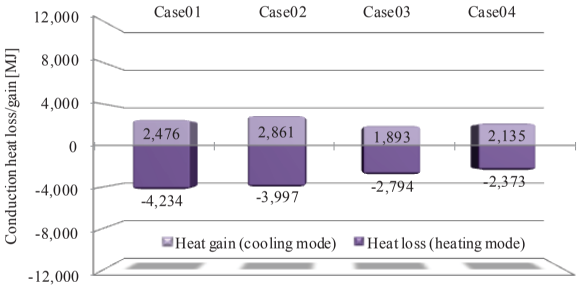


(b) Annual cooling load

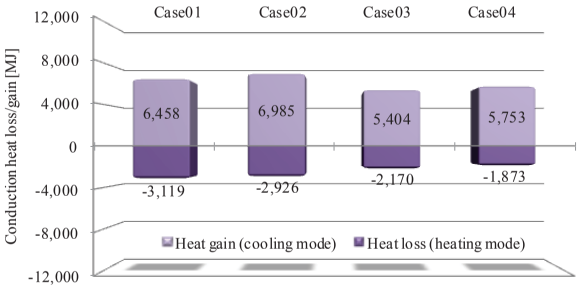
Fig. 5 Annual heating/cooling loads



(a) Tokyo, Japan

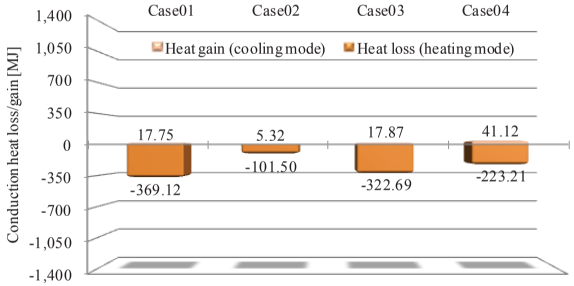


(b) Seoul, Korea

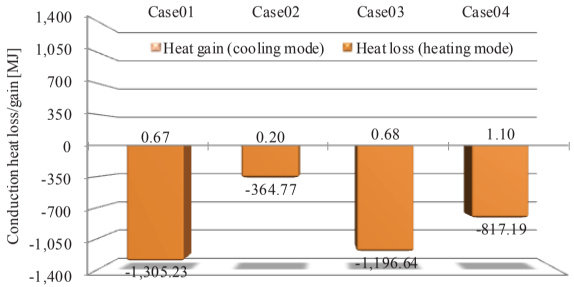


(c) Sapporo, Japan

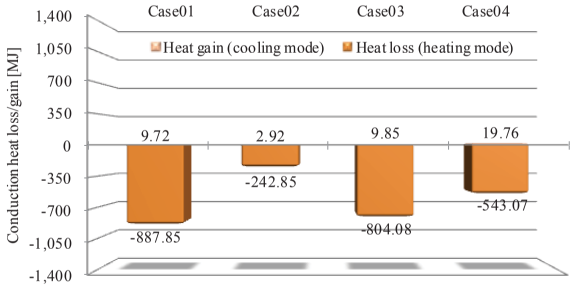
Fig. 6 Air-conditioning load due to heat conduction



(a) Tokyo, Japan



(b) Seoul, Korea



(c) Sapporo, Japan

Fig. 7 Air-conditioning load due to ventilation

Table 1 Calculated cases

Case1	General ventilator	○
	Heat recovery ventilator	×
	Heat pump system	×
	Dynamic insulation	×
Case2	General ventilator	×
	Heat recovery ventilator	○ (with 70% efficiency)
	Heat pump system	×
	Dynamic insulation	×
Case3	General ventilator	○
	Heat recovery ventilator	○ (with 70% efficiency)
	Heat pump system	○ Returning air : exhaust air from living room Mixed air : exhaust air from living room
	Dynamic insulation	×
Case4	General ventilator	○
	Heat recovery ventilator	×
	Heat pump system	○ Returning air : exhaust air from living room Mixed air : exhaust air from living room
	Dynamic insulation	○ (applied only to the window frames)

Table 2 Boundary conditions of building envelopes

	U-value [W/(m^2·K)] (building envelope)			
	Floor	Tatami [7]	Wall	Ceiling
Tokyo	0.403	0.344	0.385	0.294
Sapporo	0.208	0.191	0.254	0.167
Seoul	0.208	0.191	0.254	0.167

Table 3 Boundary conditions of windows

(a) B.C. of living room

	Glazing	Window frame			Shading
	U-value [W/(m²·K)]	U-value [W/(m²·K)]		Area rate [%] (frame/window)	Internal shad. factor
		Case 1, 3	Case 4		
Tokyo	2.54	5.68	0.00	15.00	0.50
Sapporo	1.26				
Seoul	1.26				

(b) B.C. of the other room

	Glazing	Window frame		Shading
	U-value [W/(m²·K)]	U-value [W/(m²·K)]	Area rate [%] (frame/window)	Internal shad. factor
Tokyo	2.54	5.68	15.00	0.50
Sapporo	1.26			
Seoul	1.26			

Table 4 Boundary conditions for CFD simulation

Indoor temperature	22 [°C]
Outdoor temperature	0, -2, -4, -6, -8, -10, -12, -14, -16, -18, -20 [°C]
Indoor/outdoor pressure difference	-10 [Pa]
Porosity of insulation material	0.5 [-]
Area of porous material	0.0816 [m²]
Velocity of porous material	0.002 [m/s]

Table 5 Schedule

(a) Family schedule

Room	Day	Occupants												
		AM	0-1	1-2	2-3	3-4	4-5	5-6	6-7	7-8	8-9	9-10	10-11	11-12
		PM	12-13	13-14	14-15	15-16	16-17	17-18	18-19	19-20	20-21	21-22	22-23	23-24
LDK	Weekly	AM							1	2	1	1		
		PM	1	1			1	2	2	3	3	2	1	1
	Weekend	AM									3	2	2	2
		PM	2	1			2	3	3	4	2	2	1	
Children room	Weekly	AM	1	1	1	1	1	1	1					
		PM									1		1	1
	Weekend	AM	1	1	1	1	1	1	1	1	1	1	1	1
		PM					1	1	1		1	1	1	1
Children room 2	Weekly	AM	1	1	1	1	1	1	1					
		PM							1			1	1	1
	Weekend	AM	1	1	1	1	1	1	1	1		1	1	1
		PM	1								1	1	1	1
Bed room	Weekly	AM	2	2	2	2	2	2	1					
		PM												1
	Weekend	AM	2	2	2	2	2	2	2	1				
		PM												2

(b) Air-conditioning schedule

Room		Preset temperature	
		Heating mode	Cooling mode
Living rooms	Wake time	20°C	27°C / 60%
	Sleep time	-	28°C / 60%
	Unused time	-	-
The other rooms		-	-

※ Living rooms : LDK(Living, Dinning, Kitchen), Japanese room, Children room, Bed room

(c) Equipment (ventilator) schedule

Room	Day		Supply / Exhaust air flow [m^3/h]											
		AM	0-1	1-2	2-3	3-4	4-5	5-6	6-7	7-8	8-9	9-10	10-11	11-12
		PM	12-13	13-14	14-15	15-16	16-17	17-18	18-19	19-20	20-21	21-22	22-23	23-24
Kitchen	Weekly	AM							75					
		PM	75						150	150				
	Weekend	AM						150			75			
		PM	75						150					
1F Rest room	Weekly	AM							6	2		0.8		
		PM	0.8				0.8	0.8	0.8	0.8	0.8	2.0		2.8
	Weekend	AM								4.0	4.0		1.2	1.2
		PM					2.0	0.8		2.0	0.8		2.0	0.8
Bath room	Weekly	AM												
		PM										50	25	100
	Weekend	AM												
		PM						75	25			25	25	100

Table 6 Annual air-conditioning load relative to Case 1

	Case 1	Case 2	Case 3	Case 4
Tokyo	100%	102%	85%	86%
Seoul	100%	97%	80%	78%
Sapporo	100%	90%	73%	66%

Natural Ventilation in Thai Hospitals: A Field Study

Vorapat INKAROJRIT

Faculty of Architecture, Chulalongkorn University, Bangkok 10330 Thailand

Abstract

Natural ventilation has been appraised as the main strategy in environmental control of airborne infection in resource-limited healthcare facilities. While natural ventilation offers a low-cost alternative in diluting and removing contaminated air, its' performance in actual settings is not fully understood. This paper reports a cross-sectional field study of six hospitals in Thailand with an emphasis on ventilation performance of naturally-ventilated hospital wards and AII rooms. The results showed that ventilation rates of 3-26 ACH could be achieved in hospital wards. Higher ventilation rates of 16-218 ACH were found in AII rooms. Our measurements also showed that a few locations within hospital wards had little or no air movement due to existing hospital ward designs. This study concludes that natural ventilation is suitable for resource-limited hospitals in tropical climates when windows are opened and exhaust fans are installed. Design guidelines that promote natural ventilation were discussed.

Keywords: Natural ventilation, Environmental control, Field study, Ventilation rate, Hospital design, Infection Control

Introduction

Nowadays, airborne infection of Tuberculosis (TB) is the cause of illness and death in many countries around the world. Although the prevalence and death rates have been falling in the past several years, the number of new TB cases is still rising slowly especially in the Southeast Asia region. Inpatients and health-care workers (HCWs) are at particularly high risk of infection with TB because of frequent exposure to patients with infectious TB disease. To minimize TB infection, the World Health Organization (WHO) and the U.S. Centers for Disease Control and Prevention (CDC) has proposed guideline for infection control through three-level hierarchy of control including administrative control, environmental control and personal respiratory protection. Natural ventilation is one of the strategies in environmental control of airborne infections that should be maximized in resource-limited health-care facilities [1-6].

Natural ventilation uses natural forces, i.e. pressure and thermal difference to drive air through buildings. While natural ventilation may offer a low-cost alternative in diluting and removing contaminated air when compare with mechanical ventilation, the pattern of air movement, however, is unreliable and hard to predict.

Previous researches have tried to understand the pattern of air movement in hospitals. Currently, there are many studies that examined various aspects related to the design and performance of ventilation system in health-care facilities through simulation [7-12]. The results from these simulation studies, however, had not taken into account of additional factors that may be found in actual settings such as the effect of opening windows and doors, the use of mechanical fans, and the impact from building occupants' behavior that could influence the pattern of ventilation. Thus far, there are only a limited number of studies that evaluate ventilation performance of actual naturally-ventilated hospitals. For example, Qian et al [6] showed that high ventilation

rate could be achieved in naturally-ventilated isolation room in Hong Kong and installation of exhaust fan could create enough negative pressure when the natural forces are not sufficiently strong. Escombe et al. [13] found that opening windows and doors provided median ventilation of 28 ACH from eight hospitals in Lima, Peru. Both of the above-mentioned studies used a tracer gas concentration decay technique in determining air exchange rate. Recently, World Health Organization (WHO) published a comprehensive guideline for natural ventilation implementation [3]. Examples of naturally-ventilated health-care facilities were briefly described. Results from literature review showed that existing design guideline describes general hospital designs criteria that foster natural ventilation strategy. However, ventilation performance during normal operational condition had not been documented.

In summary, ventilation performance in actual hospital has not been examined thoroughly. If designers better understood factors that affect ventilation performance in actual settings, then it would be possible to design better naturally-ventilated hospital that can effectively control airborne infection.

The research described in this paper is a part of a larger study on enhancing occupational health surveillance in Thai Hospital. This research was funded by the Global Fund (Round 8) for fighting AIDS, Tuberculosis and Malaria and Thailand-US Centers for Disease Control and Prevention. The objectives of this study are to gain more understanding on current environmental control procedure in Thailand and to evaluate the effectiveness of using natural ventilation for airborne infection control. The ultimate goal is to develop a simple method for evaluating ventilation performance and to provide practical recommendations that promote the use of natural ventilation in resource-limited hospitals.

Methods

Settings

To achieve the research's objectives, we conducted a three-day visit to six hospitals in various part of Thailand during November 2009 – March 2010. The case study hospitals were selected based on two preliminary criteria. First, the hospital must have a substantial number of TB cases per year in the area. Second, as a part of the Global Fund project, hospitals in different part of Thailand were selected as a representative for each region of Thailand.

Case study hospitals in this paper were constructed between 1980s-1990s. For each hospital, ventilation related data were collected from outpatient department, general hospital ward, ICU ward, airborne infection isolation room (AII), TB/HIV Clinic, and emergency room. This paper only presents data from naturally-ventilated hospital wards and AII rooms were reported.

Building configurations

Room and window dimensional data were gathered from available construction drawings. In case that printed documents could not be located, room and window dimensional data were measured on-site. Flows of healthcare workers (HCWs) and TB patients through various spaces were documented based on observation and series of interview. These dimensional data were later used to create floor plans of targeted departments. Locations of TB patients in hospital ward and mechanical fans were marked on floor plans for functional analysis.

Ventilation measurement

In this assessment, simplified method for documenting ventilation performance in the field was developed. Air velocity data and airflow direction were measured at various spots in the targeted departments using a thermal anemometer (Velocicalc Model. 9535-A) and ventilation smoke tube kit (MSA Part No. 458481). These data were later used for the generation of preliminary air flow diagrams and analysis. This study also documented direction of airflow between the targeted and adjacent spaces and location of fresh air intake and exhaust.

Calculation of air change rate

The method for air change rate measurement was similar to method that was used in Aluclu and Dalgic's study [14] where the air velocity data were measured and averaged from three to six spots at the center of the opening.

In order to calculate air change rate, WHO [2] suggested that, as an approximation, the rate of air change per hour (ACH) for wind-driven natural ventilation through a room with two opposite openings, can be calculated as:

$$ACH = \frac{0.8 \times v_{air} \times a_{inlet} \times 3600}{volume} \qquad \text{(Eq. 1)}$$

where

ACH = air change rate (measured as volume of room air change per hour)

v_{air} = average air velocity at inlet (m/s)

a_{inlet} = area of smaller inlet (m^2)

$volume$ = volume of room (m^3)

Finally, calculated air change rates were compared with CDC guideline [4] for determination of ventilation performance.

Building Survey

The architectural and ventilation data were collected during normal building operation hours. Position and operational behavior of windows, doors, and mechanical fans in hospital wards were not adjusted. For AII rooms, however, we examined ventilation performance in an empty room in which windows and doors were opened and closed to measure the effect of openings on ventilation performance. Exhaust fans were switched under the closed window position. We spent approximate two hours at each location for data collection. Permission to take photograph of building occupants and to measure ventilation performance was granted prior to measurement session.

Data Analysis

Field study data were represented in two forms. First, for hospital wards, air velocity data, air flow direction and location of TB patient (if they were placed in the hospital ward) were mapped onto the building floor plan. Second, configurations and ventilation performance of hospital wards and AII rooms were tabulated for comparison and analysis.

Results and Discussion

Hospital wards: Building configurations and ventilation performance

Figure 1-9 shows building floor plan of nine inpatient wards from six case study hospitals. The data showed that these hospital wards share similar planning characteristics.

First, the majority of these wards were oriented on the cardinal axis where the shorter sides (elevator lobby & fire exit) of the ward faced east-west and the longer side (bed area) faced north-south direction. It was hypothesized that these wards were designed in response to local climate (i.e. to catch the local wind and to avoid direct solar penetration). Building occupants enter these hospital wards from the entrance door on the "shorter side" of the floor plan. The entrance doors were kept open most of the time and they would be closed during non-visiting hours.

Second, the windows and doors on the patient side of the wards typically consisted of six sets of jalousie window and a door per structural bay. Insect screen was installed at each window. Based on our interview, these doors were kept open at all time while the windows would be opened or closed by patients who reside next to them. Since the time of our field study was in the winter season of Thailand, a few of the windows were closed. Although, the assumption is that these windows are expected to be opened all year round since the weather in Thailand is hot and humid.

Third, the nurse stations and single-room (special) wards usually occupied one side of the ward except for ward E1 and E3 where the nurse stations were placed next to the entrance. It was found that inpatients' beds were typically arranged in rows of four to six on the opposite side of the nurse station. Based on the interview, TB patients who had been treated would be moved to and placed at the far corner of the main ward. The locations of TB patients within each are marked on Figure 1-9.

Finally, it was found that all nurse stations and single-room ward had air-conditioning system installed. Therefore, the windows and doors in these areas were kept close most of the time except for a few hours after sunset for energy conservation.

Results from the field study showed that ceiling fans and/or wall-type fans were installed in the main ward area. In a few hospitals, occupants were free to turn these fans on/off to maintain their comfort status. While most hospitals have ceiling type fan or wall-type fan installed, two of the hospital installed exhaust fan to increase ventilation rate within the ward. At inpatient ward of hospital C, the fans were place at the upper portion of internal window (see Figure 10). This exhaust fan was found to flush air from the ward out to the corridor on the back side of the ward. For hospital D (see Figure 11), the exhaust fans were installed at the upper portion of the jalousie windows to flush the air from the ward to outdoor air space. Additional fans were installed inside the ward to push air toward the building envelope.

Table 1 describes building configurations and ventilation performance of hospital wards. The data showed that the number of beds in hospital ward ranges between 28-47 beds per ward. All of these hospitals have floor-to-ceiling height of 3.0-3.5 m. The results showed that calculated air change ranges between 3.08-26.80 air-change per hour (ACH) were found in these wards. High ventilation rates (17.75 and 26.80 ACH) were found in hospital wards which had exhaust fans installed. Low ventilation rates which are lowered than the CDC recommended value were found in hospital wards in which the air inlets and outlets were small in size and not aligned.

Airborne infection isolation room: Building configuration and ventilation performance

Figure 12 shows typical floor plans of naturally-ventilated airborne infection isolation (AII) rooms that were found during the field study. Typical floor plan consisted of a single-bed or a double-bed room, each with its own toilet (see Figure 12). Table 2 describes building configuration and ventilation performance of airborne infection isolation rooms from 4 hospitals. Data showed that when all openings were fully open, the ventilation rates were between 65-218 ACH. When the door/windows on one side were closed and the exhaust fans were turned on, the measured ventilation rates ranged between 16-36 ACH which was higher than CDC recommended value of 12 ACH.

Effect of windows and doors

It was found that the design of most hospital wards in this study did not promote the use of natural ventilation strategy. Since these hospitals were built in the early 1980s, it was hypothesized that no air-conditioning systems were installed in the nurse station area at that time. In the past windows and doors of nurse station would be opened to maximize natural ventilation. Nowadays, air-conditioning systems were installed in these nurse stations which lead to the permanent closure of windows and doors in these areas. Since effective natural ventilation relies on opening of windows and doors on the opposite side of the space, it was found that the air-conditioned nurse stations blocked path of natural wind. In many hospital wards, there was no natural air inlet or outlet except for the entrance door.

In addition, field study data showed that windows on the patient side were controlled by the building occupants who reside next to those windows. Since the temperature at the perimeter zone fluctuate more than the interior zone, a few of these windows were found closed during the time of investigation. Furthermore, a few of these windows and doors were malfunctioned, i.e. they could not be closed nor opened. Together with the installed insect screen, path of natural ventilation were blocked for multiple reasons. This leads to a lower than expected air change rate in many of the hospital wards.

Effect of exhaust fan on ventilation performance

It was found that there were two hospital wards with exhaust fans. These hospital wards were found to achieve higher ventilation rate than hospitals without exhaust fan. The airflow direction, shown by smoke visualization, showed that when the exhaust fans were turned on, the air flow outward in a good fashion. However, since the wind direction changes all the time, ventilation rate could be lowered due to the natural wind that flow against the exhaust direction.

For inpatient ward of hospital D, the contaminated air was moved toward the back corridor which connects the main ward with isolation rooms and staff rooms. This configuration could present a great risk to the HCWs and patients who suffer from low-immune function in the isolation room.

This research suggests that since natural ventilation is unreliable and unpredictable, mechanical fan should be installed to increase air change rate. Furthermore, the location of exhaust fan/duct should be carefully design to maximize the potential of natural ventilation.

ACH vs. Air movement

Results from our study clearly demonstrate that high air change rate could be achieved via natural ventilation. However, while the ACH criterion had been satisfied, analysis of spot air velocity data showed a few locations within the hospital wards with little or no air movement (less than 0.3 m/s [15]). These areas were found at the corner of the ward and, sometime, in the middle of the ward. Data analysis showed that lay-out of the existing floor plan, the location of existing air inlets/outlets which were not aligned, and the installation of interior curtain/partitions may block or divert airflow within interior space.

Figure 13 showed Floor plan and airflow direction of airborne infection isolation (AII) ward at hospital F. Since the upper portion of the AII rooms in this ward were left opened (see Figure 14), this results in possibly contaminated air moving from the upstream ward to the downstream ward.

Therefore, it is suggested that while air change criterion is a compulsory measure that needs to be satisfied in infection control, additional attention should be given to spot measurement of air velocity as well as monitoring of air movement. Locations with no air movement should be avoided, especially for the placement of TB patient within the hospital wards.

Conclusion

This paper presented a field measurement study on the performance of natural ventilation in six hospitals in Thailand. Design guidelines that promote natural ventilation for airborne infection control were discussed. The results showed that ventilation rates of 3-26 ACH could be achieved in hospital wards. The highest ventilation rates were found in hospital wards which had exhaust fans installed. For the AII rooms, high ventilation rates were found for both opened and closed window position. Our measurements also showed that a few locations within hospital wards had little or no air movement due to existing hospital ward designs.

The results confirmed that high ventilation rate could be achieved via natural ventilation and it is suitable for resource-limited hospitals in tropical climates. However, due to its unpredictability, this research suggests that mechanical ventilation system should be installed to supplement the natural ventilation.

As a cross-sectional field study, however, data collected were representative of the assessment date only. Data may not necessary represent typical operational circumstance. In addition, due to the limitation of available equipments and the availability of study sites, this field study only inspected preliminary ventilation performance under actual settings. Further studies are needed to improve our holistic understanding of factors that affect ventilation performance in actual settings. In pursuing this research further, we plan to expand the study to examine ventilation performance during other months of the year. The effect of windows and doors would also be investigated.

Acknowledgements

The work described in this paper was supported by a grant from the Global Fund for fighting AIDS, Tuberculosis, and Malaria (Round 8). The authors would like to thank Bureau of Tuberculosis, Thailand-US Centers for Disease Control and Prevention, and all Hospital staffs for their invaluable support in making this research possible.

References

1. World Health Organization, *Guidelines for the Prevention of Tuberculosis in Healthcare Facilities in Resource-Limited Settings*, WHO, 1999.

2. World Health Organization, *Infection prevention and control of epidemic- and pandemic-prone acute respiratory diseases in health care: WHO Interim Guidelines*, WHO, 2007.

3. World Health Organization, *Natural Ventilation for Infection Control in Health-care Settings,* WHO, 2009.

3. WHO, *WHO Policy on TB Infection Control in Healthcare Facilities, Congregate Settings, and Household*, WHO, 2009.

4. Center for Disease Control and Prevention, *Guidelines for Environmental Infection Control in Healthcare Facilities*, US Department of Health and Human Services Centers for Disease Control and Prevention, Atlanta, Georgia, USA, 2005.

5. Li, Y., Leung, G.M., Tang, J.W., Yang, X., Chao, C.Y.H., Lin, J.Z., Lu, J.W., Nielsen, P.V., Niu, J., Qian, H., Sleigh, A.C., Su, H.J.J., Sundell, J., Wong, T.W., and Yuen, P.L., "Role of ventilation in airborne transmission of infectious agents in the built environment – a multidisciplinary systematic review," Vol. 17, *Indoor Air*, 2007, pp. 2~18.

6. Qian, H., Li, Y., Seto, W.H., Ching, P., Ching, W.H., and Sun, H.Q., "Natural Ventilation for Reducing Airborne Infection in Hospitals," Vol. 45, *Building and Environment*, 2010, pp. 559~565.

7. Cheong, K.W.D., and Phua, S.Y., "Development of ventilation design strategy for effective removal of pollutant in the isolation room of a hospital," Vol. 41, *Building and Environment*, 2006, pp. 1161~1170.

8. Qian, H., Li, Y., Nielsen, P.V., and Hyldgaard, C.E., "Dispersion of exhalation pollutants in a two-bed hospital ward with a downward ventilation system," Vol. 43, *Building and Environment*, 2008, pp.344~354.

9. Tang, J.W., Li, Y., Eames, I., Chan, P.K.S., and Ridgway, G.L., "Factors involved in the aerosol transmission of infection and control of ventilation in healthcare premises," Vol. 64, *Journal of Hospital Infection*, 2006, pp.100~114.

10. Méndez, C., San José, J.F., Villafruela, J.M., and Castro, F., "Optimization of a hospital room by means of CFD for more efficient ventilation," Vol. 40, *Energy and Buildings*, 2008, pp.849~854.

11. Rui, Z., Guangbei, T., and Jihong, L., "Study on biological contaminant control strategies under different ventilation models in hospital operating room," Vol 43, *Building and Environment*, 2008, pp.793~803.

12. Perino, M., "Short-term airing by natural ventilation – modeling and control strategies," Vol. 19, *Indoor Air*, pp.357~380.

13. Escombe, A.R., Oeser, C.C., Gilman, R.H., Navincopa, M., Eduardo, T., Pan, W., Martinez, C., Chacaltana, J. Rodriguez, R., Moore, D.A.J., Friedland, J.S., and Evans, C.A., "Natural Ventilation for the Prevention of Airborne Contagion," Vol. 4, No. 2, *PLOS Medicine*, 2007, pp.309~316.

14. Aluclu, I., and Dalgic, A., "A Case Study on Natural Ventilation Characteristics of the Diyarbakir Surici (Old City) Municipality Building in Turkey," Vol. 40, *Building and Environment*, 2005, pp.1441~1449.

15. Gong, N., Tham, K.W., Melikov, A.K., Wyon, D.P., Sekhar, S.C., and Cheong, K.W., "The Acceptable Air Velocity Range for Local Air Movement in The Tropics," Vol. 12, No. 4, *International Journal of Heating, Ventilating, Air-Conditioning and Refrigerating Research*, 2006, 1065~1076.

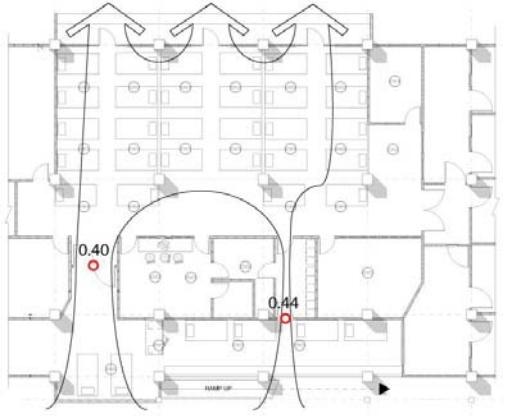


Fig. 1 Floor plan and ventilation data of hospital A inpatient ward



Fig. 2 Floor plan and ventilation data of hospital B inpatient ward

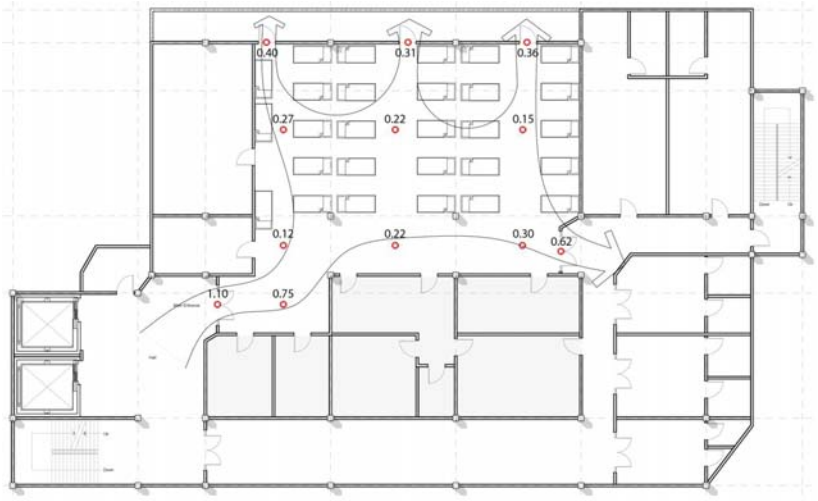


Fig. 3 Floor plan and ventilation data of hospital C inpatient ward



Fig. 4 Floor plan and ventilation data of hospital D inpatient ward

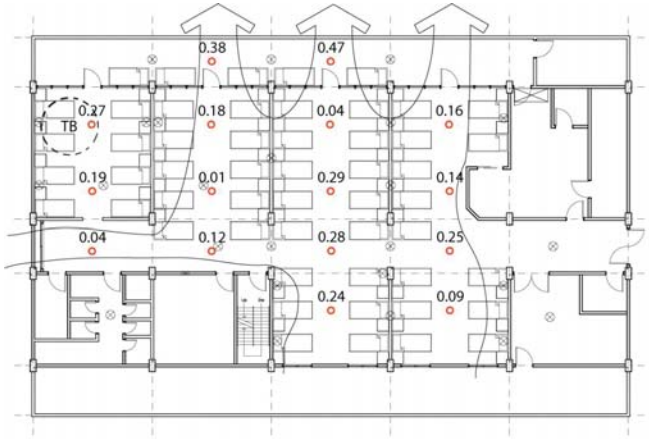


Fig. 5 Floor plan and ventilation data of hospital E inpatient ward#1

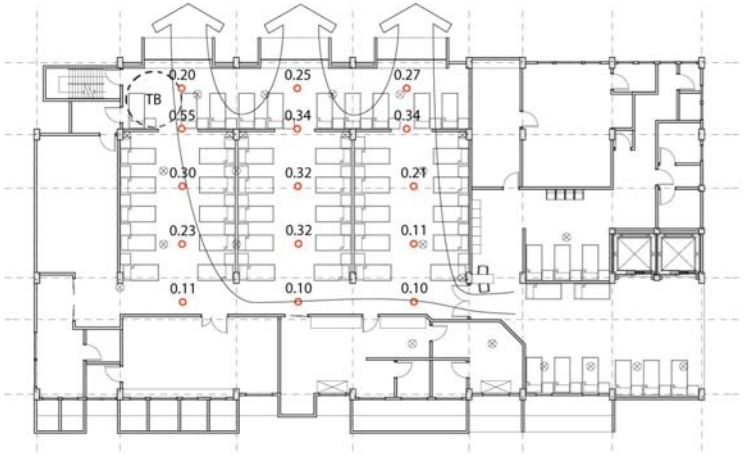


Fig. 6 Floor plan and ventilation data of hospital E inpatient ward#2

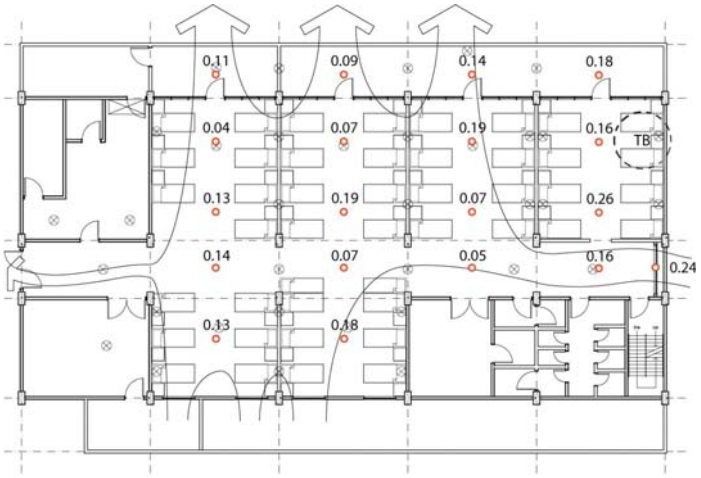


Fig. 7 Floor plan and ventilation data of hospital E inpatient ward#3

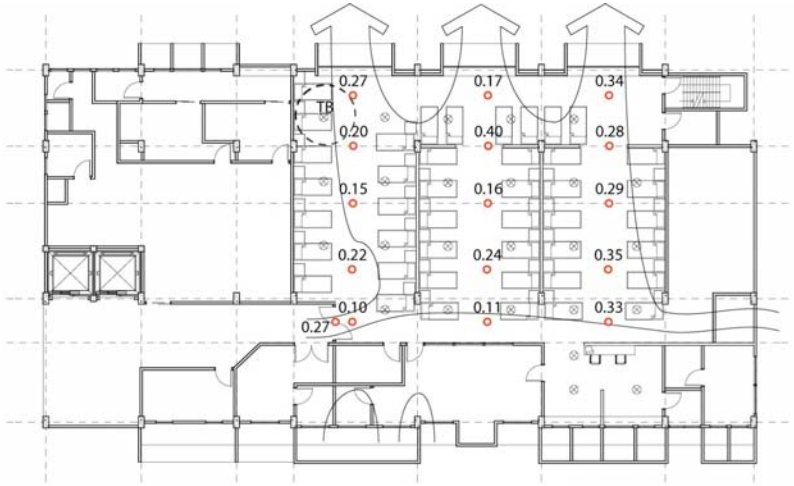


Fig. 8 Floor plan and ventilation data of hospital E inpatient ward#4

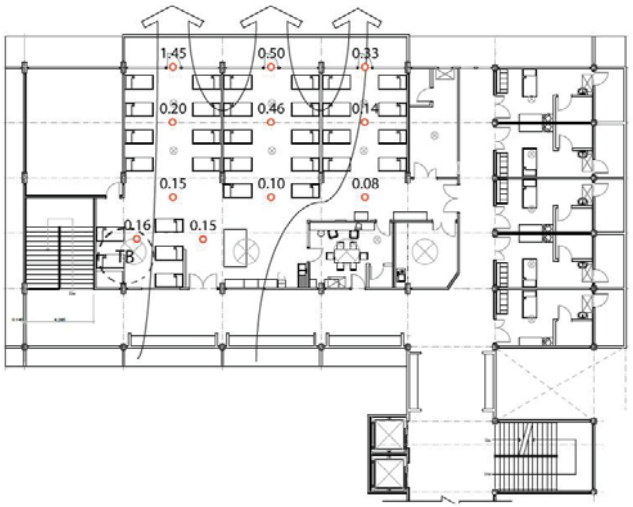


Fig. 9 Floor plan and ventilation data of hospital F inpatient ward



Fig. 10 Industrial type exhaust fan that was installed in the inpatient ward of hospital C



Fig. 11 Exhaust fans that were installed in the inpatient ward of hospital D



Fig. 12 Typical floor plans of naturally-ventilated airborne infection isolation (AII) room

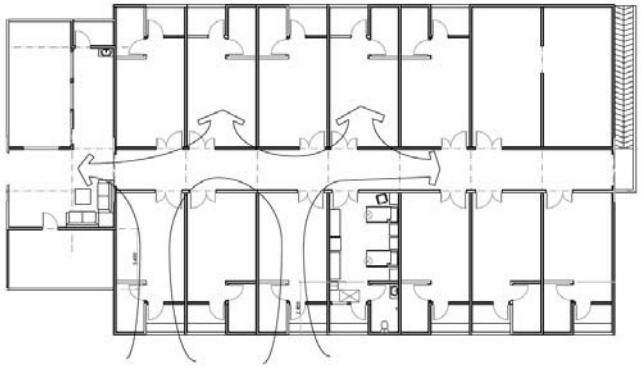


Fig. 13 Floor plan and airflow direction hospital F airborne infection isolation (AII) ward



Fig. 14 A central type corridor of AII ward at hospital F

Table 1 Building configurations and ventilation performance of hospital wards

Hospital	No. of Beds	Volume (m^3)	Area of smaller opening (m^2)	Average air flow at opening (m/s)	Calculated Air Change Rate (ACH)	Additional ventilation system
A	28	428	6	0.42	16.98	Ceiling Fans
B	38	931	4	0.52	6.43	Ceiling Fans
C	28	714	4	1.10	17.75	Exhaust Fans
D	47	980	8	1.14	26.80	Exhaust Fans
E1	47	897	6	0.63	12.14	Ceiling Fans
E2	40	955	4	0.32	3.86	Ceiling Fans
E3	43	897	4	0.24	3.08	Ceiling Fans
E4	43	955	4	0.27	3.26	Ceiling Fans
F	31	805	6	0.75	16.10	Ceiling Fans

Table 2 Building configurations and ventilation performance of AII rooms

Hospital	No. of Beds	Volume (m^3)	Area of smaller opening (m^2)	Average air flow at opening (m/s)	Calculated Air Change Rate (ACH)	Additional ventilation system
B	1	44	3	0.45(open)	88.36	3x12" exhaust fans
C	1	46	3	0.35(open)	65.74	None
D	1	62	2	0.18(close)	16.72	8" and 12" exhaust fans
F	2	63	2.40	1.99 (open) 0.36 (close)	218.33(open) 36.50 (close)	2x Ceiling Fans

Measurement of temperature distribution and CO_2 concentration in a space-heated classroom

Shuzhao Liu[1], Hiroshi Yoshino[1], Akashi Mochida[1]

[1] Tohoku University, School of Engineering, Sendai, Japan 980-8579

Abstract

The winter thermal environment and indoor air quality in classrooms has been reported to be very poor in Japan. In this study, an air-conditioned, mechanically ventilated classroom was surveyed. Air temperature, globe temperature and the concentration of CO_2 were monitored before, during and after the three-hour occupancy by 35 adults. Airtightness and airflow rates of the ventilation system were also measured. With the outdoor air of about 0ºC and the thermostat temperature setting of 30ºC, the vertical difference in air temperature exceeded 10ºC, while the horizontal difference was under 2.5ºC. After half an hour of occupancy, CO_2 concentration exceeded 1500 ppm in the respiration zone, and it reached 2500 ppm from the respiration zone to the middle of the room height for a consecutive 1.5-hour. The concentration decay showed that the air change rate was 0.82 ach. It was far from the national criterion of 2.2 ach.

Keywords: classroom, temperature, CO_2

1. Introduction

Due to the poor performance of airtightness and heat insulation, the vertical temperature distribution in classrooms in the heating season is usually large, which often causes very

serious problems related to thermal comfort [1]. It has also been reported that the CO_2 concentration in classrooms often exceeded the criterion of 1500 ppm during lessons due to low ventilation rates [1][2]. In university classrooms, occupants have complained of large temperature distribution and poor indoor air quality.

With the objective aimed at improving the thermal environment and performance of ventilation in classrooms, the actual condition of the indoor environment of a space-heated classroom with ceiling-concealed air conditioners and ventilation fans was investigated. This paper reports the measurement results of the distributions of air temperature, globe temperature and CO_2 concentration during the occupancy.

2. Investigated classroom and measured items

Investigated classroom

The classroom investigated was situated among the middle rooms of a one-storey building at Tohoku University in Sendai, Japan. It was 7.9 m wide, 9.1m long and 3.0 m high and had 60 seats. Two air conditioning units (AC) with the maximum heating capacity of 5.91 kW each were concealed in the ceiling. Two ventilation fans with heat exchangers were equipped in the north façade. *Figure 1* shows the floor plan. *Table 1* shows the materials of the building components.

Measured items

The survey included a measurement of the airtightness of the whole room and building components, the inflow and outflow rates of the ventilation fans, the thermal profile of the airflow from the AC, the indoor and outdoor air temperatures, the indoor globe temperatures, and the CO_2 concentrations of indoor and outdoor air.

3. Methods of measurements

The airtightness of the whole room and building components

The airtightness of the classroom was measured by an airtightness meter (KNS-4000II), under the depressurization method. The leakage area for each building component was estimated by the difference of the total leakage area before and after the component was sealed with vinyl films.

The supply/exhaust flow rates of the ventilation fans

With the diffuser removed, the supply and exhaust flow rates of the two ventilation fans in the north façade were measured by an airflow meter (Swema Flow 65). The measurements were conducted under the high and low operation modes of the fans when the doors were open and closed.

The thermal profile of the airflow from the air conditioners

To obtain the thermal profile of the airflow from the AC, an infrared camera (Avio TVS-610) was used. Below the symmetrical center line of the AC's diffusers, a piece of vinyl film was tensioned between two poles, which were held and pulled by two people. After 10 minutes in

this state, an infrared image of the surface temperature was taken. Since the film is thin, the surface temperature could be regarded as the same as the air temperature around it.

The air temperature and globe temperature

As shown in *Figure 2*, thermometers with loggers (TR-72 in set) were used to monitor the indoor and outdoor air temperatures. The vertical air temperature distributions were monitored at the middle and rear of the center aisle with the room height. At 1.0 m above the floor, the horizontal distribution was monitored near the south doors, the north window, the front fan, and at the front of the middle aisle. As a reference, the outdoor air temperature was also monitored at the north balcony by a thermometer in a hand-made aluminum duct that sheltered it from solar radiation and snow/rain. At the places where the horizontal distribution of indoor air temperatures were monitored, globes including T-type thermocouples were also set up. The log rate was every five minutes.

The indoor and outdoor CO_2 concentration

In the middle of the center aisle, CO_2 meters with loggers (JMS-301 in set) were set up with the height of the room. The outdoor concentration was monitored at the north balcony. The log rate was every one minute.

4. Results of the measurements

Airtightness of the room and building components

Table 2 shows the equivalent leakage areas of building components. The total leakage area of the room is 570 cm^2, which is 8 cm^2 per square meter of floor area. The leakage area of the walls, ceiling and floor occupied nearly 2/3 of the total.

The supply/exhaust flow rates of ventilation fans

Table 3 shows the measured supply and exhaust flow rates of the ventilation fans under the conditions of high/low running modes when the doors were open and closed, with the specification flow rates under high running mode as a reference.

Despite the same specification value for both supply and exhaust flow rates, measurements showed that the outflow rate was much larger than the specified value while the inflow rate was smaller, resulting in a large difference in the flow rates between supply and exhaust. The difference in the airflow was caused by the infiltration through the cracks of the room.

The thermal profile of the airflow from the air conditioners

With the set point temperature of 30ºC and downward direction of airflow supplied from AC, infrared images of the airflow from the AC running at high, medium and low wind speed modes were shown in *a*, *b* and *c* of *Figure 3*, respectively.

In medium wind speed mode, due to the relatively low speed and large buoyancy, the airflow went up to the ceiling immediately after it was jetted out, resulting in a large temperature difference. In this case, the occupied zone was not heated and the zone around foot level was

left cold. This problem became more serious in low mode. This phenomenon is due to the poor thermal performance of the building

Variation of indoor air temperature due to occupancy

The indoor thermal environment was measured under conditions with the set point temperature of 30ºC, downwards blowing at high speed, and the ventilation fans operated in high mode. The indoor air temperature changes in the periods before, during and after the three-hour of occupancy by 35 adults is shown in *Figure 4*.

At the center and the rear of the room, the vertical temperature difference was over 10ºC, between the lowest near the floor and the highest near the ceiling. The temperature at the center of foot level was under 20ºC. As for the heat released from the occupants, the temperature rose during the occupancy in the zone under 1.5 m. At all heights under 1.5 m, the temperature changed following the outdoor air, which means that the temperature control of the AC of the occupied zone was limited.

No large horizontal distribution in the air temperature was seen throughout the room at the height of 1.0 m.

Difference of air temperature and globe temperature

Figure 5 shows the difference between the globe temperature and air temperatures, at the height 1.0 m over the floor.

The globe temperature was about 2ºC higher than the air temperature in the middle of the room. It was about 1.5ºC lower than the air temperature near the door. These are respectively due to the radiation from the air conditioners and the ceiling around them, and the cold inside surfaces of the doors.

Variation of CO_2 concentrations

Figure 6 shows the variation of CO_2 concentrations in the middle of the classroom.

It was found that, after about half an hour of occupancy, CO_2 concentration at the respiration zone (1.0 m over the floor) exceeded the nation's criterion [3] of 1500 ppm for classrooms. The value increased and it reached 2500 ppm after a consecutive 1.5 hours of occupancy.

Distributions of temperature and CO_2 concentration along room height

Figure 7 gives the vertical distributions of air temperature and the concentration of CO_2, based on the averaged values between 11:00 am – 12:00 am.

The air temperature increased with the height. The lowest and highest temperatures appeared near the floor and the ceiling respectively. This phenomenon can be easily understood when thinking of the fact that the main source of heat was the AC in the ceiling. Because the thermal performance of the building was poor, due to the buoyancy effect, warm air tended to rise up. On the other hand, the concentration of CO_2 showed a different pattern of distribution. The peak was not seen near the ceiling. It seems reasonable to think that after CO_2 was

respired by occupants at higher temperature than the ambient air, it was transported upwards due to the buoyancy effect, and tended to be accumulated on the way up. At the same time, in the areas under the ceiling, where the fans were installed, the indoor air was diluted by the fresh air from the ventilation fans. Eventually, the peak was reached at about 1.5 m above the floor.

Air change rate estimated by the decay of CO_2 concentration

Figure 8 shows the normalized concentration decay with the elapsed time. It is estimated that the air change rate of the room was 0.82 ach, which is very close to the value obtained by the exhaust flow rate measurement of the ventilation fans.

5. Conclusions

The following conclusions were obtained by the detailed measurement of temperatures, CO_2 concentration, airtightness etc in a space-heated classroom with ceiling AC.

1. The airtightness of the classroom was 8cm^2 per square meter of floor area. Equivalent area of cracks in walls, ceilings and floors are dominantly larger than in the doors and windows.

2. The air temperature near the floor was over 10ºC lower than that near the ceiling. It was under 20ºC at foot level. The poor performances of the building insulation and airtightness accounted for the large temperature difference.

3. The peak concentration of CO_2 appeared at about the middle of the room height. In the respiration zone, the concentration exceeded the national criterion of 1500 ppm after about half an hour of occupancy.

4. It was estimated from the CO_2 decay that the air change rate was 0.82 ach, which was far below the national criterion of 2.2 ach for classrooms.

References

1. Daisey J. M., Angell W. J., Apte M. G., Indoor air quality, ventilation and health symptoms in schools: an analysis of existing information, Indoor Air, Volume 13, Issue 1, pp53-64, 2003

2. Iwashita Go, Hanada Y., Yoshino H., Discussion on the Indoor Air Quality in Classroom of the Elementary Schools without Heating Equipments During Winter Season based on the Window Opening and the CO_2 Concentrations (in Japanese), AIJ Journal, No.618, pp61-67, 2007

3. Ministry of Education, Culture, Sports, Science and Technology (MEXT), Japan, Standard for school environmental sanitation, 2007

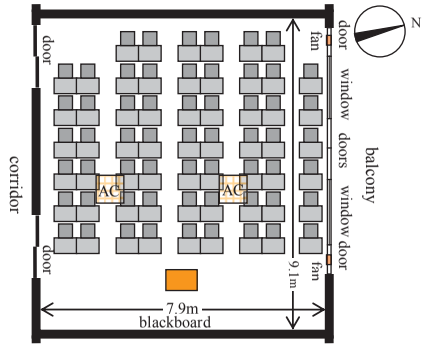


Figure 1 Plan of the surveyed classroom investigated

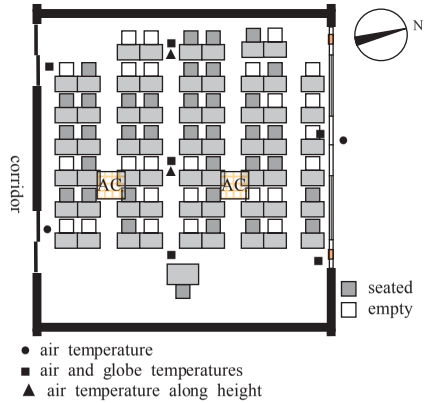
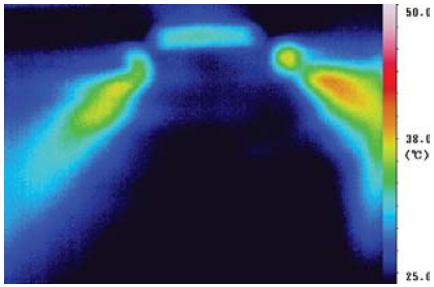
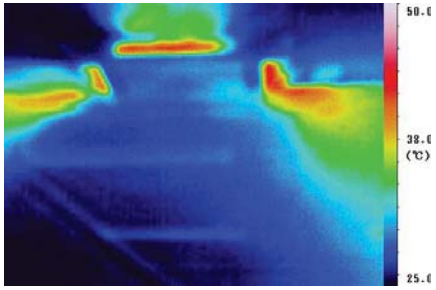


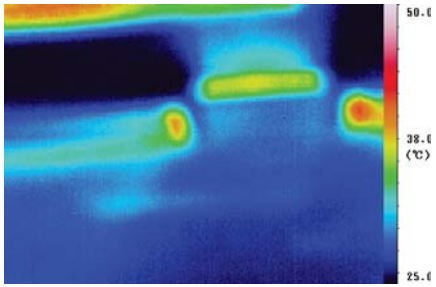
Figure 2 Location of measuring points



a) Wind speed: High

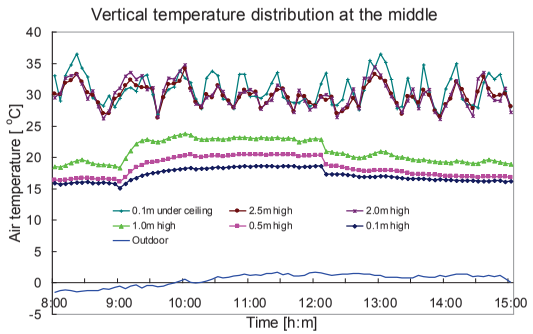


b) Wind speed: Medium



c) Wind speed: Low

Figure 3 Infrared images of airflows from air conditioners



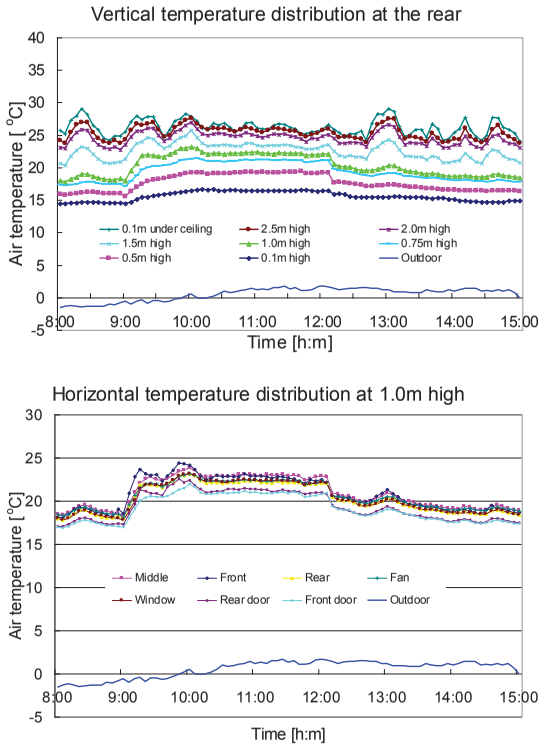


Figure 4 Vertical and horizontal distributions of air temperature

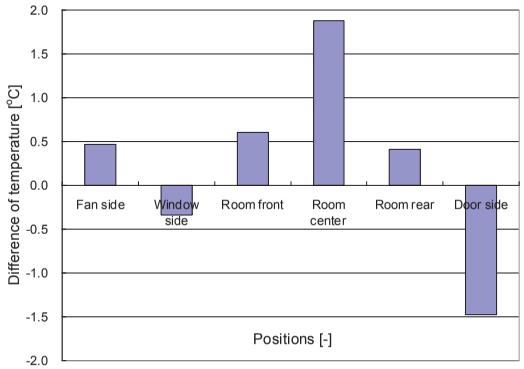


Figure 5 Difference between globe temperature and air temperature

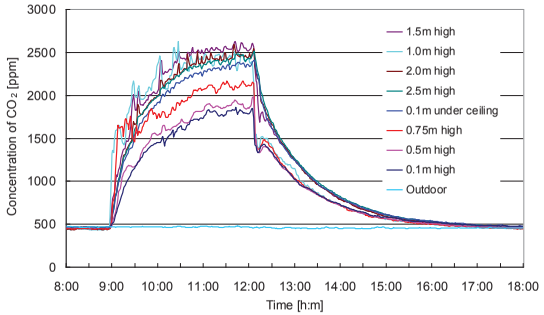


Figure 6 Variation of CO_2 concentration

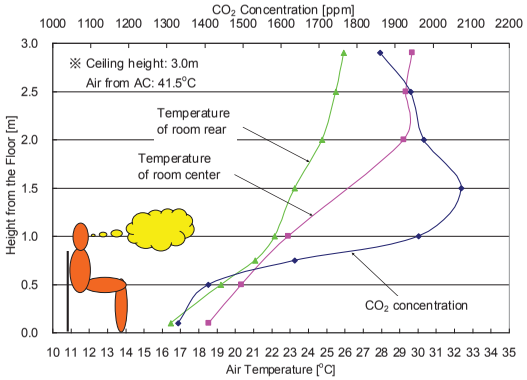


Figure 7 Vertical distributions of temperature and CO_2 concentration

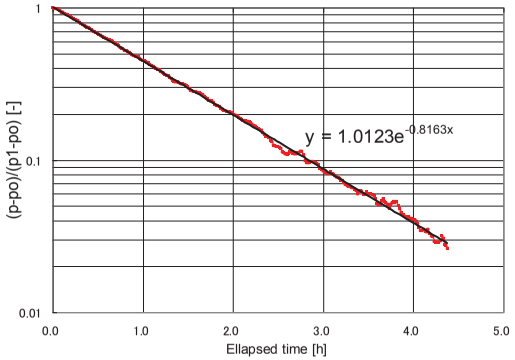


Figure 8 Normalized CO_2 concentration decay

Table 1 Components of the room envelope

Components	Materials
Window glasses	Double glazed: 5mm+6mm+5mm
Doors	Sliding doors with insulation material sandwiched by steel plates
Partition walls	Glass wool with 50mm thickness sandwiched by plaster boards 15mm thickness
Outer walls	North wall: insulation board with 120mm thickness South wall: insulation board with 120mm thickness
Floor	Tile carpet upon 80mm of concrete
Ceiling	Lowered ceiling with noise-absorption decoration board δ=12mm

Table 2 Equivalent areas of cracks [cm^2]

Components	Equivalent area		Total
South door	82	192	570
South window	14		
North door	82		
North window	14		
Others: walls, floor, ceiling	378		

Table 3 Flow rates of ventilation fans [m^3/h]

Measured articles	Status of doors	High mode		Low mode	
		Exhaust	Supply	Exhaust	Supply
Front fan	closed	93.1	53.7	19.0	15.8
	open	95.6	53.6	19.1	13.6
Rear fan	closed	93.0	51.7	18.6	16.9
	open	95.7	51.6	20.3	13.9
Specification	–	65		–	–

EXHAUST EFFECTIVENESS BASED ON RESIDUAL LIFETIME OF CONTAMINANT IN A VENTILATED SPACE

Hwataik Han[1], Kyung-Jin Jang[2], Si-Hyung Lim[1], and Jungkyung Kim[1]

[1] Kookmin University, Seoul, Korea 136-702

[2] Samgong Ltd., Gyeonggi-do Korea 450-030

Abstract

Exhaust effectiveness indicates how effectively contaminated air can be removed from a space, whereas air change effectiveness indicates how effectively distribute fresh air into the space. It is intended to describe the exhaust effectiveness based on the residual-life-time of contaminant in the context of logical extension of supply effectiveness based on LMA. It is proved theoretically that the room-mean values of LMA and LMR are identical, even though their local distributions are different from each other depending on inlet/outlet configurations. It is necessary to define ventilation effectiveness clearly so as to distinguish supply and exhaust effectiveness in describing local distributions in a room. Overall ventilation effectiveness, however, need not be distinguished, since both of the room averages of supply and exhaust indices are identical. They are dependent on the airflow pattern only, but not on the contaminant distribution in the space.

Keywords: Ventilation Effectiveness, Supply Effectiveness, Exhaust Effectiveness, Local Mean Age(LMA), Local Mean Residual-life-time(LMR), Tracer Gas experiment

Nomenclature

α_p : Local supply index
ε_p : Local exhaust index
$<\alpha>$: Room supply effectiveness
$<\varepsilon>$: Room exhaust effectiveness
C : Concentration of tracer gas
$C_{ex}^{\ p}$: Concentration at exhaust with a tracer source at P
$C_{ex}^{\ sup}$: Concentration at exhaust with a tracer source at supply outlet
$C_p^{\ sup}$: Concentration at P with a tracer source at supply outlet
$\overline{C}_p$: Concentration at P with a uniformly distributed tracer source in the space
$<C^p>$: Room average concentration with a tracer source at P
θ_p : Local mean age at P
φ_p : Local mean residual-life-time at P
$<\theta>$: Room average of LMA
$<\varphi>$: Room average of LMR
$\dot{M}$: Contaminant generation rate
$\dot{m}$: Contaminant generation rate per unit volume
Q : Volumetric airflow rate
t : Time
τ_n : Nominal time constant (=V/Q)
V : Room volume

Introduction

Ventilation effectiveness has been defined in various ways by many investigators. The term, "ventilation efficiency" was first used by Yaglou and Witheridge [1]. They defined it as the ratio of the carbon dioxide concentration in a room to that in the extract duct. The ventilation was considered to be effective when the exhaust air contains a large amount of the contaminant before it spreads out into the room. This definition has been a corner-stone for various definitions of ventilation efficiencies since.

Meanwhile, mathematical concepts of age and residence time were introduced to investigate the mixing characteristics in reactors by chemical engineers such as Danckwerts [2] and Spalding [3]. They mentioned the similarity between mixing of gases in reactors and the mixing of air in ventilated rooms. It was Sandberg [4] who first applied the concept of age of air to ventilation studies. He summarized various definitions of ventilation efficiency including relative efficiency, absolute efficiency, steady state efficiency, transient efficiency, etc. The sooner the supply air reaches a point in the room, the better the air change effectiveness at that point. Nowadays, the concept has been widely accepted by my organizations throughout the world including ASHRAE and AIVC [5-6].

In the ASHRAE Handbook [5], it is stated that ventilation effectiveness is a description of an air distribution system's ability to remove internally generated pollutants from a building, zone, or space. Whereas air change effectiveness is a description of system's ability to deliver ventilation air to a building, zone, and space. Namely, it is possible to understand the ventilation effectiveness indicates exhaust effectiveness and the air change effectiveness supply effectiveness. There are definitions of air change effectiveness based on the concept of age of air, but no definitions for ventilation effectiveness in the standard.

It is necessary to define clearly what to mean and how to obtain ventilation effectiveness. It is the objective of the present paper to provide one to one analogy of exhaust effectiveness with supply effectiveness using the concept of the residual life time of contaminant generated in a space. The meanings of local and overall values of exhaust effectiveness need be understood appropriately in conjunction with the previous definitions of ventilation effectiveness.

Definitions of ventilation effectiveness

Age and residual-life-time

The age of air is the length of time required for the supply air to reach an internal point of interest. As air can reach the point through various paths, the mean value of the ages at the point is called local mean age (LMA). Likewise, the length of time required for the air or contaminant located at an internal point to reach the exhaust is called the residual-life-time. The mean value through various paths is local mean residual-life-time (LMR). Local mean age represents the freshness of supply air, so that it can be used as local supply index at the point. Local mean residual-life-time represents the quickness of removal of the contaminant generated at the point, and can be used to represent local exhaust index. The LMA and LMR respectively represent the local supply and exhaust effectiveness at the point of the room. It should be stressed they depend on the room airflow pattern only but should not be dependent on the source distribution of a contaminant in the space, unless the contaminant concentration alters the airflow characteristics of the room.

Supply and exhaust effectiveness

A complete mixing condition is considered to be a reference condition on which we can define ventilation effectiveness. The nominal air change rate is the volumetric airflow rate divided by the room volume. The inverse of the air change rate is the nominal time constant.

$$\tau_n = V/Q \qquad \text{(Eq. 1)}$$

The local supply and exhaust indices are defined as the ratios of local mean age and the local mean residual-life-time compared to the nominal time constant, respectively. These local indices can be over 100% and as large as infinity.

$$\alpha_p = \tau_n/\theta_p \qquad \text{(Eq. 2)}$$

$$\varepsilon_p = \tau_n/\varphi_p \qquad \text{(Eq. 3)}$$

where the subscript P is the location of interest. Notice that the LMA at the exhaust means the total residence time of supply air in the space, and it is the same with the LMR at the supply. It can be noticed that these values are the same with the nominal time constant.

$$\theta_{ex} = \varphi_{sup} = \tau_n \qquad \text{(Eq. 4)}$$

Therefore, the local supply index can be understood as the ratio of the LMA at the exhaust to that at the point, and the local exhaust index as the ratio of the LMR at the supply to that at the point. The overall room effectiveness can also be defined similarly.

$$<\alpha> = \tau_n/<\theta> = \theta_{ex}/<\theta> \qquad \text{(Eq. 5)}$$

$$<\varepsilon> = \tau_n/<\varphi> = \varphi_{sup}/<\varphi> \qquad \text{(Eq. 6)}$$

where < > means the spatial average over the entire space. It will be proved later in this article that the room averages of LMA and LMR are identical. Therefore, the overall room supply effectiveness and exhaust effectiveness should be the same. We may not need terminology to distinguish between the overall values. We may simply call it overall ventilation effectiveness. Supply effectiveness and exhaust effectiveness are meaningful only for local values. The corresponding concepts are summarized in Table 1.

Table 1 Corresponding concepts for supply and exhaust effectiveness

Supply Effectiveness	Exhaust Effectiveness
Age of Air θ_p = Local Mean Age at P $<\theta>$= Room Average of LMA	Residual Life Time of Air φ_p = Local Mean Residual-life-time at P $<\varphi>$= Room Average of LMR
Local Supply Index $\alpha_p = \tau_n/\theta_p$ $= \theta_{ex}/\theta_p$ = LMA at exhaust/LMA at P	Local Exhaust Index $\varepsilon_p = \tau_n/\varphi_p$ $= \varphi_{sup}/\varphi_p$ = LMR at supply/LMR at P
Overall Room Supply Effectiveness $<\alpha>= \tau_n/<\theta>$	Overall Room Exhaust Effectiveness $<\varepsilon>= \tau_n/<\varphi>$

Measurement methods

Local supply index

In order to obtain LMA or LMR numerically or experimentally, transient concentration responses should be monitored after a tracer gas is injected. There are three commonly used ways of injecting a tracer gas, i.e. step-up, step-down, and pulse methods. The equations to calculate these values from concentration responses are different from one injection method to another, but the results should be the same. Here we will use a step-up method for most of the discussion.

The local mean age can be obtained by integrating the area above the concentration curve divided by the steady state concentration after a step-up tracer injection as follows:

$$\theta_p = \int_0^\infty \left(1 - \frac{C_P{}^{\sup}(t)}{C_P{}^{\sup}(\infty)}\right) dt \qquad \text{(Eq. 7)}$$

where the subscripts indicate the monitoring point, and the superscripts indicate the injection point. Note the steady state concentration, $C_P{}^{sup}(\infty)$, is uniform regardless of the location P, since a tracer is injected at a supply.

Another method to obtain the LMA distribution is to calculate the steady concentration distribution with uniformly distributed constant volumetric sources in the space. The equivalency of these methods has been shown numerically by Han [9]

$$\theta_p = \frac{\overline{C}_p(\infty)}{\dot{m}} \qquad \text{(Eq. 8)}$$

where $\dot{m}$ is the tracer generation rate per unit volume. In the equations above, C does not have a superscript but an over-bar, which means a uniform tracer injection throughout the entire space. The LMA at exhaust can be expressed similarly by replacing the subscript 'P' with 'ex'. Therefore, the local supply index, which is the ratio of the LMA's at exhaust and at P is calculated by the ratio of the steady concentrations with over-bars at those points. This method is especially useful for numerical calculations, since the distribution of LMA can be obtained from a single steady state concentration calculation rather than from lengthy transient calculations.

$$\alpha_p = \frac{\overline{C}_{ex}(\infty)}{\overline{C}_p(\infty)} \qquad \text{(Eq. 9)}$$

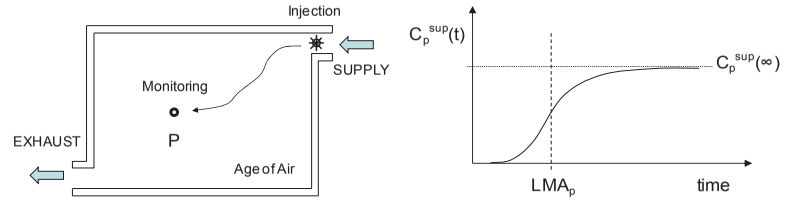


Fig. 1 Transient step-up method used to determine local mean age

Local exhaust index

Similarly, the local mean residual-life-time can be obtained from its definition as is shown in Fig. 2. The tracer should be injected at P and the transient concentration should be monitored at the exhaust.

$$\phi_p = \int_0^\infty \left(1 - \frac{C_{ex}{}^P(t)}{C_{ex}{}^P(\infty)}\right) dt \qquad \text{(Eq. 10)}$$

where the subscripts indicate the monitoring point and the superscripts indicate the injection point. The steady state concentration at the exhaust $C_{ex}{}^p(\infty)$ should be equal to $\dot{M}/Q$, as the mass should be balanced in the room. The equation can be derived as follows.

$$\phi_p = \frac{1}{\dot{M}} \int_0^\infty \dot{M} - QC_{ex}^p(t)\,dt = \frac{< C^p(\infty) > V}{\dot{M}} = \frac{< C^p(\infty) > \tau_n}{C_{ex}^p(\infty)} \qquad \text{(Eq. 11)}$$

where $\dot{M}$ is the contaminant generation rate at P. The first term in the integral is the total generation rate and the second term is the rate of contaminant leaving the room through the extract duct. The sum of the difference up to a steady state results in the amount of contaminant left in the room, which is called as the internal hold-up. It is the product of the average concentration of the room times the room volume. [4]

Therefore, the local exhaust index can be obtained either from the definition of the LMR ratio or by the ratio of the room average concentration to the exhaust concentration when a source is located at P.

$$\varepsilon_p = \frac{C_{ex}{}^{p}(\infty)}{< C^{p}(\infty) >} \qquad \text{(Eq. 12)}$$

It looks quite similar with the classical definition of ventilation efficiency introduced by Yaglou and Witheridge [1]. They defined ventilation efficiency also as the concentration ratio, but for a given contaminant source, and considered it as an overall efficiency of the room, not as a local efficiency at the source location. It should be stressed that the ratio shown in the equation is not the room exhaust index but the local exhaust index in case a source is located at P. A similar definition has been also proposed as the removal effectiveness by several authors [7-8]. Although there have been some studies on the measurements of LMA [10], the distributions of LMR have rarely been measured experimentally [11].

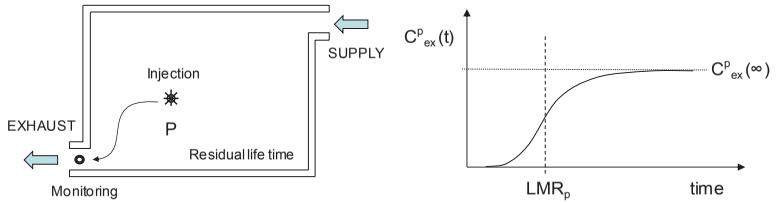


Fig. 2 Transient step-up method used to determine local mean residual-life-time.

Overall room ventilation effectiveness

The room average effectiveness should be the spatial average of local values over the entire space. The spatial average of LMA can be obtained in two different ways as was mentioned earlier; transient and steady ways. The steady method indicates it can be obtained from the spatial average of the steady state concentration under the steady condition with uniform generation from the Eq. 9.

$$< \theta >= \frac{< \overline{C}(\infty) >}{\dot{m}} \qquad \text{(Eq. 13)}$$

Therefore, the overall supply effectiveness is the ratio of the exhaust concentration to the room mean concentration as is shown in Table 2.

In order to obtain overall exhaust effectiveness, LMR should be obtained at every internal point to calculate its spatial average over the entire space. Unlike the method used for the previous age measurements, however, a monitoring point should be fixed at the exhaust, and a tracer should be injected at every point in the space repeatedly. The concentration response by simultaneous tracer injections can be obtained by superimposing every injection source present over the entire space, since the concentration equation is linear. Therefore, the room average exhaust effectiveness is the ratio of the exhaust concentration to the room average concentration with a uniformly distributed source superimposed in the space, which is exactly the same as the steady method used to determine overall supply effectiveness.

This concludes the proof that the overall supply effectiveness is equal to the overall exhaust effectiveness. Table 2 summarizes the methods that can be used to obtain local supply and exhaust indices and overall room effectiveness.

$$< \varepsilon >=< \alpha > \qquad \text{(Eq. 14)}$$

Table 2 Methods to obtain local supply and exhaust indices and overall effectiveness

	Supply Effectiveness	Exhaust Effectiveness
Local index	Definition: $\alpha_p = \frac{\tau_n}{\theta_p}$	Definition: $\varepsilon_p = \frac{\tau_n}{\phi_p}$
	Method 1. By step-up generation at supply - Transient concentration at P - Steady concentration at P $\alpha_p = \frac{\tau_n}{\int_0^\infty \left(1 - \frac{C_P{}^{sup}(t)}{C_P{}^{sup}(\infty)}\right) dt}$ where $\tau_n = V/Q$	Method 1. By step-up generation at P - Transient concentration at exhaust - Steady concentration at exhaust $\varepsilon_p = \frac{\tau_n}{\int_0^\infty \left(1 - \frac{C_{ex}{}^{P}(t)}{C_{ex}{}^{P}(\infty)}\right) dt}$ where $\tau_n = V/Q$
	Method 2. By uniform generation in space - Steady concentration at P - Steady concentration at exhaust $\alpha_p = \frac{\overline{C}_{ex}(\infty)}{\overline{C}_P(\infty)}$	Method 2. By step-up generation at P - Steady concentration at exhaust - Steady room average concentration $\varepsilon_p = \frac{C_{ex}{}^{P}(\infty)}{< C^{P}(\infty) >}$
	Definition: $< \alpha >= \frac{\tau_n}{< \theta >}$	Definition: $< \varepsilon >= \frac{\tau_n}{< \phi >}$

Overall effectiveness	Method 1. By step-up generation at supply - Transient concentration at exhaust - Steady concentration at exhaust $<\alpha>=\frac{\tau_n^{\ 2}}{\int_0^\infty t\left(1-\frac{C_{ex}^{\ sup}(t)}{C_{ex}^{\ sup}(\infty)}\right)dt}$ Method 2. By uniform generation in space - Steady room average concentration - Steady concentration at exhaust $<\alpha>=\frac{\overline{C}_{ex}(\infty)}{<\overline{C}(\infty)>}$	Method 1. By simultaneous step-up generations at every P in space - Steady concentration at exhaust - Steady room average concentration $<\varepsilon>=\frac{\overline{C}_{ex}(\infty)}{<\overline{C}(\infty)>}$ Therefore, $<\varepsilon>=<\alpha>$

Conclusions

1. Ventilation effectiveness can be categorized into two concepts; supply effectiveness and exhaust effectiveness. Supply effectiveness represents the performance of supply air distribution in a space, whereas exhaust effectiveness represents the performance of contaminant removal from the space.
2. As local supply index is defined based on local mean age, local exhaust index can be defined as the local mean residual-life-time to the nominal time constant. It represents how the contaminant generated at the point can be removed effectively. It can be obtained from transient concentration measurements at the exhaust after injecting a tracer gas at the point of interest. This is equivalent to the ratio of the concentration at the exhaust to the room mean concentration. The distribution of local exhaust index is different from that of local supply index, but closely related to airflow patterns in the space.
3. Unlike local indices, the room average exhaust effectiveness is identical to the room average supply effectiveness, which can be called as ventilation effectiveness. It depends not only on supply-exhaust configurations, but also on air change rate. Experimentally, it can be obtained by taking the 0th and the first moments of the concentration curve at the exhaust after injecting a tracer at the supply. Numerically, it is more convenient to take the ratio of the steady state exhaust concentration to the room average concentration with a uniformly distributed source in the space.

Acknowledgments

This work was supported by Source Technology Development Program 2009 of the Ministry of Education, Science and Technology in Korea.

References

1. Yaglou, C. P., Witheridge W. N., “Ventilation Requirements,” ASHVE Trans., 42, 1937, pp. 423-436.

2. Danckwerts, P. V., “Local Residence-Times in Continuous-Flow Systems,” Chemical Engineering Science, 9, 1958, pp. 78-79.

3. Spalding, D. B., “A Note on Mean Residence-Times in Steady Flows of Arbitrary Complexity,” Chemical Engineering Science, 9, 1958, pp. 74-77.

4. Sandberg, M., “What is Ventilation Efficiency,” Building and Environment, 16, 2, 1981, pp. 123-135.

5. ASHRAE, “ASHRAE Handbook - Fundamentals, American Society of Heating, Refrigerating, and Air-Conditioning Engineers,” Atlanta, GA, USA, 2009.

6. AIVC, “A Guide to Air Change Efficiency,” Technical Note AIVC28, Air Infiltration and Ventilation Centre, Coventry, United Kingdom, 1990.

7. Sandberg, M., Sjoberg, M., “The Use of Moments for Assessing Air Quality in Ventilated Rooms,” Building and Environment, Vol. 18, No. 4, 1983, pp. 181-197.

8. Skaaret, E., “Contaminant removal performance in terms of ventilation effectiveness,” Environmental International, Vol. 12, Issues 1-4, 1986, pp. 419-427.

9. Han, H. “Calculation of Ventilation Effectiveness Using Steady-State Concentration Distributions and Turbulent Airflow Patterns in a Half Scale Office Building,” Proc. of International Symp. on Room Air Convection and Ventilation Effectiveness, 1992, pp. 187-191.

10. Han, H., Kuehn, T. H., and Kim, Y. I., “Local Mean Age Measurements for Heating, Cooling, and Isothermal Supply Air Conditions,” ASHRAE Trans. Vol. 105, Pt. 2, 1999, pp. 275-282.

11. Han, H., Choi, S. H., and Lee, W. W., “Distribution of Local Supply and Exhaust Effectiveness according to Room Airflow Patterns,” International Journal of Air-conditioning and Refrigeration, Vol. 10, No. 4, 2002, pp. 177-183.

Improvement of Temperatures Stratification caused by Air-conditioner by means of Ceiling Fan in Classroom

Natsuka Wakamatsu[1], Yoshihisa Momoi[1], Toshio Yamanaka[1], Kazunobu Sagara[1], Hisashi Kotani[1]

[1] Affiliation, Osaka University, Dept. of Architectural Engineering, Japan

Abstract

This paper discusses on the indoor thermal environment controlled by the air-conditioners and the ceiling fans under the heating condition. An experiment which measured the temperature and the indoor wind velocity was conducted in the classroom with the ceiling fans. The preset temperature was 24°C, and the airflow direction of the ceiling fans was upward. The rotational speed of the ceiling fans were changed (90-300rpm). Questionnaires to the occupants were also conducted to figure out the problem when the ceiling fans were used in the classroom. As a result, followings are shown: (1) It is confirmed that the ceiling fan is beneficial to moderate the vertical temperature difference. (2) If several ceiling fans are installed symmetrically in the classroom, there might be an increase in air velocity at the center of the classroom. (3) When the rotational speed of the ceiling fan is ordinary, noisiness does not matter.

Keywords: Ceiling fan, Air-conditioner, Classroom, Heating condition

Introduction

Recently, the number of schools which are equipped with air-conditioners has been rapidly increasing in Japan. Meanwhile, energy saving attracts attention behind environmental concerns. Ceiling fans are often used for providing cooling and comfort as well as air-conditioners, but they consume low amount of energy in comparison with air-conditioners. The proper use of ceiling fans in an air-conditioned room can result in better thermal comfort and energy savings. In summer season, ceiling fans will save energy when they move air at an acceptable speed without compromising thermal comfort and allow a higher preset temperature. Also in moderate season, they can potentially avoid the use of air-conditioners and extend the period of time without the air-conditioners. In winter season, the vertical temperature stratification tends to be formed in an air-conditioned room. This temperature stratification can be moderated by means of ceiling fans. It may be able to allow a lower preset temperature.

The purpose of this study is to make a balance between comfort and energy saving by using a ceiling fan, and to establish the air conditioning system which combines air-conditioners and ceiling fans in a classroom. Study of ceiling fan is referred in some papers include the study for the large room with a high ceiling using ceiling fans (Momoi et al. 2003) and the study for office room with air-conditioners and ceiling fans. However, the large room or the office room has different room characteristics from the classroom, such as a shape, amount of heat generation and indoor ventilation properties. Although, there are some report which study about effect of ceiling fan in cooling condition (Rohles et al. 1983), measurement of flow characteristics of a ceiling fan (Chiang et al. 2007) or simulation of thermal environment(Ho et al. 2009), there are few report which study about effect of ceiling fan in heating condition or conducts questionnaire survey.

As a first step, the experimental measurement and the questionnaire surveys were conducted at the classroom under the heating condition, in order to clarify the effect of the ceiling fan in winter season. This paper reports the results of the air velocity and temperature distributions, PMV (predicted mean vote), and the findings of the problems when the ceiling fans are used in the classroom.

Method

Experiment

The experiment was conducted at the classroom of Osaka University in January of 2010. Figure1 shows the picture of classroom. The floor plan is shown in Figure2. The dimensions of classroom are 7000(W) mm x 8000(D) mm x 2700mm (H). This classroom has 4 ceiling

fans of 1100 mm in diameter which are installed symmetrically in the room. The packaged air-conditioner is almost set up at center of the room. Table1 shows the experimental items. The outdoor temperature and the corridor temperature were measured in order to understand the external environment to the object room. The indoor temperatures of occupied zone were measured at a distance of 730mm from the floor (the desk height) with the thermometers. The indoor temperatures of vertical distribution were measured at 10 points in the horizontal direction (shown in Fig.2 a ~ j), and 6 points in the vertical direction (at a height 100, 600, 1100, 1700, 2200, 2600mm from the floor) to each horizontal measurement points (shown in Fig.3) with type-T thermocouples. The wind velocities were measured at a distance of 1100mm from the floor with constant-temperature anemometer. The globe temperatures were measured at a distance of 730mm from the floor as well as the occupied zone temperatures.

Table2 shows the experimental conditions. The fixed condition was followings: preset temperature of the air-conditioner was kept at 24°C, supply air direction of the air-conditioner was downward, air volume from the air-conditioner was 1000m^3/h, and airflow direction of the ceiling fans was upward. Rotational speed of the ceiling fans was set up as a parameter. Case1 is the condition that ceiling fans were stopped. Case2 to Case5 are the conditions that the rotational speed was changed.

Table1. Experiment items

Measurement Item	Mark	Measuring Instrument	Number
Outdoor Temperature	☆	Thermo Recoder	1
Corridor Temperature	☆		1
Indoor Temperature(Occupied Zone)	★		17
Indoor Temperature(Vertical Distribution)	●	Thermocouple	60
Indoor Wind Velocity	◇	Anemometer	13
Globe Temperature	▲	Globe thermometer	2

Table2. Experimental conditions

Case	AC	CF	
		Airflow direction	Rotational speed
1	24℃	Upward	-
2			Soft (90rpm)
3			Low (150rpm)
4			Middle(200rpm)
5			High (300rpm)



Figure1. Ceiling fans in the classroom

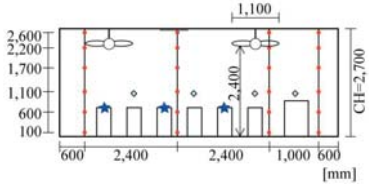


Figure3. B-B' section and measurement point

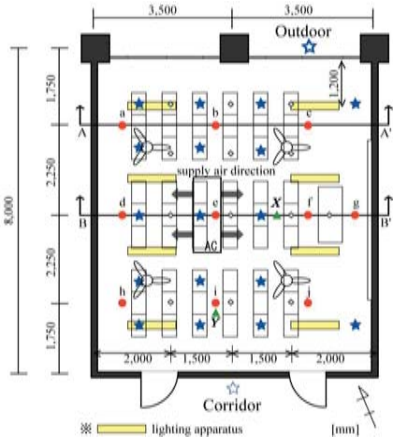


Figure2. Floor plan and measuring point

Questionnaire Survey

Questionnaires to the occupants were conducted in February of 2010 at the same classroom that the experiments were carried out. The purpose of this survey is to figure out the problems when the ceiling fans are used in the classroom. Subjects of the survey are the students who are using the classroom usually. Preset temperature, air volume, and air direction of the air-conditioner were 22°C, 1000m^3/h, and downward, respectively. Rotational speed and air direction of the ceiling fans were kept at "low" and the upward direction which are usual in

the winter. The questionnaires were conducted after the lesson, and they covered 7 sections: (a) individual attribute, (b) noisiness, (c) flicker of light, (d) sense of air flow, (e) thermal sensation vote, (f) problem of ceiling fan, (g) free description.

Results and Discussion

Experimental Results

Indoor wind velocity distribution

Figure4 shows the measurement results of wind velocity distribution. Although Case2 is rarely different from Case1 where the ceiling fans were stopped, in most cases the higher rotational speed, the greater wind velocity is generated. In Case3 - Case5, the wind velocity distribution is highest at middle of the room. The airflow pulled up by the ceiling fan sweeps along the ceiling, collides with the other airflow generated by the adjacent ceiling fan, and turns downward (Fig.5). Therefore, it is considered that the wind velocity increases at center of the room. In order to prevent this phenomenon, it is necessary to examine the number of ceiling fans and the installation position of ceiling fans.

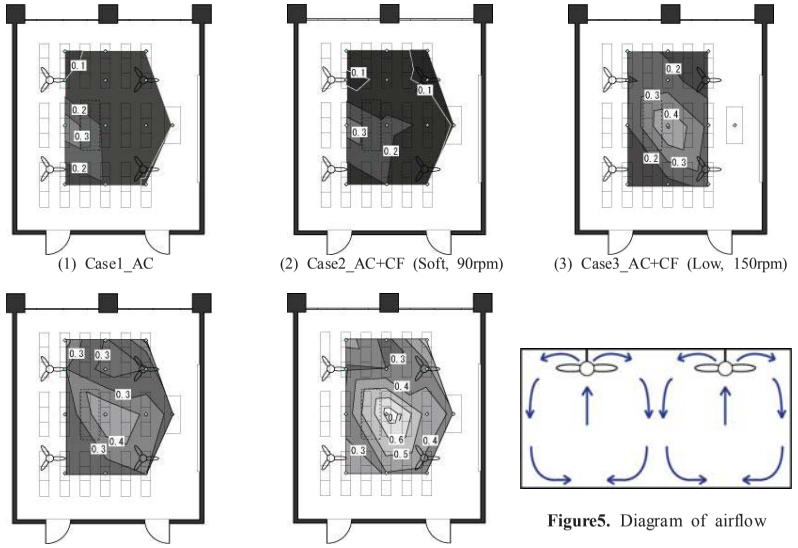


Figure4. Wind velocity distributions

Figure5. Diagram of airflow

Vertical temperature distribution

Figure6 shows the outdoor and corridor temperature. The each experimental condition was almost the same external condition during the experiment. The outdoor temperature was approximately 7^{o}C, wile the corridor temperature was approximately 14^{o}C.

Figure7 shows the measurement results of vertical profile of temperature at the window side, the middle and the corridor side. The results of window side, middle and corridor side are the averaged values from the measurement points from a to c, from d to g, from h to j, respectively. In Case1 where the ceiling fans were stopped, there are 3 ~ 5^{o}C difference in

temperature between 100mm and 1100mm from the floor. Operating the ceiling fans, the difference of temperature is reduced because the temperature at 100mm and 600mm from the floor is increased, wile the temperature at 1700, 2200 and 2600mm from the floor is decreased. The temperature at 1100mm from the floor is almost constant. Compared to the effect of ceiling fans in the horizontal position, the moderation effect of the vertical temperature difference at the corridor side is more effective than at the window side.

Figure8 shows the measurement results of vertical temperature distribution in A-A' section and B-B' section. In Case1, the temperature stratification is formed in the room. In A-A' section, the temperature stratification disappears when the ceiling fans are operated. The higher rotational speed, the more beneficial to moderate the vertical temperature difference. In B-B' section, however, it represents that the airflow from the air-conditioner does not spread horizontally but turns downward. This will be caused by the downdraft from the ceiling fans. Therefore it will need to consider the positional relation between the air-conditioner and the ceiling fans.

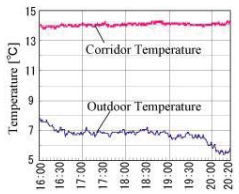
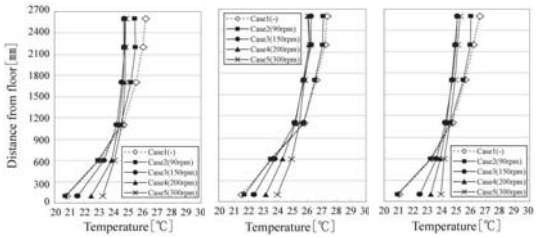


Figure6. Outdoor and corridor temperature



(1) Window side (2) Middle (3) Corridor side

Figure7. Vertical profile of temperature

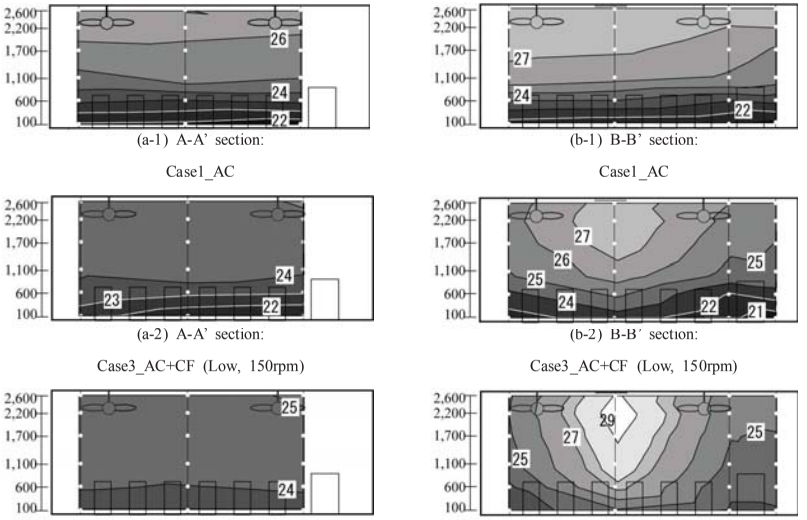


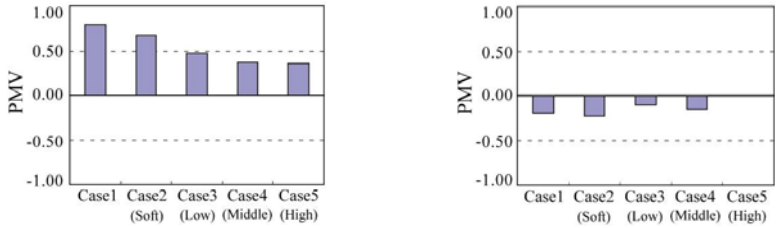
Figure8. Vertical temperature distribution

Predicted Mean Vote

Figure9 shows the calculated results of PMV in the position of *X* and *Y* (refer to Fig.2). PMV values were calculated for a seated, quiet person (with metabolic rate of 1.0met) dressed in winter attire (with clothing insulation of 1.0clo). The results of the each experimental condition are expressed by the averaged values in 30 minutes.

At the position of *X*, an increase in rotational speed of ceiling fans decreases PMV values because of the growing wind velocity (PMV=0.8 in Case1, and PMV=0.35 in Case5). In

contrast, PMV values in the position of *Y* increases as the rotational speed is increased (PMV=-0.2 in Case1, and PMV=0 in Case5). It is considered that the reason is the increase of temperature. At the both positions, as rotational speed of the ceiling fans increases, PMV values approach zero.



(1) Position of *X* (2) Position of *Y*

Figure9. Predicted mean vote

Questionnaire Results

The number of subjects is 36 students (17 male, 16 female and 3 unknown). Ages of the students ranged from 20 to 22 years. Clothing insulation ranged from 0.49 to 1.73clo (the average is 0.92clo).

Figure10 shows the questionnaire results of noisiness. The most answer is "neutral". It forms a simple majority. And nobody answered "loud" or "very loud". Therefore when rotational speed of the ceiling fan is "low" which speed is general in the winter, noisiness will be not such a big problem.

Figure11 shows the questionnaire results of flicker of light. The most answer is "not flicker". But combined "slightly flicker" and "flicker" form a simple majority. So, the flicker of light will become something of a problem in using ceiling fans in the classroom. To prevent this problem, it will be required to give attention to the positional relation between the lighting apparatus and the ceiling fans.

Figure12 shows the questionnaire results of airflow sensation. The number of students who answered "sensible" or "very sensible" is nearly 60 percent. Many of them felt airflow. The question; "Where did the airflow come from?" was asked only if they felt airflow. As the results of this question, the most answer is "air-conditioner" followed by "ceiling fan". Also the results of free description, there is the answer that "It's very uncomfortable to get some air from the air-conditioner directly." Airflow sensation is primarily influenced by airflow from the air-conditioner.

Figure13 shows the questionnaire results of thermal sensation. The most answer is "neutral", and the answer of the warm side ("hot", "warm" and "slightly warm") is more than that of the cool side ("cold", "cool" and "slightly cool"). Figure14 shows the questionnaire results of thermal comfort sensation. The most answer is "slightly comfortable" followed by "neutral". The thermal comfort at that time was almost good condition.

Figure15 shows the questionnaire results of problem of ceiling fan. The most answer is "unsightly", followed by "flicker of light" and "an oppressing feeling". Nobody answered "loud noise", "paper is blown away by wind" and "airflow is uncomfortable". From this, the visual influence such as flicker or oppressive feeling will have a tendency to bother occupants.

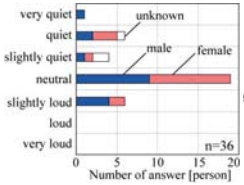


Figure10. Nosiness

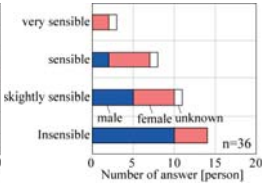


Figure12. Airflow sensation

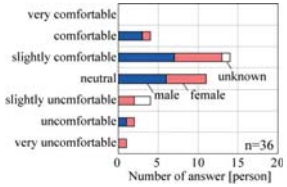


Figure14. Satisfaction

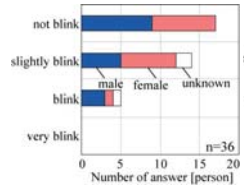


Figure11. Flicker of light

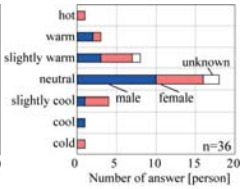


Figure13. Thermal sensation vote

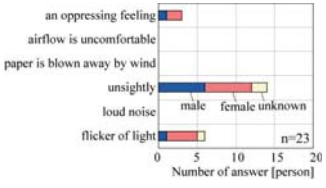


Figure15. Problem of ceiling fan

Conclusions

This paper reports the results of the experiments and the questionnaires, both of which conducted in the classroom under the heating conditions. As a result, the following remarks were obtained.

- It is confirmed that the ceiling fan is beneficial to moderate the vertical temperature difference, and the higher rotational speed, the more beneficial to improve the vertical temperature stratification.
- If several ceiling fans are installed symmetrically in the classroom, there might be an increase in airflow velocity at the center of the classroom and the supply air from air-conditioner will be not spread horizontally but turns downward.
- When the rotational speed of the ceiling fan is ordinary, noisiness does not matter. It will be required to give attention to the visual influence such as flicker or oppressive feeling to install ceiling fans at the classroom.

Acknowledgments

Our gratitude is expressed to the Panasonic Ecology Systems Co. for their cooperation.

This work was partially supported by Grant-in-Aid for Scientific Research of the Ministry of Education, Culture, Sports, Science and Technology, Japan, Young Scientists (B) 2009-No.21760449 (Representative, Y. Momoi).

References

1. Y. Momoi, T. Yamanaka, H. Kotani, K. Otaka, S. Horikawa, "Control of Airflow Pattern and Temperature Distribution in Large Rooms using Ceiling Fan," *The 7th International Symposium on Ventilation for Contaminant Control*, 2003, pp.145~150.

2. F.H. Rohles, S.A. Konz, B.W. Jones, “Ceiling Fans as Extenders of the Summer Comfort Envelope,” *ASHRAE Transactions* Vol.89, Part1A, 1983, pp.245~263.

3. H.C. Chiang, C. Pan, H.S. Wu, B.C. Yang, “Measurement of Flow Characteristics of a Ceiling Fan with Varying Rotational Speed”, *Clima 2007 WelBeing Indoors*.

4. S.H. Ho, L. Rosario, M.M. Rahman, “Thermal comfort enhancement by using a ceiling fan”, *Applied Thermal Engineering*, 29, 2009, pp.1648-1656.

Experimental Assessment of Humidity Controlling the Performances of Moisture Adsorbing/Desorbing Building Materials

Hea-Jeong Kim [1,2] Yun-Gyu Lee [2] Kyoo-Dong Song[3]

[1]Hanyang University, Dept. of Sustainable Architectural Engineering, Seoul, Korea 133-791 [2] Korea Institute of Construction Technology, Building Planning and Environment Research Division, Goyang, Seoul, Korea 411-712 [3]Hanyang University, ERICA Campus. Dept of [3]School of Architecture and Architectural Engineering, Ansan, Korea 426-791

Abstract

The climate of South Korea is that of high temperatures and high humidity in the summer season and low temperatures and low humidity in the winter. Humidifiers and dehumidifiers are used to create a cool indoor environment, and the demand for building materials with moisture adsorption/desorption functions is increasing. To investigate the performance of moisture adsorption/desorption new mineral fiber boards, a chamber test and mock-up test were performed and compared to mineral fiber boards. As a result of the chamber test and mock-up test, the new mineral fiber board showed the effect of maintaining indoor humidity regularly through humidity adsorption/desorption by the chamber test and mock-up test.

Keywords: Moisture adsorption/desorption property, Interior surface materials, Mineral fiber board, Chamber test, Mock-up room test, Relative humidity

Introduction

Relative humidity levels influence indoor environmental quality and occupants’ thermal comfort. At a very low humidity level, there may be complaints of dry noses, mouths, eyes,

and skin, and increases of respiratory illnesses [1]. In particular, various types of porous building materials with moisture adsorption/desorption properties have been introduced to the market in countries which have a hot and humid climate. Previous studies have been conducted to evaluate the hygric buffering capability of various types of building materials as follows: Abadie and Mendonca [2] have evaluated moisture performance of building materials commonly found in buildings, including concrete and cement, plasterboard, brick, particle, fiberboards and wood. In the NORDTEST project[3], an experimental protocol has been proposed that specifies a moisture buffer value that includes in its definition the surrounding air vapor concentration variation [2, 4, 5]. Other experimental methodologies to evaluate the hygrothermal performance of building materials have been proposed by the Japanese Industrial Standard (JIS) [6] and the International Standards Organization (ISO) [7]. The purpose of this study is to evaluate and compare the moisture adsorption/desorption performances of interior building materials through chamber tests and mock-up room tests.

2. Methods

2.1. Tested building materials

The ordinary mineral fiber board was manufactured as a ceiling board and it was made of mineral fibrous wool as its base material together with some additives. It was manufactured through mixing, molding, drying, cutting, carving, surface finishing and spraying procedures. This mineral fiber board was evaluated as a good fire resistant, sound absorbing, and thermal insulation material [8].

The new mineral fiber board was made of mineral fibrous wool and activated China clay as an additive. Due to its high degree of microporosity, the activated China clay has a high capacity of moisture adsorption/desorption capacity within the normal indoor temperature and relative humidity ranges. Therefore, the new mineral fiber board can control the indoor relative humidity level by adsorbing moisture when the indoor moisture level is high and by desorbing when it is low [9, 10].

The gypsum board is widely used for surface material of interior walls and ceilings in the construction industry. It was manufactured through the process such as calcining gypsum into plaster, producing slurry from the plaster, and passing the slurry through machines for shaping, setting, and cutting into a board.

Table 1 Physical properties of tested materials

2.2. Measurements in Chamber

The moisture control performances of the three different materials were measured in a test chamber which was built in accordance with the ISO 24353:2008(E). The test chamber suggested in the ISO standard, which includes an electronic balance, a moisture-proof box with a programmable air conditioner and a thermometer. Fig. 1 shows the actual test chamber

used in this study and it consists of an electronic balance, a moisture-proof box with a thermostat, a temperature sensor, a humidity gauge, and a humidifier.

For preconditioning and testing of a specimen, the ambient temperature was set to 23±0.5℃, and the ambient relative humidity was maintained to 50±1% of the value of relative humidity of 50%.

Fig. 1 Exterior and interior views of test chamber

Then, moisture adsorption/desorption tests were performed by maintaining the relative humidity levels inside the chamber as shown in Table 2. First, moisture adsorption test was carried out at 75% RH for 12 hours. Then, desorption test was performed at 50% RH for additional 12 hours.

During the 24 hour moisture adsorption/desorption tests, the mass change of the test specimen was measured at a 10 minute interval to the nearest 0.01g. Then, the mass was recorded at the end of the first 12 hour period as the result of moisture adsorption process, and at the end of the second 12 hour period as the result of desorption process.

Table 2 Relative humidity levels inside chamber

2.3. Measurements in mock-up rooms

The hygric performances of the interior building materials were also tested in mock-up rooms. Fig. 2 shows the exterior view and floor plans of the mock-up rooms. As shown in Table 3, the ordinary mineral fiber boards were installed for the ceilings of the rooms 1 and 3, while the new mineral fiber boards were installed for the ceilings of the rooms 2 and 4. The walls and floors of the four mock-up rooms were finished by gypsum boards.

Three different measurement conditions were setup in the four mock-up rooms. In the first case, electric humidifiers were operated in the rooms 1 and 2 in order to simulate high-humidity summer conditions. In the second case, open water basins were placed in the rooms 1 and 2. In the third case, no humidifier or open water basin was used in the mock-up rooms 3 and 4 in order to simulate low-humidity winter conditions. Fig. 2 shows the three different humidification methods in the mock-up rooms. Then, the indoor humidity levels and temperatures with the new mineral fiber board and ordinary mineral fiber board were measured under the three different conditions by a temperature/humidity logger (Sato, SK-L200TH-II) placed outside the rooms. Fig. 3 shows the whole measurement schedule in the mock-up rooms.

In the mock-up case 1 (with electric humidifiers), the rooms 1 and 2 were measured for six days from February 28 to March 5, 2008. The room temperatures in both rooms were maintained at 21℃ to 24℃ by radiant floor heating. The electric humidifier in each room

was operated for two days and the average humidification rate was 0.125 ℓ/h. In the mock-up case 2 (with open water basins), the rooms 1 and 2 were measured for 28 days from March 10 to April 6, 2008. The room temperatures in both rooms were also maintained at the same temperatures as in the case 1. In each room, about three liters of water was naturally vaporized from the open water basin over the 28 days at an average vaporization rate of 0.0045ℓ/h.

In the mock-up case 3 (with no humidifier), the rooms 3 and 4 were measured for 39 from February 28 to April 6, 2008. In this case, the room temperatures in the two rooms were maintained at about 21℃ to 26 ℃. The room temperature was a little higher than that of the rooms 1 and 2 because no sensible heat was transformed into latent heat due to no moisture source.

Table 3 Mock-up room conditions for three measurement cases

Fig. 2 Mock-up rooms

Fig. 3 Humidification methods in mock-up rooms

Fig. 4 Measurement schedule in mock-up rooms

3. Results

3.1. Results from Chamber measurements

Fig. 5 shows the mass changes in the three specimens during the moisture adsorption and desorption processes inside the chamber. As shown in the figure, a dramatic change in the mass was noted with the new mineral fiber board between the adsorption and desorption processes. The performances of moisture adsorption and desorption can be clearly explained by Table 4 which shows the measured masses and calculated moisture contents from the chamber tests.

Fig.5 shows the moisture adsorption and desorption contents for this case, and the values of the new mineral fiber board were always higher than those of the other materials.

The moisture adsorption/desorption rate calculated by ISO 24353 in the measured moisture adsorption/desorption contents during the 24 hour test period. As clearly indicated the graphs, most of the moisture was adsorbed and desorbed during the first three hours of each process.

Table 4 Results from chamber measurements

Fig. 5 Mass changes in specimens during moisture adsorption and desorption processes in chamber measurements

3.2. Results from mock-up room measurements

Fig. 6 shows the relative humidity profiles for mock-up case 1 in which the ceilings of rooms 1 and 2 were treated by the ordinary mineral fiber board and the new mineral fiber board, respectively, and an electric humidifier was operated in each room. As shown in the figure and Table 5, the average relative humidity of the room 2 with the new mineral fiber board was about 13.9%p lower than that in the room 1. Fig. 7 shows the relative humidity profiles for mock-up case 2 where open water basins were placed in the rooms 1 and 2. As shown in the figure and Table 5, the average relative humidity of room 2 was 11.9%p lower than that of room 1.

From the measurement cases 1 and 2 where the artificial humidification was maintained to simulate a high-humidity summer condition, it was proven that the new mineral fiber board could be an effective dehumidifier during the summer season.

Fig. 8 shows the relative humidity profiles of mock-up case 3, measured during the same period as the case 1, in which the ceilings of rooms 3 and 4 were treated by the ordinary mineral fiber board and the new mineral fiber board, respectively, and no humidifier was operated in each room. As shown in the figure, the average relative humidity of room 4 was 8.2%p higher than that of room 3.

From these measurements, it was proven that the newly developed mineral fiber board could be an effective humidifier during the low-humidity winter seasons. Considering that variety of humidity increasing activities, such as cooking, dish washing and cloth drying occur in housings during the winter season, the new mineral fiber board will effectively adsorb indoor moisture generated from these activities, then desorb it back to the space when indoor humidity level is low.

Table 5 Test results with mock-up rooms

Fig.6 Relative humidity profiles of case 1(with electric humidifier)

Fig.7 Relative humidity profiles of case 2 (with open water basin)

Fig.8 Relative humidity profiles of case 3 (natural condition)

4. Conclusion

Relative humidity levels influence indoor environmental quality and occupants' thermal comfort. As an effective way of controlling relative humidity fluctuations without adding energy costs, various types of porous building materials with moisture adsorption/desorption properties have been widely introduced to the market in countries with a hot and humid climate. In this study, the adsorption/desorption properties of an ordinary mineral fiber board,

a newly developed mineral fiber board, and a gypsum board were investigated and compared by a series of chamber tests and mock-up room tests. From the chamber test, it was found that the moisture content of adsorption/desorption process of new mineral fiber board was about three times as great as that of ordinary mineral fiber board. In the mock-up room tests, the effects of the interior building materials on indoor humidity were investigated under three different conditions with electric humidifiers, open water basins, and no moisture source. From the measurement cases where the artificial humidification was maintained to simulate a high-humidity summer condition, it can be said that the new mineral fiber board can be an effective dehumidifier during the summer season. On the other hand, in the mock-up rooms with no moisture source, the indoor humidity level with new mineral fiber board was higher than that with the ordinary mineral fiber board. The results indicated that the moisture adsorbing/desorbing building materials can help maintain the comfort indoor humidity levels throughout different seasons so that the energy for humidification and dehumidification could be saved. In this study, the performance of one kind of moisture absorbing/desorbing material was evaluated by using accurately controlled chamber and mock-up rooms. Therefore, further studies are needed to evaluate its performance in the real-scale housing unit and to evaluate the performance of various building materials.

Acknowledgement

This research was supported by a grant (06ConstructionCoreB02) from the Construction Core Technology Program, funded by the Ministry of Construction & Transportation of the Korean government.

REFERENCES

1. N. Lechner, “Heating, Cooling, Lighting, Design Methods for Architects,” John Wiley & Sons, Inc., 2000.

2. Abadie MO, Mendoncav KC., “Moisture performance of building materials: From material characterization to building simulation suing the Moisture Buffer Value concept,” Building and Environment 2009, pp. 388-401.

3. Rode C. “Moisture buffer of building material,” Depart of Civil Engineerign, Technical University of Dnemark, Report R-126, 2005.

4. Rode C. Peuhkuri R, Time B, Svennberg K, Ojanen T. “Moisture buffer value of building material”. Journal of ASTM International 2007,VOL 4(5).

5. Janssen H. Roels S, “Qualitative and quantitative assessment of interior moisture buffering by enclosures,” Energy and Buildings 2009,VOL41,pp.382-294.

6. JIS A 1470-1, “Test method of adsorption/desorption efficiency for building material to regulate indoor humidity” Japan: Japanese Industrial Standard ; 2002.

7. ISO 24353. “Hygrothermal performance of building materials and products – Determination of moisture adsorption/desorption properties in response to humidity variation. International Standard Organization” ; 2008.

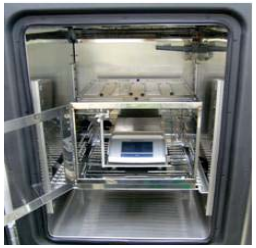
8. Sophie K. Thompson, Eileen M. “Asbestos: Mineral and fibers. Chemical health and Safety” VOL4, pp.21-23.

9. Eloussaief E. Benzina M. Efficiency of natural and Acid-activated clays in the removal of Pb(II) from aqueous solutions. Journal of hazardous Materials2010; 178:753-757.

10. Haneed B.H., “Equilibrium and kinetics studies of 2,4,6-trichlorophenol adsorption onto activated clay,” Physicochemical and Engineering Aspects2007,307,pp.45-52



a) Exterior view

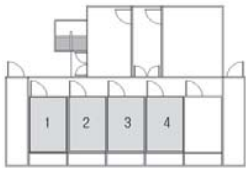


b) Interior view

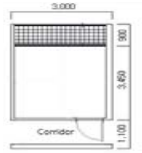
Fig. 1 Exterior and interior views of test chamber



a) Exerior view



b) floor plan



c) floor plan detail

Fig. 2 Mock-up rooms



a) electric humidifier

(rooms 1 and 2)



b) open water basin

(rooms 1 and 2)



c) none

(rooms 3 and 4)

Fig. 3 Humidification methods in mock-up rooms

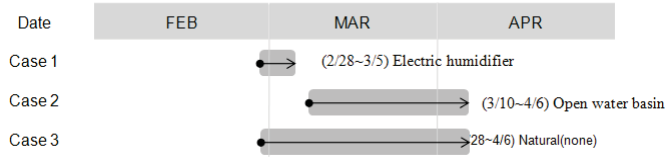


Fig. 4 Measurement schedule in mock-up rooms

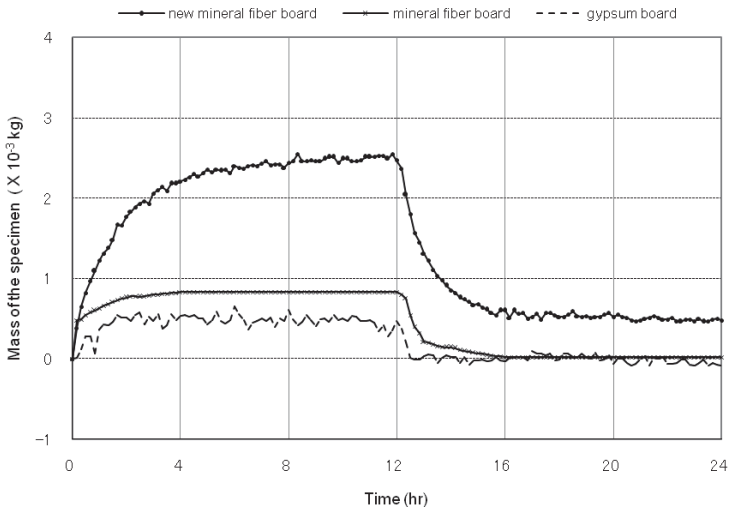


Fig. 5 Mass changes in specimens during moisture adsorption and desorption processes in chamber measurements

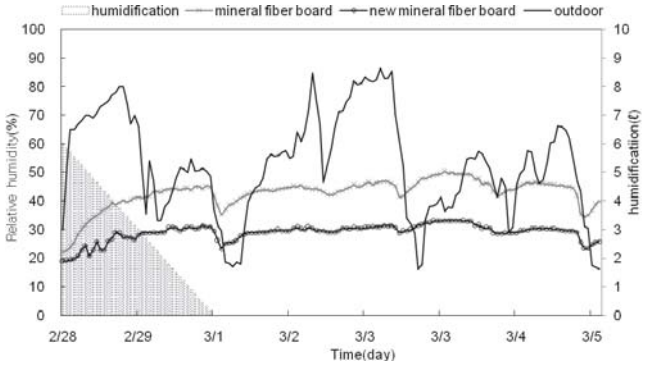


Fig.6 Relative humidity profiles of case 1(with electric humidifier)

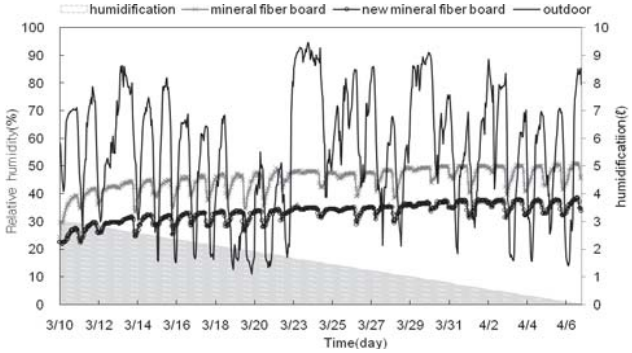


Fig.7 Relative humidity profiles of case 2 (with open water basin)

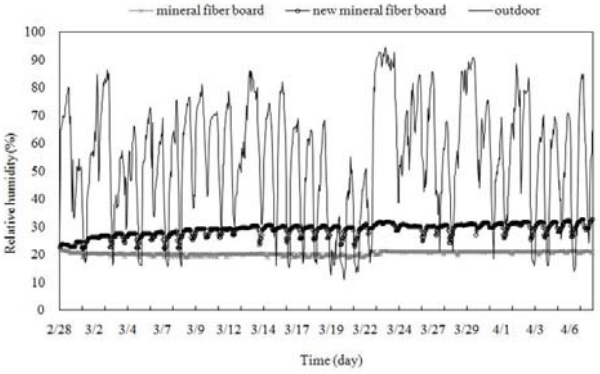


Fig.8 Relative humidity profiles of case 3 (natural condition)

Table 1 Physical properties of tested materials

Product	Material	Thickness (m)	Density (kg/m³)	Moisture content (%)
Mineral fiber board	Mineral fibrous wool	0.012	300	1.3
New mineral fiber board	Mineral fibrous wool + Activated China clay	0.012	340	2.3
Gypsum board	Gypsum	0.0095	610	0.2

Table 2 Relative humidity levels inside chamber

Relative humidity (%)		
Preconditioning	Moisture adsorption process	Moisture desorption process
	Step 1	Step 2
50	75	50

Table 3 Mock-up room conditions for three measurement cases

	Case 1		Case 2		Case 3	
No.	Room 1	Room 2	Room 1	Room 2	Room 3	Room 4
Humidification Method	E.H	E.H	O.B	O.B	N	N
Ceiling	M	N.M	M	N.M	M	N.M
Floor	G	G	G	G	G	G
Wall	G	G	G	G	G	G

E.H : Electric humidifier O.B : Open water basin,

M: Mineral fiber board N.M : New mineral fiber board

G : Gypsum board N : Natural(none)

Table 4 Results from chamber measurements

Category	Mineral fiber board	New mineral fiber board	Gypsum board
A(㎡)	0.0625	0.0625	0.0625
m_o (10^{-3}kg)	0.00	0.00	0.00
m_a (10^{-3}kg)	0.83	2.47	0.47
m_d (10^{-3}kg)	0.02	0.48	0.00
$\rho_{A,a}(g/m^2)$	13.3	39.5	7.5
$\rho_{A,d}(g/m^2)$	13.0	31.8	9.1
$\rho_{A,s}(g/m^2)$	0.3	7.7	-1.6

Table 5 Test results with mock-up rooms

		Average Temperature (℃)	Average Relative humidity (%)	Average Absolute humidity (kg/kg`)
Case 1	Mineral fiber board	22.9±1.1	42.8±5.2	0.0074±0.0008
	New mineral fiber board	22.8±1.1	28.9±3.0	0.0049±0.0005
	Outdoor	4.9±3.7	53.0±17.9	0.0027±0.0008
Case 2	Mineral fiber board	21.9±1.2	45.0±4.2	0.0073±0.0005
	New mineral fiber board	22.1±1.1	33.1±3.5	0.0054±0.0005
	Outdoor	10.6±4.3	55.6±21.6	0.0041±0.0012
Case 3	Mineral fiber board	23.7±2.0	20.5±0.7	0.0036±0.0003
	New mineral fiber board	23.4±1.8	28.7±2.4	0.0050±0.0005
	Outdoor	9.2±4.7	54.8±20.7	0.0038±0.0012

Characteristics on indoor air pollutant emission from wood-based flooring by environmental-friendly natural adhesive using CNSL

Jeong-Hun Lee[1], Sumin Kim[1*]

[1] Building Environment & Materials Lab, School of Architecture, Soongsil University, Seoul, Korea 156-743

* Corresponding Author E-mail: skim@ssu.ac.kr

Abstract

To discuss the reduction of formaldehyde and volatile organic compound (VOC) emissions from engineered flooring, cashew nut shell liquid (CNSL)-formaldehyde (CF) resin and CF/PVAc resin were applied for the maple face of the veneer bonding on plywood. The CF resin was used to replace urea-formaldehyde (UF) resin in the formaldehyde-based resin system in order to reduce formaldehyde and VOC emissions from the adhesives used between the plywoods and fancy veneers. For the CF/PVAc resins, 5, 10, 20 or 30% of PVAc was added to the CF resin. The CF/PVAc resins showed better bonding than the commercial natural tannin adhesive with a higher level of wood penetration. The standard formaldehyde emission test and a VOC analyzer were used to determine the formaldehyde and VOC emissions, respectively, from the engineered floorings. The CF resin and CF/PVAc resin systems with UV coating satisfied the E1 and E0 grades of the Korean Standard. TVOC emission was slightly increased by the PVAc addition.

Keywords: Environment-friendly resin, Cashew nut shell liquid (CNSL), Formaldehyde, TVOC, Wood-based flooring

Introduction

CNSL, an agricultural by-product of the cashew nut processing industry and a renewable resource, is a source of a long chain, m-substituted phenol which promises to be an excellent monomer for polymer production [1]. CNSL contains four major components: 3-pentadecenyl phenol (cardanol), 5-pentadecenyl resorcinol (cardol), 6-pentadecenyl salicylic acid (anacardic acid) and 2-methyl, 5 pentadecenyl resorcinol (2-methyl cardol) [2]. About 90% consists of anacardic acid, cardanol and cardol is CNSL [3]. Cardanol, which can be obtained by thermal treatment of CNSL, is a phenol derivative mainly composed of the meta substitute of a C15 unsaturated hydrocarbon chain with one to three double bonds [4,5]. Double vacuum distillation of CNSL yields pure cardanol at 50% yield[6]. The greatest problem of formaldehyde and TVOC emissions in engineered flooring is caused by the face of the fancy veneer bonding. UF resin is still used in industry in large quantity. The author's previous work [7] suggested the suitability of Tannin as a renewable resource for surface bonding in engineered flooring. In this study, to reduce formaldehyde and VOC emissions from the resin for bonding the face of the fancy veneer on engineered flooring, the UF resin was replaced by natural CNSL.

Experimental

The plywood and decorative veneer used for fabricating the test samples were supplied by Easywood Co., Ltd., South Korea. The decorative veneers were 0.5 mm thick maple, while 7mm-thick plywoods manufactured in China were used. Polycardanol, which was prepared

by enzyme-catalyzed oxidative polymerization, was kindly supplied by Hyundae Paint Co. Ltd, Korea. Figure 1 depicts the chemical structure of the polycardanol used in this work.

A formaldehyde solution of 40% weight of solid per unit volume of liquid and hexamine as a hardener were added to make the CF resin. The CF resin was polymerized by adding 1 ml of sodium hydroxide solution to the resin mixture. In the second stage of the experiment, 1 ml of 15% hexamine was also added [3]. Blends of various CF/polyvinyl acetate (PVAc) compositions were prepared. To make the CF/PVAc hybrid resin, 5, 10, 20 or 30 wt % of PVAc was added to CF and the mixture was stirred for 20 min. The engineered floorings for the formaldehyde and VOC emission tests were manufactured using natural tannin adhesive and CF/PVAc hybrid resin. After the resin was spread on the plywood, 0.5mm-thick maple fancy veneer was bonded by cold- and hot-pressing.

The formaldehyde emissions from the engineered floorings bonded with each blend were determined with a desiccator in accordance with the JIS method using a glass desiccator [9]. To determine VOC emissions we used a VOC analyzer. The VOC analyzer is a portable device to measure the four main aromatic hydrocarbon gases: toluene, ethylbenzene, xylene and styrene [10, 11].

Results and Discussion

Before surface coating, the formaldehyde emissions from the products glued with CF resin was already less than E1 grade (under 1.5 mg/L) of the formaldehyde emission level in the Korean Standard, even though the CF resin contained formaldehyde, as shown in Figure 2. The CF/PVAc hybrid adhesives samples showed a similar tendency to that of the CF resin. When the surface was coated with a UV-curable, urethane acrylate coating for flooring, the emission level was reduced to much less than half and satisfy the requirement of E0 grade. In the CF/PVAc resin system, the role of PVAc was to avoid generating formaldehyde emission, by replacement of CNSL with hexamine, and to increase the initial bonding strength through PVAc's high viscosity and room temperature curable property. Figure 3 presents the concentrations of the four indicated VOCs from the engineered flooring bonded with each resin system, as determined by the VOC analyzer. Xylene was the highest detected compound in all samples, followed by ethylbenzene and toluene. Styrene, however, was not detected at all in any of the systems. However, TVOC emission of the PVAc-added CF resin system was slightly increased compare to that of the CF resin.

Conclusions

The surface bonding strength of the CF/PVAc resins was higher than that of the CF resin. The bonding strength was maximized for the CF/PVAc resin with a PVAc content of 20%. By desiccator method, the formaldehyde emission, which presented similar emission data for

the CF and CF/PVAc resins, was lowered with the PVAc addition, and further reduced when coated with a UV-curable urethane acrylate. The formaldehyde emission level was sufficiently reduced to satisfy the E0 grade of the Korean Standard. In the case of the CF/PVAc resin, the VOC emission measured by the VOC analyzer was slightly increased by the PVAc addition. In conclusion, the CF/PVAc resins were successfully applied as environmentally friendly adhesives of surface bonding for manufacturing engineered flooring.

Acknowledgments

This work was supported by the Grant of the Korean Ministry of Education, Science and Technology (The Regional Core Research Program/Biohousing Research Institute). This work was supported by the Biohousing Research Center.

References

1. H.P. Bhunia, G.B. Nando, A. Basak, S. Lenka, P.L. Nayak, Synthesis and characterization of polymers from cashew nut shell liquid (CNSL), a renewable resource III. Synthesis of a polyether, Eur. Polym. J. 35(1999)1713-1722

2. H.P. Bhunia, G.B. Nando, T.K. Chaki, A. Basak, S. Lenka, P.L. Nayak, Synthesis and characterization of polymers from cashew nut shell liquid (CNSL), a renewable resource II. Synthesis of polyurethanes, Eur. Polym. J. 35(1999):1381-1391.

3. L.Y. Mwaikambo, M.P. Ansell, Cure characteristics of alkali catalysed cashew nut shell liquid-formaldehyde resin, J. Mater. Sci. 36(2001)3693-3698.

4. R. Ikeda, H. Tanaka, H. Uyama, S. Kobayashi, A new crosslinkable polyphenol from a renewable resource, Macromol. Rapid Comm. 21(2000)496-499.

5. Y.H. Kim, E.S. An, S.Y. Park, B.K. Song, Enzymatic epoxidation and polymerization of cardanol obtained from a renewable resource and curing of epoxide-containing polycardanol, J. Mol. Catal. B-Enzym. 45(2007)39-44.

6. H.P. Bhunia, R.N. Jana, A. Basak, S. Lenka, G.B. Nando, Synthesis of polyurethane from cashew nut shell liquid (CNSL), a renewable resource, J. Polym. Sci. Pol. Chem. 36(1998)391-400.

7. S. Kim, Environment-friendly adhesives for surface bonding of wood-based flooring using natural tannin to reduce formaldehyde and TVOC emission, Bioresour. Technol. 100(2009):744-748.

8. S. Kim, H.-J. Kim, Evaluation of formaldehyde emission of pine and wattle tannin-based adhesives by gas chromatography. Holz Roh. Werkst. 62(2004)101-106

9. S. Kim, J.-A Kim, J.-Y. An, H.-J. Kim, S.D. Kim, J.C. Park, TVOC and formaldehyde emission behaviors from flooring materials bonded with environmental-friendly MF/PVAc hybrid resins. Indoor Air 17(2007)404-415.

10. J.-Y. An, S. Kim, J.-A Kim, H.-J. Kim, Development of Simple Test Method using VOC analyzer to Measure Volatile Organic Compounds Emission for Particleboards. Mokchae Konghak 34(2006)22-31. (in Korean)

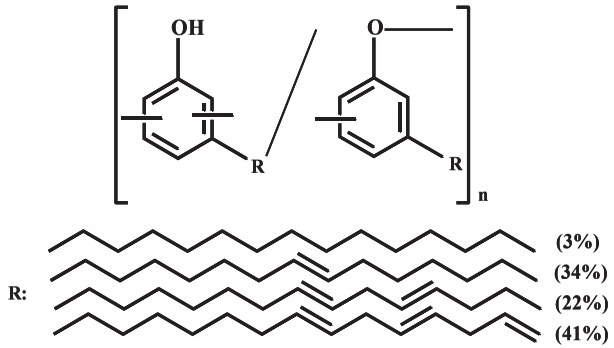


Fig. 1 Chemical structure of polycardanal

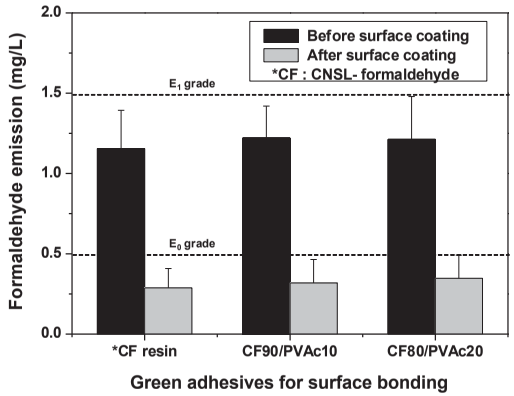


Fig. 2 Formaldehyde emission from engineered flooring bonded with CNSL-formaldehyde (CF) resin and CF/PVAc green adhesives as determined by the desiccator methodl

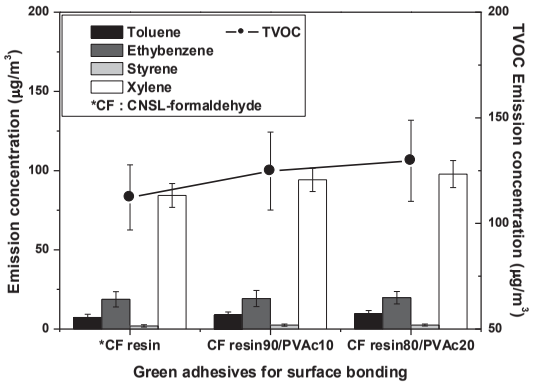


Fig. 3 VOC emission concentrations (toluene, ethylbenzene, xylene and styrene) from engineered flooring bonded with CNSL-formaldehyde (CF) resin and CF/PVAc green adhesives as determined by the VOC analyzer

Environment-friendly Hwangtoh composites using water soluble resin for interior materials

Jisoo Jeon[1], Sumin Kim[1]*

[1] Building Environment & Materials Lab, School of Architecture, Soongsil University, Seoul, Korea 156-743

* Corresponding Author E-mail: skim@ssu.ac.kr

Abstract

The objective of this research was to develop environment-friendly Hwangtoh binder for application of Hwangtoh for interior wall finishing materials in the housing. To mix with Hwangtoh powder, water soluble MPU resin with EVA, PVA, CaCO3 and inorganic fillers were designed. Far infrared ray irradiation, TVOC emission behavior, surface bonding strength and surface crack behavior were studied by comparing to epoxy/Hwangtoh blend as control. To utilize the advantage of Hwangtoh such as high absorbency, self-purification, deodorizing, sanitizing properties and radiation of far infrared rays in the filed of modern housing, this study was the foundation to develop environment-friendly binder for Hwangtoh.

Keywords: Environment-friendly, Hwangtoh, Finishing materials, TVOC, Far infrared rays

Introduction

Sick house syndrome is a serious problem with the air quality caused by indoor contaminants in the home and work place [1,2]. Public interest in healthy housing with eco-friendly materials has sharply increased recently. There has been growing concern regarding healthy housing using environment-friendly materials. Hwangtoh is one of the representative healthy and environment-friendly materials with the properties of high absorbency, self-purification, deodorizing and sanitizing properties [2,3].

This paper presents the developed Hwangtoh wall finishing materials with environmental-friendly water soluble resin which have good characteristics such as far-red frequency irradiation, low VOCs emission, good bonding property and habitat without surface crack.

Materials

To blend water soluble MPU adhesive, EVA(ethylene-vinyl acetate copolymer) emulsion was used from Air Product, Korea. 70 parts of EVA and 20 parts of PVA was blended. Commercial PVA from DC chemical(Seoul, Korea) was used. The blend was mixed by mechanical stirring for 10 min. 50 parts of $CaCO_3$ was added to blend. As additives 10 parts of silica and a part of carboxyl acid was added. After anti forming agent was added, water was added to control solid content was 50%.. This MPU was used as base resin. 10wt% of isocyanate-based compound was used as curing agent. Finally, Hwangtoh wall finishing materials were blended as shown Table 1. Inorganic additive was compound of $CaCo_3$, clay and silica. To compare with these water soluble resin, epoxy resin and hwangtoh blend was used as control.

Methods

A rack was constructed with the top and two sides containing FIR sources. The FIR sources were constructed from a ceramic-coated sheet of aluminum, and the opposite side of the sheet was heated by an electric heater. FIR emitted from the ceramic-coated sheet ranged from 5 to 25 μm with a maximal intensity of 8 to 12 μm. The temperature in the rack was approximately 40°C. These temperatures were continuously monitored with a sensor placed in the rack. These equipments were supplied by Sagano Co. Ltd (Kobe, Japan). Irradiation rate and irradiation energy at 40 °C were detected.

The 20 L small chamber was supplied with purified and humidified air at a ventilation rate of 0.5ACH through an air-flow of 0.01m3•h-1. In this paper, TVOC was defined by conversion of all areas of the peaks between C_6 and C_{16} to concentrations using the toluene response factor. Any peak area under ten was defined as the limit of detection. The gas was sampled by absorption on Tenax-TA, 7 days after the sample specimens were installed into the 20L small chamber, according to the regulation from the Ministry of the Environment, Korea.

The bonding strength between the Hwangtoh wall finishing blends and concrete panel was tested with a Universal Testing Machine (UTM, Hounds Co.) in the tensile mode. On the concrete panel (100mm × 200mm), Hwangtoh wall finishing blends and Hwangtoh/epoxy were spread as thickness of 5mm. These samples were dried at room temperature for 24 hours. The crack on the surface was checked.

Results

FIR has several benefits for human body; it 1)stimulates enzyme activity and metabolism, 2) promotes the killing of many pathogenic (disease causing) bacteria, viruses, fungi and parasites, 3)relieves nervous tension and relax autoneuro muscles 4)promotes rebuilding of injured tissue and 5)strengthens the Immune System [4,5]. FIR irradiation of Hwangtoh wall finishing materials blends are shown in Table 2. Hwangtoh with MPU resins shows higher Irradiation rate at 5~20um than Epoxy/Hwangtoh blend. Hwangtoh is one of good ceramic materials which emits high far infrared ray. Although epoxy, chemical binder, interrupted irradiation of far infrared ray, MPU binders showed higher irradiation rate dew to water soluble binder contain much lower percentage of chemical compound than only chemical binder. In the case of irradiation energy, MPU-B and MPU-C was higher than Epoxy/Hwangtoh blend. From these results, water contain rate in Hwangtoh finishing materials leads far infrared rays irradiation from Hwangtoh ceramic.

In Figure 1, TVOC emission from Epoxy/Hwangtoh blend and MPU/Hwangtoh blends by 20L chamber method is shown. TVOC emission results from MPU/Hwangtoh blends were too low to be concerned about indoor air pollution. In Korea, the Ministry of Environment

provides guidelines of formaldehyde and VOC emissions from building materials. Because a gypsum board is used as interior material for construction of buildings and houses, the emission of indoor air pollution materials such as formaldehyde is important. However, there was much lower formaldehyde emission and TVOC emission factor was under the 'Excellent' grade as defined by KACA [6,7]. Epoxy resin is one of major synthetic resins manufactured in the world. It emits VOCs during the production and use. Because epoxy resin emits VOCs, Epoxy/Hwangtoh blend shows higher TVOC emission result than MPU/Hwangtoh blends. As interior building materials, the MPU/Hwangtoh blends can be used without indoor air pollution problems because there is water soluble resin. From these results, MPU/Hwangtoh blends should be considered for wall finishing materials for interior because water soluble resins are the most practical approaches used to lower the emissions of VOC.

Because adhesion failure was appeared between the Hwangtoh wall finishing blends and concrete panel the surface bonding strength was well measured in this test. The results of the surface bonding properties are shown in Figure 2. Although the bonding strength of Epoxy/Hwangtoh blend showed highest among the samples, the bonding strength of water soluble MPU/Hwangtoh blends samples were increased as water contents were increased. Finally, the bonding strength of MPU-C/Hwangtoh blend reached to almost similar lever with epoxy/Hwangtoh blend. We found the reason of this result from the surface crack behavior.

As increasing water content in MPU/Hwangtoh blends, the surface crack was reduced and disappeared on surface of Hwangtoh finishing. Water made decreasing viscosity of MPU/Hwangtoh blend. Lower viscosity led vigorous mobility of Hwangtoh particle and resin. As interior wall finishing material, reduction of surface crack is important factor. With water contents, surface cracks of MPU/Hwangtoh blends could be controlled.

Conclusions

Water soluble MPU resins manufactured with EVA, PVA and CaCO3 were successfully applied to Hwangtoh for environment-friendly interior wall finishing materials. Irradiation rate and irradiation energy of far infrared ray of MPU/Hwangtoh blends were higher than those of epoxy/Hwangto blend as control. TVOC emission of MPU/Hwangtoh blend was satisfied the excellent grade of TVOC by Korea Air Clean Association. By the contents of water in the blend, the crack on cured surface of MPU/Hwangtoh blends was controlled. Reduction and disappearance of crack on cured surface led good bonding strength between MPU/Hwangtoh blend and concrete panel.

Acknowledgement

This research was supported by the Basic Science Research Program through the National Research Foundation of Korea(NRF) funded by the Ministry of Education, Science and Technology (NO.R11-2010-0001867)

References

1. Menzies, D., Bourbeau, J. (1997) Building related illnesses. New Eng. J. Med. 337, 1524-1531..

2. Lee, S.-W., Yang, Y.-S., Ahn, T.-H., Bae, C.-S., Moon, C.-J., Kim, S.-H., Song, S.-Y., Hwang, H.-Z., Kim, J.-C. (2007) Subacute toxicity evaluation in rats exposed to concrete and Hwangto building environments. Environ. Toxicol. 22(3), 264-274.

3. Yang, K.-H., Hwang, H.-Z., Kim, S.-Y., Song, J.-K. (2007) Development of a cementless mortar using Hwangtoh binder. Build. Environ. 42(10), 3717-3725.

4. Ishiyama, M., Miyazono, Y., Sasamoto, K., Ohrkura, Y., Ueno, K. (1997) A highly water-soluble disulfonated tetrazolium salt as a chromogenic indicater for NADH as well as cell viability. Taranta 44, 1299-1305.

5. Udagawa, Y., Nagasawa, H. (2000) Effects of far-infrared ray on reproduction, growth, behaviour and some physiological parameters in mice. In Vivo 14(2), 321- 326.

6. Kim, S., Kim, J.-A., An, J.-Y., Kim, H.-J., Kim, S.D., Park, J.C. (2007) TVOC and formaldehyde emission behaviors from flooring materials bonded with environmental-friendly MF/PVAc hybrid resins. Indoor Air 17, 404-415

7. Kim, S., Kim, H.-J., Moon, S.-J. (2006) Evaluation of VOC emissions from building finishing materials using a small chamber and VOC analyser. Indoor Built. Environ. 15(6)

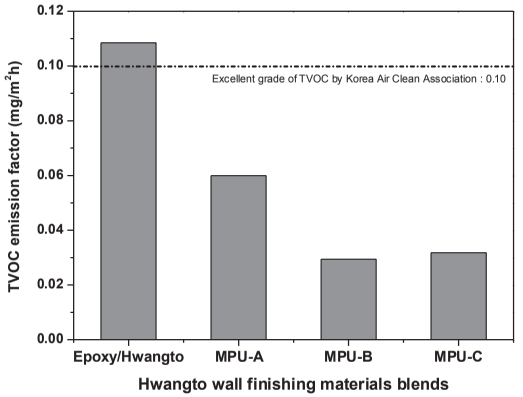


Fig. 1 TVOC emission of Hwangtoh wall finishing materials blends

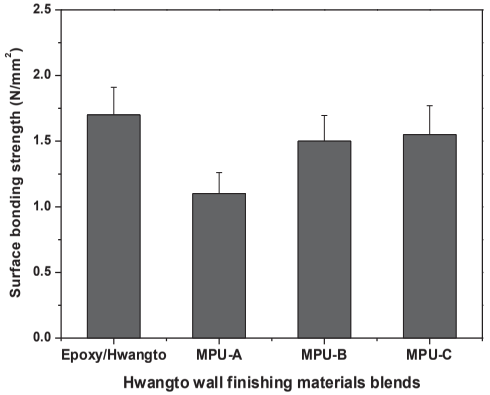


Fig. 2 Surface bonding strength of Hwangtoh wall finishing blends

Table 1 Hwangtoh wall finishing materials blending ratio (wt%)

	MPU	Isocyanate-based curing agent	Inorganic additive	Hwangto flour	Water
MPU -A	1	0.1	1	1	1.0
MPU -B	1	0.1	1	1	1.22
MPU -C	1	0.1	1	1	1.29

Table 2 Far infrared ray irradiation of Hwangtoh wall finishing materials blends

		Epoxy/Hwangto blend	MPU -A	MPU -B	MPU -C
Far infrared rays irradiation (at 40 ^{o}C)	Irradiation rate (at 5~20um)	0.895	0.992	0.990	0.991
	Irradiation energy (W/m^2)	3.70×10^2	3.70×10^2	3.72×10^2	3.71×10^2

Adaptation process of human olfactory under continues exposure to odor of ethyl acetate based on subjective estimation of odor intensity

H. Nagatsugu[1], T. Yamanaka[1], K. Sagara[1], H. Kotani[1], Y. Momoi[1] and A. Takemura[2]

[1] *Department of Architectural Engineering , Graduate School of Engineering , Osaka University , Japan*

[2] *Department of Odor and Aroma Design , School of Informatics , Daido University , Japan*

Abstract

This study was aimed at making a model which predicted olfactory sensation. Firstly, it was conducted the experiment, which odor was exposed to subjects constantly and subjects evaluated odor, to investigate the olfactory adaptation process. As a result, it was turned out odor intensity decreasing exponentially as time. Secondly, validity of the previous theoretical model (Osako,1991) was investigated by comparing the evaluation. As a result, it was found out that the validity of the previous model might be better in the case discriminating the adapting intensity from the after adapted.

Keywords: Odor, Subjective evaluation, Adaptation model

1. Introduction

Olfactory adaptation is well known as the decrease phenomenon of olfactory sensitivity by continuous smelling. In order to predict momentary evaluation accurately in our life, it is necessary to consider the unsteady variation of olfaction, because the adaptation and the recovery are repeated according to the variation of odor concentration as our movement. For example, even if there is odor visitors cannot accept, occupants never sense the odor due to the olfactory adaptation in the office. Therefore, it is also important to take account of the occupants' olfactory response in the case of being exposed to unsteady odor concentration.

However, it is necessary to know the response of olfaction under constant exposure to odor before the case of exposed unsteady state response. Thus, the purpose of this study is to clarify the adaptation response of human olfactory in time series by means of perceived intensity under continuous exposure to the odor with the constant concentration. In this study, the experiment was conducted to measure the odorous sensitivity by the subjective evaluation of the odor intensity on continuous scale. As an odor, ethyl acetate was used because it was controlled by Odor Control Law in Japan. As subjects were exposed to the odor for a long time, therefore the odor must have little effect on health. The safe odor concentration was determined accounting for the health effect.

The subjective was applied for examining the theoretical models for perceived intensity. One is the model presented by Osako which is based on the rate of increasing number of odorant-receptor combination, and the other is the model by Overbosch based on the power law. In this paper, the investigation about the former model by Osako is examined.

2. Methods

Subjects

A total of five subjects (one male student and four female students) from the age of 22 through 23 years old participated in the experiment.

Method

The experiments were conducted from May 13 to June 11, 2010 in the laboratory whose interior was decorated with stainless steel plates (Fig.1). In the tests, the sufficient ventilation rate was maintained by keeping the windows open to some extent. The temperature was ranged from 19.2 to 24.9^{o}C, the humidity ranged from 27.0 to 76.0%. Ethyl acetate was used as the odor for the tests. The subjects were exposed to the odor continuously. Fig.2 shows the odor presentation device. The method of presenting the odor was as follows. Firstly, the air in the next room where the temperature controlled was extracted by the fan. Secondly, the supplied air became odorless air after passing through the active carbon deodorant device. Thirdly, ethyl acetate was injected to the odorless air. Forth, the subjects in the laboratory (the right side in Fig.1) start to smell the mixed air supplied through the flexible duct made of aluminum. Before the experiments, the subjects were exercised the test once.

The time schedule is shown in Fig. 3. At first, the subjects were given the instruction before the start of the experiment. Then they smelled the odorless air for 5minutes. After that, subject were asked to evaluate the intensity of the odor every 30s. In total, the subjects evaluate the odor intensity for 21 times. There are two methods of breathing for the subjects. Table 1 shows the odor concentration and the breath methods. One is the method that the subjects are inhale and exhale only through nose. The other is the method that the subjects

inhale through nose and exhale through mouth. They were instructed to breathe naturally in either method. he divided time spans can bring better accuracy than using overall time span.

3. Results and Discussion

3.1 Experimental Results

Fig.5 shows the relation between the exposing time and the odor intensity for each trial, under the condition of exposed concentration and the breath method. In this figure, the evaluation results by five subjects are listed in each graph. The evaluation by subject A seems different from the results by other subjects. This difference is considered to reflect that subject A has different perception of the intensity scale in comparison with the other subjects. It is considered, therefore, the evaluation by subject A should be excluded from the following discussions in this paper.

Fig.6 shows the relation between the exposing time and the average of odor intensity under each condition. In this figure, the mean value of the evaluations and the range of ±σ (standard deviation) at each exposing time is listed. In the case of the ethyl acetate of 1.0ppm, the odor intensity decreases to “No odor” within 3 minutes. In the case of 7.0ppm, the odor intensity decreases and becomes around “Weak” in not more than 5 minutes. In the case of 20ppm, the odor intensity also decreases, but it seems to take more time than the cases of the other small concentration to reach about “Weak”. These results indicate that, so-called adaptation may be caused at any odor concentrations. In the previous studies, also the same tendency as this one was presented, therefore, obtained data can be applied to the past theoretical model of olfactory adaptation. In this study, the model presented by Osako (1991) was selected. The model is hereafter called “Osako model”.

3.2 The olfactory model

Osako model is based on the rate of odorant-receptor combination with the odorant molecules. The combination of the odorant molecules (*S*) with the receptors (*P*) were expressed as the following equation 1, which expresses the state of equilibrium.

$$S + P \underset{k_2}{\overset{k_1}{\rightleftarrows}} (SP)_{act} \rightarrow (SP)_{inact} \qquad \text{(Eq.1)}$$

The dotted line on the right side in Eq.1 shows that the active compound $(SP)_{act}$ becomes inactive compound $(SP)_{inact}$ after transmitting the electric pulses In addition, considering the actual breathing method, it is supposed that the odorant molecules will be combined with receptors during inhalation, but they may leave during exhalation. The variation of the number of combined odorant molecules with the receptors $x(t)$ is presented in Fig.7. Based on this assumption, the equations about the combination rate can be derived. Using $x'_{(t)}$ as the combination rate of the odorant molecules with the receptors during inhalation of n times from the start of exposing, Eq.2 can be written for the inhalation period. In similar way, Eq.3

can be derived for the period of exhalation. It is assumed that people exhales through their nose. Fig. 8 shows the fluctuation of combination rate calculated by the Eq.2 and 3.

$$x'_{(t)} = k_1 CN \exp\left[-(k_1 C + k_2)\{t + t_k - n(t_A + t_B)\}\right] \quad \text{(Eq.2)}$$

$$x'_{(t)} = -k_1 x'_{[(A+1)t_A + At_B]} \exp\left[-k_2\{t - (A+1)t_A - At_B\}\right] \quad \text{(Eq.3)}$$

$$I = \alpha x'_{(t)} \quad \text{(Eq.4)} \qquad I = In\left[\alpha x'_{(t)}\right] \quad \text{(Eq.5)}$$

Odor intensity can be determined in two different ways. The one way is to assume the linearity as Eq.4, the other way is to apply Weber-Fechner's law as Eq.5. If the parameters (α, t_A, t_B, k_1, k_2, N and C) in Eq.2, Eq.3 and Eq.4 can be identified by regression based on the experimental data, it is possible to establish the olfactory prediction model. In the previous report (Nagatsugu et al., 2010), t_A and t_B were fixed at 1s because t_A and t_B, that is, the time intervals have little effect on the calculated odor intensity using this model. Additionally, in order to simplify the calculation, α was assumed to be 1.0 and N was estimated to be 10000. Furthermore, C, which means the concentration of the mucus on olfactory epithelium, was regarded to be equal to the odorant concentration in the experiment. By regarding the rest parameters (k_1 and k_2) variables, these variables were identified by least-square method using experimental data. In this calculation, "No odor" was substituted by 0, and "Overpowering" was substituted by 1.

Fig.9 demonstrated the comparison between the change of calculated odor intensity based on Eq.4 and the experimental values, which is the mean value of five subjects except subject A.

The experimental data and the regression line seems to be almost conformable, however, there can be seen a little discrepancy at the start and end of exposing time. Therefore, in order to get better conformance of the model, it was tried to shorten the time span for regression. Fig.10 shows the result of the changing the time span for regression obtained by both of exponential model (Eq.4) and the logarithmic model (Eq.5), and Table 2 shows the residuals of both equations for each condition. From this table, it was made clear that the exponential model is more applicable than the logarithmic ones. Therefore, future investigations will be made by means of the exponential model (Eq.4).

In Osako model, actual breathing method was taken into account. However, it seems not necessary to distinguish inhaling process from exhaling process. That is, it is possible to apply simpler exponential model as Eq.6.

$$x'_{(t)} = \alpha \exp\left[\beta t\right] \quad \text{(Eq.6)}$$

Fig.11 shows the comparison between Osako model and the simple exponential model. There is little difference between them. Additionally, Fig.12 presents the comparison between the two exhaling method, nose exhaling and mouth exhaling. It can be said that there is also little difference between them. Thus, it is concluded that detailed Osako model is not needed to predict the decreasing process of odor intensity due to adaptation caused by continuous exposure to odor.

In Fig.13, two kinds of regression results obtained from the data in divided time spans and overall time span are drawn using simple exponential equation (Eq.6). It is found that the divided time spans can bring better accuracy than using overall time span.

Conclusions

As a result of the experiment of exposing subjects to odor constantly, it was made clear that adaptation is caused quickly, and adaptation will take longer time if the odorous concentration is higher.

Applying Osako model to the experimental data was successful, but exponential model brought better applicability than Weber-Fechner's law.

Additionally, simpler model ignoring breathing process was investigated. Consequently, it is concluded that Osako model is not needed to predict the decreasing process of odor intensity due to adaptation caused by continuous exposure to odor.

References

1. M.Osako(1991):Study on evaluation of environmental odor based on modeling of olfaction", Ph.D thesis Kyoto university (in Japanese)

2. Collegium Odor Control Law: Handbook Odor Control Law, Ver.4, 2005

3. P.Overbosch: A theoretical model for perceived intensity in human taste and smell as a function of time, Chemical Senses, Vol.11, no.3, pp.315-329, 1986

4. H.Nagatsugu, T.Yamanaka, K.Sagara, K,Hisashi, Y,Momoi and T,Takemura: Olfactory Adaptation in Odor Subjective Evaluation (Part2)Application of Olfactory Adaptation Model to Time Variation Properties of Odor Intensity, Summaries of technical papers of annual meeting of AIJ, prepublished 2010 (in Japanese)

5. U. Berglund: Dynamic properties of the olfactory system, Ann.N.YAcad.Sci., 237, pp.17-27, 1974

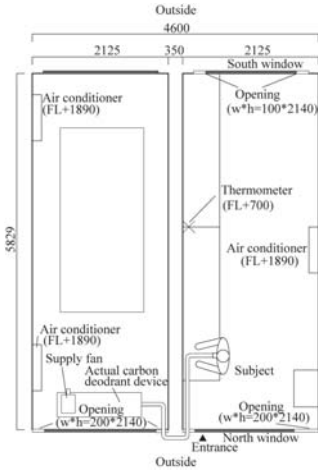


Fig.1 Laboratory plan

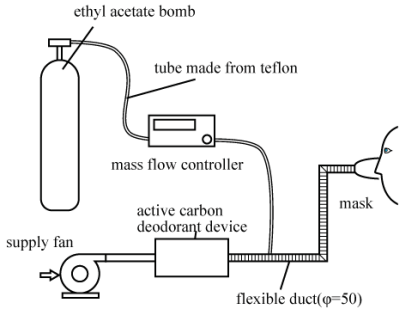


Fig.2 Odor presentation device

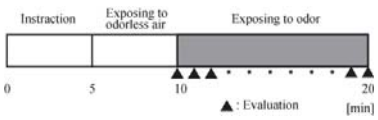


Fig.3 Time schedule



Fig.4 Scale of odor intensity and evaluation value of intensity

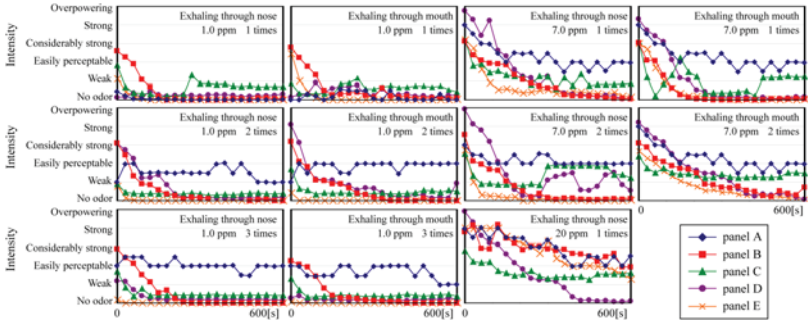


Fig. 5 Relation between exposing time and odor intensity for each trial, under condition of exposed concentration and breathing method

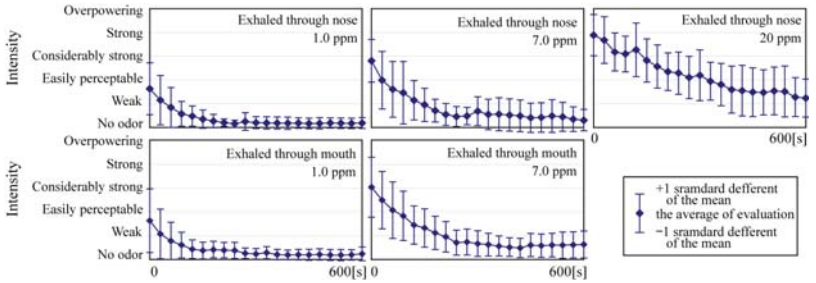


Fig.6 Relation between exposing time and average of odor intensity under each condition

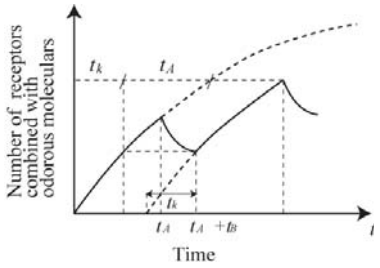


Fig.7 Conceptual graph of the number of the concentration for the Osako model

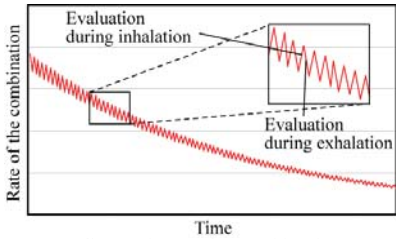


Fig.8 fluctuation of combination rate calculated by the Eq.2 and Eq.3 by Osako model

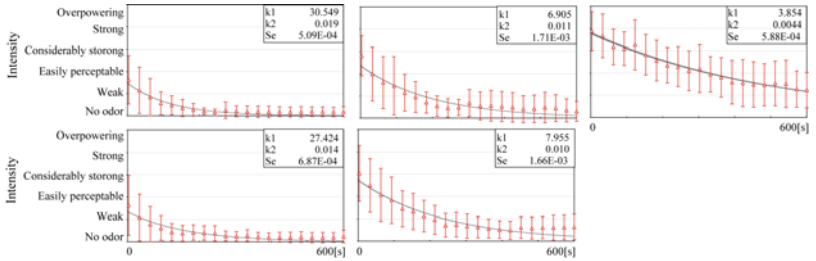


Fig.9 Comparison between change of calculated odor intensity based on Eq.4 and experimental values, which is mean value of five subjects except subject A

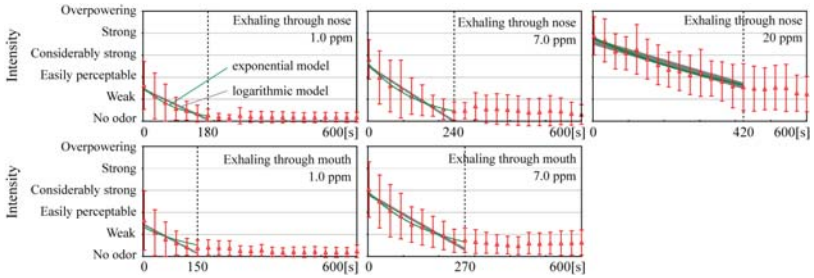


Fig.10 Result of changing time span for regression obtained by both of exponential model (Eq.4) and logarithmic model (Eq.5)

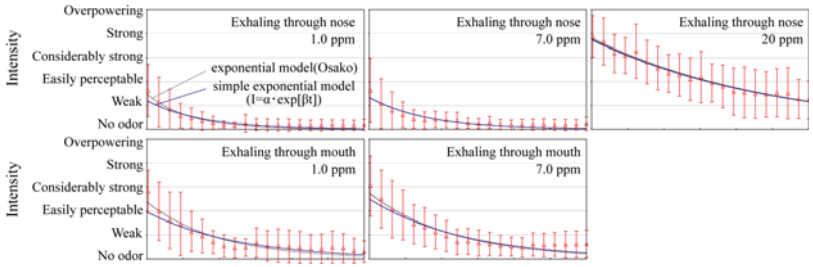


Fig.11 Comparison between Osako model and simple exponential model

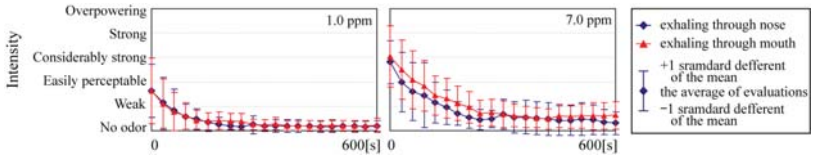


Fig.12 Comparison between two nose exhaling and mouth exhaling

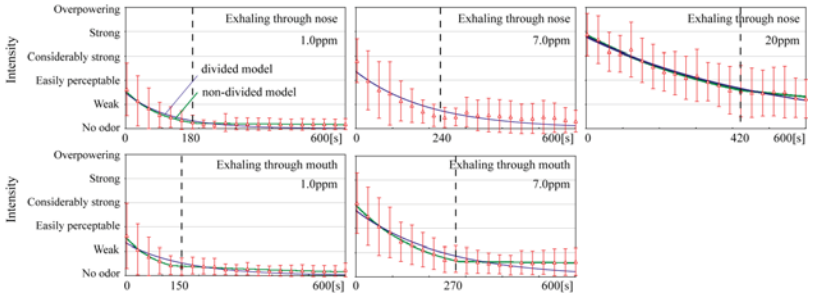


Fig.13 Two kinds of regression results obtained from data in divided time spans and overall time span using simple exponential equation (Eq.6)

Table 1 Odor concentration and the breathing methods

the method of the breath	Odor Concentration		
	1.0ppm	7.0ppm	20ppm
Exhaling through mouth	3 trials	2 trials	1 trial
Exhaling through nose	3 trials	2 trials	0 trial

Table 2 Residuals of regression lines

Concetration	Exhaling method	Exponential	Logarithmic
1.0ppm	nose	2.10E-05	6.45E-03
	mouth	1.26E-03	8.41E-03
7.0ppm	nose	2.11E-04	4.27E-02
	mouth	8.76E-05	2.41E-02
20ppm	nose	6.11E-04	1.07E-01

Experimental Investigation and Accuracy Study of CFD Analysis for Airflow around Cross-Ventilated Building

K. Asai [1], H. Kotani [2], T. Kobayashi [3], T. Yamanaka [2], K. Sagara [2] and Y. Momoi [2]

[1] Department of Architecture, The University of Tokyo, Japan
[2] Department of Architectural Engineering, Osaka University, Japan
[3] Department of Architecture and Urban Design, Ritsumeikan University, Japan

Abstract

In predicting flow rate of a building ventilated by wind, the orifice equation is usually used. This conventional method cannot work for the building provided with large openings. Therefore, the final goal of this study is to establish a new prediction method of the cross-ventilation rate, which is based on energy balance inside the stream tubes passing through/around a building. In determining stream tubes, it is beneficial to use CFD. In this study, the accuracy of CFD analysis is studied. Three turbulence models are used in the simulation; i.e. Standard k-ε Model Reynolds Stress Model, and Large Eddy Simulation. As a result, we can state the accuracy of Large Eddy Simulation is better than other CFD models.

Keywords: Cross-Ventilation, CFD analysis, Wind Tunnel Test

Introduction

In designing a building ventilated naturally by wind, the flow rate of a room under the wind must be known. The flow late of a cross- ventilated building is usually predicted by using so-called orifice equation based on Bernoulli's principle. In this method, the discharge coefficients obtained from the chamber method, and the wind pressure coefficients from a sealed building model are usually used. Ishihara (1969) showed this method could underestimate the flow rate of the building if the openings are large. Several studies on this problem have been conducted for a long time.

Murakami et al. (1991), Kato (2004) proposed "Power Balance Model". In this method, flow rate is predicted based on energy balance inside stream tube. They proposed a model of the stream tube passing through/around a building and divided it into the control volumes. The final goal of this work is to establish a new prediction method based on "Power Balance Model".

Kobayashi et al. (2008) have analyzed the stream tubes passing through/around the room using a rectangular model. To study more realistic condition, a multiple room building was used as a test object in this paper. In analyzing stream tubes, CFD seems to be effective. To analyze the stream tubes in the future work, the previous wind tunnel experiments are simulated by CFD analysis. By comparing measurement and CFD results using several turbulence models, the accuracy of the CFD simulation is to be studied. This paper focuses on the airflow around a cross-ventilated building, which includes such complicated flow field as separation and wake region.

CFD Analysis Method

Based on the previous wind tunnel test (Kotani et al. (2010)), CFD analyses were conducted. A test model shown in **Figure 1** was used for the analyses. The test model has a configuration of the building assumed to be composed of nine one-room residences of square array. The model is exposed to a free wind of 10 m/s. Five cases were simulated varying the parameters of the side length of the openings (L). The condition of the opening size was L=15, 30, 45, 60, and 90 mm. (For all cases, model has the side walls whose thickness is 6.0 mm, and 0.8 mm thick end walls were provided for the central residence to obtain sharped edge opening.) **Figure 2** gives all the cases, which are the same as those of wind tunnel test. In this study, two RANS models (Reynolds Averaged Navier-Stokes Equation) and LES (Large Eddy Simulation) were used. The summary of CFD analysis is shown in the following section.

Summary of CFD analysis

Standard k-ε Model (SKE) and Reynolds Stress Model (RSM) were used as RANS turbulence models. In the calculation of RSM, results of SKE were used for the initial condition. Assuming vertical and horizontal symmetry to reduce the calculation load, the computational domain was a quarter part of the working section of the wind tunnel. The mesh layout is shown in **Figure 3**. LES simulation using Smagorinsky-Lilly model was also conducted. The results of SKE were used for initial condition in LES simulation. The time step was set at 10^{-5} seconds. The calculated results during 0.8 seconds (8,000 time steps) from the beginning have been deserted regarding this term as the period of transition. As main calculation, unsteady flow was calculated for 15,000 time steps (1.5 seconds); i.e. 2.3 seconds in total. The calculation domain was equal to that of RANS model. Since it was unsteady analysis, however, the whole space of the wind tunnel was calculated. Summary of CFD analyses by RANS and LES are shown in **Table 1**.

Results and Discussion

Flow Field inside/around Model

From **Figure 4** to **Figure 6** shows the velocity distributions on the central cross section (Y=0) obtained from PIV measurement and CFD analysis. Here, only the cases of L=15, 45, and 90 mm are shown. As for LES, the time-average velocity was calculated based on the computational results for 1.5 seconds of main calculation.

In the result of PIV, the velocity vectors inside the model could not be estimated accurately. This is because some part of the laser sheet was reflected by the side wall of the model, which was made of acrylic board. For all the cases, the measurement shows a large

circulating flow around the separation region and a wake generated on the leeward side. This tendency has been well simulated in the results of LES simulation. As for the SKE, in the cases of smaller openings, the tendency is simulated generally better, but in larger opening case, is not simulated well. In addition, SKE tends to underestimate the size of the separation region. RSM could not predict the circulating flow in the separation region. The measurement shows that the airflow traveling in positive direction and negative direction collide with each other on the leeward side. RSM makes a prediction that the positions of collision is shifted more downstream, which means RSM has a tendency to overestimate the size of the wake region. In LES results, a circulating flow in the separation region is well simulated. The flow circulation on the leeward side of the model could also be well simulated. Although the negative flow on the leeward side was not simulated only in the case of L=90 mm, the results in LES seems to be much better than other CFD results using RANS model.

Velocity Profiles around Model

Figure 7 shows the profiles of velocity magnitude around the side wall of the model obtained from PIV measurement and CFD analysis. Since the profiles are almost the same, in all cases, only the case of L=45 mm is shown.

In the line of X=0, 30 mm, PIV measurement shows the moderate velocity gradient if compared with the results of CFD. In this study, Recursive Cross-correlation Method was used in PIV algorithm. Using this method might underestimate velocity gradient because information in the target interrogation window was influenced by the surrounding interrogation. The result of SKE shows poor agreement in all turbulence models and tends to underestimate the size of the wake region. On the other hand, RSM and LES show relatively good agreement with the experiment.

Velocity and Pressure along a Center Line

Figure 8 shows static pressure, X-component of velocity, and turbulent kinetic energy along a central line through the model obtained from the measurement by I-type hot wire anemometer and CFD analysis. The horizontal axis shows dimensionless X-coordinate divided by the model length. In the result of velocity, the vertical axis is normalized by a reference velocity of 10 m/s, which is the velocity far upstream of the model. In the results of X-component of velocity and turbulent kinetic energy, the LES results simulating the measurement by I-type hot wire anemometer (described as “LES-simulated I-type hot wire”) were shown together. This is because I-type hot wire measures resultant value of X-component and Y-component of velocity as an absolute value.

X-component of instantaneous velocity was assuming as follows;

$$v_{Hotwire} = \sqrt{u^2 + v^2} \qquad (1)$$

To estimate turbulent kinetic energy, each component of fluctuating velocity was assumed to be the same as;

$$k = \frac{1}{2}(\overline{u'^2} + \overline{v'^2} + \overline{w'^2}) = \frac{3}{2}\overline{u'^2} \qquad (2)$$

Assuming that I-type hot wire was measuring two component of velocity, turbulent kinetic energy was estimated as;

$$k = \frac{3}{2}(\frac{1}{2}\overline{v_{hotwire}^2}) = \frac{3}{4}\overline{v_{hotwire}^2} \qquad (3)$$

Static Pressure

The vertical axis indicates the dimensionless static pressure. Measured static pressure is divided by the reference dynamic pressure measured simultaneously at the point of pitot tube in order to ignore the effect of temperature fluctuation. Then, the dimensionless pressure was normalized by divided by the dimensionless total pressure at the most windward point.

For all cases, all turbulence models simulate the static pressure on the windward side of the model accurately. SKE has a tendency to overestimate static pressure particularly inside the model and on the leeward side. RSM overestimates the static pressure on the leeward side compared with the result of the measurement. LES result agrees with the measurement better than the results of other two models.

X-component of Velocity

X-component of velocity on the windward side was well simulated by RANS and LES. On the leeward side, the results of CFD analysis were quite different from the experimental results. This is because I-type hot wire cannot evaluate the negative velocity. The result of SKE disagrees with experimental result in the model. As for RSM, the larger openings are, the more out of agreement from the experimental result is. It is believed that RSM tends to overestimate the size of the wake region. The LES-simulated I-type hot wire predicts that the position of velocity weakening exists more windward in the case of L=90 mm, but it could be said that velocity field was well simulated. Therefore, it would appear that the result of LES simulation is relatively precise.

Turbulent Kinetic Energy

In the experimental result, turbulent kinetic energy was produced on the leeward side of the model. On the other hand, SKE shows the maximum turbulent kinetic energy at the windward opening. It is generally known SKE overestimates turbulence kinetic energy at the

collision point, the region of great velocity gradient (see Murakami et al. (1990)). The result of the LES-simulated I-type hot wire was much similar in the tendency to the experimental result, though underestimation of the turbulence kinetic energy is seen in the case of larger openings. Actually, it is expected turbulent kinetic energy is higher on the leeward side.

Conclusions

In this paper, the previous wind tunnel test using PIV measurement was simulated by CFD analysis. By comparing measurement and CFD results using several turbulence models, the accuracy of the CFD simulation was studied. The conclusions are listed as follows:

(1) Standard k-ε Model (SKE) could not simulate the velocity and pressure field well.

(2) In the results of Reynolds Stress Model (RSM), velocity profile around the model was well simulated. However, RSM has a tendency to overestimate the size of the wake region.

(3) LES showed the best agreement with the experimental results.

In the future work, the stream tube passing through/around the building should be analyzed based on LES simulation shown as highly accurate model.

Acknowledgments

This research was partially supported by the Ministry of Education, Science, Sports and Culture, Grant-in-Aid for JSPS Fellows (Representative T. Kobayashi (20-912)), Japan Society for the Promotion of Science, 2009.

References

1. Ishihara M., “Building Ventilation Design”, Asakura shoten, 1969. (In Japanese)

2. Murakami S., Kato S., Akabayashi S., Mizutani K., and Kim Y. D., “ Wind Tunnel Test on Velocity Pressure Field of Cross-Ventilation with Open Windows”, ASHRAE Transactions, Vol.97, Part 1, pp.525-538, 1991.

3. Kato S., “Flow Network Model based on Power Balance as Applied to Cross-Ventilation”, *The International Journal of Ventilation*, Vol.2, No.4, pp.395-408, 2004.

4. Kobayashi T., Sagara K., Yamanaka T., Kotani H., Takeda S., and Nishimoto N., “Power Transportation Analysis inside Stream Tube of Cross-Ventilated Building”, *Proceedings of the 29th AIVC Conference*, Vol.1, pp.249-254, Kyoto, Japan, 2008.

5. Kotani H., Kobayashi T., Asai K., Tanaka Y., and Shiozaki Y., “Velocity Measurement Inside and Outside a Cross-Ventilated Building by Means of PIV”, *Submitted to the 31st AIVC Conference*, Seoul, Korea, 2010

6. Murakami S., Mochida A., and Hayashi Y., “Examining the k-ε Model by Means of a Wind Tunnel Test and Large-Eddy Simulation of the Turbulence Structure around a Cube”, *Journal of Wind Engineering and Industrial Aerodynamics*, Vol.35, pp.87-100, 1990.

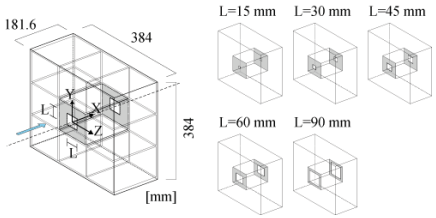


Figure 1 Test Model **Figure 2** Analysis cases

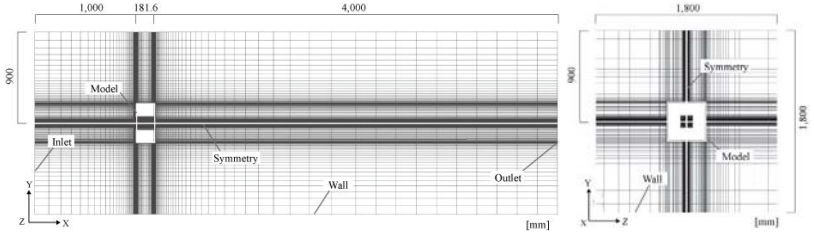


Figure 3 Mesh Layout

Table 1 Summary of CFD Analysis

RANS (Reynolds Averaged Navier-Stokes Equation)		
CFD Code		Fluent 6.3
Turbulence Model		Standard k-ε Model (SKE) Reynolds Stress Model (RSM)
Algolithm		Implicit Method (SIMPLE)
Discretization Scheme for Advection Term		QUICK
Boundary Condition	Inlet	Volocity : 10m/s Turbulent Intensity : 1% Turbulent Length Scale : 126mm
	Outlet	Gauge Pressure : 0 [Pa]
	Walls	Walls : Generalized Log Low Symmetry : free slip
Total Number of Cells		L=15mm : 1,612,128 L=30mm : 1,612,648 L=45mm : 1,685,808 L=60mm : 1,685,808 L=90mm : 1,619,688

LES (Large Eddy Simulation)		
CFD Code		Fluent 6.3
Turbulence Model		Large Eddy Simulation (Smagorinsky-Lilly Model)
Algolithm		Implicit Method (SIMPLE)
Discretization Scheme for Advection Term		Central Difference
Time Step		0.0001s (10kHz)
Transition Term		8,000 time step (0.8sec.)
Boundary Condition	Inlet	Velocity : 10m/s (Constant)
	Outlet	Gauge Pressure : 0 [Pa]
	Walls	Warner & Wengle linear power law
Smagorinsky Coefficient		0.1
Total Number of Cells		L=15mm : 1,893,060 L=30mm : 2,050,240 L=45mm : 2,024,400 L=60mm : 2,026,160 L=90mm : 2,028,240

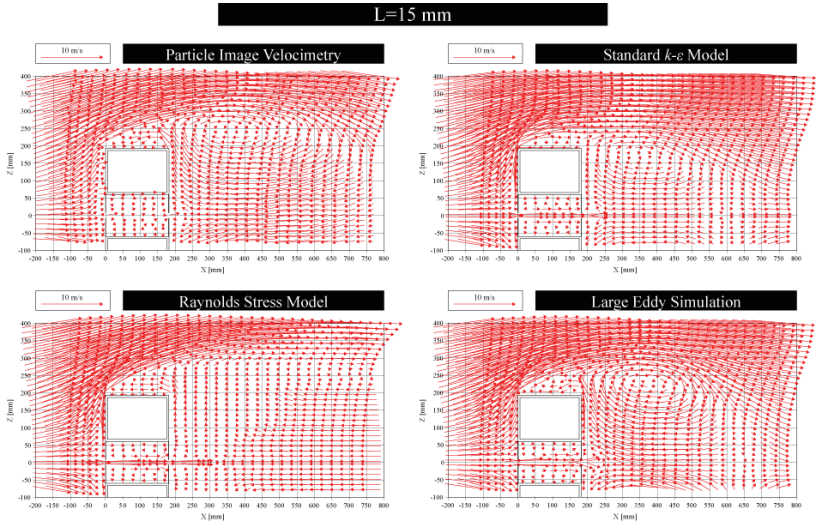


Figure 4 Velocity Vector for L=15mm

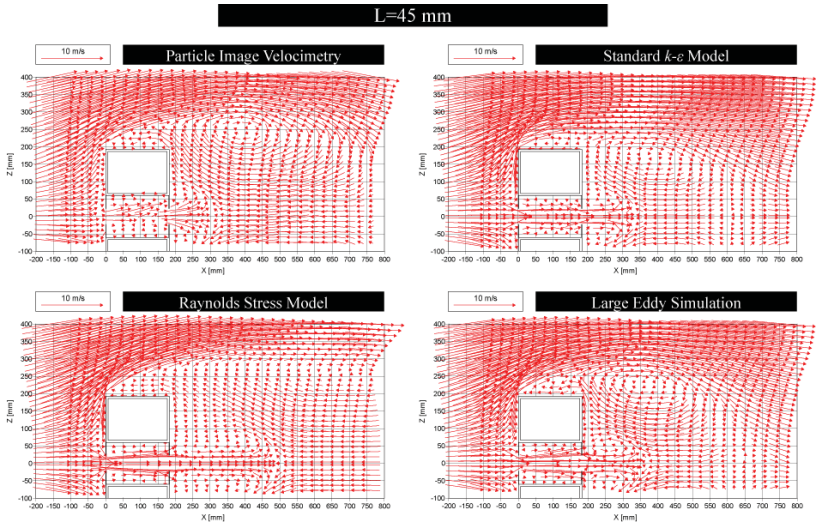


Figure 5 Velocity Vector for L=45mm

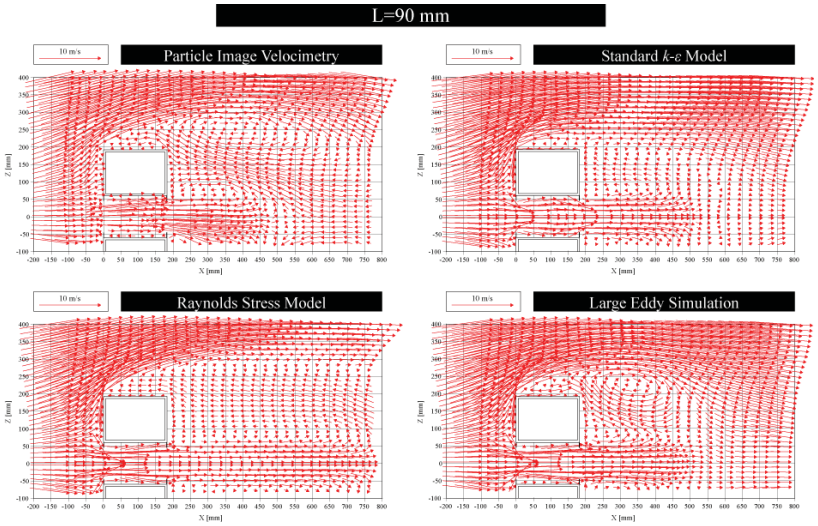


Figure 6 Velocity Vector for L=90mm

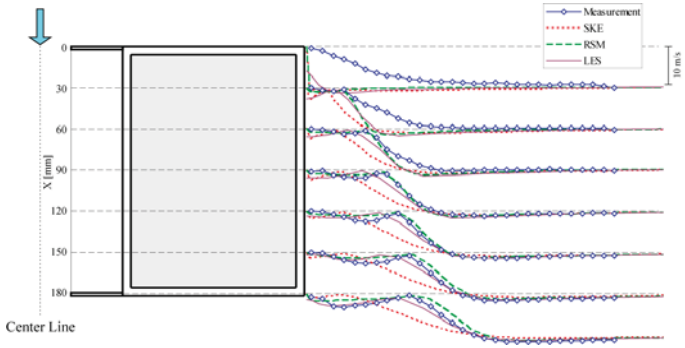


Figure 7 Profile of Velocity Magnitude

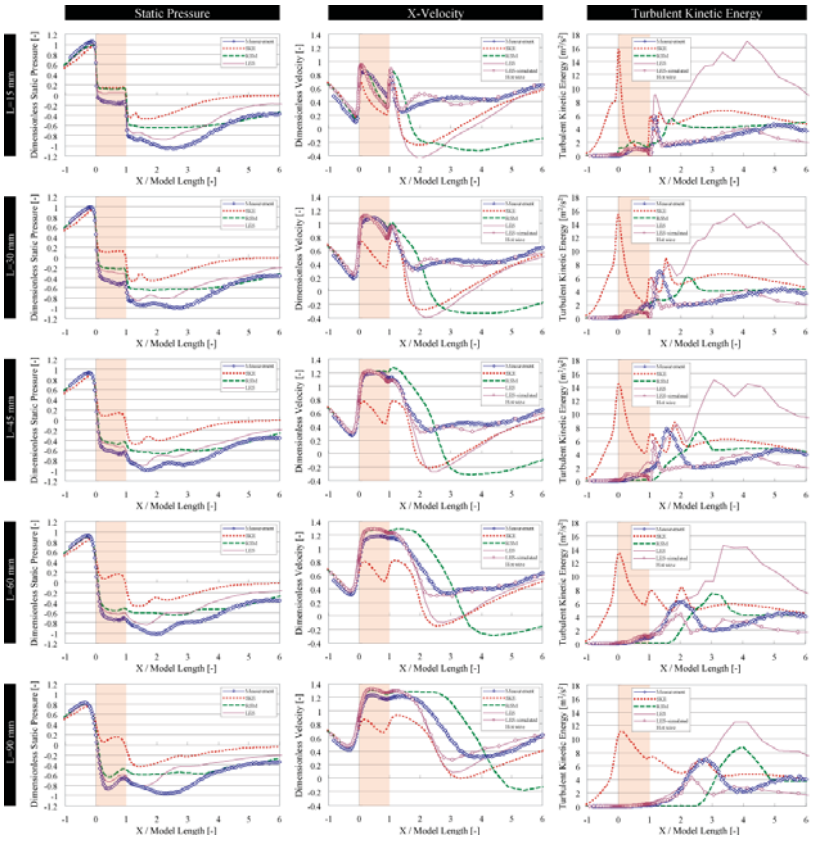


Figure 8 Static Pressure, X-component of Velocity, and Turbulent Kinetic Energy along a Central Line through the Model

Thermal Environment Generated by Occupant's Opening Control of Window at Naturally Ventilated Building

K. Kami[1], H. Kotani[1], T. Yamanaka[1], Y. Momoi[1], K. Sagara[1], T. Sakaguchi[2], and K. Tanaka[2]

[1] Division of Global Architecture, Graduate School of Engineering, Osaka University, Osaka, Japan , 565-0871
[2] Takenaka Corporation

Abstract

A field survey in a natural ventilated school building was carried out. The purpose of this study is to figure out the occupant's evaluation of thermal comfort as the result of opening control, which seems to be affected by the outdoor and indoor air condition.

Occupant's active use of natural ventilation system instead of air conditioner is a key to the performance for energy saving of building. The analysis of the data shows that windows were more actively controlled as occupant's knowledge about natural ventilation system increased. The result of this study suggests that understanding about the system leads more active control of window and less use of air conditioner, which play a grate role in saving energy.

Keywords: Natural ventilation, Occupant's utilization, and Thermal comfort

Introduction

Recently the buildings with natural ventilation system are more and more increasing for utilization of natural energy and saving energy. In such buildings, it is expected that comfortable thermal environment will be obtained by using common means of control, e.g. operable windows. Raja et al [1] has shown that occupants who have grater access to control devices report feel less discomfort than who have less access.

This paper shows the natural ventilation of the school building using staircases as natural ventilation chimneys. Longitudinal surveys in the natural ventilated school building in the west part of Japan were carried out. The building consists of four floors and central corridor, the total floor space is 4098m^2. In this building, controls such as windows are adjusted by occupants. The natural ventilation system uses wind driving force of negative pressure on the rooftop of wind chimneys and buoyancy force caused by the heat generation by occupants in lecture rooms. Komatsu et al [2] calculated ventilation rate brought by natural ventilation through chimneys using wind tunnel test.

The goal of this study is to provide the guidelines for planning and running of naturally ventilated buildings. In this study, the potential of the chimney and the occupant's use of windows had been focused on. Since this building is a school building, the surveys were conducted on exhibit, expecting the educational effect on occupants to raise their awareness. During 2008-2009, field surveys were conducted in spring and fall, when the natural ventilation system may have the biggest effect. Tsumura et al [3] calculated the wind pressure coefficient using wind tunnel test, Fujimoto et al [4] measured air change late in the building, and Wakamatsu et al [5] reported the occupants' use of windows. This paper presents the

result of the analysis on the occupancy evaluation of thermal environment as well as indoor and outdoor temperature.

Method

Figure 1 shows the natural ventilation system of the building. Each room has four kinds of natural ventilation controls, (upper-windows and lower-windows opened to outer side, doors and transoms opened to corridor). Outdoor air flows into rooms through windows first, and then flows to corridor through transoms. Finally, indoor air flows out through rooftop of the chimney. The floor plan of second and third floor is shown in Figure 2.

In 2008, one survey period was set in each of spring and fall. In 2009, three survey periods were set in each of those seasons. Before the survey in fall 2009, an educational activity using posters (see Figure 3) about the natural ventilation system of the building had been taken. The poster has the elucidations about the natural ventilation system, recommended degrees of temperature and simplified thermometer. The posters were posted on the doors of each room and the notice boards. The aim of this activity was to encourage the occupants to use controls. This paper shows the result of the survey in 2009.

As for the understanding of occupants, one questionnaire (hereinafter called understanding questionnaire) was conducted each survey period. And for the thermal evaluation of occupants, one questionnaire (hereinafter called thermal questionnaire) was conducted each day. Table 1 shows the survey periods and the number of the respondents of questionnaires in 2009.

In 2009, visual evaluations of using controls (opening checks) were conducted every two hours during 9 am to 5 pm, every day in second and third period of each survey season. “Opening-percentage” was identified for upper-windows or transoms on the basis of percentage of opening area of them. And utilization of natural ventilation system is examined using opening-percentages of student’s rooms and teacher’s rooms. Student’s rooms are the north side rooms mainly used by students, and teacher’s rooms are the south side rooms used by teachers. The definition of Opening-percentages used in this paper is shown in Figure 4.

In Figure 2, the rooms in which indoor temperatures were measured are shown. Outdoor temperatures were measured in the north and south side on the first floor of the building and the average of the measurements is used as outdoor temperature in this paper. Temperatures were averaged per one hour for the value of every two hour (the time of opening checks), and averaged per eight hours for the value of each day.

Results and Discussions

The consciousness of inhabitants

Figure 5 shows the result of understanding questionnaire to present the occupants' level of understanding about natural ventilation system. The result in 2008 is also shown in the figure as the reference. However, the result in the spring and fall in 2009 is compared here because the students are changed in every spring. Students' understanding level was improved between the spring and the fall, 2009. This may be partly because of educational effect, which is arisen from exhibited surveys and educational activity. Given that teachers had been in the building for years and already received explanations about natural ventilation, it's not surprising that the teachers' understanding level is high in spring as well as in fall.

Relation between outdoor air temperature and Opening-percentage

Figure 6 shows the relation between outdoor air temperature and opening-percentage in 2009 of upper-window and transom. Outdoor air temperatures here are the values averaged per one hour. Opening-percentages here are the values of "Opening-percentage for outdoor air temperature" (see Figure 4).

Opening-percentages had increased from spring to fall, especially about upper-window in student's rooms and transom in teacher's rooms. Their changes from spring to fall in student's rooms may be caused by the improvement of understanding. As for teacher's rooms, educational activity seems to have motivated teachers to open transoms. Upper-windows in teacher's rooms may have been frequently opened in spring as well as in fall.

Indoor air temperature as the results of opening control

To figure out the effect of natural ventilation, the data is analyzed based on the result in each room. Figure 7 shows the relation between outdoor or indoor temperature and "Opening-percentage of each room" (see Figure 4) in 2009. Both of air temperatures here are the values averaged per one hour, and indoor temperatures are the values in each room. The height in these graphs shows the total number of the rooms for each control and for every time of opening checks. The number of the rooms where the windows or transoms were closed is not shown in the graphs. These graphs show the result of teacher's rooms in fall, where controls were actively used and it expected that larger effect could be obtained.

Indoor air temperatures appear to be kept at 22 deg C or higher. Focusing on relation of the temperature and the number of the rooms where opening-percentage of transom is 100%, the number of the rooms is highest when outdoor air temperature was 21 deg C, although the highest values are seen when indoor air temperature was 27 deg C. It follows that the low outdoor temperature has small effect in many of the rooms where transoms are largely opened. The point is that inhabitants may use transoms for ventilation when it is too cold to largely open the windows opened to outdoor, and they prevent indoor environment from getting too cold.

Occupant's evaluation of indoor environment

To make analysis on occupant's thermal sensation, Figure 8 shows the relation between indoor temperatures and the occupant's evaluation using the result of thermal questionnaire. Indoor temperatures here are the values averaged per eight hours from 9 am to 5 pm. The result is averaged over every responses collected in rooms where indoor air was measured as same temperature. For the comparison of two seasons, it must be noticed that the way of asking in questionnaires is different from each season. In spring, occupants were asked about the thermal sensation under the situation of using natural ventilation, although they were asked about before and after opening the windows in fall.

About the evaluations in fall, it is clearly shown in the graph that opening windows is related with thermal sensation. Despite the indoor air had been measured as almost same temperatures, evaluations in fall take the cooler value than in spring when using the natural ventilation; however the difference in way of asking might be involved with the difference in the result. As one of possible reason, the ventilation rate may have increased because of the increasing use of controls, and occupants could feel wind velocity. As the other possible reason, occupants could imagine rooms as ventilated by understanding the natural ventilation system and that impression let them to feel cooler. However, as the advantages of opening control, occupants may expect not only to feel cooler but also to enjoy fresh air.

Conclusions

The results presented show that occupants controlled the opening area of devices (windows and transoms here) so as to achieve indoor thermal comfort. The use of them was more active in fall than in spring. It is therefore suggested that understanding how to use or how affect the natural ventilation system is strongly related to the occupant's utilization and energy saving performance of the building. Showing survey to occupants and the educational activity have profound effects on occupant's utilization.

As for occupant's evaluation of indoor environment, it is shown that opening the windows is strongly related with thermal sensation. Not only lowering the temperature but also the airflow and fresh air may be gotten as the effects of opening windows. Those effects might let occupant to achieve thermal comfort and sense of satisfaction.

Although the different climate in each season could influence the result, the educational effect could achieve. The point is that educational activity in the school building encouraged occupants to use natural ventilation, and then might augment the occupant's comfort. Use of controls enhances natural ventilation, and energy saving performance of the building may also be improved. Taking into account that occupants partly replace by others every year in school building, continuing activity is necessary for the efficient use of natural ventilation system and saving energy.

References

1. Raja, I. A., Nicol, J. F., McCattney, K.J., and Humphreys, M. A., “Thermal comfort: use of controls in naturally ventilated buildings,” *Energy and Buildings*, Vol.33, 2001, pp.235-244

2. Komatsu, Y., Sagara, K., Yamanaka, T., Kotani, H., Lim, E., and Watanabe, H., “Study on airflow around Building Roof for Design of Natural Ventilation by Chimney –Part2 Wind Velocity Distribution above Building Roof-,” *Advanced building ventilation and environmental technology for addressing climate change issues*, Volume1, 2008, pp.243-248.

3. Tsumura, Y., Kotani, H., Sagara, K., Yamanaka, T., Momoi, Y., Fujimoto, T., Wakamatsu, N., Sakaguchi, T., and Tanaka, K., “Natural Ventilation Performance of School Building with Staircase Chimney Part 5. Study on Ventilation Routs by Measurement Results and Tunnel Test” *Summaries of technical papers of Annual Meeting Architectural Institute of Japan. D, Environmental engineering, Volume 2009: pp.763-764. (in Japanese)*

4. Fujimoto, T., Kotani, T., Sagara, K., Yamanaka, T., Momoi, Y., Tsumura, Y., Wakamatsu, N., Sakaguchi, T., and Tanaka, K., “Natural Ventilation Performance of School Building with Staircase Chimney Part 4. Summary of Measurement Survey and Relation between Outdoor Wind Velocity and Ventilation Rate through Chimney” Measurement Results of Wind Pressure Coefficients by Wind Tunnel Test” *Summaries of technical papers of Annual Meeting Architectural Institute of Japan. D, Environmental engineering, Volume 2009: pp. 761-762. (in Japanese)*

5. Wakamatsu, N., Kotani, H., Sagara, K., Yamanaka, T., Momoi, Y., Fujimoto, T., Tsumura, Y., Sakaguchi, T., and Tanaka, K., “Natural Ventilation Performance of School Building with Staircase Chimney Part 6. Thermal environment and Window Operation of Occupants” *Summaries of technical papers of Annual Meeting Architectural Institute of Japan. D, Environmental engineering, Volume 2009: pp.765-766. (in Japanese)*

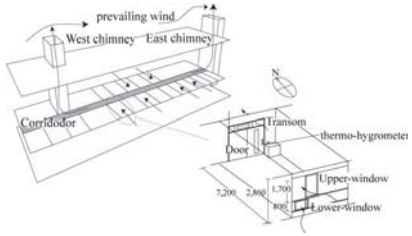


Fig. 1 Natural ventilation system

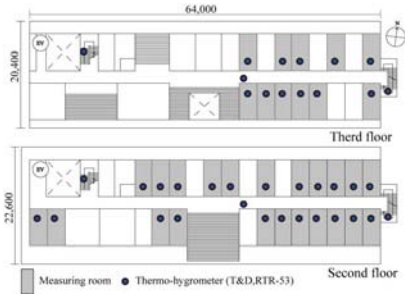


Fig. 2 Floor plan of second and third floor



Fig. 3 Poster for educational activity

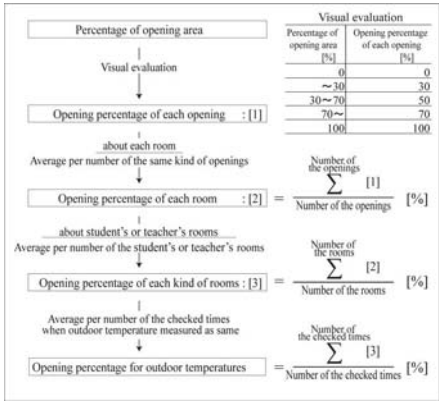


Fig. 4 Definition of Opening-percentages

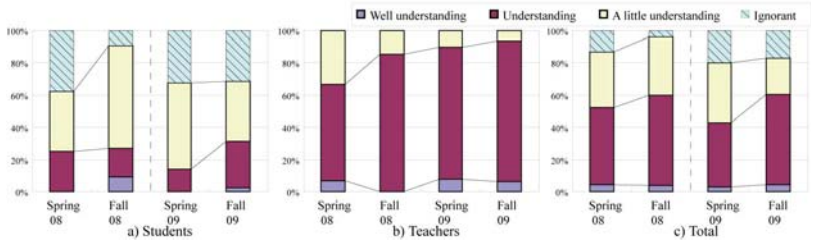


Fig. 5 Result of understanding questionnaire

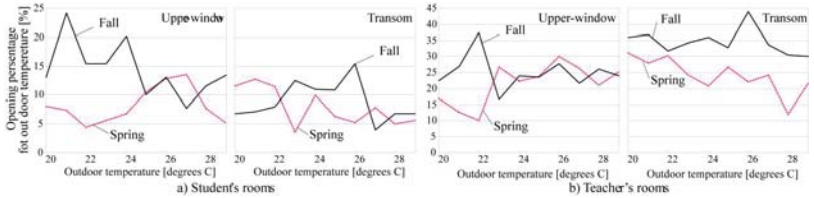


Fig. 6 Relation between outdoor temperature and Opening-percentage for outdoor temperature

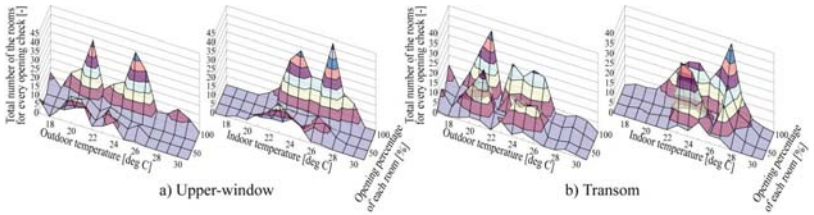


Fig. 7 Relation between air temperatures and Opening-percentage of each room

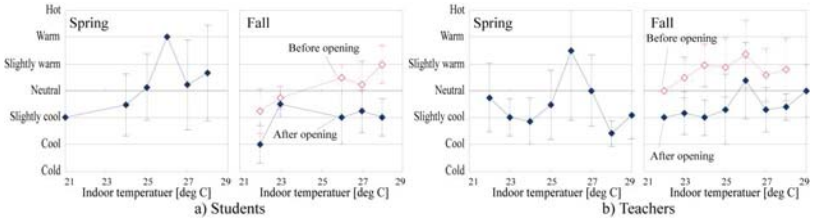


Fig. 8 Relation between indoor air temperatures and the occupant's evaluation

Table 1 Survey periods and the number of the respondents

Spring in 2009		First period 5/18～5/22					Second period 6/1～6/5					Therd period 6/29～7/3				
Respondent days		5/18	5/19	5/20	5/21	5/22	6/1	6/2	6/3	6/4	6/5	6/29	6/30	7/1	7/2	7/3
The number of respondents	Thermal questionnaire	35(14)	28(12)	26(11)	29(15)	27(11)	43(17)	29(12)	29(12)	30(14)	29(11)	31(14)	33(16)	20(9)	23(11)	23(12)
	Understanding questionnaire					33(11)					37(14)					33(13)

Fall in 2009		First period 9/16～9/25					Second period 9/28～10/2					Therd period 10/19～10/23				
Respondent days		9/16	9/17	9/18	9/19	9/20	9/28	9/29	9/30	10/1	10/2	10/19	10/20	10/21	10/22	10/23
The number of respondents	Thermal questionnaire	52(12)	21(12)	20(12)	21(11)	20(13)	17(7)	19(7)	23(10)	22(10)	21(9)	17(10)	15(8)	18(10)	18(10)	16(8)
	Understanding questionnaire					30(13)					22(10)					18(10)

The number of the teachers involveed in respondents is shown in parentheses

Study of cross- ventilated indoor air flow characteristics by frequency analysis

Tomoyuki ENDO[1], Takashi KURABUCHI[2] and Toshihiro NONAKA[3]

[1] Kanto Gakuin University, College of Engineering, Department of Architecture, Mutsuurahigashi 1-50-1, Kanazawa-ku, Yokohama-city, Kanagawa, Japan 236-8501
[2] Tokyo Science University, Tokyo, Japan
[3] Tostem Corporation, Tokyo, Japan

Abstract

In Japan where is located at the hot humid climate region, houses have been built considered hot summer life from ancient times. It is said that comfortable and cool feelings by cross-ventilation were more important. However, the characteristics of cross-ventilated air flow are unclear, and that it has yet to be revealed how they affect the psychological and physiological factors that influence comfortable feeling. So, in this study, time-series data of cross-ventilated indoor air flow velocity were measured by field measurement at the actual detached house in Japan. Various turbulence statics of cross-ventilated indoor air flow were investigated by with frequency analysis (FFT). As a result, they were observed that wind velocity, eddy size and power spectrum configuration are different in and out of the cross-ventilated air flow pathway.

Keywords: Cross ventilation, Air flow characteristic, Turbulence static, Wind velocity, Turbulent velocity, Power spectrum, Characteristic time, Eddy size, Frequency analysis

Introduction

In Japan where is located at the hot humid climate region, houses have been built considered hot summer life from ancient times. It is said that comfortable and cool feelings by cross-ventilation were more important. Recently, the momentum of incorporating outdoor air into the house by cross-ventilation in good time of ambient conditions as summer night from the view point of energy saving. However, the characteristics of cross-ventilated air flow are unclear, and that it has yet to be revealed how they affect the psychological and physiological factors that influence comfortable feeling. So, in this study, time-series data of cross-ventilated indoor air flow velocity were measured by field measurement at the actual detached house in Japan and investigations about cross-ventilated indoor air flow characteristics were carried out taking temporal and spatial fluctuation of observed data by three-dimensional ultrasonic anemometer into consideration. In particular, various turbulence statics[1] of cross-ventilated indoor air flow were investigated by analysis of observed air flow data using frequency analysis[2] (FFT).

Measurement Method

Fig. 1 shows the overview of detached house to be measured. The house is suburban two-storied building in Noda city, Chiba prefecture, Japan. The measurement was performed in July, 2009. Fig. 2 shows the surrounding buildings of the house. South side and east side of surveyed house are bordered by road. There are plan and section of that house in Fig. 3. The room where measurement was carried out is southeast one. For the measurement of

indoor air flow velocity, nine ultrasonic anemometers were set up on a plane in Fig. 3. The ultrasonic anemometer probes were adjusted at 1100mm height above the floor and the time interval for data collecting is 0.1 second. Also, outdoor wind velocity and wind direction were measured on the roof of detached house. Indoor air flow in about 20 seconds when the wind velocity and wind direction on the roof were stable became the target of the frequency analysis (FFT). Fig. 4 and Fig. 5 show the time-series data of outdoor wind velocity and wind direction investigated.

Analysis Method

Turbulent flow field consist of many different size air cloud are called eddy. Eddies possess properties differing from surrounding air and behave in a group. It is thought that various physical quantities such as wind velocity are similar to each other in same eddy. Many eddies move with respect to one another randomly on the mean flow and the fluctuation of air flow are generated. Therefore it is thought that fluctuation of air flow depend to a large part on the size and the mean velocity of eddy. There are turbulent velocity, eddy size and characteristic time and so on as these turbulence statics of air flow. Here are analysis methods in this study. The power spectrum displayed with respect to each frequency of indoor air flow is derived from measured wind velocity data by fast Fourier transformation. Then, the autocorrelation function is computed by the inverse Fourier transformation. And that the characteristic time is calculated from the autocorrelation function result. The outlines of turbulence statics definition for in this study are showed as described below.

Synthesized wind velocity: This wind velocity is synthesized in consideration of three-dimensionality from unidirectional wind velocity component of X, Y and Z directions as described Eq.1.

$$V = \sqrt{V_X{}^2 + V_Y{}^2 + V_Z{}^2} \qquad \text{(Eq. 1)}$$

V : Synthesized wind velocity (m/s), V_X : Wind velocity of X direction (m/s), V_Y : Wind velocity of Y direction (m/s), V_Z : Wind velocity of Z direction (m/s)

The wind velocity in this study is indicates synthesized wind velocity.

Turbulent velocity: It is thought that measured wind velocity V is broken down to time averaged wind velocity $\overline{V}$ and fluctuating wind velocity v as described Eq.2.

$$V = \overline{V} + v \qquad \text{(Eq. 2)}$$

$\overline{V}$: Time averaged wind velocity (m/s), v : Fluctuating wind velocity (m/s)

The standard deviation of fluctuating wind velocity v is called turbulent velocity.

Characteristic time: Characteristic time is the time scale individualize turbulent flow field. The time scale represents the averaged time when they are in the same eddy or the time when eddy pass a certain one point. Therefore, characteristic time is considered a time which retain correlation that autocorrelation function is 1 such as Fig.6 and is described as Eq.3.

$$T = \int_0^{\tau_0} R(\tau)\, d\tau \qquad \text{(Eq. 3)}$$

T : Characteristic time (s), τ : Elapsed time (s), $R(\tau)$: autocorrelation function, τ_0 : Elapsed time that autocorrelation function become 0.

Eddy size: Eddy size is described as Eq.4 and it is expressed as a product of mean wind velocity and characteristic time. This indicates length scale of turbulent flow fields.

$$A = \overline{V} \times T \qquad \text{(Eq. 4)}$$

A : Eddy size (m)

Wave number: Wave number is an indicator of eddy number per unit length. If the eddy is on the mean flow, it is thought that the frequency is influenced by the mean wind velocity. Wave number k is obtained by the removal of the effect of mean wind velocity (Eq.5).

$$K = \frac{2 \times \pi \times n}{\overline{V}} \qquad \text{(Eq. 5)}$$

K : Wave number (rad/m), π : Circular constant, n : Frequency (Hz)

Results and Discussion

Fig.7 and Fig.8 show the time-series data of wind velocity of indoor air flow in analysis object time. Each measurement point is divided into that in the cross-ventilated air flow pathway or that out of pathway groups from synthesize wind velocity result. The tendency that change in wind speed is different between the both is clearly observed.

Fig.9 shows the power spectrum displayed with respect to each frequency. There is the fluctuation form as general characteristics. There is the about hundredfold difference of energy between points A and B lie near opening window. There is the about tenfold difference of energy between points D and E lie near the center of the room. However, there is the little difference of energy between points G and I lie near the outlet of indoor air flow.

Fig.10 shows the cumulative frequency distribution of the power spectrum displayed with respect to each frequency. In the low-frequency region, the tendency that the power spectrum energy out of cross-ventilated air flow pathway is lower than that on the pathway is observed. However, remarkable difference was not observed except point A.

Fig.11 shows the cumulative frequency distribution of the power spectrum displayed with respect to each wave number. In the result displayed with respect to each wave number, there is remarkable difference between air flow on pathway and that out of pathway as compared with the result displayed with respect to each frequency. Eddies those size are up to 10

[rad/m] make up about from 30 to 60 percent of the whole at the point A and point D. However, they make up about 95 percent of the whole at the point B and point E. There is remarkable difference in the depth direction from opening window in the room. Eddies those size are up to 1 [rad/m] make up about 60 percent of the whole at the point B lie in front of the window. However, they make up about 40 percent of the whole at the point E lie near the center of the room and about 25 percent of the whole at the point I lie near the outlet of indoor air flow. From above results, the tendency that large size eddies are dissipated as heat converting to small size eddies as going to back of the room can be observed. Eddies those size are over 100 [rad/m] are observed and mean wind velocity is small in the region out of the cross-ventilated air flow pathway. From above results, it is found that very small size eddies remain in that place.

Table 1 shows the results of turbulence statics such as turbulent velocity, characteristic time and eddy size. Eddy size in the cross-ventilated air flow pathway are about from 0.2 [m] to 0.8 [m], but they are about from 0.02 [m] to 0.09 [m] out of the cross-ventilated air flow pathway. There are remarkable differences between in and out of cross-ventilated air flow pathway.

Conclusions

In this study, cross-ventilated air flows were measured by three-dimensional ultrasonic anemometer and investigation about indoor air flow characteristics were carried out by frequency analysis (FFT). Some turbulence statics such as eddy size were adopted as evaluation index. Cross-ventilated air flow pathway was assumed by measured wind velocity results and the differences of turbulence statics between air flow in the pathway and that out of the pathway. Investigations of the turbulence statics change along the cross-ventilated air flow pathway were carried out. As a result, there were differences in characteristic time and power spectrum in addition to wind velocity between the air flow in cross-ventilated air flow pathway and that out of the pathway. There is remarkable difference in the power spectrum displayed with respect to each wave number and the tendency that large size eddies of indoor air flow are dissipated converting to small size eddies as going to outlet of air flow from opening window. For the future, the measurement and the investigation of air flow characteristics which cross the opening window will be occurred.

References

1. Nobuyuki Kobayashi, “Basic study about the air flow characteristics of closed space”, Doctoral thesis, The University of Tokyo, 1974.

2. Yorihiko Osaki, “Approach of spectral analysis for earthquake motion, New edition”, Kajima Institute Publishing, 1994.



Fig. 1 Overview of detached house to be measured

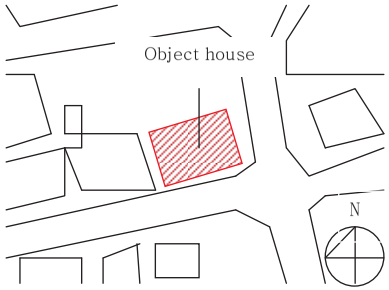


Fig. 2 Surrounding buildings of the house

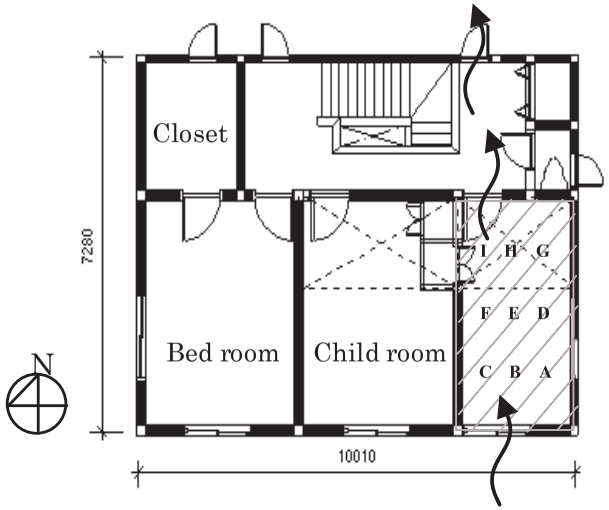


Fig. 3 Plane of the house

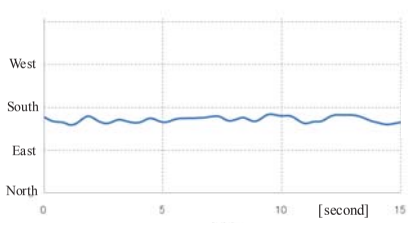


Fig. 4 Outdoor wind direction

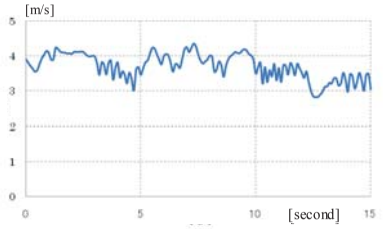


Fig. 5 Outdoor wind velocity

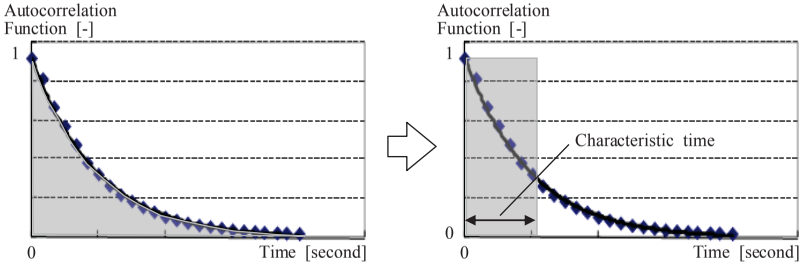


Fig. 6 Basic concept of characteristic time

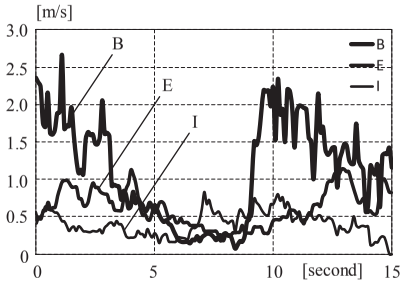


Fig. 7 Synthesized wind velocity in the pathway

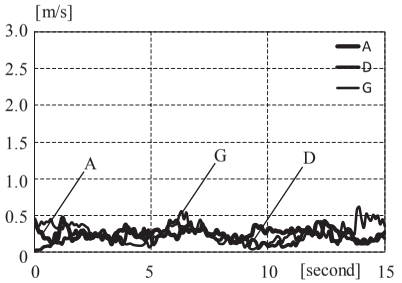


Fig. 8 Synthesized wind velocity out of the pathway

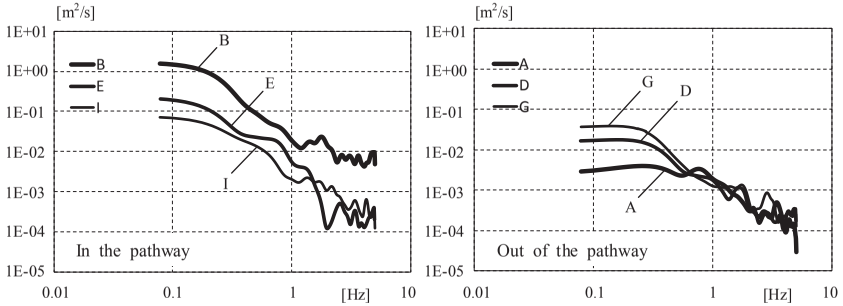


Fig. 9 Power spectrum displayed with respect to each frequency

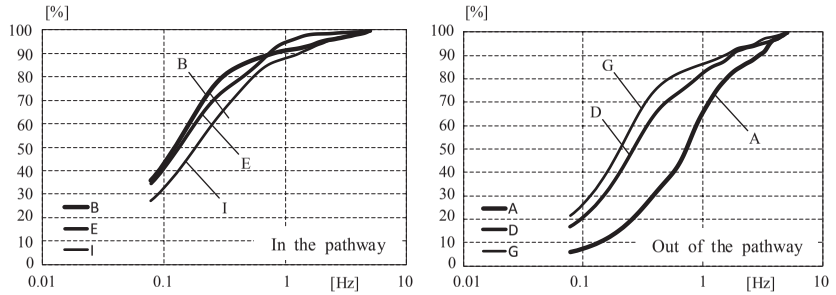


Fig. 10 Cumulative frequency distribution of the power spectrum displayed with respect to each frequency

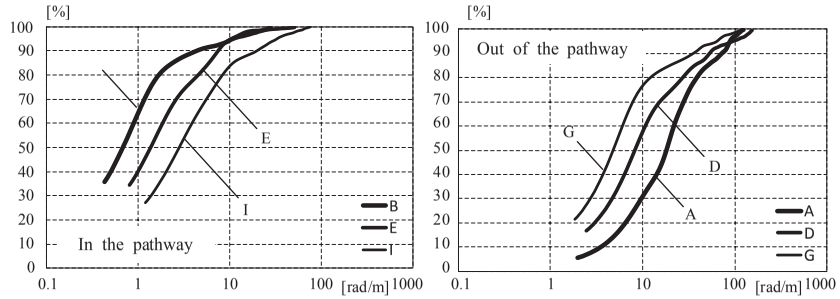


Fig. 11 Cumulative frequency distrbution of the power spectrum displayed with respect to each wave number

Table 1 Turbulence statics results

In the pathway	B	E	I
Turbulent velocity [m/s]	0.68	0.25	0.17
Mean wind velocity [m/s]	1.13	0.61	0.41
Characteristic time [s]	1.26	1.30	0.93
Eddy size [m]	0.85	0.32	0.15
Out of the pathway	A	D	G
Turbulent velocity [m/s]	0.07	0.10	0.13
Mean wind velocity [m/s]	0.25	0.20	0.26
Characteristic time [s]	0.24	0.58	0.72
Eddy size [m]	0.02	0.06	0.09

The effect of ventilation rates and window areas on building energy use

Hyoin Kim[1], Geun Young Yun[1]

[1] Kyung Hee University, Department of Architectural Engineering, Yongin, Korea 446-701

Abstract

Natural ventilation is an effective method for energy conservation while potentially improving indoor air quality. Furthermore, a window has a significant impact on energy consumption. The purpose of this study is to reduce building energy use by changing ventilation rates and window areas. We analyzed the energy consumption and CO_2 emissions according to ventilation rates and window areas through using a computer program, HEED 3.0. The reference model had two windows of 1.2m×1.5m, and assumed there was no ventilation except for the minimum ventilation rate of 0.35 ACH. In order to determine the combined effects of changes in ventilation rates and window areas, three ventilation rates; 1.0 ACH, 5.0 ACH, 20.0 ACH, and three window areas were studied. The findings were as follows: annual energy consumption was reduced by 10.6%, CO_2 emissions by 16.7% compared with the reference model by changing ventilation rates and window areas.

Keywords: natural ventilation, ventilation rates, window areas, building energy consumption

Introduction

Building energy conservation has been of increasing importance. Controlling of ventilation rates and window areas influences considerably on building energy use. The aim of this study is to contribute positively to building energy performance. Therefore, we will evaluate building energy use and CO_2 emissions according to ventilation rates and window areas using a computer program, HEED 3.0

Methods

The reference model was a room of 5m×7m×2.6m, located in Kangnung, Korea. There were two windows of 1.2m×1.5m which were oriented southwest and northeast. Table.1 presents the properties of the window.

Table 1 The properties of the window

	Composition	U-value
Window	▪ Clear double pane with Low-E coating in plastic frame ▪ Cavity : 12mm	2.1 W/m^{2}K

This study investigated two parameters to reveal relationships between energy consumption, and ventilation rates and window areas. HEED 3.0 was used to estimate building energy use. Table.2 details parameters in this study.

Table 2 The details of parameters

Parameters	Levels	Remark
Ventilation rates	1 ACH	Minimum natural ventilation
	5 ACH	Good natural ventilation
	20 ACH	High natural ventilation
Window areas	7.2 m^2	1.2m x 3.0m, 1.2m x 3.0m
	5.4 m^2	1.2m x 3.0m, 1.2m x 1.5m
	3.6 m^2	1.2m x 3.0m

Results and Discussion

Figure 1 shows the variation in energy consumption according to changes in ventilation rates. The heating and lighting energy consumption were not changed significantly. However, the cooling energy was reduced by decrease of ventilation rates. The high ventilation rates of 20 ACH reduced cooling energy use and resulting CO_2 emissions by 39%, while heating energy was increased by 7% compared to the energy consumption for the reference model.

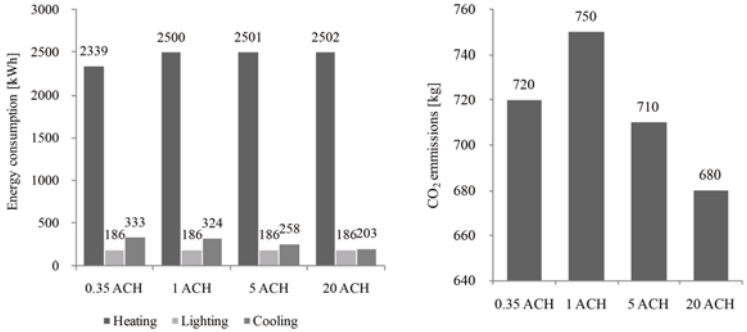


Fig. 1 The variation in energy consumption according to changes in ventilation rates

Figure 2 shows the variation in energy consumption according to changes in window areas. When a window area was reduced to 3.6m^2 from 7.2m^2, the annual energy consumption and CO_2 emissions were reduced by 13%.

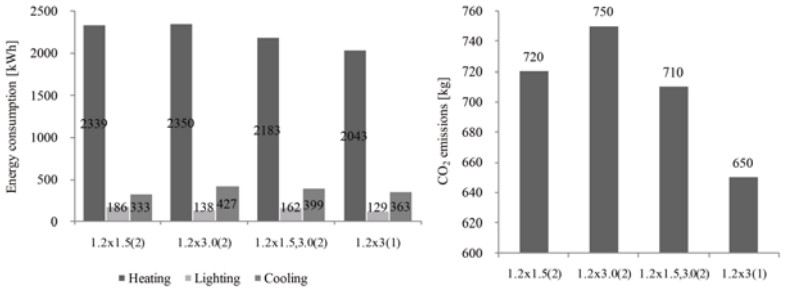


Fig. 2 The variation in energy consumption and CO_2 emissions according to changes in window areas

The combination of 20 ACH and a window of 3.6m^2 was the most energy efficient alternative. Reducing a glazing area and increasing a ventilation rate of a base case model is an effective method to reduce the total energy consumption. As shown in figure 3, both increasing a ventilation rate to 20 ACH and changing a window area of 3.6m^2 resulted in reducing the annual energy consumption by 10.6% and CO_2 emissions by 16.7% in comparison with the reference model.

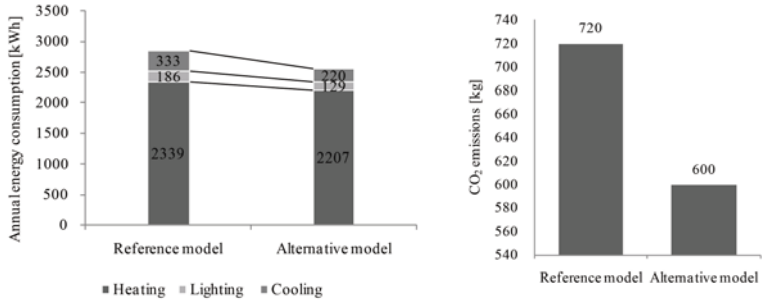


Fig. 3 The annual energy consumption and CO2 emissions of alternative model

Conclusions

The higher ventilation rates reduced the amount of electricity required for cooling. The heating and cooling energy consumption were reduced with a decrease in window areas. It is important to consider a combined effect of reducing window areas on ventilation rates, lighting energy requirements, and cooling energy consumption in the design process of a non-domestic building.

Acknowledgments

This research was supported by Basic Science Research Program through the National Research Foundation of Korea(NRF) funded by the Ministry of Education, Science and Technology (2010-0007722).

References

1. Seppanen, O. A., et al., "Association of Ventilation Rates and CO_2 Concentrations with Health and Other Responses in Commercial and Institutional Buildings," Vol. 9, No. 4, *Indoor Air*, 1999, pp.226~252.

2. Yoo, H.C., et al., "The optimal window system of office building considering energy efficiency," Vol. 25, No. 4, *Journal of the Korean Solar Energy Society*, 2005, pp.53~60.

Performances of new innovative domestic ventilation systems in combination with low temperature floor heating

Erwin Roijen[1], Peter Op 't Veld[1], Ad van der Aa[1]

[1]Cauberg-Huygen Consulting Engineers, the Netherlands

Corresponding email: p.optveld@chri.nl

SUMMARY

In extended laboratory measurements, the combination of new innovative domestic ventilation systems with low temperature heating is investigated, using the advanced EnoTemp measurement equipment. These measurements took place in the framework of a large Dutch demonstration project for these innovative domestic ventilation systems. The main conclusion of the laboratory measurements is that self-regulating façade grilles form a good combination with low temperature heating in terms of thermal comfort. The air flow is regulated in such a way that moderate air velocities in the living zone are created with substantial lower air velocities in comparison with conventional grilles.

INTRODUCTION

Legislation and building regulations always have been the main driving force to stimulate innovations in domestic ventilation systems and especially for the development of advanced energy-efficient ventilation systems. The most recent developments of the European ventilation industry concern new systems and new principles have a certain meaning and impact for the EPBD[1]. In the long term sustainability will also feature in the housing sector, as well as for new as existing housing. Also indoor air quality, thermal comfort throughout the year and the acoustic environment play more and more an important role. In current practice conventional natural ventilation grilles in facades can cause complaints concerning thermal comfort, especially in combination with modern low temperature heating systems like floor heating. This results in reluctance by designers and real estate developers to apply either sustainable heating or certain types of ventilation techniques. This is a missed opportunity for sustainable development in general. However, in the most recent developments of domestic ventilation products all quality aspects are included. Next to it there are different alternatives for energy efficient ventilation, not only with regard to manufacturers but also with regard to ventilation principles. Both in terms of advanced natural ventilation as mechanical ventilation, there are solutions available and there are applications in all possible situations, both for new and existing housing. A number of these solutions have been developed within the European RESHYVENT project[2] (2002 -2004).
In practice, it has been noted that the combination of a decentralised, unheated air supply in combination with a floor heating system can lead to comfort problems with users. Draft with traditional air supply by grids in the facade in combination with radiator heating is a more or less accepted phenomenon. Older buildings in which this combination occurs generally have a large and continuous heat supply, which, to an extent, compensates for the draft that is created, by the convection and heat radiation of the radiators. However, in well insulated houses with a low heat demand and low system temperatures there is insufficient mixing of the incoming cold air with heated air. Particularly during strong winds on the facade large volumes of (cold) air enters the living zone, which can cause draft problems if there are no compensating measures.

Self regulating grids
Despite the extensive experience with natural air supply and floor heating, the level of discomfort has not been closely studied and quantified. This is why the level of thermal comfort with decentralised air supply was studied in a laboratory setting under controlled conditions. In a broader context, the research question was whether a good level of comfort can be achieved with the combination of low temperature heating systems with advanced (natural) ventilation systems, more particularly with self-regulating facade grids
The purpose of a mechanical self-regulating air supply is to provide a constant volume of air supply, regardless of the strength and direction of the wind (wind pressure on the facade). If there is no wind, the self-regulating facade grid (SR grid) is fully open and the nominal air flow taken in by the vent is delivered to the building. If the wind pressure increases, a flap in the grid will close mechanically which limits the increase of incoming air volume. This reduces unwanted, large (and in winter cold) air volumes. The required air volume can also be regulated electronically. By using servo steering in the grid and a control device in the vent the volume of air inflow and outflow can be adjusted. This device can control on:

- Time: ventilation will take place during specific time intervals based on a time schedule to be entered.
- Presence: ventilation takes place during specific time intervals based on the detected seizure.
- CO_2: ventilation takes place based on the level of CO_2, as a measure of indoor air quality.

Based on flow measurement in the grid, a servo-controlled flap can be positioned so that the exact required air volume is supplied. Using this technology a true horizontal pressure flow diagram can be realised. This method also reduces unwanted, large (and in winter cold) air volumes.

Low Temperature Heating and thermal comfort
A floor heating system was used as the main heating in the study. Rooms with floor heating as the main heating do not have convection. Floor heating does provide a significant radiation compensation for cold facade surfaces. Inflow of outside air via the facade, limited heating capacity per square metre of floor surface, low mixing in the air space and the determining factor of the air inflow, increase the chances of local discomfort. Comfort problems that may arise with (unheated) air supply via the facade in combination with floor heating as the main heating are:

- Draft, caused by high air supply volumes via the grid. Conventional configurations with an HT radiator under the window mix the convection air with the cold outside air, thus heating it.
- Down draft, convection of relatively cold air along glass surfaces in the facade, in particular with low supply speeds.
- Cold radiation, caused by relatively cold glass surfaces in the facade (radiation).

These three aspects are difficult to distinguish in practice and can occur simultaneously. It can therefore be difficult to determine the main cause of the comfort complaints, and it is easy to draw incorrect conclusions with regard to the role of the heating and ventilation system. Down draft and cold radiation will occur in particular with facades with a lot of glass; natural air supply via facades with a high glass ratio is thus extra critical. The air permeability of the facade and facade elements is also important. Comfort/discomfort is determined using the Fanger equations and the dimensionless parameters PMV and PPD[3].

METHODS

The assessment of the thermal comfort with various types of natural air supply was done using the experimental setup in the climate room of Cauberg-Huygen RI bv, the Netherlands. A facade was simulated with an indoor and outdoor climate in the climate room, figure 1.



Figure 1: The climate room with test facade and measuring equipment.

The Dutch standard NEN1087:2001[4] provides a method for the assessment of thermal comfort. It includes the following:

- the air supply variation should not be greater than 10% of the nominal value;
- the air supply temperature should be 20 (± 2) K lower than the average air supply of the room;
- a three-dimensional measuring grid according to NEN1087:2001.

The outdoor air is simulated by cooling the room on the other side of the facade to 0°C. This simulates a winter situation where cool air flows into the heated room via the grids. This is done at an overpressure of 10 Pa (+/- 5 m/s wind speed) and 25 Pa (+/- 7.5 m/s wind speed). A wind pressure of 25 Pa was chosen to remain within the normal functional range (1..25 Pa) of SR grids. Temperature and air speed were measured using EnoTemp ClimaCubes. These measure in the x, y and z direction. What is special is that the temperature and air speed was measured using sound. The ClimaCubes emit short sound pulses between the sensors. This way, the temperature and air speed can be measured accurately and without contact based on the receipt of the sound in the sensors.

The ClimaCubes are fitted to a movable and height-adjustable measuring beam. A grid of 3 x 16 measuring positions was laid out on the floor. Measurements were taken at 12 different heights for each measuring point. Thus, there were a total of 576 measurements in a 3D grid with a mesh opening of 20 to 25 cm. The results were graphically represented in 2D and 3D graphs using appropriate software. The graphs represent temperature, air speed and air flow.

RESULTS

Table 1 contains a numerical overview of the results. The results are based on the total 3D measuring grid, i.e. including the measuring points outside the living area towards the facade, which in fact are outside of the assessment criteria of NEN1087. Table 2 shows the results for the measuring points inside the living area. Figures 2, 3 and 4 are graphic representations of the flow pattern. Next, the flow patterns have been converted into the Draft values and these are graphically represented in Figures 5, 6 and 7.

Table 1: Numerical overview of thermal comfort – total grid

Comfort criteria	Facade grid type	Standard	Passive mechanical self-regulating		Active / electronic self-regulating	
	Wind pressure on facade	10 Pa	10 Pa	25 Pa	10 Pa	25 Pa
Air speed	Average	0.24 m/s	0.08 m/s	0.10 m/s	0.05 m/s	0.06 m/s
	Maximum	1.77 m/s	0.56 m/s	0.69 m/s	0.38 m/s	0.31 m/s
Air temperature	Minimum	8.8°C.	17.5°C.	15.2°C.	19.9°C.	22.1°C.
	Average	16.7°C.	21.2°C.	21.3°C.	22.1°C.	23.9°C.
	Maximum	19.4°C.	22.9°C.	23.2°C.	23.2°C.	25.3°C.
PMV	Minimum	-5.5	-1.0	-2.0	-1.3	-1.0
	Average	-1.3	-0.1	-1.0	0.1	0.4
	Maximum	-0.6	0.7	0.3	0.4	0.7
Draft value	Average	45 %	13 %	17 %	6 %	6 %
	Maximum	100 %	87 %	100 %	82 %	76 %

Table 2: Numerical overview of thermal comfort – living area

Comfort criteria	Facade grid type	Standard	Passive / mechanical self-regulating		Active / electronic self-regulating	
	Wind pressure on facade	10 Pa	10 Pa	25 Pa	10 Pa	25 Pa
Air speed	Under 0.20 m/s	32 %	76 %	81 %	87 %	88 %
	0.20 to 0.24 m/s	12 %	7 %	2 %	6 %	5 %
	Over 0.24 m/s	56 %	17 %	17 %	7 %	7 %
PMV	Minimum	-3.4	-1.0	-1.3	-1.3	-0.5
	Average	-1.5	-0.1	-0.2	0.0	0.3
	Maximum	-0.7	0.7	0.3	0.4	0.7
Draft value	Average	62 %	11 %	13 %	7 %	8 %
	Maximum	100 %	64 %	75 %	82 %	76 %

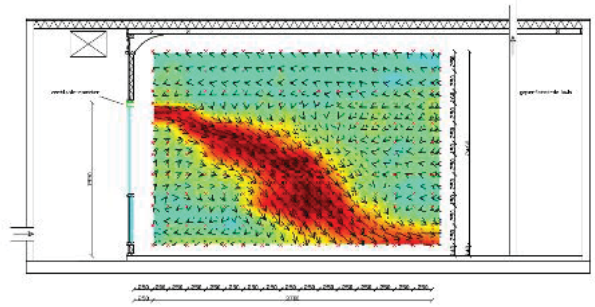


Figure 2: Flow pattern unregulated grid, pressure difference 10 Pa.

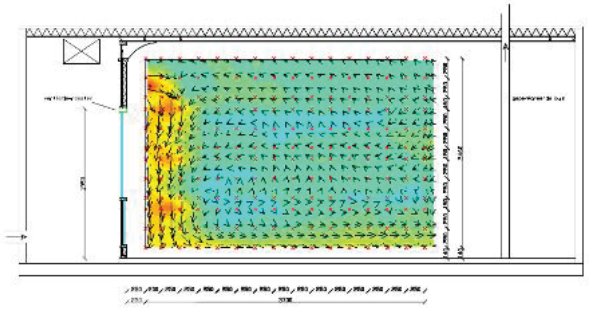


Figure 3: Flow pattern passive regulation, pressure difference 25 Pa.

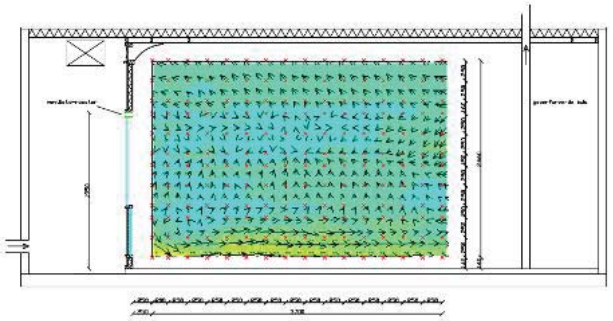


Figure 4: Flow pattern active regulation, pressure difference 25 Pa.

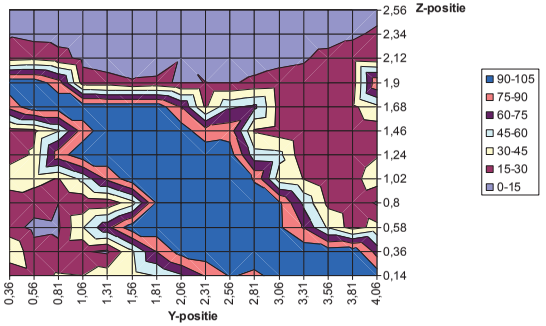


Figure 5: Draft value standard grid, wind pressure 10 Pa.

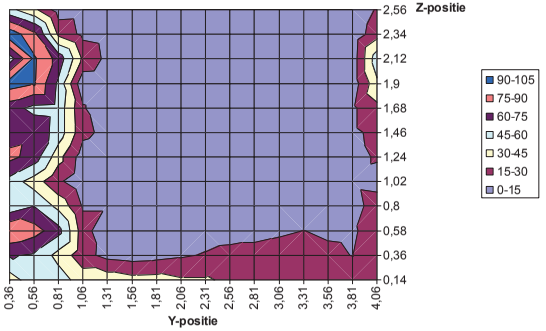


Figure 6: Draft value mechanical self-regulating grid, wind pressure 25 Pa.

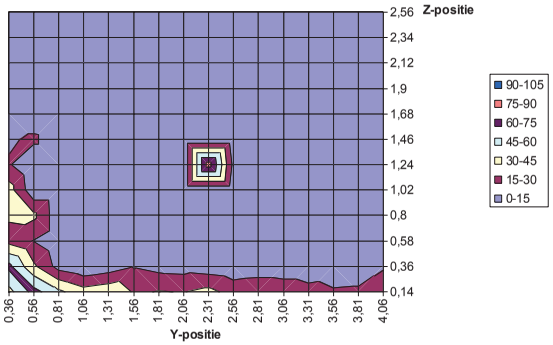


Figure7: Draft value electronic self-regulating grid, wind pressure 25 Pa.

From the figures and the table it can be concluded that with a standard facade grid air flows occur with high air speeds in the room as a result of the created pressure difference, causing local discomfort with, in particular, a high likelihood of draft complaints. With a passive (mechanical) self-regulating facade grid the average air speed is limited to 0.10 m/s, even

with a large pressure difference. With a pressure difference of 10 Pa the climate is almost thermal neutral (PMV ≈ 0). The chance of draft complaints is limited to less than 20%, even with a high pressure difference.
With an active (electronic) self-regulating facade grid the average air speed is limited (even with a high pressure difference) to 0.06 m/s, which is very low. With a pressure difference of 10 Pa the climate is almost thermal neutral (PMV ≈ 0). The chance of draft complaints is limited to less than 10%, even with a high pressure difference. With the self-regulating facade grid there is a limited disturbance of the indoor temperature, while with a standard ventilation grid there is so much inflow of cold air that space cools down noticeably. With all grid types air speeds of 0.20 m/s or higher are created at the outflow opening, but these are mostly outside of the living space.
Air velocity is particularly important for thermal comfort. As regards air speed, the electronic self-regulating grid has the best results and the number of measuring points with a high air speed is clearly lower than with the unregulated grid. The high air velocities occur mainly at a low height above the floor.

DISCUSSION

Using the innovative measuring equipment and the specially fitted climate room is possible to determine the air flows and the thermal comfort in a room with high accuracy. The collected data provide an insight into the effect of decentralised supply installations on thermal comfort. In line with practical experience, the climate room study shows a substantial chance of draft complaints with a standard facade grid. This is mainly due to the high air volumes at higher wind pressure on the facade. The self-regulating grids of Alusta that were studied limit the air volume to such an extent that comfort is average to good, also without radiator heating. In general we can conclude that self-regulating facade grids provide a clear advantage with regard to comfort. The difference between mechanical and electronic facade grids is particularly noticeable near the facade (outside of the living area). For this reason the difference between mechanical and electronic facade grids will mainly show in the form of energy savings. Dutch ISSO publication 92[5] provides general guidelines for the application of facade grids in houses.
This study shows that self-regulating facade grids also provide a good comfort with a wind pressure of 25 Pa. In practice, higher wind pressures can occur, in particular with high rise buildings and near the coast. The question is whether a self-regulating facade grid can control the air inflow sufficiently under such conditions and to what extent other air leakages in the facade will play a role. The innovative, acoustic measuring set allowed us to register even small air leakages in the regulating unit of the self-regulating facade grids. These measurements showed that the facade grids close to such an extent with high wind pressure on the facade that the outside air enters via minimal openings in the facade elements.

Possibilities for the future
The results of this study will allow improvements to be made at the product and project levels. Producers of ventilation and heating systems, but also project developers and designers, can, when in doubt, have the comfort level of a particular combination of facade design, heating and ventilation system measured before realisation of the project. This allows them to choose an alternative, if necessary. This will provide more security and will prevent unexpected results.
The main point of interest is that the pressure-air volume properties of an SR grid are really flat. There is now a requirement for self-regulating facade grids to have flat pressure-air flow properties up to a pressure difference of 25 Pa, while thermal comfort must also be guaranteed with higher pressure differences. According to the manufacturer, electronic self-regulating grids offer the advantage at high wind speeds (100 Pa) that they can (actively) close completely; sufficient air inflow will remain through infiltration in the facade. Quality assurance and possible certification of the self-regulating properties are thus crucial for preventing complaints in the application of facade grids in critical situations. This study focused on a standard facade with parapet; further investigation with facades made entirely out of glass can provide new insights into the effects of cold radiation and ice-traps on the comfort level with all forms of decentralised air supply. The role of air permeability of the facade needs to be established in more detail. Natural air inflow must therefore always be seen in relation to the quality of the facade and the heating supply system.
The ventilation grids investigated here have a different inflow opening in the SR version than the standard grids, namely pointed upwards in relation to the standard horizontal air stream. The effect of this on the air streams due to improved induction and mixing has not been studied closely, but appears important in preventing draft complaints. Finally, the metadata can possibly be used as input for computer simulations (CFD computations) for validating the simulations and improving them where necessary.

ACKNOWLEDGEMENT

This research took place in the framework of the Dutch EOS DEMO programme. The funding by the Ministry of Economic Affairs is gratefully acknowledged.

REFERENCES

1. EPBD, Directive 2002/91/EC of the European Parliament and of the Council of 16 December 2002 on the energy performance of buildings.
2. EC FP5 RESHYVENT Cluster Project on Demand Controlled Hybrid Ventilation in Residential Buildings with Specific Emphasis on the Integration of Renewables, report No: RESHYVENT-WP11-D11.5
3. Fanger, P O. 1970. Thermal Comfort. Danish Technical Press.
4. NEN 1087: 2001, Ventilation in dwellings and residential buildings, Requirements and determination methods, NNI, the Netherlands
5. ISSO Publication 92, Ventilation systems with decentral supply and central exhaust in dwellings and residential buildings, ISSO, the Netherlands
6. Roijen, E., 2009, Climate camber research thermal comfort decentral air supply and low temperature heating, Cauberg-Huygen report 20051291-42

Prediction of Plume above Residential Cooking Range by means of CFD analysis

Yuji TSUMURA[1], Hisashi KOTANI[1], Toshio YAMANAKA[1],

Kazunobu SAGARA [1] and Yoshihisa MOMOI [1]

[1] Dept. of Architectural Engineering, Osaka University, Suita 565-0871 Osaka, Japan

Abstract

Recently, Island kitchen is installed in many houses in Japan. In the island kitchen, the cooking range is placed on the island unit, and the center hood is located above the cooking f low in the room. In such a kitchen environment, there is a possibility that cross winds or other disturbing flow may reach the cooking zone. For this reason, pollutant fumes from the cooking range may be diffused to residential zone. CFD analysis is an effective measure for comprehending such a diffusion of the thermal plume. In comprehending the diffusion of the thermal plume above the cooking range by CFD analysis, a variety of plume models are prop osed as boundary conditions. In this study, "Pot-side wall jet model" is proposed. The velocity and temperature around the pot side are measured, and the profiles are regressed t o formula of two-dimensional jet flow. This means that the thermal plume with high temperature from the gas cooking range is modeled. This paper aims to demonstrate the usefulness of Pot-side wall jet model in analyzing the thermal plume in the large laborato ry where a gas cooking range with a pot is only installed. In this paper, the results of CFD analysis are compared with the experimental results.

Keywords: CFD analysis, Residential Cooking Range, Thermal Plume

Introduction

In order to predict the diffusion of the thermal plume by CFD analysis, the accuracy of the simulated thermal plume is very important. In predicting the plume, a variety of plume models are used as boundary conditions [1] [2] [3]. In this study, "Pot-side wall jet model" is proposed, where the velocity and temperature profiles are approximated by experimental formula of two-dimensional jet flow. The main purpose of this paper is to demonstrate the accuracy and the usefulness of Pot-side wall jet model in analyzing the island kitchen environment. In this paper, three modeling methods are applied for predicting the thermal plume above the range in CFD analysis. One is "Pot-side wall jet model" (hereinafter called Pot-side model), another is "Velocity fixed plume model" (Velocity model) and the other is "Heat generation model" (Heating model).

In Pot-side model, velocity and temperature around the pot are fixed. This means that the thermal plume with high temperature from the cooking gas range is modeled. On the other hand, in Velocity model, the heat generation rates are given on the side of pot, and the velocity at the height of 100mm from the top of pot is fixed. In Heating model, thermal plume is modeled simply by the heat generation rates given on the side of pot.

CFD analysis is designed to compare the experimental results. The velocity and temperature profiles from a gas cooking range are measured at the height of 100mm, 200mm, 300mm, 500mm, and 700mm above the top of the pot .The details can be found in the previous study [4]. The analyzed results by three modeling methods are compared with the measured velocity and temperature of the thermal plume above the pot.

2. Method

2.1 CFD Analysis

CFD analysis is designed to be compared with the experimental results. In order to figure out the characteristics of thermal plume, the measurements were conducted in a large laboratory where no range hood was equipped [4]. Figure 1 shows the calculated domain for CFD analysis. The calculated domain is based on the shapes and dimensions of the laboratory. Table 1 shows summary of CFD analysis. Boundary conditions for the laboratory are shown in table 2. The magnitude of the velocity of supply air was well-argued to avoid both the backflow at the ceiling and the disturbance beside the range. Boundary conditions around pot in each modeling method are described in the following chapters.

CFD analysis and experiments are conducted on the pot of 200mm diameter in boiling situation with the gas range, whose heat inputs are 4.2kW and 1.13kW.

2.2 Pot-side Wall Jet Model

Velocity and temperature around pot were measured by Laser Doppler Velocimetry (LDV) and thermocouple [4]. The measured velocity and temperature are approximated by a regression formula of two-dimensional wall jet, which is proposed by Tamura and Kotani. In Equation (1), vertical component of velocity and temperature rise are presented as a function of the horizontal distance from wall.

$$\frac{\phi}{\phi_m} = 1.479\eta^{1/7}\left[1 - erf\left(0.6776\eta\right)\right] \quad \cdots \text{(Eq.1)}$$

$$\left[\begin{array}{ll} \phi = u\ (\text{Velocity [m/s]}), & \eta = x / b_{1/2} \\ \quad \text{or } t\ (\text{Temperature rise [℃]}\ \ ※1[\text{mm}] \leqq x) & b = \text{Characteristic length} \\ \text{error function: } erf(x) = \dfrac{2}{\sqrt{\pi}} \int_0^x e^{-t^2} dt & \end{array}\right]$$

The form of the Equation is proposed by Verhoff cited in the textbook of mechanical engineering [5]. In addition, Φ_m is the maximum value of the velocity and temperature. Half maximum of full width $b_{1/2}$ is calculated by least squares. The conceptual diagram of two-dimensional wall jet is shown in Figure 2. Parameters used in modeling are shown in Table 3.

In this model, pot-side area where velocity and temperature were measured is defined to be out of the analysis domain (This pot-side area is termed “Pot-side Zone”). The upper surface of Pot-side Zone is defined as an inlet condition and the lower surface is defined as an outlet condition (Figure 3). In this model, the heat transfer by radiation is not considered (Table 4). Because its heat generation is considered to be determined by the velocity and temperature at the water surface of the pot and the upper surface of Pot-side Zone. Boundary conditions around pot are shown in Table 5.

2.3 Velocity Fixed Plume Model

This model follows the modeling method proposed by Kondo et al. [2]. Figure 4 and Table 6 show the detail and boundary conditions around the pot, respectively. The heat generation rates are given on the side of pot. And axial velocity at the height of 100mm from the top of pot is fixed. The fixed value is decided by approximating the measured results by a regression

formula. Table 7 shows the coefficient of the formula. In addition, radiation is taken into account in this model. Therefore, the temperature at the surface of pot is adjusted to be around 100℃ by means of fixing the heat transfer coefficient at the side of pot. The heat transfer coefficients in the case of heat input of 4.2kW and 1.13kW are determined as 10000 W/(m^2K) and 1000 W/(m^2K), respectively. In this model, heat transfer by radiation is considered.

2.4 Heat Generation Model

Figure 5 and Table 8 show the detail and boundary conditions around the pot in Heat generation model. It is well known that using this kind of modeling methods may underestimate the diffusion of the plume and the width of plume smaller. This model follows the modeling method applied in the previous study [6]. In this model, heat transfer by radiation is not considered.

3. Results and Discussion

Profiles of vertical component of velocity and temperature rise at the each level are shown in Figure 6 and Figure 7.

3.1 Experimental Results

It should be noticed that the maximum temperature rise becomes lower as the measurement height increases. In contradiction to temperature, the maximum velocity becomes higher as the height increases from 100mm to 700mm.

3.2 CFD Analysis in Case of 4.2kW

In Heating model, the maximum magnitudes of temperature and velocity are higher than experimental results. And the width of plume is smaller than experimental results. In Velocity model, it is observed that difference in velocity between CFD and experiment becomes larger as the level becomes higher. This difference seems to come from the disagreement of temperature rise. Temperature above pot is higher than experimental result. Temperature around pot has a great influence in the development of thermal plume. In Pot-side model, both velocity and temperature are in better agreement with experimental results than those in other two models.

Figure 8 shows the distribution of temperature in each model in the case of heat input of 4.2kW. In Pot-side model, it is observed that the width of plume is larger and temperature is lower than those in other models. Besides, in Velocity model, it is observed that temperature around range is a little high. The reason is thought that heat transfer by radiation is considered in Velocity model.

3.3 CFD Analysis in Case of 1.13kW

The profiles of each model have similar characteristics to those in the case of heat input of 4.2kW (Figure 7).

4. Conclusion

The accuracy of the simulated thermal plume is very important in predicting the diffusion of the thermal plumes above the cooking gas range by CFD analysis. It is observed that both velocity and temperature in applying Pot-side rising air model are in better agreement with experimental results than those in other models. So, it can be said that Pot-side rising air model is a higher accuracy modeling method. It also can be said that Pot-side rising air model is a versatile model because it is more suitable than other models when cross winds or other disturbances reach the cooking zone.

After this study, we are scheduled to improve the accuracy of Pot-side rising air model and expand its versatility.

5. Acknowledgements

The authors are grateful to Ms. Asako Tamura who is the former graduate student of Osaka University and Osaka Gas Co., Ltd for supporting the part of this research.

6. Reference

1. Momose T., Yamanaka T., Kotani H., and Yamamoto A. “Modeling and Measurements of Plume above Commercial Cooking Stoves”, *J. Environ. Eng., AIJ*, No.567, pp.49-56, 2003 (In Japanese)

2. Kondo Y., Abe A., Miyafuji A., Aizawa Y., and Akagi K. “CFD Modeling of Thermal Plume over a Cooking Pot and Experiments under Heating Condition”, *J. Environ. Eng., AIJ*, Vol.73 No.634, pp.1383-1390, 2008 (In Japanese)

3. Sakaguchi J., Akabayashi S., Tomioka S., and Tomaru E. “Study on the thermal environment and air flow distribution in the house kitchen by CFD analysis: Part 1 Study on the temperature, air flow and contaminant distribution above the cooking heater” *Summaries of technical papers of Annual Meeting of AIJ*. D-2: pp.673-674, 2008 (In Japanese)

4. Tamura A., Kotani H., Sagara K., Yamanaka T., and Momoi Y. “Capture Efficiency of Ceiling-mounted Hood in Island Kitchen: Part 3 Simulation Method of Plume from Residential Kitchen Range by CFD analysis” *Summaries of technical papers of Annual Meeting of SHASE Kinki Chapter*., pp.5-8, 2009 (In Japanese)

5. Shakochi T. “Jet Flow Engineering – Fundamentals and Application” *Morikita Publishing Company*, 2004 (In Japanese)

6. Tamura A., Sagara K., Yamanaka T., and Kotani H. “Ventilation Performance of Residential Kitchen Range Hood –Capture Efficiency of Island Hood”, *Proceedings of AIVC 29th Conference, Kyoto Japan,* pp.14-16, 2008

Table 1
Summary of CFD Analysis

CFD Code	FLUENT6.3
Turbulence Model	Standaard k-εModel
Density	Imcompressive-ideal gas
Algorism	Steady State (SIMPLEC)
Discretization Scheme for Advection Term	Second Order Upwind

Table 2
Boundary Conditions for Laboratory

Wall Condition		General Log-Low, Adiabatic
Inlet	Supply -Opening	0.02[m/s], 18[℃] k=0 [m^2/s^2], ε=0 [m^2/s^3]
Outlet	Ceiling	Pressure : 0 [Pa] (For Backflow: 18[℃], k=0 [m^2/s^2], ε=0[m^2/s^3])

Table 3
Parameters for Modeling in Pot-side model

	temperature (t)		velocity (u)	
	t_m [℃]	$b_{1/2}$ [mm]	u_m [m/s]	$b_{1/2}$ [mm]
4.2 kW	372.9	0.022	0.95	0.022
1.13kW	88.5	0.011	0.44	0.014

Table 4
Consideration of Heat Transfer by Radiation

Pot-side model	unconsidered
Velocity model	Discrete Ordinates Method
Heating model	unconsidered

Table 5 Boundary Conditions around Pot in Pot-side model

		Heat Input	
		4.2[kW]	1.13[kW]
Inlet	Water -Surface	0.0408[m/s]	0.0136[m/s]
		Temperature: 100[℃] (※material: Water Vaper) $k=6.00\times10^{-6}$ [m^2/s^2], $\varepsilon=1.72\times10^{-7}$ [m^2/s^3]	
	Upper Surface of Pot-side Zone	Teperature and Velocity are calcurated by an experimental formula of two-dimensional wall jet (Eq. 1)	
Outlet	Lower Surface of Pot-side Zone	Magnitude of Velocity is equivalent at Upper Surface of Pot-side Zone	

Table 6 Boundary Conditions around Pot in Velocity model

		Heat Input	
		4.2[kW]	1.13[kW]
Inlet	Water -Surface	0.0408[m/s]	0.0136[m/s]
		Temperature: 100[℃] (※material: Water Vaper) $k=6.00\times10^{-6}$ [m^2/s^2], $\varepsilon=1.72\times10^{-7}$ [m^2/s^3]	
Heat Flux	Pot Side	66182[W/m^2]	14908[W/m^2]
		Area of Heat genarating surface: 3.77×10^{-2} [m^2]	

Table 7 Coefficient of Regression Function in Heating model

($y=a+b|x|+c|x|^2+d|x|^3+e|x|^4+f|x|^5$ ※x: horizontal distance from the center of pot [mm])

Heat Input	Coefficinent					
[kW]	a	b	c	d	e	f
4.2	4.982×10^{-1}	-1.546×10^{-2}	1.015×10^{-3}	-1.564×10^{-4}	8.906×10^{-8}	-1.740×10^{-10}
1.13	3.569×10^{-1}	-6.597×10^{-3}	4.875×10^{-4}	-1.005×10^{-5}	7.413×10^{-8}	-1.836×10^{-10}

Table 8 Boundary Conditions around Pot in Heating model

		Heat Input	
		4.2[kW]	1.13[kW]
Heat Flux	Pot Side	49632[W/m^2]	11181[W/m^2]
		Area of Heat genarating surface: 5.03×10^{-2} [m^2]	

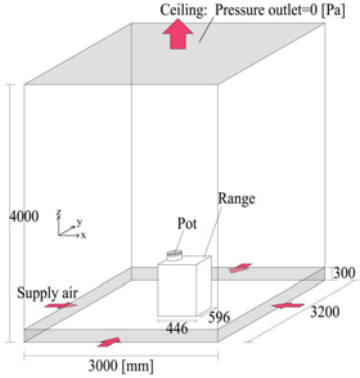


Fig. 1 Calculated Domain

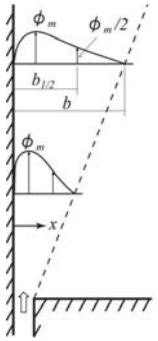


Fig. 2
Flow Model of Two Dimensional Wall Jet

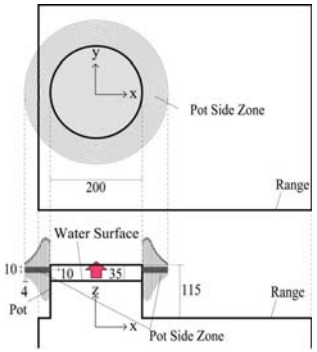


Fig. 3 Detail around Pot in Pot-side model

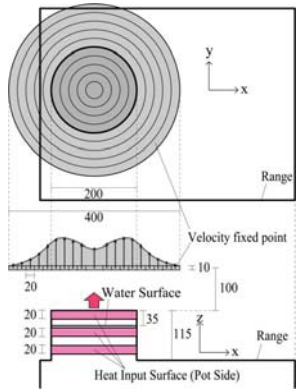


Fig. 4 Detail around Pot in Velocity model

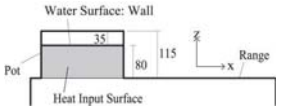
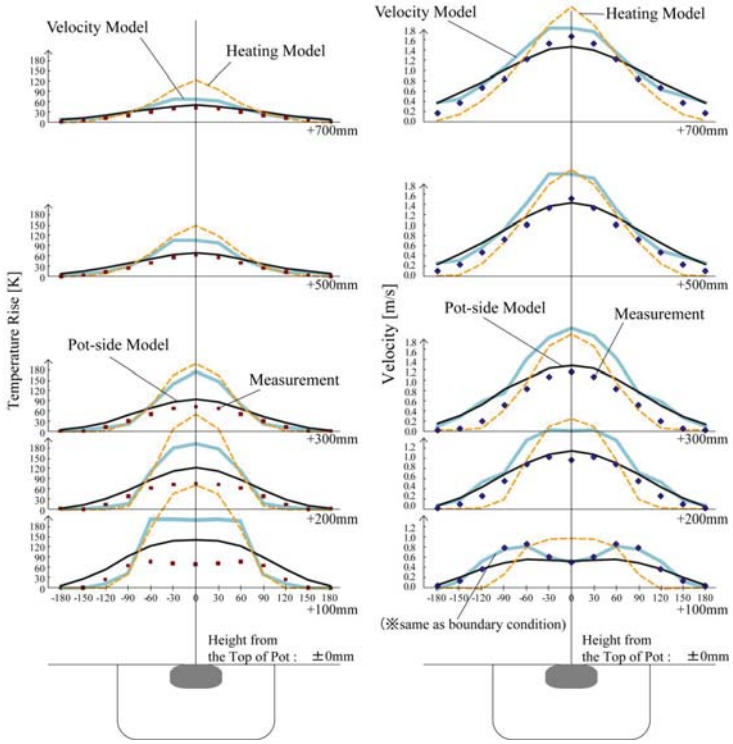
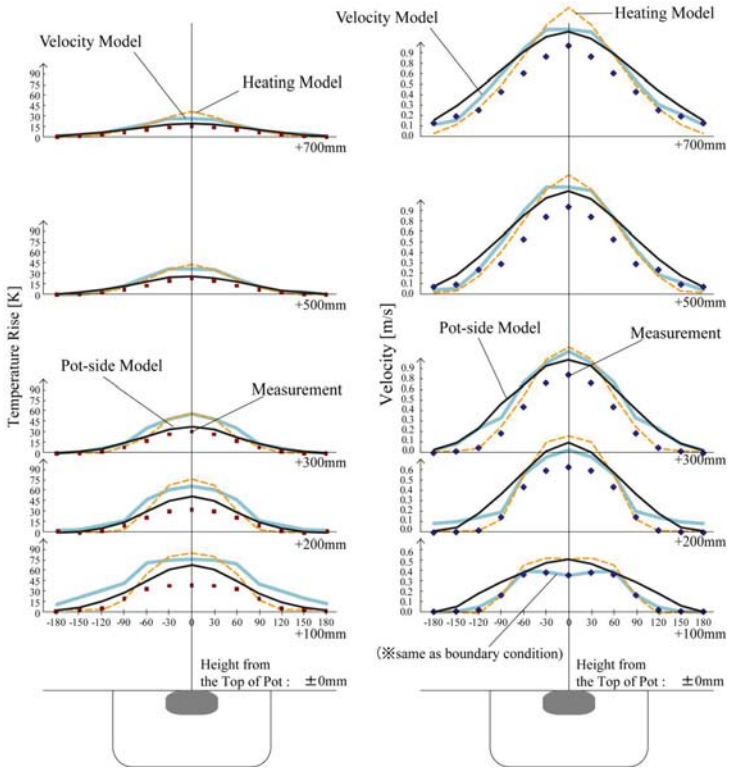


Fig. 5 Detail around Pot in Heating model



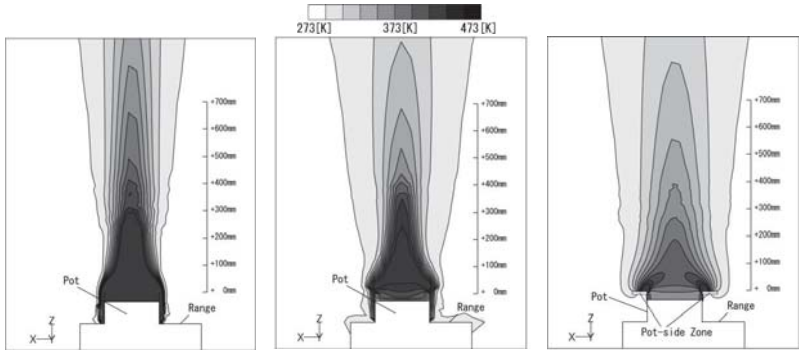
a) Temperature Rise **b)** Velocity

Fig. 6 Distributions of Temperature and Velocity (4.2kW)



a) Temperature Rise **b)** Velocity

Fig. 7 Distributions of Temperature and Velocity (1.13kW)



a) Heating Model **b)** Velocity Model **c)** Pot-side Model

Fig. 8 Temperature Distribution on Vertical Section (4.2kW)

Influence of Partition Curtain on Vertical Profile of Temperature and Contaminant Concentration in Sickroom with Displacement Ventilation

T. inagaki[1], T. Yamanaka[1], K. Sagara[1], H. Kotani[1],
Y. Momoi[1], T. Yamashita[2] and N. Choi[3]

[1] Osaka University
[2] SANKI Engineering Co.,Ltd
[3] The Tokyo Electric Power Company, Inc.

Abstract

For patients, the sickroom is a place where they receive medical treatment and also a living space where they spend most of time in a day. Therefore, good indoor air quality and comfort should be kept in sickroom.
We propose to use the displacement ventilation as a means of obtaining high indoor air quality in sickrooms. The purpose of the study is to examine the validity of this system. This paper shows the experiment results and CFD analysis results to examine the effect of partition curtain in the displacement-ventilated room.

Keywords: Displacement ventilation, Sickroom, Curtain, CFD analysis, Prediction model

1. Introduction

The mechanism of displacement ventilation is referred in many textbooks or papers (e.g. REHVA, 2002, Skistad. H, Mundt. E, Nielsen. P, Hagstrom. K, Railio. J). The prediction model of vertical temperature profile is presented by Nielsen and Mundt. It is known that the contaminant interface is formed at the height where supply airflow rate is equal to the total airflow rate of the plumes from the heat sources such as persons. Therefore, contaminant concentration profile can be predicted briefly. The relationship between the ventilation heat loss and contaminant concentration in the lower zone was investigated previously (Yamanaka and Kotani et al. 2001). It is, however, necessary to predict the effect of cool wall on the pollution of the air in the lower zone for occupants. The approach to predict the vertical profile of temperature and contaminant concentration was examined by means of macro-model (Higashimoto and Yamanaka et al. 2003). As observed above, a lot of studies for displacement ventilation are researched, but displacement ventilation for sickroom has not been studied enough.

Most sickrooms in Japan have four beds, and there is a problem of the odor from patients or diapers. Therefore the authors have proposed to use the displacement ventilation for sickroom. This study is intended to examine the applicability of the displacement ventilation system for sickroom. In the previous study, the temperature and contaminant concentration profile in displacement-ventilated room were figured out. But, the actual sickroom has partition curtains to keep patient's privacy and it is predicted that the curtain has great influence on the temperature and contaminant concentration profile. This paper shows the experiment results and CFD analysis results to examine the effect of partition curtain in the full-scaled sickroom with displacement ventilation. In addition, the experiment results were compared with the calculated results by zonal model presented by the authors before.

2. Experiment method

Experiments are performed in a full-scale displacement-ventilated room. The test room has 2.68m heights, 3.0m widths and 3.0m length, as shown in Fig.1. The floor, ceiling, and walls are insulated with 50mm thick polystyrene foam. The supply inlet is a half-cylinder displacement-type diffuser (kranz Q-ZH) located along the wall on the floor. The exhaust outlet is a 200 ϕ hole located in the corner on the ceiling. A mannequin with heating-cable is used as a human simulator. Heat generation rate of the mannequin is maintained at 40W as sensible heat load of sleeping human. The each end of a 100% polyester cloth with a thick of 0.5mm is fixed to the wall as a curtain.

Fresh air is supplied at 22 ^{o}C from the diffuser, and the surroundings of the test room are kept at 22 ^{o}C. CO_2 was emitted at the chest of heated mannequin as tracer gas. CO_2 flow rate is controlled at 0.5L/min by mass flow controller. Room air temperature, wall surface temperature and CO_2 concentration are measured at steady state.

Fig.2 shows measurement points of temperature and CO_2 concentration. Air temperature is measured at 9 points (P1~P9) in horizontal plane and at 22 points vertically, that is 198 points in total. Wall surface temperature (Wa~Wl) is measured at 6 points vertically (i.e. 72 points for all). CO_2 concentration (P1~P3, P6~P9) is measured at 12 points vertically (i.e. 84 points for all).

As parameters of the experiment, supply flow rate and bottom height of curtain were changed. Table 1 shows the experimental conditions. The results of the experiment performed at 2006 are quoted, and the conditions without curtain are added in the table.

3. Experiment results

Table 2 shows balance of heat flow. The experimental results are expressed by mean value in equal height of the measurement points (P1, P2, P7 and P8) inside of the curtain and the measurement points (P3, P6 and P9) outside of the curtain.

3.1 Influence of Curtain on vertical profile of temperature and contaminant concentration

The horizontal axis of graph of temperature means the temperature difference from supply air temperature, and that of concentration means measured concentration minus supply air concentration which is normalized by the concentration difference between supply and exhaust.

Fig.3 and Fig.4 show the measured results of vertical profile of temperature and contaminant concentration respectively, under the condition of supply airflow rate of 100m^3/h. Fig.3 shows thermal stratification is little formed outside of curtain (that is, the smaller zone without bed) when curtain is present. It is considered to be that the thermal plume from the mannequin is interrupted by the curtain. From Fig.4, it is seen that the concentration is high at

a low position when curtain is presence. It is considered that the pollutant descends to the floor with downdraught along cool walls because conduction heat loss through perimeters is relatively large in this case. Then, there is a tendency that the concentration interface level falls inside curtain (the zone with a bed) and rises outside curtain (the zone without a bed) when the curtain is present. This is because that the supply air flowing into inside of curtain is decreased and that the outside space of curtain is filled with fresh air supply.

Fig.5 and Fig.6 show the measured results of vertical profile of temperature and contaminant concentration respectively, under the condition of supply airflow rate of 200m^3/h. Fig.5 shows thermal stratification is little formed outside of curtain as is the case in supply air of 100m^3/h. In Fig.6, it is seen that the concentration interface level falls inside curtain and rises outside curtain as is the case in supply air 100m^3/h.

3.2 Influence of Bottom Height of Curtain

Fig.7 and Fig.8 show the measured results of vertical profile of temperature and contaminant concentration respectively when supply airflow rate is 200m^3/h.

From Fig.7, it can be said that the difference of vertical temperature gradient is not so large in all cases. However, the temperature profile is slightly high when bottom height of curtain is 125mm.

Fig.8 shows concentration gradient inside of curtain is low when bottom height of curtain is 125mm. The supplied air flowing under curtain into inside of curtain is decreased and the supplied air flowing over curtain into inside of curtain is increased when the opening area under the curtain is small. Therefore, it is considered that the concentration interface is not formed clearly because of the mixture of fresh air and contaminated air when bottom height of curtain is 125mm. Then, there is a tendency that the measured values outside curtain approach the value of the case without curtain as bottom height of curtain rises. Therefore, it can be said that bottom height of curtain has large influence on the distribution of supply airflow rate into inside and outside of curtain.

4. CFD analysis

4.1 Analysis Method

CFD simulation is carried out in order to examine more detailed flow patterns in the room. The test room where experiments are performed is replicated as analyzed room. Fig.9 shows the analyzed room, and Fig.10 illustrates the mesh layout. The standard k-ε model is used as a turbulence model. Table 3 shows the analysis method. As for the boundary condition, the generalized log low is applied for the velocity, and the measured temperatures are provided for wall surface temperature. The heat emission rate of mannequin is 20W on the assumption

that the convection heat accounts for 50% of total sensible heat load of sleeping human. Table 4 shows the boundary conditions of CFD analysis.

4.2 Results

Fig.11 and Fig.12 show temperature and velocity distribution obtained by CFD as for the condition of Q_s=200m^3/h and Y_{cb}=125mm.

In Fig.11(1), supply airflow and thermal plume from the heated mannequin are interrupted by the curtain. Therefore, the supply air flowing into the inside of curtain is decreased and the outside space of curtain is filled with fresh air.

In Fig.11(2), (3) and Fig.12, the cool supply air flowing over curtain into the inside of curtain is mixed with warm air inside curtain. This phenomenon explains the reason why the concentration interface is not formed clearly in the experiments in the previous chapter.

5. Validation of Zonal model

5.1 Outline of Zonal Model

In order to predict vertical profile of contaminant concentration inside curtain, the zonal model presented in the previous study is applied. This model is based on the balance of contaminant flow by convection and diffusion. Fig.13 shows the outline of the model. In this model, the room is divided into four zones vertically direction and "interface layer" (with layer(2) and (3)) including the contaminant interface is assumed. This layer has a width of W, and there is diffusive transfer of contaminant across the interface. Fundamental equations for this model are as follows.

The contaminant balance of the layer (2) can be expressed by

$$Q_{dr(y_u)}\left\{(C_u-C_d)(1-\frac{\eta}{2})+C_d\right\}-3600(D+D_t)\frac{\partial C}{\partial y}A_f=Q_{dr(y_u)}C_u$$

The contaminant balance of the layer (3) can be expressed by

$$Q_{ur(y_d)}\left\{(C_u-C_d)(\frac{1-\eta}{2})+C_d\right\}=-3600(D+D_t)\frac{\partial C}{\partial y}A_f+Q_{ur(y_d)}C_d$$

As the value of diffusion coefficient ($D+D_t$), 0.0005[m^2/s] is used, from the previous study.

The following equation can be derived from the balance of contaminant in layer(4).

$$\left(Q_s+\sum_{k=1}^{m}Q_{d_k(y_d)}\right)C_d=\left(\sum_{k=1}^{m}Q_{d_k(y_u)}\right)C_u+\left(\sum_{k=1}^{m}Q_{d_k(y_l)}-\sum_{k=1}^{m}Q_{d_k(y_u)}\right)\left\{(C_u-C_d)(1-\frac{\eta}{2})+C_d\right\}+\left(\sum_{k=1}^{m}Q_{d_k(y_d)}-\sum_{k=1}^{m}Q_{d_k(y_l)}\right)\left\{(C_u-C_d)(\frac{1-\eta}{2})+C_d\right\}$$

The contaminant balance of the whole room can be expressed by

$$C_u=C_e=\frac{NM}{Q_s}$$

By solving these balance equations as a set of simultaneous equations of y_u, y_d, C_u and C_d, these variables can be obtained.

The lying patient on the bed is considered as a line heat source. In the previous study, the length of the line source is 0.5m and the source is located 0.8m below the human. The airflow rate of plume from the patient can be expressed by

$$Q_{P(y)}=82.43y+24.72$$

From the previous paper, the vertical airflow rate along a wall due to national convection can be calculated by cumulating the following increment of airflow rate.

$$\Delta Q_{u(y)}=\Delta Q_{d(y)}=13.176\left|\Delta T\right|^{\frac{2}{5}}y^{\frac{1}{5}}l\ \Delta y$$

In this paper, the model calculation is performed on the assumption that all the supply air flows into inside of curtain on that the two-third of supply air flows into inside of curtain based on the area ratio of both area divided by the curtain.

5.2 Calculation results

Fig.14 shows the comparisons of the calculation results of vertical profile of contaminant concentration with experimental one in the case that curtain is present. The experimental results are averaged values of the same height. In this figure, the calculation (1) is the result by $Q_{si}=Q_s$ and the calculation (2) is the result by $Q_{si}=2/3Q_s$.

Fig.14 (1) ~ (4) show that calculation (2) coincides with the experimental result when supply airflow rate is $100m^3/h$ or $200m^3/h$. However, fig.13 (5) shows the calculated result doesn't coincide with experimental one when supply airflow rate is $300m^3/h$.

5.3 Prediction by Means of Identified Supply Airflow Rate into Inside Curtain Area

In this section, vertical profile of contaminant concentration inside curtain is predicted by the supply flow rate identified from contaminant balance. The contaminant balance of the inside of curtain can be expressed by

$$Q_{si}=\frac{NM}{Cui}$$

Therefore, supply air flowing under curtain into inside of curtain can be identified from the measured contaminant concentration above interface layer inside curtain.

Fig.15 shows the comparisons of the calculated results of vertical profile of contaminant concentration with experimental ones in the case that curtain is present. The identified supply flow rate and the ratio of that to actual supply flow rate are written in each figure. Fig.15 (1), (4) show calculated result coincides with the experimental result successfully in the case of $Q_s=100m^3/h$ and $Y_{cb}=250mm$ or the case of $Q_s=200m^3/h$ and $Y_{cb}=400mm$. In other case, however, contaminant interface levels obtained by calculation are higher than experimental ones and both ones don't coincide. In general, the increase of supply flow rate raises

contaminant interface height, so it is supposed that the identified supply flow rate is larger than the actual supply flow rate. This is because that the concentration isn't measured at measurement points of P4 and P5 shown in Fig.2 and the high concentration over pollution source (that is mannequin) isn't accounted for. When supply flow rate is small or bottom height of curtain is high, the horizontal profile of concentration above interface layer is considered to be uniform as little supply air is supposed to flow over curtain into inside of curtain. Therefore, supply flow rate is identified accurately and calculated results coincide with experimental ones even though the concentration over pollution source wasn't measured.

6. Conclusions

−When the curtain is present, the contaminant interface height rises inside curtain and falls outside curtain.

−When bottom height of curtain is small, the contaminant interface inside of curtain is not formed clearly.

−The CFD analysis shows that supply air flows over curtain into inside of curtain in the case of Q_s=200m^3/h and Y_{cb}=125mm.

−The calculated results by means of zonal model coincided successfully with experiment results if supply flow rate is small or bottom height of curtain is high enough.

Acknowledge

The authors wish to thank Mr. Yamane (SANKI Engineering Co.,Ltd) who helped us with experiments.

References

1. Skistad. H, Mundt. E, Nielsen. P, Hagstrom. K, Railio. J : Displacement ventilation in non-industrial premises, REHVA, 2002

2. Etheridge. D, Sandberg. M : BUILDING VENTILATION-Theory and Measurement-",JOHN WILEY&SONS,pp446~469,1996

3. Nielsen. P : DISPLACEMENT VENTILATION- theory and design, Aalborg University, pp.7-12, 1993

4. Skistad. H : DISPLACEMENT VENTILATION, RESEARCH STUDIES PRESS LTD., p10, 1994

5. Nielsen. P : Temperature Distribution in a Displacement Ventilation Room,5th International Conference on Air Distribution in Rooms, ROOMVENT'96, pp.323~329, 1996.7

6. Mundt E : TEMPERATURE GRADIENT MODELS IN DISPLACEMENT VENTILATED ROOMS,5th International Conference on Air Distribution in Rooms, ROOMVENT'96, pp.331~337,1996.7

7. Yamanaka. T, Kotani. H, Higashimoto. T : Effect of cooled or heated wall on vertical distribution of temperature and contaminant concentration in rooms with displacement ventilation ,(In Japanese), Journal of Architecture, Planning and Environmental Engineering (Transactions of AIJ) , No.550, pp.17-23, 2001,6

8. Higashimoto. H, Yamanaka. T, Kotani. H, Hanano. H : Profile of temperature and contaminant concentration in displacement ventilated room with cold wall –application of block-model with plume from heat source–, (In Japanese) Journal of Architecture, Planning and Environmental Engineering (Transactions of AIJ) , No.571, pp.47-53, 2003.9

9. Yamanaka. T, Kotani. H : Zonal Models to Predict Vertical Contaminant Distribution in Room with Displacement Ventilation Accounting for Convection Flows along Walls, ROOMVENT 2007, Helsinki, Finland.

10. Hamaguchi. T : Semi-Personal Air-conditioning System for Sickroom by Displacement Ventilation with Radiant Panel-properties of plume from slumber human and prediction of contaminant concentration- (In Japanese), academic dissertation of Osaka University, 2001

11. Iwamura. A : Semi-Personal Air-conditioning System for Sickroom by Displacement Ventilation with Radiant Panel- Influence of Radiant Panel and Location of Outlet- (In Japanese), academic dissertation of Osaka University, 2007

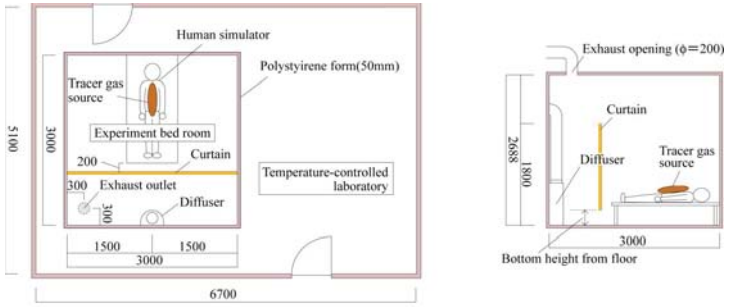


Fig.1 Experiment bed room

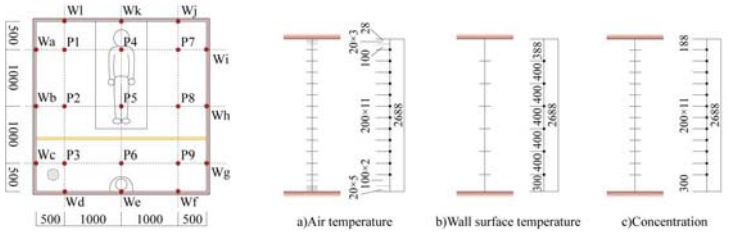


Fig.2 Measurement Points

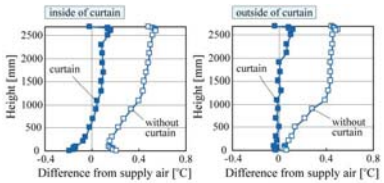


Fig.3 Vertical temperature distribution (Q_s=100m^3/h)

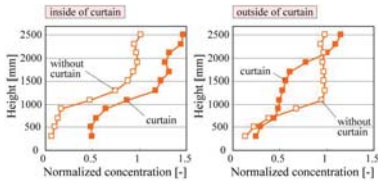


Fig.4 Vertical concentration distribution (Q_s=100m^3/h)

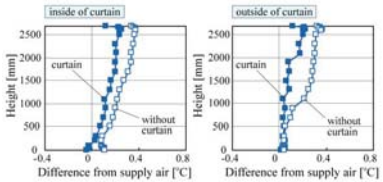


Fig.5 Vertical temperature distribution (Q_s=200m^3/h)

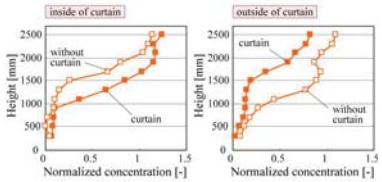


Fig.6 Vertical concentration distribution (Q_s=200m^3/h)

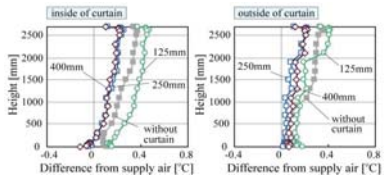


Fig.7 Vertical temperature distribution (Q_s=200m^3/h)

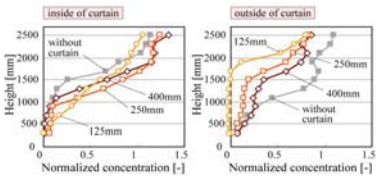


Fig.8 Vertical concentration distribution (Q_s=200m^3/h)

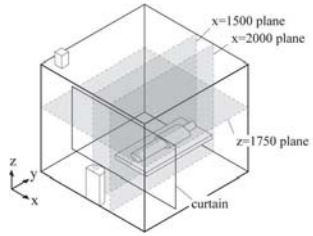


Fig.9 Analyzed room (Q_s=200m^3/h, Y_{cb}=125mm)

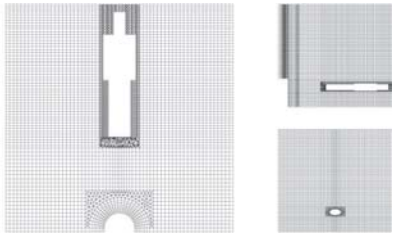
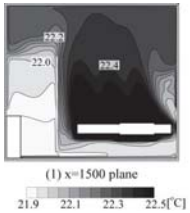


Fig.10 Mesh layout





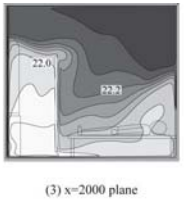


Fig.11 Temperature distribution

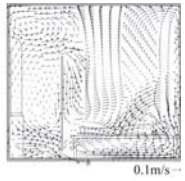


Fig.12 Velocity distribution (x=2000 plane)

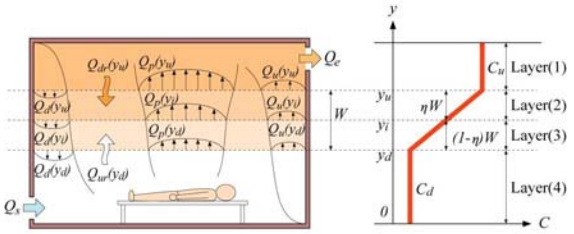


Fig.13 Outline of the zonal model

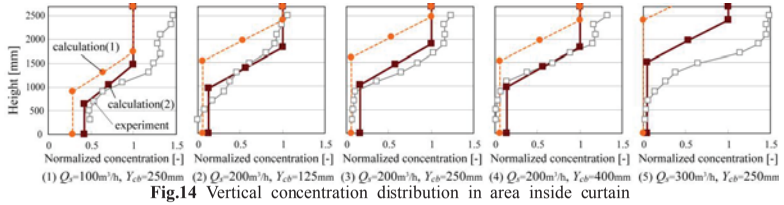


Fig.14 Vertical concentration distribution in area inside curtain

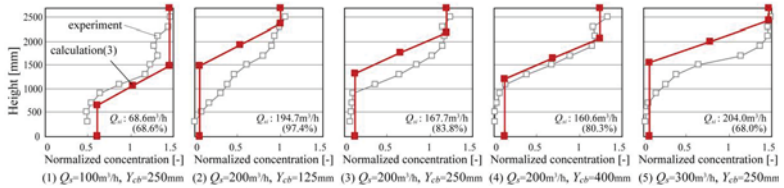


Fig.15 Vertical concentration distribution in area inside curtain

Table 1 Experimental conditions

		without curtain	curtain (bottom height from floor)		
			125mm	250mm	400mm
Supply airflow rate	100m^3/h	○		○	
	200m^3/h	○	○	○	○
	300m^3/h			○	

Table 2 Heat balance

Supply airflow rate	100m^3/h	200m^3/h			300m^3/h
bottom height from floor	250mm	125mm	250mm	400mm	250mm
Heat Value of Human Simulater [W]	40	40	40	40	40
Ventilation Heat Loss [W]	-3.64	-20.29	-11.40	-15.63	-20.69
Conduction Heat Loss [W]	-24.95	-5.34	-13.55	-7.17	-0.01
Total Heat Balance [W]	11.41	14.36	15.05	17.20	19.31

Table 3 Analysis method

CFD code	Fluent6.3
Turbulence model	Standard k- ε model
Density	Incompressible ideal gas
Calculation algorithm	Steady state (SIMPLE)
Discretization scheme	QUICK
Number of mesh	64×73×57

Table 4 Boundary conditions

Wall	Generalized log law
inlet	0.1179m/s, 21.88℃
	k = 3(UI)^2/2 (I=3%)
	$\varepsilon = C_\mu^{3/4} k^{3/2}/L$ (L=0.005m)
outlet	Pressure 0 [Pa]
Heat generation from human	14.5W/m^2 (total 20W)

【Symbol】

A_f	: Floor area [m^2]	$Q_u(y)$	: Upward airflow rate of the wall at height of y [m^3/h]
C_e	: Contaminant concentration of the exhaust air [-]	$Q_d(y)$	: Downward airflow rate of the wall at height of y [m^3/h]
C_u	: Contaminant concentration above the interface layer [-]	$Q_{ur}(y)$	: Upward airflow rate at height of y [m^3/h]
C_d	: Contaminant concentration below the interface layer [-]	$Q_{dr}(y)$	: Downward airflow rate at height of y [m^3/h]
C_{su}	: Contaminant concentration above the interface layer inside of curtain [-]	ΔT	: Temperature difference between wall and room temperature [℃]
D	: Diffusion coefficient by molecular [m^2/s]	W	: Vertical width of interface layer [m]
D_t	: Diffusion coefficient by turbulence [m^2/s]	y	: Height above floor [m]
l	: Horizontal width of the wall [m]	Δy	: Vertical width of small wall part [m]
M	: Contaminant emission rate per heat source [m^3/h]	y_u	: Height of the upper edge of interface layer above the floor [m]
N	: The number of the human [-]	y_i	: Height of contaminant interface [m]
Q_s	: Supply airflow rate [m^3/h]	y_d	: Height of the lower edge of interface layer above the floor [m]
Q_e	: Exhaust airflow rate [m^3/h]	Y_{cb}	: Bottom height of curtain [m]
Q_{su}	: Supply airflow rate flowing into inside of curtain [m^3/h]	η	: Height ratio of the interface in interface layer [-]
$Q_p(y)$	: Air flow rate of the plume of the person at height of y [m^3/h]	$\partial C/\partial y$	: Vertical gradient of concentration within the interface layer [/m]

CFD Analysis on Capture Efficiency in Commercial Kitchen using Low Radiative Cooking Equipment with Concentrated Exhaust Chimney

Koki TOYOMURA[1], Hisashi KOTANI[1], Toshio YAMANAKA[1], Yoshihisa MOMOI[1], Kazunobu SAGARA[1] and Shota TAKANO[2]

[1] Dept. of Architectural Engineering, Osaka University, Osaka, Japan

[2] SHIMIZU CORPORATION, Tokyo, Japan

Abstract

In a commercial kitchen, a large ventilation rate is needed and energy consumption can be large because a large amount of effluence of heat and moisture need to be removed. To improve kitchen environment and to save the energy, low radiative cooking equipment with concentrated exhaust chimney was developed. Although a ventilation rate may be decreased by using this equipment, the effluence needs to be captured well. To predict indoor air and thermal environment of commercial kitchen using this equipment, CFD analysis is useful. In the previous study, the capture efficiency of the hood was measured when this new equipment is used. In this paper, CFD simulation was carried out in order to analyze capture efficiency of the equipment with reproducing the measurement. CFD results of various conditions were compared with measured ones. CFD results were agreed well with measured ones for many cases.

Keywords: *Commercial Kitchen Ventilation, CFD Analysis, Capture Efficiency, Combustion Gas, Cooking Effluence*

Introduction

In commercial kitchen, a large amount of heat and moisture are generated and they must be removed. Since the gas cooking equipment involves combustion, a kitchen in which gas cooking equipment is used requires sufficient supply of oxygen for the combustion process. Hence, a large ventilation rate is required to meet the combustion and ventilation requirements resulting in high energy consumption.

A performance of the exhaust hood is important to remove contaminant and keep good air quality. The capture efficiency of hood has been examined previously under various room conditions. For example, Wolbrink and Sarnosky [1] defined capture efficiency as the ratio of moisture captured by the hood to moisture produced by the source. Li et al.[2] proposed new definition of capture efficiency which includes the air exchange between the cooking zone and the room zone in a two-zone mixing model. The capture efficiency of the standard canopy hood for exhaust gas and contaminant generated by cooking above the commercial cooking stoves and fryers were measured on two kinds of heat sources of natural gas and electromagnetic heat by Yamanaka et al.[3]. In addition, Momose et al. [4] investigated the influence of a moving person on the capture efficiency.

Recently, low radiative cooking equipment with concentrated exhaust chimney has been developed to improve the kitchen environment and conserve the HVAC energy requirements. A cross-section of the low radiative equipment is shown in **Fig.1**. The low radiative equipment has two advantages. Firstly, the surface temperature of the equipment is lower than that of the conventional equipment. This reduces radiation heat emission toward workers

and room surface. Secondly, generated combustion gas is exhausted effectively by using concentrated exhaust chimney. This reduces the diffusion and overflow of effluences to the room, which also contains the heat and CO2 waste gas from combustion. Consequently, the required exhaust flow rate can be reduced by these advantages. Although a ventilation rate may be decreased by using this equipment, there is no design guideline of ventilation system under operation of this type of equipment. Therefore the purpose of this study is to prove the ventilation performance of these equipments, and build up a design guideline of ventilation system under operation of them. To predict indoor air and thermal environment of commercial kitchen using this equipment, Computational Fluid Dynamics (CFD) analysis is useful. Authors [5] carried out CFD analysis on capture efficiency of the canopy hood for combustion gas and cooking effluence under operation of one kind of equipment operating in a laboratory. However, the simulation accuracy of exhaust plume was not so high suspect. Authors [6] also carried out simplified CFD analysis on indoor thermal environment under operation of three kinds of equipment operating in a room. However, this analysis disagrees with experimental result [5] due to the error in the boundary conditions. In this paper, first we carried out CFD analysis on capture efficiency of the canopy hood under operation of one kind of equipment in a large laboratory. We used measured data of exhaust air [7] and temperature [8] as boundary conditions of the analysis. Comparing with experimental result [5], simulation accuracy is checked. Secondly applying these boundary conditions, we carried out CFD analysis on indoor thermal environment under operation of three kinds of equipment operating in a room which has supply and exhaust air like a real kitchen.

1. CFD Analysis on Capture Efficiency of the Hood in Large Space

1.1 Outline

CFD simulation was carried out in order to analyze the capture efficiency of the hood for combustion gas and cooking effluence under operation of one kind of the low radiative equipment in a laboratory. The laboratory measurements were carried out by Authors [5]. CFD outline is shown in **Table 1**.

1.2 Methods

As an analyzed room, experiment room of the study is simulated. The experimental space is in large of experimental building and the leakage from the hood is exhausted at ceiling height around the hood and it doesn't capture again. Analyzed room is shown in **Fig.2-Fig.3**. The applications used for this analysis were low radiative range, fryer and kettle. A calculated domain is 4600*4200*3000mm space including a 1200*1200*500mm (2400*1200*500 in the case of kettle) canopy-type exhaust hood in the center. The height of the bottom of the hood is 2000mm. This is common used in the real kitchen. Each application is set under the center of hood. Initial Setting of indoor air temperature is 20 deg.C.

The standard k-ε model (SKE) and RNG k- ε model (RNG) are used as turbulence model. In order to exhaust contaminant from cooking equipment, the hood has a exhaust opening (300*300mm) at the center in the case of range and fryer, and it has two of them in the case of kettle. Assuming that the leakage from the hood is exhausted at ceiling height around the hood, the pressure at ceiling height is fixed as 0 Pa. The air is supplied from the lower part of surroundings walls (from floor to height 800mm). Supply air flow rate is 2 times of exhaust flow rate from exhaust opening at hood. As for the wall boundary condition, the generalized log law was applied for the velocity and adiabatic for thermal condition. Boundary conditions of the room are shown in **Table 2**. This CFD analysis was carried out under five conditions of exhaust flow rate, that is 20KQ (Case1), 30KQ (Case2), 40KQ (Case3), 0.3m/s of the face velocity at the bottom of the hood (Case4) and 0.4m/s of the face velocity (Case5) for each item of equipment. This method conforms to BL method [9] and is authorized as standard measuring method to determine the capture efficiency of a hood in JAPAN. Where, K is the Theoretical combustion gas flow rate per input [m3/(h・KW)] and Q is the gas input[KW]. These conditions are the same as the previous experiment. The analyzed exhaust and supply flow rate are shown in **Table 3**.

1.3 Boundary Conditions of the Equipments

The equipment models are shown in **Fig.4**. Boundary conditions of temperatures of cooking equipment surface, water vapor from the cooking pot and exhaust air from the exhaust opening were applied to the analysis. Since the radiative heat is very small compared to other heat transfer, it is not considered in this analysis. Air flow rate and temperature of combustion gas and ambient air to cool the equipment is based on the measurements. Latent heat of vaporization is calculated based on measured amount of vapor generation rate from the water per hour. Temperatures of cooking equipment surface were based on measured data. These boundary conditions of the equipment were shown in **Table 4-Table 6**.

2. CFD Analysis on Indoor Thermal Environment

2.1 Outline

CFD simulation was carried out in order to analyze indoor thermal environment of the room that three kinds of the low radiative cooking equipments with concentrated exhaust chimney are operated. The laboratory measurements were carried out by Authors [10]. By comparing CFD to Experiment, we validate the accuracy of CFD simulation. CFD outline is shown in **Table 7.**

2.2 Method

As an analyzed room, experimental room of the previous study is simulated. A plan, cross-section and perspective drawing of the analyzed room are shown in **Fig.5**. In the room of 4500*3500*2500mm, a low radiative kettle, range and fryer are installed from the left. Boundary conditions of the each equipment are the same as chapter 1 (see **Table 4-Table 6**). The air is supplied from the three ceiling inlets and exhausted from three exhaust openings (350*350mm) of the hood (900*3500mm).

SKE is used as turbulence model. As for the wall boundary condition, the generalized log law was applied for the velocity and surface temperatures were based on measured data [10]. Simulation conditions of the equipment are shown in **Table 4-Table 6**. This CFD analysis was carried out under five conditions of exhaust flow rate, that is 20KQ (Case1), 30KQ (Case2), 40KQ (Case3) and 0.3m/s of the face velocity at the bottom of the hood (Case4) which is same as the experiment of the previous study TAKANO el at. [10]. The analyzed exhaust and supply flow rate are shown in **Table 8**.

3. Result and Discussion

3.1 Capture Efficiency of the Hood in Large Space

The capture efficiency η is calculated as follows.

$$\eta = \frac{Q_H}{Q_H + Q_c} \quad \text{(Eq.1)}$$

Where

Q_H: Contaminant flow rate exhausted through the hood [kg/s]

Q_c: Contaminant flow rate exhausted at ceiling height around the hood [kg/s]

In order to obtain capture efficiency, passive contaminants are released from a cooking pot as cooking effluence and from exhaust opening of the equipments as combustion gas. The capture efficiency obtained from CFD analysis and experimental is shown in **Fig.6**. With regard to CFD analysis result of both SKE and RNG, the capture efficiency of combustion gas (η_{gas}) and cooking effluence (η_{cook}) in the cases over Case4 of all equipments is 100%. This agrees with the experiment result. In addition, both η_{gas} and η_{cook} of RNG are higher than that of SKE. This is because that as to SKE, an updraft from the pot tends to spread water-vapor into the air. As for η_{cook} of Kettle for Case1-Case3, RNG agrees with the experimental result very well. As for η_{gas} of Kettle for Case1-Case3, however, both SKE and RNG are lower than experimental result. In comparison with SKE, RNG is close to experimental result. In general, SKE overestimates turbulence kinematic energy k around impinging stream [11]. In this simulation of the kettle, SKE overestimates turbulence kinematic energy k around a top panel of the hood. As for η_{gas} and η_{cook} of range for Case1-Case3, SKE and RNG are slightly higher than experimental result, but these can follow the experimental tendency. Flow rate exhausted from exhaust chimney opening may be overestimated. As for η_{gas} and η_{cook} of fryer for Case1-Case3, SKE agrees with the experimental result very well and RNG is slightly higher than experimental result. However,

experimental result are not so accurate between Case3 (311m3/h) and Case4 (1512m3/h). This is because that experimental result has no data between them and it is largely-spaced (see **Fig.6**). Further measurements will be needed in the future. If it is assumed that measured data is higher than linearly-interpolated line between them, RNG may agree with experimental result.

In conclusion, some disagreements were seen due to the error in the boundary conditions or the turbulence model, but capture efficiency by CFD were agreed well with measured results for many cases. Thus, it seems that CFD model for each equipment in this section is faithful.

3.2 Indoor thermal environment

The vertical distributions of temperature in A-A', B-B' and C-C' section (see **Fig.5**) of CFD simulation and measure data [10] are shown in **Fig.7**. As for all exhaust flow rates, the larger exhaust rate is, the lower indoor air temperature is and the smaller air temperature difference between the top and the bottom of the room is. These agree with the experimental result very well. This is because that the amount of heat removed from the room by the hood depends on exhaust rate. Especially, as to low exhaust flow rate, room air temperature of upper area is high due to a lot of heat leakage from the hood. This indicates that we can estimate indoor thermal environment in the room accurately. To estimate them accurately, we can use section the data of 3.1 (see **Table 4-Table 6**) for boundary conditions of these equipments.

Experimental measurement point of temperature is shown in **Fig.8** and correlation charts between CFD temperature and experiment temperature are shown in **Fig.9**. As for most points, error is from -2deg.C to +2deg.C, and CFD is broadly consistent with experiment. As for some points of low temperature zone, temperature of CFD is lower than that of experiment. These points are close to the equipments. A minor change in the air movement may have significant effect upon the temperature, so the future researches are needed. **Fig.10** shows the vertical temperature distribution of the room that is the average of the measurement points with the same height. CFD is consistent with experiment well. Although, as to the lower area, temperature of CFD is a slightly lower than that of experiment, this is the same tendency as shown in **Fig.9**.

Conclusions

In this paper, two CFD simulations are carried in order to estimate capture efficiency of the hood and indoor thermal environment in the room operated the low radiative cooking equipments with concentrated exhaust chimney. By comparing the CFD result with the past experimental result, the paper indicates that the CFD conditions of the equipment in this paper are faithful, and we can estimate indoor thermal environment accurately in the room operated the low radiative cooking equipments with concentrated exhaust chimney by using them.

Acknowledgments

This measurement was supported by Ms.Shiho CHIHARA (former graduate student, Osaka University) and Osaka Gas Co., Ltd., and this is gratefully acknowledged.

References

1. Wolbrink, D. W., Sarnosky, J. R. Residental Kitchen Ventilation – a guide for the specifying engineer. ,ASHRAE Transactions 98(1), pp.1219-1226, 1992

2. Li, Y., Delsante, A. Derivation of Capture Efficiency of Kitchen Range Hoods in a Confined Space. ,Building and Environment, Vol.31, No. 5, pp. 461-468, 1996

3.Yamanaka, T., Satoh, R., Kotani, H., Momose, T., and Tanaka, R. Capture Efficiency of Exhaust Hood above Cooking Stoves and Fryer under Horizontal Disturbing Airflow in Commercial Kitchen. Proce edings of Healthy Buildings 2000, vol.2:719-724, 2000

4. Momose, T., Satoh, R., Yamanaka, T., and Kotani, H. Influence of Air Current and Movement of A Person on Capture Efficiency of Kitchen Hood. Proceedings of Healthy Buildings 2000, vol.2:713-718E, 2000

5. S. Takano, T. Yamanaka, H. Kotani, K. Sagara, Y. Momoi, and C. Iwasaki , Capture Efficiency of Exhaust Hood for Commercial Kitchen using Low Radiation Cooking Equipment with Concentrated Exhaust, Ventilation 2009, the 9th International Conference on Industrial Ventilation In CD-ROM Paper 1039 2009.10

6. S. Takano, K. Sagara, T. Yamanaka, H. Kotani, Capture Efficiency and Indoor Thermal Environment inside Commercial Kitchen using Low Radiative Cooking Equipment with Concentrated Exhaust Part.2 CFD Analysis on Indoor Thermal Environment, Technical Papers of Annual Meeting, The Society of Heating, Air-Conditioning and Sanitary Engineers of Japan, pp.1061-1064, 2008.8 (In Japanese)

7. K. Toyomura, T. Yamanaka, H. Kotani, Y. Momoi, K.Sagara and S. Takano, Indoor Air and Thermal Environment of Commercial Kitchen using Low Radiative Cooking Equipment with Concentrated Exhaust Part 5.Air Flow around exhaust stack for boundary conditions of CFD analysis, Technical Papers of Annual Meeting, Kinki Branch of The Society of Heating, Air-Conditioning and Sanitary Engineers of Japan, pp.57-60 2010.03 (In Japanese)

8. K. Toyomura, H. Kotani , T. Yamanaka , Y. Momoi, K. Sagara, Capture Efficiency and Indoor Thermal Environment inside Commercial Kitchen using Low Radiative Cooking Equipment with Concentrated Exhaust Part.6 CFD Analysis based on measured data of exhaust air, Technical Papers of Annual Meeting, The Society of Heating, Air-Conditioning and Sanitary Engineers of Japan, 2010.9 (Pre-publication, In Japanese)

9. The Center for Better Living., Ventilation Units (for Kitchen Use), Method of Testing Performance of Quality Housing Components, BLT VU-1:2005 (In Japanese)

10. S. Takano, K. Sagara, T. Yamanaka, H. Kotani, S. Chihara, Capture Efficiency and Indoor Thermal Environment inside Commercial Kitchen using Low Radiative Cooking Equipment with concentrated Exhaust,Advanced building ventilation and environmental technology for addressing climate change issues, Volume1, pp.171-176,2008.10

11. S. Murakami, A. Mochida, Y. Hayashi, S. Sakamoto, Numerical Study on velocity-pressure field and wind forces for bluff bodies by k-ε, ASM and LES, 8th International Conference on Wind Engineering, 1991.07

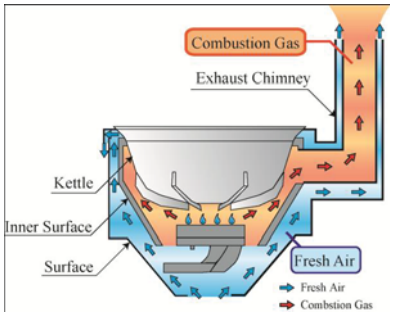


Fig.1 Outline of Low Radiative Cooking Equipment (Example of Kettle)

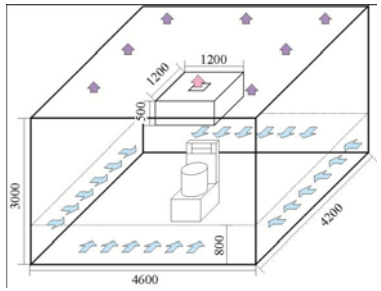


Fig.2 Analysis Room (Overall View)

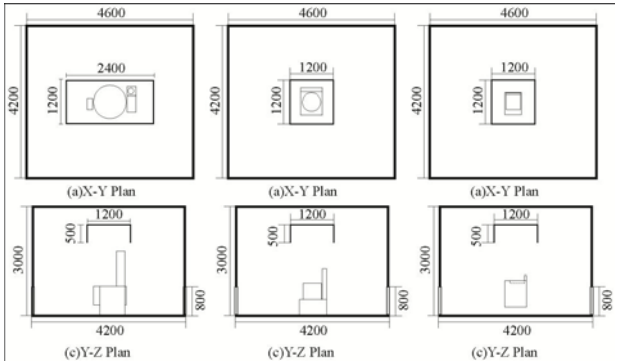
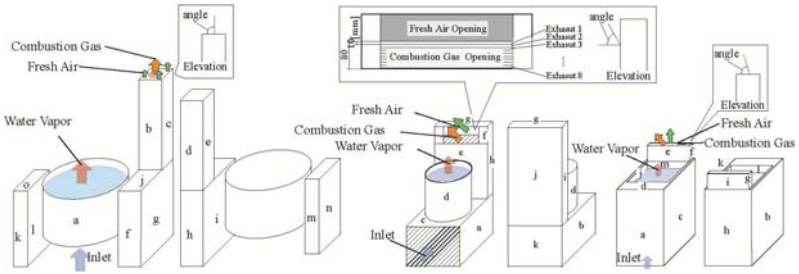


Fig.3 Analysis Room (Plan and Section)



(a)Kettle (b)Range (c)Fryer

Fig.4 Equipment Conditions

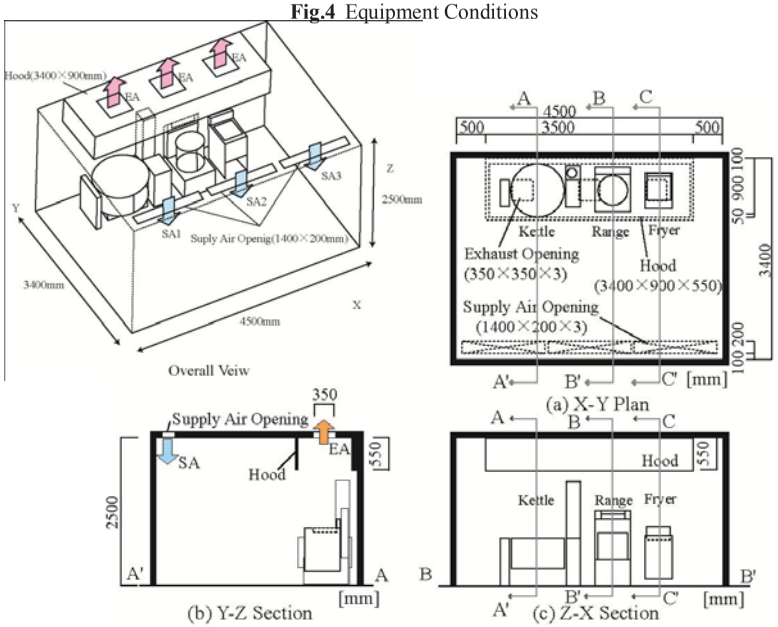
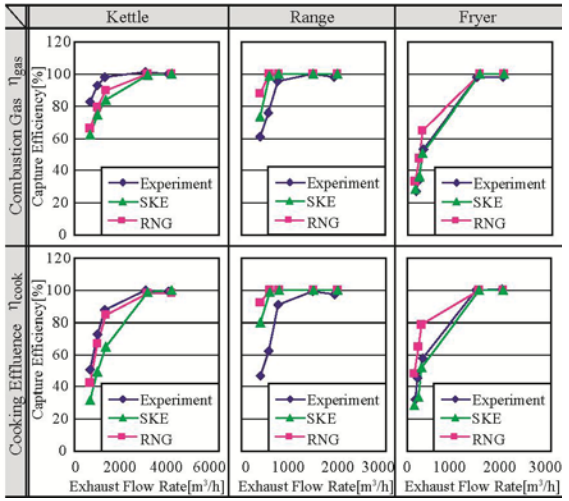


Fig.5 Analysis Room



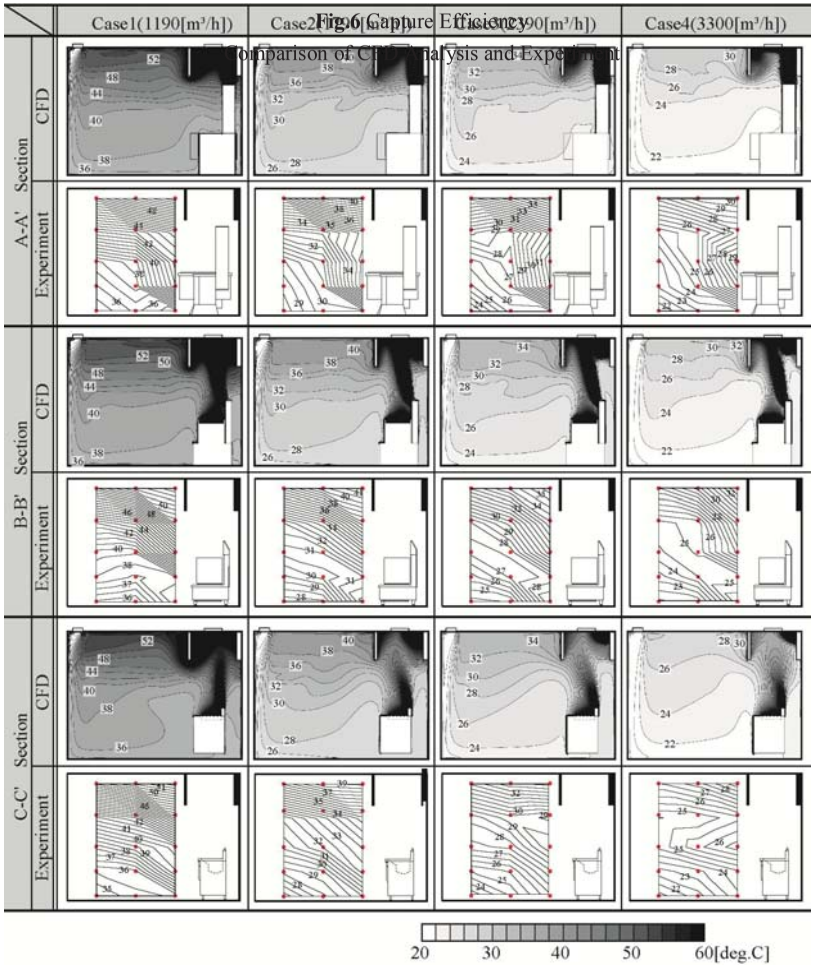


Fig.7 Vertical Distributions of Temperature in A-A', B-B' and C-C' Section
Comparison of CFD Analysis and Experiment

Fig.6 Capture Efficiency
Comparison of CFD Analysis and Experiment

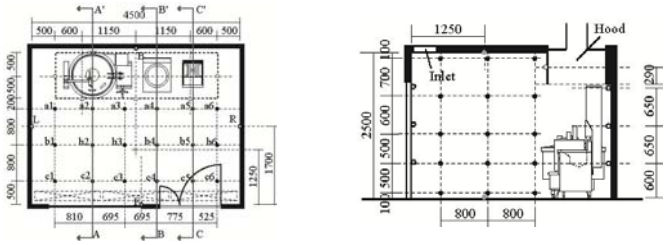


Fig.8 Experimental Measurement Point of Temperature

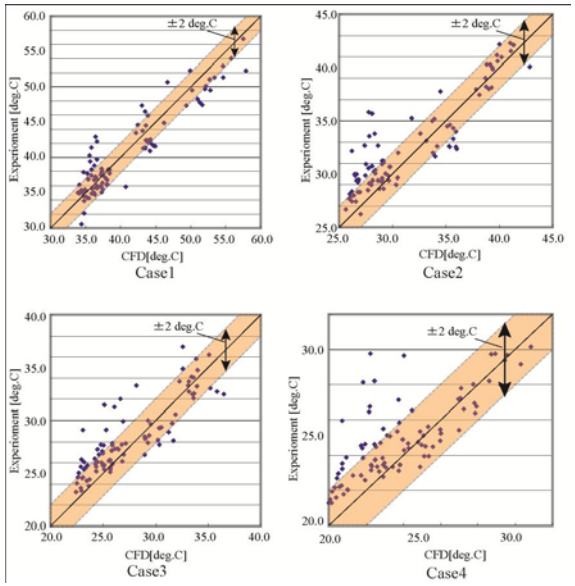


Fig.9 Correlation Chart between CFD and Experiment

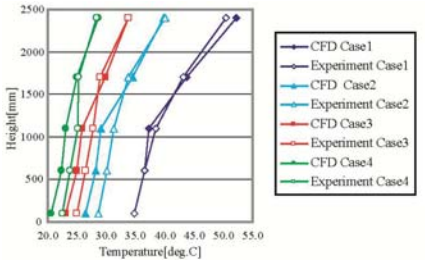


Fig.10 Vertical Temperature Distribution (Plane Measurement Point Average)

Table 1 CFD Outline

CFD code	Fluent 6.3
Turbulence Model	Standard k-ε Model
	RNG k-ε Model
Algolism	SIMPLE
Discretization Scheme	QUICK
Calculated Domain	4600*4200*3000mm

Table 2 Boundary Conditions of Room

Supply and Exhaust Flow	Inlet	θ=293.15[K], See Table 3
	Outlet	See Table 3
	Ceiling	Pressure 0 Pa
Wall		Generalized log law Adiabatic

Table 3 Parameter of Supply and Exhaust Flow Rate

		Exhaust Flow Rate of Hood[m³/h]	Supply Flow Rate[m³/h]
Kettle	Case1-K	649.1	1298.3
	Case2-K	973.7	1947.4
	Case3-K	1298.3	2596.6
	Case4-K	3033.1	6066.1
	Case5-K	4044.1	8088.2
Range	Case1-R	388.7	777.5
	Case2-R	583.1	1166.2
	Case3-R	777.5	1555.0
	Case4-R	1503.8	3007.6
	Case5-R	2005.1	4010.1
Fryer	Case1-F	155.7	311.4
	Case2-F	233.5	467.0
	Case3-F	311.4	622.7
	Case4-F	1503.8	3007.6
	Case5-F	2005.1	4010.1

Table 4 Surface Temperatures of Equipments

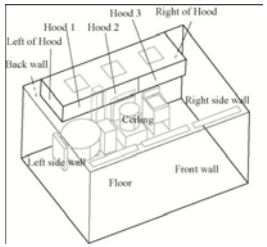
		temperautre[K]
Kettle	a	312.89
	b - e	309.19
	f - o	295.09
Range	a,b	311.26
	c	332.43
	d	372.73
	e	387.16
	f	340.55
	h	321.93
	g	317.80
	i	321.93
	j	308.10
	k	297.97
Fryer	a	309.20
	b,c	313.11
	d	337.36
	e	312.19
	f,g	316.98
	h	298.60
	i	309.98
	j -1	337.04

Table 5 Inlet Conditions of Equipment

		Velocity[m/s]	k[m²/s²]	ε[m²/s³]	Angle[°]	Temperature[K]	Length[m]
Kettle	Combustion Gas	3.07	9.41E-02	8.11E-01	90	662.09	0.08
	Fresh Air	0.68	4.61E-03	2.93E-03	90	339.08	0.24
	Inlet	0.14	1.88E-04	6.42E-06			0.9
	Pot	0.0217	4.72E-06	2.67E-08	90	373.15	0.9
Range	Combustion Gas	※See Table 6			60.00	698.57	0.08
	Fresh Air	0.68	4.62E-03	1.01E-02	54.32	351.92	0.07
	Inlet	0.15	2.18E-04	1.40E-05			0.51
	Pot	0.0224	5.02E-06	5.29E-08	90	373.15	0.5
Fryer	Combustion Gas	0.93	8.68E-03	4.04E-02	57.43	409.87	0.045
	Fresh Air	0.44	1.90E-03	1.25E-02	90	340.57	0.015
	Inlet	0.07	4.93E-05	1.50E-06			0.52
	Pot	0.0233	5.41E-06	7.38E-08	90	373.15	0.4

Table 6 Exhaust Conditions of Range

	Velocity[m/s]	k[m²/s²]	ε[m²/s³]
Exhaust 1	5.04	2.54E-01	3.75E+00
Exhaust 2	3.98	1.58E-01	1.85E+00
Exhaust 3	2.91	8.48E-02	7.24E-01
Exhaust 4	1.83	3.36E-02	1.81E-01
Exhaust 5	0.69	4.70E-03	9.46E-03
Exhaust 6	0	0	0
Exhaust 7	0	0	0
Exhaust 8	0	0	0



Name of the Surface

Table 7 CFD Outline

CFD code	Fluent 6.3
Turbulence Model	Standard k-ε Model
Algolism	SIMPLE
Discretization Scheme	QUICK
Calculated Domain	4500*3400*2500mm

Table 8 Parameter Supply and Exhaust Flow Rate

Supply Air Temperature[deg.C]		18
Exhaust Flow Rate [m³/h]	Case1	1190
	Case2	1790
	Case3	2390
	Case4	4400

Table 9 Surface Temperatures of Room

Wall name	Height	Case1 [deg.C]	Case2 [deg.C]	Case3 [deg.C]	Case4 [deg.C]
Left side wall	1590-2500mm	40.1	31.3	25.6	22.7
	900-1590mm	33.9	26.9	25.1	22.5
	0-900mm	31.7	26.2	24.3	21.9
Right side wall	1590-2500mm	42.5	32.6	28.6	25.7
	900-1590mm	38.3	31.0	27.8	25.1
	0-900mm	35.1	28.9	25.7	23.3
Front wall	1590-2500mm	36.9	28.6	25.2	22.1
	900-1590mm	34.2	27.3	24.5	21.9
	0-900mm	32.9	26.8	24.1	21.5
Back wall	1590-2500mm	48.2	39.4	35.1	32.1
	900-1590mm	40.2	34.8	32.9	29.1
	0-900mm	36.3	31.1	29.7	26.3
Left of Hood		58.6	45.8	40.1	32.1
Hood 1		57.2	44.2	37.9	31.4
Hood 2		66.9	55.8	50.2	44.3
Hood 3		65.8	53.8	46.5	42.6
Right of Hood		68.3	52.8	43.8	37.1
Ceiling		40.7	34.4	31.6	27.6
Floor		28.9	26.4	25.8	24.6

A Proposal of Hybrid Ventilation System Using Stack Effect in High-rise Buildings

Sungmin Yoon[1], Jungmin Seo[1], b, Joonghoon Lee[2], and Doosam Song[3]

[1] Graduate School, Sungkyunkwan Univ., 300 Chunchun-dong, Suwon 440-746, Korea
[2] Institute of Technology, Samsung C&T Corporation, Seoul, Korea
[3] Dept. of Architectural Eng., Sungkyunkwan Univ., 300 Chunchun-dong, Suwon 440-746, Korea

Abstract

This study proposes the hybrid ventilation system and its design methods for high-rise buildings. The proposed hybrid ventilation system uses natural driving power for ventilation based on air flow in the whole building and indoor and outdoor pressure distributions. Furthermore, it solves the troubles of the conventional natural or mechanical ventilation systems. This paper presents theories and a process for duct design for natural ventilation which forms the basis of a hybrid ventilation system in high-rise buildings. Also, the validity of the proposed design method will be analyzed by simulations.

Keywords: Hybrid ventilation, Natural ventilation, Stack effect, High-rise residential building, Duct design.

1. Introduction

Recently with rising demands for environmentally friendly building and increasing interest in indoor air quality, interest in hybrid ventilation that combines natural and mechanical ventilation is also increasing. Hybrid ventilation can overcome the problems of conventional ventilation systems and guarantee proper ventilation rate in each target space while saving energy consumption for ventilation. In this respect, hybrid ventilation is being actively applied and researched.

Meanwhile, as high-rise buildings increase domestically and internationally, stack effect has become a remarkable and is greatly influencing the ventilation performance of each floor. In spite of this fact, stack effect is generally not considered during the design phase of ventilation systems, and many problems of mechanical ventilation system caused by stack effect are being reported.

This study proposes a hybrid ventilation system in high-rise residential buildings that takes into consideration the pressure distribution and air flow in and outside the building, and attempts to establish a method of duct design which forms the basis of this system. Accordingly, this paper discusses the theory and process of duct design to maximize the performance of natural ventilation. Furthermore, the validity of the proposed duct design method will be verified through the network simulation technique.

2. Outline of hybrid ventilation system

The proposed hybrid ventilation system sets the supply/exhaust paths by taking into consideration the pressure distribution and air flow in a high-rise building by stack effect and

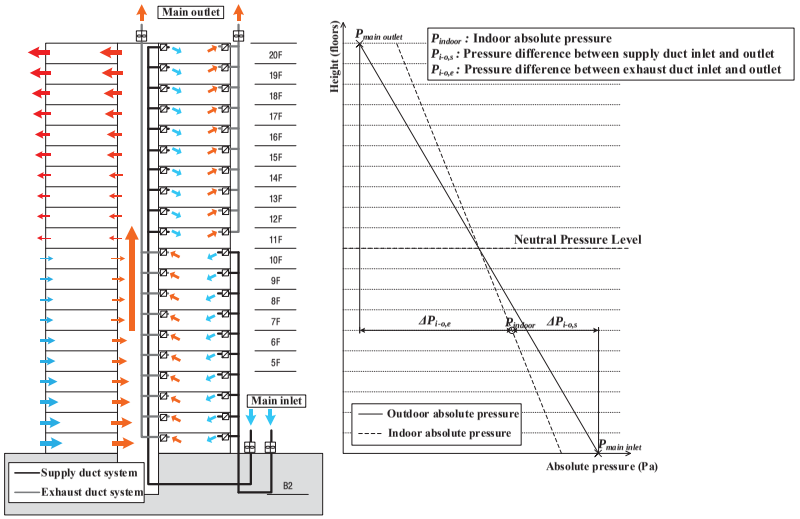


Fig. 1 Outline of the Hybrid ventilation system using stack effect in high-rise building

reverse stack effect. This enables natural driving power (stack effect) to be used for ventilation as much as possible to reduce energy consumption. When natural driving power is insufficient, the supply and exhaust fans are operated as auxiliary means so that constant ventilation will be always guaranteed for each household.

In high-rise buildings, such pressure distribution and airflow as shown in Fig. 2 are generated by the stack effect due to temperature difference between the inside and outside of the building. Therefore, if we construct the ventilation system based on the pressure distribution and airflow in Fig. 2, it is possible to supply fresh air to every room with minimum energy consumption. Meanwhile, to maximize the ventilation driving power by

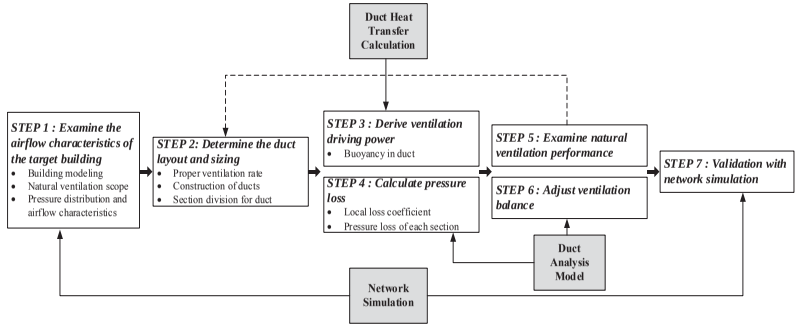


Fig. 2 Design process of duct in hybrid ventilation system

stack effect, “the construction of supply/exhaust ducts that reflect air flow and minimize pressure loss” is most important.

3. Duct design process

This chapter describes the process of duct design which forms the basis of the hybrid ventilation system design. Fig. 2 shows the duct design process along with review contents and method for each step.

3.1 STEP 1: Examine the air flow characteristics of the target building

3.1.1 Building modeling

Examine the pressure distribution and airflow characteristics in the target building by stack effect through building modelling.

3.1.2 Determination of natural ventilation scope

Through climate analysis, determine the temperature difference between inside and outside (ΔT) which the cause of the stack effect in the building. Based on this, examine the possibility of natural ventilation of each floor of the target building and determine the natural ventilation scope. Within this scope, set as the design temperature condition that is minimum temperature difference (ΔT) to arouse the driving force for ventilation.

3.2 STEP 2: Determine the duct layout and sizing

3.2.1 Determination of the proper ventilation rate

Determine the ventilation rate based on the ventilation code by country or the air pollutant concentration of the target space. The determined ventilation rate is set as the design air flow rate in the duct design step.

3.2.2 Construction of the duct layout

As shown in Figure 1, determine the duct layout to achieve maximum ventilation driving power in consideration of the air flow and pressure distribution in the building by stack effect.

Decide the duct size according to the ventilation demand. In order to achieve the maximum ventilation driving power for the supply/exhaust ducts, the ducts must be constructed in such a manner to maximize the pressure difference between duct inlet and outlet ($\Delta P_{i\text{-}o}$) and the buoyancy in the duct (ΔP_{se}). Thus, in order to achieve the maximum pressure difference between duct inlet and outlet ($\Delta P_{i\text{-}o}$), based on the indoor and outdoor pressure distributions, the outside air inlet must be placed at the point of the maximum absolute pressure of outside air and place the outlet of the indoor air in the exhaust duct at the point of minimum absolute pressure of outside air. In addition, to achieve buoyancy (ΔP_{se}) in the duct through heat exchange on the path, the supply duct must be placed in the vertical space of the building from the outside air inlet through underground, and the exhaust duct must be also placed in the vertical space of the building. The supply inlet and exhaust outlet for each room must be installed on the basis of the air flow direction by stack effect so as to improve ventilation efficiency.

3.2.3 Section division for duct

To calculate the buoyancy and pressure loss of the duct for each household, the air flow rate in the duct, cross sectional area, and shape changing are main factors to consider how to divide sections of the duct.

3.3 STEP 3: Derive ventilation driving power

To achieve a certain ventilation rate for each household using natural power, we must consider the pressure difference (ΔP) which provides the ventilation driving force for the duct construction proposed in this study. Assuming that the temperature inside the duct is constant and the air is stationary state and non-compressive, the pressure difference based on the Bernoulli's equation is defined as the following expression (Eq. 1). This can be used to derive the ventilation driving power for supply/exhaust ducts in each household.

$$\Delta P = P_i - P_o + \rho g(H_i - H_o)$$
$$\Delta P = \Delta P_{i-o} + \Delta P_{se} \quad \text{(Eq. 1)}$$

where P_i is the absolute pressure at duct inlet, P_o is the absolute pressure at duct outlet, ρ is the density of air within duct, g is the acceleration due to gravity, H is the elevation, ΔP is the pressure difference that lead to air movement, $\Delta P_{i\text{-}o}$ is the pressure difference between duct inlet and outlet, and ΔP_{se} is the thermal gravity effect.

$$\Delta P_{se} = \sum_{i=1} \Delta p_{se_i} \quad \text{(Eq. 2)}$$

where Δp_{se} is the thermal gravity effect of location i.

The pressure difference between duct inlet and outlet for the supply/exhaust ducts in each household ($\Delta P_{i\text{-}o}$) can be derived from the difference of absolute pressures between the inlet and outlet of the duct on the pressure distribution in and outside the building which was investigated in STEP 1. The buoyancy in the supply/exhaust duct (ΔP_{se}) can be obtained by the sum of the buoyancy values for the vertical section which corresponds to the supply/exhaust path of each household as shown in expression (Eq. 2). To determine the buoyancy in each vertical section of the duct, this study used the calculation module for the duct heat transfer presented in ASHRAE for duct design as shown in expressions (Eq. 3) and (Eq. 4) [1]. From the average outlet and inlet air temperatures of each section of the duct that have been calculated through these expressions, we can derive the buoyancy for each section.

$$t_l = \frac{t_e(y-1) + 2t_a}{(y+1)} \quad \text{(Eq. 3)}$$

$$y = \frac{0.5DV\rho c_p}{UL} \quad \text{(Eq. 4)}$$

where t_l is the temperature of air leaving duct, t_e is the temperature of air entering duct, t_a is the temperature of air surrounding duct, and D is the diameter of duct, L is the duct length, U is the overall heat transfer coefficient of duct wall, and c_p is the specific heat of air.

3.4 STEP 4: Calculate pressure loss

This step determines the pressure loss of the supply/exhaust ducts for each household. The calculation of pressure loss uses the analysis model created on the basis of the basic equation for air flow in the duct.

3.4.1 Basic equation for air flow in the duct

With the Darcy-Weisbach Equation, we can express the pressure loss in the duct as expression (5):

$$\Delta p_t = \left(f \frac{L}{D} + \sum C \right) \frac{\rho V^2}{2} \quad \text{(Eq. 5)}$$

where Δp_t is the total pressure loss due to friction and dynamic losses, f is the friction factor and C is the local loss coefficient.

The air flow rate can be represented by expression (Eq. 6) based on the cross sectional area of the duct and expression (Eq. 5). Here, the friction coefficient was determined with the Colebrook's equation.

$$Q = VA$$
$$Q = \sqrt{\frac{2A^2 \Delta p_t}{\left(fL/D + \sum C \right) \rho}} \quad \text{(Eq. 6)}$$

where Q is the air flow rate and A is the cross-sectional area of duct.

3.4.2 Calculation of pressure loss

The total pressure loss of the supply/exhaust ducts for each household is determined by first calculating the pressure losses in each section of the duct divided in STEP 2 using the basic equation for air flow of the duct as shown in expression (Eq. 7) and adding to them the pressure loss of the sections corresponding to the supply/exhaust paths of each household.

Because the duct air flow equation is nonlinear, this study used the MATLAB fsolve function for solving nonlinear equation to obtain the numerical answer.

$$\Delta p_{t_i} = \Delta p_{f_i} + \sum_{j=1}^{m} \Delta p_{ij} + \sum_{k=1}^{n} \Delta p_{ik}$$
$$\Delta P_t = \sum_i \Delta p_{t_i} \quad \text{(Eq. 7)}$$

where Δp_{ti} is the net total pressure loss for i-section, Δp_{fi} is the pressure loss due to friction for i-section, Δp_{ij} is the total pressure loss due to j-fittings for i-section, Δp_{ik} is the pressure loss due to k-equipment for i-section, and ΔP_t is the total pressure loss between duct inlet and outlet.

3.5 STEP 5: Examine natural ventilation performance

Examine whether the design air flow rate can be achieved from the ducts constructed in such a manner to attain maximum ventilation driving power for each household. If the pressure loss in the duct determined above is equal to the natural ventilation driving power of each household, the design air flow rate for this target space can be attained by natural driving power only. Therefore, the criterion for the supply/exhaust ducts of each household was defined as the difference between the ventilation driving power and the pressure loss as shown in expression (Eq. 8). If this is not satisfied, the duct specification in STEP 2 must be changed to satisfy this criterion

$$\Delta P - \Delta P_t \geq 0 \quad \text{(Eq. 8)}$$

3.6 STEP 6: Adjust ventilation balance

Even if the expression (Eq. 8) is satisfied in the previous step, the proposed ventilation system causes ventilation imbalance by the location (height) of each household and the supply and exhaust air flow rates differ by household because it uses stack effect and buoyancy in the duct as ventilation driving power. Thus, this step solves the ventilation imbalance between households and between supply and exhaust through adjustment of the ducts by installing a damper. As shown in expression (Eq. 9), the opening rate of the damper is adjusted to make the total pressure loss become equal to the ventilation driving power for the supply/exhaust ducts of each household so as to achieve the same air flow rate (design air flow rate) for the supply/exhaust ducts of all households. Expression (Eq. 9) is a function of the damper's local loss coefficient. The solution is derived through numerical analysis. The derived solution is the local loss coefficient of the damper. Determine the opening rate of the damper based on this.

$$\Delta P = \Delta P_t(C_d) \quad \text{(Eq. 9)}$$

where C_d is the damper loss coefficient based on opening rate.

3.7 STEP 7: Validation with network simulation

In order to determine whether the proposed ventilation system achieves the proper ventilation rate meeting the design conditions and whether the ventilation rate is identical between supply and exhaust and between different households, add ducts to the building model used in STEP 2 and check the results.

4. Case study

This chapter verifies the validity of the design method presented in chapter 3. For this validity verification, the pressure distribution in the whole building, air flow characteristics, the duct construction (layout, dimension) determined in chapter 3, heat exchange characteristics, and pressure loss have been simulated, and the duct for natural ventilation was designed in accordance with the design method presented above. Then, it is determined whether the proper ventilation rates of the analyzed households are achieved as designed.

4.1 STEP 1

The building to which the design method of this study was applied was a typical flat type apartment building in Korea with 2 floors underground and 20 floors above ground. The underground part is used for parking lots and the above ground part is used for residences. There are two households with the size of around 100m^2 on each floor. The elevator shaft is located between the two households and the stairwell is interfacing with the outer wall of the corridor.

According to the proposed design process, the natural ventilation scope based on stack effect was determined. Natural ventilation was made possible in every household for the ducts of the appropriate sizes determined in consideration of the allowable indoor wind velocity and the heat exchange efficiency of the ducts. To enable ventilation driving power in this case, the indoor and outdoor temperature difference (ΔT) must be at least 17℃. In other words, if the indoor temperature is set to 22℃[2], the outside air temperature must be 5℃ or lower to give ventilation driving power. Thus, in Suwon City which was analyzed in this study, the percentage of the area that allowed natural ventilation through stack effect was approximately 30%.

Natural ventilation performance was analyzed for three households on the 11th to 13th floors which are roughly located at the neutral zone of the building and the pressure difference by stack effect is relatively small. The air flow characteristics in the building and the pressure distributions in and outside the building were derived using CONTAMW which is a network simulation tool. As shown in Fig. 3, each floor of the analysis model consists of the inside space of the household, corridor, and elevator. Each space was modeled as one zone without any internal sections. For the stairwell and elevator shaft space, the nodes are vertically connected. The interior temperature was set to 22.0℃, and the exterior temperature was set to 5℃ as described above. Although wind velocity and direction affect the indoor and outdoor pressure distributions, they were not considered in this case study. The air leakage data for each component used the results of a previous study, which are shown in Table 1.

The analysis results in Fig. 4 show the pressure differences which form the basis of air flow in each section. In the lower floor part below the 9th floor which is the neutral zone, air flows from the outside into the interior space of each household, and air moves upward through the stairwell, and the elevator shaft. In the higher floor part, on the contrary, the air rising from the lower floor part moves into the inside of each household due to the high pressure of the stairwell and the elevator shaft. In this case study, on the 11th to 13th floors which are the target area for the analysis of natural ventilation performance, because they are located at upper part of the neutral zone, the air rising through the stairwell and the elevator shaft flows into the households through the corridor and flows out through the exterior walls.

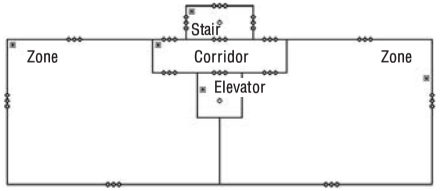


Fig. 3 Analysis model plan

Table 1 Air leakage data

Building component	Air leakage data	Source
Exterior wall	$EqLA_{10}$[a]1.21 cm^2/m^2	[3]
Residential entrance door	$EqLA_{10}$70 cm^2/item	
Elevator door	$EqLA_{10}$ 325 cm^2/item	
Stairwell door	$EqLA_{10}$ 120 cm^2/item	
Swing door located on lobby and basement floors	430 CMH at 50 Pa	[4]

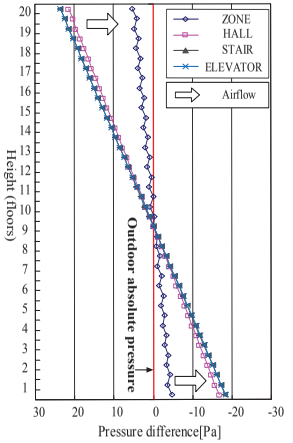


Fig. 4 Pressure distribution

4.2 STEP 2

In accordance with the ventilation standards for domestic residential buildings, the target ventilation rate for each target space was set to 0.7 times/h. Since the volume of each household is 360m^3, the target ventilation rate is 252CMH. The ducts were constructed as shown in Fig. 5 to raise ventilation efficiency depending on the pressure distribution and indoor air flow of the target building. The outside air inlet was located on the ground, and the outlet of the indoor air through the exhaust duct was located at the top of the building. The depth of the underground duct was decided as 5m in consideration of the point where underground temperature is stabilized[5]. The elevator shaft was decided as the vertical space in the building for the passage of the supply/exhaust ducts because it can minimize the length of the supply inlet and exhaust outlet to the households and the temperature is relatively high because it does not interface with the outside air. The locations of the supply inlet and exhaust outlet for each room were decided on the basis of the air flow direction for the households on the 11th to 13th floors as described above. The supply inlet was installed at the doorway of each household, and the exhaust outlet was installed at the exterior wall to improve the ventilation efficiency in the household. Fig. 5 shows the indoor and outdoor pressure distributions in the whole building, and indicates on the absolute pressure line the pressure differences ($\Delta P_{i\text{-}o}$) between the inlet and outlet of the supply/exhaust ducts for each household on the 11th to 13th floors. Fig. 6 shows the determined sections of ducts and the calculation results for each section in the following step.

4.3 STEP 3

As input conditions for outlet temperature calculation for each section of the duct, the underground temperature was set to 12℃[5], and the temperature of the shaft for heat exchange of the duct was set to 22℃. For the heat transfer coefficient, the value of ASHRAE was used. From these outlet and inlet temperatures for each section, the buoyancy of each section of the duct was derived. The ventilation driving power calculated using them are summarized in Fig. 6 and Table 4. In this case study, the temperature for all sections of the exhaust duct was set to 22℃ because the temperature of the air discharged from the room is equal to the temperature of the elevator shaft which is the path of the exhaust duct. Table 2 shows the input conditions for heat exchange for each section of the supply duct and the calculated outlet temperatures.

Table 2 Heat transfer calculations for supply duct

Duct Section	Airflow, *CMH*	Duct Size, *mm ϕ*	Duct length, *m*	Velocity, *m/s*	[a]heat transfer coefficient, *W/m^2·K*	Inlet Temperature, ℃	Outlet Temperature, ℃
1	756	500	53	1.1	3.5	5	14.7
3	504	500	3	0.7	3.4	14.7	15.3
5	252	250	3	1.4	3.5	15.3	15.6

Note) [a]Uninsulated sheet metal (1997 ASHRAE handbook—fundamentals. Chapter 32.)

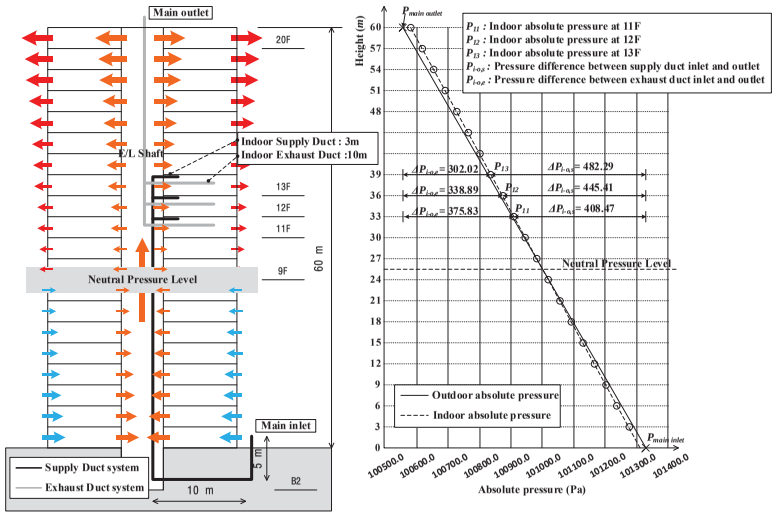


Fig. 5 Air flow and construction of ducts in the target building

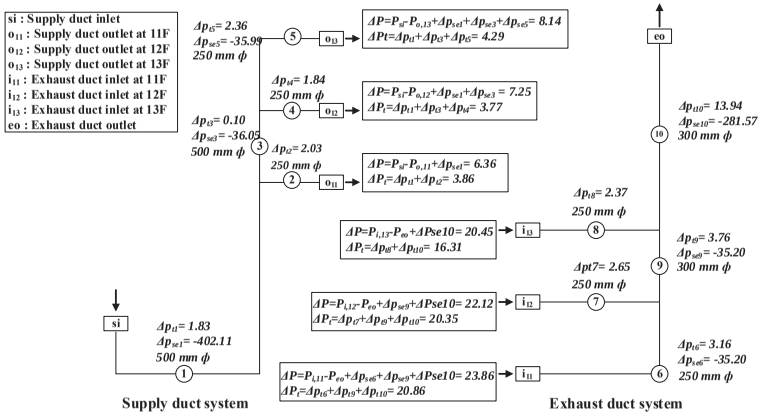


Fig. 6 Sections for calculation of pressure losses in the duct and the calculation results for each section

4.4 STEP 4

Table 3 shows the input conditions for pressure loss calculations for each section of the duct and the calculation results. The total pressure loss for the supply/exhaust ducts of each household are summarized in Fig. 6 and Table 4.

Table 3 Pressure loss calculations

[a]Duct Section, *i*	Airflow, *CMH*	Duct Size, *mm* ϕ	Duct length, *m*	Summary of Local Loss Coefficients	Friction Factor, dimensionless	Section Pressure Loss(Δp_{t_i}), Pa
1	756	500	53	0.13	0.023	1.83
2	252	250	3	1.33	0.025	2.03
3	504	500	3	0.16	0.025	0.10
4	252	250	3	1.18	0.025	1.84
5	252	250	6	1.29	0.025	2.36
6	252	250	13	1.29	0.025	3.16
7	252	250	10	1.17	0.025	2.65
8	252	250	10	0.94	0.025	2.37
9	504	300	3	1.38	0.022	3.76
10	756	300	24	1	0.021	13.94

Note) [a]See figure 6

4.5 STEPS 5 and 6

We examined on the basis of expression (Eq. 8) whether the design air flow rate can be satisfied for the ducts using the natural ventilation driving power and the total pressure loss for the supply/exhaust ducts of each household. It was found that the proper ventilation rate for each household analyzed could be achieved. However, the ventilation rate varied by household due to the pressure difference by stack effect and the difference in buoyancy inside the duct by height. Therefore, a damper was installed at the end of the duct to each household (sections 2, 4, 5, 6, 7, and 8 in Fig. 6) so that the air inflow rate could be adjusted by the opening rate of the damper. The local loss coefficient according to the opening rate of the damper was determined using expression (Eq. 9), which is shown in Table 4. Table 4 shows the values calculated in each step of the case study.

Table 4 Step results

	STEP 3			STEP 4	STEP 5	STEP 6
Floor	Pressure difference between i and o ($\Delta P_{i\text{-}o}$), Pa	Thermal gravity effect (ΔP_{se}), Pa	Pressure difference (ΔP), Pa	Total pressure loss (ΔP_t), Pa	ΔP-ΔP_t, Pa	Local loss coefficient
11F S	408.47	-402.11	6.36	3.86	2.50	2.01
11F E	375.83	-351.97	23.86	20.86	3.00	2.47
12F S	445.41	-438.16	7.25	3.77	3.48	2.80
12F E	338.89	-316.77	22.12	20.35	1.77	1.46
13F S	482.29	-474.15	8.14	4.29	3.85	3.09
13F E	302.02	-281.57	20.45	16.31	4.14	3.40

4.6 STEP 7: result

This step examines whether the ducts determined above achieves the proper ventilation rate for each household as designed, and can solve the ventilation imbalance between households through dampers. For this purpose, the duct was additionally modeled in the network model in Fig. 3. The basic input conditions for the network model were set to the same values as those in STEP 2. For the boundary conditions of the ducts, the temperature of each duct section and the local loss coefficient of the damper which were determined above were used. Table 5 shows the input conditions for the duct model. The calculations of the ventilation rate of the supply/exhaust ducts for each household are shown in Fig. 7. The error range compared to the design air flow rate 252CMH was around 1%. The ventilation rates of the households and the supply/exhaust ducts were almost identical to the design air flow rate. Thus, the ducts designed by the proposed design method achieved the proper ventilation rate

of each household by natural driving power and solved the ventilation imbalance of the conventional ventilation systems.

Table 5 Summary of duct model parameters (CONTAMW)

Duct Flow Element Model : Darcy-Collebrook resistance		
Model Parameters	Roughness	0.03 *mm*
	Shape	Circle
	Diameter	Figure 6
Segment Data	Duct segment length	Figure 5
	Sum of loss coefficients	Tables 3 and 4
Junction Data	Relative elevation	Elevation of Duct Section
	Tmperature	Outlet Temperature
		in Table 2

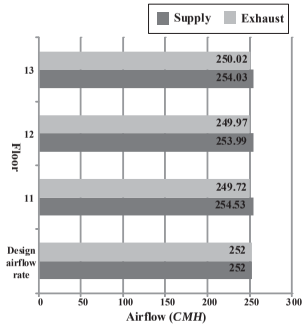


Fig. 7 Comparison of design air flow rate and simulation results.

Acknowledgments

This work is supported by Sustainable Building Research Center of Hanyang University which was supported the SRC/ERC program of MEST (grant # R11-2005-056-02004-0).

References

1. ASHRAE. 1997 ASHRAE handbook—fundamentals. Atlanta: American Society of Heating, Refrigerating and Air-Conditioning Engineers; 1997. p. 32.14-32.15.

2. SAREK. SAREK handbook. The Society of Air-Conditioning and Refrigerating Engineers of Korea; 2001. p. 1.2-1.3.

3. Jae-Hun Jo et al., Characteristics of pressure distribution and solution to the problems caused by stack effect in high-rise residential buildings, Building and Environment 42 (1) (2007) 263-277.

4. Pedersen CO, Fisher DE, Spitler JD, Liesen RJ. Cooling and heating load calculation principles. American Society of Heating, Refrigerating and Air-Conditioning Engineers; 1998. p. 131–52.

5. Leigh. SB, Jung. HS, A Study for Developing Design Tools and Guidelines to Prevent Surface Condensation in the Underground Space. AIK, 2002, p.249-58.

Simple error reduction in tracer-gas field-measurements of air handling units

Peter G. SCHILD[1]

[2] SINTEF Building & Infrastructure, Oslo, Norway. Peter.Schild@sintef.no

Abstract

Tracer gas measurements are an unparalleled means of measuring air recirculation, leakage, and air flow rates in air handling systems [1-5]. *However, such measurements are subject to significant measurement uncertainty in field conditions. A common problem is imperfect mixing of tracer gas.*

One method of error minimization is to use a constrained regression model based upon mass conservation equations. This technique is widely used in multizone tracer gas studies. The method reported in this paper uses robust regression (least trimmed weighted squares) to solve the mass flow rates in air handling units (AHU) for balanced ventilation, including any recirculation/leakage in the AHU, external short-circuiting, and ex-/infiltration caused by imbalance. The method is simple enough to implement in spreadsheet software, and works even when measurement data from one or more of the sampling points, or one of the two dosing points, has to be rejected as erroneous.

Keywords: Tracer gas, Measurement, Air flow, Leakage, Recirculation, Infiltration, Ventilation, Building

1. Introduction

1.1 Background for this study

The method presented in this paper was developed to analyse tracer gas data in an IAQ audit of AHUs in schools [6]. The measurement challenges included:

- Short ducts between dosing points and sampling points, in particular, fresh air ducts.
- Many ducts connected directly to an AHU via a plenum box, each with a different flow rate. This makes it difficult to achieve a homogeneous tracer concentration in the air flowing into the AHU using just one tracer gas injection pump.
- Uneven distribution of tracer gas in air leaving the AHU, due to incomplete mixing of recirculated air inside the AHU. If a plenum box distributes this air to multiple ducts, the ducts will have different concentrations of tracer gas. It is practically impossible to measure the volume-averaged concentration accurately with just one sampling tube and no knowledge of the flow rates in the different ducts connected to the plenum box.

The above challenges made it difficult to accurately estimate mass flow rates and recirculation fractions using conventional simple methods, as data from important tracer gas sampling points occasionally had to be rejected.

1.2 Error minimization in earlier studies

Some studies have focused on ways to maximize mixing of tracer gas at injection and sampling points in ducted ventilation systems [3],[10],[11]. Another means of error reduction

is to use numerical techniques to estimate the mass flows more accurately, which is the main focus of this paper. Conventional tracer gas measurements in air handling units (AHU), for example described in [7],[8], use simple equations to estimate recirculation fractions, typically equations 1 & 3 below. Such calculations do not exploit the assumption of mass conservation of the whole system. Roulet *et al.* have analyzed errors for different ways of estimating AHU recirculation fractions [9]. In multizone tracer gas studies the air flows are generally resolved by matrix operations of mass balance equations; see Chapter III in [12]. Measurement uncertainties can lead to calculating fictitious negative flows or flows between non-connected zones, This problem has been solved with constrained least squares (enforcing positive flows) [12],[14],[15] or Bayesian methods [12],[13].

1.3 Definitions of recirculation fractions

The relations here are valid for measurements of AHUs with negligible casing leakage (Fig.1).

- Recirculation in the AHU of extract air to supply air:

$$R_{32,AHU} \equiv \frac{\dot{m}_{32,AHU}}{\dot{m}_2} = \frac{\dot{m}_{32,AHU}}{\dot{m}_{12} + \dot{m}_{32,AHU}} = \frac{c_2 - c_{1b}}{c_{3b} - c_{1b}} \quad \text{(Eq. 1)}$$

- Total recirculation of extract air to supply air (i.e. combination of recirculation in AHU and short-circuiting outside the building, from exhaust to fresh air inlet):

$$R_{32,tot} \equiv \frac{\dot{m}_{32,tot}}{\dot{m}_2} = \frac{\dot{m}_{32,AHU} + \dot{m}_{32,out}}{\dot{m}_{12} + \dot{m}_{32,AHU}} = \frac{c_2 - c_o}{c_{3b} - c_o} \quad \text{(Eq. 2)}$$

- Recirculation in the AHU from fresh air intake to exhaust air outlet. This can be significant in AHUs with rotary heat exchanger with a purge sector.

$$R_{14,AHU} \equiv \frac{\dot{m}_{14,AHU}}{\dot{m}_4} = \frac{\dot{m}_{14,AHU}}{\dot{m}_{34} + \dot{m}_{14,AHU}} = \frac{c_4 - c_{3b}}{c_{1b} - c_{3b}} \quad \text{(Eq. 3)}$$

- Total short-circuiting outside, from exhaust air to fresh air intake:

$$R_{41,out} \equiv \frac{\dot{m}_{41}}{\dot{m}_1} = \frac{\dot{m}_{41}}{\dot{m}_{12} + \dot{m}_{14,AHU}} = \frac{c_{1a} - c_o}{c_4 - c_o} \quad \text{(Eq. 4)}$$

1.4 Conventional method of estimating mass flow rates in AHUs

The equations below can be used to estimate all the mass flow rates based upon the tracer gas concentrations and dosing rates (d_1, d_3), and the recirculation fractions calculated above. The same approach is used by Roulet & Vandaele (Section V.3 in [12]), and by Manz *et al.* [16], though both of these assume slightly different flow networks or fan locations, and dosing/sampling points compared to this study (Fig.1). The flow network for Fig.1 is given here:

$$\dot{m}_1 = \dot{d}_1 / (c_{1b} - c_{1a}) \quad \text{(Eq. 5)}$$

$$\dot{m}_3 = \dot{d}_3 / (c_{3b} - c_{3a}) \quad \text{(Eq. 6)}$$

$$\dot{m}_2 = \frac{\dot{m}_1 - R_{14,AHU}(\dot{m}_1 + \dot{m}_3)}{1 - R_{32,AHU} - R_{14,AHU}} \quad \text{(Eq. 7)}$$

$$\dot{m}_4 = \dot{m}_1 + \dot{m}_3 - \dot{m}_2 \quad \text{(Eq. 8)}$$

$$\dot{m}_{32,AHU} = R_{32,AHU}\ \dot{m}_2 \quad \text{(Eq. 9)}$$

$$\dot{m}_{12} = \dot{m}_2 - \dot{m}_{32,AHU} \quad \text{(Eq. 10)}$$

$$\dot{m}_{14,AHU} = R_{14,AHU}\ \dot{m}_4 \quad \text{(Eq. 11)}$$

$$\dot{m}_{34} = \dot{m}_4 - \dot{m}_{14,AHU} \quad \text{(Eq. 12)}$$

$$\dot{m}_{41} = R_{41,out}(\dot{m}_{12} + \dot{m}_{14,AHU}) \quad \text{(Eq. 13)}$$

- Net (useful) air exchange rate, corrected for internal recirculation inside AHU, i.e. independent of external short-circuiting:

$$\dot{m}_{net,AHU} = \max\{\dot{m}_{12}, \dot{m}_{34}\} \quad \text{(Eq. 14)}$$

- Net useful air exchange rate for the whole ventilation system (corrected for both internal recirculation and external short-circuiting):

$$\dot{m}_{net,syst} = \max\{\dot{m}_{12}, \dot{m}_{34}\} - \dot{m}_{32,out} \quad \text{(Eq. 15)}$$

- ...where $m_{32,\text{out}}$ is the part of the external short-circuiting (m_{41}) that leads extract air back to the supply air duct:

$$\dot{m}_{32,out} = \frac{\dot{m}_{41}}{1 + \frac{\dot{m}_{14,AHU}}{\dot{m}_{12}\,\dot{m}_{34}}\left(\dot{m}_{12} + \dot{m}_{34} - \dot{m}_{41} + \dot{m}_{14,AHU}\right)} \quad \text{(Eq. 16)}$$

- Resultant infiltration rate (exfiltration if negative) due to imbalance of flows in AHU.

$$\dot{m}_{\text{infil}} = \dot{m}_{34} - \dot{m}_{12} \quad \text{(Eq. 17)}$$

2. New method

2.1 Regression model description

The main objective of this study was to use constrained robust regression to provide a Maximum Likelihood estimate of the mass flows, and automatically omit suspect readings (outliers). The regression takes advantage of the fact that the system of mass conservation equations is over-determined, such that data from individual sampling or dosing points can be omitted if they are found to be too uncertain.

Fig.1 illustrates the flow paths in the studied ventilation systems.

2.2 Assumptions and preconditions

- AHU casing leakage is assumed negligible in relation to the recirculation flow rates.
- Duct leakage is assumed negligible in the ducts between the tracer gas dosing points and the AHU.

- Steady air flow rate (CAV). VAV systems should be manually overridden during the test.
- Perfect mixing of tracer gas (uniform concentration across over cross section) at the sampling points used in the regression analysis, and at points of entry into the AHU.
- It is assumed that all flow paths have a negligible time delay, except for the flow though the building from the supply duct to the extract duct. Quasi-steady concentration conditions are therefore assumed during each sampling interval at all sampling points.
- Because of the short measurement period, as mentioned above, we do not attempt to estimate the air exchange efficiency or total exchange rate in the building (i.e. resolve both flows Q_{03} and Q_{30} in [12]), however, infiltration/exfiltration caused by imbalance in the AHU (i.e. the difference between supply & exhaust flow) is calculated.

2.4 Algorithm for reconstructing concentrations and estimating flow rates

The equations below are used iteratively to find the optimum value for the five mass flows m_{12}, $m_{32,AHU}$, m_{34}, $m_{14,AHU}$, and m_{41} shown in Fig.1. . Equations 18-26 below estimate the correct concentrations at all measuring points (also the ones where we lack good measurements of the response variables). An iterative process finds the mass flows that result in the smallest deviation between estimated and measured values of tracer gas concentration

The explanatory variables (boundary conditions) are concentrations c_o (background) and c_{3a} (extract duct), and dosing rates d_1 and d_3, all of which must be measured accurately.

$$R_{41,out} = \frac{\dot{m}_{41}}{\dot{m}_{12} + \dot{m}_{14,AHU}} \quad \text{(Eq. 18)}$$

$$R_{14,AHU} = \frac{\dot{m}_{14,AHU}}{\dot{m}_{34} + \dot{m}_{14,AHU}} \quad \text{(Eq. 19)}$$

The following calculations are done for each logging interval (i) in the time series to estimate the likely tracer gas concentrations:

$$\hat{c}_{3b,i} = c_{3a,i} + \frac{\dot{d}_{3,i}}{\dot{m}_{34} + \dot{m}_{32,AHU}} \quad \text{where } \dot{d}_{3,i} \text{ is zero when no dosing} \quad \text{(Eq. 20)}$$

$$a_i = \frac{\dot{m}_{34}\,\hat{c}_{3b,i} + \dot{m}_{41}\,\dot{d}_{1,i}/(\dot{m}_{12} + \dot{m}_{14,AHU})}{\dot{m}_{34} + \dot{m}_{14,AHU}} \quad \text{where } \dot{d}_{1,i} \text{ is zero when no dosing} \quad \text{(Eq. 21)}$$

$$b_i = c_{o,i}\left(\frac{\dot{m}_{12} + \dot{m}_{14,AHU} - \dot{m}_{41}}{\dot{m}_{12} + \dot{m}_{14,AHU}}\right) \quad \text{(Eq. 22)}$$

$$\hat{c}_{1a,i} = \frac{a_i\,R_{41,out} + b_i}{1 - R_{41,out}\,R_{14,AHU}} \quad \text{(Eq. 23)}$$

$$\hat{c}_{1b,i} = \hat{c}_{1a,i} + \frac{\dot{d}_{1,i}}{\dot{m}_{12} + \dot{m}_{14,AHU}} \quad \text{where } \dot{d}_{1,i} \text{ is zero when no dosing} \quad \text{(Eq. 24)}$$

$$\hat{c}_{2,i} = \frac{\dot{m}_{12}\,\hat{c}_{1b,i} + \dot{m}_{32,AHU}\,\hat{c}_{3b,i}}{\dot{m}_{12} + \dot{m}_{32,AHU}} \quad \text{(Eq. 25)}$$

$$\hat{c}_{41,i} = \frac{\dot{m}_{34}\,\hat{c}_{3b,i} + \dot{m}_{14,AHU}\,\hat{c}_{1b,i}}{\dot{m}_{34} + \dot{m}_{14,AHU}} \quad \text{(Eq. 26)}$$

The sampled concentration data in thus study had a normal distribution, i.e. with zero kurtosis and skewness. However, it is heteroscedastic, i.e. the standard deviation is not constant but

increases with magnitude of tracer gas concentration, with an exponent of approx. 0.7; see Fig.2. This may partly be explained by the fact that higher concentrations are associated with lower volume flow rate, lower turbulence, and thus poorer mixing. Therefore a weighted least-squares estimator has been used, where the weighting function is the reciprocal of the variance of the difference between the estimated and measured concentrations. The error residuals are therefore all normalized.

Least Trimmed Sum of Squares (LTS) robust regression is basically ordinary least squares regression in which the largest residuals are omitted [17]. Equation 27 shows the LTS function, where the j is the j^{th} order of all the normalized residuals ranked in order of magnitude, and the trimmed subsample size (h) must satisfy $5\times N/2 < h \leq 5\times N$ where N is the number of intervals in the time series (i) and 5 is the number of response concentrations (k).

$$LTS = \sum_{j=1}^{h} \left[r_{[j]}^2 \right] \text{ where residual } r_{[j]} = r_{k,i} = \frac{c_{k,i} - \hat{c}_{k,i}}{\hat{\sigma}_{k,i}} \text{ and std.dev. } \hat{\sigma}_{k,i} \propto \hat{c}_{k,i}^{0.7} \qquad \text{(Eq. 27)}$$

Where the normalized residuals for the five reconstructed concentrations (response variables) are estimated thus:

For c_{1a}, c_{1b}, c_2: $$r_{k,i} = \frac{\left| c_{k,i} - \hat{c}_{k,i} \right|}{\hat{\sigma}_{k,i}} \quad \text{where} \quad \hat{\sigma}_{k,i} \propto \hat{c}_{k,i}^{0.7} \qquad \text{(Eq. 28)}$$

For c_{3b}: $$r_{3b,i} = \frac{\left| c_{3b,i} - \hat{c}_{3b,i} \right|}{\hat{\sigma}_{3b,i}} \quad \text{where} \quad \hat{\sigma}_{3b,i} \propto \hat{c}_{3b,i}^{0.7} \cdot \sqrt{2 - \frac{\hat{c}_{3b} - \hat{c}_{3a}}{\hat{c}_{3b}}} \qquad \text{(Eq. 29)}$$

For c_4: $$r_{4,i} = \frac{\left| c_{4,i} - \hat{c}_{4,i} \right|}{\hat{\sigma}_{4,i}} \quad \text{where } \hat{\sigma}_{4,i} \propto \hat{c}_{4,i}^{0.7} \cdot \sqrt{1 + \min\left[1, \frac{\max\left\{ \hat{c}_{1b,i}, \hat{c}_{3b,i} \right\}}{\hat{c}_{4,i}} \right]} \qquad \text{(Eq. 30)}$$

LTS was chosen due to its resistance to outliers in both the explanatory and response variables [18]. The amount of trimming (h) can be adjusted manually after studying a normalized plot of the residuals (Fig.3). The objective is to reject only sample data that is obviously erroneous. Anywhere from 80% to 95% are a typical values, but 100% may be used if there are no suspect data, in which case the method is identical to ordinary least squares.

Since it is impractical to solve LTS by 'brute-force', i.e. searching through all possible combinations of subsamples, efficient specialized search algorithms are used to provide near optimal solutions efficiently [18]. The search method used in this study was generic multivariate optimization (e.g. "Solver" tool in popular spreadsheet software), to minimize the error function (Eq. 28). The optimization must constrain the mass flows to be non-negative.

The iteration requires realistic initial guesses for the estimated parameters (m_{12}, $m_{32,AHU}$, m_{34}, $m_{14,AHU}$, and m_{41}). Equations 9 to 13 above are used to estimate these five mass flow rates based on the supply and exhaust fan rated/commissioned flow rates (m_2 and m_4 respectively), together with estimated recirculation fractions estimated with equations 1, 3 and 4.

2.5 Instrumentation and measurement procedure

An example of suitable instrumentation is a photoacoustic multi-gas monitor with continuous (multiplexed) monitoring in 6 channels. Sampling points should not be located inside the AHU, but rather be in the ductwork leading to or from the AHU, with sufficient distances to allow for good mixing [10]. The background concentration c_o is not measured on its own channel, but is ascertained by measuring in all 6 channels for a period before dosing starts.

This method can be carried out with continuous injection of one tracer gas (dosing at one location at a time, say 1 hour at each), or simultaneous injection of two different tracer gases at locations d_1 and d_3. In the case of using only one tracer gas (e.g. SF_6), one should inject at d_1 before d_3. When dosing has ceased at d_3, sampling should continue on all 6 channels for some length of time while the tracer gas concentration in the building decays. This step-down period can be used in the regression. A special feature of this decay period is that the tracer gas in the return duct(s) is better mixed compared to injection at d_3. The multiplexed samples must be interpolated in time (assuming an exponential curve during step-down), to obtain simultaneous values for each of the 6 channels, i.e. for each sampling point every 6^{th} value is a measurement while the other 5 are interpolated.

2.7 Limitations

Concentrations c_o and c_{3a} should not have systematic errors, as they are explanatory variables! The latter variable (c_{3a}) poses a challenge when dosing at d_3 if there are multiple extract ducts collected via a short plenum chamber, each with a different concentration. One solution is to close all ducts but one, or dose in all of the connecting ducts, neither of which are easy to do. Alternatively, if c_{3a} is erroneous, then the samples from a step-down period will be particularly valuable, or one can conduct a full regression (i.e. no trimming) to improve the estimates of the main flow rates but at the cost of the accuracy of the recirculation fractions. Measurement of c_2 must be accurate for at least half its samples; this is because there is no unique solution if c_2 is not used in the regression.

3. Results and discussion

Tests using synthetic measurement data containing deliberate outliers show that the method manages to trace these and eliminate them from the analysis, and thus perfectly recreate the mass flows, within the limitations mentioned above.

Further work: The next step is to extend the method to estimate variance in the mass flows and recirculation fractions. This should also take into account uncertainty in the explanatory

variables as well as instrumentation uncertainty. There is also a need to assess the uncertainty due to ignoring casing leakage. This can be done either analytically or by appropriate bootstrapping method for time series data.

Estimation accuracy can be further improved by taking covariance into account, for example correlation in time for the time series data during periods with steady-state conditions [13]. The method could also be combined with a priori information on measured flow rates and their variance, for example venturi-type fan inlets, such as described in [13].

4. Conclusions and further work

This study has demonstrated the application of robust regression using least trimmed weighted squares to improve the estimates of the various mass flows in air handling units for balanced ventilation, including recirculation, leakage and infiltration due to imbalance. The method provides constrained estimates of the mass flows (non-negative and conserved), and at the same time omits outliers from tracer gas measurements. The method can equally be used for measurements of CO_2, or water vapour recirculation in AHUs. The model can be applied to analyze air handling units with any degree of recirculation. Tests using synthetic measurement data show that the method provides better estimates than conventional simple methods for analysing tracer gas data in the presence of outlier data. It is simple enough to be implemented on spreadsheet software. Improvements to the method have been suggested.

Nomenclature

a_i , b_i	Intermediate parameters used in mass flow reconstruction algorithm [mg/kg]
c	Tracer gas concentration (gravimetric) [mg/kg]
$\dot{d}$	Dosing rate [mg/h]
$\dot{m}$	Mass flow rate [kg/h]
R	Recirculation ratio [-]

Subscripts:

1,2,3,4	Fresh, Supply, Return (extract), Exhaust air ducts
a,b	Location upstream or downstream of dosing, respectively
i	Sample number, for tracer gas concentration that is logged at regular intervals
k	Channel number of tracer gas sampling

Acknowledgements

The study was financed by Undervisningsbygg (UBF) and Utdannelsesetaten (UDE) in Oslo. The Norwegian energy agency Enova supported authorship of this paper.

References

[1] Roulet, C-A.; Foradini, F.; Cretton, P. “Use of tracer gas for disgnosis of ventilation systems”, *Proceedings, Healthy Buildings 1994*, Budapest, Vol.2, pp 521-526

[2] Roulet, C-A.; Foradini, F.; Deschamps, L. “Measurement of air flow rates and ventilation efficiency in air handling units”. *Proceedings, AIVC 20th Conference and Indoor Air 99*. Vol.5, 1999

[3] Cheong, K.W. “Airflow measurements for balancing of air distribution system — tracer-gas technique as an alternative?” *Building and Environment*, Vol.36 (2001), pp.955–964

[4] Roulet, C-A.; Heidt, F.D.; Foradini, F.; Pibiri, M-C. ”Real heat recovery with air handling units”. *Energy and Buildings*, Vol.33 (2001), pp.495-50

[5] McWilliams, J. *Annotated Bibliography 12, Review of Airflow Measurement Techniques*. Belgium: AIVC – Air Infiltration and Ventilation Centre. 2002 [also doc. LBNL-49747]

[6] Petersen, A.J.; Bryn, I.H.; Schild, P.G.; Haugen, E.N.; Nilsson, G.; Høydahl, K. *Roterende varmegjenvinnere i skoler*. Oslo: Erichsen & Horgen AS, Rapport 002. 2008

[7] Standard EN 308:1997, *Heat exchangers. Test procedures for establishing the performance of air to air and flue gases heat recovery devices.*

[8] “*Ventilation measurements and other tracer-gas applications”*. Ballerup, Demnark: Innova AirTech Instruments AS (now: LumaSense Technologies AS), booklet

[9] Roulet, C-A.; Zuraimi, M.S.; Sekhar, S.C.; Tham, K.W. “Tracer gas measurement of airflow rates in spaces with several air-handling units, recirculation, or large time constants”. *HVAC and R Research*, Vol.12 (2006), No.3, pp 477-496

[10] Offermann, F.J.; Robertson, J.P.; Webster, T. “The impact of tracer gas mixing on airflow rate measurements in large commercial fan systems”. *Proceedings: Indoor Air 2002*. pp 320-325

[11] Silva, A.R.; Afonso, C.F. “Tracer gas dispersion in ducts—study of a new compact device using arrays of sonic micro jets”, *Energy and Buildings*, Vol.36 (2004), pp.1131–1138

[12] Roulet, C-A.; Vandaele, L. “*Airflow Patterns Within Buildings: Measurement Techniques*”. AIVC Technical Note 34. Air Infiltration and Ventilation Centre, 1991

[13] Sherman, M.H. “On the estimation of multizone ventilation rates from tracer gas measurements”. *Building and Environment*, Vol.24 (1989), No.4, pp.355–362 (also doc. LBL-25772)

[14] Okuyama, H.; Onishi, Y.; Tanabe, S.; Kashihara, S. “Statistical data analysis method for multi-zonal airflow measurement using multiple kinds of perfluorocarbon tracer gas”. *Building and Environment*. Vol.44 (2009), No.3, pp 546-557

[15] Miller, S.L.; Leiserson, K.; Nazaroff, W.W. “Nonlinear least-squares minimization applied to tracer gas decay for determining airflow rates in a two-zone building”. *Indoor Air*, Vol.7 (2004), No.1, pp.64-75. [DOI 10.1111/j.1600-0668.1997.t01-1-00008.x]

[16] Manz, H.; Huber, H.; Helfenfinger, D. “Impact of air leakages and short circuits in ventilation units with heat recovery on ventilation ef®ciency and energy requirements for heating”. *Energy and Buildings*. Vol.33 (2001), pp. 133-139

[17] http://en.wikipedia.org/wiki/Least_trimmed_squares

[18] http://en.wikipedia.org/wiki/Robust_regression

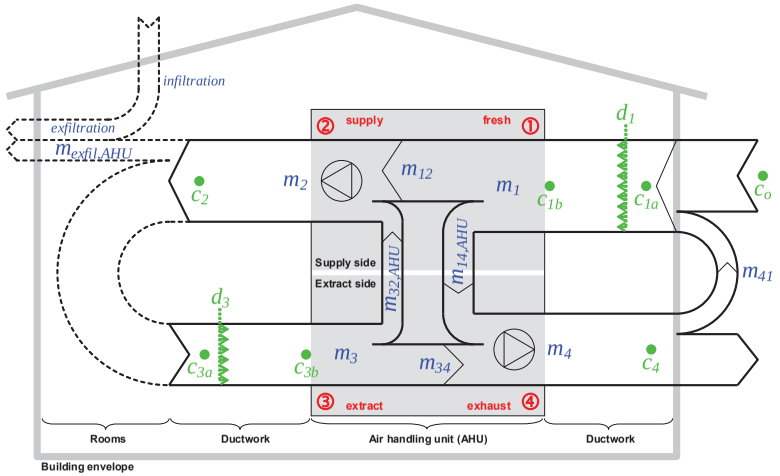


Fig. 1. Illustration of mass flow balance solved by the AHU model in this paper. Zero casing leakage is assumed. "*d*" is dosing probe, "*c*" is sampling point, "*m*" is mass flow. All mass flows are non-negative except $m_{exfil,AHU}$ which may be negative.

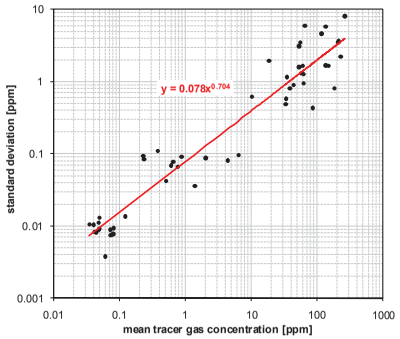


Fig. 2. Standard deviation as a function of tracer gas concentration in the field tests. This relationship is not assumed to be universally valid, but should be checked in each study.

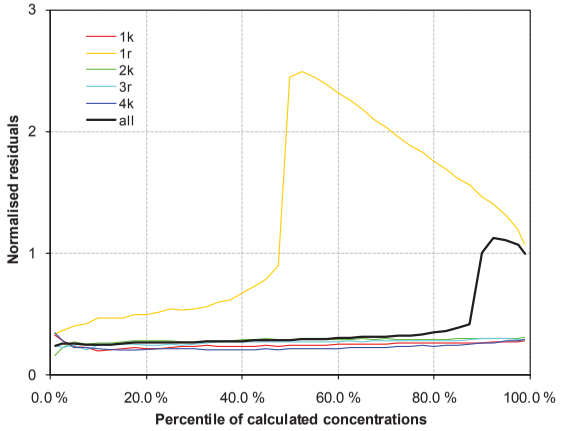


Fig. 3. Probability density of the normalized residual time series data at each sampling point, divided by an expected normal distribution. A horizontal flat line means that the data is normally distributed. Each sampling point is a different coloured line. Values above 1 are omitted (trimmed) in LTS algorithm. The thick black line is the entire data set for all sampling points.

Investigation of the Usage of Ground Source Heat Pump System on Wall Heating

O. Kincay[1], U. Akbulut[1], Y. Yoru[1], O. Acikgoz[1], H. Karakoc[2]

[1]*Department of Mechanical Engineering, Yildiz Technical University, Besiktas Campus, 34349 Istanbul, Turkey*

[2]*School Of Civil Aviation, Anadolu University, Eskisehir, Turkey*

Abstract

Wall heating systems are more preferable heating systems than other conventional systems due to their low temperature operating ranges. These systems are equipped with heating serpentines or panels where the water is circulated and the serpentines are mounted on the walls of rooms. Ground source heat pump systems are todays one of the useful renewable energy based heating systems.

In this study, daily analysis of a wall heating (radiant heating) system fed by a vertical type ground-coupled heat pump system is investigated and parameters of the system in a month (Feb. 2010) are recorded in 1 second intervals. As a result, temperatures of the wall heating system are investigated with inlet and outlet temperatures of the heat pump system. The mean heat transfer rate to the TEST room is found 1.017kW where 4.28 kW is the inlet energy rate and 3.26 kW is the outlet energy rate.

Keywords: *Analysis, Renewable Energy System, Ground Source, Heat Pump, Wall Heating*

Introduction

Wall heating systems are more preferable heating systems than other conventional systems because of its low temperature operating ranges. It is equipped with heating serpentines or panels where water is circulated and serpentines are mounted on the walls of rooms. Ground source heat pump systems are today's one of the useful renewable energy based heating system and renewable energy source based systems such as heat pump systems can be easily used in wall heating systems.

Ground-source heat pump (GSHP) systems are widely used because of their potential of energy-efficiency, environmental friendly behavior. Heat pumps are a kind of renewable energy source based energy systems which are powered with electricity. Especially usage of vertical type ground source heat pumps (V-GSHP) in heating and cooling purposes reduces energy consumption due to their high efficiency. In several studies, geothermal energy for heating and cooling systems was examined (1) (2). However, in the world, there exists large difference between climate conditions of countries. Also overall Coefficient of Performance (COP) changes due to the systems used in conjunction with the GSHP (3) (4) (5) (6). A good approach is to combine GSHP systems with the systems which work in low temperature values and ranges. This is an opportunity for energy saving.

Wall heating system is a kind of extremely simple installation which reduces investment and operating costs. It has significant advantage on increasing thermal comfort and wall heating system can be easily conjunct to a renewable energy source. In this system, heat transfer occurs from the radiant panels which are installed inside the wall to the room. Heat transfer mechanism can be classified into two sections such as radiation and natural convection. At least 60% of heat transfers by radiation with this system. Several studies in literature examined the amount of transferred heat from the radiant panels. Min et al. (7) identified natural convection coefficient of a room which is heated from walls. Schutrum and Vouris (8), represented the effect of the size of room is irrelevant except too large rooms like hangars and depots. Pamelee and Huebscher studied on the effect of forced convection coefficient on this system and suggested an increased convection coefficient for heat transfer calculations (9). Wall heating system can be used for cooling too. Some radiant panels can be mounted on ceiling if heat transfer surface area is insufficient. It will be practical and cheaper to install only one system for heating and cooling purposes. Imanari (10) compared radiant ceiling panel system with a conventional air handling unit in terms of thermal comfort, energy demand and total cost. He represented that radiant ceiling panel system provides comfort and energy saving. Vangtook (11) (12) made experimental and simulation studies on a radiant cooling system which is used with natural ventilation for very hot and humid climate. All 8

studies in literature about radiant heating and cooling system emphasized that this system is comfortable and economical.

In the study of Kincay et.al.; wind, solar and geothermal energy sources are discussed and the study is focused on the Hybrid Renewable Energy Systems (13). Hepbasli and Ozgener are presented energy and exergy analysis of a GSHP system with a 50 m vertical 1.25 in. nominal diameter U-bend ground heat exchanger (14). In the previous study of Yoru et al. a DISS-An C++ code with Artificial Neural Network (ANN) library is developed by authors to obtain results of energy and exergy analysis of a real vertical ground source heat pump system (15).

In this study daily analysis of a wall heating system fed by a vertical type ground-coupled heat pump system is investigated and parameters of the system are recorded in 1 second intervals. In wall heating system radiant panels mounted in the walls and their surface areas are sufficient for both heating and cooling purposes. Besides a V-GSHP system is conjunct to this system as a renewable energy supply.

System Description

The investigated wall heating system (Fig.1a) and vertical ground source heat pump system (Fig1.b) are located in Renewable Yildiz Energy House at Davutpasa Campus of Yildiz Technical University, Istanbul.



Fig.1 : (a) Wall heating serpentines (b) The investigated heat pump system

Wall heating systems are built in 3 different rooms of Renewable Yildiz Energy House and a saloon of a hall for heating and cooling applications.

Heat pump system with a 1.7kW scroll type compressor feeds this system. Two vertical 65m pipes were used to supply ground source water heat to the water heat pump. On the wall heating 14 mm inner diameter and 16 mm outer diameter polyetilen pipes are used. Total pipe length mounted to walls is 441m and the detailed information are given in Table 1.

Table 1: Size of heating serpentines mounted to walls

ROOMS	SIZE	QUANTITY	LENGTH (m)	TOTAL (m)
ROOM I	150x200	3	25	75
	75x200	3	15	45
	50x130	1	7	7
ROOM II	150x200	2	30	60
	75x200	3	15	45
	50x130	1	7	7
	150x200	2	25	50
ROOM III	150x200	4	25	100
	75x200	3	15	45
	50x130	1	7	7
SALOON	190x70	20	17	340
	60x140	8	11	88
	60x70	2	5	10

The compressor was controlled by an inverter to meet the need of cooling load under actual GSHP operating conditions. The boreholes were drilled down to 65 m under the ground to obtain the stable temperature of circulating water in the ground heat exchanger. The parameters such as the outdoor air temperatures, inlet-outlet temperatures, mass flow rates of both ground heat exchanger and circulating water were monitored. The heating

performance of the GSHP system was determined by measuring the input power and heating capacity.

Hybrid renewable energy system is designed for the energy requirement of 92 m^2 place. This system is original, because of different renewable energy sources as components of a conventional energy source and automatic control system.

Analysis

In the analysis of the system, the following assumptions were made for the Ground-source heat pump system;

- The system is steady state in 1 second intervals
- The efficiency of the evaporator and condenser assumed constant $(\eta_{cond} = \eta_{eva} = 0.85)$
- 3 pumps in the system are equivalent and have same power. *(W_p1=W_p2=W_p3=0.132 kW)*
- R410a flow rate is calculated and assumed constant during a second

In the energy analysis of the heat pump system mass balance equation and first law of thermodynamics law were used. Thereby COP of the heat pump system and all its components can be derived. Basically general mass and energy balance equations for a steady-state and steady-flow process are given as follows, respectively,

$$\dot{m}_{in} - \dot{m}_{out} = 0 \quad (1)$$

and

$$\dot{E}_{in} - \dot{E}_{out} = 0 \quad (2)$$

The investigated vertical gorund source heat pump system has 3 different flow cycles; ground source water (gsw) cycle , R410a refrigerant cycle and heating water cycle. The heat transfer rate in the evaporator is

$$Q_L = \dot{m_{gsw}} C_p (h_6 - h_7) \quad (3)$$

where Cp is the specific heat of the water–antifreeze solution, $\dot{m}$ is the mass flow rate of the water/antifreeze solution. The heat rejection rate in the condenser is calculated

$$Q_H = \dot{m}_{hw} C_p (h_{11} - h_{10}) \quad (4)$$

Efficiency of compressor is found from

$$\eta_{comp} = \dot{m}_{r410a} (h_2 - h1) / \dot{W}_{comp} \quad (5)$$

and for the analysis of a cubic TEST room, simply inlet and outlet energies of wall heating system are calculated from the obtained data. Therefore heat transfer to the TEST room can be found

$$\dot{Q} = \dot{E}_{out} - \dot{E}_{in} \quad (4)$$

where E is calculated by means of inlet and outlet temperatures of heating water.

Results

After modeling the system and analysis of given data, energy results are found by using thermodynamic equations in DISS-An application. Results are shown by both graphics and tables. In general 2,230,856 data lines (25 parameters per line) were obtained from the heat pump system and 2,418,000 data lines (5 parameters per line) were obtained from the wall heating system.

All energy calculations of both heat pump system and wall heating system are made by a DISS-An C++ code generated by authors (15). Daily data obtained from the heat pump and wall heating systems are shown in Figure 2.

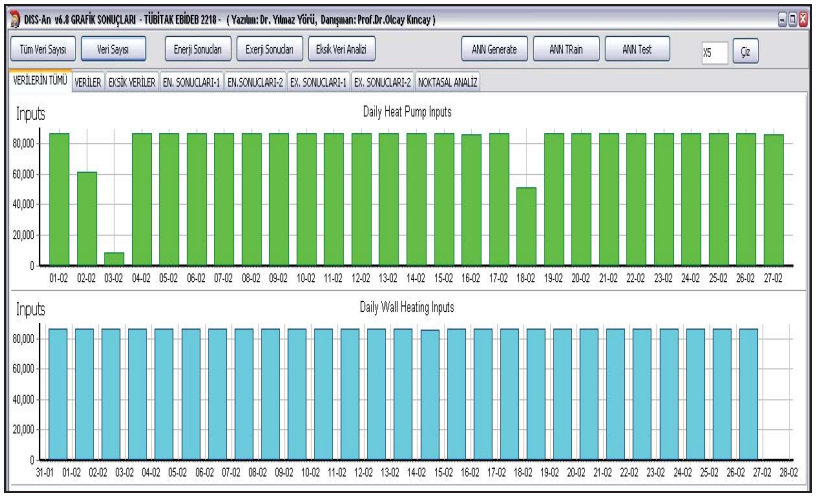


Figure 2 : Daily data obtained from the heat pump system and wall heating system (Feb. 2010)

DISS-An application is good at both displaying inputs and results beside its energy and exergy analysis. An example daily screen shot for the inputs of the heat pump system were shown in Fig. 3. It is easy to see when the heat pump started to operate and when stopped.

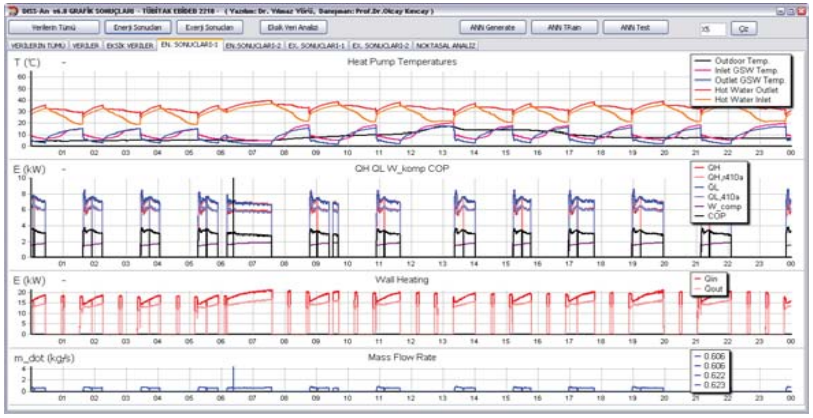


Figure 3: An example daily screen shot for the inputs of the heat pump system (16 Feb. 2010)

According to input data of wall heating system (Fig. 4), average inlet and outlet temperatures of heating water are found 30.9 °C and 25.54 °C, respectively. Average temperature of Test room is measured as 20 °C while average temperature of outdoor temperature is 7.8 °C.

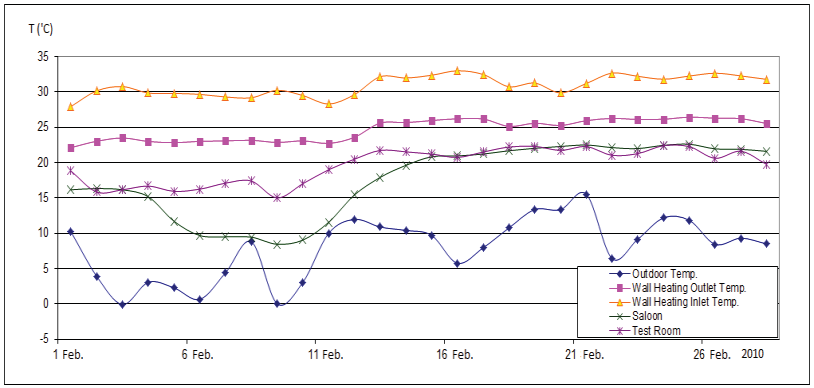


Figure 4: Average results of monthly data of wall heating system (Feb. 2010)

As a result from the obtained data of Feb. 2010, the mean heat transfer rate to the TEST room is found 1.02kW where 4.28 kW is the inlet energy rate and 3.26 kW is the outlet energy rate and hourly graph is shown in Fig. 4.

Totally, the wall heating system with heat pump is delivered 683 kWh energy to the test room in the investigated month.

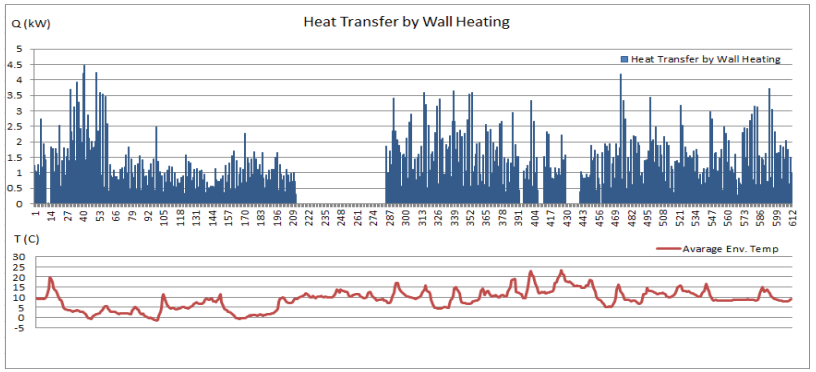


Figure 5 : Hourly heat transfer rate (Feb. 2010)

Conclusion

According to analysis, wall heating system is beneficial when used with a heat pump system and it may be developed by using hybrid renewable energy sources (solar, wind, geothermal) etc. Alternative solutions are recommended to reduce greenhouse effect due to CO_2 emissions and unhealthy combustion products of fossil fuels (CO, SO_X , NO_X , PbO_X) with this project. Besides reducing the usage of fossil fuels and effective usage of renewable energy sources of country will provide economical and environmental benefits in terms of the sustainable energy usage concept.

Acknowledgement

The authors gratefully acknowledge the financial support from the Scientific Research Projects Administration Unit of Yildiz Technical University (YTU-BAPK / 27-06-01-03, 2007) and TUBITAK- BIDEB for the support of this research on the ANN based exergy analyses of the radiant heating system.

Nomenclature

$\dot{E}$	energy rate (kW)	*Abbreviations*	
h	specific enthalpy (kJkg^{-1})	COP	Coefficient of Performance
$\dot{Q}$	*heat transfer rate* (kW)	GSHP	ground source heat pumps
s	specific entropy (kJkg^{-1}K^{-1})	V-GSHP	vertical type ground source heat pumps
$\dot{m}$	*mass flow rate*		
T	temperature (K or ˚C)		
t	target value (-)		
ψ	specific exergy (kJkg^{-1})		
ε	exergetic efficiency		
Indices			
hw	heating water		
in	inlet		
gsw	ground source water		
out	outlet, output		
r410a	refrigerant R410a		

References

1. Hwang, Y., Lee, J., Jeong, Y., Koo, K., Lee, D., Kim, I., Jin,S., Kim, S. *Cooling Performance of a Vertical Ground-Coupled Heat Pump System Installed in a School Building.* Renewable Energy, Vol. 34, 2009, pp. 578-582.

2. Michopoulos, A., Bozis, D., Papakostas, K., Kyriakis, N.A. *Three-years Operation Experience of a Ground Source Heat Pump System in Northern Greec.* Energy and Buildings, Vol. 39, 3, 2007, pp.328~334.

3. Sanner, B., Karytsas, C., Mendrinos, D., Rybach, L. *Current Status of Ground Source Heat Pumps and Underground Thermal Energy Storage in Europe,.* Geothermics, Vol. 32, 4-5, 2003, pp. 579-588.

4. Yang, W., Zhou, J., Xu, W., Zhang, G. *Current Status of Ground Source Heat Pumps in China.* Energy Policy, Vol. 38, 1, 2010, p. 323~332.

5. Lee, J. *Current Status of Ground Source Heat Pumps in Korea.* Renewable and Sustainable Energy Reviews, Vol. 13, 6-7, 2009, p. 1560~1568.

6. Bi, Y., Guo, T., Zhang, L., Chen, L. *Solar and Ground Source Heat-Pump System,".* Applied Energy, Vol. 78, 2, 2004, p. 231~245.

7. Min, T.C., Schutrum, L.F., Parmelee, G. V., Vouris, L.O. *Natural Convection and Radiation in a Panel Heated Room* s.l. : ASHAE Transactions 1956, p. 62:337.

8. Schutrum, L.F., Vouris, J.D. *Effects of Room Size and Non Uniformity of Panel Temperature on Panel Performance.* s.l. : ASHVE Transactions, ASHVE Transactions, 1954, p. 60: 455.

9. Pamelee, G.V., Huebscher, R.G. *Forced Convection Heat Transfer from Flat Surfaces." ,* s.l. : ASHVE Transactions, ASHVE Transactions, 1947, p. 53: 245.

10. Imanari T., Omori T., Bogaki K. *Thermal Comfort and Energy Consumption of the Radiant Ceiling Panel System: Comparison with the Conventional All-Air System,* Energy and Buildings, Vol. 30, 2, 1999, p. 167~175.

11. Vangtook, P., Chirarattananon S. *An Experimental Investigation of Application of Radiant Cooling in Hot Humid Climate.* Energy and Buildings, Vol. 38, 4, 2006, p. 273~285.

12. Vangtook, P., Chirarattananon S. *Application of Radiant Cooling as a Passive Cooling Option in Hot Humid Climate,",* Energy and Buildings, Vol. 42, 2, 2007, pp. 543~556.

13. Kincay, O., Utlu, Z., Agustos, H., Akbulut.U, Acikgoz, O. *Combining Trend of Renewable Energy.* Sigma-Journal of Engineering and Natural Sciences, Vol. 27, 1, 2009, pp. 60-82.

14. Hepbasli A, Ozgener O. *Energy and exergy analysis of a ground source (geothermal) heat pump system*1, Energy Management, Vol. 45, 2004, pp. 737~753.

15. Yoru Y., Akbulut U., Kincay O., Karakoc T.H. *Dynamic exergy analysis of a real vertical ground source heat pump system by using Fast Artificial Neural Network Library (FANN).* Denizli: 5th International Ege Energy Symposium and Exhibition (IEESE-5), 2010, Abstract P.131, Full Paper CD: ieeese214

Thermostat/Hygrometer vs ANN-Based Predictive/Adaptive Environmental Control Strategies

Jin Woo Moon[1] and Jae D. Chang[2]

[1] Chonnam National University, School of Architecture, Gwangju, Korea 500-575
[2] University of Kansas, School of Architecture, Design, & Planning, Lawrence, KS 66045 USA

Abstract

This study tested the feasibility of employing artificial neural network (ANN)-based predictive and adaptive control logics to improve thermal comfort and energy efficiency through a decrease in over- and under-shooting of control variables. Three control logics were developed: (1) conventional temperature/humidity control logic, (2) ANN-based temperature/humidity control logic, and (3) ANN-based Predicted Mean Vote (PMV) control logic. Analysis of the thermal chamber tests revealed that the ANN-based predictive temperature/humidity control logic provided greater periods of thermal comfort than that of the conventional logic by 0.3 to 5.1 percentage points for air temperature and 0.2 percentage point for humidity as well as a reduction in over-shoots and under-shoots. In addition, the ANN-based PMV control logic provided significantly better PMV conditions than both temperature and humidity based control logics. In most cases, ANN-based controls demonstrated a reduction in electricity consumption by 11.3% to 14.0% compared to non-ANN-based control logics, resulting in reduced fan usage and air circulation.

Keywords: thermal comfort, humidity control, artificial neural network, predictive control, adaptive control

Introduction

With its simplicity, thermostat- and hygrometer-based controls are the most widely used thermal control methods for residential buildings. However, this conventional method presents two problems in maintaining a comfortable indoor thermal environment. The first issue is the inability to take into account the building's thermal inertia and the control system's time lag associated with over and undershoots of thermal factors beyond the comfort range. This can lead to unnecessary system operation and energy consumption. The second problem arises from limiting performance to just two thermal variables (air temperature and humidity) when a number of other variables impact thermal comfort as evidenced in calculating the PMV (Predicted Mean Vote).

To address problems caused by over- and undershoots, new approaches to predictive control have been studied using artificial intelligence such as ANN (Artificial Neural Network). Yeo et al. (2003) developed an ANN model for predicting the optimal start time of a heating system for restoring interior temperature to a comfortable level by the start of business hours. Yang et al. (2000) designed a similar model but for predicting the amount of time for interior temperature to drop down to the lower limit of the comfort range. Employing these control logics with the heating system resulted in improved thermal comfort and energy efficiency for the test office buildings. For residential thermal controls, Morel et al. (2001) and Lee et al. (2002) applied ANN models to residential water heating systems and radiant floor heating systems. Gouda et al. (2006) investigated Fuzzy-ANN incorporation for a radiant heating device resulting in a significant reduction of temperature overshoots and energy consumption

compared to the PI controller. ANN models were also applied for the optimal control of cooling devices. Ben-Nakhi et al. (2002) developed an ANN model for predicting end-of-setback moment for air-conditioning resulting in accurate control and ease of use.

Moon et al. (2009) investigated PMV control in residential buildings using ANN. The researchers developed a thermal control framework and ANN-based advanced logics for conditioning based on air temperature, humidity, and PMV. The performance of the control logics with setback were numerically tested using the IBPT (International Building Physics Toolbox). The tests identified the potentials for improving thermal conditions using ANN-based environmental controls.

Objectives

This study aimed at experimentally testing the performance of the three control logics developed by Moon et al. (2009) and identifying the optimal logic in terms of thermal comfort and energy efficiency. The tested control logics were: (1) conventional temperature and humidity control logic, (2) ANN-based temperature and humidity control logic, and (3) ANN-based PMV control logic. The ANN-based logics are predictive and adaptive methods of control. Experimental data from this study coupled with the previous study's computational analysis can provide further evidence of the potential of the proposed control logics for residential thermal control.

Methods

The three control logics tested for this study are shown in Figures 1, 2, and 3. Figure 1 shows the process for a conventional non-ANN-based temperature and humidity control logic. Figure 2 shows the process for a predictive and adaptive ANN-based temperature and humidity control logic. This model independently controls air temperature and humidity using ANN predictions from two ANN models, temperature and humidity. Figure 3 shows the process for a predictive and adaptive ANN-based PMV control logic. For this study, the following values were applied in calculating the PMV, 1.0 Met and 1.0 clo for winter and 1.0 Met and 0.5 clo for summer. Three identical feed-forward and back-propagation ANN models were developed for this study and details are provided in Table 1. Since there is not a fixed scientific solution for the design of an optimal ANN model, this study employed the empirical solutions proven in the previous studies [Moon J. W. et al (2009), Datta, D. et al (1997), Kalogirou, S. A. et al (2000), Yang I. H. et al (2003), Yang, J. et al (2005), MathWorks (2005)]. The logics were developed using Matlab's Neural Network toolbox.

The control logics were tested in a thermal chamber built inside a climate controlled building. Figures 4 and 5 illustrate the layout of the thermal chamber and structure of the applied

control system. A radiant water heater, air conditioner, humidifier and dehumidifier were used to control the indoor climate. The control logics were tested under two conditions, heating/humidification (winter) and cooling/dehumidification (summer), for five days each with setbacks. Setbacks employ night and daytime setback of thermal factors to conserve energy. Figure 6 shows the comfort ranges and periods of the setback for air temperature, humidity and PMV.

Results and Discussion

The performances of the control logics were analyzed in terms of (1) duration of comfort period, (2) ratio and magnitude of overshoots and undershoots, and (3) energy consumption.

Duration of Comfort Period

Figures 7 and 8 show the duration the three control logics were able to maintain the comfort range under both heating/humidification and cooling/dehumidification operations. The ANN-based temperature/humidity control logic improved the comfort period of air temperature by 5.1 percentage points (86.2% to 91.3%) compared to the non-ANN-based temperature/humidity control logic during heating/humidification operations and by 0.3 percentage point (93.1% to 93.4%) during cooling/dehumidification operations. This difference between the heating and cooling operations was due to the greater time lag of the radiant heating system compared to the cooling system. Improvement over humidity was only 0.2 percentage point (98.0% to 98.2%) during heating/humidification operation. For cooling/dehumidification operation both logics maintained humidity comfort for 100% of the time. The ANN-based PMV control logic better maintained optimal PMV values (-0.5 to +0.5) than the two other temperature/humidity based control logics. Comfort was maintained 85.3% and 58.7% of the time during the heating/humidification and cooling/dehumidification operations respectively.

Overshoots and Undershoots

Overshoots and undershoots of air temperature and humidity were analyzed using Equations 1 and 2. The stability of thermal comfort factors for the non-ANN- and ANN-based control logics were compared using the ratio and magnitude of the over and undershoots.

$$R\ (\%) = N_O / N_T * 100 \qquad \text{(Eq. 1)}$$

Where,

R: Ratio of overshoots or undershoots outside the specified comfort range

N_O: number of overshoots or undershoots outside the specified comfort range

N_T: total number of overshoots or undershoots

$$M\ (^{\circ}C*\text{minutes or } \%*\text{minutes}) = \sum(\Delta \times t) \qquad \text{(Eq. 2)}$$

Where,

M: magnitude of overshoots or undershoots outside the specified comfort range

Δ: degree of overshoots or undershoots outside the specified comfort range

t: duration time of overshoots or undershoots outside the specified comfort range

The ratios of overshoots and undershoots for air temperature using the non-ANN-based control logic were all 100.0% while the ANN-based control logics mostly resulted in an average of 80.9% (Table 2). The magnitude of shoots was also reduced by the ANN-based control logic except for the overshoots during the cooling/dehumidification operation in which it increased from 1.90°C to 2.03°C*minutes (Table 3). Analysis of the ratio and magnitude of overshoots and undershoots indicates that the ANN-based control logic can better maintain consistant thermal conditions within the user specified ranges when using heating/cooling equipment having some time-lag.

Energy Consumption

Compared to the non-ANN-based control logic, the ANN-based temperature/humidity control logic saved energy on heating by 11.3% (from 10,425Wh to 9,250Wh) and humidification by 14.0% (from 300Wh to 258Wh) during the heating/humidification operation (Figure 9). For the cooling/dehumidification operation, the energy savings and reduced fan operation was 11.7% (from 962Wh to 849Wh) (Figure 10). ANN-based PMV control logic consumed more energy during both heating/humidification and cooling/dehumidification operations than the ANN- and non-ANN-based temperature/humidity control logics (Figures 9 and 10).

Conclusions

The main findings of this study are six fold.

- The predictive temperature/humidity control logic using ANN maintained more comfortable air temperature conditions than the conventional non-ANN-based temperature/humidity control logic. The predictive logic was more effective when applied to cooling/heating equipment with a large thermal lag effect, such as a radiant water heater.
- On the other hand, the comfort period of humidity was not significantly improved by the predictive logic. This may have been due to the humidity sensor's accuracy being only ±2%. Normal averaging method is suggested to reduce errors associated with collected sensor data.
- ANN-based PMV control logic better maintained optimal PMV conditions that the temperature/humidity based control logics.
- The predictive temperature and humidity control with ANNs stabilized better the thermal conditions than the conventional logic. The ratio and magnitude of over- and undershoots

of air temperature and humidity were generally reduced by the predictive logic even though an exceptional case for a device with insignificant time lag effect (A/C).

- ANN-based temperature and humidity control logics were generally more energy efficient. In particular, it was more energy efficient when using equipment with a higher thermal lag such as a radiant water heater.
- PMV-based control logic consumed more energy than temperature/humidity based control logics for both operating conditions due to the higher specified comfort range for PMV during the heating/humidification operation and the narrower comfort range for PMV during the cooling/dehumidification operation.

In conclusion, the predictive control of air temperature and humidity using ANN-based control logics has great potential for enhancing thermal comfort and energy efficiency in residential buildings. However, while the predictive control of PMV using ANN-based control logics improved overall thermal comfort, energy efficiency was lower than the ANN- and non-ANN-based air temeprature and humidity control logics. Thus, further study is warranted in investigating the value of improving thermal comfort (i.e. increased productivity) at the expense of increased energy consumption brought about by the ANN-based PMV control logic.

Acknowledgments

This work was supported by a grant from the Korean Ministry of Education, Science, and Technology (The Regional Core Research Program/Biohousing Research Institute) and the Biohousing Research Center.

References

1. Yeo, M. S. and Kim, K. W. "Application of artificial neural network to predict the optimal start time for heating system in building," *Energy Conversion and Management,* Vol. 44 (2003) pp. 2791-2809.
2. Yang, I. H., Yeo, M. S., and Kim, K. W. "Application of artificial neural network to predict the optimal start time for heating systems in building," *Energy Conversion and Management,* Vol. 44 (2003) pp. 2791-2809.
3. Morel, N., Bauer, M., El-Khoury, M., and Krauss, J. "NEUROBAT, a predictive and adaptive heating control system using artificial neural networks," *International Journal of Solar Energy*, April 2001, Vol. 21, pp. 161-201.
4. Lee, J. Y., Yeo, M. S., and Kim, K. W. "Predictive Control of the Radiant Floor Heating System in Apartment Buildings," *Journal of Asian Architecture and Building Engineering*, Vol. 1 n. 1, March. 2002, pp. 105-112.
5. Gouda, G. G., Danaher, S., and Underwood. C. P. "Quasi-adaptive fuzzy heating control of solar buildings," *Building and Environment,* Vol. 41 (2006) pp. 1881-1891.
6. Ben-Nakhi, A. E. and Mahmoud, M. A. "Energy conservation in buildings through efficient A/C control using neural networks," *Applied Energy,* Vol. 73 (2002) pp. 5-23.
7. Moon, J. W., Jung, S. K., and Kim, J. J. "Application of ANN (Artificial-Neural-Network)

in Residential Thermal Control," 11th International Building Performance Simulation Association Conference, Building Simulation 2009, University of Strathclyde, Glasgow, July 27-30, 2009, pp. 64-71.

8. Datta, D., Tassou, S. A., and Marriott, D. "Application of neural networks for the prediction of the energy consumption in a supermarket," Proceeding of CLIMA 2000 Conf, Brussels (Belgium), 1997, pp. 98-107.

9. Kalogirou, S. A. and Bojic, M. "Artificial neural networks for the prediction of the energy consumption of a passive solar building," *Energy* 25 (2000) pp. 479-491.

10. Yang, I. H. And Kim, K. W. „Development of Artificial Neural Network Model for the Prediction of Descending Time of Room Air Temperature," *International Journal of Air-Conditioning and Refrigeration*, Korea, Vol.12, n. 11 (2000-11).

11. Yang, J., Rivard, H., and Zmeureanu, R. "On-line building energy prediction using adaptive artificial neural networks," *Energy and Buildings,* Vol. 37 (2005), pp. 1250-1259.

12. MathWorks. MATLAB 14. Available from: http://www.mathworks.com; (Dec. 10, 2005)

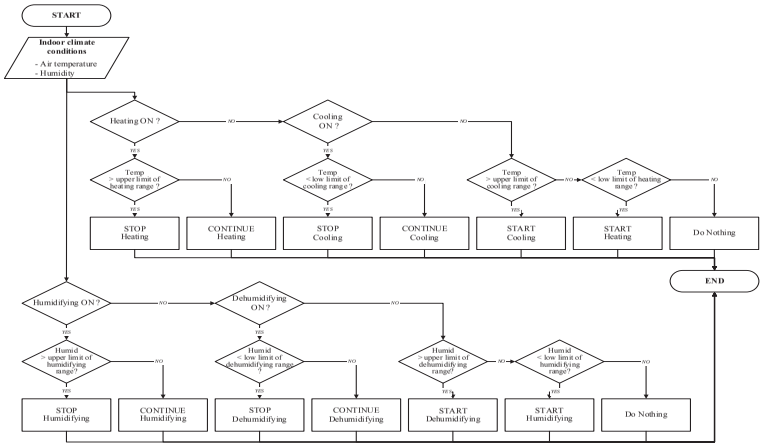


Fig. 1 Conventional non-ANN-based temperature/humidity control logic

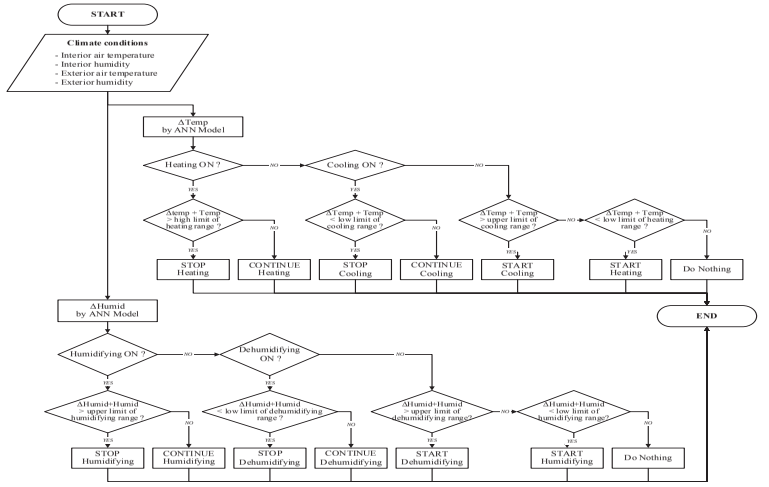


Fig. 2 ANN-based temperature/humidity control logic

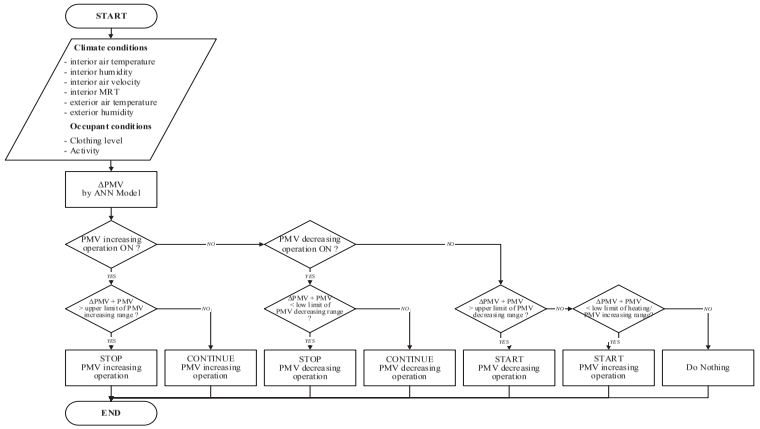


Fig. 3 ANN-based PMV control logic

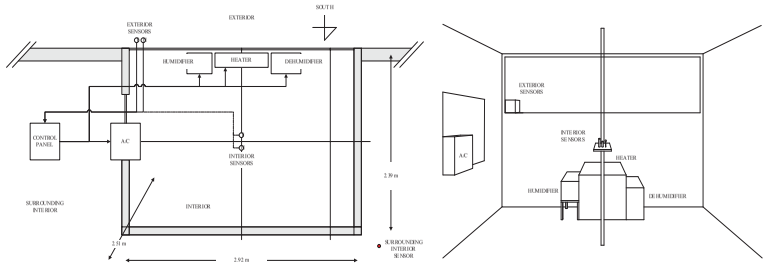


Fig. 4 Plan (left) and perspective (right) of thermal chamber

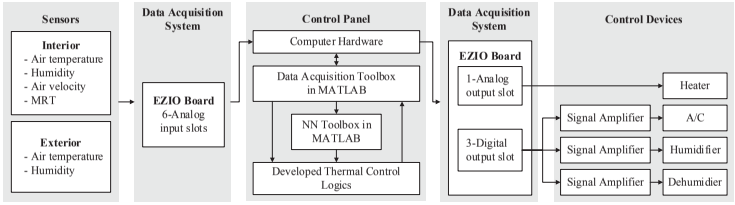


Fig. 5 Structure of the applied system

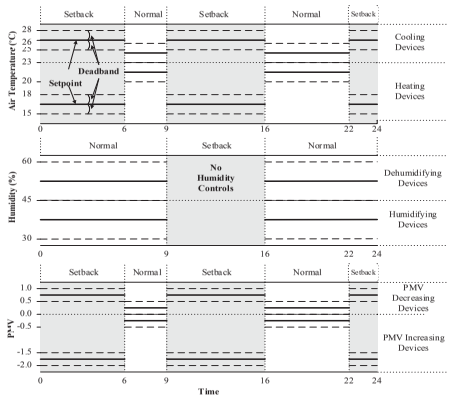


Fig. 6 Comfort ranges and periods of setback for air temperature, humidity, and PMV

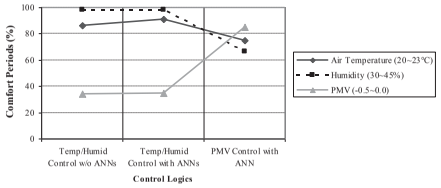


Fig. 7 Duration of comfort period during heating/humidification

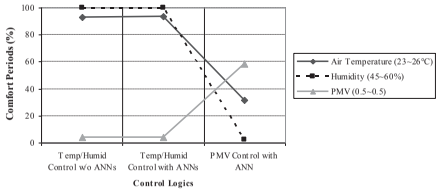


Fig. 8 Duration of comfort period during cooling/dehumidification

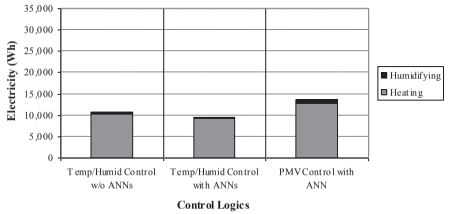


Fig. 9 Energy consumption (Wh) during heating/humidification operations

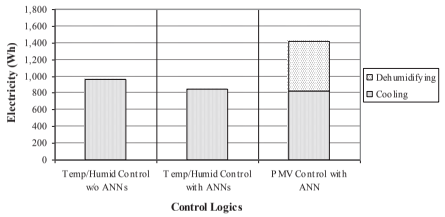


Fig. 10 Energy consumption (Wh) during cooling/dehumidification operation

Table 1 Description of developed ANN models

Structure	Input Layer	► Number of neurons: 8 1. exterior air temperature 2. exterior air temperature change from the preceding hour 3. exterior humidity 4. exterior humidity change from the preceding hour 5. interior air temperature 6. interior air temperature change from the preceding ten minutes 7. interior humidity 8. interior humidity change from the preceding ten minutes
	Hidden Layer	► Number of neuron: 17 using $N_h = 2 \times N_i + 1$ [Datta, D. et al (1997), Yang, J. et al (2005a)] Where, N_h: number of hidden neurons N_i: number of input neurons
	Output Layer	► Number of neuron: 1 (ΔTemperature, ΔHumidity, and ΔPMV, respectively)
Training Method		► Number of data set: 160 using $N_d = (N_h - (N_i + N_o)/2)^2$ [Kalogirou, S. A. et al (2000)] Where, N_d: number of data sets N_i: number of input neurons N_h: number of hidden neurons N_o: number of output neurons ► Obtained from the pre-test ► Type: sliding-window method ► Training goals: 0.1°C for air temperature 0.1% for humidity 0.1 for PMV ► Epoch: 1,000 times ► Learning rate: 0.75 ► Momentum: 0.9 ► Algorithm: Levenberg-Marquardt [MathWorks (2005)]

Table 2 Ratio (%) of overshoots and undershoots of thermal factors outside the specified comfort ranges.

Seasons	Thermal Factors	Ratios of Shoots	Control Logics	
			Temp/Humid Control w/o ANNs	Temp/Humid Control with ANNs
Heating & Humidifying	Air Temperature	Overshoots (%)	100.0	**66.7**
		Undershoots (%)	100.0	**88.9**

Season	Humidity	Overshoots (%)	100.0	**85.7**
		Undershoots (%)	100.0	**85.7**
Cooling & Dehumidifying Season	Air Temperature	Overshoots (%)	100.0	**75.0**
		Undershoots (%)	100.0	**83.3**
	Humidity	Overshoots (%)	-	-
		Undershoots (%)	-	-

Table 3 Magnitude of overshoots and undershoots of thermal factors outside of specified comfort ranges.

Seasons	Thermal Factors	Magnitudes of Shoots	Control Logics	
			Temp/Humid Control w/o ANNs	Temp/Humid Control with ANNs
Heating & Humidifying Season	Air Temperature	Overshoots (°C*minutes)	29.43	**9.21**
		Undershoots (°C*minutes)	-10.34	**-9.17**
	Humidity	Overshoots (%*minutes)	5.99	**5.39**
		Undershoots (%*minutes)	-2.55	**-2.06**
Cooling & Dehumidifying Season	Air Temperature	Overshoots (°C*minutes)	**1.80**	2.03
		Undershoots (°C*minutes)	-3.66	**-2.75**
	Humidity	Overshoots (%*minutes)	-	-
		Undershoots (%*minutes)	-	-

A Study on the Hybrid Air-conditioning system Coupled with Radiant Floor Cooling and Ventilation System

Jaehyung PARK[1], Joowook KIM[1] and Doosam SONG[2]

[1]Graduate School of Sungkyunkwan University, Suwon 440-746, Republic of Korea
[2]Dept. of Architectural Eng., Sungkyunkwan University, Suwon 440-746, Republic of Korea

Abstract

In this study, the concept of the Hybrid air-conditioning system utilizing convection and radiation heat exchange will be suggested. In this paper, the heat removal characteristics of Hybrid air-conditioning system will be described by theoretical review and experimental methods. Also the ratio of cooling load removed by Hybrid air-conditioning system could be divided as radiation and convection heat exchanges.
The methods could be used to system design of Hybrid air-conditioning system.

Keywords: Hybrid Air-conditioning system, Radiant floor cooling, Energy

Introduction

The survival of the human race is being threatened by the increase of various disasters from climate change such as global warming, and globally concerted efforts are being made to cope with these problems. In architecture, demand for energy reduction is rising, and many studies are being conducted to find measures to save cooling and heating energy in buildings in particular. On the other hand, with the rising demand for improvement of the quality of life and comfortable indoor environment, energy use in buildings is growing. In this context, as a

comfortable cooling and heating system with energy efficiency energy, a hybrid air-conditioning system which combines the conventional radiant floor cooling system with ventilation system is being spotlighted.

As an existing study on hybrid air-conditioning systems, Song et al. (2004) [1] proposed a cooling system that combines radiant floor cooling, dehumidification, natural ventilation, and free cooling, and examined the possibility of indoor environment adjustment and energy saving effects of the proposed system through experiments. However, they did not investigate the calculation method for heat removal by convection and radiation which is the most important for actual application of a hybrid air-conditioning system to buildings.

There are some studies that reported on heat removal by convection and radiation mainly through simulations [2], but there are few examples that investigated it through experiments. Olsen and Carli (1995) [3] determined the heat transfer characteristics and heat removal by different indoor temperatures of a radiant floor cooling system through experiments. Furthermore, Fisher and Pederson (1997) [4] established a calculation method for convective heat transfer coefficient and heat removal according to the changes in air flow rate of a forced convection system. Mcadams et al. investigated the characteristics of natural convection according to differences in indoor temperature.

This study aims to establish a theoretical equation for heat removal of the hybrid air-conditioning system that combines convection and radiation heat exchange on the basis of the findings of Olsen, Fisher, Mcadams, and others, and present a calculation method for heat removal features by convection and radiation of the hybrid air-conditioning system.

Outline of the Hybrid Air-conditioning System

The hybrid air-conditioning system for consists of a radiant floor cooling system utilizing floor hot water coils which installed in residential building in Korea and a cooling/dehumidifying ventilation system attached to walls.

In summer season, the radiant floor cooling system is used and chilled water is supplied to the ventilation system for cooling/dehumidifying the outside air which introduced indoors for ventilation. When indoor humidity increases and condensation occurs on the floor, the outside air inlet is closed and the inside air is circulated which removes humidity from the inside air. In mid-season when the outside air condition is relatively favorable to control indoor environment, the outside air is directly brought to the inside to remove indoor heat and contaminant. Furthermore, under the condition where natural ventilation is possible, outside air is brought in through natural ventilation; otherwise, mechanical ventilation is used. If room temperature cannot be controlled by the radiant floor cooling system only due to rapidly

increasing outside air temperature and internal cooling load, the ventilation system removes surplus load to control the room temperature to a comfortable level.

The hybrid air-conditioning system proposed in this study removes indoor heat through convective and radiant heat exchange. To define the heat removal performance of this system, therefore, it is important to investigate the characteristics of convective and radiant heat exchange.

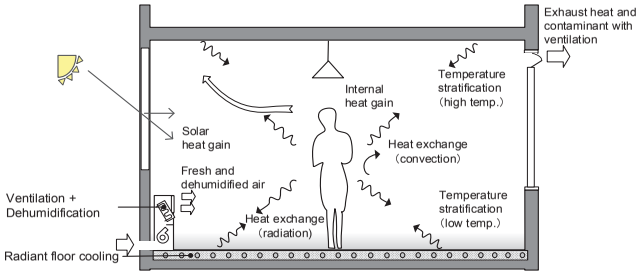


Fig. 1 Concept of hybrid air-conditioning system

Calculation of Heat Removal by the Hybrid Air-conditioning System

1) Calculation of heat removal by radiant floor cooling

The total heat transfer of radiant floor cooling system can be divided into the radiant heat exchange between surface and surrounding walls, the convective heat exchange between the cooling surface and the ambient air. But it is very difficult to calculate these two values simultaneously because their mechanisms are different.

Table 1 Parameter and variable

Q_{rad}	radiant heat transfer(W/m^2)
$Q_{f,conv}$	forced convective heat transfer(W/m^2)
$Q_{n,conv}$	natural convective heat transfer(W/m^2)
Q_{floor}	total radiant heat transfer(W/m^2)
h_{rad}	radiant heat exchange coefficient(W/m^2K)
$h_{f,conv}$	forced convective heat exchange coefficient(W/m^2K)
$h_{n,conv}$	natural convective heat exchange coefficient(W/m^2K)
T_f	absolute temperature of floor surface(K)
T_i	absolute temperature of surface i(K)
T_{room}	Average indoor temperature (K)
T_o	Absolute temperature of outdoor(K)
$T_{f,s}$	absolute temperature of centilation system(K)
$X_{f,s}$	absolute humidity of centilation system(kg/kg')
X_o	absolute humidity of outdoor(kg/kg')
ε_i	emissivity of the other surface
ε_f	emissivity of floor surface
Σ	Stefan－boltzmann constant($5.67\times10^{-8}W/m^2K^4$)
$F_{A_f-A_i}$	view factor between floor surface A_f and surface A_i
C	specific heat water(J/m^3K)
q_w	water floor rate(m^3/s)
Q	air floor rate(m^3/s)

Thus, in the case of radiant floor cooling, it is important to determine the characteristics values of the convective or radiant heat transfer (for example, convective heat transfer rate, convective heat transfer rate, etc.). The indoor heat removal of the radiant floor cooling system is defined by the following expression (1):

$$Q_{floor} = Q_{n,conv} + Q_{rad} \quad \text{(Eq. 1)}$$

For calculation of the heat exchange by floor radiation in the radiant floor cooling system, if we assume that the whole surface is gray, the heat flux of other surfaces than the floor surface can be expressed as follows [5]:

$$Q_{rad} = \varepsilon_f \sigma T_f^4 - \sum_{j=1}^{N} \varepsilon_f \sigma T_i^4 F_{A_f - A_i} \quad \text{(Eq. 2)}$$

Here, the emissivity of the gray surface of the internal wall is 0.9～0.95. The above expression can be linearized as follows:

$$Q_{rad} = \varepsilon_f \sigma \sum_{j=1}^{N} \theta_{f,i} (T_f - T_i) F_{A_f - A_i} \quad \text{(Eq. 3)}$$

Here, $\theta_{f,i}$ which can be expressed as

$$\theta_{f,i} = \frac{T_f^4 - T_i^4}{T_f - T_i} \quad \text{(Eq. 4)}$$

is the temperature difference between the floor surface and other surfaces determined by experiments. $\theta_{f,i}$ can be changed to the constant θ. Therefore, expression (4) can be converted to expression (5):

$$Q_{rad} = \varepsilon_f \sigma \theta \sum_{j=1}^{N} (T_f - T_i) F_{Af-Ai} \quad \text{(Eq. 5)}$$

$$Q_{rad} = h_{rad} \sum_{j=1}^{N} (T_f - T_i) F_{Af-Ai} \quad \text{(Eq. 6)}$$

F_{AF-Ai} is the view factor between the floor surface and all the other surfaces. The radiant heat exchange coefficient h_{rad} can be expressed as follows:

$$h_{rad} = \varepsilon_f \sigma \theta \quad \text{(Eq. 7)}$$

For the convective heat transfer of the radiant floor cooling and heating system, heat exchange results from the heat transfer by natural convection which is caused by the temperature gradient between the floor surface and ambient temperatures rather than from the heat transfer by forced convection caused by forced outside condition difference. Because the flow velocity of the natural convection is much lower than that of the forced convection, the convective heat transfer rate must be, too. But this must be considered because it is essential for determination of the heat transfer characteristics.

According to many papers and reports on heat transfer, the heat transfer by natural convection can be expressed as a function of the temperature difference ΔT between the floor (T_f) and the indoor air (T_{room}) [3, 6].

In particular, the heat transfer of radiant floor cooling can be simply expressed as expression (8) in consideration of the length of the floor surface.

$$h_{n,conv} = 0.59(\Delta T/L)^{0.25} \quad \text{(Eq. 8)}$$

Therefore, this study calculated the heat removal by natural convection in the radiant floor system by defining of the heat transfer coefficient as a function of ΔT as in expression (8). The heat removal by natural convection can be expressed as expression (9):

$$Q_{n,conv} = 0.59(\Delta T/L)^{0.25}(T_{room} - T_f) \quad \text{(Eq. 9)}$$

2) Calculation of the heat removal by the ventilation system

The heat removal by the ventilation system which corresponds to the forced convection can be defined as follows:

$$Q_{f,conv} = h_{f,conv}(T_{room} - T_s) \quad \text{(Eq. 10)}$$

3) Calculation of heat removal through experiment

① Space for experiment

For the space for experiment, the test cell in the architectural environment laboratory of the Sungkyunkwan University was used. It has the dimensions of 2.2(m) 2.2(m) 2.4(m). With the exclusion of the ondol-floor(0.224$W/m^2°C$), the ceiling and walls are composed of 2(cm) veneer board+16(cm) Styrofoam+2(cm) veneer board (0.232$W/m^2°C$). The southern surface of the test cell is interfacing with the outside of the laboratory and all the other surfaces are interfacing with the inside of the laboratory. To minimize the effect of outside air and the indoor load variations by sunlight, a 5cm thick Styrofoam was attached to the southern surface of the laboratory. X-L pipes were buried in the floor for ondol, and cool water was circulated inside the test cell by a loop pump for radiant cooling.

② Details of experiment

The temperature of the supplied chilled water during radiant floor cooling is controlled by the temperature setting of the heat exchange. The heat exchange is controlled by flow changes via a 3-way valve which was controlled by DAQ system using LABVIEW program running on a PC. Based on the lower limit of comfortable floor surface temperature determined by Olsen [3], the lower limit of the floor surface temperature was set to 21℃. The hybrid ventilation system is a convective cooling and heating system that supports cooling, heating, and ventilation. In this experiment, the ventilation system was operated in cooling mode in order to find the heat transfer rates of the ventilation system and the radiant cooling system, and the indoor set point was converged to 26℃. To measure the heat conducted from the walls, this study installed a heat flow meter. To measure the heat that flowed into the test cell, the feed and return water temperatures and the flow rate of the pump were determined. Furthermore, to determine heat removal by the ventilation system, supply air velocity and supply air temperature were measured.

The indoor temperature measuring points are shown in Fig. 2 and 3. To maintain constant heat flow through the walls interfacing with the indoor side excluding the surface interfacing the outside air of the test chamber, the temperature of the external space was set to 28℃

using the an air conditioner. For the cooling het source, a 2HP compression refrigerator was used. The total system was controlled by the LABVIEW program.

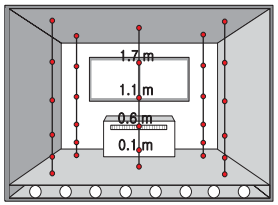


Fig. 2 Vertical temperature measuring points in the test cell

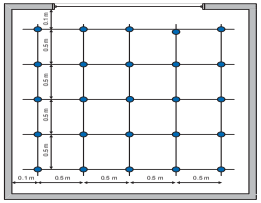


Fig. 3 Floor temperature measuring points in the test cell

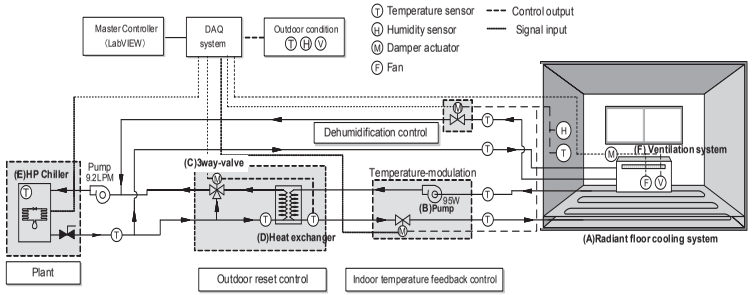


Fig. 4 Test cell system configuration

③ Calculation of heat removal

The hybrid air-conditioning system takes long until the temperature in a structure becomes constant because it is combined with radiant floor cooling. Thus, this experiment examined the heat transfer rate and heat removal of the system in the state where the indoor floor temperature converged to a constant temperature and in the state where the indoor temperature converged to the set point.

Assuming that the target space is in steady state, the heat input/output elements can be defined as follows: Q_w is the heat transferred from the cool water pipes to the room in the radiant floor cooling system; Q_{vent} is the indoor heat removal of the ventilation system which is transferred from the supply air velocity to the room; Q_{ki} is the heat conducted from each wall toward the outside; Q_{down} is the heat loss conducted downward from the cool water pipes; and Q_{inf} is the heat of the outside air supplied to the room by the infiltration the outside air. Therefore, the indoor energy equilibrium equation by the hybrid air-conditioning system becomes as follows:

Table 2 Measurement item

	Measurement item	Measuring instruments	Measuring interval
Indoor and outdoor temperatures and humidity	Indoor temp. (vertical) -30points	Thermocouple (K-type thermo couple) + data-logger	10sec
	Wall temp. – 12 points		10sec
	Floor temp. – 25 points		10sec
	Indoor humidity (at 0.6m)	SK-SATO	10sec
	Indoor humidity (at 0.1m)	KIMO thermo-hygrometer	10sec
Wind velocity, temperature, and humidity of the ventilation system	supply air velocity, temperature and humidity -2 points (outlet, room center)	Hotwire anemometer (KANOMAX)	10sec
Heat flow rate	Wall heat flow rate - 5points Under-floor heat flow rate - 1 point	Heat flow meter + data-logger	10sec
Cool water temperature	Cool water supply and return temperatures	Water temperature meter (testo)	10sec
Outside air conditions	Temperature·humidity,·wind	Weather station	1 min

	velocity·wind, direction		
Infiltration	Measurement of indoor infiltration using CO2 concentration decay method	CO2 meter	5min

$$Q_{tot} = Q_w + Q_{vent} - Q_{ki} - Q_{down} - Q_{inf} \quad \text{(Eq. 11)}$$

Where

$Q_w = cq_w(T_s - T_r)$

$Q_{vent} = q_S + q_L, \quad q_S = 0.24 \times 1.2 \times q(T_{f,s} - T_{room}), q_L = 597.3 \times 1.2 \times q(X_{f,s} - X_o)$

$Q_{inf} = 0.24 \times 1.2 \times q(T_{room} - T_o)$

Heat (Q_{ki}) and heat loss (Q_{down}) can be measured by the heat flow meter, and the heat loss by infiltration (Q_{inf}) can be defined by the calculation of infiltration quantity by the CO2 concentration decay method.

Expression (11) is the energy equilibrium equation for calculation through experiments.

As described above by literature review about radiant floor cooling and convective heat exchange, the indoor energy equilibrium equation can be expressed as follows in consideration of the radiation, forced convection, and natural convection:

$$Q_{tot} = Q_{rad} + Q_{f,conv} + Q_{n,conv} \quad \text{(Eq. 12)}$$

Therefore, based on expressions (11) and (12), the energy equilibrium equation from theory and experiment can be expressed as follows:

$$Q_{tot} = Q_{rad} + Q_{f,conv} + Q_{n,conv} = Q_w + Q_{vent} - Q_{ki} - Q_{down} - Q_{inf} \quad \text{(Eq. 13)}$$

In expression (13), the convective heat transfer of the hybrid air-conditioning system can be expressed as follows:

$$Q_{f,conv} = Q_w + Q_{vent} - Q_{rad} - Q_{n,conv} - Q_{ki} - Q_{down} - Q_{inf} \quad \text{(Eq. 14)}$$

Therefore, the convective heat transfer rate of the ventilation system which is essential for determination of the capacity of the hybrid air-conditioning system is as follows:

$$h_{f,conv} = \left[\frac{Q_{vent}+Q_w-\left\{h_{rad}\sum_{j=1}^{N}(T_f-T_i)F_{Af-Ai}\right\}-0.59(\Delta T/L)^{0.25}(T_{room}-T_s)-Q_{ki}-Q_{down}-Q_{inf}}{(T_{room}-T_s)}\right] \quad \text{(Eq. 15)}$$

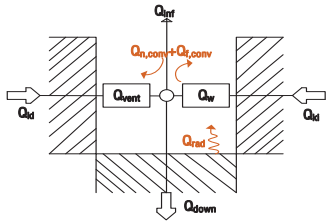


Fig. 5 Heat transfer exchange of Hybrid air-conditioning system

Meanwhile, the view factors (F_{AF-Ai}) between the floor surface and all the other surfaces for definition of the radiant heat exchange are as shown in Table 3.

Table 4 shows the values of θ that have been calculated by substituting in the expression (4) the surface temperatures and the floor temperature which have been determined through experiments.

Table 5 shows the radiant heat exchange ratios calculated by expression (7) based on the internal surface emissivity (0.9～0.95) and different θ values. Thus, the mean value of the radiant heat transfer coefficient was 5.53(W/m^2K). Furthermore, the heat transfer coefficient of natural convection based on the floor surface temperature of radiant cooling calculated by expression (8) was 0.72 (W/m^2K). This is within the general range of natural convective heat transfer coefficient which is 0.4～0.8(W/m^2K) in temperature range between 0 and 10℃[6].

Table 6 shows the values of convective heat transfer coefficients of the ventilation system calculated by expression (15). The heat exchange coefficients by forced convection were indicated by dividing the measured wind velocity of the system to 1.0, 1.5, and 2.0(m/s). The convective heat transfer coefficient was 3.56~4.35(W/m^2K).

Figure 6 shows the heat removal values of the hybrid air-conditioning system which were determined with the convective heat transfer ratio of the ventilation system and the convective and radiant heat transfer ratios of the radiant cooling system that have been calculated above.

The heat removal by radiation of the radiant floor cooling system was 42.745(W/m^2K), the heat removal by natural convection was 3.32(W/m^2K), and the heat removal of the ventilation system (forced convection) per unit area was 41.23(W/m^2K).

Table 3 View factor of experimental space

	View factors					
	Ceiling	East wall	West wall	South wall	North wall	Window
Floor	0.178	0.206	0.206	0.138	0.206	0.067

Table 4 Surface temperature

T_f(℃)	T_i(℃)	θ(K^3)
21.2℃	25.3	1.05×10^8
	25.4	
	26.6	
	25.7	
	27.1	1.06×10^8

Table 5 Radiant heat transfer

σ(W/m^2K^4)	E	θ(K^3)	h_{rad}(W/m^2K)
5.67×10^{-8}	0.9	1.05×10^8	5.36
		1.06×10^8	5.41
	0.95	1.05×10^8	5.65
		1.06×10^8	5.71

Table 6 Forced convection heat transfer

Air Velocity(m/s)	T_s(℃)	T_{room}(℃)	$h_{f,conv}$(W/m^2K)	$Q_{f,conv}$(W/m^2)
1.0	15.5	26.5	3.56	32.04
1.5	15.1	26.1	3.82	37.1
2.0	14.7	25.5	4.35	43.82

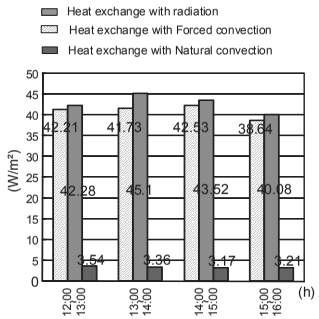


Fig. 6 Heat removed by Hybrid air conditioning system

Conclusions

In order to establish the design methodology of the hybrid air-conditioning system that combines convection and radiation heat exchange, this study presented methods for calculating the heat transfer rate such as convective heat transfer rate, radiant heat transfer rate and for calculating the heat removals by convective and radiant heat exchanges through experiments on the basis of relevant theoretical equations. The findings from this study enable the determination of system capacity which is essential for application of the hybrid air-conditioning system to actual buildings.

Acknowledgments

This work was supported by the SRC/ERC program Most(grant R11-2005-056-02004-0) of the Sustainable Building Research Center.

References

1. Song, D. S., “Performance Evaluation of a Radiant Floor Cooling System Integrated with Dehumidified Ventilation,” Applied Thermal Engineering, 2008, Volume 28, Issues 11-12, Pages 1299-1311.

2. Song, D. S., Kato, S., “Radiational Panel Cooling System with Continuous Natural Cross Ventilation for Hot and Humid Regions,” Energy and Building, 2004, Volume 36, pp. 1273-1280.

3. Olsen, B. W., Bonnefoi, F., Michel, E., Carli, M. de, "Heat Exchange Coefficient between Surface and Space by Floor Cooling Theory or a Question of Definition," ASHRAE Transaction, 1995, pp.685-687.

4. Fisher, D. E., Pedersen, C. O., "Convective Heat Transfer in Building Energy and Thermal Load Calculation," ASHRAE Transaction, 1997, pp.137-148.

5. Fanger, P. O., "Thermal Comfort," Krieger publishing company, Florida, 1982.

6. Khalifa, A. N., "Natural Convective Heat Transfer Coefficient - A Review:: I. Isolated Vertical and Horizontal Surfaces," Energy Conversion and Management 42, 2001, pp. 491-504.

7. Helmut, E., Feustel, Corina S., "Hydronic Radiant Cooling-Preliminary Assessment," Energy and Building, 1995, Volume 22, pp.196-198.

Energy-saving Effect of Thermal Energy Storage Using Introduced Outdoor Air

Yuka Asano[1], Masashi Yamagiwa[1], Kazunobu Sagara[1], Toshio Yamanaka[1], Hisashi Kotani[1], Yoshihisa Momoi[1], and Tomohiro Kobayashi[2]

[1]Osaka University, Dept. of Architectural Eng., JAPAN
[2]Ritsumeikan University, Dep. of Architecture and Urban Design, JAPAN

Abstract

Recently, buildings with thermal energy storage system have increased because of its economic advantage. In thermal energy storage system using introduced outdoor air, building masses are used as thermal storage media and cooled by outdoor air introduced by a mechanical fan in night-time. In spring and autumn, the cooled building masses can work to reduce cooling load in day-time. In this study, the stored heat was calculated by using simple heat transfer models for various building masses, and the energy performance of this system was evaluated quantitatively by system simulation. It was found that the optimized flow rate of outdoor air can be obtained by comparing the electric power consumption by a mechanical fan with the reduced cooling load because the mechanical fan is the only device requires electric power in night-time.

KEY WORDS: Simulation, Outdoor air, Thermal energy storage

Introduction

Thermal energy storage system has become popular in Japan because of lower electricity charge at nighttime. Thermal energy storage system using floor slabs, beam structures and office furniture (building masses) as storage media can reduce the initial cost and the installation space in comparison with water or ice storage system having large tanks. Furthermore, the thermal energy storage system using outdoor air can save energy because cool outdoor air in nighttime is introduced to cool building masses.

This paper presents the heat transfer models of each building mass and introduces an actual thermal energy storage system using outdoor air. In this system, building masses are cooled by outdoor air during nighttime and cool the return air from office room during daytime. The cooled building masses can reduce cooling load. However, it is difficult to evaluate the actual performance of thermal energy storage system having various building masses because the heat transfer between the building masses and introduced outdoor air is very complicated. In this paper, the building heat transfer simulation incorporating each heat transfer model was conducted, and it was found that the optimum outdoor air rate introduced by mechanical fan can be obtained by this simulation.

Heat Transfer Models

The concrete floor slab has the largest heat capacity in various building masses, and temperature of return air from the room is affected by time lag of temperature in concrete slab. Therefore, the heat capacity of concrete slab has been considered in system simulation to evaluate the effect of stored heat in concrete slab. In case that heat capacity of building masses excluding concrete slab is considered in simulation, temperature of these building masses has been simply regarded as uniform and equal to the room air temperature, and time lag of temperature in building masses has been ignored. In this study, however, heat capacity of building masses such as beam structures and office furniture is assumed to contribute the

heat transfer between the building masses and introduced outdoor air, and simple heat transfer models which can evaluate heat flux at surface of building masses accurately are suggested.

In simulating heat transfer for the building masses relatively thin, the surface heat flux can be assumed as one-dimensional. Here, the concrete slab was regarded as thin building mass. The temperature in the slab can be calculated by the following unsteady heat conduction equation,

$$\rho c_p \frac{\partial \theta(x,t)}{\partial t} = \lambda \frac{\partial^2 \theta(x,t)}{\partial x^2} \quad \text{(Eq. 1)}$$

The heat flux on concrete slab surface can be written as follows:

$$q_l = h\left(\theta(0,t) - \theta_r\right) \quad \text{(Eq. 2)}$$

The heat capacity of other building masses is not as large as that of concrete slab. If the temperature distribution in all building masses is calculated by using Eq.1, the building heat transfer simulation becomes complex and time-consuming. Therefore, simple heat transfer models are applied to the building masses (furniture and beam structures) excluding concrete slab and the heat through surface of building masses can be calculated easily. Here, the desk board is analyzed as building furniture. Heat transfer model of desk board is based on the assumption that temperature distribution in desk board is assumed to be quadratic, and this model is called the quadratic model.

The quadratic temperature distribution of building mass can be written as follows:

$$\theta(x,t) = \alpha(t)x^2 + \beta(t)x + \gamma(t) \quad \text{(Eq. 3)}$$

$\alpha(t), \beta(t), \gamma(t)$ are unknown coefficients of quadratic function. At the surface of desk board ($x=0$), the boundary condition is as follows:

$$\lambda \frac{\partial \theta(x,t)}{\partial x} = h\left(\theta(0,t) - \theta_r\right) \quad \text{(Eq. 4)}$$

As the boundary condition at the center of desk board ($x=l$) perfect insulation was applied and written as

$$\lambda \frac{\partial \theta(l,t)}{\partial x} = 0 \quad \text{(Eq. 5)}$$

The time integration of heat flux through surface is equal to the stored heat in desk board from surface to center of desk board at time t, and the heat balance equation for the board can be written as follows:

$$\int_0^t h\left(\theta(0,t) - \theta_r\right) A dt = -\int_0^l \frac{\lambda}{a}\left(\theta(x,t) - \theta(x,t)\right) A dx \quad \text{(Eq. 6)}$$

From these equations, (Eq.4) - (Eq.6), $a(t), b(t), c(t)$ can be represented the functions of mean temperature in desk board, $\bar{\theta}(t)$. The change rate of $\bar{\theta}(t)$ and the heat flux exchanged at the surface of desk board can be expressed respectively as follows:

$$\frac{\partial \bar{\theta}(t)}{\partial t} = \frac{3ha}{l(hl + 3\lambda l)}\left(\theta_r - \bar{\theta}(t)\right) \quad \text{(Eq. 9)}$$

$$q_2 = \frac{3h\lambda}{hl + 3\lambda l}\left(\bar{\theta}(t) - \theta_r\right) \quad \text{(Eq. 10)}$$

Two models, an unsteady conduction equation model and a quadratic model, are compared under the conditions of **Table1** in order to verify the accuracy of quadratic model. **Fig.1** shows the variation in heat flux calculated by these two models. The difference between the

unsteady conduction equation model and the quadratic model are very small in thin furniture. From the result, the quadratic model can be used as heat transfer model of thin furniture instead of the unsteady conduction equation model.

Table1
Condition in heat transfer model of desk board

Variable	Value
θ_r [°C]	18
$\theta(x,0)$ [°C]	28
λ [W/m·K]	0.15
h [W/m²·K]	5.0
ρc_p [kJ/m³·K]	714
l [m]	0.05

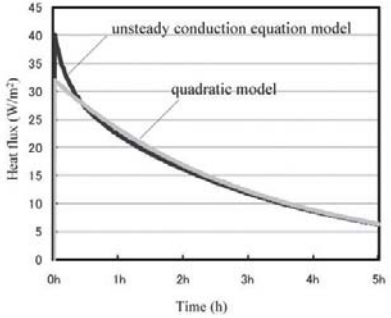


Fig.1 Comparison of heat flux by two models

In the heat transfer model of beam structure, the quadratic model can be used as heat transfer model of fire protection covering beam structure, and mean internal temperature weighted by each heat capacity of steel or fire protection covering material is used. Temperature of beam structure itself is assumed to be uniform because of high heat conductivity of steel. In the heat transfer model of sprinkler piping in ceiling chamber, the internal temperature is assumed to be uniform because of high heat conductivity.

System Simulation

A building heat transfer simulation is conducted in order to calculate energy-saving performance of this system. The outline of a building adopted thermal energy storage system by outdoor air is shown in **Table2** and the typical floor plan is shown in **Fig.2**. In cooling building masses in the ceiling chamber, the mechanical fan in air-handling-unit introduces outdoor air. The outdoor air is supplied to ceiling chamber through the return duct and cools the concrete slab, beam structures and sprinkler piping. Then the air is introduced into the office room through air supply openings which are used as suction port at the time of air-conditioning in daytime, and the introduced air cools the office furniture. Finally, the air is exhausted from natural ventilation openings above windows.

Building use : office, parking, substation, DHC plant
Total floor area : 106,000m²
Stories : 5 stories in underground and 41 stories on the ground
Air handling units in each floor : two units for ambient (8,200m³/h), four units for task(6000m³/h), one unit for EV hall

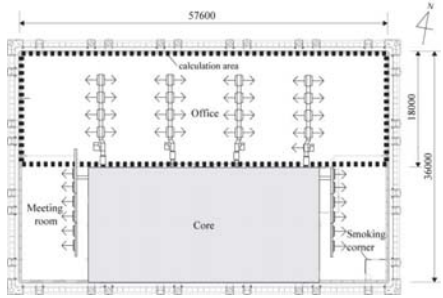


Fig.2 Typical floor plan

The energy saving performance was studied by the building heat transfer simulation surrounded by a dotted line shown in **Fig.2**. From 18:00 to 3:00 (Non-operating period), the outdoor air is not introduced anywhere and the air conditioners are turned off. From 3:00 to 8:00(Storage period), the natural outdoor air is introduced to the ceiling camber by mechanical fan and the openings for natural ventilation are opened. From 8:00 to 18:00(Air-conditioning period), the air conditioners keep the room air temperature at preset temperature.

Fig.3 shows the schematic of heat transfer between the air introduced from outside and the building masses. The room air temperature is assumed to be uniform and constant in air-conditioning period and the supplied outdoor air temperature into ceiling chamber is assumed to be the same as the measured outdoor air temperature from 18:00 May 20th to 18:00 May 21st, 2008 in the storage period (**Fig.4**).

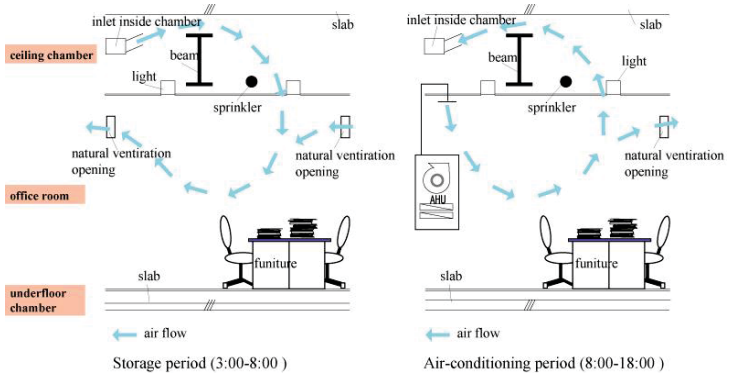


Fig.3 Schematic air flow pattern in heat transfer simulation at storage period and at air-conditioning period

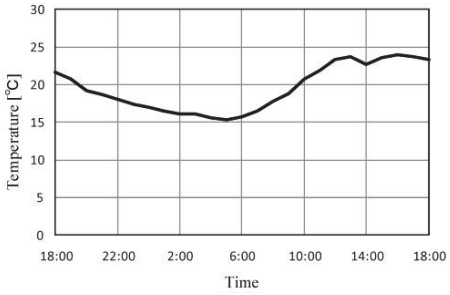
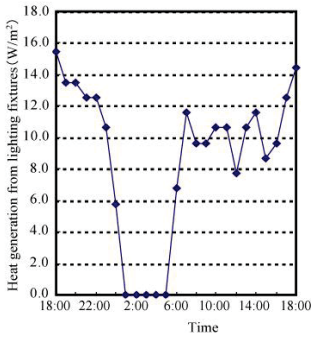


Fig.4 Outdoor air temperature from 18:00 May 20th to 18:00 May 21st, 2008

In this building, the air is supplied into the office room through slits in lighting fixtures. Therefore, the effect of heat generation from lighting fixtures should be considered. The heat generation from lighting fixture was assumed to be equal to measured electric power consumption from 18:00 on May 20th to 18:00 on May 21st in 2008. **Fig.5** shows the heat generation from lighting fixtures calculated from the measured electric power consumption. **Fig.6** shows the distribution of. In this simulation, 20% of heat from lighting fixtures was released into the office room air, and 20% was radiated to the surface of furniture (desk board). The 60% of heat from lighting fixtures is assumed to be heat up the air in ceiling ch



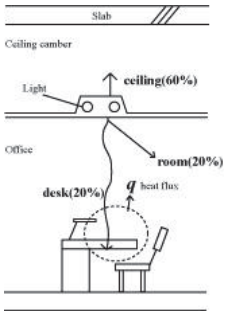


Fig.5 Heat generation from lighting fixtures

Fig.6 Distribution of lighting heat

Performance Evaluation

In evaluating of energy saving performance, the air flow rate introduced from outside by mechanical fan is important factor because the energy was only used by a mechanical fan in the storage period. The electric power required by mechanical fan is also increase if the air

flow rate increase. The optimized outdoor air flow rate can be found by comparing electric power consumption for the fan with the energy consumption for the air-conditioning. The released heat in building masses divided by the coefficient of performance (COP) is the energy consumption in the air-conditioning period by the cooled building masses. The value of COP is 2.35 that is the COP of DHC plant that supplies energy to this building. The energy reduction in the air-conditioning period by the cooled building masses is obtained by subtracting the electric power required for the fan from the effect of thermal energy storage. **Table3** shows the condition of this system simulation and **Table4** shows the condition of heat transfer models in this system simulation.

Table3 Calculation conditions in simulation

Case	Value
Room temperature during air-conditioning[°C]	25.5
Supply airflow rate during building thermal storage[m^3/s]	3.8
Airflow rate from natural ventilation openings during building thermal storage[m^3/s]	2.0
Supply airflow rate during air-conditioning[m^3/s]	1.6
Constant internal heat generation in storage period.[W/m^2]	4.0

Table4 Conditions of building elements in heat transfer models in simulation

Element	Heat conductivity[W/mK]	Volumetric specific heat[kJ/m^3K]	Thickness[mm]	Division number
slab	1.0	10000	150	10
furniture	0.15	714	100	-
beam				
steel	51.5	3713	18	-
fire protection material	0.095	384	65	-
sprinkler piping(water)	-	4168	-	-

Results and Discussion

Table5 shows the stored heat and energy consumption in the air-conditioning period by the cooled building masses. The data of electric power consumption of a mechanical fan are obtained by Building and Energy Management System (BEMS). The electric power consumption of mechanical fan in the storage period is 21.8 kWh. In **Table5**, "Storage mode" means that the building is both ventilated naturally and introduced outdoor air by the mechanical fan under the condition of **table3**. In storage mode, the building masses cooled by outdoor air can work to reduce cooling load and energy consumption of air conditioning system. However, in non-storage mode, the building masses are warmed by internal heat generation, and the building masses work to increase cooling load. According to **Table5**, the energy reduction in the air-conditioning period by the cooled building masses in Storage mode is 52.2kWh, and the difference of energy consumption of air-conditioner between Non-storage mode and Storage mode is 91.3kWh under the calculation conditions in Table3 and Table4.

Table5 Stored heat and Energy consumption in air-conditioning period

	Stored heat(kWh)		Energy consumption(kWh)	
	Storage mode	Non-storage mode	Storage mode	Non-storage mode
slab	-82.4	59.4	-35.1	25.3
furniture	-49.3	23.0	-21.0	9.8
beam structure	-31.2	9.8	-13.3	4.2
sprinkler piping	-10.8	-0.2	-4.6	-0.1
		fan	21.8	0.0
		total	-52.2	39.2
		deference	91.3	

Optimum operation of this system can be regarded as an operation of using the minimum energy. In this system, the energy reduction is determined by the balance of electric power consumption of mechanical fan. The electric power consumption of mechanical fan is proportional to the third power of air flow rate introduced from outside by mechanical fan , and the air flow rate introduced from outside by mechanical fan that makes the energy reduction in the air-conditioning period by the cooled building masses maximum can be obtained. **Fig.7** shows the relationship between the saved electric power and the air flow rate introduced from outside by mechanical fan. When the value of air flow rate is 0 m^3/s, the building is only ventilated naturally at storage period. According to **Fig.7,** the energy reduction per day by the cooled building masses reaches maximum value when the air flow rate introduced from outside by mechanical fan is about 3 m^3/s.

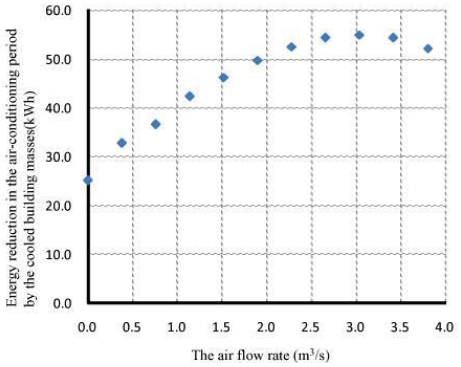


Fig.7 Relationship between the energy reduction per day by the cooled building masses and the air flow rate introduced from outside

Conclusions

In this paper, a simple heat transfer model of building masses, in which temperature distribution is assumed to be quadratic, is presented. By using this model, the surface heat flux of building masses can be obtained easily. In this thermal energy storage system simulation, the quadratic model can be used to calculate the surface heat flux of building masses such as desk board. The unsteady conduction equation model can be used to calculate the surface heat flux of concrete slab because of its large heat capacity. According to this system simulation, the thermal energy storage system using introduced outdoor air has the potential to increase the energy reduction in the air-conditioning period by the cooled building masses

Nomenclature		
θ_r	preset room temperature	[°C]
$\theta(x,t)$	building mass temperature	[°C]
$\bar{\theta}(t)$	mean building mass temperature	[°C]
x	distance from the surface of a building mass	[m]
λ	building mass heat conductivity	[W/m·K]
h	heat-transfer coefficient	[W/m^2·K]
ρ	density of building mass	[kg/m^3]
c_p	specific heat under constant pressure	[J/kg·K]
l	thickness of building mass×1/2	[m]
A	calculation area of the building	[m^2]
A_f	area of office space	[m^2]
q_1	heat flux of unsteady conduction equation model	[W/m^2]
q_2	heat flux of quadratic model	[W/m^2]
q_l	heat load from lighting fixture	[W/m^2]
W_l	he electric power consumption for lighting	[W]
W_a	energy reduction in the air-conditioning period by the cooled building masses	[kWh]
Q_a	Cooling heat load from building masses	[kWh]

References

1. Ushio,T., Sagara,K., Yamanaka,T., Kotani,H., Yamagiwa,M., Yamashita,T and Horikawa,S., "Task Ambient Air Conditioning System with Natural Ventilation for High Rise Office Buidling (Part1:Outline of System and Thermal Environment in Working Zone)" *Healthy Buildings 2006*, pp.269~274, 2006.

2. Ishino,H. and Kouri,K., "A Study on the Thermal Effect of Internal Furniture in Office Building," *Journal of Architecture*, Planning and Environment Engineering(Transactions of AIJ), No.372, pp.59-66, 1987.

3. Kumata.Y., Yamagiwa.M., Sagara.K., Yamanaka.T., Kotani.H., and Momoi,Y., " Operation Method Study of Building Thermal Energy Storage by Outdoor Air with Heat Transfer Simulation" *Summaries of Technical Papers of Annual Meeting Architectural Institute of Japan 2010*, pp7-8, 2010. (in Japanese)

Field Survey on Indoor Thermal Environment in Small to Medium Sized Building with Packaged Air Conditioners

Haruka NAKASONE[1], Hisashi KOTANI[1], Yoshihisa MOMOI[1],

Kazunobu SAGARA[1] and Toshio YAMANAKA[1]

[1] Department of Architectural Engineering, Osaka University, Japan

Abstract

Recently, a lot of multiple packaged unit system is adopted in small to medium sized buildings in Japan. This system enables to control each packaged air conditioner (PAC) individually because multiple packaged units are placed decentrally. However, it is not clarified sufficiently how indoor environment is formed when PAC is working. This paper shows the measurement results of indoor thermal environment in a medium sized building with PAC in all season for the purpose of clarifying the current status of indoor environment and its issue. In indoor thermal environment, there was no issue throughout the year though measurement conditions made difference in temperature and humidity distribution. In indoor units operation, it was clarified that supply air temperature of PAC is different from each PAC and way. In addition, it was clarified that short circuit of supply air from PAC to inlet of the ventilation devices happen.

Keywords: multiple packaged unit system, field survey, indoor thermal environment

1. Introduction

Recently, energy consumption in civilian sector is increased in Japan. Saving of energy consumption in general buildings is required as a solution of global warming. Thus, energy conservation law concerning buildings is changed from a total floor space of more than 2000 m^2 to more than 300 m^2 [1]. However, the running situation of the air conditioners in real buildings are not clarified, because they don't have monitoring control system

such as central monitor system. Furthermore, it is not applicable in small to medium sized buildings though standards of indoor environment are established in building hygienic maintenance law for large sized buildings of a total floor space of more than 3000 m^2 [2]. Therefore, standards of indoor environment in small to medium sized buildings are needed and the way to conserve the energy consumption under keeping a comfortable indoor environment has to be discussed. In addition, it is not enough though some field surveys has been done on indoor thermal environment with packaged air conditioners (PAC). [3]

This study is intended for small to medium sized buildings with PAC because a lot of multiple packaged unit system is adopted in such small sized buildings. This system enables to control each PAC individually because multiple packaged units are placed decentrally. However, it is not clarified sufficiently how indoor environment is generated when PAC is running.

This paper shows the measurement results of indoor thermal environment in a medium sized building with PAC in all season for the purpose of clarifying the current situation of indoor environment and its issue.

2. Method of investigation

Measurements were taken in summer (Jul.21 to Sep.4, 2009), moderate season (Oct.13 to Nov.6, 2009) and winter (Feb.8 to Mar.5, 2010). The office room, the target of this study, is located in the 5th floor of 7-storied office building in Osaka, Japan. There are adjacent buildings in the east-west direction, the parking in the north direction and the road in the south direction. Table1 shows building summary. The air conditioning system of this building is so-called multiple packaged unit system, and there are 6 indoor units of 4-way ceiling mounted cassette type (PAC1-6) in the office room. Cooling capacity is 9.0kW (PAC1, 3, 5) and 7.1kW (PAC2, 4, 6), while heating capacity is 10.0kW (PAC1, 3, 5) and 8.0kW (PAC2, 4, 6). Thermostats of room temperature are in indoor units. In addition, there are 3 ventilation equipments (VENT1-3) which have 2 inlets and 2 outlets. They are switchable for total heat exchanger mode (HEX) and desiccant mode (DEC). Figure1 shows 5th floor plan and measurement points of horizontal temperature and humidity. Table2 shows measurement items. Measurement conditions are determined by the setting temperature and ventilation mode. Table3 and 4 shows measurement conditions of representative weeks in summer (Aug.17 to Aug.21, 2009), moderate season (Nov.2 to Nov.6, 2009) and winter (Feb.15 to Feb.19, 2010). Aug.17 and Nov.2 is representative days of 27°C&HEX, and Feb.15 is a representative day of 22°C&HEX because measurement conditions are same for Aug.17 and 18, Nov.2 and 3, Feb.15 and 16.

Table 1 Building summary

Use	Office
Total floor area	2614m^2
Office area(5F)	216m^2
Stories	7F
Number of packaged air conditioner per office room	6
Number of total heat exchanger / desiccant per office room	3

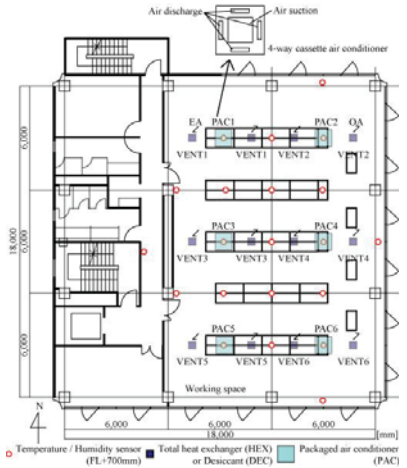


Figure 1 Building Plan

Table 2 Measurement items

Measurement item	Number of measurement points	Measurement interval
Temperature/Humidity (Horizontal distribution)	20	5min.
Temperature/Humidity (Vertical distribution)	Interior:5, Perimeter:5	5min. (FL+100,600,1100,1700,2900mm)
Temperature/Humidity (Packaged air conditioner)	Air inlet:6, Air outlet:6	5min.
Temperature/Humidity (Total heat exchanger)	Air inlet:6, Air outlet:3	5min.
PMV	2	10min.
CO_2 concentration	2	10min.
Horizontal illuminance	10	1min.
Vertical illuminance	2	1min.

Table 3 Measurement conditions (cooling)

Summer	Autumn	Setting temperature	Ventilation system
Aug.17, 18	Nov.2, 3	27°C	Total heat exchanger (HEX)
Aug.19	Nov.4	26°C	Total heat exchanger (HEX)
Aug.20	Nov.5	27°C	Desiccant (DEC)
Aug.21	Nov.6	26°C	Desiccant (DEC)

Table 4 Measurement conditions (heating)

Winter	Setting temperature	Ventilation system
Feb.15, 17	22°C	Total heat exchanger (HEX)
Feb.18	20°C	Total heat exchanger (HEX)
Feb.16	22°C	Desiccant (DEC)
Feb.19	20°C	Desiccant (DEC)

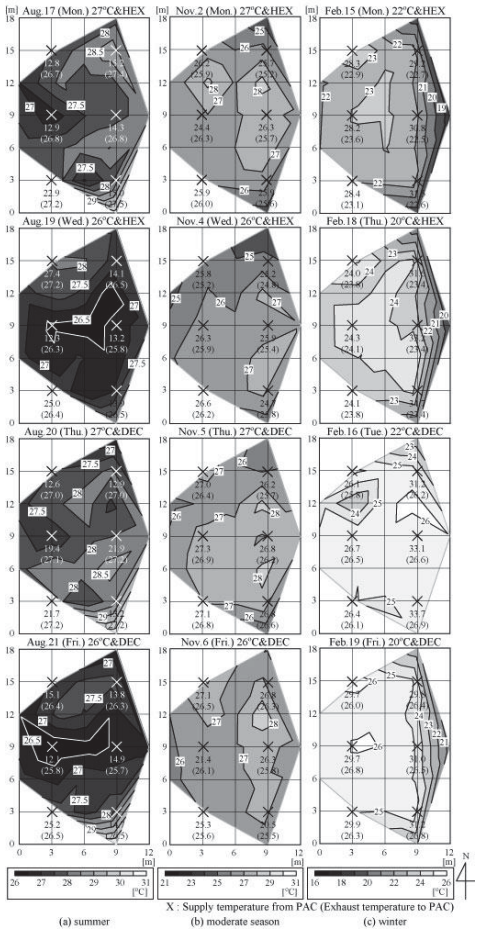


Figure2 Horizontal temperature distribution
((a) summer, (b) moderate season, (c) winter)

3. Indoor thermal environment

3.1 Indoor temperature distribution

Figure2 shows horizontal temperature distribution (FL+700mm) in summer, moderate season and winter respectively which is average of 2 hours (15:00 to 17:00). This figure is indicated as coordinate where southwest point of office room is origin coordinate (see Figure1). X-mark means PAC1-6 and values under the each X-mark represent each average temperature of supply and exhaust air. Supply air temperature shows one-way temperature in summer and average of 4-way temperature in moderate season and winter.

In summer (Figure2 (a)), room temperature is higher than setting temperature by 1°C. Specifically, room temperature is about 27.5 to 28.5°C at 27°C of setting temperature, about 26.5 to 28°C at 26°C of setting temperature. Decrease in temperature around center of the office room is especially larger than any other parts of room by 1 to 1.5°C which is resulted from operational situation of PAC3 and 4 because decrease in temperature is small on Aug.20 when PAC3 and 4 is under on-off control. It is also similar to PAC1. PAC2 and 6 is always cooling, while PAC5 is under on-off control. HEX and DEC make no difference in temperature distribution.

In moderate season (Figure2 (b)), setting temperature makes no difference since room temperature is about 26 to 28°C at 27°C of setting temperature and about 25 to 28°C at 26°C of setting temperature. It is caused by rare PAC operation because of little cooling load. Compared with summer survey, it is inclined to be smaller effect of solar radiation in the south direction and greater effect of ambient temperature in the north direction.

In winter (Figure2(c)), room temperature is about 20 to 23°C at 22°C of setting temperature on Feb.15 and room temperature is higher than setting temperature by about 3 to 6°C in other days. It is thought that PAC is heating operation on Feb.15 and room temperature was out of control in other days because of forced heating operation though cooling operation was needed actually. In addition, supply air temperature is high in these days. This is because there is heating demand not in this room, but in the other room where indoor units are connected with same outdoor units. Therefore, more analysis is needed in the near future. It is needed to pay attention to switch of operation in the room where internal load is large such as the target of this study because there are cooling demand and heating demand at the same time.

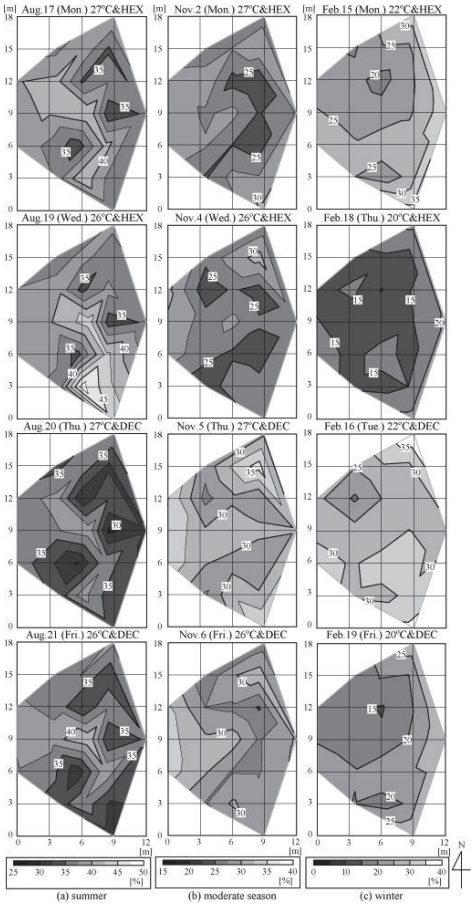


Figure3 Horizontal humidity distribution
((a) summer, (b) moderate season, (c) winter)

3.2 Indoor humidity distribution

Figure3 shows horizontal humidity distribution (FL+700mm) in summer, moderate season and winter respectively which is average of 2 hours (15:00 to 17:00).

In summer (Figure3 (a)), setting temperature makes no difference in humidity distribution. However, room relative humidity in DEC is lower than in HEX. Specifically, room relative humidity is about 35 to 45% in HEX and about 30 to 40% in DEC. This is the effect of dehumidification in DEC.

In moderate season (Figure3 (b)), there is no effect of dehumidification because ambient humidity was low. However, all relative humidity in this room is lower than 40%.

In winter (Figure3(c)), room relative humidity in DEC is higher than in HEX by about 5 to 10%. This is the effect of humidification in DEC. However, it is inclined to be low relative humidity in this room. It is resulted from no humid operation because there was not heating demand but cooling demand.

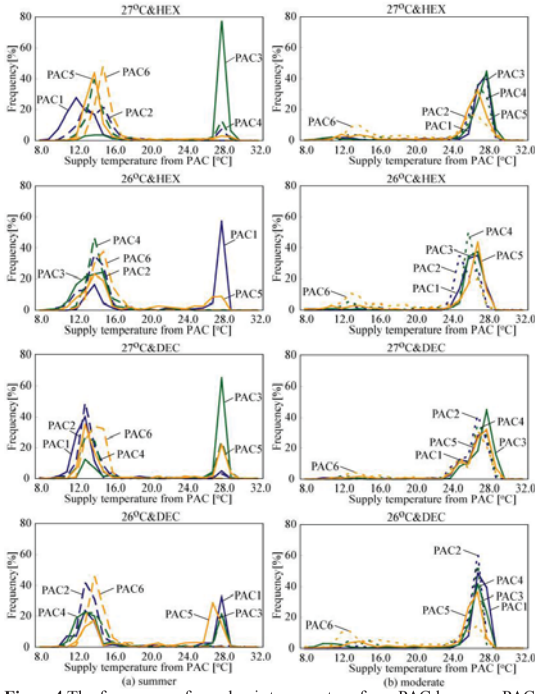


Figure4 The frequency of supply air temperature from PAC by every PAC
((a) summer, (b) moderate season)

4. Indoor units operation

4.1 Supply air temperature from PAC

(1)Difference from PAC

Figure4 shows the frequency distribution of supply air temperature of PAC by every measurement conditions when it is working hours (9:00 to 17:00) in summer and moderate season. The values of supply air temperature at intervals of 5 minutes are one-way temperature in summer and 4-way temperature in moderate season.

In summer (Figure4 (a)), supply air temperature is 12 to 14°C when the thermostat is on, and 27 to 28°C when the thermostat is off. In addition, supply air temperature is different from each PAC. It is thought that there is a mutually complementary relationship between PAC1 and 3. The thermostat is likely to be off in PAC3 when on in PAC1 at 27°C of setting temperature, while the thermostat is likely to be off in PAC1 when on in PAC3 at 26°C of setting temperature. PAC2 and 6 in the perimeter zone is cooling almost all the time. Supply air

temperature of PAC4 and 5 is different from HEX and DEC. The thermostat is likely to be on in HEX, while the thermostat is likely to be on and off in DEC.

In moderate season (Figure4 (b)), supply air temperature is 26 to 28°C almost all the time. PAC6 is sometimes cooling because it locates at south direction. Compared with summer survey, measurement conditions make no difference because thermostat is inclined to be off.

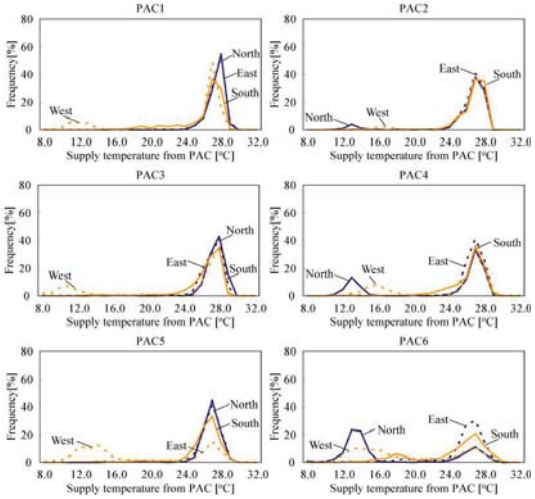


Figure5 The frequency of supply air temperature from PAC by every ways

(2)Difference from ways of supply air

Figure5 shows the frequency distribution of supply air temperature of PAC by every ways of supply air when it is working hours (9:00 to 17:00) in moderate season. In moderate season, the thermostat is likely to be off (see Figure4), however, it is different from ways of supply air. Supply air temperature of PAC1, 3, 5 in the interior zone is 10 to 13°C at the west direction, 26 to 28°C at the other direction. Supply air temperature of PAC2, 4, 6 in the perimeter zone is 12 to 14°C at the north and west direction, 26 to 28°C at the other direction. Though PAC6 is higher frequency of cooling than PAC2 and 4, it is different from supply air temperature and frequency by ways. This can cause by the positional relationship between internal heat exchanger of PAC and outlets. Especially, it can cause in moderate season when refrigerant mass flow rate is low because of low cooling load. This chapter is clarified supply air temperature of PAC is different from each PAC and way, however, there is no effect of indoor thermal environment.

4.2 Short circuit of Supply Air from PAC

Figure6 shows the diagram of airflow from PAC and VENT. It is thought that there is airflow from two directions into inlets of VENT. One is airflow mixed by supply air from PAC and indoor air, the other is airflow which comes from PAC directly. Because of this effect, it is expected that exhaust air temperature to VENT is lower than to PAC. This paper considers short circuit of supply air from PAC in summer when this effect is great.

Figure7 shows relation between exhaust air temperature to PAC2 and VENT2 to the west of PAC2 in case of 27°C&HEX when it is working hours (9:00 to 17:00).

Exhaust air temperature to PAC is 26 to 28°C that is plus or minus 1°C of setting temperature, while exhaust air temperature to VENT is lower than setting temperature by 4°C. Therefore, there is possibility that short circuit of supply air from PAC to inlet of VENT happens. This effect is shown in the other relation between exhaust air temperature to PAC and to VENT.

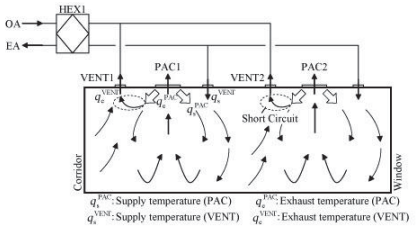


Figure6 The diagram of airflow from PAC and VENT

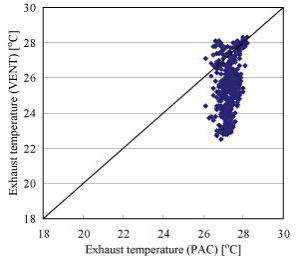


Figure7 Relation between exhaust air temperature to PAC2 and VENT2

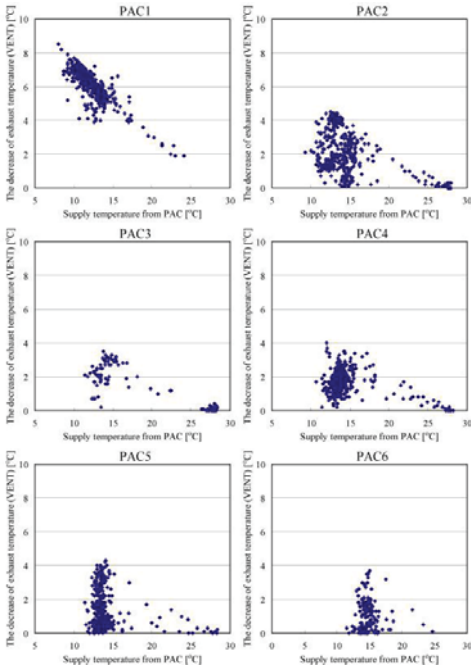


Figure8 Relation between supply air temperature from PAC and the decrease of exhaust air temperature to VENT

Figure8 shows relation between supply air temperature from PAC and the decrease of exhaust air temperature to VENT (Exhaust air temperature to PAC ($=q_e^{PAC}$) - Exhaust air temperature to VENT ($=q_e^{VENT}$), see Figure6). There is possibility that short circuit of supply air from PAC to inlet of VENT happens if the decrease of exhaust air temperature to VENT is greater than 0°C because exhaust air temperature to PAC is plus or minus 1°C of setting temperature (see Figure7). All decrease of exhaust air temperature to VENT is about 4°C when supply air temperature from PAC is 12 to 14°C. For this reason, short circuit is likely to happen. Especially in PAC1, decrease of exhaust air temperature to VENT is the greatest up to 9°C. Short circuit ratio is defined as the ratio of short circuit (decrease of exhaust air temperature to VENT>2°C) to PAC operating (supply air temperature from PAC<20°C). However, not all supply air from PAC short-circuits because it is different from supply air flow rate of PAC and exhaust air flow rate of VENT. However, more consideration is needed for this definition because the definition of 2°C is just a supposition.

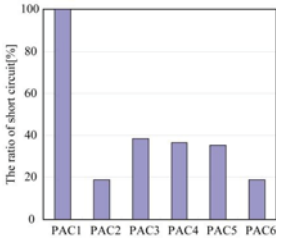


Figure9 The ratio of short circuit

Figure9 shows the ratio of short circuit from outlets of PAC to inlets of VENT on Jul.28 to Aug.28. Compared with PAC1-6, the ratio of short circuit is highest in PAC1. It is thought that supply air from PAC may short-circuit. More consideration is needed for short circuit in the future because many factors affect short circuit. In addition, consideration including heat-transfer efficiency is needed because there is heat recovery in HEX.

5. Conclusion

There was no issue in indoor thermal environment throughout the year though measurement conditions made difference in temperature and humidity distribution. In indoor units operation, it was clarified supply air temperature from PAC is different from each PAC and way. In addition, it was clarified that short circuit of supply air from PAC to inlet of VENT happens. More detailed indoor environment by means of CFD analysis is recommended in the future study.

Acknowledgments

A part of this study was done in study group for energy management in small to medium sized buildings, Kinki Branch of The Society of Heating, Air-Conditioning and Sanitary Engineers of Japan. Authors would like to appreciate everyone concerned.

References

1.Web Pages and On-line Material: (for illustration), "Japan Energy Conservation Handbook 2009," *ECCJ*, http://www.asiaeec-col.eccj.or.jp/databook/2009e/index.html (Jul.27, 2010).

2.Web Pages and On-line Material: (for illustration), "Building hygienic maintenance law," *Ministry of Health Labour and Welfare,Japan*, http://law.e-gov.go.jp/htmldata/S45/S45HO020.html (Jul.27, 2010). (in Japanese)

3. Anna Won, Toru Ichikawa, Satoshi Yoshida and Satoru Sadohara, "Study on Running Performance of a Split-type Air Conditioning System Installed in the National University Campus in Japan," *Journal of Asian Architecture and Building Engineering*, vol.8, no.2, November 2009, pp.579-583

Evaluation on the Availability of Treated Sewage Water as an Unused Energy Source in a Super High-rise Complex Building

Jae-Han Lim[1], and Seung-Yeong Song[2]

[1] Assistant Professor, Ewha Womans University, Dept. of Architecture, Seoul, Korea 120-750

[2] Associate Professor, Ewha Womans University, Dept. of Architecture, Seoul, Korea 120-750

Abstract

Because the super high-rise complex building would be designed vertically with a mixed-use space, a large amount of unpurified domestic sewage could be discharged continuously outside the building site. The waste heat from the sewage water can be used for low temperature heating and high temperature cooling sources for HVAC system such as radiant heating and cooling system, and domestic hot water services. This study aims to evaluate the availability of treated sewage water as an unused energy source in a super high-rise complex building. For this purpose, current sewage treatment methods were analyzed to clarify the alternatives of heat source, and thermal energy potentials were evaluated according to the quantity of treated water and seasonal temperature variation. In conclusion, it was forecasted that the treated sewage water could be more effective for using the heating sources rather than the cooling sources because the temperature differences in spring and winter between treated sewage water and outdoor air was larger than those in summer. Also the thermal energy potentials were estimated from 20,900 MJ/day to 62,700 MJ/day according to the building use patterns.

Keywords: Super High-rise Complex Building, Unused Energy Source, Treated Sewage Water, Heat pump, Low Temperature Heating and High Temperature Cooling

Introduction

Because the super high-rise complex building would be designed vertically with a mixed-use space, a large amount of unpurified domestic sewage could be discharged continuously outside the building site. Sewage water from baths and showers, washing machines in

buildings has a various temperature ranges between about 13 and 30 °C. Because the temperature of sewage water is relatively higher than outside air temperature with the seasons and is changed little, which is usually in less than 10°C, the sewage water has been regarded as suitable heat sources for HVAC system. Especially, the waste heat from the sewage water can be used for heat sources for low temperature heating and high temperature cooling system such as radiant heating and cooling, and domestic hot water services. Also with the recent advancement of heat pump technology, it has been considered as rational use of unused energy sources in buildings. This type of energy source has been considered as green energy sources and mainly used for district heating, heating and cooling energy for the building located near the sewage disposal plant.

This study aims to evaluate the availability of treated sewage water as an unused energy source in a super high-rise complex building. For this purpose, current sewage treatment methods were analyzed to clarify the alternatives of heat source, and thermal energy potentials were evaluated according to the quantity of treated water and seasonal temperature variation.

Application of treated sewage water in super high-rise complex building

Normally the sewage water has been discharged in every building stock. And the sewage water was moved through the drain pipe in city and finally to the sewage disposal plant. As sewage entered the plant, large solid bodies such as wood and gravel were screened out. Grit and sand were then removed by settling or screening with finer mesh. The remaining sewage passed into primary sedimentation tanks that suspended solid-type sludge settles out. The remaining sewage was aerated and mixed with microorganisms to decompose organic matter. A secondary sedimentation tank allowed any remaining solids to settle out. The remaining liquid effluent was discharged into a body of water. Sludge from the sedimentation tanks may be disposed of in landfills, dumped at sea, used as fertilizer, or decomposed further in heated tanks (digestion tanks) to produce methane gas to power the treatment plant.

The thermal energy from sewage water could be obtained by three methods depending on where the energy is extracted, i.e the in-house energy recuperation, energy recovery from raw sewers, energy recovery from treated wastewater after the sewage treatment plant. The energy potential of treated sewage water was much higher than that of raw sewage water. Unfortunately, the large energy potential of treated sewage water could not be used in many locations because the sewage treatment plants were located outside building stock, where no consumers for the heat were available.

Treated sewage water could be used for domestic hot water supply and heating and cooling for building HVAC system. As numerous pilot examples have shown, the combined use of treated sewage water for heating and cooling with thermal storage system and conventional

heat sources such as chillers and boilers normally provides an extremely economical supply of energy. Generally, sewage water heat pump can use the treated water in winter of the temperature 11-15 °C, in summer of the temperature 17-21°C. This makes the sewage water heat pump to operate efficiently by 20% in comparison of conventional air-conditioning heat pump system. Commercially available heat pump systems usually use heat from the ambient air or from the discharge of an air conditioner to heat water for household use. These systems are impractical or infeasible in cold winter season of Korea. Because conservation is particularly important in the colder climates, an alternative system is desirable.

Sewage water is collected from sinks, showers, and washing machines and is stored in an insulated storage tank. Particulates and other sediment, such as hair or lint, are filtered from the sewage water before the sewage water is circulated to an evaporator. In the evaporator, the sewage water transfers its heat to a refrigerant. The temperature of the refrigerant, which leaves the evaporator, is further increased in a compressor. Then, the heated refrigerant transfers its heat to household water in a condenser and the household water is stored. In application of treated sewage water in super high-rise complex building, an improved sewage water storage tank, including a conical mesh to treat the inlet sewage water to remove sediment, such as hair, lint, and other particulates is used in several cases. The treated sewage water is circulated to the evaporator by drawing warm sewage water from the top of the storage tank. After passing through the evaporator, the cooled sewage water is recycled to the storage tank, where it enters to displace warmer water upwardly in the tank. The conical mesh can be easily cleaned with a jet ejector nozzle which flushes the particulates from the mesh into the tank. In the evaporator, heat is exchanged between the sewage water and a refrigerant. The entering sewage water ordinarily has a temperature of about 35° C. while the refrigerant will be a liquid-gas mixture at about 4° C. The refrigerant gains heat so that it exits as a pressurized gas at about 4° C. In the compressor, saturated refrigerant vapor leaving the evaporator is superheated to achieve a high-pressure gas. This gas is passed through the condenser, where the refrigerant transfers its heat to inlet household water. The water exits via pump into an insulated storage tank. The refrigerant is re-circulated to the evaporator through a throttling valve, expansion valve, or capillary tube, completing its heat pump cycle.

Estimation of thermal energy potential in treated sewage water

Thermal energy potential is the theoretically estimated energy quantity in unused energy sources. So this is calculated with Eq.1.

$$E = W \times C_p \times \Delta T \quad \text{(Eq. 1)}$$

Where E = Thermal energy potential [kJ/day]

W= mass [kg/day], i.e. mass flow rate of treated sewage water

C_p = specific heat of treated sewage water [kJ/kg·K] (approximately 4.18)

ΔT = available temperature drop [K or ºC], i.e. temperature difference between supply and return of treated sewage water

Available energy potential is the quantity of usable energy by considering the current physical and technical limitation. So this is calculated by assuming that the sewage water heat pump can be applied to the heating and cooling purposes. This is calculated with Eq.2 and Eq.3.

$$E_c = E \times \frac{COP_c}{(COP_c+1)} \quad \text{(Eq. 2)}$$

$$E_h = E \times \frac{COP_h}{(COP_h-1)} \quad \text{(Eq. 3)}$$

Where E_c = Available cooling energy potential [kJ/day]

COP_c= Coefficient of performance in cooling operation [-]

E_h = Available heating energy potential [kJ/day]

COP_h= Coefficient of performance in heating operation [-]

Results and Discussion

1. Analysis of sewage water temperatures

Because the performance of heat pump system can be affected by the part-load conditions and the temperature variations of treated sewage water, it is necessary to design the capacity of system appropriately according to the characteristics of building loads and temperature variation of sewage water. In this study, we have aimed at evaluating the energy potential of treated sewage water as an unused energy source, so at first the temperature variation of treated sewage water in real test building has been measured year-round. Test facility was composed of sewage water heat pump, submerged pump, indoor terminal units, control panel, and sewage disposal facility (See Fig.1). In measurement results, as shown in Table 1, the sewage water temperature has been changed according to variation of the outdoor air temperature. In summer seasons, the sewage water temperature was larger than the outside air temperature, but the temperature fluctuation of sewage water during the day was smaller than that of outside air. Also it was forecasted that the treated sewage water could be more effective for using the heating sources rather than the cooling sources because the temperature differences in winter between treated sewage water and outdoor air was larger than those in summer.



Fig. 1 Photos of pilot project system in test building

Table 1 Comparison of outdoor air temperatures[1)] and sewage water temperatures

Date	Outdoor air temperature (°C) [1)]			Sewage water temperature (°C)		
	Average	Maximum	Minimum	Average	Maximum	Minimum
16 March (A)	1.9	6.0	-0.8	10.6	11.2	9.4
16 April (B)	8.2	15.4	0.2	18.3	22.5	12.0
16 May (C)	18.8	27.2	9.5	21.1	21.8	19.8
16 June (D)	22.8	27.9	17.3	28.1	28.4	25.8
16 July (E)	24.8	29.2	22.6	28.8	29.1	28.6

[1)] Outdoor air temperatures were obtained from the databases of Korea Meteorological Administration (KMA).
(http://www.kma.go.kr/weather)

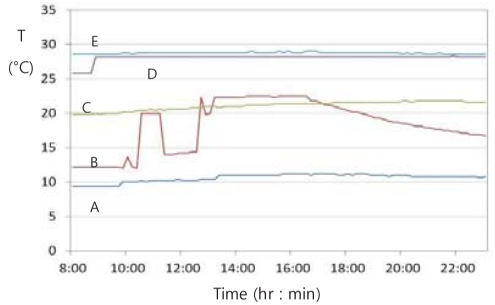


Fig. 2 Results of temperature fluctuation of treated sewage water

2. Analysis of sewage water flow rates

Sewage water flow rates in super high-rise complex building can be varied according to the total floor areas, use patterns, operation schedule, etc. Also it can affect the energy potential of treated sewage water. In the conceptual design stage, it is appropriate that the energy potential of treated sewage water and the capacity of system would be estimated according to the total floor areas because it is easy to understand the scale of overall system and communicate it with other experts. So we have used the basic estimation methods of discharge rates of sewage water according to the building usage pattern to evaluate the flow rates of treated sewage water. [1] As shown in Table 2, the discharge rates of sewage water were estimated according to the building usage, and that could be converted into the values for each floor area. In results, the discharge rate of sewage water in residential building was

10 L/m^2, that in office 15 L/ m^2, that in accommodation facility and restaurant 60 L/m^2, that in cultural facility 16 L/m^2.

Table 2 Discharge rates of sewage water according to the building usage[1)]

Building usage \ Discharge rates		Discharge rates of sewage water per day	Converted value according to the floor area
Residential building	Detached house	200 L/person	10 L/m^2
	Apartment building	200 L/person	10 L/m^2
Office building	Office	15 L/m^2	15 L/m^2
	Efficiency apartment	200 L/person	10 L/m^2
Accommodation facility (Hotel etc.)		250 L/person	60 L/m^2
Marketing facility (Shopping mall, store etc.)	Restaurant	60 L/m^2	60 L/m^2
	Department store	30 L/m^2	30 L/m^2
Cultural facility		16 L/m^2	16 L/m^2

1) Estimation methods of discharge rates of sewage water according to the building usage (Ministry of Environment, Notification No. 2007-178), Republic of Korea.

3. Analysis of thermal energy potential and available energy potential of treated sewage water

As previously mentioned, thermal energy potential and available energy potential of treated sewage water could be estimated by using the mass flow rate of treated sewage water, specific heat of treated sewage water, available temperature drop, and coefficient of performance in heating and cooling operation. Generally, the building usage pattern of international high-rise buildings over 150 meters has been changing as shown in Table 3. [2] In Table 3, we could see that the majority of high-rise buildings were destined for office use in 1980 and 1995. The current percentage in this use pattern was only 47.3%. Where buildings under construction were concerned, the figure drops to 26.8% of the total. At the same time we could see that the residential building was now becoming the most widely built pattern with 47.3% of the total currently under construction. Most of all, we also could find a steady rise of the mixed-use building, rising from 5.3% in 1980 to 11.0% today. With 17.7% currently under construction, we could anticipate a bright future for this building type. The mixed-use high-rise building would be more and more popular. So in this study, we have assumed the building use pattern in super high-rise complex building like the cases in Table 4 for estimating the discharge rates of sewage water.

Table 3 Percentages of Building usage of international high-rise buildings over 150 meters[1)]

Usage \ Year	1980	1995	2008 Plus those under construction	Those under construction only
Office	84.7 %	78.3 %	47.3 %	26.8 %
Mixed-use	5.2 %	6.6 %	11.0 %	17.7 %
Residential	5.2 %	9.6 %	35.3 %	47.3 %
Hotel	4.9 %	5.5 %	6.4 %	8.2 %

1) Georges Binder, The international Skyscraper: Observations, CTBUH Journal, 2008 Issue 1, pp. 20-30.

Table 4 Assumption of building usage in super high-rise complex building

Building usage	Case 1	Case 2	Case 3	Case 4
Residential	0.5	0.5	0.4	-
Office	0.5	-	0.3	0.5
Accommodation (Hotel)	-	0.5	0.3	0.5

Also we have assumed that the general coefficient of performance (COP) of heat pump system was 4 and the available temperature drop was 5°C to estimate the thermal energy potential and available energy potential of treated sewage water sources in super high-rise

complex buildings. In results, when the total floor area is 800,000 m^2, the total discharge rate of sewage water was about from 10,000 Ton/day to 30,000 Ton/day. If we assumed that 10 percentage of this discharged sewage water would be treated for grey water in building, we could use the treated sewage water about from 1,000 Ton/day to 3,000 Ton/day for unused energy source. In this case, the thermal energy potentials were estimated from 20,900 MJ/day to 62,700 MJ/day according to the building use patterns.

Table 5 Thermal energy potential and available energy potential of treated sewage water sources in super high-rise complex building

Category		Assumption : Total floor area is 800,000 (m^2)			
		Case 1	Case 2	Case 3	Case 4
Discharge rate of sewage water (Ton/day)		10,000	28,000	21,200	30,000
Treated rate of sewage water (Ton/day)		1,000	2,800	2,120	3,000
Thermal energy potential (MJ/day)		20,900	58,520	44,308	62,700
Available energy potential (MJ/day)	Cooling	16,720	46,816	35,446	50,160
	Heating	27,867	78,026	59,077	83,600

Conclusions

This study aims to evaluate the availability of treated sewage water as an unused energy source in a super high-rise complex building. For this purpose, current sewage treatment methods were analyzed to clarify the alternatives of heat source, and thermal energy potentials were evaluated according to the quantity of treated water and seasonal temperature variation. In conclusion, it was forecasted that the treated sewage water could be more effective for using the heating sources rather than the cooling sources because the temperature differences in spring and winter between treated sewage water and outdoor air was larger than those in summer. Also the thermal energy potentials were estimated from 20,900 MJ/day to 62,700 MJ/day according to the building use patterns.

Acknowledgments

This research is supported by a grant (Code#'09 R&D A01) from Cutting-edge Urban Development Program funded by the Ministry of land, Transport and Maritime Affairs of Korean government.

References

1. Ministry of Environment, "Estimation methods of discharge rates of sewage water according to the building usage", *Notification* No. 2007-178, Republic of Korea.

2. Georges Binder, "The international Skyscraper: Observations", *CTBUH Journal*, 2008 Issue 1, pp. 20-30.

3. N.C. Baek, U.C.Shin, J.H. Yoon, Kovler, K., "A study on the design and analysis of a heat pump heating system using wastewater as a heat source", Vol. 78, No. 3, *Solar Energy*, 2005, pp.427~440.

4. Felix Schmid, "Sewage Water: Interesting Heat Source for Heat Pumps and Chillers", *Swiss Energy for infrastructure plants*, 2008.

School Eco-Renovation Method for Improvement of Thermal Environment in Large Workshop of High School without Air-Conditioning System

Junya YAMADA[1], Toshio YAMANAKA[1], Kazunobu SAGARA[1],
Hisashi KOTANI[1], Yoshihisa MOMOI[1], and Saori YASUI[1]

[1] Dept. of Architectural Engineering, Osaka University, Suita 565-0871 Osaka, Japan

Abstract

In recent years school buildings, containing the workshop in high school, are old in Japan. Therefore most of them need renovating. Any air-conditioning systems are not often installed in the workshops. Workshops without air-conditioning systems often have bad indoor thermal environments. Since bad thermal environment is exhausting and *likely to cause some accidents, eco-renovation method for improvement of thermal environment is required. In this paper, various kinds of eco-renovation methods are examined by CFD simulation. The examined methods are insulation of the PC roof and the walls to decrease the surface temperature, and utilization of more ventilation rate in summer.*

Keywords: Workshop, Thermal environment, CFD simulation, Eco-Renovation.

1. Introduction

In Japan many schools have old buildings because they were built during the 60's - 70's of high economic growth. In the old school buildings any ecological systems are not considered.

To change this situation, Japanese government started a project named "School Eco-Renovation and Environmental Education Program" since 2005. This project helps the old school buildings to be renovated ecologically, and it is expected that through the renovation students come to know well about "Energy and Environment Matter." More than twenty schools have been renovated as models of this policy since 2005 in Japan [1].

In addition, most of the workshops of school have bad thermal environments because they are not equipped with any air-conditioning systems. Since bad thermal environment is exhausting and likely to cause some accidents, improvement of the thermal environment is required.

In this study eco-renovation method of a large workshop in a high school is proposed in order to improve the indoor thermal environment. The target workshop is in a building which school, as a model of the "School Eco-Renovation and Environment Education", has. Therefore the method is based on passive control without air-conditioning system. This paper shows that comparison between measurement and simulation by Computational Fluid Dynamics (CFD), and the effect of the insulation of the Prestressed Concrete (PC) roof and walls and the increase of ventilation rate will be examined.

2. Measurement

A measurement research of the thermal environment in large workshop was carried out to compare with simulation results. The large workshop to be investigated is a workshop of a technical high school in Osaka. The plan and sections of the workshop are shown in Figure 1.

The top height of the workshop is 6.6 m. The roof is made of PC (Pre-Stressed Concrete) and covered with waterproof sheets with silver coating. Three ventilation fans are installed on the east and west walls respectively. No air-conditioning system is installed in this workshop. In summer, the workshop is used with all windows open to introduce natural wind. In the workshop there are some turning machines and milling machines.

Measurements of the thermal environment were conducted between on the 6th to the 19th September 2009. Measurement points are shown in Figure 1. The measurement points are located in the center of workshop. Measurement points of air temperature are 10 points and that of surface temperature are 3 points (floor: 1 point, ceiling: 2 points). Air temperature and surface temperature were measured with thermocouples.

To determine the boundary conditions of CFD analysis a measurement the ventilation rate of mechanical fans was measured by tracer gas method on the 19th September 2009. During the measurement only two windows on the west wall were opened (see Fig. 2 CFD analysis domain). The airflow rate was calculated from the concentration of tracer gas. SF_6 was used as tracer gas and emitted at four points near the floor.

3. CFD Analysis

3.1 Model and Cases

The calculation domain for CFD simulation is shown in Figure 2. However in the real workshop the top height of the center is higher than that near the wall (see Fig. 1(b)), in CFD analysis all the ceiling height is assumed to be the same throughout the workshop. Outdoor air is supplied from 20 windows on the east and the west walls and exhausted from six ventilation fans. In this analysis, only convective heat transfer is considered and radiative heat transfer is not calculated. The temperatures and convective heat transfers of the ceiling, floor and east and west walls are set at constant values. All the surfaces in this model, except for ceiling, floor and east and west walls, are assumed to be adiabatic. In this model 37 heat generation panels are at floor, on the small rooms and on the north wall (see Fig. 2). They are caused by the solar radiation from the top lights. All heat generation in the room is exhausted only through six ventilation fans. The conditions of CFD analysis conditions are shown in Table 1.

Analysis cases are showed in Table 2. Case 0 is the case for comparison between measurement and simulation by CFD. The set temperatures in case 0 are based on the measurement results at 14:00 on the 19th September 2009. Case 1 is the case only for simulation at 14:00 on the hottest day of the year, the 15th July 2009. The set temperatures in case 1 are based on calculation of zonal model [2]. Case 2 and 3 are the cases of insulation of the ceiling to decrease the ceiling temperature. Case 4 is the case of increased ventilation rate. In the case 4, the airflow rate of ventilation fans is twice as much as that of real building. Case 5 is the case of insulation of the walls. In case 5, the east and west walls are heat insulation.

Case 6 is the case that all methods, insulation of the ceiling and the walls, and increased ventilation rate are applied. Only in case 0, outdoor air is supplied from two windows on the east wall (see Fig. 2) on the assumption of the condition at 14:00 on the 19th September 2009.

3.2 Boundary Conditions

Boundary conditions are shown in Table 3. The velocity boundary conditions are applied to the windows and ventilation fans. In case 0 – 3 and 5 the velocity at the ventilation fan is 1.67 m/s reflecting total exhaust airflow rate in the workshop is 9000m^3/h. In case 4, the velocity at the ventilation fan is 3.33 m/s reflecting total exhaust airflow rate in the workshop is 18000m^3/h. At the ceiling, floor, and east and west walls, heat transfer are assumed. Convective heat transfer coefficients of ceiling, floor and walls are 2.33 W/m^2K, 4.66 W/m^2K and 3.5 W/m^2K respectively [3]. The amount of heat emission of each panel on the assumption of solar radiation is 0.81 times as much as the horizontal solar irradiance, considering the transmission of the top light glazings of 0.9, and the solar absorption of the floor, of 0.9.

The mesh system is shown in Figure 3. The number of the mesh division is 953,120 (296x70x46). It has finer mesh near the walls and ceiling.

4. Results and Discussion

4.1 Comparison between measurement and CFD analysis

Vertical temperature distributions obtained by the measurement and CFD analysis are shown in Figure 4. Under the same boundary conditions, the temperatures of CFD analysis are calculated on the same position as the measurement. The vertical temperature distribution of the measurement is almost uniform from the floor to the ceiling. The temperature of calculation (case 0) is approximately lower than that of measurement by 2 deg C from the floor to 2000 mm height. This difference of temperatures between measurement and calculation is considered to result from the electric fans used at the measurement.

The contours of calculated temperatures (case 0) are shown in Figure 5. The electric fans are not considered on CFD analysis. As Figure 5 indicates, the temperature of measurement points is lower than that of the surroundings. On the other hand, during measurement on the 19th September, several electric fans were used in order to stir up the indoor air for tracer gas method. Since the indoor air was mixed by the fans, the temperature distribution of measurement was supposed to be uniform.

Although there is a little difference between measurement and calculation at a low height of the room, temperature distributions in Figure 4 show almost good agreement.

4.2 Effect of improvement methods

The vertical temperature distributions of CFD calculations are shown in Figure 6. As the results of case 1, 2 and 3 indicate, the temperatures decrease at a high height of the room because of the insulation of ceiling. The temperature of case 3 at a low height of the room is approximately 1 deg C lower than that of case 1. Though the decrease of the temperature by the insulation of ceiling results in the decrease of the air temperature of the room, the difference between case 1 (no improvement method) and case3 (the insulation of ceiling) is not large.

In Figure 6, case 4 shows the effect of increased ventilation rate. The temperature of case 4 shows 1.5 deg C lower values than that of case 1 at all heights of the room. Increased ventilation rate results in the larger difference of the air temperature compared with that in the case of the insulation of ceiling.

In Figure 6, case 5 shows the effect of the insulation of walls. The temperature of case 5 at a high height of the room is approximately 1 deg C lower than that of case 1 although there is little difference of the air temperature at a low height of the room. Therefore, the insulation of walls can bring in the decrease of the air temperature at a high height of the room.

Case 6 shows the effect of all improvement methods, insulation of ceiling and walls and more ventilation rate. The temperature of case 6 is approximately 2 deg C lower than that of case 1. As the supply air temperature is 34 deg C, the air temperature at a low height of the room is 1 deg C higher than that of supply air.

SET* distribution at a 1,100 mm height of the room in all cases are shown in Figure 7. The 11 assumption of amount of clothing, metabolic rate and relative humidity are 0.6 clo, 1 met and 50% respectively. MRT for the calculation of SET* of case 1, 2, 3 and 4 is the average temperature of ceiling, east and west walls and floor, while that of case 5 and 6 (insulation of walls) is the average of temperature of ceiling and floor. SET* of case 1 (no improvement method) indicates more than 40.0 deg C in the room. SET* of case 5 (insulation of walls) is higher than that of case 1 (no improvement method). This is because MRT of case 5 (the average temperature of ceiling and floor) is higher than that of case 1 (the average temperature of ceiling, floor and east and west walls) since the temperature of ceiling is much higher than that of floor and east and west walls. SET* of case 2 and 3 (insulation of ceiling) are lower than that of case 4 (increased ventilation rate) and 5 (insulation of walls). This result shows that insulation of ceiling is more effective in decreasing sensory temperature in the occupancy area than the insulation of walls or increased ventilation rate.

5. Conclusions

The effects of some of the improvement methods on the indoor thermal environment were examined in this paper. It was turned out that the insulation of ceiling is the most effective improvement method and the essential method to decrease the sensory temperature in the occupancy area. In addition to the insulation of ceiling, the increase of velocities in the room is

a good way to decrease sensory temperature, too. Although the improvement of thermal environment is achieved by increasing ventilation rate of mechanical fans in this paper, it can be achieved by natural ventilation as the effective way of energy saving.

Although it is not easy to do the time-series analysis of the indoor thermal environment by CFD, CFD is quite useful for the analysis of the distributions in the room, for example, of temperature, velocity and SET*. It is also proved that the method to combine CFD analysis with calculation of zonal model is so effective and successful.

Acknowledgments

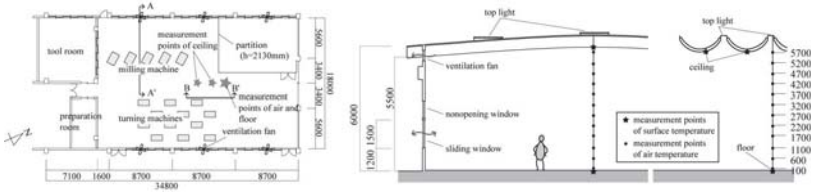
The authors are grateful to the relative parties of the high school for their cooperation.

References

1. Web Pages and On-line Material: "eco-flow / School Eco-Renovation and Environmental Education Program." http://www.ecoflow.go.jp/en/ (July 25, 2010)

2. Yasui S., Yamanaka T., Sagara K., Kotani H., Momoi Y., Yamada J., *"Indoor Thermal Environment and Vertical Temperature Gradient in Large Workshop of School without air-conditioning,"* Submitted to *the 31st AIVC Conference*, Seoul, Korea, 2010

3. Togari S., Arai Y., Miura K., "*A Simplified Model for Predicting Vertical Temperature Distribution in a Large Space,*" *ASHRAE Transactions*, 1993, Part 1, pp.84-99



(a) Plan (b) A-A' section (c) B-B' section

Figure 1 Plan and Sections of the workshop and Measurement Points

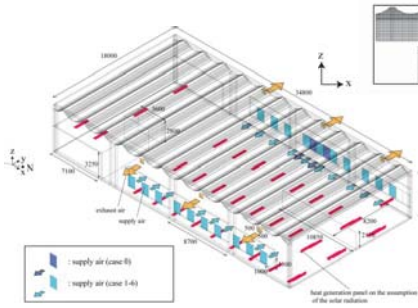
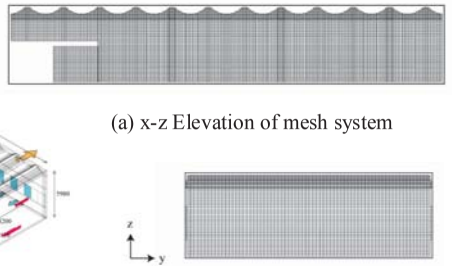


Figure 2 CFD analysis domain



(a) x-z Elevation of mesh system

(b) y-z Elevation of mesh system

Figure 3 Mesh System

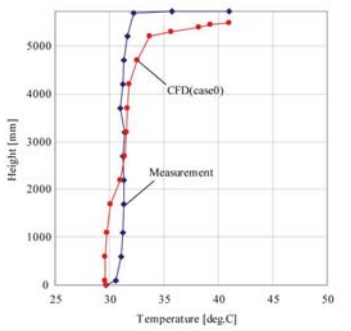


Figure 4 Vertical temperature distributions

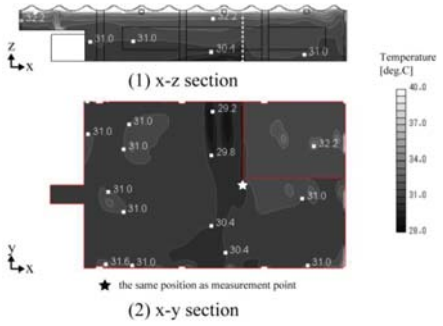


Figure 5 Counters of temperature obtained by CFD (case 0)

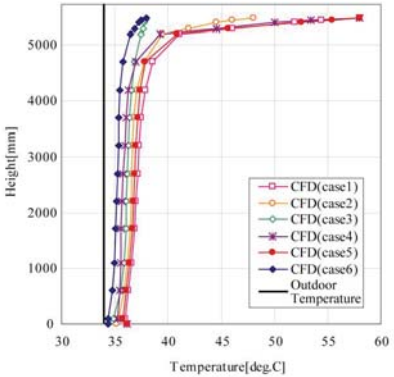


Figure 6 Vertical temperature distributions obtained by CFD analysis

Table 1 CFD analysis conditions

code	STREAM for Windows Version8
Turbulence Model	Standard k-ε Model
Algorithm	SIMPLEC
Scheme for Convective Term	1st order upwind scheme

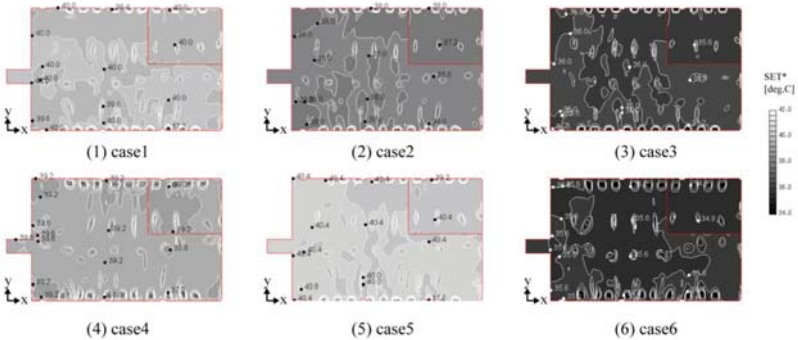


Figure 7 SET* distribution (at 1,100mm height)

Table 2 Cases for CFD simulation

	assumption case	improvement method	surface temperature [deg.C]			supply air temperature [deg.C]	ventilation rate [m³/h]
			ceiling	floor	the east and west walls		
case 0	simulation at 14:00 on the 19th September 2009	X	41	29.7	32	28.6	9000
case 1	simulation at 14:00 on the hottest day of the year, the 15th July 2009	X	58	36.2	40.6	34	9000
case 2		insulation of ceiling	48	35.2	37.8	34	9000
case 3			38	34.4	35.1	34	9000
case 4		increased ventilation rate	58	36.2	40.6	34	18000
case 5		insulation of walls	58	36.2	X	34	9000
case 6		all the methods	38	34.4	X	34	18000

Table 3 Boundary conditions

flow	supply air	velocity boundary condition
	exhaust air	velocity boundary condition
walls		Standard Log-low
thrmal	ceiling	heat transfer coefficient: 2.33[W/m²K]
	floor	heat transfer coefficient: 4.66[W/m²K]
	east and west walls	heat transfer coefficient: 3.5[W/m²K]
heat generation		37 panels: 15247.7 [W] (in total)

Indoor Thermal Environment and Vertical Temperature Gradient in Large Workshop of School without air-conditioning

Saori YASUI[1], Toshio YAMANAKA[1], Kazunobu SAGARA[1], Hisashi KOTANI[1], Yoshihisa MOMOI[1], and Junya YAMADA[1]

[1] Dept. of Architectural Engineering, Osaka University, Suita 565-0871 Osaka, Japan

Abstract

The purpose of this study is to figure out the characteristics of thermal environment in a workshop at school in Japan and to propose the improvement method of the thermal environment without air-conditioning systems. In this paper, measurement results of thermal environment in the workshop and calculation results of vertical temperature gradient are shown. In the measurement results, indoor air temperature became very high in summer. Solar radiation was the main factor raising the temperature of PC roof, and large vertical temperature gradient was formed. The calculation results of zonal model shows the good agreement with the measurement results for vertical temperature gradient. Then some improvement methods of the thermal environment was investigated with the calculation model, and the investigations showed that insulating PC roof is effective method to decrease indoor air temperature.

Keywords: Large space, Workshop, Measurements, Zonal model, Case study

1. Introduction

It is important to keep students' thermal comfort by fresh air supply and heat removal in workshop of school without any air-conditioning system. In large space, it is difficult to control various factors composing indoor environment, therefore, working space often has poor thermal conditions. The target of this study is the large workshop at school, where no air-conditioning system is installed to get out of large cost for energy consumption. The purpose of this study is to figure out the characteristics of thermal environment in the large workshop at school in Japan and to propose the improvement method of thermal environment without air-conditioning systems. Thermal measurements of existing workshop and case studies of some improvement methods with zonal model are conducted. As zonal model, Togari et al. have developed simplified prediction model of vertical temperature distribution in an atrium [1] [2] [3]. In that model, air flows along wall surfaces and air streams from outlets are considered for unsteady-state heat analysis. In this paper, the calculation method considering stack ventilation for unsteady-state is presented.

2. Thermal Measurement of Existing Workshop in a High School

2.1 Outline of Measured Building

The measurement was conducted in a workshop at high school. The plan and section of the workshop are shown in Fig.1~3. The classes of machine practical are given in this workshop. A curved heavy PC roof covers the workshop and 39 fixed skylights are on the top of the roof. The workshop wasn't installed with any air-conditioning systems, and the ventilation method is cross ventilation through side windows and mechanical ventilation with 6 axial fans on the top of outer walls (See in Fig. 2).

2.2 Method of Measurement

The measurement was carried out from 6 Sep. to 19 Sep. 2009. The all classes were hold as usual, and the windows were openable freely for teachers and students through the measurement period. Measurement items and instruments are shown in Table 1, and measurement points are shown in Fig. 1 and 3. Vertical temperature gradient and the surface temperature on the ceiling and the floor were measured at the location e (See in Fig. 1). Measurement heights at other locations were 1100mm.

2.3 Measurement Results

Measurement results on three representative days are shown in Figs.4~6. The conditions of each result are shown in Table 2. Fig.4 shows the result of Case A. The fans on the outer wall didn't operate on these three days. Fig.4 (a) shows the diurnal change of temperature and amount of solar radiation on a horizontal plane. It can be seen that indoor air temperature was much higher than outdoor and reached to 40 deg. C in the afternoon. Fig. 4 (b) shows the change of vertical temperature gradient. Large temperature gradients were formed and temperature on ceiling was over 50 deg. C. Fig.5 shows the results of Case B. In Case B, side windows must have been opened from 8:30 to 14:00 and from 18:30 to 21:00. In Fig. 5 (b), decrease of temperature due to cross ventilation was seen below 3000mm height. However, the ceiling temperature has kept high and stagnant hot air zone exists near the ceiling. Fig. 6 shows the results of Case C. In Fig. 6 (b), the ceiling temperature doesn't rise as Case A or B, and temperature gradient wasn't formed. Figs. 4~6 indicate that the main cause of hotness in the workshop is supposed to be the ceiling heated by solar radiation and stagnant hot air near the ceiling. Thus insulation of the roof and heat removal in higher part of the workshop can be efficient method to improve the thermal environment in summer.

3. Calculation of Vertical Temperature Gradient

3.1 Description of Calculation Model

Fig.7 shows the modeling of the workshop. It consists of PC roof, indoor air, floor and ground. Actually the roof is curved, but the roof is modeled as a plane for simplification, and the walls are assumed to be insulated. Each part of the workshop is divided into a limited number of zones with only horizontal boundaries, and the temperatures are calculated using forward difference. Calculation nodes are shown in Fig. 8. The heat balance equations can be written generally for each node:

$$C\rho_j \Delta x_j \frac{\theta^{n+1}_{j(i)} - \theta^{n}_{j(i)}}{\Delta t} = \lambda_j \left(\frac{\theta^{n}_{+j(i-1)} - \theta^{n}_{j(i)}}{\Delta x_j} - \frac{\theta^{n}_{j(i)} - \theta^{n}_{j(i+1)}}{\Delta x_j} \right) \quad \text{(Eq.1)}$$

At the surfaces of roof, ceiling and floor, heat transfers by convection and radiation. The heat balance equation of the top node of the roof is written as follows:

$$C\rho_{pc}\Delta x \frac{\theta_{pc(1)}^{n+1}-\theta_{pc(1)}^{n}}{\Delta t} = h_o\left\{\left(\theta_o^n+\theta_\delta^n\right)-\theta_{pc(1)}^{n}\right\}+\lambda_{pc}\left(\frac{\theta_{pc(2)}^{n}-\theta_{pc(1)}^{n}}{\Delta x_{pc}}\right) \quad \text{(Eq.2)}$$

where $\theta_e = \frac{A_s J}{h_o}$

The heat balance equations for surfaces of ceiling and floor are as follows:

$$\lambda_{pc}\left(\frac{\theta_{ceil}-\theta_{pc(nx)}}{\Delta x_{pc}/2}\right) = h_{ic}\left(\theta_{ceil}-\theta_{a(1)}\right)+\varphi_{cf}h_{ir}\left(\theta_{ceil}-\theta_{fs}\right) \quad \text{(Eq.3)}$$

$$h_{ic}\left(\theta_{a(nx)}-\theta_{fs}\right)+\varphi_{fc}h_{ir}\left(\theta_{ceil}-\theta_{fs}\right) = \lambda_f\left(\frac{\theta_{fs}-\theta_{f(1)}}{\Delta x_f/2}\right) \quad \text{(Eq.4)}$$

For calculation of air temperatures, if upper zone temperature is lower than lower zone temperature, mixing due to the buoyancy becomes active. Therefore it is possible to assume $\theta_{a(i)} \approx \theta_{a(i-1)}$ [1]. In this case, large value of λ_t (apparent thermal conductivity of indoor air, $\lambda_t = 20$ [W/mK]) is used in a calculation

program for convenience. As boundary conditions, outdoor temperature and solar radiation are given by measurement or meteorological data near the workshop and the temperature at the bottom node of ground is given 16 deg. C all day. Physical properties of each part and heat transfer coefficients are shown in Table 3, 4.

3.2 Modeling of the heat transfer by stack ventilation

If side windows and skylights are opened, reduction of indoor air temperature is expected due to stack ventilation. When the workshop is ventilated, airflow at boundary of zones must be considered. Fig.9 shows the diagram of airflow distributions. Ventilation rate is calculated with pressure difference between skylights and the center height of side windows. The pressure difference and ventilation rate are as follows:

$$\Delta P = \rho_o g H - \sum_i \rho_{a(i)} g \Delta x_a \quad \text{(Eq.5)}$$

$$Q = C_D A \sqrt{\frac{2}{\rho}\Delta P} \quad \text{(Eq.6)}$$

The air inflow rates entering each zone are modeled following two kinds:

(1) zones above side windows : all of Q flows into the zones

(2) zones below the top of side windows : Q from outside is equally distributed to these zones

These air flow patterns are shown in Fig. 9. Then terms of heat transfer caused by airflow are added to Eq. 1:

(1) zones above side windows

$$C\rho_{a(i)}\Delta x_a \frac{\theta_{a(i)}^{n+1}-\theta_{a(i)}^{n}}{\Delta t} = \lambda_t \frac{\theta_{a(i-1)}^{n}-\theta_{a(i)}^{n}}{\Delta x_a} - \lambda_t \frac{\theta_{a(i)}^{n}-\theta_{a(i+1)}^{n}}{\Delta x_a} + C\rho_{a(i+1)}^{(1)} Q\theta_{a(i+1)}^{n} - C_{vp}\rho_{a(i)} Q\theta_{a(i)}^{n} \quad \text{(Eq.7)}$$

(2) zones below the top of side windows

$$C\rho_{a(i)}\Delta x_a \frac{\theta^{n+1}_{a(i)}-\theta^{n}_{a(i)}}{\Delta t} = \lambda_t \frac{\theta^{n}_{a(i+1)}-\theta^{n}_{a(i)}}{\Delta x_a} - (\lambda_t)\frac{\theta^{n}_{a(i)}-\theta^{n}_{a(i-1)}}{\Delta x_a} \quad (1)$$
$$+C\rho_o \frac{Q}{N}\theta^{n}_{o} + C\rho_{a(i+1)}\left(\frac{nx_a - i}{N}Q\right)\theta^{n}_{a(i+1)} - C_p\rho_{a(i)}\left(\frac{nx_a + 1 - i}{N}Q\right)\theta^{n}_{a(i)}$$

(Eq.8)

3.3 Calculation Cases

Calculation cases are shown in Table 5. The vertical temperature gradients were calculated for September and July. The results of Case 1(in September) were compared with measured data to validate the calculation model. As solar radiation and outdoor temperature in July is lager than September, various cases of calculation are for July (Case 2~11) in order to predict the effect of some improvement methods of thermal environment in the hottest conditions.

3.4 Calculation Results

3.4.1 Comparing with measured data

The results of calculation and measurement for Case 1 are given in Fig.10 and 11. Fig.10 shows the diurnal change of solar radiation and the air temperature. It is can be seen that the calculated ceiling and floor surface temperature showed good agreement with measurement temperature. For the indoor air temperature, the calculation results were higher than measurement from evening to early morning on each day. It is likely that no heat loss through the walls existed because of insulating assumption, and then indoor temperature didn't decrease so much at night in calculation. In the morning, calculation and measurement air temperatures were similar relatively. Fig.11 shows the vertical temperature gradient on 7 Sep. 2009. Actually, the height of ceiling is different between calculation and measurement, but ceiling temperatures of both methods are shown at the same height for convenience. In Fig.11, calculation and measurement results were quite similar except at 18:00. Therefore this calculation model can be available to predict the vertical temperature gradient at the hottest time of day.

3.4.2 Effect of roof insulation

Fig.12 shows the vertical temperature gradient in Case 2, 6, 8 and 10. It is comparing the thermal effect of the roof insulation. All calculations are at 16:00 on 15 July. It can be seen in Fig.12 that roof insulation was able to decrease the ceiling and indoor air temperatures very much. Comparing Case 6 and Case 8, high reflective paint (As=0.2) is more efficient than polystyrene foam. If both polystyrene foam and high reflective paint were adopted, the vertical temperature gradients would be little and the temperature in occupancy area would decrease to near outdoor temperature.

3.4.3 Effect of stack ventilation

Fig.13 shows the ventilation rate in Case 3~5, and Fig.14 shows the vertical temperature gradient for Case 2~ 5. The opening areas of the skylights were varied, and in Case 2, all side windows and skylights were closed. Lager the opening area of skylight is, grater the ventilation rate is (See in Fig.13). It can be seen in Fig.14, when any small areas of skylights were opened, indoor air temperature decrease widely and the amount of decrease in air temperature didn't depend strongly on the opening area of the skylights in the range of opening area assumed in the calculation. However, ceiling surface temperature didn't decrease so much as the air temperature.

Fig.15 shows the vertical temperature gradient in Case 3, 7, 9 and 11, and Fig.16 show the comparison of ventilation rates in time series. In Case 7, 9 and 11, the workshop is ventilated and the roof is insulated or painted with high reflective paint. It can be seen in Fig.16, the ventilation rates decrease due to insulation or high reflective paint in the afternoon. However, the amounts of decrease in air temperature Case 7, 9 and 11 are larger than Case 3 (See in Fig. 15).

4. Conclusions

In the thermal measurement results in the workshop, where no air-conditioning system is installed, indoor temperature became too high and large vertical temperature gradient was formed. It is thought that the cause of hotness is the solar radiation. The authors constructed the zonal model for calculation, and the model is useful to predict the vertical temperature gradient at the hottest time of day. In the calculation results of zonal model, it was made clear that the roof insulation and stack ventilation were the efficient method to decrease indoor air temperature. Although it is true the roof insulation can reduce ventilation rate, it is not necessary to mind that. When roof insulation and heat removal in higher part of workshop are combined, indoor temperature can be decreased much and become almost equal to outdoor temperature.

Acknowledgments

The authors would like to appreciate the cooperation of relevant parties of the high school.

Nomenclature

i : node number,	h_o : outdoor total heat transfer coefficient [W/ m^{2}K],
j : material name,	h_{ic} : indoor convective heat transfer coefficient [W/ m^{2}K],
Δt : time [s],	h_{ir} : indoor radiant heat transfer coefficient [W/ m^{2}K],
Δx_j : division width of material j [m],	A_s : solar absorptance [-],
n : time step,	J : amount of solar radiation [W/m^2],
nx_j : division number of material j [-],	φ_{cf} : shape factor for floor on ceiling [-],
N: number of zones below the top of side windows, [-]	φ_{fc} : shape factor for ceiling on floor [-],
$\theta_{j(i)}$: temperature at node i of material j [deg. C],	ΔP : pressure difference between side windows and skylights [Pa],
$C\rho_j$: specific heat per volume of material j [J/m^{3}K],	ρ_o : outdoor air density [kg/m^3],
λ_j : thermal conductivity of material j [W/mK],	$\rho_{a(i)}$: indoor air density at node i [kg/m^3],
θ_o : outdoor temperature [deg. C],	g : acceleration of gravity [m/s^2],
θ_e : equivalent temperature of solar radiation [deg. C],	H : height from center of side windows to skylight [m],
θ_{ceil} : surface temperature of ceiling [deg. C],	C_D: discharge coefficient [-],
θ_{fs} : surface temperature of floor [deg. C],	A : opening area [m^2],
λ_a : apparent thermal conductivity of indoor air [W/mK],	Q : ventilation rate [m^3/s]

References

1. Togari S, Arai Y, Miura K, "*A Simplified Model for Predicting Vertical Temperature Distribution in a Large Space,*" *ASHRAE Transactions*, 1993, Part 1, pp.84～99.
2. Arai Y, Togari S, Miura K, "*Unsteady-State Thermal Analysis of a Large Space with Vertical Temperature Distribution,*" *ASHRAE Transactions*, 1994, Part 2, pp.396～411.
3. Takemasa, Y, Togari, S, Arai, Y, *"Application of an Unsteady-State Model for Predicting Vertical Temperature Distribution to an Existing Atrium,*" *ASHRAE Transactions*, 1996, Part 1, pp.239～247.

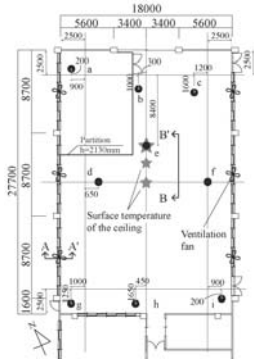


Fig. 1 Plan of the workshop

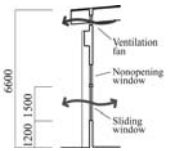


Fig. 2 Section A-A'

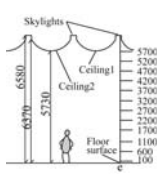


Fig. 3 Section B-B'

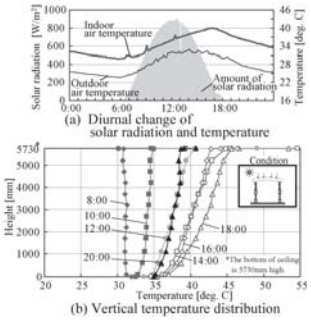


Fig. 4 Thermal measurement result (Case A)

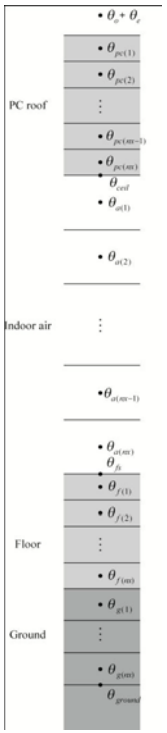


Fig. 8 Calculation nodes

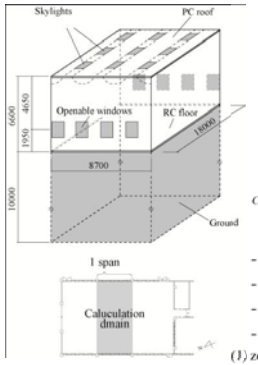


Fig. 7 Modeling of the workshop [mm]

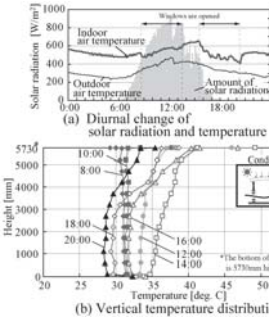


Fig. 5 Thermal measurement result (Case B)

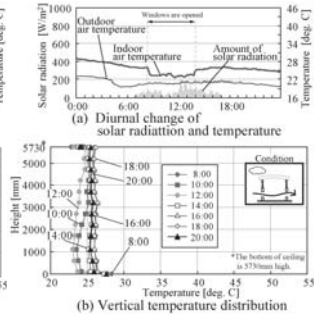


Fig. 6 Thermal measurement result (Case C)

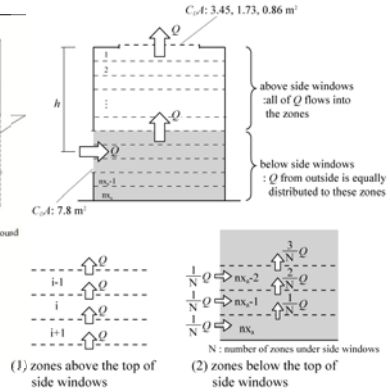


Fig. 9 Airflow by stack ventilation

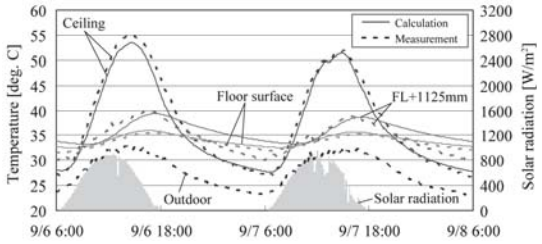


Fig. 10 Comparing calculation and measurement for diurnal change of indoor air temperature in September

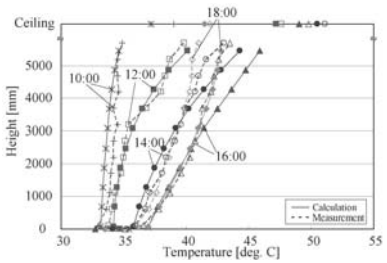


Fig. 11 Calculated and measured vertical temperature gradient in Case1(2009.9.7)

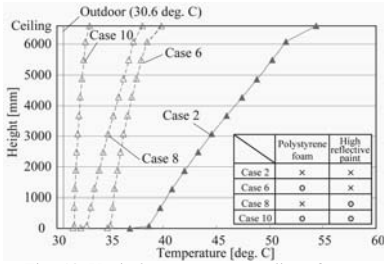


Fig. 12 Vertical temperature gradient for Case 2, 6, 8 and 10 (2009.7.15 16:00)

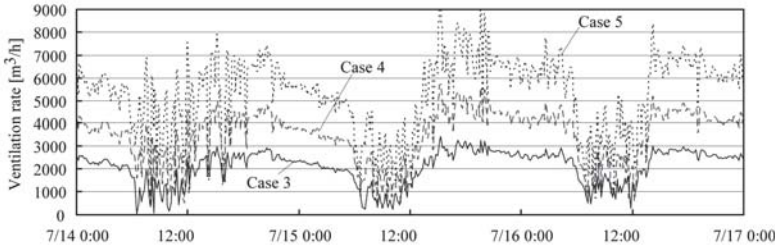


Fig. 13 Diurnal change of ventilation rate for Case 3~5

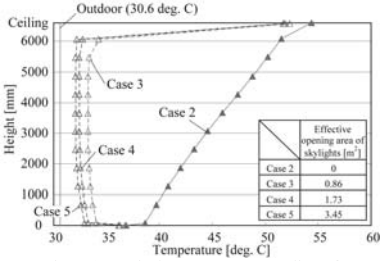


Fig. 14 Vertical temperature gradient for Case 2～5 (2009.7.15 16:00)

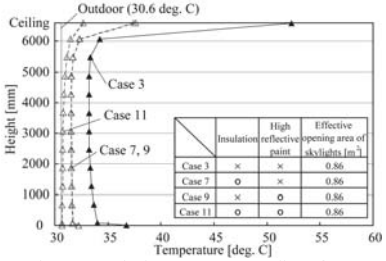


Fig. 15 Vertical temperature gradient for Case 3, 7, 9 and 11 (2009.7.15 16:00)

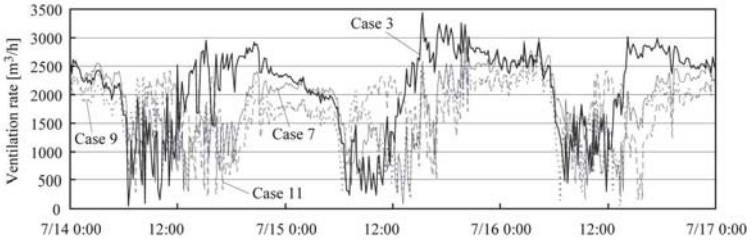


Fig. 16 Temporally change of ventilation rate for Case 3, 7, 9 and 11

Table 1 Measurement item and instrument

Measurement item	Measuring instrument	Number	Mark
Indoor air temperature, Humidity	Portable thermohygrometer T&D / RTR-53	8	●
	0.32mmϕ T type thermocouple	12	
Surface temperature of ceiling	0.32mmϕ T type thermocouple	2	★
Surface temperature of floor	0.32mmϕ T type thermocouple	1	
Outdoor air temperature, Amount of insolation, Wind direction, Wind velocity	Compact meteorological data acquisition system SEC / Weather Bucket TA-WL-2S	1	

Table 2 Condition of measurement results

	Date	Solar Radiation	Windows
Case A	2009.9.6	Large	Close
Case B	2009.9.8	Large	Open
Case C	2009.9.15	Small	Open

Table 3 Physical properties

(a) PC roof

Item		Value
l	m	0.075
λ	W/mK	1.5
ρ	kg/m^3	2400
C	J/kgK	800

(b) Indoor air

Item		Value
l	m	6.6
λ_t*	W/mK	1.16
$C\rho$	J/m^{3}K	1173.6

*λ_t : Apparent thermal conductivity

(c) RC floor

Item		Value
l	m	0.15
λ	W/mK	1.4
ρ	kg/m^3	2200
C	J/kgK	880

(d) Ground

Item		Value
l	m	10
λ	W/mK	1.85
$C\rho$	J/m^{3}K	3916000

(e) Polystyrene foam

Item		Value
l	m	0.02
λ	W/mK	0.037
ρ	kg/m^3	28
C	J/kgK	1300

Table 4 Heat transfer coefficient

Item			Value	
Outdoor total heat transfer coefficient	h_o	W/m^{2}K	23	
Indoor convective heat transfer coefficient	h_{ic}	W/m^{2}K	1.13	Natural convection, heat flow : downward
			3.99	Natural convection, heat flow : upward
			2.33	Natural ventilated, heat flow : downward
			4.66	Natural ventilated, heat flow : upward
Indoor radiant heat transfer coefficient	h_{ir}	W/m^{2}K	4.97	

Table 5 Calculation Case

September

Roof : Standard Paint As=0.8		Effective Opening Area of Skylights			
		0.00 m2	0.86 m2	1.73 m2	3.45 m2
Thickness of Polystyrene Foam	0 mm	Case 1	X	X	X
	20 mm	X	X	X	X

July

Roof : Standard Paint As=0.8		Effective Opening Area of Skylights			
		0.00 m2	0.86 m2	1.73 m2	3.45 m2
Thickness of Polystyrene Foam	0mm	Case 2	Case 3	Case 4	Case 5
	20mm	Case 6	Case 7	X	X

July

Roof : High Reflective Paint As=0.2		Effective Opening Area of Skylights			
		0.00 m2	0.86 m2	1.73 m2	3.45 m2
Thickness of Polystyrene Foam	0mm	Case 8	Case 9	X	X
	20mm	Case 10	Case 11	X	X

A Study of Design principle and Technology performance applied in Passive House

- Focused on cases of the apartment type of Passive Houses in European -

Sung-Eun, Shin [1], Soo-Am Kim [2], Yong-Sang Yoon[3], Sung-Ok Lee [4]

[1] Dept.Building&Urban Research. Korea Institute of Construction Technology, Geyeonggi-Do, Republic of Korea, 411-712

[2] Dept.Building&Urban Research. Korea Institute of Construction Technology, Geyeonggi-Do, Republic of Korea, 411-712

[3] Dept.Building&Urban Research. Korea Institute of Construction Technology, Geyeonggi-Do, Republic of Korea, 411-712

[4] Dept.Building&Urban Research. Korea Institute of Construction Technology, Geyeonggi-Do, Republic of Korea, 411-712

Abstract

Recently, the role of the architecture which is corresponding to climate change and saving energy has been important. This study drew factors about design principle, technology performance on passive house, focusing on apartment and multi-family house cases in Europe. The dwelling type of Korea and climate, however, are different from the European styles, and therefore it is necessary to develop energy efficient design, technology and details that is applicable to Korea's apartment. Under this circumstance, this study aims at providing the fundamental data for drawing design principle, technology performance, details applicable to domestic apartment and climate condition for passive house in Korea. Therefore, this case study is intended to explain three topics: strategy, energy performance, and details.

Keywords: Passive House, Passive Design principle, Energy performance

Introduction

Major global conversation topics in the 21st Century would be “climate change” and “energy saving” above all. During the life cycle a building is designed, constructed, and operated, influence of on the environment and the amount of energy consumed relating to the building are enormous indeed. In view that the building sector occupies 30 ~ 40% of the world’s energy consumption (IEA: International Energy Agency, 2005) and 45% of the world’s CO2 emissions (UNEP, 2007), it is inevitable to develop the design technique and technology that enables to secure health and comfort of the building occupants and save energy as well. Under these international circumstances, the concepts such as Passive House, Self-sufficient House, Zero Energy House, etc. have been developed. Of them, passive house has been actively studied in Germany and Central Europe since the mid 1990s, and more than 8,000 passive houses have been built since then.

Objectives

This Study is aimed at the analysis of design technique, concept, and energy saving technologies of the foreign advanced countries in order to grasp design principle and architectural technology components necessary to suggest optimized energy-saving housing model that can be applied to domestic apartment house in introducing such advanced passive technology and components. In Korea, based on the classification by housing types in 2005, the ratio of apartment house in the entire residences reaches 53%, marking the highest. In order to embody the housing model in ultra en

house that occupies a majority of total housing types, the decision on the design variables that influence on the performance of building at the planning phase should be made in compliance

with energy performance in accordance with quantitative objective and systematic design guide line rather than the experience of architect or generally known knowledge only. Therefore, the analysis of information and data on the major strategy and performance applied to the foreign advanced ultra energy saving type apartment houses being carried out in this study would be a very important indicator.

Method of Research and Description

As the method of study, passive house research report and apartment house example and reports that were disclosed by Passive Association were collected.

This study is intended to explore the concept of passive house, analyze foreign examples and research data, and finally derive passive design strategy and component technology applied to the design principle of the passive house.

The case study selected is a model passive house (ultra energy saving house) distribution project - European CEPHEUS (Cost Efficient Passive Houses as European Standards) Project aimed at the distribution of passive house, through which a variety of passive house concept was verified and tested. Of them, five CEPHEUS Projects that fall under the apartment type except detached house and five buildings that have been recently completed out of the PHs built since 2001 were selected in addition.

Definition and Performance Standard of Passive

German Passive House Institute(2001) defines passive house as 'the building that provides pleasant indoor environment in summer and winter without the necessity of traditional mechanical cooling/heating equipment', which means energy saving to the maximum by minimizing the loss of thermal energy by actively utilizing natural energy. In 1988, Germany Passive House Institute considers less than 15kWh/㎡.year for heating energy and less than 120kWh/㎡.year for total energy consumed by the building including cooling/water heating/electricity (primary energy consumption) as the prerequisite of passive house.

Passiv haus standard was enacted first in 1995, which forms the most basic standard of Passive.

Besides, the design condition required for Germany's passive house is as shown in Table 1.

Table 1. Passive House Performance Standard

Space Heating Demand	≤ 15 kWh/㎡.year
Primary Energy Demand	≤ 120 kWh/㎡.year
Air Tightness	≤ 0.6
Window Frame/Glass Average U-value	6 h-1 @ 50pa
Energy Ventilation Efficiency of Ventilation System ηHR	75%

Passive Design Principle and Integral Design

Passive house maximizes energy saving passive components used by the building, while minimizes the active components such as renewable energy utilized, etc. The energy saving in the building sector is one of the most important parts out of the objectives of passive house. The passive house design principles are first, Super insulation and Design without thermal bridge; second, Heat recovery and Indoor air quality; third, Passive solar gain; fourth, Electric efficiency; and fifth, On-site renewable to be considered.

To meet these passive house standards, integral plan of interaction between superior design and components is important, that is, it is the key to integrate technology and design to accomplish passive house suitable for climate, land, building type, scale of the region where the building is built. In the passive house Institute, they provide PHPP (Passive House Planning Package) as the planning tool that can be used at the energy design stage of Passive House. PHPP is the integral package program under a simple calculation method that helps design the passive house, which principally calculates periodic heat load by applying a

special boundary condition by super insulation without normal heating system and adopts Heating Degree Hours based on 20℃ for the standard indoor temperature in its estimation of yearly energy consumptions of the building. When designing passive house, PHPP Software is used for the calculation of Energy Balance.

Analysis of overseas passive house design and energy performance

[Table 2] shows building type, dwelling unit, area, and structure of the passive houses selected in Sweden, Germany, and Austria.

Besides, the characteristic of passive house was explored from two aspects of passive strategy and energy performance of each case.

Table 2. Architectural Overview of Passive Houses

Project Title		Building Type	Dwelling unit	Treated Floor Area(㎡)	Construction
01 Germany, Hannover,Kronsberg		Terraced house	32	3,576	Mixed construction (timber wall, roof, prefab con'c core)
02 Germany, Frankfurt, Hessen, St.Jakob		Multy-family house (2002)	19 (A,B Block. 5F)	1,927	Mixed construction. (timber, masonry)
03 Germany, Kassel		Apart ment (1999)	31	3,055	Solid (masonry) + external insulation
04 Austria, Wolfurt		Multy-family house (1999)	10	1,296	Mixed construction (steel skeleton, con' c ceiling, timber wall)
05 Austria, Lodenareal		Apart ment (2009)	361	28,316	Solid (massive construction)
06 Utendorfgass, Vienna		Apart ment (2006)	60	-	Reinforced concrete
07 Austria, Kuchi		Multy-family house (2000)	25	1,798	Mixed construction (steel column, RC slab)
08 Austria, Hallein		Apart ment (2000)	31	2,318	Mixed construction. (steel skeleton, timber)
09 Samer Mosl, Salzburg		Apart ment (2006)	60	-	Timber Construction (prefabricated wall)
10 Sweden, Gothenburg, Hamnhuset		Apart ment (2008)	116 (4~5F)	-	Mixed construction. (wall-con'c, pillar-steel)

Table 3. Major performances of overseas passive houses

CASE		1	2	3	4	5	6	7	8	9	10
Orientation		South	South & East	East & West	South & West	South & East	South	North & East	South & East	North & East	South, East
U-Value	Wall	0.13	0.11	0.13	0.12	0.13	0.13	0.13	0.11	0.11	0.14
	Roof	0.1	0.1	0.11	0.10	0.11	0.1	0.1	0.11	0.11	0.1
	Window	0.75	0.8	0.6	0.83	0.85	0.8	0.7	0.7	0.6	-
Heating Energy		14.2	13	17.2	21.4	14.5	14.5	22.9	12.4	12.5	12
Primary Energy		72.1	119.9	133	56.5	112	118	126.6	-	-	60
Airtightness		0.3	0.3	0.35	0.33	0.2	0.4	0.23	0.58	0.46	-
Heat Recovery Efficiency		99%	84%	85%	79%	90%	-	80%	80%	○	82%
Window System		Triple Low-e, Wood AL. Frame	Triple Low-e, G 53%	Triple Low-e, PVC Frame	Triple Argon Gas glass, Super Insulation frame	Triple Glass	Triple Glass	Triple Glass	Triple Argon Gas glass	Triple Low-e, Wood AL. Frame	Triple Low-e, Wood AL. Frame
Balcony		Separat-ion from external wall -Heat bridge prevent ion	Steel Struc-ture	Separat ion from externa l wall - Heat bridge prevent ion	NO	Preven tion of heat bridge betwee n balcon y and slab	Steel Struc -ture	Steel Struc -ture	Steel Struc -ture	Steel Struc -ture	Heat bridge preventi on
Solar heat/ Photo voltaic system		Collector 126㎡	-	-	Collector 62㎡	Collector 1,050 ㎡	-	Panel 75㎡	Collector 120㎡	Collector 200㎡	Collector 193㎡

Results and Discussion

1. Passive Design Technique & Core Technical Components

Design principle and strategy to be considered in passive house design can be divided into Passive components and Active components. Design principle and plan applied in European passive cases are mainly reviewed from the range as below.

○ Passive components

Passive components minimize energy loss by improving the building energy performance.

As far as not cooling the space artificially, there exist the components generating heat only in the building such as sunlight coming in through the window, heat being generated from human body, heat coming from lighting fixture, heat coming out from the operation of electric equipment, etc. It is the passive house and its components to calculate insulation that enables to maintain the heats being generated like this inside the building and airtight condition. The component technologies mainly applied to the cases are as shown in [Fig.1].

Orientation		Maximization of solar radiation gain, minimization of load, south bound arrangement if possible 20% of energy is saved when arranging the orientation to the South
Super Insulation		Reinforcement of insulation by three times based on domestic standard. Heat transmission coefficient: 0.15 W/m2K for building shell, 0.11 W/㎡K for roof
Space Heating		Traditional heating method : replacing into waste heat recovery system by ventilation; Condensing boiler, geo thermal heat pump, etc.
Building Shape		Minimizing Area/Volume Ratio - High Compact form (Compactness Design) Energy saving in consideration of the ratio of lateral to longitudinal length
Triple-glazing window		Low-E triple glazing, Filling Argon gas, High-insulation High performance window frame, Window area south-bound ratio 40~60%, U-value : 0.8W/㎡K
Airtightness		n 50<0.6 ac/h Minimizing the energy loss through air infiltration to secure high air-tightness performance
Heat Recovery		Recovery ratio 75% or more
Thermal Bridge		Air-tightness, window to be installed within shell insulation line, Minimizing the heat exchange around window frame, High-performance insulation, development of details at the junction
Natural ventilation		Building type/wall/opening/inner partition/dual structure/roof ventilation system, etc.
Shading		Southern side awning system for controlling solar heat in summer season, fixed awning, variable awning, awning using trees
Passive Solar Gain		Arrangement at south bound to increase solar radiation gain, hot water supply, power generation Review of location and type of window, consideration of acquisition/loss of sunlight energy depending on window area ratio
Thermal Mass		Applying interior materials such as PCM, etc.

Fig. 1 Extraction of major passive component technologies

○ Active components

Active components produce clean energy through the introduction of new & renewable energy, consisting of solar heat water heating, heating, geothermal, sewage source heat, pellet boiler, wind power generation, fuel cell, co-generation, etc. In the case of solar heat/photovoltaic, it can replace only the energy used by the entire building in part. Therefore, the passive architecture that minimizes the use of energy centered on Europe came to emerge. The followings shown in [Fig. 2] are the active components applied to the case of passive in Europe;

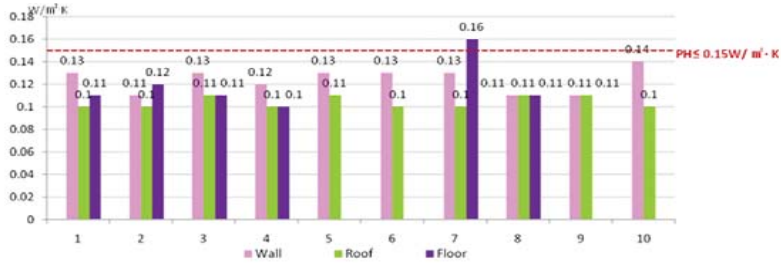
New/Renewable Energy		New/renewable energy (solar heat, photovoltaic, biomass, wind power, etc.)
Geo thermal Heating & Cooling System		Geo thermal Heating & Cooling System - Outdoor air by geo heat using under ground duct, preheating, pre-cooling
Pellet Boiler		Heating/Water Heating System / Co-Generation System

Fig. 2 Major Active Component Technology

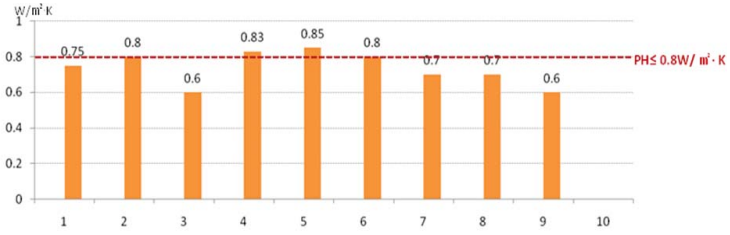
2. Application of Technical Performance

[Fig. 3] is the energy performance level accomplished in each case from which the range of technical performance implemented to the actual passive house can be found.

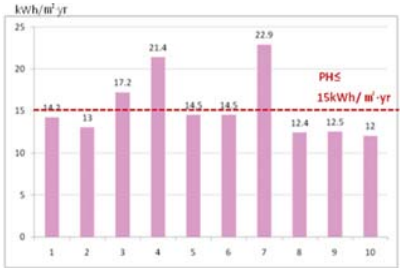
That is, several components of the selected cases exceeds the performance conditions of passive house, but most of them meet the performance within the range of technical solutions suggested by Promotion of European Passive Houses (PEP) in accomplishing Passive House.



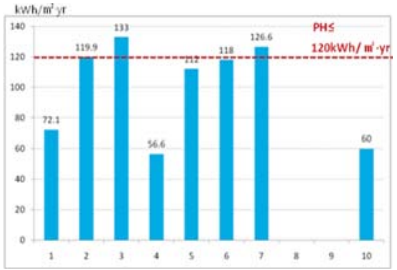
[U-Value - Wall/Roof/Floor]



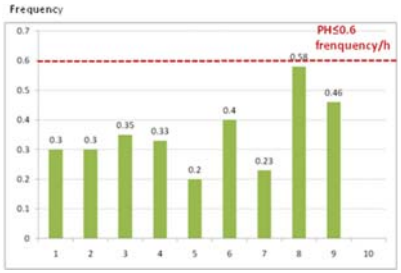
[U-Value - Window]



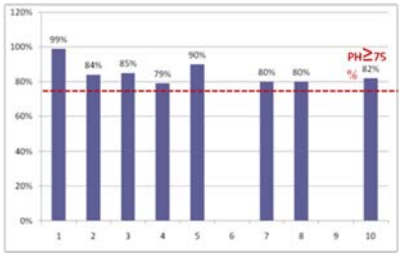
[Heating Energy Requirement]



[Primary Energy Requirement]



[Frequency of ventilation]



[Heat exchanger efficiency]

Fig. 3 Performances of Overseas Passive Houses

Conclusions

In this study, the concept of passive house was established and the major energy technical components applied to passive house was grasped through the exploration of the overseas cases. Each case was found to follow the passive technology that minimizes energy loss and load with high-performance insulation, high-efficiency window, and air-tightness performance basically reinforced, which incorporates active components of new and renewable energy suitable for regional climate in most economic and efficient manner.

Unlike the general building process, the process of energy saving-concept building aimed at the building's energy reduction includes the analysis of a variety of design variables as well as energy performance of each component technology from the early stage of design. That is, it is characterized with that arrangement for ultra energy saving design, essential design guideline of building design such as space plan, elevation, etc.,. and quantitative analysis to absolutely meet the energy performance are intensively reviewed from the planning stage. In view of the domestic situation that 'mandatory requirement for public office to maintain 1st class energy efficiency' and 'total annual energy use' are being introduced, it is necessary to verify how energy is reduced in a quantitative manner from the planning stage different from

the existing design method, and the architects need to actively participate in such change the requirement.

Acknowledgments

This work was supported by the Korea Research Council for Industrial Science and Technology funded by the Korea government (Ministry of Knowledge Economy) (B551179-09-04-00)

References

1. Wolfgang Feist. Passive House Institute, Final Technical report CHPHEUS-Project Information No. 36, 2001.7
2. Wolfgang Feist.et.al, Passive House Planning Package 2007, PHI, 2007
3. Jurgen Shnieders.CHPHEUS-measurement results from than 100dwelling units in passive houses.ECEEE, 2003
4. Passive-on project, Passive Home Training Module for Architects and Planners.
5. Promotion of European Passive House(PEP), Passive House Solution, 2006
6. Web Pages and On-line Material: http://www.greenspec.co.uk

Prediction of mass transfer rate on the surface of tested building material using CFD analysis

Janghoo SEO[1]

[1] Chosun University, School of Architecture, Gwangju, Korea 501-759

Abstract

We developed an airflow control unit for small chambers for uniformly controlling airflow on the surface of tested building material in the small chambers. We will present the mass transfer rate on the surface of tested building materials corresponding to an actual building in order to exactly evaluate the performance of the reduced amount and concentration of released chemical materials with the small chambers. We measured the airflow velocity on the surface of building materials in the small chamber with the developed airflow control unit and the fan speed for airflow control. We reviewed the distribution of water vapor concentration in the small chamber by means of CFD (Computational Fluid Dynamics) and estimated the mass transfer rate on the surface of building material to confirm test reliability.

Keywords: small chamber, mass transfer rate, CFD analysis

Introduction

For measuring the amount of chemical materials released from building materials and the like, many countries including Korea have instituted laws or specifications for measurement methods applicable to their own country. For measuring the amount of chemical materials released from building materials, small chambers are generally used, considering the

advantages of easy experiments, expenses, etc. Meanwhile, in Korea, KS M ISO 16000-9 was instituted and publicized as a criterion for the small chamber law to specify small 20-liter chambers (ADvanced Pollution and Air Quality Chamber: ADPAC) for measuring the amount of released chemical materials. In Japan, the small 20-liter chambers are generally used for measuring the amount of released chemical materials (JIS A 1901) and for evaluating the performance of reduced concentration of materials for reducing the concentration of chemical materials (JIS A 1905-1, 2) as well.

The aforementioned small chambers keep the mass transfer rate for water vapor diffusion on the surface of tested building material uniform at approximately 2 to 3m/h, which is far below the mass transfer rate of 9 to 18m/h (12 to 18m/h in the method of evaluating performance of reduced chemical material concentration) recommended in JIS A 1901, JIS A 1905-1,2, etc. This means that actual material transfer in the small chamber is different from the inside of an actual architectural space.

In order to settle the aforementioned problems in this study, we developed an airflow control unit for small chambers for uniformly controlling airflow on the surface of tested building material in the small chambers. We will present the mass transfer rate on the surface of tested building materials corresponding to an actual building in order to exactly evaluate the performance of the reduced amount and concentration of released chemical materials with the small chambers. We measured the airflow velocity on the surface of building materials in the small chamber with the developed airflow control unit and the fan speed for airflow control. We reviewed the distribution of water vapor concentration in the small chamber by means of CFD (Computational Fluid Dynamics) and estimated the mass transfer rate on the surface of building material to confirm test reliability.

Configuration of the airflow control unit and the small chamber

The airflow control unit consists of a case made of SUS 304 and a Teflon fan to avoid chemical materials to be adsorbed and decomposed and is shown in Figure 1.

The fan for generating uniform airflow in the airflow control unit was installed on the bottom of the chamber in order to minimize the influence of air flow formed by air supply and exhaust of the chamber as shown in Figure 2. In the chamber, 3 types of mechanical ventilation are performed and can be controlled to keep wind velocity uniform on the surface of the tested building material according to fan rotation. To avoid pollutants to be generated by the fan in the chamber, the fan rotates by means of magnetic force in connection with the driving unit out of the chamber. The area for installing the tested building material in the airflow control unit is 0.043m^2, which corresponds to the product loading factor of 2.2 m^2/m^3.

Method

The example of analyzing the airflow field on the basis of average wind velocity (U_{center}) in the center of the airflow control unit and the wind velocity (U_{fan}) of the fan is shown in Table 1. The temperature and the number of ventilations in the small chamber was set to 28°C and 0.5 times/h, respectively. With respect to the average wind velocity U_{center} in the airflow control unit, the airflow field was analyzed for 5 cases from 8.27×10^{-4}m/s(U_{fan} =0.01m/s) to 3.57×10^{-1}m/s(U_{fan} =4m/s). For each case, the Reynold's number (=U_0L_0/ν: U_0 is an average wind velocity in the airflow control unit[m/s]. L0 is a half of the internal height of airflow control unit (Line X×1/2, shown in Figure 3)[m]) was 1, 10, 160, 350 and 600, respectively.

The airflow field was subject to 3 dimensional analysis with the low Reynold's number type *k-ε* model (Abe–Nagano model). The wall coordinate (y^+) of the first mesh on the surface of the building material in the airflow control unit is at most 1. Numerical analysis was carried out only for the 1/2 of the space as shown in Figure 2(a), considering symmetry of the analyzed object. The boundary condition of CFD analysis is shown in Table 2.

After analyzing the airflow field, the boundary condition of evaporation dominating building materials was given on the side where the building material was provided, as a model of releasing chemical materials. The surface of the evaporation dominating building material was modeled with liquid of a simply single component. The model of building material was water (distilled water) and water evaporation from the liquid surface to the air, that is, the mass transfer rate was reviewed on the surface of the building material. Diffusion field analysis was carried out, assuming the isothermal state (28°C) without considering latent heat on the surface of building material in the surface model of the building material for this analysis. The surface concentration of the building material was set to being uniform (C_s=constant) to use the water saturation concentration as a boundary condition. In this study, it was assumed that water is a passive contaminant to calculate the distribution of water concentration, and water (vapor) diffusion in the air is expressed as a diffusion equation (1). The water (vapor) diffusion coefficient in the air was calculable by means of the equations (2) to (4).

$$\frac{\partial \overline{C}_1}{\partial t}+\frac{\partial \overline{U}_j \overline{C}_1}{\partial x_j}=\frac{\partial}{\partial x_j}\left(\left(D_a+\frac{\nu_t}{\sigma_t}\right)\frac{\partial \overline{C}_1}{\partial x_j}\right) \quad \text{(Eq. 1)}$$

$$\log_{10} P_w=\frac{A-B}{(C+T)}-3 \quad \text{(Eq. 2)}$$

$$C_0=\rho_a\frac{M_1}{M_2}\frac{P_w}{P-P_w} \quad \text{(Eq. 3)}$$

$$D_a=\frac{6.7\times10^{-8}\times T^{1.83}}{P}\times\left[\left(\frac{T_{c1}}{P_{c1}}\right)^{\frac{1}{3}}+\left(\frac{T_{c2}}{P_{c2}}\right)^{\frac{1}{3}}\right]^{-3}\sqrt{\frac{1}{M_1}+\frac{1}{M_2}} \quad \text{(Eq. 4)}$$

where,

C_1 : pollutant concentration at a spatial point (μg/m^3)

D_a : molecular pollutant diffusion coefficient (m^2/s)

U_j : wind velocity (m/s)

v_t : eddy viscosity (m^2/s)

σ_t : turbulent Schmidt's number (-)

P_w : water vapor pressure (Pa)

A, B, C : empirical constant (A:7.7423, B:1554.16, C:219)

T : temperature (°C)

C_0 : saturation concentration (g/m^3)

ρ_a : air density (g/m^3)

M_1, M_2 : molecular weight

P : atmospheric pressure in the chamber (Pa)

T_{c1}, T_{c2} : critical temperature (°C)

P_{c1}, P_{c2} : critical pressure (Pa)

The water (vapor) diffusivity D_a in the air calculated by means of equations (2) to (4) is $2.30\times10^{-5}m^2/s$ and the water concentration at the small chamber supply is zero (0).

Results and Discussion

Figure 4 shows the average velocity vector (case 3) of airflow in the airflow control unit and the small chamber. The air supplied from the small chamber supply is mixed with the air in the small chamber just before reaching the airflow control unit. It is seen that the mixed air flows uniformly from the upper part to the lower part of the airflow control unit.

Table 3 shows the velocity of released water on the surface of building material and the mass transfer rate. Figure 5 shows correlation among the airflow velocity, the velocity of released water in the airflow control unit and the mass transfer rate in the airflow control unit.

For the case 1 where the Reynold's number is 1, the average velocity of released water is $3.29g/m^2\cdot h$. As the Reynold's number increases to 10 and 160, the velocity of released water increased to $4.07g/m^2\cdot h$ (case 2) and $4.49g/m^2\cdot h$ (case 3). It is considered that the increased Reynold's number depending on the increased central wind velocity in the airflow control unit contributes to smooth diffusion of the material in the airflow control unit, thus to make the difference (gradient) between the water surface and the water concentration in the air

larger. Meanwhile, in cases 4 and 5, although the Reynold's number increased as in Figure 5, the average velocity of released water did not increase and was kept almost at a constant number. It is considered that, although airflow due to fan rotation occurs, the materials in the airflow control unit are completely mixed when the airflow in the airflow control unit reaches at a given velocity and a water concentration difference between on the water surface and in the air is not caused any more. The result of average mass transfer rate exhibits similarity to the result of average release velocity. The mass transfer rate of case 3 where the Reynold's number is 160 and case 4 where the Reynold's number is 350 was 14.43m/h and 18.07m/h, respectively, and it is estimated to be similar to the material transfer phenomenon in an actual architectural space. In particular, case 3 analyzed with the same condition as that of the experiment did not exhibit significant difference from the mass transfer rate measured in the experiment. For case 5 where the Reynold's number is 600, the mass transfer rate was predicted to be 21.55m/h which is slightly above the specification of JIS and the like.

Table 3 and Figure 6 show the result (the average concentration (C_s) on the surface of building material released side is 1) of non-dimensionalizing the chamber exhaust concentration and the concentration distribution in the chamber on the basis of the surface concentration of the building material.

In case 3, the concentration at the chamber exhaust for the surface concentration of the building material became 0.98, so that it is seen that the water concentration in the chamber reached almost saturation and it was almost the same as the measurement result checked in the experiment. In cases 1 and 2, the water concentration in the airflow control unit exhibited uniform distribution, but a slight concentration difference from the concentration distribution in chamber outside of the airflow control unit was observed. A small concentration boundary layer was formed by means of airflow caused by the fan around the surface of the building material. Meanwhile, in case 3 where the mass transfer rate is 14.43m/h, a concentration boundary layer was observed, e.g. a certain concentration gradient was formed around the surface of the building material.

If the wind velocity is not strong on the surface of the building material as in cases 1 and 2, non-uniform concentration distributions (35 to 90% of the surface concentration of the building material) were exhibited in the small chamber. Since the small chamber method of installing the building material as an experiment sample in a small chamber to test release or evaluate performance of reduced concentration assumes complete mixture, it is considered that it is desirable to control airflow in the chamber to form uniform concentration distribution higher than a certain level.

Conclusions

In this study, we developed an airflow control unit for small chambers for controlling the mass transfer rate to be constant on the surface of tested building material in a small chamber. We presented the mass transfer rate on the surface of tested building material corresponding to an actual architectural space for which the amount of released chemical material and performance of reduced concentration can be exactly evaluated. The conclusion derived on the basis of such results is described in the following.

When installing an airflow control unit in a small chamber to control fan speed (U_{fan}) at 1m/s (U_{center}=9.31×10^{-2}m/s, Reynold's number of 160), the mass transfer rate of water vapor diffusion was shown approximately 12m/h for the experiment number, and 14.43m/h for the numerical analysis. Therefore, it is considered that the numbers are the most similar to the mass transfer rate in an actual architectural space. Therefore, it is expected that application of the airflow control unit and the airflow velocity proposed in this study will contribute to achieving an even higher level of measuring the amount of released chemical materials and evaluating performance of reduced chemical material concentration of reduced pollutant concentration materials. When using the airflow control unit in the small chamber, it was seen that the velocity of released materials and the mass transfer rate highly depended on the airflow velocity by the fan, that is the Reynold's number. Increasing the Reynold's number depending on the increased airflow velocity of the fan resulted in smaller concentration difference (gradient) of the materials on the surface of building material and in the air thus to enable smooth material diffusion in the chamber. However, it is necessary to be careful because the amount of release from tested samples might be overestimated when measuring the amount of released chemical materials.

Acknowledgments

This work was supported by the Biohousing Research Center and the Grant of the Korean Ministry of Education, Science and Technology. (The Regional Core Research Program / Biohousing Research Institute)

References

1. K. Kim et al., “A Study on Prediction of an Indoor Volatile Organic Compound and Formaldehyde Considering the Emission Characteristics of Interior Finishing Materials”, *Journal of AIJ, Planning & Design*, 21(12), 2005, pp.255-260.

2. D. Kim et al., “An Analysis of Convective Mass Transfer Coefficient of Material surface in Small Chamber Simulation Method”, *Proceedings of Annual conference of AIK*, 23(1), 2005, pp.243~246.

3. J. Seo et al., “Study on Measurement of Mass Transfer Coefficient and Compounds Emitted from Electrical Appliances and Furniture Using Large Test Chamber Method”, *Journal of AIJ, Planning & Design*, 23(7), 2007, pp.287-294

4. H. Yu et al., “A Study on the Emission Characteristic of Formaldehyde and TVOC from Indoor Finishing Materials”, *Journal of AIJ, Planning & Design*, 21(7), 2005, pp.141-148

5. K.Han et al., “A Study on the Improvement of Emission Test Method for Paints”, *Proceedings of Annual conference of AIK*, 27(1), 2007, pp.833~836.

6. Handbook of chemistry (1999), *The society of chemical engineers*, Japan.

7. J Seo, S Kato (2007). A new way to reduce pollutant? Adsorptive materials and VOCs, *AHSRAE IAQ APPLICATION*, 8(3), pp.9-12.

8. J Seo, S Kato, Y Ataka and S Nagao (2006). Measurement and CFD analysis on decreasing effect of toluene concentration with activated carbon and adsorptive building material, *Proceedings of Healthy building* 2006, 5, pp.101-106.

9. K Abe, T Kondoh and Y Nagano (1994). A new turbulence model for predicting fluid flow and heat transfer in separating and reattaching flows. Flow field calculations, *Int. J. Heat Mass Transfer*, 37(1), pp.139-151.

10. R Funaki, S Tanabe and H Tanaka (2003). The performance test of a small chamber for the measurement of aldehydes and VOCs emission rates from building materials and the comparison of formaldehyde emissions between two different chambers, *Journal of environmental engineering*, AIJ, 572, pp.47-54.

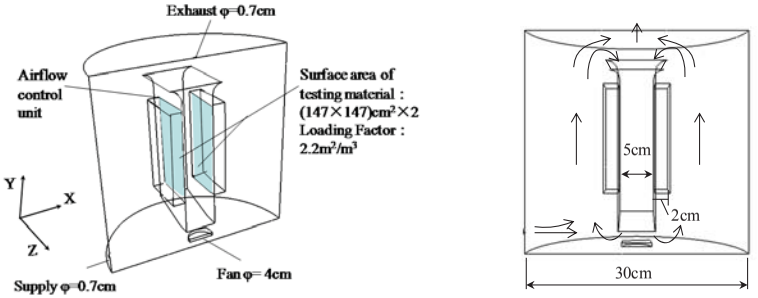
11. S Murakami, S Kato, Q Zhu, S Tanabe and K Ito (2001). Physical modeling and numerical analysis of VOCs emission from building materials (Part 27) CFD analysis of VOCs emission within ADPAC, *Summaries of tech. paper of annual meeting AIJ*, D-2, pp.811-812. (In japanese)

12. Z Qingyu, S Kato, Y Ataka (2004), Examination of influence of mass transfer coefficient on emission rate in medium density fiberboard by test chamber experiment and CFD analysis : Study on test chamber method for measuring emission rate of formaldehyde, *Journal of environmental engineering*, No.582, pp.67-74. (In japanese)



(a) Front view (b) Side view

Fig. 1 Airflow control unit



(a) Airflow control unit and small chamber (b) Airflow in small chamber

Fig. 2 Simplified view of airflow control unit and small chamber

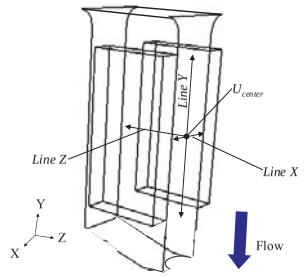


Fig. 3 Point for measuring wind velocity in airflow control unit

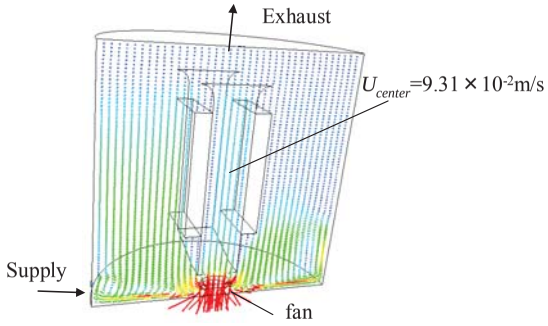


Fig. 4 Velocity vector (cross section X-Y) : case 3

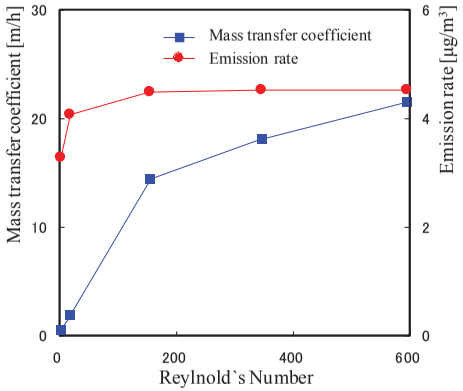
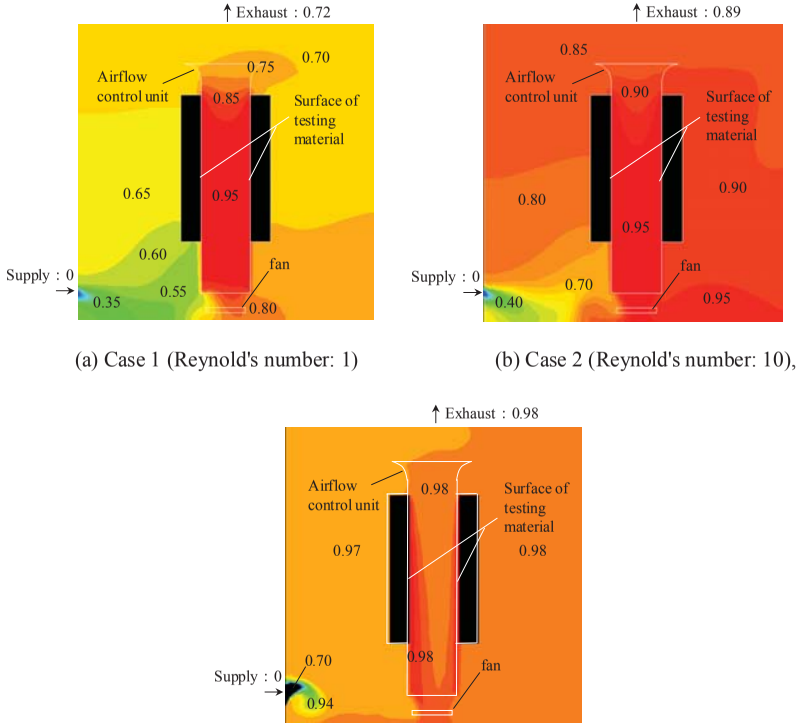


Fig. 5 Correlation between airflow velocity and mass transfer rate/released velocity in the airflow control unit



(a) Case 1 (Reynold's number: 1) (b) Case 2 (Reynold's number: 10),

(c) Case 3 (Reynold's number: 160)

Fig. 6 Distribution of water (distilled water) concentration in the small chamber (C/C_S), cross section X-Y

Table 1 Cases of numerical analysis (Temp: 28°C)

Case	U_{center} (U_{fan}) [m/s]	Reynold's [U_0L_0/v]	Ventilation rates[h^{-1}]	Release model
1	8.27×10^{-4} (0.01)	1	0.5	Evaporation dominating building material (distilled water)
2	3.86×10^{-3} (0.05)	10		
3	9.31×10^{-2} (1)	160		
4	2.07×10^{-1} (2)	350		
5	3.57×10^{-1} (4)	600		

Table 2 Conditions of numerical analysis

Turbulent flow model	Low Reynold's number type k-ε model (Abe-Nagano model)
Number of meshes	270,690
Scheme	Space difference : Second order upwind
Inflow boundary	$U_{x,in}=7.2\times10^{-2}$m/s, $U_{y,in}=0$, $U_{z,in}=0$ $k_{in}=3/2\cdot(U_{in}\times0.05)^2$, $\varepsilon_{in}=C_\mu\cdot k_{in}^{3/2}/L_{in}$ $L_{in}=1/7L_o$, $L_o=7.0\times10^{-4}$m
Outflow boundary	U_{out}=Mass flow, k_{out}, ε_{out}=free slip
Fan boundary	U_{fan}=0.01, 0.05, 1, 2, 4 (m/s)
Wall boundary	No-slip
Analysis of diffusion field	Considering 3-dimensional symmetry, only the 1/2 of the chamber area was analyzed. After airflow field analysis, the water (distilled water) saturation concentration on the surface of building material was set to the condition of C_s=constant to analyze pollutant diffusion in the chamber.

Table 3 Result of predicting average release velocity and average mass transfer rate

Case	U_{center} [m/s]	Reynold's number [U_0L_0/v]	C_{out}/C_s	C_s	Average release velocity [$g/m^2\cdot h$]	Average mass transfer rate [m/h]
1	8.27×10^{-4}	1	0.72	1 (constant)	3.29	0.61
2	3.86×10^{-3}	10	0.89		4.07	1.89
3	9.31×10^{-2}	160	0.98		4.49	14.43
4	2.07×10^{-1}	350	0.99		4.52	18.07
5	3.57×10^{-1}	600	0.99		4.53	21.55

Sensitivity Analysis of Parameters affecting Indoor Air Quality related to HCHO and TVOC Reduction

Mi Yeon Kim[1], Hae Jin Kang[1], Jin Chul Park[2], Eon Ku Rhee[2]

[1] Graduate Program, Dept. of Architecture, Chung-Ang University, Seoul, Korea 156-756
[2] Professor, Dept. of Architecture, Chung-Ang University, Seoul, Korea 156-756

Abstract

The objective of the study is to analyze the relative performance of factors affecting indoor air quality in multi-residential buildings in Korea. A study of the factors affecting indoor air quality is essential for establishing indoor air quality management strategies effectively. To observe the indoor air quality response following a modification of a given parameter sensitivity analysis was performed. The factors examined for the analysis include; wall+ceiling paper, adhesive for wall/ceiling paper, floor material, adhesive for floor material, and ventilation rate. The experimental design system which offers main effects among the design parameters with a few experiments was used to decrease the number of experiments. The simulation for indoor air quality was undertaken using a validated equation. Then, ANOVA(Analysis of Variance) was performed to evaluate the relative importance of each parameter affecting the indoor air quality. The result of the study indicates that the indoor air quality may be influenced most by adhesive for wall/ceiling paper, followed by ventilation rate and adhesive for floor material.

Keywords: Indoor Air Quality, Sensitivity Analysis, ANOVA, Residential Building

1.Introduction

As the importance of indoor air quality is increased in Korea, recommended standards and relevant regulations have been being established. Particularly in newly built residential

buildings having 100 or more units, total volatile organic compounds (TVOC) and formaldehyde (HCHO) should be measured and notified to residents mandatorily prior to occupation. In order to meet recommended standards, the designer and engineers have a tendency to apply almost all IAQ strategies such as eco-labeled interior materials, ventilation, and bake-out in addition. However careless application of IAQ strategies can lead to overuse of cost or materials ineffectively. This is due to the lack of information of relative importance of factors affecting indoor air quality and of factor characteristics. Therefore, a study of the parameters affecting indoor air quality is essential for better establishing strategies of indoor air quality improvement.

2. Research Scope and Methodology

The scope and methods of this study are summarized as follows in the order of progress of sensitivity study. However, there are no formal rules and well-defined procedure for performing sensitivity analysis for indoor air quality, because the objectives of each study are different and building description are quite complicated. In most cases, perturbation technique and sensitivity methods are being used to study the impacts of parameters on different simulation outputs, compared to a base case situation. Then, the results are interpreted and generalized so as to predict the likely response of the performance.

1) Selection of parameters of indoor air quality

Important parameters of the indoor air quality are identified and analyzed from the point of view of intensity reduction of HCHO and TVOC. In order to identify major parameters for HCHO and TVOC applicable to multi-residential buildings, relevant research was reviewed.

2) Establishing base case reference and simulations

To formulate a base case reference, a survey of multi-residential buildings located in Soul was conducted. The equation for the basis of simulation is selected. The equation is approved and used in the Ministry of Environment. In order to secure the validity of equation, actual data of several residential buildings are compared with the result of the equation.

3) ANOVA(Analysis of Variance)

To obtain the factors largely affecting HCHO and TVOC reduction, sensitivity analysis and ANOVA(analysis variance) were conducted. The system of experimental design which offers information about the main effect among the parameters with a few experiments was used to decrease the number of simulations.

3. Identification of relative importance factors applicable to multi-residential buildings

Before performing the analysis, it is essential to understand what parameters are to be studied. A list of the parameters was prepared, and they represented a variety of different factors encountered in multi-residential building design and construction. They are categorized

according to applicable sequences ; design stage and construction stage. In each stage, different sub-parameters are divided as shown in Table 1. As shown in Table1, ventilation strategies can be applied in every stage. However, all strategies in terms of ventilation are integrated into total ventilation rate. Bake-out is excluded from analysis due to theoretical uncertainty and largely-fluctuated results depending on the conditions during the bake-out. Therefore, it was finally determined to include; wall+ceiling papers, adhesive for wall/ceiling papers, floor material, adhesive for floor material, ventilation rate.

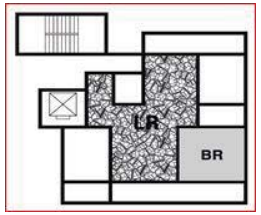
Table 1 Parameters affecting to HCHO, TVOC reduction

Applicable Stage	Category		Parameters
Design	Interior Materials	Finishing Materials	Wall+Ceiling paper
			Floor materials
			Adhesive for Wall/Ceiling paper
			Adhesive for Floor materials-
	Ventilation Strategy	Natural ventilation	Space Planning
			Opening Size & Location
		Forced Ventilation	Ventilation System
Construction	Ventilation Strategy	Natural Ventilation	Ventilation Periods, Ventilation Quantity
		Forced Ventilaton	
	Bake-out	Bake-out	Bake-out temperature, Periods

4. The base case reference for simulation

The base case model forms a very important part in the analysis because all subsequent calculation and analysis are based on the comparison with it. A base case multi-residential building has been established from a survey in Seoul. The characteristics of base case model was determined by careful examination of typical design. Brief description and the plan of the base case building is given in Table 2.

Table 2 Brief description of building and Plan

Plan			
	Total Area		108.9 m^2
	LR	Volume	100.8m^3
		Wall-Ceiling Area	130.1 m^2
		Floor Area	42.0 m^2
	BR	Volume	39.4 m^3
		Wall-Ceiling Area	55.4 m^2
		Floor Area	16.4 m^2
Ventilation	Ventilation Rate		0.7/h
Outdoor Air	HCHO		6.00 mg/m^3/h
	TVOC		101.90 mg/m^3/h

The total area of the base case is 108.9 m^2 . Among the space, the living room and bed room in which good level finishing materials in eco-label mark are applied are selected for sensitivity analysis. The ventilation rate is 0.7/h, the minimum standard in a multi-residential building. The outdoor HCHO and TVOC intensity was 6.00 mg/m^3/h and 101.90 mg/m^3/h.

5. Experiment Design and Simulation

To determine the relative importance of each parameter on HCHO and TVOC reduction, all other parameters should be fixed and one parameter should be changed diversely to review how the results change. However, even if the five parameters presented in Table 4 are

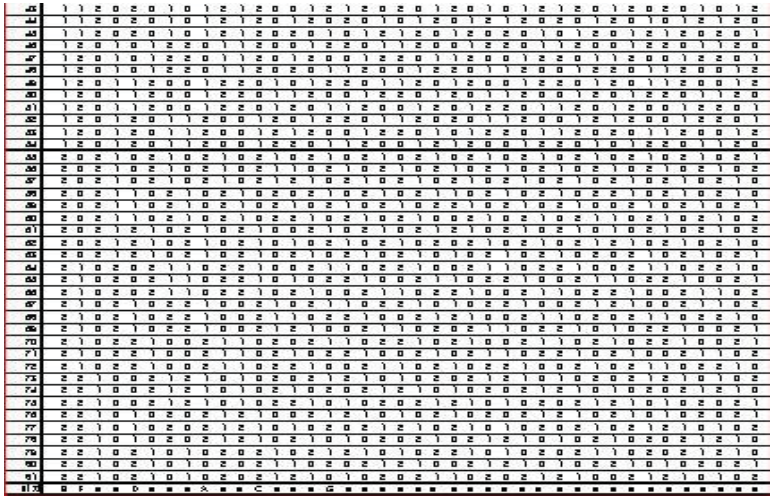
changed in only three levels, as many as 3^5(=279) simulations will be required, making the analysis almost impossible.

Table 3 Brief description of building and Plan

Categorize	Parameters	Level		
		1	2	3
Finishing Materials	Wall+Ceiling paper	General	Good	Excellent
	Floor materials	General	Good	Excellent
	Adhesive for Wall/Ceiling paper	General	Good	Excellent
	Adhesive for Floor materials	General	Good	Excellent
Ventilation Rate		0.5/h	0.7/h	0.9/h

However, if a design of experiment called Orthogonal Arrays is used, the same results as the calculation of entire simulation can be induced by only implementing small number of simulations. According to the Orthogonal Arrays it is possible to reduce the number of simulation up to 27($L_{27}(3^{13})$). However to secure p-value in statistical analysis, the reduced number of simulation was limited to 81 as partly shown in Table 5.

Table 5 Orthogonal Arrays($L_{81}(3^{40})$)



For simulation, the equation which is used in the Ministry of Environment for chamber test is selected. The equation is shown in <Eq. 1>. Because <Eq. 1> was developed to figure out the emission intensities of material in the small chamber, < Eq. 1> is re-established by implementing the binomial theorem of < Eq. 2>.

$$EF = \frac{(C_t - C_{t_b.t}) \times Q}{A} = \frac{(C_t - C_{t_b.t}) \times nV}{A} = (C_t - C_{t_b.t}) \times q = (C_t - C_{t_b.t}) \times \frac{n}{L} \qquad \text{(Eq. 1)}$$

A	Area of materials (㎡)
Ct	HCHO and TVOC intensity during 't' hours in the chamber (㎎/㎥)
Ctb,t	HCHO and TVOC intensity during 't' hours in the empty chamber (㎎/㎥)
EFa	Emission intensity per area(㎎/㎡. h)
n	Ventilation rate (/hr)
Q	Ventilation rate in the chamber(㎥/h)
q	Ventilation rate per area(㎥/㎡. h)
t	't' hours after starting experiment
V	Volume of the chamber(㎥)

$$C_t = \frac{\sum(EF_a \times A)}{n \times V} + C_{t_b.t} \quad \text{(Eq. 2)}$$

A	Area of materials (㎡)
Ct	HCHO and TVOC intensity during 't' hours in the chamber (㎎/㎥)
Ctb,t	HCHO and TVOC intensity during 't' hours in the empty chamber (㎎/㎥)
EFa	Emission intensity per area(㎎/㎡.h)
N	Ventilation rate (/hr)
Q	Ventilation rate in the chamber(㎥/h)
Q	Ventilation rate per area(㎥/㎡.h)
T	't' hours after starting experiment
V	Volume of the chamber(㎥)

In order to secure the validity of IAQ simulation, actual indoor air quality data of several residential buildings were compared with results of < Eq. 2>. Based on the results, it was identified that differences were within 10% (0.2%-9%).

6. Analysis of variances(ANOVA)

ANOVA were conducted with the results of simulations. The relative importance of each parameter was obtained by the following equation

$$P_{A_0} = \frac{Y_1+Y_2+Y_3+\cdots+Y_{27}}{27} - T_m$$

P_{Ai}	Affections of each parameters on i level.
Y_i	HCHO or TVOC intensity of each experiment
T_m	Total average of HCHO or TVOC intensity of 81 experiments

The result of the study indicates that, in terms of the contribution to TVOC reductions, adhesive for wall+ceiling paper was found to have the best contribution(49.9%(LR), 53.9%(BR)) followed by ventilation rate(31.9%(LR), 31.2%(BR)) and floor adhesive (7.3%(LR), 6.4%(BR)). As for HCHO, it was found that the contribution of reduction is greater as the following order; adhesive for wall+ceiling(59.3%(LR), 60.5%(BR)), ventilation rate(22.3%(LR), 22.4%(BR)) and floor-adhesives(8.0%(LR), 7.1%(BR)). It is considered that the other parameters' contributions are small enough to be negligible. (Table 6,7)

Table 6 The contribution rate to TVOC reduction

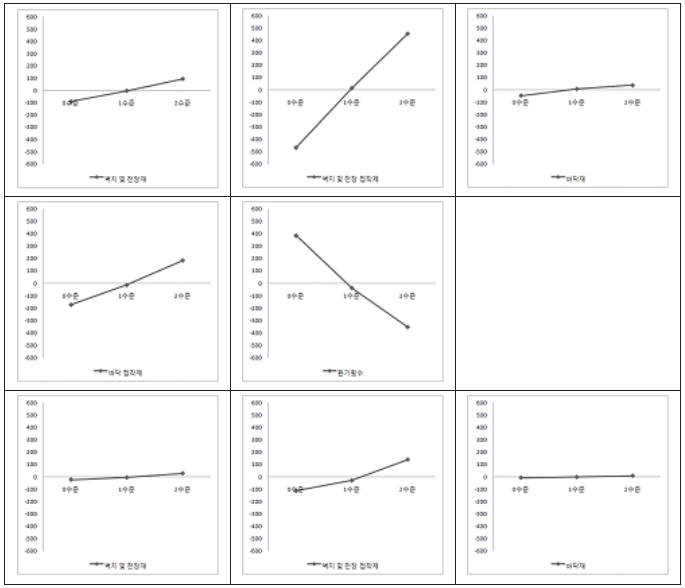
			Contribution to TVOC reduction in LR				Contribution to TVOC reduction in BR		
			0	1	2		0	1	2
A	Wall+Ceiling papers	1.8	-90.4	-2.8	93.2	1.5	96.8	-32.4	-64.4
B	Adhesive for Wall/Ceiling papers-	49.9	-467.0	13.2	453.8	59.3	-523.3	0.0	523.0
C	Floor materials	0.3	-46.8	8.0	38.8	0.1	-20.5	-5.1	25.6
D	Floor Adhesive	7.3	-171.6	-12.6	184.2	8.0	-188.9	15.7	173.2
E	Ventilation Rate	31.9	385.2	-35.0	-350.2	22.8	416.5	-37.9	-378.6

Table 7 The contribution rate to HCHO reduction

			Contribution to TVOC reduction in LR				Contribution to TVOC reduction in BR		
			0	1	2		0	1	2
A	Wall+Ceiling papers	1.5	96.8	-32.4	-64.4	1.5	96.8	-32.4	-64.4
B	Adhesive for Wall/Ceiling papers-	53.9	-112.0	-28.0	140.0	60.5	-122.1	-30.5	152.7

C	Floor materials	0.0	-7.2	-1.8	9.0	0.0	-7.2	-1.8	9.0
D	Floor Adhesive	6.4	-43.9	-6.8	50.7	7.1	-45.0	-6.4	51.4
E	Ventilation Rate	31.2	83.2	-7.6	-75.7	22.3	88.9	-8.1	-80.8

In figure 1, the contribution rates are illustrated in the gradient in graph. The more factors contribute to HCHO and TVOC reduction, the steeper the gradient is inclined. In the graph, 0 corresponds to the average intensity of HCHO and TVOC. Positive (+) values indicate that values are larger than the average intensity, and negative (-) values mean that values are smaller than the average intensity.



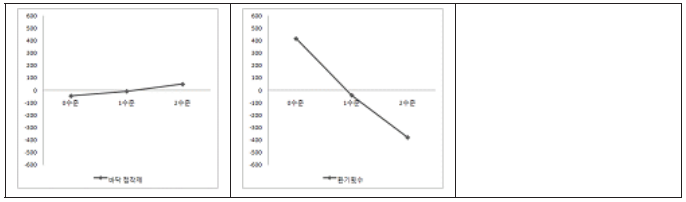


Fig. 1 Graph of the contribution rate

7. Conclusion

The objective of this study is to derive relative importance of factors which affect to reduce indoor HCHO and TVOC intensity. The HCHO/TVOC sensitivity analysis and ANOVA were conducted and the following conclusions were derived.

1) Through a literature search, the main factors affecting HCHO, TVOC are selected. The factors examined for the analysis include: wall+ceiling papers, floor materials, adhesive for wall/ceiling papers, adhesive for floor materials, ventilation rate.

2) For predicting HCHO, TVOC intensity, the equation which is approved and used by the Ministry of Environment is used. The equation is re-established because the original equation is made for testing the emission in the small chamber. The difference between equation and actual data was shown less than 10% and the reliability of the equation was secured.

3) By using orthogonal arrays, the number of simulations is reduced to 81. With the results of simulation, analysis of variance is conducted. As a results, adhesive for wall/ceiling paper was found to have the most contribution followed by ventilation rate and floor-adhesive.

Acknowledgments

This research was supported by a grant(06ConstructionCoreB02) from Construction Core Technology Program funded by Ministry of Construction & Transportation of Korean government.

References

1. Go Eun-Hee, A Study on the Prediction of the Concentrations of Newly Built Multi-family Residential Buildings' Indoor Pollutants in Relation to the Selection of Finishing Materials, Master's Thesis, The Graduate School, Chung-Ang University, 2005
2. The number of times of ventilation in newly built multi-family residential buildings noticed to be legislated by the Ministry of Land, Transport and Marine Affairs to become effective as of January 2006.
3. The Ministry of Environment, indoor air quality process test method, 2004, p172

Analytical estimation of optimal minimum airflow for air circulation

Jin-Hyeon Park[1], Choon-Dong Kim[2], Young-Hum Cho[3], Dong-Ho Choi[4], Jeong-Hoon Yang[5]

[1] Yeungnam University, Graduate School, Dept. of Architecture, Gyeongsan, Korea 712-749
[2] Catholic University of Daegu, School of Architecture, Gyeongsan, Korea 712-702
[3] Kumoh National Institute of Technology, School of Architecture, Gumi, Korea 703-701[1]
[4] Catholic University of Daegu, School of Architecture, Gyeongsan, Korea 712-702
[5] Yeungnam University, School of Architecture, Gyeongsan, Korea 712-749

Abstract

Space conditions are directly controlled by terminal boxes in variable air volume (VAV) air handling unit (AHU) systems. The terminal box either modulates airflow or adjusts discharge air temperature. Conditioned space will have thermal discomfort by less air circulation if the airflow and discharge air temperature are not suitable. The objective of this study is to estimate an optimal value of the airflow and discharge air temperature, which maintains room thermal comfort. This paper is conducted to determine the optimal room airflow and discharge air temperature and verify the impact of room airflow and discharge air temperature on thermal stratification through CFD (Computational Fluid Dynamics) simulations.

Keywords: Air circulation, Thermal comfort, CFD simulation, VAV, AHU

Introduction

Terminal boxes control space conditions in variable air volume (VAV) air-handling unit (AHU) systems. Terminal boxes may cause occupant discomfort if the airflow and discharge air temperature are not suitable. During the winter period stratification and short-circuiting

can be cause of thermal discomfort. The higher the supply air temperature above the space temperature, the lower air circulation.

In ASHRAE standard 62, the room temperature difference should not exceed 15°F(-9.4 °C) to avoid excessive temperature stratification. The supply air temperature is no higher than about 90°F(32.2°C) which limit assumes 75°F(23.9°C) space temperature. But, some zone may require higher supply air temperature to meet peak heating load requirements with low minimum airflow setpoint. Liwerant (2008) suggested the maximum leaving-air temperature (LAT) is 90°F(32.2°C). A LAT above 90°F(32.2°C) will result in stratification and/or short-circuiting. To maintain a LAT of 90°F(32.2°C), minimum (heating) airflow can be adjusted upward. It will have high reheating energy consumption and AHUs will consume more fan power. Therefore, it should be studied to determine an optimal value of the airflow and discharge air temperature, which maintains room thermal comfort and save energy.

The objective of this study is to determine the optimal room airflow and discharge air temperature on thermal stratification. The analytical estimation of optimal value is conducted by numerical simulations and verified by results of temperature and velocity distributions.

Determined minimum value of the inlet air velocity

A balance of a momentum flux of the natural convection and the air flow into the room from the VAV terminal boxes was a basic solution.

Momentum flux of the natural convection

When heat is added to an air and the air density varies with temperature, an airflow can be induced due to the force of gravity acting on the density variations. The importance of buoyance forces in a mixed convection flow can be measured by the ratio of the Graf and Reynolds numbers:

$$Gr = \frac{g \cdot \beta \cdot (T_s - T_\infty) \cdot L^3}{\nu^2} \quad (1)$$

$$\mathrm{Re} = \frac{V \cdot L}{\nu} \quad (2)$$

$$\frac{Gr}{\mathrm{Re}^2} = \frac{g \cdot \beta \cdot (T_s - T_\infty) \cdot L}{V^2} \quad (3)$$

Generally, the combined effects of free and forced convection must be considered when $(Gr/\mathrm{Re}^2) \approx 1$. If the inequality $(Gr/\mathrm{Re}^2) << 1$ is satisfied, free convection effects may be neglected and forced convection is negligible if $(Gr/\mathrm{Re}^2) >> 1$. When this number approaches or exceeds unity, you should expect strong buoyancy contributions to the airflow. Conversely, if it is very small, buoyancy forces may be ignored.

Buoyancy influences within room spaces flow patterns may be significant and it is appropriate to include a gravity term in the vertical component :

$$g \cdot (\rho - \rho_{\infty}) \tag{4}$$

According to the Boussinesq approximation,

$$\rho = \rho_{\infty} \cdot (1 - \beta \cdot (T - T_{\infty})) \tag{5}$$

The buoyancy term in the momentum equation,

$$\dot{F}_{a,room} = -\rho_{a,box} \cdot \beta \cdot (T_{a,room} - T_{a,box}) \cdot g \tag{6}$$

Momentum flux of the air flow into the room

For the air stream blown into the room, the momentum flux can be calculated by the following equation,

$$\dot{F}_{a,box} = \dot{m}_{a,box} \cdot V_{a,box} = \rho_{a,box} \cdot A_d \cdot V_{a,box}^{\ 2} \tag{7}$$

Determination of the minimum value of the inlet air velocity

In order to maximize air circulation, the following relation can be found:

$$\dot{F}_{a,box} \geq \dot{F}_{a,room} \tag{8}$$

$$\rho_{a,box} \cdot A_d \cdot V_{a,box}^{\ 2} \geq -\rho_{a,box} \cdot \beta \cdot (T_{a,room} - T_{a,box}) \cdot g \tag{9}$$

Consequently, a minimum value of the inlet air velocity can be expressed as

$$V_{a,box} \geq \sqrt{\frac{\beta \cdot (T_{a,box} - T_{a,room}) \cdot g}{A_d}} \tag{10}$$

Figure 1 shows a relation between a discharge air temperature and room air temperature and resulting minimum inlet air velocity. Figure 2 shows a relation between a discharge air temperature and inlet diameter of terminal box and resulting minimum airflow to prevent a short air circulation.

NUMERICAL SIMULATION

Simulation condition

A simulation model was developed with FDS. The Building and Fire Research Laboratory at NIST has developed a computational fluid dynamics (CFD) fire model using large eddy simulation (LES) techniques. This model, called the NIST Fire Dynamics Simulator (FDS), has been demonstrated to predict the thermal conditions resulting from a compartment fire. A CFD model requires that the room or building of interest be divided into small three-dimensional rectangular control volumes or computational cells. The CFD model computes the density, velocity, temperature, and pressure and species concentration of the gas in each cell. Based on the laws of conservation of mass, momentum, species and energy, the model

tracks the generation and movement of fire gases. The basic sets of governing equations are written as follows:

Conservation of Mass :

$$\frac{\partial \rho}{\partial t} + \nabla \cdot \rho \cdot u = 0 \tag{11}$$

Conservation of momentum (Newton's second law) :

$$\frac{\partial}{\partial t}(\rho \cdot u) + \nabla \cdot \rho \cdot u \cdot u + \nabla \cdot p = \rho \cdot f + \nabla \cdot \tau_{ij} \tag{12}$$

Conservation of energy (First law of thermodynamics) :

$$\frac{\partial}{\partial t}(\rho \cdot h) + \nabla \cdot \rho \cdot h \cdot u = \frac{Dp}{Dt} + \dot{q}''' - \nabla \cdot q + \Phi \tag{13}$$

Geometry and a coordinate system of the model are shown in Fig. 3. The model for the simulation is selected as the office as the field experiments to verify simulation results. The one wall of model faces to the south. Boundary conditions that were assumed for numerical simulations are presented in Table 1.

Simulation method

CFD simulations of temperature and velocity distributions are done. Details of 8 simulation items with varying inlet air values and outside air temperature are presented in Table 2. The discharge air temperature was calculated by room load when the room air temperature was maintained at 75°F(23.9°C). Simulation 1~4 was conducted to verify the determined minimum inlet air velocity according to discharge air temperature. Minimum airflow of Simulation 5 is set twice as lower and that of Simulation 6 is set twice as higher as determined minimum value. Calculations were repeated until the room air temperature was maintained its setpoint at height points of 5 ft(1.52 m).

Validation of the models

The FDS originally describes the transport of smoke and hot gases during a fire in an enclosure. Most of the validation work has evaluated the model's ability to predict the transport of heat and exhaust products from a fire through an enclosure. Initial comparisons with experimental data collected in a controlled environmental test chamber [Yuan et al. 1998] have produced encouraging results, while identifying the importance of issues such as representation of boundary conditions at the inlet diffuser and modeling of the heat transfer boundary condition at room walls. Room airflow applications were considered by Emmerich and McGrattan [1997, 1998]. In general, the FDS code is able to produce results that agree reasonably with the experimental data. However, a systematic modeling approach that considers the problem solving technique employed by the code is essential to obtaining the best results.

To verify the simulation results, measurements were performed by vertical difference of the room air temperature. Three data loggers were installed at 6.5 ft(2.0m), 3.6 ft(1.1m) and 0.3 ft(0.09m) above the floor. The height where the room air temperature is controlled is 3.6 ft(1.1m), the height at which room temperature controllers are generally installed. Simulations were conducted by same measurement condition. Two discharge air temperatures 82.5 °F(28.1°C) and 86.0 °F(30.0°C) were applied in the analysis. Figure 4 shows the comparison data between measurement and simulation data at different height. The simulation results can predict the performance within 5% of experimental results. In a simplified simulation, which is modeled by Fire Dynamics Simulator (FDS), the simulated results agree reasonably with the predicted results.

Simulation results and discussion

Figure 5 shows the CFD simulation results of the temperature distribution at XY plan along the y=5 ft(1.52m) in the room for all cases. Figure 6 shows the velocity distribution for case 1, 2, 5 and 6 to see the impact of room airflow and discharge air temperature on thermal stratification. If the minimum airflow is lower than determined value (case 5), it can be poor air circulation in the room and cold air temperature near the occupant can be comfort issue.

The results show that the type of temperature profile ensures a suitable thermal comfort for occupants with minimum airflow of case 1~4 as shown Figure 7. The vertical distribution is kept lower than the value proposed by the study on comfort as the vertical temperature difference is below 5.4 °F(-14.8°C) between the head and ankles (3.6 ft(1.1m) and 0.3 ft(0.09m) above the floor) (ASHRAE 1992; Olesen, B.W. 2002).

CONCLUSION

In this study, optimal minimum airflow for air circulation of single duct VAV Terminal boxes are determined. The analytical estimation of optimal value is conducted by numerical simulations and verified by results of temperature and velocity distributions. The results are as follows:

(1) Determined value of minimum airflow is confirmed by results of CFD simulations.

(2) Determined minimum airflow can prevent occupants from short air circulation.

(3) The vertical distribution is kept lower than the value proposed by the study on comfort.

NOMENCLATURE

Gr – Grashof number

Re – Reynolds number

β - thermal expansion coefficient

g - acceleration due to gravity

$\dot{m}_{a,box}$ - mass air flow rate of terminal box, lbm/hr(g/s)

ρ - the local air density, lbm/ft3(kg/m^3)

ρ_∞ - the constant effective mean air density, lbm/ft3(kg/m^3)

ν - viscosity

V - velocity

$\dot{F}_{a,box}$ - momentum flux of terminal box

$\dot{F}_{a,room}$ - buoyancy term in the momentum equation

$T_{a,room}$ - room air temperature

$T_{a,box}$ - discharge air temperature

f - external force vector (excluding gravity)

h - enthalpy; heat transfer coefficient

p : pressure

$\dot{q}'''$: heat release rate per unit volume

t : time

$u = (u, v, w)$: velocity vector

Φ : dissipation function

ρ : density

τ_{ij} : viscous stress tensor

Acknowledgments

This research was supported by a grant (Code# '06 R&D B03) from Cutting-edge Urban Development Program funded by Ministry of Land, Transport and Maritime Affairs of Korean government.

References

1. ASHRAE, "Thermal environmental conditions for human occupancy," *ASHRAE Standard*, 1992, pp.55.

2. ASHRAE, "Ventilation for Acceptable Indoor Air Quality (IAQ)," *ASHRAE standard*, 2004, pp.62.

3. Emmerich S.J., and K.B. McGrattan, "Application of a large eddy simulation model to study room airflow," 104(1), *ASHRAE Transactions*. 1998, pp.1~9.

4. Int-Hout, D., "Air Distribution For Comfort and IAQ," *HPAC Engineering*, 1998.

5. Liwerant, E., "VAV-Box Selection, Code Conformance : Demystifying the application of cooling-with-reheat VAV terminals," *HPAC Engineering*, 2008.

6. McGrattan, K., “Fire Dynamics Simulator (Version 4) User’s Guide,” *NIST Special Publication 1019*, 2008,

7. Olesen, B.W., “Introduction to thermal comfort standards and to the proposed new version of EN ISO 7730,” Vol. 34, *Energy and Buildings*, 2002, pp.537~548.

8. Taylor, S. T., J. Stein, “Sizing VAV Boxes,” Vol. 46, No. 3, *ASHRAE Journal*, 2004, pp.30~35.

9. Webster, T., 2002, “Thermal stratification performance of underfloor air disstibution (UFAD) systems,” *Indoor Air*, 2002.

10. Yuan, X., Q. Chen, L.R. Glicksman, Y. Hu, and X. Yang. 1999. “Measurements and computations of room airflow with displacement ventilation,” Technical Report RP -949, *American Society of Heating, Refrigerating, Air-Conditioning Engineers.*

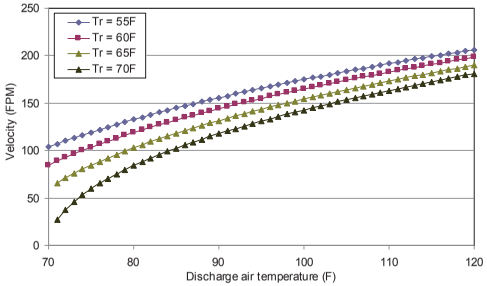


Fig. 1. Minimum inlet air velocity according to discharge air temperature

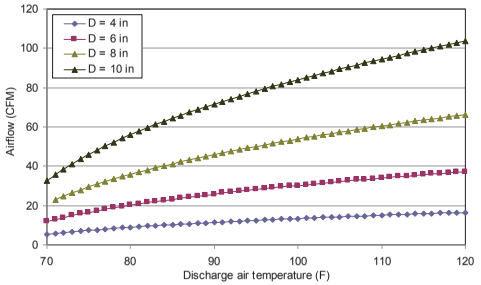


Fig. 2. Minimum airflow according to discharge air temperature

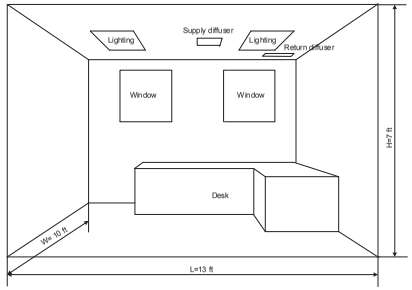


Fig. 3. model for the simulation

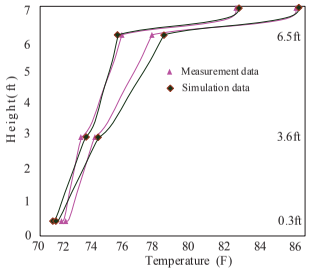
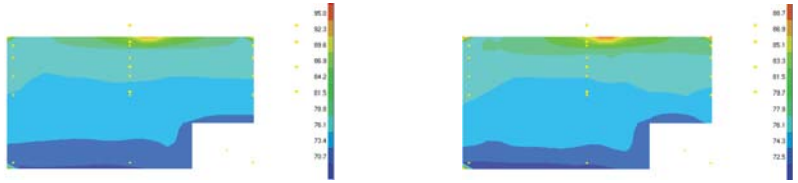
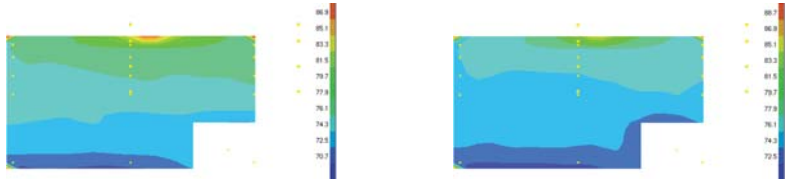


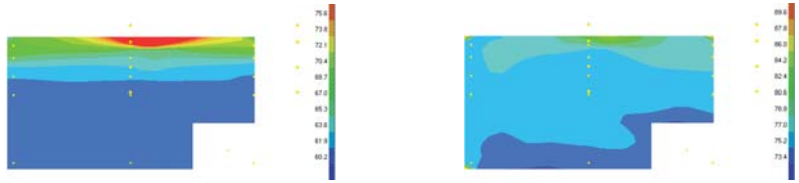
Fig 4. Comparison data for verification of simulation results



Case 1 Case 2

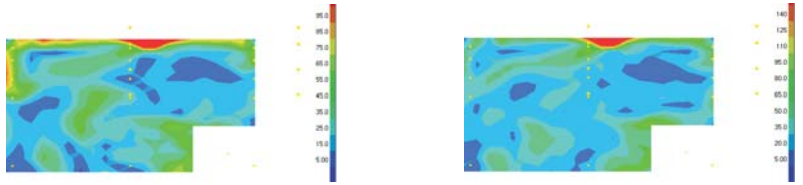


Case 3 Case 4

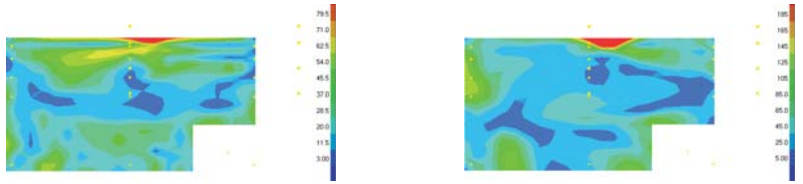


Case 5 Case 6

Fig 5. Room air temperature contours (XY plan along the y=5 ft(1.54m), unit : °F)



Case 1 Case 2



Case 5 Case 6

Fig 6. Velocity contours (XY plan along the y=5 ft(1.54m), unit : m/s)

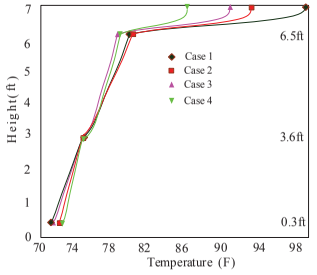


Fig 7. Vertical room air temperature

Table 1. Input data for the simulation

Item	Input data	
Simulation model	Location	Omaha, Nebraska
	Model room	Office rooms
	Floor area	12.08m^2 (3.96*3.04 m)
	Volume	25.77m^3 (3.96*3.04*2.13m)
	Occupancy	1 person
Initial condition	Room air Temperature	12.8°C / 18.3°C
Boundary condition	Outside air temperature	-12.2°C / -1.1°C
	Discharge temperature	30.7°C ~51.1°C
	Supply air velocity	0.38m/s , 0.76m/s , 1.01m/s , 1.52m/s
	Supply diffuser	Louvered face diffuser with 127mm inlet diameter

Table 2. Simulation items.

	Ta, out (°C)	Room load (W)	Va,box (FPM m/s, CFM L/s)	Ta,dis (°C)
Case 1	-12.2°C	147W	0.76m/s, 9.63L/s	37.2°C
Case 2	-12.2°C	147W	1.01m/s, 12.84L/s	34.1°C
Case 3	-1.1°C	101W	0.76m/s, 9.63L/s	33.3°C
Case 4	-1.1°C	101W	1.01m/s, 12.84L/s	30.9°C
Case 5	-12.2°C	147W	0.38m/s, 4.81L/s	51.1°C
Case 6	-12.2°C	147W	1.52m/s, 19.25L/s	30.7°C

Evaluation on the Daylighting performance of 'generative façade components' In the digital simulation

Hwang Yi[1]

[1] SAMOO architects & engineers, Sustainable Design Team, Seoul, 135-839, Korea

Abstract

The aim of this study is to find out a role of the computer simulation on sustainable design projects and development of façade elements with results of daylighting simulation and energy performance. 3D components of façade modeling get to realized in Rhino 3d with some help of Paracloud encoding. With simulation program of Ecotect and eQuest, thus, the result will show influencing factors of each generative components on the radiation & daylighthing factors. And not only that, the result will move to further arguments which is how many factors are related in design of generative skin and which factors should be mainly considered in development façade elements of a sustainable building.

Keywords: performative envelope, generative component, daylighting analysis, digital energy simulation

Introduction

Recently, the better to get realized a sustainable design in architecture, the more collaborations with variety of parts are required. Environmental architecture needs some kind of mechanism about down to earth building elements that allow it to become sustainable.

Correspondingly, there is a trend to contrive integrated process at the early stage of design in architecture. One of this kind of architect's effort seems to appear as a development of the performative building envelopes which is something to do with strong interests among some architects about an innovative building façade. It gives rise to make a building dress up with digitally designed facade which each composing elements are designed through so called 'algorithmic' digital design processes. However, there is need to examine how well these façade design functions environmentally in real and further, to investigate the energy saving effect itself. Thus, digital simulation plays a significant role on this stage of design. In this study, it is the main stream to prove relationship between results of simulation, in particular, solar radiation and daylight analysis, and develop performative components on facade.

Objectives

As a way of examination environmental efficiency of component design, The Main idea is the reification of relationship among three counter parts - daylight efficiency, solar radiation energy performance.

Method

In order to proceed a quantitative comparison of the environmental performance, it selects a real, but simulated in this paper, target building - As shown in both Fig.1 and Fig.2, the head office of SAMSUNG electronics corp. in Seoul. Presuming that it would be renovated recently, the analysis is conducted within ranges of digital manipulation, focusing on alternating of façade of typical floor. And the several simulation tool are suggested - ParClould Modeler and Rhino as generative component design and solar analysis, DOE-2 for energy simulation, ECOTECT of solar and daylight calculation tool.

A three step process is followed for using both ECOTECT and eQuest. First, baseline set up. a digital modeling of the target building is made in ECOTECT (Fig. 3, Fig. 4), which is set up with a 'baseline design' to follow the criteria of ASHRAE 90.1-2007 Appendix G.
It is followed by solar analysis in ECOTECT in the limits of fundamental design factors shown in architectural drawing (Fig.5) with present climate condition. The offset distance of an analytical plane (analysis grid in Ecotect) set to 1.5m above the finish level of typical floor.(see Fig.7) In analytical plane, the void and core parts are excluded. External glasses consists of all low-E double glazing of which are SG 28%, Conductivity 1.65 (Table 2)
Secondly, proposed design analysis. Two different types of façade components are suggested. Each application is ordered as proposed design1 and 2.(Fig. 10 and Fig. 15) The proposed design 1 consists of one components –CASE 1.(Table 4). Proposed design 2 is made up with three different kinds of elements – No.5 to 7 in CASE2. A significant difference between 1 and 2 is the weaving method of façade. Proposed design 1 refer to uniform repetition of one

component. However, It is combination that three elements are applied to proposed design 2. It means, with both ParaCloud Modeler 1.0.4 and Rhinoceros, that intensity of solar radiation on the façade analyzed and it made combination of each elements optimized by its result(Fig 14). For example, in the point of high solar intensity on the façade, components with smaller size fenestration are applied.

All properties of proposed design, including overall size of façade, are the same with the baseline design shown in Table 2 to 3, Except one thing – fenestration and its ratio.

Third phase is the analysis of energy consumption. Considering estimation that daylight control affects directly on the energy consumption of artificial lighting, Annual Energy use on the whole building was checked on each case –baseline, proposed 1 and 2 by using DOE-2. Boundary conditions are illustrated through Table 5 through 8.

Results and Discussion

The 'effective' glazing portion of the façade of the target building is 67.7% (*glass mullion should be considered horizontal/vertical louver). Table 1 shows the interesting result. As though Proposed design 1 has similar fenestration ratio with baseline, its illumination on the floor is multiplied from 325.97 to 596.57 (83% increment). And in the case of proposed design2, the fenestration ratio is decreased by about half. However, the result of daylight level shows just 3% decrement. Solar radiation on the floor ,measured during a year, shows slight difference but a bit. It reaches at a point at least over 80% of the maximum daylight autonomy value within the scene.

Table 1 Final Result of Analysis

		Illumination lx	Insolation kWh/m^2·yr	Fenestraion %	Electricity consumption
Baseline design		325.97	82.13	67.7	20,260MWh
Proposed design	case1	596.57	83.19	61.3	21,660MWh
	case2	577.36	79.53	34.4	19,432MWh

More focusing on the energy comsumption, though the variation of fenestration, insolation and energy consumptions are relatively stable without fluctuation. Through Fig. 19 to 21,The green and yellow area corresponds to the 'daylight area' whereas purple indicates a shortage of daylight. Leading much daylight on the floor not necessarily refers to excessive consumption of energy. Proposed case 1 and case2, though difference of fenestration, their energy consumption are relatively constant.

Conclusions

In brief, This simple set of models show uniformly distributed fenestration bring about daylight efficiency with little regard to any increment of energy consumption - the efficient inflow daylight with little increment of insolation. Moreover, better performative result of optimized arrangement is caused by both elimination of unnecessary numbers of glazing and more glazing on the south elevation.

References

1. International code council, “2009 International Energy Conservation Code and ANSI/ASHRAE/IESNA Standard 90.1-2007 Energy Standard for Building Except Low-Rise Residential Buildings,” ICC, U.S., 2009

2. John Carmody, et al., “Residential Windows,” 3rd ed., W W Norton & CO., 2007

3. Diego I. Ibarra, Christoph F. Reinhart, “DAYLIGHT FACTOR SIMULATIONS – HOW CLOSE DO SIMULATION BEGINNERS ‘REALLY’ GET?,” Building Simulation 2009 Conference, Glasgow, Scotland, 2009.

4. Web Pages and On-line Material: Energy Information Administration , “ Annual Energy Review 2008”, EIA, http://eia.doe.gov (2008).

5. Bradley, E., Kummert, M., McDowell T., “Experiences with and Interpretation of Standard Test Methods of Building Energy AnalysisTools,” The Bi-Annual Conference on IBPSACanada,eSIM 2004, Vancouver.

6. Reinhart C F, Mardaljevic J and Rogers Z.,“Dynamic Daylight Performance Metrics for Sustainable Building Design,”Leukos 3(1):1-20, 2006.



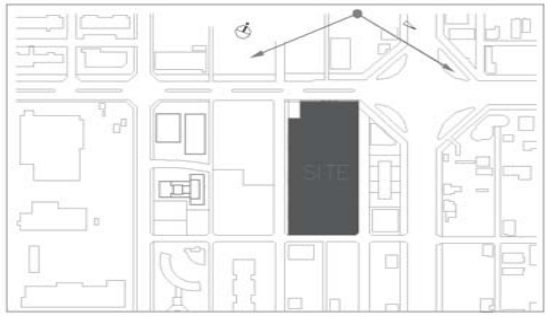
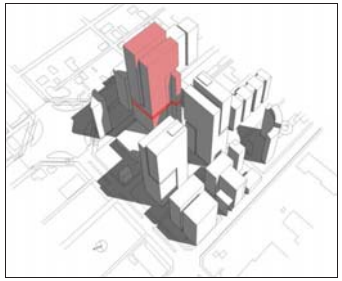
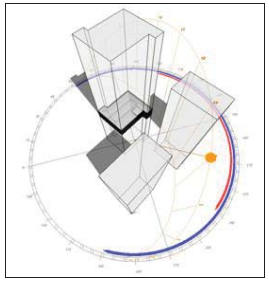


Fig. 1 (left) Target building : the headquarter of SAMSUNG.
Fig. 2 (right) The site plan of the building





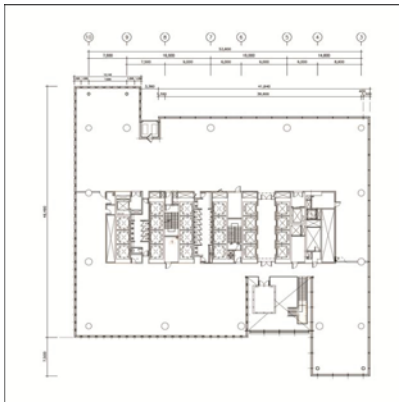


Fig. 3 (above left) Shadow map of target building and Typical floor (marked in red color)
Fig. 4 (above right) Orientation and Daily Sun-path of the building
Fig. 5 (below) Typical floor plan (17F)

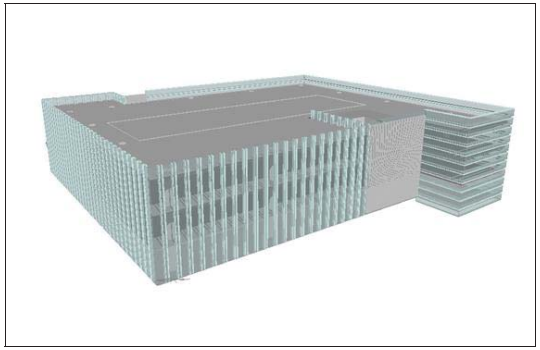


Fig. 6 Digital Baseline modeling of typical floor(16F~18F) in ECOTECT

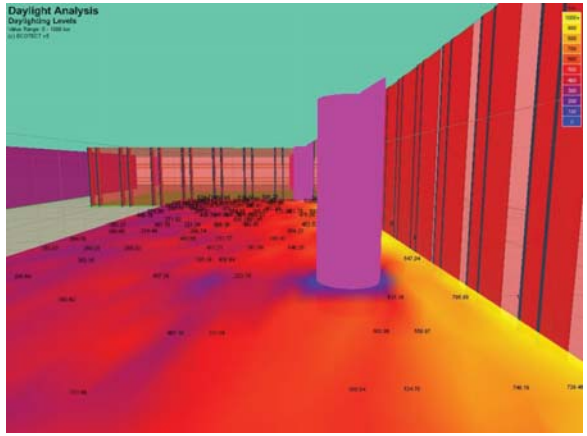


Fig.7 3D Interior view of Illumination levels in baseline modeling

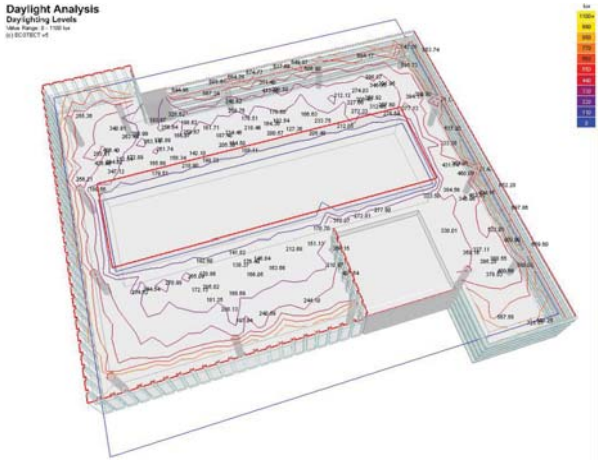


Fig.8 Illumination levels in baseline modeling (average 325.97 lx)

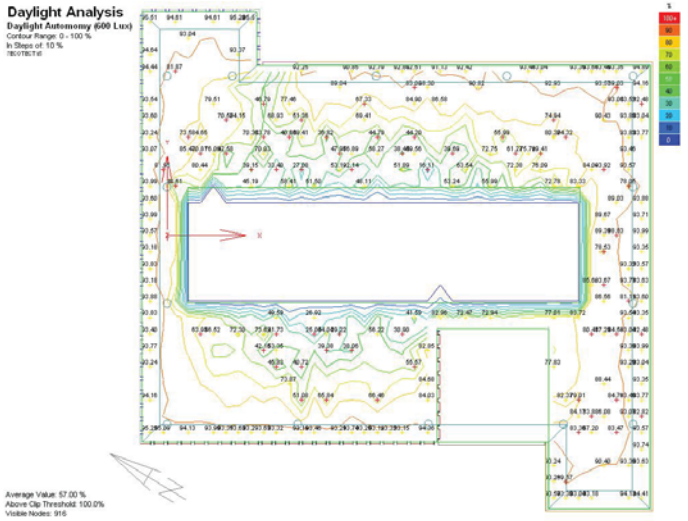


Fig. 9 Daylight Autonomy above 600lx in baseline modeling (average 57%)

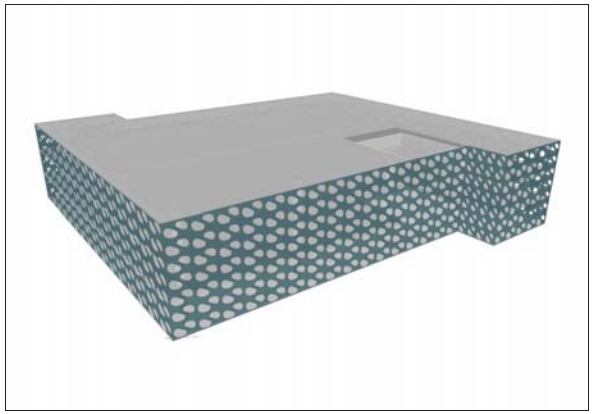


Fig.10 Proposed façade design - alternative 1

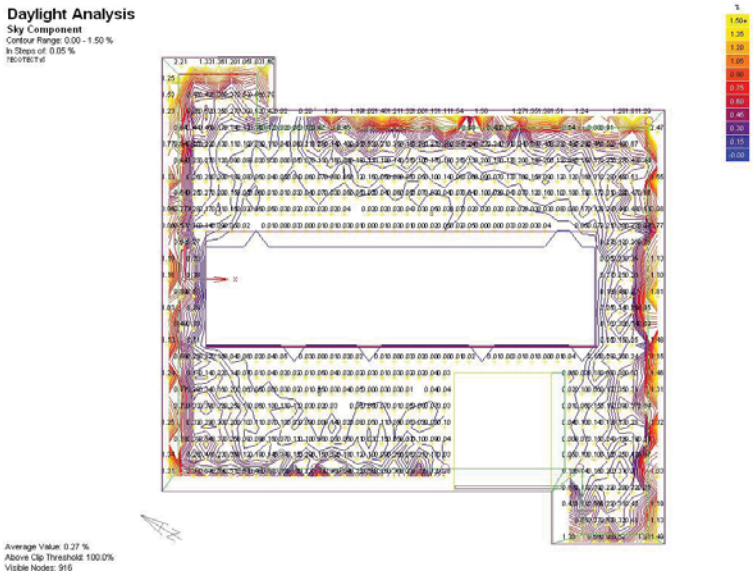


Fig.11 Sky component distribution in Proposed façade design 1(average 0.27%)

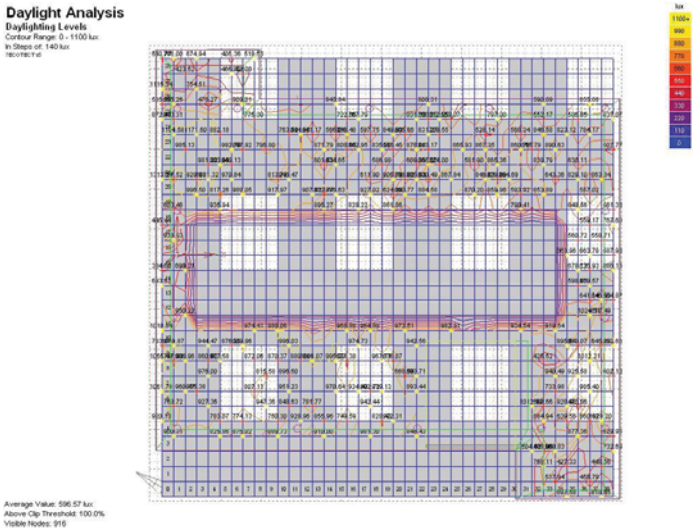


Fig.12 Illumination level in Proposed façade design 1 (average 596.57lx)

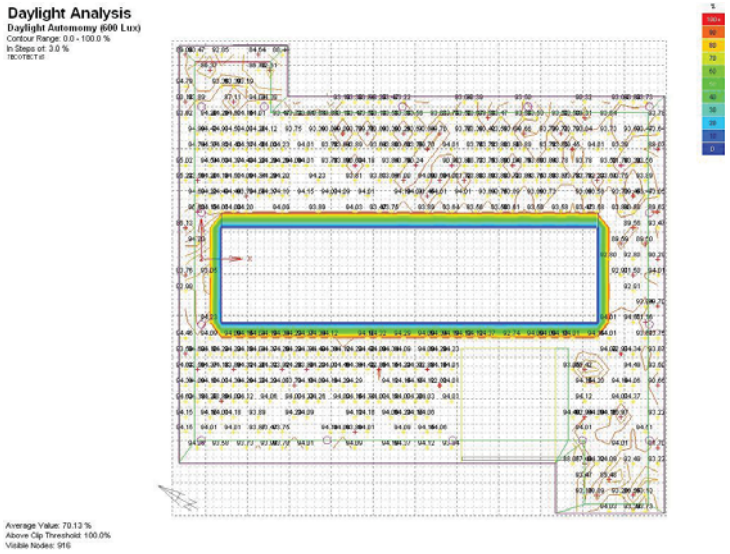


Fig.13 Daylight Autonomy above 600lx in Proposed façade design 1(average 70.13%)

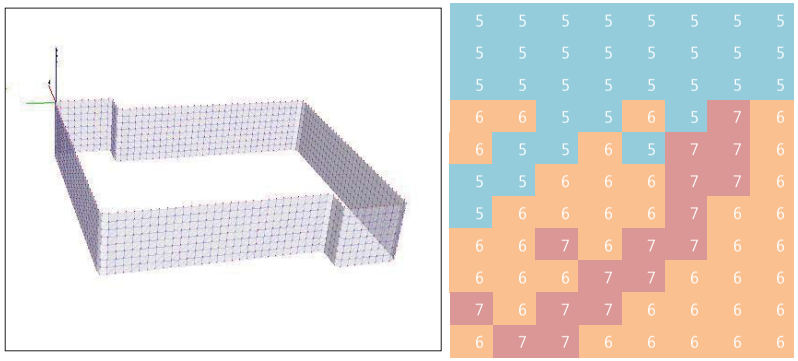


Fig.14 Solar optimization process of proposed design2 in ParaCloud Modeler

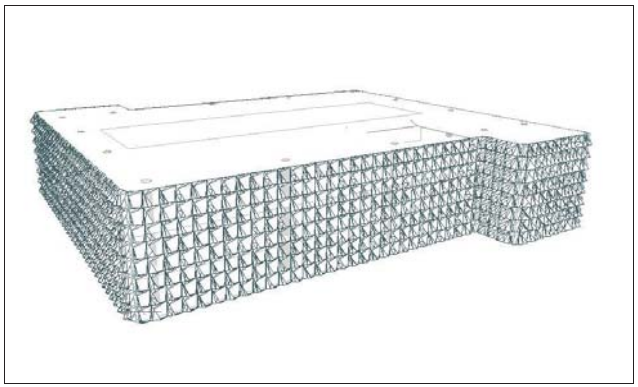


Fig.15 Proposed façade design - alternative 2

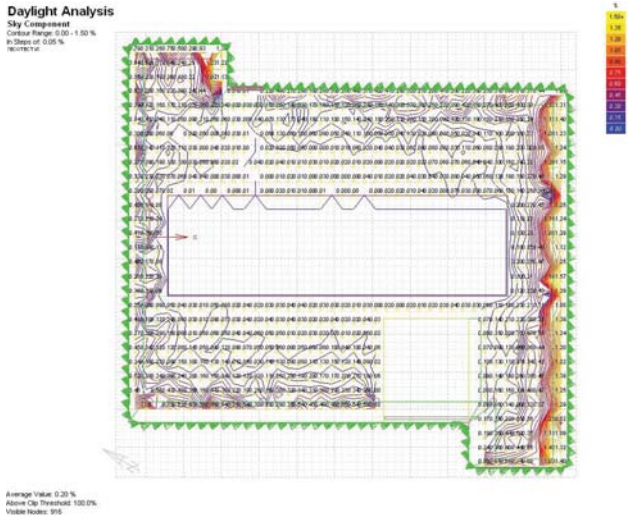


Fig.16 Sky component distribution in Proposed façade design 2(average 0.2%)

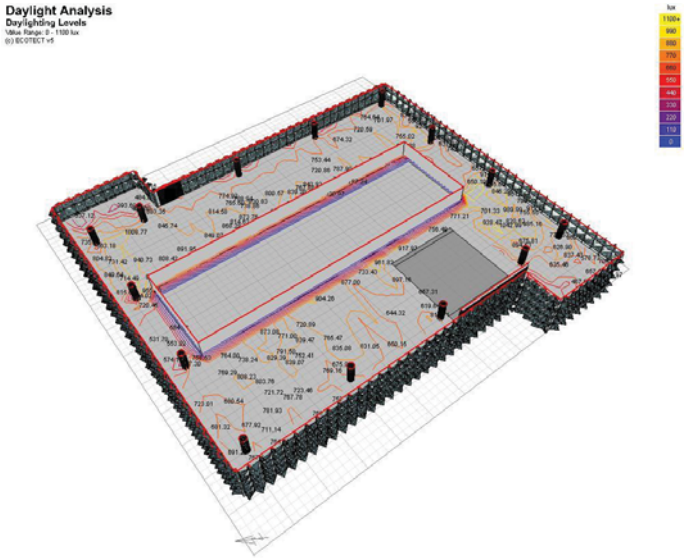


Fig.17 Illumination levels in Proposed façade design 2 (average 325.97 lx)

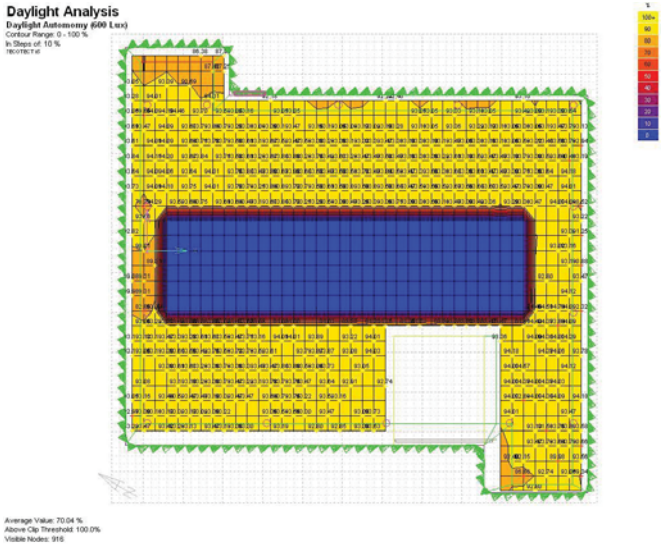


Fig.18 Daylight Autonomy above 600lx in Proposed façade design 2(average 70.04%)

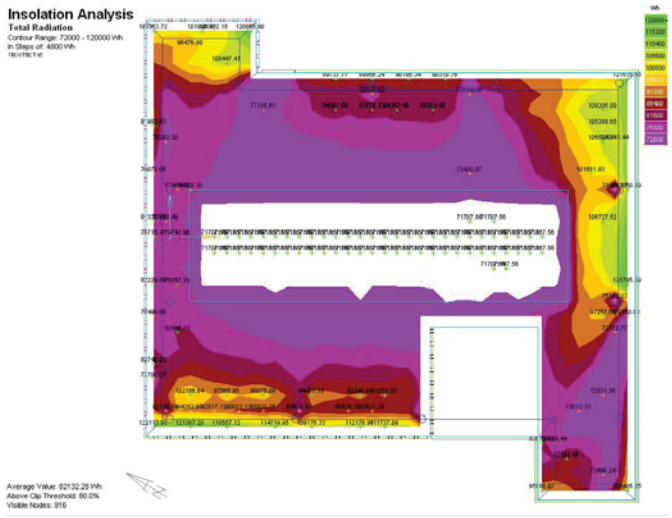


Fig.19 Insolation distribution in baseline design (average 82.13 kWh/m^2·yr)

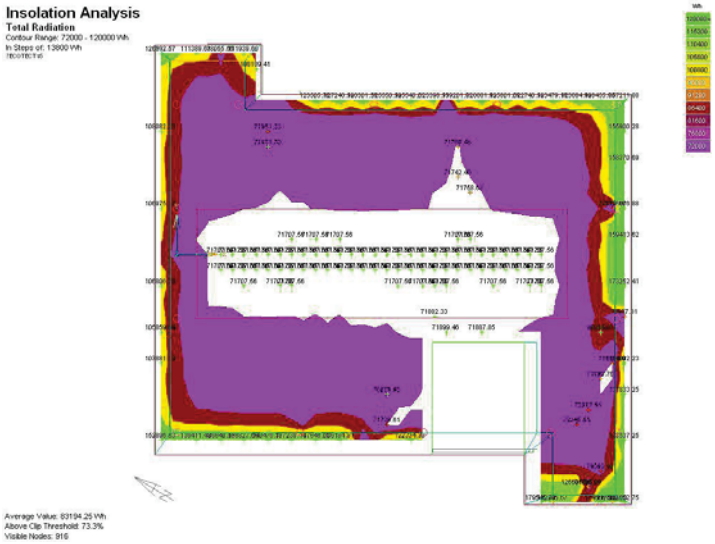


Fig.20 Insolation distribution in Proposed design 1 (average 83.19 kWh/m^2·yr)

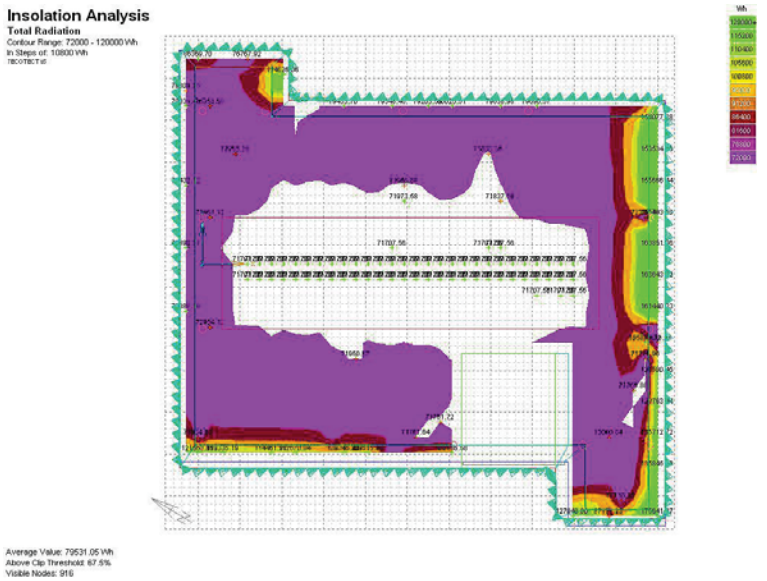


Fig.21 Insolation distribution in Proposed design 2 (average 79.53 kWh/m^2·yr)

Table 2 CurtainWall detail Input data

VRE1 – 46 (Reflective Double glazing, low solar gain low-E)

U-value	1.65 W/m^2 K (0.29 Btu/ft^{2}h °F)
SHGC	28% (= SC 0.32 X 0.87)
Visible Transmittance	43%
Refractive Index of Glass	1.9

Table 3 Premium Reflective Films Input data

No.	Visual Ray		SC	Solar Heat Cut off	Ultra Violet Cut off
	Reflectance	Transmittance			
RS-440	42%	36%	0.38	66%	99%
SRS-220	**55%**	**15%**	**0.25**	**78%**	**99%**
SRS-220-EXSR	63%	15%	0.22	81%	99%

Table 4 Information of component cases and elements

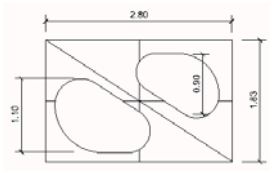
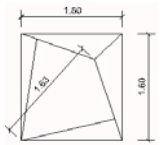
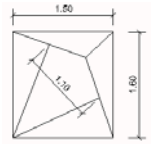
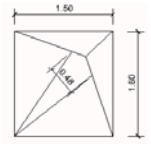
Case1		Case 2		
		 No.5	 No.6	 No.7
Horizontal Projection Area	5.12 m^2	2.40 m^2		
	Fenestration ratio (%)			
	61.3	56.6	37.5	16.0
Material	Aluminum Panel THK 12	Aluminum Panel THK 12	Aluminum Panel THK 12	Aluminum Panel THK 12
Glazing	Window properties are the same with baseline design.			

Table 5 Portion of each space program on typical floor and CFM

Area Type	Percent	Max occup.	CFM. /per
Office	51.0 %	150	20
Stroage	2.0%	22.5	20
Corridor	11.4%	150	7.5
Meeting room	1.0%	450	22.5
Mech. / Elec. Room	21.8%	450	67.5
Copy room	1.0%	187.5	93.75
Restroom	4.5%	52.5	55.0
Lobby	7.3%	150	15

Table 6 Operation Schedule

DAY1 (Typical)	Weekday	8 – 6h (90%)
DAY2	Weekend(Saturday)	9 – 14 h (30%)
DAY3	Holiday	Off

Table 7 Boundary condition of HVAC

Cooling Source	**Heating Source**
-Steam turbine Centrifugal Chiller w/CHW loop. (Individual Chiller pump) COP: 6.0	**- Smoke Fire-tube packaged Boiler** (forced draft) w/ HW loop - **Steam boiler** (forced) - Effi. : 88% / 90%
Single Zone AHU / Ducted VAV sys. (Variable Speed fan)	Fuel : Natl gas
CHW loop Head: 899 ft / ΔT : 14°F	

Table 8 Setpoints of Heating and Cooling source

Thermostat Setpoints	*Occupied*	*Unoccupied*
Cooling Setpoints °F	80.6	86.6
Heating Setpoints °F	66.2	60.2
Design Temperatures	Indoor	Supply
Cooling Design Temp °F	78.8	58.8
Heating Design Temp °F	68.0	88.0

Filtering technology for air purification in HVAC

Henggen SHEN*, Yiren WU

School of Environment Science & Engineering, DongHua University Shanghai 200051, P. R. China

Abstract: this paper is mainly present the filtering technology for air purification in the process of ventilation and air conditioning. By the means of reviewing the related research we have made in this area, several effective programs for PM10 filtration are introduced from the view of experimental testing and practical applications. However, the selection and screening of fiber filter material has yet to be standardized, and the development of new multi-functional and energy efficient fiber filter material is pressingly required. So in the conclusion part, several views are proposed to provide new ideas for the further development of filtering technology in the process of ventilation and air conditioning.

Keywords: filtering technology; PM10; air purification; HVAC

* Corresponding author: School of Environment Science & Engineering, DongHua University Shanghai 200051, P. R. China. E-mail: shenhg@126.com.

0 Introduction

Over the decades, the air quality and environmental problems have attracted most of people's attentions. Hence, the air purification with filtering technology played an essential role in the ventilation and air conditioning process. Basically, the traditional filtering technology mainly focuses on the particulate matter control. For China, soot and automobile exhaust are the two major sources contributing to air pollution. In particular, nearly one-fifth of cities in China have been faced to the serious air pollution problems at present, and more than one-third of the 113 major cities in China could not achieve the secondary standard of national air quality [1]. The ambient respirable particulate matter (PM 10) is considered as the most deleterious pollution for inhabitant health and circumstance, which could cause the respiratory disease by adhering to the bronchial wall or alveolar wall. Moreover, PM 10 could be the vector of the harmful compounds, bacteria and virus in most cases, causing disease by respiration procedure. Owing to its seriousness, it is indicated in national "HVAC (heating, ventilation and air conditioning) design handbook" (GB50019) that the PM10 has been regarded as the essential air pollution which should be under control and the concentration of PM10 should not extend to 0.15 mg/m^3. Meanwhile, the subject "Investigations on prevention of particular matter pollution and thoughts of control approach" has been involved in " the twelfth Five-Year National Environmental Protection Plan " by 2010 [2].

Actually, the control of PM10 should serve to two respects: one is to people's health and the other is to craft, which namely means the products produce and equipments should be protected, and the energy utilization should be improved. Although the mature technologies of air purification protecting the craft have been mainly utilized in electronics and pharmaceutical industries [3], the existing air cleaning technique cannot solve all of the issue to certain extent. At present, the air purification issues still involved in inhabitant health, craft protection and energy utilization improvement fields, such as the spread of bacteria virus (SARS), the capacity

constraints of heat exchanger by dirt, and the influence of fluid flow rate in pipe when the higher speed causing fray and lower speed inducing blockage.

In this paper, we mainly focus on the description of our research results on filtering technology application in certain fields, including the purification of indoor air circulation, the fresh air filter installation in air conditioning units, fresh air filter utilizations in industrial environment. Moreover, innovate filtering technologies and strategies are promoted to purify air during ventilation and air conditioning process. As for filtering technology, there are also some researches for individual respiratory protection, which can be seen in other papers [4][5][6][7][8].

1 Cyclic purification for internal air

Currently, most of the household air conditioners are only installed with the simple filter screens and low efficient filter, which are seldom applied with air purification procedure. Due to the lack of device arresting the PM10 effectively, it could not ensure the concentration of PM10 of the internal air could achieve the standard. Hence, it is obligatory to amend the internal purification system. The most efficient approach is to add the filtering material to the filter screen, which is similarly with wearing the mask for the air conditioner.

Accordingly, the test bench measuring the filtering capability of filtering material for PM10 has been set up based on the PM10 index of modified HVAC design handbook. Furthermore, this test bench could test the performance of filtering material under variety of filtering velocity, such as the filtering efficient with weight calculation and resistance to PM10. The experimental device is illustrated in Figure2-1 below.

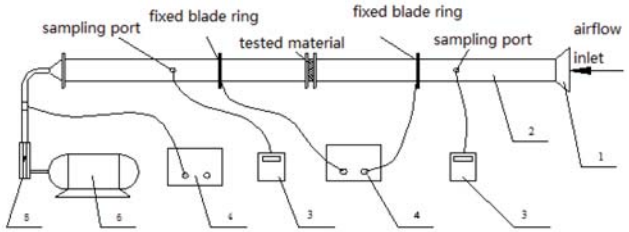


Fig. 2-1 schematic diagram of the testing bench for the filter materials performance

1-current collector，2-testing tube（φ50mm），3- TSI 8520 DustTrak^{TM} Aerosol Monitor，4- DP1000-II digital micromanometer，6- LZB rotameter，7- oil-free vacuum pump

(a) Air duct system: air duct system is made of organic glass steel, which is divided into two steps, and its diameter is 50mm;

(b) Dynamic system: the dynamic system utilize oil-free vacuum pump as resource;

(c) Measurement system: TSI 8520 DustTrak^{TM} Aerosol Monitor is used for measuring the concentration on weight calculation of particular matter of aersol, DP1000-II digital micromanometer is used for measuring the resistance, LZB rotameter is used for controlling the flow volume of filtering air;

(d) Weld fume system: using Aersol or the Talcum Powder with the diameter of 1μm.

Compared to the various non-woven filtering material samples including melt-blown, acupuncture and compound by the performance test, it could be concluded that the charged acupuncture fiber has the best filtering characteristic, which is also with the high efficient and low resistance feature. Through the electrets treatment for filtering material, the carrier would be deposited on the fiber, thus it could become the fiber electrets with charged permanently. In ordinary, the filtering material is relying on the original mechanical barrier to suspend the particular material. However, this kind of filtering material could capture the electrical material by the appeal of Coulomb force, besides it could induce the neutral particles to become polarity and then absorb the PM10. In fact, according to this approach, it could purify the phase of the sub-micro particles more efficiently, which could improve the efficiency several times [9][10]. In comparison with the conventional

filtering material, the innovated filtering material is cheaper, more flexible and less resistance, which could lessen the use of materials, could be folded in hinge deformation. With consideration of its advantages, the 150g/m3 charged acupuncture fiber was utilized in the household air conditioner. It could be concluded by practical application that the filtering effect modified significantly since this kind of material installation. For instance, the filtering efficiency to the PM10 could achieve 71% ~73.6%, meanwhile to the PM2.5 it could reach 68.4% ~ 70.2% and to PM1.0 it arrive at 66.3% ~ 69.6%. In view of the high filtration efficiency, it could reach the merit standard immediately even if in the heavily polluted conditions. Nevertheless, in terms of the initial resistance is slightly higher to the air conditioner, resulting in reducing fan velocity and low wind speed of supply and return air. Thus, it made the cooling procedure longer, but did not influence the original performance of air conditioners [11].

3 Fresh air filter installation in air conditioning units

When the concentration of outdoor respirable particulate matter does not meet the standard, the introduction of fresh air may become another source of pollution rather than improve indoor air quality. Therefore, adequate emphasis should be put forward on fresh air filter technology, which belongs to disposable filtration, during the process of ventilation and air conditioning.

We tested the performances of common used bag filters in Central Air Conditioning System, and comparative analyzed the data [12][13][14]. We have found that the efficiency of bag fibers made of ordinary fiber material increases with the increasing of the particle size, and also the amount of the dust accumulated on the filter. But for the electret filter, the variation regulation of filtration efficiency is different for its different filtering mechanism. Data shows that the filtration efficiency is higher than those ordinary ones and of clean state is highest. With the accumulation of the dust, firstly a slight increase in the filtration efficiency, then partly declines, and then increases again. We soaked electret filtering material in the isopropyl alcohol solution, and made the charge fiber material attenuate permanently, leading to the fierce reduction of filtration efficiency while the resistance remained unchanged. Therefore, to reasonably use the charged fiber filters, the filtration efficiency reduction caused by charge neutralization should be taken into account.

Assuming that particles are uniformly distribute, indoor cleaning mode was established. If particles are uniformly distributed, the indoor particulate instantaneous concentrations can be calculated as followed:

$$N_t = \left[N_0 - \frac{Mn(1-S)(1-\eta_n)+G}{n-nS(1-\eta_r)} \right] e^{-[1-S(1-\eta_r)]nt} + \frac{Mn(1-S)(1-\eta_n)+G}{n-nS(1-\eta_r)} \quad (3\text{-}1)$$

N_t — concentration of indoor dust at a time t，mg/m3；

N — stable concentration of indoor dust，mg/m3；

N_0 — original concentration of indoor dust，mg/m3；

V — volume of the house，m3；

n — air changes，time/h；

G — dust generation volume per-unit indoor space ，mg/(m3.h)；

M — atmospheric dust concentration，mg/m3；

S —— return air ratio，%；

η_1 ——filter efficiency for fresh air，%；

η_2 ——filter efficiency for return air，%；

η_3 ——filter efficiency for terminal equipment，%；

The stable concentration of indoor dust can calculated as followed:

$$N = \frac{Mn(1-S)(1-\eta_n)+G}{n-nS(1-\eta_r)} \quad (3\text{-}2)$$

Compared the example of the applications of the electret fresh air filter with the existing fresh air filter with the equation 3-2, the result shows that the existing fresh air filter cannot meet the national requirements that PM10 should be less than 0.15 mg/m^3 while the electret fresh air filter can[15][16].

4 Fresh air filter for industrial environment

It is well known that China is an industrialized nation, thus it is necessary to filter the fresh air in the industrial environment for workers' health, which plays a key role in the production process.

Using positive pressure cleaning equipment to effectively clear particles in the atmosphere and improving the fresh air with the air-conditioning system are believed to be the main technology for "foggy yarn" in the textile industry. A kind of positive pressure cleaning equipment is provided for "foggy yarn"[17][18].The equipment with polypropylene electret filter material has the feature of compact structure, high filtration efficiency, low filtration resistance and long life. The filtration efficiency reaches 80.9% for the particles PM2.5, with filtration resistance 95pa in clean conditions. The filtration efficiency becomes 78.3% for the particles PM2.5, with filtration resistance 180pa after a half year when the filter needs to be replaced. The filter for fresh air is installed as showed in figure4-1.

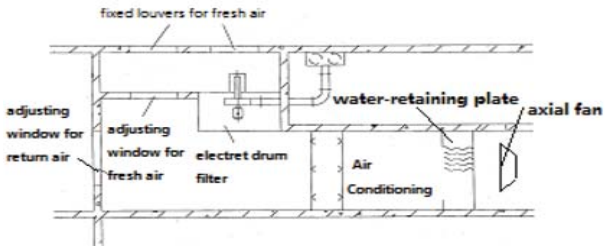


Fig. 4-1 Planar graph of electret drum filter

The working principle is that after the ambient air filtered through the drum filter, some of particulate matters would be intercepted by electret filtering material, and collected regularly by the rotative suction nozzle, then through the dusting fan sent to the dust box to be separated between dust and air. The dust which adhered to the surface of the dust bag would fall into the ash container by regular mechanical vibration, then compacted and collected by the extrusion press. The separation of air would be through the drum filter again. The air after dealing with filtering would be compound with the return air of the spun yarn workshop by axial fan. After that it need be processed in spray chamber. Then it enter the spun yarn workshop through the water-retaining plate, air main and branch duct.

The result of the practical test for the spun yarn workshop show that, compared with the other three production areas, the A area installed the air convection ventilation and purification devices, and the atmospheric environment influence of particulate matter is very less, the concentration of the fine particulate matters (PM2.5) is very low. At the same time, the generation rate of the deficient "foggy yarn" is much lower than the other three areas. The productive process of the "foggy yarn" affects by ambient air, in different ambient air conditions, the result of this device for prevention and control of the "foggy yarn" still need to be tested in practice.

5 Conclusion

As for the increasing requirement of air quality, the application of the filtration technology in the process of ventilation and air conditioning has drawn widespread attention. However, the selection and screening of fiber filter material has yet to be standardized, and the development of new multi-functional and energy efficient fiber filter material is pressingly required. Several views are proposed:

(1) As health is more important than comfort, closer attention should be paid on human health in the design of HVAC;

(2) Among China's current standards , "Indoor Air Quality Standard "(GB / T 18883-2002) is related to the concentration limits of PM10 ≤ 0.15mg/m3 in civil buildings, but it's just a recommended standard, and the technical means for ensuring the compliance of PM10 is still no clear. Therefore, the selection of fiber filter and filtering material in the actual projects needs to be pressingly standardized;

(3) The filtering technology used in industrial ventilation should be further concerned, and the development of high temperature resistant filtering material is significant;

(4) Development of energy-efficient fiber filtering material, low resistance, high efficiency and long life, is an important direction of the fiber filtering material research;

(5) Not be limited to particulate matter control, the advantage of the different characteristics of fiber material itself may be taken to achieve cooperative control of harmful gases;

(6) For the building-energy-saving requirements, fiber filtering material with appropriate comprehensive features (large surface area , small size, good performance in heat transfer, etc.), may directly service to the heat exchange parts of ventilation and air conditioning system, which can recover the exhausted heat meanwhile reduce the harmful emissions, thus provide a new solution for energy use and recycling.

Reference:

[1] (http://news.china.com.cn/rollnews/2010-09/06/content_4141268.htm) Ministry of Environmental Protection

[2] The institute for public selection undertaking unit for "The twelfth Five-Year National Environmental Protection Plan". 2010 .05

[3] Xu Zh. L., Technologies and principles of air cleaning, Shanghai, Tongji University Press, 1998, 86－116

[4] Shen H. L Yang. G Liu. H Wang. L Cai. S Liu and Y Lu, Performance of a new mask material in filtering ambient aerosols for medical staff, *Acad J Sec Mil Med Univ*, 2003, 24(6): 629-31.(in Chinese)

[5] Yang L., Shen H. G., Wu G. 2007, " Racial Differences in Respirator Fit Testing: A Pilot Study of Whether American Fit Panels are Representative of Chinese Faces ", *Ann Occup Hyg*. 51(4): 415-421.

[6] Yang L., Shen H. G[I]. 2005. "The Assessment on The Leakage of Simple Respiratory Protection in Ambient Air", *Proceedings of Indoor Air 2005*, Beijing, Sep. 2005, Vol.I (2): 1011-1015.

[7] Yang L., Shen H. G[II]. 2005. "Quantitative Study on the Relationship between Leakage Volume of N95 Respirators and Inhaled Airflow against PM10, PM2.5 and PM1.0", *Proceedings of 6th International Scientific Conference of International Occupational Hygiene Association*, Johannesburg, Sep. 2005, 231-236.

[8] Yang L., Shen H. G. 2007, "Performance Evaluation of Electret Fiber, Non-woven and Cotton Fiber used for Respirators Challenged with Polydisperse Ambient Aerosols", in Proceedings of 2007 International Forum on Biomedical Textile Materials, May 2007, Shanghai, 114-117.

[9] Chen, C. Y., Filtration of Aerosols by Fibrous Filters, Chem. Rev., 1955, 55, 595

[10]A.C.Payatakes, Model of Aerosol Particle Deposition in Fibrous Media with Dendrite-Like Pattern.Application to Pure Interception during Period of Unhindered Growth, Filtration & Separation., 1976, 13, 602-608

[11]Wang H. Y. 2004, "Performance of the filter materials on PM10", Master thesis (in Chinese)

[12] JIS B 9908-1991, Air Filter Units for Ventilation，Japanese Standards Association，2001

[13] Dorman, R. G., In High Efficiency Air Filtration ,Buterworth, London, 1964

[14] Ronard G.Stafford and Harry J.Ettinger. Comparison of Filter Media Against Liquid and Solid Aerosols. American industial hygiene association Journal, V32,No.5,309~326,1971

[15] Tan L.L.2005, "The experimental investigation of the fibrous material and fibrous filter for particulate matter control in building environment", Master thesis (in Chinese)

[16]Yu X. 2005, "Investigation of Test and Application of Fibrous Filter for Particulate Matter Control in Civil Air Conditioning System" , Master thesis (in Chinese)

[17]Zhang W. 2005, "Study on Technology of Eliminating the Foggy Yarn in the Cotton Mill", Master thesis (in Chinese)

[18] Zhu H., Shen H. G., Zhang W. "Causes and Prevention of the Foggy Yarn in the Cotton Mill", Building heat energy, ventilation and air conditioning, 2004, 23(1), 80－83

Effective flow area estimation test using CO2

Ken Iwamoto, Koji Fujita, and Takayuki Matsushita

Dept. of Architecture, Graduate School of Eng., Kobe Univ., Kobe, Japan 657-8501

Abstract

We developed a method for estimating effective flow areas not only in the external wall of a house but also in the internal walls between rooms using only one type of tracer gas. This method is based upon the following hypotheses: (1) the temperature and tracer-gas concentration in the room is homogenous, (2) the air in the room is in a windless state, (3) there is no error in the measurement of tracer-gas concentration. However, we know that in reality, these hypotheses are not entirely true. To check the effects of discrepancies between the hypotheses and actual conditions on the estimated results, we set up a miniature model experiment. As a result of this experiment, it was clarified that the present estimation method yields a reasonable estimate of the discharge coefficient even when there is a certain amount of discrepancies between the hypotheses and actual conditions.

Keywords: Effective flow area, Air leakage area, Discharge coefficient, Estimation, Newton's method, experiment, miniature model.

Introduction

To quantify air flow rate through leakage area in a wall under any conditions, it is necessary to determine the effective flow area in the wall. Practical method exists for estimating effective flow area on the basis of the relation between pressure difference and air flow rate [1]. However, this method has mostly been used to estimate effective flow areas in the external walls of a house and not those in the internal walls between rooms.

We developed a method for estimating effective flow areas not only in the external wall of a house but also in the internal walls between rooms using only one type of tracer gas [2]. The effective flow area is calculated by multiplying the discharge coefficient of the wall and the area of the wall. Therefore, if the discharge coefficient is known, we can obtain the effective flow area. The theoretical basis of the estimation method is as follows. The discharge coefficients and the pressure in the rooms - which are unknown variables - are determined using a set of equations, which are balance equations for mass and tracer-gas concentration in the rooms. Here, mass and tracer-gas concentration balance equations are considered so as to include the same number of unknown variables as the number of equations. These equations form a nonlinear system, which can be solved using Newton's numerical method.

This method is based upon the following hypotheses: (1) the temperature and tracer-gas concentration in the room is homogenous, and (2) the air in the room is in a windless state (still). However, we know that in reality, the above hypotheses are not entirely true. Further, it is possible that measuring errors may affect the estimated effective flow areas. To check the effects of discrepancies between the hypotheses and actual conditions on the estimated results, we set up a miniature model experiment.

Experimental setup

Figures 1 shows the diagram of the miniature model used in the experiment. The experiment was carried out in an experimental room. The airflow inside the experimental room was maintained under quiet conditions. The miniature model had four cubic rooms, each with sides 0.4-m long. In each internal wall, i.e., a wall between rooms, and external wall, i.e., a wall separating a room from the external environment, 25 holes with a diameter of 6.5 mm were bored such that there were five holes in the vertical and horizontal directions; neighboring holes were separated by a distance of 0.065 m. The discharge coefficients of the walls in which holes had been bored were estimated using the effective flow area estimating method [2]. Here, the discharge coefficient of a wall is defined as shown in Equation 1. We assume that the air flow rate is proportional to the square root of pressure difference across an opening as long as there is no vertical distribution of pressure difference. The effective flow area was calculated by multiplying the discharge coefficient of the wall and the area of the wall.

$$\alpha_w = \frac{\sum_{i=1}^{25} \alpha_i A_i}{A_w} \qquad \text{(Eq. 1)}$$

where:

α_w : discharge coefficient of a wall (-), $\left(= \frac{Q_0}{A_w} \left(\frac{\rho}{2} \right)^{0.5} (p_r)^{a-0.5} \right)$ [1],

Q_0 : air leakage coefficient ($m^3/(s\ Pa^a)$) [1],

a : air flow exponent (-) [1],

p_r : reference pressure difference (Pa) [1], (in Japan, 9.8 Pa),

α_i : discharge coefficient of hole "i" (-),

A_w : area of wall (m^2),

A_i : opening area of hole "i" (m^2).

CO_2 was used as the tracer gas. Figure 2 shows the location of the heating element (Nichrome wire), the location of the mixing fan, the point at which the CO2 was supplied, and the points at

which temperature and the CO2 concentration were measured. The fans were installed to maintain uniform temperature and CO_2 concentration distributions in each room.

Heat generation and the supply of CO2 were carried out under the three conditions listed in Table 1.

The temperature in each room was measured using T-type thermocouples at heights of 0.02 m, 0.20 m, and 0.38 m at the center of each room. The CO_2 concentration in each room was measured using Non-dispersive infra-red analyzers. The CO_2 concentration at a height of 0.20 m was measured throughout each experiment and that of 0.02 m and 0.38 m was measured just before the end of each experiment, the condition of which is listed in Table 1. The repeatability of the analyzers for full scale (volume standard concentration 5,000 ppm) was ±80 ppm. In each room, one such device was used to measure the CO_2 concentration; thus, four measuring devices were used in total. A plastic tube with a diameter of 6 mm, through which air flowed at a rate of 0.5 l/min, was used for aspiration of air during the measurement of the CO_2 concentration; the circulated air reached its original location after the measurement process was completed. The CO2 concentration of the external air was measured both before and after the CO2 concentration inside the room had been measured. The measured temperatures and concentrations were recorded by a data logger at 1-s intervals.

Results

Figure 3 depicts the changes in temperature and CO_2 concentration at height of 0.2 m under three conditions. The temperature in a room is represented by the average of the values measured at the three measuring points in that room.

The final values of the changes in temperature and concentration, as shown in Figure 3, were considered to be their steady-state values. (We considered that the steady state had been achieved when the change in concentration was less than 30 ppm for 3 min.) These values are listed in Table 2. This table also includes the temperature and concentration values under steady-state conditions at the three heights. The difference between the temperatures observed at the high and low points was 2.9–8.1°C in the heated rooms and 0.1–1.6°C in the other rooms. Further, the difference between the concentrations at the high and low points ranged up to 120 ppm (mass standard).

These average temperature of the three heights, average concentration of the three heights, and the volume of CO_2 supplied in each room, as well as the width and height of each wall were input into the program that uses the effective flow area estimation method [2], and the discharge coefficient of each wall was estimated. The allowed values of errors that satisfied the mass and concentration balance equations were respectively set to 2.0×10^{-5} kg/s and 8.0×10^{-9} kg/s.

Table 3 lists the estimated discharge coefficient of each wall. The validity of these discharge coefficients was verified by using the method described below. The change in CO_2 concentration in each room was simulated by inputting information into an airflow network calculating program [3]; the information that was input included the above-mentioned discharge coefficients, the dimensions of the miniature model, the volume of CO_2 supplied, and the changes in the temperature in each room. The validity of the estimated discharge coefficients was evaluated by comparing the calculated concentration change with the measured concentration change.

Figure 4 shows the calculated and measured values of the changes in CO_2 concentration. Since the calculated and measured values are roughly equal under all conditions, it is confirmed that the estimated values of the discharge coefficients that are listed in Table 3 are approximately correct.

Summary and conclusions

We developed a method for estimating effective flow areas not only in the external wall of a house but also in the internal walls between rooms using only one type of tracer gas [2]. This method assumes that the distribution of temperature and tracer-gas concentration in the room is completely uniform, the airflow inside the room is maintained under quiet conditions, and there are no errors in the measurement of temperature and concentration. To check the effects of discrepancies between the hypotheses and actual conditions on the estimated results, we set up a miniature model experiment.

As a result of this experiment, it was confirmed that the values of the discharge coefficients of the walls that were estimated by this method can be used to explain the experimental values of the changes in the CO2 concentration. Thus, it was clarified that the present estimation method yields a reasonable estimate of the discharge coefficient even when there is a certain amount of error in the measurement of concentration and the distribution of temperature, the concentration in the room is not perfectly uniform, and the air in the room is not in a quiet state. Further investigation is required to quantify the errors in the estimated discharge coefficient values; these errors may be caused by concentration measurement errors, nonuniform temperature and concentration distributions, and air circulation in the room.

Acknowledgments

This work was supported by MEXT KAKENHI (No. 21760450).

References

1. ISO 9972, Thermal performance of buildings - Determination of building air permeability of buildings - Fan pressurization method, 2006.5.

2. K. Fujita, K. Iwamoto and T. Matsushita, “Effective flow area estimation method using a gas”, Proceedings of 31th AIVC international conference in Seoul, 2010.10.

3. J. Rao and F. Haghighat, “A Procedure for Sensitivity Analysis of Airflow in Multi-zone Buildings”, Building and Environment, Vol.28, No.1, 1993, pp.53-62.

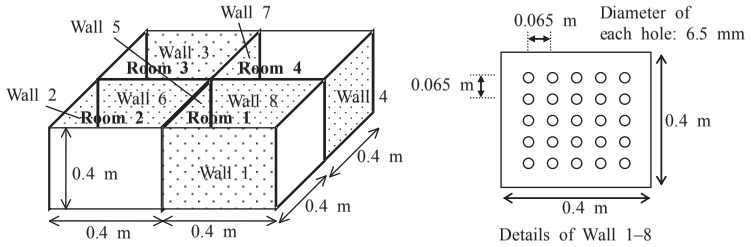


Fig. 1 Diagram of miniature model

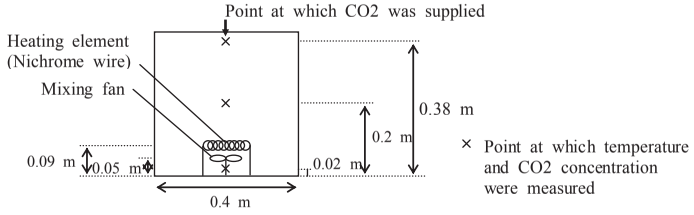


Fig. 2 Vertical cross section of a room

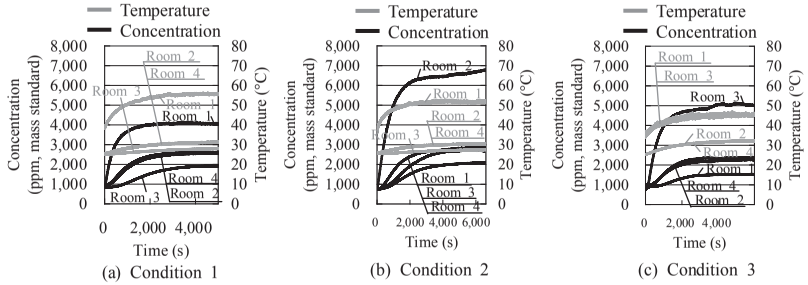


Fig. 3 Changes in temperature and CO_2 concentration

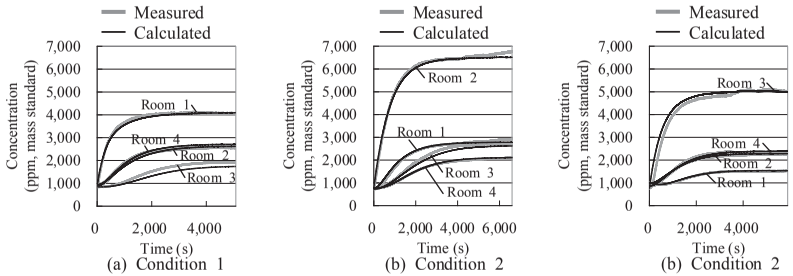


Fig. 4 Calculated and measured values of changes in CO_2 concentration

Table 1 Conditions for heat generation and supply of CO2

	Heating				Supply rate of CO2 (g/h)			
	Room 1	Room 2	Room 3	Room 4	Room 1	Room 2	Room 3	Room 4
Condition 1	heated	-	-	-	1.944	-	-	-
Condition 2	heated	-	-	-	-	1.944	-	-
Condition 3	heated	-	heated	-	-	-	1.944	-

Table 2 Values of the steady-state temperature and CO2 concentration

	Temperature (°C)				CO2 concentration (ppm, mass standard)			
	Room 1	Room 2	Room 3	Room 4	Room 1	Room 2	Room 3	Room 4
Condition 1 ave.	55.27	31.27	27.97	31.23	4,020	2,540	1,923	2,635
0.38 m height	59.3	31.8	28.0	31.7	4,068	2,555	1,925	2,650
0.20 m height	55.3	31.8	28.1	31.2	4,045	2,548	1,919	2,621
0.02 m height	51.2	30.2	27.8	30.8	3,948	2,517	1,926	2,634
Condition 2 ave.	51.80	30.37	27.33	30.27	2,928	6787	2,702	2,115
0.38 m height	51.3	30.4	27.3	30.6	2,937	6,839	2,683	2,118
0.20 m height	57.1	30.5	27.3	30.2	2,914	6,776	2,685	2,101
0.02 m height	47.0	30.2	27.4	30.0	2,931	6,748	2,738	2,126
Condition 3 ave.	45.37	32.27	45.77	32.10	1,524	2,249	5,009	2,395
0.38 m height	46.6	32.3	46.4	32.4	1,534	2,243	5,016	2,403
0.20 m height	45.8	32.4	50.0	32.1	1,521	2,262	5,015	2,386
0.02 m height	43.7	32.1	40.9	31.8	1,519	2,242	4,996	2,395

Table 3 Estimated discharge coefficients

Wall No.	1	2	3	4	5	6	7	8
Estimated value	0.002870	0.002047	0.002500	0.001858	0.002119	0.001529	0.001505	0.001727

PCM cold storage under various ventilation conditions

Pavel CHARVAT and Milan OSTRY

Brno University of Technology, Brno, Czech Republic

Abstract

Cold storage is a way to deal with peak cooling loads. Cold storage integrated with building structures is independent of the approach used for building cooling – it can be used with passive cooling as well as mechanical cooling. High thermal storage capacity in a narrow temperature interval makes phase change materials (PCMs) a suitable medium for cold storage in built environments. A set of experiments was performed with the aim to investigate performance of PCM cold storage in building structures under various ventilation strategies. The experiments were carried out in two identical test rooms located in an attic of a building. The main problem of PCM cold storage in building structures is the discharge (rejection) of heat. Three ventilation strategies were used to reject heat from cold storage. These strategies were: natural ventilation, mechanical supply of unconditioned outdoor air and mechanical supply of air-conditioned air.

Keywords: ventilation, phase change materials, cold storage

Introduction

The increasing use of air-conditioning in Europe and throughout the world leads to higher consumption of electricity in the buildings. Buildings already account for most of the electricity consumption in the developed countries. Modern architecture favors light-weight building structures and transparent building envelopes. Such buildings have a very low thermal mass and the external and internal heat gains immediately translate into the increase of indoor temperature (causing discomfort of the occupants). That makes air-conditioning unavoidable in many cases.

Another trend that can be seen today is the increasing use of air-to-air air-conditioning systems (e.g. variable refrigerant flow systems). The air-to-air systems are being installed in the types of buildings where only chilled-water systems were used in the past. Modern air-to-air air-conditioning systems are easy to install, boast with high COP, and most of them can operate in the space heating mode. Those features make them a really good option in the climates where space cooling dominates but space heating is also needed during a certain part of the year. Unlike the chilled-water systems, where ice thermal storage can be employed to deal with the peak cooling loads, the thermal storage capacity has to be provided by the building itself in case of the air-to-air air-conditioning systems. That is where cold thermal storage in building structures can be employed.

PCM thermal storage

Matter can exist in three phases – solid, liquid and gas – and the transition from one phase to another is associated with transfer of latent heat. Phase change is more or less an isothermal process (more for pure chemical elements less for mixtures of substances). The liquid-gas

phase change has been successfully used in many technical applications (steam turbine cycles, vapor compression cycle, etc.). The utilization of solid-liquid phase change is much less common in technical applications and its most promising potential can be seen in the area of thermal storage. Unlike sensible heat storage, where the amount of stored heat is proportional to the change in temperature of the heat storage medium, latent heat storage allows to store huge amount of heat at almost constant temperature.

The expression phase change material (PCM) generally refers to a material with high heat of fusion that is used for thermal storage purposes. The phase change materials have become a well established category in the material science and they are finding their way to application in many new areas. A number of phase change materials suitable for heat storage applications have been identified and many more materials are being developed. Sharma et al. (2009) presents a review on thermal energy storage with phase change materials. The obvious advantage of PCMs in thermal storage is their high thermal storage capacity in a very narrow temperature interval. This advantage can be utilized in cold thermal storage in building structures. Unlike ice thermal storage that operates at rather low temperatures, the PCM cold storage can operate at room temperature and thus to contribute to higher energy efficiency of air-conditioning systems.

Selection of a suitable PCM for cool thermal storage in building structures is not an easy task. Organic PCMs do not suffer from phase separation during phase change and deterioration of their properties with the undergone number of melting cycles is relatively small – Shukla et al. (2009). On the other hand, organic PCMs have relatively low density and thermal conductivity. Also, their flammability can pose a fire hazard in some situations. Inorganic PCMs offer relatively high values of heat of fusion (latent heat) per unit of mass and their thermal conductivity is generally better than that of the organic PCMs. Hydrated salts, that represent the most common inorganic PCMs, contain water and they have to be kept in airtight containers as not to change the water content. One of the main problems with the hydrated salt PCMs is their tendency for supercooling – cooling below the melting temperature without changing the phase. Supercooling of hydrated salts can be considerably reduced when a small amount of nucleating agent is added to the PCM. The nucleating agent initializes crystallization and thus suppresses the supercooling effect.

The advantage of PCM thermal storage in comparison to sensible heat storage can be observed in the chart in Figure 1. The chart shows the results of an environmental chamber experiment with the aluminum containers filled with the Rubitherm® SP 25 blend. The blend has a melting temperature of 26°C and congealing temperature of 25°C. The heat storage capacity in the temperature range 15/30°C is 180 kJ/kg. One of the containers in this experiment was filled with water instead of the PCM in order to obtain comparison between

latent heat and sensible heat storage. The air temperature in the chamber was increased to 29°C at the rate of 0.1 K per minute and afterwards it was maintained at 29°C for 10 hours. Then the air temperature in the chamber was decreased to 20°C (at the rate of 0.1 K per minute) and kept at that level for another 10 hours. As can be seen, the temperature of water-filled container followed very quickly the air temperature in the chamber while it took almost 12 hours for the container filled with Rubitherm® SP 25 blend to reach temperature of 29°C. The phase change is not distinctly visible in the melting period. There is a distinct change in the slope of the temperature curve at about 26°C (apparently caused by the phase change) but there is no temperature plateau so well known from the theory. The phase change is much better recognizable in the congealing period. A slight supercooling at the initialization of congealing can be seen in the chart but it is rather small.

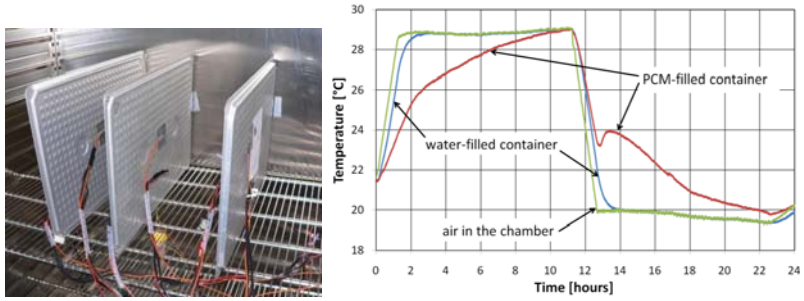


Fig. 1 Comparison of latent heat and sensible heat thermal storage

Experimental facility

Investigations of the performance of PCM cold storage integrated with building structures were carried out in two test rooms located in the attic of one of the university buildings (Figure 2). Each of the test rooms has a floor area of 14.9 m^2 and volume of 29.4 m^3. The test rooms have the same shape and dimensions. The walls of the test rooms are thermally insulated with 200 mm of mineral wool. Internal and external surfaces are covered with gypsum wall boards. A vapor barrier is installed under the internal covering.

The light-weight partition between the rooms is insulated with 400 mm of mineral wool in order to minimize heat transfer between the rooms. The clearance height of the rooms is 2300 mm. The light-weight ceiling is also covered with gypsum wall boards and insulated with 200 mm of mineral wool. There is a skylight in each of the room. The skylights are operable and are facing south west.

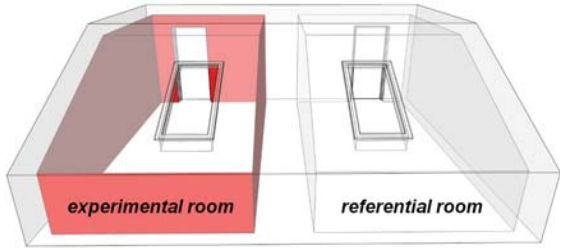


Fig. 2 Test rooms

In total 240 containers filled with the PCM were installed in one of the test rooms (the room will be referred to as the experimental room). The containers were installed on walls and the ceiling (Figure 3). The total latent heat storage capacity is approximately 36 MJ. An air handling unit is installed at the test rooms. The unit is fitted with a direct evaporator for mechanical cooling of supply air. The air supply (by means of a textile air diffuser) is situated under the ceiling and the exhaust air is extracted through the grills at the bottom of the wall. Air supply through the wall mounted grills located at the ceiling is also possible.



Fig. 3 Experimental room with PCM filled panels

Three ventilation scenarios were investigated: natural ventilation, mechanical supply of unconditioned outdoor air and mechanical supply of air-conditioned air.

Scenario 1 (natural ventilation): No energy is needed to provide ventilation in natural ventilation case but the air change rate cannot be controlled. The configuration of the test rooms does not allow cross ventilation and single-sided ventilation through the skylights is not very efficient.

Scenario 2 (mechanical ventilation with unconditioned air): The use of mechanical ventilation allows control of the ventilation rates. A minimum ventilation rate was maintained during daytime and a high air change rate was used overnight. Unconditioned outdoor air was used all the time.

Scenario 3 (mechanical ventilation with air-conditioned air at night): The minimum ventilation rate was provided during daytime (with unconditioned outdoor air) and air-conditioned air was supplied to the rooms at night.

Results and Discussion

As expected, the scenario 1 (natural ventilation) was not very effective in combination with cold storage in the tested configuration (Figure 4). The daily temperature swing in both rooms was rather small, though some stabilizing effect of additional thermal on the indoor temperature in the experimental room can observed. The experiments were carried out in early June when the highest outdoor air temperatures were relatively low (rarely exceeding 30°C). The air change rates could not be measured in this scenario, but considering the

moderate decrease of temperature in the rooms overnight the air change rates had to be quite small.

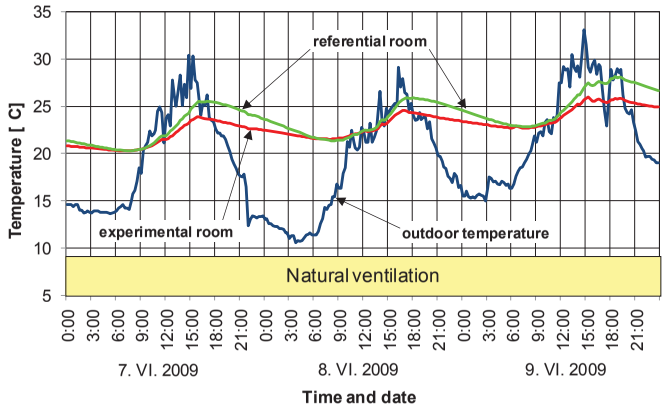


Fig. 4 Scenario 1 – all-time natural ventilation

The scenario 2, in which unconditioned outdoor air was supplied into the rooms (Figure 5), showed better results than natural ventilation. The controller of the air handling unit did not allow control of the air flow rate with regard to the outdoor temperature, therefore, a time schedule for air flow rates was used. The air handling unit operated at minimum capacity from 6 A.M. to 8 P.M. and over the night it operated at the maximum capacity. The decrease of indoor temperature in both rooms was much steeper when passive cooling by intensive mechanical ventilation was used at night than in case of natural ventilation. Even better results could be achieved with a better location of the air intake of the air handling unit. The air intake was located at the roof and the outdoor air drawn into the intake had a higher temperature than was the outdoor air temperature at a nearby (distance of 100 m) weather station. This can be one of the problems when using night ventilation passive cooling technique in urban areas (urban heat island).

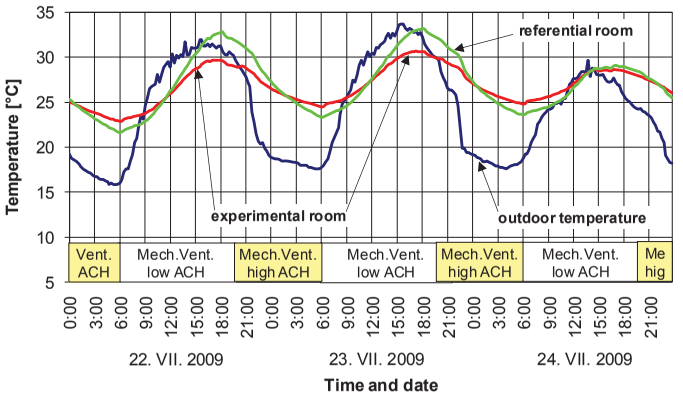


Fig. 5 Mechanical ventilation with unconditioned outdoor air

The best results were achieved in scenario 3 when air-conditioned air was supplied into the rooms at night (Figure 6). The air supply time schedule was similar to scenario 2: mechanical ventilation with the air handling unit operating at minimum capacity was used from 6 A.M. to 8 P.M. The unconditioned outdoor air was supplied to the rooms during this period. Mechanical cooling of supply air was used overnight (from 8 P.M. to 6 A.M.). There can be seen a steep decrease in indoor temperature when the air-conditioning was enabled.

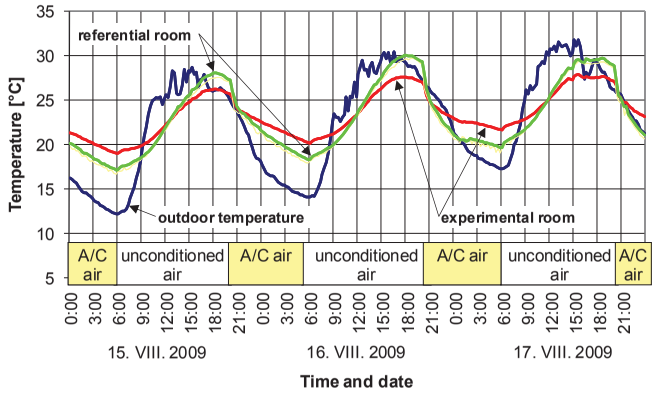


Fig. 6 Mechanical ventilation with air-conditioned air at night

Conclusions

Many office buildings with light-weight building structures suffer from overheating on hot sunny days in summer. As a consequence, mechanical cooling has to be used to maintain acceptable level of thermal comfort for the occupants. That leads to the peaks in electricity consumption on hot summer days. The consumption peaks can be reduced by application of energy saving measures. The reduction of heat gains (proper solar shading, use of low-consumption office equipment, etc.) should be the first step in the reduction of cooling load. Other measures can follow; thermal storage and passive cooling among them. This article deals with the use of latent heat cold storage integrated in building structure. As demonstrated, this approach can be used with both passive and mechanical cooling.

The experiments carried out in the test rooms showed that passive cooling by intensive night-time ventilation may not be sufficient for discharge (rejection) of latent heat from thermal storage on hot sunny days. That does not mean that passive cooling by night time ventilation is unsuitable in combination with PCM cold storage. It rather indicates that a close attention has to be paid to passive cooling and its limits (e.g. in connection to urban heat island). The experiments carried out in the test rooms showed that temperature of outdoor air supplied to the rooms was a few degrees higher than outdoor temperature measured at the nearby weather station. There is usually not a universal solution to any problem and the same applies to building cooling. Each cooling technique should be employed in the situation that suites it the best. Passive cooling can be used under favorable conditions and mechanical cooling can kick in when passive cooling becomes insufficient. Many buildings today use sophisticated building management system that make it possible to implement control strategies that would employ passive and mechanical cooling in a manner that minimizes energy consumption and operating costs.

Acknowledgments

This work was supported by the project BUT No. FAST-S -10-33 ”Efficient latent heat storage in structures of low-energy buildings” and the contribution itself by the project of Czech Ministry of Education No. OC10051.

References

1. Artmann, N., Manz, H., Heiselberg, P., (2007) Climatic potential for passive cooling of buildings by night-time ventilation in Europe, Applied Energy, Volume 84, pp. 187-201.

2. Artmann, N., Jensen, R.L., Manz, H., Heiselberg, P. (2010) Experimental investigation of heat transfer during night-time ventilation, Energy and Buildings, Volume 42, Issue 3, Pages 366-374.

3. Breesch, H., Bossaer, A., Janssens, A., (2005) Passive cooling in a low-energy office building, Solar Energy, Volume 79, pp. 682–696.

4. Eicker, U., Huber, M., Seeberger, P., Vorschulze, C., (2006) Limits and potentials of office building climatisation with ambient air, Energy and Buildings, Volume 38, pp. 574–581.

5. Liu, H, Awbi H.B., (2009): Performance of phase change material boards under natural convection, Building and Environment, in press doi:10.1016/j.buildenv.2008.12.002

6. Ryu, H.W., Hong, S.A., Shin, B.C. and Kim, S.D. Heat transfer characteristics of cool-thermal storage systems. Energy Vol. 16, No.4 pp.727-737, 1991

7. Shukla, A., Buddhi, D. and Sawhney, R.L. (2009): Thermal cycling test of few selected inorganic and organic phase change materials, Renewable Energy, Vol. 33, pp. 2606– 2614

8. Sharma, A., V.V. Tyagi, Chen, C.R., Buddhi, D. (2009) Review on thermal energy storage with phase change materials and applications, Renewable and Sustainable Energy Reviews Vol. 13, pp. 318–345.

Study on the Feasibility of Heat Pump Desiccant System Combined with Cogeneration System in Heating and Humidification Mode

Beungyong Park[1], Sihwan Lee[1], Shinsuke Kato[2], Yujin Nam[3]

[1] Graduate Student, The University of Tokyo, Dept. of Architecture, Tokyo, Japan 153-8505
[2] Professor, The University of Tokyo, Institute of Industrial Science, Tokyo, Japan 153-8505
[3] JSPS Research Fellow, The University of Tokyo, IIS, Tokyo, Japan 153-8505

Abstract

Recently, in order to reduce energy consumption in the building sector, many air-conditioning systems have been proposed and applied to real buildings. Of particular note, air-conditioning systems that treat sensible and latent loads separately have been assessed as efficient in hot and humid climates. In this study, a highly efficient desiccant system combined with a cogeneration system and a heat pump desiccant system has been developed. The main concept of this system is to utilize the waste heat from the other systems, namely the cogeneration system and the solar heat system, to assist the desiccant material to recover, and to function in concert with the desiccant and heat pump systems. This paper describes a feasibility study into the proposed system, which was conducted based on an annual energy simulation, and assessed the system's performance under various conditions. The case studies were conducted using an energy simulation tool, TRNSYS 16, with comparison to a general ventilation system, a heat recovery ventilator and a heat pump desiccant system, respectively. The sensible and latent loads, indoor air temperature and relative humidity in all cases were calculated using an energy simulation. It was found that the proposed system could save more energy than these other conventional systems through its more efficient use of waste heat.

Keywords: Cogeneration, Heat-pump system, Desiccant system, Energy simulation, Ventilation

Introduction

The energy consumed by heating, ventilating, and air-conditioning (HVAC) systems accounts for about 40% of all energy consumption in the building sector, which equates to 39% of civilian energy consumption [1, 2]. Accordingly, the building sector is obliged to reduce its energy consumption while maintaining control over the humidity in buildings. Moreover, desiccant-based systems represent an environmentally friendly technology by utilizing the capabilities of sorbents to control the moisture content in air [3]. Air-conditioning systems that treat sensible and latent loads separately have already been proposed and applied. Several advanced studies have been conducted on desiccant materials, their progress in system configurations, and hybrid desiccant air-conditioning systems using solar energy and recovery energy [4]. Moreover, a novel self-regenerating heat pump system was recently developed by directly attaching sorbents to the heat exchangers of a new type of heat-pump desiccant (HPD) system [5, 6]. Aynur et al. evaluated the performances of the heating and humidification mode and dehumidification mode in the field [6, 7, 8]. The heat-pump desiccant system was concluded to consume less energy than variable refrigerants. Nevertheless, there remain some concerns about undesirable side effects, such as poor ventilation of the return air and an imbalance in the air volume. There is a high possibility that the compressor of heat pump could automatically shut down when hot and cold air is supplied to a HPD system.

Objectives

In this study, we proposed a highly efficient desiccant system combined with a cogeneration system and a HPD system (CHPD). The main feature of this system is a more efficient design of HPD system through outdoor air supply for both pre-heating and pre-humidification. This study focuses on the CHPD system that is able to satisfy the need for a comfortable indoor environment while saving energy. In order to evaluate the performance of proposed system were conducted using TRNSYS 16.

Methods

1. System description

The operational mechanism is illustrated in Figures 1. The proposed system is combined with a hot-water desiccant system and HPD system. This system will increase its focus on the energy efficiency solutions based on cogeneration and solar water heat. The HPD system, uses a type of refrigerant (R410a), consisted of two heat exchangers with adsorption material, an expansion valve, a four-way value, a hermetic scroll compressor, and ducts attached. A detailed explanation of the HPD system can be found in Reference [7]. The hot-water desiccant system consists of a water pump, a four-way valve, a three-way valve and two heat

exchangers also covered with water-vapor-absorbing desiccant materials. In the first cycle (Fig. 1 (a)), hot water (60°C) flows into the left heat exchanger and raises its temperature. Humid warm outdoor air (OA2) is supplied to the evaporator of the HPD system as the supply air. At that stage, the supplied air and dehumidified return air (X) mix. The moisture in the humid air (VII) is absorbed by the evaporator surfaces of the HPD system, and is exhausted outdoors in the exhaust air (VIII). This process is expected to support a poor airflow rate from return air and to prevent automatic shutdown of the heat pump's compressor when cold air is supplied. The pre-heated outdoor air (OA1) is supplied to the condenser of the HPD system as supply air. However, the supplied air (IX) is more humid and hot, it makes a warm and humidity indoor environmental conditions. When the evaporators of the HPD system and hot-water desiccant systems need to be restored, the second cycle (Fig. 1 (b)) comes into effect. The position of each air damper and valves will be change.

2. Analysis conditions and instrumentations

In order to evaluate the various system performance conditions, several case studies were conducted using energy simulations, which were compared with conventional ventilation systems, such as general ventilation, heat recovery ventilator, HPD system and CHPD system. The analysis of simulation case was explained in Table 1. The total sensible and latent loads were simulated between the energy request and the admitted variation of indoor air temperature and relative humidity. Figure 2 is a schematic plan of the office as simulation model. The detailed simulation conditions are shown in Table 2. The office is located in Kumagaya, Japan. This office was installed a mechanical ventilation system to achieve a ventilation rate of 0.5 times per hour. The indoor air temperature and relative humidity were specified based on ASHRAE comfort ranges [3]. Table 3 shows detailed information on the HPD system, total and latent capacities, power consumption, and humidification rate. Besides, this research assumed specific capacities for the hot water desiccant systems that were half those of the HPD system, but the air exchange rate is the same at 57.4 m^3/h. The evaluation of CHPD system was carried out from November to March. During this heating period, the average outdoor air temperature and absolute humidity were found to be 7°C and 34 g/kg respectively. This was a stand-alone operation by the ventilation and combined heating and cooling systems, but the heating and cooling systems only operated from 9:00 to 18:00 except on weekends. No heating or cooling was provided when the building was vacant.

3. Evaluation methodology

Modeling of desiccant air-conditioning systems has been studied extensively in previous research during past decades [9, 10]. It is difficult to make a simulation model that can factor in the influence of control strategy parameters, such as the mass of desiccant, the heat

exchange surface areas, heat transfer coefficient, and regeneration temperature. Moreover, most of the results involved limited study of rotary desiccant systems, and the HPD system is a new type of heat exchange system with adsorption material attached to the wheel. In this instance, this study decided to adapt a model for the simulation. It is easy to apply parameters for operating data from the enthalpy capacity, sensible capacity, latent capacity and electrical energy consumption provided in the manufacturer's catalogues [11]. Accordingly, this study determined the supply temperature and humidity using the following equations.

$$\dot{Q}_{sen} = \dot{m}_{OA-SA} \cdot c_p \cdot (T_{SA} - T_{OA}) \quad \text{(Eq. 1)}$$

$$\dot{Q}_{lat} = \dot{m}_{OA-SA} \cdot (w_{SA} \cdot h_{gSA} - w_{OA} \cdot h_{gOA}) \quad \text{(Eq. 2)}$$

$$\dot{Q}_{total} = \dot{Q}_{sen} + \dot{Q}_{lat} \quad \text{(Eq. 3)}$$

$$h_g \cong 2500.9 + 1.82 \cdot T \quad \text{(Eq. 4)}$$

where C_p [kJ/kg·K] is the specific heat, h_g [kJ/kg] is the enthalpy of air, h_{gSA} [kJ/kg] is the enthalpy of supply air, h_{gOA} [kJ/kg] is the enthalpy of outdoor air, $\dot{m}_{OA-SA}$ [kg/s] is the air mass flow rate to supply air from outdoor air, $\dot{Q}_{sen}$ [kW] is the capacity of sensible heat, $\dot{Q}_{lat}$ [kW] is the capacity of latent heat, $\dot{Q}_{total}$ [kW] is the capacity of total heat, T_{SA} [ºC] is the supply air temperature, T_{OA} [ºC] is the outdoor air temperature, w_{SA} [kg /kg] is the humidity ratio of supply air, w_{OA} [kg /kg] is the humidity ratio of outdoor air.

A load demand is calculated based on set-temperature and set-humidity to make a good environmental condition. The supply air and humidity are giving the tendency equation from, load capacity. Here shows a tendency equation at 22ºC ~ 24ºC and 40%RH ~ 50%RH in Figure 3. Tendency of supply air and humidity from the load capacity data is shown here. Moreover, Figure 4 shows a flow chart of the load calculation for the general ventilation system and Figure 5 is for heat recovery ventilator. Figure 6 shows a flow chart of the load calculation to include discrimination for HPD system while Figure 7 is for CHPD system.

Results and discussion

The simulation results for temperature and humidity are shown in Figure 8 and Figure 9 during both stand-alone and heating/cooling-assisted operation from January 9th to January 15th. It is including the weekend of January 14th and 15th. The hot water desiccant assisted HPD system provided the best thermal condition. It was found that, the HPD system maintained an indoor temperature of 12ºC ~ 19ºC with humidity of 56 g/kg ~ 74 g/kg. The CHPD system maintained an indoor temperature of 15ºC ~ 25ºC and humidity of 62 g/kg ~ 78 g/kg. The CHPD system can reduce the sensible heat load and latent heat load by about 61% from Case 1. The general ventilation system consumed more energy, at about 1,698 kWh (sensible load: 1,358 kWh, latent load: 339 kWh). The HPD system managed to reduce

that by about 47%RH, while the CHPD system achieved about a 61%RH reduction. Moreover, the HPD system by itself consumed about 4,114 kWh, whereas the one integrated into the CHPD system used 1,759 kWh. The demand load, sensible load and latent load is shows in Figure 10. As seen from Figure 11, which shows the electrical energy consumption by the HPD system, it was found that the combination of a hot-water desiccant system, pre-heating and pre-cooling, and HPD system could save energy. Figure 12 shows the comparison of the indoor thermal environment as operating ventilation system

Conclusions

This paper presents the development of a highly efficient desiccant system combined with a cogeneration system and a heat-pump desiccant system (Case 4). A feasibility study of the proposed system was conducted based on an annual energy simulation. Through this case study, the system performance was estimated under various conditions. The calculation results from the simulation are shown as follows:

1. The CHPD system maintained an indoor temperature and relative humidity of 18^{o}C ~ 24 ^{o}C and 50%RH ~ 70%RH respectively through ventilation as a stand-alone operation.

2. The general ventilation system consumed more energy at about 1,698 kWh (sensible load: 1,358 kWh, latent load: 339 kWh). The CHPD system had 61%RH less energy consumption (sensible load: 565 kWh, latent load: 105 kWh). The HPD system was about 47%RH less.

3. The electrical consumption of the CHPD's HPD element (Case 4) was 57%RH less than that of the HPD system by itself (Case 3).

It was determined that the proposed system can achieve better energy savings than the other conventional systems through the efficient use of waste heat. In future, a more detailed simulation including the operations schedule and the system capacity will be estimated by calculating the annual performance factor. Furthermore, an experimental analysis using full-scale equipment will be conducted in a real office building.

Acknowledgment

This study was made possible by the financial support received from the Tokyo Gas Engineering Co., Ltd, Japan.

References

1. U.S Department of Energy, 2009 Building Energy Data Book, 10, 2009.

2. Payne FW., “Energy Management Control System Handbook,” Fairmont Press, 1984.

3. ASHRAE, “Handbook of Fundamentals American Society of Heating, Refrigerating and Air-conditioning Engineers”, Atlanta, USA (Chapter19), 1989.

4. D. La, Y. j. Dai, Y. Li, R.Z. Wang, T.S. Ge., “Technical Development of Rotary Desiccant Dehumidification and Air Conditioning: A review,” Volume 14, Issue 1, Renewable and Sustainable Energy Reviews, January 2010, pp. 130-147.

5. Shuji IKEGAMI, Nobuki MATSUI., “Heat Exchanger which Directly Supports Adsorbent for High Efficiency Desiccant, ” JSME annual meeting, Japan, 2007(3), pp. 23-24.

6. T.N. Aynur, Y. Hwang and R. Radermacher., “A Heat Pump Desiccant unit for Dehumidification and Humidification, ”12th International Refrigeration and Air Conditioning Conference at Purdue West Lafayette, IN, USA (2008), pp.1–8.

7. Tolga Nurettin Aynur, Yunho Hwang, Reinhard Radermacher., “Field Performance Measurements of a Heat Pump Desiccant unit in Heating and Humidification mode,” Volume 42, Issue 5, Energy and Buildings, May 2010, pp678-683.

8. T.N. Aynur, Y. Hwang, R. Radermacher., “Integration of Variable Refrigerant Flow and Heat Pump Desiccant Systems for the Heating Season,” Energy and Buildings, 2009.

9. Pascal Stabat, Dominique Marchio., “Heat-and-mass transfers modelled for rotary desiccant dehumidifiers”, Volume 85, Issues 2-3, Applied Energy, February-March 2008, pp. 128-142.

10. G. Panaras, E. Mathioulakis, V. Belessiotis., “Achievable working range for solid all-desiccant air-conditioning systems under specific space comfort requirements”, Volume 39, Issue 9, Energy and Buildings, September 2007, pp. 1055-1060.

11. http://ec.daikinaircon.com/ecatalog/DKCB010/index.html

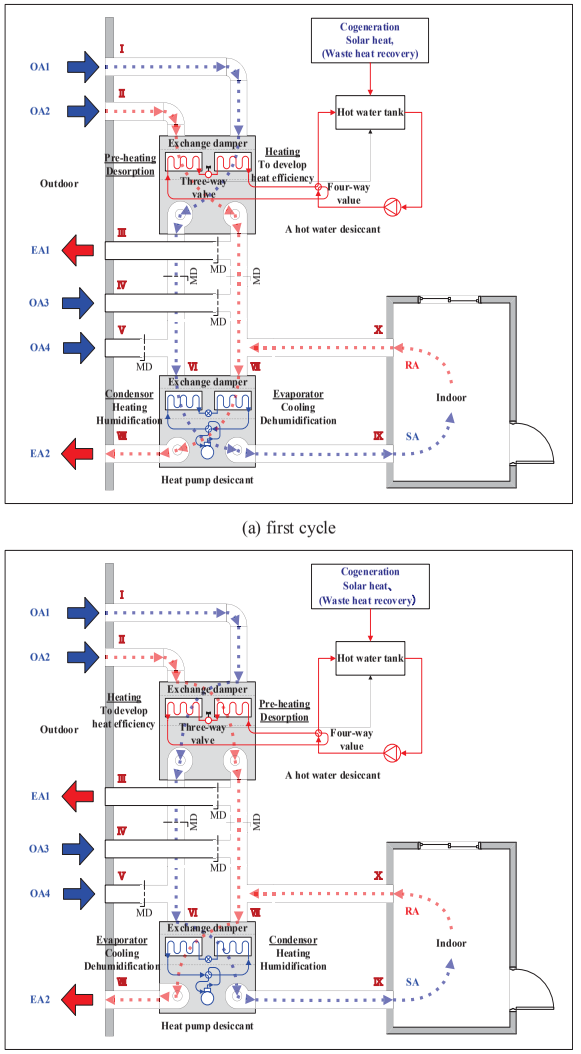


Figure 1 Operation diagram of the CHPD system

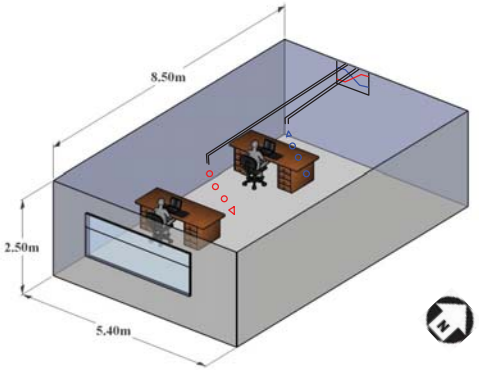


Figure 2 Schematic plan of the office

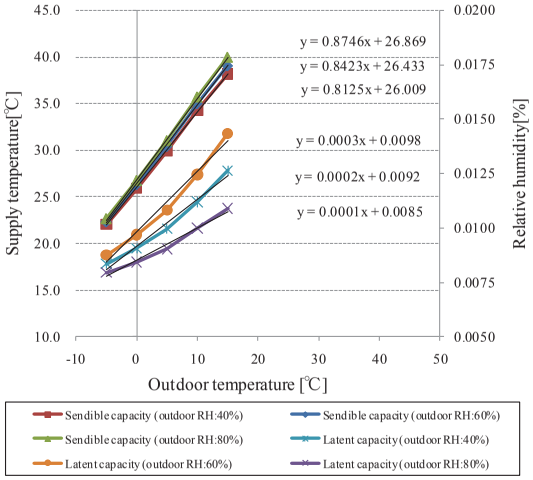


Figure 3 Tendency of supply air and humidity from the load capacity

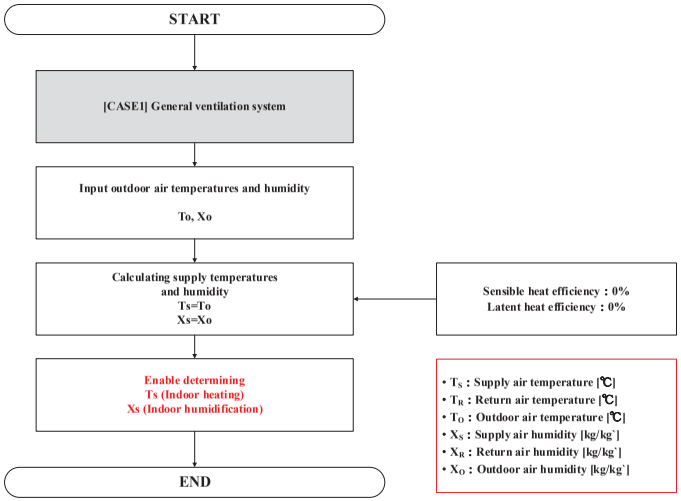


Figure 4 Flow chart of load calculation of the general ventilation system

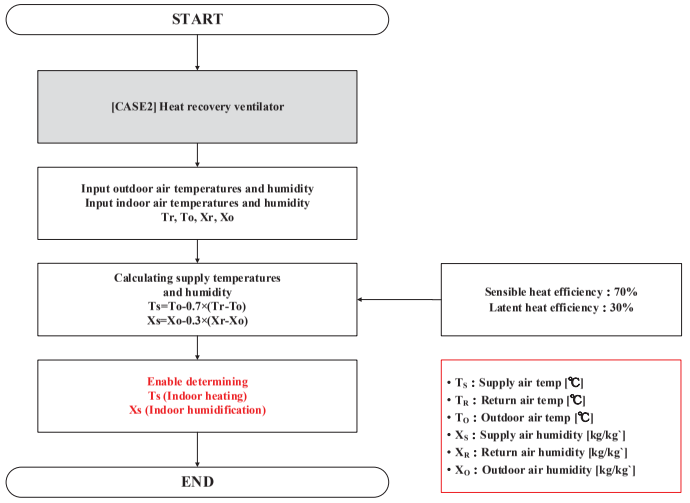


Figure 5 Flow chart of load calculation of the heat recovery ventilator

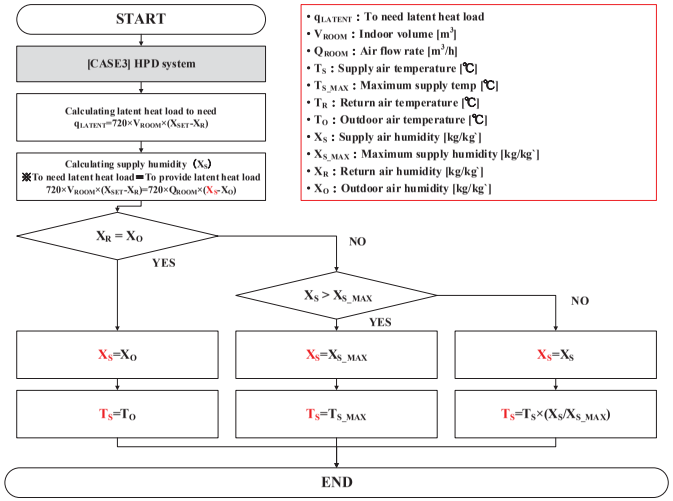


Figure 6 Flow chart of load calculation of the HPD system

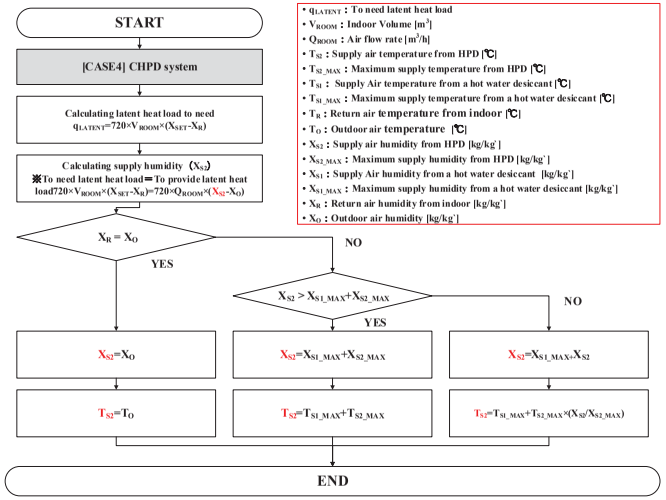
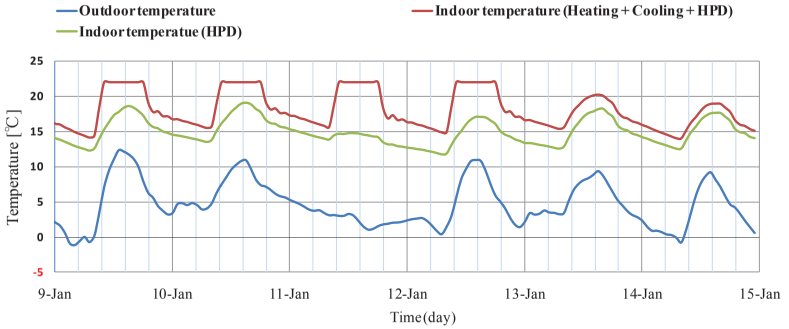
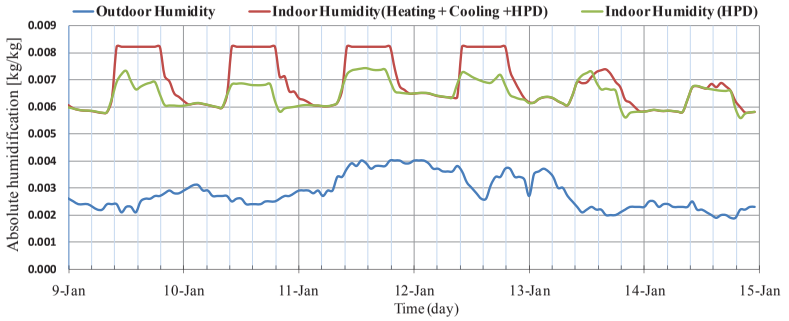


Figure 7 Flow chart of load calculation of the CHPD system

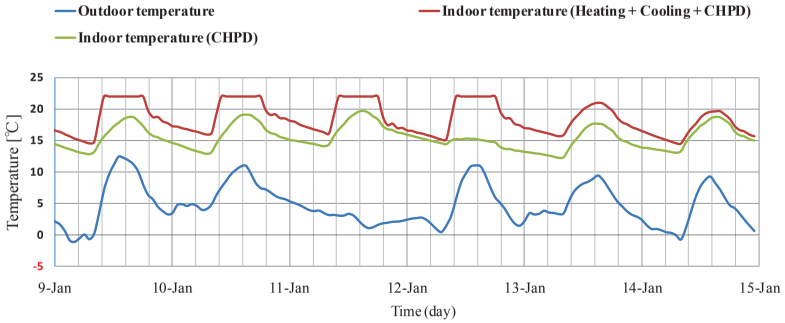


(a) Temperature distributions of indoor

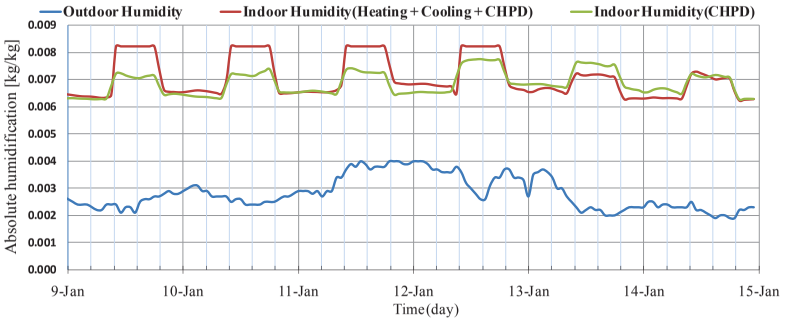


(b) Humidity distributions of indoor

Figure 8 The simulation results of Case 3



(a) Temperature distributions of indoor



(b) Humidity distributions of indoor

Figure 9 The simulation results of Case 4

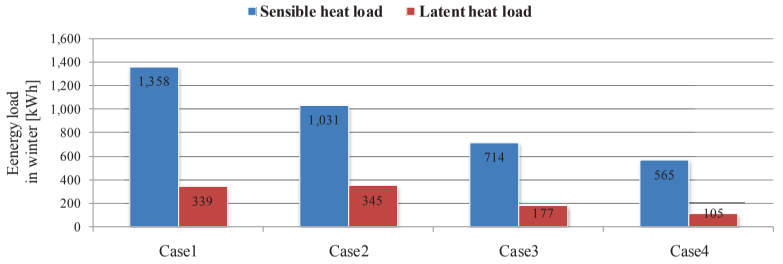


Figure 10 Case study : To request of energy load for target environment in winter

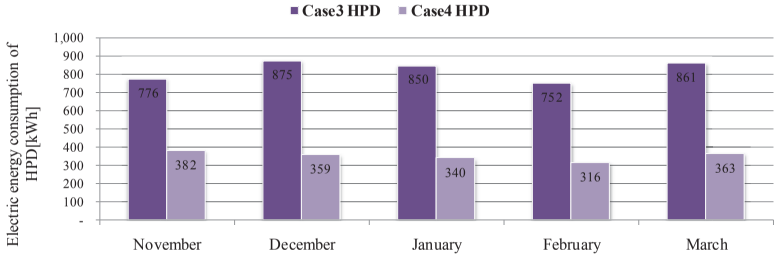


Figure 11 Compare to electric energy consumption of HPD system

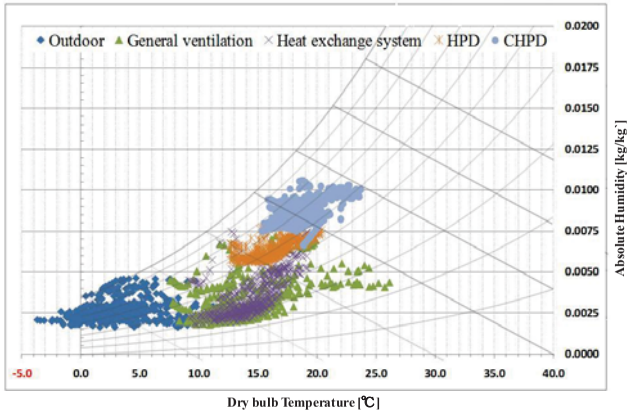


Figure 12 Comparison of the indoor thermal environment by Cases

(The indoor temperature and humidity show the provided indoor conditions by ventilation on January)

Table 1 Analysis of Cases

	Analysis of system	Reference
Case1	General ventilation system	Sensible efficiency : 0% Latent efficiency : 0%
Case2	Heat recovery ventilator	Sensible efficiency : 70% Latent efficiency : 30%
Case3	HPD system	Operation data from manufacture's catalogues
Case4	CHPD system	The capacity of Hot water desiccant System is 50% of HPD system and Here, HPD system is also used operation data from manufacture's catalogues.

Table 2 Simulation condition model and building details

Target model	Depth 5.4m × Width 8.5m × Height 2.5m
Control condition And operation schedule	Operation schedule : 08~18hours Set temperature, relative humidity : 22 [ºC], 50[%] From November to March
Weather data	AMeDAS* weather data, Kumagaya city, Japan
Heat transfer coefficient	Wall : 0.49 [W/m^2·K], Floor : 2.00 [W/m^2·K], Window : 5.69 [W/m^2·K], Window frame : 8.17 [W/m^2·K]
Air change rate	0.5 times per hour (57.4 [m^3/h])
Internal load	Two computers (0.42 [kW/h]), Two persons (0.3 [kW/h])

* AMeDAS : Automated Meteorological Data Acquisition System, developed by the Japan Meteorological Agency

Table 3 Specification of the heat pump desiccant system

Amount of airflow		500 [m^3/h]
COP		3.78 [kg/h], 4.13
Heating and Humidification	Total heat capacity / Latent heat capacity	7.1/ 4.4 [kW]
	Power consumption	1700 [W]
Indoor conditions		22[ºC], 50[%]
Outdoor conditions		0[ºC], 50[%]

Air Leakage Tests for the requirements of the LEED in two high-rise residential buildings

Hyun Kook Shin[1], Hyun Cho[2], Kwan Woo Kim[2], Hoi Soo Seo[2], Jae Hun Jo[1]

[1] Chungbuk National University, Dept. of Architectural Engineering, Cheongju, Korea
[2] POSCO E&C Corp., Incheon, Korea

Abstract

Air leakage test was carried out according to ASTM E779-03, Standard Test Method for Determining Air Leakage Rate by Fan Pressurization to meet the requirements of the LEED-NC v2.2(EQp2). Air leakage tests for quality assurance can be performed once all work on the air barrier has been completed and all windows and doors have been installed in two high-rise residential buildings. Test units selection was carried out in accordance with the following guidance, California's 2001 Energy Efficiency Standards. That is, 1 in 7 dwelling units was sampled, and dwelling units were grouped for testing according to unit size and type. Finally, we completed pressurization and de-pressurization tests for 240 residential units and the final readings were a level of 0.87 square cm per square meter of surface area or less.

Keywords: Airtightness, Blower door, LEED, Residential Building

Test building descriptions

Two high-rise residential buildings in Korea are selected as the test buildings for airtightness measurements. Both buildings are now constructed and have similar types of inter-walls and

slabs. But there is a quite difference in the exterior walls; one is a curtain wall system, the other is a punched window. These residential buildings are similar to tower shaped-office buildings in various aspects; they generally have a central core, elevator shafts and stairwells, are surrounded by corridors, and have 4 to 5 residential units on each floor. General information regarding these two buildings is given in Table 1.

Table 1 Test building summaries

Classification	A	B
Building address	Yeonsu-gu, Incheon, SOUTH KOREA	
Number of stories	2 basements , 47 stories	2 basements , 11~33 stories
Test date	Feb. 2010 ~ Jun. 2010	Apr. 2010 ~ Sep. 2010
The estimated year of construction	Nov. 2010	Dec. 2010
Ventilation system	balanced ventilation	
Air view		

Test method and conditions

Dwelling unit air infiltration performance shall be tested to required standards as outlined in LEED-NC Reference Guide under EQp2 Option 3. Dwelling units must be constructed to a level of air infiltration performance such that blower door testing carried out in accordance with ASTM E779-03 results in readings of air infiltration at a level of 1.25 square inches of leakage area per 100 sq. ft. of surface area or less (0.87 square cm per square meter of surface area). Both “Preliminary” and “Final” Blower Door Testing shall be performed to full test requirements as described in ASTM E779-03 “Standard Test Method for Determining Air Leakage Rate By Fan Pressurization” Should any units fail the Blower Door Test procedure – to exceed allowable air leakage parameters as outlined herein (excluding “preliminary” Blower Door Testing) – the re-testing procedure for failed units shall adhere to the requirements as outlined in the Residential Manual for Compliance with California’s 2001 Energy Efficiency Standards, Chapter 4 “Compliance Through Quality Construction.” Pressure differential testing shall be required where entry doors into dwelling units from common corridors are not weather-stripped. Pressure differential testing shall be required to demonstrate a pressure differential of an average of 5Pa and at all times at least 1Pa as measured at 10 second intervals for a 15 minute period of time. Testing shall be performed as per test conditions outlined in the LEED-NC v2.2 Reference Guide (Second or Third Editions). Test shall be based on “worst case conditions” of transport of air from dwelling unit to adjacent spaces, with all entry doors and windows closed. Testing shall be performed as per previously described sampling methodology, and can be performed on same units identified for “Final Blower Door Testing.”

The envelope air tightness test was carried out in accordance with the following standards: ASTM E779-03 "Standard Test Method for Determining Air Leakage Rate by Fan Pressurization" The building was pressurized and depressurized using a blower door system. The blower door system comprises of a portable fan capable of supplying 40,776/hr at 50 Pascal's. The fan was set up in the entrance door of the test residential unit. Pressure differences across the fan and the building were measured using a digital manometer (Retrotec DM-2A) at the start, during and the end of the test. Air temperatures were measured using a Data Logger TH-101. Measurements were taken at the start and end of test. Wind

speeds at the start and end of the test were measured using a TESTO 445. Barometric pressure readings were taken using a PTB220 Class A.

Table 2 Test equipments

Equipment Type	No.
Blower door set: Retrotec 2200 Fan	2
Blower door set: Retrotec 3300SR Fan	3
Retrotec DM 2A Manometer	3
Digital thermometer: Data Logger TH-101	3
Multi-function meter: TESTO445	1
Digital barometer: PTB220 Class A	3
Smoke generator	1
Notebook	3
2-way radios	6

Table 3 Openings and temporary sealing conditions

Detail	Response
All external door and windows	Closed
All internal doors	Open
All extracts (check kitchen and bathroom(s) extracts and the oven hood)	Sealed
All drainage traps (check all toilet sinks)	Sealed
Combustion appliances	Off
Ventilation openings	Sealed
Dryer	No



Fig. 1 Supporting photos of the air leakage test



Fig. 2 Supporting photos of the temporary sealing

Checking test limits

Section 8.4 of the ASTM E779-03: The product of indoor-outdoor temperature difference and building height must be less than 200m℃. In this case, the building is a dwelling house with a floor to ceiling height of 3.1m (4.8m for penthouse). The indoor-outdoor temperature

difference during the test is 1~7℃. Multiplied together, these temperature difference give 3.1m × (1~7℃) = 3.1~21.7m℃ (4.8m × (1~7℃) = 4.8~33.65m℃ for penthouse), therefore, this test passed. The average wind speed is 1m/s or less, and the average outdoor temperature is 15℃, thus meeting the specifications of 8.5 of the ASTM E779-03. Ten pressure difference and flow measurements are made between 10 and 60 Pa, thus meeting the requirements of 8.10 of the ASTM E779-03.

Test units selection

Test units selection was carried out in accordance with the following guidances: 'Reference Guide - Blower Door Test' and 'California's 2001 Energy Efficiency Standards, Chapter 4, Compliance Through Quality Construction'. That is, 1 in 7 dwelling units was sampled, and dwelling units were grouped for testing according to unit size and type.

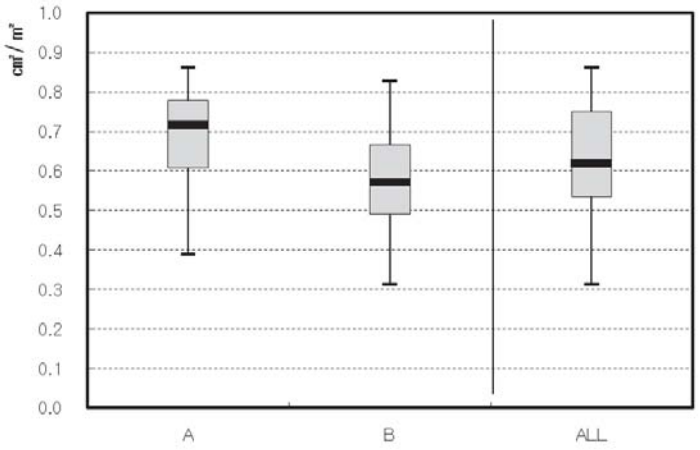


Fig. 3 Airtightness results

Conclusions

Air leakage tests of two high-rise residential buildings were carried out according to ASTM E779-03 "Standard Test Method for Determining Air Leakage Rate by Fan Pressurization" to meet the requirements of the LEED-NC v2.2(EQp2). Air leakage tests for quality assurance can be performed once all work on the air barrier has been completed and all windows and doors have been installed. Finally, we completed pressurization and de-pressurization tests for 240 residential units and the final readings were a level of 0.87 square cm per square meter of surface area or less which are the 'pass'.

Acknowledgments

This research is supported by a grant from High-Tech Urban Development Program, Super-Tall Building R&D Project (VC-10), funded by the Ministry of land, transport and maritime affairs.

References

1. ASHRAE, 1997 ASHRAE Handbook-Fundamentals. Atlanta: American Society of Heating, Refrigerating and Air-Conditioning Engineers, Inc., 1997.

3. ASTM, ASTM E779-03 "Standard Test Method for Determining Air Leakage Rate by Fan Pressurization" American Society for Testing and Materials, U.S.A., 2004.

4. ATTMA, ATTMA TS1-Measuring Air Permeability of Building Envelopes, 2007.

5. ISO, ISO 9972:2006 Thermal performance of buildings -Determination of air permeability of buildings-Fan pressurization method, 2006.

6. CMHC, Energy Audits of High-rise Residential Buildings, Technical Series 97-100, 1996.

7. Max H. Sherman, The Use of Blower Door Data, LBL Report No. 35173, 1998, 03.

8. Max H. Sherman, & Darryl J. Dickerhoff, Airtightness of U.S. Dwellings, ASHRAE Transaction, Vol. 104, 1998.

9. The Energy Conservatory, Operational Manual for Minneapolis Blower Doors, The Energy Conservatory, 1993.